SERI/TP-351-431

SSEA

Proceedings

Systems Simulation and Economic Analysis

January 23-25, 1980
San Diego, California

Sponsored by:
Systems Development Division
Office of Solar Applications
Department of Energy

Coordinated by:
Solar Energy Research Institute

DISCLAIMER

NOTICE

SERI/TP-351-431

DISTRIBUTION CATEGORIES
UC-59,60 & 63

CONFERENCE 800101

SYSTEMS SIMULATION AND ECONOMIC ANALYSIS

CONFERENCE PROCEEDINGS

JANUARY 23-25, 1980

BAHIA HOTEL

SAN DIEGO, CALIFORNIA

SPONSORED BY:

SYSTEMS DEVELOPMENT DIVISION
OFFICE OF SOLAR APPLICATIONS
DEPARTMENT OF ENERGY

COORDINATED BY:

SOLAR ENERGY RESEARCH INSTITUTE

CONFERENCE CHAIRMAN

LAWRENCE M. MURPHY, PH.D.

PREFACE

SECOND SYSTEMS SIMULATION AND ECONOMIC ANALYSIS CONFERENCE (SSEA)

January 23-25, 1980

The SSEA conference is currently the only open forum for comprehensive solar systems analysis. This conference provides an excellent opportunity to enhance and evaluate the coordination of various technical, economic, and policy disciplines.

Interest and participation in this conference has grown rapidly since the inception of the concept two and one-half years ago. More than 175 individuals participated during this meeting. Some 75 technical and economic presentations were given in the two and one-half day conference. Photovoltaics, wind, process heat, and thermal electric as well as solar heating and cooling (SHAC) systems were discussed. Continued growth and participation is expected, not only in the area of SHAC (the major emphasis of this year's conference) but also in other solar technologies as well. Clearly, as newer technologies such as ocean thermal and photochemical concepts evolve closer to the applications stage, systems issues are expected and encouraged to be aired in this program.

The importance of including and coordinating numerous disciplines on specific needs of industry emerged from the conference. The keynote speaker, Dr. Fred Morse, emphasized the imperative to rapidly accelerate the implementation of solar energy systems by understanding and assisting the solar industry. Dr. Morse felt that the industry needs assistance now and cannot wait until all analysis development is complete. As an analogy, Dr. Morse pointed out that flying was feasible long before comprehensive analysis and predictive capabilities were available for aircraft. Thus, the interactive combination of application and analysis has proved beneficial to the advancement of the aircraft industry where a significant portion of the research and analysis effort supported the needs that were first identified by industry. Similarly, the expertise in this group might be best focused on the resolution of needs identified by the solar industry. Therefore, speakers were asked to address whom their research benefits, directly, how it is expected to be used, and how it will eventually assist the solar industry.

During the conference, session chairpeople were asked to provide their insights regarding both the technical and general content of the conference. The following discussion is based on those comments.

There was general agreement that the meeting was quite useful. For example, it was pointed out that the opportunities for personal and professional interaction and the comprehensive review of current activity related to simulation and analysis was valuable for all participants. Particularly helpful is the opportunity to provide peer review and criticism for all DOE funded projects that may or may not be on sound technical ground. The present format also offers DOE officials, contractors, and other professionals the unique opportunity to discuss current and future programmatic and policy issues. For instance, many open evening discussions were held on issues like the national controls plan, the national cooling plan, and the best methods of meeting industry needs.

This conference re-emphasized a number of unresolved specific issues that include:

- There is a need for a widely acceptable and precise definition of validation. The requirements of the various user groups should be understood and these users should be keenly aware of what validation is as well as the limitations of current analysis approaches.
- The controls community still disagrees about the relative merits of various control types. Further, one expert suggested that the controls community does not thoroughly understand the significance of various contractors' work.
- There is still disagreement on the relative merits of various solar water heater system configurations, based on experiments and analysis. An example is the controversy surrounding one tank and two tank systems. This issue appears resoluble by more carefully studying insulation and tank placement. Other controversies concerning reliability do not seem as easily resolved.
- Builders, designers, and engineers need simple, hybrid (combined active, passive, and conservation) analysis methods. There is currently no simple* method of analyzing, much less optimizing, a mix of solar and conservation measures.
- Use of appropriate simulation tools should be encouraged. Government policy that advocates simulation methods that are more complex and time-consuming than the user needs should be examined. Further, when model developers advocate the widespread use of simulation methods, two points should be kept in mind. First, because people in industry usually develop modeling tools

*A case can be made that no simple or complex method can adequately handle the general hybrid problem.

specific to their needs, simple tools often provide the most assistance to them. Second, the more complex methods often do not, as is often assumed, offer greatly increased accuracy, but offer instead a better understanding of the physics involved.

- The need to use a comprehensive standard set of assumptions was also cited. Often issues arise because assumptions are not clearly stated, and comparisons either cannot be made or are inappropriately made. The identification of crucial assumptions, the establishment of an acceptable comparative methodology, and a standard reporting format are needed. The SERI Standard Assumptions document is a significant step in that direction, but it must be further refined and extended to all solar technologies.

The value of the Second Systems Simulation and Economic Analysis Conference has been established and the original, defined goals have been met. In addition to the speakers and session chairpeople, many have contributed to the success of this conference, which was supported by the Systems Development Division, Office of Solar Applications, DOE. The assistance of Drs. Fred Morse, J. Michael Davis, Sam Schweitzer, and Roger Bezdek is gratefully acknowledged. The members of the SERI Training Development and Conference Branch, namely, Vicky Curry, Kate Blattenbauer, Donna Post, Yvonne Bishop, Zo Milne, and Judy Hulstrom, are also cited for their excellent administrative and coordination effort.

L. M. Murphy, Ph. D.
Conference Chairman

TABLE OF CONTENTS

Session IA

Dr. William Beckman
University of Wisconsin
Chairperson

SYSTEMS SIMULATION I

SYSTEM ANALYSIS FOR MULTIZONE BUILDINGS

J. Ottenstein, J.W. Mitchell and W.A. Beckman
Solar Energy Laboratory
University of Wisconsin
Madison, WI 53706

ABSTRACT

An analysis of the application of solar energy to multizone buildings is performed using TRNSYS with a model of a variable air volume system formulated for the purpose. The model includes conventional heating and cooling equipment, heat recovery chiller, economizer cycle, and storage tank. Solar collectors and an absorption chiller are then added to the building. The results lead to a number of conclusions about the feasibility of solar energy systems for multizone buildings.

INTRODUCTION

Solar heating and cooling of residential buildings is a topic that has been extensively researched [1, 2]. However less work has been done on applications of solar energy for multizone buildings. These buildings have different energy use characteristics than residential buildings due to the fact that as buildings size increases, the volume increases at a faster rate than the envelope area. Internal heat generation is proportional to the volume of the building while infiltration and transmission heat losses are proportional to the envelope area. Thus, as building size increases, cooling loads increase faster than heating loads.

Another characteristic of a multizone building is that the heating and cooling system must control individual zones which have widely different thermal loads. It is common to provide simultaneously heating to one zone and cooling to another. This requires systems and controls that are more complex than those used in residential applications.

In this paper, a method is presented for simulating the thermal response of multizone buildings with TRNSYS [3]. The building model and system HVAC models are described. These models are exercised with and without solar collection systems added to the base HVAC system. Several conclusions regarding the interaction of the systems and the feasibility of solar energy systems for multizone buildings are discussed. These results are described in more detail in [4].

COMPONENT MODELS

Building Models

The TRNSYS component model for the building devides the structure up into thermally similar zones. Each of these zones is treated as having uniform rates of environmental heat flows, energy generation, ventilation, etc. These are shown schematically in Fig. 1. The zones on the periphery are designated by their compass directions. The remaining zones are a top story with a roof, and a totally interior core region. These divisions do not allow a detailed representation of the loads in each individual room. Rather, they are suitable for an overall assessment of the thermal interaction between solar and HVAC systems and the building.

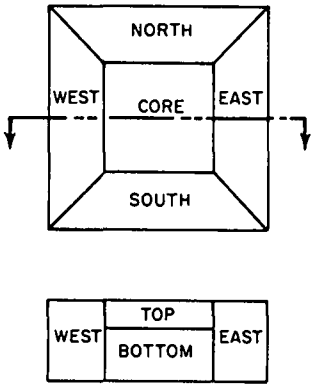

Fig. 1 Building Zones

In the results presented in this study, a particular three-story building was simulated in the Madison, WI climate. The building is 30m by 30m in cross section and 11m high, and divided into six zones. It is occupied five days a week from 8 AM to 6 PM. The lights and ventilation system are on only during occupied hours. There is assumed to be no outside air infiltration, and no humidification is provided.

Conduction gains and losses through external walls and roofs are modeled using the transfer function method described in ASHRAE [5]. Window solar gains are calculated directly from incident solar radiation. The heating and cooling loads are calculated from these losses and gains using the room transfer function method [4,5].

The necessary inputs for the model are given in Table 1 along with the characteristics for the particular building. The building is represented with a minimum of detail.

HVAC System Model

It was decided that the variable air volume (VAV)

Table 1
Building Description
3 Story Building, 30m x 30m x 11m High

Walls: ASHRAE Wall No. 1
$U = 0.579\ W/m^2°C$
$\alpha = 0.5$
$\varepsilon = 0.8$
20% of area is double glazed windows
$U = 3.4\ W/m^2°C$
$\tau = 0.8$
Roof: ASHRAE Roof No. 8
$U = 0.522\ W/m^2°C$
$\alpha = 0.5$
$\varepsilon = 0.8$
Capacitance: Thermal 6.2×10^8 J/°C
Moisture 1.1×10^5 kg
Internal construction is medium
Internal Loads: Lights: $21.5\ W/m^2$
People: $10\ m^2$/person
Sensible - 75 W/person
Latent - 55.6 W/person
Ventilation Requirements:
Outside Air: 0.00283 kg/sec-person (5 cfm/person)
Ventilation: 1 Air Change/hr
Exhaust: 0.0569 kg/sec (100 cfm) for each perimeter zone

system is the most appropriate for use with solar energy systems. The variable air volume system has very low energy consumption, which is important because any air conditioning system that is used in conjunction with a solar system must be energy conserving. Energy is conserved because reheat is reduced to a minimum and fan power is reduced. Outside air can also be used for cooling purposes (economizer cycle). Variable air volume systems are presently being installed on about 50% of all new buildings.

Figure 2 shows the generalized variable air volume system for which the component model was developed. A zone thermostat controls the flow rate of air entering each zone by means of a damper. This flow rate has a maximum determined by design, and a minimum due to ventilation requirements. In addition to these parameters, the design conditions for the interior, the fan pressure drop-flow characteristics, the desired supply air temperature, and the chiller characteristics are required.

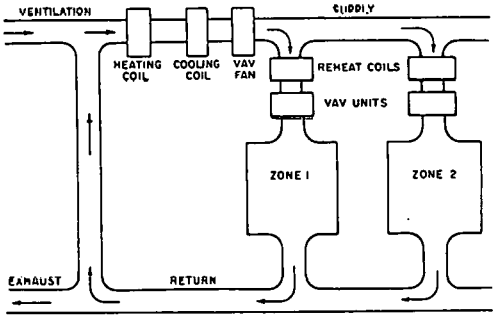

Fig. 2 Variable Air Volume System

Control System Model

Energy rate control and temperature level control are both commonly used in simulations of building performance. The advantage of energy rate control is that a single determination of the time dependent heating and cooling load of each zone can be made, stored on mass storage, and re-used in subsequent simulations. Simulations run with energy rate are lower in cost than temperature level control, which is important when a large number of zones are simulated. However energy rate control is not entirely realistic in that actual systems are temperature level controlled. Temperature level control provides a more detailed and realistic simulation of the load supply interaction. However, since the load is dependent on the heating and cooling system, it is no longer possible to calculate the load one time only and re-use that data in subsequent simulations, and thus simulations cost more than with energy rate control.

SIMULATION RESULTS

Comparison of Energy Rate Control and Temperature Level Control

Simulations were run to compare energy rate control and temperature level control. A month simulation of the cooling load of the six zone building with a time-step of one hour uses about 11 cpu-seconds in temperature level control. During the heating season, the differences in calculated loads were negligible. Calculated cooling loads for three summer months are given in Table 2. Since the actual cooling loads are highly sensitive to many additional variables such as building capacitance, glass transmittance, lights, solar radiation, etc., either value is probably representative. The difference in calculated cooling load between energy rate control and temperature level control is small enough to be neglected in building simulations.

Table 2
Comparison of Energy Rate and Temperature Level Control

Month	Energy Rate Control	Temperature Level Control	Percent Difference
Jun	139.9 GJ	133.6 GJ	+4.5%
Jul	149.4 GJ	150.9 GJ	-1.0%
Aug	122.2 GJ	129.6 GJ	-5.7%

Building Loads

The weekly cooling load, heating load, chiller work, lighting energy, and internal heat generation over the course of the year are presented in Fig. 3. Internal heat generation includes lights and sensible and latent loads from people. The cooling load is significantly greater than the heating load but chiller energy is significantly less than the heating energy required. Over half of the cooling load is due to internal heat generation. Heating and cooling loads are not coincident due to two factors. First, the economizer cycle provides cooling when the ambient temperature is low. Second, the large capacitance of the building allow energy from lights, people, and solar radiation to be stored in the

building structure for heating at night.

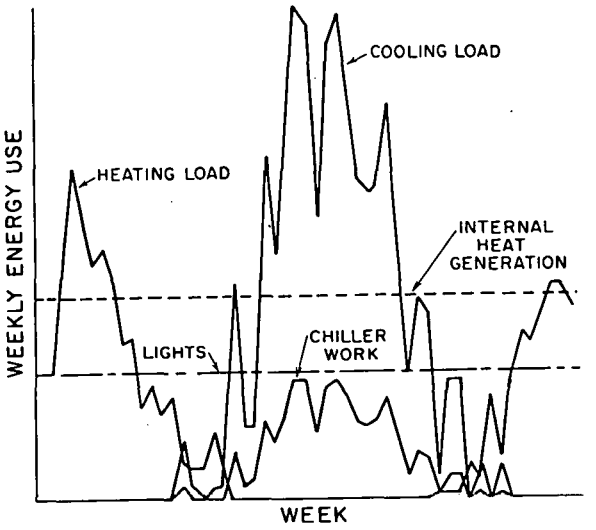

Fig. 3 Weekly Building Energy Use

Table 3 is a summary of the building energy usage by source. The building simulated is a small, well insulated, tightly constructed building in Madison, Wisconsin, a location with winters much colder than most places in the U.S. The cooling load is larger than the heating load because of internal heat generation. This reduces the potential for solar heating systems. Lighting levels are low by past standards but lighting energy is larger than the sum of all other energy requirements. The cooling load caused by solar radiation can be reduced by the use of reflective glass and overhangs. Fan energy is a significant fraction of chiller energy. These characteristics would be general for many areas of the country.

Table 3
Summary of Base System

Type of Use	Energy Usage (GJ)
Lights	543.9
Fuel	339.5
Fans	31.6
Chiller	126.8

Heat Recovery System

The heat recovery system is a heat pump which uses the interior of the building as its heat source. The heat pump COP is high because the source temperature is high, although the heat source is limited by internal loads. Storage tanks are needed if the recoverable energy is to become a large fraction of the heating load. Large load heat exchangers are needed to keep the supply water and tank temperatures low so that the required cut-off temperature will be low and the chiller COP high. Heat recovery systems dump energy that is not needed by the use of the economizer cycle.

The influence of storage volume on the performance of the heat recovery system during the heating season is shown in Fig. 4. For storage sizes in the range of daily storage, there are reductions in auxiliary heating and purchased energy. Chiller work increases due to the greater transfer of energy between the storage tank and building interior. The heat recovery system can provide a significant fraction of the heating load. Storage tanks significantly increase the amount of energy recovered. Heat recovery systems are physically compatible with solar systems in that storage is required; however, the heat recovery system reduces the heating requirement.

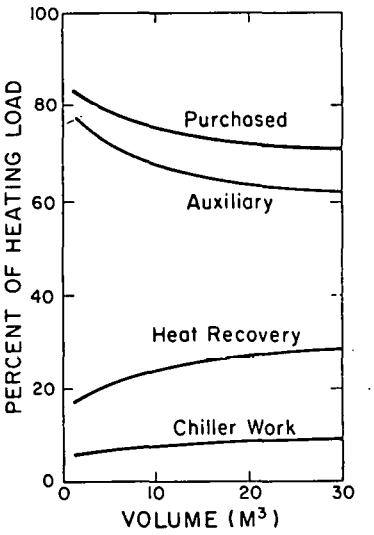

Fig. 4 Heat Recovery System Effect of Storage Volume

Solar-Heat Recovery System

A solar energy system was added to the VAV system as shown in Fig. 5. Solar energy transfers heat to the storage tank for use in heating. An absorption chiller is also provided to allow solar energy to be used for cooling. The heat pump can reject the cooling load to either the storage tank or to the cooling tower, as desired. In winter, the heat recovery chiller acts as a heat pump which uses the interior of the building as a heat source to heat perimeter zones. In summer, it acts as an ordinary chiller.

The operation of the system is controlled by tank temperature. In cold weather, the tank temperature is generally low, and the heat pump is used to provide cooling. This cooling load together with solar energy is transferred to the storage tank where it is used in the perimeter heating system. During warmer seasons, more energy is supplied to the tank than is needed by the load. When the tank temperature rises to a specified cut-off temperature, the air conditioning system switches to the economizer cycle. Heating is provided by the solar energy through the storage. When the ambient air temperature is greater than the supply air temperature of the air conditioning system, the economizer cycle cannot be employed. The absorption chiller is operated from the tank. Any cooling load not met

by the absorption chiller is met by the auxiliary chiller.

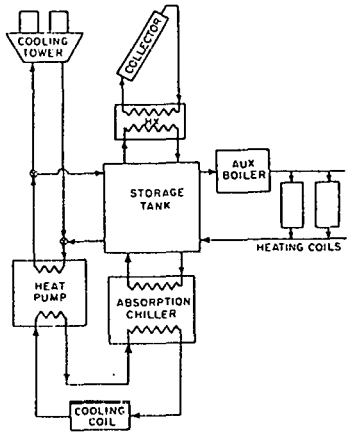

Fig. 5 Solar Heat Recovery System

Table 5 shows the monthly fraction of the heating load met by solar energy, recovered energy, chiller work, and auxiliary energy for a system with a collector area of $200m^2$ and a storage tank volume of $30m^3$. Adding a solar system to a heat recovery system reduces the amount of purchased energy required. However, it also reduces the amount of cooling energy recovered, but also reduces the chiller work required. These interactions need to be considered in the design of any building.

Table 5
Solar Heat Recovery System
Heating Season Performance
Collector Area - $200m^2$
Storage Tank Volume - $30m^3$
Cut-off Temperature - 50°C

	F_{Solar}	$F_{Chiller\ Work}$	$F_{Heat\ Rec.}$	F_{Qux}
Oct	100.0	0	0	0
Nov	51.1	5.3	15.7	28.6
Dec	38.8	5.8	17.8	37.6
Jan	27.4	5.2	15.6	51.8
Feb	42.1	5.3	15.9	31.0
Mar	89.9	2.0	5.4	2.8
Apr	96.1	1.0	2.6	0
Yr	49.6	4.65	13.9	32.0

Table 6 shows the effect of collector area on the recovered energy and Fig. 6 shows the effect of storage volume and collector area on the fraction of the heating load met by solar. Increasing the collector area causes a large reduction in recovered energy because the collected solar energy raises the average tank temperature above the set temperature for heat pump heat rejection. This allows the economizer cycle to be employed which reduces the recovered energy.

The solar energy system helps meet the cooling load, and its contribution can be defined in two ways. The cooling fraction by solar can be defined as the fraction of the cooling load met by the solar operated absorption chiller, or it can be defined as the fraction of the electrical chiller work saved by solar energy. The second definition shows how much purchased energy is really saved. In general, the two definitions will not equal.

Table 6
Solar Heat Recovery System
Effect of Collector Area on Recovered Energy
Storage Volume - 150 L/m^2

Collector Area	Recovered Energy % of Heating Load
0 ($10m^3$ storage)	25.6
$200m^2$	13.6
$400m^2$	8.45
$600m^2$	3.21

Table 7 presents the monthly performance for one collector size, while Table 8 compares the yearly averages for three collector areas. The results indicate that the fraction of work saved is slightly less than the fraction of cooling load met. The difference tends to be most pronounced in spring and fall when the cooling load and wet-bulb temperatures are low. The reason for this is that the solar system meets a high fraction of the cooling load when the COP of the electrically driven chiller is high.

Table 7
Solar Heat Recovery System Performance
Cooling Season
$200m^2$ Collector Area
$30m^3$ Storage Volume

Month	Fraction of Cooling Load Met by Solar	Fraction of Chiller Work Saved by Solar
Apr	61.9	51.0
May	45.3	43.8
Jun	23.5	23.1
Jul	19.5	19.7
Aug	24.4	24.1
Sep	49.3	48.1
Oct	56.6	54.2
Nov	71.8	72.5
Yr	28.9	27.9

Table 8
Solar Heat Recovery System Performance
Cooling Season
150 L/m^2 Storage

Collector Area (m^2)	Fraction of Cooling Load Met by Solar	Fraction of Chiller Work Saved by Solar
200	28.9	27.9
400	52.5	51.2
600	69.6	68.3

SUMMARY

Models for the heating and cooling loads in multizone buildings have been developed for use with TRNSYS. This model allows the use of preprocessed loads in further simulations under energy rate control. With temperature level control, hour-by-hour load calculations are required. Both approaches require a minimum amount of information about building

characteristics, and are suitable for exploring different system concepts.

A model of a variable air volume air conditioning system has been developed. The model includes a mechanical chiller, cooling tower, heat recovery heat exchanger, and a variety of control options. Solar collection systems and absorption cooler can readily be added. This allows determination of performance of a variety of alternative systems.

The simulations revealed a number of interactions between the various components of the solar-heat recovery system. First, the initial cost of the solar system is proportionately less than that for residential units due to year around collection and shared costs among the various systems. Heat recovery systems are compatible with solar systems in that both require storage tanks and heat exchangers. Second, heat recovery chillers may reduce the size and cost of a solar system, but also reduce the solar savings. Third, recommended storage volumes per collector area established for solar heating systems appear to be adequate for solar heating and cooling systems as well. Fourth, the rated capacity of the solar driven absorption chiller has a significant effect on the amount of solar cooling. In addition, the high COP of electrically driven chillers and the low COP of absorption chillers will usually make electrical auxiliary less expensive then fuel auxiliary. Fifth, there are detrimental interactions between the economizer cycle and the heat recovery system. Sixth, solar heating and cooling systems will be most economically feasibility in situations where large heating and cooling loads occur. Seventh, the need for seasonal simulations as opposed to design point analyses in assess overall system performance is demonstrated.

ACKNOWLEDGEMENT

This work has been supported by the Solar Heating and Cooling Research and Development Branch, Office of Conservation and Solar Applications, U.S. Department of Energy.

REFERENCES

[1] W.A. Beckman, S.A. Klein, and J.A. Duffie, Solar Heating Design, John Wiley and Sons, New York (1977).

[2] J.A. Duffie and W.A. Beckman, Solar Energy Thermal Processes, John Wiley and Sons, New York (1974).

[3] Solar Energy Laboratory of the University of Wisconsin, TRNSYS - A Transient Simulation Program, Engineering Experiment Station Report 38, (1978).

[4] J. Ottenstein, "Application of Solar Energy in Multizone Buildings, M.S. Thesis, University of Wisconsin (1979).

[5] ASHRAE Handbook of Fundamentals, American Society of Heating, Refrigerating, and Air Conditioning Engineers, New York (1977).

NOTES

Dup

SERI DOE-2 SOLAR SIMULATOR STUDY

By
Anthony Eden, P.E. and
David A. Simms*

Solar Energy Research Institute
Golden, Colorado

ABSTRACT

This paper discusses the Solar Energy Research Institute's (SERI) analysis of the solar energy simulator section of DOE-2, a public domain computer program that allows users to explore the energy-use patterns of proposed and existing buildings and their heating, ventilating, and air conditioning (HVAC) systems. This computer program contains a solar energy simulation portion called Component-Based Simulator (CBS) incorporated into the HVAC Plant (large equipment) section. SERI is investigating the adequacy and sensitivity of DOE-2's solar portion when various active solar energy systems and combinations of solar components are interfaced with standard space conditioning systems or used in a stand-alone mode. The components have been assembled into typical configurations and parametric test runs have been performed examining the problems associated with the program and the characteristics of the output for eventual comparison with other energy analysis computer programs.

INTRODUCTION

To provide analysis methods that would help designers reduce energy consumption and to furnish an evaluation tool for the Building Energy Performance Standard (BEPS), the Department of Energy (DOE) has been developing a computer code to model the energy consumption and air conditioning systems designs of proposed structures. Development work on the computer program called DOE-2 has been funded by DOE at Lawrence Berkeley Laboratory (LBL) and Los Alamos Scientific Laboratory (LASL) [1]. Included within DOE-2, CBS deals with the possible solar energy subsystems of such structures. This paper will discuss SERI's investigation of CBS as a part of DOE-2 and as a stand-alone computer program. The report will describe the large DOE-2 program and CBS components and outline the SERI plan, as well as give examples of preliminary results. Finally, the paper will discuss the use of other computer codes for comparison to CBS output.

GENERAL DESCRIPTION

DOE-2 is a large computer program primarily designed to aid the architect and mechanical engineer when evaluating the future performance of air conditioning systems in new buildings. The version of the code being used at SERI is DOE-2.0A that will be current until DOE-2.1 is published and released in March, 1980 [2]. LBL and LASL are performing formal research into the operations and continued development of DOE-2 [3]. SERI is investigating the computer program in support of BEPS as part of its inquiry into all solar analysis methods with a copy of the code on the CDC 6600 computer located at the Water & Power Resources Service Computer Center near Denver, Colo. SERI is scrutinizing the solar energy aspects of DOE-2 and CBS because the program is being emphasized as a design tool and evaluation method. SERI is also investigating many other solar energy computer codes to include the national solar energy code center.

DOE-2 is a very powerful computer code, capable of analyzing many different HVAC systems over a full year. The simulations of DOE-2 are mostly directed at the HVAC loads, systems, plant, and economics as illustrated by the major portions of the program shown in Fig. 1. As one can see in this simplified diagram, DOE-2 consists of five major programs, the first being the Building Design Language (BDL) Processor with its material and weather libraries containing ASHRAE Test Reference year (TRY) data [1]. Since DOE-2 was designed to allow simplified entry of the many variables needed to describe a building and its operation, BDL is necessary to analyze the user input instructions and to control subsequent simulation portions of the program called Loads, Systems, Plant, and Economics (LSPE). After the BDL processor has prepared the input for the program, data is sent to all the other elements that are used sequentially through the process of computer overlays.

Within the LSPE construction of DOE-2, Plant, which contains CBS, is the focus of the SERI investigation into the program's active solar energy system simulation capabilities. Other research at SERI will study the passive solar aspects of Loads and Systems. Within Plant, CBS is attached to the energy supply simulation allowing solar energy to be used as if it were another conventional energy source. As the HVAC data is passed to Plant from Systems through the Modified Hourly Data as shown in Fig. 1, one can program Plant to decide how to meet the energy demand most efficiently, which may include the use of available solar energy if CBS systems are programmed into the Plant options.

Investigation of CBS through Plant, while tied to the main program, can be very time consuming and expensive; however, once a sample structure has been modelled and run through DOE-2, the Systems output can be stored in a separate file for direct use by Plant. Therefore, one can accomplish later runs that involve changes only in CBS by

*This work was supported by Systems Development Division, Office of Solar Applications, DOE.

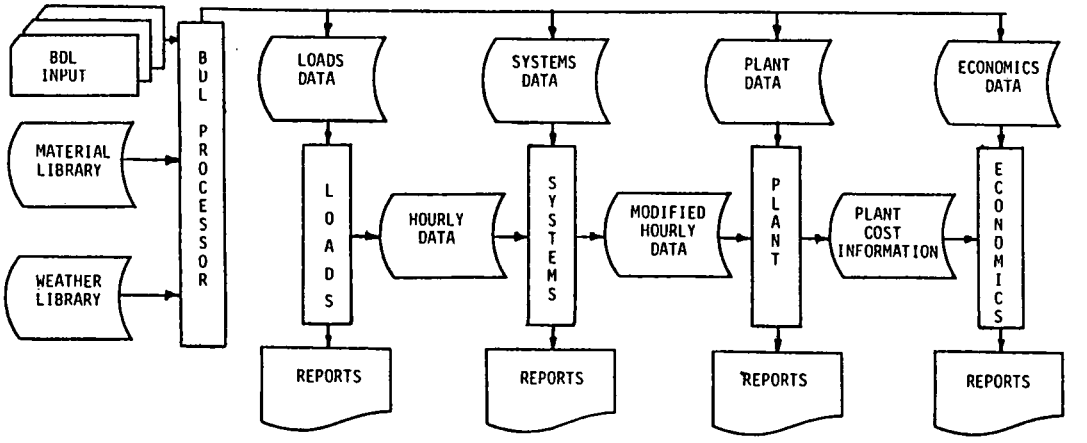

Figure 1
DOE-2 Program Outline

running Plant alone and by using previously saved Systems data files as input. Also, one can examine the reports from Loads and Systems for the HVAC load characteristics and those can be modelled separately to produce a file containing hourly loads. Both of these file-creating techniques allow one to use CBS in a stand-alone mode without needing to execute the entire DOE-2 program, thus saving time and money. One may use the degree-day simulator component available in CBS to perform the heating load calculations and to allow a parametric study of the code without using the main DOE-2 program.

CBS DESCRIPTION

The CBS portion of DOE-2 consists of many modelled active solar energy components designed to permit easy assembly by the user into various liquid and air configurations. This code structure allows flexibility in the solar energy systems design when the subsystem is still conceptual. SERI investigation of CBS is very extensive, but only a few example components will be discussed (see Figs. 2, 3, 4, and 5). CBS contains many more components than just these few illustrations including many preconnected into subsystems [2]. Figure 2 shows a collector model component consisting of four smaller components programmatically connected into this configuration. Using the procedures in CBS [2], the programmer can either use these connections of collectors, relief valves, pumps, and heat exchanger models or can chose to further divide the system into each individual component if more detail and flexibility is desired. One should refer to the CBS documentation [2] for a complete description of the possible combinations and configurations available in the computer program.

Figure 3 shows the fully mixed, unstratified storage tank component included in the DOE-2.0A version of CBS. As modelled in the figure, the fully mixed tank receives the output energy data from the collector model and simulates the reaction of a storage tank to that energy. The storage tank component then passes output data to one of the selected HVAC subsystems. Figures 4 and 5 show two possible configurations for these subsystems—one designed primarily for a commercial building and the other for a residence. As one can see in Fig. 4, the commercial system offers the designer a number of options when selecting the heating coil connections within a HVAC system. Also shown are the connections for the auxiliary system and a fresh air make-up. The residential system in Fig. 5, which has the necessary connections for the auxiliary energy system, is less complex than a real system would be in actual use.

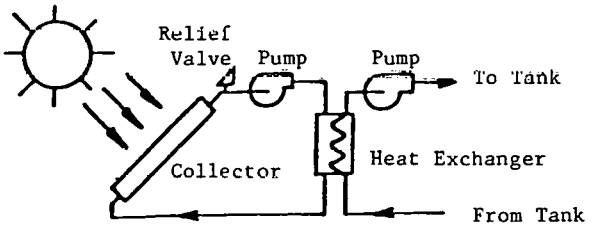

Figure 2
Collector System Model [2]

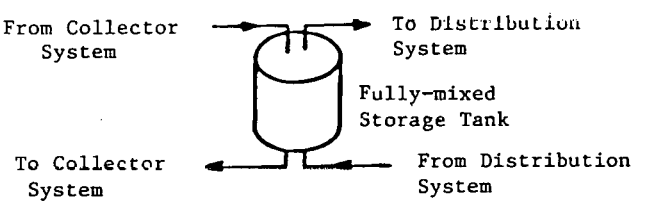

Figure 3
Storage Tank Model [2]

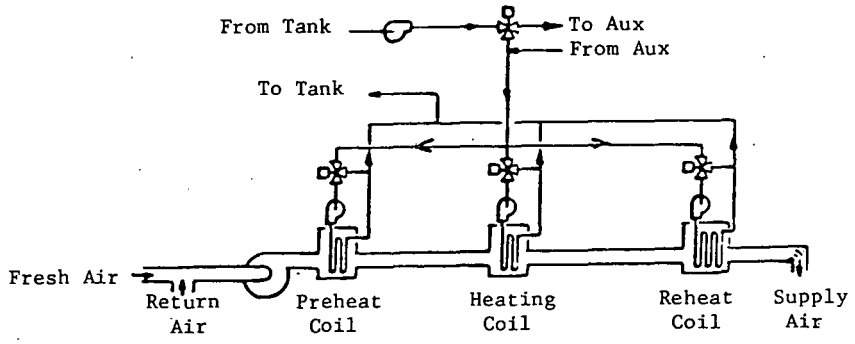

Figure 4
Commercial Distribution System Model [2]

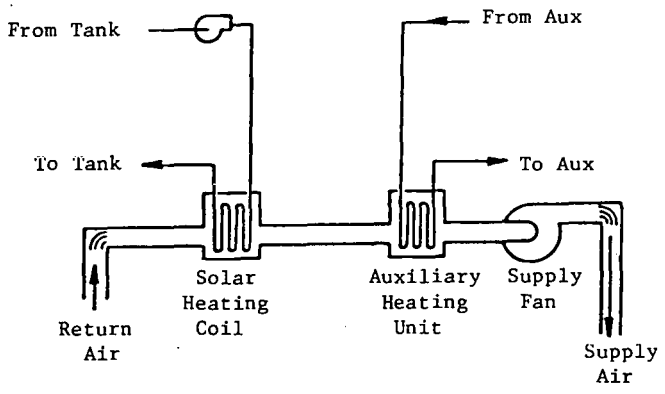

Figure 5
Residential Distribution System Model [2]

Once the solar energy system is configured by the selection and assembly of the components, the programmer chose which CBS component to use as the controller, insolation model, report format, and load simulator. As discussed previously, the load can come from a file created by a run of a DOE-2 sample, from a file of loads from any hourly simulation program, or from a degree-day load calculator. The entire program is then run for a complete year, and the results are available for study or comparison to other designs or other programs.

MODELLING APPROACH AND RESULTS

The Systems Analysis and Testing Program [4] at SERI is directing the evaluation of CBS to determine its sensitivity to various parametric changes and to compare its output to programs such as TRNSYS [5]. The researchers at SERI developed a baseline solar building model and solar energy system combination shown in Fig. 6 for the parametric studies. The basic building is patterned after Sample 3A from the DOE-2 Sample Run Book [1]. Researchers ran the complete DOE-2 program and simplified the thermal energy load output with the degree-day component into a "heating only" load. Further studies can build on this thermal energy base case. The solar energy systems were then added to the roof as shown in Fig. 6 to begin the CBS testing.

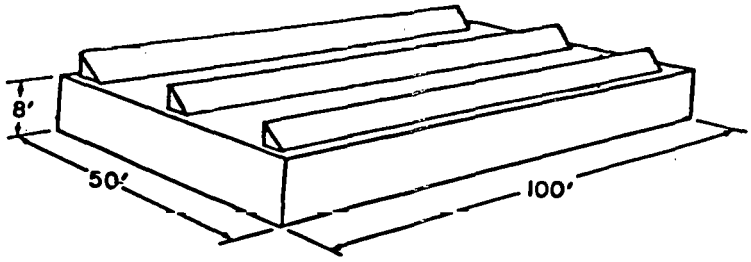

Figure 6
Simple Building with Collectors

The first systems tested were flat-plate collectors using liquid as a transfer medium. The city chosen was Chicago and the weather was the TRY data contained in the Weather Library. The weather data is prepared by a separate DOE-2 weather processor into a format compatible with the program. Future plans call for sensitivity studies that compare variations in site, systems design, and system types.

An example of the capabilities of CBS and one of many possible reporting formats is shown in Table 1. As one can see in this table, the program can analyze modelled solar energy systems and list the various outputs of interest to researchers. The data presented are summaries of the simulation of each hour collected into daily and then monthly reports. The trends of this system's performance can be noted and as the parameters are changed, these effects can also be observed. For this specific run, the liquid collector area was 4000 ft^2 of nonselective, single-glazed panels; the storage tank volume was 8000 gal. of water; and the ethylene-glycol water mixture flow rate was 100 gpm. Through the variation of these and other parameters, output can be generated and then plotted as shown in Figs. 7 and 8. Figure 7 illustrates the parametric analysis of a liquid collector system using collector area as a parameter and maintaining the ratios shown for flow rate and tank volume. As one can see, the addition of collector area shows the diminishing return in increases of average solar fraction. Figure 8 shows the relationship of an optimum flow rate with the average solar fraction while holding collector area and tank volume constant. These two figures demonstrate the direction of the research at SERI on CBS.

Table 1. SOLAR SYSTEM PERFORMANCE SUMMARY

	Total Incident Energy (Million Btu)	Total Collected Energy (Million Btu)	Total Heating Load (Million Btu)	Total Solar Heating (Million Btu)	Avg. Stor. Temp. (F)	Max. Stor. Temp. (F)	Min. Stor. Temp. (Fi)	Avg. Collector Eff. (%)	Avg. System Eff. (%)	Avg. Part Solar (%)	Avg. Solar Bldg. Load Ratio	Total Solar Elec. Load (kWh)
Jan.	112.853	17.613	23.815	7.513	103.8	128.6	97.7	15.6	6.7	31.5	4.74	126
Feb.	126.075	23.616	19.896	10.354	106.3	126.9	98.2	18.7	8.2	52.0	6.34	150
Mar.	160.584	27.540	12.487	12.487	131.3	150.9	111.9	17.2	7.8	100.0	12.86	146
Apr.	195.977	20.920	7.146	7.146	197.4	200.7	141.6	10.6	1.6	100.0	62.29	119
May	193.832	16.281	1.085	1.085	190.9	200.9	174.0	8.4	0.6	100.0	178.61	128
June	204.565	16.548	0.031	0.031	198.0	201.9	192.1	8.1	0.0	100.0	999.00	131
July	229.639	14.692	0.000	0.000	197.3	201.5	192.2	6.4	0.0	100.0	999.00	131
Aug.	210.159	14.432	0.000	0.000	196.8	201.6	190.0	6.9	0.0	100.0	999.00	135
Sept.	196.561	11.782	0.680	0.680	194.6	200.9	186.5	6.0	0.3	100.0	289.20	105
Oct.	160.418	16.586	2.643	2.643	177.1	188.6	160.1	10.3	1.6	100.0	60.70	107
Nov.	118.594	15.092	9.530	9.487	139.0	188.6	99.6	12.7	8.0	99.6	12.44	107
Dec.	95.871	13.634	16.851	4.723	101.3	110.4	97.4	14.2	4.9	28.0	5.69	130
	2005.077	208.638	90.165	52.149	160.5	201.9	97.4	10.4	2.6	57.8	22.24	1514

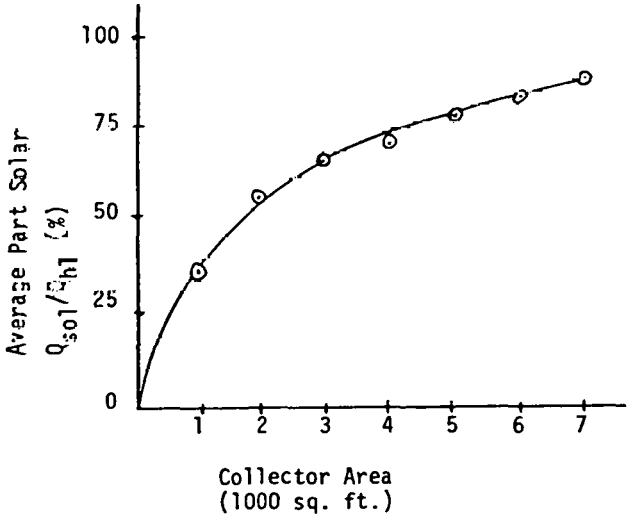

Figure 7
Plotted Parametric Output (Collector Area)

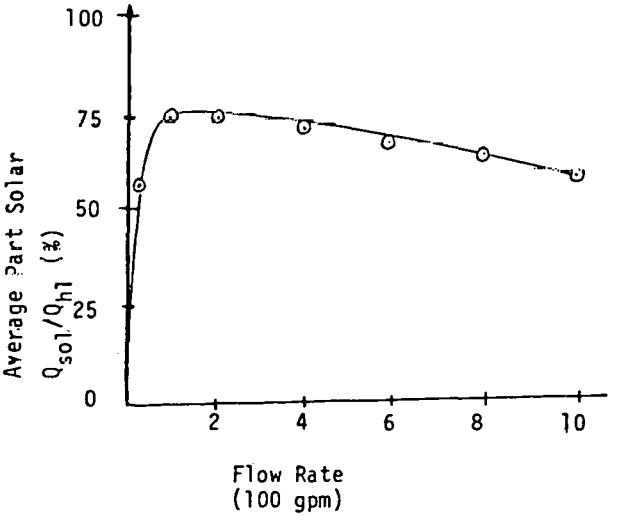

Figure 8
Plotted Parametric Output (Flow Rate)

FUTURE PLANS

Parametric analysis of CBS is being performed at SERI. Detailed comparison to TRNSYS output is a near-term objective. The plans of the Systems Analysis Branch reflect a strong desire to become thoroughly familiar with the operations of CBS both within the DOE-2 Plant and as a stand-alone modelling technique. TRNSYS appears to be the choice for the comparison of CBS to another code because of its widespread availability, its exposure in the technical community, and its generally accepted modelling accuracy. CBS is only one of many codes SERI is investigating or planning to examine closely. The researchers will compare CBS and TRNSYS outputs for agreement over a wide spectrum of solar energy systems and component combinations. Also, the researchers will vary chosen parameters to determine the changes in output of both programs and to compare any differences to develop confidence with CBS capabilities. This will be especially critical when CBS is used with DOE-2 as an evaluation tool for BEPS and to fulfill SERI's mission to become the national solar energy code center. SERI investigations of CBS support the further development of general solar energy expertise at the institution through the technical knowledge gained by the research personnel. Continued research into the operations of this and other codes supports the national planning effort for code development. All aspects of the various solar energy codes can be examined and the best of those can be highlighted for continued research. SERI is an institution that is not directly involved with developing CBS or DOE-2 and, as such, can exercise the codes and objectively report results for purposes of both research and application.

Finally, by keeping abreast of solar simulation advancements, SERI can aid LBL and LASL in determining the direction of code development by having firsthand knowledge of any shortcomings in the code and by being directly involved in future solar energy research. Such advice would be helpful by avoiding delays in program upgrading and improvements, and by having solar energy experts involved early in the conceptual phase of code development. This approach should soon benefit the modelling and analysis of proposed hybrid active/passive systems. Many other areas of investigation by LBL and LASL are possible for CBS with adequate assistance, advice, and technical knowledge from SERI.

CONCLUSION

This report has examined CBS both when used as a part of DOE-2 and when used in a stand-alone mode. A few components of CBS have been discussed as well as some typical output from a parametric study of a liquid collector system. The report also covered some of SERI's future plans for investigating the capabilities of CBS and the effects of that research on the development of the code.

REFERENCES

1. Building Analysis Group, DOE-2, LBL-8688,8689,8678, Energy and Environment Division, Lawrence Berkeley Laboratory, California, July 1979.

2. Building Energy Analysis Group, DOE-2, Version 2.1 (Draft Document), Energy and Environment Division, Lawrence Berkeley Laboratory, California, March 1980.

3. M. A. Roschke, B. D. Hunn, and S. C. Diamond, A Component-Based Simulator for Solar Systems, U.S. Department of Energy, Conference on System Simulation and Economic Analysis for Solar Heating and Cooling, San Diego, California, June 1978, pp. 8-10.

4. C. J. Bishop. Systems Analysis and Testing Program, SERI/PR-35-313, p. 7, July 1979.

5. S. A. Klein, et al., TRNSYS, A Transient System Simulation Program. Solar Energy Laboratory, University of Wisconsin, June 1979.

SYSTEMS ANALYSIS OF THE THERMAL PERFORMANCE OF OPERATING SYSTEMS

Dan S. Ward
Solar Energy Applications Laboratory
Colorado State University
Fort Collins, Colorado 80523

ABSTRACT

The principal objective of any design method or system analysis procedure is to present predicted or measured performance in an unambiguous format so that potential improvements in the operation of the system, comparisons of different operating modes, and other operating experience can be realistically evaluated. An important qualification is the availability of sufficient detail in the design method and/or sufficient data in the system's analysis to allow for definitive conclusions on the relative merits of different solar designs and/or operating conditions.

This paper will present and discuss a performance evaluation criteria which the author considers as the minimal requirement for a realistic analysis of the operating performance of a solar heating and cooling system.

INTRODUCTION

In the analysis of the operating performance of a solar heating and cooling system, two distinct approaches are utilized. The first approach constitutes the design method whereby the operating performance of a given system is predicted. Traditionally the design methods developed by the solar heating and cooling community have been directed toward the goal of predicting the non-renewable energy savings obtained by use of a solar system (and/or the fraction of a specified heating or cooling load to be met by the solar system). This number could then be utilized in turn to estimate the economic feasibility of a given solar installation.

While such calculations are certainly useful, another important reason for the validation of a design method has tended to be overlooked. In fact, one of the principal reasons for making design calculations is to evaluate the relative performance of two or more similar but distinct design alternatives. And in order to evaluate the relative performance of different designs, it is necessary to consider more than a single parameter, such as (f). Design methods must, in fact, be sufficiently detailed so that relatively 'minor' design variations do not inadvertently lead to 'major' decreases in the performance of the system and that the parameters utilized to evaluate the system are not strongly dependent upon the sheer size of the system.

Similarly, the second approach in analyzing the operating performance of a solar heating and cooling system is not merely to validate a design method or calculate cash savings (or loss) to date, but to determine the performance of components and subsystems as well as complete solar systems. The major objective of any system analysis procedure should be to present actual performance data in an unambiguous format and to provide a clear, careful analysis of the data. Emphasis must be placed on the practical evaluation of the data, effective potential improvements in the operation of the system, comparisons of different operating modes (when applicable), and other operating experiences.

In both approaches to analyzing a system's predicted and/or measured performance, it is essential that the design method and/or system's analysis procedure be in sufficient detail to ensure a realistic evaluation. In general, the minimum information which should be included in undertaking an analysis of a system's performance consists of predicted or measured values of: (1) Incident daily solar radiation on the plane of the collector; (2) Daily useful heat collection by the collector; (3) Daily useful heat delivered to storage (or load); (4) Daily useful heat delivered from storage to space heating load; (5) Daily useful heat delivered to DHW heating load; (6) Daily useful heat delivered to space cooling load; (7) Actual cooling accomplished (i.e., heat actually removed from the conditioned space); (8) Dailv average heat losses from solar system (thermal storage, piping and/or ducting, etc.); (9) Electrical power usage by the solar system for operation (i.e., does not include auxiliary energy usage); (10) The quantitative degree of confidence or accuracy of the data (i.e., the estimated error); and (11) The basic design parameters of the system.

In addition, it is important to include information or data on solar collector efficiencies (instantaneous and daily), solar collector operating threshold (i.e., the minimum solar insolation rate necessary for the collection of useful heat), overall solar system efficiencies or effectiveness, and quantitative effects of control system modifications.

In order to adequately evaluate the operating performance of solar heating and cooling systems, it is not possible to limit our 'figure to merit' to a

single number. While the COP of an absorption chiller is indicative of the overall performance of a particular unit design, no such simple number is available in solar systems. Rather, it is necessary to utilize several parameters to categorize solar heating and cooling system designs in order to account for variations in: (1) Individual component variations in performance within a complete solar system; (2) Solar and climatological factors (i.e., the total amount, relative direct/diffuse/reflective components, and time-dependence of solar radiation as well as temperature and weather conditions affecting the heating/cooling load); (3) Specific building designs and/or type of applications of solar heating and/or cooling units; (4) Quality of overall system design, specifications and installation; and (5) Control modes, maintenance, reliability of equipment and other associated factors.

The purpose of this paper is to present a suggested set of parameters which will account for these variations in design and provide unambiguous answers to specific design questions. These parameters are defined in detail in the Performance Evaluation Criteria section and are further elaborated on in the section titled Example System.

PERFORMANCE EVALUATION CRITERIA

Performance parameters which meet the requirements discussed above include:
(1) System overall efficiency, η_S
(2) System thermal efficiency, η_{ST}
(3) Solar coefficient of performance, SCOP
(4) Solar controlled coefficient of performance, SCCOP
(5) Utilizability (ϕ)/solar operating threshold, I_C
(6) Solar heat delivered to load, Q_S
and the 'bottom line'
(7) Actual savings in non-renewable energy resources, Q_C or Q_H

Each of these parameters are defined by the following:

η_S = Average daily solar heating and cooling system efficiency over a specified period (typically 1 month), dimensionless

η_{ST} = Average daily solar heating and cooling system thermal efficiency over a specified period (typically 1 month), dimensionless

SCOP = Solar coefficient of performance, dimensionless

$$= \frac{\text{Total useful heating and/or cooling by solar (daily average)}}{\text{Total electrical power usage to operate the solar system (daily average)}}$$

SCCOP = Solar controlled coefficient of performance, dimensionless

$$= \frac{\text{Total, controlled, useful heating and/or cooling by solar (daily average)}}{\text{Total electrical power usage to operate the solar system (daily average)}}$$

$\bar{\phi}$ = Average daily utilizability over a specified period (typically 1 month), dimensionless

$\bar{I}_C$ = Average daily solar operating threshold, i.e., the minimum solar radiation intensity over a specified period (typically 1 month) at which the solar system can collect useful energy, kJ/m^2·hr

$\bar{Q}_S$ = Average daily solar heat delivered to load over a specified period (typically 1 month), kJ/day

$\bar{Q}_C$ = Average daily savings in non-renewable energy resources over a specified period (typically 1 month) by the solar cooling system, kJ/day

$\bar{Q}_H$ = Average daily savings in non-renewable energy resources over a specified period (typically 1 month) by the solar heating system, kJ/day

These parameters can be defined quantitatively with:

$$\eta_S = \frac{\bar{Q}_u^A - \bar{Q}_L^{Ext} - \beta\bar{Q}_L^{Int} - \varepsilon\bar{E}}{A_C\bar{I}_T}(COP)_{HC} \qquad (1)$$

where:

$\bar{Q}_u^A$ = Average daily useful heat collection by the solar collector array over a specified period (typically 1 month), kJ/day [see eqn. 14]

$\bar{Q}_L^{Ext}$ = Average daily solar system heat losses to the exterior of the conditioned space over a specified period (typically 1 month), kJ/day

$\bar{Q}_L^{Int}$ = Average daily solar system heat losses to the interior of the conditioned space over a specified period (typically 1 month), kJ/day

β = Factor to account for the degree of usefulness/non-usefulness of heat losses to the interior of the conditioned space, dimensionless [see eqn. 18h and 18c]

ε = Factor to convert the electrical energy usage to its thermal energy equivalent, dimensionless [see eqn. 19]

$\bar{E}$ = Average daily electrical power required to operate the solar system over a specified period (typically 1 month), kJ(elec)/day

$\bar{A}_C$ = Area of the solar collector array, m^2

$\bar{I}_T$ = Average daily integrated solar radiation per unit area on the tilted surface of the solar collector array over a specified period (typically 1 month), kJ/day·m^2

$(COP)_{HC}$ = Coefficient of performance of the heating or cooling unit (e.g., COP of an absorption chiller), dimensionless

$$\eta_{ST} = \frac{\bar{Q}_u^A - \bar{Q}_L^{Ext} - \bar{Q}_L^{Int}\beta}{A_C\bar{I}_T}(COP)_{HC} \qquad (2)$$

$$SCOP = \frac{\bar{Q}_u^A - \bar{Q}_L^{Ext} - \bar{Q}_L^{Int}\beta}{\bar{E}}(COP)_{HC} \qquad (3)$$

$$SCCOP = \begin{cases} SCOP \text{ for the condition } \beta \geq 1 & (4) \\ \dfrac{\overline{Q}_u^{A} - \overline{Q}_L^{Ext} - \overline{Q}_L^{Int}}{\overline{E}} (COP)_{HC} \text{ for } \beta < 1 & (5) \end{cases}$$

$\overline{\phi}$ is defined by Klein [1]. However, it is recommended that the following definition be used for $\overline{I}_c$:

$$\overline{I}_c = \frac{F_R U_L}{F_R(\overline{\tau\alpha})} (\overline{T}_{f,i} - \overline{T}_a + \Delta T_{control}) \quad (6)$$

where:

F_R = Solar collector heat removal factor, dimensionless

U_L = Solar collector heat loss coefficient, kJ/hr·m2.°C

$(\overline{\tau\alpha})$ = Average daily value of the collector transmissivity/absorptivity product over a specified period (typically 1 month), dimensionless

$\overline{T}_{f,i}$ = Average daily inlet fluid temperature to the solar collector array when operating over a specified period (typically one month), °C

$\overline{T}_a$ = Average daily ambient temperature when the solar system is actively collecting solar energy over a specified period (typically 1 month), °C

$\Delta T_{control}$ = Differential set point between the solar collector outlet and thermal storage temperatures which is used to control the on/off functions of the solar collector array heat transfer medium pump and/or blower, °C

$$\overline{Q}_c = [\, \overline{Q}_u^{A} - \overline{Q}_L^{Ext} - \overline{Q}_L^{Int} \beta - \xi \overline{E} \,] (COP)_c \quad (7a)$$

$$\overline{Q}_H = [\, \overline{Q}_u^{A} - \overline{Q}_L^{Ext} - \overline{Q}_L^{Int} \beta - \xi \overline{E} \,] (COP)_H \quad (7b)$$

Based on these defining equations, we note several specific relationships:

$$\eta_S = \eta_{ST} \{ 1 - \frac{\xi (COP)_{HC}}{SCOP} \} \quad (8)$$

$$SCOP = \eta_{ST} (\frac{A_c \overline{I}_T}{\overline{E}}) = \frac{\overline{Q}_s}{\overline{E}} (COP)_c \quad (9)$$

$$\eta_{S(cooling)} = \frac{\overline{Q}_c}{A_c \overline{I}_T} \quad (10)$$

$$\eta_{S(heating)} = \frac{\overline{Q}_H}{A_c \overline{I}_T} \quad (11)$$

$$\eta_{ST(cooling)} = \frac{\overline{Q}_c + \xi \overline{E} (COP)_c}{A_c \overline{I}_T} \quad (12)$$

$$\eta_{ST(heating)} = \frac{\overline{Q}_H + \xi \overline{E} (COP)_H}{A_c \overline{I}_T} \quad (13)$$

As supporting definitions we define:

$$\overline{Q}_u^{A} = \begin{cases} A_c F_R (\overline{\tau\alpha}) \overline{I}_T \overline{\phi} C_n & \text{(design)} \quad (14a) \\ \dot{m} C_p (\overline{T}_{f,o} - \overline{T}_{f,i}) & \text{(experimental)} \quad (14b) \end{cases}$$

where:

C_n = Factor to account for multiple solar collector modules in series flow configurations, dimensionless [see eqns. 20a, 20b, 20c]

$\dot{m}$ = Average daily mass flow rate through solar collector array over a specified period (typically 1 month), kG/hr

$\overline{T}_{f,o}$ = Average daily outlet fluid temperature of the solar collecting array when operating, °C

$$\overline{Q}_s = \overline{Q}_u^{A} - \overline{Q}_L^{Ext} - \overline{Q}_L^{Int} \beta \quad (15)$$

i.e.,

$$\eta_{ST} = \frac{\overline{Q}_s}{A_c \overline{I}_T} (COP)_{HC} \quad (16)$$

$$\overline{Q}_{HC} = (\overline{Q}_s - \xi \overline{E}) (COP)_{HC} \quad (17)$$

$\beta_{\text{(heating season)}}$ = Fraction of heat lost to the conditioned space which is not useful (18h)

Define the building heating load, Q_{Load}, as:

$$Q_{Load} = (UA)_L (T_r - T_a)$$

where T_r is the thermostat room temperature setting and $(UA)_L$ is the building heat loss coefficient. The building internal heat generation, Q_I, is:

$$Q_I = Q_I(solar) + Q_I(non\text{-}solar)$$

where:

$$Q_I(solar) = \overline{Q}_L^{Int}$$

when:

(1) $Q_{Load} < Q_I(non\text{-}solar)$, $\beta = 1$

(2) $Q_{Load} \geq Q_I$, $\beta = 0$

(3) $Q_I(non\text{-}solar) < Q_{Load} < Q_I$; $0 < \beta < 1$

$$\beta_{\substack{\text{cooling} \\ \text{season}}} = \left[1 + \frac{1}{(COP)_c} \right] \quad (18c)$$

$$\xi = \{ \frac{\eta_f / \eta_e}{(COP)_{Conv}} \} \text{ whichever is greater} \quad (19)$$

where:

η_f = Average daily conventional unit efficiency of converting non-renewable energy resources into useful heating and/or cooling, dimensionless

η_e = Electrical power generation, distribution and transmission efficiency, dimensionless

$(COP)_{Conv}$ = Coefficient of performance of conventional heating and/or cooling unit, dimensionless

Note that $\overline{Q}_L^{Ext}$ and $\overline{Q}_L^{Int}$ include both operating heat losses [i.e., of the form $(UA)_L(T_{op}-T_a)$] and heat capacitance losses when not operating [i.e., of the form $(cV\rho)(T_{op}-T_{non\text{-}op})$].

Finally, C_n has been defined by Ward [2] and is defined here for convenience. For no heat losses in the interconnection(s) between collector modules in series flow configurations:

$$C_2 = 1 - \frac{A_c}{4}\frac{F_R U_L}{\dot{m}C_p} \qquad (20a)$$

$$C_3 = 1 - \frac{A_c}{3}\frac{F_R U_L}{\dot{m}C_p} + \frac{A_c^2}{24}\left[\frac{F_R U_L}{\dot{m}C_p}\right]^2 \qquad (20b)$$

For an interconnection heat loss coefficient of $(UA)_{LI} \neq 0$, the collected useful heat, Q_u^A, must be reduced by an additional amount equal to $(UA)_{LI}(T_{f,i}-T_a)$, i.e.,

$$Q_u^A = Q_u^{A'} - (UA)_{LI}(T_{f,i}-T_a) \qquad (20c)$$

where $Q_u^{A'}$ is calculated using equation (14).

In order to show the importance of this Performance Evaluation Criteria, it is useful to consider an example system.

EXAMPLE SYSTEM

CSU Solar House III is an integrated solar energy system supplying useful heat from a solar collector to a residential-style building for space and DHW heating and space cooling. A water/ethylene glycol mixture is used as the heat transfer liquid with a single cover selective surface, flat-plate solar collector and thermal storage tank (approx. 1200 gal. of water). During the cooling season the heated water from thermal storage is pumped to the generator of a 2-ton lithium bromide absorption chiller for space cooling. The chiller uses solar heat to operate the unit, which cools by removing heat from water in an evaporator and discharging this heat to the exterior of the building. The resulting chilled water is pumped to a cooling coil for space cooling. Auxiliary heating and cooling are supplied by an electric boiler. An automatic control system provides for all functions of the system operation.

In the spring of 1979, the solar heating and cooling system of Solar House III was redesigned and extensively modified. The purpose of the modification was to increase the overall system performance. Data analyzed for the 1978 cooling season provided ample evidence that, for solar cooling to be competitive with conventional methods, significant system changes would have to be implemented. Based on this analysis and other experience gained in operating an absorption cooling system, the following recommendations were made: (1) Reduce parasitic power consumption; (2) Reduce length of piping runs and piping heat losses; (3) Decrease the cooling load from uncontrolled heat losses by relocating the thermal storage tank exterior to the conditioned space; (4) Install an air-to-air heat pump as an auxiliary source of heating and cooling (replacing an electric boiler); and (5) Reduce the complexity of the system design and controls.

The first two objectives were accomplished by optimizing the placement of the system components, thus minimizing the length of interconnecting piping (the total piping length was reduced by over 400 ft). In addition, the number of valves, elbows and other flow restrictions were reduced. The combination of these improvements with the use of higher efficiency pumps allowed the total pumping horsepower to be reduced from 2.31 to 0.74.

The thermal storage tank was moved to an attached tank room and insulated with 4 inches of polyurethane foam. While the use of an attached tank room does not completely eliminate the negative effects of internal heat loss during the cooling season (because of conduction and infiltration from the tank room), it does allow these losses to be utilized during the winter through controlled venting of heated air. The result of these modifications on the location and amount of heat loss can be seen in Table 1, lines 6 through 9b. It should be noted that the heat losses have a more pronounced effect during the cooling season since twice the amount of heat lost to the conditioned space must be supplied to the chiller to restore the space to its original condition (assuming $COP_{chiller} = 0.5$).

A significant fact is that the principal system components (collectors, chiller, storage tank, etc) remain the same for the two-year period. Therefore this study was directed primarily toward improving system performance through design improvements.

The result of these modifications is summarized in Table 1. This table lists a number of system performance parameters and their value for August 1978 and 1979. The greatest improvement was found to be in the reduction of electrical power usage, which declined from 59.0 to 22.5 MJ/day. This 61% reduction, coupled with the increase in useful heat delivered to load (Q_u^A) of 50 MJ/day and a reduction in thermal losses, caused the solar coefficient of performance (SCOP) to increase from 1.59 to 6.1.

The full effect of reducing electrical power consumption cannot be appreciated until the electrical savings are converted to their equivalent thermal energy. For this analysis, the conversion of one KJ electrical power is approximately 2.4 KJ thermal power. Applying this conversion shows that piping modifications account for an average savings of 87 KJ/day of thermal energy over the previous system. This result shows the need for great care in piping design and pump selection.

The thermal losses from storage and piping, shown in Table 1, were somewhat reduced from 1978 yet were still significantly greater than predicted. An analysis of these losses shows that approximately 25% of the tank losses occur by conduction through the tank legs. Additionally, the possibility of an optimistic R value for the tank insulation and unexpected thermosyphoning in the heat exchange and DHW loops also contribute to the loss.

The system thermal efficiency, η_{ST}, increased from 8.7% to 13.1%. This increase can be primarily attributed to the removal of the thermal storage from the conditioned space. The overall system efficiency increased from 0.4% to 10.2% and this increased degree of improvement is due to the threefold increase in the system SCOP.

Another important parameter to consider is Q_C, the actual savings of non-renewable energy. It is to be noted that, by optimally designing the system, the "real" energy savings (electrical and thermal) were increased from a low of 4.4 MJ/day in August 1978 to 108 MJ/day in 1979.

COMPARISON OF ACTUAL TO PREDICTED PERFORMANCE

During the summer of 1979 an attempt was made to model the performance of the two systems. Two methods were used to arrive at these predictions. The first, using the $\overline{\phi}$-f-chart formulas by Klein [1] was done for both systems utilizing data inputs from August 1978 and 1979. These results are shown in column 2 of the table. Next, a more detailed analysis (1979 only) was made which customized the predictions to the specific system by considering additional inputs such as heat losses, their location, and parasitic power use.

An examination of the table shows a fair degree of agreement between actual performance the $\overline{\phi}$-f-chart prediction in the collection related categories which is, of course, the essential function of $\overline{\phi}$-f-chart. However, the closeness of the agreement for the 1979 season is suspect because of DHW use, which was not accounted for in the $\overline{\phi}$-f-chart calculation. The discrepancy between $\overline{\phi}$ and actual performance for 1978 does not have the DHW complication and is therefore a better indication of the accuracy of $\overline{\phi}$-f-chart. Here the error was an overprediction of 16%.

$\overline{\phi}$-f-chart does not consider system heat losses or electrical usage, however, and thus correlation between other parameter predictions and actual performance is limited. Comparison of values of Q_u shows a discrepancy of 211 MJ/day (130%) in 1978 and 145 MJ/day (70%) for 1979. This discrepancy is almost entirely due to lack of consideration of heat losses which can be devastating in a cooling system. Examination of the prediction which includes heat losses shows a reduction of the Q_u error to an acceptable level (in this case, 21%).

A factor which even more severely limits $\overline{\phi}$-f-chart's usefulness as a design tool is its inability to differentiate between systems whose thermal and electrical use characteristics, and thus performance, vastly differ. For example, $\overline{\phi}$-f-chart predicts that η_S for both August 1978 and 1979 will be approximately 20%. In actuality, the 1978 figure was 0.4% and increased to 10.2% in 1979. The $\overline{\phi}$-f-chart model not only predicts a system efficiency twice the maximum achieved, but fails to predict the significant difference in efficiencies for the two systems. Once again, the detailed model shows much better correlation. These results clearly show the need for consideration of additional system related variables in forming accurate performance modeling.

CONCLUSION

Solar heating and cooling feasibility depends on the specific design and installation variables, such as parasitic power consumption, thermal losses, domestic hot water use, control strategies, building configuration, and many other factors. Therefore an accurate estimation of the performance of a solar cooling system must necessarily include a careful calculation/consideration of these variables.

REFERENCES

[1] Klein, S.A., "Utilizability of Solar Collectors". Solar Energy, Vol. 21, No. 5, 1978.

[2] Ward, D.S. and Oberoi, H.S., "Collector Modules in Series Flow", Technical Note, Submitted to Solar Energy, December 1979.

[3] Ward, D.S., Oberoi, H.S., and Grebe, J.M., "Improving Performance of Solar Cooling Systems". Proc. Second Annual Solar Heating and Cooling Systems Operational Results Conf., Colorado Springs, November 1979.

ACKNOWLEDGEMENT

This work has been supported by the U.S. Department of Energy, Office of Solar Applications, Office of the Assistant Secretary of Conservation and Solar Energy.

TABLE 1. CSU SOLAR HOUSE III PERFORMANCE DATA/PREDICTIONS [3]

	Parameter (1)	$\bar{\phi}$-f-chart Prediction (2) 1978	$\bar{\phi}$-f-chart Prediction (2) 1979	Experimental Performance (3) August 1978	Detailed Model Prediction (4) Aug 1979	Experimental Performance (5) 2-26 Aug 1979
	1. $\bar{I}_T$ MJ/day·m^2	18.4	18.0 (a)	18.4	18.0 (a)	18.0
	2. $\bar{I}_T$ (during operations)	--	--	11.3	11.1 (c)	13.9
	3. $\bar{Q}_u^A$ MJ/day	365.7	350.2(c)	315.5	309.1 (c)	357.9
	4. η_c (during operations)	--	--	47.6%	47.6% (a)	43.9%
	5. η_c (daily)	33.9%	33.2% (c)	29.3%	29.3% (a)	33.9%
	6. $\bar{Q}_L^{Ext}$ (piping) MJ/day	0	0	14.7	15.2 (t)	17.8
	7. $\bar{Q}_L^{Ext}$ (storage)	0	0	19.1	13.9 (t)	35.9
	8. $\bar{Q}_L^{Int}$ (piping)	0	0	9.8	7.4 (t)	12.7
	9a. $\bar{Q}_L^{Int}$ (storage)	0	0	38.1	4.6 (t)	9.6
	9b. $\bar{Q}_L^{Int}$ (storage + preheat)	0	0	38.1*	20.1 (t)	21.4
	10a. $\bar{Q}_{Load}$ (total)	365.7	350.2	233.8*	268.0 (c)	300.2 +
	10b. $\bar{Q}_{Load}$ (chiller)	365.7	287.9	233.8	205.7 (c)	237.9
	11. $\bar{Q}_{Cooling}$	219.4	172.7	141.5	123.4 (c)	125.4
	12. $(COP)_c$	0.60 (a)	0.60 (a)	0.605	0.600 (a)	0.527
	13. Total solar system electrical power	--		59.0	18.3 + 5.1 (DHW)	22.5
Collector Parameters	14. $\bar{I}_c$ MJ/hr·m^2	1.12	1.12	1.16 (e)	1.03 (a)	0.98 (e)
Collector Parameters	15. ϕ	0.424	0.415	0.406 (e)	0.448	0.471 (e)
Collector Parameters	16. $(COP)_c$	0.60	0.60	0.605	0.600 (a)	0.527
Collector Parameters	17. β	0	0	2.65	2.67	2.90
System Parameters	18. $\bar{Q}_s$ MJ/day	365.7	350.2	233.8	205.7	237.9
System Parameters	19. η_{ST}	20.3	22.3	8.7%	14.1%	13.1%
System Parameters	20. SCOP = SCCOP	∞	∞	1.59	6.4	6.1
System Parameters	21. $\bar{Q}_c$ MJ/day	219.4	172.7	4.4	113.8	108.0
System Parameters	22. η_S	20.3	22.3	0.4%	10.8	10.2

(a) Assumed
(c) Calculated
(e) Calculated from experimental data
(t) Theoretical
* No DHW in 1978
\+ 5.1% error in storage heat balance

Dup

ANALYSIS OF COMMUNITY SOLAR SYSTEMS FOR COMBINED SPACE AND DOMESTIC HOT WATER HEATING USING ANNUAL CYCLE THERMAL ENERGY STORAGE

F.C. Hooper, J.D. McClenahan and J.D. Cook*
University of Toronto

F. Baylin, R. Monte and S. Sillman*
Solar Energy Research Institute

ABSTRACT

A simplified design procedure is examined for estimating the storage capacity and collector area for annual-cycle-storage, community solar heating systems in which 100% of the annual space heating energy demand is provided from the solar source for the typical meteorological year. Hourly computer simulations of the performance of these systems were carried out for 10 cities in the United States for 3 different building types and 4 community sizes. These permitted the use of design values for evaluation of a more simplified system sizing method.

Results of this study show a strong correlation between annual collector efficiency and two major, location-specific, annual weather parameters: the mean air temperature during daylight hours and the total global insolation on the collector surface. Storage capacity correlates well with the net winter load, which is a measure of the seasonal variation in the total load, a correlation which appears to be independent of collector type.

INTRODUCTION

Most designs of solar heating systems utilizing low-temperature storage for space heating and domestic hot water are based on a "short term" storage capacity that can meet loads for no more than a few days during periods of insufficient collectible insolation. The economically optimal ratio of thermal storage capacity to collector area for such designs is typically between 200 and 400 KJ/m^2°C (i.e., for water, 1.25 to 2.5 gal/ft^2) [1].

Solar heating systems with annually cycled storages having storage capacity-to-collector area ratios typically 50 times greater than comparable "short term" systems have recently gained considerable acceptance as an important design alternative. For certain building types and climates these may offer the least cost per unit energy delivered over the life cycle of the system. The simplified f-Chart design procedure for "short term" systems is not applicable to "long term" systems, which are characterized by a slowly varying annual storage temperature. Thus there is a need for simplified design procedures for determining optimal configurations for such systems.

This paper examines parameters that have been found to be useful for annual storage system design. To provide the necessary data base, hourly simulations of these systems were performed. Three building types and four community sizes for each of ten locations in the United States were examined [2].

For each case, two collectors (a flat plate and an evacuated tube), set at two collector tilts, one equal to latitude and one to latitude plus 10 degrees, were examined.

The weather input data consisted of hourly air temperatures and insolation values taken from the typical meteorological year (TMY) data base for the site [3]. Global radiation incident on the inclined collector surface was calculated using Hay's anisotropic model for the sky diffuse component [4].

The criteria for the final system design for each case were (1) to provide 100% of the annual community space heating load and at least 85% of the annual community domestic hot water load from the solar source, and (2) to ensure a tank temperature cycle that rose close to the maximum permitted (design maximum) temperature of 80° C (176° F) and fell close to the lowest useful (design minimum) temperature of 32° C (90° F) over the year. This provided a stable basis for comparisons between sites and between systems.

DESIGN CONSIDERATIONS

In sizing the collector and storage for a given load, location, and collector type, two factors should be considered:

- the maximum and minimum storage temperatures reached over the annual cycle of the heat storage reservoir, and
- the total amount of uncollectible insolation over a full annual cycle of operation.

To be economically competitive, annual storage solar heating systems designed to provide 100% of a space heating load must maximize the utilization of both the collector and the storage subsystems.

*This work has been supported by the Solar Heating and Cooling Research and Development Branch, Office of Conservation and Solar Applications, U.S. Department of Energy.

The collector is underutilized if the storage tank temperature is equal to its maximum design temperature when there is further collectible insolation available. That is, collectible insolation cannot always be delivered either to storage or to load and some must be wasted. The storage is underutilized if the storage temperature never reaches the maximum design storage temperature or never falls to the minimum design temperature over one year of operation.

Ideally, the designer should size the storage and collector so that all collectible insolation is either stored or used directly in meeting a coincident load, and so that the storage temperature reaches both design limits at least once during the year of operation. A system which never reaches the minimum storage temperature has in effect been sized to meet a larger heat load than it is servicing. The performance of a system which exactly achieves the maximum and minimum design storage temperatures, with no uncollectible insolation, is said to be unconstrained; other systems are storage-constrained or collector-constrained.

The approach to system design and to the sizing of subsystems should be consistent with the objective of minimizing the capital investment required to meet a given load. The solar acquisition cost, or initial investment cost, is considered to be a function of the costs of three independent parameters: storage and distribution system, collector field, and storage insulation. That is,

$$C(M_T,A_C,V_I) = K_0M_T + (K_1M_T)^{2/3} + K_2A_C + K_3V_I + K_4 \quad (1)$$

where K_0,K_1,K_2,K_3,K_4 are constants for a given optimization. This cost evaluation follows the example of Hollands and Orgill [5].

For relatively large systems, very high storage efficiencies can be achieved with relatively small investments in storage insulation (see Table 1), while providing 100% of the space heating load from the solar source. Typically, storage insulation costs represent no more than 5% of the total solar acquisition cost. Since our estimates of the total solar cost may be in error by at least this amount, it is reasonable for large systems to lump storage insulation costs into the constant term K_4 of eq. 1.

Table 1. INSULATION COST AS A PERCENTAGE OF TOTAL COST FOR LARGE ANNUAL STORAGE SYSTEMS

Site: Boston, Massachusetts
Weather Data: Typical Meteorological year (TMY)
Loads: 0.2 - 9.0 MJ x 10^7

Case	Total Cost ($x10^{-6})	Insulation Cost (%)	Storage Efficiency
1	0.71	3.8	92.2
2	1.43	3.4	94.0
3	1.97	2.7	95.6
4	2.47	2.9	95.9
5	3.81	2.4	96.9
6	4.84	2.7	97.1
7	5.19	2.8	97.0
8	9.11	2.2	98.0
9	11.52	2.5	98.2
10	23.76	2.6	98.7

Hooper and Cook [6] have shown that the solar acquisition cost for annual storage solar space heating systems is effectively minimized when collector and storage subsystems are sized to achieve unconstrained performance; that is, unconstrained sizing corresponds closely to cost-optimal sizing. Storages and collector arrays are thus sized approximately optimally over a considerable range of collector and storage cost assumptions. Furthermore, it was concluded that annually cycled solar systems appear to be most economic in providing large fractions of large space heating loads.

These results suggest that we should seek design methodologies that would allow sizing of large annual storage solar heating systems meeting 100% of the average annual space heating requirements with unconstrained operation. This requires a knowledge of the design and site-specific factors for unconstrained sizing derived from previous computer simulation experiments. The initial storage sizing requires specification of the total annual load and of the mean and limit storage temperatures. The initial collector sizing requires a knowledge of the total annual heating load to be met, the total annual storage heat loss, the overall annual collector efficiency, and the total annual insolation falling on the tilted plane of the collector. Further refinements and generalizations of this design method should follow when more detailed statistical analysis of the results of these simulation experiments become available.

INITIAL SIZING

Storage

For annual storage solar heating systems providing 100% of the space heating load and none of the domestic hot water (DHW) load and operations in northerly locations, it has been observed from previous simulations that the optimal storage mass is approximately related to the total load by the ratio:

$$K \equiv \frac{M_T C_p (T_T - T_{TMIN})}{\text{Annual Heating Load}} \cong 0.3 \quad (2)$$

where M_T = mass of storage media,

C_p = specific heat of the storage media,

T_T = mean annual storage temperature, and

T_{TMIN} = minimum design storage temperature.

However, the optimal storage sizing is also sensitive to other parameters that are functions of site specific

conditions and design requirements. For example, storage sizing should also depend on the distribution of the total load over a year of operation and on the extent to which collectible insolation can meet immediate heating requirements.

Collector

The collector area required is given explicitly by

$$A = Q_T / (I_T \cdot CE) \qquad (3)$$

where Q_T = total load to be met by solar including storage loss,

I_T = total insolation per unit collector surface for one year, and

CE = annual collector efficiency.

Thus, an accurate estimate of the collector requirements depends on a determination of the annual collector efficiency. This depends, among other factors, on the climate and the collector characteristics. Initial simulations were required to determine this parameter.

COMPUTER SIMULATION

Operation

The simulation uses an hourly time step beginning on April 1 for a one-year period. The space heating season for all cases was defined as the period from September 15 to May 15. Outside of this period, the space heating load is assumed to be zero.

For each time step, the program operates in the following stepwise manner. The storage heat loss is calculated first, using the tank temperature at the start of the hour. The resultant new tank temperature is then used in calculating the collector heat gain for the hour. Based on this new temperature, the domestic hot water load supplied by solar energy is determined. The space heating load supplied by solar energy is then calculated and the corresponding tank temperature is checked to ensure that it is less than or equal to the maximum design temperature. Any excess energy is rejected before the beginning of the next hour.

Weather Input

Inputs to the simulation include hourly values for air temperature and for total insolation on the inclined collector surface. The parameters necessary to provide the input data are air temperature, total irradiance on a horizontal surface, normal incidence direct irradiance, and a daily snow indicator for determining albedo. These are taken from the typical meteorological year (TMY) weather data base [3]. Hay's anisotropic model [4] was used to calculate the diffuse component of the total insolation on the tilted surface.

Heating Loads

The computer simulation does not treat the space heating and domestic hot water systems as separate. The cold water supply to the domestic hot water system is preheated with heat drawn from the thermal storage tank by means of a heat exchanger, assuming a fixed temperature drop. Supply water temperature to the DHW system varies between locations, usually depending upon the local average temperature of shallow groundwater. The DHW delivery temperature is fixed for all cases at 49°C (120°F). The DHW load, expressed in gallons per day per building unit, is a constant which, of course, differs for building types. The hourly DHW load varies throughout the day in a fixed manner.

A constant heat load factor is used to determine the hourly space heat demand during the heating season. The design (effective) thermostat setting depends on the assumed internal heat generation for each building type.

Collectors

Slope-intercept data chosen for a typical flat plate and for an evacuated tube collector were used for efficiency calculations. The slope and intercept values used for the flat-plat collector were 6.104 $W/m^2°C$ and 0.711, respectively; for the evacuated tube they were 1.170 and 0.447. These efficiencies were reduced by a constant factor to account for collector performance deterioration due to dirt accumulation, selective surface aging, and other factors. The collector inlet temperature was assumed to be 1.1°C less than the mean tank temperature to allow for temperature stratification in the tank. For the case when the collector was out of operation in the previous hour, the control strategy was that the collector would be brought into operation for the following hour if the collector characteristic curve showed an efficiency greater than zero at an inlet temperature taken as 7.1°C above the mean tank temperature. When the collector was already in operation, it would be withdrawn from operation over the next hour if the curve indicated an efficiency less than zero at an inlet temperature taken as 4.1°C above the mean tank temperature.

Storage

The storage tank is assumed to be well mixed and unstratified. A below-ground storage tank with top flush with the surface of the ground was assumed. The shape of the tank was taken as cylindrical, with vertical axis and with radius equal to depth. The insulation along the tank wall and floor is specified for all tank sizes to have a maximum 22-cm (R50) thickness of polyurethane insulation and is so distributed that the heat loss is equal for all points on the tank surface. The lid insulation thickness is specified as 33 cm (R60) of fiberglass.

An effective thermal resistance for each of the tank sizes was calculated based on a more detailed finite-difference transient soil heat transfer model. The model assumes a horizontal isothermal boundary in the soil at a depth 10% greater than that of the tank floor and a vertical isothermal boundary in the soil at a distance from the tank wall equal to 1.1 times the tank radius. The Equivalent Thermal Resistance (ETR) values used in the tank heat loss calculations for this study are shown in Fig. 1 as a function of tank radius.

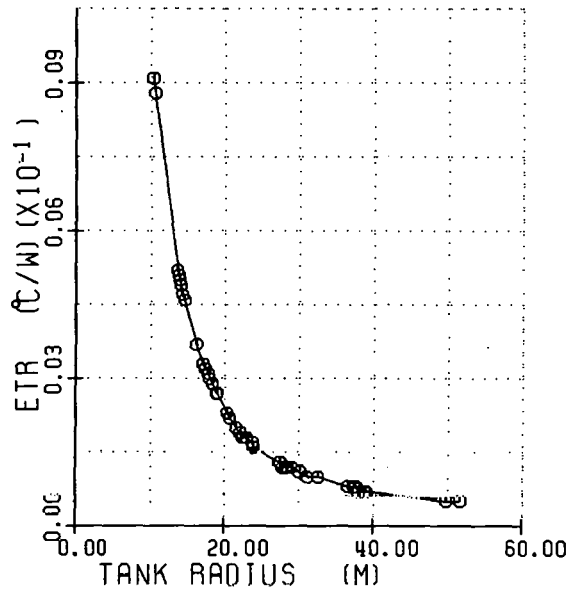

Fig. 1. The Equivalent Thermal Resistance (ETR) to Heat Flow from the Thermal Storage as a Function of the Tank Size for Tanks with Depth Equal to Radius. Soil Conductivity Taken as 1.73 W/m^{2}°C.

The maximum temperature that the storage water is permitted to attain at the end of any hour is 79.4°C (175°F). When the storage temperature exceeds this maximum, solar energy must either be used to service the heat load or be dumped.

SIMULATION RESULTS

The design objective requires that collector and storage be sized to permit unconstrained system performance. In this way all the cases simulated were operationally equivalent, at least to the extent that unconstrained sizing is achieved. Within the time limitations on the project it was not possible to meet this objective precisely, resulting in some systems having to reject small amounts of collectible insolation and in some systems not being able to utilize fully their storage capacities. This variation from the objective was kept to a minimum so that a valid general correlation could be determined for future system design purposes. Differences in sizings from location to location may be largely attributable to differences in site-specific, weather-related parameters and to design requirements, such as collector characteristics, rather than to inconsistencies in overall system operations.

Figure 2 shows the variation in K (initial storage sizing criteria defined in eq. 2) with the percentage DHW

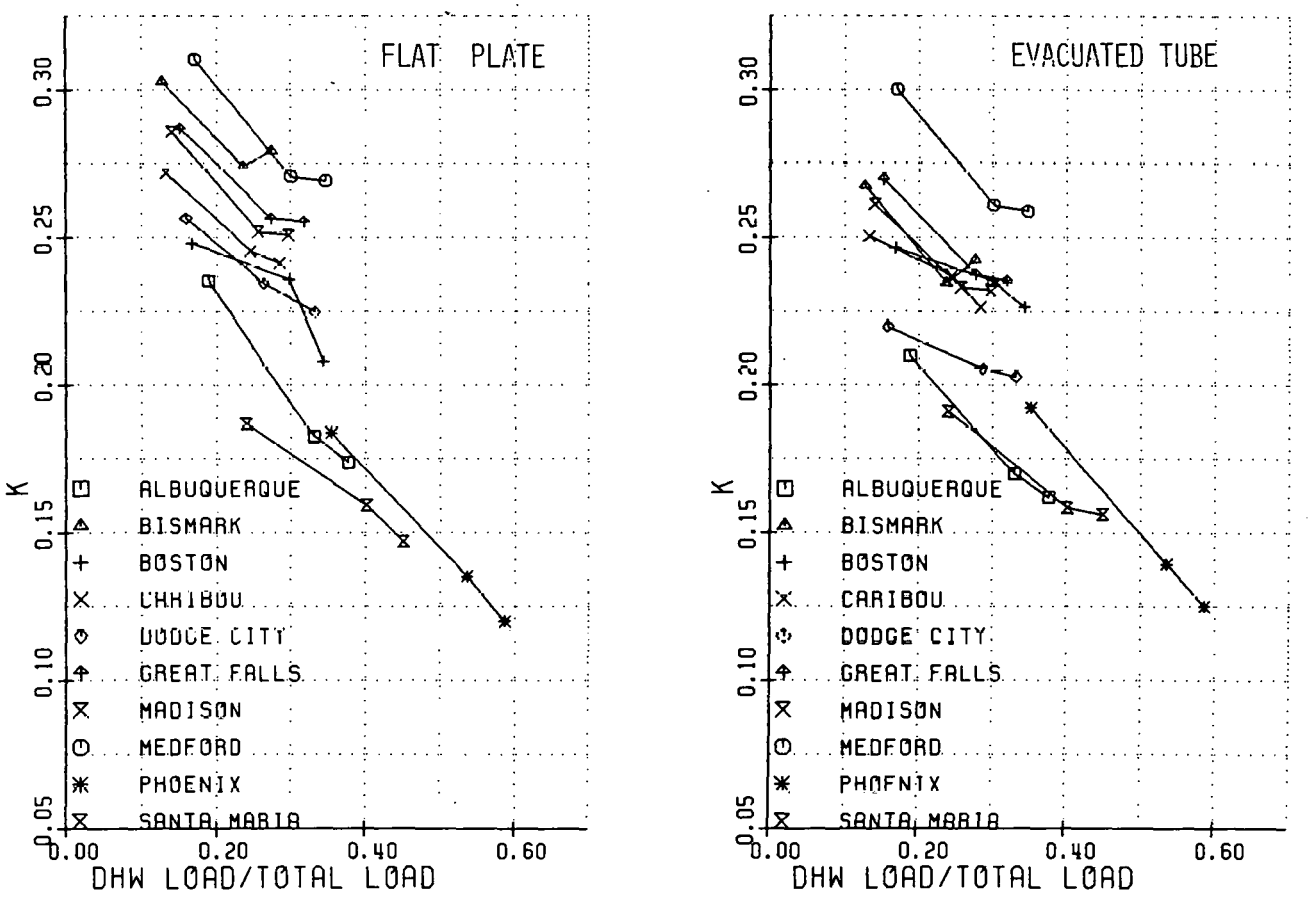

Fig. 2. Initial Storage Sizing Criteria vs. % DHW Load

load for the different locations. Although the general trend at any location shows a decreased need for storage as the domestic hot water load fraction increases, this in itself is not sufficient for design purposes. Similar results were presented by Baylin et al. [2] where storage volume was expressed as a function of total winter load. The difference in K values between locations shows the need for relating storage size to some other factor able to account for the variation in load and insolation throughout the year.

Results presented by Baylin et al. [2] show a good correlation between storage size and net winter load, net winter load being the integrated monthly difference between the heat load and collector gain for the winter period defined as the months of November, December, January, and February. Figures 3 and 4 show this relationship, identifying three points for each location. The points for each location represent the three different building types, always sequenced from left to right as the 200-unit apartment building, the 10-unit condominium, and the single-family residence. The storage to net winter load ratio appears to be generally independent of location and collector characteristics.

The annual collector efficiency required for sizing collector area is shown in Figs. 5 and 6 as nearly linear relationships with the site-specific weather parameters of average annual daylight air temperature (TA) and total annual incident insolation per unit collector area (I). Annual collector efficiencies are found to be essentially constant for a particular location regardless of the building type or system size. However, the relationship between the efficiency, the air temperature, and the insolation is some function of the specific collector characteristics, and different correlations would apply for collectors with characteristics substantially different from those of the chosen collectors.

CONCLUSIONS

A general correlation has been shown between the annual collector efficiency, a simple function of the annual incident insolation on the collectors, and the average ambient air temperature during the daylight hours. This has been done for only two solar collector characteristic performances, but a simple extension of the work to include the range of slopes and intercepts usually encountered in commercial collectors will yield an empirical correlation which should be of direct use in the preliminary or approximate design of large annual storage systems operating in the unconstrained (optimal) manner.

A useful general correlation has also been shown between the storage size and the net winter heat load that appears to be independent of the collector characteristics assumed for the classes of systems studied.

Examination of the performance curves shows the effect of the local climate upon annual storage system performance. As would be expected, the annual average collector efficiencies are lower in colder and cloudier regions, although the sensitivity to these factors is dependent upon the collector selected.

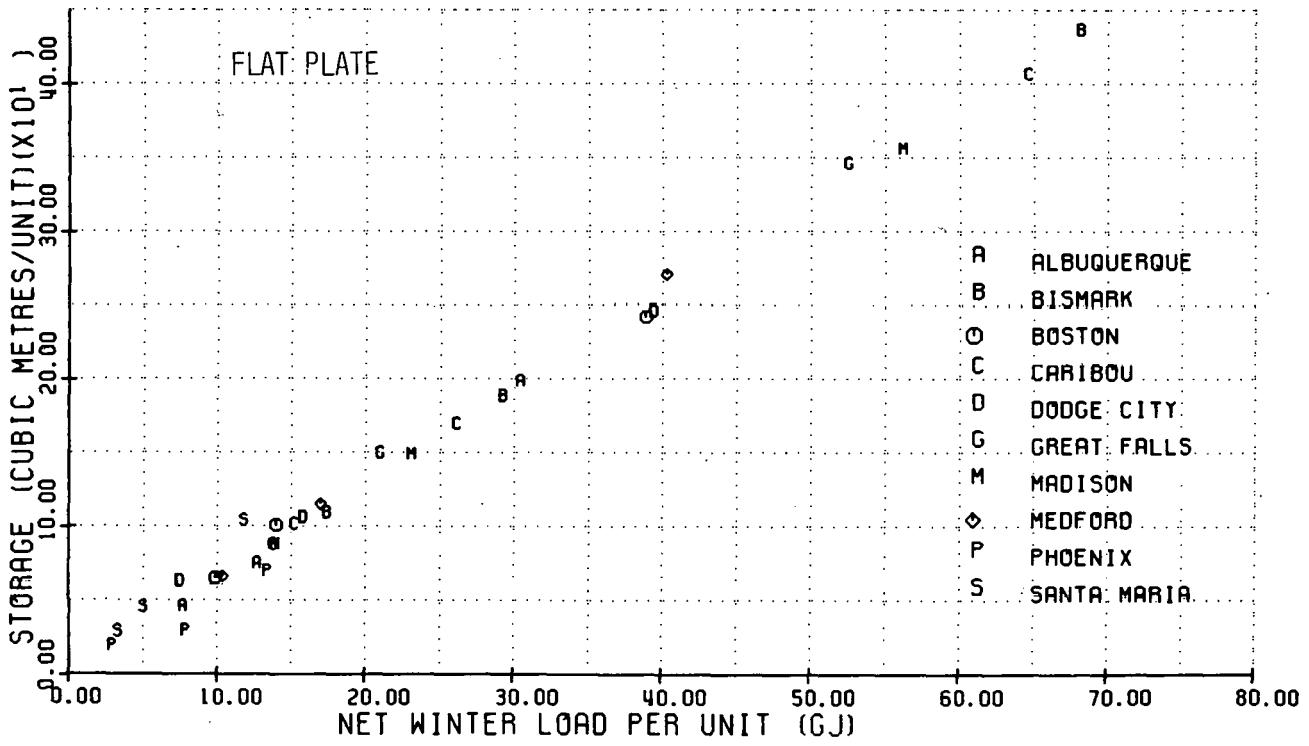

Fig. 3. Storage Size vs. Net Winter Load Correlation for Systems With Flat-Plate Collectors

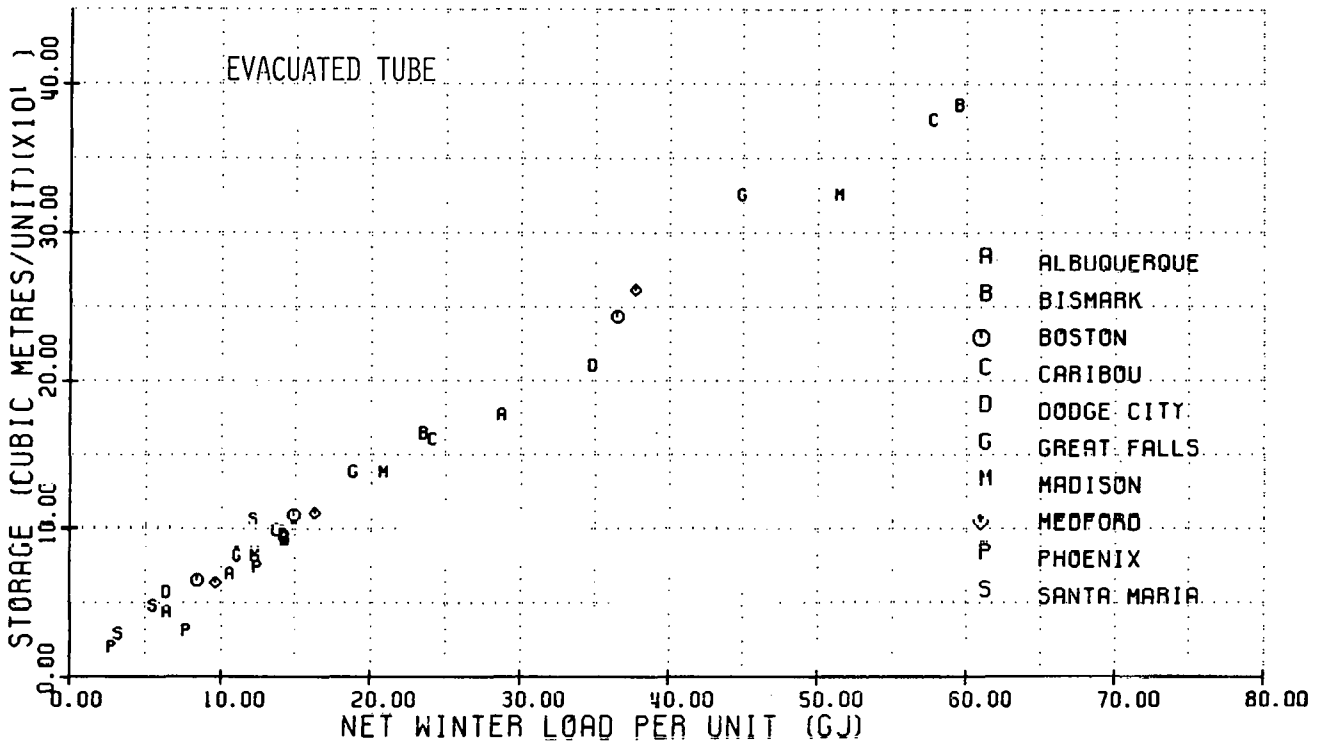

Fig. 4. Storage Size vs. Net Winter Load Correlation for Systems With Evacuated-Tube Collectors.

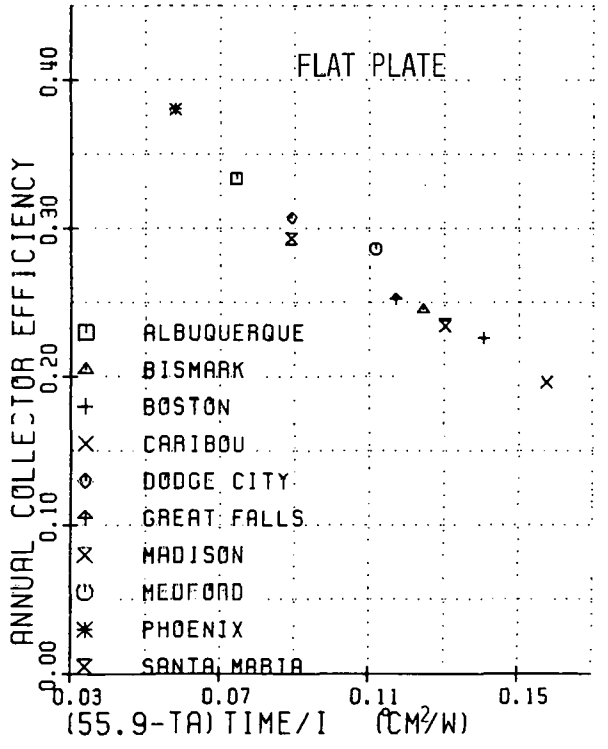

Fig. 6. The Annual Average Collector Efficiency as a Function of the Annual Incident Insolation and the Average Ambient Air Temperature During Daylight Hours for Evacuated-Tube Collectors.

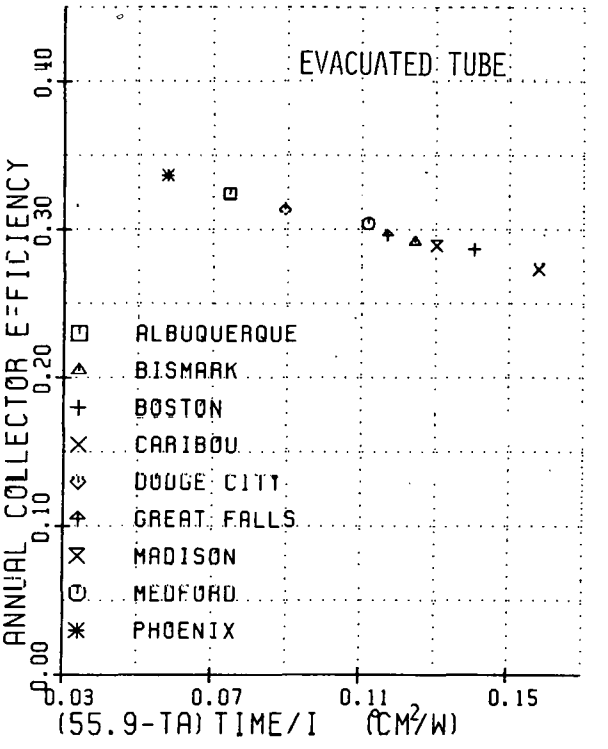

Fig. 5. The Annual Average Collector Efficiency as a Function of the Annual Incident Insolation and the Average Ambient Air Temperature During Daylight Hours for Flat-Plate Collectors.

REFERENCES

1. W. A. Beckman, S. A. Klein, J. A. Duffie. Solar Heating Design by the f-Chart Method. J. Wiley and Sons. 1977.

2. F. Baylin, R. Monte, S. Sillman. "Sensitivity Analysis of A Community Solar System Using Annual Cycle Thermal Energy Storage." Proceedings of Second Miami International Conference on Attractive Energy Sources. Miami, FL; Dec. 10-13, 1979.

   For detailed results, see: F. Baylin, R. Monte, S. Sillman. Annual Cycle Thermal Energy Storage For a Community Solar System — Details of Sensitivity Analysis. SERI report in preparation.

3. I. J. Hall et al. "Generation of Typical Meteorological Years For 26 Solmet Stations." ASHRAE Transactions, Vol. 85, Part 2. 1979.

4. J. E. Hay. "An Analysis of Solar Radiation Data for Selected Locations in Canada." Climatological Studies No. 32. Atmospheric Environment Service, Toronto; 1978, p. 6.

5. K. G. T. Hollands, J. F. Orgill. Potential for Solar Heating in Canada. University of Waterloo Research Institute, Report #77-01, Waterloo, Ontario; 1977.

6. F. C. Hooper, J. D. Cook. "Design of Annual Storage Solar Space Heating Systems." Proceedings of the Symposium for Solar Energy Fundamentals and Applications. 72nd Annual AICHE Meeting, San Francisco, CA; Nov. 25-29, 1979.

NOTES

COMPARISON OF ACTUAL AND SIMULATED PERFORMANCE OF THE ARLINGTON HOUSE SYSTEM

M.A. Daugherty, J.W. Mitchell and J.A. Duffie
Solar Energy Laboratory
University of Wisconsin
Madison, WI 53706

ABSTRACT

The performance of a solar energy system on a small residential building at Arlington has been evaluated through experiment and simulation. The house system incorporates Owens-Illinois evacuated tabular collectors with air as the working fluid. A large pebble bed storage unit is used to store off-peak electric auxiliary and solar energy. Auxiliary energy is supplied by the utility only between 10 PM and 8 AM. Domestic hot water is provided by an air-water heat exchanger supplying a preheat tank.

Data for two periods have been analyzed in detail to determine actual system performance. TRNSYS simulations have then been done for the same periods using the measured solar radiation on a horizontal plane and the measured ambient temperature. Leakage and duct losses are found to have a major effect on the results, and these are included in the simulations. Comparisons are made of integrated energy quantities and rock bed temperatures. The data and the simulations agree quite closely for the two data periods simulated.

INTRODUCTION

Simulations provide a useful and efficient means of evaluating and comparing the performance of solar heating systems. Models of complex systems are built from separate models for the various components of the system. These component models are developed from detailed studies of the components and many have been well validated by comparison with experimental data. The validity of using component models to simulate an entire system has not been as extensively studied.

This paper compares the measured and simulated performance of the Arlington Solar House. The simulations were done using TRNSYS [1]. The parameters used in the component models have been determined from a combination of experimental and analytical techniques. Weather data taken at the house during the test period were used to drive the simulation. The performance of the system in terms of total energy quantities and the dynamic response of some components are determined and compared to the data.

The comparison of measured and simulated performance establishes the validity of this system simulation. This is a complex system with a large number of components and a complex control strategy; it is clear that such systems can be successfully simulated.

ARLINGTON HOUSE SYSTEM DESCRIPTION

The Arlington House is an air-based system as shown schematically in Fig. 1. The collectors are evacuated tubular collectors with a selective surface on the absorber tube. The rock bed is used as a combined energy storage system for both collected solar energy and auxiliary energy from an electric duct heater. The system is unique in that the auxiliary heater supplies heat directly to the storage and only during the off peak hours of the utility (10 PM-8 AM). This auxiliary supply does not heat the house directly but is used to ensure that the energy in the rock bed is sufficient to meet the expected demand. Thus, the storage is charged each night with the sufficient energy to provide heat to the house during the next on-peak 16 hour period.

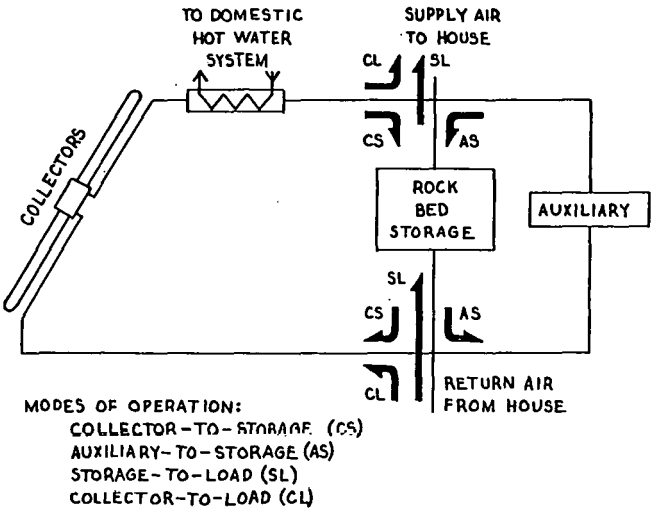

Fig. 1 Arlington House System Schematic

When direct solar is not available to meet the load, the house is heated by using the energy stored in the rock bed. Domestic hot water heating is provided by a heat exchanger in the collector return duct and a preheat-storage tank in combination with a conventional electric water heater. A more detailed description of the system is given by Erdmann [2] Persons [3] and Wallace [4].

The control strategy for the house is given in Table 1. During winter, both house and hot water heating are provided, while hot water heating only is provided in summer. A two stage thermostat is employed

to initiate house heating. First stage heating is provided when the house temperature drops below the first set temperature. Air is circulated through the house directly from the collector if solar energy is available (CL mode), and from the storage if solar energy is not available (SL_1). Second stage heating initiates if the house temperature drops below the second set temperature. Air circulates from storage through the house even if solar energy is available (SL_2). During off peak hours, the average rock bed temperature is compared to a set temperature to determine if charging from auxiliary (AS) is required.

The availability of solar energy is determined through three differential controllers. In winter, the air flow through the collectors initiates when the collector temperature is higher than the collector supply temperature at the discharge of the rock bed by a predetermined value. The low loss coefficient for the collectors means that this temperature may be high and not reflect air temperature during solar collection. Accordingly, the control is switched to a second differential controller that compares the delivery temperature entering the rock bed with the discharge temperature. In summer, the comparisons are made with the preheat tank temperature instead of the discharge temperature.

Table 1
Control Strategy

	Mode					
Input	CL	CS	SL_1	SL_2	AS	CW
Winter	Yes	Yes	Yes	Yes	Yes	No
$T_{house}<T_{set1}$	Yes	No	Yes	X	No	X
$T_{house}<T_{set2}$	No	X	No	Yes	X	X
Solar Available*	Yes	Yes	No	X	No	Yes
Off Peak Period	X	X	X	X	Yes	X
Charge Store	X	X	X	X	Yes	X

*Solar available if

$$T_{collector} > T_{supply} + T_{set1} \quad (\tau<5 \text{ min})$$
$$T_{delivery} > T_{supply} + T_{set2} \quad (\tau<5 \text{ min})$$

Modes:
- CL - collector to load
- CS - collector to storage
- SL_1 - storage to load, first stage heating
- SL_2 - storage to load, second stage heating
- AS - auxiliary to storage
- CW - collector to domestic hot water

Simulation Model

The Arlington house heating system was modeled and simulated using TRNSYS [1]. Special component models were written to simulate the collectors and control system. The rest of the system, including the house load, rock bed, pre-heat tank, electric duct heater, electric water heater, windows for passive gain, pump, fan, heat exchanger, dampers, and ducts were modeled using standard TRNSYS components. Table 2 presents the components used. In order to accurately model this system many more components are required than for typical simulation studies. The source of inputs and parameters for the simulations are listed in Table 3. Where available, values were taken directly from manufacturers specifications.

Table 2
TRNSYS Components Used in the Simulation

Name	Type	Quantity Used
Standard Components		
Radiation Processor	16	3
Rock Bed	10	1
One-Node House	12	1
Window	35	1
Overhang	34	1
Heat Exchanger	5	1
Preheat Tank	4	1
Water Heater	4	1
On/Off Auxiliary Heater	6	1
Fan	3	1
Damper	11	3
Tee Piece	11	3
Duct	31	2
Pump	3	1
Forcing Functions	14	1
Nonstandard Components		
Collector	-	1
Controller	-	1

Table 3
Source of TRNSYS Inputs

Forcing Functions:
- Weather
- Domestic Power Consumption
- Hot Water Loads

Previous Steady State Experiments:
- Rock Bed UA and Parameters (Persons [2])
- Water Heater Parameters (Manufacturer Specs)
- Heat Exchanger Effectiveness (Manufacturer Specs)
- Flow Rates (Measured)
- Duct Heater Power Consumption (Manufacturer Specs)

Building Plans:
- Overhang Dimensions
- Window Dimensions

Engineering Calculations:
- Inlet and Outlet Duct UA
- Pre-heat Tank UA

Dynamic Calibration Experiments
- House UA
- Collector Efficiency Plot Intercept Value
- Rock Bed Set Temperature
- Temperature Differential Required to turn Collector on

Values for four of the system parameters were not directly available. These parameters are the house loss coefficient UA, the intercept of the collector efficiency plot, the rock bed set temperature, and the temperature differential required to turn the collector on. Since the exact value of these four parameters could not be directly determined, it was necessary to use the simulation to determine their values. This was done by using two separate data periods. First, estimates were made for each of the four parameters. The simulation was then run on the first data period and the values of the four parameters were adjusted until the simulation results agreed with the data. The values determined in this

way were close to the estimates made earlier. Then the simulation program, using the same values for all parameters, was run for the second data period.

In the case of house loss coefficient, a design value was available and this was used as a base. It was modified to take into account the differences between design and construction. Adequate modeling information was not available on the collector performance to allow the data to give the daily performance. These data provided initial estimates for use with the model developed by Eberlein [5].

In the initial simulations, the minimum rock bed temperature for control was assumed to be 35C as set on the controller. It became apparent that the actual set temperature was higher than this. The actual temperature was based on the average of five temperatures located in the rock bed. However, as shown by Persons [2], these sensors were located in a region of low air flow and did not accurately represent the rock bed energy. It was found that a value of 52C more accurately represented the actual controlled temperature.

The collector model used in the simulations did not include thermal capacitance. The actual collectors and the sensors have appreciable capacitance which creates a significant delay on the time at which the collectors are turned on. This effect is modeled by increasing the collector turn on temperature so that the turn on times for the actual operation and simulations agree.

A major source of uncertainty in the modeling concerned the location of air leakage into and out of the solar-house system. In experiments, Erdmann [2] determined that the mass flowrate out of the collector was 15% larger than that into the collector. Ambient air was found to be leaking into the collectors and manifolds. In the simulations leakage was all assumed to occur at the collector inlet as indicated in Fig. 2. The collector inlet temperature was then determined by a mass weighted average of the supply air at its temperature and the leakage air at ambient temperature. It was more difficult to determine the path the leakage air took when it left the system. Various alternatives are shown in Fig. 2. Path (a) was the route assumed in the simulation. The leakage flowrate at the return temperature transferred energy into the heated space. Then the leakage flowrate at the house temperature was transferred to ambient as an energy loss from the heated space. The three other possible paths for the leakage (b,c, and d) were investigated and these will be discussed later.

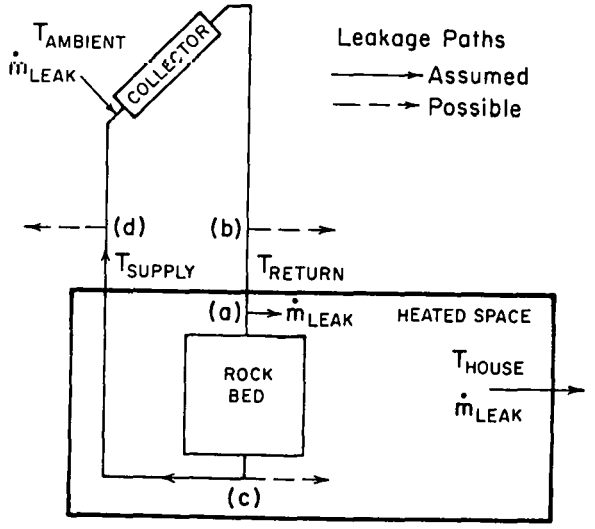

Fig. 2 Schematic of Paths for Duct Leakage

Simulation Results

The data and simulation results for the two periods are compared in Table 4. As stated earlier, four parameters were adjusted to achieve the agreement shown for period 1. The test is, then, the agreement between the two results for period 2. The agreement between simulation and measured for collected energy, auxiliary supplied, and water heating auxiliary is within 6% of the input energy. This agreement establishes confidence in the system model and the choice of parameters.

Table 4

Period 1
13 Noon-Noon Days
Feb. 25 - Mar. 10, 1978

	Data	Simulation	Difference Based on $Q_{collector}$
$Q_{collector}$	4.04 GJ	3.99 GJ	1.3
Q_{aux}	2.91 GJ	2.93 GJ	0.5
$Q_{water\ aux}$	0.19 GJ	0.19 GJ	--

Period 2
12 Noon-Noon Days
Mar. 11 - Mar. 23, 1978

	Data	Simulation	Difference Based on $Q_{collector}$
$Q_{collector}$	2.55 GJ	2.61 GJ	2.4
Q_{aux}	1.59 GJ	1.43 GJ	6.2
$Q_{water\ aux}$	0.19 GJ	0.20 GJ	0.4

As another evaluation of the simulation predictions, some dynamic outputs from the simulation were examined and compared to data. Figure 3 is a plot of house temperature as a function of time. The relatively smooth periods with peaks and without the oscillations represent day time during which the load is being met by the passive solar contribution. The regular oscillations represent night time when energy is supplied from storage. The frequency of the oscillations in the simulations is lower than that of the data, indicating that the actual lumped house capacitance is smaller than the value used in the simulation. The temperature from the simulation represents the average temperature of the entire house. The temperature plotted as data represents the south half of the house where essentially all of the passive contribution enters through the south facing windows. Thus, the temperature increases in the data are larger than those

in the simulation. Nevertheless, the model is able to fairly accurately represent the history of the room temperature.

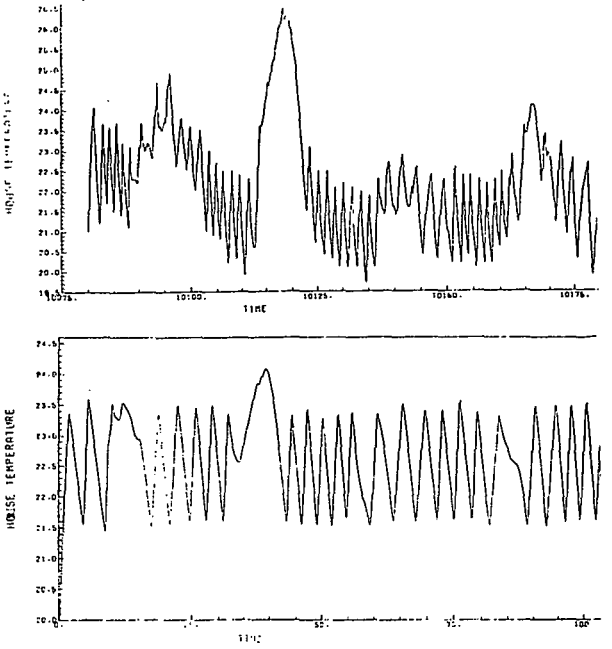

Fig. 3 House Temperature as a Function of Time. Top is Measured Response and Bottom is from Simulation.

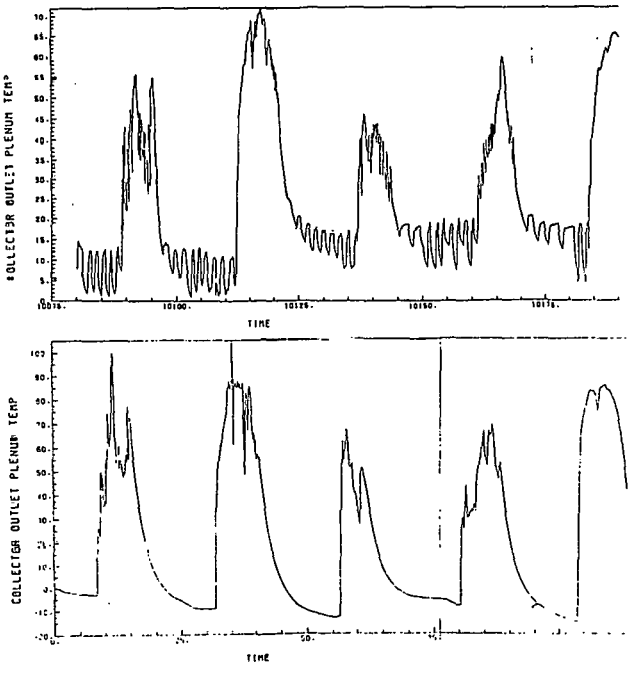

Fig. 4 Collector Outlet Temperature as Function of Time. Top is Measured Response and Bottom is from Simulation

Figure 4 shows the measured and simulated collector outlet temperature as a function of time. The simulation parallels the data very closely although the actual temperatures are somewhat lower than simulated. The measured energy is the same in the simulation and the data, which indicates that the flowrate in the simulation was lower than that actually occured in the house. This is due to the difficulty of determining the actual house flowrate in the various modes of operation. The oscillations in the data at night are due to the heating system cycling on and off during the night. The leaky dampers allow warm air to enter the collectors in some of the modes of operation.

Simulations were performed to determined the effects of air leaks out of the house by paths b, c, and d as shown in Fig. 2. Table 5 presents the effect the path has on system performance. By dumping all of the leakage air directly to the outside ambient before the rock bed as in path b, the net gain from the collectors is considerably reduced. To meet the load, the auxiliary power then increases as shown. If air leaks occur after the entire flowrate has passed through the bed as in paths c and d, much less energy is lost from the systems. Since the air leaving the bottom of the rock bed is at a temperature near room temperature, there is virtually no change in performance between leakage via paths c and d. These results demonstrate the need to accurately determine leakage routes in actual systems.

Table 5
Effects of Leakage Path on Energy Flows

Leakage Path	$Q_{collector}$	Q_{aux}	Percent Difference from Path (a) $Q_{collector}$	Percent Difference from Path (a) Q_{aux}
(a)	2.26 GJ	2.94 GJ	-	-
(b)	1.76 GJ	3.37 GJ	-22	+15
(c)	2.51 GJ	2.87 GJ	+11	-2
(d)	2.52 GJ	3.07 GJ	+12	+4

CONCLUSIONS

The Arlington house system has been modeled using standard and non standard components. The system is quite complex and requires a large number of components and parameter values. Previous steady state experiments are used to provide values for most of the parameters. Air leakage is found to have a significant effect on the results, and the location of leaks must be determined accurately. Dynamic experiments are used to determine values of four critical parameters. Simulations using weather data that does not include the parameter evaluation periods are found to yield performance results in good agreement with that measured. This produces confidence in the system model, and in the use of simulations to evaluate systems.

ACKNOWLEDGEMENTS

This work has been supported by the Solar Heating and Cooling Research and Development Branch, Office of Conservation and Solar Applications, U.S. Dept. of Energy.

REFERENCES

[1] Solar Energy Laboratory, University of Wisconsin, TRNSYS - A Transient Simulation Program, Engineering Experiment Station Report 38, (1979).

[2] D.R. Erdmann, "Thermal Performance of the Arlington House," M.S. Thesis, University of Wisconsin (1979).

[3] R.W. Persons, "Rock Bed Storage Performance, Arlington Solar House," M.S. Thesis, University of Wisconsin (1978).

[4] L. Wallace, "Description, Problems, and Performance Data of the Arlington Solar House," M.S. Thesis, University of Wisconsin (1979).

[5] M.B. Eberlein, "Analysis and Performance Predictions of Evacuated Tubular Solar Collectors Using Air as the Working Fluid," M.S. Thesis, University of Wisconsin (1976).

Session IB

Clair Ellis
Aerospace Corporation
Chairperson

SYSTEMS ECONOMICS I

CONSERVATION AND SOLAR: WORKING TOGETHER*

by

J. Douglas Balcomb
Los Alamos Scientific Laboratory
Los Alamos, New Mexico 87545

ABSTRACT

Although it is often stated that proper building design consists of first doing energy conservation and then doing solar, a methodology for best allocating limited resources between the two has not been developed. This article provides a simple procedure, based on local cost estimates and local weather data, which minimizes annual auxiliary building heat. The procedure is then extended to identify the point of minimum life-cycle dollar savings given assumptions of future fuel costs, financing, discounting to present value, inflation rates, resale value, taxes, etc. The same methodology can be used to identify the minimum net energy required of a building considering the energy embodied in construction materials, energy expended in construction, and operating energy over an assumed lifetime. Numerical examples are given.

EXAMPLE

Consider, for a moment, the results on Fig. 1. This graph refers specifically to cost data developed by Robert Taylor for Model 1, a 1370 sq ft house under construction in the La Vereda Subdivision[1] (Susan and Wayne Nichols' new project) and to weather data of Santa Fe, New Mexico. Along the horizontal axis is plotted the incremental cost of conservation over and above the cost of conventional construction (2 x 4 frame) with R11 insulation, single windows, no perimeter insulation, and 6 inches of fiberglass in the ceiling; the local 1979 norm. Along the vertical axis is plotted the incremental cost of passive solar consisting of a mix of 16" thick, unvented, poured-concrete Trombe wall and mass-backed greenhouse. Both are insulated at night with R9 shutters. The curved lines on the figure show energy savings, compared to the conventional non-solar house which consumes 71.8 million Btu/year for heating.

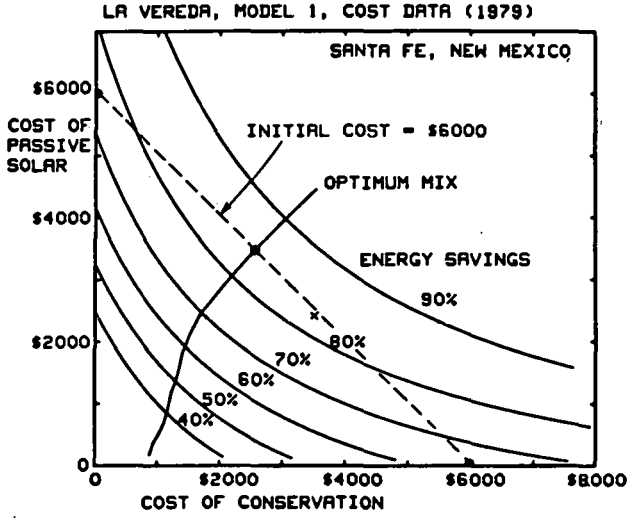

Fig. 1. Savings in energy, compared with conventional construction, obtainable with different investments in energy conservation (added insulation, double glazing, etc.) and passive solar (Trombe wall). The dotted line is for a total initial investment of $6000 for both. The x corresponds to the La Vereda Subdivision, Model 1, as designed.

For example, if one were to spend $6000 for conservation, the savings would be 63%. The same $6000, spent on passive solar would result in a 74% savings. These two points are plotted on Fig. 1. The dotted line connecting these points corresponds to a constant initial investment of $6000, split up in various ways between conservation and passive solar, and shows that an optimum allocation (yielding a maximum energy savings) lies at the point where the dotted line is tangent to one of the energy savings curves. The maximum energy savings that can be achieved with a $6000 investment is 85% corresponding to $2550 spent on conservation and $3450 spent on passive solar.

Suppose that the builder wanted to spend more or less than $6000 on such energy-reducing strategies. The line marked "optimum mix" shows how he or she might allocate the funds. Up to an initial investment of about $800, all should be spent on conservation. But above this value, most additional expenditures should go toward

*Work performed under the auspices of the U.S. Department of Energy, Office of Solar Applications.

passive solar. Beyond $4000, further investment should be divided about equally between the two strategies. (This line is called an "expansion path" by economists).

LIFE-CYCLE CONSIDERATIONS

How far along the "optimum mix" line does it make economic sense to proceed? The present value of the stream of future costs can be computed for each point on Fig. 1. The "life-cycle" savings (expressed as an equivalent reduction in present costs) can be computed by subtracting all costs (conservation, passive solar, and future fuel) from the present equivalent cost of fuel required for the conventional house (at the zero-zero point of Fig. 1). Unfortunately, this requires knowledge of many imponderables -- future fuel costs, financing arrangements, discount rates, inflation rates, resale value, taxes, etc., which depend on such discrete assumptions as maintaining passage through the Straits of Hormuz and continued friendly relations with Saudi Arabian leadership, as well as the more predictable domestic economy.

Suppose I proceed unabashed with the following assumptions: backup heating is electric baseboard at current rates of 7¢/kWhr, escalation rate of electric energy cost is 8%, loan interest rate is 10%, loan period is 30 years, period of financial analysis is 10 years (time of resale), resale value of conservation and solar investment escalates at 4.5%, down payment fraction is 15%,

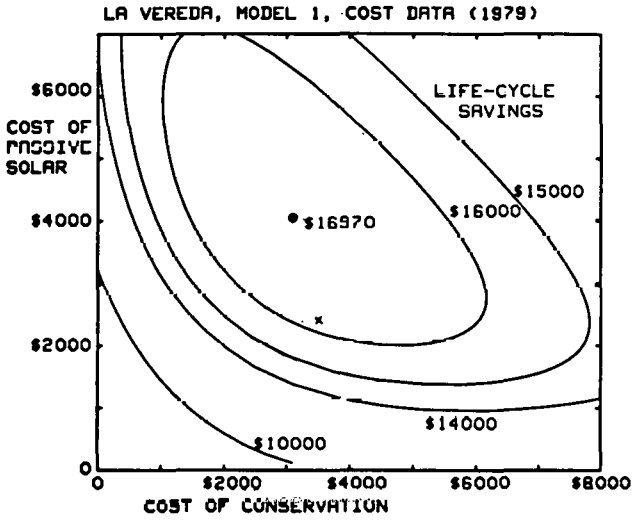

Fig. 2. Life cycle savings (in present dollars) compared to the conventional house. (The coordinates are the same so that Fig. 2 can be overlaid on Fig. 1.) Backup heat is electric. The maximum savings is $16970. The life cycle cost of heating the conventional house is $26650 (in present dollars) which can be reduced to $2520 by an initial investment of $7120 in conservation and solar.

discount rate is 7%, inflation rate is 6%, marginal income tax rate is 25%, property tax rate is 2%, and operation and maintenance is 1% of the total incremental cost. Then the fixed charge rate is .0831 and the fuel cost levelizing factor is 1.500.[2] With 6007 degree-days in Santa Fe, the equivalent "do nothing" cost is $26650 for fuel! (in present dollars).

Life-cycle fuel costs with conservation and solar are obtained and life-cycle savings, overlaid on the same coordinates as Fig. 1, are plotted on Fig. 2. The "global optimum", which is the point of maximum life-cycle savings, always lies on the "optimum mix" line. A life-cycle savings (in present dollars) of $16970 can be realized by expending $7160 on energy savings strategies ($3110 for conservation and $4050 for passive solar). If a different set of assumptions are made which change the fixed charge rate or fuel costs, then the global optimum will move, but it always lies along the "optimum mix" line! Thus the designer can't go too far wrong in designing to this line.

PROCEDURE

How can the designer find the optimum mix for particular given local construction costs and local weather? Proceed as follows:

Step 1. Estimate the incremental cost of conservation. I assume that cost varies inversely with L, the heating load coefficient, and recommend that the designer establish the scaling constants based on discrete "point" calculations. That is:

$$\text{Cost of conservation} = b/L - C_c$$

where L = heating load coefficient, Btu/F-day

The conservation constants, b and C_c can be determined from cost and heating load analyses of two widely different conservation levels. The first level should be a conventional building and the second a very well insulated building. The load is calculated for each and the incremental cost of going from the first to the second is calculated. Heating load coefficients can be determined from steady-state design-load calculations using the following approximate formula:

$$L = \frac{24 \times (\text{design heating load, Btu/hr})}{(\text{inside temperature} - \text{design temperature, F})}$$

where: design heating load = calculated heating rate required to maintain the building at a fixed inside temperature if the outside temperature is equal to the design temperature, in the absence of other internal heat sources or solar gains.

Then the values of b and C_c can be determined from:

$b = (\text{incremental cost})/(1/L_2 - 1/L_1)$
$C_c = b/L_1$

where: L_1 = heating load coefficient for conventional building
L_2 = heating load coefficient for well insulated building.

For example, Robert Taylor estimated Model 1 would cost $3512 more than conventional construction for 2 x 6 framing with 5-1/2" insulation plus insulating sheathing, foam perimeter insulation, double-glazed windows, and more ceiling insulation, reducing the heating load coefficient from 11948 Btu/DD to 5932 Btu/DD. Therefore:

$b = 3512/(1/5932 - 1/11948) = 4.13 \times 10^7$
$C_c = 4.13 \times 10^7/11948 = \$3463$

Step 2. Estimate the incremental cost of solar. I assume that this varies linearly with solar collection area, as follows:

$\text{cost of solar} = a A + C_a$

where C_a is a fixed cost (usually employed for active solar systems) and A is the solar collection area. The constant a can best be determined from a careful estimate of the incremental cost for a particular size of collection area. Then,

$a = (\text{solar add-on cost} - C_a)/(\text{net collection area})$

For example, Taylor estimated an add-on cost of $1414 for 250 sq ft of combined Trombe wall and mass-backed greenhouse on Model 1.* Thus:

$a = 1414/250 = \$5.66/\text{sq ft}$

since the fixed-cost component is assumed to be zero (C_a=0). To this I added another $4.00/sq ft to account for adding movable insulation. This is not strictly needed in Santa Fe but since I plan to study this design in northern climates later in the article it is convenient to insert it here. Therefore: a = 5.66 + 4.00 = $9.66/sq ft. (At these costs, night insulation is cost effective in Santa Fe.)

Step 3. Determine the solar performance curve for the local climate. This can be done using the F-Chart method for an active system or the LASL Solar/Load Ratio method for a passive system or through a detailed simulation analysis. In any case, the results should be expressed as solar savings fraction, F, versus the load/collector ratio, LCR.

LCR = L/A (Btu/DD-sq ft)
F = function of LCR

For example, for a Trombe wall with R9 night insulation in Santa Fe, I find the following values:[3].

LCR	F	LCR	F
214	0.1	27.8	0.6
101	0.2	21.5	0.7
64 5	0.3	16.1	0.8
46.4	0.4	10.7	0.9
35.5	0.5		

Step 4. For different values of F, estimate the derivative D and the function R, defined as follows:

$D = dF/d(1/LCR)$
$R = 1 + LCR(1-F)/D$

Step 5. For the same values of F, calculate optimum pairs of A and L using the following equations:

$L_o = \sqrt{b\ LCR/(a\ R)}$
$A_o = L_o/LCR$

Step 6. Determine costs from the scaling equations:

cost of conservation = $b/L_o + C_c$
cost of solar = $a A_o + C_a$
initial investment = sum of the two

The results are shown in Table I.

The designer may wish to stop at this point, selecting a point in the table consistent with initial cost constraints and energy saving expectations.

Global Optimization

If it is desired enter the world of life-cycle optimization, then proceed with Steps 7 and 8

Step 7. Determine the constant h, defined as follows:

$$h = \frac{\text{cost of backup heat, levelized over the accounting period, \$/Btu} \times \text{degree days}}{\text{(fixed charge rate)}}$$

For example, with the values given earlier:

$h = (1.5 \times .07/3413) \times (6007)/(.0831) = 2.23$

For a detailed discussion of the financial factors, see references 2 or 5.

Step 8. Calculate a/h and find the point where D = a/h. (See Step 4 for the definition of D).

For example, with the previous values:
D = a/h = 9.66/2.23 = 4.34

*The printed paper in the Proceedings (reference 1) contains an addition error which was corrected by Taylor in the oral presentation at the Fourth Passive Solar Conference. The cost of the passive house is $62151 rather than $65629, leading to a passive solar incremental cost of $1414.

The point where this occurs is at F = 0.820 and LCR = 15.0, as can be seen by interpolation in Table I. The corresponding values of L and A are given by:

$$L_o = \sqrt{b/(a/LCR + h(1-F))} = 6285 \text{ Btu/DD}$$
$$A_o = L_o/LCR = 419 \text{ sq ft.}$$

At this point the costs are as follows:

		Optimum	Model
cost of conservation	=	$ 3110	$ 3512
cost of solar	=	4050	2415
initial costs	=	7160	5927
future costs*	=	2520	4458
total, life cycle cost	=	9680	10385
reference future cost**	=	26650	26650
life cycle savings	=	16970	16265

This is the global optimum shown on Fig. 2. The corresponding values for Model 1 in La Vereda are given in the second column (assuming the use of night insulation). The solar savings fraction is 0.663 and the dollar savings are within $700 of the optimum indicating a good design. More could have been spent on passive solar except that the building is architecturally constrained and additional collection area would be difficult to fit in.

NET ENERGY

The same methodology can be applied to locate the net energy global optimum or constrained optimum. To accomplish this, costs are all reckoned in source-energy Btu and the same scaling laws are used. The same formulae are employed except that:

$$h = (\text{building lifetime}) \times (\text{degree days})/\eta$$

where: η = primary energy efficiency

$$= \frac{\text{energy delivered to load}}{\text{energy resource depletion}}$$

For example, if Model 1 costs an extra 92.3 MMBtu to add conservation and an extra 53.2 MMBtu to build the passive solar,[4] then:

$b = 1.087 \times 10^{12}$ Btu^2/DD
$C_c = 91$ MMBtu
$a = 0.213$ MMBtu/sq ft

For a 30 year building lifetime and $\eta = 0.25$

$h = 30 \times 6007/.25 = 720840$

at the optimum, $D = a/h = 0.30$
which corresponds to F = 0.962 and LCR = 6.0

The corresponding values of L_o and A_o are given by

$L_o = 4137$ Btu/DD
$A_o = 687$ sq ft

Energy costs are (all referred to source energy):

cost of conservation	=	172 MMBtu
cost of passive	=	147 MMBtu
initial cost	=	319 MMBtu
future cost	=	111 MMBtu
total life cycle cost	=	430 MMBtu
reference cost	=	8612 MMBtu
life cycle savings	=	8182 MMBtu

The net energy optimum calls for far greater initial investment and energy savings than the dollar optimum and leads along a slightly different expansion path calling for proportionally larger initial investment in solar than is called for by the economic optimum path.

Returning to the previous example, the dollar life-cycle optimum (L = 6285, A = 419) corresponds to an initial investment of 82 MMBtu for conservation and 89 MMBtu for passive solar for a total of 171 MMBtu. The annual energy savings (referred to source energy) is 65 MMBtu so that the energy payback time is only 2.6 years.

The general conclusion is that net energy optimization, although philosophically more palatable than economic optimization, tends to lead to very low energy designs which are probably beyond practical consideration for most buildings in terms of the required initial investment. Furthermore, the economic optimum makes good net energy sense being only slightly less effective than the global net energy optimum.

SENSITIVITY NEAR THE OPTIMUM

Precision in actually designing to the optimum is not essential. If the design lies within about 20% of the indicated values of A and L, this is probably close enough. Further precision is not warranted by the accuracy of the assumptions. The shape of the optimum is a fairly flat-topped mountain with steep sides allowing a wide latitude around the peak without great loss in savings. Thus in Fig. 2, anything within the $15000 life-cycle savings contour is a reasonable design.

In practice such leeway is essential, especially for the energy conservation expenditure, since materials are only available in specific sizes. It is usually somewhat easier to adjust solar collection area although this also comes in unit sizes. One would be foolish to make an architectural compromise in the design for the sake of a few square feet of collection area, just to zero in on a particular desired area. It is more important to understand the nature of the tradeoffs involved and to design "in the neighborhood" of the optimum.

Furthermore, the assumed cost scaling laws are only a rough guide to actual costs. Different conservation strategies will lead to different

*future cost = $h(1-F)\,L = 2.23 \times (1-0.820) \times 6285 = \$2520$.
**reference future cost = $hL_1 = 2.23 \times 11948 = \$26650$.

TABLE I. OPTIMUM MIX VALUES FOR EXAMPLE PROBLEM

F, solar savings fraction (percent)	LCR (Btu/DD-sq ft)	D (Btu/DD-sq ft)	R	L (Btu/DD)	A (sq ft)	Cost of Conservation ($)	Cost of Passive Solar ($)	Total Initial Cost ($)	Energy savings, compared to conventional house (percent)
10	214	20.3	10.5	9340	44	959	422	1381	29.6
20	101	18.4	5.4	8946	89	1153	856	2009	40.1
30	64.5	17.2	3.62	8723	135	1272	1306	2578	46.9
40	46.4	16.0	2.74	8503	183	1394	1770	3164	57.3
50	35.5	14.1	2.26	8202	231	1572	2232	3804	65.7
60	27.8	11.2	1.99	7721	278	1886	2688	4574	74.2
70	21.5	8.01	1.81	7136	332	2325	3206	5531	82.1
80	16.1	4.93	1.65	6446	402	2944	3880	6824	89.2
90	10.7	1.99	1.54	5458	510	4104	4927	9032	95.5

TABLE II PASSIVE SYSTEM PERFORMANCE - Values of LCR and D vs SSF for six cities for three passive system types.

The six system types are abbreviated as follows:

WW - Water Wall
WWNI - Water Wall with Night Insulation (R9)
TW - Trombe Wall
TWNI - Trombe Wall with Night Insulation (R9)
DG - Direct Gain
DGNF - Direct Gain with Night Insulation (R9)

			SSF = .1	.2	.3	.4	.5	.6	.7	.8	.9
MEDFORD OREGON		WW	134	57	34	22	15	9	5	-	-
42.4 N	L	WWNI	222	100	62	44	32	25	19	14	9
4930 DD	C	TW	130	56	32	20	13	8	4	-	-
T(JAN)=37	R	TWNI	209	94	58	40	29	22	16	12	7
		DG	118	42	-	-	-	-	-	-	-
		DGNI	227	102	62	42	30	21	15	10	5
		WW	11.3	9.4	7.4	5.4	3.5	1.9	.6	-	-
		WWNI	20.2	16.9	15.9	13.6	11.4	9.0	6.3	4.2	1.6
	D	TW	11.2	8.7	6.4	4.5	2.9	1.6	.6	-	-
		TWNI	18.7	16.2	14.2	12.1	9.8	7.4	5.2	3.0	1.1
		DG	9.0	4.5	-	-	-	-	-	-	-
		DGNI	19.9	17.2	14.4	11.8	8.9	6.5	4.1	2.0	.5

			SSF = .1	.2	.3	.4	.5	.6	.7	.8	.9
NASHVILLE TENNESSEE		WW	124	56	32	22	16	11	8	4	-
36.1 N	L	WWNI	207	98	61	42	32	25	20	16	11
3696 DD	C	TW	122	54	32	21	14	9	6	3	-
T(JAN)=38	R	TWNI	195	92	57	40	30	23	17	13	8
		DG	108	41	15	-	-	-	-	-	-
		DGNI	212	98	60	42	31	23	17	11	7
		WW	11.2	8.8	7.2	6.1	4.8	3.2	1.6	.3	-
		WWNI	19.4	17.6	14.8	13.4	12.6	10.7	8.6	5.6	2.3
	D	TW	10.8	8.8	6.8	4.9	3.3	2.0	1.1	.4	-
		TWNI	18.3	16.0	14.0	12.7	10.9	8.8	6.2	3.8	1.5
		DG	8.5	4.9	.8	-	-	-	-	-	-
		DGNI	19.8	16.7	14.6	12.5	10.3	7.5	5.0	2.8	.9

			SSF = .1	.2	.3	.4	.5	.6	.7	.8	.9
SANTA MARIA CALIFORNIA		WW	327	164	107	77	58	46	35	26	17
34.9 N	L	WWNI	448	224	148	108	83	66	53	42	30
3053 DD	C	TW	311	152	97	67	49	36	27	19	12
T(JAN)=50	R	TWNI	423	211	138	100	76	59	46	34	23
		DG	383	185	116	79	55	38	26	16	7
		DGNI	485	241	156	112	85	65	50	36	24
		WW	32.7	32.3	29.1	25.7	22.4	19.1	13.2	7.6	2.8
		WWNI	44.8	44.8	42.6	37.4	33.8	29.6	24.9	15.9	6.8
	D	TW	30.9	28.2	24.8	20.2	15.9	12.0	8.4	5.1	2.6
		TWNI	42.3	41.6	37.8	34.0	30.3	23.9	17.1	10.5	4.4
		DG	37.7	33.6	28.3	21.5	15.5	10.3	6.0	2.7	.6
		DGNI	48.5	46.9	42.3	37.7	32.0	24.3	17.1	10.4	4.3

			SSF = .1	.2	.3	.4	.5	.6	.7	.8	.9
ALBUQUERQUE NEW MEXICO		WW	178	84	53	37	28	21	16	11	6
35.0 N	L	WWNI	270	130	83	60	46	37	30	23	17
4292 DD	C	TW	171	80	50	34	24	17	12	8	5
T(JAN)=35	R	TWNI	255	122	78	56	43	33	26	19	13
		DG	183	82	47	29	16	-	-	-	-
		DGNI	283	135	86	61	46	35	26	19	12
		WW	16.8	14.9	13.3	12.1	10.3	8.0	5.0	2.5	.5
		WWNI	26.3	24.5	22.1	20.5	19.1	16.9	13.6	8.7	3.6
	D	TW	16.0	14.2	11.9	9.2	7.0	4.9	3.2	1.8	.8
		TWNI	24.5	22.5	20.6	19.1	16.6	13.3	9.5	5.8	2.4
		DG	16.5	13.3	9.3	5.6	2.6	-	-	-	-
		DGNI	27.1	24.6	22.3	20.0	16.6	12.5	8.6	5.1	1.9

			SSF = .1	.2	.3	.4	.5	.6	.7	.8	.9
BOSTON MASSACHUSETTS		WW	81	35	20	13	9	5	-	-	-
42.4 N	L	WWNI	159	73	46	32	24	19	15	11	8
5621 DD	C	TW	85	36	21	13	8	4	-	-	-
T(JAN)=29	R	TWNI	150	69	43	30	23	17	13	10	6
		DG	49	-	-	-	-	-	-	-	-
		DGNI	158	72	44	30	22	16	11	8	4
		WW	6.8	5.3	4.2	3.1	2.0	.8	-	-	-
		WWNI	14.1	13.2	11.5	10.3	9.3	7.7	6.1	4.0	1.6
	D	TW	7.2	5.5	4.1	2.6	1.4	.5	-	-	-
		TWNI	13.5	12.1	10.8	9.6	8.1	6.5	4.5	2.7	1.0
		DG	2.9	-	-	-	-	-	-	-	-
		DGNI	14.0	12.1	10.6	8.9	7.1	5.0	3.2	1.6	.4

			SSF = .1	.2	.3	.4	.5	.6	.7	.8	.9
MADISON WISCONSIN		WW	62	25	13	7	-	-	-	-	-
43.1 N	L	WWNI	137	62	39	27	20	15	12	9	6
7730 DD	C	TW	67	27	15	8	3	-	-	-	-
T(JAN)=17	R	TWNI	130	59	36	25	19	14	11	8	5
		DG	-	-	-	-	-	-	-	-	-
		DGNI	133	59	36	24	17	12	8	5	2
		WW	4.9	3.4	2.3	1.1	-	-	-	-	-
		WWNI	12.3	10.7	9.6	8.3	7.3	6.2	4.6	3.0	1.1
	D	TW	5.5	3.9	2.4	1.2	.1	-	-	-	-
		TWNI	11.7	10.2	8.9	7.7	6.5	5.1	3.5	2.1	.8
		DG	-	-	-	-	-	-	-	-	-
		DGNI	11.7	9.8	8.2	6.8	5.2	3.5	2.1	.9	.1

Compiled by C. Dennis Barley [3].

mixes of wall, ceiling, infiltration, and other loads which do not necessarily lead to a one-to-one relationship between cost and overall heating load coefficient. However a conservation sub-optimization should be made to best allocate a fixed initial expenditure between the various conservation options leading to a minimum heating load coefficient (as discussed by Barley[5].). Even if a detailed sub-optimization is carried out, the resulting initial investment in conservation will not be a smooth function of heating load coefficient but rather a step-wise discontinuous approximation to the inverse scaling law assumed. For this reason, it is recommended that the point calculations used for determining the cost constants be for two designs at quite different conservation levels.

VARIATION WITH CLIMATE

Variations with climate can be readily studied. LASL has used data for 216 sites around the U. S. (SOLMET) and also data for sites in southern Canada to study these variations. The cost data for the La Vereda building were used to identify the optimum value for each site.

Mapping these results shows that passive solar is an economically viable strategy, working with conservation, throughout the U. S. and southern Canada. It is significant that a mixed strategy beats out both a conservation-only and a solar-only strategy throughout the U.S.

Table II gives LCR and D tables for six cities for three passive system types.

VARIATIONS IN COST DATA

Cost data will vary with locale, building type, whether construction is new or retrofit, and passive solar type. It is difficult to characterize such variations since they depend on so many variables.

One example which has been studied in some detail is the case of the retrofit of a particular existing masonry building. The results, although different in detail, support the general conclusions of this article.[6] Costs are higher, but energy savings are greater and a mixed strategy beats a single strategy throughout all U.S. climates.

SUMMARY

A practical solution was obtained by assuming suitable simple scaling laws for costs, namely that costs scale linearly with passive solar collection area and inversely with heating load coefficient. These are reasonable assumptions if not extended over too wide a range.

As an alternative to the 8-step procedure outlined, one can estimate values of cost scaling constants for a particular situation (steps 1, 2, and 3) and then calculate the global optimum values of (steps 7 and 8). This provides an indication of the maximum initial investment that is economic. If this investment is outside the budget, then a constrained optimum can be calculated (steps 4, 5, and 6).

The next step is to choose an energy conservation strategy which will lead to a value of L which is within about 20% of the indicated optimum. (This might well be the case analysed to determine the constants b and C_c, in which case one simply has confirmed that this was an economically intelligent choice.) The last step is to select the passive solar collection area on the basis of maintaining LCR at the optimum value.

Selection of the actual design might well be on criteria other than cost optimization. The value of the analysis is to inform the designer of the neighborhood of the optimum and the magnitude of the savings achievable as one possible basis for a selection.

The net energy analysis indicates that payback times are short (2-3 years) and that a mixed conservation and solar strategy also makes sense in terms of minimizing net energy impact as well as maximizing dollar savings.

References

1. R. D. Taylor, "Energy Savings and Incremental Costs for Conservation and Passive Solar Construction", Proceedings of the 4th National Passive Solar Conference, Kansas City, pp 674-676. AS/ISES, Killeen, TX. (Oct. 1979)

2. D. Balcomb, et. al., "Passive Solar Design Handbook , Chapter E, "Economic Analysis" by S. Noll and D. Barley, to be published by DOE.

3. D. Balcomb, et. al., "Passive Solar Design Handbook , Appendix F, "Tables of LCR and D vs SSF", by D. Barley to be published by DOE.

4. B. M. Hannon, R. G. Stein, B. Z. Segal, D. Serber and C. Stein, "Energy Use for Building Construction", CAC Document No. 228, CAC, University of Illinois at Urbana-Champaign (Feb. 1977).

5. D. Barley, "Load Optimization in Solar Space Heating Systems", Solar Energy, Vol. 23, pp 149-156, Pergamon Press (1979).

6. D. Balcomb, "Energy Conservation and Passive Solar" accepted for publication in Energy and Buildings.

SIMULATION AND COST OPTIMIZATION OF THE SOLAR ASSISTED ANNUAL CYCLE ENERGY SYSTEM (ACES)†

J. WARD MAC ARTHUR
ENERGY RESOURCES CENTER
HONEYWELL INC.
2600 RIDGWAY PARKWAY
MINNEAPOLIS, MN 55413

DEAN W. FINN-CARLSON
TOUCHE ROSS AND COMPANY
780 NORTHSTAR CENTER
MINNEAPOLIS, MN 55402

KHANH H. NGUYEN
LOCKHEED ELECTRONICS CO. INC.
1830 NASA ROAD 1
HOUSTON, TX 77058

ABSTRACT

A detailed, dynamic computer simulation has been developed to determine the cost optimized solar assisted Annual Cycle Energy System (ACES). This model evaluates the two systems that form the core of recognized quality ACES: the ice-maker heat pump and the dual source evaporator. In addition to simulating the ACES system, the computer program can simulate combinations of four conventional heating and cooling systems: gas fired furnace, oil fired furnace, air-to-air heat pump, or a central heating/cooling (electric) system. This capability permits a meaningful evaluation of the cost-effectiveness of the ACES system, based on the present worth of all cash outlays, discounted over the appropriate system lifetime. Included in the economic model is time-of-day pricing, a feature which provides a realistic evaluation of the effect of thermal storage on life cycle costs.

Three building types in three different climatic regions have been analyzed. The results document the cost-effectiveness of the Full, Minimum and Cost Optimized ACES when compared to four conventional heating and cooling systems.

INTRODUCTION

Residential and commercial buildings account for approximately one-third of the total energy consumed in the United States. Over 70 percent of this energy is used for space conditioning (heating and cooling) and the production of domestic hot water. In the past, space heating and hot water needs (the two largest consumers have been supplied directly by oil and natural gas. However, the prices of these fuels have increased sharply in the last six years and show no signs of leveling off in the near future. In addition, spot shortages of petroleum caused by the world political situation have raized the spector of not being able to secure traditional fuels at any price. The only remaining conventional energy form is electricity; however, it carries a stiff conversion penalty: only one-third of the energy input to a power plant is converted to usable electricity. An approach to minimize the impact that this shift to electricity could have on our national energy needs is the ACES concept.

This concept is centered around an existing energy efficient device, the ice-maker heat pump, [1,2] which creates ice as a by-product of space and water heating. Under the ACES concept, this ice is stored and then used in summer to provide almost electricity-free cooling. The capability of this system to use water's heat of fusion as a heat source in the winter and a heat sink in the summer permits an effective utilization of interseasonal energy transfer.

Previous work [3,4,5 6] indicates that the ACES concept has the potential for reducing building energy consumption. This paper illustrates the extent to which building energy consumption can be reduced and determines the economic feasibility of the ACES. Since the economically rational consumer will purchase an ACES only if it will save money when compared to conventional HVAC systems, widespread use of ACES will depend on its economic desirability. This study has undertaken an investigation of the relationship between energy consumption and the economic performance of the ACES. A full description of this work can be found in Reference [7].

†*The information contained in this paper has been extracted from the study entitled "The Economic Evaluation of the Annual Cycle Energy System," which was performed for Oak Ridge National Laboratory under contract number 7470.*

The objective of this report was to determine the energy effectiveness and economic viability of the ACES concept. To perform this task proficiently, the ACES was studied in three building types in three climatic regions and compared to a number of conventional systems. The different classes of buildings include:

- Single-Family Residence
- Multi-Family Residence
- Commercial Office Building

The application of ACES to each building type was studied in three regions chosen to represent major climatic conditions in the continental United States. The locations include:

- Minneapolis, Minnesota
- Atlanta, Georgia
- Philadelphia, Pennsylvania

For each building type in each location, the economic evaluation of the ACES was based on a comparison of the present worth of the ACES to the present worth of a number of conventional systems currently in extensive use. They include:

- Electric resistance heating, electric air conditioning, and electric domestic water heating.
- Air-to-air heat pump and electric domestic water heating.
- Oil-fired furnace, electric air conditioning, and electric domestic water heating.
- Gas-fired furnace, electric air conditioning, and gas domestic water heating.

The single-family and multi-family residential ACES were compared to all four conventional systems in the three regions. Due to the limited use of commercial air-to-air heat pumps, the commercial ACES was compared only with the other three conventional systems in each area.

ACES OPERATIONAL CONCEPT

At its most basic level, the Annual Cycle Energy System concept consists of extracting heat from a storage tank by a unidirectional heat pump. As the heat is extracted during the heating season, or at other times to provide domestic hot water, ice to be used for air conditioning during the summer is formed within the tank.

The water's heat of fusion is available as a heat source in winter and a heat sink in summer. It is this interseasonal transfer of energy that allows both the heating and cooling outputs of the heat pump to be used to satisfy building loads. This unique ACES feature results in an annual coefficient of performance (COP) considerably higher than that of a conventional system.

In northern areas of the United States, where heating loads predominate, storage of all of the ice produced during the heating season would result in excess ice at the end of the summer. To prevent the accumulation of the excess ice, a collector/convector panel is used to supply solar and convective energy as needed and as available to melt ice.

In climates where cooling loads predominate, the ACES configuration utilizes a bin sized to store all of the ice generated during the heating season. This ice will not be sufficient to meet all summer cooling needs; after the stored ice has been depleted, the ACES heat pump is operated at night to generate ice to meet the cooling requirements of the next 24-hour period. The heat extracted from the water by heat pump operation is rejected to the environment by an air-cooled fan coil. Two advantages of nighttime compressor operation are that the dissipation of waste heat is more efficient at lower nighttime temperatures and that off-peak electric power rates may be utilized in those areas where they are in effect.

System Definition

For the purpose of this study, three ACES configurations were defined. Each incorporates an electrically driven unidirectional heat pump and a water-ice storage tank. The ice-maker plates of the heat pump are located above the ice storage tank, and flake or sheet ice upon harvest will fall by gravity into the storage bin.

The ACES configurations analyzed in this study are defined as follows:

- Full ACES--This configuration provides the heating, cooling, and domestic hot water demands of the building while minimizing total energy consumption. The water-ice storage volume is selected to maximize interseasonal energy transfer. The Full ACES utilizes an electrically driven unidirectional heat pump, a water source evaporator (ice-maker), water-ice storage tank, provision for producing and storing hot water, and solar panels and outdoor air coils as needed.
- Minimum ACES--This configuration satisfies the heating, cooling, and domestic hot water demands of the building under the restriction of minimum water-ice storage capability, which is defined as storage sufficient to provide heating for 12 consecutive sunless days during the coldest month. The components of the system are the same as for the Full ACES.

- Cost-Optimized ACES--This configuration provides heating, cooling, and domestic hot water for the building at minimum total cost over the life of the system. It may contain all of the components of the Full ACES and may, in addition, incorporate an air source evaporator that is automatically used when it is more cost-effective for the system to operate an an air-to-air heat pump than as a water-to-air heat pump. The use of stored sensible heat as well as heat of fusion is considered to be an option for reducing life cycle costs.

METHODOLOGY

The three-step methodology employed in the Economic Evaluation of ACES is illustrated in Fig. 1. The first step was to develop a data base containing the structural and operational characteristics of the study buildings, component operating characteristics and/or costs (for both ACES and conventional systems), energy costs (including time-of-day rate schedules for electricity), energy price escalation scenarios, general economic parameters and typical year weather.

The second step was to synthesize or develop the necessary analysis packages. For each building type, a computer program was developed that would:

- Calculate the time-dependent dynamic heating, cooling and domestic hot water loads.
- Size the ACES components for the Full and Minimum ACES.
- Determine annual energy consumption by simulating the interactions between the building, the weather and the HVAC/hot water system.
- Evaluate the economic effectiveness of the various systems in terms of life cycle costs.

The final step was to use these programs to define and evaluate the various system/building location combinations. At each location, a determination was first made as to the type of solar panel (absorber, single-glazed, or double-glazed) that resulted in lowest system life cycle costs. The identified types were then used for the ACES evaluation at that location. Once the life cycle costs for the Full and Minimum ACES were determined, the configuration and life cycle cost of the Cost Optimized ACES were determined by parameter variation. Four parameters were varied independently:

- Ice tank size
- Collector area
- Changeover temperature
- Tank insulation

If the Cost Optimized ACES employed a water source heat pump, no changeover temperature was used. If a dual source heat pump was used, the changeover temperature marked the point at which the heat pump ceased using ambient air as a heat source and switched to using the water in the ice tank as a heat source.

COMPUTER PROGRAM

Figure 2 illustrates the executive flow of the computer program used to simulate and evaluate the ACES and conventional heating and cooling systems. This computer program, ACESIM, is comprised of four modules:

- Loads Module (LODMOD)
- Design Module (DESMOD)
- Simulation Module (SIMMOD)
- Economic Module (ECOMOD)

The first module calculates the time dependent thermal loads imposed on the user-specified structure. If these loads have been previously determined, the loads module can be bypassed.

The second module reads the required load information from a permanent record file or from the loads module and determines the size of various ACES components. If the ACES components have already been correctly sized or if the user wishes to evaluate "off-sized" components, this phase can be bypassed.

The third module reads information generated by the first two modules and simulates either an ACES system or one of the four conventional systems. Its output is the time dependent history of all gas, oil, and electric consumption of the system being simulated.

The final model reads the energy use history of the simulated system, all capital equipment costs, and projected escalation rates, discount rates, and time-dependent utility rates. The final program outputs are present worth of all cash outlays for the system (discounted over an appropriate system lifetime) and payback of incremental ACES cost compared to conventional systems.

Included in the dynamic model are directional heat flows through walls, roofs, ceilings, basement, internal partitions, tank and surrounding ground as well as the time-dependent boundary conditions that include direct and diffuse radiation impingent on any surface. The equations defining heat flow are coupled to one another and to the global energy equations defining system response.

RESULTS AND CONCLUSIONS

The results of the Economic Evaluation of ACES are summarized by building type. The following areas are reviewed:

- ACES component configurations.
- Annual COP of ACES and conventional systems.
- Economic characteristics of ACES and conventional systems.

All results are presented in terms of two possible ACES equipment cost scenarios: today's cost of prototype systems (1978) and system costs resulting from extensive commercialization (1982).

Results for the Single-Family Residences

Table 1 contains a description of the Full, Minimum, and Cost Optimized ACES for the three regions. Examination of this table yields the following conclusions:

- The optimum level of tank insulation depends on the interaction of climatic extremes and the relative magnitude of heating and cooling loads. Heat in-leakage to the ice tank can be significant.
- The type of solar collector used is a function of the climatic location.
- Solar collectors are not an economically attractive means of melting excess ice.
- Dual source heat pumps are used in all locations in the Cost Optimized ACES.

Table 2 characterizes the various HVAC systems by location. Important results are that:

- The Cost Optimized ACES are economically superior to both the Full and Minimum configurations.
- The Full ACES are the most energy efficient of the systems analyzed because they maximize interseasonal energy transfer.
- The ACES can be three to four times more energy efficient than conventional systems.
- When compared to the Cost Optimized ACES, the maximized interseasonal energy savings of the Full ACES do not economically justify the required storage capital costs.
- Under current equipment cost constraints residential ACES are not in general cost-competitive with conventional systems.
- Using the reduced price scenario, residential ACES are economically superior to conventional systems (oil, heat pump, electric and sometimes gas).
- Reduction in ACES investment costs results in a more energy efficient Cost Optimized ACES.
- The energy saving capability of the ACES with seasonal COP as high as 3.69 is extremely favorable (this is not an upper limit of the ACES COP; it is merely the highest value found in this study).
- Cost savings in the residential sector could be greatly enhanced by utilizing a high side storage system (hot tank). This configuration would reduce significantly on-peak utilization during the heating mode.

One final observation should be made regarding the application of ACES in residential buildings. ACES are much more energy efficient than current systems that use electricity to provide space heating and cooling and domestic hot water. The ACES has a large potential to reduce significantly national consumption of source energy if electricity is the fuel of the future.

Results for the Multi-Family Residences

In Minneapolis, where the heating load far exceeds the cooling load, heat in-leakage to the ice tank provides free ice melting. The type of solar collector that should be used is also dependent on location. However, solar energy is still not a cost-effective method of getting rid of excess ice. In cases where loads are not balanced, the most cost-effective method of getting rid of excess ice is simply not to produce any. This is accomplished by using ambient air as a heat source for a longer time.

All of the observations made for single-family residential ACES applications hold for multi-family applications. The various ACES configurations result in significant annual energy savings, but at a cost that is unacceptable for systems installed at today's prototype prices. However, under the reduced equipment price scenario the economic picture is very favorable. As was the case with the single-family residences, component cost reductions result in a more energy efficient Cost Optimized ACES.

Results for the Commercial Buildings

Table 3 presents the ACES configurations for the Full, Minimum and Cost Optimized systems. The observations for residential ACES relative to configurations still apply. However, the commercial ACES differs significantly from the residential systems when the discussion turns to economic attractiveness.

Table 4 presents the characteristics of the study systems in each location and each system's annual COP. Once again, ACES delivers significant energy savings. The important difference between residential and commercial systems is that commercial systems are economically superior to oil, gas and electric systems at today's equipment prices in all locations. The major reason is that the commercial ACES, with both high and low side storage, can take maximum advantage of off-peak rates. In addition, the ACES can be used to reduce significantly the magnitude of on-peak demand. Thus, the ACES is an economically feasible load shed/demand control device in commercial applications.

REFERENCES

[1] H. C. Fischer and E. A. Nephew, Application of the Ice-Maker Heat Pump to an Annual Cycle Energy System, ASME Paper 76-WA/ENER-4.

[2] V. D. Baxter, Intermediate Report on the Performance of Plate Type Ice-Maker Heat Pumps, ORNL/CON-23, Oak Ridge National Laboratory, Oak Ridge, TN, October, 1978.

[3] R. A. Biehl, et al., "Energy Bank," Heating, Piping and Air Conditioning, Volume 49, Number 1 (January, 1977) pp. 53-60.

[4] F. C. Hopper, Solar Space Heating System Using Annual Heat Storage, Dep. Ntis, PC A04/MF A01 (August, 1977).

[5] R. G. Werden, "Modified Annual Cycle Energy System," presented at the Second Annual Heat Pump Technology Conference, Stillwater, OK (October, 1976).

[6] M. H. Sumerville, et al., "The Design and Analysis of a North Dakota Annual Cycle Residential Solar Heating System," Bulletin #77-04-EES-01, Engineering Experiment Station, University of North Dakota, Grand Forks, ND.

[7] J. W. MacArthur, Final Report on the Economic Evaluation of the Annual Cycle Energy System, ORNL/CON-7470, Oak Ridge National Laboratory, Oak Ridge, TN (October, 1979).

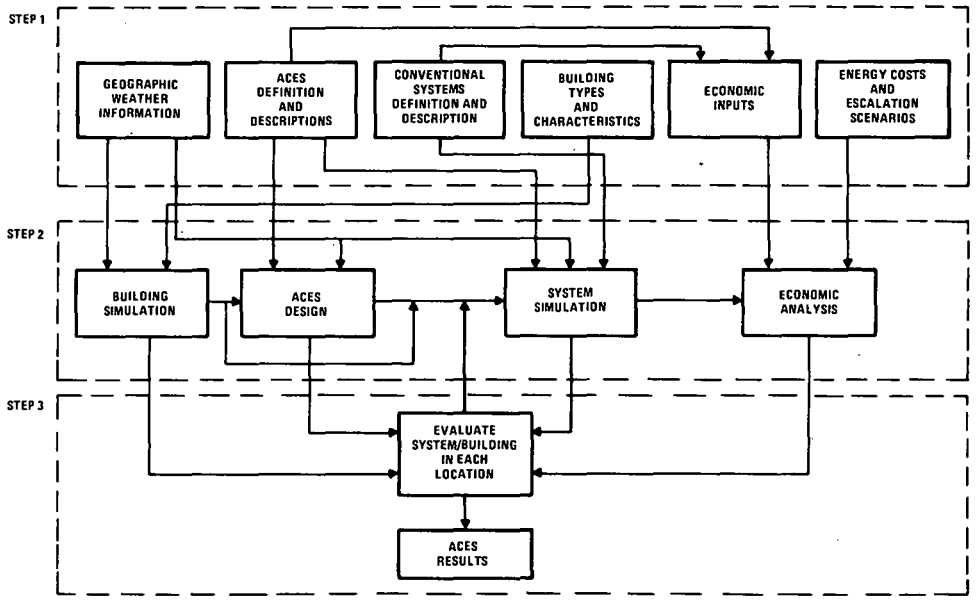

Fig. 1. ACES Study Methodology

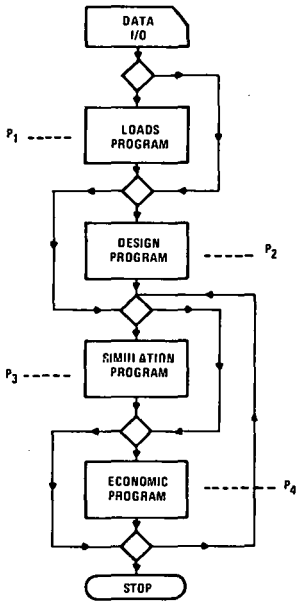

Fig. 2. ACESIM Executive P-Level Routine

Table 1. Single-Family ACES Configurations

SYSTEM TYPE AND LOCATION	SYSTEM CHARACTERISTICS						
	TANK INSULATION	TANK SIZE (FT^3)	COLLECTOR AREA (FT^2)	COLLECTOR TYPE	HEAT PUMP TYPE	CHANGEOVER TEMPERATURE(^oF)	ELECTRIC BACKUP
MINNEAPOLIS							
FULL	YES	2592	504	SG	WS	NONE	NONE
MINIMUM	YES	1800	558	SG	WS	NONE	NONE
COST OPTIMIZED							
- 1978 INSTALLATION	NO	2048	0	NONE	DS	15	YES
- 1982 INSTALLATION	NO	2048	0	NONE	DS	15	YES
ATLANTA							
FULL	YES	5000	0	NONE	WS	NONE	NONE
MINIMUM	YES	648	54	ABS	WS	NONE	NONE
COST OPTIMIZED							
- 1978 INSTALLATION	YES	648	0	NONE	DS	30	NONE
- 1982 INSTALLATION	YES	2312	0	NONE	DS	40	NONE
PHILADELPHIA							
FULL	YES	3872	90	ABS	WS	NONE	NONE
MINIMUM	YES	1152	252	ABS	WS	NONE	NONE
COST OPTIMIZED							
- 1978 INSTALLATION	YES	1152	0	NONE	DS	20	NONE
- 1982 INSTALLATION	YES	2312	0	NONE	DS	30	NONE

NOTE: SG = SINGLE GLAZE, DG = DOUBLE GLAZE, ABS = ABSORBER, WS = WATER SOURCE, DS = DUAL SOURCE

Table 2. Characteristics of the Single-Family HVAC Systems

HVAC SYSTEM HEATING PLANT/ COOLING PLANT	PHILADELPHIA					ATLANTA					MINNEAPOLIS				
	INSTALLED COST		ANNUALIZED COST			INSTALLED COST		ANNUALIZED COST			INSTALLED COST		ANNUALIZED COST		
	1978	1982	1978	1982	COP	1978	1982	1978	1982	COP	1978	1982	1978	1982	COP
NATURAL GAS/ ELECTRIC[1]	1692	1692	1017	970	.74	1692	1692	732	705	.91	2122	2122	907	887	.70
OIL/ELECTRIC[2]	1870	1870	1226	1136	.87	1870	1870	844	780	1.06	2020	2020	1084	1011	.81
AIR-TO-AIR HEAT PUMP[2]	2776	2776	1253	1156	1.68	2860	2860	882	809	1.69	3606	3606	1233	1134	1.53
ELECTRIC/ ELECTRIC[2]	1710	1710	1485	1366	1.09	1710	1710	937	861	1.25	2130	2130	1453	1341	1.05
FULL ACES[3]	15899	7631	1700	1029	3.43	13200	6346	1262	727	3.50	22520	22520	2372	1330	3.20
MINIMUM ACES[3]	14622	7018	1668	1042	3.10	10357	4969	1183	738	2.44	22800	10944	2408	1353	3.13
COST OPTIMIZED ACES	8646	5032	1250	895	2.6/2.9*	7686	4784	1000	698	2.3/2.6*	10097	4846	1416	923	2.43

1. Natural gas fired domestic hot water heater
2. Electric domestic hot water heater
3. Desuperheater domestic hot water heater

*Cost Optimized ACES has a different configuration in 1982; therefore, a different COP.

Table 3. Commercial ACES Configurations

SYSTEM TYPE AND LOCATION	SYSTEM CHARACTERISTICS: TANK INSULATION	TANK SIZE (FT^3)	COLLECTOR AREA (FT^2)	COLLECTOR TYPE	HEAT PUMP TYPE	CHANGEOVER TEMPERATURE(^oF)	ELECTRIC BACKUP
MINNEAPOLIS							
FULL	YES	78732	0	NONE	WS	NONE	NO
MINIMUM	YES	16251	3078	SG	WS	NONE	NO
COST OPTIMIZED*							
- 1978 INSTALLATION	YES	16251	0	NONE	DS	-10	YES
- 1982 INSTALLATION	YES	16251	0	NONE	DS	-10	YES
ATLANTA							
FULL	YES	24876	0	NONE	WS	NONE	NO
MINIMUM	YES	10302	465	ABS	WS	NONE	NO
COST OPTIMIZED*							
- 1978 INSTALLATION	YES	10302	0	NONE	DS	20	YES
- 1982 INSTALLATION	YES	10302	0	NONE	DS	20	YES
PHILADELPHIA							
FULL	YES	78732	0	NONE	WS	NONE	NO
MINIMUM	YES	17603	3628	ABS	WS	NONE	NO
COST OPTIMIZED							
- 1978 INSTALLATION	YES	17603	0	NONE	DS	20	YES
- 1982 INSTALLATION	YES	17603	0	NONE	DS	20	YES

NOTE: SG = SINGLE GLAZE, DG = DOULBE GLAZE, ABS = ABSORBER, WS = WATER SOURCE, DS = DUAL SOURCE

Table 4. Characteristics of the Commercial Building HVAC Systems

HVAC SYSTEM HEATING PLANT/ COOLING PLANT	PHILADELPHIA: INSTALLED COST 1978	INSTALLED COST 1982	ANNUALIZED COST 1978	ANNUALIZED COST 1982	COP*	ATLANTA: INSTALLED COST 1978	INSTALLED COST 1982	ANNUALIZED COST 1978	ANNUALIZED COST 1982	COP*	MINNEAPOLIS: INSTALLED COST 1978	INSTALLED COST 1982	ANNUALIZED COST 1978	ANNUALIZED COST 1982	COP*
NATURAL GAS/ ELECTRIC[1]	57130	57130	18877	17516	.98/.86	66330	66330	28749	26890	1.17/1.12	69220	69220	16315	15272	.89/.78
OIL/ELECTRIC[2]	56205	56205	18288	16880	1.19/1.01	65690	65690	28229	26527	1.55/1.29	68470	68470	16293	15123	1.09/.93
ELECTRIC/ ELECTRIC[2]	56628	56628	19697	18082	1.47/1.20	64730	64730	32350	30095	1.84/1.48	66930	66930	17702	16372	1.38/1.13
FULL ACES[3]	147465	144465	17659	16073	3.45/2.41	106483	104292	23905	21771	3.20/2.42	148358	145085	17384	15847	3.32/2.35
MINIMUM ACES[3]	182064	138801	19343	16576	2.55/1.94	129753	107589	25073	22420	2.77/2.17	182376	149548	20417	17573	2.42/1.86
COST OPTIMIZED ACES[3]	85867	82867	16576	15085	2.72/2.03	81649	78654	23694	21495	2.87/2.23	80084	78317	14486	13388	1.82/1.45

1. Natural gas fired domestic hot water heater
2. Electric domestic hot water heater
3. Desuperheater domestic hot water heater

*First value of COP does not include air distribution energy consumption; second value does.

NOTES

Dup

AN OPTIMIZATION TECHNIQUE FOR MINIMIZING THE COST OF SELF-POWERING INDUSTRIAL HVAC SYSTEMS

David S. Cowen Edward J. Daniels
Energy Systems Analysis
Institute of Gas Technology
Chicago, Illinois

ABSTRACT

This paper presents a generalizable cost optimization technique for designing industrial heating, ventilating, and air conditioning (HVAC) systems that include components that produce both power and heat. The intent of the paper is to show that intuition — design based on only the initial capital costs of the subsystems or components — could result in a less than optimal operating system. The analysis reveals that as the total cost of owning and operating HVAC systems becomes increasingly sensitive to costs other than initial capital costs, optimization techniques become essential.

INTRODUCTION AND SUMMARY

This paper provides a generalizable cost optimization technique for designing industrial heating, ventilating, and air conditioning (HVAC) systems that include their own power and heat source. Such a source could be a fuel cell, a solar thermal-electric hybrid system, a Stirling engine-generator, or any other cogeneration system. This technique optimizes the size of HVAC components, given their operating parameters and capital and operating costs, and the base-load electric power and heat requirement for the industrial user. In essence, this paper proposes integrating the various methods of producing electrical and heat energy in the most cost-effective fashion.

The methodology is as follows: Equipment specifications are utilized to produce n equations in n unknowns describing system performance. An additional equation sums the unit capital and operating costs of each component. The performance equations are simplified to one unknown, and substituted into the "Z" or cost equation. This equation is differentiated with respect to that unknown, and a minimum solution is found. The remaining minima are found by substitution of this known value into the performance equations.

Statement of the Problem

A fuel cell manufacturer wishes to design a factory that utilizes phosphoric acid fuel cells to generate heat and electricity. The baseline electrical requirement is projected to be 800 kW(e), while the process heat requirement is 810 kW(th). The design day winter heating load is 300 kW(th). (For the sake of simplicity, we stipulate no cooling requirement, although this would be an interesting variation on the problem.)

Three heating appliances are available for the system (Fig. 1):

- An electric heat pump
- A heat exchanger (shell and tube-type)
- An electric furnace.

Heat is to be provided in the form of steam at 121°C (250°F).

The problem is as follows: Given the operating characteristics and annualized capital and operating costs of each component, what is the optimum size of each component such that the minimum annual total cost for the entire heating system is achieved?

Specifications and Assumptions

The analysis is based upon the following information:

- Two fuel cells are to be used. The size of the first is fixed at 800 kW(e). The second provides additional power for peaking and/or downtime of the first fuel cell. This may be considered a "remote-location" example. Electricity grids and gas pipelines are not accessible.
- The phosphoric acid fuel cell produces five units of thermal energy [177°C (350°F) gas] for every four units of electrical energy (DC converted to AC at an assumed 100% efficiency).
- Ten percent of the 177°C (350°F) heat from the first fuel cell can be recovered as 82°C (180°F) heat.
- The heat exchanger is assumed to be 100% efficient.
- Components of any size are assumed to be available.

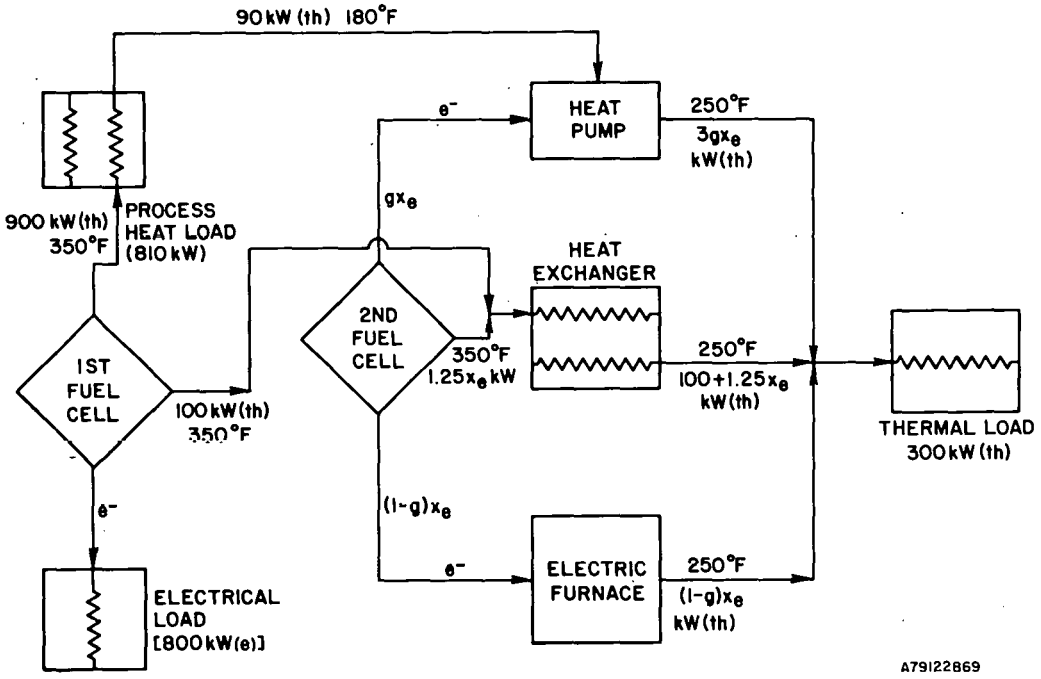

Fig. 1. Schematic of Industrial HVAC System

- The coefficient of performance (COP) of the heat pump is 3.0.
- The heat pump absorbs heat at 82°C (180°F) and produces heat at 121°C (250°F) (operates at 40% of Carnot cycle COP).
- The electric furnace is assumed to be 100% efficient in converting electricity to heat.
- System losses of pressure and heat are considered negligible.

Cost Data

The capital cost data shown here (Table 1) are based upon official statements or projections.*

Table 1. Annualized Costs

	Capital	Operating
Heat Exchanger	20	0
Electric Furnace	25	400
Heat Pump	150	400

The units are in late 1979 dollars per kilowatt. The operating costs reflect the annualized charge for electricity from the fuel cell at $0.05/kWhr.

* EPRI, private communication, December 7, 1979; Rockwell International, Cost Algorithms, 76-019-49-72, Atomics International Division.

No credit for by-products (thermal or otherwise) is taken in this charge for electricity from the fuel cell. No maintenance costs are assumed in these operating costs. The plant factor is 90% (downtime 10%) for all three components and the fuel cells.

We utilize the cost information and the equipment specifications to develop the performance equations and the cost equations for the components of the system (Table 2). The system constraint shown as equation 4 sets the boundary for the solution. The problem is now to minimize the sum of the system components (the Z equation) costs provided the system requirements are met (equation 4). For the system under consideration, the solution to the problem yields not only the minimum but also the value of g in the system. If g is not 0, then a heat pump is included in the minimum cost system. The solution is presented in the Appendix.

Using the solved value of g of 0.38462, we can solve for the other variables as follows:

$$x_e = \frac{200}{2g + 2.25} = 66.242$$

$$Z_{min} = \$1.460 \times 10^6$$

$$x_{hp} = 3g\, x_e = 76.434$$

$$x_f = (1-g)\, x_e = 40.764$$

$$x_{hx} = 100 + 1.25\, x_e = 182.802$$

$$x_{hp} + x_f + x_{hx} \overset{\checkmark}{=} 300.000$$

Table 2. System Equations

1. Heat Pump Performance

$$x_{hp} = 3g\ x_e \quad (COP = 3)$$

where g = fraction of electric output of second fuel cell to drive heat pump

x_e = electric output [kW(e)] of second fuel cell

$$x_{hp} \leq 90 + g\ x_e \quad \text{(energy out} \leq \text{energy in)}$$

2. Heat Exchanger Performance

$$x_{hx} = 100 + 1.25\ x_e$$

where x_{hx} = heat output [at 121°C (250°F)] of heat exchanger in kW

3. Furnace Performance

$$x_f = i\ x_e$$

where $i = 1-g$

x_f = heat output of furnace in kW

4. System Constraint

$$x_{hp} + x_f + x_{hx} = 300$$

5. Cost Equations

Heat Pump: $cost_{hp} = (150 + 400g\ x_e)\ x_{hp}$

Heat Exchanger: $cost_{hx} = 20\ x_{hx}$

Furnace: $cost_f = (25 + 400i\ x_e)\ x_f$

$$\Rightarrow Z = (150 + 400g\ x_e)\ x_{hp} + 20\ x_{hx} + (25 + 400i\ x_e)\ x_f$$

Discussion

Intuition might have led the HVAC designer to a different choice of component sizes than the mathematical approach would indicate. If we look at the capital costs (Table 1), the heat pump would seem too expensive on that basis. The designer might therefore reject the heat pump and just use the electric furnace and the heat exchanger. This would result in a system cost of $3 million, $1.3 million over the actual minimum using a heat pump (Fig. 2). Of course, it is possible the designer's intuition is fortified by the knowledge that the heat pump provides thermodynamic and economic benefits by using low-grade heat. So he would include a heat pump — but what size is best? Choosing the wrong size could also result in annual million-dollar losses (Fig. 2).

This example could be made more complex and perhaps more realistic by considering other possible fuel sources or prime movers. Of course, burning propane or No. 2 fuel oil is cheaper than having a second fuel cell; however, this may not be true 20 years hence, particularly for remote location sites. Also, the system could be expanded to include these energy sources and boilers for using them. Thus, the methodology would remain the same.

Conclusion

Despite capital costs several times higher than the competition, the heat pump has a useful place in this fuel-cell-driven HVAC system (heating mode only in this example). As the example becomes more complicated (with, for instance, addition of cooling or discrete size components), the economic risks tend to become higher. Hence, where the total cost of owning and operating energy-conversion components becomes increasingly sensitive to costs other than the initial capital cost of the component, and/or as the total system becomes more complex, optimization techniques similar to that presented here must be employed. The consequences of relying on intuition alone are too great.

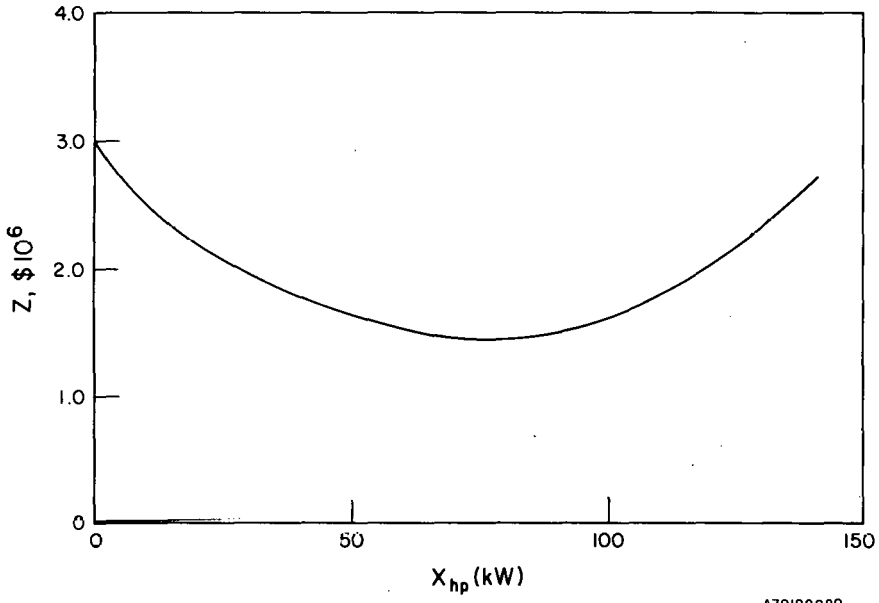

Fig. 2. System Costs Versus Heat Pump Size

APPENDIX

Computer algorithms can be employed especially for more complex systems. However, this example is solved by hand for exposition. The minimum of the Z function is found and then the values of all of the variables are solved at that minimum.

Minimize $Z = (150 + 400g\ x_e)\ x_{hp} + 20x_{hx} + (25 + 400i\ x_e)\ x_f$

subject to:

$$x_{hp} + x_f + x_{hx} = 300 \quad (1)$$

$$x_{hp} = 3g\ x_e \quad (2)$$

$$x_{hp} \leq 90 + g\ x_c \quad (3)$$

$$x_{hx} = 100 + 1.25x_c \quad (4)$$

$$x_f = i\ x_o \quad (5)$$

- $x_{hp} + x_f + x_{hx} = 300$

By substitution of equations 2, 4, and 5,

$$x_e = \frac{200}{2g + 2.25} \quad (6)$$

- $Z = (150 + 400g\ x_e)\ x_{hp} + 20x_{hx} + (25 + 400i\ x_e)\ x_f$

By substitution of equations 6, 2, 4, and 5,

$$Z = x_e^2\ (1600g^2 - 800g + 400) + x_c\ (425g + 50) + 2000$$

- $\frac{dZ}{dg} = 2x_e \frac{dx_e}{dg} (1600g^2 - 800g + 400) + x_e^2 (3200g - 800) + (425g + 50) \frac{dx_e}{dg} + 425x_e$

- $x_e = \frac{200}{2g + 2.25}$

$$\frac{dx_e}{dg} = -400\ (2g + 2.25)^{-2}$$

- $\frac{dZ}{dg} = 2 \left(\frac{200}{2g + 2.25}\right) \left[\frac{-400}{(2g + 2.25)^2}\right] X\ (1600g^2 - 800g + 400) + \left(\frac{200}{2g + 2.25}\right)^2 (3200g - 800) + \left[\frac{-400}{(2g + 2.25)^2}\right] (425g + 50) + 425 \left(\frac{200}{2g + 2.25}\right)$

$\frac{dZ}{dg} = 0$ (for minimum)

$$\Rightarrow -(400)^2\ (1600g^2 - 800g + 400) + (2g + 2.25)\ (200)^2\ (3200g - 800) + (2g + 2.25)\ (-400)\ (425g + 50) + (2g + 2.25)^2\ (425)\ (200) = 0$$

$$\Rightarrow -16\ (1600g^2 - 800g + 400) + 4\ (2g + 2.25)\ (3200g - 800) - 0.04\ (2g + 2.25)\ (425g + 50) + 8.5\ (2g + 2.25)^2 = 0$$

$$\Rightarrow -2.56 \times 10^4 g^2 + 1.28 \times 10^4 g - 6400 + (8g + 9)\ (3200g - 800) - (2g + 2.25)\ (17g + 2) + 8.5\ (4g^2 + 9g + 5.0625) = 0$$

$$\Rightarrow -2.56 \times 10^4 g^2 + 1.28 \times 10^4 g - 6400$$

$$+ 2.56 \times 10^4 g^2 + 2.24 \times 10^4 g - 7200$$

$$- 34g^2 - 42.25g + 4.5$$

$$+ 34g^2 + 76.5g + 43.03 = 0$$

$$3.523 \times 10^4 g - 1.355 \times 10^4 = 0$$

$$g = \frac{1.355}{3.523} = 0.38462$$

Second Derivative

$$\frac{dZ}{dg} = \left[\frac{10^4}{(2g + 2.25)^3}\right] (3.523g - 1.355 \times 10^4)$$

$$\frac{d^2Z}{dg^2} = \frac{10^4 (3.523)}{(2g + 2.25)^3}$$

$$+ 10^4 (3.523g - 1.355 \times 10^4) (-6) (2g + 2.25)^{-4}$$

$$= [(2g + 2.25) (3.523) - 21.14g + 8.13 \times 10^4]$$

$$\times \frac{10^4}{(2g + 2.25)^4}$$

$$= (7.05g + 7.93 - 21.14g + 8.13 \times 10^4)$$

$$\times \frac{10^4}{(2g + 2.25)^4}$$

$$= \frac{(10^4) (- 14.09g + 8.13 \times 10^4)}{(2g + 2.25)^4}$$

Real and positive for $0 \leq g \leq 1$

$\therefore$ Z minimum in the relevant range.

RS:vz

NOTES

Session IIA

Dr. Bryon Winn
Solar Environmental Engineering Corporation
Chairperson

CONTROLS I

CONTROL STRATEGIES FOR DUAL TEMPERATURE SOLAR HOT WATER SYSTEMS: AN EXPERIMENTAL COMPARISON

R.L.T. Wolfson and H.S. Harvey

Department of Physics
Middlebury College
Middlebury, Vermont 05753

ABSTRACT

Two identical solar collector systems were operated side by side for a 67 day period. Data acquisition and control of both systems were accomplished by a minicomputer. Each system included two storage tanks. One system's control strategy kept its two tanks at the same temperature, simulating a single tank. The other system employed a dual temperature strategy designed to allow greater flexibility in adjusting to varying insolation. The dual temperature strategy showed a modest 4% gain in energy delivered to a load.

INTRODUCTION

Dual temperature storage capability in solar collector systems permits the use of flexible control strategies resulting in more effective utilization of available insolation. Dual temperature storage can be regarded as a means of artificially enforcing a chosen degree of stratification or as a way of expanding and contracting storage volume as conditions dictate. In any event, dual temperature storage allows closer matching of load requirements with insolation as each varies.

Complex control strategies are often evaluated and even optimized using numerical simulations. But there remain difficulties with simulations capable of covering long time periods while properly handling short time scale events associated with control operations such as valve and pump cycling, and with heat capacities of system components. Experiments with real hardware include all these effects. Except for control of meteorological inputs, a real system may be made nearly as flexible as a numerical simulation through computer control and data acquisition. Finally, side by side operation of identical systems under different control strategies permits direct experimental comparison of performance under given meteorological inputs. This paper describes the results of an experiment in which dual temperature control strategy is compared with a more conventional strategy.

EXPERIMENTAL APPARATUS

At Middlebury College a pair of identical solar collector systems is operated side by side, exposed to the same meteorological inputs, but under different control strategies. Data acquisition and control for both systems are handled by a minicomputer (DEC PDP 11V03) so that changes in control strategy may be accomplished by simple software modification. The systems are amply provided with temperature sensors (Fenwal UUT43J1 curve matched thermistors) and other environmental sensors as well as with computer controlled solenoid valves and pumps, so that a wide variety of control strategies may be tested. Each system consists of a single flat plate collector (Columbia Chase model 4394) with 2.1 m^2 net area, pump, valves and other plumbing, a large storage tank of 151 liter (40 gal.) capacity, and a small storage tank of 57 liter (15 gal.) capacity. Systems are pressurized to 1.4×10^5 nt/m^2 (20 psi). Flow rate during circulation is 0.05 liters/second (0.8 GPM). Figure 1 shows a diagram of one of the two identical systems. Inclusion of two tanks in each system allows implementation of dual temperature control strategies.

CONTROL STRATEGIES

During the fall of 1979, an experimental test of a dual temperature control strategy was conducted. Both systems were operated with identical criteria for switching circulation. Pumps were turned on when collector plate surface temperature exceeded the temperature at the bottom of either storage tank by a turn-on differential of 6° C. Circulation was stopped when collector outlet temperature fell within a 2° C turn-off differential of the bottom of the cooler storage tank. In system A valve switching was used to maintain the two tanks within 1° C of each other, thus simulating a single unstratified tank. (There was, however, considerable stratification within the individual tanks, necessitating the large number of thermistors in

the tanks.) With circulation on, system B's control strategy attempted to heat the small tank toward a target temperature of 45° C as long as collector outlet temperature exceeded the temperature at the bottom of the small tank by more than 2° C; if this condition was not met, circulation was switched to the large tank. If target temperature was reached in the small tank, the large tank was heated to target temperature, whereupon both tanks were kept within 1° C of each other as in system A. Prior to the experiment both systems were operated under the single temperature strategy for several weeks to confirm that they behaved identically.

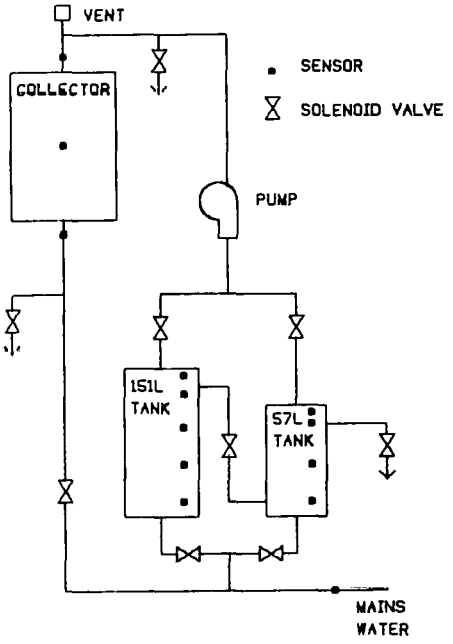

Fig. 1. System diagram of one of two identical systems. Not shown are relief valves, expansion tank, hand valves, as well as load draw tank which is common to both systems. All valves are NC configuration except for dump valves near collector which are NO to provide freeze protection.

120 liters, constituting more than half the system volume of 208 liters (55 gal.) were drawn from each system daily. At 0700 and 1700 hours 50 liters were drawn, while 20 liters were drawn at 1200 hours. Loads were drawn in 10 liter quanta, alternating between the two systems. Circulation was stopped when water was actually being drawn from a system, and valving configured so that water drawn from the top of the small tank was replenished with water flowing from the top of the large tank into the bottom of the small tank. The large tank, in turn, was replenished with mains water flowing into its lower section. Prior to each load draw mains water was run down the drain until its temperature stabilized, so that makeup water temperature was the same for both systems. Because only discrete multiples of 10 liters could be drawn with the present equipment, no attempt was made to mix hotter and cooler water to achieve a desired load temperature. Rather, the solar heated water was assumed to fall short of the desired load temperature, here taken as 50° C. This assumption is generally appropriate for any reasonably sized solar hot water system in our Vermont location during all but the summer months. Load temperature was monitored almost continuously as water left the storage tank. An average load temperature was then calculated.

Switching differentials, target temperature, load draw schedule, and other control parameters were chosen on the basis of early experience with the system. No attempt has yet been made to optimize these parameters.

The rationale for the dual temperature control strategy is twofold. First, heating a relatively small volume of water quickly may make delivery near desired load temperatures more likely. In this sense the dual temperature strategy seeks to maximize energy quality rather than quantity. On the other hand the presence of a large volume of cool water means the dual temperature system may meet the circulation criterion during periods of of marginal insolation when the single temperature system does not, although energy collected at such times is of lower quality.

A simple analysis based on extreme cases should serve to illustrate situations in which the dual temperature strategy is both a realistic and practical alternative to the single temperature strategy. First, consider the case when total daily load is far less than the volume of the small tank alone. Here the dual temperature system operates primarily as a single tank system, with the small tank alone being active. The small tank is adequate to meet load needs, and because of its smaller volume it delivers hotter water. This case is uninteresting from a practical standpoint because it implies simply that the storage capacity of the two tanks together, and indeed of the small tank alone, is grossly oversized in relation to the load. However, the case does show that the dual temperature system excels in some parameter range, albeit due to poor system engineering. At the other extreme, when the daily load vastly exceeds the storage capacity of both tanks, lower collection efficiencies associated with hotter storage and the insignificance of the smaller tank volume relative to the load combine to eliminate any advantage possessed by the dual temperature strategy. Between these extremes lies the range of interest. As meteorological inputs vary the flexibility of the dual temperature system means that it may often, although not always, provide hot water better matched to load requirements. That it might do so in a single day, starting from cold storage, is evident. Whether

any long range advantage persists depends on meteorology, load requirements, and details of the control parameters.

EXPERIMENTAL RESULTS

The present experiment was begun on 12 October, 1979; this paper reports results through 17 December. Data from all sensors were taken approximately every five seconds and averaged over 10 minutes. The 10 minute averages, along with status of system control signals, were stored on a floppy disk. Every two weeks the disk was dumped to a larger computer for analysis. A data summary was also printed hourly as the experiment proceeded, and control signal status was always available through an LED display on the data acquisition and control interface unit. Absolute accuracy of temperature and energy measurements except for outdoor ambient was approximately 1%. However, comparisons between the two systems could be made to better than 0.5%.

Insolation was measured with an Eppley model PSP pyranometer mounted in the collector plane, oriented south and inclined at 45°. The inclination angle is approximately the site latitude. Pyranometer output was connected through a precision instrumentation amplifier to the data acquisition system.

Insolation during the experimental period was mediocre, averaging 39% of clear sky values for this time of year. A plot of daily insolation is shown in Fig. 2.

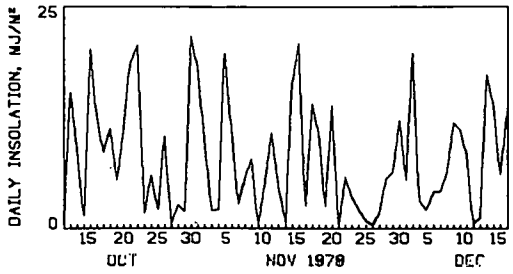

Fig. 2. Daily insolation, in megajoules per square meter, measured in the collector plane.

Although load temperatures and calculated solar load fractions were low, the extreme variability of the insolation probably worked to the advantage of the dual temperature strategy because the systems usually started from low temperatures on the occasional days of high insolation. More generally, since the dual temperature system is designed for flexibility in the face of varying inputs, the experimental period represents the sort of conditions under which the dual temperature strategy should be effective.

Data for each day was summarized in graphical form permitting detailed analysis of the operation of each control strategy. Figure 3 shows a day when the dual temperature strategy did substantially better.

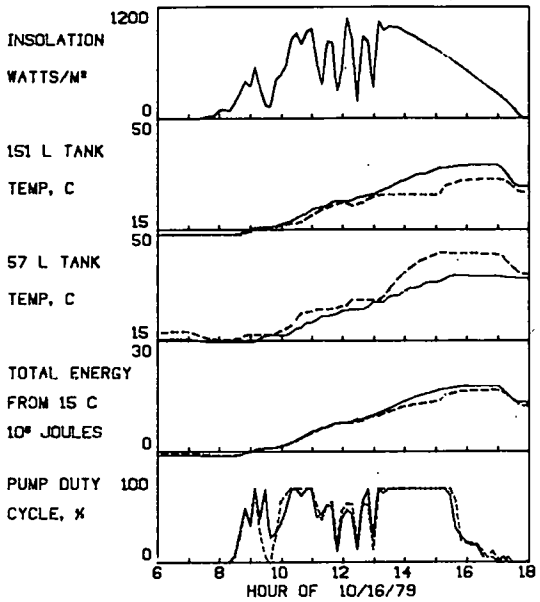

Fig. 3. Data summary for 16 October, 1979. Insolation is measured in the collector plane. Solar fraction is calculated on the basis of a desired load temperature of 50° C and a starting temperature of 15° C, and is the fraction of the load actually supplied by the solar system. All energies are measured in megajoules, based on zero at 15° C.

Notice that system B, the dual temperature system, collected only 2.5% more energy than system A, but delivered 38% more to the load. The difference in performance is due to the availability of hotter water from system B's smaller tank, a fact which becomes clear when one looks at the plots of tank temperatures. 16 October, the day shown in Fig. 3, is an exceptionally good day for the dual temperature strategy. This is because of low starting temperatures, a result of poor insolation on the preceding days, and the high insolation on this day. However, intermittent morning sunshine meant that the dual temperature strategy did not become fully effective until about noon. This can be seen because system B's large tank did heat during the morning, indicating insufficient insolation to heat the small tank continually. Furthermore,

the dual temperature strategy achieved target temperature in the small tank at about 1500 hours, and again switched to heating the large tank. Thus the effect of differential tank heating was achieved largely in the three hour period between noon and 1500 hours. Although one might expect substantially better results on a clearer day, analysis of plots like Fig. 3 shows that truly differential heating never occurs for more than about three hours, so that 16 October is close to optimum for the dual temperature strategy with present operating parameters and hardware.

An objection to the dual temperature strategy is that although the small tank supplies hotter water at the first load draw since it was heated, it is replenished with colder water than its counterpart in the single temperature system. This effect is seen clearly at the 1700 hour load draw in Fig. 3, where the temperature of system B's small tank falls sharply, while system A's hardly changes. System A's large tank, on the other hand, falls more than system B's. Meanwhile the energy contents of both systems fall by the same amount, and indeed track nearly identically all day. On this particular day both systems end the day on an equal footing, but there are occasions when system B ends up at a disadvantage. Energetically, this loss is due to the relative inefficiency of the higher collection temperatures experienced in system B. Because of it, one should expect system A to outperform system B on days of low insolation following days when system B did better. Figure 4 shows such a day, which occurred two days after the day of Fig. 3. (The intermediate day was one in which system B delivered 6% more energy than system A.) Notice that system B actually collected more energy, although it delivered less to the load. While the difference in system performance is not substantial, a number of such days following a single good day for system B can nearly offset the gains made by the dual temperature strategy. Similarly, a long overcast stretch puts the two systems on an equal footing, and further dilutes the average gain of the dual temperature system.

The net result of the experimental comparison between the two control strategies is summarized in Table 1, which shows average performance for the entire 67 day experimental period and for two subsets of this period.

TABLE 1. SYSTEM PERFORMANCE

Data Subset	Average Insolation, $MJ/M^2/Day$	Energy Delivered, MJ/Day Sys. A	Sys. B	Sys. B Gain
All	8.0	5.40	5.63	4%
#1	14.0	3.83	4.43	16%
#2	7.0	5.14	4.97	-3%

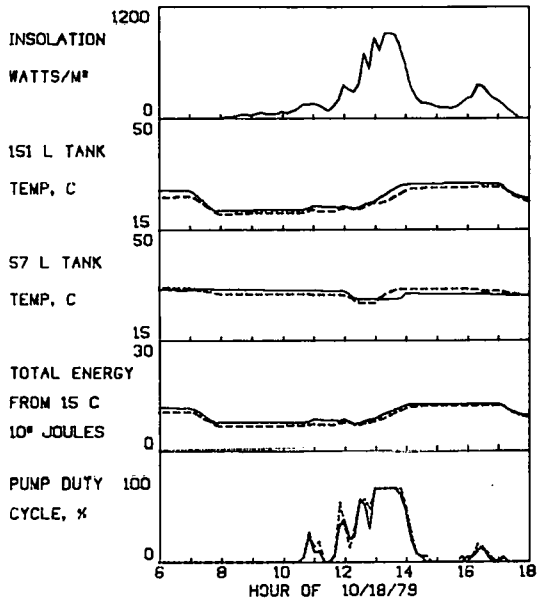

SOLAR INPUT/SYSTEM, MJ 17.8 AV.AMB.TEMP. 10.3

	SYSTEM A——	SYSTEM B---
ENERGY COLLECTED, MJ	5.8	6.2
ENERGY DELIVERED	7.9	7.7
SOLAR FRACTION	.45	.44

Fig. 4. Data summary for 18 October, 1979. That energy delivered exceeds energy collected indicates that load was supplied partly from energy collected on previous days.

For the entire run the dual temperature strategy achieved 4% better performance than the single temperature strategy, as measured by the amount of energy delivered to the load. For both systems the solar fraction was low, being 32.4% for system A and 33.7% for system B. The average duty cycle for system A's pump was 17.8% between 0600 and 1800 hours, compared with 18.6% for system B, so that system B was collecting energy more of the time. Despite the higher duty cycle, system B collected less than 1% more energy than system A, because of losses due to higher collection temperatures. Thus system B's advantage in load energy delivered is due not to more energy collected but to the availability of higher temperature water in the small tank.

To clarify the nature of those days on which the dual temperature system excelled, two subsets of data were considered. Subset #1 was somewhat arbitrarily defined as those days on which the solar fraction of load supplied by system B exceeded that of system A by 0.02 or more. (This is roughly equivalent to system B's delivering at least 0.40 MJ more than system A.) There were 14 such days, representing the best performances of

the dual temperature strategy relative to the single temperature strategy. As Table 1 indicates, average insolation for these subset #1 days was nearly double the average for the entire run, but energy delivered to the load was substantially less. This suggests that the dual temperature strategy does best on sunny days following long periods of poor insolation, when water temperature is low. Further confirmation of this trend is made by noting that only three of the 14 subset #1 days followed within two days of another subset #1 day. There were a number of occasions when subset #1 days were followed by other days of high insolation, but except for the three cases mentioned, those subsequent days were not exceptional ones for the dual temperature strategy. The dual temperature system clearly thrives on extreme variability in insolation on a daily time scale.

Subset #2 shown in Table 1 consists of those days when system A delivered more energy than system B. Again, there were 14 days in this subset. 12 of the 14 followed within two days of a subset #1 day, showing that gains made by the dual temperature strategy are somewhat offset during subsequent days. Of the two exceptions, one followed immediately after a day that almost qualified for subset #1, and the other occurred three days after a subset #1 day. Although average insolation for subset #2 was slightly below average for the entire run, subset #2 days varied from completely overcast to nearly clear, suggesting that their proximity to subset #1 days, rather than meteorology, determined system performance.

The analysis by subsets shows that the dual temperature control strategy must be evaluated over many days. For the insolation pattern during this experimental run, that evaluation shows the superiority of the dual temperature strategy.

CONCLUSION

The dual temperature control strategy examined in this experiment showed a modest gain of 4% in energy delivered compared with a more conventional strategy. This gain is attributable to the increased flexibility with which the dual temperature strategy responds to changing insolation. This simple experiment, in which no attempt was made to optimize control parameters, suggests that complex control strategies, based perhaps on microprocessor control systems, may contribute to a modest improvement in solar collector system performance.

ACKNOWLEDGMENTS

Thanks are due to David Gustafson for his work on the design and early construction of our data acquisition and control interface, and to Arthur Thorne for his high quality work on the design and installation of the system plumbing. This work was supported by the U.S. Department of Energy under contract EM-78-S-4719.

ENHANCEMENT OF PERFORMANCE OF ACTIVE SOLAR SYSTEMS BY OPTIMAL CONTROL AND SYSTEM IDENTIFICATION TECHNIQUES

C. A. Baer and D. V. Pryor
Graduate Students
Mechanical Engineering
Colorado State University
Fort Collins, CO 80523

C. B. Winn
Professor
Mechanical Engineering
Colorado State University
Fort Collins, CO 80523

Loren Lantz
SEEC
2524 E. Vine Dr.
Fort Collins, CO 80521

ABSTRACT

Optimal controllers of the second kind can provide significant increases in the amount of useful energy gained as compared to that provided by bang-bang controllers. Theoretical increases range from 5% up to over 50% depending upon the climatological data used [1]. The purpose of this paper is 1) to investigate practical considerations which may cut into this increased performance and 2) to offer possible solutions to these implementation type problems.

CONTROL SYSTEM DESCRIPTION

Optimal controllers of the second kind represent controllers that maximize the difference between the useful energy collected and the pumping costs associated with collecting solar energy [1]. This is equivalent to maximizing the cost functional

$$J = \int_{t_o}^{t_f} \{Q_u(\dot{m}) - P(\dot{m})\}dt$$

where Q_u represents useful energy gained, $\dot{m}$ is mass flow and P represents parasitic losses due to operating the pump. If one assumes that the parasitic losses are a function of $\dot{m}^3$, the optimal control strategy is

$$\dot{m} = F'^2 W_L A_c/[2C_p(F'-F_R)]$$

where

$$F_R = F' - (3C_5/C_4 f)^{1/4}$$

If insolation is measured, f can be determined from

$$f = A_c[H_T(\tau\alpha) - U_L(T_s-T_A)]$$

If the outlet temperature is measured instead, f can be calculated from

$$f = \dot{m}C_p(T_o-T_s)/F_R$$

if the pump is on and

$$f = A_c U_L(T_o-T_A)$$

If the pump is off.

It is worthwhile to try to gain some intuition in the above formulation before proceeding. Substituting into the $\dot{m}$ equation we get

$$\dot{m} = F'^2 U_L A_c/2C_p\left(\frac{3C_5}{C_4 f}\right)^{1/4} \quad (1)$$

or

$$\dot{m} = k\left(\frac{\dot{m}}{F_R}\right)^{1/4}(T_o-T_s)^{1/4} \quad (2)$$

Whereas the bang-bang type controllers select $\dot{m}$ to be full on or full off based upon ΔT, and proportional controllers pick $\dot{m}$ as a constant times ΔT, the optimal controller will select $\dot{m}$ as a function of ΔT and the mass flow at that particular moment. That is, the optimal controller uses information concerning available energy as well as ΔT to determine the new $\dot{m}$. Ostensibly, this could seem like a distinct advantage over the straight proportional controller. One must remember, however, that the proportional controller will get available energy information albeit, indirectly. That is, a relatively large ΔT indicating that a large mass flow is required would soon decrease if the available energy was low. While the optimal controller would determine this immediately by virtue of using $\dot{m}$ in the feedback equation, the proportional controller will effectively find this out as ΔT decreases. Furthermore, inconsistent outputs such as large ΔT's and low mass flow rates will only occur when the system is first turned on or if the inputs are changing dramatically. During normal operation, ΔT is itself an indication of available energy since mass flow is determined by it. In the dynamically slow world of solar systems, then, one would not expect to see much difference between proportional and optimal controllers of the second kind. In fact, proportional controllers may have an advantage in some cases.

IMPLEMENTATION OF THE OPTIMAL CONTROLLER

In order to put the problem of implementation in perspective, it is necessary to get some idea of how this version of the optimal controller compares with other types of controllers, in

particular bang-bang and proportional controllers. The computer model for this simple comparison consisted of a single collector with storage inside a small insulated building. The collector was run for low, average, and high solar insolation days. Insolation and ambient temperatures were modelled with simple sign waves. All controllers were "tuned" to some extent and had the same maximum flow rates, 100 kg/hr. Results are shown in Table 1.

The performance increases expressed as a percent gain of optimal over the other controllers are in Table 2.

The point to be made here is that the optimal controller shows significant gains over the bang-bang controller; however, the increase over the performance of the proportional controller is minimal. Therefore, any problems incurred during the implementation of the optimal controller which result in the incorrect amount of gain for mass flow determination will make the system performance inferior to the proportional controller. With this in mind, let us consider the control equation, Eq. (1).

There are two major assumptions made for the implementation of the optimal controller. First is that one assumes that all the parameters involved are known and that they are constant. Secondly, the assumption was also made that pump losses were proportional to $\dot{m}^3$. The validity of these assumptions determines how truly optimal the system performs; therefore it is worthwhile to see how these systems react to variations of the nominal parameters. The parameter of Eq. (1) which would have the largest variance is the heat loss coefficient U_L. Variations of 50% or more may be possible due in large part to the wind conditions. Table 3 gives results for performance while varying U_L ±50% from the nominal conditions for the different controllers.

The point to be made here is that the optimal controller still performs quite well as compared to the bang-bang controller, however, the proportional controller actually performs better in some instances. The proportional controller, which was tuned for the medium insolation days, keeps the same value for feedback gain. The optimal controller was also tuned for the same typical day, but the variation in the U_L value from the nominal value used in the controller gain is enough to affect its performance the small amount indicated above. The percent increase in performance over the proportional controller is now +.5% to -.9%.

The other assumption made during the development of the optimal controller is that the pump losses are proportional to $\dot{m}^3$. This is more than likely a good assumption for large systems with heat exchangers. In many cases, however, the flow in the collectors will be laminar and therefore the losses will be proportional to $\dot{m}^2$ for at least part of the system. How this affects the various control systems is quite minimal for energy proportional to $(\dot{m})^{2.5}$. For the optimal versus the proportional controllers were within .3% of one another. And, as one might expect with lower pump energy charges, the bang-bang controller fairs better than before, reducing percentage increases of Table 2 to 24%, 2%, and ~ 0% for low, medium and high insolation respectively.

Using the computer model as a basis, then, we can thus far conclude that under nominal conditions, the optimal controller will outperform bang-bang controllers, by a substantial margin and outperform proportional controllers by a very slight amount. For off-nominal conditions, proportional and optimal controllers still outperform the bang-bang controller, but the difference between the former two controllers is even smaller than before with the advantage sometimes going to the proportional controller. The remaining question to be asked, then, is would it be worthwhile to try to enhance the performance of the optimal controller by having an up-to-date value of U_L such as could be provided by an observer?

To determine the potential enhancement by using observer techniques on U_L is a two part problem. First, how much could the performance be improved? Secondly, is U_L observable using the present data or would it require additional measurements. An indication of the answer to the first question is to note the variation of the $(\dot{m}/F_R)^{1/4}$ term of Eq. (2) as a function of U_L. This will give the amount of variation in the feedback gain for the optimal controller. For

$$(\dot{m}/F_R)^{1/4} = \left(\frac{\dot{m}}{\frac{\dot{m}C_p}{U_L A_c}\left(1 - \text{Exp} - \frac{F'U_L A_c}{\dot{m}C_p}\right)}\right)^{1/4}$$

The normalized results for three different mass flows are shown in Table 4.

One can see that even if one had correct values, the effect on results would be minimal. Computer simulations also show little or no improvement. In answer to the second question one can formulate the observer in the following manner.

$$f_1 = \dot{x}_1 = \dot{T}_s = \frac{\dot{m}k_2}{x_2}\left(1 - \exp - \left(\frac{k_1 x_2}{\dot{m}}\right)\right.$$

$$\left.[(x_3 - x_2(x_1 - T_A) - UA(x_1 - T_A)]\right.$$

$$f_2 = \dot{x}_2 = \dot{U}_L = 0$$

$$f_3 = \dot{x}_3 = H_T(\tau\alpha) = 0$$

$$y = \begin{matrix}1 & 0 & 0\end{matrix}\begin{pmatrix} x_1 \\ x_2 \\ x_3 \end{pmatrix} + \text{input terms}$$

TABLE 1. ENERGY CALCULATIONS

Controller	Daily Insolation ($kwh/m^2 day$) 2.0 (LOW)			4.8 (MEDIUM)			9.0 (HIGH)		
	E_{COLL}	E_{PUMP}	E_{NET}	E_{COLL}	E_{PUMP}	E_{NET}	E_{COLL}	E_{PUMP}	E_{NET}
Bang-bang	4319	1279	3039	15830	2300	13529	32412	2692	29719
Proportional	5296	65	5231	15920	318	15601	32321	898	31422
Optimal	5399	149	5250	15948	344	15604	32128	586	31542

TABLE 2. PERFORMANCE GAIN OF OPTIMAL CONTROLLER

Controller	Daily Insolation ($kwh/m^2 day$) 2.0 (LOW)	4.8 (MEDIUM)	9.0 (HIGH)
Bang-bang	72%	15%	6.1%
Proportional	.3%	0%	.4%

TABLE 3. EFFECTS OF VARIATIONS ON U_L

	-50%	-25%	0%	25%	50%
Bang-bang					
Low Insolation	4027	3506	3039	2605	2205
Medium Insolation	15294	14383	13529	12735	12014
High Insolation	32485	31057	29719	28468	27310
Proportional					
Low Insolation	6613	5884	5231	4643	4111
Medium Insolation	17756	16630	15601	14651	13766
High Insolation	34490	32894	31422	30052	28764
Optimal					
Low Insolation	6550	5866	5250	4696	4191
Medium Insolation	17717	16617	15604	14669	13802
High Insolation	34687	33057	31542	30130	28810

TABLE 4. NORMALIZED EFFECT OF U_L VARIATIONS

	MASS FLOW (kg/hr) 100	50	10
U_L = +50%	1.005	1.004	1.02
U_L = Nominal	1	1	1
U_L = -50%	.998	.991	.951

Note that the first equation is nonlinear and that the state variable $H_T(\tau\alpha)$ must be included since it is not being measured. To determine the observability, linearize the equation and then apply the observability criterion. Doing this in general terms we get

$$\frac{\partial \bar{f}}{\partial \bar{x}} = \begin{matrix} \frac{\partial f_1}{\partial x_1} & \frac{\partial f_1}{\partial x_2} & \frac{\partial f_1}{\partial x_3} \\ 0 & 0 & 0 \\ 0 & 0 & 0 \end{matrix}$$

The observability matrix becomes

$$\begin{matrix} 1 & 0 & 0 \\ \frac{\partial f_1}{\partial x_1} & \frac{\partial f_1}{\partial x_2} & \frac{\partial f_1}{\partial x_3} \\ (\frac{\partial f_1}{\partial x_1})^2 & \frac{\partial f_1}{\partial x_1}\frac{\partial f_1}{\partial x_2} & \frac{\partial f_1}{\partial x_1}\frac{\partial f_1}{\partial x_3} \end{matrix}$$

The rank of this matrix is two and therefore not of full rank. Mathematically, this means the system is not observable. Intuitively, it means that an observer can not tell the difference between the sun going behind a cloud (lower $H_T(\tau\alpha)$ and the wind increasing (H_L increasing). Note that if we were to measure $H_T(\tau\alpha)$ the top row of the observability matrix would become (1 0 1) and the system would be observable subject to the values of state variables at the particular time. The net result, then, is that it would require more instrumentation for a very minimal amount of increased performance.

CONCLUSIONS

Optimal controllers of the second kind can provide a substantial performance increase over that of the conventional bang-bang controller even when considering that some parameters may be off nominal. The performance difference between the optimal and proportional controllers, however, is very slight and off nominal conditions do not affect this conclusion to any significant degree. If observer techniques were to be employed to determine particular parameters used in the optimal controller, additional instrumentation would be necessary and the payoff would be minimal.

NOMENCLATURE

F' = collector efficiency factor
U_L = collector heat loss coefficient
A_c = collector area
c_p = specific heat of fluid
F_R = heat recovery factor
f = available energy
T_o = collector outlet temperature
T_s = storage temperature (inlet temperature)
T_A = ambient temperature
H_T = incident insolation
$(\tau\alpha)$ = transmissivity - absorbtivity factor
UA = heat loss coefficient x area of storage

REFERENCES

[1] C.B. Winn and Dwight E. Hull, III, "Optimal Controllers of the Second Kind," Proc. of First Workshop of Control of Solar Energy Systems for Heating and Cooling, (1978).
[2] A. Gelb (ed.), Applied Optimal Estimation, M.I.T. Press, Cambridge, MA, 1974.
[3] J.A. Duffie and W.A. Beckman, Solar Energy Thermal Process, Wiley-Interscience Publication, John Wiley and Sons, New York, 1974.

ANALYTIC TECHNIQUES FOR DEVELOPMENT OF CONTROL STRATEGIES FOR PASSIVE SOLAR BUILDING

by

Peter R. Herczfeld and Robert Fischl
DREXEL UNIVERSITY
Department of Electrical Engineering
Philadelphia, PA 19104

and

Matthew Fischer
U.S. ARMY CORADCOM
Ft. Manmouth, NJ

ABSTRACT

~~In this paper~~ a formalism is developed, using analytic techniques, for incorating the control problem of passive solar energy systems with the design procedures. The model emphasizes structures consisting of composite walls and demonstrates how their dynamics are related to the control. The general approach is well suited for application of classical frequency domain control theory.

The theory is augmented by several examples, which demonstrates the interaction between the control functions and the building dynamics. The frequency domain analysis provides physical insight into the thermal response of passive solar buildings. It is shown that composite wall structures can reduce the undesired high daily temperature swings of building without effecting the overall heat gain.

INTRODUCTION

Passive solar energy systems have been succesful in reducing the heating and/or cooling loads of buildings by utilizing the time variation of climatic forces, particularly the solar flux. Some of the exisiting passive structures experience large daily temperature swings [1], which have to be compensated for by the introduction of managed heat sources and/or sinks or some other form of controllers. Usually the control stategy in passive buildings is not part of the design but on afterthought. Controllers interact with the building dynamics like any other driving forces and therefore should be an integral part of the design.

In this paper a formalism is developed which properly accounts for the control function. The emphasis is not on the derivation of a particular control strategy but on the physical insight into the interaction of control forces with the building dynamics.

Developing a simple, yet integrated approach to the design and control of passive solar buildings requires an intimate knowledge of the complex interalations of the solar inputs, the thermal response of the building, and the control mechanisms employed. Within such an approach, the design aspect involves selection of proper building materials and generation of building specifications (e.g. orientation). The control aspect relates synthesis of daily control strategies for both auxiliary powered devices (such as heat sources or attic fans) and more passive devices (such as window covers or night insulation). For both design and control, it is imperative to have available a dynamic model for the entire passive solar system.

The model to be used in this study is based on the premise that more rigorous, analytic approach will lead to a more accurate, more physically understandable solution which is adaptable to design and control studies and which yields a more efficient computer code for specific calculations.

In Section II a general model for the thermal response of the passive building will be introduced. The differential equation for the "room temperature" will be solved using Laplace transform technique. Submodels representing the heat flow through composite walls and the control fucntion will be derived. Section III includes three examples of the utility of the general approach. A brief summary is presented in Section IV.

II. PASSIVE SOLAR ENERGY MODEL

A model for the room temperature θ_R of a simple enclosure consisting of walls (including windows), a roof and a floor may be described by a first order differential equation of the form*

$$C_R \frac{d}{dt} \theta_R = \sum_p A_p \phi_p + C \qquad (1)$$

Here, C represents a control mechanism or managed heat sources. The summation indicates the totality of heat flows into the room through each side of the enclosure where A_p is the surface area of the side. The room temperature is, in general, a function of space and time but, for the present discussion we shall limit ourselves to a room with spatially uniform temperature.

Each of the terms on the r.h.s. of Eq.(1) are themselves modelled by various time dependent expressions. Some are described by relatively simple algebraic relations while other submodels require ordinary or partial differential equations.

The general approach to the solution of Eq.(1) is conceptually straight forward:

i. Take the Laplace transform with respect to time of Eq.(1) and of the expressions describing the various submodels. In particular,-Eq.(1) in frequency domain becomes:

$$C_R[s \hat{\theta}_R - \theta_{R_0}] = \sum_p A_p \hat{\phi}_p + \hat{C} \qquad (2)$$

ii. Solve the submodel expressions in the frequency domain.

iii. Substitute submodel solutions into Eq.(2) and solve for $\hat{\theta}_R$.

iv. Use this expression to analyze the control problem in the frequency domain or take the inverse transform to the time domain.

* A list of symbols is provided in Appendix A

Before we proceed with the examination of the submodels it should be pointed out that equation (1) could be expanded to include additional terms representing various physical phenomena (e.g. heat generated by lights and machinery, etc.). Each of these terms would be treated as an additional submodel leaving the entire approach unchanged.

In the modeling of the enclosure extensive consideration will be given to composite wall structures. It is hoped that by properly distributing the capacitive and resistive materials within the wall one can influence the time delays and the temperature fluctuations in the interior of the building.

A. Submodel for the Heat Flow Through a Composite Wall

Let us consider the heat transfer through a composite wall (the p-th wall) shown in Fig. 1. Each of the slabs have different thermal characteristics and the entire wall is driven by time dependent forcing functions, F_{pe} and F_{pi}, at the exterior and interior surfaces.

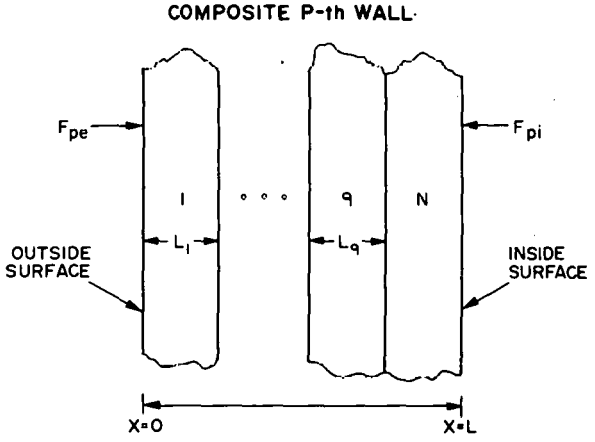

Fig. 1. Composition of the p-th wall consisting of slabs with different thermal characteristics. F_{pe} and F_{pi} are the external and internal driving functions

The thermal diffusion equation characterizing the q-th slab of the p-th wall is written:

$$\frac{\partial}{\partial t}\theta_{pq} = \frac{1}{(RC)_{pq}}\frac{\partial^2}{\partial x^2}\theta_{pq} \tag{3}$$

The first step in obtaining a solution is to take the Laplace transform with respect to time;

$$(s\,\hat{\theta}_{pq} - \theta_{pqo}) = \frac{1}{(RC)_{pq}}\frac{\partial^2}{\partial x^2}\hat{\theta}_{pq} \tag{4}$$

where θ_{pqo} represents the initial temperature distribution within the q-th slab. Extending the technique of Pipes [2] the general solution of Eq.(4) for the temperature and heat flow may be written in matrix form:

$$[\hat{E}_{pq}] = [X_{pq}][C_{pq}] + [\hat{P}_{pq}] \tag{5}$$

where

$$[\hat{E}_{pq}] = \begin{bmatrix} \hat{\theta}_{pq} \\ \hat{\phi}_{pq} \end{bmatrix} \tag{6}$$

$$[X_{pq}] = \begin{bmatrix} \cosh \alpha_{pq} x & \sinh \alpha_{pq} x \\ -\frac{1}{Z_{pq}} \sinh \alpha_{pq} x & \frac{1}{Z_{pq}} \cosh \alpha_{pq} x \end{bmatrix} \tag{7}$$

$$[C_{pq}] = \begin{bmatrix} A_{pq} \\ B_{pq} \end{bmatrix} = \text{coefficient vector} \tag{8}$$

and finally

$$[P_{pq}] = \begin{bmatrix} \theta_{pqo} \\ \hat{\phi}_{pqo} \end{bmatrix} = \text{initial condition} \tag{9}$$

The homogeneous boundary conditions at the interface between slabs q and q+1 are:

$$[\hat{E}_{pq}] = [\hat{E}_{pq+1}] \tag{10}$$

and at the two ends of the wall we have innomogeneous boundary conditions:

at x=0

$$[\hat{E}_{pe}] = \begin{bmatrix} \hat{\theta}_{pe} \\ \hat{\phi}_{pe} \end{bmatrix} = \begin{bmatrix} \hat{\theta}_{pe} \\ h_e(\hat{F}_{pe} - \hat{\theta}_{pe}) \end{bmatrix} \tag{11}$$

x=L,

$$[\hat{E}_{pi}] = \begin{bmatrix} \hat{\theta}_{pi} \\ \hat{\phi}_{pi} \end{bmatrix} = \begin{bmatrix} \hat{\theta}_{pi} \\ h_i(\hat{F}_{pi} - \hat{\theta}_{pi}) \end{bmatrix} \tag{12}$$

Repeated applications of the boundary conditions yields a relation between the fluxes at the two ends of the wall:

$$[\hat{E}_{pi}] = [Y_p][\hat{E}_{pe}] + [P_{pi}] \tag{13}$$

where

$[P_{pi}]$ = initial condition

$[Y_p]$ = overall heat transfer matrix

$$= \prod_q [Y_{pq}] \tag{14}$$

and

$[Y_{pq}]$ = heat transfer matrix of the q-th slab

$$= \begin{bmatrix} \cosh(\alpha_{pq} L_q) & Z_{pq} \sinh(\alpha_{pq} L_q) \\ \frac{1}{Z_{pq}} \sinh(\alpha_{pq} L_q) & \cosh(\alpha_{pq} L_q) \end{bmatrix} \tag{15}$$

The overall transmission matrix $[Y_p]$ appears complicated but it is ideally suited to computation by digital computer. Expression (13) can be further manipulated to yield the desired expression, providing for the heat flow and temperature in terms of the forcing functions:

$$[\hat{E}_{pi}] = [T_p][\hat{F}_p] + [P_{pi}] \qquad (16)$$

where

$$[\hat{F}_{pe}] = \begin{bmatrix} \hat{F}_{pe} \\ \hat{F}_{pi} \end{bmatrix} = \text{driving force vector} \qquad (17)$$

and

$$[T_p] = \begin{bmatrix} T_{11} & T_{12} \\ T_{21} & T_{22} \end{bmatrix} = \frac{h_i}{D} \begin{bmatrix} h_e/h_i & (y_{11}-h_e h_{12}) \\ h_e & (y_{21}-h_e y_{22}) \end{bmatrix} \qquad (18)$$

with

$$D = h_i y_{11} - h_i h_e y_{12} + h_e y_{22} - y_{21}^{*} \qquad (19)$$

The heat transfer matrix $[T_p]$ is general, it holds for composite walls. single slab walls, windows, etc; and for the limiting case of s approaching zero (s→0) it yields the well known steady state heat transfer coefficients.

A proper extension of the above discussion and particularly of equations (16) or (13) would provide for the temperature and the heat flux at any position within the wall.

Equation (16) represents the desired result of this submodel and it can be substituted into Eq.(2) to yield:

$$C_R \hat{\theta}_R = \sum_p A_p [T_{p21} \hat{F}_{pe} + T_{22} \hat{F}_{pi}] + \hat{C} + [C_R \theta_R + \sum_p A_p \phi_{poi}] \qquad (20)$$

B. Control Submodel

Two different classes of control mechanism must be distinguished. The first class of devices effect changes in the structure of the enclosure. Various night insulations and window covers belong to this class of devices. Since these mechanisms introduce a sudden variation in the composition of the wall structure their analysis requires a re-examination of the submodel for the heat flow through composite walls. In particular the heat transfer matricies $[Y_p]$ and $[T_p]$ will reflect the change in wall composition. The initial conditions in Eq.'s (13) and (16) will facilitate the preservation of continuity in the presence of these sudden changes.

The second class of control mechanisms consist of auxiliary powered devices such as air conditioners, heaters, attic fans, etc. The submodels for these falls into two categories, those that are explicitly dependent on the room temperature and those that are not. The attic fan, for example, is modeled by

$$C = (\dot{M}C_p)(\theta_R - \theta_a) = \dot{C}_R(\theta_R - \theta_a)$$

where θ_a is the ambient temperature.

Each of the other controllers can be represented by a similar type of expression for C or $\hat{C}$ and can be substituted into equation (2) or (20).

* The y terms here are elments of the matrix defined in Eq.(13).

III. Examples

The results of section II are general and abstract. The purpose of this section is to illustrate, through some representative examples, how this method provides for a better physical insight into the thermal dynamics of the building and the operation of the controller, and that it yields results that agree with ones obtained by different technique. Three related examples will be considered sharing the following simplifying conditions:

a) All initial conditions are zero - $\theta_{Ro} = \phi_{po} = 0$

b) The internal driving function will be the room temperature - $F_{pi} = \theta_R(t)$ for all p.

c) All the walls (assumed to be six) will be identical in size and composition. In particular three different wall compositions, consisting of concrete and insulating glass, will be considered as shown in Fig. 2. The thermal characteristics of the slabs are listed in Table 1.

	R(hr m°C)/KJ	C(KJ/m³ °C)	L(m)
concrete	0.385	1245.1	0.15
insulating glass	4.76	142.75	0.05

h_i = 24.54 KJ/hr m² °C h_e = 122.7 KJ/hr m² °C

Table 1 - Thermal Characteristic of the Concrete and Insulator Slabs and the Surface Heat Transfer Coefficients.

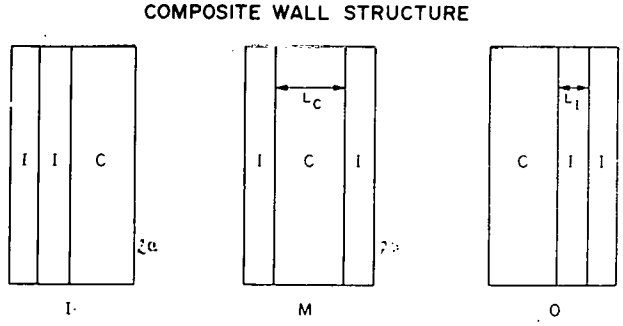

Fig. 2. Illustration of composite wall structure consisting of concrete and insulating glass. In Fig. 2a the concrete is in the inside (I), in Fig. 2b the concrete is in the middle (M), and in Fig. 2c on the outside (O).

Based on these conditons Eq.(20) takes the following form:

$$C_R s\hat{\theta} = A_w[T_{21} \sum_p \hat{F}_{pe} + T_{22} \sum_p \hat{F}_{pi}] + \hat{C} \qquad (21)$$

The threee examples, presented below, are based on this equation. The emphasis is on the technique and the physical understanding not as the particular number generated.

Example 1 - Heat flow through a composite wall into a room. For this problem it is assumed that the controller maintains the room at a constant temperature, 21°C and the external driving function is defined by:

$$F_{pe} = \begin{cases} \theta_{solair} & p=1 \\ 21°C & p\neq 1 \end{cases} \qquad (22)$$

where the solair temperature is given in terms of a Fourier series (see Table 2). This particular problem have been treated by M.S. Sodha et.al. using Fourier analysis.

For this example equation (21) reduces to:

$$\hat{C} = A_w T_{21}[(5)(21°C)\delta(s)+\hat{\theta}_{solair}] + A_w T_{22}[(6)(21°C)\delta(s)]$$

The frequency spectrum of the heat transfer functions, $|T_{21}|$ and $|T_{22}|$, for the three wall structures are shown in Fig. 3. For the present example T_{21} is more significant since the room is driven through the external wall, however for a direct gain building, for example, T_{22} would be more important. All three spectra for T_{21} have the same low frequency value, the total thermal resistance of the wall, which is unaltered. Of the three spectra, the one with the concrete in the middle has the fastest drop-off suggesting a damping of the high frequency fluctuations. By the same argument, when the concrete is on the outside, the fluctuations will be the most prevalent. The time dependance of the heat flux into the room which is the heat load for the controlled heat sink (air conditioner) was calculated and depicted in the Fig. 4. As expected from the shape of the spectra, spectra, the wall with the concrete in the middle has the least fluctuation. These results are in agreement qualitatively and quantiatively with the ones published by M.S. Sodha. [3]

Example 2 - Uncontrolled (floating) Room Temperature.

In this example the controller function is zero (C=0) and the room temperature is allowed to float. One of the walls is driven externally by θ_{solair}. The ex external forcing functions acting on the other walls are arbitrarely set to a DC value (21°C), which helps to isolate the effect of the θ_{solair} on the room temperature. Thus the external forcing functions are:

$$F_{pe} = \begin{cases} \theta_{solair} & p=1 \\ 21°C & p\neq 1 \end{cases} \qquad (23)$$

With the above conditions the room temperature in frequency domain becomes

$$\hat{\theta}_R = R_{21}[5(21°C)\ \delta(s) + \theta_{solair}] \qquad (24)$$

where

$$R_{21} = \frac{T_{21}}{\beta s - \delta T_{22}} \qquad (25)$$

and

$$\beta = C_R/A_w \qquad (26)$$

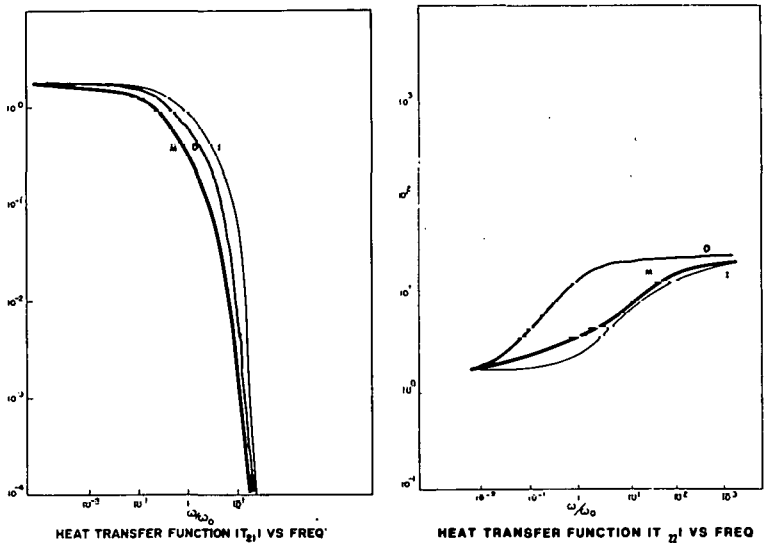

Fig. 3. Heat transfer functions T_{21} and T_{22} vs normalized frequency. In these curves and all subsequent curves the letters I,M, and O identify the position of the concrete slabe within the composite wall. For definition of I,M, and O and O see Fig. 2.

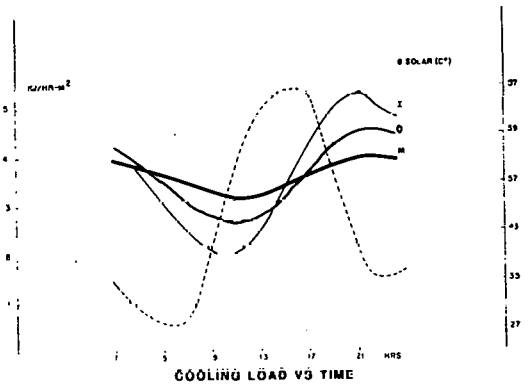

Fig. 4. Time dependence of heat flux through composite wall. The dotted line is θ_{solar}.

The frequency spectra of $|R_{21}|$ for three wall st structures are presented in Fig. 5. Based on these curves one can predict that the fluctuation in the room temperature will be the most pronounced when the concrete is in the inside. the smallest when the concrete is in the outside. The room temperature curves, Fig. 6, confirm this ascertion. The temperature fluctuations are small because of the large thermal resistance of the enclosure however the relative temperature variations for the three different wall structures are indication of the thermal dynamics of the room.

A simple parametric variation of $|R_{21}|$ with β shows that as the thermal capacity of the room is increased relative to the area of the wall driven by θ_{solair}, the temperature fluctuations will be damped, as expected. The dependence of $|R_{21}|$ on β at the frequency corresponding to a period of 24 hours is shown in Fig. 7.

Example 3 - Forced Infiltration

The final example is an extension of the one discussed above. The room is heated from the outside by θ_{solair}; the external forcing functions are defined by eq.(23). It is further assumed that the room temperature is moderated by a steady exchange of air between the interior of the enclosure and the ambient (e.g. an attic fan). The control function is given by:

$$C = (\dot{M}_{cp})_R\,(\theta_R - \theta_a) = \dot{C}_R(\theta_R - \theta_a) \qquad (27)$$

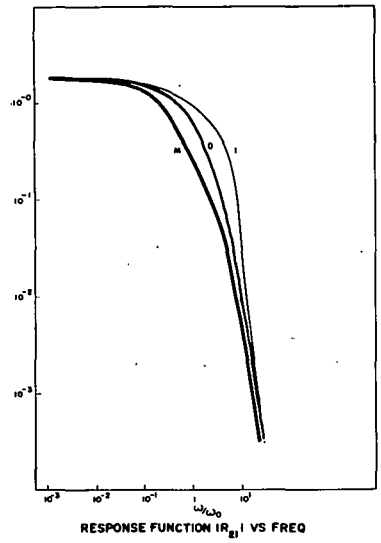

Fig. 5. Room response spectra, R_{21}, with β=1.

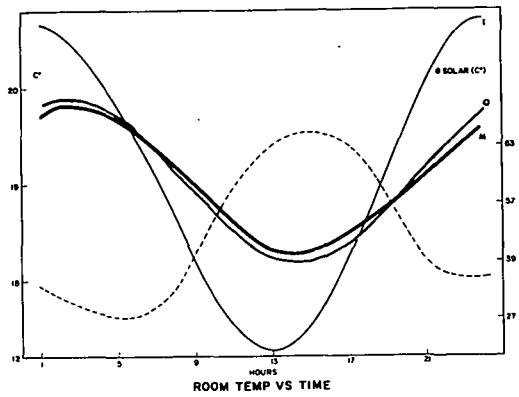

Fig. 6. Room temperature and θ_{solar} vs time.

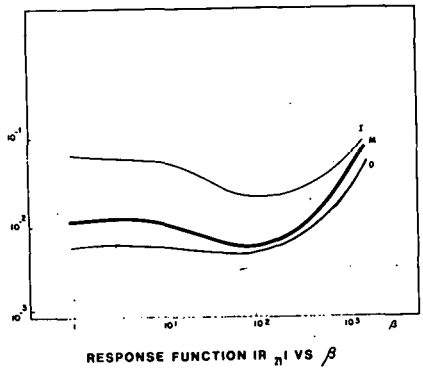

Fig. 7. Dependence of R_{21} on β.

where θ_a is the ambient temperature assumed to have a sinnsoidal time depdendance with a peak at 3:00 P.M. in the afternoon.

$$\theta_a = 20 - 10\cos(\omega_o t - \pi/4). \qquad (28)$$

We introduce a new parameter α, which is the ratio of the time rate of air mass that is being circulated between the interior of the structure and the enviroment to the total air mass of the room:

$$\alpha = (\dot{M}_{cp})_R\,/(M_{cp})_R = \dot{C}_R/C_R \qquad (29)$$

The room temperature is frequency domain now takes on the form:

$$\hat{\theta}_R = R'_{21}[5(21°C)\,\delta(s) + \hat{\theta}_{solair}] + R_c\,\hat{\theta}_a \qquad (30)$$

where

$$R'_{21} = \frac{T_{21}}{\beta(s+\alpha) - 6T_{22}} \quad \text{and} \quad R_c = \frac{\alpha}{\beta(s+\alpha) - 6T_{22}} \qquad (31)$$

The frequency depdendence of the room response function R_{21} and the control response function R_L are displayed in Fig.'s 8 and 9. Based on the frequency depdendence of these response functions, one can predict again that the wall construction with the concrete in the middle will yield the time variation in the room temperature. The calculated time depdendence of the interior temperature (Fig. 10) concurs this predictions.

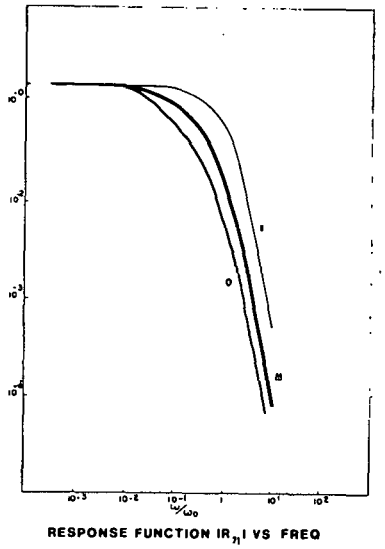

Fig. 8. Room response spect a R''_{21} with β=1 and α=1.

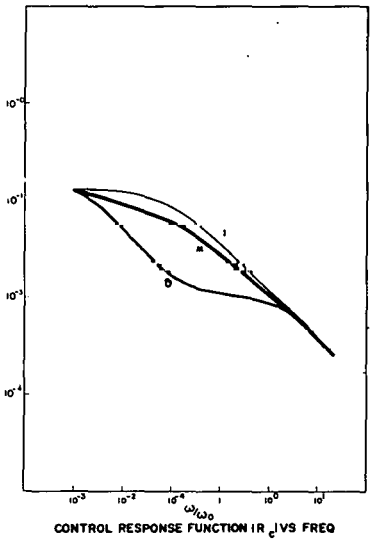

Fig. 9. Control response spectra R_c with β=1 and α=1.

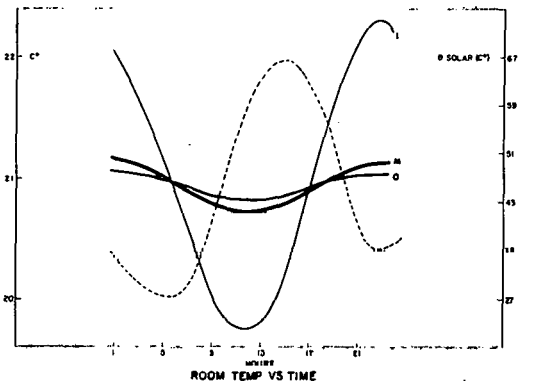

Fig. 10. Room temperature and θ_{solar} vs time.

$$\theta_{solair} = \sum_{n=0}^{6} A_n e^{j(n\omega_o t - \phi_n)}, \text{ with } \omega_o = \frac{2\pi}{24}\ hr^{-1}$$

where

n	0	1	2	3	4	5	6
A_n	44.6	19.0	4.4	1.5	0.8	0.5	0.2
ϕ_n	0	4.0	1.1	1.6	6.2	6.2	5.7

Table 2: Solair Temperature

IV. Summary

A formalism, based on analytic derivations, is presented which integrates the design and control problems of passive solar energy systems. The formalism aacounts for both discontinuous type of control mechanisms, such as window covers and night insulation and for auxiliary power driven devices like heaters and attic fans. For studies involving specific control devices or general control optimization utilizing classical frequency domain control theory this approach (particularly eq.(20)) is well suited.

Through some selected examples it is demonstrated that the control function interact with the building dynamics, and therefore must be made part of the over all design procedure. These examples also illustrate the effect of composite wall structures on the building response which may be exploited in design. First of all, as seen from the examples, examination of the response spectra enables one to predict the time dependence of the temperature variations of the room, and furthermore, this prediction can be related to the sequencing of the building materials. A careful examination of the examples show that each design and/or control change effects the shape of the spectra. Therefore the frequency domain analysis not only provdie a physical insight but can also be utilized for systematic design and control studies.

List of Symbols

- θ = Temperature
- $\phi_p = -\frac{1}{K_p}\frac{\partial}{\partial x}\theta_p$ = heat flow in p-th wall
- R = Thermal resistance
- C = Thermal Capacitance
- $C_R = (M\ c_p)_R$ = Thermal capacity of the room.
- $\alpha = \sqrt{RC_s}$ = Operational characteristic impedance
- A_w = Surface area of wall
- h_i, h_e = Interior and exterior heat transfer coefficients
- S = Laplace transform variable = $j\omega$
- ω = Angular frequency
- $\omega_o = \frac{2\pi}{24hr}$

SOLAR FLAT PLATE COLLECTOR CONTROL SYSTEM SENSITIVITY ANALYSIS

P.R. Herczfeld, R. Fischl and S. Konyk, Jr.
DREXEL UNIVERSITY
Electrical Engineering Department
Philadelphia, PA 19104

Abstract

This paper is concerned with problems related to the implementation of on/off controllers. A dynamic collector loop model is used to investigate of the controller performance in terms of the sensitivty of pump cycling and net energy collected with respect to control set points, flow rate, sy system parameters and climatic conditions. Criteria are developed for the selection of the control set points in terms of system parameters such as time constants, flow rate, and climatic conditions. Finally effect of the sensor location on the controller action is investigated.

1. Introduction

The increased use of solar energy for heating and cooling applications focused attention on the control problem associated with active solar energy systems. Most of the recent work in the control of solar energy systems concentrated on various optimization processes from the theoretical and/or simulation perspective [1-6]. In this paper the results of recently developed work is presented where the emphasis is on the practical aspect of the control problems. Simple questions are asked "where shall I put my sensors?" or "what should be the appropriate values of the control set points?". Answers to these questions may not lead to the implementation of optimal controllers but lead to a class of good suboptimal controllers which avoid strategies that can seriously degrade the performance of the active solar energy systems.

Current control design methods treat the collector loop and load loop independently (loosely coupled via the storage) and use either on/off or proportional control in each subsystem separately. On the collector side, the control goal is to maximize the net energy delivered to the storage tank, while on the load side the control objective is to use as much heat from the storage as possible subject to the load temperature settings.

This paper is concerned with the control of liquid flow rate in the collector loop using an on/off feedback controller. In order to determine the on/off set points and sensor locations, it is imperative that the collector loop model reflects the dynamics under control action. Recent work [7] showed that the dynamics of the components of the collector loop (i.e., collectors, transport piping and storage) are best described by distributed parameter models, namely a set of partial differential equations, since they reflect the pump cycling phenomena experienced in the field when implementing on/off control strategies [8]. These criteria for designing "good" on/off controllers which maximize the net energy delivered to the storage while minimize the number of short term pump on/off cycles. This trade-off criteria is given in terms of controller and system parameters such as control set points, sensor location collector time constans, time delays around the loop, flow rate, pump losses and climatic conditions.

2. System Model

The simplest model which provides for an accurate description of the performance of liquid flat plate collectors is Klein's Plug Flow Model (PMF) [9]. The distributed parameter model of the described by the normalized partial differential equation given below:

$$\frac{\partial T_{fc}(\xi,t)}{\partial t} = (1-\gamma)\frac{1}{\tau_{fc}}[\alpha_c f(t)-(T_{fc}-T_a)] + \gamma\frac{1}{\tau'_{fc}}[\alpha_c f(t)-(T_{fc}-T_a)]-\gamma\frac{1}{\tau_{tc}}\frac{\partial T}{\partial \xi}fc \quad (1)$$

(The list of symbols is provided at the end of the paper.) A closed form analytic solution of Eq.(1) is given by:

$$T_{fc}(\xi,t) = \gamma[F'(t)-e^{-\frac{\tau_{tc}}{\tau'_{fc}}\xi}F'(t-\tau_{tc}\xi)U((t-\tau_{tc}\xi) + e^{-t/\tau'_{fc}}A_1(\xi-t/\tau_{tc})U(\xi-t/\tau_{tc}) + e^{\frac{\tau_{tc}}{\tau'_{fc}}\xi}A_2(t-\tau_{tc}\xi)U(t-\tau_{tc}\xi)] + (1-\gamma)[f(t)+e^{-t/\tau_{fc}}A_1(\xi)] \quad (2)$$

where

$$F(t) = \frac{1}{\tau_{fc}}\int_0^t [\alpha_c f(\lambda)+T_a(\lambda)]e^{-(t-\lambda)/\tau_{fc}}d\lambda \quad (3)$$

In the above equation $F'(t)$ is the same as $F(t)$ with τ_{fc} replaced by τ'_{fc}; $A(\xi,0)$ is the initial condition; (i.e. inlet temperature); $A_2(t)=T_{fc}(0,t)$ is the boundary condition, $U(\cdot)$ is the unit step function.

The solution given in Eq.(2) has been discussed in previous papers [7]. It does reflect the collector dynamics as observed experimentally including pump cycling [8] as seen in Fig. 1.

This same model was also utilized in control optimization studies recently [10]. In this paper this very same model will be used for a sensitivity analysis. However before we can proceed with the sensitivity studies it is necessary to expand on the discussion of the boundary conditions, $A_2(t)$.

Under stagnant conditions ($\gamma=0$) a temperature difference exists between the various system components (i.e. collector, transport and storage) because of the differences in thermal constants and solar absorbance. If one assumes that each component is isothermal then one obtains step discontinuities at the boundaries between the components. In reality, the temperature and its first derivative across the boundaries are smooth and the transition (or boundary) region extends specially into the component. In order to reflect this phenomena, the temperature $T(\xi)$ across the boundary region $0\leq\xi\leq1$ is modeled by:

$$T_f(\zeta) = \beta(T_1-T_0)\ \xi^2(1-\zeta) + T_0 \qquad (4)$$

where $\beta = 6.75$, $T_0 = T_f(\zeta=0)$ and $T_1 = T_f(\zeta=1)$

represents the stagnant temperatures of the component at the inlet and outlet, respectively. Hence, in the sensitivity studies, $T_f(\zeta)$ is used for the boundary condition A_2.

3. Parametric Sensitivity Studies

In order to establish the tradeoff between the energy collected, J_1, and pump cycling, J_2 it is necessary to establish the dependence of these performance indices on the various system and control parameters. This was established via a sensitivity analysis in which the set of parameters varied is denoted by the vector $\underline{\phi}$ and classified as follows:

$$\underline{\phi} = \begin{cases} \underline{\phi}_c - \text{Control parameters} \\ \underline{\phi}_s - \text{System Parameters} \\ \underline{\phi}_w - \text{Climatic Parameters} \end{cases}$$

where

$$\underline{\phi}_c = \begin{cases} \Delta T_{off}=T_{off}-T_s - \text{pump turn-off set-point(°C)} \\ \Delta T_{on}=T_{on}-T_s - \text{pump turn-on set-point (°C)} \\ \mathring{m} - \text{collector fluid flow rate (kg/hr)} \end{cases}$$

$$\underline{\phi}_s = \begin{cases} \tau_{tc} - \text{system dynamic time constant} \\ \tau_{fc} - \text{system static time constant} \end{cases}$$

$$\underline{\phi}_w = \begin{cases} I_0 - \text{peak solar insolation (kj/m}^2\text{-hr)} \\ \Delta T_{ia} = (T_s-T_a) = \text{storage to ambient temperature difference (°C)} \end{cases}$$

In addition to the parameters $\underline{\phi}$, there are a number of parameters denoted by $\underline{\zeta}$, which are held constant, namely,

- ω = Radian frequency of solar insolation (rad)
- T_i - Initial temperature of collector (°C)
- t_o - Time of sunrise (hr)
- $\tau\alpha$ - Collector transmittance obsorbtance product

The sensitivity of the system performance (J_1 and J_2) was investigated by systematically varying each parameter of ϕ about a base line system given in Table I. This was accomplished by first evaluating the collector outlet temperature as a function of time (using Eq.(2)) as shown in Fig.1 and then evaluating J_1 and J_2 for each parameter value. (A detailed description of the computational algoirthm is given in [11]).

Figures 2a-c illustrates the effect on the net energy collected and pump cycling due to variation of the control parameters ΔT_{off}, ΔT_{on} and $\mathring{m}$; while Fig.2d shows the effect due to variation in system time constant, τ_{fc}. Note that these figures depict the system performance only during the morning hours (6 to 10.5 hrs.) since the tradeoffs are most significant in this time period under clear day conditions. The results of the parametric sensitivity analysis can be summarized as follows:

* The most important parameter in terms of both energy collection and reduction of cycling is the turn-off set point, ΔT_{off}. This should be set as low as possible (usually limited by parasitic pump losses).
* The flow rate, for the on/off controller, should be reasonably high for good collection efficiency.
* The turn on set point, ΔT_{on}, can be set high without significantly affecting energy collection while markedly reducing pump cycling.

4. Control Set Point Selection

The sensitivity analysis presented above, gives valuable insight into the performance of the collector controlled by an on/off controller which can be exploited to derive simple, practical expression for the set point ΔT_{on} in terms of ΔT_{off} so as to reduce the chance of cycling without greatly affecting the energy collection. If one allows the collector temperature to rise under stagnant conditions until the solar flux is strong enough to maintain the steady state temperature rise in the collector (under flow) above ΔT_{off}, then cycling disappears, at least for a clear sky day. Thisconcept can be used to calculate approximately the desired turn-on temperature as follows.

Under flow conditions the steady state temperature rise across the collector is

$$\Delta T_{fc} = T_{fc}(1,t) - T = \frac{\tau_{fc}}{\tau_{fc}} [\alpha_c f(t) - (T_s - T_a)] \quad (5)$$

On the other hand under stagnant conditons, difference between the collector outlet temperature and the storage temperature stagnant can be obtained from Eq. (2), namely

$$T_{fc}(1,t) - T_s = F(t) + e^{-t/\tau_{fc}} A_1(1) - T_s \quad (6)$$

Assuming a clear sky and a slow variation of T_a and T_s as a function time, one can compute from Eq.(5) the time $t=t_{off}$ when $\Delta T_{fc} = \Delta T_{off}$. If $t=t_{off}$ is now substituted into Eq.(6) the desired trun on set point is obtained:

$$\Delta T_{on} = T_{fc}(1,t_{off}) - T_s \quad (7)$$

If the system is well defined, in particular if ΔT_{off}, τ_{fc}, τ_{fc}, α_c, T_s and T_a are known, then ΔT_{on} can be calculated numerically. Alternatively one can solve for t_{off} and hence for ΔT_{on} analytically, but that leads to a lengthy transcendental algebraic expression. However if it is assumed that the collector capacitance under stagnant and flow condition are equal or reasonably close then a relatively simple expression for ΔT_{on} results, neamely;

$$\Delta T_{on} = \left[\frac{1}{1+\omega^2 \tau_{fc}^2}\right] [F \omega \tau_{fc} (\alpha_c^2 - F^2)^{1/2}] \quad (8)$$

where

$$F = \Delta T_{off} \tau_{fc}/\tau_{tc} + (T_s - T_a)$$

A simple parametric study of the above relation was pweformed Fig. (3) illustrates the dependence of ΔT_{on} on $(T_s - T_a)$, on the flow rate $\dot{m}$ (related to τ_{tc}), on the system time constant, τ_{fc}, and on the peak solar insolation, I_o, for various ΔT_{off} values. It is understood that ΔT_{off} has been selected as low as possible. In general this implies

$$\Delta T_{off} = P(\dot{m})/\dot{m}$$

where $P(\dot{m})$, is the pumping power to maintain flow rate $\dot{m}$[ ]. These curves in conjunction with Eq.(8) may be used to select the proper value of ΔT_{on} for a particular system, at a particular location.

5. Sensor Location

From the above discussion is is seen that the selection of control set points ΔT_{on} and ΔT_{off} is crucial to the performance of the controller. The question arises what effect the sensor location may have on the actual measurement of these set points and hence on the operation of controller. In theory the collector outlet temperature is sensed at the top of the collector, $\zeta=1$, which represent the highest temperature in the collector if boundary effects are ignored. However if the boundary between the collector and the storage (or piping) is accounted for than one will have a non-uniform temperature profile at the top of the collector as shown in Fig. (4). We have simmulated the performance of the controller for a number of different sensor locations which are shown in Fig. (4). The results are summarized in Fig. (5) which shows the first turn-on time, t_{on}, and the total energy collected until 10:00 A.M. as a function of sensor location. These examples assume clear sky conditions and that the set points ΔT_{off} and ΔT_{on} are selected in accordance with the previous discussion. The results indicate that the optimal sensor location is at the beginning (i.e. upstream) of the boundary region. If the sensor is located downstream from this point then the system turns on at a latter time, thus reducing the useful energy gain. Note that this is equivalent to raising the turn on set point ΔT_{on}. If, however the sensor is located upstream from the optimal position then the collector area will appear smaller than it actually is. This will cause cycling and a reduction in the energy collection.

6. Summary

Utilizing the dynamic collector loop model a sensitivity analysis of the performance of the on/off controller was carried out. The controller action was evaluated in terms of control parameters, namely turn-on and turn-off set points and flow rate, the system parameter ($_{fc}$), and climatic variations, the peak insolation (I_o) and ambient temperature (T_a). Based on this analysis criteria for the selection of control set points was developed. Finally the relation between sensor location and controller action was investigated. It was found that improper sensor location may markedly degrade control performance.

ACKNOWLEDGEMENT

This work has been supported in part by the Solar Heating and Cooling Research and Developement Branch, Office of Conservation adn Solar Applications, U.S. Departmetn of Energy, under contract E-8-77-5-02-4512.

References

1. Proceedings of the Workshop on the Control of Solar Energy Systems for Heating and Cooling, pp. 19-21, May 23, 1978.

2. M. Kovarik, P.E. Lesse, "Optimal Control of Flow in Low Temperature Solar Heat Collectors", Solar Energy, Vol. 18, pp. 431-435, 1976.

3. A.H. Eltimsahy,E.A. Santos, Jr.,"A Suboptimal Controller for Domestic Solar Heating System Utilizing a Time Varying Price for Electricity", Proc. of the 1977 Annual Meeting AS/ISES, pp. 9.19-9.22, Orlando, PA., June 6-10, 1977.

4. L.B. Anderson, H.E. Pauch, "Application of Optimization Techniques to Solar Heating & Cooling" , J. of Energy, Vol. 1, No. 1, pp 18-24, 1977.

5. D.R. Farris et. al. ,"Energy Conservation by Adaptive Control for a Solar Heated Building", Submitted to 1977 Internationl Conference on Cybernetics and Society, Sept. 19-21, 1977, Washington, D.C.

6. C.B. Winn, D.E. Hull, "Optimal Controllers of the Second Kind", Proc. of the 1978 Annual Meeting AS/ISES, pp 493-498, Denver,CO., Aug. 1978.

7. A. Orbach, P.R. Herczfeld,R. Fischl, "Flow Control in Solar Heating and Cooling Applications",P Proc. of the 1978 Annual Meeting, AS/ISES, Vol. 2, pp 488-492.

8. T.M. Conway, "Fluid Flow-Control Strategies in Flate-Plate and Evacuated Tube Collectors",American Section of the ISES, Proc. 1977 Annual Meeting, Orlando, PA., Vol. 1, pp 9.11-9.14, June 6-10, 1977.

9. S.A. Klein et al., "Transient Considerations of Flate-Plate Solar Collectors", T.A.S.M.E., J. of Eng for Power, pp 109-113, April 1974.

10. R. Fischl, P.R. Herczfeld, A. Orbach, S. Konyk Jr., "Control and Sensitivity Analysis of Liquid Flate-Plate Solar Collector Systems", Proc. of the 18th IEEE Conference on Decision and Control, Ft. Lauderdale, Fla., Dec. 1979.

11. P.R. Herczfeld, R. Fischl, "Final Report DOE Contract E-8-77-5-02-4512", Submitted to Solar Heating and Cooling Research and Development Branch , Office of Conservation and Solar Applications, U.S. Department of Energy.

NOMENCLATURE

T_{fc}	Temperature of fluid in the collector
T_s	Temperature of mixed storage
T_a	Ambient temperature
$I(t)$	Solar flux on collector surface
I_o	Maximum solar flux on collector surface
$f(t) = I(t)/I_o$	Normalized solar flux
x	Distance along collector tubing
L	Length of tubing in collector
$\xi = x/L$	Normalized distance along collector tubing
C_c	Lumped capacitances of collector
A_c	Surface area of collector
U_L	Heat loss coefficients of collector
$\dot{m}_c$	Mass flow rates in collector
$(\tau\alpha)_c$	Transmittance-absorptance product of collector
c_p	Specific heat of fluid

$$\alpha_c = \frac{I_o(\tau\alpha)_c}{U_{Lc}}$$

$$\tau_{fc} = \frac{C_c}{U_{Lc} F'} \quad ; \quad \tau_{tc} = \frac{C_c A_c}{\dot{m}_c c_p}$$

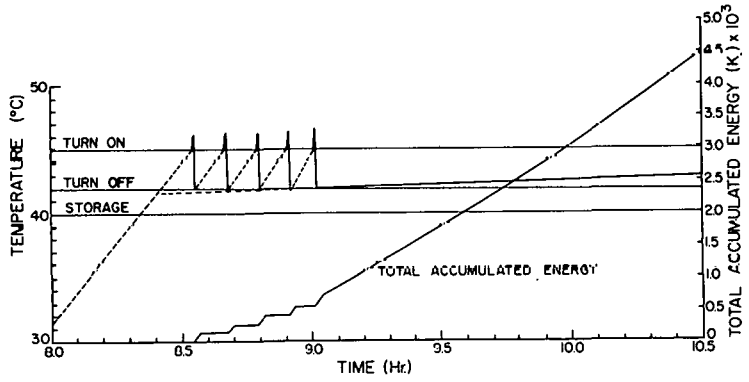

Fig. 1: In this figure the collector output temperature and accumulated energy are plotted as functions of time. The dotted portion of the collector output temperature corresponds to stagnant condition while the solid line corresponds to flow condition. This particular run shows cycling. It should be noted that there is energy collection during cycling however at a lower efficiency.

Table I: Baseline system parameter values.

Nominal Values of Parameters			Climate	Set Points
$C_c = 10.22 \frac{kj}{C\text{-}m^2}$ $W = 1.0$ m $\dot{m}_c = 227.19 \frac{kg}{hr}$	$U_L = 18.65 \frac{kj}{m^2\text{-}C\text{-}hr}$ $(\tau\alpha) = .8281$ $C_p = 4.19 \frac{kj}{kg\text{-}C}$	$F' = .95$ $L = 2.0$ m $A_c = 2.0\ m^2$	$T_a(t) = 0$ C $I(t) = I_o \sin\omega(t-6)$ $I_o = 3000 \frac{kj}{m^2\text{-}hr}$	$\Delta T_{on} = 5$ C $\Delta T_{off} = 2$ C $\Delta T_h = 3$ C

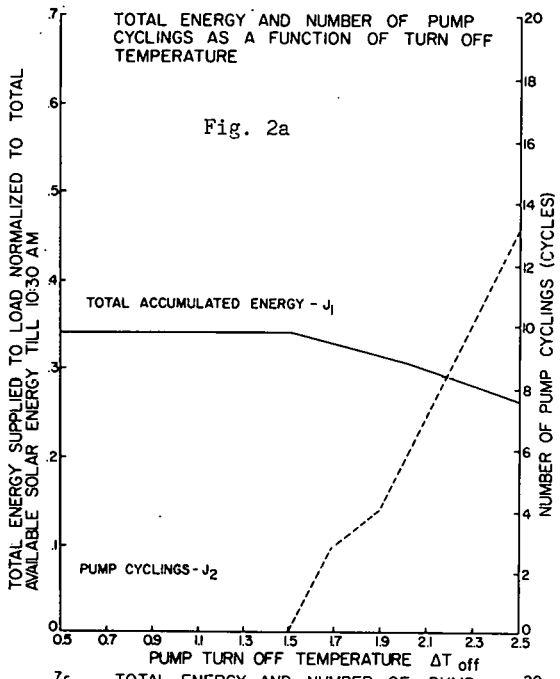

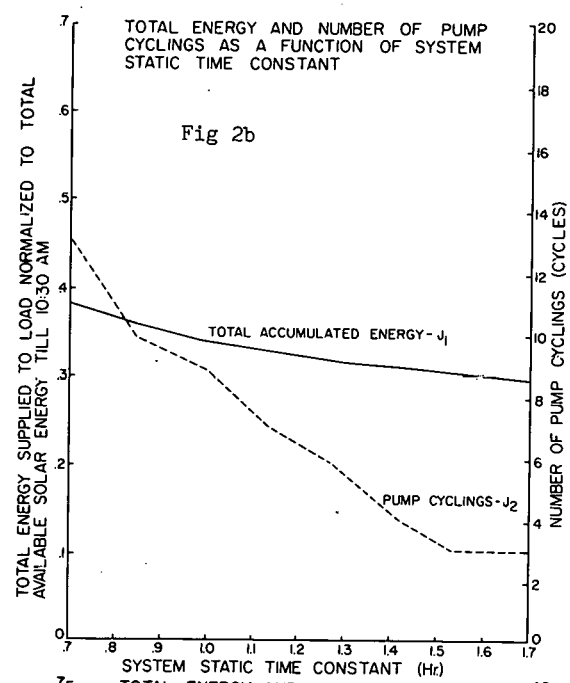

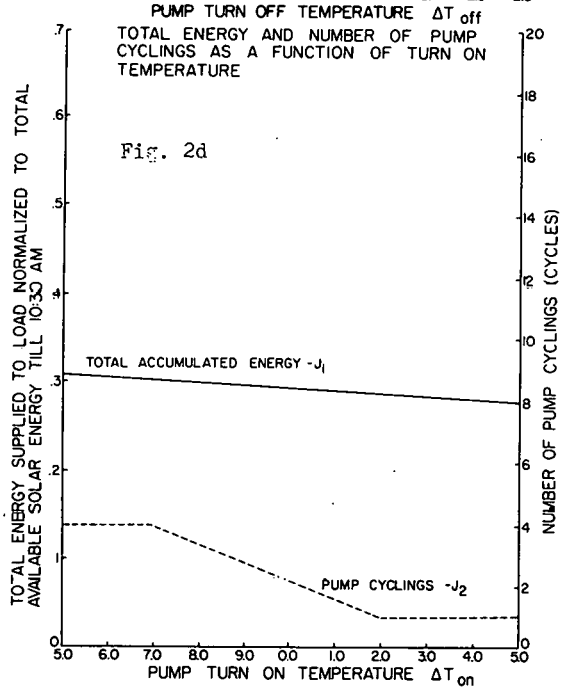

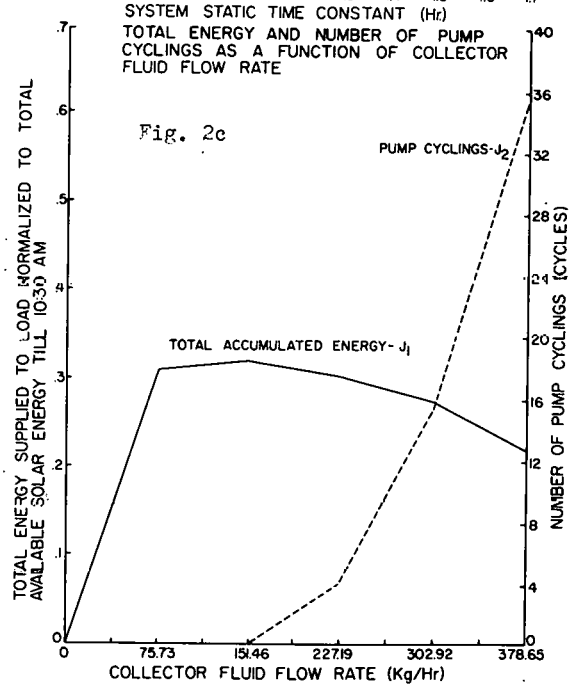

Fig 2: The above figures (a,b,c,d) illustrate the results of the parametric sensitivity analysis of the controller performance in terms of cycling ,J_2, and energy collection ,J_1.

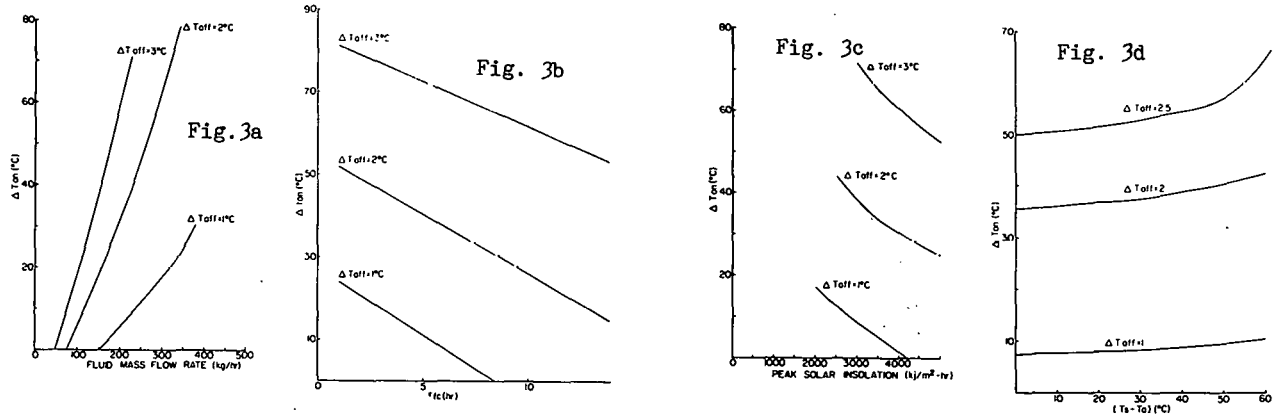

Fig. 3: The above figures illustrate the parametric vareation of ΔT_{on} with respect to flow rate (a), system time constant (b), peak insolation (c), and ambient temperature (d).

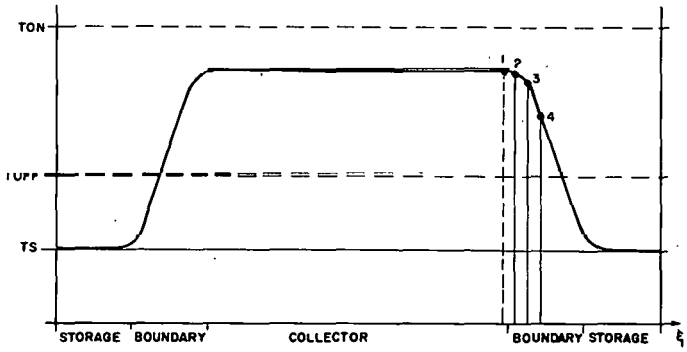

Fig. 4: Collector loop showing transport, boundary, and sensor locations.

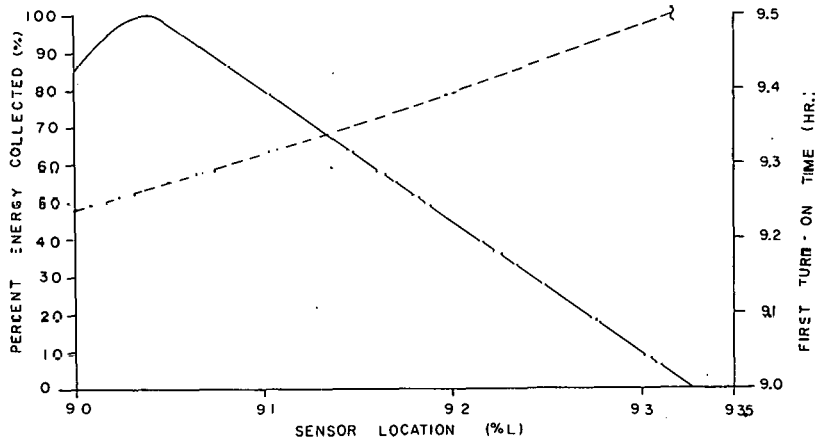

Fig. 5: Collected energy and first turn-on time vs. sensor location.

Session IIB

Dr. William Kennish
TPI Inc.
Chairperson

VALIDATION I

REAL-WORLD VALIDATION OF SHAC MODELS

Louise S. Morrison*
Solar Energy Research Institute
Golden, Colorado 80401

ABSTRACT

This paper proposes a statistical approach to validation of SHAC models. It includes a definition of validation, an explanation of its purposes, and a description of the statistical aspects of experimental design. It proposes a study to validate design codes with statistical samples of real-world systems. Also included is a summary of present SHAC validation methodologies and studies as well as recommendations for future activity.

INTRODUCTION

In designing a validation study it is essential to consider carefully the following: (a) the definition of validation being used, (b) the user community and purposes of the validated model, (c) the method of selecting the test systems/components, (d) the instrumentation of the test systems/components, (e) the statistical aspects of the study including interpretation of results, (f) the generalization of results, and (g) the expected impact of the study.

PRELIMINARY CONCEPTS

A major decision in the experimental design of SHAC validation studies is the intended degree of control of the test system/component environment.

Controlled Data and Environment

In a controlled environment, design and performance data is obtained from a system/component that fits the model assumptions. The system/component is well designed, well installed, and fine-tuned for optimal performance. Load and weather data are collected at the site together with the performance data so that the driving forces of the model are known. A modeling expert using the actual weather and load data obtains the model prediction "after-the-fact." The input data to the model is referred to as controlled data.

Uncontrolled Data and Environment

In an uncontrolled environment, design and performance data is obtained from a system operating in a "real-world" or field environment. A model user of uncertain expertise predicts performance for a system that may only minimally fit the model assumption, whose quality of design and installation is uncertain, and whose existing performance level is not altered for the study. Load and weather data are not collected at the site; instead user-estimated or model-supplied data is used. The model prediction is usually made before the performance data is collected. The input data to the model is referred to as uncontrolled data.

The intent of most software/hardware studies has been to test a model with highly controlled data; however, systems malfunctions and instrumentation problems have limited the degree of control obtained. The intended degree of control has great impact, since the experimental design is radically different for a controlled approach than for an uncontrolled approach.

"After-the-Fact" Prediction

In validation studies using controlled data, "model prediction" is a misleading expression because the prediction is made "after-the-fact" using load and weather data that was collected at the site together with the performance data. This type of study verifies that the modeled performance agrees reasonably well with the real performance.

"In-Advance" Prediction

In validation studies using uncontrolled data, "model prediction" really means prediction. The model is used with estimates of load and weather data to forecast "in advance" how a system will perform for the next few years.

DEFINITION OF VALIDATION

A major problem in SHAC validation has been a lack of consensus about its definition and purposes. The definition of validation which will be used in this paper is as follows. A model is defined as validated for a group of systems/components operating in a particular environment if performance predictions are not significantly different from measured performance values for a sample of systems/components that has been selected from the set in a statistical manner. The degree of significance of results required for validation is a decision of the researcher and is addressed later in a section on experimental design.

*This work was supported by Systems Development Division, Office of Solar Applications, DOE.

According to this definition, no SHAC model has been validated with systems/components in general. However, each of the various SHAC models has been validated with a few systems/components operating in a controlled environment. (This is the default case, in which the set of test systems/components is a statistical sample of itself but is not selected to be a statistical sample of a larger set.)

VALIDATION PURPOSES

Models Validation with Controlled Data

Researchers, engineers, economists, and others desire systems and component models that have been validated with controlled data for purposes which include the following:

- to make comparative performance predictions similar to the EPA mileage ratings for cars;
- to compare system/component performance with standards such as BEPS (Building Energy Performance Standard);
- to perform sensitivity studies to optimize physical systems; and
- to examine system/component effects of shading, snow cover, etc.

In all these cases, generalization of results applied to uncontrolled data is uncertain, but some confidence is obtained.

Models Validated With Uncontrolled Data

Installers, distributors, architects, homeowners and others desire techniques which have been validated with uncontrolled data for purposes which include the following:

- to estimate the economic feasibility of an installed system; and
- to optimally size the system collector array and other components.

A STATISTICAL APPROACH TO EXPERIMENTAL DESIGN

A very brief discussion of this topic is presented here; for a detailed description see Cohen [1].

In a statistical approach an attempt is made to select data that is representative of some larger set so that one knows how much confidence can be placed in the results and so that generalization of results can be justified. No matter what data is used, there is an emphasis on careful experimental design.

Data Selection and Generalization of Results

Ideally, a model validator would identify a population of systems/components and select a rigorous statistical sample from the population according to random, stratified, or other sampling methods. For example, one sampling strategy would select randomly from all existing SHAC systems, another would weight the sample to be representative of a potential SHAC systems distribution. A decision would be made whether to collect data in a controlled or uncontrolled environment. Any restrictions imposed on the sample would be identified, such as systems which are working, systems that fit the model assumptions, etc. Results would generalize only to those systems/components in the population that meet the limitations imposed on the sample and that are operating in a similar environment.

Most validation studies do not state the method of selecting the test systems/components. Occasionally, one reads that systems were selected "randomly," but random selection has a precise mathematical meaning and should not be used unless actually employed. It is often assumed that results generalize even though it is not known how the test systems/components came to the attention of the validators.

Interpretation of Results

The results of a validation study can be interpreted statistically in a number of ways. For each system/component, a calculation of (predicted-measured)/predicted could be made for a parameter such as solar fraction. The mean and standard deviation of these values could be used to establish a confidence interval on model output. The size of the sample and the value of the confidence limits are interrelated. A discussion of these aspects of experimental design can be found in books on sampling theory.

It is often desirable to consult a statistician for assistance in experimental design and interpretation of results. Research today involves expertise in many disciplines in order to solve the really difficult problems.

Error Sources

Many sources of error contribute to differences between model prediction and measured performance, including error due to unmodelled parameters, inaccurate estimates for modelled parameters, inaccurate measurement of performance, etc.

Sensitivity studies have been done with controlled data to determine confidence intervals for a model prediction due to individual sources of error. However, because of the magnitude and number of sources of error, it appears impossible to combine the contributions of individual sources of error to obtain a confidence interval for all error.

In a validation study with uncontrolled data, all error is combined in a single confidence interval because sources of error are not eliminated or minimized in the experimental design. This is desirable for "real-world" validation purposes since the homeowner or installer is primarily interested in the bottom line, which is the range of system performance that can be expected based on a model prediction.

STATISTICAL APPROACHES IN OTHER DISCIPLINES

Other disciplines recognize the need for a statistical approach for problems similar to validation. Opinion sampling in politics and market research is done with rigorous statistical techniques. Even so, results often do not generalize as expected; in a classic example, in the 1948 Presidential election Dewey was predicted as the victor

over Truman when a telephone survey underrepresented the many farmers who had no phones.

Medical experimenters use double-blind experiments to minimize the unconscious biases of a researcher. In such an approach, neither the researcher nor the test subject knows whether the subject is in the experimental group or the control group. Solar researchers are naive if they think they can carry out validation studies in an unbiased manner without taking specific measures to minimize personal bias.

INSTRUMENTATION

Obtaining adequate data has been a significant problem in validation. Performance and data acquisition difficulties have occurred during data collection, and measurement error has been large. The cost of presently used instrumentation schemes has dictated that only a few types of systems/components be monitored. The average cost of installed instrumentation for a system monitored by the National Solar Data Network is approximately $40,000, and data processing of the information is prohibitively expensive.

Existing data may be able to serve many of the needs of statistically sound validation studies. However, new data may be required to permit the use of relatively large samples of systems/components. There should be an investigation of inexpensive instrumentation plans (often devised by those without federal funding) and a study of the requirements which can be met by data of reduced precision.

Examples of inexpensive instrumentation plans for validating design codes with SDHW systems are given in Cohen [1]. In one scheme, Btu meters are proposed that cost less than $350 and that have a claimed accuracy of $\pm$ 3%. Drawbacks include potential difficulties in using inexpensive Btu meters, such as imprecise measurements of temperatures and flow rates, degradation due to lime build up, circuit failures, etc.

PERFORMANCE MEASUREMENTS

Solar fraction is the most common performance measurement utilized in validation studies. This indicator can be defined in many different ways for active systems, and its interpretation is especially difficult for passive systems. Because of the ambiguity of the expression, quantities such as solar contribution, auxiliary fuel contribution, or displaced fuel should be used in validation studies.

PROPOSED VALIDATION STUDY

A needed validation study would test the ability of design codes to predict "in-advance" for a typical solar space heating system operating under "real-world" conditions. An example outlining how this might be done is given in the following sections.

Data Selection

The population of residential SHAC systems in a region would be estimated by the utility companies. Meter readers would record addresses of domestic solar energy systems, and mailings would be sent to homeowners requesting their participation in the study. A firm experienced in statistical sampling would select a representative sample of the identified systems. Site visits would be made to determine systems performance according to model-independent criteria, and restrictions for excluding systems would be established. Results would generalize to all systems meeting the chosen criteria. Design and load data would be estimated using information available to the average model user. Weather data would be obtained for the year of the study from an appropriate design code weather data city.

Performance Predictors

For each design code, performance would be predicted "in-advance" using design weather data and "after-the-fact" using the weather data that occurred during the year of the study.

A group of engineers, architects, and others who have had SHAC experience in the region would be selected. Each person would use engineering judgment (without design code usage) to estimate performance for the set of systems. It would be determined if the members of the group have previously used a design code.

Other techniques used by the industry (such as "rules-of-thumb" and nomographs) would be identified. Performance predictors used in foreign countries would be appraised, since design codes are not applied universally. These identified techniques would be utilized to predict performance for the test systems.

The sample of systems would be instrumented as inexpensively as possible to obtain essential performance values. Measurements would be taken for the test sytems, and comparisons would be made with the various predictors. A statistical analysis would be made of the results.

Analysis of Results

The HVAC industry has developed assumptions about the thermal performance of residential heating and cooling of buildings, and SHAC models have for the most part incorporated these basic assumptions. Software/software validations studies often result in the modification of the models to make the models agree more closely.

If the study shows that design codes are adequate predictors, it will justify their usage for "real-world" purposes. Otherwise, the research community should do one or more of the following:

- re-examine the basic assumptions of the design codes to determine which assumptions need to be extensively reworked to increase "real-world" predictive capability;
- develop new models with different assumptions that better serve "real-world" predictive use;
- recommend that design codes be used strictly for studying systems under controlled conditions;
- recommend the use of engineering judgment or other techniques for "real-world" predictive purposes; or

- encourage "real-world" usage of design codes for learning purposes only in developing engineering judgment.

Actually, most researchers agree that design codes are poor predictors of "real-world" performance. Precise prediction may be an impossible task for a SHAC model, since weather and load data is unpredictable. Some feel that the industry should be encouraged to use SHAC models until a better alternative is developed. Unfortunately, some members of the solar industry do not employ sufficient engineering judgment in design code application. Whether or not the study is implemented, disseminators should state clearly the limitations of design codes in making absolute predictions.

The study would indicate needed improvements in systems design, manufacture, installation, maintenance, and instrumentation. A sociological survey of the system owners would give commercialization information. The data base of residential SHAC systems woud be valuable for many applications. At present, there is not even a good estimate of how many residential systems are installed.

A pilot project should be implemented to give experience in creating a statistically valid experimental design. From sampling theory, it has been estimated that approximately 20 systems would suffice for a statistical sample of SHAC systems in a state such as Colorado.

SHAC VALIDATION EFFORT

Methodologies

Theoretical approaches for validation of SHAC simulations and design codes have been proposed by Cohen [1], Kennish and Knasel [2], Lantz and Winn [3], Winn et al. [4], and others. Because validation is such a difficult and many-faceted problem, it is probable no single approach suffices.

Kennish's methodology addresses the validation of models with controlled data for "after-the-fact" prediction. He stresses a practical approach by recommending use of existing data, limited numbers of test systems/components, software/software studies, and component validation. Kennish is particularly interested in performing sensitivity analyses of design code inputs. There is little emphasis on statistical experimental design.

Cohen enlarges the validation picture to include studies with uncontrolled data for "in-advance" prediction and emphasizes a statistical approach in studies with either controlled or uncontrolled data. Cohen's major concern is careful experimental design. He recommends using statistical samples of systems/components and stresses software/hardware studies and system validation. Cohen presents an idealized approach which he recognizes may be difficult and expensive to implement, but he feels that the researcher should be aware of the ideal and recognize the extent to which actual studies depart from it. See Cohen [1] for a detailed description of Kennish's and Cohen's methodologies.

Studies

As stated previously, SHAC models have been validated with a limited number of systems/components operating in limited kinds of controlled environments. Generally, model predictions have compared favorably to measured performance when using controlled data; at times the models were modified until agreement was reached.

In most comparisons there has been little description of the experimental design and minimal statistical interpretation of results. In few, if any, studies have the test systems/components been selected as a statistical sample of a larger set taking into account factors such as geographical location, installer, system type, etc. Therefore, it has been difficult to determine the extent to which the results of these experiments generalize. In addition, studies have attempted to generalize from systems operating in a controlled environment to those in an uncontrolled environment. Sources of error, such as typical installation problems, have been missed. This has been a very frustrating approach and has made validation appear to require an unending series of studies.

Software/software studies have been done extensively, and models have generally compared well with each other when using controlled data or have been modified to do so. When models correlate highly, undue confidence in them sometimes results, even though none of the models has been validated with performance data.

Many validation studies have incorporated a defense of the models and a defense of solar technology. Attempts have been made to interpret reality to fit the model rather than the reverse. "Real-world" validation needs have been grossly ignored because validators have anticipated the many uncertainties of field systems.

The results of the validation studies give confidence that SHAC models can predict performance for systems/components operating in a controlled environment. However, they give little evidence that SHAC models can predict performance "in-advance" for field systems.

Bibliographies

SAI has summarized some of the SHAC validation efforts in Refs. [2] and [5] and ADL has compiled a validation bibliography [6]. Results of validation studies are often difficult to obtain since they are presented in memos, working group minutes, technical reports, and performance papers.

MAJOR RECOMMENDATIONS

- Validation studies should be done with greater emphasis on careful experimental design and on statistical interpretation of results.
- The first step in a validation study should be the preparation of a study plan which includes (a) the definition of validation being used, (b) the user community and purposes for which the validated model is intended, (c) the method of selecting the test systems/components, (d) the instrumentation of the test systems/components, (e) the statistical aspects of the study including interpretation of results, (f) the generalization of results, and (g) the expected impact of the study. This information also should be stated in the study results.

- Validation studies with controlled and uncontrolled data complement each other and studies of each type are needed. More software/hardware studies with controlled data are needed because of the poor quality and limited scope of the data used in present studies. Software/hardware studies with uncontrolled data, such as the study proposed here, should be implemented.
- Proposed software/software studies should be examined to ensure their potential contribution. These studies take computer and staff time, generate reports, and at times are little more than busy work.
- Sensitivity studies should concentrate on the sources of error, such as load estimates, which are of large magnitude.
- The use of solar fraction as a performance measurement in validation studies should be deemphasized.
- Persons operating the National Solar Data Network (NSDW) and other data collection programs should consider defining populations of solar energy systems and instrumenting a statistical sample. They should also investigate inexpensive instrumentation schemes and data requirements which can be met by data of reduced precision.
- EPRI should encourage utility companies to participate in a nationwide census of residential solar energy systems.
- Researchers should be honest with disseminators in expressing the limitations of design codes to make absolute predictions for "real-world" systems.
- There should be increased communication between the research community and the solar industry. Model developers need industry input to design relevant and useful models. The industry needs input from the researchers to understand the available tools and how to apply them.

ACKNOWLEDGEMENT

The author wishes to acknowledge the inspiration of Joel Cohen, the assistance of L. M. Murphy, and the exchange of ideas with Bill Kennish.

REFERENCES

1. Cohen, J. S. Statistical Problems in Design Code Validation. Technical Report. Solar Energy Research Institute, Golden, CO. In progress.

2. Knasel, T. M. and Kennish, W. J. Validation Methodology for Solar Heating and Cooling Simulation Models. Final Report. Science Applications, Inc., McLean, VA. March 1978.

3. Lantz, L. J. and Winn, B. C. "Validation of Solar Radiation Computer Models." Proceedings: Conference on Systems Simulation and Economic Analysis for Solar Heating and Cooling, San Diego, CA. 1978.

4. Winn, B. C., Parkinson, B. W. and Duoung, Nguyen. "Validation of Solar Systems Simulation Programs." Proceedings of the 1978 Annual Meeting, American Section of ISES, Denver, CO. Vol. 2.1, August 1978. pp. 120-124.

5. Knasel, T. M., Mansoor, Y. and Kennish, W. Validation Status of Solar Heating and Cooling Systems Models. Final Report SAI-79-855-WA. Science Applications, Inc., McLean, VA. March 1979.

6. Arthur D. Little Co., Building Energy Analysis Computer Programs with Solar Heating and Cooling System Capabilities, Report EPRI ER-1146, ADL, Cambridge, MA 02140, August 1979.

NOTES

FIELD VALIDATION OF THE DEROB SYSTEM:

THE BRUCE HUNN RESIDENCE*

Francisco Arumí-Noé, Ph.D.
David O. Northrup, M. Arch.**
Michael Wysocki, M. Arch.

Numerical Simulation Laboratory
School of Architecture
University of Texas
Austin, Texas

ABSTRACT

Hourly thermal performance data for the Bruce Hunn residence in Los Alamos, New Mexico, a medium sized passive solar structure with a Trombe wall system, are compared with hourly data simulated for 7 days, Dec. 27 thru Jan. 2. Macro and micro climatic weather data for the Los Alamos site for this 7 day period were utilized (Fig. 1).*** The simulation was carried out on CDC6400 at the University of Texas at Austin.

INTRODUCTION

DEROB is a powerful, and flexible system of programs capable of the full dynamic simulation of buildings of arbitrary geometries. The system can correctly interpret the presence of shading devices and can handle up to 7 thermally coupled volumes (i.e. coupled via conduction, radiation, and convection energy exchange).[1] The system was developed at the University of Texas at Austin in '72-'73, and has been undergoing continuous revision and evolution ever since. DEROB version III was used for this study.

INTERIOR AMBIENT TEMPERATURE

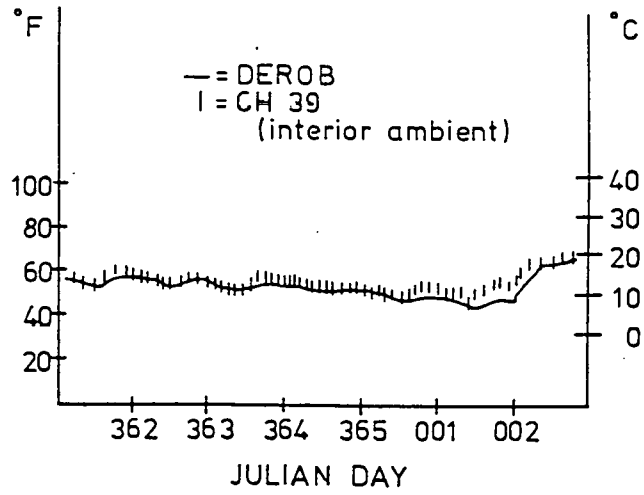

Fig. 2

TEST STRUCTURE

The Hunn residence is a two-story Trombe wall structure composed of 9 major rooms. The house was originally designed to use the Trombe wall for its entire heating load, coupling it with a duct system and rock bin for heat transport and storage, but due to construction defects this has not occurred.[3] The residence currently uses the radiant energy from the glazed Trombe wall supplemented by a mechanical heat source. The hourly data recorded at the Hunn residence, in addition to the microclimatic weather data, were inside air temperatures (Fig. 2), temperatures for the spaces in front of the Trombe wall (Fig. 3), wall surface temperatures and internal wall temperatures (Fig. 4).

TROMBE WALL AIR TEMPERATURE

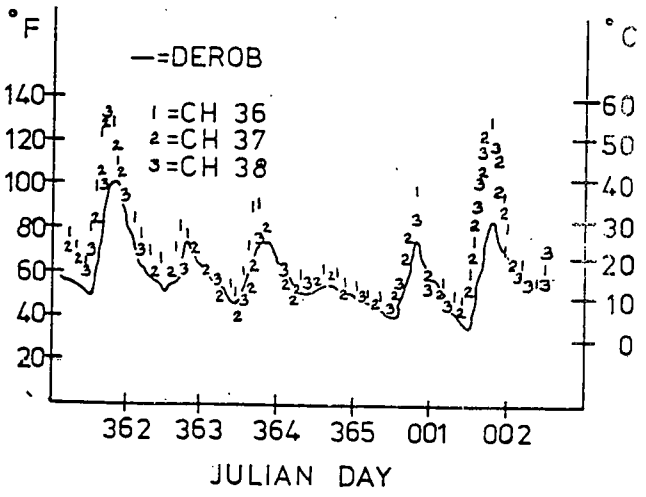

Fig. 3

* This work has been supported by the Solar Heating and Cooling Research and Development Branch, Office of Conservation and Solar Applications for the Department of Energy.

** David Northrup is now employed with Science Applications Incorporated in McLean, Virginia.

*** Denotes illustration at end of paper.

TROMBE WALL TEMPERATURE RAKES

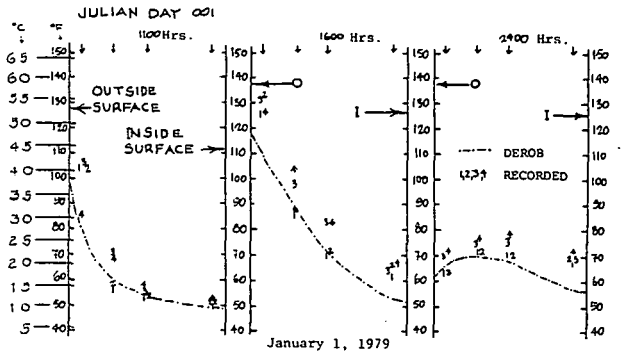

Fig. 4

RESULTS

The structure as simulated was modeled with 5 thermally coupled volumes and 41 surfaces (Fig. 5).*** DEROB was setup to output wall and air temperatures that roughly correspond to the location of the temperature-recording probes in the structure. The simulation results show that temperatures predicted by the DEROB system for room air and Trombe wall temperatures show a very close correlation with the recorded temperatures. 79% of the wall temperatures are within 2.8°C of the predicted values (Fig. 6) and 94% of the air temperatures are within 2.8°C of the predicted values (Fig. 7) with a maximum deviation of 4.2°C. Statistical analysis of the room air temperatures shows that the mean of the absolute values of the differences between predicted and actual values was 1°C with a standard deviation of 1°C, for an accuracy of 3%. For the air space in front of the Trombe wall, 58% of the recorded temperatures lie within 5.8°C of the predicted values (Fig. 8).

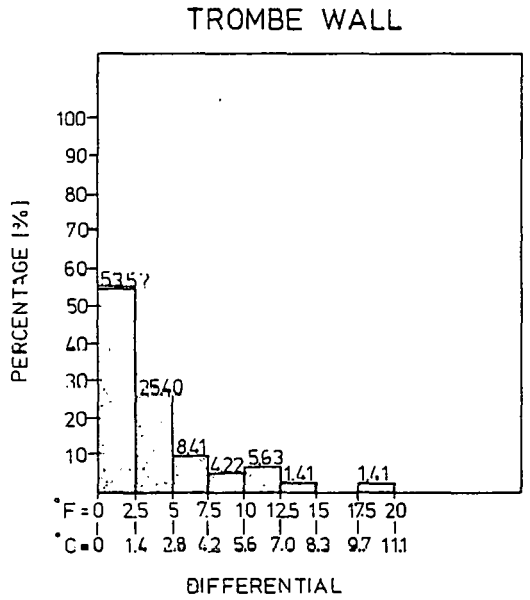

Fig. 6

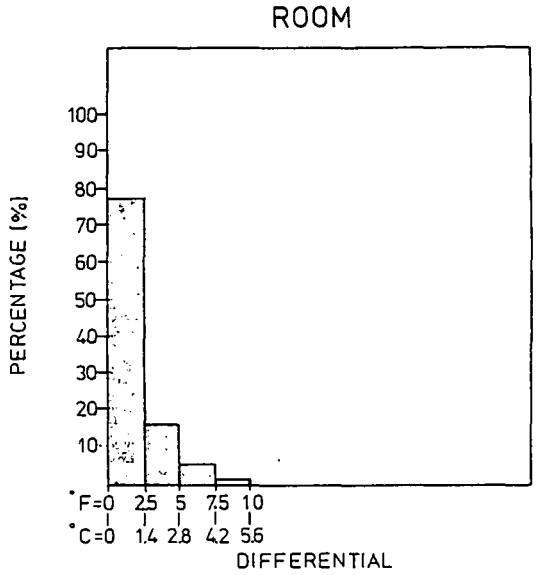

Fig. 7

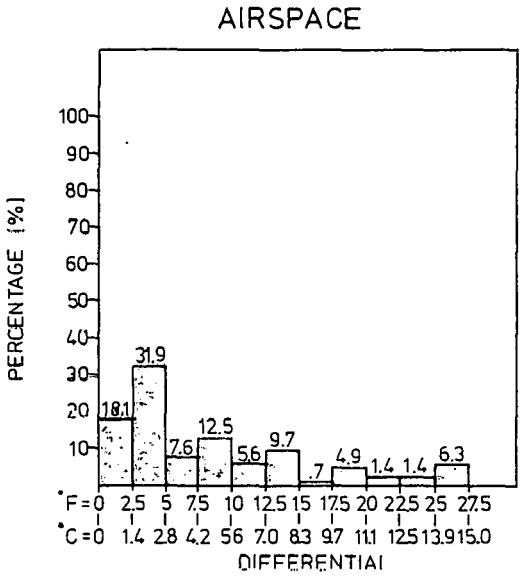

Fig. 8

CONCLUSIONS

The DEROB system has previously been tested against 7 small-scale structures and the Balcomb residence utilizing empirical data collected by the Los Alamos Scientific Laboratory (LASL).[4,5] These validation studies have tested the DEROB system's ability to accurately simulate a variety of functional and geometric conditions often met when dealing with passively heated and cooled buildings (e.g. Direct Gain systems, water walls, vented and unvented Trombe walls, convective loops and multi-space structures).

The successful nature of the validation studies during DEROB's testing phase has been sufficient to justify the limited distribution of DEROB, complete with User's Manual and logic documentation. [6] Further validations, extensions and user oriented refinements are planned, the research effort being aimed at developing DEROB into an accurate and flexible tool for aid in the design and analysis of passive solar buildings.

References

1. Arumí, F. N., "An Introduction to the Numerical Simulation Laboratory at the University of Texas," Energy and Buildings, Vol. 1, No. 2, p. 147 (1977).
2. Arumí, F. N., "Multi-Space Coupling Algorithm of the DEROB System," Heat Transfer in Energy Conservation, (1977).
3. Arumí, F.N. and Northrup, D. O., "The Bruce Hunn Residence as Simulated by the DEROB System," submitted to 1980 ASHRAE Symposium in Denver, Colorado, June 23-27, 1980.
4. Arumí, F. N., "Field Validation of the DEROB/PASOLE System," Passive Solar Takes Off, Vol. 3, p. 152 (1979)
5. Arumí, F. N. and Northrup, D. O., "A Field Validation of the Thermal Performance of a Passively Heated Building as Simulated by the DEROB System." Energy and Buildings, Vol. 2, No. 1 (1979).
6. Arumí, F. N., Bernstein, M., McAdams, K., and Wysocki, M., The DEROB III System: Users Manual (Vol. I), Explanatory Notes and Theory (Vol. II) and Flowcharts, Listings and Cross-Reference Maps for DRBDIG, DRBGF, DRBLUM, DRBSOL, DRPWAL, DBROLEN (Vol's. III-VIII), (1979).

WEATHER DATA

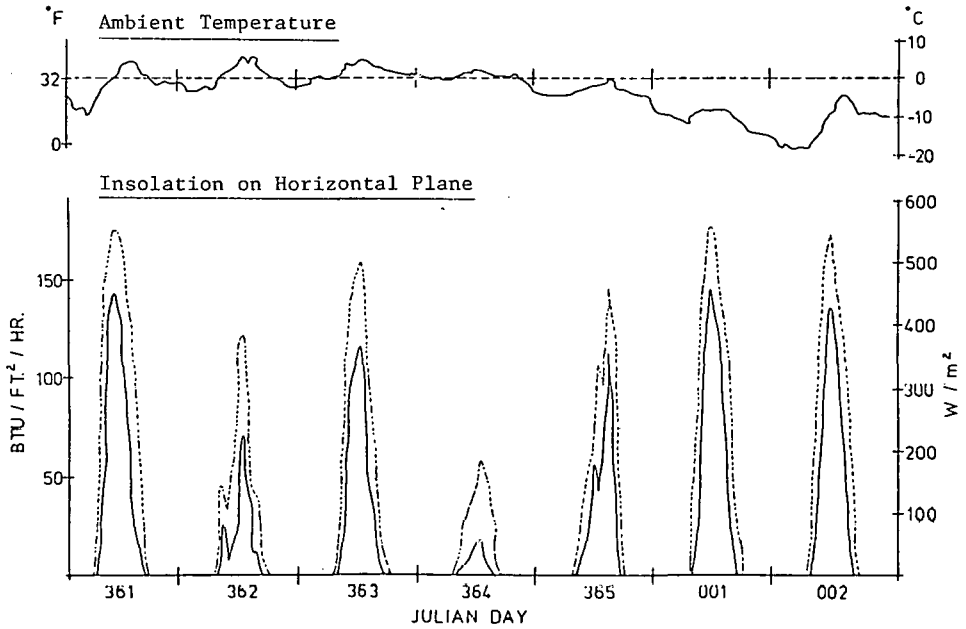

Fig. 1

DEROB Model of the Hunn Residence

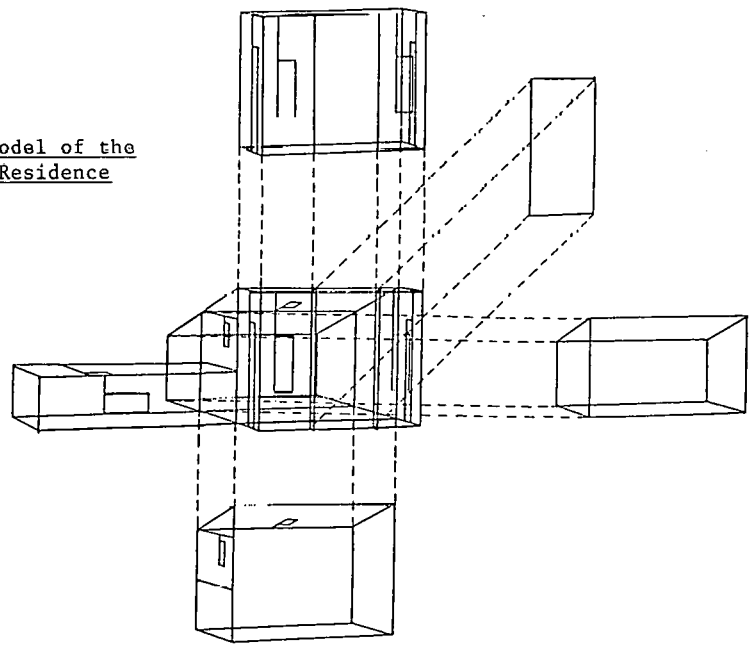

Fig. 5

Dup

VALIDATION OF SOLAR SYSTEM SIMULATION CODES BY THE INTERNATIONAL ENERGY AGENCY

James C. Hedstrom
Los Alamos Scientific Laboratory
Los Alamos, NM

Thomas L. Freeman
Altas Corporation
Santa Cruz, CA

ABSTRACT

Validation of active solar energy system simulation codes by the International Energy Agency using data from the Los Alamos Study Center is described. Two rounds of comparisons of predicted to measured performance were completed. In the first round, all participants were given detailed system description data and a period of measured hourly weather and loads data with the corresponding measured hourly performance data. In the second round, the participants were given minor changes to the system description and a second period of measured weather and loads data without the corresponding measured hourly performance. In the first round, each of the participants was able to predict the results provided. However, this required an undocumented series of adjustments to the user input and the models and comparisons of measured and predicted results. Agreement of measured and predicted results were nearly as good in the second round except for two codes that predicted significantly erroneous results. As a result of this exercise, errors and shortcomings have been found and corrected in most of the codes and confidence in the ability of all codes to model real systems has been increased. However, the questions of a workable methodology for validation and the means of dealing with user error remain unanswered.

INTRODUCTION

The International Energy Agency (IEA) Task 1 group on solar system modeling and simulation has conducted comparisons of performance predictions of several active solar simulation codes to each other and to a carefully measured experiment. Each code has been run by the representative from the IEA participating country where the code was developed, who, in most cases, was personally involved in developing the code. The codes and the corresponding countries are:

INSOL	Belgium
SVS	Denmark
Philips	Germany
Faber	Great Britain
FTP	Italy
Nikken	Japan
LASL	USA
TRNSYS	USA

In the first phase of the validation, representative residential liquid and air-based systems were defined in detail with the cooperation of all participants. A tape of year-long hourly weather data for three very different climates with space heating loads precalculated by NBSLD was distributed to each participant. In the first series of comparisons, several problems and discrepancies were encountered. The most significant of these was caused by the differences in the radiation tilting algorithms employed by the various codes. For subsequent runs of the comparison, the group agreed upon a common means of calculating radiation on tilted surfaces. As the participants iteratively ran their simulations and compared results, nearly all of the original discrepancies disappeared. In the process, a variety of user input and modeling errors, oversimplifications and other shortcomings were identified in each of the codes. In the end, all codes predicted the same annual "percent solar" to within ±2 percent and nearly identical hourly profiles of energy collected, auxiliary energy and tank temperature. These results are fully documented in a report published by the IEA[1].

The second phase of the validation was to make comparisons on real systems. The Los Alamos Study Center was selected as the first system on which to do simulation code validations. This paper presents the results of this second phase.

Two separate rounds of comparison were undertaken in this exercise using two separate, two-week-long periods of winter time measured hourly meteorological and loads data. In the first round, hourly measured performance data was included with the meteorological and load forcing functions supplied to the participants. A detailed description of the system was provided[2]. In the second round, the system description data was changed slightly[3] and a two-week period of forcing function data from another month was distributed without any of the measured performance data.

Figure 1. LASL Study Center

A photograph of the Study Center is shown in Figure 1. The 716 m^2 collector is in one planar array tilted 35° from the horizontal. The photo shows how shading occurs from the building on the east and the concourse to the west of the collector. A schematic of the system in Figure 2 shows the solar system for heating and cooling and the HVAC system. The present study involves only the heating supply system which includes the solar collector, heat exchanger, the large vertical storage tank, the steam auxiliary heat exchanger, and the associated piping.

A schematic of the collector is shown in Figure 3. The collector has a black chrome selective surface and is single glazed with water-white glass. The collector fluid is paraffinic oil, which is circulated through a tube and shell heat exchanger. Water is circulated through the tube side of the heat exchanger and then into a 71.6 m^3 (10,000 gallon) steel tank. Water from the tank is circulated to 55 terminal boxes with reheat coils throughout the 5500 m^2 (60,000 ft^2) building. Each terminal box has its own thermostat. When the storage tank temperature is inadequate to heat the building, the water is circulated through an auxiliary steam heat exchanger.

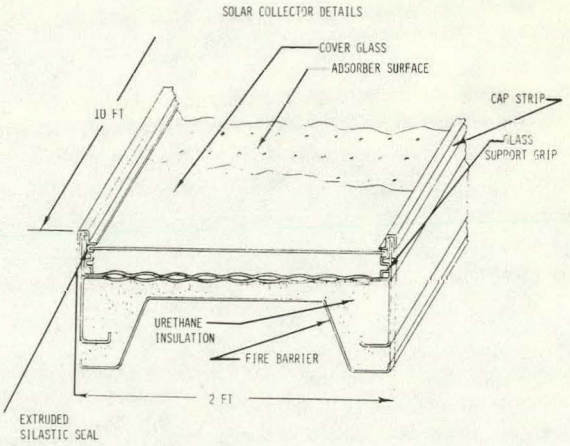

Figure 3. Collector Schematic

MODEL INFORMATION

Collector

The participants were provided with all the physical parameters that were known for the collector. These included collector area, absorber properties, glazing properties, fluid heat transfer coefficient, back side and end heat loss coefficients, collector mass, and shade factors from the adjacent structures. A measured efficiency curve obtained from the LASL Collector Testing Laboratory was also available. Collector manifold piping dimensions were specified along with their mass and heat loss coefficients. Physical properties and flow rates of the paraffinic oil used in the collector loop were given.

Heat Exchanger

The heat exchanger model, tube number, tube diameter, surface area, and mass were made available. A correlation of the heat exchanger heat transfer coefficient which was derived from measured data was provided.

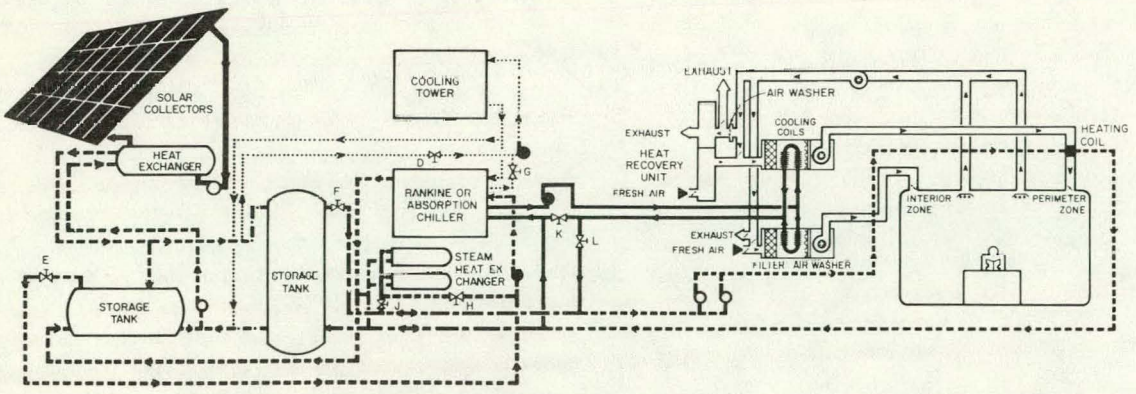

Figure 2. Schematic of Study Center Mechanical System

Storage Tank

The size, volume, and surface area of the tank was given. The heat loss coefficient of the tank insulation was suggested. Because the apparent tank heat loss was much larger than the tank coefficient would predict for the first data period, an increase by a factor of four was suggested. The losses were more in line with expectations for the second period so the use of the normal tank coefficient was recommended.

A daily measured tank heat loss determined by a heat balance on the tank (taking into account the change in energy stored in the tank) is shown in Figure 4. Although the scatter in the data is large (because of the difference between two large numbers and because there are only four temperature measurements in the tank) the difference between the two periods is evident. The reason for this difference is unknown, but could be due to changes in instrumentation or possibly, thermocirculation in the piping. The domestic hot water system (which was not operating during the second period due to a failure in the flow meter) could also be a factor.

Specifications of the tank inlet and outlet piping were given.

Auxiliary

The Study Center switches to auxiliary heat from steam heat exchangers whenever the storage tank drops below a setpoint. This setpoint is a function of outside temperature. The functional relationship was determined from the data and provided to the participants. The controller has hysterisis and is not perfectly repeatable, sometimes causing different auxiliary operation than the provided function would predict.

Collector Controller

The on and off differential settings between the collector absorber temperature and the storage temperature were given.

DATA INFORMATION

The Study Center is monitored with a PDP-11 computer and a PDP-ISC Data Acquisition System. Data has been acquired on the system since November 1977, and has been reported in (4) and (5).

First Period

The first set of data provided to the IEA participants

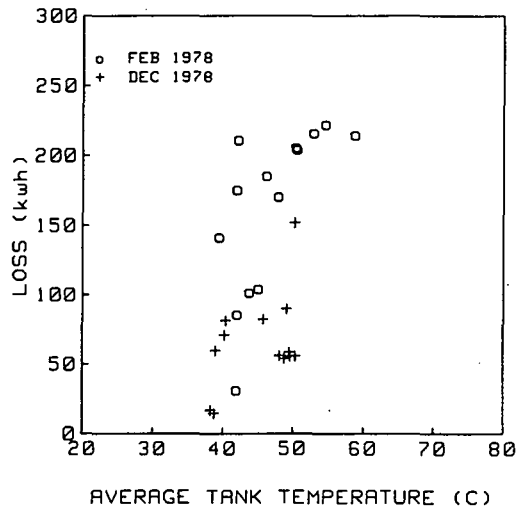

Figure 4. Daily Measured Tank Loss (By Energy Balance)

was the period from February 1-14, 1978. These data were supplied in August 1978, and the results of the simulation were reported at the IEA Task I meeting held in Palermo in December 1978.

The weather data consisted of hourly averages of horizontal insolation, solar radiation on the collector plane, ambient temperature, wind velocity and direction, building heating load and domestic hot water load.

The participants were also provided with measured results so they could make their own comparisons and do a certain amount of fine tuning to achieve the known result. These data included the hourly averaged collector heat output, heat exchanger output, tank energy input, tank energy output, auxiliary heat and the average tank temperature.

Second Period

For the second round of comparisons a second two-week period of data was distributed - this time without the measured results. The period selected was December 18-31, 1978. It included an initial cloudy two-day period followed by eight sunny days ending with four more cloudy days. It was cold during this period, and the building loads were high.

The weather data were provided to the participants in January 1979, the hourly results were due back at LASL for detailed comparison in April 1979, and the comparisons were presented the next IEA Task I meeting in Tokyo in May 1979.

TABLE I

TWO WEEK ENERGY COMPARISON
February 1-14, 1978

	QINC	QCOUT	QSIN	QSLOSS	QSOUT	QAUX	QLOAD	QDHW	% SOLAR
DATA	46509	14557	-	-	11843	5382	17274	333	69.4
USA (TRNSYS)	46509	14750 (1.3)	14750	2330	12420 (4.87)	5277 (-1.95)	17274	333	70.0 (0.6)
DENMARK	44765	15193 (4.37)	15193	3001	12192 (2.95)	5245 (-2.55)	17274	333	70.2 (0.8)
GREAT BRITAIN	46509	13432 (-7.73)	12951	810	12141 (2.52)	5208 (-3.23)	17274	333	70.4 (1.0)
USA (LASL)	46509	14548 (-.06)	14446	1547	12360 (4.37)	5208 (-3.23	17274	333	70.4 (1.0)
JAPAN	46509	13719 -5.76	13511	443	12509 (5.62)	5047 (-6.22)	17274	333	71.3 (1.9)

Energy Units: kWh
( ) Per cent deviation from measured

TABLE II

TWO WEEK ENERGY COMPARISON
December 18-31, 1978

	QINC	QCOUT	QSIN	QSLOSS	QSOUT	QAUX	QLOAD	QDHW	% SOLAR
DATA	44792	15137	14901	-	14237	10822	24717	0	56.2
GREAT BRITAIN	44793	12882 (-14.9)	12456 (-16.41)	36	12425 (-12.73)	12496 (15.47)	24717	0	49.4 (-6.8)
JAPAN	44793	14293 (-5.57)	14089 (-5.45)	375	13593 (-4.53)	11362 (4.99)	24717	0	54.0 (-2.2)
BELGIUM	44793	14364 (-5.1)	14061 (-5.64)	380	13306 (-6.54)	11262 (4.06)	24717	0	54.4 (-1.8)
USA (TRNSYS)	44933	14773 (-2.41)	14351 (-3.69)	352	14215 (-.15)	10988 (1.53)	24717	0	55.5 (-.7)
USA (LASL)	44792	14786 (-2.32)	14696 (-1.38)	396	14283 (.32)	10707 (-1.07)	24717	0	56.7 (.5)
DENMARK	42863	16652 (10.01)	16652 (11.75)	415	16281 (14.36)	8436 (-22.1)	24717	0	65.9 (9.7)

Energy Units: kWh
( ) Per cent deviation from measured

RESULTS

First Period

The results from this first period were obtained and compiled by the various participants at the Palermo meeting. In most cases detailed hourly or daily results were not available for direct comparison. The two-week summary of results is presented in Table I. The parameters in the table are defined below.

QINC	Incident solar on the collector plane
QCOUT	Collector output
QSIN	Storage input
QSLOSS	Storage losses
QSOUT	Storage output
QAUX	Auxiliary
QLOAD	Building space heating load
QDHW	Domestic hot water load
% SOLAR	Percent solar, [100%(QLOAD - QAUX)/QLOAD]

The measured results are labeled DATA on the first line of the table. The percent deviation of the calculation from the measured parameter is given below each calculated value in parenthesis. The participants are listed from low to high percent solar.

For this period, all simulators were able to predict within 1.9 percentage points of the overall measured percent solar value of 69.4 percent. The collector efficiency for this period is 31.3 percent. The calculated values deviated as much as 2.5 percentage points low from this value (or 7.7 percent low on a absolute basis). Many of the simulators made compensating adjustments to the storage loss coefficient as seen by the wide range of calculated storage losses. This parameter, of course, was not well defined, as mentioned previously.

Second Period

The two-week results for the second period are given in Table II. Four of the simulators predicted within 2.2 percentage points of the measured percent solar value of 56.2 percent, which was nearly as accurate as in the first period analyzed. However, the participants from Great Britain predicted 49.4 percent solar or 5.8 points low, and the Danish participants predicted 65.9 percent or 9.7 points high. The exact reason for their deviations at this time is unknown but presumably is due to user error since agreement in the first round, and in previous IEA comparison exercises, was much better.

The measured collector efficiency for the second period was 33.7 percent and the same four simulators predicted within 1.8 percentage points of this value (or 5.6 percent on an absolute basis). The British calculation was 15 percent low on collector output, and the Danish calculation was 10 percent high, both of which are consistent with the discrepancies of the overall simulation results.

Since the participants did not have a measured result for comparison, LASL had suggested they use the given tank insulation coefficient. All simulators predicted approximately the same tank heat loss except the British, who were low by a factor of 10. This is possibly due to an error in converting units but is certainly user error of some kind.

The bar graph in Figure 5 shows the day-to-day variations of measured and calculated daily storage input energy. On a daily basis most simulators were in good agreement although Great Britain was consistently low and Denmark was consistently high. The daily auxiliary energy as shown in Figure 6 shows the same trends as the storage input energy graph.

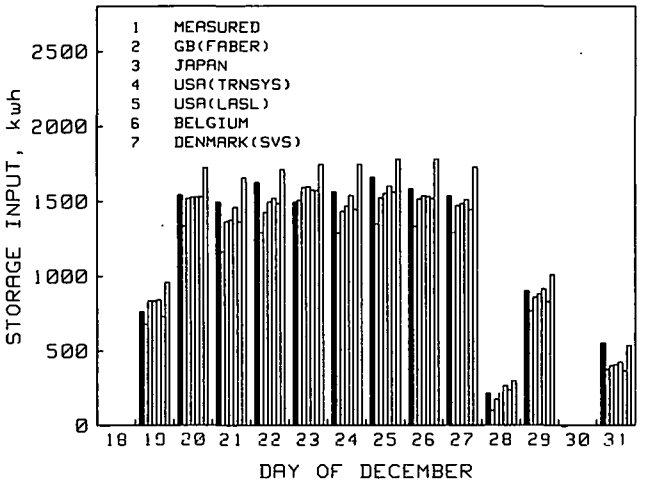

Figure 5. Comparison of Daily Storage Input Energy

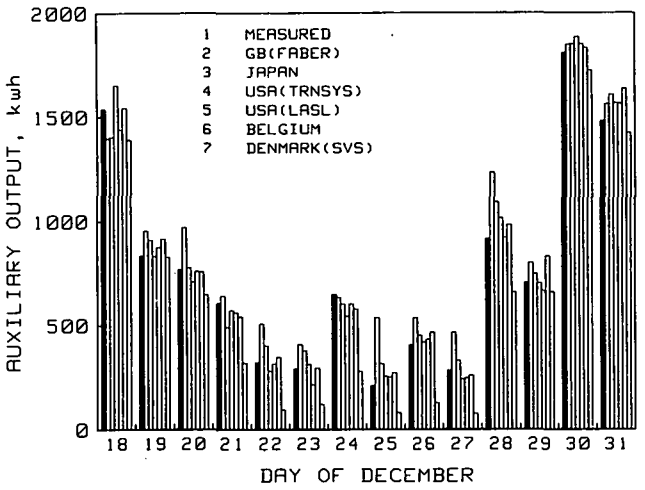

Figure 6. Comparison of Daily Auxiliary Requirements

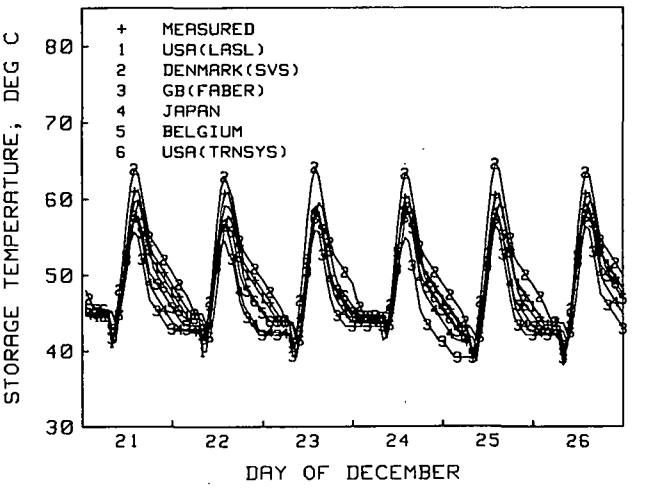

Figure 7. Six Day Plots of Hourly Storage Temperatures

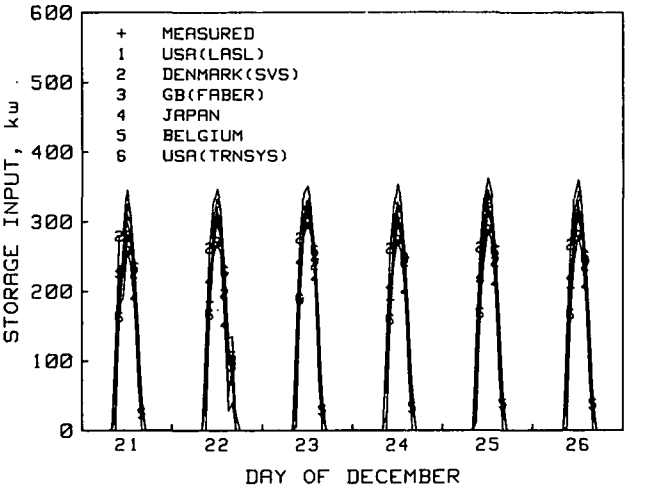

Figure 8. Six Day Plots of Hourly Storage Input Energy

The standard deviations between daily calculated quantities and measured quantities are given in Table III. Four of the simulators were within 10 percent of all energy quantities, while two others were outside this band.

TABLE III

DAILY STANDARD DEVIATION
December 18-31, 1978

	QCOLL %	QSIN %	QSOUT %	QAUX %	TSAVE %
Great Britain	17.5	19.2	17.8	21.8	6.3
Japan	9.2	9.2	9.9	11.9	4.6
Belgium	8.1	8.4	8.5	9.1	3.5
USA (TRNSYS)	6.9	7.4	4.7	8.3	2.5
USA (LASL)	5.9	5.5	5.1	6.5	2.0
DENMARK	11.8	13.6	17.0	25.7	4.2

Hourly plots of average storage temperature and storage input energy are shown in Figures 7 and 8 for the six-day period from December 21-26, 1978. The Danish and British participants are again high and low respectively. Phase shifts between various simulations do not seem to be a particular problem.

CONCLUSIONS

It has been shown that all the programs involved in this study are capable of predicting the measured performance of a solar heating system although major questions concerning an appropriate validation methodology remain.

This software-hardware, and previous IEA software-software, comparisons have shown that the potential for user error is large in the preparation of input for any of the codes involved in the comparisons. In practice the effects of user error contribute much more uncertainty to results than any remaining errors or differences in the modeling approaches or algorithms. No hard data is available on the extent of iterative input adjustment in the first round of this exercise but it is the experience of the authors that three or four iterations are typically required before results are obtained that are within the error tolerance capability of the codes. It must be recognized that a "typical" user is likely to make far more mistakes than the "experts" who ran each of the codes in this study.

A second point is that the two-round comparison methodology allows users to infer the values of some key parameters in the first round simulation (sometimes called the "training" period) rather than calculate them from information normally available to a user. Data arrived at in this empirical way may mask one or more important effects not properly accounted for in the model. The inferance of the tank loss coefficient In this exercise is an example of this problem. The apparent losses from the measured data were much higher than expected, possibly due to thermosyphoning or some other unmodeled phenomena. The range of tank losses predicted by the codes in the first round shows that most participants used the tank loss coefficient parameter to adjust their results. Thus not only was the actual cause of the unexpectedly high losses falsely attributed, but other modeling inaccuracies or user errors were compensated for in the tank loss coefficient.

A final problem relates to the lack of sufficient code output data to completely identify the sources of differences. In a "system" simulation, the performance of all "components" is interrelated such that an error in one component creates disagreement between measured and predicted results in all components. Either "stand-alone" component tests are required or more short term data must be measured in the experiment and output by the codes for comparison. As an example, hourly measured and simulated collector input and output data could be plotted in the efficiency vs. $\Delta T/I$ format to validate the collector "component" in this "system" test.

In summary, this validation exercise, and others like it, are valuable for locating and correcting significant modeling errors and lack of modeling capability. They are not appropriate, however, for defining the error bounds on the codes. Dealing with inevitable user error in a validation methodology is a tricky problem but the idea of eliminating its effects with a preliminary "training round" of comparisons has serious shortcomings.

The IEA has provided a valuable forum for comparing and improving the consistency of solar simulation codes used throughout the world. The LASL Study Center has been established as an appropriate system for performing code comparisons and the consistency and quality of the performance data has been established for future validation efforts.

References

1. International Energy Agency Solar Heating and Cooling Program - Task 1 - Investigation of the Performance of Solar Heating and Cooling Systems - A Modeling and Simulation Report on Subtask A - Edited by Ove Jorgensen (October 1979).
2. Validation Information for the Study Center - Information Package from J.C. Hedstrom to IEA Participants 8/23/78.
3. Validation Information for the Study Center - Phase II - Letter from J.C. Hedstrom to IEA Participants 1/16/79.
4. H.S. Murray, J.C. Hedstrom, and J.D. Balcomb, "Solar Heating and Cooling Performance of the Los Alamos National Security and Resources Study Center," CCMS/ISES Conference Proceedings, Dusseldorf, April 19-20, 1978.
5. J.C. Hedstrom, H.S. Murray, J.D. Balcomb, "Solar Heating and Cooling Results for the Los Alamos Study Center," Conference on Solar Heating and Cooling Systems Operational Results, Colorado Springs, Colorado, November 27-30, 1979.

THE SEA-LAB PASSIVE TEST BUILDING PROJECT

James R. Clinton

Solar Energy Analysis Laboratory
4325 Donald Ave.
San Diego, CA 92117

ABSTRACT

A group of eight passive test buildings is being constructed at an inland San Diego County site. Purposes of the project include side-by-side comparison and demonstration of the various passive solar heating and cooling techniques and validation of calculational models. Different passive systems including Trombe wall, water wall, direct solar gain, roof pond, sunspace, clerestory and "high mass" concepts will be incorporated into individual 16 ft. by 16 ft. two room buildings. An eighth standard construction building is fitted with an active solar system and will be used for comparison and control purposes.

The buildings are fully instrumented and monitored with an on-site computer based data acquisition system. A special feature of the instrumentation allows actuation of devices like fans and dampers under software control.

One activity associated with this project is the validation of thermal network simulation models. Comparisons with component models as well as overall seasonal performance checks will be conducted.

Construction began during January 1980 with all buildings scheduled to be operational for the start of the 1980 cooling season.

PROJECT CONCEPT

Present quantitative knowledge of the operating performance of passive solar buildings has come from either occupied buildings,(1) or from test cells.(2) While data from these sources has been extrememly useful in establishing the value of passive techniques, a number of gaps remain. Data from complex buildings is very difficult to reconcile with simple performance models, especially with the considerable uncertainties due to occupant behavior, and test cells cannot cover the range of conditions occurring in larger structures.

This project is funded by the San Diego Gas and Electric Company and the Southern California Gas Company. Additional support for modeling is provided by the Solar Heating and Cooling Research and Development Branch, Office of Conservation and Solar Applications, U. S. Dept. of Energy, through a contract with the Energy Center of the University of California, San Diego.

This project consists of structures of intermediate size which will serve to test the primary passive concepts on a uniform basis. Each of the buildings, described in detail below, is fitted with one major passive solar feature and is as similar to the other buildings as is feasible. The two room design allows investigations of the important problem of heating rooms not equipped with passive solar features. Of the eight small buildings, one is a conventional control building and seven test various generic passive concepts:

- Conventional Design Control Building
- Trombe Wall with Vertical Underfloor Rock Bin
- Water Wall with Hydronic Slab Heating
- Direct Gain with Horizontal Underfloor Rock Bin
- Sunspace with Horizontal Underfloor Rock Bin
- Clerestory with Massive Wall
- High Mass Construction (Tilt-Up Concrete)
- Roof Pond

The project is located at site about 50 miles northeast of San Diego with approximately 2500 Heating Degree Days and average summer high temperatures in the low 90's. Even though space conditioning requirements are modest in this climate, excellent test conditions are assured because a range from cool and cloudy through warm and sunny (overheating) can occur at any time during the heating season. This fact allows convenient investigation of designs with solar fractions near 100%, and such designs offer stringent test conditions for model comparisons.

Since typical buildings in this region are minimally insulated, space heating normally takes more energy per heating degree day than in most harsher climates, in spite of the sunny weather. New construction in Southern California proceeds at a rapid pace so great opportunities exist for implementation of passive designs on a large scale. Demonstration of the various concepts to builders and architects is an important goal of this project and the reason that standard construction practices are employed to the greatest extent possible.

TEST BUILDINGS

The test buildings are of standard wood frame and concrete floor slab construction, except that the high mass building has tilt-up concrete walls. The 16 ft. by 16 ft. floor area is equally divided into two rooms. Rooms not containing major passive solar features are heated primarily be convection through open doorways. Some of the buildings are also equipped with underfloor rock bins or hydronic slab tubing. Roof trusses allow non-bearing room partitions and interior walls may therefore be easily added or removed for some experiments. Ceilings are insulated with standard R-19 fiberglass blankets and walls are insulated to R-11. Window area is 18% of the floor area in the conventional building and of equal or corresponding area in the other buildings. Regular windows are single glazed in keeping with standard practice in this region, but all glazing associated with passive features is double glass.

Auxiliary heating is supplied to the buildings by a circulating hot water system. Each building is equipped with a fan coil unit with the fan controlled by a room air thermostat. Heat addition is measured by the temperature drop across the coil and the flow rate of the circulating water. The system includes a water chiller so that cooling can be supplied with the same loop during the cooling season. During the heating season, fan-off heat losses from the fan coil units provide for a reasonable and measured amount of internal heat gain to the buildings. During the cooling season, internal gains will be provided by electric resistance heaters.

A movable, modular building is also in place at the site to house the instrumentation and auxiliary equipment and provide an area for personnel and informative displays.

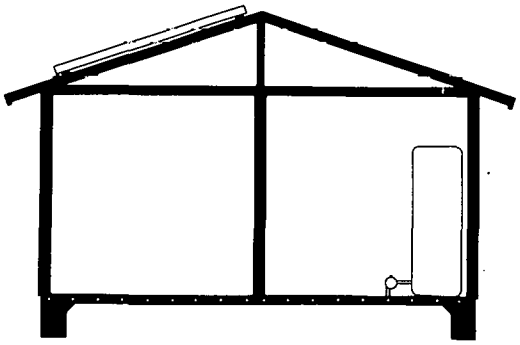

Fig. 1 CONVENTIONAL BUILDING

The conventional control building is shown schematically in Fig. 1. Its primary function is to provide a comparison with the passive solar buildings. Also, it is equipped with an active solar system with roof mounted collectors. Storage for the active system is provided by an indoor water tank.

Heat delivery from the solar system can be accomplished by a fan coil unit or by tubes embedded in the slab. One goal of the project is to better understand the implications of various means of adding off-peak energy to the buildings and the floor slab tubes provide one possible option.

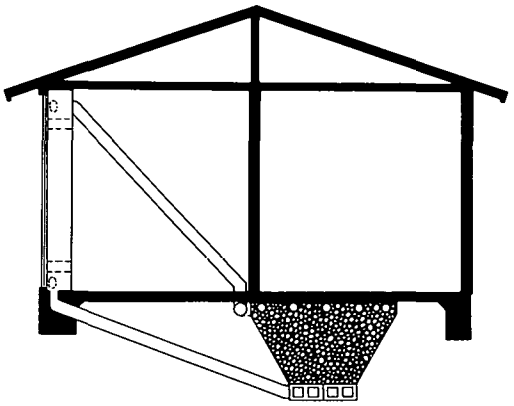

Fig. 2 TROMBE WALL BUILDING

The Trombe wall building is shown in Fig. 2. The wall is equipped with exterior double glazing and vents into the room. Half of the wall is constructed with concrete blocks (reinforced and solid grouted) and other half is solid reinforced concrete. Since the total area of the wall is nearly 50% of the floor area, most experiments will be conducted with half of the wall exposed and the other half insulated to the same level as the wood frame walls. Other sizings can also be investigated in this manner.

Air from the wall surface—glazing space can be ducted into the room or into a vertically fed rock bin located under the floor in the north room. Various control strategies will be implemented. The most straightforward is to duct heat into the room if needed to meet the thermostat setting and then store excess heat in the rock bin. Under normal operation, the rock bin heats the floor passively, but because the effective thermal conductivity of rock bins in the no-flow condition is low, provision has also been made for active discharge.

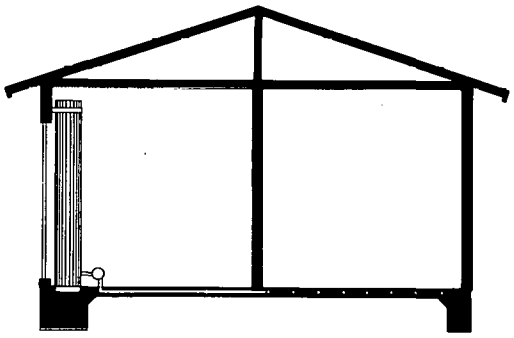

Fig. 3 WATER WALL BUILDING

The water wall building, shown in Fig. 3, compares two types of water containers. One side of the wall is fitted with five 13 in. diameter cylindrical tanks. The 5 in. spaces between tanks allows for some direct solar gain. The other side if fitted with two 12 in. deep rectangular tanks. As in the Trombe wall building, the large south wall relative to the floor area means that only half the wall needs to be exposed to achieve a reasonable solar aperture.

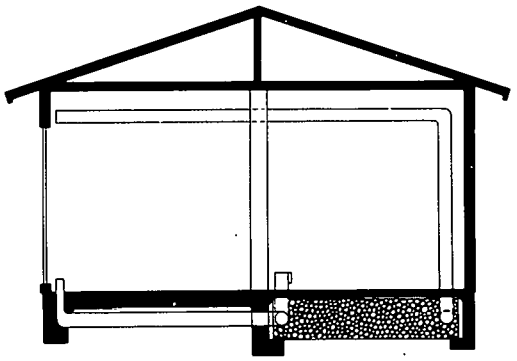

Fig. 4 DIRECT GAIN BUILDING

The direct gain building is shown in Fig. 4. The floor slab in the south room is 8 in. thick compared to the 4 in. thickness of all other floor slabs. The interior wall is 8 in. solid grouted concrete block and provides additional heat storage capacity.

The rock bin under the north floor is not used in the normal operation of this building because air from a living space is generally not sufficiently warm to heat a rock bin. However, equipment is fitted to the large south window to allow the installation of and opaque hot air collector system. It is envisioned that as the south room becomes overheated, the collectors would become operational and transfer excess heat to the rock bin.

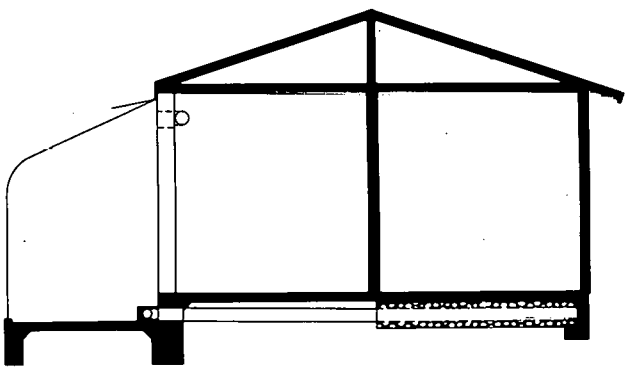

Fig. 5 SUNSPACE BUILDING

The sunspace building, shown in Fig. 5, is fitted with a commercially available attached greenhouse. An 8 in. solid concrete block wall separates the sunspace from the south room. A door in this wall can be opened to directly heat the interior.

Excess heat from the sunspace is ducted to the horizontally fed rock bin under the north room. This rock bin can be actively discharged and, during the cooling season, can be cooled with outside air at night.

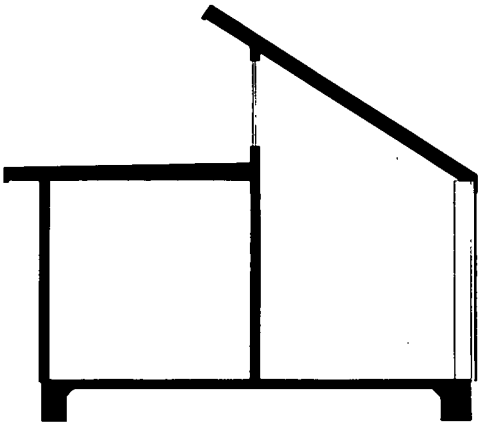

Fig. 6 CLERESTORY BUILDING

The clerestory building shown in Fig. 6 is intended to test one method of direct gain passive heating in designs which preclude the use of the south wall. Also, clerestories provide a means of heating north rooms.

The north wall of the building is of 8 in. concrete block construction. The flat roof facing the clerestory aperture is to be fitted with reflectors. Designs for reflectors which also serve as movable night insulation are under study.

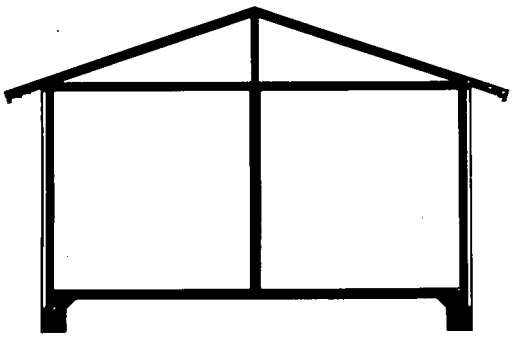

Fig. 7 HIGH MASS BUILDING

The walls of the high mass building shown in Fig. 7 are of a concrete—foam construction. The walls are factory cast and transported to the site for assembly. This method offers a reasonable cost alternative to concrete block or conventional concrete wall construction. The climate in this region is such that a large thermal time constant can provide a large decrease in both heating and cooling requirements.

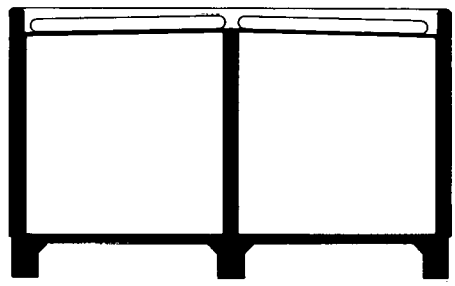

Fig. 8 ROOF POND BUILDING

The roof pond building is shown in Fig. 8. As an alternative to the concrete block construction used in other roof pond buildings, this test building has wood frame construction. Walls are built with 2 by 6 studs to accomodate the additional roof load.

The means for covering the water bags has not yet been fixed. A number of designs which allow both proper winter and summer operation are being considered.

INSTRUMENTATION

The instrumentation system takes data from the sensors installed in the buildings and can actuate various devices under software control. A microprocessor based computer controls a digital voltmeter and scanner. The scanner accomodates 120 channels of sensor input and 20 channels of actuator output.

Globe and air temperature in each room of the buildings is monitored as well as other temperatures of interest. Platinum thermometers are used as temperature sensors to achieve the level of reproducibility necessary for accurate temperature difference measurements. Two precision pyranometers monitor the horizontal and vertical solar radiation at the site and a pyrheliometer monitors the direct radiation. A third pyranometer is available for measurements of radiation at other orientations or radiation on interior surfaces. Wind speed and direction and ambient temperatures are also monitored.

Most temperature measurements are conducted every 20 min. This period corresponds to the time increment used in the thermal network simulation method (3) which will be used to compare experimental results to simulation results. Measurements of temperature difference across the fan-coil units and solar radiation instrument readings are taken every minute and averaged for the 20 minute time step. Data is stored on magnetic disks, with a telephone link included to provide a daily check on data reliability.

REFERENCES

1. R.P. Stromberg and S.O. Woodall, Sandia Laboratories Report SAND 77-1204, August, 1977. "Passive Solar Buildings: A Compilation of Data and Results."

2. J.D. Balcomb, R.D. McFarland and S.W. Moore, Proc. of the 2nd National Passive Solar Conference, Philadelphia, March, 1978. "Passive Testing at Los Alamos."

3. James R. Clinton, Proc. of the 4th National Passive Solar Conference, Kansas City, October, 1979. "The SEA-PASS Passive Simulation Program."

Session IIIA

Dr. Dan Ward
Colorado State University
Chairperson

SYSTEMS SIMULATION II

Dup

FEASIBILITY EVALUATION FOR SOLAR INDUSTRIAL PROCESS HEAT APPLICATIONS

S. A. Stadjuhar
Solar Energy Research Institute
Thermal Conversion Branch

ABSTRACT

An analytical method for assessing the feasibility of Solar Industrial Process Heat applications has been developed and implemented in a flexible, fast-calculating computer code—PROSYS/ECONMAT. The performance model PROSYS predicts long-term annual energy output for several collector types, including flat-plate, nontracking concentrator, one-axis tracking concentrator, and two-axis tracking concentrator. Solar equipment cost estimates, annual energy capacity cost, and optional net present worth analysis are provided by ECONMAT. User input consists of detailed industrial process information and optional economic parameters. Internal program data includes meteorological information for 248 U.S. sites, characteristics of more than 20 commercially available collectors representing several generic collector types, and defaults for economic parameters. Because a full-scale conventional back-up fuel system is assumed, storage is not essential and is not included in the model. Although the software is neither a dynamic simulation nor a detailed design tool, it yields the advantages of speed and flexibility and provides a method for uniform comparison of diverse solar equipment, IPH applications, and locations. Recent updates in performance calculations, the collector array sizing algorithm, and system cost estimates have improved the accuracy of the PROSYS/ECONMAT evaluation. Efforts in IPH model comparison and PROSYS/ECONMAT validation have been initiated. The PROSYS/ECONMAT code has been used in a variety of the case studies, in-depth applications analyses, and generic system studies. Examples of such analyses demonstrate the capabilities of the model.

INTRODUCTION

The industrial sector is the largest single U.S. energy consumer, using 37% of the total national energy demand. From 50% to 70% of this energy is for industrial process heat (IPH) used in the preparation and treatment of manufactured goods and produce [1]. Industry thus provides a potentially large market for solar technology but only if the quantity and quality of energy required by IPH applications can be provided by solar energy.

Although industrial process heat requirements span a broad temperature range, a significant amount of heat is used at temperatures that can be provided by currently available solar technology. At least 27% of the IPH requirement is for temperatures below 300°C (550°F) and can be supplied by commercial collectors [2]. Using solar energy for preheat and technological developments to supply higher temperatures will increase the percentage of potential solar contribution to as much as 50%.

Solar energy for process heat can be supplied directly or through a heat transfer fluid such as hot water, hot air, or low-pressure steam. To effectively meet the wide range of IPH temperatures, many generic collector types are required, as shown in Fig. 1. Because of the diverse temperature requirements, system configurations, and the variety of available collectors, it is important to select the appropriate solar equipment for the specific IPH application. Considerations in the selection of the most effective solar equipment must include process requirements, meteorological effects, solar system characteristics, and economic factors, as illustrated in Fig. 2. Because of the number of variables and computations involved, the evaluation can be performed most efficiently with a computerized analysis.

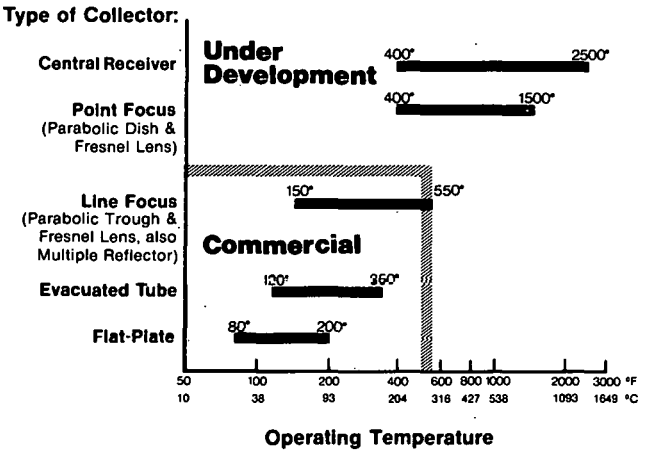

Figure 1. Typical Operating Temperature Ranges of Solar Collectors

EVALUATION PROCEDURE

Software developed for the analysis of solar IPH applications includes the performance model PROSYS, the economic evaluation ECONMAT, and several attendant data bases. Figure 3 shows the basic relationship of these

components and the flow of the evaluation procedure. The main features of the PROSYS/ECONMAT code are summarized in Table 1 and expanded in the following sections.

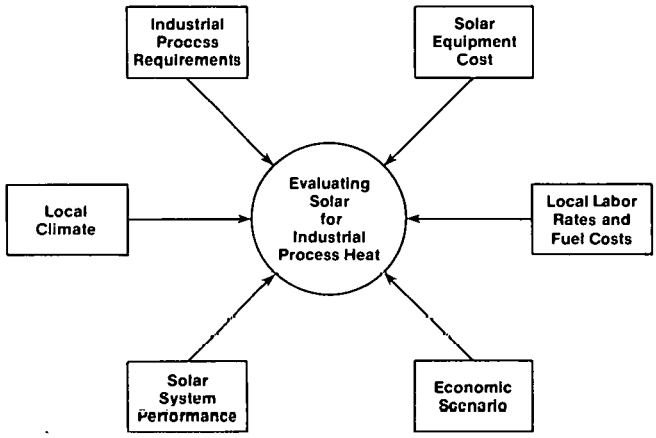

Figure 2. Key Variables in Evaluation of Solar Industrial Process Heat

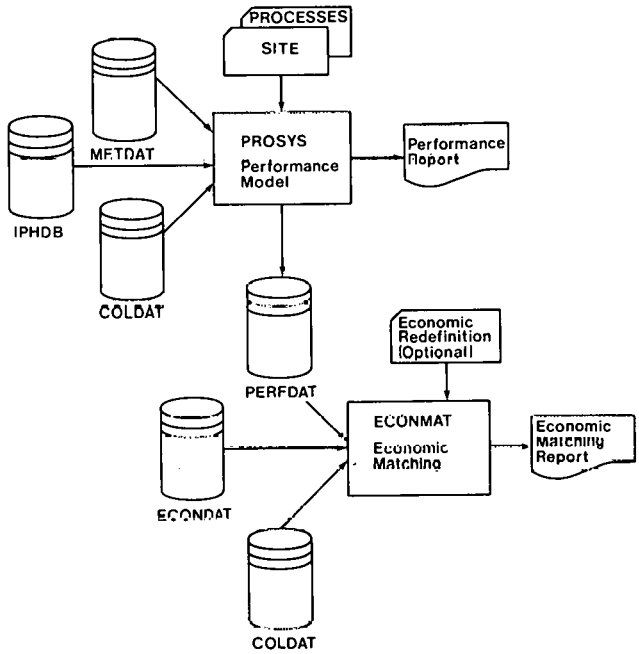

Figure 3. Flow of Evaluation Procedure

DATA BASES

Characterization and analysis of solar IPH applications require site-specific meteorological data, detailed industrial process information, solar equipment performance and cost data, and appropriate economic parameters. This information resides on four data bases - METDAT, IPHDB, COLDAT, and ECONDAT.

Table 1. Features of the PROSYS/ECONMAT Code

Purpose:	Provide method to assess feasibility of solar IPH applications.
User Input:	Detailed industrial process information and optional economic parameters.
Internal Data:	Meteorological information for 248 U.S. sites.
	Characteristics of several generic collector types.
	Defaults for economic parameters.
Program Output:	Long-term average performance prediction for each collector process combination.
	Estimate of solar system cost and annual energy capacity cost. Optional present worth analysis.
Advantages:	Flexible, high-speed evaluation.
	Uniform comparison of diverse solar equipment, IPH applications, and locations.
Restrictions:	Nondynamic analysis.
	Not a detailed design tool.
	Conventional fuel backup assumed, no consideration of storage.

The meteorological data base (METDAT) specifies the quantity and quality of the available solar radiation at 248 U.S. locations as determined by availability of SOLMET and ERSATZ data [3]. Values are given for a typical day each month and include long-term average daily total radiation on a horizontal surface, clearness number, daytime ambient average temperature, and cloudiness index K_T for each location.

The industrial process heat data base (IPHDB) is composed of entries for specific processes and contains for each of them: temperature, heat rate, and flow rate requirements; conventional fuel source and efficiency; and appropriate system types in order of applicability (3 of a possible 6). Each entry is identified as a four-digit standard industrial classification (SIC) and an optional alphanumeric character if subprocesses are given.

At the present time, 20 collectors are represented in the collector data base (COLDAT). Of these, eight have performance data derived through tests at the facilities of Sandia Laboratory, Albuquerque [4]. Both performance and cost information is given for each collector, including optical efficiency, concentration ratio, heat-loss coefficients, internal blocking and shading factors, F.O.B. costs, auxiliary costs, and installation labor. Generic collector

types represented in COLDAT include flat plate, compound parabolic concentrator, linear fresnel lens, parabolic trough, line focus, and parabolic dish.

The economic data base (ECONDAT) contains site-specific information on labor rates and conventional fuel costs, including coal, natural gas, fuel oil, electricity, and propane. Fuel costs often vary with usage amount, contract status (firm, interruptible, etc.), and use schedule. In cases where such detailed information is known, the data base values can be overridden through card input.

PERFORMANCE MODEL PROSYS

In order to assess the feasibility of solar energy for a specific industrial process, it is first necessary to calculate the amount of energy that can be delivered by the available solar equipment while satisfying the process requirements. The analytical performance model applies a method developed by Rabl and Collares-Pereira that predicts the long-term average energy delivered by several generic collector types. This procedure is based on the classical utilizability concept originated by Hottel, Whillier, Liu, and Jordan [5,6] for flat-plate collectors. Rabl and Collares-Pereira have generalized and simplified the method by including other collector types and defining the utilizability with respect to the day rather than the hour [7,8].

Collectors that are modeled include the two-axis tracking concentrator, single-axis concentrator, nontracking concentrator (compound parabolic concentrator), and flat-plate collector. The calculated deliverable energy per unit area for a single collector is adjusted to include losses normal to larger systems. Six system types are modeled, including direct hot water, fluid/water heat exchange, direct hot air, fluid/air heat exchange, flashed steam and unfired steam generator.

The analytical model is implemented in the computer program PROSYS (Process Heat System Model), yielding a tool with which a varity of solar equipment configurations can be evaluated. PROSYS is neither a dynamic simulation nor a means of detailed system design, but instead a method of predicting long-term average performance. While the nondynamic nature of the model imposes some limitations, it yields the advantages of speed and flexibility. The model provides an efficient method for preliminary appraisal of solar energy for industrial applications, a standard procedure to compare generic collector types, and a rapid means of performing a large number of parametric studies.

ECONOMIC EVALUATION ECONMAT

The basic calculation of the economic analysis is the estimation of the total solar equipment cost. To allow comparison of systems differing in size and annual energy output, an energy capacity cost [$/(GJ/yr)] is calculated by dividing the total equipment cost by the annual delivered energy. Additional economic evaluation may include calculation of life-cycle levelized energy cost, net present value, simple payback period, and break-even fuel price [9,10].

The computer program ECONMAT implements the analysis using the precalculated performance data from PERFDAT, the collector costs from COLDAT, and labor rates from ECONDAT. Given the process demand heat rate and the collector peak delivery rate, the collector array is sized such that all energy supplied by the solar system is used by the process and no excess energy is produced. Total solar equipment cost is estimated including collector, auxiliary equipment, installation, and system costs.

The optional net present value analysis depends on economic factors that may vary from case to case. The software contains typical default values for economic parameters, such as 12% internal rate of return; 6% general inflation rate; 5% add-on fuel escalation rate; annual operation, maintenance, property tax, and insurance at 2% of initial investment; 50% corporate income tax rate; 20-year system lifetime; and 20% tax credit. Appropriate local fuel price is obtained from ECONDAT. All default economic factors, including fuel price and labor rate, may be overridden by user input.

To allow system size variation for a specific process and to demonstrate the economy of scale effect, all calculations are shown for ten incremental energy levels. A large number of computations are required to evaluate each process-system-collector combination at ten energy increments, and a large output results. To facilitate analysis, an option is provided to print only the results for the most economic collector per system.

ANALYTICAL RESULTS

The analytical tools PROSYS/ECONMAT allow comparison of a variety of collectors for diverse process requirements and quick selection of the solar equipment most suitable in both cost and performance for a specific process. The software can be used for many types of analysis merely by varying the information in the data bases. A ranking of solar IPH applications for a given location can be generated by using an IPHDB containing average parameter values for many "typical" industrial plants. Conversely, actual case studies that provide detailed process breakdown, preheat potential, and/or process reconfiguration can be analyzed with an IPHDB containing specific process data.

A subprocess can be characterized and its solar potential appraised over the entire U.S. region in an in-depth analysis. For example, consider a pastuerization process at 169°F operating six days per week, producing approximately 3000 gal/hr, with process heat provided by a conventional steam boiler at 65% efficiency. Evaluation of solar process heat provided by horizontal parabolic trough collectors tracking about the N-S axis in an indirect hot water configuration was performed for 27 locations [11]. Figure 4 shows the required fuel price in 1979 $/MBtu for a 10-year payback for 1979, 1985, and 1990 system start-up times.

An assortment of parametric sensitivity studies can be performed, including studies of the effects caused by changes in collector characteristics, costs, and economic factors. A comparison of the performance of five collector types over a range of temperatures is illustrated graphically in Fig. 5.

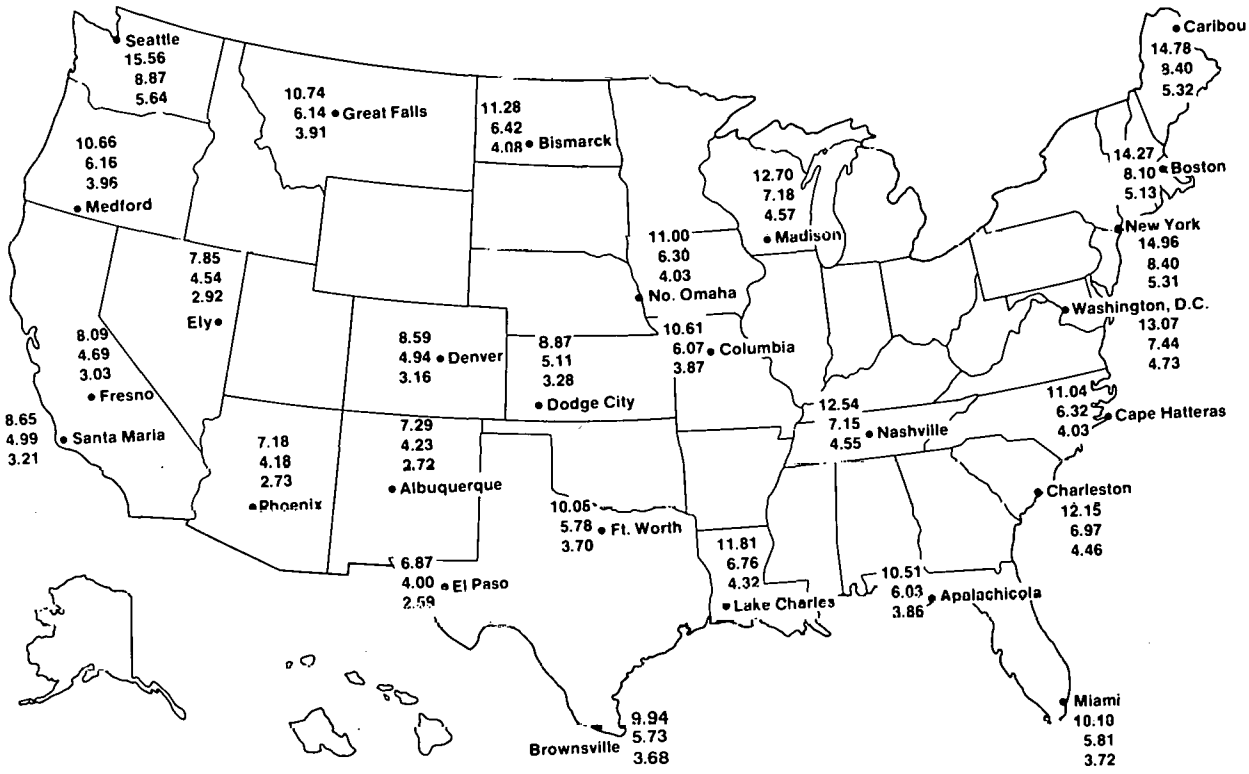

Figure 4. Required Fuel Price in 1979 Dollars/MBtu for a Ten Year Payback.
(Upper Number—1979 Startup: Middle Number—1985 Startup;
Bottom Number—1990 Startup)

CONCLUSIONS

The industrial process heat sector appears to be a large potential market for solar energy applications. Because of the variety of process requirements and available solar equipment, the evaluation of solar technology for IPH is a complex procedure most easily accomplished by the use of computerized analysis. The PROSYS/ECONMAT software was originated to provide this capability.

Extensive application in end-use matching, case studies and in-depth analysis has provided excellent review and program checkout. Improvements in performance calculations and system cost estimates, and updates in collector data, will improve model accuracy. The software provides a powerful analytical tool for an efficient method in appraising the feasibility of solar technology for industrial process heat applications.

The work described herein has been sponsored by the U.S. Department of Energy under contract EG-77-C-01-4042. More complete information on this project is in a SERI report on industrial process end-use matching [12].

ACKNOWLEDGEMENT

The author gratefully acknowledges the continued advice and contributions of Ken Brown, Doug Hooker, Ken May, and Ron West in the development of PROSYS/ECONMAT.

REFERENCES

1. Copeland, R. J., Technology Development Needs for High Temperature Process Heat, SERI/TR-35-047, Solar Energy Research Institute, Golden, CO, August 1978.

2. Fraser, M. C., Analysis of the Economic Potential of Solar Thermal Energy to Provide Industrial Process Heat, ERDA/InterTechnology No. 00028-1, InterTechnology Corporation, Warrenton, VA, 1977.

3. Cinquemani, V., Input Data for Solar Systems, USCOMME-NOAA-Asheville, N.C. 12/78/1000, National Climatic Center, Asheville, NC, November, 1978.

4. Dudley, V. E., Summary Report: Concentrating Solar Collector Test Results, Collector Modular Test Facil-

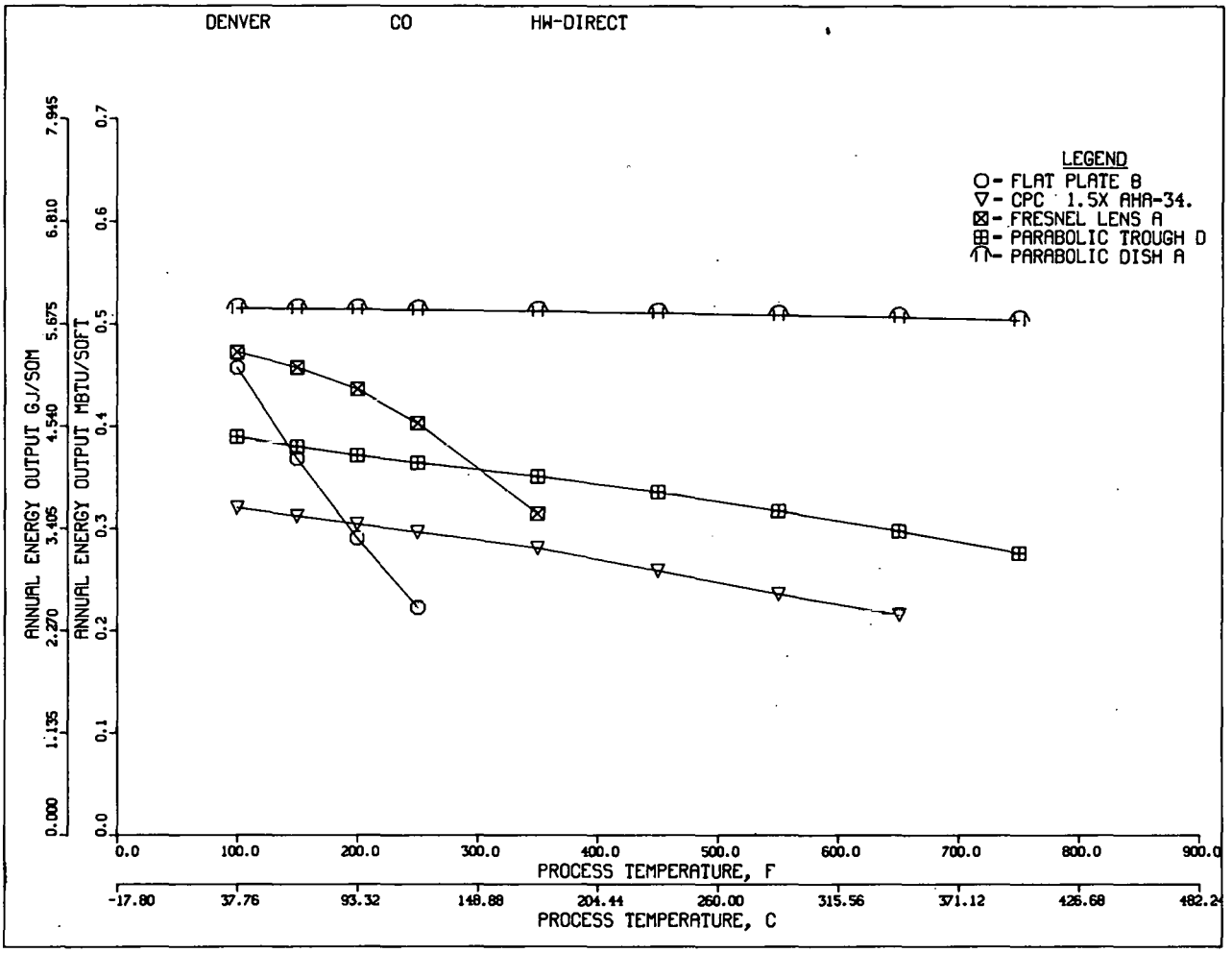

Figure 5. Annual Energy Output of Several Collector Types over a Range of Temperatures

ity, SAND 78-0815, Sandia Laboratories, Albuquerque, NM, May, 1978.

5. Hottel, H. C. and Whillier, A., "Evaluation of Flat-Plate Solar Collector Performance," Transactions of the Conference on the Use of Solar Energy: The Scientific Basis, Vol. II, Part I, Section A, pp. 74-104 (1955).

6. Liu, B. Y. H. and Jordan, R. C., "A Rational Procedure for Predicting the Long Term Average Performance of Flat-Plate Solar-Energy Collectors," Solar Energy 7, 53 (1963).

7. Collares-Pereira, M. and Rabl, A., "Simple Procedure for Predicting Long Term Average Performance of Nonconcentrating and of Concentrating Solar Collectors," Solar Energy 23, No. 7 (1979).

8. Collares-Pereira, M., and Rabl, A., "Derivation of Method for Predicting Long Term Average Energy Delivery of Solar Collectors, Solar Energy 23, No. 7 (1979).

9. Dickinson, W. C. and Freeman, H. J., An Economic Methodology for Solar Assisted Industrial Process Heat Systems: The Effects of Government Incentives, UCRL-52254, Lawrence Livermore Laboratory, Livermore, CA, June 1977.

10. Dickinson, W. C. and Brown, K. C., Economic Analysis of Solar Industrial Process Heat Systems: A Methodology to Determine Annual Required Revenue and Internal Rate of Return. UCRL-52814. Livermore, CA: Lawrence Livermore Laboratory, August 1979.

11. Brown, K. C. et al., Industrial Applications Analysis, Market Characterization and System Definition for Several Industries, Proceedings 1979 Industrial Process Heat Conference, SERI/TP-353-467, Solar Energy Research Institute, Golden, CO, Oct. 1979.

12. Brown, K. C., et al., End-Use Matching for Solar Industrial Process Heat, SERI/TR-34-091, Solar Energy Research Institute, Golden, CO, Jan. 1980.

NOTES

COMPUTER-AIDED SOLAR THERMAL SYSTEMS ANALYSES FOR INDUSTRIAL PROCESS HEAT (IPH) APPLICATIONS

S. Sundaram, C. F. Roos and B. G. Eldridge
Jacobs-Del Solar Systems, Inc.
251 South Lake Avenue
Pasadena, California 91101

ABSTRACT

We have developed a computer-simulation program to analyze our approach to the solar production of industrial process heat. Ours is a modular program--or system of programs--which offers several advantages over other simulation programs. It is easy to learn, requires little debugging and reduced run time, and provides its analysis at a lower cost than do other such programs developed by universities and the national laboratories to study solar thermal energy systems. It enables us to study all aspects of the solar production of industrial process heat, as well as space heating and cooling. The system, Solar Thermal Systems Simulation (STSS), uses an IBM System VM370 under CMS environment; it is written in FORTRAN IV. STSS, which includes main programs, subroutines and data files, will be validated and refined during the operation of a Jacobs-Del Solar Systems, Inc. project. This DOE-funded project, a demonstration of the solar production of industrial process steam, is being conducted at The Home Laundry in Pasadena, California.

INTRODUCTION

Supplying low- to intermediate-temperature process heat (200^{o}-600^{o} F) for industrial use in the United States requires roughly 4×10^{15} BTU/year, which is approximately 5% of the nation's total energy consumption. The need to supplement existing, Industrial Process Heat energy sources with a source which is virtually non-depletable, such as solar energy, is acute; our fuel consumption rate is growing 3% per year, and our production of crude oil and natural gas is declining.

Solar systems are now being used for some Industrial Process Heat applications. We at Jacobs-Del Solar Systems, Inc. have developed a computer-simulation program to analyze our approach to the solar production of Industrial Process Heat. Ours is a modular program, or system of programs, which enables us to study all aspects of the solar production of IPH, as well as space heating and cooling. This paper describes the analytical basis for the development of the STSS, which will be validated and refined during the operation of a DOE-funded demonstration project at The Home Laundry in Pasadena, California.

SIMULATION MODEL

The Solar Thermal Systems Simulation Model will allow us to evaluate candidate solar systems and, eventually, to achieve an economically competitive IPH system which will offer both significant energy savings and environmental advantages. A functional diagram of the STSS is shown in Figure 1.

The three major components of the STSS are a field performance program, a thermal losses in pipes and equipment program and an economics program. The field performance program determines the amount of usable energy which an array can collect under varying conditions. The second STSS program estimates thermal losses in pipes and storage tanks during a 24-hour day. The STSS economics program considers factors such as capital investment, life expectancy, operating and maintenance costs, taxes, functional efficiency, etc. in the process of evaluating an IPH system.

The Field Performance Program

The field performance program determines the amount of usable energy an array can collect under varying conditions. These conditions can be categorized into three groups: the first group includes those conditions which affect collector efficiency; the second group is composed of conditions which affect one collector by itself, and the third group covers the conditions of interrelationships of all of the collectors within the array. Direct solar radiation, ambient temperature, inlet and outlet fluid temperatures and wind velocity over the receiver tube are first-group conditions. The conditions in the second group are collector orientation, tilt angle, length, etc. The third group of conditions are those which determine the effect of one row of collectors on the next row: orientation, tilt angle, spacing between collectors, width of collectors, physical dimensions of collectors, size and latitude of the array.

Many of the above conditions vary hourly; consequently, values are computed hourly and summed daily, monthly and annually by the STSS. Average hourly values for different months are computed and printed.

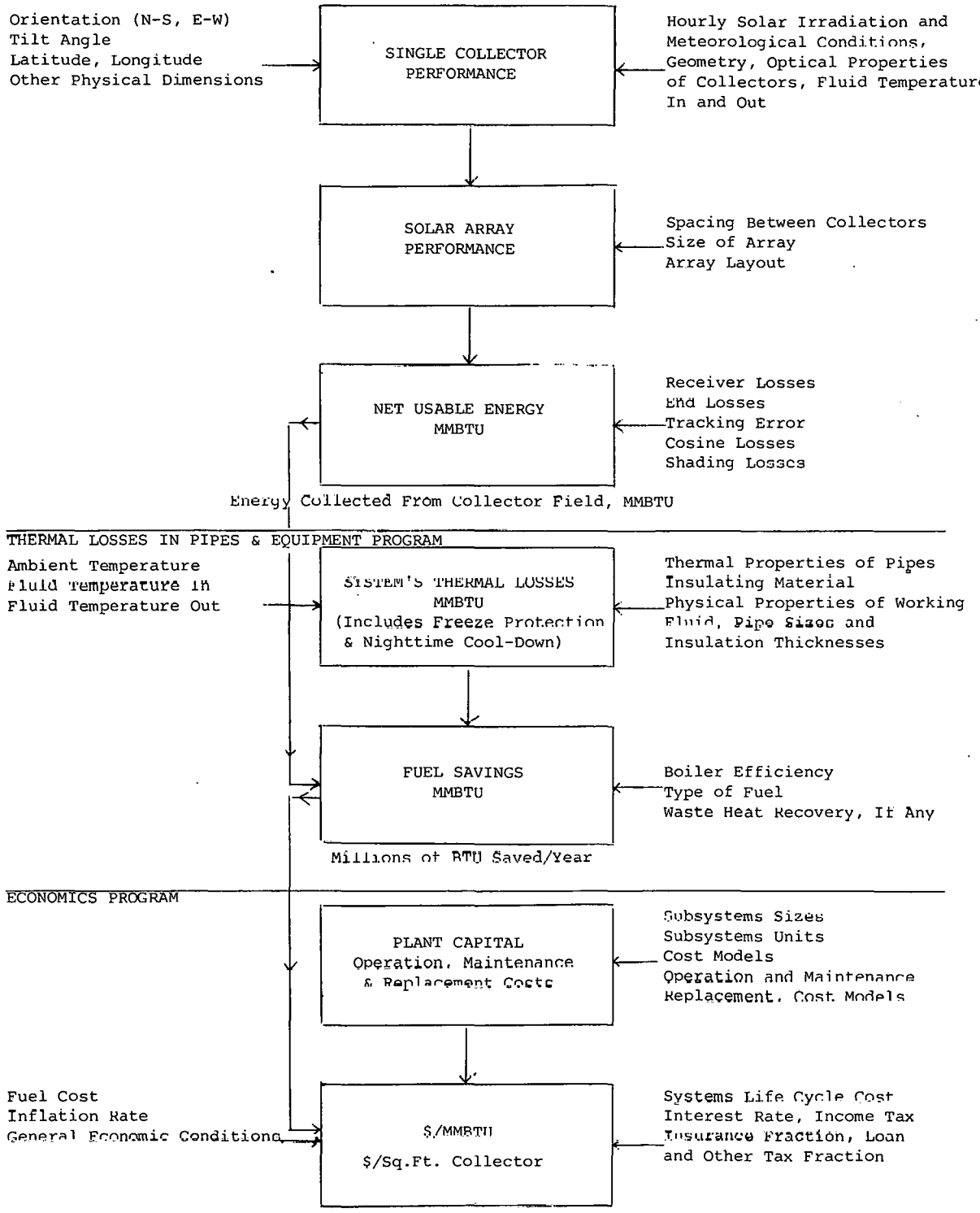

Figure 1. STSS Computer Program Flow Chart

Receiver Tube Losses. We have developed a heat transfer model for receiver tube losses. It considers the annulus, i.e., the gap between the absorber tube and the glass envelope, as well as the gap pressure. The analytical factors which were considered in the model are described in the following discussion.

The receiver tube is subject to heat losses from the absorber tube due to convection and radiation, from the glass wall as a result of conduction, and from the outside of the glass because of convection and radiation. If the annular gap is small, conduction losses are large; if the annular gap is large, convection losses are large. Therefore, it calculates the optimal gap width to balance these losses. Evacuation of the annular gap limits heat loss to radiative energy loss only and eliminates the effect of wind on receiver heat loss. This is applicable for evacuated receiver tubes.

Cosine, End and Shading Losses; Tracking Error. The STSS computes the sun's position hourly. Altitude and azimuth angles provide data to compute the angle of incidence over the end of the collector. From the angle of incidence, cosine losses, end losses and end shading losses are determined based on the physical dimensions of the collector. These losses pertain to each collector and are expressed per square foot of collector. For parallel rows of collectors, these factors are independent of orientation, spacing, tilt angle and width of collector.

Tracking error is taken into account by considering the intercept factors--the amount of solar energy expected to hit the receiver tube, as predicted by manufacturing tolerances.

The Thermal Losses in Pipes and Equipment Program

We have developed subroutines to estimate a solar system's 24-hour thermal losses through insulated pipes during three time periods or modes of operation: warm-up mode, solar energy collection mode and nighttime cool-down mode. Two programs, STEADY STATE and QUASI-TRANSIENT, cover the different operational conditions which exist during the three modes. We have implemented the model in FORTRAN IV on the IBM System VM370 under CMS environment.

The STEADY STATE program calculates heat losses during the solar energy collection mode; the QUASI-TRANSIENT program approximates the variations of fluid temperature characteristic of the cool-down and warm-up modes of operation.

The Economics Program

The STSS Economics Program evaluates factors such as system capital investment, finance charges, insurance rates, fuel savings, depreciation, energy tax credits (state and federal), life expectancy, operating and maintenance costs, etc.

CONCLUSION

The advantages of the STSS over other simulation models were enumerated earlier. In addition to these operational considerations, we are pleased by the fact that analysis of the engineering and cost data provided by the STSS model during its period of operation at The Home Laundry will permit us to improve system design and to decrease system cost. This, certainly, will foster the commercialization of process heat applications. The data gathered should also provide justification for much-needed reform of tax policies applicable to solar systems.

ACKNOWLEDGMENTS

The study leading to this report was supported by the Basic Resources Division of the Jacobs Engineering Group, Pasadena, California.

REFERENCES

1. M. W. Edenburn and N. R. Grandjean, "Energy System Simulation Computer Program--SOLSYS," Sandia Laboratories, Albuquerque, New Mexico, SAND75-0048, June 1975.

2. M. E. Fewell and N. R. Grandjean, "User's Manual for Computer Code SOLTES-1, Simulator of Large Thermal Energy Systems," Sandia Laboratories, Albuquerque, New Mexico, June 1979.

3. A. C. Ratzel, et. al., "Techniques for Reducing Thermal Conduction and Natural Convection Heat Losses in Annular Receiver Geometrics," Heat Transfer in Solar Energy Systems, ASME Winter Annual Meeting, Atlanta, Georgia, pp. 17-24, November 1977.

4. D. Q. Kern, Process Heat Transfer, 1st Edition, pp. 20-25, McGraw Hill, New York (1950).

5. S. Sundaram, C. F. Roos and B. G. Eldridge, "Solar Systems Losses Through Insulated Pipes," To be communicated.

6. E. F. Nogotov, Applications of Numerical Heat Transfer, 1st Edition, McGraw Hill, New York (1978).

NOTES

FLAT-PLATE PHOTOVOLTAIC ARRAY SIMULATION AND DESIGN ANALYSIS*

R. W. Weaver**
Jet Propulsion Laboratory
Pasadena, California

ABSTRACT

As part of the Jet Propulsion Laboratory's Low-cost Solar Array Project, a comprehensive program of flat-plate solar array design and cost optimization has been carried out. The objectives of these studies have been to improve reliability and reduce costs of arrays. Two simulation methodologies were developed. The first allows the analyst to determine the probable power loss due to cell or module failure for various array circuit designs. This method has been computerized and used to analyze various circuit designs with differing levels of series/paralleling. The second method was developed to determine the life-cycle cost of energy produced by a specific system design. This simulation also indicates which failure replacement strategy should be used to insure minimum life-cycle cost.

INTRODUCTION

The objective of the design analyses performed by the Jet Propulsion Laboratory's Low-Cost Solar Array Project is to determine the minimum life-cycle cost of energy produced by photovoltaic arrays. Two prime elements of life-cycle cost are the costs associated with building and operating the system and the amount of energy produced by the system over the period being considered. These elements vary with the type of application.

The energy produced by a photovoltaic (PV) system is a function of the solar energy incident upon the array over the life of the array and the series/parallel electric network design. Considerable work has been done to determine the array tilt angle and azimuth setting to optimize the incident solar energy. Those results are incorporated into this analysis. An analysis of the series/parallel electric network was performed to determine the energy losses as a function of the cell failure rate, module size and network design. This analysis was performed using a computer program that simulates PV modules with various series/parallel connections and computes the resulting current-voltage curves based on the above factors.

The results of power loss analysis and the estimated costs are used in a life-cycle cost determination program. The minimum life-cycle energy cost is used as the final criterion to define optimum network design and replacement strategy. This analysis directly integrates array structures costs, panel costs, module costs, replacement strategies, series/paralleling tradeoffs, module size tradeoffs, cell reliability performance, and several other factors. The conclusions presented provide design guidelines for future flat-plate photovoltaic modules.

CIRCUIT DESIGN

The analysis of array circuit designs is an important step in the development of design guidelines for PV systems. Component reliability and fault-tolerant designs are critical in the production of low-cost energy, particularly in a relatively complex developing technology. The design of PV array circuits must therefore take into account the probability of circuit component failures and provide a means for minimizing energy losses when failures do occur.

Definitions

A PV module consists of solar cells electrically connected in series and/or parallel. A string of cells connected in a pure series arrangement is referred to as a series string or substring. When series strings are wired in a parallel configuration, they are called parallel strings and a group of parallel strings connected at their end points is called a series block. Modules are grouped together in panels for structural purposes, forming an array. A branch circuit is composed of a group of series blocks between the positive and negative termination points of a power conditioner. Therefore, an array is a collection of branch circuits. The series blocks may be whole modules or parts of modules. In the former case, series blocks are connected by

* This paper presents the results of one phase of research conducted at the Jet Propulsion Laboratory, California Institute of Technology, and sponsored by the U. S. Department of Energy, through an agreement with NASA.
**Member Technical Staff, Low-cost Solar Array Project, Energy Technology Engineering Section .

connectors external to the modules; in the latter, some series blocks are connected by internal module wirings, while groups of series blocks are connected externally. No distinction is made in the type of connections involved in this discussion. Figure 1 presents examples of a module and a branch circuit using the above definitions.

Failure Probabilities

Since PV technology is still in the developmental stage, methods and techniques of cell and module production are continually changing. For this reason long-term in-service data regarding the rate of failure of various array components do not exist, and failure probabilities must be treated parametrically. Open-circuit failures result in the largest power loss per failure and are therefore the only type considered here.

For any given circuit design all failures are considered to have a binominal distribution. The following steps are used to determine the probabilities of various states of array failure.

The appropriate substring failure density to be used for a given array design is determined from the following equation:

$$F_{ss} = 1 - (1-F_c)^{N_c} \qquad (1)$$

where:

F_{ss} = substring failure density

F_c = cell failure density

N_c = number of cells per substring

The relationship between cell failure density and substring failure density is shown in Fig. 2. An increase in the number of cells per substring for a fixed cell failure density results in an increase in the probability that a substring will fail. When a particular circuit design is to be analyzed, the number of cells per substring, the cell failure density and the substrings per series

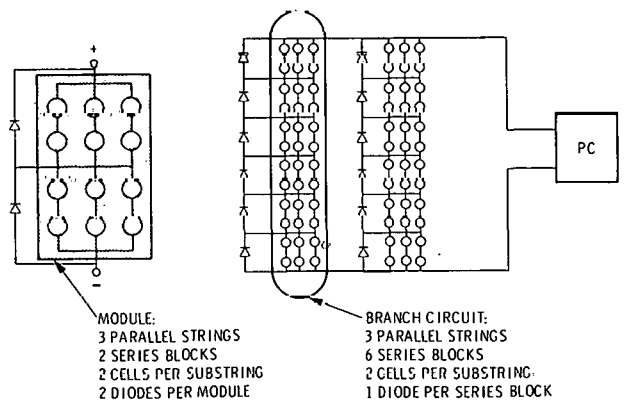

Fig. 1. Series-Parallel Nomenclature

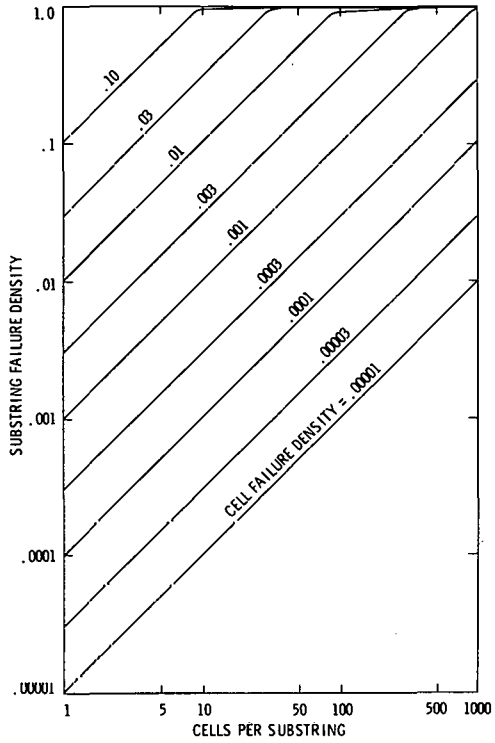

Fig. 2. Cell Failure Density as a Function of Substring Failure Density

block are specified. The number of substrings that fail within a series block governs the power output of the branch circuit and thus of the whole array. The effect of increased substring failure density on the number of substrings failed within a series block are shown in Fig. 3 for a series block containing 8 substrings. As the substring failure density increases the probability of additional substring failure increases.

Using the above failure probability technique, the state of failure of a branch circuit can be defined for any specific circuit design. The results are used in the circuit simulation program to determine the power losses due to failures as a function of substring failure density.

Circuit Simulation and Power Loss

The circuit simulation method involves the use of a computer model with appropriate statistical analyses to calculate cell and module I-V curves based on the following equation:

$$I = I_{sc}\left(1 - e^{\left(\frac{1.74}{0.87 - FF}\right)\left(\frac{V}{V_{oc}} - 1\right)}\right) - \frac{V}{R_{sh}} \qquad (2)$$

where:

I = current of element at voltage V

I_{sc} = short-circuit current

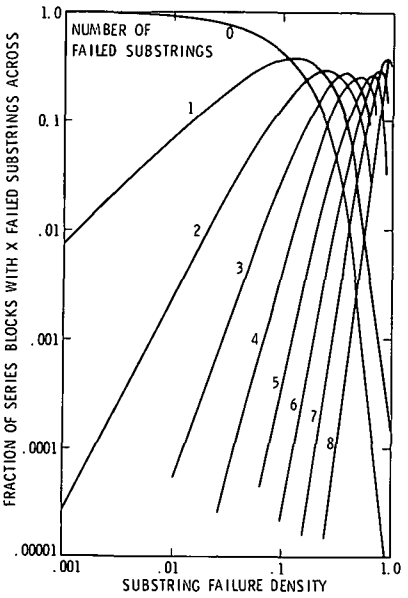

Fig. 3. Fraction of Series Blocks as a Function of Substring Failure Density, Eight Substrings Total

FF = fill factor

V_{oc} = open-circuit voltage

R_{sh} = shunt resistance

The photovoltaic parameters are those commonly measured for cells and modules.

The computer model simulates various circuit designs with and without bypass diodes by adding the I-V curves of the component elements. An element is any cell or combination of cells located in a module or branch circuit. Failures can be introduced by adding I-V curves of the elements containing the types of failures being considered.

The locations of multiple failures are significant when the number of failures is not large enough to saturate the array system. Thus, the most likely location of multiple failure has an important effect on array performance. The statistical treatment of failure location has been performed in conjunction with the computer model but not internal to it. The output of the statistical model is used to define the number of cells most likely to fail for a given wiring configuration.

The output of the circuit-design computer model provides the I-V curve of the resultant combination of elements along with the maximum power of the combination. These results are combined with a statistical evaluation of the state of a given photovoltaic system to determine the most probable power output under given failure rates.

For each state of the system the branch circuit power loss fraction is plotted as in Fig. 4.

The array power loss is determined by summing the power losses for branch circuits having one failed substring, a maximum of two failed substrings, and so on. In the summation each power loss is weighted by the fraction of branch circuits having series blocks (at least one) with a maximum of the corresponding number of failed substrings. In other words, this fraction of branch circuits will have series blocks with numbers of failed substrings up to and including the maximum.

The end result of applying this method is the generation of a family of curves giving array power degradation as a function of the number of series blocks and parallel strings per branch circuit. Power degradation is plotted against the substring failure density. An example of this is shown in Figures 5 and 6 for the case of eight parallel strings. The two figures allow a comparison of the results obtained with and without bypass diodes. Similar results have been generated for branch circuits with one, four and 16 parallel strings and for different diode placement. For a more detailed discussion of this simulation methodology see Ref 1.

LIFE-CYCLE COST

The life-cycle cost methodology provides a means of integrating the results from a variety of diverse flat-plate solar array design studies and to draw conclusions relative to optimum module and array mechanical and electrical circuit configurations. Because of the strong interaction between module size and replacement cost, any analysis of module size must also consider the expected degree and timing of module replacement. This is further tied to the entire question of module reliability, definition and module failure and replacement criteria, and reliability engineering features, such as series/parallel, bypass diodes, and redundant solar cell electrical contacts.

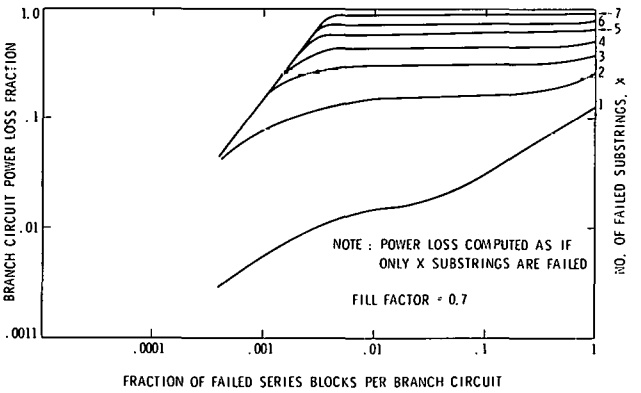

Fig. 4. Branch Circuit Power Loss as a Function of Failed Series Blocks for Eight Parallel Strings, Without Diodes

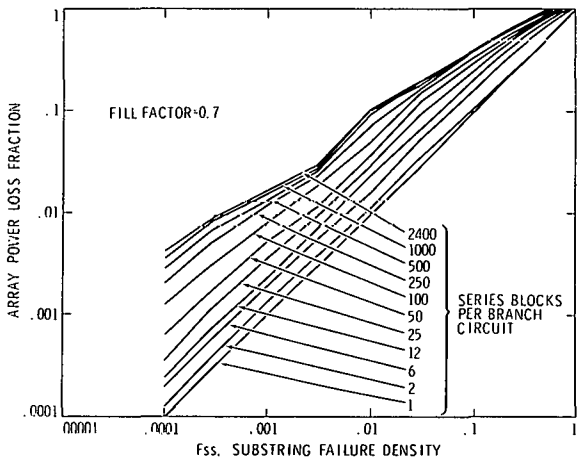

Fig. 5. Array Power Loss as a Function of Substring Failure Density, for Eight Parallel Strings, Without Diodes

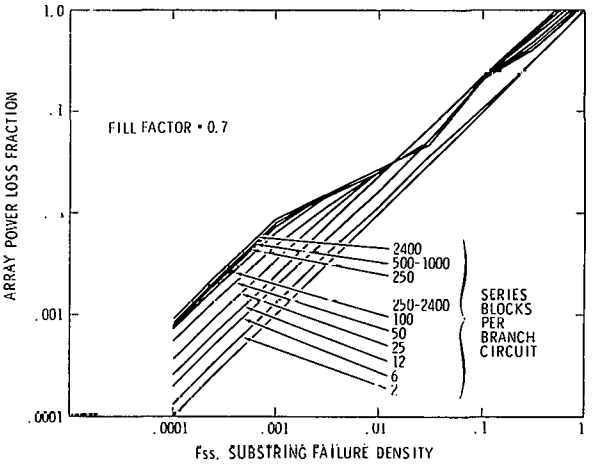

Fig. 6. Array Power Loss as a Function of Substring Failure Density, for Eight Parallel Strings, With One Diode per Series Block

Conversely, any analysis for the selection of optimal reliability engineering features must include consideration of replacement costs, and therefore of the size of the modular replacement unit.

In the selection of the optimum mechanical and electrical configuration for a flat-plate module for a large ground-mounted photovoltaic array, for example, complete analysis should, as a minimum, address the following interactions: 1) module superstrate (glass) thickness and material cost versus size, 2) module efficiency (perimeter area effect and encapsulant transmission) versus size, 3) module efficiency loss due to cell mismatch versus circuit configuration, 4) module assembly cost versus size and circuit configuration, 5) module manufacturing yield cost (larger modules have higher probability of containing faulty parts, but greater circuit redundancy reduces losses associated with faults), 6) module shipping and handling and installation cost versus size, 7) support structure cost versus module size and efficiency, 8) field cabling costs versus module size and efficiency, 9) system power degradation versus electrical circuit reliability as influenced by series/paralleling, bypass diodes, multiple cell contacts, etc., and 10) module life-cycle replacement cost versus module size and system power degradation. Review of these interactions indicates the complexity of the problem.

Cost Elements and Performance Parameters

Based on work carried out previously (2,3,4), the photovoltaic array cost elements were identified. Table 1 presents these elements for three different module sizes; the module is a glass solar cell sandwich with no frame.

Module yield cost is the amount that must be added to the price of a module to pay for modules scrapped during final assembly, shipping, and installation due to broken cells or circuit failures. The module failure criterion is based on controlling electrical mismatch in the array and assumes that a module is rejected if its power loss is greater than 10% of the average peak power output for all modules. The yield cost value in Table 1 is for a circuit failure density of 1 per 1000 solar cells, and is dependent on the level of module circuit redundancy.

Another important area of cost dependency involves parameters which alter module or array electrical efficiency. Changing efficiency directly leverages the total quantity of modules and the support structure required, and thus directly affects the initial plant cost. Two efficiency dependencies are important in the present analysis: a) decreased border on smaller modules (1), and b) decreased cell mismatch losses associated with high degrees of series/paralleling (3). The effect of

TABLE 1. COST DEPENDENCIES FOR ARRAY ELEMENTS

ELEMENT	UNITS (1975 $)	MODULE SIZE (ft x ft) 2 x 4	4 x 4	4 x 8
INITIAL:				
MODULE DIRECT COST	$/m^2	60	60	60
MODULE YIELD COST*	$/m^2	0-5	0-8	0-23
• MODULE SUBTOTAL	$/m^2	60-65	60-68	60-83
PANEL FRAME	$/m^2	24	18	15
PANEL WIRING	$/m^2	2-4	2-3	1-2
• PANEL SUBTOTAL	$/m^2	26-28	20-21	16-17
PANEL INSTALLATION	$/m^2	1	1	1
INSTALLED ARRAY STRUCT	$/m^2	22	22	22
• ARRAY TOTAL	$/m^2	109-116	103-112	99-123
PER REPLACEMENT ACTION:				
FAULT IDENTIFICATION	$/PANEL	4	4	4
PANEL SUBSTITUTION LABOR	$/PANEL	21	21	21
MODULE REPLACEMENT LABOR	$/MOD	12	12	12
REPLACEMENT MODULE PARTS (INC 1% INVENTORY COST)	$/m^2	61-66	61-69	61-84

*1 CELL FAILURE PER 1000 DURING ASSEMBLY/SHIPPING/INSTALLATION

these and other system performance dependencies are summarized in Table 2.

Except for the module efficiency entries, the majority of the figures in Table 2 reflect nominal values required in the life-cycle energy cost calculations and have little impact on the relative comparisons which result from the analyses. The cost elements and performance parameters along with power loss values obtained from the electric circuit simulation program are used as input to the life-cycle cost program.

Example Application

As an example application of the life-cycle cost simulation, the following circuit design is proposed:

8 parallel substrings per series block

(Cells per substring) x (number of series blocks) ≡ 2400*

Cell failure rate of 0.0001 per year

Using the life-cycle cost program, it is possible to answer the question "What fraction of the initial power remains at the end of each year if 4 ft x 8 ft modules containing 320 cells are used and no failures are replaced?"

The effects of increasing the number of series blocks are plotted in Fig. 7. The selection of one series block would result in a 50% power loss in the first three years and is therefore an unacceptable design choice. On the other hand,

TABLE 2. NOMINAL LIFE-CYCLE PERFORMANCE PARAMETERS

	MODULE SIZE (ft x ft)		
INITIAL ARRAY EFFICIENCY	2 x 4	4 x 4	4 x 8
ENCAP. CELL EFFICIENCY	0.15	0.15	0.15
NOCT EFFICIENCY	0.92	0.92	0.92
PACKING EFFICIENCY	0.89	0.91	0.93
ARRAY EFFICIENCY SUBTOTAL	0.123	0.126	0.128
BALANCE-OF-PLANT EFFICIENCY			
ELECTRICAL EFFICIENCY	0.92		
MODULE SOILING EFFICIENCY	0.92		
BALANCE-OF-PLANT SUBTOTAL	0.85		
BALANCE-OF-PLANT COSTS (1975$)	150 $/kW		
DISCOUNT RATE (OVER INFLATION)	10%		
ANNUAL INSOLATION	1825 kW-h/m^2/yr		

*This defines the voltage level of the system when the cell voltage is specified.

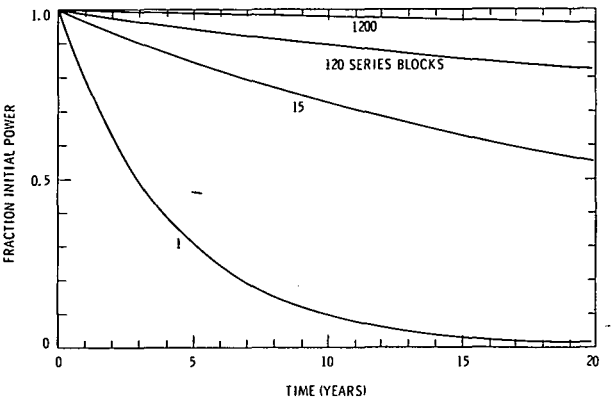

Fig. 7. Array Power Degradation for Eight Parallel-String Branch Circuits

use of the 1200 series blocks design would result in losses of only 5% over the 20-year life. The life-cycle cost of energy for this example is shown in Fig. 8.

It is apparent (Fig. 8) that the optimum configuration for an array of 4 ft x 8 ft modules in eight parallel-string branch circuits is 240 or more series blocks, with no module replacement. Figure 9 compares this result with similar results for 2 ft x 4 ft and 4 ft x 4 ft modules. As seen in Fig. 9 both smaller module sizes result in higher system energy costs because of the higher support structure cost for small modules. Also, the cost reduction due to yield-cost improvements occurs at a higher number of series blocks because of the fewer cells per module. If, for some

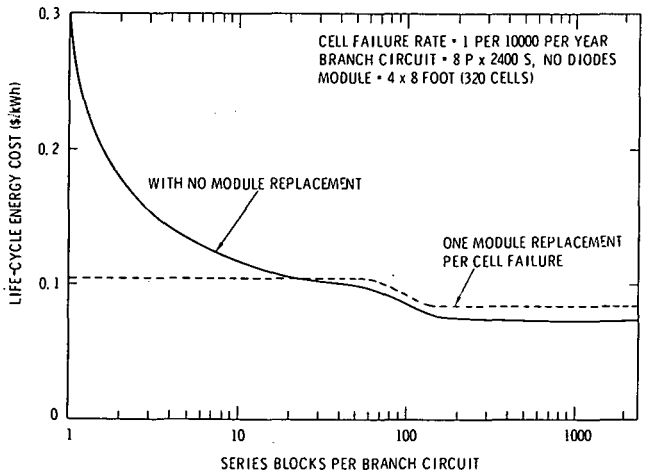

Fig. 8. Life-Cycle Energy Costs for Eight Parallel-String Branch Circuits

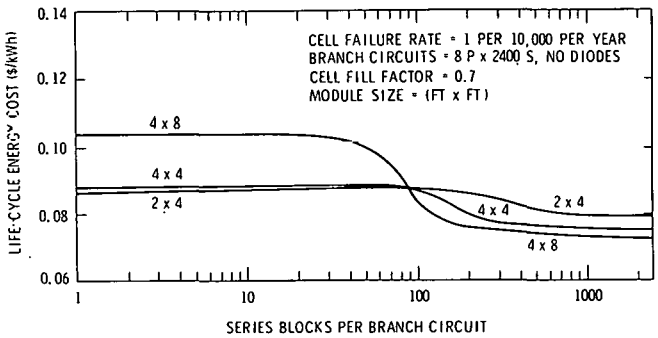

Fig. 9. Minimum Life-Cycle Energy Costs for Various Module Sizes

reason, a low degree of series/paralleling is utilized together with a full replacement strategy, the smaller modules are preferred over the larger 4 ft by 8 ft modules. This is because of the higher replacement cost for large modules and the similarly higher yield costs when no module internal series/parallelling can be utilized.

Figure 10 illustrates the key argument against the adoption of this low-series/paralleling, full-replacement strategy by indicating the effect of a higher cell failure rate. As can be seen, the low series/paralleling configurations are much more sensitive to higher-than-expected failure rates than are the high series/paralleling configurations.

The effects of varying other circuit design factors are shown in Figs. 11 through 13. In Fig. 11 the fill factor of the cells in the circuit was varied and the results indicate that the lower of the two tends to be better for optimization purposes. Figure 12 depicts the effects of varying the number of substrings in parallel in a series block and Fig. 13 shows the effects of utilizing bypass diodes in the circuit. An indepth discussion of the life-cycle cost simulation method for design optimization can be found in Ref. 5.

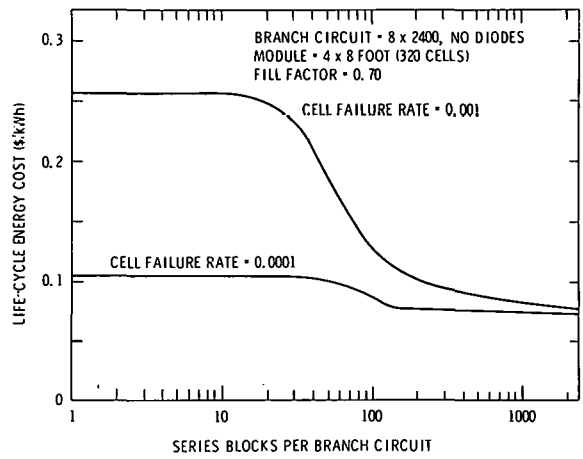

Fig. 10. Minimum Life-Cycle Energy Cost Versus Failure Rate

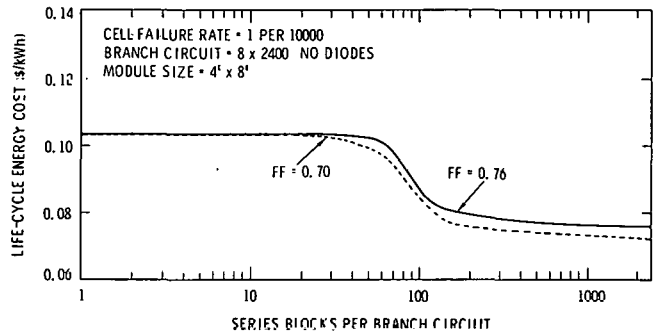

Fig. 11. Minimum Life-Cycle Energy Cost Versus Cell Fill Factor

CONCLUSIONS

The techniques described herein are proving to be very useful in analyzing photovoltaic designs. The simulation methodologies are sufficiently accurate to provide comparative results for the design selection process. Specific design guidelines drawn from this work are:

(1) The fewer cells that are connected in substrings the smaller the power loss per expected failure.

(2) The paralleling of substrings further reduces power loss when a large number (greater than $\approx$ 100) of series blocks are employed.

(3) The use of bypass diodes reduces cell overheating when failures occur.

(4) Increasing the number of series blocks per branch circuit reduces the life-cycle cost.

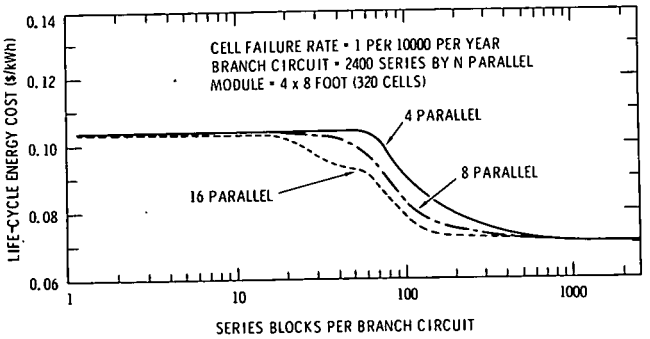

Fig. 12. Minimum Life-Cycle Energy Cost Versus Degree of Paralleling

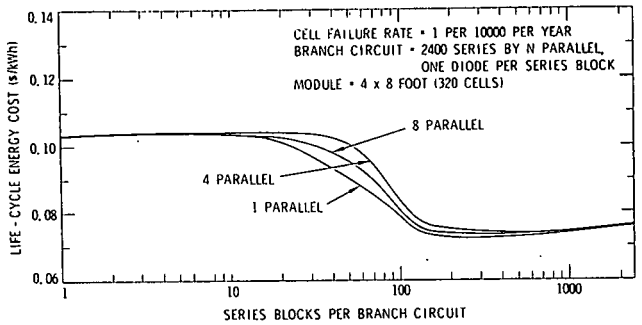

Fig. 13. Minimum Life-Cycle Energy Cost with Bypass Diodes

REFERENCES

1. C. Gonzalez, and R. Weaver, "Circuit Design Considerations for Photovoltaic Modules and Systems," presented at 14th IEEE Photovoltaics Specialists Conference, San Diego, California, January 7-10, 1980.

2. Bechtel Corporation, "Engineering Study of the Module/Array Interface for Large Terrestrial Photovoltaic Arrays," Final Report prepared for Jet Propulsion Laboratory under contract number 954698, June 1977.

3. Bechtel National, Inc., "Module/Array Interface Study," Final Report prepared for Jet Propulsion Laboratory under contract number 954698, August 1978.

4. R. G. Ross, Jr., "Photovoltaic Design Optimization for Terrestrial Applications," Proceedings of 13th IEEE Photovoltaics Specialists Conference, Washington, D. C., June 5-8, 1978, pp. 1067-1073.

5. R. G. Ross, Jr., "Flat-Plate Photovoltaic Array Design Optimization", presented at 14th IEEE Photovoltaic Specialists Conference, San Diego, California, January 7-10, 1980.

NOTES

METHOD FOR PREDICTING LONG-TERM AVERAGE PERFORMANCE OF PHOTOVOLTAIC SYSTEMS

Y. Gupta and S. Young
Science Applications, Inc.
8400 Westpark Drive, McLean, VA 22102

ABSTRACT

Based on the utilizability concepts of Liu and Jordan, an analytic model has been developed to predict the long-term average performance of grid-connected photovoltaic power systems. In contrast with hourly simulation, the methodology utilizes insolation probability distributions and correlations to evaluate long-term PV system performance, including energy flows from array directly to load, through storage to load, and to the utility for sellback systems. The method has been validated by comparison with hourly simulation results and can be adapted for rapid computer simulation or for hand-held programmable calculators.

INTRODUCTION

Based on the utilizability concepts of Hottel, Whillier, and Liu and Jordan, an analytic model has been developed to predict the long-term average performance of grid-connected PV systems. This model stands in contrast to other PV system evaluation techniques. Clear day and/or average day methods for estimating solar system performance result in large errors because they do not address the day-to-day stochastic fluctuations of insolation. Hourly simulation methods, on the other hand, provide detailed information but require extensive computer evaluations over many years to average yearly weather fluctuations of 10 percent or more, and the hourly meteorological data that is required may not be available in many locations. Moreover, hourly simulation methods require a significant amount of expertise and expense which often precludes their use for the design of small systems. As a result, solar thermal system designers have long used utilizability methods based on statistical correlations of long-term insolation probability distributions developed by Hottel, Whillier, and Liu and Jordan. However, these methods do not directly apply to PV systems since the collector efficiency relations are significantly different, and the match between array output and load demand is extremely important, particularly for utility sellback configurations. This paper derives a methodology for integrating insolation probability distributions to estimate photovoltaic system performance for design purposes.

METHODOLOGY OVERVIEW

The method adapts the utilizability techniques of Liu and Jordan [1] to estimate for each month, the long-term performance of the photovoltaic system, including array output, energy flows from array directly to load, and energy flows through storage to the load or to the utility for sellback. The monthly performance results can then be used in a conventional present worth analysis to determine system economics and sizing. An overview of the methodology is provided in Fig. 1.

Inputs for the methodology consist of monthly meteorological data, photovoltaic system parameters, load data, and economic data. Compared to a detailed hourly simulation, the Liu and Jordan approach has the advantages of automatically averaging over yearly fluctuations, of requiring only monthly rather than hourly meteorological data, and of being computationally much simpler. Elements of the methodology are described below.

WEATHER DATA

Weather data required for the methodology consists of monthly values of average daily total horizontal radiation $\bar{H}$, average clearness index

$$\bar{K} = \bar{H}/H_o \qquad (1)$$

(where H_o is the daily extraterrestrial horizontal radiation), average daytime temperature $\bar{T}$, and average wind speed $\bar{W}$. The radiation data are required to estimate hourly insolation on the collector, and the temperature and wind speed data are used to estimate array efficiency. The clearness index $\bar{K}$ characterizes cloudiness and atmospheric transmittance and provides a basic correlating parameter for estimating diffuse radiation and insolation probability distributions. Additional weather data may be required to determine electric loads; presently, load data are assumed as an input.

INSOLATION MODEL

The insolation model estimates hourly horizontal radiation and diffuse radiation based on correlations developed initially by Liu and Jordan [1] and later extended by Collares-Pereira and Rabl [2].

The first step is to separate total radiation into its direct and diffuse components. Figure 2 plots the ratio of daily horizontal diffuse radiation H_d to daily horizontal total radiation H as a function of the daily clearness index K. The solid curve represents the average value of H_d/H to be expected

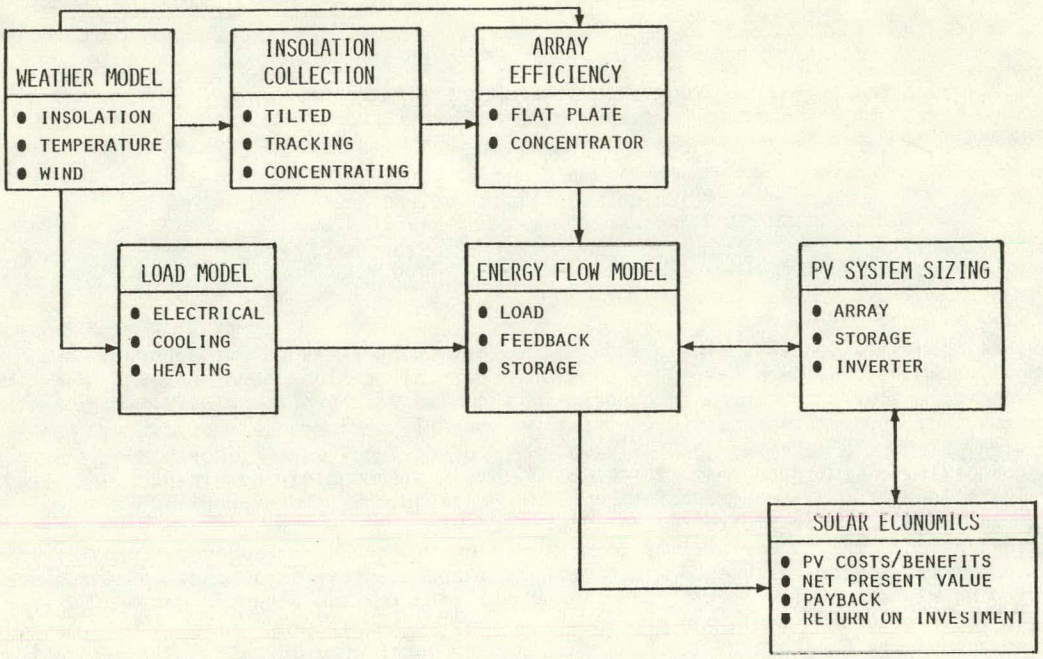

Fig. 1. Methodology Overview for Evaluation of Photovoltaic Power Systems

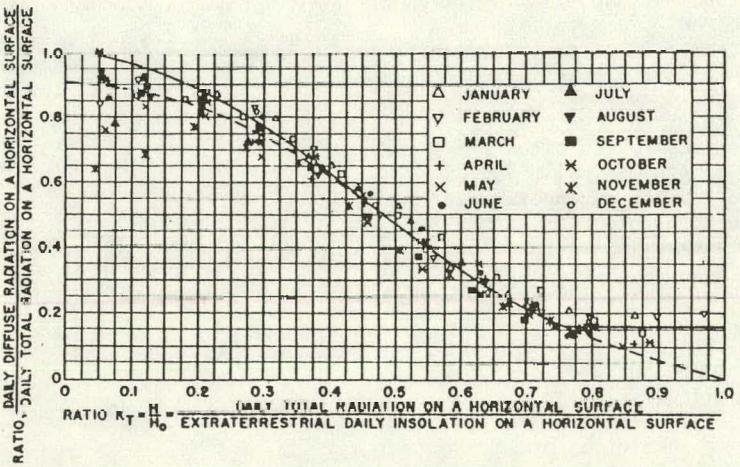

Fig. 2. Diffuse Radiation Correlation [2]

Liu and Jordan [1] have developed generalized probability distribution curves which characterize the fraction of days which occur with different amounts of insolation. They have shown that the form of these curves depends only on the value of the average clearness index $\overline{K}$. Figure 4 shows, for each $\overline{K}$, a plot of K versus the cumulative fraction F of days having total horizontal radiation which does not exceed the corresponding K value. In probability notation, the cumulative distribution function F(x) is defined for each month as:

$$F(x) = \text{Prob}\{K \leq x\} \tag{10}$$

and is characterized by the single parameter $\overline{K}$. It should be noted that by definition of expectation, the distribution function must satisfy:

$$\overline{K} \equiv \mathcal{E}(K) = \int_0^1 dF \bullet K(F) \tag{11}$$

where K(F) is K as a function of F in Fig. 4. Based on the probability distribution F and the insolation correlations given previously, it is possible to compute the average daily radiation incident on the collector by integrating the expected hourly radiation over time t and over the distribution of daily K values:

$$\overline{I} = \int_{-t_s}^{t_s} dt \int_0^1 df \bullet \mathcal{E}[i(t)|K] \tag{12}$$

where i(t) is a function of $r(t)$, $r_d(t)$, $q(t)$, $q_d(t)$, H, and H_d; and H and H_d are functions of K=K(F) which in turn is a function of F. The integration is performed using Simpson's rule, with linear interpolation of the K(F) values provided in Table 5 of Liu and Jordan [2]. The array electrical output is then $A \cdot \overline{\eta} \cdot \overline{I}$, where A is the array area.

The electric energy output of the array may at times exceed the on-site electric demand. Because the electric energy used directly for on-site loads is valued differently from excess energy which is sold back to the utility (or sent to battery storage with an efficiency loss), it is necessary to compute the solar excess fraction, i.e. the fraction of the array electrical output which exceeds the demand and is available for sellback or for storage. The expected value of the daily excess fraction is given by:

$$\mathcal{E}(EF) = \frac{1}{A\eta\overline{I}} \bullet \int_{-t_s}^{t_s} dt \; \mathcal{E}[A\eta i(t) - d(t)]^+, \tag{13}$$

where $A\eta i(t)$ represents the electrical output of the array at time t, d(t) is the daily electric demand at time t, and the plus sign indicates that only the positive part (i.e., the excess) contributes to the expectation. Rearranging terms and expresssing the expectation in terms of the F curves yields:

$$\mathcal{E}(EF) = \int_{-t_s}^{t_s} dt \bullet \frac{\overline{i(t)}}{\overline{I}} \bullet \phi(t) \tag{14}$$

where $\phi(t)$ is given by

$$\phi(t) = \int_0^1 dF \bullet \mathcal{E}\left[\left(\frac{i(t)}{\overline{i(t)}} - \frac{d(t)}{A\eta\,\overline{i(t)}}\right)^+ \Big| K\right]. \tag{15}$$

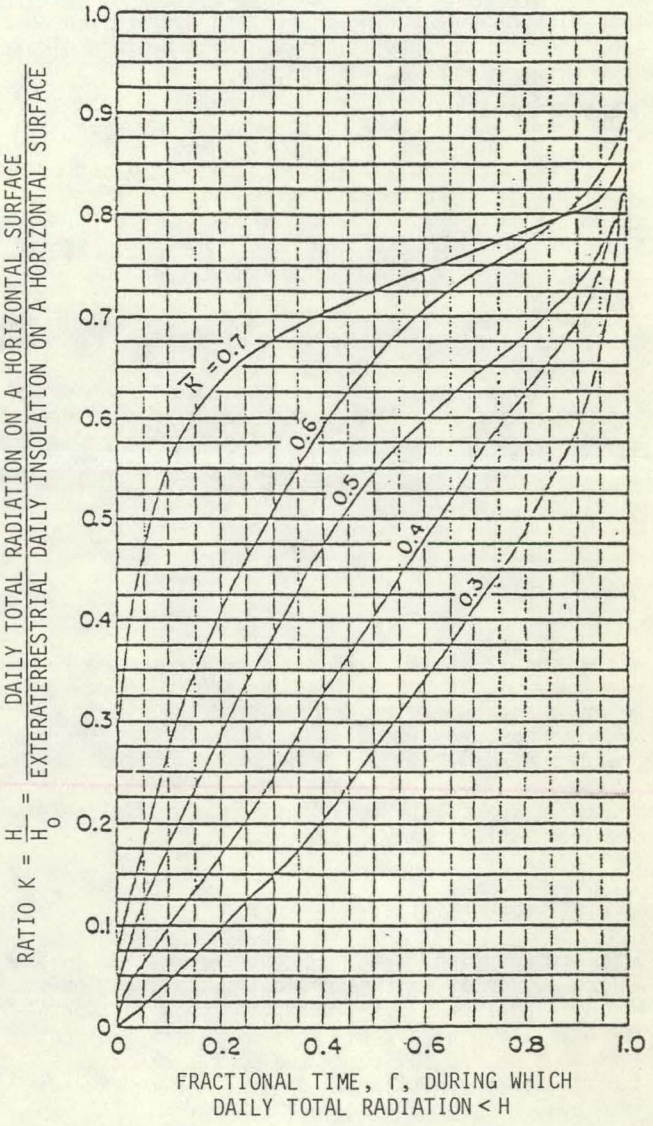

Fig. 4. Cumulative Distribution Curves for Daily Insolation [1].

on those days when the clearness index is K. In probability notation, the curve represents the conditional expected value of H_d/H given K, denoted by:

$$\mathcal{E}[H_d/H \mid K]. \tag{2}$$

Collares-Pereira and Rabl [2] have derived a general correlation for the diffuse fraction given by:

$$\mathcal{E}[H_d/H \mid K] = \begin{cases} 1.188-2.272K+9.473K^2-21.856K^3+ \\ \quad 14.648K^4, \text{ for } .17<K<.8 \\ .99 \text{ for } K\leq .17. \end{cases} \tag{3}$$

The above should not be confused with similar correlations developed for the monthly average daily diffuse radiation $\bar{H}_d$ during the entire month given that the average total radiation is $\bar{H}$ with average clearness index $\bar{K}$; this is denoted by:

$$\mathcal{E}[\bar{H}_d/\bar{H} \mid \bar{K}]. \tag{4}$$

The latter expected value should be calculated by integrating the correlation given above for $\mathcal{E}(H_d/H|K)$ over the insolation probability distribution for the month, and the results are not necessarily consistent with published correlations for $\bar{H}_d/\bar{H}$.

Next, the hourly radiation must be estimated based on the daily totals. Figure 3 shows a plot of the hourly diffuse radiation as a function of the daily diffuse radiation. Again, this represents a conditional expectation given the daily diffuse radiation H_d. A close approximation is provided by a formula based on the extraterrestrial hourly to daily ratio [1]:

$$q_d(t) \equiv \mathcal{E}[h_d(t)/H_d|H_d] = \frac{\pi}{24}\,\frac{\cos w - \sin w_s}{\sin w_s - w_s \cdot \cos w_s} \tag{5}$$

where w is the solar hour angle corresponding to time t and w_s is the sunset hour angle. A similar relation exists for the ratio:

$$q(t) = \mathcal{E}[h(t)/H|H] \tag{6}$$

of hourly to a daily total horizontal radiation as provided in Reference [2].

INSOLATION COLLECTION

Standard equations are used to determine the insolation available to the collector as a function of hourly diffuse and total radiation on a horizontal surface. In general, the radiation i(t) incident at time t on the collector can be expressed as a function of the horizontal diffuse and total radiation by:

$$i(t) = r(t)\bullet h(t) - r_d(t)\bullet h_d(t) \tag{7}$$

where r(t), $r_d(t)$ are conversion factors which depend on the time of day t, the latitude L, the declination δ, and the collector type. The above formulation may be used for both flat plate and concentrating collectors. The conversion factors for a flat plate array facing south, for example, are given by [1]:

$$r(t) = r_b(t) + \rho(1-\cos\beta)/2 \tag{8}$$
$$r_d(t) = r_b(t) - (1 + \cos\beta)/2$$

where

$$r_b(t) = \frac{\cos(L-\beta)\cos\delta\,\cos w + \sin(L-\beta)\,\sin\delta}{\cos L\,\cos\delta\,\cos w + \sin L\,\sin\delta} \tag{9}$$

and β is the tilt angle, ρ the ground reflectance.

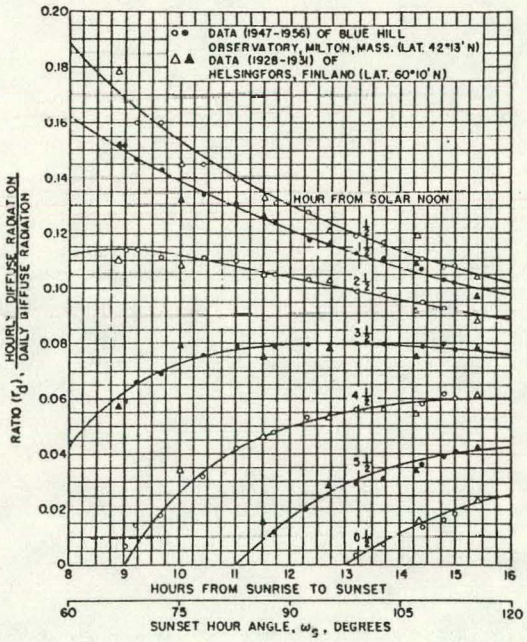

Fig. 3. Hourly Diffuse Radiation Correlation [2]

ARRAY EFFICIENCY

A simplified array efficiency model has been developed which determines the average array electrical efficiency $\bar{\eta}$ as a function of ambient temperature, wind speed, and incident radiation. The photovoltaic array efficiency equations and steady state energy balance equations were first solved to derive an equation for the cell temperature rise above ambient, T_c-T, as a function of ambient temperature, incident radiation, wind speed, and module heat loss coefficients. The form of the equation was then used to develop an approximation for array efficiency based on nominal efficiency data and cell temperature data (e.g., NOCT). Details of the derivation and validation are provided in Reference [3]. It should be noted that in contrast to solar thermal collectors, photovoltaic array efficiency is not strongly dependent on temperature, and moreover it decreases (approximately linearly) as ambient temperature increases.

Again, the integration is performed using Simpson's rule and linear interpolation of the K(F) curves. The function $\phi(t)$ represents the hourly excess fraction at time t and corresponds in concept to the utilizability function of Liu and Jordan. By rearranging the terms in the equation for ϕ, it is possible to show that ϕ depends on only three parameters: the clearness index $\bar{K}$; the hourly demand to solar ratio

$$X = \frac{d(t)}{A\,\eta\,\overline{i(t)}}; \qquad (16)$$

and the hourly collection parameter ratio

$$Z = \frac{q_d(t).r_d(t)}{q(t).\ r(t)} \qquad (17)$$

This makes it possible to develop generalized curve fits for the ϕ function which can be used directly without re-performing the numerical integrations for expected value.

SYSTEM ECONOMICS

Standard economic analysis techniques are applied to evaluate the present worth of system costs, annual operation and maintenance costs, and electric energy savings based on the monthly photovoltaic system performance calculated previously.

CONCLUSIONS

A methodology has been developed to evaluate the performance and economics of photovoltaic power systems by integrating over monthly insolation distribution curves which are correlated in terms of the monthly average clearness index $\bar{K}$. The required meteorological data consists of long-term monthly averages. Because the performance calculations are computed on a monthly rather than hourly basis it is possible to rapidly evaluate a large number of system configurations and sizes for system optimization.

ACKNOWLEDGEMENT

This work was supported by the U.S. Department of Energy, Division of Distributed Solar Technology, under Contract #13-2281 with Sandia Laboratories, Albuquerque, NM. Acknowledgement is given to Dr. Gary Jones, Sandia Technical Representative.

NOMENCLATURE

A general convention used for insolation variables is that capital letters denote daily total values (e.g., H), while lower case letters with time t in parentheses denote hourly values at that time (e.g. h(t)), and a bar over any variable indicates the long-term average value over all days in a given month (e.g., $\bar{H}$ or $\overline{h(t)}$ in January).

A	= Array area, m^2
β	= Collector slope angle, degrees
δ	= Declination, degrees
$\bar{\epsilon}$	= Expected value in a given month
η	= Array efficiency
F	= Fraction of days for which K does not exceed a specified value
H, H_d, H_o	= Daily total, diffuse, and extra-terrestrial radiation on a horizontal surface, $kWh/m^2.d$ respectively
I	= Daily radiation incident on the collector, $kWh/m^2.d$
i(t)	= Hourly radiation incident on the collector, $kWh/m^2.h$
K	= Clearness index = H/H_o
L	= Latitude, degrees
$q(t), q_d(t)$	= Hourly fraction of daily total and diffuse radiation, respectively
ρ	= Ground reflectivity
$r(t), r_d(t)$	= Conversion factors from horizontal radiation to radiation incident on the collector
T	= Ambient temperature, ^oC
t	= Solar time from noon, hr
T_c	= Cell temperature, ^oC
t_s	= Solar sunset time, hr
ϕ	= Hourly excess fraction
w	= Solar hour angle = $2\pi t/24$, radians
w_s	= Solar sunset angle, radians
X	= Demand to solar ratio = $d(t)/\overline{A\eta i(t)}$
Z	= Collection Parameter = $q_d(t)r_d(t)/q(t)r(t)$

REFERENCES

[1] B. Liu and R. Jordan, "A Rational Procedure for Predicting the Long-Term Average Performance of Flat-Plate Solar Energy Collectors," Solar Energy 7, 53-74 (1963).

[2] M. Collares-Pereira and A. Rabl, "The Average Distribution of Solar Radiation Correlations between Diffuse and Hemispherical and between Daily and Hourly Insolation Values," Solar Energy 22, 155 (1979).

[3] S. Young and D. Edelman, "A Simplified Method to Calculate Photovoltaic Array Output Based on Manufacturer's Data," draft technical paper for Sandia Laboratories, Contract #13-2281, to be published in final report (1979).

NOTES

PERFORMANCE STUDIES OF COMBINED PHOTOVOLTAIC/THERMAL SOLAR HEATING AND COOLING SYSTEMS

S. R. Venkateswaran, Research Assistant
D. K. Anand, Professor

Solar Energy Projects
Department of Mechanical Engineering
University of Maryland
College Park, Maryland 20742

ABSTRACT

This paper presents a simulation study of combined photovoltaic/thermal (PV/T) solar collector-series heat pump systems for heating and cooling applications. A computer program incorporating detailed performance models for the PV/T collector, electrical and thermal storage, heat pump and building load is developed to simulate the year-round operation of such a system. System simulations are made for three US locations to study the effect of important design parameters on the collector and overall system electrical and thermal performance.

The long term performance is found to be relatively insensitive to electrical and thermal storage size over most of the range of values of practical interest. The collector area, orientation and performance parameters as well as the geographical location dependent weather and building loads have a significant effect on the system performance that is critical from the point of view of design. Combined PV/T collector-heat pump systems are found to have the maximum potential for energy savings in cold regions with high thermal loads.

INTRODUCTION

The search for alternate energy sources has spurred the study of various solar heating and cooling systems aimed at reducing the consumption of non-renewable energy resources. Solar thermal collectors can be used to supply some of the thermal requirements of a building. Direct photovoltaic generation of electricity, expected to become economically viable by the mid 1980's can be used for the electric power requirements. An alternative to these individual schemes for supplying all the building energy demands is the combined photovoltaic/thermal (PV/T) collector, which essentially combines a photovoltaic module and a solar thermal collector in a single unit. It can be expected that PV/T collectors would cost less and require significantly reduced space than a combination of separate photovoltaic and thermal collectors providing the same power.

Extensive analytical and experimental studies of solar thermal and photovoltaic systems have been undertaken but little work has been accomplished with combined PV/T collector systems. Florschuetz [1] has extended the Hottel-Whillier-Bliss model for the thermal analysis of flat plat collectors to the analysis of combined PV/T collectors, involving simple modifications of the conventional HWB model parameters with the additional assumption that the electrical output varies linearly with cell temperature. Evans, Facinelli and Otterbein [2] have developed an extended TRNSYS-type subroutine which has been used to simulate PV/T collector performance under varying ambient and flow conditions. More recently, the thermal and electrical performance of an air type and liquid type combined PV/T collector has been experimentally evaluated by Hendrie [3], yielding close correlations with theoretical results.

A number of conceptual design and systems analysis of PV/T collector systems have been carried out for the US Department of Energy. A MIT Licoln Laboratory study [4] concluded that PV/T collector systems provide the least cost options for residences in cold climates, while all-photovoltaic systems are the most cost effective for regions characterized by high air conditioning loads. Also that heat pump systems minimize auxiliary energy consumption. A Westinghouse Corporation study [5] of residential photovoltaic systems concluded that both hybrid and all photovoltaic systems are superior to separate photovoltaic and thermal collector systems. The use of on-site electrical and thermal storage is considered essential.

The purpose behind this work is twofold. The first is to simulate and compare under varying operating conditions, the thermal and electrical performance of a combined PV/T solar collector-series heat pump system when applied to the heating and cooling of a building. Design parameters of importance are the collector area, flow rate, performance parameters, orientation; electrical and thermal storage size; control temperatures for direct and heat pump heating and location dependent weather and building energy loads. A detailed computer simulation program is developed incorporating performance models for the solar collector, storage components, heat pump, electrical power conditioning equipment, service water heating module and building load. Based on system simulations for Washington, D.C.,Madison, Wi. and Phoenix, Az., the critical design parameters are isolated and broad guidelines developed

for system design and optimization. Results are based on a comparison of long term performance indices including electrical and thermal solar fractions, collector efficiencies and component COP's.

The second part of this work develops a general design procedure for the PV/T collector-series heat pump system that may be used to estimate the monthly solar fractions for a given load. This paper presents the results of the first part of the study. The design procedure will be the subject of a forthcoming paper.

SYSTEM DESCRIPTION

The PV/T collector-heat pump system is designed to supply the space heating and cooling, service hot water and miscellaneous electrical loads of a 112 m^2 (1200 ft^2) all-electric residential building A schematic of the system is shown in Fig. 1.

The primary solar energy collection function is accomplished by a combined PV/T collector of a very basic design, consisting of a liquid cooled flat plate thermal collector with silicon photovoltaic cells affixed on its absorber surface. The photovoltaic cells are arranged in a conventional series-parallel configuration covering the entire absorber plate area. These PV/T collectors are used to supply the energy demands of a well insulated single family residence of 1200 ft^2 floor area. The collector panels are mounted on the roof, facing south. The building has an estimated UA of 850 KJ/hr-^oC (448 Btu/hr-^oF) and is maintained at a set temperature of 20^oC (68^oF). Heat gains due to occupants, lighting and infiltration are taken into account. The annual space heating and cooling loads are estimated as 54.9 GJ (52.0 MmBtu) and 30.0 GJ (28.4 MmBtu) for Washington, D.C., 91.2 GJ (86.4 MmBtu) and 20.8 GJ (19.7 MmBtu) for Madison, 14.3 GJ (13.6 MmBtu) and 94.0 GJ (89.1 MmBtu) for Phoenix, respectively.

Thermal Subsystem

The thermal energy collection loop consisting of the solar collector, heat exchanger, relief valve, hot storage tank, pumps and controllers, transfers the collected solar heat to the liquid storage tank. The tank is treated as fully mixed with a thermal loss factor of 23.4 KJ/hr-^oC (12.3 Btu/hr-^oF). Collector and heating circuit piping thermal losses are ignored.

The system operates in the heating or cooling mode depending on the nature of the building space load. A thermostatic deadband of ±5^oC (±9^oF) prevents frequent mode switching under marginal conditions. Direct heating is supplied from thermal storage, when the tank temperature is above a set value. Otherwise, a heat pump supplies the demand with the hot storage as the evaporator heat source. Auxiliary heat is provided by induct resistance coils. If the storage temperature falls below a minimum, 3^oC (37.4^oF), both direct and heat pump heating are deactivated and the electric auxiliary supplies the entire demand. The cooling load is met entirely by the heat pump rejecting heat to the ambient. There is no provision for auxiliary cooling and the machine has to be adequately sized to meet the expected summer loads. Figure 2 shows the capacity and electrical input for the heat pump in the heating and cooling modes. The heating COP of this machine varies from 2.4 to 3.9 over the evaporator source temperature range of 0 to 40^oC (32 to 104^oF) and the cooling COP from 2.9 to 1.8 for ambient temperatures of 20 to 45^oC (68 to 113^oF). This heat pump is typical of a current technology, high effeciency device and is used for all the simulations.

The service water heating module consists of a preheat tank into which solar heat is transferred from the main storage tank and a main supply tank which is maintained at supply temperatures through auxiliary resistance heating. An average daily hot water demand of 400 kg (882 lb) at 55^oC (131^oF) is assumed based on the requirements of a four person family.

Electrical Subsystem

The electrical subsystem supplies the heat pump electrical input, space heating and service water auxiliary loads and the diversified building electrical demand. This includes loads associated with lighting and other household appliances and is represented by a single location independent daily profile [6] applicable to an average four member family. The electrical subsystem incorporates a maximum power tracker that monitors the power output of the photovoltaic array and continuously adjusts its voltage to operate at the maximum efficiency point.

The intermittant nature of the photovoltaic power supply makes it essential to have electrical storage capability in the system. Although various advanced storage cells are under development, at present only lead acid batteries are commercially available for this purpose. The electrical storage module used for the system simulations consists of a 96 cell lead acid battery with a capacity of 48 kwh, operating at an average voltage of 200V. The battery efficiency is set at 84%, which is typical of state-of-the-art deep discharge lead acid batteries.

The rest of the power conditioning equipment consists of a regulator that monitors the battery state of charge and regulates the charging rates of the battery. It prevents over charging or discharging of the battery and controls priorities on recharging the battery as opposed to sending array power to the load. A power inverter is a necessary power conditioning component to convert the battery or array DC output to AC. A Bechtel Corporation study [7] of power conditioning alternatives suggests that line commutated inverters operating in parallel with the utility should be used for photovoltaic power systems since this would virtually eliminate switching transients and utilize the solar output more fully.

In order to simulate the electrical performance, an operational control strategy is necessary to interface the array, battery, utility and load. This should be one that most effectively utilize the available solar output and prolongs battery life. The regulator monitors the battery state of charge, the photovoltaic output and electrical demand and institutes the appropriate energy flow path. When the battery is near fully charged condition, the regulator will "dump" excess array output through shunt resistors. Otherwise excess array output is used to partially recharge the batteries. When a specified minimum battery state of charge is reached, the regulator will prevent further discharge by switching to utility power. In addition, once this minimum state of charge is reached, first priority on the use of the array generated power is given to recharging the battery to some specified state of charge.

Details of the mathematical models appear in further detail in reference 8.

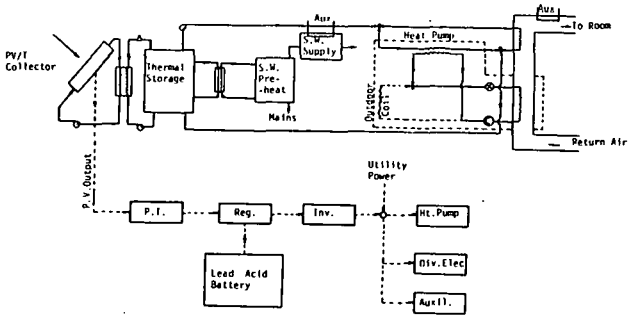

Figure 1 - Combined Photovoltaic/Thermal Collector- Series Heat Pump Schematic

SYSTEM SIMULATIONS

A computer program is developed to simulate the year-round performance of the PV/T solar collector-heat pump system described in the preceeding section. A detailed listing of the program and input variables is given in reference 8.

In order to evaluate the effect of system design parameters on the long term performance, a series of simulations are made over the period of one year, with the design parameters being varied in an orderly fashion. Other variables are maintained at baseline values representing state-of-the-art components found in literature. The design parameters of interest include the collector area, flow rate, orientation and performance constants; electrical and thermal storage size, control temperatures and location dependent weather and building loads. Performance measures averaged over a monthly or yearly basis are compared. A simulation timestep of one hour is used in every case. Hourly insolation, ambient dry bulb temperature and wind speed data characteristic of three US locations (Washington D.C., Madison and Phoenix) are read from TMY tapes to drive the simulations. The three locations are chosen to represent a diversity of weather and building load patterns. Madison is characterized by high winter heating loads while Phoenix is subject to high summertime air conditioning loads with Washington, D.C. somewhere inbetween. The performance indices used as indicators of the system electrical and thermal performance are detailed in the next section.

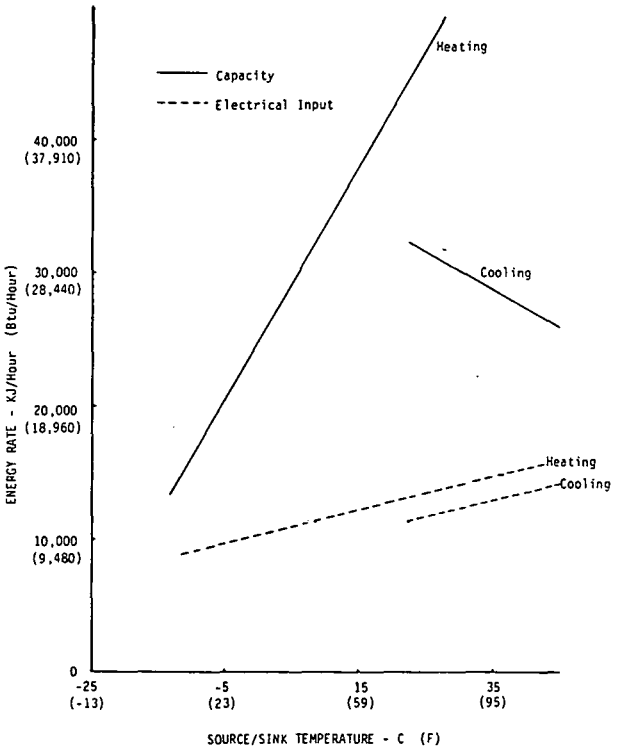

Figure 2 - Heat Pump Operating Characteristics for Heating and Cooling (Carrier Model 50YQ030)

Performance Measures

The indices of major interest in this work are those based on long term integrated energy quantities. Besides the collector electrical and thermal efficiency and the heat pump COP, these include:

a) Thermal Solar Fraction (f_{th}): The thermal solar fraction is an indicator of the thermal subsystem performance and can be defined as:

$$f_{th} = (QLT - QAUXT - WHPH)/QLT \quad (1)$$

where: $QLT = QSW + QSH$ (2)

Here, the effective thermal load (QLT) that the system tries to satisfy is the sum of

the service water (QSW) and space heating (QSH) loads. The fraction of this thermal load not supplied by the solar thermal subsystem either by direct or heat pump heating appears as auxiliary space heat and service water load (QAUXT) and heat pump electrical input (WHPH).

b) Electrical Solar Fraction (f_e): The fraction of the system electrical load satisfied by solar (f_e) is given by:

$$f_e = (QLE - QUTIL)/GLE \quad (3)$$

Where QUTIL is the required utility backup power. The effective electrical load (QLE) that the system sees is the sum of the service water and space heating auxiliary (QAUXT), the heat pump electrical input in the heating (WHPH) and cooling (WHPC) modes and the diversified building electrical load (QDIV).

$$QLE = QAUXT + WHPH + WHPC + QDIV \quad (4)$$

c) Net Solar Fraction (f): The single most informative indicator of the hybrid system performance is the fraction of the total load (QL) met by solar. Considering the total system energy load as the sum of the space heating, space cooling, service water and diversified load leads to defining of f as:

$$f = (QL - QUTIL)/QL \quad (5)$$

where:
$$QL = QSW + QSH + \frac{QSC}{COP_c} + QDIV \quad (6)$$

d) System COP (COP_s): This is an indicator of the overall system energy conversion efficiency and is defined as the fraction of the incident collector insolation that is available at point of use as either electrical or thermal energy.

$$COP_s = (QL - QUTIL)/QI \quad (7)$$

where QI = total solar radiation incident on the collector.

Results

The simulation results are summarized in the conclusions. Some of the more interesting results are presented below in greater detail. Although the results shown in this paper are primarily based on simulations for Washington, D.C., those for Madison and Phoenix lead to the same general conclusions and are available in reference 8.

In order to generate data on sizing of the storage components, a series of simulations are made to study the sensitivity of the system performance to changes in the electrical and thermal storage capacity. The direct effect of changing battery capacity is on the electrical subsystem performance. Figure 3 presents the variation of F_e with the battery capacity for 50, 75 and 100 m^2 (538, 807 and 1075 ft^2) collector area systems located in Washington, D.C. Insufficient battery capacity results in a sharp increase in the photovoltaic energy dumped. As the collector size goes up, this increasing imbalance between array output and demand causes further degradation of the electrical performance at low battery sizes. However, above 250 ampere-hours any additional capacity does not result in any significant increase of F_e. These results demonstrate the need to incorporate electrical storage capability in the system and to optimize its size for any particular application, in order to best utilize the available photovoltaic output.

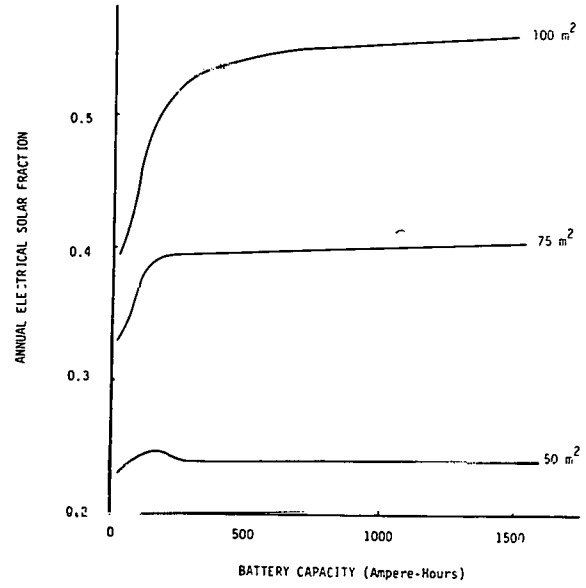

Figure 3 - Annual Electrical Solar Fraction (F_e) vs. Battery Capacity (Washington, D.C.)

Figures 4 and 5 show the effect of flow rate (G) and thermal loss coefficient (U_L) on the electrical (η_e) and thermal (η_{th}) efficiencies of the collector. As expected, low values of U_L result in higher thermal efficiencies due to reduced heat losses from the collector. But the resulting higher absorber plate temperature causes a deterioration of the electrical output.

Similar collector efficiency plots showing the effect of the ($\tau\alpha$) product for a 1, 2, and 3-cover system and the photovoltaic cell reference efficiency (k_1) are presented in Fig. 6 and 7. η_e increases linearly with k_1 as expected while η_{th} suffers a drop because a smaller fraction of the incident energy is available for thermal conversion. However, increasing the transmittance of the covers or the absorptance of the photovoltaic cells improves both η_e and η_{th}, because a larger fraction of the incident solar radiation is available for conversion. But the resulting increase in the average collector temperature would tend to offset some of this improvement. These results indicate that single-glazed low performance flat

plate collectors of inexpensive design coupled with efficient photovoltaic modules would serve the purpose of achieving efficient photovoltaic conversion while providing reasonable thermal output.

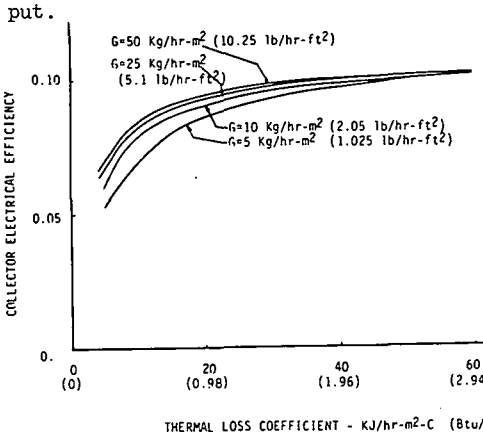

Figure 4 - Effect of Fluid Flowrate (G) and Thermal Loss Coefficient (U_L) on the Collector Electrical Efficiency

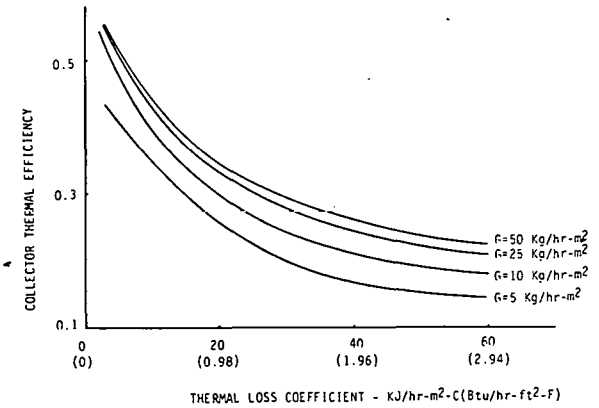

Figure 5 - Effect of Fluid Flowrate (G) and Thermal Loss Coefficient (U_L) on the Collector Thermal Efficiency

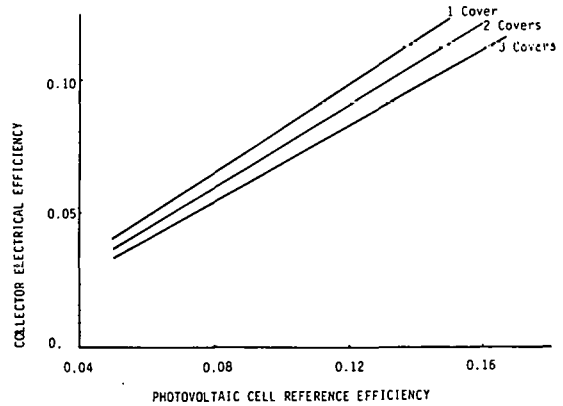

Figure 6 - Effect of Transmittance-Absorptance Product and Photovoltaic Cell Reference Efficiency on Collector Electrical Efficiency

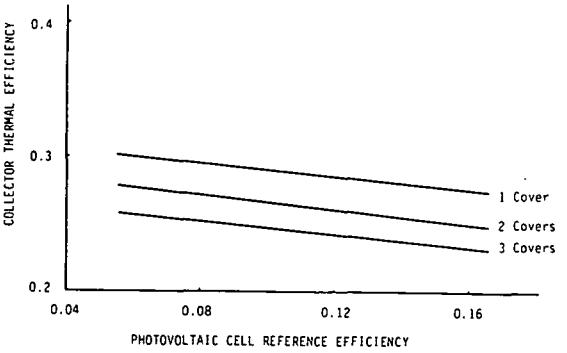

Figure 7 - Effect of Transmittance-Absorptance Product and Photovoltaic Cell Reference Efficiency on Collector Thermal Efficiency

Figure 8 presents the energy savings per unit collector area achieved by installing the PV/T collector system in Washington, D.C., Madison Phoenix. The maximum energy savings are attained in Madison over most of the range of collector areas of practical interest. Madison is characterized by high thermal loads and results in maximum utilization of the PV/T collector output. In the case of Phoenix which is subject to lower thermal loads all year round, the system tends to be thermally oversized most of the time. This results in elevated storage temperatures and lower collector efficiencies except at very small collector areas where there is more of a balance between supply and demand.

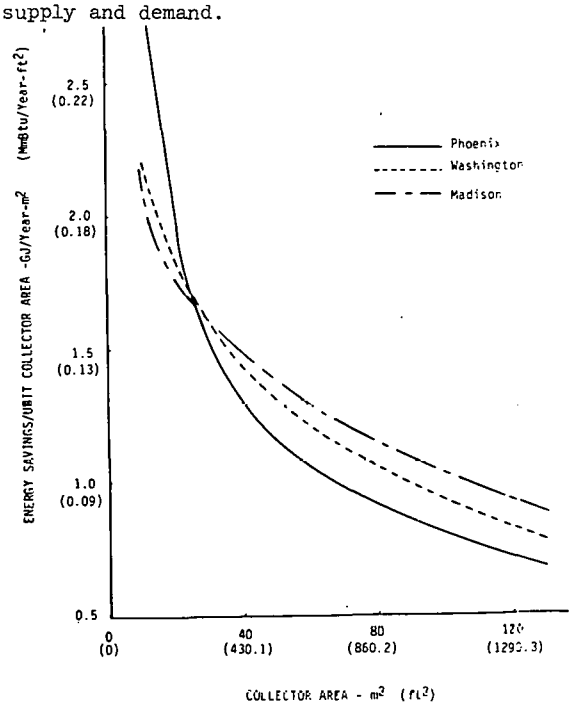

Figure 8 - Comparison of Annual Energy savings per Unit Collector Area for Madison, Washington and Phoenix

CONCLUSIONS

1) The electrical and thermal storage capacities as well as the collector flowrate are found to have only a small effect on the long term performance of the PV/T collector-heat pump system over a wide range of values of practical interest. However, very small values of the battery capacity, thermal storage size and collector flowrate below 250 ampere-hours, 100 kg/m^2 (20.5 kg/ft^2) and 50 kg/hr m^2 (10.3 lb/hr ft^2) respectively, tend to penalize long term performance.

2) From point of view of maximizing photovoltaic output, expensive collector thermal designs with low heat loss coefficients and employing multiple glazings are not justified.

3) A minimum storage temperature of 30°C (86°F) for direct space heating minimizes auxiliary energy usage.

4) Combined PV/T collector systems have the potential for achieving maximum energy savings in cold climates characterized by high thermal loads.

5) The long term system performance is found to drop off rapidly at small collector areas because 'starvation' of the heat pump evaporator results in poor utilization of the series heat pump capability. Large collector areas however lead to elevated storage temperature and degraded collector efficiencies, because the system tends to be thermally oversized a lot of the time. The optimum system size can be determined by examining system costs, fuel savings and other economic factors.

ACKNOWLEDGEMENT

This work is supported by the Department of Energy, Division of Conservation and Solar Applications and the Computer Science Center of the University of Maryland.

NOMENCLATURE

f - Monthly solar fraction
F - Annual solar fraction
G - Collector fluid flowrate per unit area (kg/hr-m^2)
k_1- Photovoltaic cell reference efficiency
U_L- Collector thermal loss coefficient (KJ/hr-m^2-°C)
η - Collector efficiency
$(\tau\alpha)$- Collector transmittance - absorptance product

Subscripts

e - Electrical
th - Thermal

REFERENCES

1. L.W. Florschuetz, "Extension of the Hottel-Whillier-Bliss Model to the Analysis of Combined Photovoltaic/Thermal Flat Plate Collectors", Sharing the Sun Joint Conference, Vol. 6, Winnipeg (1979).

2. D.L. Evans, et al., "Combined Photovoltaic/Thermal System Studies", SAND78-7031, Arizona State University, August 1978.

3. S.D. Hendrie, "Evaluation of Combined Photovoltaic/Thermal Collectors", 1979 ISES International Congress, Atlanta, May 1979

4. E.C. Kern, M.C. Russel, "Hybrid Photovoltaic/Thermal Solar Energy Systems", MIT, Lincoln Laboratory Report No. COO-4577-1, March 1978

5. Westinghouse Corporation, "Conceptual Design and System Analysis of Photovoltaic Systems", ALO-2744-13, May 1977.

6. General Electric Company, "Conceptual Design and System Analysis of Photovoltaic Systems", ALO-3686-14, March 1977.

7. Bechtel Corporation, "Energy Storage and Power Conditioning Aspects of Photovoltaic Solar Power Systems", Volume 1, COO/2748-75/TI, October 1975.

8. S.R. Venkateswaran, "Simulation Study of Combined Photovoltaic/Thermal Solar Heating and Cooling Systems, MS Thesis, Mechanical Engineering Department, University of Maryland, College Park, November 1979.

Session IIIB

Dr. J. Douglas Balcomb
Los Alamos Scientific Laboratory
Chairperson

SYSTEMS ECONOMICS II

ECONOMICS OF SOLAR DOMESTIC HOT WATER HEATERS IN CALIFORNIA

M. F. Young

J. W. Baughn

Department of Mechanical Engineering
University of California
Davis, California 95616

ABSTRACT

A comparison of the cost-effectiveness of four types of Solar Domestic Hot Water (SDHW) systems is presented for five (5) locations throughout California using a net present worth (NPW) analysis with inflation. Computer simulations were previously performed to obtain the annual auxiliary energy requirements for a prescribed hot water load. The systems considered are two-tank thermosyphon (2TT) and pumped (2TP) and one-tank thermosyphon (1TT) and pumped (1TP). The accuracy of the computer simulation was previously verified by comparison to experimental data on each of the four types of systems.

It was found that when the SDHW systems are compared to a conventional electric hot water system, the NPW is always positive, with or without a tax credit, for the locations considered. The 2TT was found to have the highest NPW with the 2TP quite close.

When a SDHW system is compared to a conventional natural gas hot water system the NPW is negative in most locations without a tax credit but for most of the systems the NPW becomes positive with the California 55% tax credit.

It appears that most SDHW systems are now cost-effective in most California locations with the present tax credit.

INTRODUCTION

Solar energy can significantly contribute to that 4% (~ 1.5 million barrels/day) of the total national energy in the U.S. which is used by domestic hot water heaters [1]. A variety of Solar Domestic Hot Water (SDHW) systems are currently competing in the marketplace. The best design for a particular location depends on a combination of climate, cost, efficiency, reliability and hot water usage.

The objective of the present work is to compare the cost-effectiveness of thermosyphon and pumped SDHW systems for different climatic conditions and load demands. To accomplish this, annual solar contributions for each system were predicted by analytical models. These models were previously verified by comparing analytical results with experimental data. Computations were then performed for five different locations in California [2]. Input weather/radiation data, as well as hot water load distribution and size, were varied for each simulation. Annual solar contribution predictions have been previously presented for other locations in California [3,4].

Both passive (thermosyphon) and active (pumped) solar systems are considered in this work. Thermosyphon systems, sometimes called natural circulation systems, eliminate the need for pumps and their corresponding controls. As discussed in [5], the flow occurs naturally due to the density differences between the hot fluid in the collector and the cooler fluid in the storage tank and downcomer. Fluid in the storage tank must be mounted at or above the collector. Furthermore, since thermosyphon systems generally use the potable water directly in the collector, freeze protection may be problematic. No consideration of freeze protection or its effect on the selection of thermosyphon versus pumped systems is given in the present paper.

For both passive and active systems, designs with either one or two tanks can be used. With one-tank designs, solar energy and auxiliary heat are both added to the potable water which is stored in a single tank. Two-tank systems have a separate solar storage tank, the outlet of which is connected to a conventional hot water heater (the solar system acting essentially as a preheater for the conventional hot water system).

SOLAR DOMESTIC HOT WATER SYSTEMS

The four SDHW systems considered in the present work are: 1) Two-tank pumped (2TP), 2) Two-tank thermosyphon (2TT), 3) One-tank pumped (1 TP), and 4) One-tank thermosyphon (1TT). A diagram of the 2TP system is shown in Fig. 1 (the second tank (conventional hot water heater) is not shown). The 2TT system differs from the 2TP system only in the deletion of the pump and valve, the requirement for an elevated tank, and usually the use of slightly larger diameter interconnecting piping. The 1TT system is shown in Fig. 2. For this system the auxiliary heater is in the storage tank. A diagram of the 1TP system is shown in this case and the fluid in the solar collector loop can be a 50/50 solution of antifreeze and water.

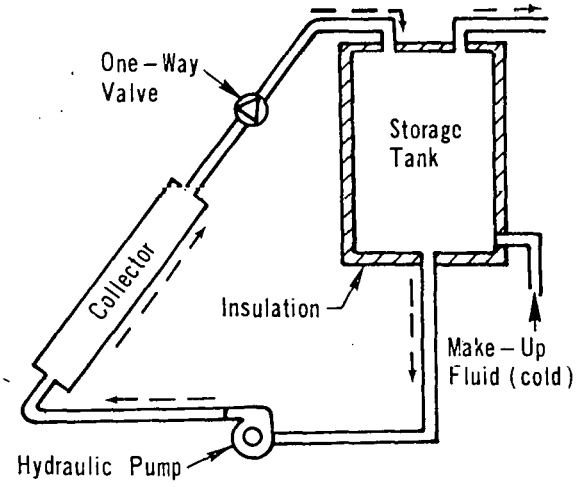

Fig. 1 Diagram of Two-Tank Pumped System (Delete Pump and Valve for Two Tank Thermosyphon)

ANALYTICAL MODELS AND EXPERIMENTAL RESULTS

A versatile computer program, SHOW (Solar Hot Water) was developed to numerically simulate these four solar systems. System parameters, climate conditions and load demands are required inputs for system simulations. Collector flow rates are either calculated, (in the case of the thermosyphon systems) or are input (for the pumped systems). Collector inlet/outlet temperatures, as well as storage tank temperatures and auxiliary energy requirements, are outputs from the computer program. Fifteen vertical nodes were normally used in the storage tank simulation and the effects of flow into and out of the tank, auxiliary heat addition, heat conduction between nodes and tank heat losses are included. The flat-plate collector model uses experimental performance data which are correlated as recommended by ASHRAE [7]. An expanded description of these models is given in [2] with further details [3].

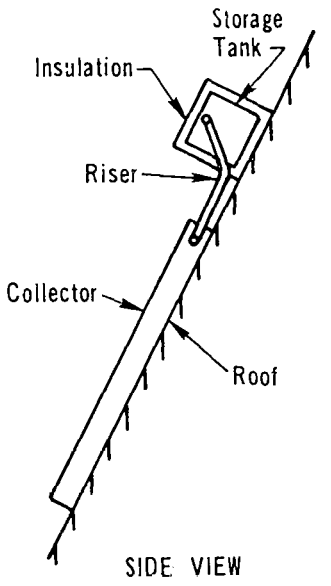

Fig. 2 Diagram of One-Tank Thermosyphon System

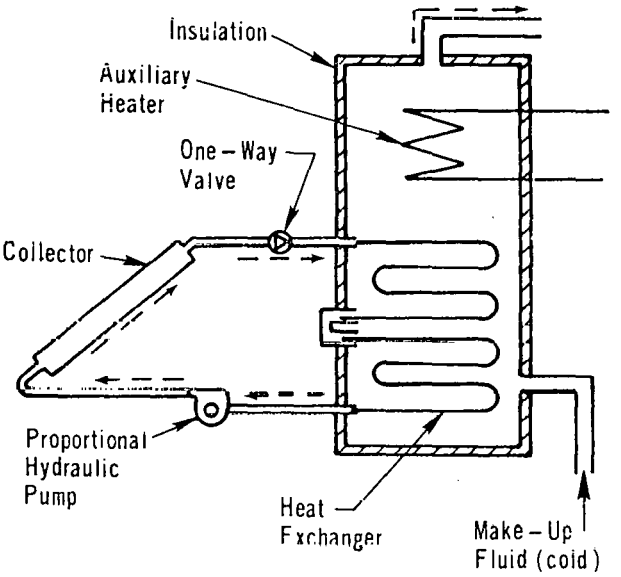

Fig. 3 Diagram of One-Tank Pumped System

To establish the validity of the analytical models, experiments were performed using four commercially available SDHW systems. System parameters (capacity and dimensions of the various components) are discussed fully in [3,4]. Tests were performed for a wide range of climate conditions and for two different load profiles which are shown in Fig. 4. With Load Profile #1 (LP1) most of the hot water is used in the evening, while with Load Profile #2 (LP2) the use is entirely during the daytime. Comparisons of analytical and experimental collector inlet and outlet temperatures and auxiliary energy for

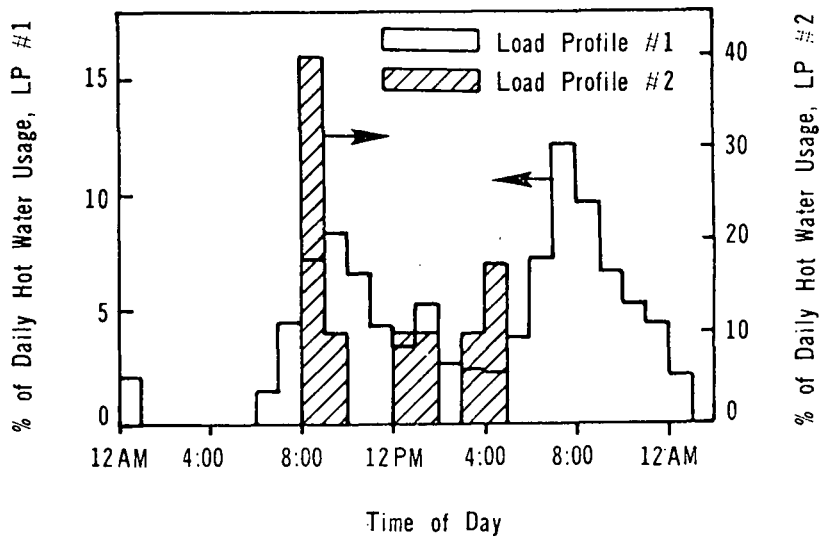

Fig. 4 Water Demand Load Profiles

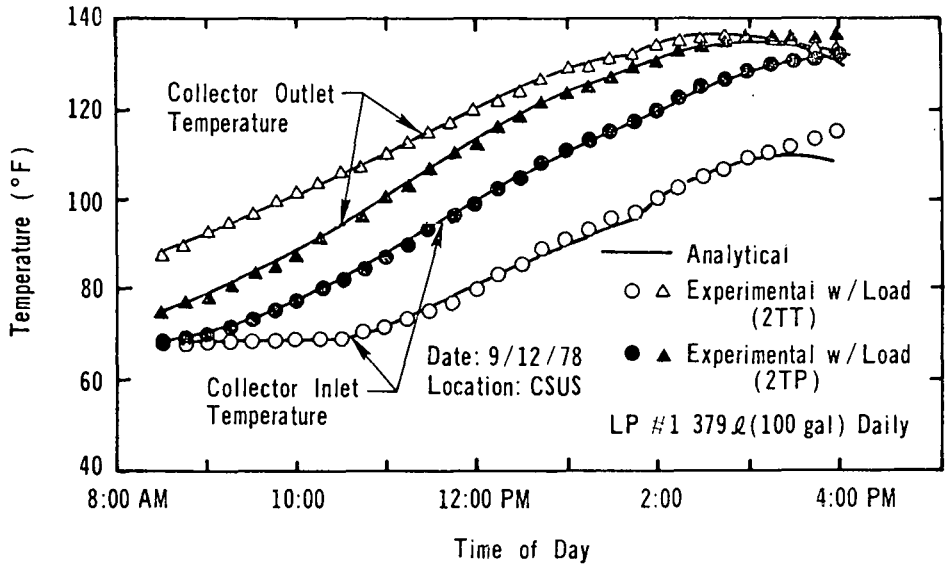

Fig. 5 Comparisons of Analytical and Experimental Collector Temperatures with LP1 and a Total Daily Load of 379 liter (100 gal.)

the four systems are presented in [3,4]. In almost all cases, the agreement is excellent. A sample comparison of these results is given in Fig. 5 which shows analytical and experimental values of collector inlet and outlet temperatures for the 2TT and the 2TP systems using LP1 with a total daily load of 379 liters (100 gallons).

ECONOMIC ANALYSIS

Economic decisions are often made using a Net Present Worth (NPW) calculation. In a NPW analysis, all benefits and costs are brought back to a common time, the present. A positive NPW represents larger overall system benefits than cost during the assumed lifetime of the system. It usually represents an attractive economic situation. Further details of the economic analysis are given in [3].

For example, in the present study the NPW is given by

$$\text{Present}_{\text{inflation}} = \sum_{I=1}^{\text{Life}} \frac{BC(I)_{\text{inflation}}}{(1+r)^I} \qquad (1)$$

where

$$BC(I)_{\text{inflation}} = \text{Save}(I)\,(1+r)^I - \left[\frac{\text{Loss}(I) + L}{(1+r)^I} + \left\{(1+r)^I \left[M(I) + \text{Ins}(I) + \text{Replace}(I) + \text{Aux}(I)\right]\right\}\right]$$

and Save (I) = Savings in fuel costs at year I
L = Loan payment at year I
Loss (I) = Loss of interest on down payment at year I
M (I) = Maintenance costs at year I
Ins (I) = Insurance costs at year I
Replace (I) = Replacement costs at year I
Aux (I) = Auxiliary fuel costs at year I
r = Inflation rate at year I

RESULTS

These computed annual solar contributions for the four systems described above and for five different locations in California are given in Table 1. The weather/radiation conditions used in these simulations are presented in [3,4].

In order to facilitate the economic comparisons, a Base Case is established. Economic parameters for the Base Case are shown in Table 2. NPW results after inflation for a 238.88 liter (75 gallon) daily load distributed according to LP1 are shown in Table 3. The values not in parentheses are for the base case results. Values in parentheses are with the California's 55% Tax Credit taken into account. Initial capital cost data are given in [3]. The results show positive NPW values for all locations and all systems investigated.

TABLE 1. YEARLY PERCENT SOLAR FOR A 238.88 LITER (75 GALLON) DAILY LOAD DISTRIBUTED ACCORDING TO LP1.

	System			
Location	2TP	2TT	1TP	ITT
El Centro	89(83)*	90	78(72)*	79
Los Angeles	63(58)	63	54(49)	56
Richmond	58(53)	58	52(47)	51
Sacramento	66(61)	66	58(53)	56
San Diego	73(68)	73	64(59)	65

* Numbers in parentheses are for pump energy taken into account.

TABLE 2. ECONOMIC PARAMETERS FOR BASE CASE ANALYSIS

Construction:	Retrofit
Tax Credit:	None
System Life:	20 years
Loan Duration:	10 years
Loan Interest Rate:	12%
Minimum Attractive Rate of Return:	5.5%
Maintenance Costs:	0
Replacement Costs:	$1.50/ft^2 of collector area
Replacement Increment:	5 years
Insurance Costs:	1% of Capital Cost
Initial Fuel* Cost:	4.5¢/KWHR
Down Payment on Loan:	10% of capital and installation cost
Back-up system Cost:	0
Escalation Rate of Maintenance:	0%/yr
Escalation Rate of Insurance:	0%/yr
Escalation Rate of Fuel:	1%/yr
Inflation Rate:	12%/yr

* based on an electrical water heater

The system with the largest NPW value for a particular location is usually the most cost-effective system. The most-cost effective system for each location is designated with a line under its NPW value. Table 3 shows that the NPW increases considerably but that the relative order does not change with 55% tax credit. The 2TT is seen to be the most cost-effective system at all locations investigated when a 238.88 liter (75 gallon) daily load is required and distributed according to LP1. Results from [3] indicated that the 2TT system is the most economical SDHW system at the five locations considered above for all daily load sizes less than 278.5 liters (100 gallons) and for both LP1 and LP2. For daily loads greater than or equal to 278.5 liters (100 gallons) distributed entirely during the daytime (LP2) the 2TP system was found to have the highest NPW at all of the above locations.

The effect of using natural gas rather than electric auxiliary heaters was investigated. The NPW results after inflation for a 238.88 liter (75 gallon) daily load distributed according to LP1, are shown in Table 4. An effective (cost of energy to heat water) natural gas cost of 1.5¢/KWHR was used in the calculation (see [3]). This is based on 26¢/Therm and a gas hot water heater efficiency of 50% compared to an electrical hot water heater efficiency of 83%.

CONCLUSIONS

When the SDHW systems are compared to a conventional electric hot water system, the NPW is always positive, with or without a tax credit. The 2TT was found to have the highest NPW with the 2TP quite close.

TABLE 3. NPW VALUES AFTER INFLATION FOR A 238.88 LITER (75 GALLON) DAILY LOAD DISTRIBUTED ACCORDING TO LP1
SYSTEM COST USED FOR DETERMINING NPW ARE GIVEN IN APPENDIX A

Location	2TP	2TT	1TP	1TP
El Centro	$2820*($3360)**	$3190($3710)	$1920($2660)	$2130($2940)
Los Angeles	1620(2160)	1900(2420)	818(1560)	1040(1850)
Richmond	1380(1920)	1660(2180)	722(1470)	797(1610)
Sacramento	1770(2310)	2050(2560)	1010(1750)	1040(1850)
San Diego	2100(2640)	2380(2900)	1300(2040)	1470(2280)

* Values not in parentheses are Base Case results.

** Values in parentheses are with the California 55% Tax Credit.

TABLE 4. NPW VALUES AFTER INFLATION FOR A 238.88 LITER (75 GALLON) DAILY LOAD DISTRIBUTED ACCORDING TO LP1, FUEL COST = 1.5¢/KWHR

Location	2TP	2TT	1TP	1TP
El Centro	$173($713)*	$325($842)	$-377($369)	$-382($428)
Los Angeles	225(315)	-105(412)	-743(2.39)	-748(61.3)
Richmond	-305(235)	-18.5(333)	-75(-29.5)	-828(-18.3)
Sacramento	-178(362)	-57.1(460)	-679(66.1)	-748(61.3)
San Diego	-66(474)	54.4(572)	-584(162)	-605(205)

* Values in parentheses are with the California 55% Tax Credit.

When compared to a conventional natural gas hot water system the NPW is negative in most locations without a tax credit but for most of the systems it becomes positive with the California 55% tax credit.

It appears that most SDHW systems are now cost-effective in most California locations with the present tax credit.

REFERENCES

[1] Study of Energy-Saving Options for Refrigerators and Water Heaters - Volume 2: Water Heaters, Arthur D. Little, Inc., May 1977.

[2] J.B. Bergquam, M.F. Young, J.W. Baughn, Comparative Performances of Passive and Active Solar Domestic Hot Water Systems, Fourth National Passive Solar Conference, Kansas City, Missouri, October 1979.

[3] M.F. Young, Solar Domestic Hot Water Heaters - A Comparative Study and Storage Tank Investigation, Ph.D. Dissertation, University of California, Davis, 1979.

[4] J.B. Bergquam, M.F. Young, S. Perry, and J.W. Baughn, A Comparative Study of SDHW Systems in California, Report to the California State Energy Commission, June 1979.

[5] J.W. Baughn and D.A. Dougherty, Experimental Investigation and Computer Modeling of Solar Natural Circulation Systems, Proceedings of the 1977 Annual Meeting, AS/ISES, June 1977.

[6] J.W. Baughn and D.A. Dougherty, Effect of Storage Height on the Performance of a Natural Circulation (Thermosyphon) Hot Water System, 2nd National Proceedings of the Passive Solar Conference, March 1978.

[7] Method of Testing Solar Collectors Based on Thermal Performance, Proposed Standard 93-P, ASHRAE, pg. 21, 1976.

APPENDIX A - SYSTEM COMPONENT COSTS

In this appendix, cost estimates of the various components of each system are given. These "capital" or "first" costs were used in determining the NPW. Capital costs were obtained from retail vendors while installation costs were estimated after several surveys.

2TT (Two Tank Thermosyphon System):

Capital Costs:

66 gallon storage tank w/o electric heater	$ 195.96
30 gallon electric hot water heater	$ 100.80
4' x 10' single glazed non-selective collector	$ 387.00
Piping and insulation	$ 50.00
	$ 733.76
Retro-fit Installation: 30 hrs. at $25/hr	$ 750.00
Total Cost	$1483.76

2TP (Two Tank Pumped System):

Capital Costs:

66 gallon storage tank w/o electric heater	$ 195.96
30 gallon electric hot water heater	$ 100.80
4' x 10' single glazed non-selective collector	$ 387.00
Stainless steel pump	$ 171.00
Differential controller	$ 66.67
Piping and insulation	$ 50.00
	$ 971.43
Retrofit Installation: 20 hrs at $25/hr	$ 500.00
Total Cost	$1471.43

1TP (One-Tank Pumped System):

Capital Costs:

80 gallon storage tank with heat exchangers, electric heater, 1/2 h.p. pump and proportional controller	$1010.67
4' x 10' single glazed non-selective collector	$ 387.00
Piping and insulation	$ 50.00
	$1447.67
Retrofit Installation: 20 hrs at $25/hr	$ 500.00
Total Cost	$1947.67

1TT (One-Tank Thermosyphon System):

Capital Costs:

Two 4' x 5' flat-plate single glazed non-selective collectors, 80 gallon storage tank with electric heater and interconnecting pumping	$1695.00
Piping and insulation	$ 50.00
	$1745.00
Retrofit Installation:	$ 300.00
Total Cost	$2045.00

Dup

A COMPARATIVE ANALYSIS OF SIX GENERIC SOLAR DOMESTIC HOT WATER SYSTEMS

Robert Farrington
Darryl Noreen
L. M. Murphy
Solar Energy Research Institute
Golden, Co.*

ABSTRACT

Results were analyzed from experiments on six solar domestic hot water systems tested at National Bureau of Standards. Use of pumps, fans, controls, and solenoid valves in the pumped systems resulted in high parasitic energy consumption. Storage losses from double tank systems were greater than expected due to poor storage tank insulation. Direct systems performed better than indirect systems as expected. The thermosyphon delivered the most solar energy to the hot water load for the lowest initial cost. The air system performed poorly due to the parasitic energy consumption and poor heat transfer across the air-to-water heat exchanger. Reliable freeze protection needs to be developed for direct systems, especially thermosyphon systems, to take advantage of direct heat transfer.

INTRODUCTION

The Solar Energy Research Institute (SERI) analyzed experimental data provided by the National Bureau of Standards (NBS) of six solar domestic hot water systems (SDHW).[1] The objective of this study is to aid users and designers in understanding existing systems and their relative benefits.[2,3,4,5] The systems tested in this study, selected as typical of those being installed at the time,** were exposed to the same climatic conditions and supported approximately the same thermal load. These systems, therefore, do not necessarily reflect the state of the art nor were they optimized to meet the thermal load. The six systems tested are shown in Fig. 1 and a description of each system is given in Table 1.

Table 1. SYSTEM DESCRIPTION

System	Collector Area m^2 (ft^2)	Solar Storage Tank ℓ (gal)	Auxiliary Tank ℓ (gal)
Single[a] Direct[b]	33.3 (36)	310 (82)	- (--)
Double, Direct	5.0 (54)	310 (82)	159 (42)
Single, Indirect	5.0 (54)	310 (82)	- (--)
Double, Indirect	5.0 (54)	310 (82)	159 (42)
Air System	7.3 (80)	310 (82)	159 (42)
Thermosyphon	5.0 (54)	250 (66)	- (--)

[a]Single or double describes the type of system based on the number of tanks.
[b]Direct or indirect refers to the method of heat transfer.

*This work was supported by the Systems Development Division, Office of Solar Applications, DOE.
**Results discussed in this report are based on the performance evaluations of only those systems tested; therefore, the authors discourage generalizing these findings to apply them to systems with different thermal characteristics.

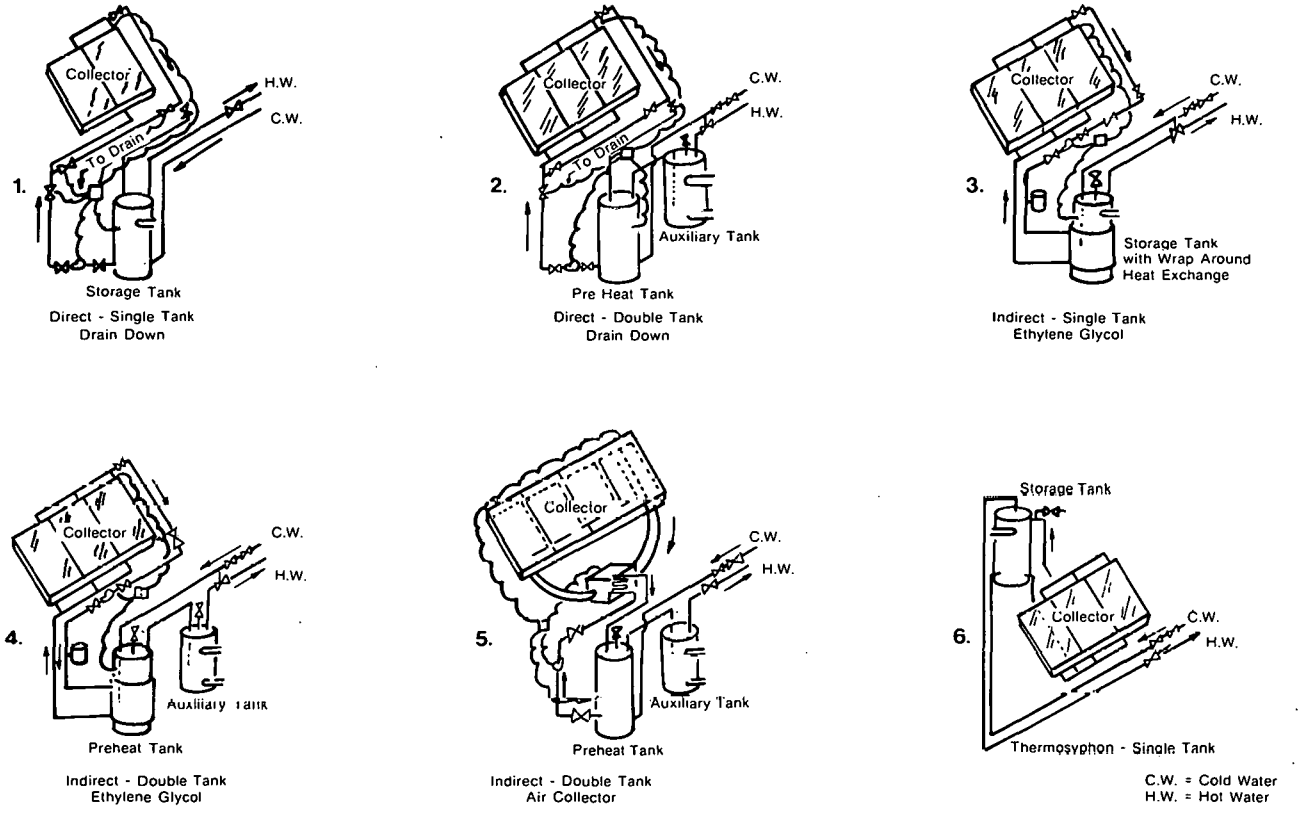

Figure 1. Six Common SDHW Systems Currently In Use

SYSTEM PERFORMANCE

This study included analysis of collector, piping, and storage tank losses as well as energy consumed by pumps, controls and solenoid valves (parasitic energy consumption), and auxiliary heating necessary to meet the load. The thermal efficiency was calculated as well as the system efficiency. The solar fraction was calculated for each system as well as a net solar fraction. When an electric backup was used, the system efficiency and net solar fraction were also calculated considering the energy used at the fossil-fueled generating plant (assumed at 33% efficiency).*

The results from the thermal and system analyses are shown in Table 2.

Table 2. SYSTEM PERFORMANCE[a]

System	Thermal Efficiency (%)	System Efficiency (%)	Solar Fraction (%)[b]	Net Solar Fraction %
Single, Dir.	28.2	21.4 (7.8)	40.9	31.1 (11.4)
Double, Dir.	17.9	12.5 (2.0)	39.8	28.1 (4.6)
Single, Ind.	22.1	19.6 (14.7)	48.6	43.1 (32.3)
Double, Ind.	17.1	14.6 (9.4)	37.9	32.2 (20.9)
Air System	6.6	3.1 (-4.0)	21.7	10.1 (-13.2)
Thermosyphon	23.3	22.6 (21.2)	50.2	48.8 (45.7)

[a]Figures in parenthesis represent values if parasitic energy consumption were considered as energy required at a fossil-fueled electric generating plant.
[b]Collector areas must be considered when comparing solar fractions.

*For definitions of terms used, see nomenclature in back of report.

The double tank systems had lower efficiencies than the single tank systems because the additional tank provided a greater heat transfer area for heat loss. These tanks had 1.07m^2°C/W (R6.1) insulation. Tank losses would be reduced and thermal performance enhanced for double tank systems having greater storage tank insulation.

Indirect systems had lower efficiencies than the corresponding direct systems due to the presence of a heat exchanger and use of an antifreeze. These led to high collector inlet temperatures and therefore lower collector efficiencies. The heat transfer fluid, a mixture of ethylene glycol and water, had 80% of the heat capacitance of water.

Parasitic energy consumption is a major factor in determining the system efficiency of a solar domestic hot water system. Parasitic energy affected the direct systems more than the indirect systems because of the addition of solenoid valves for freeze protection and the double tank systems more than the single tank systems because of the longer operating time. The direct systems had two 15W solenoid valves, which used more energy than the pumps, for draindown freeze protection. (see Table 3).

Table 3. PARASITIC ENERGY CONSUMPTION

System	Hours of Operation (6 mo. total)	Estimated Energy Consumed by Pumps (kWh)	Estimated Energy Consumed by Solenoid Valves (kWh)
Single, Dir.	681.66	68.2	91.4
Double, Dir.	882.87	88.3	91.4
Single, Ind.	690.24	69.0	91.4
Double, Ind.	870.49	87.1	NA
Air System	644.94	64.5(+48.Fan)	NA
Thermosyphon	-	NA	32.4

Because a greater temperature difference existed across the collectors of the double tank systems, they operated longer than the single tank systems. The greater temperature difference resulted from water (or antifreeze) which had never been heated by the auxiliary heating coils entering the collectors at a lower temperature.

The efficiencies of the single and double tank direct systems decreased 24% and 30%, respectively, due to the parasitic energy consumption. The efficiencies of the single and double tank indirect systems decreased 11% and 15%, respectively, due to the parasitic energy consumption.

The air system, the only double-glazed system tested, did not perform well as a stand alone* solar domestic hot water system. This was due to the poor heat transfer across the air-to-water heat exchanger, resulting in high collector inlet air temperatures and large collector losses. Only 22% of the incident energy on the collectors was absorbed by the air. The efficiency of the air system decreased by 53% due to parasitic energy consumption.

Of the systems tested, the thermosyphon systems had the best overall system performance due to low parasitic energy consumption.** Thermal performance was enhanced by the direct method of heat transfer rendering it more efficient than the indirect systems.

SYSTEM ECONOMICS

The economics of solar domestic hot water systems depends on both system cost and system performance.

The initial system cost was broken down into five areas: collector costs; storage costs; pumps, controls, and solenoid valves; miscellaneous component costs (relief valves, gate valves, expansion tanks, thermometers, air vents, heat exchangers, piping, and various fittings); and installation costs. Collector costs were assumed to vary from \$81/m^2 (\$7.50/ft^2) to \$162/m^2 (\$15/ft^2). Collector costs tended to be the largest and the most variable of these and most influenced the total system cost. The other four areas of the cost breakdown were essentially fixed costs. The total installed cost for a system varied substantially depending on the collector cost used.

*As opposed to a combined water and space heating system.

**Solenoid values were added to this system midway through the testing. The degradation of the system efficiency due to the parasitic energy consumption should not, therefore, be compared directly to the other systems.

The cost per joule (Btu) delivered was calculated for the testing period. Table 4 shows the cost of delivered energy for the lowest cost for the collector ($81/m^2). The effect of parasitic energy consumption is included in column 6 and not included in column 5.

Table 5 shows the cost of delivered energy for the highest cost for the collector ($162/m^2). As in Table 4, parasitic energy is accounted for in column 6 and not considered in column 5.

Because of the cost per joule (¢/kJ) reflects only the period of testing of the above systems, a more helpful number for comparison is the cost per GJ ($/Btu) as determined using the initial cost, a system lifetime of 20 years (without system degradation), and the assumption that these systems would deliver approximately three times as much energy to the thermal load during one year of operation as they did during the testing period. Although this is a simplified method that does not include maintenance costs, uncertainties existing in the escalating costs of fuel make it useful for relative comparison of the systems and estimating the cost of energy delivered to the thermal load.

In order to facilitate comparison of those systems, we calculated a relative ranking with the best system equal to one unit of cost per GJ delivered to the thermal load. The result, shown in Table 6, includes the negative effect of parasitic energy by subtracting it from the energy delivered to the thermal load.

With further research and development parasitic

Table 4. SYSTEM ECONOMICS I[a]
[Collectors at $81/m^2 ($7.50/ft^2)]

System	Initial Cost ($)	¢/kJ (¢/Btu) (w/o parasitics)		¢/kJ (¢/Btu) (w/ parasitics)		Days of Testing
Single, Dir.	1718	.092	(.097)	.121	(.128)	127
Double, Dir.	2325	.131	(.139)	.186	(.197)	127
Single, Ind.	2397	.109	(.115)	.123	(.129)	127
Double, Ind.	2802	.164	(.174)	.193	(.204)	127
Air System	3329	.343	(.362)	.757	(.799)	127
Thermosyphon	1267	.054	(.058)	.057	(.060)	121

Table 5. SYSTEM ECONOMICS II
[Collectors at $162/m^2 ($15.00/ft^2)]

System	Initial Cost ($)	¢/kJ (¢/Btu) (w/o parasitics)		¢/kJ (¢/Btu) (w/ parasitics)		Days of Testing
Single, Dir.	2123	.114	(.120)	.150	(.158)	127
Double, Dir.	2933	.166	(.175)	.235	(.248)	127
Single, Ind.	3005	.137	(.144)	.154	(.162)	127
Double, Ind.	3410	.200	(.211)	.235	(.248)	127
Air System	4229	.436	(.460)	.962	(1.015)	127
Thermosyphon	1875	.081	(.086)	.084	(.088)	121

Table 6. COST OF DELIVERED ENERGY AND RELATIVE RANKING I
(Including parasitic energy consumption)

System	$/GJ ($/MBtu) (Collectors at $81/m^2)		Relative Ranking	$/GJ ($/MBtu) (Collectors at $162/m^2)		Relative Ranking
Single, Dir.	20.21	(21.32)	2.12	24.98	(26.34)	1.79
Double, Dir.	31.07	(32.77)	3.26	39.20	(41.34)	2.80
Single, Ind.	20.45	(21.57)	2.16	25.64	(27.05)	1.83
Double, Ind.	32.24	(34.00)	3.39	39.23	(41.38)	2.80
Air System	126.24	(133.16)	13.28	160.37	(169.16)	11.45
Thermosyphon	9.42	(9.93)	1.00	13.94	(14.70)	1.00

energy consumption can be reduced. Therefore, the cost per GJ neglecting parasitic energy consumption calculated for each system can serve as an incentive to reduce parasitic energy consumption.

The relative rating without considering parasitic energy is shown in Table 7.

The relative rankings from Table 6 and 7 are combined in Table 8. Notice in Table 8 the same order results regardless of whether parasitic energy consumption or collector cost is considered. However, considerable differences do exist among the relative rankings depending on the collector cost and the inclusion or exclusion of

Table 7. COST OF DELIVERED ENERGY AND RELATIVE RANKING II
(Excluding parasitic energy consumption)

System	$/GJ ($/MBtu) (Collectors at $81/m^2)		Relative Ranking	$/GJ ($/MBtu) (Collectors at $162/m^2)		Relative Ranking
Single Dir.	15.34	16.19	1.70	18.96	(20.00)	1.41
Double, Dir.	21.91	23.11	2.43	27.64	(29.16)	2.05
Single, Ind.	18.17	19.17	2.02	22.78	(24.03)	1.69
Double, Ind.	27.41	28.92	3.04	33.36	(35.19)	2.47
Air System	57.20	60.33	6.35	72.66	(76.64)	5.38
Thermosyphon	9.13	09.63	1.00	13.52	(14.26)	1.00

Table 8. RELATIVE SYSTEM RANKINGS

System	Collectors at $81/m^2		Collectors at $162/m^2	
	w/o parasitics	w/ parasitics	w/o parasitics	w/ parasitics
Thermosyphon	1.00	1.00	1.00	1.00
Single, Dir.	1.70	2.12	1.41	1.79
Single, Ind.	2.02	2.16	1.69	1.83
Double, Dir.	2.43	3.26	2.05	2.80
Double, Ind.	3.04	3.39	2.47	2.80
Air System	6.35	13.28	5.38	11.45

parasitic energy consumption. Systems should be compared only for a given collector cost and parasitic energy consideration because of the assumptions used in normalizing the cost of energy for the best system, i.e., the thermosyphon system. In other words, comparisons should only be made within a given column, not across rows.

CONCLUSIONS AND RECOMMENDATIONS

Results clearly demonstrate that the thermosyphon is the best choice from an economic perspective. This relative ranking is valid only for the systems tested. If freeze protection requiring sizeable parasitic energy were added to the thermosyphon system the order might change. It should be noted that pumps and solenoid valves that use less energy than the ones used in this experiment are available and are beginning to be used. Parasitic energy consumption is not negligible for systems similar to these tested. Designs should minimize parasitic energy consumption by using properly sized pumps and other parasitic equipment.

It can be concluded that single tank systems perform better than double tank systems if the tank insulating value is similar to ones in this experiment. Double tank systems may be preferred for other reasons, such as greater capacity and use of existing equipment. With different insulation schemes the double tank systems may perform better than the single tank systems.

The air system that was tested performed considerably below all the other systems. However an air SDHW may be desirable if it is coupled with an air space heating system. Care must be taken to minimize the parasitic energy consumption.

The direct systems performed more efficiently than their respective indirect systems even with large parasitic losses associated with the direct systems. With lower powered solenoid values or other

means of freeze protection the margin between the direct and indirect system can be expected to increase. Other aspects of direct systems require further study. Reliability of the freeze protection equipment needs to be considered. Corrosion due to the constant filling and draining of direct systems needs to be examined. Direct systems inherently transfer energy more effectively than indirect systems and work needs to be done to design reliable and efficient direct systems.

Although thermosyphon systems have definite advantages--low parasitic consumption (if at all), low initial cost, and operational simplicity--they also have the disadvantages of being difficult to protect from freeze damage without degrading the thermal performance. Manual or seasonal draindown freeze protection should be considered. Seasonal draindown of thermosyphons can compete economically with active direct and indirct systems.

It is our recommendation, finally, that to increase SDHW system performance on the whole, designers, manufacturers, and researchers need to concentrate on reducing parasitic energy consumption, increasing reliability of components, and maximizing the system efficiency.

NOMENCLATURE

Net solar fraction: Solar energy used at the thermal load minus the parasitic energy consumption divided by the thermal load.

Parasitic energy consumption: Energy consumed by pumps, fans, and controls and solenoid valves in a solar energy system.

Solar fraction: Percentage of the thermal load met by solar energy.

System efficiency: Solar energy delivered to the thermal load minus the parasitic energy consumption, divided by the solar energy incident on the collector surface.

Thermal efficiency: Percentage of the incident radiation used at the thermal load.

Thermal load: Thermal energy required to meet the hot water load, excluding storage tank losses.

Thermosyphon system: System which depends on density gradients for fluid circulation instead of mechanical pumps.

REFERENCES

1. National Bureau of Standards. Solar Domestic Hot Water Test Facility July-December 1978 Experimental Data. A. H. Fanney, project leader. Gaithersburg, MD.

2. Fanney, A. H. Experimental Validation of Computer Programs for Solar Domestic Hot Water Heating Systems. National Bureau of Standards, Center for Building Technology; July 1978.

3. Buckles, W. E.; Klein, S. A.; Duffie, J. A. Analysis of Solar Water Heating Systems. ISES Annual Meeting, Atlanta, GA; 1979.

4. Fanney, A. H.; Lia, S. T. "Experimental System Performance and Comparison with Computer Predictions for Six Solar Domestic Hot Water Systems." Proceedings of the 1979 International congress of the International Solar Energy Society. Atlanta, GA; May 28-June 1, 1979.

5. Farrington, R. B.; Murphy, L. M.; Noreen, D. A Comparison of Six Generic Solar Domestic Hot Water Systems. SERI RR-351-413. Golden, CO: Solar Energy Research Institute; forthcoming.

COMPARISON OF SOLAR THERMAL POWER SYSTEMS

J. J. Iannucci
Energy Systems Studies Division
Sandia Laboratories
Livermore, CA

P. J. Eicker
Heliostat Division
Sandia Laboratories
Livermore, CA

ABSTRACT

Because of past development efforts, three major candidates currently exist for solar thermal power systems: central receivers, parabolic troughs, and parabolic dishes. In this study, systems using each of these technologies have been designed and costed to provide thermal energy at 93, 149 and 316°C (200, 300 and 600°F) for end use sizes of 3, 30, 300, and 1500 MWth. Higher temperature designs were also generated for the central receiver systems. Each system was engineered to the same specifications and applications as constraints. As examples, all systems can survive the same wind speeds and are made of the same materials where appropriate at the same unit costs. The results point up the principal design differences and allow one to rank these three technologies, based on annual delivered thermal energy costs, for a range of applications and end use sizes.

INTRODUCTION

Solar energy is actively being considered for many applications in the United States. Prominent among these applications is the production of process heat at various temperatures and for diverse plant sizes. While central receivers, parabolic troughs, and parabolic dish systems each might be able to fulfill all of these needs at all temperatures and sizes of interest, certain technologies may be economically superior for certain applications. The objective of this paper is to present consistent designs, costs, and performance values for a large technology/application matrix. First order design differences and similarities are highlighted. Detailed annual performance simulations are performed and a simple economic model employed to yield levelized energy costs for each case.

The thermal energy systems examined were: 93, 149, and 316°C (200, 300, and 600°F), each at sizes of 3, 30, 300, and 1500 MWth, provided by each of the three technologies: central receivers, troughs, and dishes. In addition, designs were developed for central receivers at 510 and 1093°C (950 and 2000°F).

The design philosophy has been to create tailored systems for each technology, collector temperature, and plant output, which are mutually consistent. Each must produce thermal power at the same power ratings and temperatures. Each must survive and perform in the same environmental conditions with the same insolation. Costs and performance must be calculated by the same techniques. Here the constraints upon the design of the systems end. For example, the choice of working fluid, piping layout, pipe diameters, insulation thickness on each pipe element, pumping motors, pressure drops, thermal losses, and overnight protection are free to be chosen for each system as best suits it. Great care has been taken to be even handed with each technology, not forcing it to use techniques or materials with which it is incompatible or are needlessly expensive. As an example, pipe diameters and insulation thicknesses are chosen individually and carefully with regard to both cost and performance. Despite the consistency of the design philosophy, the resulting systems for each of the three solar technologies are quite distinct as would be expected.

Each of the systems has been divided into several subsystems which were designed in parallel. The collector subsystem consists of the reflective surface and all that is required to support and direct its motion. The receiver subsystem is the set of tubes through which the working fluid passes (and insulation around them as required) and also includes the support to hold these tubes in place. The transport subsystem is the set of piping network components necessary to connect the receivers to one another and to the end use point. Each of these subsystems and the design procedures used are described below and then the overall costs, efficiencies and delivered energy costs are given. Much more detail will be found in References 1-5.

COLLECTOR SUBSYSTEM

Each collector subsystem was designed with the following ground rules: (1) use of laminated glass mirrors of 50 m^2 aperture area; (2) the glass was bonded to steel hat sections; (3) steel support structures connect these hat sections to a drive tube; (4) harmonic drive was used for 180° motion, no provision was made for inverting; (5) the drives bolt to precast, prestressed concrete piles which are driven into place. The design process then consisted of (1) determining the area and weight of the glass surface .64 centimeters (.25 inches) thick based on f/D = .5 for dishes and f/D = .25 for troughs; (2) determining the wind loads at the

gimbal axes (to determine the required drive torque for winds of 145 km/h (90 mph) while stowed, 80 km/h (50 mph) in any orientation and 48 km/h (30 mph) while in operation); (3) determining the dimensions, weights, etc. of the main structural members to withstand wind and gravity loads (with the same maximum stresses and deflections allowed in the McDonnell Douglas heliostat design) [2].

While the wind lift and drag forces on each system are very similar, the torques are not since the center of pressure is much further from the rotational axis for curved sections. This leads to the need for stiffer (and heavier) structure (both steel and concrete) and larger drives, especially in the dish design. The cost breakdowns for each of the three collector subsystems are shown in Table 1.

Performance coefficients (optical efficiencies versus sun position) were determined and are presented in Reference 2.

TABLE 1. COST BREAKDOWN FOR DISHES, HELIOSTATS, AND TROUGHS, 1979 $.

	DISH	HELIOSTAT	TROUGH (N-S)
Mirror Surface	$ 639	$ 566	$ 697
Drives	1290	868	556
Controls & Wiring	309	381	213
Structure	893	553	646
Pedestal/Foundation	652	416	600
Installation & Other	409	349	506
Total $/Unit	$4192	$3113	$3218
Total $/m^2 Aperture	$85/m^2	$64/m^2	$66/m^2

NOTE: Costs assume established production at 25000 units per year, with 8% fee and 10% contingency included. "Other" includes checkout, assembly, maintenance equipment and transportation (exept pedestal), but not land, receivers, or piping.

RECEIVER SUBSYSTEM

Within each technology considered, the receiver subsystem needs to be more closely tailored to match the end use than was the collector subsystem (e.g., the heliostat design for any central receiver system is independent of temperature and probably independent of system size over a broad range of sizes; the receiver, however, must be designed specifically for a given temperature and power rating). All systems were constrained to have an expected life of 30 years, to operate at the designated temperatures, and to be optically consistent with the appropriate collector subsystem. Based upon these constraints, a conceptual design was developed for each receiver. The receiver dimensions were calculated and the tube sizes and insulation requirements determined. For the central receiver systems, the tower height was determined, the choice between external and cavity was made (only the highest temperature system is a cavity), and the overall dimensions of the working fluid panels derived. For the dish systems, all receivers were cavities with external insulation applied; the cavity opening was optimized with regard to optical spillage and thermal losses. The trough receiver was a simple carbon steel pipe (with selective coating) at the focal line. It was determined that a glass envelope was desirable at 300 and 600°F. While each trough reflective section was 50 m^2 in area (2 meters wide by 25 meters long), a thermal length of 200 m (400 m^2 area) was chosen to ensure turbulent flow for good heat transfer in the receiver. This was accomplished by ganging eight troughs in series [3].

The receiver costs with support struts are roughly 13 and 25 $/m^2 of collector aperture area for the lowest and highest temperature troughs, respectively. The dish receivers with support struts cost 12 $/m^2. The lower temperature central receivers cost 5 to 6.5 $/m^2 including the tower cost. The 2000°F central receiver was estimated to cost 29 $/m^2, with the 950°F system in the 11 $/m^2 range [3].

ENERGY CENTRALIZATION SUBSYSTEM

Energy centralization designates the process of energy transport once the concentrating collectors (central receivers, dishes, and troughs) have put the diffuse insolation into a transportable form. In the case of thermal collectors, this form is simply the sensible heat which has been added to a working fluid. Energy centralization entails all that must be done to accumulate all of these energies until the nameplate capacity of the plant has been piped to, or near, a single end use location. Specifically, this means laying out a complete piping network (including risers and downcomers) to connect each receiver to an end use point (and back) in the most cost effective way. A Lagrange multiplier techniques has been used to optimize (1) the pipe diameters with respect to cost and parasitic pumping power; (2) the insulation thicknesses with respect to cost and thermal losses while operating [4]. The items included in the energy centralization subsystem accounts are: field piping (installed including handling, alignment, footings, sliders, fittings, welding, expansion allowances, testing and checkout), insulation with weather protection, risers and downcomers (insulated and flexible as appropriate), pumps, valves (isolation, control, check), diagnostics, fluid, and heat tracing where necessary.

The costs of the baseline thermal energy centralization systems are summarized in Table 2. The basic cause of the dramatic cost differences is the length of piping required for each. (As an example, for the 1500 MWth case, the pipe lengths required are roughly 6, 130, and over 1000 kilometers for the central receiver, trough, and dish systems, respectively.) It should be remembered that the trough receiver tubes do double duty, hence the difference in field piping with the dishes. Details and sensitivities of all these costs to collector size, parallel and series connection, and edge vs. central collection have been determined also [4].

TABLE 2. BASELINE THERMAL ENERGY CENTRALIZATION COST SUMMARY* ($/m^2).

TEMPERATURE °C	TEMPERATURE °F	TECHNOLOGY CENTRAL RECEIVER	TROUGH	DISH
93	(200)	0.5 - 1.5	7 - 7.5	50 - 55
149	(300)	0.5 - 1.0	7 - 8	51 - 56
316	(600)	1.5 - 2.5	10 - 16	69 - 99
510	(950)	5.	---	---
1093	(2000)	9.	---	---

*All costs in rounded 1979 dollars, the ranges represent variations in system power rating from 3 to 1500 MWth.

The performance of the thermal energy centralization systems follows the same tendencies. The design point thermal losses are shown in Table 3. Another concern, the parasitic pumping power requirements, are fairly well balanced between technologies. These range (in MWh electricity required per MWh thermal produced) depending upon power rating and temperature from 0.2 to 3.7% for the dishes, 0.05 to 0.83% for the troughs, and 0.1 to 2.1% for the central receiver systems. The overnight thermal losses lead to annual energy impacts of up to 10%, 3.3%, and 0.14% for the dishes, troughs, and central receiver systems, respectively. Thus, the overall transport performance edge goes to the central receiver, the dish systems performing most poorly.

TABLE 3. BASELINE PIPING THERMAL LOSSES AT DESIGN POINT (%).

TEMPERATURE °C	TEMPERATURE °F	TECHNOLOGY CENTRAL RECEIVER	TROUGH	DISH
93	(200)	0.05 - 0.15	0.7 - 0.9	3.6 - 4.8
149	(300)	0.1 - 0.2	1.2 - 1.6	5.0 - 7.0
316	(600)	0.3 - 0.7	3.6 - 3.8	16.6 - 20.4
510	(950)	.65	---	---
1093	(2000)	.11	---	---

ENERGY PRODUCTION COSTS

The performance coefficients at off-design conditions (temperature, windspeed, sun angle, etc.) were calculated and used in the STEAEC code [6] to calculate the annual energy production from each plant design. Insolation data for Barstow, California, was used as typical of other southwest localities. The subsystem costs and performance can be combined with other known cost items, which are common to all systems, to yield delivered energy costs for process heat.

The following assumptions were used to calculate the delivered energy costs: (1) 17.75% fixed charge rate; (2) operation and maintenance costs of 2% of capital cost escalating at 8% per year; (3) balance of plant of $2500 per MW and land at 1 $/m^2 ($4000 per acre); (4) sun following dispatching with no storage; (5) 30 year payback with utility accounting, 1979 dollars. Table 4 shows preliminary estimates of the process heat costs which were determined [5].

TABLE 4. PROCESS ENERGY COSTS. ($/10^6 BTU,† 1979$)

	Size	Temperature, °C (°F) 93 (200)	149 (300)	316 (600)	510 (950)	1093 (2000)
CENTRAL RECEIVER	3 MW_t	5.60	5.60	6.20		
	30 MW_t	5.70	5.60	6.30		
	300 MW_t	6.00	5.90	6.70	7.40	19.50
	1500 MW_t	6.60	6.30	7.60		
PARABOLIC TROUGH	3 MW_t	6.50	7.00	8.70		
	30 MW_t	6.60	7.10	8.90		
	300 MW_t	6.80	7.20	9.30		
	1500 MW_t	7.00	7.30	9.80		
PARABOLIC DISH	3 MW_t	8.90	8.70	12.40		
	30 MW_t	9.30	9.00	13.40		
	300 MW_t	9.80	9.40	14.80		
	1500 MW_t	10.90	10.00	17.90		

†To convert to $/$MWh_t$ multiply by 3.413.

SUMMARY AND CONCLUSIONS

When trough, dish, and central receiver systems are designed with the same design criteria and per unit material and fabrication costs, certain similarities and differences arise. The collector subsystems are physically similar and their costs compare closely, differing primarily due to the stiffer drives and structures required in the dish systems. The receiver subsystems are quite diverse in design and cost as would be expected: the more highly concentrating systems (dishes and central receivers) have smaller and hence less expensive receivers in the lower temperature ranges. At very high temperatures, where more expensive materials are required, the receiver costs rise appreciably. The energy centralization subsystems are quite distinct from one another in cost and performance. Primarily due to the sheer lengths of pipe required (e.g., the 1500 MWth cases use 6, 130 and over 1000 kilometers for the central receiver, trough, and dish systems, respectively), the central receiver piping is least expensive and most efficient.

The bottom line delivered thermal energy costs are quite attractive across the matrix of technology, temperature, and scale. The costs are fairly independent of scale due to the effect of a slight diseconomy of solar capital cost with scale. The central receiver systems are competitive at all temperatures and sizes, appearing to be slightly superior to trough systems. The dish thermal costs are somewhat higher than the other two systems due primarily

to the cost of its piping network [1,5].

ACKNOWLEDGEMENTS

This work is the synthesis of the efforts of the authors and J. B. Woodard, J. D. Hankins, and E. D. Eason as part of the detailed technology comparison in References 1 through 5. This work was supported by the United States Department of Energy.

REFERENCES

[1] P. J. Eicker, "Design, Cost and Performance Comparisons of Several Solar Thermal Systems for Process Heat: Vol I, Executive Summary," SAND 79-8279, to be published.

[2] E. D. Eason, J. D. Hankins, "Design, Cost and Performance Comparisons of Several Solar Thermal Systems for Process Heat: Vol II, Concentrator Design Cost and Performance," SAND79-8280, to be published.

[3] J. B. Woodard, "Design, Cost and Performance Comparisons of Several Solar Thermal Systems for Process Heat: Vol III, Receiver Design, Cost and Performance," SAND79-8281, to be published.

[4] J. J. Iannucci, "Design, Cost and Performance Comparisons of Several Solar Thermal Systems for Process Heat: Vol IV, Energy Centralization Systems, Design, Cost and Performance," SAND79-8282, to be published.

[5] P. J. Eicker, J. J. Iannucci, "Design, Cost and Performance Comparisons of Several Solar Thermal Systems for Process Heat: Vol V, System Design, Cost and Performance," SAND79-8283, to be published.

[6] J. B. Woodard, G. J. Miller, "STEAEC--Solar Thermal Electric Annual Energy Calculator Documentation," SAND77-8278, January 1978.

INFLATION AND TAXES IN BENEFIT-COST ANALYSIS

J. Clair Ellis
The Aerospace Corporation

ABSTRACT

Economists have long promoted the use of the techniques of benefit-cost analysis in both public and private decision-making to enhance objectivity and economic efficiency. The analysis of solar energy systems has relied on those techniques to an unprecedented extent. Unfortunately, the varying applications of those techniques often introduce substantial uncertainty and confusion into the analysis results, particularly concerning the choice of a discount rate and the treatment of inflation and taxes. While the appropriate discount rate has been widely discussed, if not unanimously agreed upon, neither the standard textbooks nor the theoretical literature provide an integrated treatment of the latter two "real world" considerations.

This paper examines the effects of income tax considerations on the choice between real and nominal approaches to benefit-cost analysis. Substantial biases are found in both approaches as they are typically applied. The advantages and disadvantages of both approaches are discussed, as well as recent theoretical and empirical advances which may provide improvements. A generic required revenue model is used to analyze the remaining uncertainties. An example of a solar energy system to supply industrial process heat is used to illustrate and quantify those uncertainties. The implications for future benefit-cost studies are summarized and suggestions are offered which may lead to more realistic, and more modest, decision recommendations.

(Paper was not available for publication. Copies of it may be obtained directly from the author, The Aerospace Corporation, P.O. Box 92957, Los Angeles, California 90009.)

NOTES

SOLAR MODELS DATA BASE

K. A. Kramer
Data Base Analyst
Solar Energy Research Institute

Abstract

The Solar Energy Information Data Bank (SEIDB) of the Solar Energy Research Institute (SERI) has undertaken the identification and classification of models and simulations used in solar energy applications. At the present time, there is no central resource for descriptions of the variety of programs which are available. By Spring of 1980, the SEIDB will have more than 170 descriptions of solar models and simulations stored in a computer and searchable online.

This Models Data Base contains descriptions of models with wind, active solar heating and cooling, photovoltaics, solar thermal, biomass, passive solar, and ocean systems applications and technologies. The functions of the models range from optimizing the size of solar collectors to monitoring the response of an OTEC plant platform to ocean waves.

The individual models described in the data base represent varying stages of development and levels of users. Models available for single runs to the general public are described, as are models which require sophisticated programming and which are used for complex research applications.

Each record in the data base describes one solar model in three sections: background information, technical descriptions, and computer information. The background file lists the developer, access information, user level, contact names and addresses, literature references, and validation tests. The technical file contains six text fields describing in detail the model problem, analytical method, limitations, user inputs, data files, and results of the run. The computer file outlines the model's operating requirements including language, machine, core, operating system, and run time.

Users may access the information in the data base in several ways. The model name is indexed for the user who wishes to retrieve information on specific model. Technology indexes have been assigned each model for the user who wishes to see, for example, all photovoltaic or passive solar models. A user who wishes to learn about all economic models or models that provide design analysis may access the data base by numerous keywords or purpose codes. Besides descriptive indexes of the models, the user may find all models available for a single run in California or all models available for architectural applications.

Introduction

In the expanding areas of energy technology, there are major demands for information and data being made not only by the technical community, but by governmental agencies and legislative bodies, architects, manufacturers, the financial community, builders, and homeowners. A specific information need of many of these groups is for the identification ofmodels and simulations used in solar energy applications. To meet this need, the Solar Energy Research Institute (SERI), with its Solar Energy Information Data Bank (SEIDB)*, has developed a Solar Models Data Base with the goal of identifying and classifying data on models and simulations with solar applications and making this information readily available to the solar community.

Need for the Models Data Base

As in other fields, models and simulations have gained wide use and respect within the solar community during recent years and, therefore, the number of models has grown significantly. Currently, numerous models exist that analyze a variety of solar energy aspects and applications. Many of these models were developed by universities for standards and testing applications. Private industries and utilities have developed

*This research, information and data center, specified by Congress in the Solar Energy Research Development and Demonstration Act of 1974, (PL 93 473), provides a centralized and comprehensive resource directed toward furnishing valid information and data in usable forms, to meet the varied requirements of the diverse solar audience. The Solar Energy Information Data Bank includes the development of online accessible data bases of solar related information, a computer network to utilize the data bases, an information dissemination program, a solar energy information center with a collection of over 25,000 publications, and an Inquiry-Referral service.

models to test their own products or systems, and to project future needs. The Federal government has made a significant investment in model development for research and development efforts. With the myriad of useful models and simulations being developed, information about these models needs to be available to the modeling and solar communities. Government sponsored models are generally documented but these reports may not be widely advertised or distributed. Other significant models may be buried in the thesis library of a university or are being developed by a private company only for their own use. The research and development efforts in the field of solar models and simulations will be most effective when the results of the efforts are widely known. The Solar Models Data Base Program is designed to provide broad dissemination of this information.

The Solar Models Data Base serves two major needs of the solar community. First, by utilizing the data base, or corollary publications, model users can find the model or simulation that best answers their modeling needs. Secondly, model developers may access the resources to discover other modeling activity in specific areas and, thereby, avoid duplicative effort.

Model users, including builders, architects, designers, analysts, engineers and others, are continually looking for new, efficient, more precise models. A researcher developing a collector sizing model may not know that a federal grant is funding a similar project. A state may need to project gasohol demand for the next decade and not realize that another state has begun research in that area. A builder's pricing model may not account for a new Federal tax credit which a more recent model would calculate into the system price. By utilizing the data base, all these people would enhance their use and development of solar models.

Contents of the Models Data Base

The models and simulations contained in the data base are categorized by the following technologies:

Active Solar Heating/Cooling, Bioconversion, Chemical Conversion, Hybrid Systems, Low-Head Hydro, Energy General, Passive Solar Heating/Cooling, Photovoltaic (Solar Cells), Process Heat, Satellite Solar Power, Ocean Systems, Solar General, Energy Storage, Solar Thermal Power, Wind Energy Conversion. If any aspect of a model pertains to one or more of these applications or technologies, the model is eligible for inclusion in the data base. In addition, the model may simulate a variety of circumstanees surrounding a solar technology. Life cycle cost analysis, collector sizing, thermal mass sizing, and cost/benefit analysis are common model applications that can be found in the data base. Alcohol fuel demand, blade performance of a wind machine and evaluation of wave stress on an OTEC plant platform are more unique applications that can also be found in the data base.

Because of the variety of applications and technologies in the data base, the complexity of the models varies also. Models run on TI-59 programmable calculators such as TEANET are included, as are models such as SIM (Solar Insolation Model) which requires a ten seconds run per location per year on a Cyber 74. A beginning user of models may wish to see descriptions of other programmable calculator models whereas a researcher may use the data base to locate other complex photovoltaic models. Search strategies for the data base allow both users to find what they need. The contents of the data base are designed to supply all information necessary to determine if a specific model will serve an individual user's needs and if he/she can obtain and run the model. For the computer scientist, specific computer hardware requirements are listed. For the elementary user, the level of knowledge needed to run the model is described. For scientists and researchers, detailed descriptions of the purpose, analytic approach, inputs and outputs of the models are included.

Formating of the Models Data Base

A record in the Models Data Base contains three main sections; the name of the model functions as the main locator.

Section I

Model Name or Acronym	Validation Tests
Developer	Availability
Commercial Contacts	Costs
Level of User Knowledge	Sponsor
Documentation	Years of Releases
Literature References	Current User Types

Section II

Purpose of Program	Problem Definition
Inputs	Outputs
Analytic Approach	Limitations
Comparable Models	Degree of Solar Emphasis

Section III

Computor Language	Operating Systems
Type of Computer	Machine
Core Required	Run Time

The following is a sample record from the data base. F-CHART was chosen because of its familiarity to users. SERI will not attempt to validate any models included in the data base and inclusion in the data base does not denote endorsement.

Example of Information on F-Chart to be Included in The Solar Models Data Base

Model Name	:	F-CHART
Model Developer	:	University of Wisconsin
Year of Original Release	:	1976
Year of Current Release	:	1979
Program Sponsor	:	Solar Heating and Cooling Systems Development Branch, Office of Conservation and Solar Application, Department of Energy
Developer	:	University of Wisconsin, Madison, Wisconsin
Contact	:	Accounting Branch Solar Energy Research Institute 1617 Cole Boulevard Golden, CO 80401
Purpose of Contact	:	To Purchase/Order
Contact	:	Design Tool Manager Market Development Branch Solar Energy Research Institute 1617 Cole Boulevard Golden, CO 80401 (303) 231-1261
Purpose of Contact	:	For More Information
Accessibility & Cost	:	For Purpose Magnetic Tape . . . $100.00 Card Deck . . . . . $150.00 Overseas Shipping . $200.00
Documentation	:	User's Manual

Literature References

1. Klein, S. A., Bechman, W. A., and Duffie, J. A., "A Design Procedure for Solar Heating Systems," Solar Energy, 18, 113, (1976).
2. Klein, S. A., Bechman, W. A., and Duffie, J. A., "A Design Procedure for Solar Air Heating Systems," accepted for publication in Solar Energy, (1977).
3. Bechman, W. A., Klein, S. A. and Duffie, J. A., Solar Heating Design by the F-CHART Method, Wiley-Interscience, New York, (1977).
4. Hughes, P. J., et al., "F-CHART Version 3.0 Users Manual," Report 49-3 of the Engineering Experiment Station, University of Wisconsin-Madison, June (1979).
5. R. T. Ruegg, "Solar Heating and Cooling in Buildings: Methods of Economic Evaluation," NBSIR 75-712, U.S. Department of Commerce, National Bureau of Standards.

User Type	:	Architects, Utility Company, Researcher, Home Owner, Engineer, Contractor/Builder, Designers, Educators
Level of User Knowledge	:	Beginner

Program Description

Purpose of Program		Design Method, Building Energy Analysis
Problem Definition	:	F-CHART, which models liquid or air solar water heating or combined solar water and space heating systems (solar cooling or heat pump systems cannot be modeled) is capable of estimating the thermal performance and lifecycle economics to assist in the design of the system.
Analytic Approach	:	The F-CHART design method is based on standard solar heating system configurations using either liquid or air as the heat transfer medium. This method treats collector area as the main design variable but is capable of considering secondary design variable such as storage unit capacity. The F-CHARTS are the result of correlating hundreds of detailed simulations of solar heating systems.
Inputs-Data Files	:	The meteorological data required to use the F-CHART method are the long-term monthly average of daily total solar radiation on a horizontal surface or on the collector plane, the long-term monthly average ambient temperature, and the long-term monthly

average heating degree days ($65^{\circ}F$ base).

Inputs-User : The solar energy system data needed for the F-CHART includes the collector parameters, the effectiveness of heat exchangers between collector and tank and between the tank and building (for liquid-based systems), the storage capacity per unit area of collector, and the orientation of the collector.

The building heating load is incorporated either by specifying the monthly load (calculated by any standard technique) or by specifying the building overall loss coefficient (energy per degree-day concept), which is the design heating load divided by the design temperature difference. In addition, a service hot water load can be added to the heating load. Given these numbers, the fraction of monthly total loads and the fraction of the annual loads to be carried by solar energy can readily be determined for any collector area.

Outputs : There are two options in the use of the program. First, the collector area can be specified and the annual (and monthly, if desired) thermal performance is returned. If cost data are supplied, an economic assessment can also be returned. The second option is to request the program to find the economic optimum collector area. The program uses a numerical technique to optimize the collector area and returns the same information as the first option but for the optimum area. The economic optimum collector area is found by calculating the estimated value of future costs for both the solar system and the conventional system (including, if desired, the effects of escalating fuel prices, property and income taxes, tax rebates, interest, depreciation, insurance, and maintenance). The optimum collector area minimizes the sum of the present value of future cost plus the initial costs of the solar system above the costs of a conventional heating system.

Limitations : Two basis uncertainties are associated with F-CHART. First, a system must be well engineered and constructed to perform the way in which F-CHART estimates. Second, there are uncertainties in the meteorological data. Some data are long-term averages of careful measurements and will not change much; other data are subject to change.

Solar Emphasis : Primary

Computer Information

Used On :

Language : FORTRAN

Machine	Operating System	Core or Run Required
Cyber CDC or	Scope II Version 501	23000_{10} characters 54000_{8} characters

Searching the Models Data Base

Two subject keyword schemes exist for indexing individual models. A searcher may use one or more of the fifteen technologies previously described, or, utilizing a controlled vocabulary list, the searcher may use broader subject keywords to locate a model. A searcher may locate models in several other ways: by purpose of model (such as life cycle cost, component analysis, load program), user type (such as architect, economist, homeowner), accessibility to model (such as purchase, single run service, lease), or contact person or company for the model (name and address of developer, marketer, or sponsor). The following are examples of common questions answered by the data base:

Are there any models that deal with wind systems in the data base?

Which models are especially useful to utility companies? Who can I contact to use the model?

What models run in FORTRAN?

Which models give life cycle costs for solar heating and cooling applications? Is there a model called SOLTES? Describe it in detail.

Solar Model Information Sources

Several publications describing solar models currently exist. The Technology Commercialization Division of SERI, in cooperation with the Systems Analysis Branch and the Information Systems Division, has published a brochure detailing several models with solar heating and cooling applications entitled "Analysis Methods for Solar Heating and Cooling Applications: Active and Passive Systems" (SERI/SP-35-232R, January 1980). This new brochure complements earlier publications on "Analysis Methods for Wind Applications" (SERI/SP-35-231) and "Analysis Methods for Photovoltaic Applications" (SERI/SP-35-230).

To inform the modeling community about the Solar Models Data Base and to encourage designers of new models to submit information on their programs, the Information Systems Division of SERI has published Solar Models Data Base Candidates (SERI/SP-451-563). This brochure lists more than 170 models and simulations that are being considered for entry into the computerized Solar Models Data Base. In the Spring of 1980, SERI will publish an up-to-date, detailed pamphlet describing solar models with a wide range of solar technologies and applications. The Solar Models Data Base will be fully operational in March 1980 and will be available for online searches.

If a user has a special question that cannot be answered in the publications from the data base, he/she may access its online capabilities. SERI's Solar Energy Information Center, the National Solar Heating and Cooling Information Center, the four Solar Energy Regional Offices, and the Department of Energy in Washington, D.C. have direct access to the system. A user may write or call any of the offices listed below to outline their information needs.

Mid-American Solar Energy Complex
8140 26th Avenue, South
Bloomington, Minnesota 55420
(612)854-0400
SEIDB Contact: Ms. Joyce Mortison
Chief Librarian: Ms. Agnes Brown

Southern Solar Energy Center
61 Perimeter Park
Atlanta, Georgia 30341
(404)458-8765
SEIDB Contact: Mr. George Meier
Chief Librarian: Ms. Pam McElhaney

National Solar Heating and Cooling Information Center
1911 Arch Street
Philadelphia, Pennsylvania 19103
(215)448-1535
SEIDB Contact: Ms. Marcia Ballen
Chief Librarian: Ms. Gloria Fultz

Northeast Solar Energy Center
70 Memorial Drive
Cambridge, Massachusetts 02142
(617)661-3500
SEIDB Contact: Dr. David Chan
Chief Librarian: Ms. Eileen Baker

Western SUN
921 S.W. Washington Street
Suite #160
Portland, Oregon 97205
(503)241-1222
Chief Librarian: Mr. Jay Tappan

Beginning Spring of 1980, SERI will be hosting a series of SEIDB training sessions. The training session participant will receive training in the INQUIRE data base management language and will learn particulars of the SEIDB data bases.

Besides maintaining descriptions of solar models and simulations, SERI has an On-line Models Library that contains the full model in executable forms. Currently SERI is maintaining three models - F-CHART, SOLCOST, and RSVP. For additional information on the On-line Models Library or the Solar Energy Information Data Bank (SEIDB) and training opportunities for its use, please contact the following persons at the Solar Energy Research Institute (SERI), 1617 Cole Boulevard, Golden, Colorado 80401:

Network Coordinator - Training
Rafael Ubico (303)231-1032

Data Base Development Branch Chief
Howard Shirley (303)231-1204

On-line Models Library Manager
Nancy Birkenheuer (303)231-1464

Solar Models Data Base Analyst
Kate Kramer (303)231-1227

NOTES

SERI ON-LINE MODELS LIBRARY

Nancy Birkenheuer

Abstract

The Solar Energy Research Institute (SERI) Computer Center, operated by the Computer Systems Branch of the Information Systems Division, currently provides large-scale computational capability utilizing a CDC Cyber 70/Model 76, a Cyber 170/Model 720, and two CDC-2551 Communication Processors. This center is available to outside users via a value-added network. To provide additional support to the user community, a system for on-line access to computer models relating to solar applications is being developed. This project is designed to enhance and compliment the capabilities of the Solar Energy Information Data Bank (SEIDB) at SERI. The target user community for the On-Line Models Library includes Regional Solar Energy Centers (RSEC's), affiliated institutions, DOE offices and laboratories, subcontractors, universities, and internal SERI users. Models selected for the library must be complete, operational and well documented. A broad range of applications will be available, including materials research, systems analysis, passive systems, market analysis, sizing, costing, and graphics. After a formal request is approved, the user will receive access to the system through an interactive executor program. This program allows model selection and execution, and processes accounting information. The capability to produce listings and, eventually, graphics at the central site to be mailed to remote users will also be provided.

Introduction

On-line access to analytical models and related calculation tools for use by the nation's solar energy community is being provided through the scientific computational facility at the Solar Energy Research Institute (SERI). The user community is expected to include Solar Energy Information Data Bank (SEIDB) Network participants: the DOE Regional Solar Energy Centers and the National Solar Heating and Cooling Information Center, DOE solar offices, laboratories and contractors, SERI and its subcontractors, and colleges and universities engaged in related energy research.

All models offered through the On-Line Models Project are catalogued and maintained with extensive documentation on content and procedures for execution. Models currently ready, under development, or planned for conversion encompass the solar technologies of passive systems, photovoltaics, wind, solar thermal, biomass, and ocean thermal. A broad range of applications will be available, including materials research, systems design and analysis, sizing, costing, market analysis, and graphics.

The intent of the On-Line Models Project is to augment the capabilities of the SEIDB models data base which contain the descriptions and characteristics of each model. The project will also enhance the Systems Analysis Test and Validation Program Code Center (SATVA) at SERI. Models that meet the necessary criteria will be chosen from the Code Center to reside in the SEIDB Models Library.

Candidate Models

Over three hundred models which have been developed at laboratories and universities around the country, including SERI, are being evaluated for inclusion in the library. Many SERI branches, including the Computer Systems Branch, the Systems Analysis Branch, and the Solar Thermal Conversion Branch are actively acquiring and testing selected models. Members of the Computer Systems Branch are converting and enhancing the capabilities of the more promising models. A partial list of the candidate models being evaluated for inclusion in the on-line models collection is presented below:

Available in Library:

F-CHART	Solar Heating Systems Design
RSVP	Residential Solar Viability Program
SOLCOST	Residential and Commercial Solar Costing & Design

Under Development:

SIM	Simulation of Solar Irradiance Components
SOLTRAN	Solar Beam Intensity Spectrum at Earth's Surface

Other Possibilities:

BLAST	Building Thermal Loads Model
DEROB	Simulation of Passive Solar Systems Design
DOE-2	Building Thermal Loads Model
EASE-2	Economic Analysis of Solar Energy
ECONMAT	Solar System Costing Model
MITAS	General Thermal Analysis
PASOLE	Simulation of Passive Solar Systems Design
PROSYS	Process Heat System Performance Model
SIMWEST	Simulation of Wind Energy Storage Systems
SOLCEL	Simulation of Photovoltaic System Performance
SPURR	National Market Penetration Model
TRNSYS	Simulation of Transient Thermal Performance

A partial list of software to be available in conjunction with the library:

DISSPLA	Graphics Software
SPSS	Statistics Software
TSP	Time Series Software
IMSL	Math Library

Utility programs for data conversion, insolation and angle calculations, return on investment computations, and financial charting will also be available.

Computer Systems and Communications

Access to the On-Line Models Library is being provided through the SERI Computer System. The major components of this system, manufactured by Control Data Corporation, include a Cyber 70/Model 76, a Cyber 170/Model 720, a Gandalf Communication Processor, and two CDC 2551 Communication Processors (Fig.1). The system will be accessible nationwide through the data communications value-added network Tymnet.

Terminals will be connected to the communications processors via concentration devices that will account for line contention and routing, either to the scientific processor or to the remote host for data base processing. Through the use of Tymnet, most users will need only make a local call to access the SERI Computer System. Some users will also have Remote Job Entry access to the system (Fig. 2).

System Access Procedures

After a user's request for access to the Models Library has been approved by SERI, the user will be assigned a unique identification number. When the user logs on and runs the executor program for the library, several procedures will execute automatically. An accounting and a record-keeping program will ask for model selection or return a menu of models or detailed descriptions of the models. Once the model has been selected, another program will then prepare the control language for the model, run the model, and return control to the executor program. Optional data files for modeling applications, such as Typical Meteorological Year (TMY) tapes and SOLMET tapes, eventually will be provided in addition to the existing default data files for each model.

A message and suggestion file is to be provided for user comments. At the conclusion of each session, costs will be tallied and printed. The printed listings as well as the graphics outputs will be mailed to the remote user.

Resource ceilings are maintained for each user identification number to prevent unauthorized or unlimited usage. Resources per session are also limited, unless appropriate authorization is provided. Library copies of the models will be stored with read-only access.

Documentation and Standards

Each model is tested for completeness and operability before being accepted for inclusion in the Models Library. A comprehensive user's manual is also required. All SERI-introduced modifications will be tested and verified against original results. To the extent that it is practical, the program code for all models is self-documenting and has incorporated interactive data input.

Cost

SERI is currently working with DOE to determine a costing policy and rate schedule for users of the Models Library. This information will be announced as soon as it becomes available.

SEIDB Liaison Contacts

Pertinent SEIDB contacts at SERI are listed below. Interested users should feel free to contact these individuals as the need arises. Any contact for general coordination purposes should be through SERI's Network Coordinator, Rafael Ubico, who has overall responsibility for maintaining effective working relationships within the network.

Function	Name	Telephone Ext.
Network Coordinator, SEIDB	Rafael Ubico	(303) 231-1032 or FTS 327-1032
Models Library	Nancy Birkenheuer	(303) 231-1464 or FTS 327-1464
Models Data Base	Kate Kramer	(303) 231-1227 or FTS 327-1227
Document Dissemination	Steve Rubin	(303) 231-1207 or FTS 327-1207
Applications Programming & Technical Support	David Ashton	(303) 231-1251 or FTS 327-1251
Systems Programming & Network Communications	Leroy Lacy	(303) 231-1252 or FTS 327-1252

Schedule

Costing Policy Announcement	May 1980
Availability of Library Message File	Feb. 1, 1980
	Feb. 15, 1980
Additional Model Added to Library	As they become available

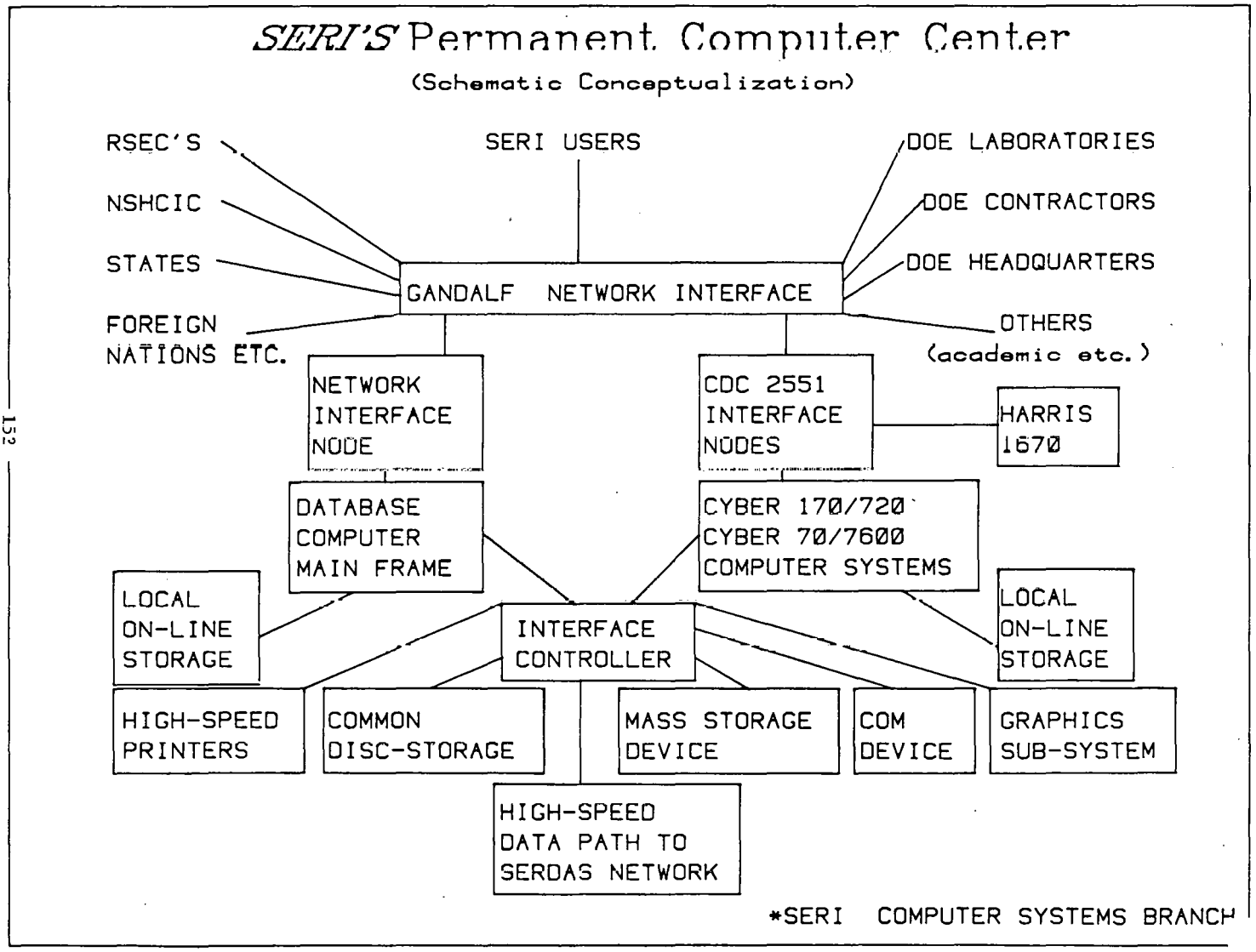
SERI'S Permanent Computer Center
(Schematic Conceptualization)
RSEC'S
NSHCIC
STATES
FOREIGN NATIONS ETC.
SERI USERS
DOE LABORATORIES
DOE CONTRACTORS
DOE HEADQUARTERS
OTHERS (academic etc.)
GANDALF NETWORK INTERFACE
NETWORK INTERFACE NODE
CDC 2551 INTERFACE NODES
HARRIS 1670
DATABASE COMPUTER MAIN FRAME
CYBER 170/720 CYBER 70/7600 COMPUTER SYSTEMS
LOCAL ON-LINE STORAGE
INTERFACE CONTROLLER
LOCAL ON-LINE STORAGE
HIGH-SPEED PRINTERS
COMMON DISC-STORAGE
MASS STORAGE DEVICE
COM DEVICE
GRAPHICS SUB-SYSTEM
HIGH-SPEED DATA PATH TO SERDAS NETWORK
*SERI COMPUTER SYSTEMS BRANCH

Figure 1

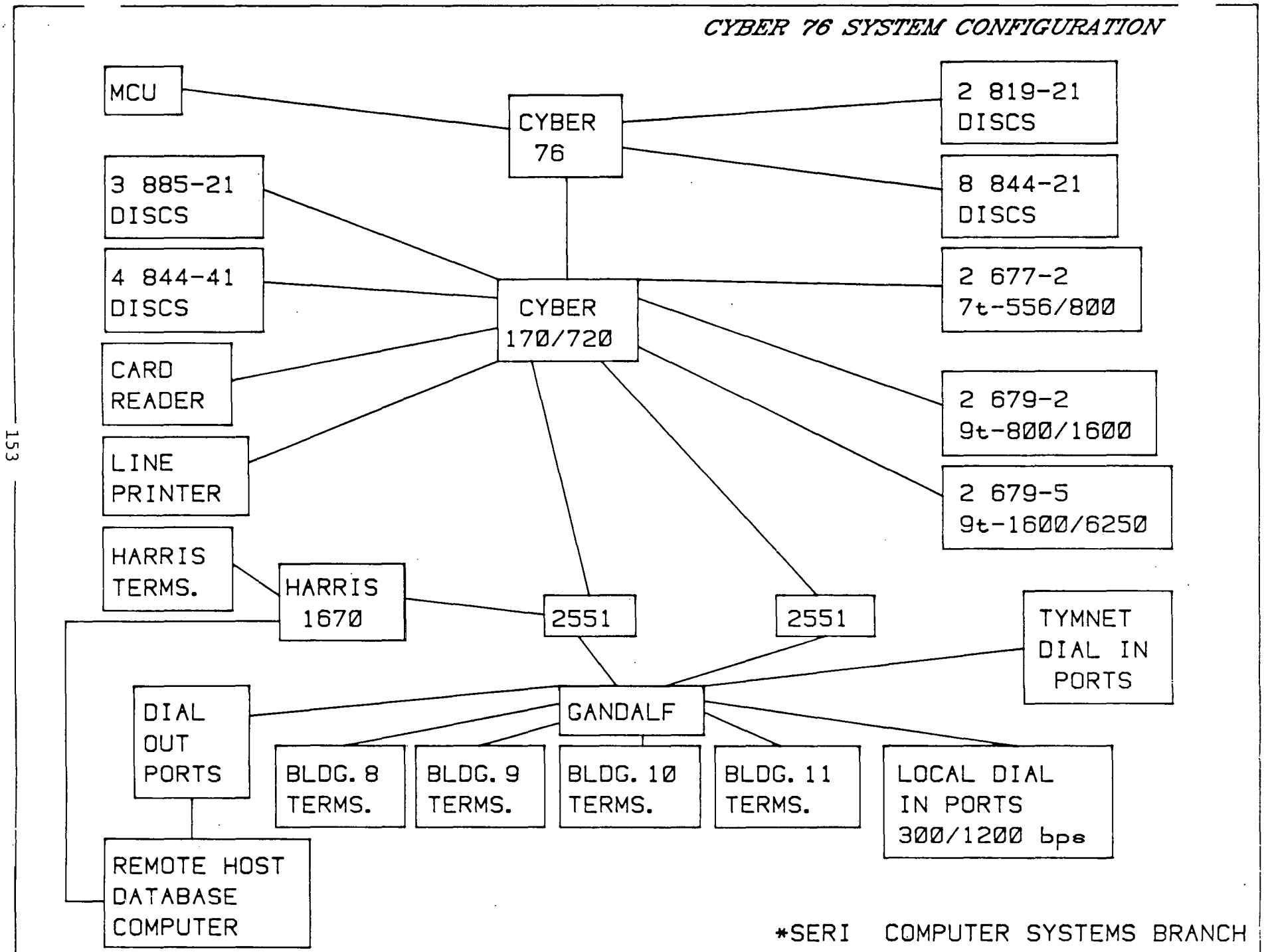
CYBER 76 SYSTEM CONFIGURATION
MCU
CYBER 76
2 819-21 DISCS
8 844-21 DISCS
3 885-21 DISCS
4 844-41 DISCS
CYBER 170/720
2 677-2 7t-556/800
CARD READER
LINE PRINTER
2 679-2 9t-800/1600
2 679-5 9t-1600/6250
HARRIS TERMS.
HARRIS 1670
2551
2551
TYMNET DIAL IN PORTS
DIAL OUT PORTS
GANDALF
BLDG. 8 TERMS.
BLDG. 9 TERMS.
BLDG. 10 TERMS.
BLDG. 11 TERMS.
LOCAL DIAL IN PORTS 300/1200 bps
REMOTE HOST DATABASE COMPUTER
*SERI COMPUTER SYSTEMS BRANCH

Figure 2

Session IVA

Dr. Mashuri L. Warren
Lawrence Berkeley Laboratory
Chairperson

CONTROLS II

IMPLEMENTATION OF AN OPTIMAL CONTROLLER OF THE SECOND KIND

Robert C. Winn
Graduate Research Associate
Solar Energy Applications Laboratory
Colorado State University
Fort Collins, Colorado 80523

C. Byron Winn
Professor
Solar Energy Applications Laboratory
Colorado State University
Fort Collins, Colorado 80523

ABSTRACT

An optimal controller of the second kind is one which maximizes the difference between the useful energy collected by a solar heating system and the associated pumping costs. This paper presents an analytical solution to the optimization problem and describes the method of implementing the microprocessor based optimal controller. The optimal controller built for Solar House II at Colorado State University, which has an air solar heating system, is described. Comparisons of system performance for a bang-bang controller with a single stage fan, an optimal controller with an infinitely variable fan, and an optimal controller with a four stage fan are presented. Also, the effect of errors in system parameters on system performance is analyzed.

INTRODUCTION

An optimal controller of the second kind is one which maximizes the difference between the solar energy collected and the associated pumping costs. This problem was first approached by Kovarik and Lesse [1]. They solved the problem numerically, but their solution could not be implemented because it was not a function of measurable states of the system and required advance knowledge of weather data. Winn and Hull presented an approximate analytical solution to the problem which can be implemented [2]. They showed close agreement between their results and the results of Kovarik and Lesse.

This paper presents an alternate approximate solution to the problem with results identical to those of Winn and Hull. The problem is further simplified so that it can actually be implemented in a practical controller. An optimal controller of the second kind has been built and is being installed in Solar House II at Colorado State University. This controller provides an alternative to the bang-bang controller as well as the proportional controller for solar heating systems.

THE OPTIMIZATION

The problem is to maximize the difference between the solar energy collected and the parasitic pumping costs, both of which are functions of collector mass flow rate, $\dot{m}$. That is, maximize

$$I = \int_0^{t_f} [C_1 Q_u(\dot{m}) - P(\dot{m})]dt \qquad (1)$$

where C_1 is a weighting factor which takes into account the difference between cost of energy to run the fan and that to provide auxiliary heating. A sufficient condition for this expression to be a local maximum is that the term

$$dI/dt = J = C_1 Q_u(\dot{m}) - P(\dot{m}) \qquad (2)$$

must be a maximum at all times.

The energy collected can be found from the Hottel-Willier-Bliss equation [3]

$$Q_u(\dot{m}) = F_R A_c [H_T \tau\alpha - U_L(T_i - T_a)] \qquad (3)$$

where

$$F_R = (\dot{m}C_p/U_L A_c)[1-\exp(-FU_L A_c/\dot{m}C_p)] \qquad (4)$$

and

A_c = collector area
H_T = solar insolation on the collectors
τ = transmissivity of the collector glazings
α = absorptivity of the absorber plate
U_L = overall collector loss coefficient
T_i = collector inlet temperature
T_a = ambient temperature
C_p = specific heat of the collector fluid
F = collector efficiency factor.

To simplify this relationship, the exponential is expressed as a Taylor series and truncated after second order terms. With this approximation, the energy collected is expressed as

$$Q_u(\dot{m}) = (F - F^2 U_L A_c/2\dot{m}C_p)A_c[H_T\tau\alpha - U_L(T_i - T_a)]. \qquad (5)$$

Now define the available energy as

$$f = Q_u/F_R = A_c[H_T\tau\alpha - U_L(T_i - T_a)] \qquad (6)$$

Hence,

$$Q_u(\dot{m}) = fF - fF^2U_LA_c/2\dot{m}C_p. \quad (7)$$

The parasitic pumping costs must also be expressed as a function of mass flow rate. The fan laws state that the power required by a fan is proportional to the cube of the flow rate [4]. This theoretical relationship will be changed by factors such as fan efficiency and changing flow regimes, which will also vary with flow rate. For this analysis, however, the parasitic pumping costs are treated as a function of the cube of the flow rate; that is,

$$P(\dot{m}) = C_2\dot{m}^3. \quad (8)$$

The problem now is to maximize

$$J = C_1fF - C_1fF^2U_LA_c/2\dot{m}C_p - C_2\dot{m}^3. \quad (9)$$

The flow rate is the only term in this expression which can vary significantly in a short period of time. Therefore, by taking the derivative of J with respect to flow rate and setting it equal to zero, the optimal mass flow rate can be determined as

$$\dot{m}_{OPT} = (C_1fF^2U_LA_c/6C_2C_p)^{1/4} \quad (10)$$

This is the same result obtained by Winn and Hull [2].

The available energy, f, is determined from either

$$f = \dot{m}C_p(T_{OUT} - T_i)/F_R \quad (11)$$

if the collector fan is on, or

$$f = U_LA_c(T_{OUT} - T_i) \quad (12)$$

if the fan is off [2]. Here, T_{OUT} is the collector outlet temperature. Thus, the optimal mass flow rate is determined from a knowledge of the system parameters, the flow rate during the last time interval, and the collector inlet and outlet temperatures.

IMPLEMENTATION

Practical implementation of this optimal control problem requires some compromises. The solution of the problem requires a fan with an infinitely variable flow rate. This is not practical; however, there are several multi-speed fans on the market. Therefore, the optimal controller picks the fan speed with the flow rate closest to the optimal flow rate. The solution of the problem also requires continuous measurement of collector temperatures and continuous updating of the optimal flow rate. This would result in cylcing which would be at the least bothersome. To avoid this problem, an arbitrary time interval between updates must be established. A microprocessor based controller may be used to make the calculations and maintain the time interval between updates.

Calculating the optimal mass flow rate as described earlier requires 8K of program storage space which is expensive. To reduce the required storage size, the calculations are replaced by a table search. The new optimal flow rate depends on the flow rate for the previous time interval and the temperature difference across the collector. For a four stage fan, there are only five possible flow rates, zero or one of the four stages. For each of these flow rates, temperature differences are determined which will result in each of the five possible flow rates for the next time interval. Thus a table is generated which, with the search program, requires less than 1K of storage. This reduction in storage reduces the cost of the controller by about half. For a system with parameters given in Table 1, the matrix shown in Table 2 results.

The optimization takes place when the controller's internal clock signals that it is time for an update. The collector inlet and outlet temperatures, which are analog signals, are converted to digital signals and subtracted. The resulting digital signal and the digital signal corresponding to the most recent flow rate are used to enter the table. A digital signal corresponding to the new optimal fan stage results and is used to send a signal to the appropriate fan stage relay.

RESULTS OF SYSTEM SIMULATIONS

The approximate analytical solution with an infinitely variable flow rate compares closely to the exact numerical solution [2]. Simulations show that an optimally controlled four stage fan system performs almost as well as the optimally controlled infinitely variable flow rate system.

Three systems were simulated; each system was assumed to have the parameters shown in Table 1. System 1 was a bang-bang control strategy with ΔT_{OFF} of 3°F and ΔT_{ON} of 20°F, system 2 was the optimal control strategy with an infinitely variable flow rate, and system 3 was the optimal control strategy with a four stage fan. The results of simulations for several different insolation conditions are shown in Table 3.

The compromised optimally controlled system, system 3, has an overall performance within 0.6% of system 2 over the entire range of insolation conditions. Both optimally controlled systems perform better than the system with the bang-bang control strategy, particularly on days with low insolation.

The optimization relies on an accurate determination of system parameters. To test the sensitivity of the optimization to errors in parameters, simulations were run with mass flow rates 10% higher than design. The results are shown in Table 4.

TABLE 1. SYSTEM PARAMETERS

Collector Area, A_c	55.76 m^2
Collector Loss Coefficient, U_L	14.4 $kJ\text{-}hr^{-1}\text{-}°C^{-1}\text{-}m^{-2}$
Specific Heat of Air, C_p	1.004 $kJ\text{-}kg^{-1}\text{-}°C^{-1}$
Weighting Factor, C_1	1.
Pumping Cost Constant, C_2	$7.716 \times 10^{-8} kJ\text{-}hr^2\text{-}kg^{-3}$
Stage 1 Mass Flow Rate, $\dot{m}_1$	1401 $kg\text{-}hr^{-1}$
Stage 2 Mass Flow Rate, $\dot{m}_2$	2659 $kg\text{-}hr^{-1}$
Stage 3 Mass Flow Rate, $\dot{m}_3$	2910 $kg\text{-}hr^{-1}$
Stage 4 Mass Flow Rate, $\dot{m}_4$	3342 $kg\text{-}hr^{-1}$

TABLE 2. SEARCH TABLE

$(T_{OUT}-T_i)$ (°C)		Fan Stage for Last Time Interval				
		0	1	2	3	4
Fan Stage for Next Time Interval	0	-∞→0.19	-∞→0.07	-∞→0.05	-∞→0.04	-∞→0.04
	1	0.19→13.4	0.07→5.2	0.05→3.0	0.04→3.0	0.04→2.7
	2	13.4→47.3	5.2→18.4	3.2→11.4	3.0→10.5	2.7→9.4
	3	47.3→75.3	18.4→29.2	11.4→18.1	10.5→16.8	9.4→14.9
	4	75.3→∞	29.2→∞	18.1→∞	16.8→∞	14.9→∞

TABLE 3. SIMULATION RESULTS

Objective Function, I (kJ/day)	Peak Daily Insolation (W/m^2)		
	400	600	800
System 1 (Bang-Bang)	114240	259545	406624
System 2 (Optimal)	134924	277351	425037
System 3 (Optimal with 4-Speed Fan)	134072	277016	424652

TABLE 4. SENSITIVITY OF SYSTEM PERFORMANCE TO FLOW RATE ERRORS

Objective Function, I (kJ/day)	Peak Daily Insolation (W/m^2)		
	400	600	800
Optimal System with 4-Speed Fan	134072	277016	424652
Optimal System with 10% Error in Flow Rate	132421	275277	422229
Bang-Bang System	114240	259545	406624

With an error in system parameters, the system does not perform optimally; however, the difference from the optimum is small. The improvement over the bang-bang system performance is still significant.

CONCLUSIONS

A controller which maximizes the difference between energy collected and pumping costs has been built. It is a microprocessor based controller which requires the collector inlet and outlet temperatures as inputs. The controller picks the optimal air flow rate and signals the fan to operate at the appropriate stage.

The decision that the controller makes depends on the values of system parameters used in the controller. If these values are in error, the performance of the system will not be optimal. Therefore, accurate identification of system parameters is important. Most of the parameters can be easily determined, but the mass flow rates for each stage and the corresponding power requirements are difficult to predict. They both depend on the fan and the system in which it is installed. The recommended implementation procedure, then, is to estimate the parameters and install the controller. Then operate the system and measure the parameters. The microprocessor can then be reprogrammed more accurately. If it is impractical to measure the parameters, a small deviation from the optimum occurs, but the system still performs much better than if controlled by bang-bang logic.

An optimal controller of the second kind is currently being installed in Solar House II at Colorado State University. The house uses air as the collector fluid and has a four speed fan installed. The performance of this optimally controlled system will be reported at a later date.

ACKNOWLEDGEMENT

This work was sponsored in part by a grant from the U.S. Department of Energy under contract number EG77-S-02-4519.

REFERENCES

[1] M. Kovarik and Lesse, "Optimal Control of Flow in Low Temperature Solar Heat Collectors," Solar Energy, Vol. 18, No. 6 (1976).
[2] C.B. Winn and D.E. Hull, III, "Optimal Controllers of the Second Kind," Solar Energy (1979).
[3] J.A. Duffie and W.A. Beckman, Solar Energy Thermal Processes, John Wiley & Sons, New York, 1974.
[4] ASHRAE, Guide and Data Book, Equipment, ASHRAE, New York, 1975.

Dup

COMPARISON OF PROPORTIONAL AND ON/OFF COLLECTOR LOOP CONTROL STRATEGIES USING A DYNAMIC COLLECTOR MODEL

Steven R. Schiller and Mashuri L. Warren

Solar Group
Energy and Environment Division
Lawrence Berkeley Laboratory
University of California, Berkeley

and David M. Auslander

Department of Mechanical Engineering
University of California, Berkeley

ABSTRACT

Common control strategies used to regulate the flow of liquid through flat-plate solar collectors are discussed and evaluated using a dynamic collector model. Performance of all strategies is compared using different set points, flow rates, insolation levels and patterns (clear and cloudy days), and ambient temperature conditions.

The unique characteristic of the dynamic collector model is that it includes the effect of collector capacitance. In general, capacitance has a minimal effect on long term collector performance; however, short term temperature response and the energy-storage capability of the collector capacitance are shown to play significant roles in comparing on/off and proportional controllers. Inclusion of these effects has produced considerably more realistic simulations than any generated by steady-state models.

Simulations indicate relative advantages and disadvantages of both types of controllers, conditions under which each performs better, and the importance of pump cycling and controller set points on total energy collection.

Results show that the turn-on set point is not always a critical factor in energy collection since the collector stores energy while it is warming up and during cycling; and, that proportional flow controllers provide improved energy collection only during periods of interrupted or very low insolation. Although proportional controllers initiate flow at lower insolation levels than on/off controllers, proportional controllers produce lower flow rates and higher average collector temperatures, resulting in slightly lower instantaneous collection efficiencies.

INTRODUCTION

Active solar heating systems are generally capitol intensive; therefore, improvements which increase system efficiency must do so with only a small incremental initial cost in order for them to help solar energy compete with other energy sources. Since improved control strategies and controllers may satisfy these criteria, researchers and manufacturers have sought to evaluate and improve solar energy system controllers[5,8,9,11,12,13,15,16].

Commercially available controllers for domestic heating systems include both on/off and proportional control of the collector fluid[16]. While some manufacturers have advertised microprocessor based control systems, none of these systems are cost effective, as yet, for residential solar energy usage. On/off controllers have had the widest application due to their simplicity and generally reliable operation. However, demonstration projects [2,3,,6,14] have shown that two problems can occur with these controllers; 1) they can cause the circulating pump to cycle on and off excessively and 2) improper selection of set points can cause low system efficiency. In response to these problems some controller manufacturers have marketed proportional flow controllers claiming improved overall system efficiencies. This project was therefore undertaken to determine the relative merits of proportional and on/off control so that solar manufacturers and designers will be able to improve system efficiencies.

DYNAMIC FLAT-PLATE SOLAR COLLECTOR MODEL

The Hottel-Whillier-Bliss (H.W.B.) collector model [7], as adapted by Klein [10] to include the effects of capacitance, is used to describe the operation of a flat-plate solar collector. The model is based upon a heat balance on a tube and fluid element within a collector, where the entire capacitance of the collector is lumped within the tubes and the circulating fluid. The heat balance is solved using numerical methods on a digital computer to describe the circulating fluid's temperature as a function of time and space. The transient heat balance for a collector element of width W_c is:

$$\partial T_{f,x}/\partial t = \gamma\left[(F'/C_A)[S - U_L(T_{f,x} - T_a)] - (\dot{m}c_p/C_A W_c)(\partial T_{f,x}/\partial x)\right] + (1 - \gamma)\left[(F'/C_A)[S - U_L(T_{f,x} - T_a)]\right] \quad (1)$$

Where: If $\gamma = 1$ pump is running

If $\gamma = 0$ pump is not running

C_A is the weighted average of the total collector capacitance. This equation is for a non-drain down collector. For a drain down system a two lump model is required since the collector and fluid capacitance would have to be treated separately.

The spatial derivative is eliminated by breaking the collector into a number of stirred tanks; thus, the time dependent temperature of the Nth node is written:

$$dT_N/dt = \gamma\left[(F'/C_A)[S - U_L(T_{f_N} - T_a)] + (\dot{m}c_p/C_A W_c \Delta x)(T_{f_{N-1}} - T_{f_N})\right] + (1 - \gamma)\left[(F'/C_A)[S - U_L(T_{f_N} - T_a)]\right] \quad (2)$$

This equation for 4 nodes was solved using the Parasol program [1] which solves differential equations through the use of the fourth-order Runge-Kutta method. The Parasol program's output is the fluid temperature at different positions and for discrete time intervals.

The model described by equation 2 is adopted for the following reasons:

1) It provides a simple and accurate description of the transient temperature distribution in a collector's circulating fluid.
2) It included the effects of collector capacitance.
3) It is derived from a well established and respected collector model.
4) Results it provides are usable and consistent with known collector operation.

COLLECTOR PARAMETERS

To compare the various control strategies using a collector computer model, appropriate parameters must be used which represent a typical flat-plate collector under the influence of common external conditions. Although a multi-node model is used for the simulations, the single node model is used to define the parameters used. These parameters are then scaled for use in a multi-node model.

In the limiting case of a single node model of the collector, equation 2, for flow conditions, can be written to demonstrate the functional dependence of the collector temperature on 1) insolation and ambient temperature, 2) fluid flow rate and 3) collector characteristics:

$$C_A dT_{out}/dt = (K_{gain})f(t) + (K_{flow})T_{in} - (K'_{flow})T_{out}$$

Where:

K_{gain} represents the collector's gain from insolation and losses to the environment
$K_{gain} = F'[S_{max} + U_L T_{a,max}]$

f(t) represents the time variation of the normalized forcing function due to insolation and ambient temperature

K_{flow} represents the fluid flow rate per unit area
$K_{flow} = \dot{m}c_p/A_c$

$K'_{flow} = \dot{m}c_p/A_c + F'U_L$; since, $F'U_L << \dot{m}c_p/A_c$

K_{flow} approximately equals K'_{flow}

C_A represents the collector/fluid capacitance per unit area

By allowing K_{gain} and K_{flow} (and K'_{flow}) to take on either HIGH or LOW values while keeping all other parameters constant, the various control strategies are compared based on a limited but comprehensive set of collector, meteorological, and flow variations which are used to define limits of operation for a typical collector. The numerical values for the parameters used are summarized in Table 1.

The dynamics associated with the storage tank and the piping are not considered to be critical for comparative results; therefore, the collector inlet temperature, T_{in}, is constant.

The solar day for all runs is 12 hours long with a peak insolation rate reached at hour 6. For modeling of a clear day (no interruptions of insolation) the insolation rate, I, is proportional to a sine wave with a 24 hour period. For a cloudy day (the view of the collector intermittently interrupted) the following equation, that was used by Close[4], determines the insolation rate as a function of time, t, in hours:

$$I = (I_{max}/2)[\sin \pi t/12)][\cos(40\ \pi t/12) + 1]$$

The ambient temperature, T_a, is proportional to a sine wave with a 24 hour period, the peak value is at the 9th hour of the solar day:

$$T_a = TO + TM * \sin(\pi t/12 - \pi/4) \qquad t = \text{hours}$$

COLLECTOR FLOW CONTROLLERS

The collection of solar energy is controlled by the flow of fluid through the collector loop. Collector outlet and storage tank temperatures are compared by a controller to determine the fluid flow rate. The difference between the collector outlet temperature and the storage tank temperature is known as ΔT and represents the temperature rise across the collector.

On/Off Flow Control

The on/off controller is a thermostat which turns the fluid circulation pump either on or off based on ΔT. The flow rate ($\dot{m}$) through the collector is defined by the following equations:

$$\dot{m} = \begin{cases} 0 & \begin{cases} \text{if } \Delta T < \Delta T_{on} \text{ and last flow} = 0 \\ \text{or} \\ \text{if } \Delta T < \Delta T_{off} \end{cases} \\ \dot{m} & \begin{cases} \text{if } \Delta T \geq \Delta T_{on} \\ \text{or} \\ \text{if } \Delta T \geq \Delta T_{off} \text{ and last flow} = \dot{m} \end{cases} \end{cases}$$

Where:

ΔT_{off} = temperature difference between fluid outlet and inlet sufficient to turn pump off.

ΔT_{on} = temperature difference between fluid outlet and inlet sufficient to turn pump on.

The region between ΔT_{on} and ΔT_{off} is known as the hysteresis zone. Because of hysteresis on/off controllers have "memory" which limits pump cycling.

Proportional Flow Control (with saturation)

In this type of feedback controller the fluid flow rate is varied as a function of the temperature rise across the collector, ΔT. The advantages of proportional controlled system are: fluid circulates at lower values of ΔT and pump cycling is minimized. The fluid flow rate through the collector can be described with the following equations:

$$\dot{m}(t) = \begin{cases} 0 & \text{for } \Delta T < \Delta T_{off} \\ K\Delta T & \text{for } \Delta T_{off} \leq \Delta T \leq \Delta T_{max} \\ \dot{m}_c & \text{for } \Delta T \geq \Delta T_{max} \end{cases}$$

Where:

$\dot{m}_c$ = maximum flow rate

K = proportional flow constant equal to ratio of the maximum flow rate to the temperature difference required for maximum flow: $K = \dot{m}_c / \Delta T_{max}$

ΔT_{max} = temperature rise across collector at which flow rate saturates to its maximum

ΔT_{off} = the temperature rise across the collector sufficient to turn off the pump or the minimum temperature rise across the collector for which it is possible and/or profitable to turn on the pump

DETERMINATION OF CONTROLLER SET POINTS

In determining proper controller set points there are two major considerations: set points must be chosen to maximize energy collection and minimize pumping power(or cost); and set points must be within the capability of the sensors used. The importance of sensor sensitivity and location cannot be overstressed since these two concerns have caused numerous problems in some solar installations.

The minimum temperature rise across the collector required for maintaining flow, ΔT_{off}, is the one that realizes an energy value collection rate equal to the energy cost of running the pump; therefore, ΔT_{off} can be shown to equal:

$$\frac{\text{(pumping power)(pumping cost)(heating system efficiency)}}{\text{(fluid capacitance flow rate)(heating cost)(pump efficiency)}}$$

This equation can be used for both on/off and proportional flow controllers. If a higher value of ΔT_{off} is used, say to meet sensitivity requirements of an uncalibrated sensor, less energy will be collected since the pump will turn on later, shut off sooner and cycle more than necessary.

Unlike ΔT_{off}, only a range of values can be determined for ΔT_{on} without knowledge of specific weather conditions. To determine an optimum range for ΔT_{on} the steady-state H.W.B. model is used to analyse a solar collector. The maximum practical value for ΔT_{on} would be one that insures that the pump never cycles. That is, ΔT_{on} is set so that after the pump turns on at some level of absorbed insolation and ambient temperature the temperature rise across the collector does not fall below ΔT_{off}. Control stability requires that the minimum ΔT_{on} be greater than ΔT_{off}. Using these criteria it can be shown that the ratio of ΔT_{on} to ΔT_{off} should be greater than unity while less than the ratio of the capacitance flowrate to the approximate collector heat loss:

$$1 \leq \frac{\Delta T_{on}}{\Delta T_{off}} \leq \frac{\dot{m} c_p}{A_c F_R U_L}$$

For typical parameters $\Delta T_{on}/\Delta T_{off}$ is calculated to be less than thirty, much larger than typical ratios of 2 - 7 used in the solar industry[2,16] that provide satisfactory results while allowing some cycling at low temperatures or insolation levels.

CONTROLLER AND SET POINT COMPARISONS:

The controllers are compared on the basis of their performance with respect to: collection efficiency, maximum steady-state efficiency, pump running time and pump cycling. These comparisons are the results of digital computer simulations using a time step of 0.001 hours for high flow rates and 0.002 hours for low flow rates. The model is implemented on a PDP 11/60 computer.

A total of six controllers are compared under 8 different sets of conditions. The four on/off controllers have the following characteristics:

A) $\Delta T_{on} = 5^{o}C(9^{o}F)$, $\Delta T_{off} = 1.7^{o}C(3^{o}F)$

B) $\Delta T_{on} = 11.7^{o}C(21^{o}F)$, $\Delta T_{off} = 1.7^{o}C$

C) $\Delta T_{on} = 5^{o}C$ with a 'perfect' timer

D) $\Delta T_{on} = 11.7^{o}C$ with a 'perfect' timer

The proportional controllers have the following characteristics:

E) full flow at $\Delta T_{c} = 5^{o}C = \Delta T_{max}$, $\Delta T_{off} = 1.7^{o}C$

F) full flow at $\Delta T_{c} = 11.7^{o}C = \Delta T_{max}$, $\Delta T_{off} = 1.7^{o}C$

The set points were picked to represent upper and lower limits of values used in industry and research. Timers are used to limit the amount of cycling; therefore, the 'perfect' timer eliminates all pump cycling.

One day simulations of different control strategies indicate how their operation varies with different set points, timers, meteorological conditions, and flow rates. Figure 1 shows a typical collector outlet temperature history generated by the model for a morning of low insolation. Table II presents the collection efficiencies, pump running times and amount of cycling for the different control strategies under the assigned conditions.

RESULTS

For the clear day cases, the collection efficiency for all but one of the controllers is approximately equal and not more than 7% below the maximum steady-state efficiency. The on/off controllers, in general, did slightly better with the on/off controllers with timers achieving the best efficiency since they run the pumps for the longest amount of time. It is doubtful that any other type of controller could do better under similar conditions. During periods of interrupted insolation though, neither proportional nor on/off controllers respond well to rapid changes in the insolation rate and the collection efficiency falls well below the maximum possible.

Proportionally-controlled collectors can collect more energy during periods of interrupted insolation and/or very low insolation than on/off-controlled systems, because the proportional controller is more sensitive to changes in insolation and ambient temperature than the on/off controller. This sensitivity also causes the proportional controller to maintain a lower average flow rate and thus operate the collector at higher temperatures. While decreasing collection efficiency, this may improve storage stratification and overall system performance.

The on set point, ΔT_{on}, for an on/off controller can have a minimal effect on energy collection as long as it is not so high that the collector pump does not come on until late in the morning. This is because of the collector's capacitance, which allows the collector to store energy when the fluid is not circulating, energy which can be later released into the fluid. The fact that the collector acts as a storage device, also leads to the result that low to moderate cycling of the pump has a minimal effect on energy collection. The effects of collector capacitance are important and cannot be considered in steady-state analysis.

The proportional controller set point for maximum flow is found to have an effect on energy collection. If this point is too high, the flow rate will never reach maximum and thus losses to ambient are increased. However, if the set point is too low, the proportional controller's sensitivity will be lost and the controller will act as a bang-bang controller.

The off set point for on/off and proportional control has simple criteria; that energy collected exceed parasitic pumping power and that the point selected meet sensor error requirements. The on set point, however, does not have simple criteria and can be defined only within a broad range.

Parasitic power required to run a circulating pump does not appear to be significant for either on/off or proportional controllers unless a large pump-motor is required, such as in a large drain down system.

CONCLUSIONS

The implications of this study for the design and evaluation of proportional and on/off control are two fold. First, the difference between a steady-state and a dynamic analysis of control strategies is significant. Future work in modeling control systems must consider collector capacitance in order to accurately describe the transient response of the fluid temperature. Second, neither on/off nor proportional control performs best for all conditions. Whether on/off or proportional control should be implemented is dependent on the weather conditions in the location being considered. It is hoped that the results of this analysis will be used as a guideline to indicate the general meteorological and flow rate conditions for which on/off or proportional control can be more advantageous.

Further work in the comparison of on/off and proportional control should include: 1) additional simulation studies using this or an improved dynamic solar system model which includes load loop dynamics, 2) experimental testing of the control strategies on facilities which can duplicate meteorological and load conditions for comparisons and 3) field tests.

ACKNOWLEDGMENTS

This work has been supported by the Systems Analysis and Design Branch, Systems Development Division, Office of Solar Applications, U.S. Department of Energy, under Contract No. W-7405-ENG-48.

SOURCES CONSULTED

1. Auslander, D.M. "A Continuous System Simulation Language Designed for LSI Economics" Mathematics and Computers in Simulation, Vol. 20 (1978): 308-313.

2. Bartlett, J.C. "Evaluation of Solar Energy Control Systems." Proceedings of the Solar Heating and Cooling Operational Results (Colorado Springs, CO: November, 1978): 419-423.

3. Cash, M. "Learning From Experience." Solar Age (Nov., 1978): 14-

4. Close, D.J. "A Design Approach For Solar Processes." Solar Energy Vol. 11, No. 2 (1967): 112-122

5. Conway, T. "Fluid Flow Control Strategies in Flat-Plate and Evacuated Tube Collectors." Proceedings of 1977 ISES Meeting (Orlando, FL): 9.11-9.14.

6. Department of Energy. "Solar heating and Cooling Project Experiences Handbook, Preliminary Report."Sept, 1978.

7. Duffie, J.A. and Beckman, W.A. Solar Energy Thermal Processes. (NY: Wiley-Interscience Publications, 1974): Chap. 7.

8. Herczfeld, P.R., et.al. "Study of Pump Cycling in the Control of Solar Heating and Cooling Systems." Proceedings of the Workshop on the Control of Solar Energy Systems for Heating and Cooling of Buildings(Hyannis, MA: May, 1978). U.S. Department of Energy.

9. Honeywell Energy Resources Center. "Cost-Effective Control Systems for Solar Heating and Cooling Applications, Final Report." (September, 1978.)

10. Klein, S.A., Duffie, J.A. and Beckman, W.A. "Transient Considerations of Flat-Plate Solar Collectors." ASME Journal of Engineering Power, 96A (1974).

11. Lewis, R. and Carr, J. "Comparitive Study on ON/OFF and Proportionally Controlled Systems." Proceedings of the Workshop on the Control of Solar Energy Systems for Heating and Cooling of Buildings. (Hyannis, MA: May, 1978). U.S. Department of Energy.

12. Orbach, A., et.al. "Optimal and Sub-Optimal Control Strategies and Sensativity Study for Solar Liquid Collector Systems." Proceedings of the 1979 ISES Annual Meeting (Atlanta, GA: May, 1979).

13. Schlesinger, R.J. "Preliminary Comparison of Proportional and Full On-Off Control Systems for Solar Energy Applications." Proceedings of the 1977 ISES meeting (Orlando, FL): 9.15-9.18.

14. Sparkes, H.R. and Raman, K. "Lessons Learned on Solar System Design Problems From the HUD Solar Residential Demonstration Program." Proceedings of the Solar Heating and Operational Results Meeting (Colorado Springs: November, 1978): 251-256.

15. Winn, B.C. and Hull, D. "Optimal Controllers of the Second Kind." Proceedings of 1978 ISES meeting (New Delhi, India): 493-498.

16. Manufacturer's Product Bulletins from:

Andover Controls, Andover, MA; Grundfos Pumps Corp, Clovis, CA; Helitrope General, Spring Valley, CA; Honeywell Energy Center, Minneapolis, MN; Independent Energy, E. Greenwich, RI; Johnson Controls Inc. Penn Division, Oakbrook, IL; March Manufacturing Inc., Glenview, IL; Natural Power, Inc., New Boston, NH; Piper Hydro Inc., Anaheim, CA; PPG Industries Glass Division, Pittsburg, PA; Rho Sigma Inc., Van Nuys, CA; Solar Control Corp., Boulder, CO.

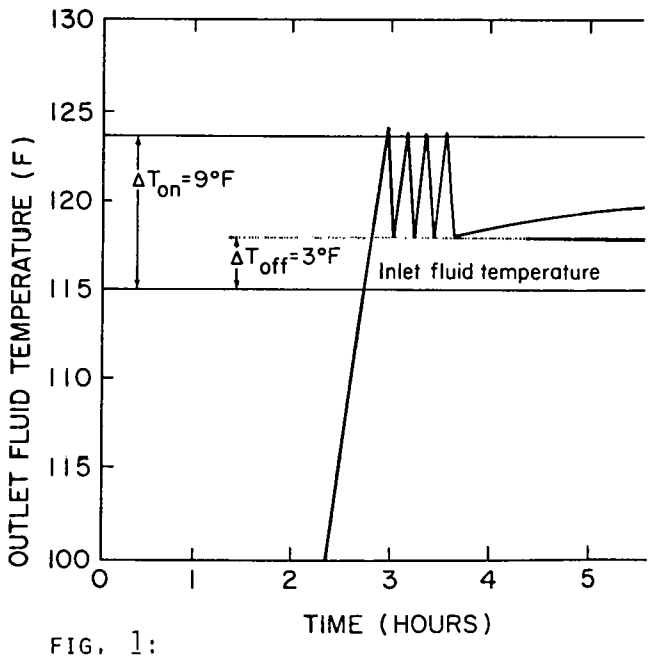

FIG. 1:
OUTLET FLUID TEMPERATURE
LOW GAIN, LOW FLOW, CLEAR DAY

TABLE I: SUMMARY OF COLLECTOR PARAMETERS AND SIMULATION RUNS

CAPACITANCE

C_A = .7 BTU/ft^2-^{o}F
= 14.3 kJ/m^2-^{o}C

HIGH GAIN

I_{max} = 300 BTU/ft^2-hr
= 946 watts/m^2

$T_{a(max)}$ = 70^{o}F
= 21.1^{o}C

HIGH FLOW

$\dot{m}c_p/A_c$ (max) = 25 BTU/ft^2-hr-^{o}F
= 511 kJ/m^2-hr-^{o}C

COLLECTOR LOSS COEFFICIENT

U_L = .7 BTU/ft^2-hr-^{o}F
3.97 watts/m^2-^{o}C

LOW GAIN

I_{max} = 150 BTU/ft^2-hr
473 watts/m^2

$T_{a(max)}$ = 50^{o}F
10^{o}C

LOW FLOW

$\dot{m}c_p/A_c$ (max) = 15 BTU/ft^2-hr-^{o}F
306 kJ/m^2-hr-^{o}C

TRANSMITTANCE/ ABSORPTANCE

$\tau\alpha$ = 0.84

INLET FLUID TEMPERATURE

T_{in} = 115^{o}F
46.1^{o}C

FIN EFFICIENCY

F' = .95 (flow)
1.0 (no flow)

TABLE II: CONTROLLER STRATEGY COMPARISONS

12 Hour Totals

CONTROL STRATEGY		HIGH GAIN[a] HIGH FLOW[b] CLEAR DAY	HIGH GAIN LOW FLOW[c] CLEAR DAY	LOW GAIN[d] HIGH FLOW CLEAR DAY	LOW GAIN LOW FLOW CLEAR DAY	HIGH GAIN HIGH FLOW CLOUDY DAY[e]	HIGH GAIN LOW FLOW CLOUDY DAY	LOW GAIN HIGH FLOW CLOUDY DAY	LOW GAIN LOW FLOW CLOUDY DAY
Maximum Steady-State Efficiency(%)		65.7	65.7	39.5	39.5	56.1	56.1	26.5	26.5
ON/OFF On=9^{o}F (5^{o}C) Off=3^{o}F(1.7^{o}C)	efficiency(%)	60.3	59.6	35.0	34.9	45.2	45.2	8.6	8.5
	pumping time(hours)	8.72	9.27	2.76	5.98	3.34	3.83	.311	.496
	times cycled	10	2	61	10	14	12	4	10
ON/OFF On=21^{o}F(11.7^{o}C) Off=3^{o}F(1.7^{o}C)	efficiency(%)	59.7	59.1	31.9	33.9	44.1	44.2	5.2	5.4
	pumping time(hours)	0.39	8.98	1.39	5.48	2.47	8.98	0.095	0.16
	times cycled	6	2	22	6	12	18	8	8
ON/OFF With perfect timer On=9^{o}F 5^{o}C	efficiency(%)	60.5	59.9	35.7	35.3	--	--	--	--
	pumping time (hours)	9.87	9.88	7.68	7.69	--	--	--	--
	times cycled	0	0	0	0	--	--	--	--
ON/OFF With perfect timer On=21^{o}F 11.7^{o}C	efficiency(%)	60.4	59.8	35.5	35.1	--	--	--	--
	pumping time(hours)	9.71	9.72	7.38	7.39	--	--	--	--
	times cycled	0	0	0	0	--	--	--	--
PROPORTIONAL Full On=9^{o}F 5^{o}C Off = 3^{o}F 1.7^{o}C	efficiency(%)	60.2	59.7	35.0	34.7	45.4	45.0	9.6	9.5
	pumping time (equiv. hours)	7.54	8.85	3.58	4.63	3.20	4.03	0.52	0.72
	times cycled	0	0	0	0	0	0	0	0
PROPORTIONAL Full On=21^{o}F 11.7^{o}C Off = 3^{o}F 1.7^{o}C	efficiency(%)	59.6	59.0	34.4	33.9	44.8	44.3	9.4	9.1
	pumping time (equiv. hours)	4.92	6.33	2.34	3.01	2.16	2.84	0.38	0.51
	times cycled	0	0	0	0	0	0	0	0

a) high gain: insolation = 2292 BTU/ft^2-day
7224 watt-hrs/m^2-day
ambient temp. = 44.4^o - 70^{o}F
6.89^o - 21.1^{o}C

b) high flow = 25 lbm/hr-ft^2
122 kg/hr-m^2

c) low flow = 15 lbm/hr-ft^2
73.2 kg/hr-m^2

d) low gain: insolation=1146 BTU/ft^2-day
3612 watt-hrs/m^2-day
ambient temp.= 32.9^o - 50^{o}F
.5^o - 10^{o}C

inlet temperature = 115^{o}F
46.1^{o}C

collector capacitance = .7 BTU/ft^2-^{o}F
14.3 kJ/m^2-^{o}C

collector loss coefficient = .7 BTU/ft^2-hr-^{o}F
3.97 watts/m^2-^{o}C

e) for cloudy day cases, the total insolation is half of the clear day values given in (a) and (d)

OPTIMAL IDENTIFICATION OF PARAMETERS IN PASSIVE SOLAR BUILDINGS

D. V. Pryor and C. A. Baer
Graduate Students
Department of Mechanical Engineering
Colorado State University
Fort Collins, CO 80523

C. B. Winn
Professor
Department of Mechanical Engineering
Colorado State University
Fort Collins, CO 80523

ABSTRACT

The use of the Kalman filter in evaluating system parameters of passive solar systems is examined. Two basic applications of the filter are discussed, in one of which the filter was driven with simulated data, while in the other, data gathered at an experimental test station was used. Results from both applications are presented and discussed. In both cases, the Kalman technique was found to be of some use, although was not without some problems, particularly in the case where real data was used. Finally, suggestions are made for possibly correcting some of the noted shortcomings of the results obtained in this study.

INTRODUCTION

The purpose of this study was to assess the usefulness of the Kalman filter as a tool in determining the system parameters of passive solar structures. The investigation focuses on two related applications, one of which determines the system parameters of a simulated, and therefore known, model. The other application uses the filter to derive parameters of an actual passive building, using recorded data of system states and forcing functions taken at the site. In the first problem, the system is a two-node model of a passive building, with one node representing the average inside air temperature, and the other representing the average temperature in an exterior wall. The second problem is also modeled as a two-node system, with one node being the average interior temperature of the building and the other the average temperature in a cylindrical water wall [1]. The building is located at the Colorado State University Solar Village.

The need for parameter identification is evident in the area of system design and controller design. Designing efficient solar systems can be enhanced by accurate knowledge of the design parameters, and by simulated comparisons among designs with different parameters. Also the effectiveness of a controller can be heavily dependent on the accuracy of the model parameters as specified to the controller. The purpose of the first application was to develop a model to generate simulated data with known characteristics, and to test the filter under controlled conditions. By starting with a model having known parameters, the performance of the filter could be observed in its effort to determine them, and knowledge of the workings of the filter itself could be gained and used in the second application. The purpose of the second application was to use the filter to estimate parameters of an unknown, but somewhat simple system, and evaluate again the effectiveness of the filter in this more complicated setting. Naturally, this application can also be seen as a stepping stone toward use of this method in highly complex systems.

The paper begins with a brief look at the Kalman filter equations, particularly as they apply to the above systems. A description of both applications is given as well as results and observations for both. Conclusions regarding the usefulness of the method, as well as its drawbacks are also presented, followed by recommendations for further study in this area.

KALMAN EQUATIONS

Before discussing the particular applications of the Kalman filter, a brief discussion of the method is in order. Throughout, the notation of the filter will be the same as found in [2], where a more lengthy discussion can also be found.

Among the earliest applications of the Kalman filter was the determination of the states of a known linear system, in the presence of process noise, measurement noise, and initial state estimate error. The method was extended to nonlinear cases, where at each time step the model is linearized about the current state estimate. The general state differential equation considered is given by

$$\dot{x}(t) = f(x(t), t) + w(t);\ w(t) \sim N(0, Q(t)) \quad (1)$$

with the measurement model given by

$$z_k = h_k(x(t)) + v_k;\ k = 1,2,\ldots;v_k \sim N(0,R_k), \quad (2)$$

where N(m,B) denotes a normal distribution with mean vector m and covariance matrix B. It is further assumed that

$$x(0) \sim N(\hat{x}_0,P(0)), \text{ and} \quad (3)$$

$$E[w(t)v_k^T] = 0 \text{ for all } k \text{ and } t, \quad (4)$$

where $\hat{x}_k$ denotes the kth estimate of the state vector. Then the propagation of the estimated state and the error covariance can be expressed as

$$\dot{\hat{x}}(t) = f(\hat{x}(t),t) \quad (5)$$

and

$$\dot{P}(t) = F(\hat{x}(t),t) + P(t)F(\hat{x}(t),t) + Q(t) \quad (6)$$

where

$$F(\hat{x}(t),t) = \left.\frac{\partial f(x(t),t)}{\partial x(t)}\right|_{x(t) = \hat{x}(t)} \quad (7)$$

At the (k-1)th time step, the state and error covariance are propagated forward to give a priori estimates at the kth time step, $\hat{x}_k(-)$ and $P_k(-)$. After the kth measurement has been taken, these a priori estimates are updated yielding

$$\hat{x}_k(+) = \hat{x}_k(-) + K_k[z_k - h_k(\hat{x}_k(-))] \quad (8)$$

and

$$P_k(+) = [I - K_k H_k(\hat{x}_k(-))]P_k(-), \quad (9)$$

where

$$H_k(\hat{x}(-)) = \left.\frac{\partial h_k(x(t_k))}{\partial x(t_k)}\right|_{x(t_k) = \hat{x}(-)} \quad (10)$$

and the Kalman gain matrix is determined to be

$$K_k = P_k(-)H_k^T(\hat{x}_k(-))[H_k(\hat{x}_k(-))P_k(-)H_k^T(\hat{x}_k(-)) + R_k]^{-1} \quad (11)$$

FIRST KALMAN APPLICATION

In the first application of the filter, the following simulated model of a building was developed (see Figure 1):

$$\dot{T}_1 = \frac{UA_{12}}{c_1}(T_2 - T_1) + \frac{k_W}{c_1}W^2(T_A - T_1) + \frac{k_{s_1}}{c_1}s_1 + \frac{1}{c_1}Q_A, \quad (12)$$

$$\dot{T}_2 = \frac{UA_{12}}{c_2}(T_1 - T_2) + \frac{UA_{2A}}{c_2}(T_A - T_2) + \frac{k_{s_2}}{c_2}s_2 \quad (13)$$

Rewriting (12) and (13) in terms of the parameters to be identified gives

$$\dot{T}_1 = \rho_1(T_2 - T_1) + \rho_2 W^2(T_A - T_1) + \rho_3 s_1 + \rho_4 Q_A \quad (14)$$

and

$$\dot{T}_2 = \rho_5(T_1 - T_2) + \rho_6(T_A - T_2) + \rho_7 s_2. \quad (15)$$

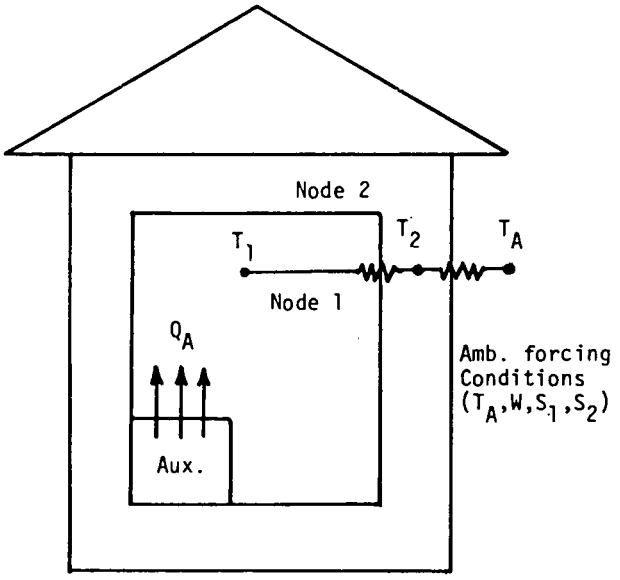

FIGURE 1. DIAGRAM OF PROBLEM 1 MODEL

Here the parameters $\rho_1,\ldots,\rho_7$ are modeled as constant states in the Kalman filter equations. The state estimation problem is therefore a nonlinear one, there being products of state variables in each equation. Setting the state vector equal to $(T_1,T_2,\rho_1,\ldots\rho_7)^T = (x_1,x_2,\ldots x_9)$, Equation (1) becomes

$$\dot{x}(t) = \begin{bmatrix} x_3(x_2 - x_1) + x_4W^2(T_A - x_1) + x_5s_1 + x_6Q_A \\ x_7(x_1 - x_2) + x_8(T_A - x_2) + x_9s_2 \\ 0 \\ \vdots \\ 0 \end{bmatrix} \quad (16)$$

It is assumed that T_1 and T_2 can be measured directly (with measurement noise, of course), so that the measurement matrix for the system described by (16) is the constant matrix

$$h_k(x(t_k)) = \begin{bmatrix} 1 & 0 & 0 & \cdots & 0 \\ 0 & 1 & 0 & \cdots & 0 \end{bmatrix}; \quad k = 1,2,\ldots$$

A simulation "truth" model was developed which generated "true" values for T_1 and T_2 on the basis of equations (12) and (13) and actual weather data which gave values of the forcing functions T_A, W, s_1 and s_2. Q_A was simulated as a function of the calculated value of T_1 and the current value of Q_A, as would normally be done by a thermostat. That is, the simulated auxiliary heat source would be turned on when T_1 was below a minimum dead-band temperature and turned off

when T_1 went above a maximum dead-band temperature. The Q_A input was left unchanged whenever T_1 was found to be in the dead-band. The Kalman filter was then set up to observe the simulated truth model, the object being to start with erroneous estimates of the system states and converge in time to values close to those used by the truth model.

Using runs of 108 hours, the filter was able to determine all but one of the seven parameters to within 8% and the remaining parameter to within 18%, where the errors in the initial guesses ranged from 27% to 67%. The initial estimates of the ρ values, as well as the final estimates after 108 hours of filtering are given in Table 1.

TABLE 1. INITIAL AND FINAL ρ ESTIMATES

	True Value	Initial Est.	% Initial Error	Final Est.	% Final Error
ρ_1	.120	.200	67.1	.122	1.8
ρ_2	.730E-11	.530E-11	-27.4	.601E-11	-17.7
ρ_3	.117E-3	.169E-3	42.8	.122E-3	4.7
ρ_4	.146E-3	.106E-3	-27.4	.143E-3	-2.3
ρ_5	.315	.445	41.5	.289	-8.4
ρ_6	.308	.208	-32.5	.286	-7.2
ρ_7	.308E-3	.210E-3	-31.7	.287E-3	-6.8

Convergence curves for the parameters ρ_1 and ρ_7 are illustrated in Figure 2.

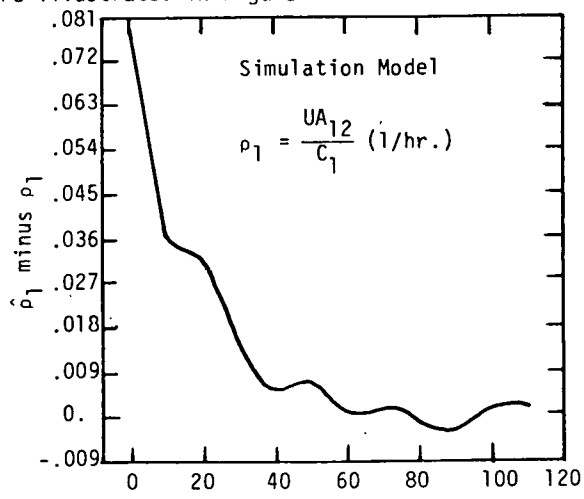

FIGURE 2.1. GRAPH OF ESTIMATE $\hat{\rho}_1$ MINUS TRUE VALUE ρ_1, VERSUS TIME

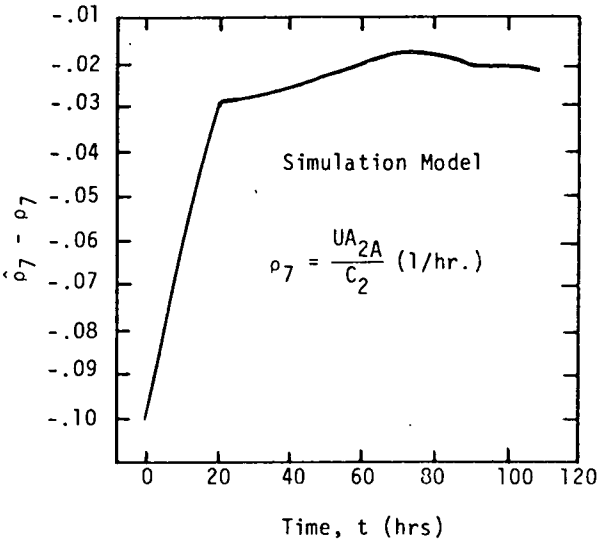

FIGURE 2.2. GRAPH OF ESTIMATE, $\hat{\rho}_7$ MINUS TRUE VALUE, ρ_7, VERSUS TIME

To test the computed values of the parameters, the simulation was rerun with the derived parameters used in place of the true parameters. The resulting output values, i.e. the T_1 and T_2 trajectories were duplicated for all time steps to within 3°F of the truth model trajectories for both T_1 and T_2. Through several numerical experiments, it was observed that the stability of the filter was quite sensitive to both process noise and initial error covariance, and indeed this sensitivity is well known to be one of the drawbacks to the use of this method [2],[3]. Also it was found that, for a highly erroneous initial guess, stability could often be salvaged at the expense of an undesirable value of the Kalman gain matrix. That is, it is desirable that the Kalman gain matrix approach zero, which indicates that the filter has confidence in its present estimates of the parameters. It was noted that when letting the Q matrix decrease with time, both the final parameter estimates and the Kalman gain matrix were improved, as well as the final value of the error covariance matrix. Finally, the fact that the filtered values of the parameters so closely reproduced the behavior the truth model may indicate a low sensitivity on the part of the system to variations in certain parameters. This may in turn account for the bias which remained in the parameter estimates, even after 108 hours of filtering, particularly the ρ_2 parameter.

SECOND KALMAN APPLICATION

The second application of the filter employed a model similar to that used in the first case. The model was of a test cell structure which contains a cylindrical water wall on the south side of the building. This structure is described in Figure 3 and [1]. The model is given by

$$\dot{T}_1 = \frac{UA_{12}}{c_1}(T_2-T_1) + \frac{UA_{1A}}{c_1}(T_A-T_1) + \frac{k_{s_1}}{c_1}s_H, \quad (18)$$

$$\dot{T}_2 = \frac{UA_{12}}{c_2}(T_1-T_2) + \frac{UA_{2A}}{c_2}(T_A-T_2) + \frac{k_{s_2}}{c_1}s_H \quad (19)$$

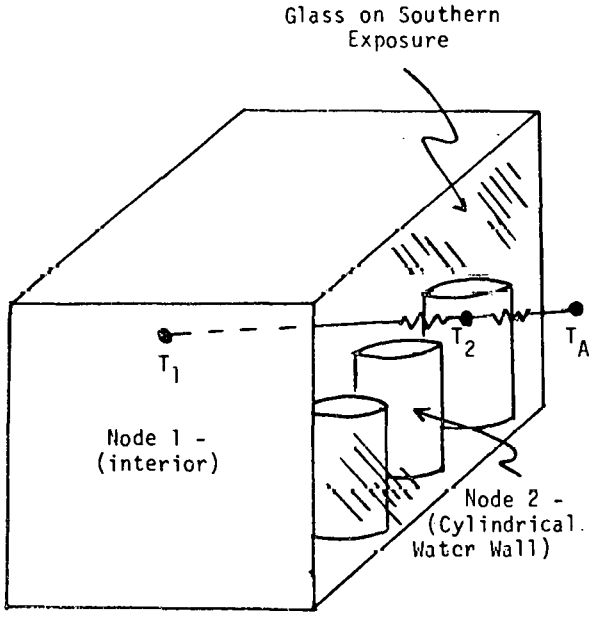

FIGURE 3. DIAGRAM OF EXPERIMENTAL TEST STATION

The following data was obtained at the site of the test cell: inside temperature (T_1), average water wall temperature (T_2), ambient temperature (T_A), and total horizontal insolation (s_H). (Shielded thermocouples were used for the temperature measurements.) Denoting the parameters as $b_1,\ldots b_6$, rewriting (18) and (19) gives

$$\dot{T}_1 = b_1(T_2-T_1) + b_2(T_A-T_1) + b_3 s_H \quad (20)$$

$$\dot{T}_2 = b_4(T_1-T_2) + b_5(T_A-T_2) + b_6 s_H \quad (21)$$

As in the first problem, the state vector is set equal to $x = (T_1,T_2,b_1,\ldots,b_6) = (x_1,x_2,\ldots x_8)$ and equation (1) for this system can now be written as

$$\dot{x}(t) = \begin{bmatrix} x_3(x_2-x_1) + x_4(T_A-x_1) + x_5 s_H \\ x_6(x_1-x_2) + x_7(T_A-x_2) + x_8 s_H \\ 0 \\ \vdots \\ 0 \end{bmatrix} \quad (22)$$

Equation (17) remains the same for this problem (except for the dimension of h_k), since we have measurements ot T_1 and T_2, but no other states. The data was filtered for 48 hours, using initial estimates obtained from hand calculations. Constant process noise for the duration of the run was also assumed. The initial and final values of the parameters are given in Table 2.

TABLE 2. INITIAL AND FINAL b ESTIMATES

	Initial Estimate	Final Estimate
b_1	.900	.250
b_2	.500	.174
b_3	.210	.055
b_4	.120	.095
b_5	.00825	.00782
b_6	.0150	.0151

The values of the estimates of the first three parameters plotted against time, as calculated by the Kalman filter, are shown in Figure 4.

As in the first problem, the final estimates were used in a simulation of equations (20) and (21), and the resulting simulated trajectories of T_1 and T_2 compared favorably (within 5°F for T_1, 8°F for T_2) with the trajectories experimentally measured. In longer simulations using the estimated parameters the comparison was somewhat worse, as was expected.

Much of the behavior of the filter exhibited in the first application was also observed in the second, but the results were not as definitive, nor was convergence as clearly demonstrated in the second case. The obvious difference in the two problems is that the order of the filter matched the order of the system in the first case and not in the second i.e. the behavior of the test cell system is certainly not completely modeled by equations (20) and (21). The insolation terms are particularly suspect in this regard. Indeed, it was noticed from the data of the third day that the insolation was highly diffuse, as opposed to the predominantly beam radiation of the first two days. The measured total horizontal radiation can be misleading in terms of the gain to the system, if the distinction is not made between beam and diffuse radiation. As expected, the filter began to exhibit irregular behavior on the third day. Also, the simulation of the test cell using the 48-hour estimates as model coefficients

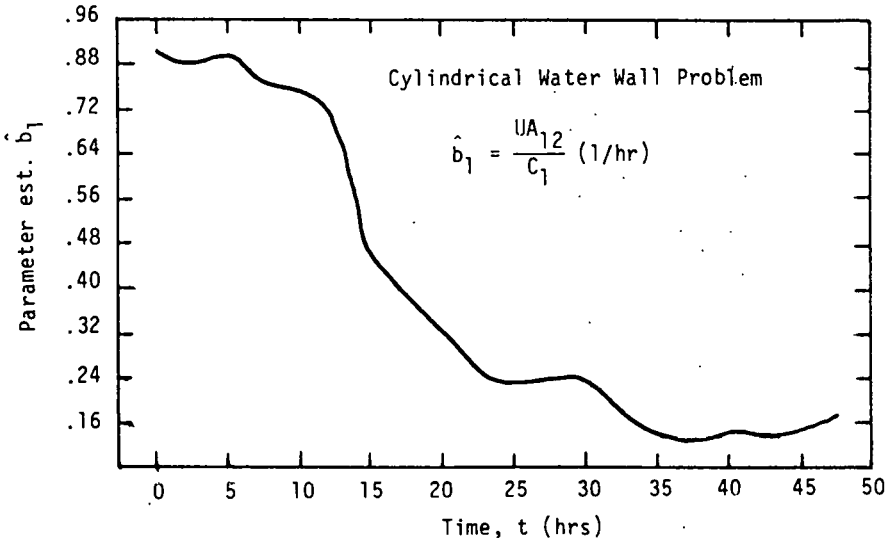

FIGURE 4.1. GRAPH OF PARAMETER ESTIMATE b_1 VERSUS TIME

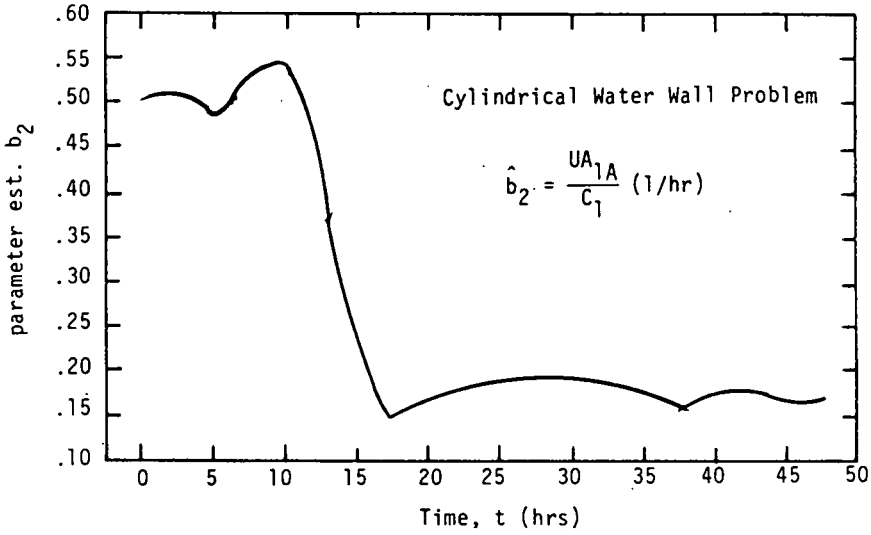

FIGURE 4.2. GRAPH OF PARAMETER ESTIMATE $\hat{b}_2$ VERSUS TIME

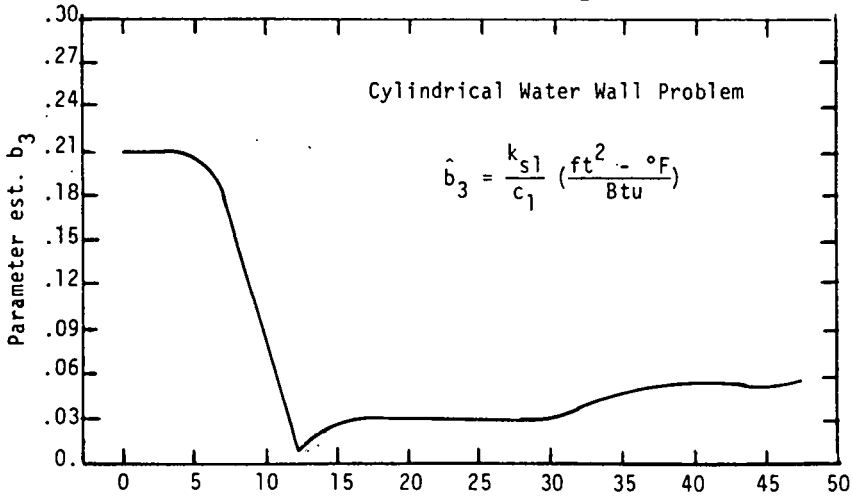

FIGURE 4.3. GRAPH OF PARAMETER ESTIMATE b_3 VERSUS TIME

indicated an overestimation of the solar gain on the third day. In view of the model inaccuracies, it should therefore be no surprise to see the filter behave deficiently in the second case as compared with the first.

CONCLUSIONS

1. As a tool for use in determining system parameters the Kalman filter can be useful, but it is not without problems. An accurate model is certainly required for the success of the filter, as demonstrated by its performance in each of the two test situations.
2. Also needed are good initial guesses of the states and noise statistics to avoid problems of instability and questionable convergence characteristics. In most cases knowledge of the physics of the system can lead to estimates which are at least somewhat close to the true parameter values.
3. Finally, wide variations in the system forcing functions and the measured states were found to enhance the performance of the filter, a fact borne out by experimenting with the simulated model in the first application.

RECOMMENDATIONS FOR FURTHER WORK

The next step to be taken to improve the effectiveness of the method in the water wall problem is to include in the filter model a radiation processor for correcting the inherent inaccuracies found in (20) and (21). Another enhancement to the methods usefulness would be to redefine the system, when one or more of the parameters has been determined with a high degree of confidence. The reformulated model would thus have fewer states to simultaneously burden the filter, and would perhaps exhibit system sensitivity to terms with lesser impact on the system. Finally, the possibility of the filter determining multiple solutions for a given set of data points, solutions which depend on filter initialization, has not been addressed.

NOMENCLATURE

$\hat{b}_1, \ldots \hat{b}_6$ - estimated parameters for 2nd system
$b_1, \ldots b_6$ - system parameters for 2nd system
c_1 - specific heat of node 1, Btu/°F
c_2 - specific heat of node 2, Btu/°F
h_k - kth value of measurement matrix
K_k - kth value of Kalman gain matrix
k_{s_1} - area bounding node 1, ft^2
k_{s_2} - area bounding node 2, ft^2
k_w - conduction constant, $Btu \cdot hr/°F \cdot ft^2$
P_k - kth value of error covariance matrix
$Q(t)$ - process noise covariance
Q_A - auxiliary heat source, Btu/hr
R_k - kth value of measurement error covariance
s_1 - effective solar insolation $Btu/hr \cdot ft^2$
s_2 - effective solar insolation $Btu/hr \cdot ft^2$
s_H - total horizontal insolation $Btu/hr \cdot ft^2$
T_1 - inside temperature, °F
T_2 - wall temperature, °F (1st problem)
- water wall temperature, °F (2nd problem)
t - time, hrs
UA_{12} - UA between nodes 1 and 2, Btu/°F·hr
UA_{1A} - UA between node 1 and outside, Btu/°F·hr
UA_{2A} - UA between node 2 and outside, Btu/°F·hr
v_k - kth value of measurement noise
W - wind speed, ft/hr
w - process noise
x - state vector
$\hat{x}$ - estimated state vector
z_k - value of the measurement vector
$\rho_1, \ldots \rho_7$ - system parameters of first system
$\hat{\rho}_1, \ldots \hat{\rho}_7$ - estimated parameters of first system

REFERENCES

[1] P.J. Burns, J. Nobe and C.B. Winn, "Thermal Radiation Calculations for a Vertical Cylindrical Water Wall," Proc. Fourth National Passive Solar Conference, Kansas City, MO (1979).
[2] A. Gelb (ed.), Applied Optimal Estimation, M.I.T. Press, Cambridge, MA, 1974.
[3] G.J. Bierman, Factorization Methods for Discrete Sequential Estimation, Academic Press, New York, 1977.

Dup

1371A/

CONTROL SYSTEM ANALYSIS FOR OFF-PEAK AUXILIARY HEATING OF PASSIVE SOLAR SYSTEMS

Hugh S. Murray*
James L. Melsa**
J. Douglas Balcomb*

ABSTRACT

A computer simulation method is presented for the design of an electrical auxiliary energy system for passive solar heated structures. The system consists of electrical mats buried in the ground underneath the structure. Energy is stored in the ground during utility off-peak hours and released passively to the heated enclosure. An optimal control strategy is used to determine the system design parameters of depth of mat placement and minimum installed electrical heating capacity. The optimal control applies combinations of fixed duration energy pulses to the heater, which minimize the room temperature error-squared for each day, assuming advance knowledge of the day's weather. Various realizable control schemes are investigated in an attempt to find a system that approaches the performance of the optimal control system.

INTRODUCTION

The auxiliary energy for passive solar heated structures may be provided by storing energy in the ground underneath the structure during utility off-peak hours. This approach is attractive to contractors because of the relative ease with which electrical resistance mats may be placed on the ground during excavation for the foundation. The use of off-peak storage released passively to the heated enclosure leads to significant control problems. Energy must be expended before it is needed to heat the structure due to the thermal lag of the storage medium. The success of this approach depends upon the development of a control system that regulates the room temperature sufficiently while using energy at a cost lower than that for a conventional electrical backup system.

A reasonably intelligent control system that can manage storage subject to the off-peak rate structure and anticipate the need for auxiliary energy will be necessary.

METHOD OF ANALYSIS

For the purpose of designing the auxiliary energy system, it is assumed that a good controller can be found to meet the system performance requirements. Generally, it has been found in this study that the design parameters are affected by the type of control used, that a simple conventional controller gives poor performance in terms of energy cost, and that the system performance is less sensitive to design parameters with an intelligent controller than with a very simple controller.

The analysis approach in this study is to use the best control that can be applied to the system. The best control is achieved with advance knowledge of the weather. For the purpose of this study, one day's advance knowledge is assumed. The off-peak period is assumed to be between 10 p.m. and 8 a.m., during which time electricity would cost one-half of the daytime cost. The ten-hour off-peak period is divided into five two-hour periods. To determine the best control, the differential equations that describe the system are solved as follows.

1. The equations are solved using actual weather data with no auxiliary energy used. This is called the unenforced response.

2. The equations are solved using auxiliary power at a constant level applied over each of the five two-hour periods during the off-peak hours. These are the forced responses.

3. It is assumed that the system equations are linear, so the unforced response can be subtracted from each of the five forced resposes to give that part of the system response due to each of the five energy pulses.

4. Again, due to the linearity of the system, the response difference due to any combination of the five individual response

*This work performed under the auspices of the U.S. Department of Energy, Office of Solar Applications.
**Notre Dame University, South Bend, Indiana.

differences can be found by addition of the individual responses, and the total system response can be found by adding the result to the unforced system response.

5. The combination of pulses that gives the minimum root-mean-square (RMS) room temperature error around 70°F over the entire day is the heat control for that day.

Naturally, the number of pulses or time divisions over the off-peak period can be made arbitrarily large, but five pulses, giving 32 combinations, is used here. Ten pulses would give 1024 combinations, for example. However, although the method is well-suited to digital computer solution, computing time becomes prohibitive for ten pulses if very many days or parameter studies are to be examined.

The daily computations were repeated over a three-month period (December, January, and February) using weather data for the Los Alamos, New Mexico, winter of 1974. The effect of the design parameters of electrical mat placement depth and installed heating system capacity were studied with soil conductivity as a variable.

SYSTEM MODEL

The system model parameters are based on a passive solar heated home under construction in the LaVereda Subdivision in Santa Fe, New Mexico, in which the buried electrical backup heating system will be used. This project is a joint venture between the Public Service Company of New Mexico, the Los Alamos Scientific Laboratory, and Communico, Inc., a Santa Fe builder, to demonstrate the use of an advanced, load-managed electrical backup heating system in a passive solar heated residence. The house under study makes use primarily of a solar storage wall and considerable direct solar gain. The electrical mats are buried a prescribed depth beneath a four-inch concrete floor slab. The mats rest on undisturbed native soil (caliche), and are covered by a compacted fine-grained fill material.

The basic constants of the system are assumed to be

Total Building Load	367 $\frac{\text{Btu}}{\text{hr.}^\circ\text{F}}$	(Int. - Amb. Temp. Diff.)
Slab conductivity (k)	0.8 $\frac{\text{Btu}}{\text{hr.ft.}^\circ\text{F}}$	
Solar Wall (Trombe wall)	16 in. concrete, dbl-glazed exterior, k = 1.0 $\frac{\text{Btu}}{\text{hr.ft.}^\circ\text{F}}$	
$\frac{\text{Solar wall area}}{\text{Building Load}}$	Ratio = 1.0	
Solar wall int. heat transfer coefficient	1.0 $\frac{\text{Btu}}{\text{hr.ft}^2\text{°F}}$	
Floor heat transfer coefficient	1.5 $\frac{\text{Btu}}{\text{hr.ft}^2\text{°F}}$	
Constant soil diffusivity $= \frac{\text{conductivity}}{\text{volumetric specific heat}}$	$\frac{0.03\ \text{ft}^2}{}$	

It is assumed that the soil is at a constant temperature of 50° five feet below the slab for the purpose of calculating downward losses. Rigid insulation limits heat loss at the periphery of the structure.

System Simulation with Perfect Control

Two standard cases were analyzed for comparison purposes. In each case, auxiliary energy is used directly in the heated enclosure at any time during the day to regulate the room temperature. In the first case, a "perfect" controller regulated the room temperature at 70°F at all times, and in the second case, a ±2°F deadband around 70°F was used to simulate a conventional thermostat control. The estimated rate differential for off-peak electricity is one-half, so to compare the totally off-peak system, a rate-adjusted energy total is calculated as

$$E_{adj} = \frac{1}{2} E_{night} + E_{day} .$$

The 90-day house energy balances for the standard cases given in Table I. The energy terms are

$E_{AUX,N}$	Auxiliary energy, night (off-peak);
$E_{AUX,D}$	Auxiliary energy, day;
E_{SD}	Direct solar energy;
E_{SW}	Solar wall energy input;
E_L	Total house energy loss; and
E_{ADJ}	Rate-adjusted auxiliary energy use.

TABLE I
SIMULATED ENERGY BALANCE

	$E_{AUX,N}$	$E_{AUX,D}$	E_{SD}	E_{SW}	E_L	F_{OP}	PS	E_{ADJ}
Perfect 70°F Controller	1568	1038	1008	1969	5583	.60	53	1822
70°, ± 2°F Deadband	1888	1024	1008	1965	5885	.65	51	1964

TABLE II
SYSTEM DAILY SUMMARY WITH OPTIMAL CONTROL

DAY	AMBIENT TEMP (°F) AVG	HIGH	LOW	ROOM TEMP (°F) AVG	HIGH	LOW	70°F RMS ERROR	CONTROL SEQ	ENERGY kWHR
1	25.8	35.0	16.0	69.3	73.5	67.0	2.2	10000	20
2	28.6	40.0	18.4	69.2	73.0	66.7	2.3	10000	20
3	27.1	36.0	16.6	69.6	73.6	67.5	2.0	11000	40
4	28.0	38.0	18.1	69.6	73.9	67.4	2.3	10000	20
5	25.9	36.0	18.1	69.1	73.1	67.0	2.1	10000	20
6	30.6	42.0	23.0	69.2	73.1	67.4	2.0	10000	20
7	38.0	44.0	28.0	69.9	73.5	67.9	1.9	00000	0
8	28.1	38.0	17.2	69.5	70.6	68.1	0.9	11101	80
9	13.8	22.0	9.0	69.4	73.7	66.7	2.2	11100	60
10	16.2	30.0	3.0	69.1	74.2	66.4	2.6	11100	60
11	18.5	30.0	7.0	69.6	73.9	67.6	1.6	11111	100
12	17.2	31.0	4.3	69.5	74.1	67.4	2.3	11000	40
13	27.1	39.0	18.2	69.1	73.6	66.7	2.5	10000	20
14	26.3	41.0	17.0	68.6	71.1	66.4	2.1	11110	80

Energy terms are in kWhr. The other terms are:

F_{OP} Fraction of auxiliary energy used off-peak, and

PS Percent solar.

Numerous simulation studies were made to determine the optimum placement depth of the electrical mats using the optimal control scheme.

A typical daily summary of the system simulation is given in Table II. This summary is for a two-week period taken from a three-month simulation. The control sequence column shows the two-hour time periods over the ten-hour off-peak period when the power is on. For example, 10000 represents power on from 10 p.m. to midnight, 00001 represents power on from 6 a.m. to 8 a.m., and so forth. The case shown in Table II uses the design parameters of 10-kW electrical capacity, 9-inch mat depth and assumptions of ground conductivity of 0.7 Btu/hr.ft.°F above the mats and the 0.5 Btu/hr.ft.°F below the mats.

The performance parameters that are used to determine the system design are seasonal RMS room temperature error, absolute minimum room temperature attained, total time spent below 65°F, total time spent above 75°F, and total electrical consumption.

The simulation studies indicate that, for this model, the performance parameters listed above become relatively insensitive to placement depth and soil conductivity at power density levels above 7.5 watts/ft^2. At power densities below this critical value, the performance of the system in terms of the listed parameters deteriorates sharply, except that less total energy is used. The house that is being built with this heating system has 1300 ft^2 of heated area, so this would indicate a design value of 9.75 kW of capacity. Actually, 10 kW was used, and this capacity is used in the remainder of the simulation examples.

Some typical results are summarized in Tables III and IV for different fill and base soil conductivities. The table headings are

D Depth, inches

E_{ADJ} Rate-adjusted energy, kWhr

t < 65 Time below 65°F, hours

t > 75 Time above 75°F, hours

Tmin Minimum room temperature, °F

TABLE III
SYSTEM PERFORMANCE SUMMARY

K_{fill} = .7, k_{ground} = .5, Btu/hr ft°F

D	E_{ADJ}	RMS	t < 65	t > 75	T_{min}
3	1600	2.16	9.5	0	64.2
6	1635	2.25	1.0	1.0	64.9
9	1710	2.27	0	0	65.3
12	1810	2.26	0	0	65.7
15	1900	2.31	0	0	65.1
18	2010	2.38	19.0	2.0	64.0

TABLE IV
SYSTEM PERFORMANCE SUMMARY

K_{fill} = .5, k_{ground} = .3, Btu/hr ft°F

D	E_{ADJ}	RMS	t < 65	t > 75	T_{min}
3	1300	2.14	3.5	3.0	64.6
6	1360	2.20	0	2.0	65.1
9	1400	2.24	0	0	65.5
12	1460	2.24	0	3.0	65.6
15	1535	2.22	0	7.5	65.6
18	1625	2.55	0	14.0	65.7

It is assumed that the fill material will have a conductivity somewhat higher than that of the undisturbed soil below the mats.

The general findings from the studies are:

1. The seasonal RMS temperature error increases with depth, but over the range of conductivities examined, exhibits a broad region of insensitivity to both depth and minimum RMS error for depths between 6 and 15 inches. Generally, for depths in excess of 12 inches, the RMS error increases rapidly with increasing depth.

2. A depth of at least 6 inches is required to obtain acceptable minimum temperatures (over $65^{o}F$). The minimum temperature also drops off rapidly for depths in excess of 12 inches.

3. The time spent below $65^{o}F$ exhibits a broad minimum (usually zero) for a depth between 6 and 12 inches.

4. Total energy consumption increases with depth. For higher base soil conductivities (above 0.6 Btu/hr.ft.^{o}F), placement depth must be less than 12 inches for the system to use less rate-adjusted energy than is used in the standard case.

If all of the cases are considered, a depth of 9 inches appears to be the optimum value for a wide range of soil conductivities for the model assumed in this study; this depth has been chosen for the project.

CONTROL SYSTEM DESIGN

Work on the design of this system is incomplete. In order to design a control system, one must find a control algorithm that gives a system performance as close to the optimal system as possible. The optimal system performance can never be attained because knowledge of the next day's weather is not attainable. An important constraint on the design is that the control hardware must be kept simple and of low cost.

An analysis of two types of systems gives the results in Table V. The two ideal systems with heat added directly to the interior are also tabulated. The $72^{o}F + 1^{o}F$ slab control system simply regulated the concrete slab temperature to $72^{o}F$ during off-peak hours. The slab reset system moves the slab control setpoint as a function of ambient temperature according to the schedule $T_{slab} = 75.0 - T_{ambient}/6.$, so that the slab setpoint is $75^{o}F$ for $0^{o}F$ ambient, and $70^{o}F$ for $30^{o}F$ ambient. The realizable schemes show poor performance compared to the optimal system, with considerable overheating. It is felt that some enhancement of the slab reset system can be realized by adding anticipation based on ambient temperature rates, and knowledge of the previous day's performance. Additional analysis in this area is continuing.

TABLE V
CONTROL SYSTEM COMPARISON

	E_{ADJ}	RMS	Tmin	t < 65	t > 75
Perfect $70^{o}F$	1822	0.0	70.0	0.0	0.0
Perfect $70^{o}F \pm 2^{o}F$	1968	---	68.0	0.0	0.0
$72^{o}F \pm 1^{o}F$ Slab Control	1887	3.0	64.2	19.3	207.6
Slab Reset	1842	2.8	64.5	14.0	196.4
Optimal	1710	2.3	65.3	0.0	0.0

CONCLUSIONS

The design method leads to a system that will perform well with considerable insensitivity to system variables that may not be well known (soil conductivity). Very simple realizable controls do not approach optimal performance, but still show energy cost savings. Cost savings for the optimal control amount to 13%. For the slab reset control, savings are 6% when compared to the ideal room temperature control with deadband. The overall results of this study indicate that with a controller possessing a small amount of intelligence, much-improved system performance can be attained. The control hardware that would be required to implement a variable setpoint controller (a simple microprocessor) could be used to implement a system which could anticipate energy needs based on previous performance history and the dynamics of ambient conditions without a significant increase in hardware complexity. Such a controller could also manage more complex off-peak rate structures than the one examined here and also accommodate peak load rate considerations.

EXPERIMENTAL TEST FACILITY FOR EVALUATION OF CONTROLS AND CONTROL STRATEGIES*.

Mashuri L. Warren, Steven R. Schiller, and Michael Wahlig

Solar Energy Group
Energy and Environment Division
Lawrence Berkeley Laboratory
University of California, Berkeley

ABSTRACT

An experimental test facility has been constructed to evaluate the operation and performance of controls for active hydronic solar energy systems. The experimental system serves to test the relative performance of different controllers and alternative control algorithms for a variety of input meteorological conditions and output load demands.

The experimental system consists of a collector loop heat input simulator, a storage tank, a load loop air channel with fan coil, an auxiliary heat source, and associated pumps and valves. The heat input simulator, the pseudo-collector, consists of a boiler with a controlled mixing valve that allows precise adjustment of the heat input from the "collectors" based on predictions of a collector loop model using solar and weather data. An automated air flow channel has been constructed to simulate the building return airflow across the heating coil in the furnace ductwork for a residential system. A single zone building load model is used to predict building energy requirements and to simulate the demand thermostat. Only the apparent temperature of the collector and the demand thermostat condition are simulated, enabling control strategy and equipment comparisons based on identical load conditions.

The test facility is well instrumented with thermocouples and turbine flow meters. Data acquisition is accomplished using a one hundred channel DORIC data logger. Data acquisition, experiment control, and the load and pseudo-collector models are under control of a HP 9825A microcomputer using flexible disks for data and program storage.

Initial experiments have been done using an LBL-developed PROM based controller to control all functions of the solar system. Preliminary energy balance tests, reported previously, indicate that the overall heat balance for the experiments is within 5% of the total heat input. The criterion for evaluation of performance of a controller and/or control strategy is the amount of auxiliary energy required to meet a given load demand. The test facility is now operational and initial test results over many hours, with simulated collector heat input and simulated building load under microcomputer control, will be reported.

INTRODUCTION

The test facility is used to experimentally evaluate the relative performance of different solar heating control strategies for a variety of input meteorological conditions and heating load demands. To allow repeated runs under identical external conditions and to make meaningful comparisons between alternative control strategies, the solar energy input to the system and the building energy load are simulated. In this paper we shall describe the test facility and the methodology of the solar heat input and building load simulators. Initial test results are also presented.

EXPERIMENTAL TEST FACILITY

The experimental solar energy system consists of a collector loop with a solar heat input simulator, a 3000 gallon storage tank, a load loop air channel with fan coil, an auxiliary heat source, and associated pumps and valves. A schematic of the system is shown in Figure 1. The system is sized to represent a hydronic solar heating system in a typical residence. The operation of the solar energy

* This work has been supported by the Systems Analysis and Design Branch, Systems Development Division, Office of Solar Applications, U. S. Department of Energy, under Contract No. W-7405-ENG 48.

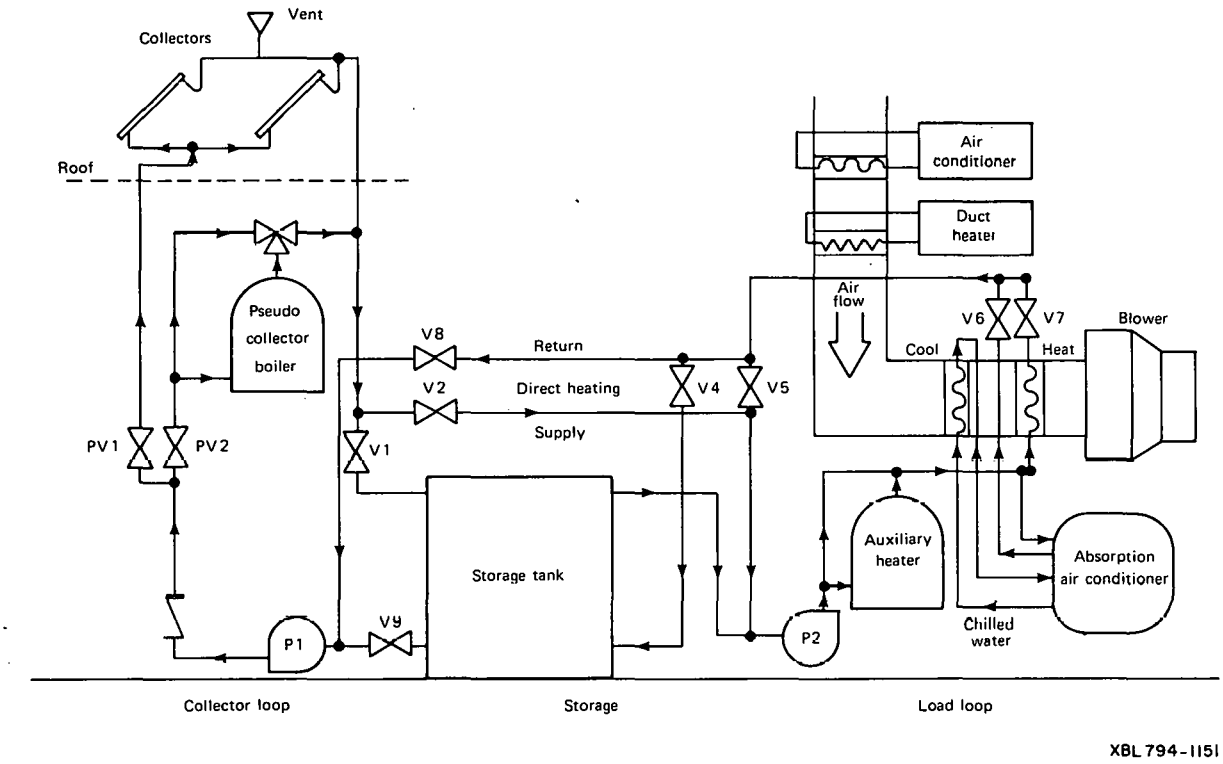

Figure 1. Solar Controls Heating and Cooling Test Facility

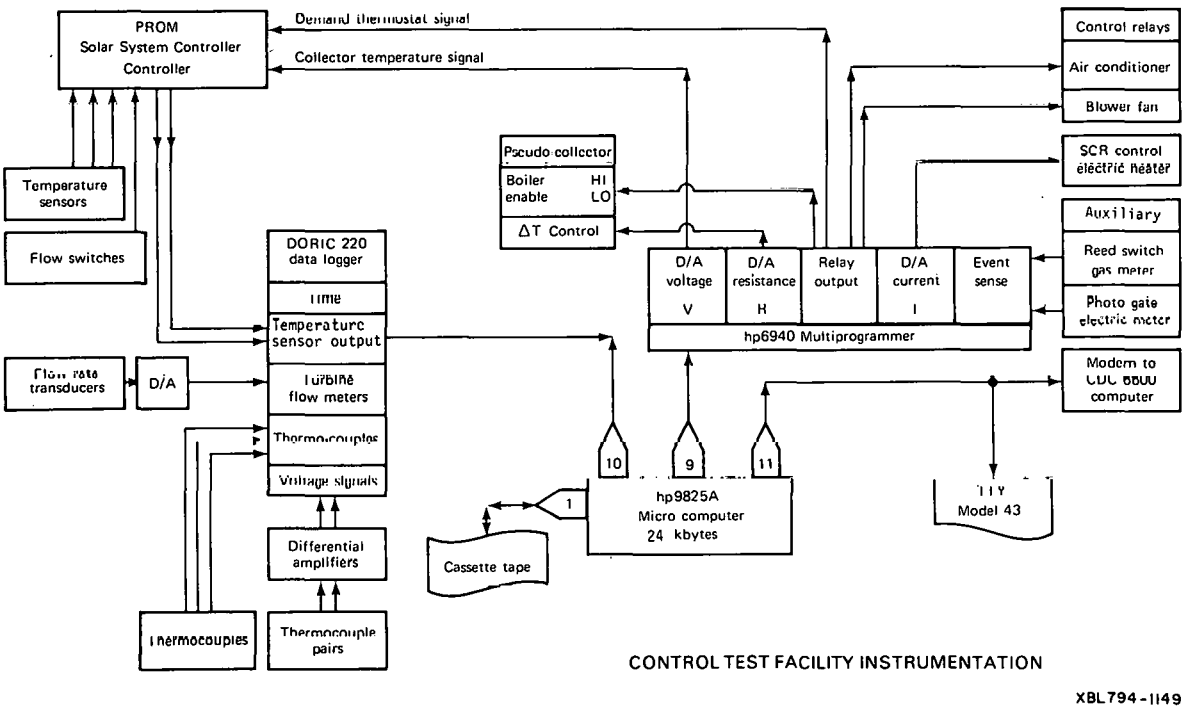

Figure 2. Test Facility Instrumentation.

system is controlled by a PROM based controller developed at LBL that uses thermostat signals and temperature sensor comparisons to address a truth table containing the control algorithm used to control system actuators. This controller has been described previously[1,2].

INSTRUMENTATION AND DATA ANALYSIS SYSTEM.

The test facility is well instrumented with thermocouples and turbine flow meters. Data acquisition is accomplished using a 100 channel DORIC data logger. Data acquisition, experiment control, and the load and pseudo-collector simulations are under control of a HP 9825A microcomputer using flexible disk for data and program storage. Software requirements for data acquisition, adjustment of the load and pseudo-collector simulators, and intermediate data analysis are extensive, exceeding the limits of the computer memory. Therefore, the software has been rewritten in an overlay mode to greatly extend the computer capability. Segments containing the main program, subroutines for operation of the datalogger and output devices, experiment initialization, data analysis and control procedures are now stored on different files and are loaded into memory from the disk as they are required. Auxiliary gas consumption for back-up heat, and parasitic power requirements for the pumps and fans, are now measured electronically. The facility instrumentation is shown in Figure 2.

SOLAR INPUT SIMULATOR (PSEUDO-COLLECTOR)

A schematic of the facility collector loop is shown in Figure 3. The solar input simulator, the pseudo-collector, is a boiler with a controlled mixing valve that allows adjustment of the input-output temperature difference. The high- and low-fire gas burners of the boiler, as well as the position of the three way mixing valve, are all controlled by the HP-9825A. Values of solar insolation, ambient temperature, the boiler inlet temperature and flow rate, along with typical collector parameters, are used to calculate the expected inlet-outlet temperature difference using the Hottel-Whillier-Bliss steady state model[3]. Initial experiments have been run using a simple increasing and decreasing insolation pattern. Work is presently underway to generate insolation values incident on the collector array using typical meteorological year, TMY, data tapes prepared for SERI by Science Applications, Inc.

Under no-flow conditions in the collector loop, the value of the collector sensor, TS-4, is set to the calculated collector stagnation temperature through an output device. When the collector loop pump is on, the collector output temperature is calculated from the collector model, and the boiler output is adjusted accordingly. The apparent collector temperature and boiler control are updated every 60 seconds.

The PROM system controller turns on the collector loop pump, P1, when the apparent collector tempera-

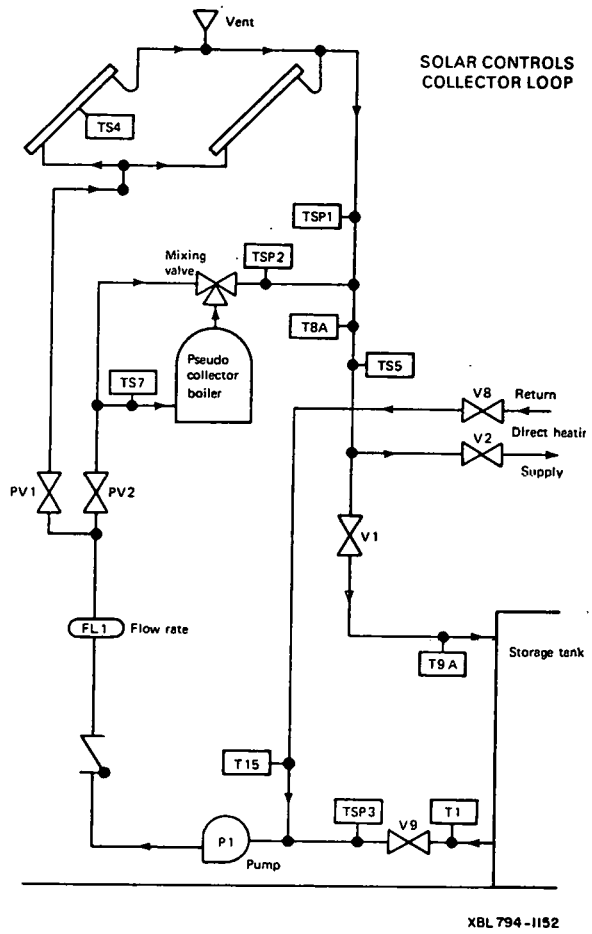

Figure 3. Solar Controls facility Collector loop showing pseudocollector boiler. The collector array is not used and the collector input is simulated using the boiler with a mixing valve.

ture reaches the "on" set point, given by the storage tank temperature plus a temperature differential, ΔT_{on} of 11 °C. The pump is turned off if the collector temperature falls below the "off" temperature, given by the storage tank temperature plus a temperature differential, ΔT_{off} of 2 °C.

Figure 4 shows the inlet temperature and the calculated and observed collector outlet temperature over a four hour period of increasing and decreasing insolation. If the collector outlet temperature under flow conditions is less than the off temperature and the collector stagnation temperature is greater than the on temperature, then the collector loop pump will cycle on and off and the collector temperature will cycle between the "on" and "off" temperatures. Such cycling is typical of solar collector systems. The steady state collector model does not adequately describe this cycling and work is underway to implement a dynamic collector model for the solar input simulator.

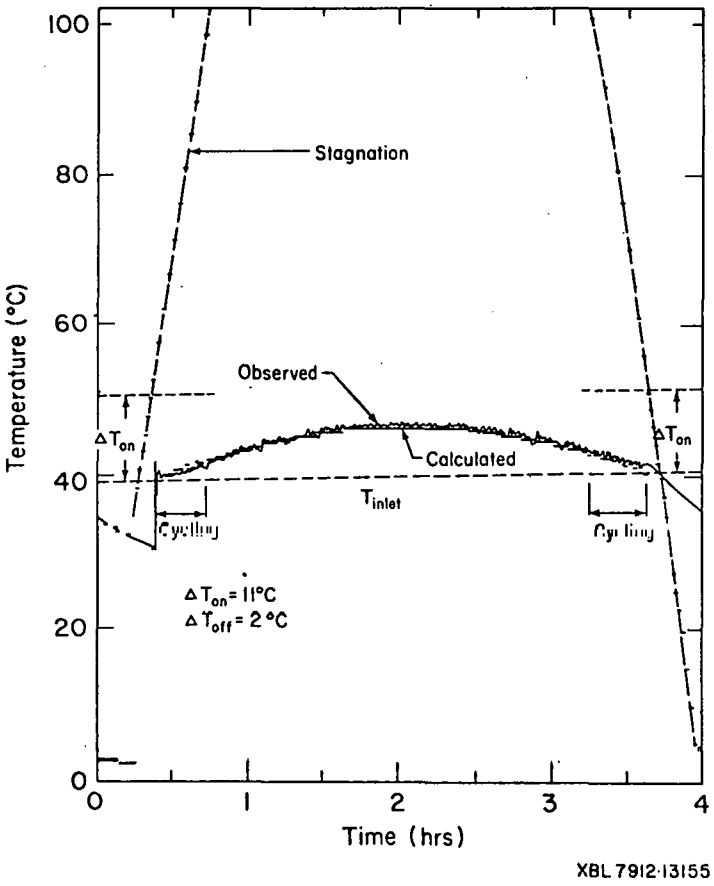

Figure 4. Pseudocollector output. Calculated temperature (no flow), Calculated outlet temperature (flow), and observed pseudocollector outlet temperature.

LOAD SIMULATOR

The load simulator is an air channel which simulates a building's heating system consisting of a return air duct, fan and heating and cooling coils. The inlet air temperature is adjusted by an electric resistance heater and an air conditioner under the control of the HP-9825A. A schematic of the building load loop and air channel are also shown in Figure 1.

The building heating requirements to be satisfied by the solar energy system are modeled in the microcomputer. A simple thermostat model is used to control the heat delivery system. As determined by McBride[4] in experimental studies, the heat delivery system is on for a fixed interval of about 5 minutes. The energy delivered to the load by the heating coil is measured and compared with the building load to determine how often heat must be supplied and whether auxiliary energy is required. Initial experiments have been run using a building effective heat loss coefficient, UA = 500 W/°C and a typical ambient temperature varying between 20 °C and 0 °C. Work is presently under way to calculate hourly building loads using a TRNSYS compatible residential building load model[5] with recommended building parameters for typical residences in four representative cities.

INITIAL RESULTS

Initial experiments have been run on the test facility to determine the accuracy of energy balance measurements for the system. The building load and collector array size represent a typical residence in Madison, Wisconsin.

Energy balances are performed during the experiment by: 1) determining the energy delivered by the pseudo-collector; 2) determining the energy stored at the beginning and end of a period; 3) determining the amount of energy delivered to the load; and 4) estimating losses from storage and piping.

Collector Loop Energy Balance.

Preliminary energy balance experiments were run with simulated solar heat input from the pseudo-collector, with the apparent collector temperature determined by the HP-9825A, and with the operation of the collector and load loop determined by the LBL electronic controller.

Energy supplied by the pseudo-collector was calculated at 60 second intervals and the amount of energy in the storage tank was calculated at 30 minute intervals as the apparent solar insolation was increased from zero to a maximum of 950 W/m^2 and then back to zero. The duration of each experiment was 4 hours.

Time period	4 hrs	4 hrs	22 hrs
Heat Input			
Q2	131.9 MJ	128.6 MJ	705.2 MJ
Q4	128.6 MJ	126.1 MJ	692.3 MJ
$\Delta Q_{storage}$	113.0 MJ	118.5 MJ	663.9 MJ
Estimated Piping Losses			
Q2 -Q4	3.3 MJ	2.5 MJ	12.8 MJ
Q_{piping}	3.7 MJ	4.9 MJ	25.2 MJ
Net Energy Balance			
$\Delta Q_{storage}$	113.0 MJ	118.5 MJ	663.9 MJ
+ Q_{piping}	3.7 MJ	4.9 MJ	25.2 MJ
+ Q_{loss}	4.6 MJ	5.6 MJ	28.4 MJ
- Q2	-131.9 MJ	-128.6 MJ	-705.2 MJ
Net Balance	-10.6 MJ	-0.4 MJ	12.3 MJ
	(-9.0%)	(0.3%)	(1.7%)

TABLE 1. Collector Loop Energy Balance Summary

An energy balance summary for two 4 hour experiments and for a 22 hour total of successive experiments is shown in TABLE 1. The change in storage tank energy, ΔQ_S, is calculated from measurements of the storage tank temperatures. Heat input from the pseudo-collector boiler is calculated using the measured flow rate and the temperature difference

between inlet and outlet. Q2, the total heat supplied to the fluid stream, is calculated using thermocouples just before and after the boiler. Q4, the heat supplied to storage, is calculated using thermocouples before the boiler and at the storage return and is slightly smaller because of piping losses.

Estimates are made for heat losses from the system piping and from the storage tank, which contains 11,400 kg of water. Previous experiments indicate that the heat loss coefficient should be approximately 25 W/°C for the collector loop piping and 24.6 W/°C for the storage tank.. Estimated piping energy losses are indicated in Table 1 and compared with the difference between Q2 and Q4 which represents about one half the estimated loss, as it accounts only for the return side of the collector loop. Additional losses are found on the supply side.

The net energy balance is calculated by subtracting the energy input from the change in energy storage and the estimated losses. The energy input during each four hour period was reproducible as shown in Table 1. The energy balance over a single four hour measurement period is not precise, primarily because of uncertainty in the storage tank energy measurements. Even though the storage tank energy change is calculated from the weighted average of 6 thermocouples, errors of the order of ± 10 MJ are produced as the stratification in the storage tank changes. However, over a long experimental run of 22 hours, the energy balance is quite acceptable.

Load Loop Energy Balance.

Preliminary energy balance experiments were run with heat delivered from the storage tank to the heating coil located in the air duct. Power discharged in the heating coil, Q_H, was measured every thirty seconds using a differential thermocouple measured across the coil and the load loop flow measurement, FL2. Power delivered to the load was typically 12 kW. The load loop experiment summarized in Table 2 was run for a period of 18 hours, with the building load calculated for a constant outdoor temperature of 0 °C and a building loss coefficient of 500 W/°C.

The overall energy balance for the 18 hour run is quite good when estimated losses from storage, from piping, and across the heating coil are compared with the changes in the stored energy.

Testing plans

Comparison tests of alternative control strategies are now beginning. The facility will be run for a series of days using typical meteorological data for Madison, Wisconsin. Improvements are underway to permit comparisons of on/off and proportional flow control in the collector loop. The test facility will a valuable resource to compare alternative control strategies for active solar systems in a controlled laboratory environment where accurate and repeatable observations can be made. Our goal is to improve the utilization of solar energy through improved controls and control strategies.

Time Period		18 hrs
Storage Tank Energy Balance		
	$\Delta Q_{Storage}$	-561.4 MJ
	ΔQ_{loss}	21.8 MJ
Piping losses (estimated)		24.3 MJ
Net delivered to load		-515.3 MJ
Measured Heat To Load	Q_H	-536.7 MJ
Net Energy Balance		-21.4 MJ (4%)

TABLE 2: Load Loop Energy Balance Summary

References.

[1] "Experimental Test Facility for Evaluation of Solar Control Strategies," by M. Majteles, H. Lee, M. Wahlig and M. Warren. Proc. Workshop on Control of Solar Energy Systems for Heating and Cooling. Hyannis, Mass. 23-25 May, 1978. (LBL-8308) Aug. 78.

[2] "Electronic Controller Development and Evaluation of Control Strategies," M. Wahlig and M. Warren. (LBL-8381) Sept. 1978. Proc. of 3rd Annual Solar Heating and Cooling Research and Development Branch Contractors' Meeting. 24-27 Sept. 1978, Washington, D.C.

[3] J. A. Duffie and W. A. Beckman, Solar Thermal Processes (New York; John Wily & Sons, 1974).

[4] Merle F. McBride, "Measurement of Residential Thermostat Dynamics for Predicting Transient Performance," ASHRAE, 85 (1979), PH-79-7A.

[5] P. J. Hughes and J. H. Morehouse, "A TRNSYS-Compatible, Standardize Load Model for Residential System Studies," Draft Report, May 1979, Science Applications, Inc.

NOTES

Session IVB

Dr. Ashley Emery
University of Washington
Chairperson

SYSTEMS ECONOMICS III

AN ANALYSIS OF THE ECONOMIC VIABILITY OF A SOLAR THERMAL POINT FOCUSING ELECTRIC PLANT FOR SANTA CATALINA ISLAND — A CASE STUDY

J. V. V. Kasper
University of California at Los Angeles
Los Angeles, CA 90024

R. B. Davis
Jet Propulsion Laboratory
Pasadena, CA 91103

ABSTRACT

The effective cost of electricity generation to the Catalina Island utility system was determined for a combined diesel/solar thermal electric plant. This cost was compared to the effective cost of electricity generation for an all-diesel electric plant, the status quo on Catalina. Breakeven solar system capital costs were calculated for various future scenarios. The Alternative Power System Economic Analysis Model (APSEAM), a cash flow computer model, was used to perform the computations. Conclusions from the analysis include:

- For the base case assumptions, the Catalina Island utility would be financially indifferent between diesel power generation and diesel/solar thermal power generation at a solar capital cost of $2475/kWe.
- The solar system breakeven capital cost is strongly dependent on the method of financing of the capital investment, varying from $1535/kWe for 100% equity financing (at a rate of 17%) to $6240/kWe for 100% bond financing (at a rate of 12%).
- The solar system breakeven capital cost for Catalina Island is quite sensitive to the specifics of the escalation rate of fuel costs over time. A constant annual fuel escalation rate of 11% over the 1980-2015 time frame has about the same impact on the solar system breakeven capital cost as a 30% escalation rate for the first three years of that time period and an 8% escalation rate thereafter.

INTRODUCTION

The effective cost of electricity generation to the Catalina Island utility system for two different electricity generation systems was determined utilizing the Alternative Power System Economic Analysis Model (APSEAM), an interactive computer model developed at the Jet Propulsion Laboratory. The Catalina Island utility system is owned and operated by Southern California Edison Company. Presently, diesel engines are used to generate electricity for Catalina Island. The power generation alternative considered in this analysis was a combined diesel/solar thermal electric plant in which the diesel plant provides the shortfall between the load requirements and solar energy production.* One solar thermal electric plant size was considered, 1000 kWe. Insolation data for Long Beach, California, and Barstow, California, were used in conjunction with an in-house simulation model** to obtain performance information for the solar thermal electric plant. Load data for a typical year were obtained from the Catalina utility system. Construction of the solar plant is assumed to commence in 1982 and commercial operation to start in 1985. Utility financial data from the past 5 years were analyzed in light of diesel system operational concepts to develop an algorithm describing the cost over time of diesel operation on Catalina. Detailed cash flows were projected for both power generation options for each year in the time period of interest, and calculated figures of merit were used to determine those sets of parameters for which either option was preferred.

POWER SYSTEM INVESTMENT ALTERNATIVES FOR CATALINA ISLAND

At present, Catalina Island has 6.2 MWe of diesel engine capacity. The maximum load is about 3 MWe, implying a reserve margin of about 100%. This reserve margin is not considered excessive due to the isolated nature of the island. There is presently a moratorium on new housing construction on the island due to water resource constraints. This is assumed to continue into the future so that all of the island's electrical needs over the next thrity years could be met by the present 6.2 MWe of diesel system capacity while maintaining a 100% reserve margin. A substantial fraction of the present cost of electricity production on Catalina Island is due to the cost of diesel fuel. In 1979, for example, the price of diesel fuel increased 85%; at the end of 1979, the price of fuel alone accounted for 5.7¢ per kilowatt-hour of electrical energy generated. Given the likelihood of future fuel price increases and fuel availability limitations, alternatives to the present

*Although the diesel system produces about 83% of the total energy requirements in the base case, it will subsequently be referred to as the makeup system.

**Gabalawi, N. El, Hill, G., Bowyer, J. M., Slonski, M. L., "A Modularized Computer Simulation Program for Solar Thermal Power Plants," JPL Internal Document 5102-80, July 1978.

electricity generation system on Catalina Island merit serious attention. An option which partially circumvents the problems of future fuel price increases and fuel availability limitations is investment in renewable energy resources such as solar thermal technology. This analysis compares the following two options for meeting the island's electrical demand in the 1985-2015 time frame: (1) Continued all-diesel operation; and (2) Investment in a solar thermal electric system, to allow for combined diesel/solar thermal power generation.

THE COST OF DIESEL SYSTEM OPERATION

Data from a Catalina Island operations report* were utilized to formulate a linear algorithm to describe the cost** of diesel system operation over time on the island:

$$\text{Annual Cost} = \left[\text{Peak Demand}\right]\left[\$157/\text{kW-yr}\right]\left[\prod_{t=1}^{N}(1+\text{ERCC}_t)\right] + \left[\text{kWh Generated}\right]\left[(\$0.01)\right]\left[\prod_{t=1}^{N}(1+\text{ERPE}_t)\right] + \left[\text{kWh Generated}\right]\left[(\$0.057)\right]\left[\prod_{t=1}^{N}(1+\text{ERFC}_t)\right]$$

where 1980 is the base year, that is, N = 0 for January 1, 1980

ERCC_t is the escalation rate of fixed costs in year t

ERPE_t is the escalation rate of non-fuel-related variable costs in year t

ERFC_t is the escalation rate of fuel costs in year t.

The constants in this expression were empirically determined so as to minimize the difference between calculated and actual costs. The average percentage difference between actual and calculated costs is 9%. Table 1 shows the actual operational costs in the 1974-1979 time frame for the Catalina Island utility system, the escalation rates experienced in that time period, and the calculated costs of diesel operation based on the algorithm.***

*"Results of Operations--Santa Catalina Island Electric 1974-1979," prepared in September 1978 for the Public Utilities Commission of the State of California by Southern California Edison.

**This cost includes the costs of major overhauls/short block replacements, periodic maintenance, operations, fuel, depreciation, customer accounting, and G&A.

***Although Catalina Island has experienced a growth in energy production in the 1974-1979 time period, new resource constraints (i.e., water) might limit future growth. In this analysis, future growth is assumed to be zero.

TABLE 1
COMPARISON OF ACTUAL AND CALCULATED COST OF UTILITY OPERATION ON CATALINA ISLAND

Time Period	ERFC (%)	ERCC (%)	ERPE (%)	kWh Generated	Calculated Costs ($)	Actual Costs ($)
1974-1975	90.0%	10%	10%	9,072,000	581,375	572,266
1975-1976	0.0	10	10	9,605,000	633,529	661,754
1976-1977	8.1	10	10	10,631,000	728,380	639,813
1977-1978	4.4	10	10	10,959,000	796,919	833,830
1978-1979	6.6	10	10	12,500,000	926,771	1,271,000
1979-1980	84.8	10	10	14,000,000	1,409,000	1,389,000

When this algorithm is used to project the cost of diesel system operation in the 1985-2015 time frame, assuming a constant annual energy requirement of 14,000,000 kWh (the number of kWh generated by the system in 1979) and a peak demand of 3000 kWe, the effective levelized price (in dollars of constant energy purchasing power over time) of diesel-generated energy is 12.43¢/kWh over that time horizon. This is the price which, if allowed to escalate each year (starting in 1980) at 10%, would generate sufficient revenues to exactly cover the costs of diesel system operation, including the return on investment.

THE SOLAR THERMAL INVESTMENT ALTERNATIVE

A solar thermal electric plant (with the existing diesel system providing required make-up power to satisfy the load) is the alternative power generation option considered in this analysis. The solar plant displaces fuel. The capacity displacement by the solar plant is assumed to be zero.

Solar System Size

A 1 MWe solar thermal electric system is considered in this analysis. The plant consists of 50 20 kWe point-focusing parabolic dishes. Each of these dishes consists of a parabolic collector which focuses the solar rays, a receiver which is mounted at the focal point of the collector, and a heat engine which converts the thermal energy into electrical energy. There is no storage.

Solar System Performance

Solar Thermal Plant Subsystem Efficiencies: The efficiency assumptions* for the solar thermal plant subsystems were as follows:

Collector/Receiver Efficiency	74%
Engine Efficiency (at 815C in, 50C out)	30%

Capacity Factor: Insolation on Catalina Island has not been adequately measured. The base case capacity factor for the solar thermal plant was approximated as follows: The in-house solar thermal simulation program, utilizing a 1977 hourly insolation tape for Barstow, California,

*These represent performance targets for 1st generation (1982) solar systems. See "Annual Technical Report, Fiscal Year 1979," November 15, 1979 (DOE/JPL-1060-30).

determined a capacity factor of 35% for a solar thermal plant located in Barstow. This capacity factor was then scaled to be appropriate for Long Beach, on the coast of California, 26 miles from Catalina. The annual amount of direct normal insolation for Barstow is 2718* kWh/m^2 and for Long Beach is 2138** kWH/m^2. Thus, an approximate capacity factor for Catalina is:

$$(35\%)(2136/2718) = 27.5\%$$

This same capacity factor was assumed for all years in the time horizon of interest.

Subsystem Lifetimes: The base case lifetimes for the various solar thermal plant subsystems were based on in-house engineering design estimates and were as follows:

Collectors:	30 years
Receivers:	15 years
Engines:	10 years
Balance of Plant:	greater than 30 years.

Base Case Solar Subsystem Costs*** (1980 dollars):

Collectors	$1600/kWe
Receivers	$ 450/kWe
Engines	$ 750/kWe
Balance of Plant	$ 300/kWe
Total	$3100/kWe

Solar System Dispatch Strategy

The solar plant is dispatched whenever it produces useable energy. The diesel system is then throttled, as necessary, in response to variations in the solar system energy output, to meet load requirements. The diesel system cost algorithm described above projects the cost of the diesel system operation in a make-up energy mode (that is, when the diesel system is throttled in response to the solar system output), if the fuel efficiency of the diesel engines in that mode is the same as at present.****

*This value was obtained from the report: "Solar Energy Measurement at Selected Sites Throughout the Southwest During 1977," R. J. Yinger, Southern California Edison Company, June, 1978, Table 2, page 16.

**This value was determined using a modified Liu and Jordon approach and the latest SOLMET values; see V. Cinquemani, et al., "Input data for Solar System," prepared by the National Climatic Center, Asheville, NC, November, 1978.

***These prices are representative of near-term technology and small (less than 50 units/yr) production rates. More advanced technology and large production rates will result in substantially lower costs.

****The basis for this assumption is the relatively constant heat rate for diesel engines when they are operated at greater than 50% of load. (Source: P. Steitz, L. G. Mayo, S. P. Perkins, "Assessment of the Potential of Solar Thermal Small Power Systems in Small Utilities," Nov. 1978, Table 3-6, p. 3 13.) When the solar system size is constrained to 1 MWe or less, a make-up mode diesel dispatch strategy can always be identified in which each of the diesel engines is either off or operated at greater than 50% of load.

RESULTS

Base Case Assumptions

Capital Investment:
- -Solar system cost: $3096/kWe
- -Salvage value: 5% of capital cost
- -Zero land cost (land is already available).
- -Depreciation schedules:
  - Federal: double declining balance
  - State: 150% declining balance
- -Depreciation Lifetimes:
  - Collectors: 30 years
  - Receivers: 15 years
  - Engines: 10 years

Capital Funding:
- -Down payment: 10% of each year's construction costs
- -Short term construction loans (@ 12%) taken during construction, with financing at end of construction period via equity (50%) and bonds (50%)
- -Equity dividend rate = 11%
- -Equity appreciation rate = 6%*
- -Bond interest rate = 12%
- -Bond lifetime = 30 years

Recurrent Costs:
- -Fuel costs = $5.10/$10^6$ Btu
- -Fixed O&M for solar plants = $2.50/kW-yr
- -Variable O&M for solar plant = $0.005/kWh
- -Other annual costs for solar plant = $1000/yr
- -Insurance costs for solar plant = $10000/yr

Incentives
- -Federal investment tax credit = 10%
- -Federal energy tax credit = 0%**
- -State solar tax credit = 25%***

*Non-dividend return to the stockholder can be realized through any mode of increase in the value of the company, i.e., through an increase in stock market value, retained earnings, or in any other component of a company's assets. Theoretically, the stockholder would realize this increase in value if the company were to be liquidated at the end of the investment time horizon and all of the company's assets distributed to its stockholders. This equity appreciation is accounted for (and paid for in a cash flow sense) by means of an annual contribution to a sinking fund. When the equity appreciation rate is adjusted to yield a net present value of zero, then the total return on equity is the sum of the dividend rate and this adjusted equity appreciation.

**The federal energy tax credit rate is 10%, but is scheduled to end in 1983. Hence, its effective rate for this analysis is 0%.

***The California tax credit, scheduled to end in 1980, is assumed to be extended to 1985.

Escalation Rates (annual)	
-Capital equipment	10%
-Fixed O&M for solar plant	10%
-Variable O&M for solar plant	10%
-Standard rate of inflation	8%
-Fuel costs*	30% for 3 yr, 9% thereafter
Investor Specific Parameters	
-Opportunity (after-tax) cost of investment	10.8%
-Other federal and state net taxable income	$10 million
Performance	
-Capacity factor	27.5%

Economic Viability Decision Criteria

The solar thermal plant investment is preferred if:

- -Net Present Value (NPV) is greater than zero (a NPV equal to zero implies that the investor is indifferent, from a purely financial standpoint, to one or the other option)(The net present value is expressed in terms of 1982 dollars)
- -Absolute cost of energy is less than 12.43¢/kWh

Base Case Results

For the base case, the net present value is -753.6K$ and the absolute cost of energy is 12.77¢/kWh. Thus, for the base case, the solar investment is not preferred, from a purely financial standpoint, to a continuation of the present mode of electricity generation on Catalina Island.

Sensitivities:

Capital Costs. Figure 1 illustrates the variation in the net present value of the solar thermal investment choice as a function of the solar system cost. As can be seen, at a capital cost of $2475/kWe, the investor would be financially indifferent between the two options.

Fuel Price Escalation Rates. Table 2 shows the sensitivity of the results to the details of the escalation rate of fuel prices and clearly indicate the need to consider year-specific escalation rates. Over a thirty-year period, a fuel price escalation rate of 11%, compounded annually, increases the price of fuel by a factor of about 23. This same factor is approximately realized if one escalates at 30%/year for 3 years and then at 9%/year for 27 years. However, the base case net present value for the former escalation scheme is

*The Autumn, 1979 "Energy Review" by Data Resources, Inc., projected nominal diesel fuel prices to increase by about 12%/yr through 1982 and at about 9.5%/year thereafter. In light of recent crude oil price increases, expected future increases, and the experience of the Catalina Utility in 1979 (85% fuel price increase), this assumption is not unreasonable.

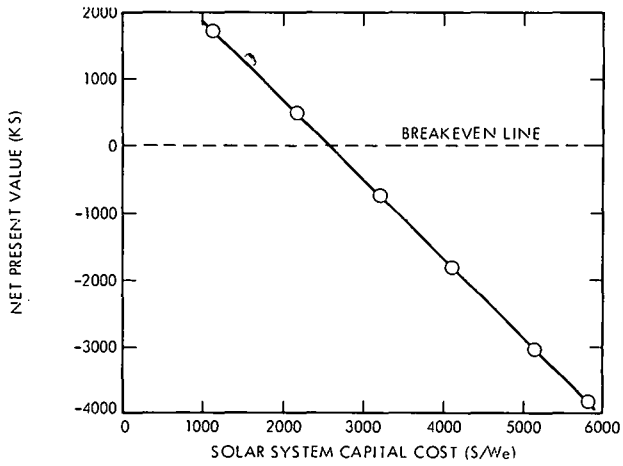

Fig. 1. Variation of Net Present Value of Solar Investment Choice with Solar System Capital Cost

TABLE 2
IMPACT OF SPECIFICS OF FUEL PRICE ESCALATION RATES ON SOLAR SYSTEM ECONOMICS

Fuel Price Escalation Scheme for 1980-2015 Time Frame	Fuel Price Increase Factor at End of 30 years	Net Present Value (K$)	Breakeven Capital Cost ($/kWe)
8% all years	10.1	-2255.4	1240
9% all years	13.3	-1973.3	1470
10% all years	17.4	-1627.6	1760
11% all years	22.9	-1202.6	2105
30% 1st 3 yrs, 8% thereafter	17.5	-1151.7	2150
30% 1st 3 yrs, 9% thereafter	22.5	- 753.6	2475
30% 1st 3 yrs, 10% thereafter	28.8	- 249.0	2890

-1202.6 K$, whereas the base case net present value for the latter escalation scheme is -753.6 K$, an improvement in the net present value of 449K$.

Performance - Capacity Factor. The sensitivity of the base case results to the capacity factor of the solar thermal plant is shown in Table 3. The data show that a given percentage change in

TABLE 3
IMPACT OF SOLAR SYSTEM PERFORMANCE (CAPACITY FACTOR) ON SOLAR SYSTEM ECONOMICS

Capacity Factor (%)	Net Present Value (K$)	Effective Cost of Energy (¢/kWh)	Breakeven Capital Cost ($/kWe)
20.0	-1617.1	13.17	1765
25.0	-1041.5	12.90	2240
27.5	- 753.6	12.97	2475
30.0	- 465.8	12.64	2715
35.0	+ 109.9	12.38	3185

capacity factor produces a concomitant percentage change in the breakeven capital cost. Thus, there is a direct tradeoff between realizing increased performance (by increased insolation or operational efficiencies) and experiencing increased breakeven capital costs.

Performance - Subsystem Lifetimes. Table 4 illustrates the effect on the net present value of

TABLE 4
IMPACT OF SOLAR SYSTEM PERFORMANCE
(SUBSYSTEM LIFETIMES) ON SOLAR SYSTEM ECONOMICS

Subsystem Lifetimes (yrs)			
Collectors:	30	24	21
Receivers:	15	12	11
Engines:	10	8	7
Net Present Value (K$)	-753.6	-1003.9	-1229.6
Effective Cost of Energy (¢/kWh)	12.77	12.89	12.99
Breakeven Capital Cost ($/kWe)	2475	2320	2200

the solar thermal investment choice due to varying the sub- system lifetimes. As can be seen, the breakeven capital cost is relatively insensitive to variations in subsystem lifetimes.

Capital Investment Financing. As expected for capital intensive investments, the economic viability of the solar plant investment is quite sensitive to the method of financing. The base case financing method is a downpayment in each year of the construction period of 10% of that year's construction costs with the remaining construction funds obtained from short-term loans each year of the construction period.

At the end of the construction period, these short-term loans are refinanced with a combination of a stock issue (50%) and a bond issue (50%). This bond/stock ratio was chosen to reflect the capitalization structure of Southern California Edison Co.* Table 5 illustrates the impact of varying the base case financing method. The extremes considered are: (1) all bond financing, at a bond rate of 12% and (2) all equity-financing, at a total return on equity of 17%. Clearly, if the Catalina Island utility were not required to finance the solar investment in line with its capitalization structure but, rather, could utilize all bond financing, even a solar system costing $6240/kWe would be economically viable.

*The capitalization structure of SCE is 48.5% debt, 37.2% common equity, 14.3% preferred stock. Source: "Costs of Capital and Rates of Return for Industrial Firms and Class A and B Electric Utility Firms," Ernst and Ernst, June 1979 (DOE/ERA-6391 1). No provision is made in this analysis for utilizing preferred stock as a source of funds.

TABLE 5
EFFECT OF FINANCING METHOD ON
ECONOMIC VIABILITY OF SOLAR INVESTMENT

Financing Method	Net Present Value (K$)	Breakeven Capital Cost ($/kWe)	Effective Cost of Electricity (¢/kWh)
All bond @ 12%	1544.1	6240	11.72
50% bond @ 12% 50% equity @ 12%	673.4	3972	12.12
All equity @ 12%	- 197.2	2906	12.52
50% bond @ 12% 50% equity @ 17%	- 753.6	2475	12.77
All equity @ 17%	-3051.3	1535	13.82

The sensitivity of these results to the return on equity (in the base case, this is 17%) is shown in Table 6. The fact that, at a percentage return on

TABLE 6
EFFECTS OF VARIATION OF RETURN
ON COMMON EQUITY ON NET PRESENT VALUE

Return on Common Equity (%)	Net Present Value (K$)
14.0%	246.9
14.9%	0
15.0%	- 28.2
16.0%	- 357.5
17.0%	- 753.6
18.0%	-1232.5
19.0%	-1814.0

equity of 14.9% (11% annual dividend, 3.9% stock appreciation), the net present value is zero implies that this is the return on equity which the Catalina utility would realize, were it to make the solar system investment choice.

Figure 2 shows the net present value of the solar thermal investment choice for three different types of long term financing as a function of the solar system capital cost. As can be seen, the effect of utilizing different financing instruments is most dramatic, the greater the capital cost of the solar thermal system. The 100% equity financing option is most costly because the required cash outlays for the payment of dividends to stockholders, and for the annual contribution to a sinking fund to reflect appreciation in the value of the company and to provide for a (theoretical) disbursement of company assets to the shareholders at the end of the investment time horizon) are not tax-deductible. On the other hand, because bond interest costs are tax-deductible, even the most costly solar system considered ($6200/kWe) is the preferred investment choice.

The policy implication of this finding is that funding-related incentive schemes are most effective when solar capital costs are greatest. Thus, incentives are more important at present since

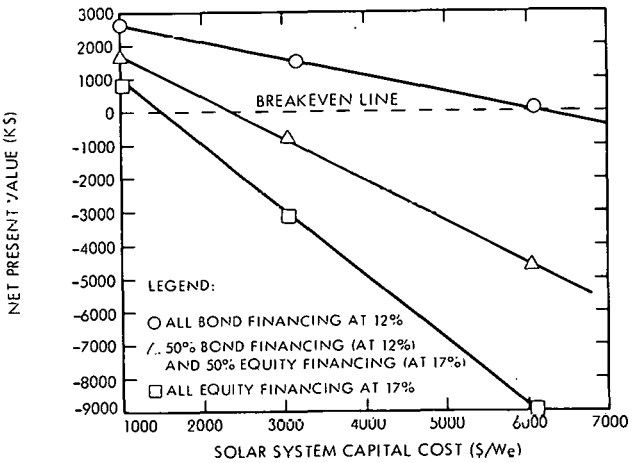

Fig. 2. Effect of Solar System Capital Cost and Financing Method on Net Present Value of Solar Investment Choice

the capital costs of solar equipment are expected to substantially drop in this decade.

Incentives. The effects of three different incentive schemes on the economics of the solar investment were considered: (1) Extension of the federal energy tax credit to the year 2016 (current law calls for this tax credit to end in 1983) and an increase in that tax credit to 25% (from the current 10%); (2) Allowance for financing of 50% of the total loan with low cost (i.e., 6%) bonds (possibly available through the Solar Bank); (3) Allowance of tax deductibility of dividend payments.

1. Federal Tax Credit--25% through the year 2016: The effect of this incentive is to increase the net present value of the base case from -753.6K$ to -162.6 K$. The breakeven capital cost increases from $2475/kWe to $2640/kWe and the effective cost of electricity decreases from 12.77¢/kWh to 12.50¢/kWh. If the federal energy tax credit were further increased to 28.9%, then the base case would have a net present value of zero. Table 7 gives the breakeven federal tax credit (i.e., that which yields a net present value of zero) as a function of the capital cost of the solar investment.

TABLE 7
VARIATION OF BREAKEVEN FEDERAL ENERGY TAX CREDIT WITH SOLAR SYSTEM CAPITAL COST

Solar System Capital Cost ($/kWe)	Breakeven Federal Energy Tax Credit (%)
2580	6.42
3096	28.86
3612	39.06
4128	46.72
4644	52.67
5160	57.43
5676	61.32
6192	64.57

2. Low Cost Bonds: When the investor is allowed to finance 50% of the loan amount with low cost (i.e., 6%) bonds (the remaining 50% being financed by an equal combination of bonds (at a cost of 12%) and equity (at a cost of 17%)), the net present value of the base case increases from -753.6 K$ to +796.7 K$, the breakeven capital cost increases from $2475/kWe to $4190/kWe, and the effective cost of electricity decreases from 12.77¢/kWh to 12.06¢/kWh.

3. Tax Deductibility of Dividend Payment by Solar System Investor: One of the major reasons for the high cost of equity financing relative to bond financing (see Table 5) is due to the fact that bond interest payments are tax deductible whereas equity dividend payments are not. If federal tax law were to be modified so as to make the dividend payments associated with solar system financing tax deductible, then the base case net present value would increase from -753.6 K$ to +646.9 K$ and the breakeven capital cost would increase from $2475/kWe to $3930/kWe.

Conclusions from Incentives Sensitivity: Of the three incentive schemes considered in this section, the low cost bond scheme is the most effective means for improving the perceived economic viability of the solar investment.

CONCLUSION

Although the all-diesel option is financially preferred to the combined solar/diesel system for the base case assumptions of this analysis, there are many incentive schemes and possible future scenarios for which investment in a solar thermal system would be financially favored. Hence, more detailed analysis of the value and role of alternative power generation technologies (such as solar thermal) for Catalina Island and all similar applications appear very much warranted.

ACKNOWLEDGMENTS

The contributions of Bob Adamson, Catalina Operations Manager, John Ballance, Moshe Barak, and Florence Glazebrook of Southern California Edison Company, and Bob Gurfield of JPL in the development of the data base for this paper is gratefully acknowledged.

The research described in this paper was carried out at the Jet Propulsion Laboratory, California Institute of Technology, and was sponsored by the U.S. Department of Energy through an agreement with NASA.

Dup

SOLSTOR RESULTS FOR A PHOTOVOLTAIC/BATTERY SYSTEM WITH TIME-OF-DAY PRICING AND SELLBACK

B. C. Caskey, Division 4744
D. L. Caskey, Division 4723
E. A. Aronson, Division 2623
Sandia Laboratories
Albuquerque, NM 87185

ABSTRACT

The Sandia Laboratories' optimizing computer code, SOLSTOR,[1] has been utilized to investigate the role of battery storage in a residential flat plate photovoltaic (PV) system. The system is connected to the utility grid and time-of-day pricing and sellback policies are considered.

The study assumes that the 1986 PV module cost goals will be met, and hence PV systems will be competitive with grid electricity. A range of battery costs is included. Systems installed in three cities (Phoenix, AZ, New York, NY, and Columbia, MO) were optimized based on minimizing the 20 year life cycle energy cost for a typical all-electric single family dwelling.

The results show that the usefulness of batteries is a strong function of the battery costs, economic conditions, time-of-day pricing ratio, and the sellback ratio. At about $100/kWh, batteries can generally lower life cycle costs. Also, the synergism of PV arrays and batteries can result in larger PV arrays.for the optimized system.

In particular, it was determined that whenever either the sellback ratio was 0.5 or less, or the peak/off-peak electric rate ratio was greater than 3:1, batteries were an economic asset in the system.

INTRODUCTION

Sandia Laboratories, in its role as lead center for the DOE development program "Batteries for Solar Applications," has considered the usefulness of storage in photovoltaic systems. The present study focuses on grid-connected residential systems, utilizing flat plate photovoltaic (PV) collectors. Future work will look at stand-alone residences, as well as larger system applications such as apartments, commercial buildings, and light industrial sites.

The study was performed using the SOLSTOR simulation program. SOLSTOR, which is described in detail in ref. 1, performs iterative hour-by-hour simulations for a year to provide the optimum system configuration for the conditions assumed. The result is that the yearly cost of energy is minimized over the assumed system lifetime.

ASSUMPTIONS

A clear understanding of the assumptions used in a study of this type is essential to interpreting the conclusions in a meaningful way. We have divided the assumptions into three categories--general economic, system related, and utility interface.

General Economic Assumptions

Individual homeowner economic parameters were used. Two solar energy related tax incentives were included--the 20% Federal tax credit, and the fact that many local governments are exempting solar installations from the property tax base. These and other general economic parameters are summarized in Table 1, below.

TABLE 1. BASIC ECONOMIC ASSUMPTIONS

Income Tax Rate	30%
Interest Rate	8.5%
Discount Rate	10%
Down Payment on System	20%*
Federal Tax Credit	20%*
Property Tax	0%
General Inflation Rate	5%
Operation and Maintenance Costs/year (based on initial capital costs)	1.5%
Price Year	1980
Base Year	1986
Year Operation Begins	1986
Lifetime	20 Years

*The 20% down payment, when combined with the 20% tax credit represents a loan leveraging situation which is probably unrealistic in the long run. Changing the down payment to 40% has only a minor effect on the results presented here.

System Related Assumptions

SOLSTOR, as run in this study, treats four components as variables. They are: 1) the flat plate PV array, 2) the battery storage, 3) the power conditioning, consisting of a max power tracker, a battery charger, and an inverter, and 4) a line powered charger for charging the batteries from utility power. Each component is characterized by an electrical efficiency and a cost. All costs in this study consist of a fixed cost plus a variable cost related to size chosen. No economies of scale were assumed. In order to simplify the computations, the cost of the line powered charger

(rectifier) was lumped into the power conditioning, and its efficiency included in the battery efficiency.

The battery storage costs are complicated by the requirement to provide battery replacements over the system lifetime. This was handled by computing the present value of all the replacements required, and using that as the cost. Battery lifetimes assumed varied from 5 years, for current lead acid technology, to 14 years for a projected advanced lead acid design. In addition, we constrained the batteries to charge/discharge rates no greater than the five hour rate (capacity/5). The costs and efficiencies used in the study are shown in Table 2, below. The PV array costs were derived from a basic module cost of 70¢/Wp (the 1986 goal).

TABLE 2. PV SYSTEM COSTS, 1980 DOLLARS*

Component	Efficiency	Fixed Cost	Variable Cost
PV Array	11%	$ 1000	$ 117/m^2
Power Conditioning	95%	200	140/kW
Battery Storage	80% (round trip)	850	270/kWh † 163/kWH † 91/kWh † 64/kWh †

*Installed costs
†Present value of replacements to provide 20-year life

The PV system is assumed to be on a well constructed house of 1520 ft^2, kept at 68°F. The PV system supplies electricity for space heating and cooling, via a heat pump, domestic hot water, and general lighting and appliance loads. In the SOLSTOR model the heat pump's coefficient of performance (COP) is varied with the outside temperature. Heating and cooling loads are calculated hourly from the weather data (Typical Meteorological Year--TMY),[2] and hot water and general loads follow a simple profile which repeats daily. Typical yearly energy consumption is about 20 MWh.

Utility Interface Assumptions

Assumptions about the utility rates and policies are of critical importance in grid-connected systems, primarily because SOLSTOR uses utility energy whenever there is an economic advantage in doing so. SOLSTOR is able to handle a fairly general set of utility rates. This can include a fixed "system charge" as well as "energy charges" which can vary seasonally and daily. Time-of-Day rates (TOD) are beginning to come into use, and appear to be the wave of the future.

Sellback of excess energy from the PV array to the utility is also a plausible scenario. We characterize sellback by a fraction which represents the percentage of the current selling price that the utility will pay the system owner for energy.

Utility rates used in this study represent actual 1979 rates in use in the study cities, carried forward to 1980.[3] TOD rates were synthesized such that the total bill for purchased energy would remain the same, if there was no change in the homeowner's use profile. These rates are shown in Table 3, below.

TABLE 3. RESIDENTIAL ELECTRIC RATES (1980$)
(¢/kWh)

	Fixed	Peak/ Off Peak = 3*	Peak/ Off Peak = 6*
Phoenix:			
Summer[1]	5.15	8.14/2.71	9.51/1.59
Winter	4.51	7.14/2.38	8.33/1.39
New York:			
Summer[2]	13.9	22.8/7.6	27.3/4.55
Winter	11.2	18.5/6.17	21.9/3.65
Columbia, Mo:	3.75	6.17/2.06	7.36/1.23

* Peak time is 9 am to 9 pm in summer, Mon-Fri.
8 am to 8 pm in winter, Mon-Fri.

[1] Summer rates effective May 1-Nov. 1.
[2] Summer rates effective May 15-Oct. 15.

STUDY PARAMETERS

Since the purpose of this study was to evaluate storage in a PV system, the prime parameters were battery cost and utility rates. The latter includes both variations in TOD price ratios and sellback ratios. The highest TOD ratio used was 6:1, representative of several TOD rates in use at the present time. (Example: Madison, WI ratio is 7.5:1 in Summmer, 5.2:1 in winter, with peak time of 10 am-9 pm. See Ref. 4.)

Battery costs used span a range of slightly over 4:1, and represent current lead acid systems ($270/kWh) at the high end, to projected advanced lead acid batteries ($64/kWh) at the low end.

Electric rate escalation is a parameter affecting the feasibility of solar systems in general. It was varied also, using 0%, 3% and 6% above inflation.

Finally, three different locations were used in the study. New York, NY represents a moderately cold region, with fair insolation and high electric rates. Phoenix, AZ is representative of a hot, sunny region with average electric rates, and Columbia, MO is characterized by a nearly equal heating and cooling load, fair insolation, and low electric rates.

In all, 432 different optimum systems were synthesized and evaluated. Table 4 lists the parameter values used. At least one simulation was run for all possible combinations.

TABLE 4. VARIABLE PARAMETERS

Location (Phoenix, AZ; New York, NY; Columbia, MO)
Electric Rate Escalation (0%, 3%, and 6% above inflation)
Battery Cost ($64, $91, $163, and $270/kWh)
TOD Ratios (1:1, 3:1, and 6:1)
Sellback Ratios (0., 0.25, 0.50, and 0.75)
432 systems

RESULTS

Since space does not permit a complete tabulation of the results for all 432 systems, representative results for all three locations are shown. (See Ref. 5 for complete report.) We have chosen a battery cost of $163/kWh and an electric rate escalation of 3% above inflation as our nominal case. For these "baseline" conditions, results for all twelve combinations of TOD rates and sellback ratios are given in Figs. 1-3. (Figures appear at the end of this paper.) Each figure provides four pieces of data for the twelve systems. First, the "Life Cycle Cost Ratio" (LCCR) is given. This is defined as the ratio of the levelized annual energy cost with the system chosen, to the levelized annual energy cost without the PV system (i.e. the loads are satisfied totally by purchased electricity). Second, the PV array size is given. The simulation was restricted to a maximum size of 150 m^2. Third, the battery size is given; the maximum allowed was 50 kWh. And fourth, there is an indication as to whether the batteries, where employed, were used in an off-peak charging mode from the utility; if so, a "Y" is indicated.

Figure 1, for New York, indicates that New York City is by far the most favorable of the three locations. This is due to the high electric rates found there. All twelve systems had a favorable LCCR, and array sizes, except for the zero sellback case, are chosen at the maximum allowed. Sizable storage is indicated in all but two cases. It is interesting to note that previous studies restricted to 1:1 TOD rates, got the same result we did for that case--namely, that storage is not beneficial for sellback ratios in excess of 0.5.[6] However, when TOD rates are assumed, all sellback ratios result in storage being beneficial. In light of the trend by utilities and regulatory bodies toward TOD pricing, these results seem quite significant. Finally, Fig. 1 shows that off-peak charging should never be done under a flat rate (TOD = 1:1) pricing system. The storage in that case, for low sellback ratios, is dedicated to the PV array. That is, it is used only to store excess PV energy.

Figure 2 (Phoenix, AZ), looks much like Fig. 1. However, the LCCR's are higher, the PV arrays are somewhat smaller, and storage is chosen in fewer cases and tends to be smaller where it is used. A TOD ratio of 6:1 is required for batteries to be used for all sellback ratios in an off-peak charging mode.

Figure 3, Columbia, MO, presents a rather bleak outlook for solar in general. Under the assumed 3% rate escalation scenario, PV systems are not even viable unless TOD rates are employed. Even then the LCCR's are close to 1 and not attractive. Only three cases involve storage.

Optimum vs. PV-only Systems

Another way to get at the influence of storage in PV Systems is to compare optimum systems, such as are shown in Figs. 1-3, to those which are optimized when constrained to have no storage. This has been done for New York, again using 3% rate escalations, but with lower battery costs ($91/kWh). The results are shown in Fig. 4, which plots LCCR's vs. sellback ratio for all three TOD ratios. The solid lines are for optimum systems, i.e. batteries are included, if warranted. The dashed lines repeat the same conditions, but storage is forced to zero size. Where the dashed and solid lines coincide for a particular case, no batteries were chosen in the optimum system.

Thus, for example, the two curves for a 1:1 TOD ratio converge at a sellback ratio of 0.5. Hence the economic benefits to be derived from storage are greatest at zero sellback and decline to zero at the 0.5 sellback point. In contrast, the 6:1 TOD ratio shows a minimum storage benefit at a sellback of about 0.35, and the benefits increase with increasing sellback from that point.

CONCLUSIONS

Several conclusions can be drawn from the results of this study. One is that the optimum array size is larger when storage is used, compared to PV-only systems. This situation occurs, in general, for sellback ratios of 0.5 or less. This could increase fossil fuel displacement and possibly accelerate PV production rates.

Second, present day lead acid battery costs of about $270/kWh over 20 years are too high for their use to be economically attractive in grid-connected residences, except for isolated cases. At a cost of $100-$150/kWh, batteries do become economically attractive in a large number of cases. These cases can be roughly categorized as follows:

1) Sellback ratios less than 0.5, or

2) Time-of-Day ratios greater than 3:1.

Third, storage in a PV system increases its flexibility. The system will be better able to cope with changing utility strategies. For example, implementation of a monthly peak demand charge would severely hurt PV-only systems, but not those with storage.

And fourth, there are cases where the batteries would not be justified on the basis of either off-peak charging alone or PV-charging alone, but are justified by having both modes available.

We have demonstrated in this study which combinations of TOD rates and sellback would justify storage in the residence, but we have not at-

tempted to predict which are likely. These factors are regionally dependent, and will also change with time. It seems clear to us, however, that sellback ratios will tend to decline as PV penetration increases, and that TOD ratios will also decline as utilities achieve better load balancing.

REFERENCES

1. "SOLSTOR Description and User's Guide," by D. L. Caskey, B. C. Caskey, and E. A. Aronson, SAND79-2330.

2. "Generation of Typical Meteorological Years for 26 SOLMET Stations," by I. J. Hall, R. R. Prairie, H. E. Anderson, and E. C. Boes, SAND78-1601.

3. "Selected Residential Electric Rates and Rate Structures in the U.S., July, 1979," by D. L. Caskey, SAND79-2110.

4. "Time-of-Day Pricing of Electricity Activities in Some Midwestern States," by J. R. Malko, D. J. Ray, and N. L. Hassig, presented at Midwest Economics Association Annual Meeting, April, 1979.

5. "Parametric Analysis of Residential Grid-Connected Photovoltaic Systems with Storage," by D. L. Caskey, and B. C. Caskey SAND79-2331.

6. "Regional Conceptual Design and Analysis Studies for Residential Photovoltaic Systems," by E. J. Buerger, T. S. Chan, R. P. Fogaroli, A. Kirpich, E. M. Mehalick, G. O'Brien, N. Shepard, G. F. Tully, R. D. Woodson, SAND78-7039.

TOD Ratio / Sellback Ratio		Life Cycle Cost Ratio			PV Array Size (m^2)			Storage Size (kWh)			Off-Peak Charging?		
		1:1	3:1	6:1	1:1	3:1	6:1	1:1	3:1	6:1	1:1	3:1	6:1
Sellback Ratio	0.	.73	.67	.56	112	96	42	31	28	38	N	Y	Y
	.25	.71	.63	.46	149	150	150	37	26	26	N	N	Y
	.50	.62	.38	.14	150	150	150	0	23	40	-	Y	Y
	.75	.42	.10	-.26	150	150	150	0	28	43	-	Y	Y

3 % Rate Escalation
$163 /kWh Storage Cost Date: 7/25/79

Figure 1. PV/Storage Study Results, New York, NY

Sellback Ratio	TOD Ratio	Life Cycle Cost Ratio			PV Array Size (m^2)			Storage Size (kWh)			Off-Peak Charging?		
		1:1	3:1	6:1	1:1	3:1	6:1	1:1	3:1	6:1	1:1	3:1	6:1
	0.	.88	.78	.72	85	64	61	24	13	14	N	N	Y
	.25	.87	.77	.69	51	60	53	0	0	16	-	-	Y
	.50	.78	.55	.44	150	150	150	0	0	26	-	-	Y
	.75	.52	.22	.03	150	150	150	0	0	26	-	-	Y

3 % Rate Escalation

$163/kWh Storage Cost Date: 7/19/79

Figure 2. PV/Storage Study Results, Phoenix, AZ

Sellback Ratio	TOD Ratio	Life Cycle Cost Ratio			PV Array Size (m^2)			Storage Size (kWh)			Off-Peak Charging?		
		1:1	3:1	6:1	1:1	3:1	6:1	1:1	3:1	6:1	1:1	3:1	6:1
	0.	>1.	1.0	.95	0	34	31	0	0	20	-	-	Y
	.25	>1.	1.0	.92	0	37	38	0	0	15	-	-	Y
	.50	>1.	.98	.90	0	47	51	0	0	15	-	-	Y
	.75	>1.	.83	.68	0	150	150	0	0	0	-	-	-

3 % Rate Escalation

$163/kWh Storage Cost Date: 8/15/79

Figure 3. PV/Storage Study Results, Columbia, MO

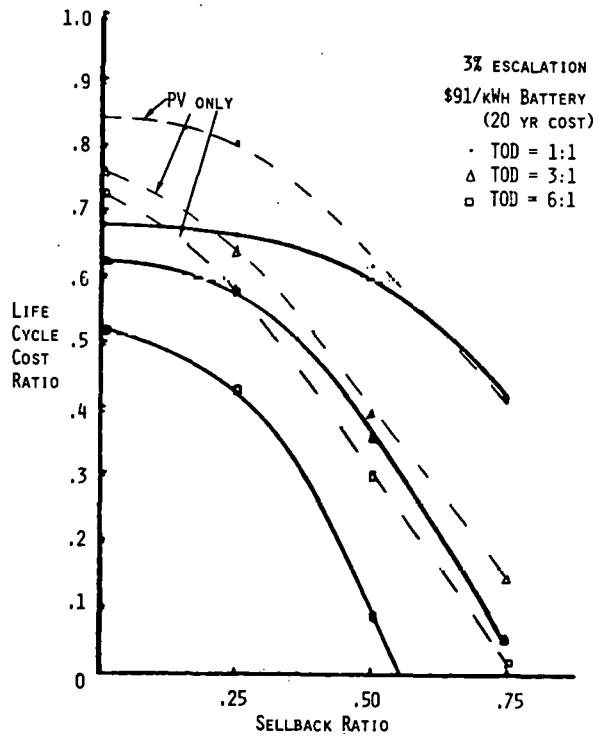

Figure 4. Optimum vs. PV-Only Systems, New York City

NOTES

ECONOMIC WORTH OF ON-SITE SOLAR ELECTRIC GENERATION IN A UTILITY GRID

Y. Gupta, R. Knowles, O. Merrill, and S. Young
Science Applications, Inc.
8400 Westpark Drive, McLean, VA 22102

ABSTRACT

Widespread utilization of solar electric technologies in parallel, or as supplements to the existing utility necessitate a detailed evaluation of their economic worth and utility impacts. Such an assessment must be performed within the context of the overall utility/solar electric system interaction, system design-cost relations, future electric energy costs, rate structures, and ownership options.

SAI has developed a methodology to evaluate in detail the utility impacts and economics of grid-connected solar electric technologies. The value of utility integrated solar plants consists of both electric generation costs and capacity costs to meet a specified reliability level and depends on a number of complex variables. The methodology and results presented here incorporate these complex variables through integration of diverse simulation techniques, including hourly solar electric system performance evaluation, probabilistic solar-subtracted load determination based on solar plant outage probabilities, mixed-integer linear programming formulation of the capacity expansion, and probabilistic determination of generation cost and loss of load probabilities.

INTRODUCTION

Solar electric power systems have the potential to supply power for industrial, commercial, institutional, and utility applications and to reduce consumption of non-renewable fossil fuels. However, widespread utilization of solar electric technologies in the United States will require that the solar systems be operated in parallel with, or as supplements to, the existing utility grid. For such systems, assumptions regarding future electric energy costs and rate structures have a major impact on solar system design and economics. Thus, in order to fully assess the economic worth of solar electric systems, it is necessary to evaluate their impacts on utility generation characteristics and to determine solar electric system design and cost relations within the context of the overall utility/solar electric energy supply system. Results of solar impact analysis are expected to assist in the development and manufacturing of appropriate solar energy systems as well as their commercial utilization by utilities, commercial/industrial and other user groups.

SAI has developed a methodology which evaluates the impacts and economics of grid-connected solar electric technologies within the overall utility context. Because solar energy varies both hourly and seasonally, reaching a peak level for only a few hours each year, solar generation is unique relative to conventional generation currently in use by most utilities. The value of solar plants integrated in a utility network is determined by both the electric generation costs and the capacity costs required to meet a specified reliability level, and depends on a number of variables—the mix and cost of conventional (non-solar) generation; the stochastic coincidence between solar generation and the electric system load; the amount of solar penetration; solar plant construction time and ownership; the energy storage capability of the solar system; and the solar system dispatch strategy. This paper summarizes the various techniques which have been developed and provides initial results for the worth of on-site photovoltaic, wind, and solar thermal electric technologies.

METHODOLOGY OVERVIEW

Grid-connected solar electric systems have an impact on utility characteristics by modifying the load to be supplied by conventional generation. This provides direct economic benefits to the utility in the form of reduced fuel and operation and maintenance costs. In addition, the resulting load may also provide capacity savings in the form of reduced installed capacity requirements, depending on the statistical reliability of the solar generation during peak load periods. The modified load will also affect the appropriate utility generating mix of base, intermediate, and peaking plants. Figure 1 illustrates these impacts and the interactions between solar electric power systems and the utility network.

The model developed by SAI provides a comprehensive analysis of the impacts of different solar electric technologies, and estimates the economic value of the solar plants to the utility, dispersed user, and third-party investor. The final output of the model is a set of estimates of the breakeven cost for solar electric technologies under different assumptions about ownership, payback period, and return on investment. The model calculates the economic benefits to dispersed users by assuming that the annual cost savings to the utility are passed on to the user via an appropriate rate structure. The precise nature of this rate structure is currently the subject of rather controversial legislation, and the formulation of this model does not require any specification beyond the

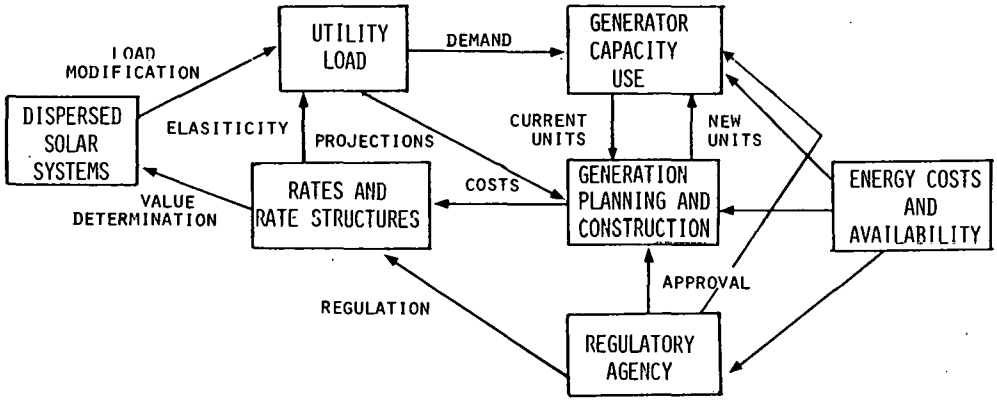

Fig. 1. Factors Affecting Solar Electric Power Systems Impact on Utility

assumption that any rate structure will spread the benefits fairly.

An overview of the model is shown in Fig. 2. The overall assessment methodology involves five separate model segments—hourly simulation of solar electric system performance; utility load projection and adjustment for the output of the solar plants; capacity expansion and mix adjustment for conventional utility generation; production costing for the resulting conventional utility mix; and finally economic analysis of the solar plant value under different ownership alternatives. Because of the extensive calculations that are involved, the models have been implemented with a modular structure so that analysis runs can be made independently of the others. The various model segments are described in what follows.

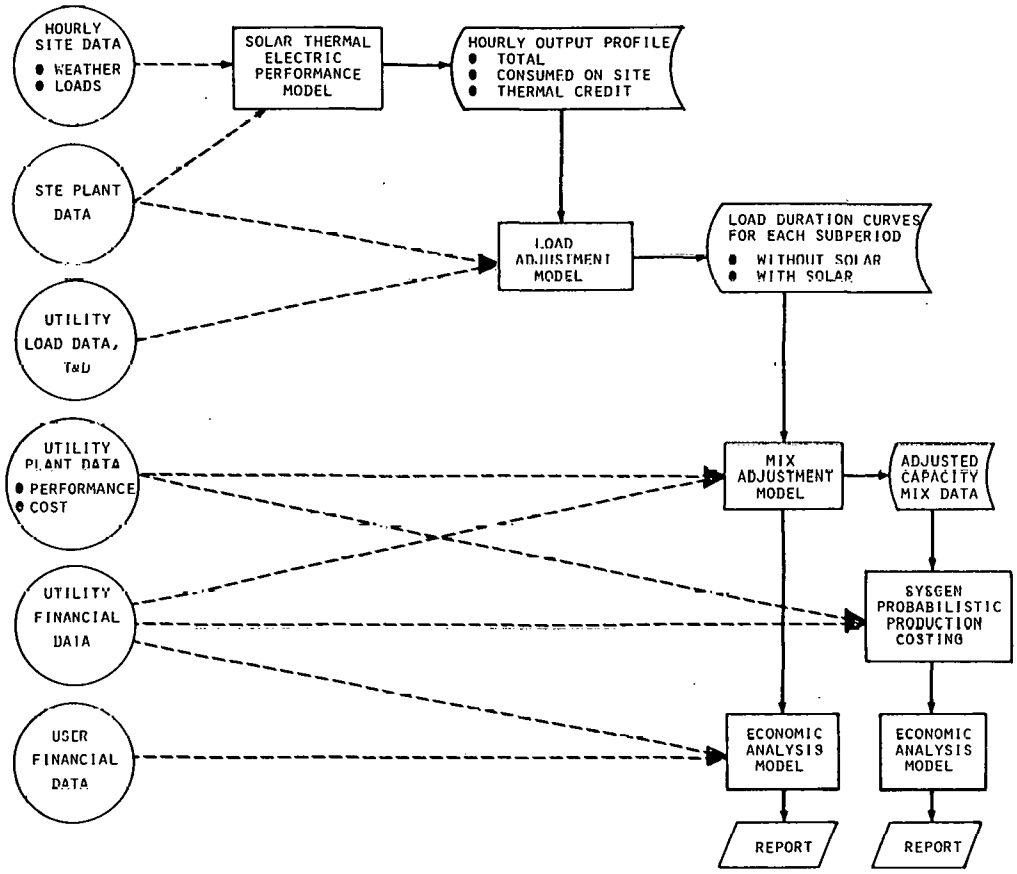

Fig. 2. Solar Electric Power Systems Impact Analysis Methodology

SOLAR ELECTRIC SYSTEM PERFORMANCE MODELS

The solar electric performance models simulate the hourly output of various solar technologies. Separate models are available for photovoltaic, solar thermal electric, and wind systems. Each model consists of subsystem component models which are used to compute steady-state efficiencies at each hour. As an example, Fig. 3 provides an overview of the simulation model for solar thermal electric power systems. At each hour the model computes steady-state energy balances, tracking losses, cosine losses, blocking and shading, reflectivity (or transmissivity), surface error losses, receiver intercept factors, receiver absorptivity, re-radiation and convection losses, thermal transport losses, storage or hybrid energy flows, and part-load turbine generator efficiencies.

Inputs for the various models comprise the following categories: hourly meteorological data on SOLMET tapes—beam and total horizontal radiation, sun position, temperature, wind speed; solar electric plant data—type, collector parameters, energy conversion parameters, storage/hybrid subsystem parameters, dispatch strategy; and hourly on-site electric demand profiles.

Outputs consist of the annual energy flows to/from various subsystems, overall plant performance summaries, thermal energy credits (where applicable) and hourly electric output files for total generation and energy consumed on-site. The model outputs can be used directly for systems analysis and design trade studies, or the hourly output files can be attached for input to subsequent analysis models.

LOAD ADJUSTMENT MODEL

The load adjustment model estimates the impact of the solar electric generation of the overall utility loads. The original load for the utility is first projected to the time span of interest, and then the outputs of the solar electric plants are subtracted on an hourly basis, taking into account the transmission and distributed benefits of on-site generation. Solar plant outputs are scaled by the number of units and capacities of the various solar systems, and then their hourly outputs are subtracted probabilistically in the sense that various combinations of solar plant outages are considered at each hour in accordance with the forced outage probabilities. The hourly results are then accumulated in the form of load duration curves for each month or season, as indicated in Fig. 4. These load duration curves are stored for both the original load projection (without solar) as well as for the solar-subtracted load. This provides a non-solar reference case which is carried along with the solar case throughout the remaining analysis, so that the differential impacts of the solar generation can be accurately measured.

MIX ADJUSTMENT MODEL

The mix adjustment model performs a capacity expansion analysis to determine the type and number of conventional generating units which should be added to the existing utility mix to meet projected electric demands at minimum total cost. This analysis is performed for both the solar case and the non-solar reference case. Inputs for the analysis include the existing utility system generating plants; the plants available for capacity expansion; characteristics of each plant type, including rated capacity, minimum operating levels, fuel type, heat rates, forced outage probabilities, maintenance requirements, fixed capital costs, and variable O&M costs; utility economic data, such as fuel costs, escalation rates, taxes, discount rate, insurance, etc.; and projected utility load data in the form of seasonal or monthly load duration curves both with and without solar.

Figure 5 presents a screening curve analysis which illustrates the considerations involved in performing the utility mix optimization. The upper curve shows annual costs for different plant types as a function of the number of hours per year which they are run; the lower curve represents the annual load duration curve. Capital-intensive plants such as nuclear or large coal have high fixed costs but low variable costs, so they are most appropriate when used as base-loaded plants that are run almost continuously. Combustion turbines, on the other hand, have low capital costs but high variable costs, so they are most appropriately used as peaking units which run only a few hours per year to meet the highest demand levels. By projecting the intersection points of the plant cost curves onto the load duration curve, as shown in the screening curve analysis of Fig. 5, it is possible to estimate the amount of capacity desired for each plant type.

The screening curve analysis does not account for the previously existing plant mix of the utility, the discrete sizes of the available plants, the minimum operating levels of the plants, the spinning reserve requirements to maintain available capacity for meeting sudden load increases, or the probabilistic forced outage characteristics of the various plants. SAI has formulated the basic capacity expansion problem as a mixed-integer linear programming problem which is solved using a standard linear programming package with branch and bound techniques for the integer variables. Figure 6 illustrates the discretization of the load duration curve into demand segments and the variable cost representation of each generator (which allows non-linear heat rates but assumes linear incremental heat rates). The variables for the linear program are the number of plants of each type to be installed, the number of plants of each type which are dispatched in each demand segment (if minimum operating levels are accounted for), and the operating level of each plant in each demand segment. The objective function of the linear program is to minimize the present worth of total fixed plus variable plant costs. Constraints for the problem include the following categories—

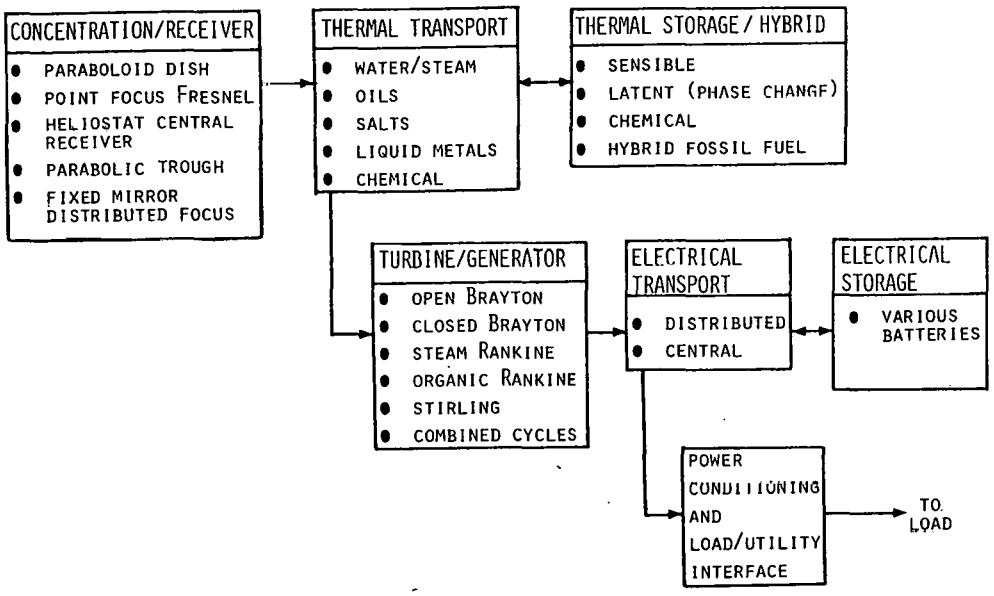

Fig. 3. Solar Thermal Electric Plant Performance Model

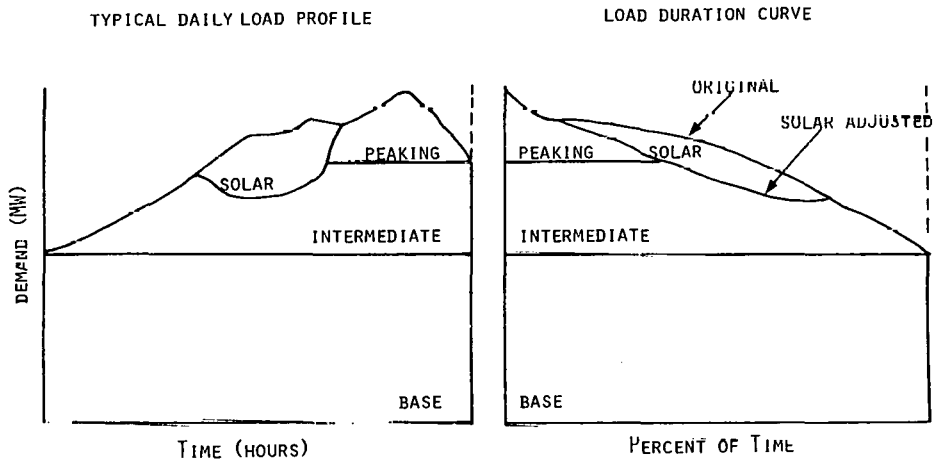

Fig. 4. Formulation of Utility Load Duration Curves

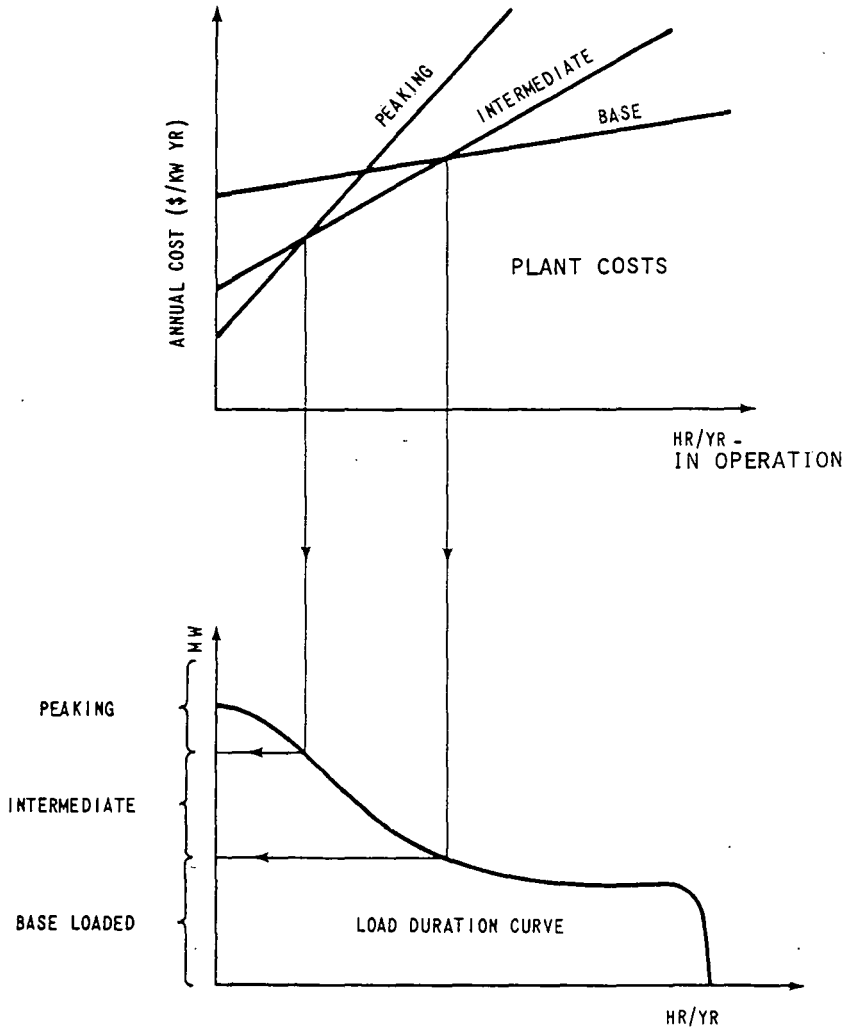

Fig. 5. Screening Curve Analysis for Mix Optimiation

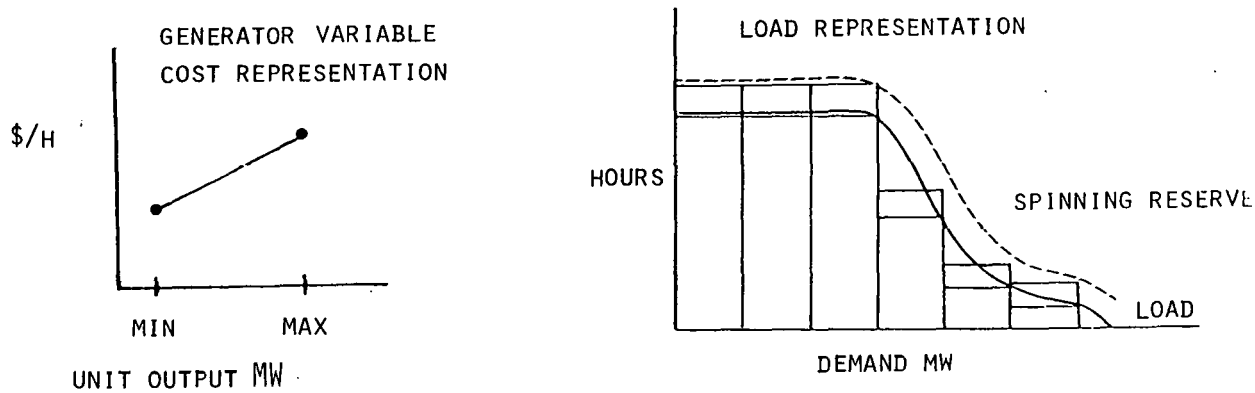

Fig. 6. Linear Programming Formulation

installed reserve margin, demand requirements, spinning reserve, plant capacity, plant availability and purchase constraints, plant energy limits (e.g., hydro), and integer variable constraints.

The solution of the linear program provides the basic capacity expansion plan; however, it assumes de-rated plant capacities without accounting explicitly for the probabilistic nature of plant forced outages. This is performed in a subsequent analysis step, which estimates loss of load probability (LOLP) using a Gram-Charlier series expansion technique to rapidly evaluate convolutions of the demand and plant outage random variables. Peaking capacity is then added or subtracted from the generation mix to meet the requiremed LOLP reliability criterion. Finally, a maintenance schedule is estimated by removing plants according to maintenance requirements so as to levelize the reserve margin, defined as the ratio of the total available plant capcity over peak demand, over all months. The final output of the mix adjustment model is the adjusted capacity mix (both with and without solar), the estimated annual production costs for each generator type and fuel type, and an estimate of the present worth of revenue requirements for the utility.

DETAILED UTILITY PRODUCTION COSTING MODEL

A detailed probabilistic production costing model, SYSGEN [1], can be used to provide a refined estimate of production costs based on the modified load duration curves and the optimized conventional capacity mix for both—the system with solar generation and the reference system with no solar generation. SYSGEN uses the standard Booth-Baleriaux algorithm to account for plant outages, in which the effective load duration curve seen by each generator is expressed as the original load duration curve plus the random outages of previous generators in the loading order. The successive load duration curves are computed using a recursive technique to perform the required convolutions, as described in Reference [1].

ECONOMIC ANALYSIS MODEL

The outputs of either the mix adjustment model and/or the detailed production cost model are then used to provide estimates of the breakeven costs of the solar plants for utility, on-site user, and third-party investor ownership alternatives. Additionally, the economic analysis can calculate the net present worth of the solar systems for various solar plant cost assumptions. The key assumption of the economic analysis is that the rate structure applied to solar system investors will reflect the difference in cost of electric service to this customer class, so that the overall savings provided by the solar plants are passed on to the investor.

CONCLUSIONS

The methodology described above provides a comprehensive and consistent analysis of the economic worth of different solar electric technologies operating in a utility network. This is an important consideration in determining solar electric system design and cost relations within the context of the overall utility/solar system interaction. Representative results of the modeling analysis will be presented at the conference for the worth of on-site photovoltaic, wind, and solar thermal electric technologies.

ACKNOWLEDGMENT

This work was partially supported by the U.S. Department of Energy under Contract #XP-9-8051-1 with SERI, and Contract #955238 with the Jet Propulsion Laboratory.

REFERENCE

[1] S. Finger, "SYSGEN Production Costing and Reliability Model User Documentation," MIT Energy Laboratory Technical Report, May, 1979.

ECONOMIES OF SCALE IN THE ACQUISTION OF SOLAR ENERGY

Charles L. Dick, Jr., PH.D.
Solar Thermal Systems Division
Exxon Enterprises, Inc.

Charles R. Grebenstein, PH.D.
Solar Thermal Systems Division
Exxon Enterprises, Inc.

ABSTRACT

The recent hypothesis that there are no economies of scale in the acquisition of solar energy is explored. A non-technical definition of the concept of economies of scale is offered as well as three examples of the use of this concept in real world situations. First, a study is cited which maintains that economies of scale existed and were exploited in U.S. electric power generation. Second, a study is cited which indicates economies of scale exist for sugarcane farmers where biomass conversion of sunlight is the solar energy process. Third, the optimal sizing of residential solar hot water systems is offered as an example of the use of scale concepts in solar thermal applications. The conclusions reached are that scale economies are important in policymaking, that scale economies do appear to exist in at least some solar energy applications and that further research in this area seems warranted.

INTRODUCTION

A hypothesis that has surfaced in the literature on alternative energy sources is that there are no economics of scale in the acquisition of solar energy [1]. The validity of this idea could have significant implications for government policy making and private sector investments. Conventional wisdom would dictate that if there are no economies of scale in the acquisition of solar energy, then large central receiver technologies which require large distribution infrastructures would seem to make little sense. Alternatively, dispersed solar technologies such as solar thermal hot water systems located on single family dwellings would seem to be the sensible choice. Logically, the existence of decreasing, constant or increasing returns to scale in the application of solar technologies should influence policy content, policy impact and investment decisions such that the technologies and applications with the most desirable economics, broadly speaking, are the ones that are promoted.

The purposes of this papér are threefold. First, to define, as clearly as possible in lay terms, the concept of economies of scale[1] and then to present three examples of the application of the concept to real world situations. Second, to examine the utility of using the results of economies of scale analysis to affect policy-making and to examine the validity of the hypothesis that there are no economies of scale in the acquisition of solar energy. Finally, to suggest areas for further research.

It is hoped that this discussion will prove useful to the various policy makers in the public sector where large sums of money will be spent to develop solar energy technologies, to economic researchers who can shed more light on the subject, and ultimately to the private sector decision makers who will allocate industry's limited financial resources.

For the purposes of this paper a broad definition of the "acquisition of solar energy" will be used. The term acquisition is assumed to mean single steps in a complete solar technology process (such as the growing of grain as part of the gasohol process) as well as the entire process (such as the collection of sunlight, conversion to steam and production of electricity by a "power tower"). The term solar energy is assumed to include such things as ocean thermal electric power generation technologies, wind power technologies, biomass technologies, etc., as well as the more traditional solar thermal and photovoltaic technologies.

[1] The terms "returns to scale" and "economies of scale" are interchangeable.

THE CONCEPT OF RETURNS TO SCALE

Economic returns to scale may be defined as the proportional amount of additional output resulting from some positive increment to the cost of production [2]. Equivalently, the concept may be expressed as the change in the cost per unit of output as more output is produced. Returns to scale are said to be increasing, constant or decreasing as the cost per unit of output decreases, remains the same or increases following an increase in output. A typical pattern of returns to scale is illustrated in figure 1.

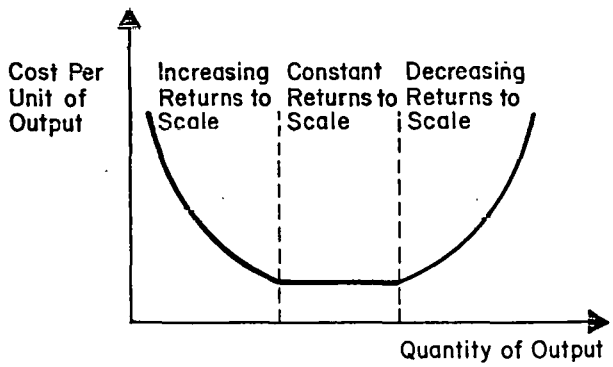

Varying Economic Returns to Scale

Figure 1

Defined in this general way, the concept can be applied in a range of situations. Individual plants, single- or multi-plant firms, single industries or industry groups may be examined. The envelope of analysis may be varied as appropriate in either a horizontal manner (e.g., across across several plants providing the same output) or a vertical manner (e.g., across different functions or steps that make up an entire process or product). It is important to remember however, that the conclusions reached about returns to scale may change as the envelope of analysis is redrawn.

EXAMPLES OF ECONOMIES OF SCALE

Presented below, for purposes of illustration, are three examples of the application of the concept of returns to scale to different real world situations.

The first example comes from the electric utility industry where considerable research has been done on returns to scale in electric power generation. Universal agreement among researchers on the nature of economies of scale in electric power generation does not exist. However, one well documented conclusion is that there were increasing economies of scale to be had during the pre-1970 decades, but that most opportunities to capture benefits from the increasing returns to scale had been exhausted by about 1970 due to growth in the size of utilities up until that time [3]. Post 1970, the returns to scale appear to be constant, and thus no benefit would accrue from further increasing the size of the generating units. This finding provides a partial explanation of the recent reversal in the historical trend of declining real prices for electricity. It is important to note, however, that the literature is considerably less robust in the analysis of returns to scale in the transmission and distribution of electric power and, perhaps most importantly, in the analysis of returns to scale for integrated electric power generation and delivery systems.

The second example is in the broad sense an application of the concept of economies of scale to a step in a solar energy technology (i.e., biomass conversion of sunlight). The government of Brazil in 1971 implemented a policy of merger, incorporation and relocation of sugar producing and refining operations. A desire for increases in efficiency through decreased costs of production among sugar producers was the motivation behind the policy. A successful outcome was based on the notion that there are in fact economies of scale to be achieved by increasing the nominal size of the sugarcane producing units. A study by Alcantara and Prato [4] of returns to scale among sugarcane producers near Sao Paulo concluded that a situation similar to the hypothetical situation illustrated in figure 1 existed for the firms they sampled. That is,

---

[2] Another common approach is to define economies of scale in terms of the proportional amount of output resulting from a uniform increment to all quantities of inputs rather than just to cost as was chosen in this case. See Giora Hanoch [2] for a technical comparison of the two approaches. Note that additional conditions of both definitions are that inputs be used as efficiently as possible and the price structure for inputs does not change over the range of input data considered.

increasing returns to scale are believed to exist for farms up to a specific size[3] measured in tons of harvested sugarcane, and that decreasing returns to scale occur beyond that size. Their conclusion was that an elightened policy for the Brazilian government to pursue would be to encourage the growth in the size of sugarcane farms up to the size where increasing returns to scale stopped accruing.

A final example of the concept of returns to scale is drawn directly from a solar thermal domestic hot water application where there is a conventional fuel auxilliary system. In this example, the analysis of proper "solar system sizing" can also be seen as a question of returns to scale. The curve in figure 2 demonstrates the relationship between the average annual per unit cost of meeting a domestic hot water load ($/MBtu/gallon of water) and the proportion of thermal energy provided from conventional versus solar sources (a so-called "percent solar fraction"). In any application it may be possible to meet most or even all of the hot water load with solar energy. However, in order to increase the percent solar fraction, additional solar energy collection and storage equipment must be introduced, that is, the scale (size) of the solar system must be increased at an increase in capital investment. For the relationship described in figure 2, returns to scale of the solar system are not constant, rather they increase, reach a maximum and decrease for an increasing percent solar fraction or equivalently for increasing sizes of the system. That phenomenon occurs principally because at a very low percentage solar contribution, the increase in capital investment for an increase in system size is more than offset by the decrease in conventional fuel costs. However, the relationship between energy output for the solar system, the system size and the required capital investment is nonlinear. A point in size is eventually reached where further increases in system size and capital investment to achieve more energy output, and thus a greater solar contribution, is no longer offset by decreasing conventional fuel costs. This means decreasing returns to scale have set in.

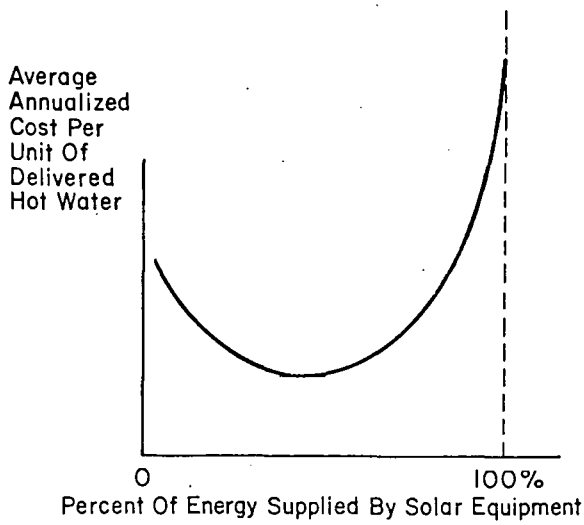

Figure 2

Returns To Scale For Domestic Hot Water Application

IMPLICATIONS FOR SOLAR ENERGY POLICIES

To summarize, a claim has been made that there are no economies of scale in the acquisition of solar energy and furthermore because of this, that policies influencing the development of solar technologies should discriminate against large central systems while favoring small dispersed ones [1]. The appropriateness or applicability these two proposals may now be examined, drawing on the discussions in foregoing sections.

Taking the latter of these two proposals first, that the absence or presence of economies of scale can support and/or help direct policies, evidence of the truth of this exists. The fact that there no longer appear to be increasing returns to scale in the generation of electric power speaks against any policy that would promote the development of electrical generating units that are larger in size than current industry practice. In the sugarcane example analysis of the economies of scale directly supports the premises of the implemented policy, that increasing the size of the farming units should lead to a decrease in the cost of production. Apparently, however, Brazilian government's incentives did not discriminate by the size of the existing farming unit. While the analysis

[3] That point was reached at an annual production of 161,000 tons of harvested sugarcane.

by Alcantara and Prato indicated that the policy would only be effective up to a certain size and that above that size, increases in the cost of production would be the likely result. This, then, is also an example of an opportunity for policy adjustment in light of the results of an economies of scale analysis. Finally, the current purchasing behavior of solar domestic hot water customers support the notion that there is nominally a "best" target percentage solar contribution design figure. In the New England area, the majority of solar domestic hot water installations are sized[4] to achieve between 35-45% solar contribution.

Examination of data related to the first premise, that there are no economies of scale in the acquisition of solar energy, has uncovered two exceptions and it is strongly suspected that additional exceptions can be found. In particular, the claim has been made [1] that since sunlight falls everywhere[5] and one corn plant is efficient as the next one, that a large assemblage of such plants is no more efficient than a small one (except for minor savings in maintenance costs) Hence, there is no economy of scale in this case, and, further, this is true for all applications of solar energy. Clearly, Alcantara and Prato's findings challenge that viewpoint. Also, as was just discussed, there are economies of scale to be considered in the design of solar domestic hot water systems. In light of this evidence, it would seem that there is sufficient justification to warrant suspicion of the premise that, a priori, there are no economies of scale in the acquisition of solar energy. Because of this, the pursuit of broad based programs and/or policies for the redesign of national energy systems, based on this premise appears to be premature. Furthermore, the lack of available economies of scale analyses, theoretical or empirical, particularly regarding entire systems of energy production, suggests that a rich opportunity for important research lies untapped.

[4] As evidenced, for example, by the results of the Long Island Lighting Company's domestic hot water program involving the installation of several hundred systems.

[5] Seemingly implicit in this statement is the notion that sunlight falls evenly everywhere which is approximately true for local regions but, of course, is not generally true.

CONCLUSIONS

Based on the foregoing discussion, three conclusions can be drawn.

First, economies of scale analysis is potentially a useful tool to help support or direct policymaking as it applied to the acquisition of solar energy. This holds true, however, if and only if the concept is applied in a manner appropriate to the issue being addressed.

Second, it is not possible to state at this time whether or not variable economies of scale exist for the acquisition of **all solar** energy technologies, although there seems to be evidence that they do exist in at least some applications.

Third, there are fruitful opportunities for research into the following areas: scale returns for individual solar technologies; scale returns for entire conventional energy systems; and scale returns for integrated solar and conventional energy systems.

REFERENCES

[1]. Commoner, Barry, The Politices of Energy New York, A.A. Knopf, 1979, pp 44, 54, 55.

[2]. Hanoch, Giora, The elasticity of scale and the shape of average costs. Am. Econ. Rev. 65(3): 492-497, June 1975.

[3]. Christensen, Laurits R., and William H. Greene. Economies of scale in U..S. electric power generation. J. Pol. Econ. 84(4): 655-676, August.1976.

[4]. Alcantara, Reinaldo, and Anthony A. Prato. Returns to scale and input elasticities for sugarcane: The case for Sao Paulo, Brazil. Am. J. Agri. Econ. 55(4): 577-583, November 1973.

THE THERMAL IMPLICATIONS OF THE CITY OF SEATTLE ENERGY CODE

A.F. Emery, C.J. Kippenhan, D.R. Heerwagen

University of Washington
Seattle, Washington 98195

ABSTRACT

Thermal analyses of single wall sections and of a simple room have been made with a large scale simulation code to determine under what conditions the special passive solar provisions in the recent City of Seattle, Washington building code reflect what would be observed for structures exposed to typical coastal and semi-arid weather patterns. The results suggest that the reduction in U values permitted for heavy wall sections are somewhat optimistic and that the daily temperatures changes estimated to occur in thermal masses located within the building envelope are overly generous for external walls and for internal frame walls and too small for internal concrete walls. The effects of external insolation on reducing effective winter U values is shown to be substantial and suggest that some provision be made to accommodate this in the code.

INTRODUCTION

The City of Seattle has recently adopted a building code [1] which applies to new and rehabilitated structures. The code is based upon ASHRAE 90-75, [2], but includes special provisions for passive designs. Structures are to have both specific section U values and overall U values which are less than those specified and to meet maximum OTTV values as dictated by ASHRAE 90-75. In computing the U value based upon an equation of the form

$$U = \frac{M A_i U_i + A_f U_f}{A_i + A_f} \qquad (1)$$

where A_i refers to a wall section i and A_f to the glazing portion we find that M is specified as a factor which ranges from 0.9 to 1.0 depending upon the weight of the section and A_f represents the uncompensated fenestration area. The M values are listed below in Table 1. Heavy sections, with their apparent storage of energy, are given as much as a 10% reduction in U value to account for a delayed release or absorption of energy. For every 7.9×10^5 j/day (750 BTU/day) of thermal storage which is contained within the insulated shell of the structure, one may reduce the fenestration area A_f by .09 square meters (1 square foot), whether this thermal storage is illuminated by sunlight or not. In computing the thermal storage, we use the equation

$$S = (W M \cdot SH) \cdot \Delta T \qquad (2)$$

where WM · SH represents the total thermal capacity of a square foot of a wall and ΔT represents an average daily temperature variation. The code specified ΔT to be 2.8°C/day (5°F/day) for heavy sections and 5.6°C/day (10°F/day) for light sections although the definition of heavy and light section is somewhat ambiguous.

Table 1

M Values

section weight		M
0-122 kg/m^2	0-25 lb/ft^2	1.00
122-195	26-40	0.96
195-342	41-70	0.93
342 and above	71 and above	0.90

Although the language of the code is very similar to the City of Davis, California code [3], the area of typical wall sections required to meet the code requirement are about 27% larger than those specified by Davis, being equivalent to 10^6 j/day (950 BTU/day). In calculating the thermal capacity of a square foot, the depth of the wall is taken to be that depth at which a resistance of R= 0.18 m^2-°C/W(1 BTU/ft^2-hr-°F) is reached, although it is not clear whether the surface resistance is to be considered.

In examining these two aspects of the code, we asked ourselves the following questions: How realistic are the M values and do they depend upon the placement of the insulation or upon the weather; are M values different for summer and winter periods; are the temperature changes of 5 and 10°F per day realistic; does radiation between the various surfaces affect any of these results? Accordingly we devised a series of numerical simulations to test the conclusions of the code. Since Northwest

buildings are primarily designed for heating loads, only the winter simulation results are presented here.

RESULTS

The Single Wall

Using standard finite element techniques, a single wall composed of insulation [k = .073 w/m-°C (0.042 BTU/hr-ft-°F), c = 795. j/kg-°C (0.19 BTU/lbm-°F), ρ = 192 kg/m^3 (12.0 lbm-ft^3)] and medium weight concrete [k = .52 w/m-°C (0.3 BTU-m-ft-°F), c = 920 j/kg-°C (0.22 BTU-lbm-°F), ρ = 1600 kg/m^3 (100 lbm/ft^3)] was constructed of such material thicknesses that its section weight varied from 60 to 500 kg/m^2 (12 to 102 lb/ft^2). One series of simulations was made with a constant insulation thickness and varying concrete thicknesses such that both WM and U varied and another series with the thicknesses adjusted to maintain a constant U value. The simulations were made for both summer and winter periods with three different weather data: 1) a weather profile which repeated every day and for which the temperature and insolation varied sinusoidally during the day; 2) weather data which is typical of the northwest coastal region (specifically Seattle) with mild temperatures and frequent overcast skies; 3) weather which is typical of Eastern Washington, which has hot clear summer and cold clear winter days. Both the Seattle and the Eastern Washington weather tapes were obtained by selecting appropriate days from NOAA weather tapes. The simulations were made by first calculating for a 3 day period to allow the temperature profile to become independent of the initial conditions and then simulating an additional 5 days. For all cases, the sinusoidal weather results gave values of M which were unity, indicating that over a day's time, storage played no part since the effect is simply one of a phase shift in the temperature profiles. The results of the two measured winter weather profiles are shown in Tables 2 and 3 for several winter days. Calculations were done both with and without set back, to simulate the two most common building use strategies and to investigate the effect of a substantial heat release to and acceptance from the building interior. The effective U is defined by calculating the hourly U values and averaging according to

$$U_{eff} = \sum_{120 \text{ hours}} \frac{Q \text{ lost from the room}}{T_{room} - T_{outside}} \qquad (3)$$

The winter results indicate that the placement of the insulation has an effect upon the M value, with inside insulation indicating that the effective U value may be higher than the steady state value and with outside insulation showing a reduced M value, but with a nonlinear trend. When no night setback is used the trend of the results tends to be the same for either location of the insulation. However, the use of setback suggests that outside placement of the insulation is to be preferred especially when solar irradiation is considered. It should be stressed that while these 5 day averages are typical of the winter weather, substantial differences are to be expected on a day by day comparison. In general, when the weather is reasonably mild and the daily variation small, as in the coastal weather, the effect is to give a value of M, based upon U_{eff} for no mass, equal to or larger than 1 except for the night setback case. On the other hand, when the weather is severe, as in the semi-arid weather, M appears to be always less than 1. From a prescriptive code point of view, those results suggest that no effect of section weight be considered because of its strong dependence upon climatic variables and operating schedules. The tables also indicate the effective temperature change of the walls, and in none of the cases, do we see anything near the 2.8°C(5°F) permitted by the code. The temperature change was determined by the equations

$$\Delta Q \text{ (due to mass)} = Q - Q \text{ (no mass) over a 24 hour period}$$

$$\Delta T = \Delta Q \text{ (due to mass)}/WM \cdot SH \qquad (4)$$

applied over the 5 day period. The effective daily temperature variation did not appear to be affected by setback or by the absorption of solar radiation. Of greater effect is the solar energy absorbed at the outer surface of the wall which tends to reduce the average heat loss, in the amount of 30 to 45%. Obviously, for summer days it will increase the heat gain (increasing U by as much as a factor of 6). However it would appear prudent to permit dwellings whose surfaces can be protected by shading in the summer to gain credit for winter insolation by permitting a reduced value of U to be used.

The Room

When a room is composed of a number of surfaces which can exchange heat radiantly, one might expect substantially different results. The simulation program, UWENSOL [4], was used to model a space composed of the following surfaces

Table 4
Composition of the Room

Wall	Description	
1	interior concrete slab floor	(500 kg/m^2 or 60 kg/m^2)
2	interior concrete slab ceiling	(60 kg/m^2 or 500 kg/m^2)
3	double glazed wall	
4	exterior concrete wall	(U = .93 w/m^2-°C, 60 or 500 kg/m^2, concrete & insulation)
5	exterior frame wall	(U = .93 w/m^2-°C, gypsum, framing, insulation, sheathing)
6	interior frame partition	(gypsum both sides)

Table 2

Ratio of U_{eff} to $U_{eff(mass = 0)}$ for Single Wall Sections

Pacific Northwest Coastal Weather

5 Day Winter Average

Section Weight (kg/m^2)	Inside Insulation		Outside Insulation		ΔT^*	
	without setback	with setback	without setback	with setback		
500	1.082	1.042	1.085	.888	.21	No Insolation
350	1.062	1.036	1.068	.890	.21	
250	1.043	1.021	1.049	.866	.26	$\frac{U_{eff(mass=0)}}{U_{steady\ state}} = 1.00$
150	1.021	1.003	1.027	.857	.23	
60	1.004	.991	1.006	.911	.16	
500	1.179	.996	1.186	.746	.21	Insolation
350	1.141	.985	1.153	.747	.21	
250	1.098	.969	1.113	.722	.25	$\frac{U_{eff(mass=0)}}{U_{steady\ state}} = .615$
150	1.036	.972	1.057	.722	.23	
60	1.002	.981	1.006	.847	.16	

* ΔT = effective daily change in the average temperature of the wall with setback

---

Table 3

Ratio of U_{eff} to $U_{eff(mass = 0)}$ for Single Wall Sections

Pacific Northwest Semi Arid Weather

5 Day Winter Average

Section Weight (kg/m^2)	Inside Insulation		Outside Insulation		ΔT^*	
	without setback	with setback	without setback	with setback		
500	.963	.949	.958	.913	.37°F	No Insolation
350	.981	.973	.978	.936	.25	
250	.988	.983	.986	.946	.24	$\frac{U_{eff(mass=0)}}{U_{steady\ state}} = 1.00$
150	.994	.991	.993	.957	.18	
60	.999	.998	.998	.984	.10	
500	.965	.925	.959	.884	.36	Insolation
350	.986	.955	.982	.909	.25	
250	.994	.970	.991	.925	.24	$\frac{U_{eff(mass=0)}}{U_{steady\ state}} = .822$
150	.999	.987	.998	.944	.18	
60	1.000	.997	1.000	.981	.10	

In performing the simulation, the glazing was south facing, the exterior surface solar absorptivities were set to unity, and the solar energy transmitted by the glazing fell only on the floor. The floor was taken as 60 or 500 kg/m^2 to investigate the effect of mass and radiation interaction and the ceiling was 500 or 60 kg/m^2, respectively for the same reason. The surfaces were either permitted or not permitted to radiate to each other. Tables 5 through 8 summarize the results. The effective U values were defined in terms of the amount of energy needed to maintain the room at a temperature of 18.3°C (65°F) from 7 a.m. to 9 p.m. with a set-back to 12.9°C (55°F). The effect of surface radiation to the glazing, with the associated energy loss through the glass is clearly indicated by the substantial increase in U_{eff} for an emissivity of 0.97 as compared to the results for zero radiation. The heavy external wall has a marginal effect since the values of U_{eff} are reduced by about 9% regardless of whether a heavy or light concrete wall absorbs the incoming solar radiation.

Table 5

Overall $U_{eff}/U_{steady\ state}$ for the Room

Pacific Northwest Coastal Weather

Surface Emissivity	Section Weight of Illuminated Concrete Floor	Section Weight of External Wall 60 kg/m^2	500 kg/m^2
.97	60 kg/m^2	.61	.56
	500	.56	.53
0	60	.41	.38
	500	.31	.33

Table 6

Daily Temperature Change of Internal Frame Wall

Pacific Northwest Coastal Weather

Surface Emiccivity	Section Weight of Illuminated Concrete Floor	Section Weight of External Wall 60 kg/m^2	500 kg/m^2
.97	60	3.3°C	3.0
	500	2.5	3.0
0 (all cases)		2.2 °C	

Table 7

Daily Temperature Change of Internal Concrete Wall

Pacific Northwest Coastal Weather

Surface Emissivity	Section Weight of Illuminated Concrete Floor	Section Weight of External Wall 60 kg/m^2		500 kg/m^2	
		Section Weight of Internal Concrete Walls			
		60	500	60	500
.97	60 kg/m^3	22.9°C	1.1	19.8	0.4
	500	7.9	4.6	5.5	3.3
0	60	28.9	0.4	28.9	0.4
	500	4.4	3.9	4.4	3.9 °C

Table 8

$U_{eff}/U_{steady\ state}$ for the External Wall in the Room

Pacific Northwest Coastal Weather

Surface Emissivity	Section Weight of Illuminated Concrete Floor	Section Weight of External Wall	
		60 kg/m^3	500
.97	60 kg/m^2	.95	.88
	500	.94	.84
0 (all cases)		.87	

Tables 6 and 7 list the daily temperature changes of the internal walls determined by solving equation (2) for ΔT. The lightweight frame wall shows a ΔT of about 2.8°C (5°F) as compared to the code permitted value of 5.6 °C (10°F). The effect of radiation and which concrete wall is illuminated is apparent. When the sun falls on the lightweight floor, its surface temperature rises substantially, and the consequent increase in radiation has a decided effect upon the internal frame wall storage. However, when the external concrete wall is heavy, its constancy of temperature acts as a damper and reduces the effect on the frame wall. Table 7 suggests that internal concrete surfaces which are directly illuminated should be credited with a ΔT close to 5.6°C (10°F) rather than the 2.8°C (5°F) permitted by the code if a heavy section is illuminated whereas 2.8°C (5°F) appears to be a good average ΔT for both heavy and light walls if light sections are illuminated. Finally table 8 indicates that the effective U value for the external wall appears to be related to its mass in about the same way that a single wall (table 2) is, and that internal radiation is not a critical factor. Similar results were found for simulations performed using the semi-arid weather profiles.

CONCLUSIONS

Simulations made with typical coastal weather and inland semi-arid weather profiles suggest that no credit for section weight should be given in computing U-values. No passive energy storage allowance for external walls should be given, while the computations of stored energy for light internal walls should be based upon a ΔT of 2.8°C (5°F) and for internal concrete walls should be based on 5.6°C (10°F) if a heavy concrete wall absorbs the solar radiation and 2.8°C (5°F) for absorption by a light concrete wall.

In general the simulations suggest that the code overestimates the storage effect in external walls and underestimates the effect for internal walls when the space temperature is held at fixed values.

1. Ordinance 108500, Seattle Code for Energy Conservation, Seattle, Washington, August, 1979.
2. Ordinance 784, Energy Conservation Performance Standards for Residential Construction, Davis, California, October, 1975.
3. Energy Conservation in New Building Design, ASHRAE Standard 90-75, New York, 1975.
4. The Incorporation of Energy Conservation Principles into the Design of State Buildings, Vol II, UWENSOL Users Manual, The Built Environment Study Teaching and Research Group, IES, Univ. of Washington, Seattle, Washington, August, 1979.

Session VA

Dr. James Baughn
University of California - Davis
Chairperson

SYSTEMS SIMULATION III

SIMULATION AND DESIGN METHODS FOR A SOLAR CENTRAL RECEIVER HYBRID POWER SYSTEM

Michael D. Walzel
University of Houston, Energy Laboratory
Houston, Texas 77004

ABSTRACT

The simulation and design of the solar collector portion of advanced sodium cooled central receiver power systems has been carried out at the University of Houston. The application is in the area of electric power generation utilizing solar thermal technology and using coal as an alternate energy source when the solar component is down. The analysis of the solar part of the system, which was analyzed separately from the coal fired system, will be presented.

Simulation methods include modeling of the sun, the action of the heliostats, and calculating the resulting flux profile on the receiver. The component cost and loss functions are involved in the design phase. This includes finding the optimum distribution of heliostats and the boundary of the collector field for a specific tower height and receiver size. This information and a figure of merit are output for several tower heights and receiver sizes. The optimum power plant size and configuration for a design point can then be selected.

INTRODUCTION

Electric power generation via a solar-coal hybrid plant has been proposed to provide either base load or intermediate load electricity for utility companies. The analysis of the solar tower part of the system was done separately, apart from the design of the coal fired system. Therefore, the two are somewhat independent as far as design, optimization, and simulation are concerned. Of course, they must be properly sized and paired, and for this purpose a solar baseline design was established. Both the coal and solar thermal energy goes into heating sodium, which then is piped to a steam generator. The steam is then sent to the turbine to produce electricity.

Two different solar power systems to be paired with the 100 MWe coal plant are considered. One has a solar multiple of .8 and has essentially no storage, while the other system has three hours of storage with a solar multiple (SM) of 1.4. We require 260 MWt to produce 100 MWe. The cycle efficiency is 43.5% which results in 113.1 MWe. This extra electric power is needed for parasitic losses such as operation of the heliostats and the plant facilities. The solar multiple is a ratio of receiver thermal power output to turbine inlet demand. Since the turbine requires 260 MWt, the 1.4 SM system will need to output 364 MWt. The .8 SM system is sized to output 229 MWt. This is because the field-receiver power ratio (FRPR) is 1.1. When the insolation is such that more than 208 MWt is achieved, the extra power is dumped.

Methods used to get answers from the optimization code are described below. The data needed and the procedures involved to produce an optical simulation are also discussed. This includes shading and blocking, and image formation. Data is retained on disc files which allow receiver interception factors to be determined for heliostats in the collector field. Component cost and losses are parameterized for the receiver, heliostats, and other hardware. The optimization finds the best distribution of heliostats and the boundary of the collector field. This is necessary because most of the cost of the solar portion of the plant is tied up in the heliostats. Therefore, one must find optimum heliostat spacings if the cost of the system per unit of energy delivered is to be truly minimized. For each combination of tower and receiver, a collector field is produced which provides the best way for the heliostats to be positioned.

A figure of merit is output for each tower-receiver-field combination and is then plotted versus the delivered thermal power at noon on autumnal equinox for an assumed insolation of 950 W/m^2. This plot reveals the optimum power plant size and configuration for a specific design point power requirement for the specified day, time and insolation. The figure of merit is the initial capital cost of the system divided by the thermal energy delivered over the course of one year ($/MWH/year). Such information allows designers to choose the cost effective system and still satisfy design constraints such as thermal power delivered, and peak flux on the receiver.

SYSTEM DEFINITION

In this section the system that is to be simulated and designed will be described. The technical approach that has been utilized is to establish a baseline concept. Revisions are made based upon these studies with the result that a cost effective system is obtained. Before the trade studies that affect the solar portion of the plant are discussed, a plant description needs to be given. This is based upon trade studies that were not performed by the University of Houston, but which affect our design goals and constraints [1]. In addition, the understanding of the various components of the plant and their function is enhanced by examining the trades and choices that were made.

For both the .8 and 1.4 SM plants, the alternative energy source was chosen to be coal rather than oil. Sodium and draw salt were considered for use as the heat transport fluid, and sodium was selected. Series versus parallel heaters were studied, and both plants will has parallel heaters. The receiver will be an external cylindrical receiver and the size is to be optimized. The number of panels which make up the cylinder is 18 for the .8 SM plant and 24 for the 1.4 SM plant. However, there will be only one valve per panel where flow control, thermal loss, and reliability were studied. Temperature leveling and thermal loss in the panels were considered and the determination was made that the sodium should pass through the receiver but once to be heated.

The 1.4 SM plant will have 300 MWeH sotrage. The hot sodium is the storage medium. The .8 SM plant will have 4.2 MWeH storage, and it will be located at the top of the tower rather than at ground level. The superheated steam will be at 538°C (1000°F). The hot sodium as it enters the steam generators is at 593°C (1100°F). The .8 SM plant will have the coal fired heater supplying at least 20% of the thermal power at all times. In the case of the 1.4 SM plant there are times when the coal heater can be shut down entirely. The heater stack is located inside the tower, and goes out through the top of the receiver. The receiver, since the heat transport fluid is sodium, can tolerate a peak flux of 1.5 MW/m^2.

The main thrust of the simulation and optimization work performed at the University of Houston is to optimize the collector field geometry, and correlate field and receiver optimums to deliver the required thermal power on the design point day with the lowest cost/benefit ratio, i.e., figure of merit. In addition to choosing the cylindrical receiver size, the tower height must also be selected. Studies were also done to determine if heliostat aiming strategies would be cost effective in trying not to exceed the receiver peak flux limit.

SIMULATION AND DESIGN METHODS

Simulation

Optical Simulation. Several phenomena must be simulated in order to give a good account of the performance delivered by a central receiver system. The sun's location must be known and the direct beam insolation must be calculated for the particular day and time in question. Next, the action of a large number of heliostats must be simulated as they reflect sunlight to the receiver at the top of the tower. The resulting incident flux on the receiver must be modeled to determine the amount of energy absorbed into the working fluid to generate the desired amount of electricity.

The solar positions and intensities used to simulate a central receiver can be obtained from a model in the code, or they can be read in as data from other sources. The times (or positions) and intensities are important because they are involved in the annual simulation of the system in which the energy of the system is integrated over one year.

The heliostats form images or solar flux densities which must be calculated in order to properly model the system [2,3,4]. These images determine how the flux is distributed on the receiver, as well as how much spillage occurs. In the course of reflecting sunlight to the receiver, the heliostats interfere with neighboring heliostats. This is called shading and blocking and occurs when the shadow of one heliostat is cast across a portion of a neighboring heliostat's reflective surface, or when part of the reflected sunlight from a heliostat strikes the back of a neighboring heliostat before it can reach the receiver.

A year's worth of shading and blocking data is kept on disc file for use with out optimization code. The collector field is divided into several cells or areas with a representative heliostat in each cell, and a variation of sixteen different neighborhoods describing heliostat spacings is included within each cell. A file is also stored containing information about the sun's positions and intensities. A nodal interception file is retained to supply the percentage amount of flux intercepted by each node or elemental area on the receiver for each of the representative heliostats in the collector field. All this data is needed in order to set up computer runs which will allow the optical simulation and performance calculations necessary to properly size and optimize the system.

Losses. There are several losses that must be accounted for before the energy in the direct normal insolation reaches the turbine to produce electricity. First, there are cosine losses due to the foreshortening of the heliostat whose reflective surface normal must bisect the angle between the sun and the receiver. Then there is loss due to the fact that only a percentage of the energy is reflected by the heliostat. Next, there is the action of shading and blocking as mentioned before. The reflected beam which travels from the heliostat to the receiver is attenuated to some extent by the air and particles within it. Then, only a portion of the receiver incident flux is absorbed into the metal. Finally, the receiver will have radiative and convective losses due to

its high temperature and exposure to the atmosphere. All of the aforementioned losses must be simulated in order to calculate the performance of the solar central receiver.

Costs. The cost of all the components needed to supply thermal energy to the steam generators needs to be modeled so that a cost effective system can be designed. Only the initial installed capital costs of the equipment needed for the solar portion of the system is required. The steam generators and turbine (electric power generating system or EPGS) are assumed to be needed by the coal system as well, so they are not considered. Neither is the cost of the thermal storage, since it was sized before the optimization of the collector field. Such costs as operation and maintenance costs can be included if desired. However, the costs usually included are those concerned with the heliostats, land, wiring, receiver, tower, and piping runs. The cost functions describing them depend primarily on component sensitivity to size and/or power level of the system.

Design

The 1.4 SM Plant. The design point constraint for the 1.4 SM plant requires that its receiver deliver 364 MWt at noon on autumnal equinox for an assumed insolation of 950 W/m^2. The optimization code accepts a specific tower height and receiver size as input and outputs the number of heliostats and the best way to distribute them in the collector field. After an initial run, variations in tower height and receiver size can be made to get closer to the design point power [5,6,7].

A time integral over one year is done to produce the optimized collector field and the annual thermal energy produced. This annual energy is divided into the initial capital cost of the system to give a figure of merit ($/MWH/year). This figure of merit allows different solar energy collection configurations to be compared on a cost/performance basis.

Referring to Figure 1, each one of the seven curves represents a different receiver and input figure of merit (FMI) combination for a tower height of 150 meters (492 feet). Our code uses an iterative approach in that the best cost/performance ratio occurs when the input figure of merit is equal to the output figure of merit. The output figure of merit is on the ordinate, while the equinox noon power is the parameter on the abscissa. A curve is created by varying the outer boundary (and thus the power level) while maintaining the same heliostat spacings. A different FMI for the same tower-receiver combination results in a different heliostat field density, i.e., a higher FMI results in a higher field density. The optimum outer boundary for the particular field density -tower-receiver combination is therefore at the minimum of the curve.

However, the minimum of a curve may not give the desired power, or if it does, it may not be the lowest figure of merit obtainable by going to another receiver size, tower height, or FMI. Since we need

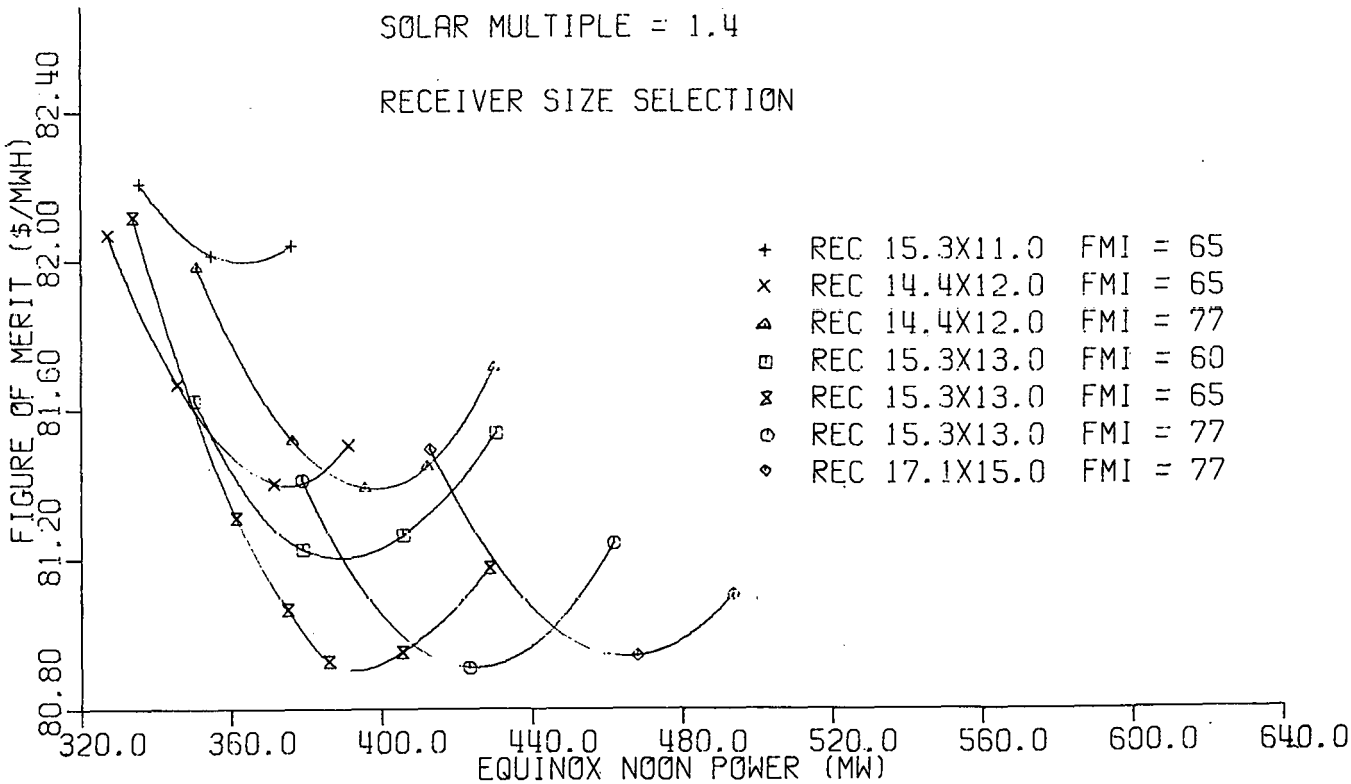

Fig. 1 Power Versus Figure of Merit for the 1.4 SM System

364 MWt for the 1.4 SM plant, it is easy to pick off which of the seven curves that has the lowest figure of merit while satisfying this constraint. It is the cylindrical receiver of height 15.3m (50.2 feet) and 13.0m (42.7 feet) diameter with FMI = 65.

If one were to draw one curve beneath these seven curves such that it was an envelope of minima, it would represent fairly well the lowest figure of merit obtainable for a 150m tower for various receivers and FMI. However, note that the minimum for all curves is fairly broad. The percentage difference between divisions on the ordinate is about one half percent, and the cost and loss may not be accurate.

The .8 SM Plant. A design effort similar to that of the 1.4 SM plant was undertaken for the .8 SM plant. Referring to Figure 2, we see the best receiver to supply 229 MWt is the 12.0m (39.4 feet) by 10.4m (34.1 feet) receiver (height and diameter, respectively). All four of these curves are for a tower of height 120m (394 feet) and FMI = 72. Again, the minimum of these curves is very broad and there is not too much difference in the figure of merit for each of the four systems shown.

However, the aiming strategy is one point aim for the two lowest curves, and the resulting flux on the receiver violates the peak flux limit of 1.5 MW/m^2. In order to flatten the flux profile at the 229 MWt level, a two point aim was instituted. Rather than having all heliostats aim at the belt of the receiver (one point aim), a high-low two point aim was used where alternating heliostats aim above and below the beltline. This lowers the peak flux, but increases spillage. The annual energy is less and the output figure of merit is therefore higher.

The apparent winning combination is the two point aim and the 13.5m (44.3 feet) by 10.4m receiver. Note that the increase in the cost/performance ratio is only slightly more than a percent over the one point aiming strategy.

Correlating Power and Field-Receiver Optimums. If one develops data as in the previous two subsections for many tower heights, an envelope of minima can be constructed for each case. If all these curves are then plotted on the same graph, one can develop their envelope of minima. This is essentially the curve shown in Figure 3. There are seven data points shown here, and they represent efforts to minimize the figure of merit for five different tower heights.

The first three points on the low power end (around 200 MW) are from a 120m tower. After that, the tower heights in increasing order are 150m, 180m (591 feet), 240m (787 feet), and 330m (1083 feet).

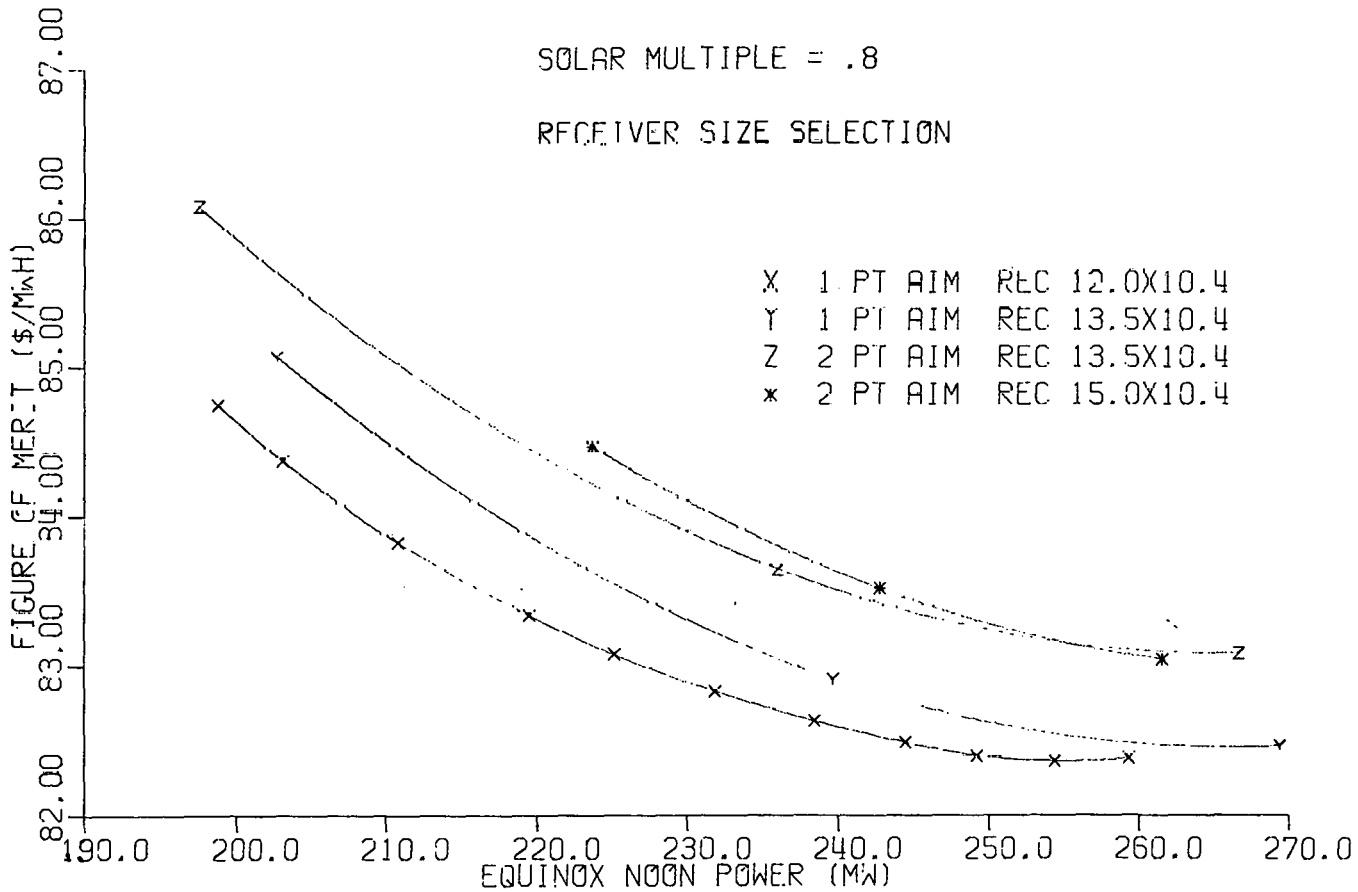

Fig. 2 Power versus Figure of Merit for the .8 SM System

This curve also has a broad minimum over a wide range of power levels. It looks as though a 180m tower and five to six hundred MWt is about optimum given the cost and loss functions employed in the simulation and analysis. However, note that an increase of less than one percent in the cost/performance ratio is the penalty for going to a 1000 MW system and a 240m tower, a system which gives about twice the power as the overall optimum 180m tower.

RESULTS

The results of this study recommend a 120m tower and a 13.5m by 10.4m receiver for the .8 SM system. A 150m tower and a 15.3m by 13.0m receiver is recommended for the 1.4 SM system. The number of heliostats for the .8 SM is 8,496 while the 1.4 SM system has 13,521. Each heliostat has $49m^2$ (528 square feet) of area so that the total mirror area for the .8 SM system is $.417km^2$ ($4.6x10^6$ square feet) and $.660km^2$ ($7.1x10^6$ square feet) for the 1.4 SM system. The land areas required for the .8 SM system and the 1.4 SM system are, respectively, $2.00x10^6m^2$ (494 acres) and $3.11x10^6m^2$ (768 acres).

The two systems will both require some type of aiming strategy to reduce the peak flux to an acceptable value. This can be done with only a small loss in cost effectiveness. Also, both systems had heliostats moved from the northern part of the field to the southern part of the collector field in an effort to reduce the north-south receiver flux ratio. This can also be done with but a nominal increase in the figure of merit.

CONCLUSION

This type of power plant will benefit utilities who are trying to get away from burning oil or gas. They will have a plant that uses solar, but which can still be used in a baseload or intermediate capacity. The system simulation and design of the plant will enable the correct size and configuration to be built in order to achieve the most cost effective plant. The optimization is needed to reduce costs and increase performance. This will help manufacturers save money and therefore bring solar central receiver power systems to the marketplace more quickly.

ACKNOWLEDGEMENTS

This work was supported in part by the United States Department of Energy Contract DE-AC03-78ET 20567. However, any opinions, findings, conclusions, or recommendations expressed herein are those of the author and do not necessarily reflect the views of DOE.

REFERENCES

[1] Solar Central Receiver Hybrid Power System, T.H. Springer, Energy Systems Group of Rockwell International, Department of Energy Contract DE-AC03-78ET 20567, Progress Reports, Final Report to be available from NTIS, (1979).

[2] M.D. Walzel, F.W. Lipps, and L.L. Vant-Hull,

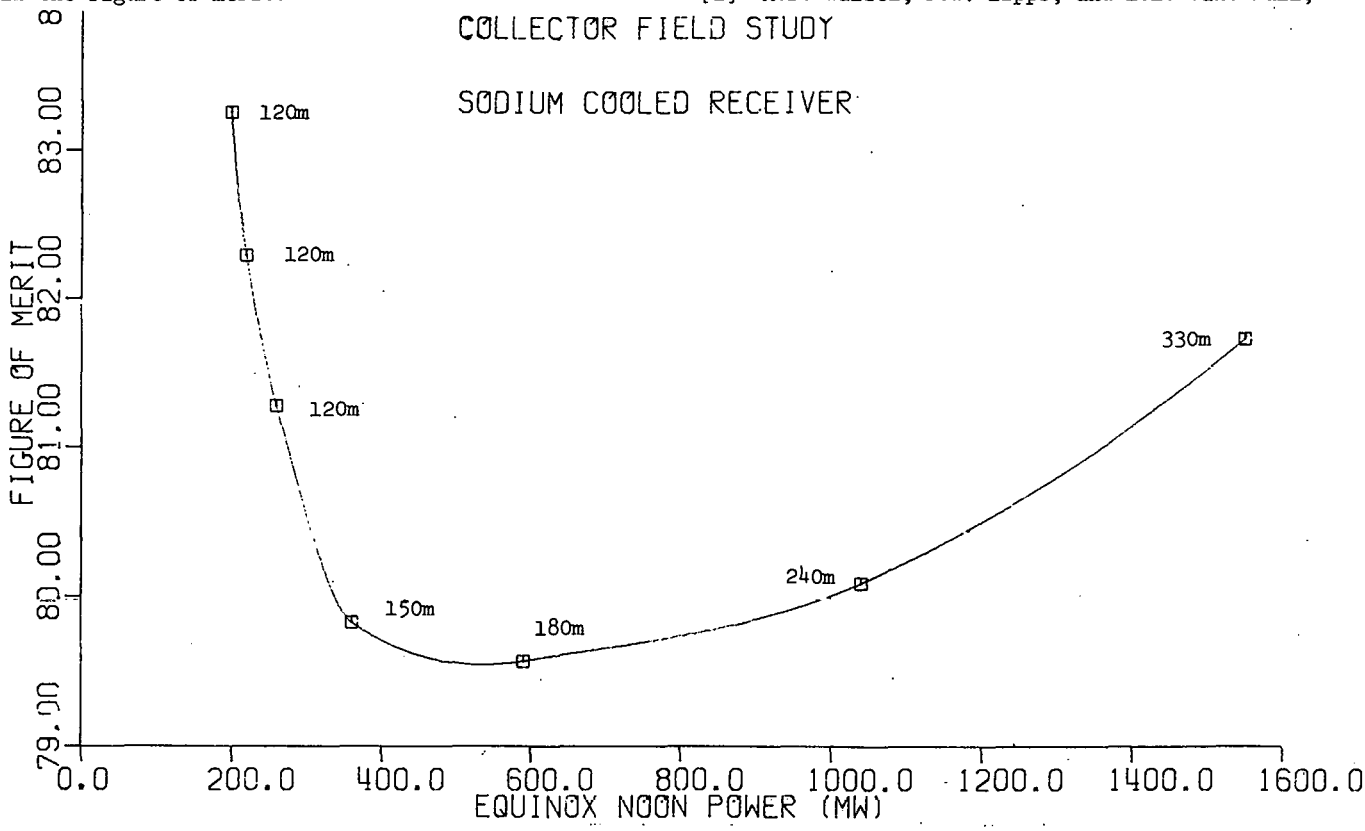

Fig. 3 Power versus Figure of Merit for the Envelope of Minima

"A Solar Flux Density Calculation for a Solar Tower Concentrator Using a Two-Dimensional Hermite Function Expansion", Solar Energy, 19, pp. 239-253, (1977).

[3] F.W. Lipps, "Four Different Views of the Heliostat Flux Density Integral", Solar Energy, 18, pp. 555-560, (1976).

[4] F.W. Lipps and M.D. Walzel, "An Analytic Evaluation of the Flux Density due to Sunlight Reflected from a Flat Mirror having a Polygonal Boundary", Solar Energy, 21, pp. 113-121, (1978).

[5] F.W. Lipps and L.L. Vant-Hull, "A Cellwise Method for the Optimization of Large Central Receiver Systems", Solar Energy, 20, pp. 505-515, (1978).

[6] M.D. Walzel and L.L. Vant-Hull, "A Comparison of Central Receivers Optimized for Advanced Receivers", Proceedings of the 1978 Annual Meeting, AS of ISES, Denver, CO., Volume 21, pp. 799-804.

[7] F.W. Lipps and L.L. Vant-Hull, "Parametric Study of Optimized Central Receiver Systems", Proceedings of the 1978 Annual Meeting, AS of ISES, Denver, CO., Volume 21, pp. 793-798.

Dup

BALDR-1: A SOLAR THERMAL SYSTEM SIMULATION

Joseph G. Finegold and F. Ann Herlevich
Solar Energy Research Institute
1617 Cole Blvd.
Golden, CO 80401

ABSTRACT

A solar thermal system simulation (BALDR-1) has been written by a team of SERI engineers. This flexible simulation was written in a modular fashion to facilitate expansion and modification. The flexibility of the simulation is derived, in part, from the use of three separate models to constitute the system simulation: FIELD, POWER, and ECON. Each model can be run independently, or they may be coupled and run as a set.

The FIELD code models the optical and thermal performance of the collector field. It has separate optical and thermal performance routines for each generic collector type. Meteorological data is read in 15-minute or hourly increments.

The POWER code models the performance of power conversion and storage components. It calculates the total thermal and/or electrical energy produced during the year for a set of plant configurations comprised of different collector field sizes, thermal storage sizes, and electrical storage sizes. The POWER code allows the selection of one of several control strategies in the dispatch of thermal and electrical storage.

The ECON code calculates the initial capital cost of each power plant configuration modelled in POWER. This capital cost is combined with operations and maintenance costs to calculate a life-cycle busbar energy cost and simple payback period for each plant.

INTRODUCTION

A system simulation, BALDR-1*, was written to model the performance of solar thermal systems. The original application was to model the performance and economics of 0.1 - 10 MW_e solar thermal electric power plants (Ref. 1). It has subsequently been used in receiver selective surface value analysis and in thermal storage value analysis, and is being adapted currently to model industrial process heat systems.

*In Scandanavian mythology, BALDR was the god of sunlight and the personification of wisdom, beauty and brightness. The version of the code is the original, hence "dash one".

The FIELD code models the optical and thermal performance of the collector field and thermal transport subsystems. The POWER code models the power conversion and energy storage subsystems. The ECON code determines the initial capital cost of the power plant and the life-cycle busbar energy cost. A flow chart of the system simulation is shown in Figure 1.

FIELD CODE

The FIELD code is a second-order simulation based on a similar code previously developed by the Aerospace Corporation with modifications by the Jet Propulsion Laboratory (JPL) (Ref. 2), and by Battelle Pacific Northwest Laboratories (PNL) (Ref. 3). The FIELD code uses meteorological data read in from SOLMET or TMY format weather tapes in 15-minute or hourly increments. Data used in the current version of FIELD are: direct normal insolation, solar time, global insolation, ambient temperature, dew point, and day of the year. The FIELD code models the performance of collector subsystems in four different ways depending on the type of collector subsystem being modelled. There are separate modules to calculate the optical and thermal performance of each generic collector type. If the need should arise to model other collector types, it is a simple matter to add additional optical and thermal performance modules.

For point focus central receiver systems (PFCR) and line focus central receiver systems (LFCR), the optical efficiency of the concentrator field is determined at each time step by a bivarient linear interpolation of tables of optical efficiency as a function of solar azimuth and zenith angles. These efficiency tables must be input and generally result from third-order simulation programs such as DELSOL (Ref. 4) and MIRVAL (Ref. 5).

The radiative losses from the receiver are calculated in the FIELD code based on the effective receiver temperature, the effective absorptivity and emissivity of the receiver and the effective normalized receiver area. The convective and conductive losses are assumed to be a constant fraction of the calculated radiative losses. The value of this fraction can be adjusted to yield receiver efficiencies similar to those predicted by third-order simulations and reconciled with experimental results. The energy incident on the receiver at each time step per unit area of collector is then equal to the product of the optical efficiency, direct normal insolation, and the time step. The energy collected at the receiver is this term minus the calculated thermal losses. The energy collected

in the collector field (ECF) is then equal to the product of the energy collected at the receiver and the thermal transport efficiency.

For the point focus distributed receiver systems (PFDR) e.g., paraboloidal dishes, and fixed mirror distributed focus systems (FMDF) e.g., hemispherical bowls, the optical efficiency is determined by explicit calculation at each time step. This calculation includes the effects due to solar azimuth, zenith, concentrator position, intercept factor, reflectivity, blockage, shadowing, edge losses and dust. The receiver thermal losses are calculated in a manner identical to that described above for the central receiver systems. The energy incident on the receiver at each time step per unit area is again equal to the product of optical efficiency, direct normal insolation and the time step. The energy collected at the receiver is the energy incident on the receiver minus the thermal losses. The energy collected from the field (ECF) is the product ot the energy collected at the receiver and the thermal transport efficiency. This may be determined per unit area of concentrator or per unit collector module.

For the line focus distributed receiver systems (troughs) with either tracking collectors (LFDR-TC) or tracking receivers (LFDR-TR), the optical efficiency is determined by explicit calculation at each time step. This calculation includes the effects due to solar azimuth, intercept factor, reflectivity, blockage, shadowing, edge losses, dust, secondary concentrator efficiency and transmissivity of receiver cover. The thermal losses of the receiver are based on a selectable fraction of the thermal losses resulting from tests of the best receiver to date (Ref. 6). This fraction allows for future improvements in receiver design such as selective coatings, evacuated covers, etc. The energy incident on the receiver at each time step per unit area is once again equal to the product of the optical efficiency, direct normal insolation and the time step. The energy collected by the receiver is the energy incident on the receiver minus the thermal losses. The energy collected from the field (ECF) is equal to the product of the energy collected at the receiver and the thermal transport efficiency.

For low concentration non-tracking systems (LCNT) e.g., CPC collector, and shallow solar ponds (SSP), the total collector efficiency is determined from a linear relationship between total efficiency and ΔT ($T_{collector} - T_{ambient}$). These relationships were based on plots of test data for advanced concept versions of each of the two collector types. (The y-intercept, T=0, is equal to the optical efficiency). The energy collected from the field (ECF) is equal to the product of the total collector efficiency (including thermal losses), insolation, the time step, and the thermal transport efficiency. For the LCNT, insolation was taken as the sum of direct normal plus diffuse divided by the concentration ratio. For the SSP, insolation was taken as direct normal plus diffuse, or global.

The variables passed to the POWER code include an array of values of ECF for each time step, dry-bulb and wet-bulb temperatures, and unit collector area.

POWER CODE

The POWER code is a second-order simulation based on the Aerospace computer code as modified by JPL (Ref. 2) and Battelle PNL (Ref. 3). POWER differs from the earlier codes primarily in that it provides the option of using different control algorithms for both the operation of power conversion equipment and the dispatch of electrical and thermal storage. There are currently two operational control algorithms: CNTRL2 and CNTRL3.

CNTRL2 models systems with storage of receiver fluid (e.g., salt, sodium, etc.) at approximately the same condition as it leaves the receiver, sometimes called series storage. CNTRL3 models systems with storage of an intermediate fluid (e.g., storage of oil for a steam receiver system). In this case, the temperature of storage is significantly below the receiver outlet temperature and a dual admission turbine is therefore modelled.

Both control algorithms share the following features not usually found in second order solar thermal system simulations.

1. Electrical and thermal storage may both be modelled for any power plant.
2. A weighting factor may be used to reduce the value of electricity delivered above plant rating to simulate hard or soft limits on plant output.
3. The decision of how to dispatch the energy from the collector field is made for the current time step; knowledge of future insolation is not used.
4. Depletion of thermal storage is limited to the value which will assure a hot start-up the following morning. The minimum allowable amount of heat in storage is then a function of the number of hours until the next anticipated morning start-up.

In addition, CNTRL2 incorporates the possibility of overload operation of the power conversion equipment for specified periods. While not currently incorporated into CNTRL3, this capability could easily be added.

CNTRL2 operates with priority on producing and delivering electricity. Thermal storage is used only when there is insufficient energy to start the engine or when there is more energy than required to produce rated power. If electrical storage is modelled it is used for leveling the plant output curve. When the engine generator output is below plant rating, the output is supplemented by energy from electrical storage.

In CNTRL3, there are three operating strategies available: electricity priority, storage priority, and peak load priority. The electricity priority strategy is identical to that used in CNTRL2. The storage priority causes thermal storage to be charged with the engine off until storage is filled to a specified fraction. Only then is the engine turned on, and the priority reverts to generation of electricity for the remainder of the day. The peak load priority option is similar to the storage charging priority except that storage is maintained at the specified fraction until a designated peak period occurs. During the peak period, the priority reverts to generation of electricity. When the peak period is over, any heat left in storage is retained for use during the following day.

Component models in POWER were written in several levels of detail according to their impact on plant performance. The engine efficiency model is a function of hot engine temperature, cooling tower temperature, and the load at each time step. The thermal and electrical energy storage residence losses are calculated based on the amount of energy in storage at each time step. The auxiliary electrical loads are calculated based on plant capacity and actual plant output at each time step. The electrical transport efficiency is based upon electrical current flow through the transport system. The component models for thermal and electrical storage charging and discharging, the electrical generator, power conditioning, the inverter and the converter currently use a constant average efficiency. The component models may be easily increased in accuracy if necessary or desirable for a particular application.

The POWER code calculates the electricity delivered to the grid at each time step and sums it for one year. The total electrical energy delivered during the year is divided by the total electricity which would have been delivered had the plant operated at rated capacity for the entire year. This yields the plant capacity factor.

This capacity factor is calculated for each plant described by an element of the three dimensional matrix of collector field sizes (AC), thermal energy storage sizes (ST), and electrical storage sizes (STE).

Matrices of the operating mode of the plant and the dispatch of electrical storage at each time step can be output. The calculated capacity factor, along with the corresponding collector field size, thermal storage size and electrical storage size, is output for use by the ECON code. In addition, the plant rated capacity and generator size are output for use by ECON.

ECON CODE

The ECON code includes two major subroutines (COST and BUSBAR) which are based on computer codes originally written by JPL (Ref. 2,7). Using the output from POWER, ECON determines a capital cost, a life cycle busbar energy cost, a simple payback period, and annual operations and maintenance (O&M) costs for each plant configuration based on either the thermal energy or the electrical energy produced.

Subroutine COST uses unit costs as inputs to determine the cost streams for both capital expenditures and O&M. Capital costs are determined for each of four subsystems: 1) collector and receiver, 2) electrical and/or thermal storage, 3) power conversion, and 4) miscellaneous (including land, thermal and electrical transport, and spares and contingencies). These costs are currently distributed over the plant construction period as a uniform series of payments. With slight modifications to the code, COST could create a nonuniform cost stream.

Operations and maintenance costs are also determined in COST. Currently, O&M is a uniform stream of annual costs for each year of the plant's lifetime. In case a specific schedule of required maintenance is known, COST can be modified to produce a nonuniform O&M cost stream. Alternatively, a periodic maintenance cost could be added onto the annual O&M cost stream currently produced by COST.

Subroutine BUSBAR is based on the Utility-Owned Solar Electric Systems (USES) model, a conventional present value analysis adapted for solar electric power plants by JPL (Ref. 8). It calculates that busbar energy cost in constant-year dollars which will generate system-resultant revenues equal to the system-resultant costs. The inputs for BUSBAR represent two types of information: system cost data and accounting information. The cost data as currently used consist of the arrays of capital costs and O&M costs which are generated in subroutine COST. Escalation rates are input for capital and O&M in addition to the general inflation rate. BUSBAR is written to handle separate maintenance charges, fuel costs and social benefits along with their appropriate rates of escalation. The ECON code also has the capability of doing only the busbar energy calculations if a net present value cost is input.

The second group of input data, the accounting information, represents the variables that are used to determine the cost of capital. From this data, the discount rate, the fixed charge rate, and the capital recovery factor are determined in BUSBAR.

An additional capability exists within ECON for producing plots of the data generated. Subroutine PLOTIT can be called to produce a graph of busbar energy cost versus capacity factor for each system. For the systems which use either thermal or electrical storage, but not both, the graph will have a set of curves, each of which represent a distinct value of collector area with points marked representing various amounts of storage (e.g., Figure 2). For the systems which use both electrical and thermal storage, a separate plot will be generated for each value of collector area. Each plot will consist of a set of curves, each representing an amount of thermal storage with points marked representing amounts of electrical storage.

COMPUTATIONAL TIME

To simulate the annual performance of a point focus central receiver system using 15-minute time steps, approximately 50 seconds of CPU time is required for FIELD and approximately 300 seconds of CPU time for POWER for a full matrix of collector areas and storage sizes for electrical output cases. ECON requires approximately 10 seconds of CPU time in the corresponding simulation.

SUMMARY

A system simulation has been written to model the performance of solar thermal power systems for both electrical and process heat applications. The models are modular allowing for easy use and modification. Annual performance and economics of most proposed solar thermal systems can be modelled by the simulation in its present form.

ACKNOWLEDGMENTS

The development of this simulation is the work of many SERI employees. The following people participated in the development of BALDR-1.

M. Buhl	J. Kowalik
S. Cronin	L. Lacy
M. Edesess	D. Madison
A. Edgecombe	R. Mitchell
J. Finegold	L. Morrison
A. Herlevich	R. O'Dougherty
M. Karpuk	J. Pagano

L. Morrison and A. Edgecombe are singled out for particularly important contributions in the early stages of model development. We also gratefully acknowledge the support of J. Thornton, Task Leader of the Small Power Systems Study, under whom this work was conducted. Funding was provided under DOE Contract EG-77-C-01-4042.

REFERENCES

1. Thornton, J., Brown, K., Edgecombe, A., Finegold, J., Herlevich, A., Kriz, T. Comparative Ranking of 1-10MW$_e$ Solar Thermal Electric Power Systems - An Executive Overview, SERI/TR-35-238, Solar Energy Research Institute, Golden, CO, September 1979.
2. El Gabalawi, N., Hill, G., Bowyer, J., Slonski, M. A Modularized Computer Simulation Program for Solar Thermal Power Plants, JPL 5102-80, Jet Propulsion Laboratory, Pasadena, CA, July 1978.
3. Bird, S. Modification of the JPL Solar Thermal Simulation Code for Use in the PNL Small Solar Thermal Power Plant Systems Analysis, Battelle Pacific Northwest Laboratory, Richland, WA, July 29, 1978.
4. Dellin, T. A., Fish, M. J. A User's Manual for DELSOL: A Computer Code for Calculating the Optical Performance, Field Layout, and Optical System Design for Solar Central Receiver Plants, SAND 79-8215, Sandia Laboratory, Livermore, CA, June 1979.
5. Leary, P. L., Hankins, J. D. A User's Guide for MIRVAL - A Computer Code for Comparing Designs of Heliostat-Receiver Optics for Central Receiver Solar Power Plants, SAND 77-8280, Sandia Laboratory, Livermore, CA, February 1979.
6. Dudley, V. E., Workhoven, R. M. Summary Report - Concentrating Solar Collector Test Results Collector Module Test Facility (CMTF) January-December 1978, SAND 78-0977, Sandia Laboratory, Albuquerque, NM, March 1979.
7. Slonski, M. L. Energy Systems Economic Analysis (ESEA) Methodology and User's Guide, JPL 5101-102, Jet Propulsion Laboratory, Pasadena, CA, February 15, 1979.
8. Doane, J., O'Toole, R., Chamberlain, R., Bos, P., Maycock, P. The Cost of Energy from Utility-Owned Solar Electric Systems: A Required Revenue Methodology for ERDA/EPRI Evaluations, JPL 5040-29, Jet Propulsion Laboratory, Pasadena, CA, June 1976.

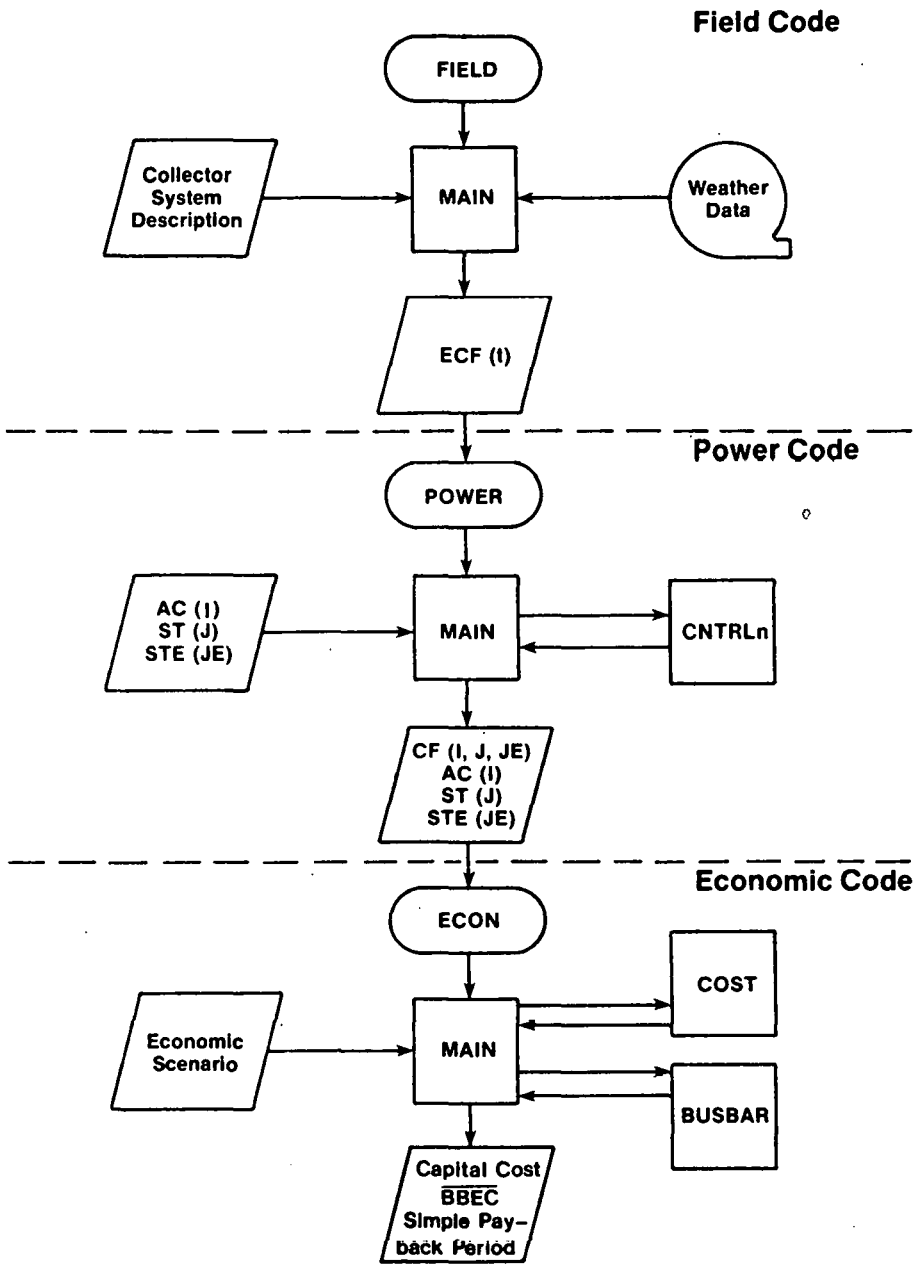

Figure 1 - Simplified flow chart for BALDR-1 performance and cost simulation codes

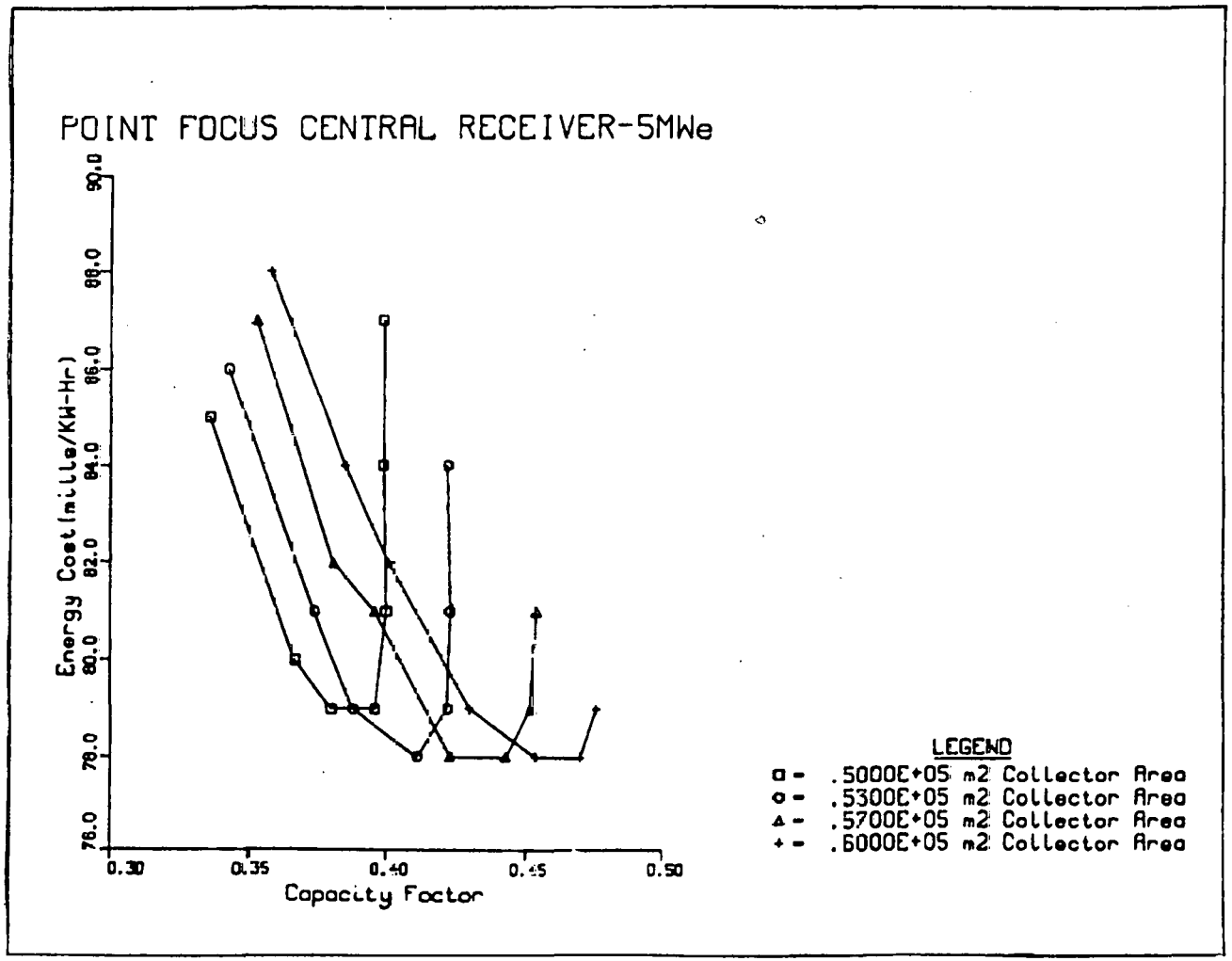

Figure 2 - Graphical Output from ECON
Each point marked on a curve represents a different amount of storage.

PERFORMANCE OF DISTRIBUTED ACTIVE SOLAR POWER SYSTEMS

Paul A. Curto
Rebecca C. Bjustrom
Arnold S. Cherdak
Marie E. Coluzzi
Frank R. Eldridge
Richard N. Manley
Willis E. Jacobsen

ABSTRACT

The performance of an active solar power system depends upon the available solar resource, equipment characteristics and load profile. A distributed solar power systems performance simulation model is developed that can handle all classes of windpower, solar thermal process heat and electricity, and photovoltaics systems. This model utilizes hourly insolation, windspeed, temperature and pressure data (derived from SOLMET tapes, available from the National Climatic Center), characterizations of over 200 classes of solar equipment components and subsystems, and hourly electrical and thermal load data for selected industrial, commercial, institutional, agricultural and residential applications (including seasonal variations). Model outputs include peak array power, annual collected energy, solar fraction, backup energy requirements, peak backup load power, excess generated energy available for sale or waste, average hourly generation profiles, and other related data. System performance can be determined for up to 72 different applications and 26 locations for various array sizes and storage capacities.

BACKGROUND

A simulation model was developed for the U.S. Department of Energy, Division of Central Solar Technology, to perform studies of generic solar power systems for use in on-site (distributed) applications. The study was originally commissioned by the Division of Solar Technology, and was scoped to handle solar thermal, photovoltaics, windpower and wood combustion technologies. The purpose of these studies was to characterize the performance of solar power systems throughout the U.S., and to estimate the costs of such systems. This paper addresses only performance.

APPROACH

Data on a variety of solar power systems hardware and conceptual/preliminary designs were gathered and analyzed to ascertain component performance characteristics and costs.

Analysis of this data led to preparation of a series of performance algorithms and configurations of the components into so-called "generic designs".

Generic designs for solar thermal, photovoltaics and windpower systems are displayed in Figures 1, 2 and 3. Tables 1, 2 and 3 provide some information regarding the equipment selections for the generic designs.

A computer model was formulated that has the capability of simulating the system hourly performance through a year. The model utilizes the performance algorithms, SOLMET weather tapes, and a series of demand profiles which characterize each application on an hourly basis. These demand profiles also change with season of the year. They are based on electrical demand profiles developed by RTI [1]. The ratio of thermal-to-electric demand was estimated from data acquired from the Census of Manufactures [2] and Battelle [3], ITC [4] and Aerospace [5] studies. This ratio was held constant for each region and SIC on a real-time basis. One such profile is shown in Figure 4, and is representative of a typical one-shift industrial application (SIC 32 -- the Standard Industrial Classification for Stone, Clay and Glass Products).

MODEL OUTPUTS

Two types of simulations are performed with the model, profile generation and stepwise system output versus demand analyses.

The profile generation provides four calculated parameters, presented as annual averages as a function of the hour of the day: single module output energy, insolation, dry-bulb atmospheric temperature, and wind velocity. Also shown is the peak module power and time at which peak power is obtained, peak insolation, peak windspeed, solar capacity factor (annual output divided by peak output sustained throughout the year), annual module output and insolation available to the collector surface. One such output file is shown in Table 4.

The analysis run model output is used for the simulations wherein a load profile and storage capacity are matched to the array output. One such file is shown in Table 5. The following output parameters relate to system performance in satisfying the given application's demand requirements:

load-the total energy demand associated with the application

usable system-the total amount of energy that is generated by the solar system and then delivered

aux-the amount of energy supplied to the load by the backup system

array waste-the amount of solar-derived energy wasted because the array supplied more than the load demanded and storage was full

solar fraction-the fraction of the total load that is supplied by solar-derived energy

useable output-the amount of solar-derived energy delivered to the end use on a normalized-to-array-area basis

total collector output for the year-all the energy delivered by the array including that which may eventually be wasted

total collector output/array size-total collector energy output normalized to total array area

peak power output-maximum thermal power delivered during the year.

The variable levels of collector array waste throughout the day or from one part of the year to another are frequently of concern. Average hourly values of solar-derived wasted energy are presented in Table 5. Energy waste occurs when the maximum storage capacity has been reached and the load will not accept all the energy then being generated. Summary parameters related to waste, i.e., peak hourly waste, waste fraction and maximum storage required are calculated and presented as well.

An additional part of the analysis simulation provides cost and performance calculations and then allows analyst intervention/interaction to direct execution back to previous areas of the simulation that he may wish to revise and examine. Cost of energy algorithms are exercised based on dependent variables such as collector type, storage capacity and power conversion capacity. Capital cost estimates provided for the analysis are also presented on Table 5 for the major subsystems and three time frames (Cost 1, 2 and 3, respectively). The capital cost of a unit of energy production capacity is an important parameter for comparing alternative energy production schemes. The capital cost of the system is divided by the amount of solar-derived energy delivered to the load and is shown as "$/kWh/yr, system delivered" on Table 5. The capital cost per unit of energy produced by the solar system, including waste, is also shown.

The computer simulation is run for a given application, collector type, geographical region, array size and various levels of storage capacity. Several simulations with various levels of storage capacity generally provide enough data to estimate the optimum level of storage for a given system array size and application. During the course of the study, over 6000 simulations were performed.

MODEL LOGIC

Power output of a generic collector module is computed hourly as a function of collector size, orientation, and efficiency; insolation; ambient temperature; air density, based on temperature and pressure; and wind velocity. The results are stored for subsequent use in energy balance analyses. Module power outputs are computed only once per census region city. Figure 5 shows the basic computer logic of the first section of the simulation.

The next step in the simulation is an energy balance analysis that computes how well the complete solar system meets the thermal or electric demand of a given application. To meet a specific demand level, the solar system is sized to an appropriate number of collector modules based on the collector output characteristics computed in the initial section of the simulation. This part of the simulation is iterative and interactive in structure so that the load profile, the number of collector modules, and storage capacity can be varied by the analyst.

Figure 6 shows the logic of the energy balance analysis routine. If the power produced by the collector array exceeds the load, storage (if not fully charged) is charged. Whenever storage is charged to capacity, any remaining excess energy is wasted. If the array power produced falls short of the load, storage (if available) is discharged. The electric utility, acting as an auxiliary power source, supplies any remaining unfulfilled demand.

This procedure permits storage to be dispatched as it is available. In addition, the model is able to simulate dispatching of storage in any of the following three modes: based on the time-of-day, based on the level of the demand, and based on both the time-of-day and the demand level. The mode in which storage is dispatched can greatly affect the overall product costs. If, for example, a utility's rate structure is based on time-of-day pricing, then storage dispatching would be restricted to the hours when the utility rates are the highest in an effort to cut costs. On the other hand, if the utility rate structure is based on peak power demand, then storage dispatching would be restricted to the times when the demand on the utility is the greatest.

The output of the entire simulation includes annual average hourly profiles of the energy supplied by the solar system, the energy supplied by the utility, and the energy that is wasted. The state-of-charge of storage (e.g., batteries) is monitored within the program and outputs of storage cycling can be obtained. The data includes distributions and averages for start-of-cycle and end-of-cycle states-of-charge.

The method used to size storage for a given collector array size involves calculating a ratio of system capital cost to delivered energy for several capacities. Then the storage size corresponding to the minimum value of the cost/performance ratio is selected.

For solar power systems without storage, the power conversion device is sized to handle the maximum array output. If the system has storage, the power conversion device is sized to meet the maximum power demand of the load or the maximum array output, whichever is larger.

RESULTS

The effect of load-matching and array and storage sizing is perhaps best demonstrated by examination of an "f-chart," or a plot of solar fraction vs. array size for varying storage capacity and a fixed application and geographic location. One such chart generated during this study is shown in Figure 7. Note that the solar fraction generally increases with increasing array size, and also increases at a given array size as more storage capacity is added. This plot, for a silicon 50X concentrator in SIC 32 (Stone, Clay and Glass Products) in Columbia, Missouri, demonstrates these effects. Up to a certain array size (350 modules), the solar fraction increases linearly. This is the "fuel-saver" range of operation. There is no waste (excess generation). Above this array size, without storage, the solar fraction saturates at about 43 percent. As storage is added, the solar fraction gradually increases to 63 percent at 1264 modules and to 78 percent at 2178 modules (8000 kWh storage capacity). For this application, the peak power demand is 747.9 kWe and the energy requirement is 3.29×10^6 kWhe per year. The energy output of the array (assuming passage through storage) would have equalled the annual load energy requirement with 2178 modules. In this case, with 8000 kWh of storage (10.7 hours at peak load), the excess generation or energy available for sale or buyback is 33.9 percent of the annual demand load.

Load matching is a critical factor impacting storage sizing and system economics. In all cases represented in the study, an "optimal" storage capacity was chosen for each array size. The technique of optimization is graphically represented in Figure 8.

In Figure 8, the system described in Figure 7 is represented as a plot of C/P index vs. solar fraction. The four curves shown display the increase in solar fraction for each of the four array sizes chosen, and each curve shows a relative minimum at some value of storage capacity. Up to 350 modules (solar fraction of 0.193) and C/P index is constant. As one increases solar fraction with optimized array area and storage capacity, the loci of optima follow an exponentially increasing curve for the C/P index. It should be noted that this plot is for ultimate (far-term) system costs.

Performance Comparison

Photovoltaic "fuel-saver" systems; i.e., systems without storage and little or no excess generation, are evaluated in Table 6 in terms of annual array output normalized per unit aperture area. Also shown in parentheses is the average annual system efficiency (system output divided by available insolation to the aperture of the collector array).

The flat panel systems using silicon actually outperform the silicon 50X concentrators in eastern U.S. locations but are significantly lower in performance relative to the 50X concentrator in higher insolation regions. The compound cell 1000X concentrator is by far the best performer in all regions. The thin-film flat panel is the lowest in efficiency and performance in all regions. Regarding efficiency variations, hotter climates generally offer lower efficiency (Phoenix, Ft. Worth, Charleston) while colder climates allow lower cell temperatures, thus higher efficiency (Boston, New York, Madison).

The performance of storage-coupled photovoltaic systems is illustrated for far-term systems in a commercial application (SIC 53-General Merchandising Stores) in Phoenix, New York and Columbia in Table 7. These represent the best, worst, and average insolation locations simulated. The same trends regarding performance ranking and geography hold as in Table 6. However, the excess generation (waste or sell back energy) becomes significant for storage-coupled systems. In general, the waste fraction increases with decreasing insolation and increasing solar multiple (ratio of peak array power to peak load power required). In New York, the worst insolation city, the waste fraction approaches one-third of total generation. In Phoenix, the waste fraction is roughly 15 percent. This effect is due to the larger solar multiple required in poorer insolation areas for which during sequences of days of high insolation, storage becomes fully charged and the array power exceeds the load requirement.

A similar presentation is made for solar thermal systems (Table 8) and wind systems (Table 9).

ACKNOWLEDGMENTS

The authors would like to thank H. A. Abelson, G. E. Bennington, and M. M. Scholl for the support and guidance during this study.

REFERENCES

[1] R. A. Whisant, et al., Research Triangle Institute, "Application Analysis and Photovoltaic System Conceptual Design for Service/Commercial/ Institutional and Industrial Sectors, Task I Report," SAND 78-7032, Sandia Laboratories, Albuquerque, New Mexico, July, 1978.

[2] Department of Commerce, "Annual Survey of the Manufacturers, 1976", M76(AS)-4.2, May, 1978.

[3] Battelle (Columbus) Laboratories, "Survey of the Applications of Solar Thermal Energy Systems to Industrial Process Heat," Vol. I, January, 1977.

[4] Fraser, M. D., "Analysis of the Economic Potential of Solar Thermal Energy to Provide Industrial Process Heat," Report ERDA/Intertechnology Corporation No. 00028-1, Warrenton, Virginia, 1977.

[5] Aerospace Corporation, "Solar Total Energy Systems Project, Final Report, ATR-78 (7692-01)-1, El Segundo, California, March, 1978.

TABLE 1

SOLAR THERMAL GENERIC EQUIPMENT CHARACTERISTICS

Solar Collector Type	Collector Orientation or Configuration	Delivered to Process	Storage Type	Power Conversion -Heat Exchanger	Auxiliary
Evacuated Tube	North-South Polar	100°C Process Heat	Water	Shell and Tube Heat Exchanger	Heater
Parabolic Trough	North-South Horizontal	100°C Process Heat	Water	Shell and Tube Heat Exchanger	Heater
Parabolic Trough	North-South Horizontal	200°C Process Heat	Oil/Rock	Shell and Tube Heat Exchanger	Boiler
Line Focus Central Receiver	North-South Polar	200°C Process Heat	Oil/Rock	Shell and Tube Heat Exchanger	Boiler
Parabolic Dish	Azimuth Elevation Tracking	250°C Process Heat	Salt/Rock	Shell and Tube Heat Exchanger	Boiler
Point Focus Central Receiver	North Field	600°C Process Heat	Salt/Rock	Shell and Tube Heat Exchanger	Combustor
Parabolic Dish	Azimuth Elevation Tracking	On-Site Electricity	Battery	Stirling Engine	Utility Or Home
Point Focus Central Receiver	North Field	On-Site Electricity	Salt/Rock	Steam Rankine	Combustor

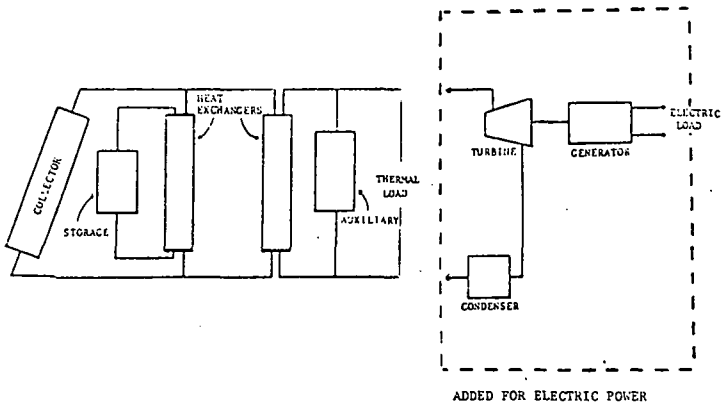

Figure 1

Solar Thermal Generic System Designs

TABLE 2

PHOTOVOLTAIC GENERIC EQUIPMENT CHARACTERISTICS

Collector Type	Collector Module Area	Collector Orientation	Photovoltaic Cell Efficiency	Collector Module Power Packing
Silicon Flat Panel	$2m^2$ cell packing factor=0.9	fixed polar	16.8% air mass 1.0 $1kW/m^2$ insolation 25°C cell temperature	285 watts
Thin Film Flat Panel	$2m^2$ cell packing factor=0.95	fixed polar	10% air mass 1.0 $1kW/m^2$ insolation 25°C cell temperature	188 watts
Silicon 50X Concentrator	$8m^2$ 1 parabolic trough	2-axis tracking	18% air mass 1.0 $50kW/m^2$ insolation 38°C cell temperature	1186 watts includes 12.5 watts for tracking
Compound Cell 1000X Concentrator	$28m^2$ array of 900 headlamp units	2-axis tracking	30% air mass 1.0 1500 kW/m^2 insolation 70°C cell temperature	6660 watts includes 215 watts for tracking and cooling

NOTE: All four generic systems use electrochemical batteries for storage and solid state power conditioners.

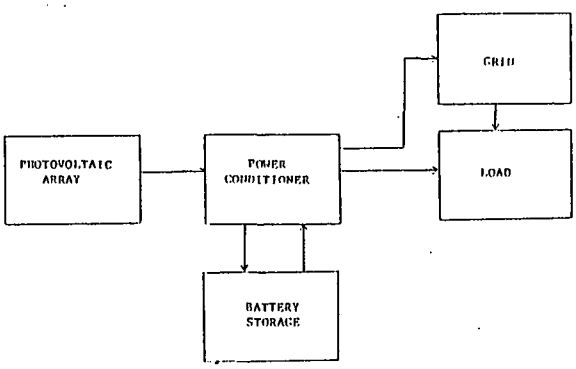

Figure 2

Photovoltaic Generic System Designs

TABLE 3

WINDPOWER GENERIC EQUIPMENT CHARACTERISTICS

	HAWT 1/					VAWT 2/	
	A	B	C	D	E	F	G
Rotor Type	2-prop.	2-prop.	2-prop.	3-prop.	3-prop.	2-blade	2-blade
Rated System Output (kW)	2500	200	40	4	8	55	8
Rated Windspeed (m/s) 3/	12.3	10.0	8.94	8.0	8.0	15.0	15.0
Rotor Swept Area (m^2)	6580	1140	299	39	78	158	29.5
Cut-in Windspeed (m/s) 3/	6.3	4.5	4.47	3.1	3.1	4.7	5.1
Cut-out Windspeed (m/s) 3/	20.1	17.9	26.8	NA 4/	NA 4/	28.2	25.4
Max. Power Coefficient	0.42	0.42	0.40	0.42	0.42	0.35	0.34
Efficiency 5/	0.75	0.75	0.75	0.75	0.75	0.83	0.75

1/ Horizontal-axis wind turbine

2/ Vertical-axis wind turbine

3/ At rotor centerline

4/ None available

5/ Combined mechanical drive plus electrical generator, at system rated output.

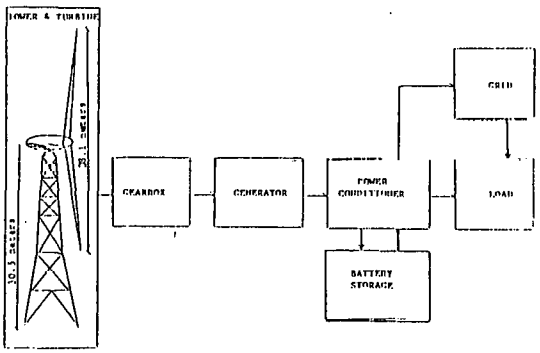

Figure 3

Windpower Generic System Designs

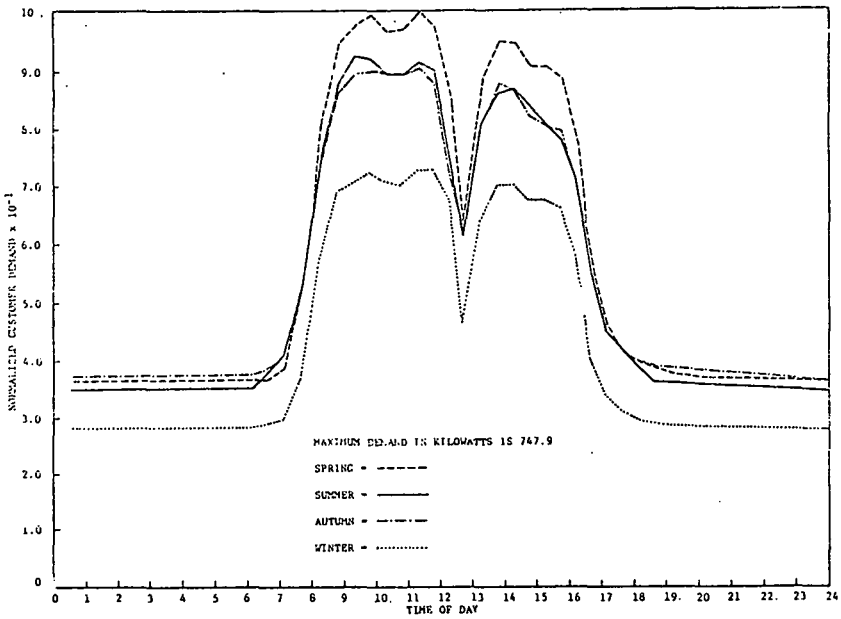

Figure 4

Seasonal Average Daily Profile
SIC 32: Stone, Clay, and Glass Products

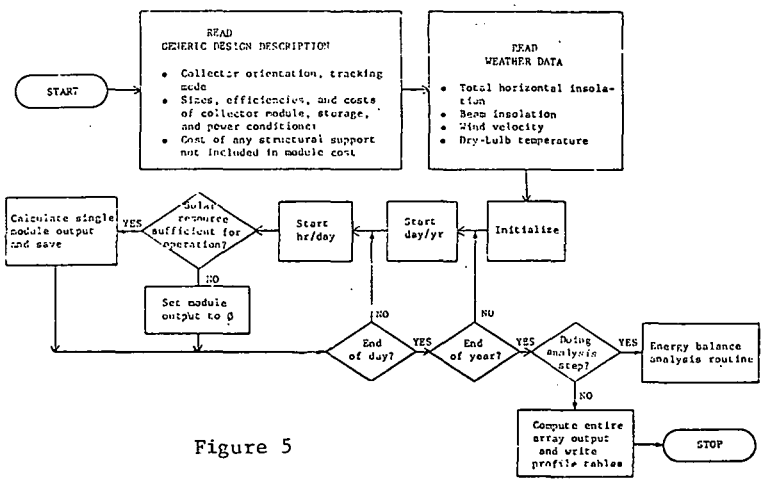

Figure 5

Flow Chart of Module Output Simulator

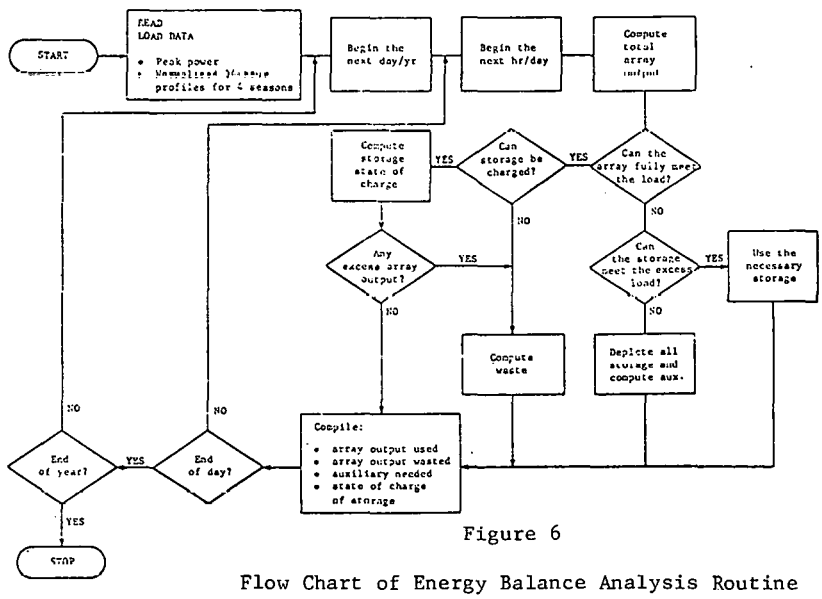

Figure 6

Flow Chart of Energy Balance Analysis Routine

TABLE 4

PROFILE GENERATION OUTPUT

NUMBER OF MODULES	ARRAY SIZE (M-SQ)	STORAGE CAPACITY (KWH)	POWER COND. (KW)	TOTAL ENERGY (KWH/YEAR) USABLE LOAD	USABLE SYSTEM	AUX.	ARRAY WASTE	SOLAR FRACTION	USABLE OUTPUT (KWH/M2/YR)
47	1.88E+03	2.60E+03	2.03E+02	1.27E+06	1.03E+06	2.42E+05	3.12E+05	0.809	5.47E+02

**NOTE : STORAGE STATE-OF-CHARGE AT THE BEGINNING OF THE YEAR = 1.000, THE MINIMUM = 0.0 AND THE END = 0.446
**THE ENERGY FROM A CHARGED BATTERY AT THE BEGINNING OF THE YEAR THAT WENT TO THE LOAD = 2.46E+03 KWH

TOTAL COLLECTOR OUTPUT FOR THE YEAR = 1.49E+06 KWH TOTAL COLLECTOR OUTPUT/ARRAY SIZE = 7.92E+02 KWH/M2/YR
PEAK POWER OUTPUT OF ARRAY = 4.17E+03 KW

PROFILE OF WASTE IN KWH

HOUR	PERIOD 1	PERIOD 2	PERIOD 3	PERIOD 4	PERIOD 5
1	0.0	0.0	0.0	0.0	0.0
2	0.0	0.0	0.0	0.0	0.0
3	0.0	0.0	0.0	0.0	0.0
4	0.0	0.0	0.0	0.0	0.0
5	0.0	0.0	0.0	0.0	0.0
6	0.0	0.0	0.0	0.0	0.0
7	0.0	0.0	0.0	0.0	0.0
8	0.0	0.0	0.0	0.0	0.0
9	0.0	0.0	0.0	0.0	0.0
10	0.0	0.0	0.0	0.0	0.0
11	0.0	0.0	0.0	0.0	0.0
12	1.28E+02	1.24E+04	1.01E+03	2.91E+02	0.0
13	7.78E+03	2.84E+04	2.33E+04	1.09E+04	0.0
14	1.62E+04	3.03E+04	3.13E+04	2.03E+04	0.0
15	1.50E+04	2.50E+04	2.56E+04	1.82E+04	5.04E+02
16	5.54E+03	1.50E+04	1.50E+04	6.39E+03	2.57E+01
17	0.0	2.17E+03	1.73E+03	0.0	0.0
18	0.0	0.0	0.0	0.0	0.0
19	0.0	0.0	0.0	0.0	0.0
20	0.0	0.0	0.0	0.0	0.0
21	0.0	0.0	0.0	0.0	0.0
22	0.0	0.0	0.0	0.0	0.0
23	0.0	0.0	0.0	0.0	0.0
24	0.0	0.0	0.0	0.0	0.0

PEAK HOURLY WASTE FOR THE YEAR = 7.91E+02 KWH WASTE FRACTION = 0.210
ADDITIONAL STORAGE NEEDED FOR NO WASTE = 1.57E+05 KWH

	STORAGE	POWER CONVER	TOTAL ARRAY	TOTAL SYSTEM	$/KWH/YR SYSTEM/DELIV	$/KWH/YR SYSTEM/TOTAL
COST 1	72042.6	30389.0	556209.	658641.	.639980	.442546
COST 2	72042.6	30389.0	278105.	380536.	.369759	.255685
COST 3	72042.6	30389.0	165403.	287835.	.279683	.193399

EFF OF POWER CONVERSION = 0.900 EFF OF STORAGE = 0.950

TABLE 5

SOLAR THERMAL SYSTEM ANALYSIS OUTPUT

HOUR	ARRAY ENERGY (KWH)	INSOLATION (KWH/M**2)	ATMOS. TEMP. (DEGREES C)	WIND (M/SEC)
1	0.0	0.0	1.571E+01	4.317E+00
2	0.0	0.0	1.526E+01	4.282E+00
3	0.0	0.0	1.484E+01	4.232E+00
4	0.0	0.0	1.449E+01	4.217E+00
5	0.0	0.0	1.419E+01	4.207E+00
6	0.0	5.225E-03	1.394E+01	4.157E+00
7	1.161E-02	5.722E-02	1.469E+01	4.368E+00
8	1.848E+00	1.888E-01	1.580E+01	4.734E+00
9	5.796E+00	3.748E-01	1.716E+01	5.103E+00
10	9.631E+00	5.464E-01	1.866E+01	5.389E+00
11	1.231E+01	6.655E-01	2.003E+01	5.538E+00
12	1.371E+01	7.239E-01	2.131E+01	5.793E+00
13	1.356E+01	7.157E-01	2.209E+01	5.719E+00
14	1.219E+01	6.548E-01	2.270E+01	5.868E+00
15	9.832E+00	5.486E-01	2.325E+01	5.932E+00
16	5.957E+00	3.700E-01	2.294E+01	5.842E+00
17	1.900E+00	1.487E-01	2.234E+01	5.494E+00
18	1.629E-02	2.878E-02	2.147E+01	5.108E+00
19	0.0	0.0	2.014E+01	4.762E+00
20	0.0	0.0	1.894E+01	4.647E+00
21	0.0	0.0	1.795E+01	4.569E+00
22	0.0	0.0	1.735E+01	4.422E+00
23	0.0	0.0	1.675E+01	4.384E+00
24	0.0	0.0	1.623E+01	4.324E+00

NOTE : THE ABOVE DATA REPRESENT AN AVERAGE DAY FOR A TYPICAL YEAR FOR 1 MODULE(S)

PEAK ARRAY POWER = 2.499E+01 ON DAY 246 HOUR 12
PEAK INSOLATION = 1.203E+00 ON DAY 246 HOUR 12

PEAK AMBIENT TMP = 3.940E+01 ON DAY 220 HOUR 13
PEAK WIND SPEED = 2.210E+01 ON DAY 171 HOUR 1
CAPACITY FACTOR FOR THE YEAR = 1.447E-01
ARRAY OUTPUT FOR THE YEAR (KWH) = 3.167E+04
INSOLATION FOR THE YEAR (KWH/M**2) = 1.835E+03

TABLE 6

ANNUAL ENERGY DELIVERED BY PHOTOVOLTAIC SYSTEMS
AND ANNUAL AVERAGE EFFICIENCY[1] (kWh/m^2)

CITY	SILICON FLAT PANEL		THIN-FILM FLAT PANEL		SILICON 50X CONCENTRATOR		COMPOUND CELL 1000X CONCENTRATOR	
BOSTON	173.1	(12.2%)	103.1	(7.3%)	180.2	(15.4%)	264.3	(22.5%)
NEW YORK	170.6	(12.1%)	101.7	(7.2%)	167.6	(15.3%)	246.2	(22.4%)
CHARLESTON	202.4	(11.9%)	121.9	(7.2%)	200.1	(14.7%)	301.3	(22.2%)
MADISON	190.6	(12.3%)	114.0	(7.3%)	201.4	(15.3%)	295.6	(22.4%)
NASHVILLE	187.6	(11.8%)	113.1	(7.1%)	190.6	(14.8%)	287.0	(22.2%)
COLUMBIA	205.4	(12.1%)	124.1	(7.3%)	231.0	(14.9%)	344.6	(22.2%)
FT. WORTH	223.7	(11.9%)	136.1	(7.3%)	256.3	(14.5%)	387.1	(22.9%)
PHOENIX	276.2	(11.5%)	171.4	(7.2%)	351.0	(13.9%)	544.1	(21.6%)
SANTA MARIA	247.5	(12.2%)	151.0	(7.4%)	290.0	(14.8%)	434.8	(21.1%)

[1]SYSTEM OUTPUT DIVIDED BY AVAILABLE INSOLATION AT APERTURE OF COLLECTOR

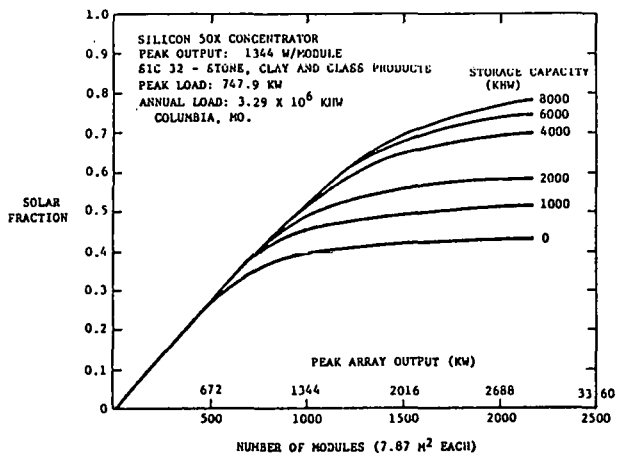

Figure 7

F Chart for Silicon 50X Concentration

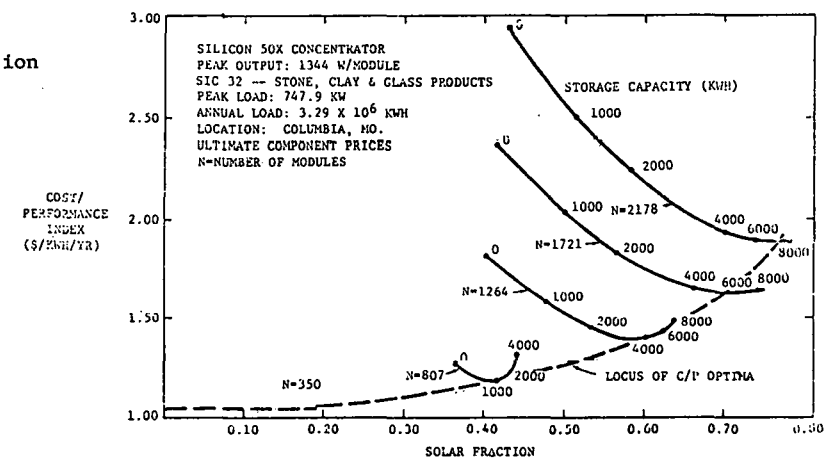

Figure 8

Storage/Array Optimization as a Function of Solar Fraction for Silicon 50X Concentrator

TABLE 7

PERFORMANCE COMPARISON OF GENERIC PHOTOVOLTAIC SYSTEMS,
ANNUAL ENERGY DELIVERED TO LOAD PER UNIT COLLECTOR AREA
($kWh/m^2/yr$)

	Silicon Flat Panel		Thin Film Flat Panel		Silicon 50X Conc.		Compound 1000X Conc.	
Location	Delivered to Load	Available for Sell Back	Delivered to Load	Available for Sell Back	Delivered to Load	Available for Sell Back	Delivered to Load	Available for Sell Back
Best (Phoenix)	216.5	29.9	134.3	20.1	261.2	62.6	412.8	88.0
Worst (New York)	106.4	43.3	63.8	28.2	100.2	54.1	154.0	70.8
Average (Columbia)	133.7	47.8	82.2	29.8	138.3	77.5	205.0	116.0

TABLE 8

PERFORMANCE COMPARISON OF SOLAR THERMAL SYSTEMS,
ANNUAL ENERGY DELIVERED TO LOAD PER UNIT
COLLECTOR AREA ($kWh/m^2/yr$)

SYSTEM TYPE / REGION	LOW TEMPERATURE		MID TEMPERATURE		HIGH TEMPERATURE		ELECTRICITY	
	EVACUATED TUBE	PARABOLIC TROUGH	PARABOLIC TROUGH	LINE FOCUS CENTRAL RECEIVER	PARABOLIC DISH	POINT FOCUS* CENTRAL RECEIVER	PARABOLIC DISH	POINT FOCUS CENTRAL RECEIVER
Best (Phoenix)	964	1230	1040	1090	1760	1020	597	439
Worst (New York)	475	687	325	400	757	359	237	172
Average (Columbia)	605	713	542	618	987	563	350	255

*Values are 30% higher in mid-temperature range; 40% higher in low-temperature range.

TABLE 9

PERFORMANCE COMPARISON OF WIND ENERGY SYSTEMS,
ANNUAL ENERGY DELIVERED TO LOAD PER UNIT AREA
($kWh/m^2/yr$)

SYSTEM TYPE 1/ / LOCATION	A Chemical Industry	B Food Processing	C Schools	D Residential (Air conditioned)	E Residential (All-electric)	F Schools	C Residential (All-electric)
Best (Boston, MA)	1090	635	460	150	260	530	270
Worst (Santa Maria, CA)	320	190	140	50	40	140	50
Average (Columbia, MO)	640	410	280	130	180	280	135

1/See Table 3 for wind machine characteristics.

Notes:
- Energy delivered to primary load only; excess wasted
- Zero storage capacity
- Reference area is rotor swept area (Table 3)
- Near-term generic wind systems

OUTPUT POWER OF WIND MACHINES

W. RICHARD POWELL

Applied Physics Laboratory

Johns Hopkins Road, Laurel, MD. 20810, U.S. A.

ABSTRACT

A new model of wind machine output power is suggested. This model not only avoids errors associated with prior models, but also allows the average power produced by a wind machine to be calculated without resort to numerical methods. The average power is expressed as a function of the "cut-in", "rated" and "maximum" speeds of the wind machine and the two parameters used to characterize wind speeds with Weibull statistics. The variation of average power and capacity factors with changes in wind-machine design is explored. These analytical results provide a useful guide for machine selection prior to more detailed analysis. An application for wind power is suggested.

INTRODUCTION

Unlike sunlight, wind power is usually more available during winter than in summer. Wind power can be combined with an electric heat pump to provide an efficient heating system. No energy storage is required if the wind driven generator can reverse the electric meter and thus "sell" excess electric power to the electric utility grid. The complex legal and technical questions associated with a grid-connected wind-energy system will not be discussed here. The purpose of this text is to provide a simple method for estimating both the annual energy production and capacity utilization factor for such a wind-power system.

The power of the wind increases as the cube of the wind speed ($P \sim V^3$). However, it is not economical to utilize fully the extreme power levels occasionally available because most of the time the generator would operate far below capacity in accordance with the cubic power law. Wind machines usually shut down and produce no power during storms for structural and safety reasons. Thus for wind speeds between V_r, the minimum speed required for the rated capacity of the generator, and V_m, the maximum operational speed, the wind machine produces its rated output power, P_r, independent of wind speed.

$$P = P_r \qquad V_r \leq V \leq V_m \qquad (1)$$

$$P = 0 \qquad V_m < V \qquad (2)$$

Because of friction or design limitations, a minimum or "cut in" wind speed, V_i, is required before any power is available. See Fig. 1.

$$P = 0 \qquad V < V_i \qquad (3)$$

Thus the output power of a wind machine is a simple function of wind speed, except in the partial power range ($V_i < V < V_r$). Output in this range is a different function of wind speed for each machine, but several reasonable analytical models can be used to estimate the power available without separate consideration of each machine.

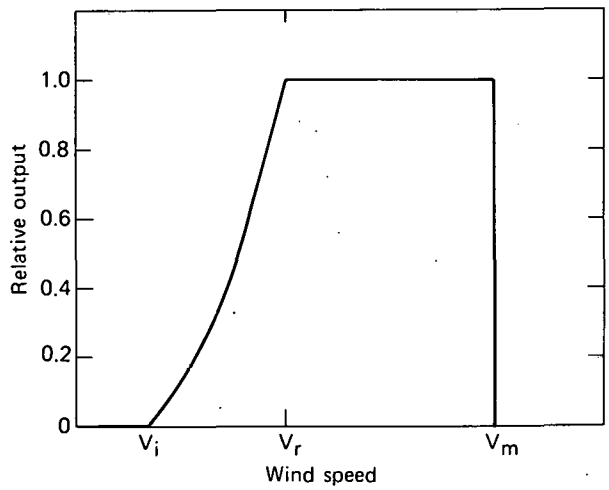

Fig. 1. Output Power vs Wind Speed

PARTIAL POWER FUNCTIONS

Usual Form

The output of a wind machine in the partial power range is usually assumed to have the form:

$$P(V) = a + bV + cV^2. \qquad V_i < V < V_r \qquad (4)$$

The simplest model asumes a linear increase in power from zero at $V = V_i$ to P_r at $V = V_r$. That is, in the simplest model,

$$a = P_r V_i/(V_i - V_r) \quad (5a)$$

$$b = P_r/(V_r - V_i) \quad (5b)$$

$$c = 0. \quad (5c)$$

This model over-estimates the power available. To correct this defect, Justus et al. [1] suggest that

$$a = P_r V_i[V_a - 2V_r(V_a/V_r)^3]/2(V_r - V_a)^2 \quad (6a)$$

$$b = P_r[V_r - 3V_a + 4V_a(V_a/V_r)^3]/2(V_r - V_a)^2 \quad (6b)$$

$$c = P_r[1 - 2(V_a/V_r)^3]/2(V_r - V_a)^2 \quad (6c)$$

where

$$V_a = (V_i + V_r)/2 \quad (6d)$$

because with this set of values for a, b, and c,

$$a + b V_i + c V_i^2 = 0, \quad (7a)$$

$$a + b V_r + c V_r^2 = P_r, \quad (7b)$$

and

$$a + b V_a + c V_a^2 = P_r(V_a/V_r)^3. \quad (7c)$$

This form usually predicts output lower than the simple linear model. Although Eq. (4) often provides a more realistic model of partial output with values of a, b and c taken from Eq. (6) instead of Eq. (5) it can also generate nonsense. Equation (4) predicts negative power output in parts of the partial power range if V_i is less than 26% of V_r when the values of a, b and c are taken from Eq. (6). See Appendix for this calculation.

New Form

The functional form given in Eq. (8) also predicts less output power than the simple linear model and is never negative.

$$P(V) = a + b V^c \qquad V_i<V<V_r \quad (8a)$$

where

$$a = P_r V_i^c/(V_i^c - V_r^c) \quad (8b)$$

$$b = P_r/(V_r^c - V_i^c) \quad (8c)$$

and c is set equal to 2 if only the mean wind speed is known. If more detailed information about the wind is known, then c is set equal to the shape parameter of the Weibull distribution best characterizing the wind speed distribution.

The Weibull distribution is a two parameter function generally useful for characterizing wind speeds. The probability density function, f(V), is given by

$$f(V) = (c/g)(V/g)^{c-1}\exp(-(V/g)^c) \quad c>0, g>0 \quad (9)$$

where c is the shape parameter and g is the scale parameter. The mean wind speed, μ, is

$$\mu = \int_0^\infty Vf(V)dV = g\Gamma(1 + 1/c) \quad (10)$$

and the variance, σ^2, is

$$\sigma^2 = \int_0^\infty (V - \mu)^2 f(V)dV = g^2[\Gamma(1 + 2/c) - \Gamma^2(1 + 1/c)]. \quad (11)$$

The mean wind speed, μ, and the standard deviation, σ, can be determined from wind speed records. Then Eqs. (10) and (11) can be used to determine the Weibull parameters c and g. See reference [2] for discussion of other methods for estimating c and g. See Fig. 2 for illustration of shape parameter effects.

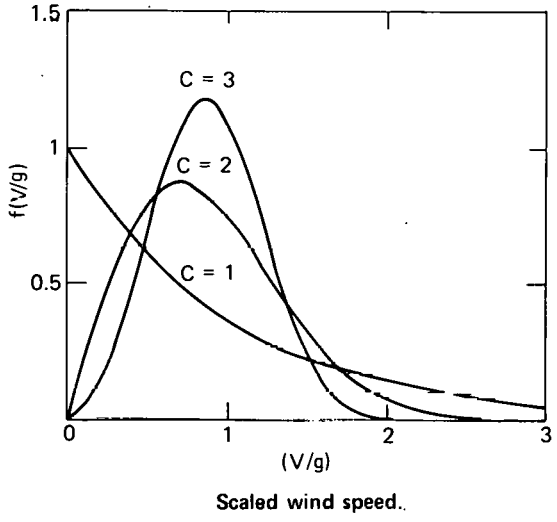

Fig. 2. The Weibull Distribution

The Rayleigh distribution is a special case of the Weibull distribution with c = 2. Often it is sufficiently accurate for analysis of wind-power systems. [3] It will be used to numerically compare the old and new forms of the partial power functions. Table 1 gives the output power at the midpoint of the partial power range, V_a, predicted by Eq. (4) with a, b, and c from Eq. (6). Table 1 also gives the results of Eq. (8) with c = 2 for various design speed ratios, (V_r/V_i). The simple linear model always predicts 50 percent output power at V_a and is not included in Table 1.

TABLE 1. PERCENTAGE OF RATED OUTPUT PREDICTED AT MID-RANGE BY OLD AND NEW PARTIAL POWER FORMS FOR VARIOUS DESIGN RATIOS

(V_r/V_i)	2	3	4	5
$a+bV_a+cV_a^2$	42.2	29.6	24.4	21.6
$a+bV_a^2$	41.7	37.5	35.0	33.3

AVERAGES

Output Power

The average output power computed with Eqs. (1), (2), (3), (8), and (9) is

$$\overline{P} = \int_{V_i}^{V_r} (a + bV^c) f(V)dV + P_r \int_{V_r}^{V_m} f(V)dV. \qquad (12a)$$

$$\overline{P} = \{P_r - a - bg^c[(V_r/g)^c + 1]\}\exp[-(V_r/g)^c] + \{P_r - a - bg^c[(V_i/g)^c + 1]\}\exp[-(V_i/g)^c] - P_r \exp[-(V_m/g)^c] \qquad (12b)$$

Capacity Factor

The capacity factor or ratio of average output to rated capacity is given in terms of the machine design parameters, V_i, V_r, and V_m and the wind parameters, c and g by

$$\overline{P}/P_r = [(V_r/g)^c - (V_i/g)^c]^{-1}\{\exp[-(V_i/g)^c] - \exp[-(V_r/g)^c]\} - \exp[-(V_m/g)^2] \qquad (13)$$

after eliminating a and b in Eq. (12b) with values from Eqs. (8b) and (8c). Numerical methods would have been required in Eqs. (12) and (13) if Eq. (4), the old form, were used instead of Eq. (8) for the partial power range.

Approximations

We can simplify Eq. (13) if we assume a Rayleigh distribution (c=2) and normalize all velocities so that the observed mean wind speed is numerically equal to $(\pi/4)^{1/2}$. This normalization reduces g to unity because $\Gamma(1.5)$ is $(\pi/4)^{1/2}$ in Eq. 10. We will further simplify Eq. (13) by assuming that the last term in Eq. (13) can be neglected. That is, we assume that the energy lost because the machine must shut down during extremely high winds is not a significant part of the total collected at other times. Thus in terms of the normalized wind machine design parameters,

$$v_i = (V_i/\mu)(\pi/4)^{1/2} \qquad (14a)$$

$$v_r = (V_r/\mu)(\pi/4)^{1/2} \qquad (14b)$$

the annual capacity factor of the wind machine is

$$\overline{P}/P_r = [\exp(-v_i^2) - \exp(-v_r^2)]/(v_r^2 - v_i^2). \qquad (15)$$

If we further assume that wind machines with different rated speeds are equally efficient when operating at their rated speeds, then the maximum output power is proportional to the cube of the rated speed. Also the annual energy yield, E, is proportional to the product of capacity factor and v_r^3. That is

$$E \sim v_r^3[\exp(-v_i^2) - \exp(-v_r^2)]/(v_r^2 - v_i^2) \qquad (16)$$

assuming that Eq. (15) can be used instead of Eq. (13) for the capacity factor.

ILLUSTRATIONS

The energy computed with Eq. (16) has a definite maximum for each (V_r/V_i) ratio as illustrated in Fig. 3. The curves in Fig. 3 have been normalized relative to the peak of the $(V_r/V_i) = 5$ case. Inspection of Fig. 3 shows that a machine designed with $V_r = 4\ \mu$ and $V_i = 0.8\ \mu$ can produce approximately 2.3 times more energy than a machine with $V_r = 2\ \mu$ and $V_i = \mu$.

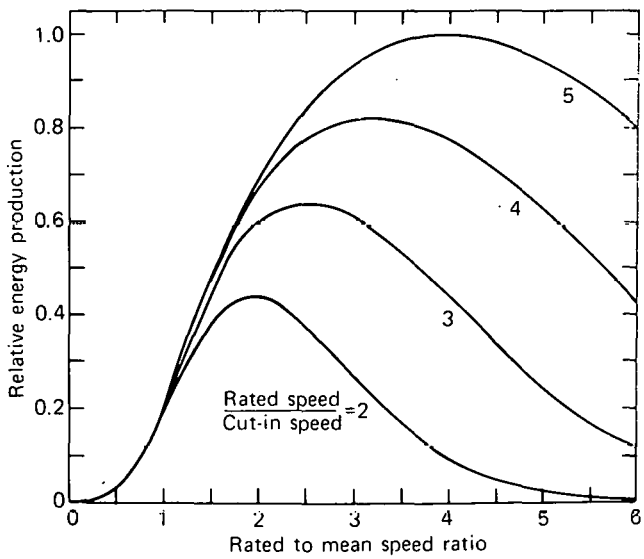

Fig. 3. Annual Energy Production

Machines with higher rated capacity produce more energy annually and should have their rated speed larger than the mean wind speed as illustrated in Fig. (3). However such machines cost more than a

machine of lower capacity, and as illustrated in Fig. (4), they are not as well utilized. Fig. (4) gives the capacity factor computed with Eqs. (14) and (15) to illustrate this point. Thus the choice of a wind machine for a particular application is a compromise between the greater energy available as rated capacity increases and the greater utilization of capital invested possible with machines of more limited capacity. Each application must be considered separately, but the analytical model developed here illustrates quantatively the choice to be made.

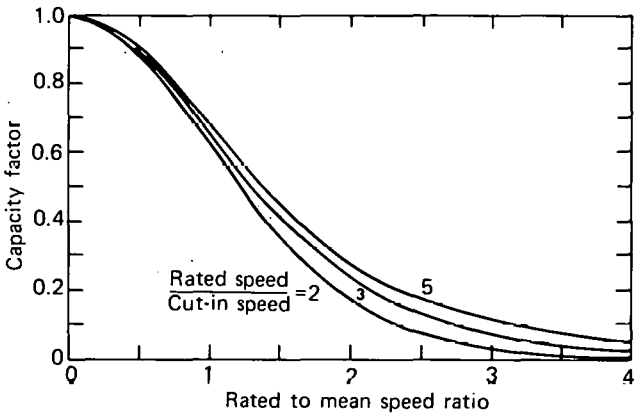

Fig. 4. Capacity Factor vs. Speed Ratio

ACKNOWLEDGEMENTS

This work was supported by the U. S. Navy under Contract N00017-72-C-4401 and by the U. S. Coast Guard Office of Research and Development.

REFERENCES

1. C. J. Justus, et al., Nationwide assessment of potential output from wind-powered generators, J. Appl. Meteor. 15, 673-678, (1976).
2. G. G. Justus, et al., Methods for estimating wind speed frequency distribution, J. Appl. Meteor. 17, 350-353, (1978).
3. J. C. Doran, et al., Accuracy of wind power estimates, Battelle Pacific Northwest Laboratories report PNL-2442, p. 18 (1977).

APPENDIX

The power at V_i is zero and the slope of the power function given by Eqs. (4) and (6) can be negative at V_i if

$$b + 2cV_i < 0 \tag{A1}$$

or since $P_r(V_r - V_a)^2$ is inherently positive if,

$$[V_r - 3V_a + 4V_a(V_a/V_r)^3] + 2[1 - 2(V_a/V_r)^3]$$

$$(2V_a - V_r) < 0 \tag{A2}$$

or,

$$(V_a/V_r)^3 < (1/4) \tag{A3}$$

or if,

$$(V_i/V_r) < 2(1/4)^{1/3} - 1 = .26 \tag{A4}$$

Thus if the "cut-in" speed is less than 26% of the rated speed, Eq. (4) with a, b and c from Eq. (6) predicts negative output power in a portion of the partial power range adjacent to V_i. Equation (4) with a, b and c from Eq. (6) can be solved for a velocity inside the partial power range, V_o, such that $P(V_o) = 0$, if $(V_i/V_r) < .26$. Equations (4) and (6) predict negative output for $V_i < V < V_o$. and positive output power for $V_o < V < V_r$. For example, if $(V_i/V_r) = .2$, the negative power portion of the range is 12% of the total range. The relative error in computed power is much smaller.

The transition between Eqs. (12a) and (12b) is facilitated by:

$$\int (c/g)\exp[-(V/g)^c]V^{c-1}dV = -g^{c-1}\exp[-(V/g)^c \tag{A5}$$

and

$$\int (c/g)\exp[-(V/g)^c]v^{2c-1}dV = -g^{2c-1}[(V/g)^c + 1]$$

$$\exp[-(V/g)^c]. \tag{A6}$$

SOLAR DISTRICT HEATING MODEL FOR AN AZIMUTH-TRACKING FLOATING CONCENTRATOR ON A SEASONAL-HEAT-STORAGE RESERVOIR

By

C. Brent Cluff, Associate Hydrologist, Water Resources Research Center
Robert B. Kinney, Professor, Department of Aerospace and Mechanical Engineering
University of Arizona

ABSTRACT

The development of a computer model which sizes the floating concentrator and seasonal heat-storage reservoir needed to operate solar district-heating and-cooling systems is reported. A prediction of the water temperature variation with time in the storage reservoir is obtained using a Fourier series type analysis.

The model has been applied to districts composed of 10, 50 and 250 individual residences. A 4459 m^2 (98,000 ft^2) circular collector on a 10.7 m (35 ft) deep reservoir will provide the 250-home subdivision with 100 percent of the space heating and domestic hot water in an average year. This is approximately 17.8 m^2 (192 ft^2) per home which is one-third that required without annual storage. This reduction in area should more than compensate for the cost of insulation and distribution of the hot water from the patented centralized collector system. A utility operated system would have the convenience and dependability that consumers are now experiencing with non-renewable sources of thermal energy.

INTRODUCTION

In most regions of the country, insolation is most abundant during the spring, summer and fall months when space heating demands are minimum. That is, the peak in the seasonal heating demand occurs at a different time than that in the solar cycle.

Annual thermal storage, providing it can be done economically, offers a means for utilizing the off-season peak periods of solar irradiation. In this concept, collected thermal energy is stored over extended periods for later distribution to the heating load. If desired, solar-powered refrigeration can also be included in the duty cycle.

A possible economical method of seasonal or annual storage of solar energy involves the joint use of a floating solar collector on a water reservoir. The reservoir would be made with sufficient depth to provide the required thermal storage.

Components of this collector-reservoir system have been under test by the principal author for the past five years [3]. The system is described in U.S. patent number 4148301 [8]. A platform, on which are mounted parabolic-trough concentrating collectors, floats on water contained in the reservoir. The reservoir is excavated so that thermal losses can be better controlled. The floating platform, which is made of light but rigid insulating material, effectively blocks evaporation and reduces heat losses to the air.

The platform rotates about a central pivot point to track the sun in the azimuthal direction. Little power is required to rotate the platform, owing to the low frictional drag exhibited by the water.

It is envisioned that annual heat storage would best serve a small community of residences, either for single or multiple families, in which the solar collection, storage, and distribution is done centrally. The concept has received considerable recent attention in Sweden, and a demonstration heating plant is now in operation, with a second one under construction [6].

In this paper, the feasibility of utilizing annual thermal storage in the Southwest is explored. A simple and straight forward computer simulation of the annual thermal cycle is developed, and conceptual designs for different sizes of single-family housing developments are presented.

COMPONENT TESTING

Several prototype floating collectors have already been built and tested at the University of Arizona. Commercially available parabolic-trough reflectors and tracking mechanisms have been incorporated into the prototypes. The first floating collector was constructed in the summer of 1977 [3]. This unit is shown in Figure 1 following the manuscript. It consists of five 0.22 x 6.10 m. (4 x 20 ft) parabolic troughs mounted parallel, adjacent to each other, on a 8.53 m (28 ft) diameter platform. The collector was manufactured by Sun Power Systems, Inc. It is tracked using a light-weight chain-link drive around the perimeter. The 0.062 kJ-sec. (1/12 h.p.) drive motor is activated using a shadow bar sensor. The platform was constructed using wax-impregnated expanded polystyrene. It is floating in a 15.2 cm

(6 inch) deep pool on the roof of the Civil Engineering Building.

A 4.27 m (14 ft) diameter dual tracking system was built for Sensor Technology, Inc. to demonstrate intermediate concentration of photovoltaic panels [3]. It was driven using a motor activated windless rope drive around the perimeter.

A third 23.8 m (256 ft^2) collector system rotating on a 7.3 m (24 ft) diameter pool 10.2 cm (4 inches) deep was constructed in the summer of 1979, as shown in Fig. 2. This unit was constructed to provide 5x-sun concentration for commercial terrestrial photovoltaic panels. The 2.44 m (8 ft) wide intermediate concentrator is a segmented parabola that evenly illuminates a 30.5 cm (12 inch) wide photovoltaic panel. The segmented design allows the use of inexpensive back surface glass mirrors. This type of concentrator can also be used to produce thermal energy for the annual storage system. This system used a center pivot tracker which simplifies the construction particularly for smaller systems. This is shown in Fig. 3. For larger systems a propeller or water jet drive with either a pivot point or peripheral braking system can be used. The prototype of this type of system has been successfully tested.

The 2.74 m (9 ft) wide Hexcel parabola collector is presently being tested in an azimuth mode. This highly efficient collector utilizing a honeycomb aluminum construction is performing satisfactorily at low sun angles experienced in the winter months. Although the aperture is 2.74 m (9 ft) the collector, when laying flat, extends only 0.61 m (2 ft) above the platform. See Fig. 4. It was the estimated annual efficiencies from this collector that were used in the simulation of the floating collector-reservoir system.

SIMULATION AND DESIGN APPROACH

The main task is to determine the size of the collector and thermal storage reservoir to be used with each housing development. The reservoir is assumed to be excavated below ground level in the shape of an inverted truncated cone. A schematic of the system is shown in Fig. 5.

The hourly and daily reservoir temperature variations are not pertinent to this study. Rather, it is the variation over an annual cycle which is of interest. Therefore, a time increment of one week was selected.

A ranch style house typical to the southwest was taken to be representative of those in the housing development. Heat transfer parameters for the structural components were determined from handbook tabulations [1], and space heating and cooling loads were determined for a single 24-hour period each week using the Total-Equivalent-Temperature-Difference method. These values were then multiplied by a factor of seven to give weekly averages.

In these calculations, the hourly difference between the assigned inside temperature which varied between 293 and 298° K (68 and 78° F) over the year and the outside air temperature was first determined. The latter temperatures were taken from historical records for Tucson. For surfaces receiving direct solar irradiation, the sol-air temperature was used in place of the outside air temperature. An average temperature difference was next computed for the 24-hour period, and this was multiplied by the U-factors and appropriate areas in order to obtain a daily total for the heat transfer to each house. This was assumed to be representative for each day of the week in question.

The heating demand was taken to be the direct heat loss from each house. In the calculation of the cooling load, a factor of 1.667 was applied to the heat gain calculated for each house in order to determine the heat energy required. This corresponds to a Coefficient of Performance for the cooling equipment of 0.60.

A level demand for domestic hot water was assumed to exist throughout the year. This amounted to 3.94×10^5 kJ's (3.74×10^5 Btu's) per house per week and corresponds to 3028 l (800 gal U.S.) raised in temperature by 286° K (56° F). Using the above procedure, the heating demand to be imposed in the thermal balance applied to the reservoir was obtained. The heating supply, provided by the solar collectors, was determined using the second law for zenith distance angles modified by A. Meinel [7]. The solar flux was further reduced by cloud factors for Tucson. Hourly insolation values were computed for a representative day of each week of the year. A collector efficiency that varied from a maximum of 58 percent to a minimum of 46 percent at a solar angle of 10° was used. This reduction in efficiency coupled with the cosine effect and reduced solar insolation results in insignificant collection of energy much below a sun angle of 10-15°. The annual heating supply used in the computer simulation was 44.8 percent of the total measured insolation for a flat surface in Tucson as given by Meinel [7]. It appears that this is realistic if a parabolic trough as efficient as the Hexcel is used.

The losses to the soil from the bottom and side of the reservoir were estimated using results for an unsteady one-dimensional heat-conduction model. The thermal penetration depth into the soil was first determined for an imposed sinusoidal temperature variation on the interface between the reservoir and soil. The period was taken to be one year. Because the temporal variation is relatively slow, it is reasonable to approximate the soil temperature distribution at any time by a linear variation from the interface temperature to the undisturbed ground temperature, the latter being allowed to vary seasonally. The thermal resistance of the wall material of the reservoir was assumed to be negligible, so that the effective U-factor for the bottom and side is given by the soil thermal conductivity divided by the penetration depth.

Having thus obtained the energy demand, supply, and losses to be imposed on the thermal reservoir, an energy balance was written and an equation was derived for the temperature of the fluid, taken to be water and fully mixed. This derivation plus numerical values used for the transfer coefficients are presented in the next section.

As previously mentioned, the reservoir size is the main quantity to be determined in the present conceptual design. This was obtained using successive approximations in the following manner. Trial reservoir dimensions and solar-collector area were selected. The week-by-week reservoir temperatures were computed and listed. Minimum and maximum acceptable temperatures were preselected to be 322 and 366° K (120 and 200° F) respectively. The former is acceptable for domestic hot-water and space heating, whereas the latter is below the normal boiling point. If the computer reservoir temperatures were not within these bounds, then new trial values for the reservoir dimensions and collector area were assumed and the calculations repeated.

The depth of the reservoir was restricted to no more than 12.2 m (40 ft) for practical reasons. The surface diameter had to be sufficient to accomodate the collector area needed.

Acceptable designs were achieved within five or six trials. It was found that for a fixed reservoir size, increased collector area generally shifted the entire temperature levels upward. On the other hand, for a fixed collector area, the larger the reservoir the smaller was the difference between the maximum and minimum temperatures. Thus a reservoir size could first be determined such that the computed difference between the temperature extremes was approximately 44° K (80° F). Then the entire curve could be shifted upward or downward by increasing or decreasing the collector area.

In this manner the design parameters for representative housing developments were obtained. Specific results will be presented and discussed in a later section.

ANALYSIS

Determination of Reservoir Temperature

An energy balance performed on the reservoir requires that the energy supplied in excess of that delivered to the load and attributed to losses must be stored as internal energy. For a fully mixed system, one has in equation form

$$mc\frac{dT_f}{dt} = \dot{Q}_{supply} - \dot{Q}_{demand} - [U_T A_T (T_f - T_a) - (U_s A_s + U_b A_b)(T_f - T_g)] \qquad (1)$$

In the foregoing, the terms in square brackets represent the losses from the top, side, and bottom of the reservoir.

The fluid temperature, T_f, is the unknown of interest. The air temperature, T_a, and ground temperature, T_g, are all prescribed functions of time and are considered known. This is true of $\dot{Q}_{supply}$ and $\dot{Q}_{demand}$ as well. The mass, m, specific heat, c, areas and U-factors are all constants.

Proceeding with the solution of Eqn. (1), it is best to rewrite it in the following general form,

$$\frac{dT_f}{dt} + \frac{b}{a} T_f = \frac{1}{a} f(t) \qquad (2)$$

where $b = (U_t A_t + U_s A_s + U_b A_b)$

$a = mc$

$$f(t) = \dot{Q}(t)_{supply} - \dot{Q}(t)_{demand} + U_t A_t T(t)_a + (U_s A_s + U_b A_b)\, T(t)_g$$

This equation can be solved in closed form. The right-hand side of Eqn. (2) is a periodic function of time, and can therefore be represented by a Fourier series as follows,

$$f(t) = A_o + \sum_{n=1}^{\infty} A_n \cos\frac{2n\pi t}{\tau} + \sum_{n=1}^{\infty} B_n \sin\frac{2n\pi t}{\tau} \qquad (3)$$

where $A_o = \frac{1}{\tau}\int_o^t f(t)\,dt$

$$A_n = \frac{2}{\tau}\int_o^t f(t)\cos\frac{2n\pi t}{\tau}\,dt$$

$$B_n = \frac{2}{\tau}\int_o^t f(t)\sin\frac{2n\pi t}{\tau}\,dt$$

In evaluating the foregoing integrals, values for f(t) were first tabulated for each week of the year, and the quadratures were calculated using Simpson's rule over the total period, τ, equal to 52 weeks.

The solution to Eqn. (2) is given by

$$T_f = e^{-bt/a}\left[\int_o^t \frac{e}{a}^{b\xi/a} f(\xi)\,d\xi + C\right] \qquad (4)$$

The first term in the brackets arises from the particular solution to the complete equation, and the constant, C, arises from the complementary solution to the homogeneous equation. Note that ξ appearing in Eqn. (4) is a dummy variable of integration.

Upon substituting Eqn. (3) into Eqn. (4), the integrations can be carried out and there results

$$T_f = e^{-bt/a}\left[\sum_{n=1}^{\infty} \frac{\left(\frac{2n\Pi}{a\tau} B_n - \frac{b}{a^2} A_n\right)}{\left(\frac{b}{a}\right)^2 + \left(\frac{2n\Pi}{\tau}\right)^2} - \frac{A_o}{b} + C\right]$$

$$+ \frac{A_o}{b} + \sum_{n=1}^{\infty} \frac{\left(\frac{b}{a^2} A_n - \frac{2n\Pi}{a\tau} B_n\right)}{\left(\frac{b}{a}\right)^2 + \left(\frac{2n\Pi}{\tau}\right)^2} \cos \frac{2n\Pi t}{\tau}$$

$$+ \sum_{n=1}^{\infty} \frac{\left(\frac{b}{a^2} B_n + \frac{2n\Pi}{a\tau} A_n\right)}{\left(\frac{b}{a}\right)^2 + \left(\frac{2n\Pi}{\tau}\right)^2} \sin \frac{2n\Pi t}{\tau} \qquad (5)$$

In the foregoing, the first term on the right-hand side represents a pure transient which disappears with increasing time. The remaining terms are the purely "steady-periodic" portion of the solution, and they are the only ones of interest to this study.

The final solution can be put into a more convenient form for computations if a trignometric identity is used to introduce the phase angle, α_n. The resulting expression becomes

$$T_f = \frac{A_o}{b} + \sum_{h=1}^{\infty} \frac{A_n/b}{\left[1+\left(\frac{2n\Pi a}{b\tau}\right)^2\right]^{1/2}} \cos\left(\frac{2n\Pi t}{\tau} - \alpha_n\right)$$

$$+ \sum_{n-1}^{\infty} \frac{B_n/b}{\left[1+\left(\frac{2n\Pi a}{b\tau}\right)^2\right]^{1/2}} \sin\left(\frac{2n\Pi t}{\tau} - \alpha_n\right) \qquad (6)$$

In this form, it is apparent that the reservoir temperature lags behind the imposed forcing function, f(t), by the angle α_n. The lag angle, equal to $\tan^{-1}(2n\Pi a/b\tau)$, is different for each of the harmonics of the forcing function. If f(t) were given by either a pure sine or cosine variation, then only the fundamental would be present, corresponding to n = 1. In the case of the present study, the first ten harmonics were retained. That is, the series were truncated after ten terms.

In the computer calculations, numerical values were substituted for the constants a and b, and the coefficients A_o, A_n, and B_n were evaluated using numerical integration. The fluid temperature was then calculated from the analytical expression derived above. Values for the various transfer coefficients needed for these calculations are presented in the next section.

Evaluation of Transfer Coefficients

The top of the reservoir (i.e. the floating platforms) was assumed to be a slab of polyurethane foam .1525 m (.5 ft) thick. The thermal conductivity was taken to be .02306 joule/s·m·K (.0133 Btu/h·ft·F). The film coefficient on the water side was assumed to be very large, and that on the air side was assigned the value 34.07 joule/s·m^2·K (6.0 Btu/h·ft^2.F). These give for the U-factor assigned to the top

$$U_t = \frac{1}{1/34.07 + .1525/.02306} = .1505 \text{ joule/s·}m^2\text{·K}$$

As discussed in a previous section, the U-factor used for the side and bottom was taken to be the thermal conductivity of the soil divided by the penetration distance of an imposed sinusoidally varying temperature at the interface between the reservoir and the soil. This penetration distance is given by $L = 5.65\sqrt{K/w}$, where K is the thermal diffusivity of the soil (taken to be .002 cm^2/s) and w is the circular frequency of the oscillation. The period of the imposed oscillation is one year or 3.1536×10^7 seconds. The penetration depth is thus $L = 5.65(.002 \times 3.1536 \times 10^7/2\pi)^{1/2}$ cm or approximately 5.65 m. For a thermal conductivity of the soil equal to .263 joule/s m K, one obtains

$$U_s = U_b = .263/5.65 = .0466 \text{ joule/s } m^2 \text{ K}$$

RESULTS

Optimum designs were obtained for a 10, 50 and 250 home subdivision for seasonal storage of solar heat for space and domestic hot water. All designs were obtained for refrigeration plus the space and domestic hot water.

In all designs an azimuth tracking parabolic array was used. This type of array collects a maximum amount of sunlight per unit area of land occupied since the entire surface is covered. The results are shown in Table 1 near the end of the article

Fig. 6 at the end of the publication is a graphical representation of the solar insolation, the domestic hot water and space heating demand for the 250 home subdivision. It also gives the average weekly temperature of the storage reservoir for this example.

The results are similar for the three sizes of subdivisions investigated. For the 10 home subdivision size, in order to keep the bottom diameter large enough to accommodate construction equipment the depth was reduced and the surface area increased. The percentage of surface area covered with a collector was reduced to 61. For the small subdivisions where excess platform area is available and the collectors can be spaced to reduce shadowing it may be more cost effective to use an altitude tracking array on the azimuth tracking platform. This dual tracking system will be more efficient particularly in the winter and should further reduce the required size of the storage. For the larger system where excess platform area is not available the simple azimuth tracking system would probably be more effective. The relation between the best type of collector and the size of subdivision needs to be researched

further. It was beyond the scope of this initial research effort.

The designs did show a significant reduction of the size of collector needed when annual storage was used in conjunction with domestic hot water and space heating; a lesser but still significant reduction was experienced when solar powered refrigeration was added.

Table 1 shows the storage efficiency (Energy Used/ Energy In x 100) ranged from 82.4 to 89.4 percent. The efficiency of the 10 home subdivision was reduced since the depth for reasons described above was made less than the other two subdivision sizes. This reduced depth increased the surface area and therefore increased the losses.

The storage losses on all systems except for the 10 home space and domestic hot water design were approximately 12 percent. This does not include the 10 percent losses that were estimated for delivery. Total losses of storage and delivery were approximately 22 percent.

The above system furnished 100 percent of the subdivisions' space conditioning and domestic hot water in an average year. Generally, solar systems are designed to furnish 60 or 70 percent in order to be cost effective. With annual storage, 100 percent systems in an average year can be achieved. For instance, centralized back up systems would only be used on space heating designs in years when the temperatures were below average in the winter. An above-average temperature in the summer might require the operation of the back up heat source in systems supplying air conditioning.

ECONOMICS

The presentation of a complete economic analysis of the floating-solar-annual-storage system is beyond the scope of this paper. The economics would depend on several factors including the site selected, the soil conditions, climate, the size of system and the spacing of the homes to be served.

There are some money saving features of the system such as the close proximity of the collector with regard to the storage. Several circulation systems through the collector into the storage could be used to reduce both pumping and piping costs. The use of the floating system rules out the installation of expensive footings that would otherwise be used in fixed altitude tracking systems. The platform would easily bolt together on the reservoir which would be previously filled with water. With the azimuth tracking system there would be a maximum collection of energy per unit of land occupied.

As compared to the value of electricity in Tucson the system would collect $500,000 worth of thermal energy per hectare (2.5 acres) per year. Due to this high rate of return the cost of land to put the system on should not be a problem.

The district heating approach would not require a backup system in each home. Only a central back-up system such as a coal or butane gas fired central boiler would be needed. This is a considerable savings. The cost of distribution of heat from a central source using a water media is not formidable. There are many "district heating" systems in Europe that are operating satisfactorily [5]. These systems are reported to have distribution heat losses of 5 to 10 percent. Experience from lining salt gradient solar ponds can be used to line reservoirs for the system under discussion [2].

A summary of a cursory economic analysis is found in Table 2. It does not include the cost of the land. The basis for this analysis is found in an Arizona Solar Energy Commission completion report [4].

DISCUSSION AND CONCLUSION

The simulation program has provided a method whereby annual storage systems using floating solar collector can be sized. The program shows that an overall efficiency much greater than open salt-gradient solar ponds can be expected.

The computer program needs to be refined to include among other things distribution losses. A simulation of the expected stratification in the reservoir would also be useful. This information is needed with regard to operation of water chillers in the summer. In order to maintain the high summer temperatures needed for these systems water would have to be taken from storage at the highest temperature. A means of selective removal at the appropriate level in the reservoir would be desirable. If necessary the collection system could be operated at a higher temperature to maintain an appropriate layer of hotter water. In the winter, as the temperature in the reservoir drops, the collector could be operated at a lower temperature to increase the efficiency.

A 15 to 20 home demonstration of the system is needed to verify the program, define any unforeseen operational problems and clarify the economics of the system.

The solar district heating system should be well accepted by both utilities and consumers. The utilities now selling non-renewable fuels could build and operate the solar district systems. Retrofitting would be more difficult than building the unit at the time of construction of the subdivision. However connecting each house to an insulated twin pipeline and installing the necessary heat exchanges would be far simpler than any other type of solar retrofit. In older neighborhoods the system could be established on a vacant lot, by closing of an appropriate street or intersection or by purchasing and clearing of a house or two. Due to the relatively high collection and storage efficiency the amount of land needed per subdivision is relatively small.

Finally, a utility owned and operated system would provide the consumer with the dependability and convenience that they are used to with their non-renewable sources of thermal energy.

ACKNOWLEDGMENTS

The authors acknowledge the help of F. Eskandani, a mechanical engineering graduate student who helped on the project.

A. Gilkes, Research Specialist, has provided considerable input to the design, construction and testing of the components of the project; his help is appreciated.

The help of Dr. T. Triffet, head of the Engineering Experiment Station and C. Glickman of the Solar Research Facility is appreciated.

Finally, the support of Jim Warnock of the Arizona Solar Commission who provided funding is gratefully acknowledged.

BIBLIOGRAPHY

[1] ASHRAE Handbook - 1977 Fundamentals, Chapter 26, Published by ASHRAE, 345 E. 47th St., New York, N.Y., 10017, 1977.

[2] Bryant, H. C. and F. Zangrando, "A Salt Gradient Solar Pond," Solar Age, April 1978.

[3] Cluff, C. B., A Floating azimuth-tracking platform - an economic method of increasing solar collector efficiency," Proceedings of the 1978 Annual Meeting, Denver, Colorado, American Section of the International Solar Energy Society, Inc., Volume 2.1.

[4] Cluff, C. B., R. B. Kinney and F. Eskandani, An Evaluation of Annual Heat Storage of Solar Energy for Arizona Subdivisions Using an Azimuth Tracking Floating Collector, Final Report to the Arizona Solar Commission, Solar Research Facility, Engineering Experiment Station, University of Arizona, August 1979.

[5] Diamant, R. M. S. and J. McGarry, Space and District Heating, London Iliffe Books Ltd., 1968.

[6] Margen, Peter, "Central Plants for Annual Heat Storage," Solar Age, October, 1978.

[7] Meinel, A. B. and M. P. Meiner, Applied Solar Energy, Addison-Wesley Publishing Company, Reading, Mass., 1976.

[8] United States Patent 4,148,301, Water-Borne Rotating Solar Collecting and Storage Ssytems. C. Brent Cluff, inventor, issued April 10, 1979.

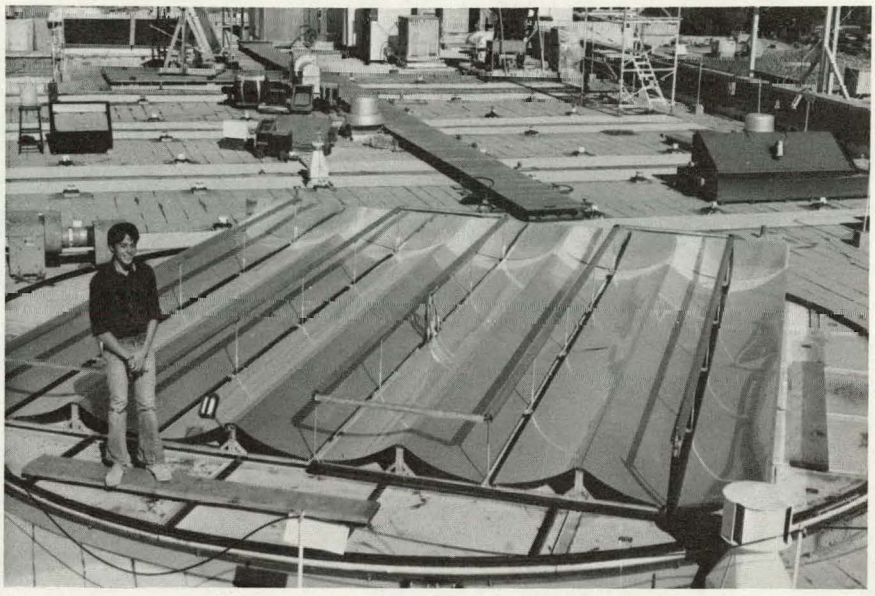

Figure 1. Floating azimuth tracking 1.22 m aluminum parabola.

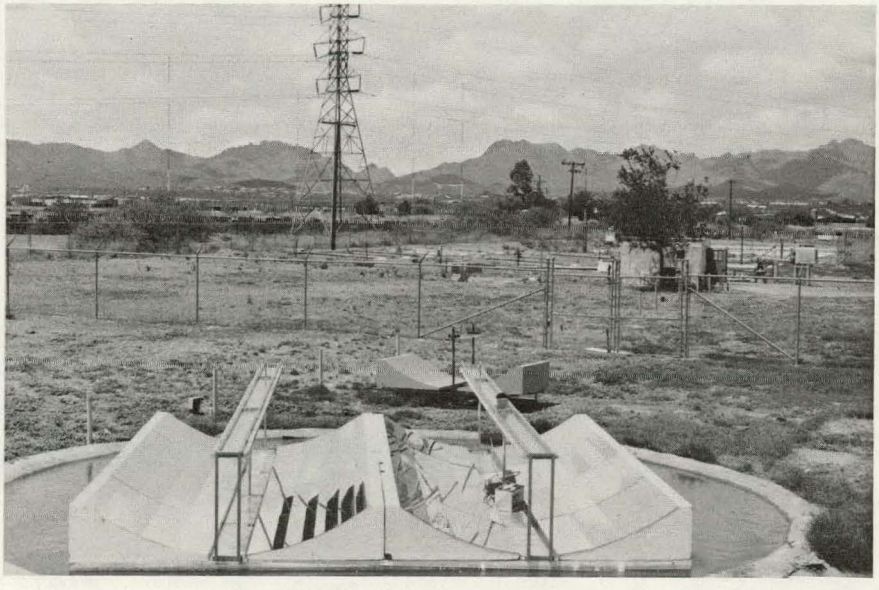

Figure 2. Floating azimuth tracking segmented parabola concentrator.

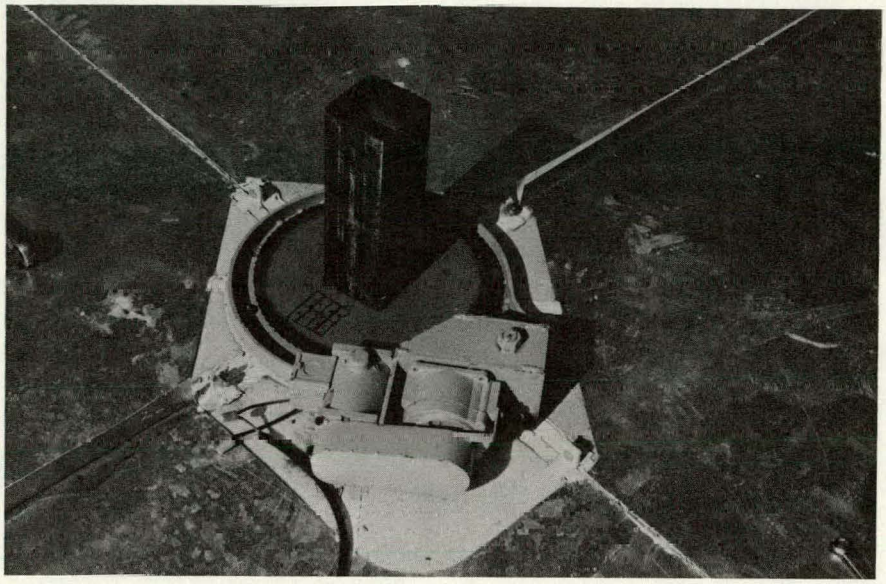

Figure 3. Center pivot drive for azimuth tracking floating platform.

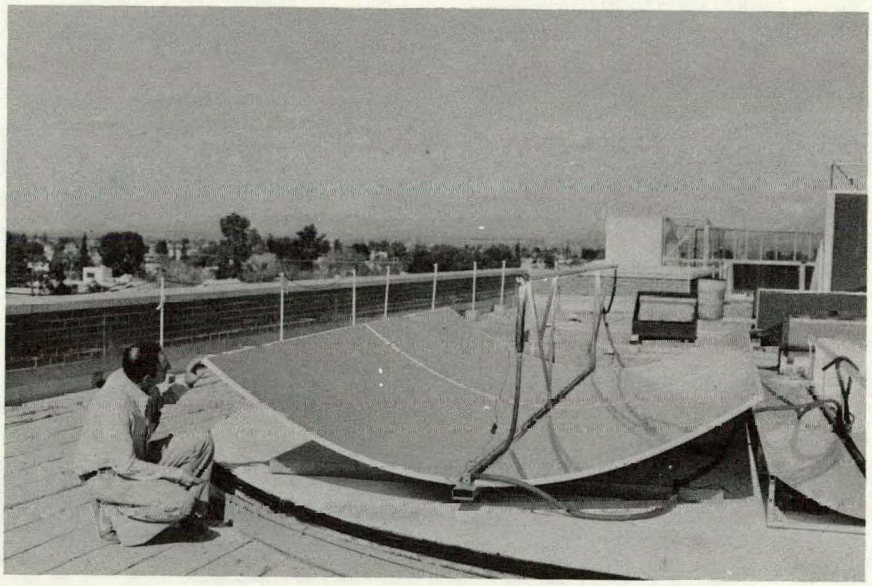

Figure 4. Hexcel parabolic collector on azimuth tracking platform.

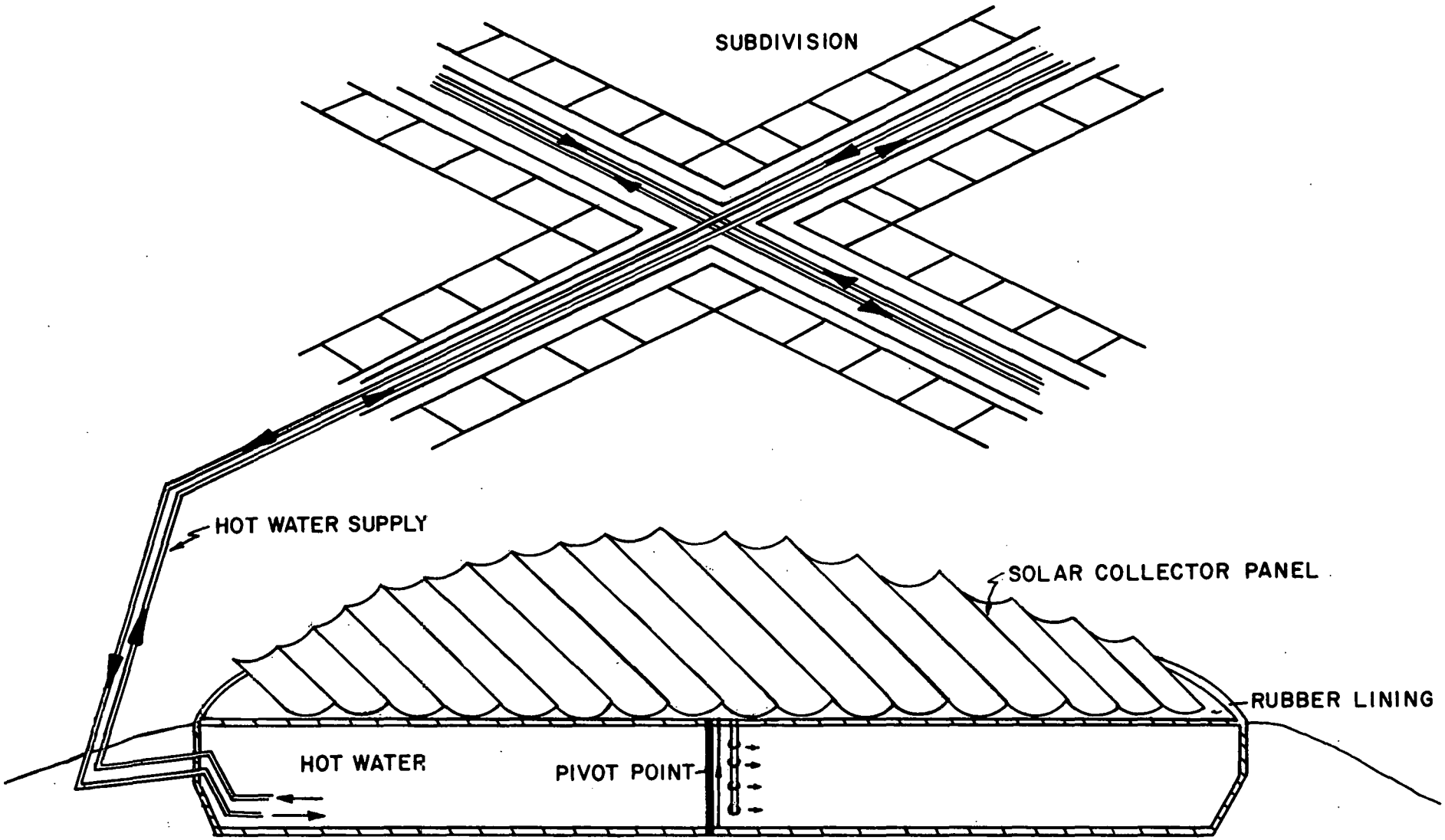

RESERVOIR SCHEMATIC OF SEASONAL CENTRAL SOLAR HEAT SYSTEM
USING FLOATING SOLAR COLLECTOR ON HEAT STORAGE RESERVOIR
ENGINEERING EXPERIMENT STATION
UNIVERSITY OF ARIZONA, FEBRUARY 1979

Figure 5

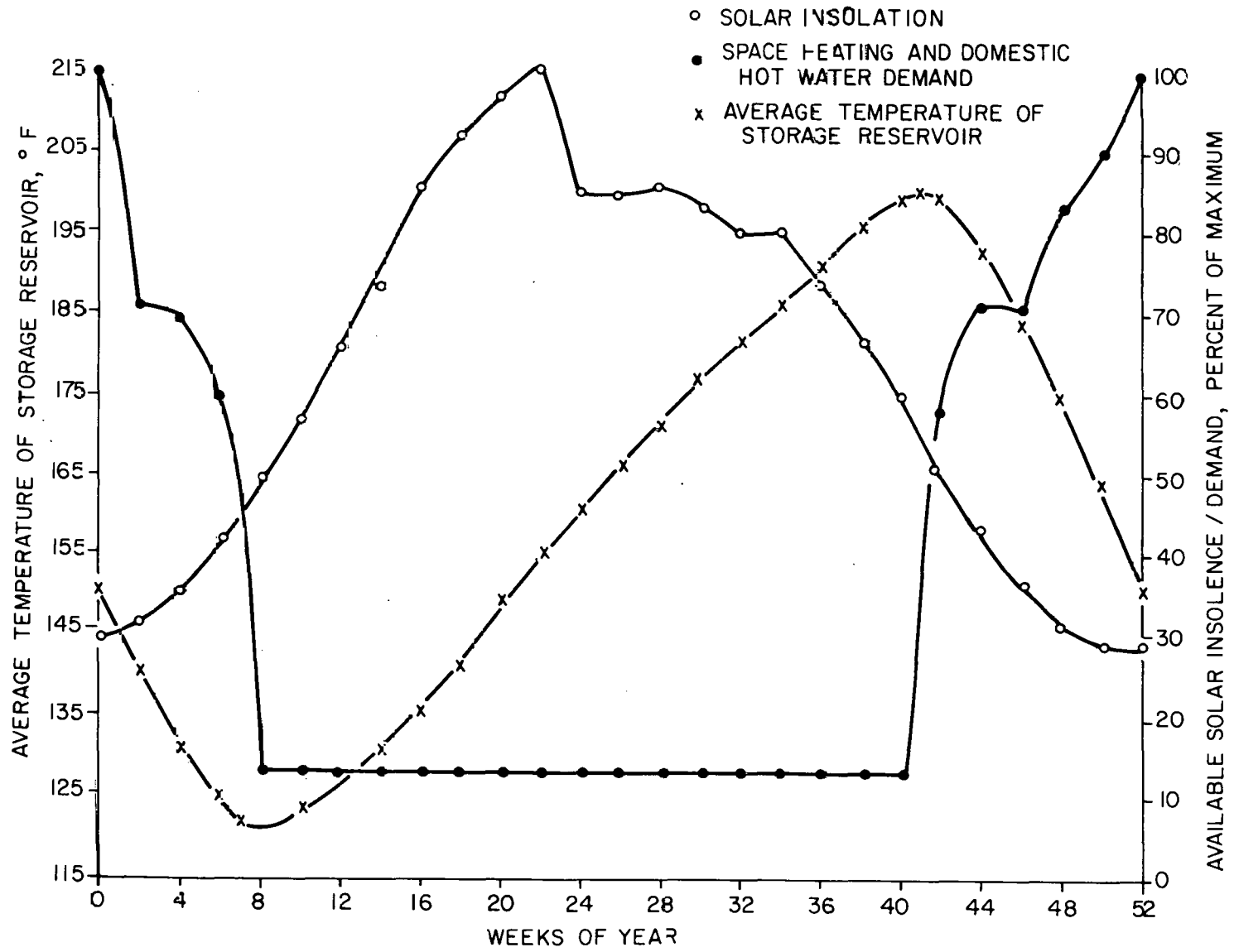

Figure 6. Graph showing relation between insolation, space heating and domestic hot water demand, and temperature of storage reservoir for a 250 home subdivision.

TABLE 1

CENTRAL STORAGE OF HEAT FOR SPACE CONDITIONING
AND DOMESTIC HOT WATER AZIMUTH
TRACKING SOLAR COLLECTOR

	Reservoir Parameters			Storage Water Temperature		Collector Area		
	Surface Area	Dia.	Depth	Min.	Max.	Total	Per House	Storage* Efficiency
	m^2	m	m	^oK	^oK	m^2	m^2	Percent
10								
Heating	319	20.1	8.5	322	367	194	19.3	82.4
Heating & Cooling	394	22.5	6.7	331	164	375	37.4	88.2
50								
Heating	1026	36.3	11.3	321	366	903	18.0	88.4
Heating & Cooling	1904	24.6	6.7	336	365	1866	37.3	88.7
250								
Heating	4680	78.0	10.7	323	366	4448	17.8	89.8
Heating & Cooling	9457	109.7	6.1	335	365	9269	37.0	89.3

* Storage efficiency is the energy output/energy input X 100.

TABLE 2

CAPITAL COSTS
SOLAR DISTRICT HEATING IN TUCSON, AZ. WITH
ANNUAL STORAGE OF 250 HOME SUBDIVISION*

	Low	High	
Parabolic Collector	$	$	
15-cm Foam Tracking Platform	38	38	
Excavating & Lining	27	27	
Circulation	5	5	
Distribution**	27	27	
Total Installed	140	205	
Engineering & Contingencies @ 40%	56	82	
Subtotal	196	287	
Royalties & Profit @ 20%	39	57	
TOTAL COST PER SQ. METER	235	344	
TOTAL COST PER HOUSE	$4182	$6123	
Tax Credits/House (State & Federal)	$2050	$3000	(Max)
Estimated Savings/House***	500	500	
NET COST PER HOUSE	$1632	$2623	
AMORTIZATION COST PER HOUSE (12% interest with a 20-year life)	$ 218	$ 352	

* Costs are per square meter of collector unless otherwise indicated.
** Distribution costs are based on a spacing of 3 homes per acre.
*** The savings is the estimated difference between the cost of gas furnace and solar heat exchangers.

Session VB

Dr. John Andrews
Brookhaven National Laboratory
Chairperson

COMPONENT SIMULATION MODELS

SOLAR "BREADBOX" SIMULATION USING D.A.T.A.'S TBBX CODE

Bruce T. Maeda Bruce Melzer

Davis Alternative Technology Associates

(D.A.T.A.)
P.O. Box 470
Davis, CA 95616

ABSTRACT

D.A.T.A. has developed a computer code for the simulation of passive or integral solar hot water heaters, sometimes referred to as "breadboxes". This code was derived from and is similar to a code used for simulating passive solar design of structures, denoted SOLSIM. Parametric simulations were run to evaluate operational influences on breadbox performance. Simulations were used to evaluate breadbox design for a breadbox installation project in Indio, California. Breadbox simulation indicates that convective/conductive gains in breadboxes are of equal magnitide to direct solar absorption. Simulations are compared to a monitored breadbox system in Davis, California.

INTRODUCTION

Historical Overview

Solar "breadbox" hot water heaters (hereafter termed breadboxes) are defined as solar water heaters which combine storage and collection in a single integrated system. They usually consist of black metal water tanks placed in an insulated box with a transparent or translucent cover. They may have an insulated shutter or lid which is operable to reduce nighttime heat losses through the cover. The "classical" system is currently considered to be the design of Zomeworks Corporation, although a wide variety of new designs have been developed. Older designs not only existed but were sold commercially from 1890 to 1941. One of these earlier designs was named the Climax water heater and was marketed throughout Southern California. Over time, this design was modified until it more closely resembled today's flat plate systems. There is reason to believe that breadbox systems could be mass-produced and be more cost effective than flat plate systems. Custom site-built systems have proven to be as cost effective as flat plates in mild climates; however, these systems require some lifestyle change by shifting hot water usage to early evening instead of late night and morning. Like flat plate systems, breadboxes are more cost effective for higher demand situations even though the solar fraction may decline. Currently breadboxes tend to be found in localized areas because a local designer or individual has promoted their use. Commercialization has begun but is still quite limited. The potential for improvements in design and production is much greater than for flat plate solar collectors.

Scientific Literature

Scientific literature regarding breadbox performance has been minimal, especially when compared to flat plate systems. A wide range of solar water heaters including a breadbox and an exposed black tank were studied by F.A. Brooks in the 1930s [1]. Some papers describe work in breadbox-like designs in other countries [2,3,4]. A few papers have been presented at recent solar conferences, especially the National Passive Solar Conferences [5,6,7]. Private publications such as Horace McCracken's "How to Build a Passive System Solar Hot Water Heater" have also given design and performance data.

The Problem

While the performance of breadboxes is generally below that of flat plate systems, the installed cost is typically one-half that of flat plate hot water heaters for site-build systems. These systems provide 100% of the hot water needs of 2-3 adults for at least six months of the year in and around Davis, California. The breadboxes act as preheaters during the remaining months of the year, contributing an overall performance of slightly over 50% [8]. While breadboxes have been tested and simulated on computers, these evaluations have not been guided by experience with operating systems and the knowledge of important design parameters which affect the system performance. Likewise, the appropriate variation of design with climate has often been ignored by researchers unfamiliar with the important performance parameters for breadboxes.

This paper presents the results of three different simulation analyses of breadbox performance. The first analysis, conducted for Sacramento, California, used parametric changes to determine the sensitivity of performance to hot water load profiles, hot water demand, and water set point temperatures. The second analysis, conducted for Blue Canyon, California, examined the potential for breadbox freezing in cold climates. The third analysis, conducted for Indio, California, evaluated seven different designs for a multifamily housing project.

COMPUTER SIMULATION PROGRAM DESCRIPTION - TBBX

The computer program TBBX is a FORTRAN IV program based on D.A.T.A.'s program SOLSIM, a passive solar building simulator. Since the basic structure of the programs are similar, the description below applies to both programs except as noted.

Program Inputs

The programs TBBX and SOLSIM both initialize the full range of input parameters with the exception of the shell element characteristics and the storage type characteristics. Immediately following initialization, input parameters are read and echoed out to the output file, which by default is a line printer. There are five general categories of inputs as can be seen from the flow chart Fig.1.

SOLSIM/TBBX Flow Chart

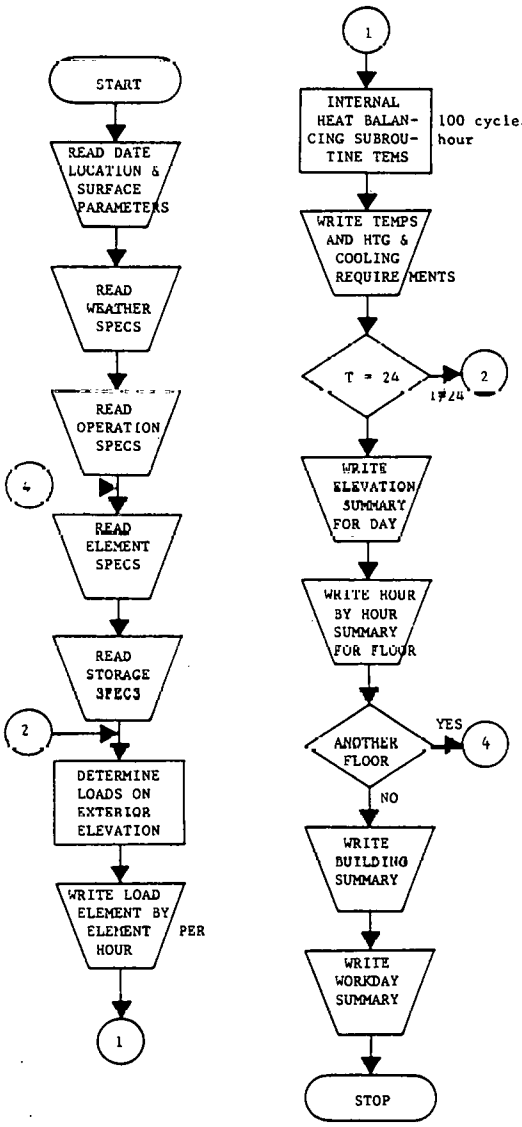

Fig. 1

The first is a general category including title, date (month and day), location (latitude, longitude, and time zone), and general shell surface characteristics (air film values, solar absorption of walls and roof). The second category is weather specifications and includes mean wind velocity, cloudiness, clearness number, cloud cover, solar reduction factor, hourly or maximum and minimum daily temperatures. Next a category of hourly operations is read in and may include a lighting schedule, mechanical heat gain schedule (or programmed back up heating), ventilation schedule, and infiltration schedule. The fourth category of input is the exterior shell characteristics which include:

1. Opaque wall area
2. The area of transparent or translucent shell surfaces
3. R value of wall
4. R value of transparent or translucent surfaces
5. Daily average shading coefficient of the wall
6. Daily average shading coefficient of the glazing
7. Orientation according to azimuth and tilt of the element
8. Construction type (TETD or CLTD type from ASHRAE Handbook of Fundamentals)
9. Portion of glazing with moveable insulation
10. R value of the moveable insulation
11. Operation schedule code number for the moveable insulation.

The final input section deals with the characteristics of heat storage type. Various heat storage elements such as water cylinders, barrels, concrete slab, roofponds, or Trombé walls may be investigated. Storage devices may be shuttered, exposed to the exterior in sun or shade, or totally enclosed within the building shell. They may vary in number and several characteristics:

1. Associated solar radiation element glazing, which tells the program where the sunlight is coming from.
2. Number of identical units
3. Surface area of each unit
4. Location flag
5. Exterior operable insulation R value
6. Interior operable insulation R value
7. Portion of surface exposed to solar radiation (daily average)
8. Portion of surface exposed to interior
9. Portion of surface exposed to exterior air temperature
10. Portion of surface exposed to lighting
11. Portion of surface exposed to north sky
12. Mass of each unit
13. Specific heat of each unit
14. Density of mass
15. Mass thickness (primarily for slabs)
16. Emissivity of mass surface

There may be up to five types of storage mass elements differing in any of these characteristics. For each storage type there are four different shutter schedules that are used in the input. One controls the exposure to exterior air temperatures and sunlight, one to interior conditions, one to exposure to the north sky for radiant cooling and the final operation schedule controls exposure to glazing for moveable insulation between glass and the thermal mass. TBBX includes a mass flow schedule for each storage type, mass source temperature,

mass flow origin code (source or other storage type), water source temperature, and desired water temperature.

Program Calculation Procedures

After reading in the input data the program begins calculations. The first calculations compute daily values mostly relating to sun angles for the day. Next the hourly calculation cycle begins. Most of the calculations are done in a subroutine denoted THERM, which does the calculation of each shell surface one by one. After the shell surface conductive and radiation heat transfers are determined, the volumetrically dependent heat exchanges such as internal loads, infiltration, and ventilation are determined. The total shell heat balance is determined from the current temperatures inside and outside the structure. This heat balance is then submitted to the internal heat balancing subroutine TEMS, to determine the new hourly mass and internal air temperature. TEMS determines the heat exchange between the mass types and the air. Virtually all transfers are mediated through the air. Short wave radiant transfers from sunlight go directly into the mass when appropriate, and long wave radiant transfers to glazing are determined separately. A schematic of these exchanges is shown in Fig. 2.

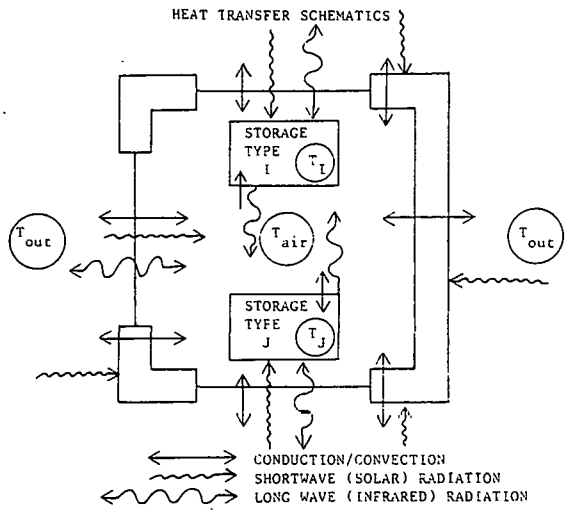

Fig. 2

This calculation methodology is not perfect but it adequately predicts temperatures and allows the evaluation of the effects of thermal mass on a wide range of characteristics. At the end of each hour the shell heat balance for each surface element, air and storage type temperatures, and total structural heat balances are printed. These are accumulated and summarized at the end of the day on a structural heat balance sheet for the day. Daily balances for each of the shell surface elements are printed. SOLSIM allows a Calcomp plot of air and mass temperatures. This feature was deleted from TBBX to save computation overhead costs. TBBX includes an automatic annualization procedure based on four to twenty-four design days per year. The greater the number of design days, the more accurate the annualization; however, the cost of the runs is over $2 per day simulated, and computation costs can become prohibitive for small, private researchers such as D.A.T.A. The design day temperatures and BTU output summary is printed on a separate output file. The annualization procedure involves the simulation of a clear and cloudy design day for each season or month. These design days are annualized by multiplying by the number of clear, partly cloudy, and cloudy days in the chosen period. Partly cloudy days are weighted with 2/3's clear day performance and 1/3 cloudy day performance because correlations of sunshine and cloudiness data indicate a similar non-linear relation between sunshine and cloud cover.

Program Validation

Only a few validation runs have been performed. SOLSIM was originally validated by comparison with data gathered at the Living Systems office in 1975. Comparisons were made with the monitored breadbox at the Nittler/Maeda Suncatcher house in Davis, California. This breadbox is monitored along with the rest of the Nittler/Maeda Suncatcher house under grant #DE-FG04-79CS30169 from the Solar Heating and Cooling Research and Development Branch, Office of Conservation and Solar Application, United States Department of Energy [8]. The mock up of performance was quite close, but parametric input changes that are physically realistic could allow substantial variation in the calculated results because of the large number of input parameters. The results of this comparison are shown in Fig. 3 below.

SIMULATION RESULTS

Breadbox Characteristics

A series of parametric runs was done for a breadbox designed by John Burton of Integral Design, Santa Rosa, California. This breadbox is designed to be site-built on a flat roof or ground mounted. It incorporates two 0.151m^3(40 gallon) gas or electric water heater tanks acting as absorption and storage, in a prismatic box with a right isosceles triangular cross section 1.83m(6') on the equal sides and 2.41m(7'11") on the hypotenuse. The width is also 1.83m(6'). The box is double glazed with slightly less then 48ft^2(4.46m^2) of Kalwall$_{TM}$ or Filon$_{TM}$ which acts as the collector. Plans for this system and a horizontal breadbox are available from Integral Design at $15 for both plans.

Parametric Runs

A series of simulations of eight design days each was run for the Integral Design breadbox using weather and climate data for Sacramento, California which is representative of most of the Great Central Valley of California and the low desert region of the southwestern United States. These simulations were run to determine the annual performance sensitivity to load profiles, thermostat set point temperature, use of shutters, and demand. The table below gives the annualized output in gigajoules (GJ) and millions of BTUs (MBTUs) for the series of runs.

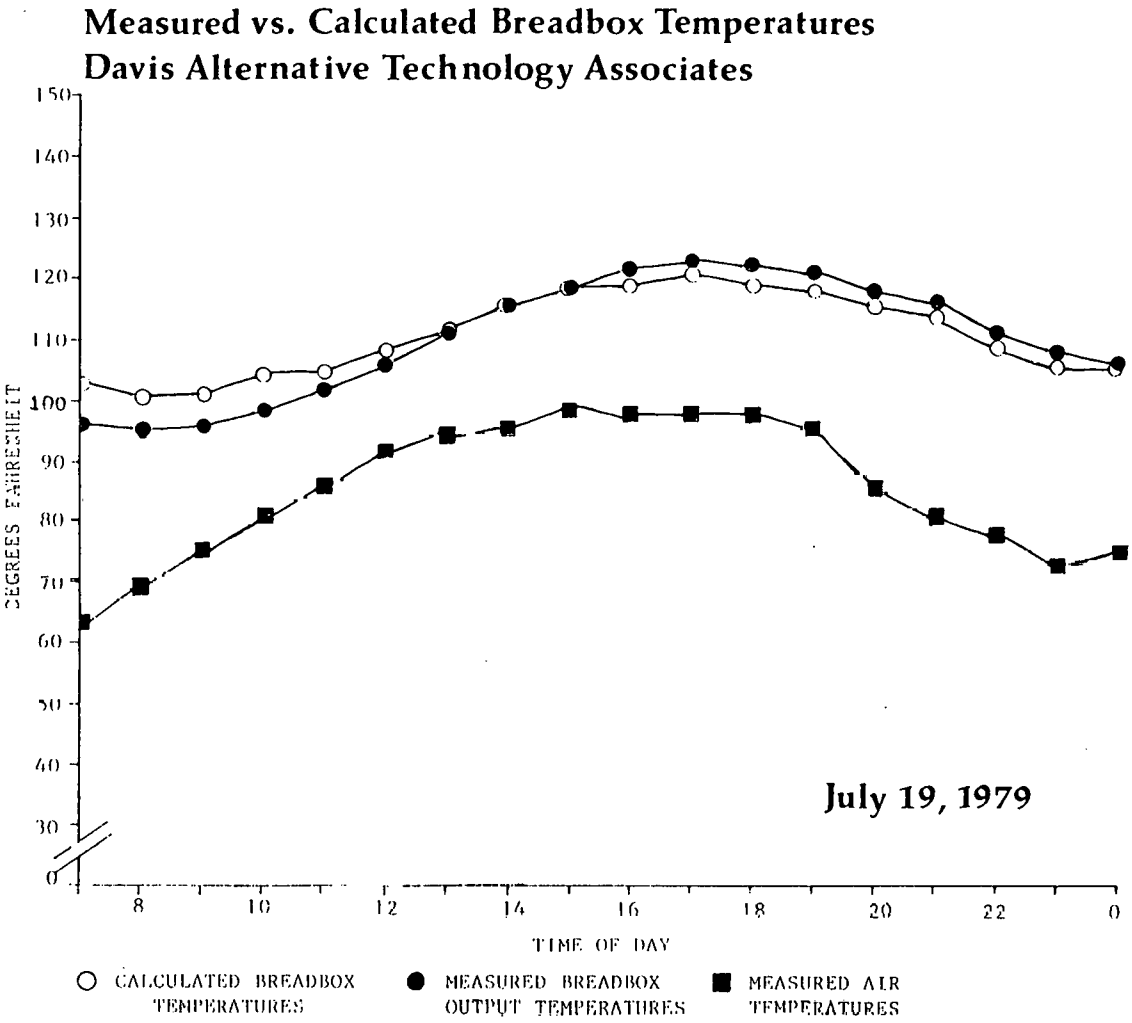

Fig. 3

Two cold climate runs were done using the base case and Blue Canyon, California data. Blue Canyon is 1609m(5280ft) in elevation and has 3160°K-days (5704°F-days) heating degree days. Blue Canyon has an average January maximum daily temperature of 6.0°C(42.8°F) and an average January minimum daily temperature of -1.2°C(29.8°F). Performance was reduced to 3.47 GJ(3.29 MBTUs) and 33% solar. The simulations indicated that the tanks would not reach freezing temperatures. The pipes, however, would have to be insulated or properly placed to prevent freezing.

Previous simulations have indicated other important design characteristics of breadboxes. The first is fundamental enough--energy has to get through the glazing to do an adequate job relative to the load. That is, the transmitted energy through the total transparent/translucent cover has to be more than two times the desired minimum output. In order to achieve adequate minimum morning temperatures in a standard residential use basis, the glazing to mass ratio should not exceed $0.01 m^3_{water}/m^2_{glazing}$ in the Central Valley of California [8].

BREADBOX DESIGN SIMULATIONS

The program TBBX was originally developed from SOLSIM as part of a contract with the California Solar Business Office, then SolarCal, which in turn was funded by the Federal Southwest Border Regional Commission to act as design consultants on a breadbox project for the Fred Young Farm Labor Housing Center in Indio, California. Under the terms of this contract, eight distinctly different designs were drafted for usage at the Labor Center. This situation was quite useful for solar breadbox application with a high afternoon load. Hot water demand was quite high, and the budget was limited to such a degree that compromises had to be made with the design of the breadbox installation. Nevertheless, the summary of the performance evaluation is quite instructive and is given as Table 3 below. Graphic depictions of the design are given in the final report for this project and are not reported here due to space considerations.

During the analysis of the eight breadbox designs, two key parameters were held constant. The ratio

Table 1

BREADBOX PERFORMANCE TABLE

Water Heater Thermostat Set Point Temperature in GJ (MBTUs)

	140 F	110 F
Base Case	2.33 (2.21) 20% solar	3.08 (2.92) 45% solar
Standard Load Profile	1.99 (1.89) 17%	2.71 (2.57) 39%
75 Gallon/Day Demand	3.83 (3.63) 22%	4.62 (4.38) 45%
Shuttered 5pm to 8am	2.95 (2.80) 26%	3.65 (3.46) 52%

The base case is defined as the afternoon/evening "shifted" load profile, 0.189m^3(50 gallons) of hot water demand per day and no moveable insulation.

The load profiles are given in Table 2 below:

Table 2

HOT WATER DEMAND LOAD PROFILES AS PERCENTAGE OF DAILY DEMAND PER HOUR

Hour	Standard %	"Shifted"* %	Hour	Standard %	"Shifted"* %
0	2.0	-	12	3.2	5.0
1	-	-	13	5.0	30.0
2	-	-	14	2.7	-
3	-	-	15	2.5	-
4	-	-	16	2.0	-
5	-	-	17	4.0	-
6	1.5	-	18	7.0	5.0
7	4.5	10.0	19	12.3	5.0
8	7.5	5.0	20	9.9	-
9	8.5	-	21	6.7	15.0
10	6.6	-	22	5.3	15.0
11	4.5	-	23	4.5	-

*Load shifted towards afternoon and evening hours and away from morning hours.

of water mass to glazing area, which was determined in earlier research to be a critical limit on performance, was held at approximately 0.06-0.08m^3 of water (1.5-2.0 gallons) per m^2(ft^2) of glazing [earlier research showed that 0.10m^3/m^2 (2.5 gallons/ft^2) of glazing is the maximum ratio, and lower ratios result in better performance]. The number of breadbox units per installation was based on using 11.1m^2(120ft^2) of effective south facing glazing per installation. For many designs two breadbox units per installation were used, although a system with a curved glazing surface (system #6) required 6 breadbox units to achieve the 11.1m^2 glazing standard.

The majority of the systems using tanks performed very similarly, with solar fractions of 30-33%. In

Table 3

BREADBOX PERFORMANCE SUMMARY SHEET
for
Fred Young Farm Labor Center
in Indio, California

System Number	Tanks/ Unit	# of Units	Total Capacity	MBTUs Annual Output	% Solar	KBTU/$
1. 2 tank vertical	2	2	21.4m^3 (160gal)	23.97	33	37.45
2. 3 tank vertical	3	2	24.1m^3 (180gal)	25.12	35	31.40
3. 2 tank plus superheater	3	1	16.1m^3 (120gal)	22.39	31	41.01
4. 2 tank horizontal	2	2	16.1m^3 (120gal)	24.01	33	43.97
5. 2 tank bubble	2	6	48.2m^3 (360gal)	62.93	76	46.68
6. Narrow diameter bubble	30'	6	35.3m^3 (264gal)	31.00	31	51.15
7. Narrow diameter triangular	16'	10	7.9m^3 (59gal)	23.78	32	82.00
8. 1 tank triangular	1	4	21.4m^3 (160gal)	13.28	19	18.14

this case most two tank systems are relatively insensitive to design variation. The two notable exceptions were system #6, using the curved glazing, and system #8, using one tank in an isosceles triangle shaped box similar to that modeled for Sacramento. The high performance of system #6 was due to the large number of breadbox units used, but the overall cost for building such a system exceeded the budget limit. The low performance of system #8 can be attributed to large heat losses from the box walls and glazing. An experimental system, developed by Horace McCracken (system #7), uses 7.62cm(3") diameter aluminum pipes to achieve a solar fraction of 32% for a low cost. While this particular system has a number of practical drawbacks, it shows that narrow diameter breadbox systems are extremely effective in high demand situations. While the results of this study are interesting, they cannot be generalized to typical residential installations because of the number of unique water demand, load profile, and climatic characteristics [9].

RESULTS

It is clear that breadboxes perform better at lower set point temperatures, shifted schedules, higher demand, and with shutters. However, reliable operable insulation designed for exterior or interior use with a breadbox has not been perfected or automated. It appears for Sacramento at least that set point temperature is more important than load profile. Higher demand for water may not increase the percent solar but does increase the cost effectiveness, since energy output increases. Just as in flat plate systems, hot water conservation and solar hot water heating with breadboxes conflict. For high demand relative to storage capacity in hot summer climates a system more closely resembling an active system is more appropriate, but overall performance per dollar tends to favor a cross between the two systems provided cost estimates of hypothetical systems are accurate.

A great deal of study of both an experimental and theoretical nature needs to be done for breadboxes, breadbox-like designs, or hybrids between flat plates and breadboxes. Breadbox design is still quite unsophisticated and could tolerate a complete redesign. The performance capability is quite real for mild climates, especially when compared to electric hot water heating, bottled gas, or fuel oil. Performance per dollar will probably exceed flat plates for even a wider climate range if sufficient research and development resources are directed towards this effort. In spite of the limited resources D.A.T.A. has been able to direct towards this research, some valuable results have been determined.

ACKNOWLEDGEMENTS

The authors wish to thank Wayne Parker and Jerry Yudelson of the Solar Business Office and the Federal Southwest Border Regional Commission for the funding that made the evaluation program development possible. We wish to thank John Burton of Integral Design, Horace McCracken, Gary Milhollen of Sun Energy Builders, Bruce Whitelam, and Marshall Hunt for sharing their knowledge and experience with breadbox design, construction, and performance. Staff help was invaluable and included graphics by Marcia Cary, typing and editing by Martha Townsend and Libby Hueter, and the work load carried by the rest of the D.A.T.A. staff, Ken Nittler, Paul Grant, and Tim Allis, which allowed this work to be reported. Our thanks also goes to the Department of Energy which funded the Suncatcher monitoring project that provided fundamental data for the validation of the computer program TBBX.

REFERENCES

1. F.A.Brooks, Solar Energy and Its Use For Heating Water in California, Bulletin 602; Agricultural Experiment Station, U.C.Berkeley, 1836

2. S.Van Straaten, "Solar Water Heaters For Low Cost Housing", Proceedings of 2nd Southeastern Conference on Application of Solar Energy; NTIS CONF. 760423; Springfield, VA 1976

3. I.Tanishita, "Recent Developments of Solar Water Heaters in Japan"; United Nations Conference on New Sources of Energy, Rome, Italy, 1961

4. G.Starr and B.Melzer, "An Evaluation of Two Breadboxes", Proceedings of the 2nd National Passive Solar Conference, Vol 2; Mid-Atlantic Solar Energy Association, Philadelphia, PA 1978

5. H.P.Gaig, "Year Round Performance Studies On A Built-In Storage Type Solar Water Heater In Jodhpur, India", Solar Energy Vol 17, pp.167-172, 1974

6. C.Heeschen,"An Inverted Solar Water Heater for Domestic Hot Water", Proceedings of the 2nd National Passive Solar Conference, Vol 2; Mid-Atlantic Solar Energy Association, Philadelphia, PA 1978

7. J.Burton,J.Reiss and L.Nelson,"A Passive Solar Retrofit in Downtown Sacramento, CA", Proceedings of the 3rd National Passive Solar Conference; American Section of the International Solar Energy Society, Newark, DE 1979

8. B.Maeda,D.Anson, and P.Grant,"Suncatcher Monitoring and Performance Evaluation Project", Proceedings of the 3rd National Passive Solar Conference; American Section of the International Solar Energy Society, Newark, DE 1979

9. B.Melzer and B.Maeda, Breadbox Design for the Fred Young Farm Labor Center in Indio; Solar Business Office, Sacramento, CA 1979

TRNSYS SIMULATION OF CHEMICAL HEAT PUMPS FOR SOLAR HEATING, COOLING, AND STORAGE

Peter O'D. Offenhartz
EIC Corporation
55 Chapel Street
Newton, Massachusetts 02158

ABSTRACT

TRNSYS-compatible subroutines for the simulation of various types of chemical heat pumps have been written and simulations for both heating and cooling are being performed for the Washington, D.C. climate. Direct comparisons between the H_2SO_4/H_2O, $CaCl_2/CH_3OH$, and NH_4NO_3/NH_3 chemical heat pumps are being carried out and, in the heating mode, comparisons with "conventional" hot water storage are being made. In all cases simulated, the solar collector is a fixed evacuated tube system.

Chemical heat pumps operate at higher solar collector temperatures (>100°C) than "conventional" solar heating systems with hot-water storage, but make up for reduced collector efficiency by having a coefficient of performance greater than unity. The trade-off between these two factors is sensitive to solar collector performance, particularly to the transmittance-absorptance product ($\tau\alpha$), to climate (the trade-off is more favorable to chemical heat pumps in warmer climates, where their cooling capability is most useful), to the control strategy, and to the design and size of the chemical heat pump. In liquid-based systems, such as H_2SO_4/H_2O and NH_4NO_3/NH_3, undersizing the system can lead to high collector temperatures, but performance remains very good.

The performance of the H_2SO_4/H_2O and NH_4NO_3/NH_3 systems was found to be quite similar, although the ammonia-based system showed some potential problems due to high concentrations of NH_4NO_3 that could lead to salt precipitation. The $CaCl_2/CH_3OH$ consistently indicated lower maximum solar collector temperatures, but at the cost of reduced coefficients of performance. In the cooling mode, which has been examined at some length, the reduced COP of the $CaCl_2/CH_3OH$ system was almost exactly balanced by the reduced collector performance (at higher operating temperatures) of the H_2SO_4/H_2O system. Thus, despite remarkably different designs, the two systems met almost exactly the same fraction of the cooling load with a given collector area. While this result is somewhat accidental -- it depends on climate, collector performance, and, above all, on storage capacity -- it indicates that differences between various chemical heat pump designs do not necessarily lead to major differences in performance.

CHEMICAL HEAT PUMP DESIGNS

In a generic sense, chemical heat pumps are absorption-cycle thermally activated heat pumps with built-in (inherent) chemical storage of thermal energy. They resemble the more well-known LiBr/H_2O and H_2O/NH_3 absorption cycle heat pumps, differing primarily in the energy storage feature. Furthermore, chemical heat pumps are generally being designed for solar heating as well as for cooling.

In the cooling mode, an important objective of chemical heat pump design has been to achieve sufficiently high absorber and condenser temperatures to permit dry heat rejection, without a cooling tower, since this is considered crucial to the residential market. This requires a relatively large heat pumping temperature gradient, i.e., temperature difference between absorber and evaporator. A large gradient is also vital for heating applications. As shown by a number of authors [1-3], the requirement for a large temperature difference between absorber and evaporator implies a large temperature difference between the generator and condenser, and hence forces the solar collector temperature to be above the normal range of flat-plate systems. Thus, it is generally agreed that chemical heat pumps will be used in conjunction with evacuated-tube, parabolic focusing, or Winston-type collectors, which can achieve temperatures in the 100-200°C range.

Under DOE sponsorship, work is in progress on two fundamentally different chemical heat pump designs, based respectively on liquid-gas and solid-gas reactions. Liquid-gas systems, exemplified by the H_2SO_4/H_2O [4] and NH_4NO_3/NH_3 [5] systems, are most similar in concept to the familiar LiBr/H_2O cycle. The basic design is shown in Fig. 1. Indeed, the fundamental difference is that LiBr is not highly soluble in water, so that a concentrated solution of LiBr cannot be used for energy storage. By contrast, H_2SO_4 and H_2O are completely miscible so that excess solar energy can be stored by concentrating the H_2SO_4 solution stored in the acid tank. Of course, as the solution becomes more concentrated, the vapor pressure of H_2O decreases, and the generator temperature (i.e., the solar collector temperature) must be increased if condensation of H_2O is to occur at a temperature suitable for heat rejection (to the residence in the heating season; to outdoor air in the cooling season). Thus, the concentration of H_2SO_4 is limited by the maximum solar collector temperature. In the NH_4NO_3/NH_3 cycle, precipitation of NH_4NO_3 will probably be limiting.

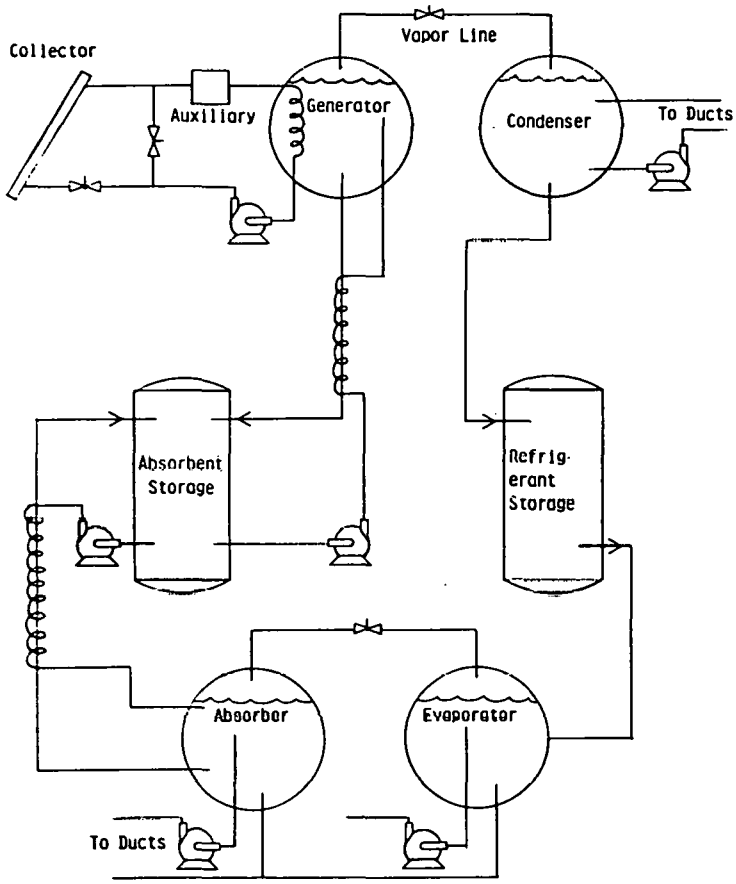

Fig. 1. Schematic Diagram of a Liquid-Based Chemical Heat Pump.

In solid-gas systems, such as the $CaCl_2/CH_3OH$ [6] and metal-hydride/H_2 [7] systems, there is little or no variation of vapor pressure with "concentration." This is a consequence of Gibb's phase rule. Thus, for a given condenser temperature, the solar collector temperature remains largely constant until the solid absorber ($CaCl_2$ or metal hydride) is fully regenerated. However, the design of a solid-phase system is quite different from the design of a liquid-based system, since it is difficult at best to circulate the solid absorber. Instead, as shown in Fig. 2, a fixed-bed absorber is used, and the heat exchange fluids are periodically switched from one bed to the other. This is somewhat more complex than in a liquid-based system, and sensible-heat recovery is not as good. For this reason, the coefficients of performance of solid-based systems will be lower.

TRNSYS-COMPATIBLE LOAD AND COLLECTOR MODULES

In order to simulate the performance of the various chemical heat pumps, it was necessary to develop TRNSYS-compatible subroutines for the major components, including the residential load. (For a number of reasons, the load module supplied with the TRNSYS package [8] was not quite suitable.) The model we used can be characterized as a single-node residence, with an overall UA of 1200 kJ/°C-hr, and a thermal capacitance of 40,000 kJ/°C. The effective UA includes infiltration, which was set at 0.75 air changes per hour. Infiltration is particularly important in the cooling mode, since the latent heat contained in the moist infiltrated air must be explicitly accounted for. Moisture "capacitance" and internal heat generation (2300 kJ/hr) were also included in the model, but internal generation of humidity and direct solar gains were not. With these latter exceptions, the model is quite similar to the one to be released by SERI [9].

The settings of an internal thermostat were used to control the chemical heat pump operation. Above 25.5°C (77.9°F), the heat pump was set to the cooling mode, and cooling was continued until the temperature fell below 25°C (77°F). Between 24° and 25°C, the heat pump was shut off; any heat of condensation that occurred during solar collection was rejected to outdoor ambient air, as in the cooling mode.

Below 24°C, the heat pump was set to the heating mode, and any heat of condensation was rejected indoors. (During the summer, heating in this mode was not permitted. Similarly, in winter, cooling was not permitted.) Heating with condenser heat was hence permitted over a wide "dead-band," allowing the heat capacity of the residence to take up excess heat during peak hours of solar collection.

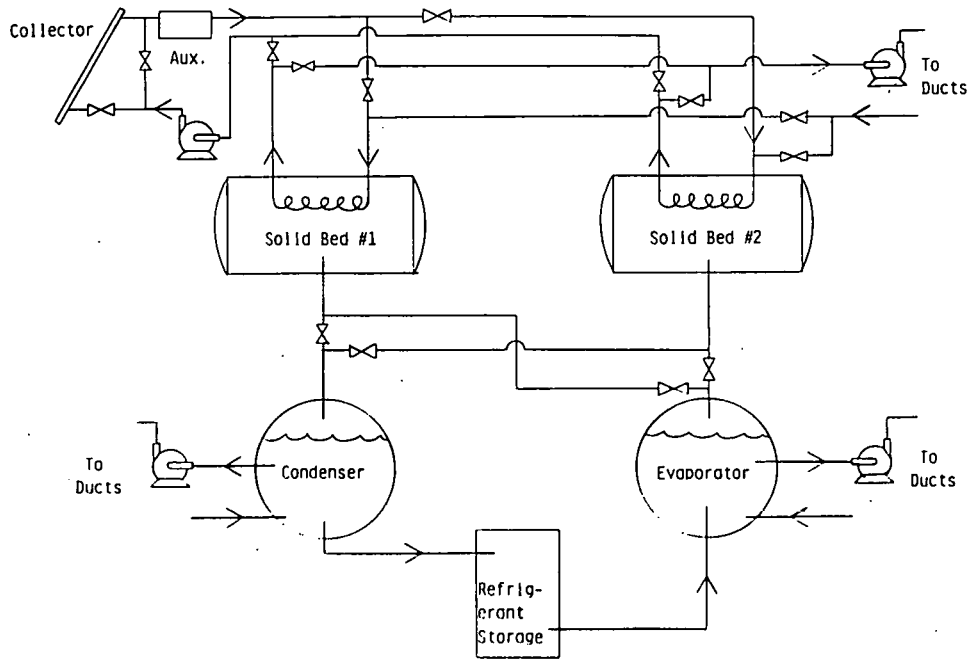

Fig. 2. Schematic Diagram of a Solid-Based Chemical Heat Pump.

When the temperature of the residence fall below 19°C, heat from the absorber was used. Finally, below 18°C, auxiliary heat was added to the generator, so that backup operation took advantage of the heat pump coefficient of performance. It should be noted that the wide condenser dead-band, similar in behavior and function to the control scheme in a passive solar residence, is vital to the operation of a chemical heat pump in the heating mode. Without the wide temperature band, it would be necessary to reject most of the heat of condensation to outdoor ambient air, and the effective coefficient of performance of the heat pump would decrease sharply toward unity.

The efficiency of the solar collector was simulated using the formula

$$\eta = A - B(T_C - T_a)/H_S$$

where T_C and T_a are respectively the average temperature of the solar collector heat exchange fluid and the temperature of the ambient air, and H_S is the solar radiation (beam and diffuse) corrected for angle of incidence. This formula unquestionably oversimplifies the collector performance curve, but the oversimplification should not be serious since the same collector performance was used in all simulations; the objective is to compare heating and cooling systems, not collectors.

The parameter A and B were set equal to 0.65 and 2.5 kJ/m^2-°C respectively. Thus, the collector efficiency was at best 65% (η = A), falling off at higher fluid temperatures. The performance of chemical heat pumps in the heating mode is sensitive to the ratio of collector efficiencies at ca. 60°C (a typical input temperature to a hot-water storage system) and at ca. 130°C (a typical input temperature to a chemical heat pump). At noon on a bright day, this ratio is approximately 1.1 in our simulations. Thus, the coefficient of performance of the heat pump must be at least 1.1 to overcome the reduced collector efficiency. In practice, the required ratio is higher (ca. 1.2), due to the effect of reduced morning and evening insolation.

TRNSYS-COMPATIBLE HEAT PUMP MODULES

TRNSYS-compatible subroutines were written to simulate the performance of both solid- and liquid-based chemical heat pumps, including appropriate controllers. Program development of the liquid-based systems was greatly facilitated by adapting a routine written for the H_2SO_4/H_2O system by Mark O. McLinden at the Solar Energy Laboratory of the University of Wisconsin [10]. The structure of the program was changed to incorporate a separate generator, condenser, absorber, and evaporator, thus permitting simulation of the heat pump in the "continuous" mode. (The original routine was written for the "batch" mode.) The program structure also permitted direct substitution of the physical-properties subroutine, so that the same program could be used for H_2SO_4/H_2O and NH_4NO_3/NH_3. McLinden's routines were used for H_2SO_4/H_2O. The latter are not nearly as accurate, however, owing to lack of data on heat capacities of NH_4NO_3-NH_3 solutions. Nevertheless, we believe the accuracy is sufficient for present purposes. The routines assume that all solutions are in thermodynamic equilibrium, i.e., that there are no pressure drops. Constant-effectiveness heat exchange (ε = 0.8) was also assumed, and the heat capacities of the fluid containers was ignored. These

assumptions are optimistic, but should not be excessively so in a well-designed system.

Program development for the solid-phase system was more complex. Since chemical kinetics are more important in solid-phase systems, equilibrium was not assumed. Instead, the ratio of absolute temperatures (absorber-evaporator or generator-condenser) was taken as constant. The resulting fluid temperatures match those observed experimentally with reasonable accuracy. Heat capacities of the containers were accounted for, since they are more important in solid-based systems. Only the $CaCl_2/CH_3OH$ system was simulated, since it is doubtful that metal hydride systems will ever be sufficiently inexpensive to be used in a storage system. (Metal hydrides are more likely to find application in heat pumps fired by fossil fuels.)

SIMULATIONS IN THE COOLING MODE

The annual temperature profile for the Washington, D.C. climate is shown in Fig. 3, together with the profiles for July and August. In the TMY data used [9], there are 1084 hours in which the temperature exceeds 25°C; of these, 331 hours are in July and 279 hours in August.

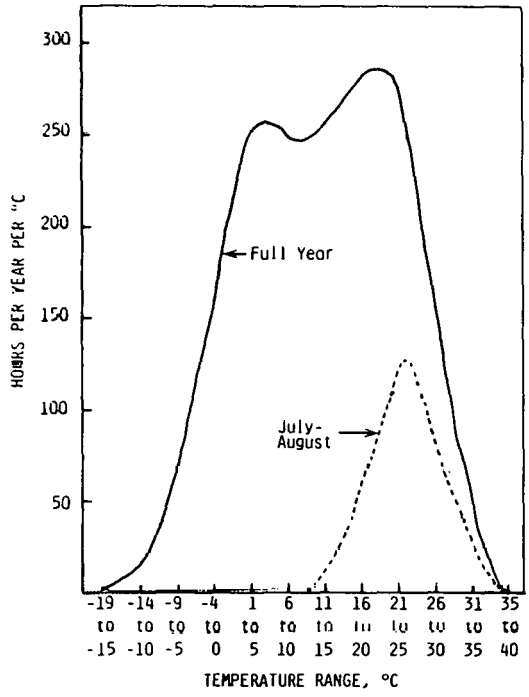

Fig. 3. Annual and July-August Temperature Profiles for the Washington, D.C. TMY.

At the present time, only the cooling simulations are near completion, and our results are limited to a comparison of the H_2SO_4-H_2O and $CaCl_2$-CH_3OH systems for the eight-day period starting July 15. The average temperature during this period was 23.7°, somewhat below the average for July (24.5°C). Temperature and insolation curves are shown in Fig. 4.

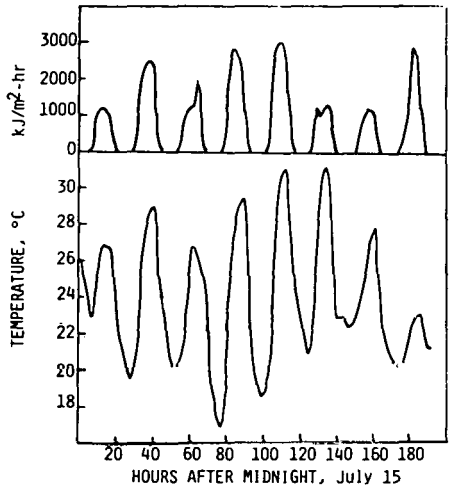

Fig. 4. Temperature and Insolation Profiles for the Period July 15-July 22, Washington, D.C. TMY.

To determine the cooling load, simulations were initially carried out with oversized collectors and chemical heat pumps. As expected, the results were the same regardless of the type of chemical heat pump employed. The average cooling load was 42,000 kJ/day; the maximum, 93,200 kJ/day on July 20. On two days, July 17 and July 22, no cooling load was indicated. The latent load averaged 40% of the total. By way of comparison, the average solar intensity incident upon the collector (oriented at latitude +15°) was 12,300 kJ/m^2-day.

The collector area was systematically reduced for both systems until they were no longer capable of meeting the full load. This occurred just below 9 m^2. The collector area was then set at 10 m^2, and the storage volumes were systematically reduced until the performance again began to decrease. It is evident from Fig. 5 that solar intensity and cooling load are by no means coincident, so that, within a limited range, one may trade storage capacity against solar collector area for a given level of performance [11].

The storage capacity of a liquid-based chemical heat pump is difficult to specify with any precision, since it depends on the temperatures at which it operates, particularly on the solar collector temperature. For this reason, we varied the volumes of the two systems. We determined in this way that the minimum storage volume of the H_2SO_4-H_2O system was roughly 0.25 m^3. This involves storage of 175 kg of 75% H_2SO_4 and 75 kg of H_2O, with adequate volume for dilution and concentration. During operation, the concentration ranged from 63% to 90% H_2SO_4, which corresponds to the cycling of 62 kg H_2O. Thus, the effective energy storage capacity was equivalent to about 140,000 kJ of cooling.

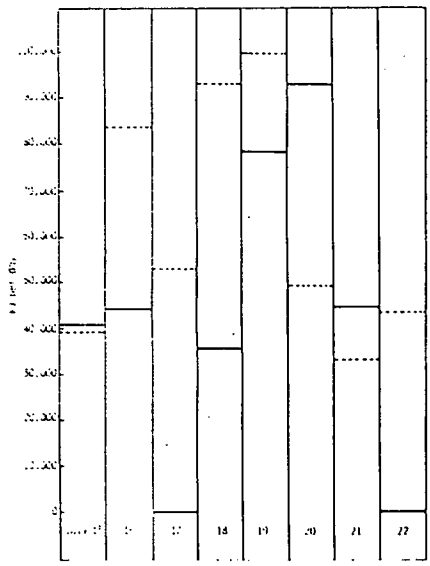

Fig. 5. Comparison of cooling load (——) with daily solar energy incident on the collector surface (---). For comparison only, the collector area is 5 m^2.

In the case of $CaCl_2$-CH_3OH, the minimum storage system consisted of 260 kg of $CaCl_2$ and 150 kg of CH_3OH. The energy storage capacity of this system is, once again, about 140,000 kJ, but the volume is about 0.60 m^3.

At these sizes, the H_2SO_4-H_2O and $CaCl_2$-CH_3OH systems met 94% and 91% of the cooling load respectively. The difference is without significance, particularly since both systems were found to be capable of meeting the full cooling load when the storage volumes were increased. What is of significance is the details of the performance of each system, since these details have practical implications for collector choice and sizing as well as choice of storage volume.

COMPARISON OF THE OPERATION OF "UNDERSIZED" STORAGE SYSTEMS

A comparison of undersized systems is important for warm climates, or cooling-only applications, where heating is not a major requirement. In these cases it is economically important, as with any heat pump, to size the components so that the cooling load is met a large fraction of the time, but not quite 100%.

A comparison of solar collector temperatures and state of charge for the two systems, sized as noted above, is shown in Fig. 6. During the first day shown, the systems behave in relatively similar fashion; in both cases, the solar collector temperature is about 105°C and, since the cooling load is somewhat greater than the insolation available, each system shows a small net decrease in its state of charge. By the end of the third day, however, major differences are evident. The $CaCl_2$-CH_3OH system is fully charged, so the collector is not

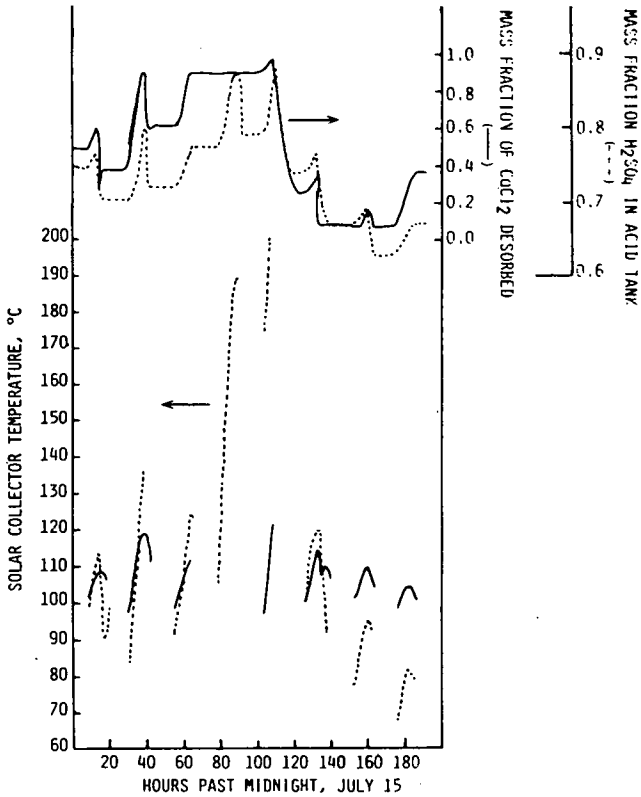

Fig. 6. Comparison of solar collector temperatures (lower curves) and state of charge (upper curves) for $CaCl_2$-CH_3OH (——) and H_2SO_4-H_2O (---) chemical heat pumps.

used for most of the fourth day. (For this reason, no solar collector temperature is shown for this system on the fourth day.) By contrast, the collector temperature of the H_2SO_4-H_2O system climbs rapidly to 190°C as the acid solution approaches 90% concentration. The same pattern is repeated on the fifth day, until decreasing insolation and increasing cooling load combine to reduce the state of charge quite sharply. Both systems run out of storage capacity on the sixth day, and the collector temperature and sulfuric acid concentrations fall to such low values that the evaporator temperature (not shown) becomes too high for effective cooling and dehumidification.

What is most remarkable about these results is the great similarity in net cooling output despite major differences in design and in solar collector temperature. The solar collector temperature for the H_2SO_4-H_2O system varies from below 70°C to nearly 200°C (the control system stopped the collector from operating above 200°C). By contrast, the solid-phase system has a more constant temperature, in the range 100-120°C. The solid-phase system has a nearly constant coefficient of performance, around 0.7, while the COP of the H_2SO_4-H_2O system varies greatly, from below 0.5 at the highest temperatures to above 1.0 at the lowest. In effect, the H_2SO_4 system responds to excess insolation by reducing its coefficient of performance, and responds to excess cooling load by increasing the

coefficient of performance (and producing a relatively warm coolant).

The effect of collector choice was examined by changing the collector parameter B from 2.5 kJ/m^2-°C to 5.0 kJ/m^2-°C, which has the effect of making the collector less efficient at higher temperature. The performance of the $CaCl_2$-CH_3OH system fell fairly sharply, so that the system met only 72% of the cooling load. The H_2SO_4-H_2O system did better, meeting 89% of the load. As seen in Table 1, the difference is not traceable to a difference in solar collector temperatures or efficiencies -- both systems evidently operated at the same average temperature -- but is due instead to the higher COP of the H_2SO_4-H_2O system. In a hotter climate, where the heat rejection temperatures are higher, the H_2SO_4-H_2O system would be forced to operate at higher concentration, and would hence have a lower COP. However, in the relatively mild climate simulated here, its cooling performance is exceptional.

OTHER COMPARISONS

We have carried out a limited examination of NH_4NO_3-NH_3 liquid-based systems, under development by Martin-Marietta Corp. [5]. While the results have not yet been checked out in detail, preliminary examination indicates a remarkable similarity between this system and the H_2SO_4-H_2O system. Collector temperatures and coefficients of performance appear nearly identical. We believe that this similarity may reflect a more fundamental similarity among all liquid-based systems: The thermodynamic behavior of such systems is variable, depending upon concentration, and automatically adjusts to the available thermal input. Thus, the coefficient of performance achieved in practice is a function of collector size and design, storage capacity, and load, and depends very little on the particular chemical system used. Solid-based systems, on the other hand, have essentially fixed behavior depending on the chemicals used. It should be noted that our simulation of the NH_4NO_3-NH_3 system did not set an upper limit on NH_4NO_3 concentration. At the present time, the exact limits on precipitation are not known, but appear to lie in the range 80-90% NH_4NO_3 by weight. At 90%, the full storage capacity could be used with a maximum solar collector temperature around 200°C. At 80%, the energy storage density would be reduced by about 30%, and the solar collector temperature would be restricted to a maximum of 150°C.

We have also examined the effect of increased storage capacity in the cooling mode. However, the study yielded little of interest: above the minimum size, all systems met the full cooling load.

Limited simulations for heating show that the collector size used for cooling -- 10 m^2 -- is far too small. This is not surprising -- in residential buildings, in all but the most southern part of the United States, the heating load is considerably greater than the cooling load. It is of interest to note, however, that chemical heat pumps can operate with a high coefficient of performance in the backup heating mode. This could be done even with a small system. Thus, a small and relatively inexpensive system, designed for solar cooling, could be used in winter as a "gas-fired heat pump" with a small solar contribution.

Further simulations in the heating mode, using far larger systems, are in progress. For budgetary reasons, these will probably be restricted to the Washington, D.C. climate. As in the cooling simulations, we will attempt to determine comparative system sizing for various fractions of load met by solar. These data should be useful in estimating cost-performance trade-offs. We also intend to examine further the small-scale system sized for solar cooling. This system could be particularly attractive as the cooling element in a passively heated residence.

CONCLUSIONS

Anyone involved in simulation studies must cautiously note that the simulations are only as accurate as the assumptions on which they are based. Furthermore, by themselves, simulations can only indicate potential performance, not cost. With these caveats in mind, we note that liquid-

TABLE 1. COMPARISON OF THE PERFORMANCE OF "UNDERSIZED" CHEMICAL HEAT PUMPS FOR THE PERIOD JULY 15-JULY 22, WASHINGTON, D.C. TMY. COLLECTOR AREA IS 10 m^2. THE THERMAL COEFFICIENT OF PERFORMANCE, DEFINED AS COOLING DELIVERED ÷ SOLAR ENERGY COLLECTED, HAS NOT BEEN CORRECTED FOR STORAGE EFFECTS. ALL ENERGIES ARE IN 10^6 kJ.

System	Size	Collector Parameter B (kJ/m^2-°C)	Solar Energy Collected	Collector Efficiency (%)	Cooling Delivered	Heat Rejected to Ambient Air	Thermal Losses	Energy Stored	Thermal Coefficient of Performance
H_2SO_4-H_2O	175 kg 75% H_2SO_4 (see text)	2.5	0.385	39.1	0.315	0.656	0.044	-0.001	0.820
$CaCl_2$-CH_3OH	260 kg $CaCl_2$ (see text)	2.5	0.440	44.7	0.305	0.667	0.071	-0.027	0.693
H_2SO_4-H_2O	as above	5.0	0.313	31.8	0.297	0.578	0.038	-0.006	0.950
$CaCl_2$-CH_3OH	as above	5.0	0.306	31.1	0.240	0.499	0.058	-0.028	0.783
H_2SO_4-H_2O	350 kg	2.5	0.440	44.8	0.310	0.685	0.043	0.022	0.703
$CaCl_2$-CH_3OH	520 kg	2.5	0.459	46.7	0.327	0.722	0.082	-0.021	0.713

based systems in general, and the H_2SO_4-H_2O system in particular, appear to offer a highly flexible and compact means of providing solar cooling and storage. Solid-based systems can perform equally well, but only at a penalty in energy density. The question that remains is one of economics. Differences in storage volume may or may not have economic implications; questions of safety (i.e., economics at an approximate level of safety) are likely to dominate, particularly since the volumes involved are quite small, well under a cubic meter. Thus, we cannot say, on the basis of simulations alone, that any given system is clearly superior.

The programs we have developed should prove quite useful for design purposes. For example, we have found that the performance of liquid based systems is sensitive to the circulation rates in the heat exchangers between the "acid" storage tank and the generator and the absorber. We set these circulators at high rates to maximize performance, but the programs could be used in an economic design study to optimize parasitic power consumption. Furthermore, it should be possible to upgrade the programs as further data become available; at the conclusion of the current contract, the routines will be made available to chemical heat pump designers to assist them in preparing for prototype development.

As these simulations indicate, chemical heat pump technology has enormous potential. Progress on the technical side has been rapid -- the program is barely three years old -- and no technical obstacles are in sight. It remains to be seen whether the technology will fit the simulations, i.e., whether component performance continues to meet current estimates and laboratory measurements. Model validation must await the first field tests. However, since chemical heat pumps are based on relatively conventional technology (but substantially new concepts), it appears unlikely that the simulations will prove far off the mark.

ACKNOWLEDGMENTS

This work was supported by Contract EG-77-C-02-4483 from the Solar Heating and Cooling Branch of the U.S. Department of Energy. Technical monitoring has been carried out by Argonne National Laboratory, under the direction of Allan Michaels. I am indebted to Mr. Michaels for his encouragement and support. I am also indebted to Ms. Jacquelyn Marston for her work in the earlier stages of the contract, and for developing models for several of the chemical heat pump components.

REFERENCES

1. P. O'D. Offenhartz, "Chemical Methods of Storing Solar Energy," Joint Conf. Am. Can. Sections of ISES, 8, 48, Winnipeg (1976).

2. W. M. Raldow and W. E. Wentworth, "Chemical Heat Pumps - A Basic Thermodynamic Analysis," Solar Energy, 23, 75 (1979).

3. W. E. Wentworth, D. W. Johnson and W. M. Raldow, "Chemical Heat Pumps Using a Slurry of Metal Salt Ammoniates in an Inert Solvent," Proc. ISES Conf., Vol. 1, p. 122, Atlanta, May, 1979.

4. C. C. Hiller and E. C. Clark, Sandia Laboratories Report No. SAND78-8824, July, 1979; C. C. Hiller and E. C. Clark, Development and Testing of the Sulfuric Acid-Water Chemical Heat Pump/Chemical Energy Storage System, Proc. 14th IECEC, Vol. 1, p. 510, Boston, August, 1979; C. C. Hiller and E. C. Clark, Development of the Sulfuric Acid-Water Chemical Heat Pump/Chemical Energy Storage System for Solar Heating and Cooling, Proc. ISES Conf., Vol. 1, p. 149, Atlanta, May, 1979.

5. F. A. Jaeger, Martin Marietta Corp., Denver Colorado, private communication.

6. P. O'D. Offenhartz, F. C. Brown, R. Mar and R. W. Carling, J. Solar Energy Engineering (ASME), in press; P. O'D. Offenhartz and F. C. Brown, Methanol Based Heat Pumps for Storage of Solar Energy, Proc. 14th IECEC, Vol. 1, p. 507, Boston, August, 1979.

7. D. M. Gruen, M. Mendelsohn and I. Sheft, Solar Energy, 21, 153 (1978).

8. S. A. Klein et al., "TRNSYS - A Transient Simulation Program," University of Wisconsin, Madison (Version 10.1).

9. C. LeBoeuf, "Standard Assumptions and Methods for Solar Heating and Cooling Systems Analyses," Solar Energy Research Institute Draft Report, September, 1979.

10. S. A. Klein and M. O. McLinden, private communication.

11. P. O'D. Offenhartz and J. M. Marston, "Analysis of Advanced Thermal Energy Storage Subsystems for Solar Heating and Cooling," Proc. Third Annual Solar Heating and Cooling Research and Development Branch Contractor's Meeting, U.S. Department of Energy, September, 1978 (CONF-780983), p. 196.

NOTES

COO 4094-79

A COMPARISON OF TWO TECHNIQUES FOR THE SIMULATION OF PV SYSTEMS*,+, ++

L. L. Bucciarelli
Massachusetts Institute of Technology
School of Engineering
Cambridge, Massachusetts

B. L. Grossman
Massachusetts Institute of Technology
Lincoln Laboratory
Lexington, Massachusetts

ABSTRACT

For several years, MIT Lincoln Laboratory has conducted computer simulations of the performance of photovoltaic solar energy systems in order to size system components, to define designs of potential economic feasibility, to test various control schemes, and to monitor the performance of working systems in the field. When used as an aid-to-design, these "hourly simulations" step through a full year's worth of insolation and weather data at a specific geographical site. These data are available on computer tapes in the SOLMET format from the National Climatic Center.

More recently, a simulation technique has been developed that does not require marching through time but instead works with probability-density functions of daily values of insolation and load as inputs while still providing estimates of the usual measures of system performance (e.g., auxiliary energy required, surplus energy thrown away, fraction of load displaced). Results obtained compare well with results previously obtained from an hourly simulation of a daytime radio station.

This technique may be used to study the effect on system performance of varying degrees of correlation of load with insolation and to test the sensitivity of economic analyses to variations in utility escalation rate (discounted for inflation), PV module and balance-of-system costs.

INTRODUCTION

MIT Lincoln Laboratory has conducted computer simulations of the performance of solar photovoltaic (PV) power systems in support of the design of these same systems. Figure 1 shows the kind of system with which the laboratory has been concerned. In the typical design, energy from the PV array flows either directly or via an energy storage subsystem to an inverter, then to the load. The system usually requires some degree of automatic control.

* This work was sponsored by the U.S. Department of Energy.
+ To be presented at the 2nd Annual Systems Simulation & Economics Analysis Conference, San Diego, CA, 23-25 January 1980.

For a system with battery storage, a controller is needed to ensure that the batteries do not overcharge. Shedding of array is initiated if excessive charge is imminent. It also protects the batteries from excessive depth of discharge, by calling for auxiliary power as needed. Not all of the net array output reaches the load: there are energy losses due to the inefficiencies of the inverter and the energy storage subsystem.

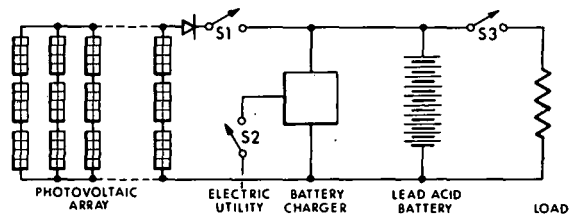

Figure 1. Typical PV system configuration.

The computer simulation used to date is an hourly simulation: time histories of the insolation incident onto the array, as obtained from a SOLMET tape, and of the prescribed load power drawn at the AC side of the inverter are inputs to the simulation. Analytical models of the current-voltage characteristics of the array, the battery, and the inverter are required.(1) The computer algorithm, through iteration, determines a value for the DC bus voltage such that Kirchoff's current law is satisfied at the DC bus node at each time instant. Having the battery current at that instant, an update of the battery state-of-charge is made (applying a charging efficiency) to obtain the state-of-charge at the start of the next hour. This process is serially repeated until one has marched, hour by hour, through an entire year.

While these hourly simulations have proven their worth in establishing confidence in system design, they do have limitations. One major complaint is that the measures of system performance obtained from a single year's run provide little information about variations in performance from one year to another. One could, of course, simulate many years to obtain this information but that process would be time consuming. Motivated by these

concerns, a simulation technique has been developed which, while crude in some respects, does take into account the stochastic nature of the sun's daily insolation and of the load placed on the system.

The essential elements of this new method, are described below. The results of applying this method to study the performance of a PV system, previously evaluated using hourly simulations, are presented and a comparison of the two methods is made.

THE METHOD

The variable of central concern in this approach is the daily net charge, or drain, on the energy storage subsystem, denoted by D. It is this variable that changes the energy storage level and occasions addition of auxiliary energy or dispensing of surplus energy. We consider the usable storage capacity to be divided into N energy levels or states. If D_i (D>0), carries the battery over the top into the (N + 2) state, surplus is created. Conversely, if D, (D<0), pulls the battery down into its lowest state, N=1, where there is no energy left in storage, auxiliary energy must be added to the system. In this study, auxiliary energy is added in sufficient measure to just make up the deficiency of the array output relative to the load.

By making two assumptions, the need to march through time is avoided. First as implied by the above, daily totals for net charge or discharge, array output, and load, are used in the analysis.

If F_i is the total array output for the ith day and G_i is the total load demanded at the DC side of the inverter, then

$$D_i = F_i - G_i \qquad (1)$$

As it stands, this approach neglects the effects of the shape of the time histories of insolation and load on performance. The match or mismatch of these profiles can be important; it determines the fraction of array energy that flows through storage and, hence, the extent of the losses incurred in that process. A first-order account of these losses can be obtained, however, by assuming a definite shape for the insolation profile and another for the load, while allowing their respective amplitudes to vary from day to day. A storage efficiency would then enter into equation (1). Similarly, an inverter efficiency could be introduced and equation (1) adjusted accordingly.

Second, the energy storage level is assumed to be a stochastic process, discrete in time (day to day) and discrete in space (N+2 states). It is further assumed that the process can be represented as a Markov chain, i.e., D_i is independent of all previous days' increment in charge or discharge energy, D_{i-k}, $k>1$. Finally, it is assumed that all states are aperiodic and positive recurrent and that the stationary distribution of the process provides a useful measure of system performance.(2)

The transition probability matrix for this system is obtained from the probability density for D_i, which, in turn, will depend on the statistics of the array output and of the load through equation (1). Having the transition-probability matrix, the vector of limiting probabilities of the storage states ,

$$|S| = \begin{Bmatrix} S_1 \\ S_2 \\ \vdots \\ S_{N+2} \end{Bmatrix} \qquad (2)$$

may be obtained using methods described in (2).

With these, and the probability density for D_i the daily increment in storage level, one can obtain estimates of the probability densities of both the daily surplus and the daily auxiliary energy requirement.

COMPARISON OF TWO SIMULATION METHODS

Hourly simulations of the performance of a PV system which has been installed at a daytime radio station in Ohio were conducted. The system includes a PV array rated at 15 kW and inclined at an angle equal to the latitude of the site and a battery subsystem with a 40-kWh rated storage capacity. A constant 4-kW, daytime only, load prescribed at the input side of the inverter, and a year's worth of insolation and temperature data, obtained from a SOLMET tape, were played through the system. The main results of the hourly simulation are summarized in Figures 2 and 3.

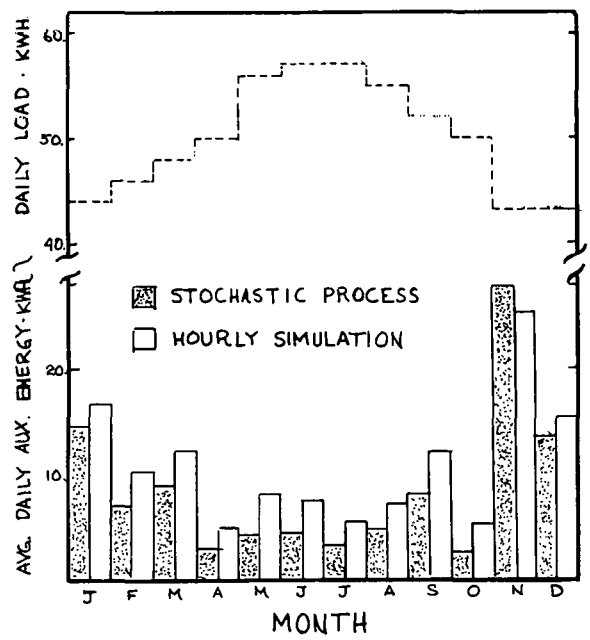

Figure 2. Load and auxiliary energy.

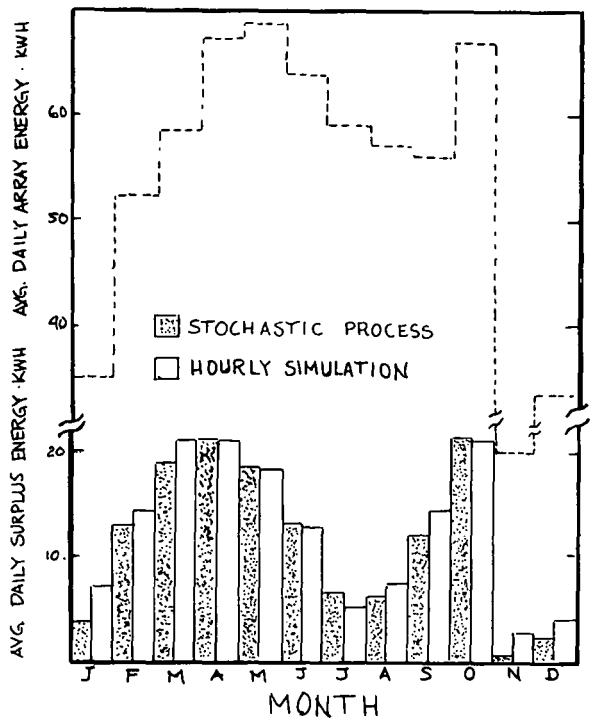

Figure 3. Array output and surplus energy.

The variation in the daily load from month to month is shown as the top segmented line in Figure 2, while the average daily array output is shown by the corresponding line in Figure 3. Comparing the top curves in Figures 2 and 3, we see that the average daily array output is greater than the daily load for all but three months of the year (January, November and December). Note that November was a particularly bleak month.

Figure 3 shows the average daily surplus energy, energy that could have been collected but had to be thrown away. Note that in general the greater the array output relative to the load the more surplus is obtained. Figure 2 shows the demand for auxiliary energy. Here, as one might expect, the greater the load relative to the array output, the greater the demand for auxiliary energy.

In applying the new method, we started not with probability densities for the sun's flux onto the array as one should (and could), but with probability densities for F_i, the daily values of array output, as obtained from the hourly simulation. This was done in order to permit a search for inadequacies in this new approach independent of any errors due to poor modeling of the array characteristics. A battery in/out efficiency was also introduced and applied when the array output exceeded the load by setting.

$$D_i = \eta_{BAT} * (F_i - G_i) \qquad \bar{F}_i - G_i > 0$$

Finally, in calculating the stationary states, the usable battery capacity of 26 kWh was divided into N=2 states.

The results of applying the new method, treating the energy storage process as a stochastic process, are also shown in Figures 2 and 3.

Expected values for the auxiliary energy, obtained from the monthly probability densities of this random variable, are shown in Figure 2. Expected monthly values for surplus, again derived from the monthly probability densities, are shown in Figure 3. The results obtained by this new method compare well with those previously obtained by means of an hourly simulation.

Typical values for the stationary distribution of the process for the months of April and December are given below. S_1 is the limiting probability of finding the system in the fully discharged state and requiring auxiliary energy. S_4 is the limiting probability of finding the system in state 4 , fully charged and requiring action to shed array.

April		December	
S_4	= 0.604	S_4	= 0.157
S_3	= 0.119	S_3	= 0.146
S_2	= 0.105	S_2	= 0.192
S_1	= 0.172	S_1	= 0.505

The probability densities for daily surplus for April and December were calculated to be:

April

Prob (Surplus = 0 kWh)	= 0.397
Prob (0 <Surplus < 6.5)	= 0.127
Prob (6.5<Surplus <19.5 ")	= 0.112
Prob (19.5<Surplus <32.5 ")	= 0.083
Prob (32.5<Surplus <45.5 ")	= 0.000
Prob (45.5<Surplus <58.5 ")	= 0.201

December

Prob (Surplus = 0 kWh)	= 0.844
Prob (0 <Surplus < 6.5 ")	= 0.072
Prob (0.5<Surplus <19.5 ")	= 0.064
Prob (19.5<Surplus <32.5 ")	= 0.020

The expected values for the surplus, shown in Fig. 3, were obtained from these probabilities. The relatively high probability associated with surplus falling in the neighborhood of 50 kWh in April reflects the high probability of the system occupying state 4 (S_4 = 0.604), and the high probability of bright clear day that month.

The probability densities for daily auxiliary energy requirement for these same months were found to be:

April

Prob (	Aux. = 0 kWh)	= 0.828
Prob (0 <	Aux. < 6.5 ")	= 0.075
Prob (6.5 <	Aux. < 19.5 ")	= 0.057
Prob (19.5 <	Aux. < 32.5 ")	= 0.025
Prob (32.5 <	Aux. < 45.5 ")	= 0.009
Prob (45.5 <	Aux. < 58.5 ")	= 0.006

December

Prob (	Aux. = 0.0 kWh)	= 0.495
Prob (0 <	Aux. < 6.5 ")	= 0.105
Prob (6.5 <	Aux. < 19.5 ")	= 0.132
Prob (19.5 <	Aux. < 32.5 ")	= 0.121
Prob (32.5 <	Aux. < 45.5 ")	= 0.147

CONCLUSIONS

The results obtained from this preliminary study of the performance of PV power systems treating the system's behavior as a stochastic process--as a Markov chain--suggest that this method might be used to advantage in place of hourly simulations. We also conclude that the energy flow process can be assumed stationary, at least to a useful, first-order approximation. Stepping through time is not necessary.

Further directions for research include: 1) studying the effect of correlation of load with insolation; 2) consideration of load profiles that extend past the daylight hours, 3) investigating different control strategies and, 4) testing of the assumption of stationarity.

REFERENCES

1. Bucciarelli, L.L., Hopkinson, R.F., "Performance of the Mead, Nebraska, 25 kWp Photovoltaic Solar Energy System and Comparison with Simulation," MIT Lincoln Laboratory, COO 4094-43.

2. Bhat, U.N., Elements of Applied Stochastic Processes, John Wiley & Sons Inc., New York 1972.

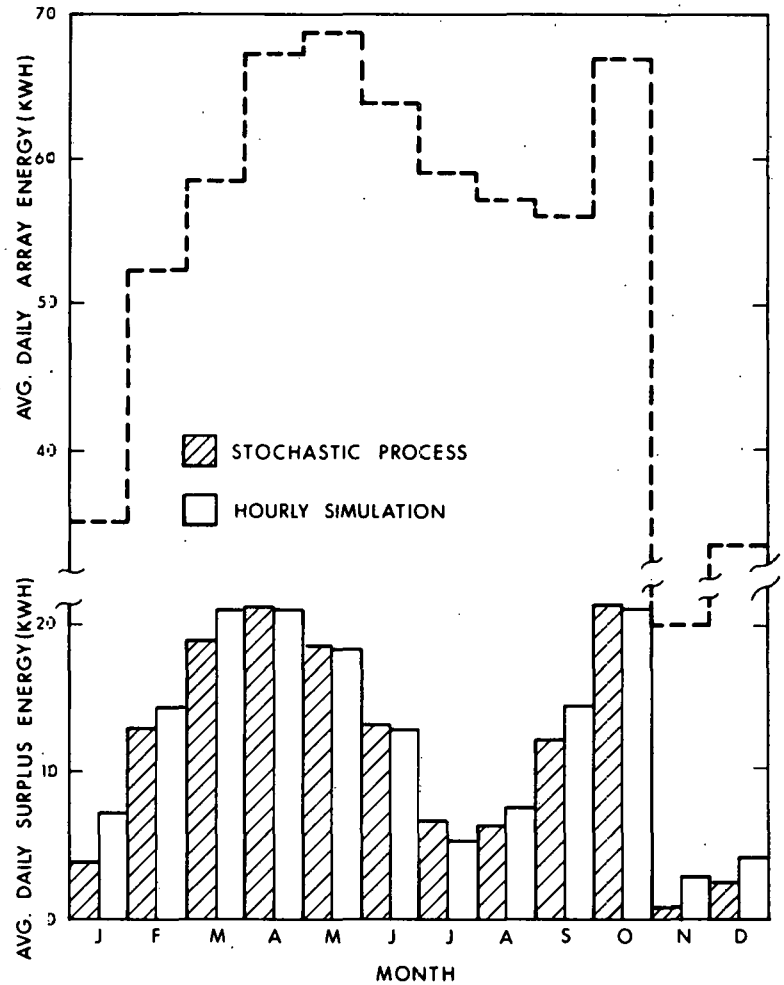
70
60
50
40
AVG. DAILY ARRAY ENERGY (KWH)
STOCHASTIC PROCESS
HOURLY SIMULATION
20
10
0
AVG. DAILY SURPLUS ENERGY (KWH)
J F M A M J J A S O N D
MONTH

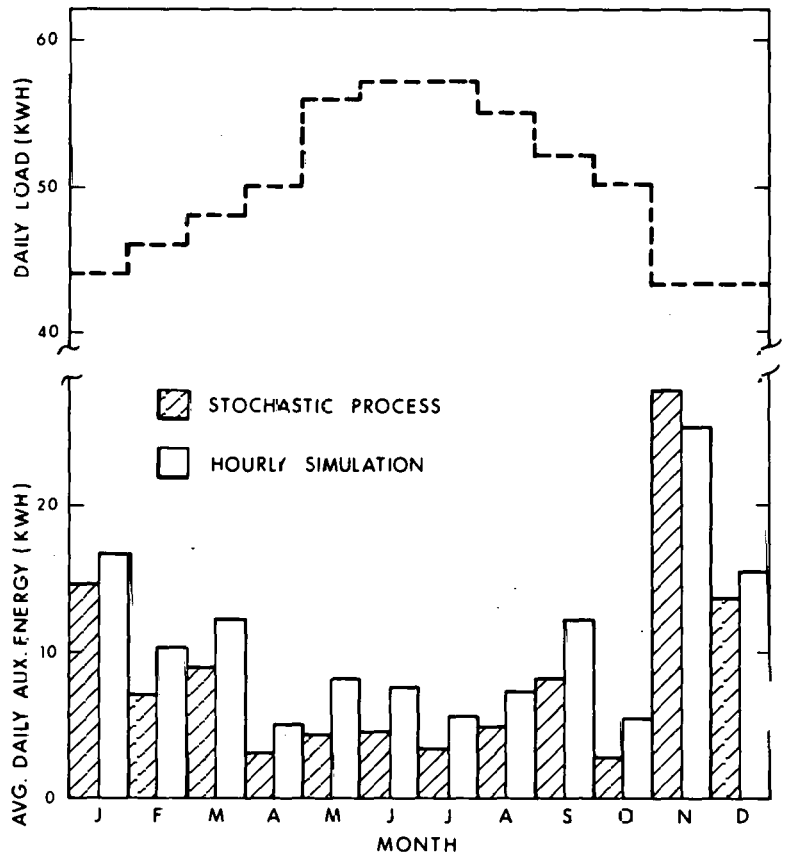
60
50
40
DAILY LOAD (KWH)
STOCHASTIC PROCESS
HOURLY SIMULATION
20
10
0
AVG. DAILY AUX. ENERGY (KWH)
J
F
M
A
M
J
J
A
S
O
N
D
MONTH

COMPUTER MODELING OF AIR LEAKAGE IN A SOLAR AIR HEATING SYSTEM

Jefferson G. Shingleton, P.E.
David E. Cassel, P.E.
Mueller Associates, Inc.
1900 Sulphur Spring Road
Baltimore, Maryland 21227

and

Michael E. McCabe, P.E.
National Bureau of Standards
Washington, D.C. 20234

ABSTRACT

A detailed TRNSYS computer model developed to permit evaluation of the effects of air leaks on the performance of a solar air heating system is described. The model was developed to define reasonable limits of air leakage for specification in performance criteria for solar heating and cooling systems in commercial and residential buildings.

The computer model, based on a physical system in the HUD demonstration program, was designed to utilize air flow rates as measured in the physical system after extensive repairs had been made to reduce air leaks. The model accounts for the existence of air leaks in the collector array, the storage container, and the control dampers for both an actually measured and various hypothetical conditions. The subroutine developed to account for collector air leakage incorporates the equations of Close and Yusoff to model collector leakage with either infiltration or exfiltration. The subroutine developed to control system model operation varies the air flow rates and leak rates for each mode of operation according to preset parameters based on the field measurements.

Hour-by-hour simulations were performed for an entire heating season for various air leakage rates. Hourly simulation results are presented to demonstrate the immediate system effects (reduced collector outlet and house supply temperatures) that are the cause of long-term system performance degradation.

Seasonal simulations performed with the model indicate that the elimination of all the measured air leakage results in a 19 percent reduction in auxiliary energy use. Short-term simulations show that collector and storage air leakage is accompanied by lower collector outlet and house supply temperatures, higher collector array operating efficiency, and increased auxiliary energy use.

INTRODUCTION

The National Bureau of Standards was directed by Public Law 93-409, the "Solar Heating and Cooling Demonstration Act of 1974," to assist the Department of Housing and Urban Development (HUD) to develop performance criteria for solar heating and cooling systems in buildings. Air leakage has been identified to have significant occurrence in the operation of air-type solar heating systems. Therefore, a study was undertaken to investigate the effect of air leakage on system thermal performance and to provide guidance in selection of recommended leakage levels for the performance criteria.

Included in the study was a review of field measurements of air leakage manufacturers' literature and performance data as well as analysis by computer simulation techniques. In order to assess the effect of air leaks on system thermal performance a computer model of a typical residential solar air heating system with air leaks was developed and hour-by-hour simulations were performed for the heating season. This paper focuses on only the computer modeling aspect of the study.

DESCRIPTION OF SYSTEM AND MODEL

The particular solar air heating system modeled was chosen on the basis of three factors. First, it is a fairly typical solar air collector system with manufactured collectors and system components for which component specifications and a system control description are available. Second, an attempt was made to seal leaks in the solar system ducts and components. Duct air leakage has been virtually eliminated with the use of sealant and tape and the system is as airtight as possible using conventional construction techniques. Third, air flow rates were measured throughout the system for each mode of system operation.

The physical system is illustrated schematically in Fig. 1. The 50.7 m^2 (546 ft^2) collector array

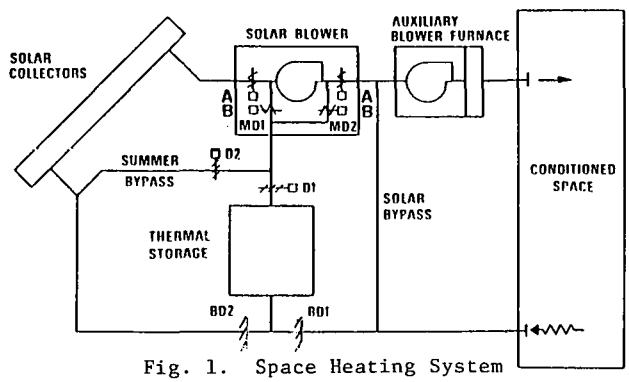

Fig. 1. Space Heating System

is mounted on the mechanical room against the south wall of the house. The mechanical room contains 9.77 m^3 (345 ft^3) of rock storage, a 29.4 kW (100,000 Btu) gas furnace with two 0.56 kW (3/4 hp) blowers and associated dampers, ductwork, and controls.

Operation of System

The system is controlled by a two-stage thermostat in the conditioned space and by temperature sensors located in the top of the rock bin, top of the collector array and in the collector inlet duct. The latter sensor was modeled to be in the bottom of the rock storage to avoid model instability when switching from one mode to another.

The control scheme is such that air is directed through the collectors to either storage or the space whenever there is a 22°C (40°F) temperature differential between collector array inlet and outlet. Once a collection mode is initiated it continues until the differential drops to 14°C (25°F). In the model the standard TRNSYS Type 2 controller performs this control function.

In the physical system when the house thermostat first calls for heat an attempt is made to heat without auxiliary. If the room temperature falls approximately 1°C (2°F) further there is a call for auxiliary heating. Two standard Type 2 controllers were used in the model to accomplish this.

System Operation Modes

The physical system operates in the seven basic modes described below. The control system in the model duplicates the control logic of the physical system to operate the model in all but the DHW mode. The DHW subsystem was not included in the model.

No Operation: If there is no collectable solar energy and there is no call for heating the system is off.

Storage-to-House: If there is no collectable solar energy and the top of storage is at least 32°C (90°F), at the first call for heating the system will operate in the Storage-to-House mode. Dampers MD1B and MD2A open, dampers MD1A and MD2B close, and both the solar system blower and the furnace blower operate to circulate air between the rock bin storage and house.

Collector-to-House: If there is collectable solar energy and a call for heating, dampers MD1A and MD2A open, dampers MD1B and MD2B close, and both the solar system blower and the furnace blower operate to circulate air between the collectors and house.

Collector-to-Storage: If there is collectable solar energy, and no call for heating, dampers MD1A and MD2B open, MD1B and MD2A close, and the solar system blower operates to circulate air between the collectors and storage.

Storage-to-House with Auxiliary Heat: If there is no collectable solar energy and either there is a call for heating and the top of storage is at a temperature of less than 32°C (90°F), or there is a call for auxiliary heating, the system will operate in this mode. The status of each damper and blower will be identical to that in the Storage-to-House mode and the auxiliary furnace will operate to boost the temperature of the air delivered to the house.

Collector-to-House with Auxiliary Heat: If while operating in the Collector-to-House mode the room temperature drops an additional 1°C, the thermostat will call for auxiliary heat and the system will be identical to that in the Collector-to-House mode except that the auxiliary furnace will operate to boost the temperature of the air delivered to the house.

DHW Preheating: The physical system includes a DHW subsystem. When the system is operating in a solar collection mode, air is always directed through the air-to-water heat exchanger in the duct between the collector outlet and the solar blower. During the heating season, the domestic hot water preheat pump operates to preheat the domestic hot water any time the system operates in a collection mode. During the summer season, Damper D2 is manually opened and D1 is manually closed to bypass storage. The system controls operate the domestic hot water preheat pump and solar blower simultaneously when there is both a demand for hot water and collectable solar energy. Their operation continues until the stored water temperature reaches 60°C (140°F) and resumes again after the stored water temperature drops 6°C (10°F). As stated earlier, the DHW subsystem was not included in the system model.

Description of Model

The model was developed using standard and modified components available in TRNSYS Version 9.2 [1] as well as new component subroutines developed for the study. All of the simulations were performed using a 15 minute timestep.

The TRNSYS information flow diagram for the model is presented in Fig. 2, included at the end of this paper.

Thermal losses for system components such as ducts and storage were included in the model. Duct heat transfer (UA) coefficients were calculated from building plans that indicated one inch of fiberglass insulation on all ductwork. For mathematical simplicity the ducts were assumed to have no thermal capacitance.

Two single-stage thermostat components were employed in the model for temperature control of both the solar and auxiliary heat sources.

The collector array was modeled as a single 50.7 m^2 (546 ft^2) collector having constant cover transmittance, constant plate absorptance and constant heat loss coefficient. The collector performance is defined by the Hottel, Whillier and Bliss equations used in Mode 1 of the TRNSYS flat plate collector model but modified to include collector air leaks. Efficiency curve intercept and slope values for the collectors were developed using results of a National Bureau of Standards test [2].

The modifications to the TRNSYS Flat Plate Collector component (Type 1) consisted of including an additional input parameter for leak air flow and changing the F_R (heat removal factor) calculation. The equations of Close and Yusoff [3] were utilized to modify the F_R factor to model an infiltration air leak that occurs continuously along the collector array.

The equations used in the collector model to calculate the heat removal factor for a collector with infiltration air leakage, as adapted from Close and Yusoff, are presented below:

$$F_R = \frac{1 - \exp\left[\left(1 - \frac{F' \cdot U_\ell \cdot A}{m_\ell \cdot C_p}\right) \ell n \left(\frac{1}{1 - \frac{m_\ell}{m_i}}\right)\right]}{\frac{U_\ell A}{m_i C_p \left(1 - \frac{m_\ell}{m_i}\right)} \cdot \left(1 - \frac{m_\ell C_p}{F' U_\ell A}\right)}$$

$$Q_u = F_R \left[\tau\alpha - U_\ell \left(1 - \frac{m_\ell C_p}{U_\ell A}\right) \left(\frac{1}{F'} - \frac{1}{F_r}\right)\right] (t_i - t_a)$$

$$\eta = Q_u / I$$

$$t_o = (\eta I A + m_i C_p t_i - m_\ell C_p t_a) / (C_p m_i - C_p m_\ell)$$

Where A = Collector Area

C_p = Fluid thermal capacitance

η = Instantaneous collector efficiency

m_i = Mass flow rate at collector inet

F' = Collector geometry efficiency factor

F_R = Collector heat removal factor

I = Rate of solar radiation incident on the collector surface per unit area

Q_u = Rate of energy collection per unit area

m_ℓ = Mass flow rate of total collector air leakage (a negative number for infiltration air leakage)

t_a = Outdoor ambient air temperature

$\tau\alpha$ = Product of the cover plate transmittance and the absorber plate absorbtance

t_i = Collection inlet temperature

t_o = Collector outlet temperature

U_ℓ = Overall energy loss coefficient

The TRNSYS blower model was modified so that the 0.56 kW (3/4 hp) blower operating energy was converted to heat and added to the air flow stream at each blower.

A TRNSYS component subroutine to model air leaks was developed for this study. It was designed to add air at a given flow rate and temperature to an existing flow stream in the case of infiltration, or to deduct air at a given flow rate and temperature from an existing flow stream in the case of exfiltration. This component was used to model leaks at the control dampers, at the storage bin, and at the inlet to the solar blower. This same subroutine was also used to model the solar bypass air flow and the net house exfiltration.

A TRNSYS subroutine that controls leaks and blowers in the system model was developed for this study. Since each leak varies in flow rate from one mode to another, this component determines the mode of system operation and adjusts the leak and blower rates appropriately at each timestep.

Weather Data And Heating Load

The particular modeled system is physically located in a climate characterized by mild winters that are usually overcast. Therefore, the solar fraction during the heating season is normally quite small. To avoid drawing conclusions on system performance in this atypical climate, the simulation was actually performed using weather data for Madison, Wisconsin. The house to which the solar system model was load-coupled is a 110 m^2 (1200 ft^2) modular townhouse of light-weight wood construction located at NBS in Gaithersburg, Maryland. This house had been previously studied for both solar [4] and conventional applications [5] under both actual and simulated weather conditions. The building heating and cooling load calculation program NBSLD [6] had been used in conjunction with hourly weather records from five international locations and NBS townhouse description data, to calculate building heating and cooling loads for the International Energy Agency Modeling and Simulation Group [7]. The Madison, Wisconsin weather-load tape was used for the simulations in this study.

To utilize temperature level control (provided by Mode 4 of the TRNSYS heating load component Type 12) the precalculated heating load was input as a negative QGAIN (time dependent heat gain). The building UA was set to zero. A building capacitance of 13,000 kJ/°C (6,800 Btu/°F) was chosen as a compromise between model realism, mathematical stability, and computational efficiency. A house energy balance was performed and the house temperature was calculated each timestep. The house temperature was then utilized by the model control system.

SIMULATION RESULTS

Long-Term Results

Seasonal simulations were performed for the system with no air leaks and with the measured air leaks. Simulations were also performed for various combinations of measured external leaks and damper leaks. The simulations indicate that the elimination of all the air leakage results in a 19 percent reduction in seasonal auxiliary energy use compared to the measured leak condition. The results of all of the simulations have been previously presented [8] and are summarized in Fig. 3. The measured air leakage is summarized in Fig. 4.

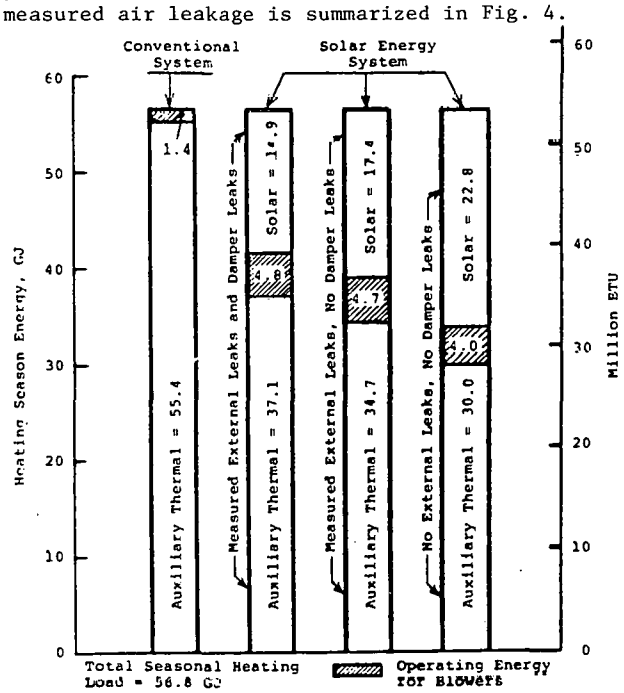

Fig. 3. Computer Simulation Results for a Solar Air Heating System in Madison, Wisconsin With and Without Measured Air Leakage

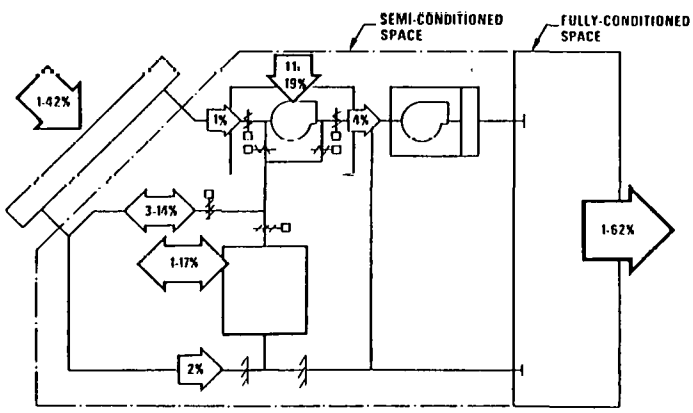

Fig. 4. Measured Component Air Leakage Summary

Short Term Results

Day-long simulations were performed with the system model to demonstrate how the short-term effects of air leakage (lower system temperatures) contribute to long-term performance degradation. The simulation period (24 hours) was the day of February 11, a relatively cold, sunny day chosen from the aforementioned weather-load tape to represent a very active day for the solar energy system. The short-term simulations were performed for both the no-air-leakage case and the 20 percent leakage case. For both simulations, the initial conditions were identical except that for the later case, the collector and storage leakage rates were both set at 20 percent of the system design air flow rate in each mode. Table 1 summarizes the flow rates used for the 20 percent leakage simulation. Blower flow rates for the no-leakage simulation were equal to those in the 20 percent leakage simulation and were extrapolated from the field measurements.

TABLE 1. SYSTEM AIR FLOW RATES FOR SIMULATED 20 PERCENT LEAKAGE RATE

MODE	AIR FLOW RATE ℓ/s (cfm)				
	Solar Blower	Furnace Blower	Collector Leakage	Storage Leakage	Net House Exfiltration
Storage-To-House	557 (1180)	902 (1910)	0	-103 (-218)	+103 (+218)
Collector-To-House	576 (1222)	900 (1907)	-103 (-218)	0	+103 (+218)
Collector-To-Storage	452 (957)	0	-103 (-218)	+103 (+218)	0

NOTES
1. Infiltration air leakage = (-)
   Exfiltration air leakage = (+)
2. Design flow rate = 516 ℓ/s (1092 cfm) = 10 ℓ/s.m^2 (2 cfm/ft^2)

Table 2 presents a summary of the results of the short-term simulations for both the no-leakage and the 20 percent air leakage case. For the system with 20 percent air leakage, 12 percent more auxiliary thermal energy was required to meet the same load than for the system with no leakage. This resulted in a 9 percentage point difference in the calculated solar fraction. The lower system temperatures in the 20 percent leak case are reflected in the 37 percent lower storage and duct heat losses.

TABLE 2. RESULTS OF SHORT-TERM SIMULATIONS

PARAMETER	VALUE	
	No Leakage	20% Leakage
Simulation Period	24 Hours	24 Hours
Load	720 MJ	720 MJ
Auxiliary Thermal Energy	510 MJ	570 MJ
Auxiliary Operating Energy	40 MJ	40 MJ
Total Auxiliary Energy	550 MJ	610 MJ
Incident Solar Radiation	1,100 MJ	1,100 MJ
Collected Solar Energy	220 MJ	240 MJ
Storage and Duct Heat Loss	19 MJ	12 MJ
Solar Fraction	0.29	0.20

To illustrate the instantaneous system performance effects for the case with 20 percent leakage rate, the system temperatures for the period from 10:00 A.M. to 7:00 P.M. are presented in Figures 5 and 6. Figure 7 shows the system operation mode for each timestep in the same period and the total daily hours of operation in each mode for both cases. The leaking system spent more solar collection time in a heating mode (rather than a storage mode) than the no-leak system. This is apparently due to the lower collector outlet temperatures in the system with collector air leakage as indicated in Fig. 5. Even though the solar collector array operated at a greater efficiency with air leakage (as evidenced by the 11 percent greater Collected Solar Energy in Table 2), it consistently delivered air at a lower temperature to both storage and the house than the collector array without air leakage.

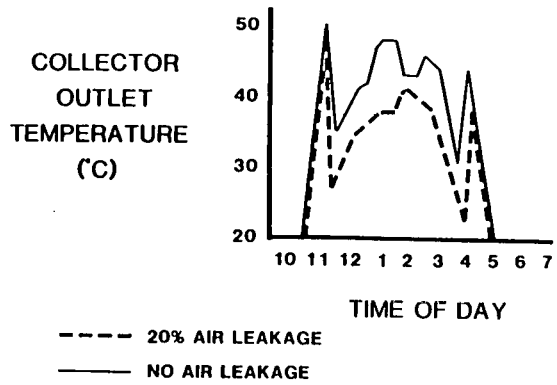

Fig. 5. Collector Outlet Temperatures for February 11 in Madison, Wisconsin

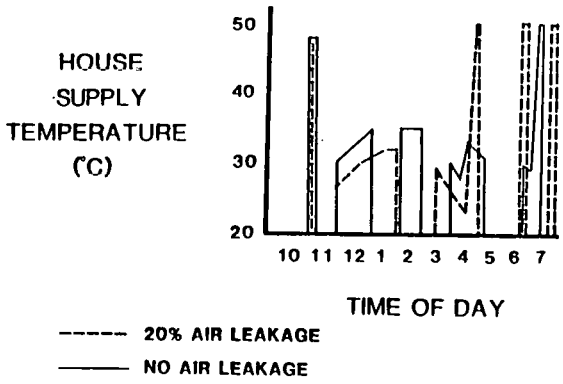

Fig. 6. House Supply Temperatures for February 11 in Madison, Wisconsin

The leaking system also spent more total hours in a heating mode than did the no-leak system and was not able to heat directly from storage without auxiliary, whereas the no-leak system was able to heat from storage without auxiliary until approximately 6:15 P.M. An examination of Fig. 6 shows that the temperature of the air delivered to the house was 4°C (7°F) lower during the collection period in the system with 20 percent air leakage.

(It should be noted that the difference between the collector outlet temperatures and the house supply temperature during periods of Collector-to-House operation is due to the mixing of house-temperature air from the bypass duct with air from the collector array directly ahead of the furnace.)

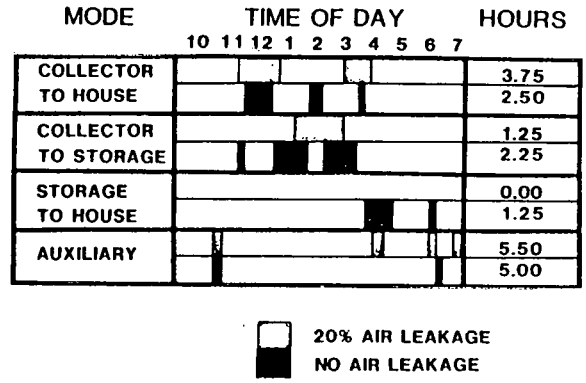

Fig. 7. System Modes and Total Hours for February 11 in Madison, Wisconsin

CONCLUSIONS

The TRNSYS model was used to simulate the performance of a solar air heating system using Madison, Wisconsin weather data for the complete heating season using precalculated loads from the NBSLD load calculation program. The NBSLD load calculation program has been shown to have very good correlation with measured data.

Short-term and long-term simulations were performed for the modeled system with no air leakage, the measured air leakage and for a theoretical 20 percent air leakage rate for the collector and storage container. The long-term simulations predict an annual savings of 19 percent in auxiliary thermal energy by eliminating air leakage. The short-term simulations were used to demonstrate the effects that result in long-term performance degradation. During the 24 hour short-term simulation period, the system with 20 percent collector and storage air leakage used 12 percent more auxiliary thermal energy than the system with no air leakage. This is a result of the significantly lower collector outlet and house supply temperatures throughout the day in the system with 20 percent air leakage than in the system with no air leakage. At a lower temperature, the collector array operated at a higher average collector efficiency with air leakage. In addition, as a result of the reduced system temperatures, the system with 20 percent air leakage spent less time in the Collector-to-Storage mode and more time in the Collector-to-House mode than did the system without air leakage. On the simulated day, the system with air leakage was not able to achieve a storage temperature high enough to support house heating directly from storage as did the system without air leakage.

FUTURE WORK

Future work on this project will be focused on three general areas. The first area consists of an evaluation of the effect of the degree of coupling between the house and the mechanical room on the degradation of system performance due to air leakage. Second, the possibility that the collector air leakage may tend to suppress a portion of the natural house infiltration and thereby reduce the equipment load will be investigated.

In the other area of work the analytical technique and some of the components described here will be used in the analysis of a method, proposed by Jones [9], that modifies FCHART collector parameters to predict the performance of a system with collector air leakage.

REFERENCES

1. TRNSYS Computer Program, Version 9.2, University of Wisconsin Solar Energy Laboratory, Madison, Wisconsin, February, 1978.

2. NBS, BSS 117, "Experimental Verification of a Standard Test Procedure for Solar Collectors," National Bureau of Standards, January, 1979.

3. D.J. Close and M.B. Yusoff, "The Effects of Air Leaks on Solar Air Collector Behavior," Solar Energy Journal, Vol. 20, No. 6, pp. 459-463.

4. J.E. Hill, T.E. Richtmeyer, "The Design and Operation of a Retrofitted Residential Solar Heating and Cooling System," National Bureau of Standards, presented at ISES Congress, July 28, 1975.

5. NBS BSS 57, "Comparison of Measured and Computer-Predicted Thermal Performance of a Four Bedroom Wood Frame Townhouse," National Bureau of Standards, April, 1975.

6. NBSIR 74-575, NBSLD, Computer Program for Heating and Cooling Loads in Buildings, National Bureau of Standards, Gaithersburg, Maryland.

7. Ove Jorgensen, Editor, IEA Draft Report on Subtask A, "Modeling and Simulation," November, 1978.

8. J. Shingleton, D. Cassel, and M. McCabe, "The Use of Operational Results to Identify Potential Improvements in the Thermal Performance of Air Solar Heating Systems and to Establish Performance Criteria," presented at the Second Annual Operational Results Conference, Colorado Springs, Colorado, November, 1979.

9. D. Jones, L. Shaw and G. Lof, "Air Leakage Effects on Active Air Heating Solar Collector System Performance," presented at the Second Annual Operational Results Conference, Colorado Springs, Colorado, November, 1978.

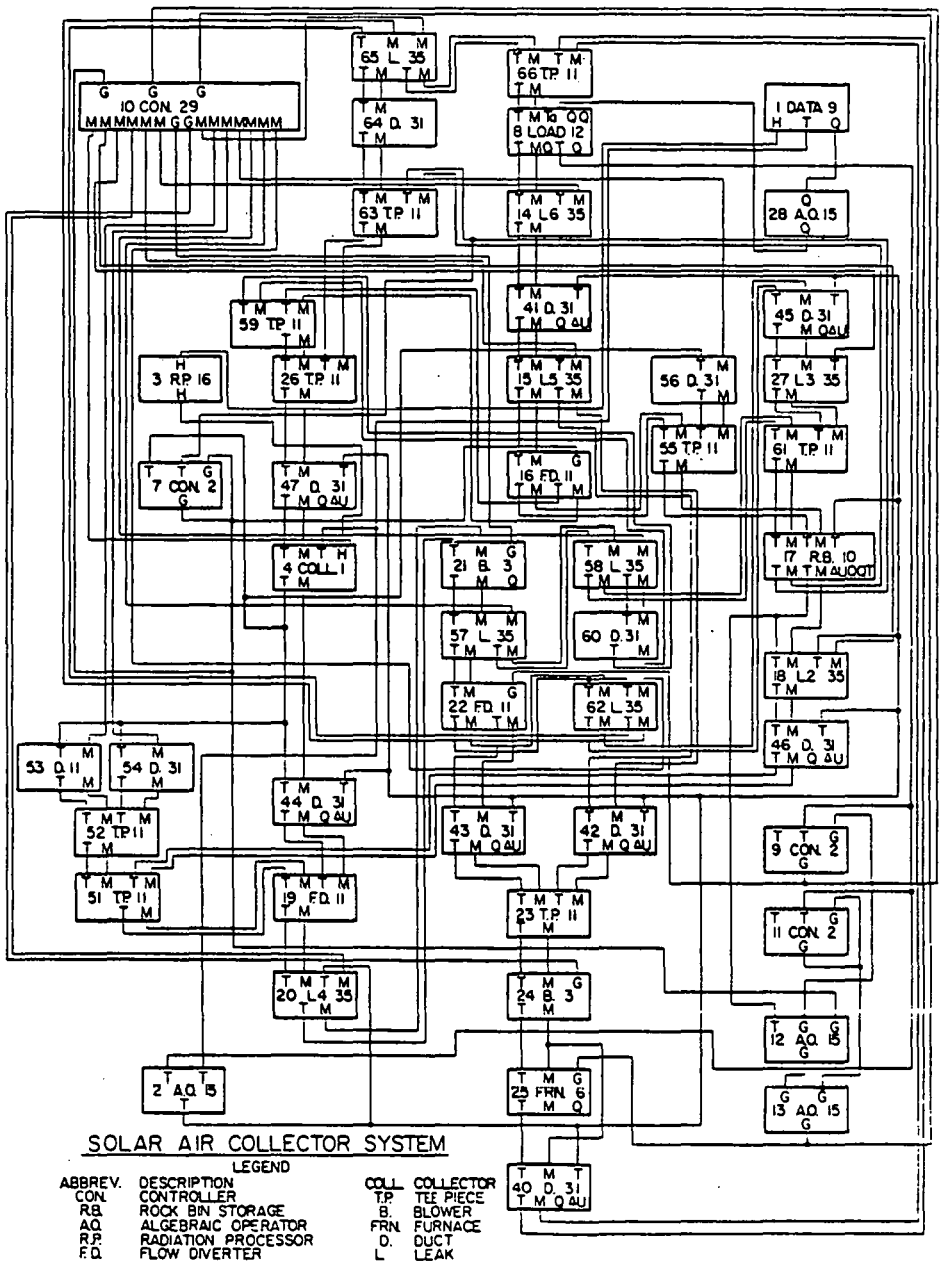

Fig. 2. TRNSYS Information Flow Diagram

NOTES

Session VIA

Thomas Freeman
Altas Corporation
Chairperson

SIMPLIFIED ANALYSIS

FCHART 4.0: THE UNIVERSITY OF WISCONSIN SOLAR ENERGY DESIGN PROGRAM

J.C. Mitchell
Solar Energy Laboratory
University of Wisconsin
Madison, WI 53706

ABSTRACT

The FCHART computer program utilizes several methods for the design of solar energy systems which have been developed at the University of Wisconsin during the last few years. These methods, outlined in the following paper, allow convenient estimation of the long-term average performance of solar space heating, water heating, heat pump, and certain industrial process heating systems. In all cases, system performance is calculated from equipment characteristics and monthly average meteorological data. The interactive program allows the user to describe the system to be analyzed easily and provide straightforward tables of performance results. Combining efficient methods of performance evaluation with system optimization and economic analysis routines, FCHART 4.0 is a convenient and powerful tool for engineers in the solar energy field.

INTRODUCTION

Design methods are tools for estimating the long term average performance of solar energy systems with minimal calculation effort. For most solar energy systems, accurate estimates of system performance require calculation at monthly intervals using monthly average weather data. Monthly design computations require several orders of magnitude less calculation time than hour-by-hour simulations and, at present, represent the most efficient approach to the design of many systems. FCHART 4.0 utilizes several methods based on monthly calculations for the design of a variety of solar energy systems.

Systems which utilize solar energy include a radiation collection device, storage capacity, mechanisms for transfer of energy to and from storage, and auxiliary energy supply equipment. Figure 1 illustrates the typical arrangement of these components and lists the examples in each category which are treated by FCHART.

The FCHART user describes a system by choosing a consistent set of components from the available options. To analyze a typical air-based space heating system, for example, one would select a flat-plate collector, air ducts, rock bed, furnace, and conditioned (heated) space. Unrealistic or unimplemented combinations such as a CPC collector with air ducts and a liquid storage tank are rejected; the program asks a series of questions which point out the available options for each component type.

System Performance and Meteorological Data

The performance of any system depends on the operating characteristics of each component, and the conditions under which the system operates. Component performance parameters may be measured, derived from theory, or obtained from equipment manufacturers. They are known quantities which are supplied to the FCHART program by the program user. In contrast, the conditions under which a system operates depend on the varying energy supply and demand. Energy demands may occur on a regular day-to-day schedule, as in an industrial setting, or may be a function of weather conditions, as in home heating. Energy supply in solar systems is invariably coupled to the weather.

The two weather indicators which are most closely related to the supply of solar thermal energy are the level of insolation and ambient temperature. Since solar systems are characteristically nonlinear in their response to conditions, it is often necessary to estimate the distribution of each of these variables in addition to obtaining monthly average daily solar radiation and monthly average ambient temperature. For systems with solar collectors, a solar radiation cumulative distribution function is useful for finding long-term average performance. Liu and Jordan [1] have shown that the distribution of radiation is a function of $\bar{K}_T$, the ratio of monthly radiation received to monthly extraterrestrial radiation. For systems which include an ambient source heat pump, it is desirable to estimate the number of hours over the month when the ambient temperature is at any given level. A triangular frequency distribution with the number of hours at each temperature dropping off linearly with distance from the mean temperature has been found to be satisfactory for this purpose (Anderson [2]).

Collector Performance

When a solar collector operates, heat is gained from the incident solar radiation and heat is lost to the surroundings. As indicated by the Hottel-Whillier model [3-5], the heat gain depends on the insolation while the heat loss is a function of the difference between ambient and collector working fluid temperatures. If the gains are greater than the losses, then useful energy collection can take place. Thus, for any given operating temperature, there is a minimum level of insolation, defined as

the critical level, above which there is net heat gain from the collector. Determining collector performance, and hence total solar energy input to a system, is facilitated by determining the fraction, $\bar{\phi}$, of the monthly radiation which is above any given critical level. Klein [6], extending the results of Whillier [7] and Liu and Jordan [8] has developed a correlation for $\bar{\phi}$ for flat-plate collectors as a function of critical level, total radiation for the month, location, collector orientation, and time of year. Collares-Pereira and Rabl [9] have developed similar correlations for CPC, 1-axis tracking and 2-axis tracking concentrating collectors.

Space Heating with Seasonal Storage

A schematic of a typical liquid-based solar space heating system is shown in Fig. 2. Collected solar energy is stored in the tank. The tank loses a fraction of the heat to the surroundings and supplies the remainder to the load according to demand. An auxiliary furnace provides space heating when the solar system cannot meet the space heating requirement. In systems with sufficient storage to save summer heat for fall or winter, the tank temperature does not vary significantly from day to day. As a result, the critical insolation level for energy collection is nearly constant over a month and the $\bar{\phi}$ correlation may be used to express the monthly energy collected as a function of average tank temperature. The performance of each component, and hence system performance, is a function of tank temperature. An iterative solution for the average tank temperature which satisfies the system energy balance yields an estimate of monthly system performance. Braun [10] has compared this $\bar{\phi}$-method with detailed simulations for a wide range of system parameters and a variety of locations and found good agreement.

Space and Water Heating with Short-Term Storage

If a system such as shown in Fig. 2 has a tank with storage capacity of less than approximately one week's energy demand, then storage temperature variations over a month are likely to be significant. This causes considerable variation in the critical radiation level for energy collection. As a result, the $\bar{\phi}$-method just described will not adequately predict system performance; another approach is required.

One alternative, the f-chart method developed by Beckman, Klein and Duffie [11], is to correlate monthly system performance with two dimensionless parameter groups, called X and Y. The first, X, is a reference collector loss divided by the system load, while the second, Y, is the total energy absorbed by the collector divided by the load. The f-chart correlation for monthly fraction of the load met by solar energy is used in FCHART for air-based space heating and for domestic water heating systems.

Another approach for closed-loop systems with short-term storage, the $\bar{\phi}$,f-chart method of Klein and Beckman [12], is applicable if energy can be delivered only when the tank is above some minimum temperature, T_{min}. Space heating, absorption air conditioning, and certain process heating systems have loads of this type. Since the tank temperature will not be drawn below T_{min}, there is a minimum critical level for collection. Hence there is a maximum fraction of the energy absorbed by the collector which can be put to use, denoted $\bar{\phi}_{max}$. The performance of this type of system may be correlated with X and the product $\bar{\phi}_{max}Y$. The $\bar{\phi}$,f-chart method is utilized in place of the f-chart algorithm for liquid-based solar space heating systems. One advantage of the method is that it allows the tank heat loss coefficient to be specified.

Heat Pump Space Heating System

Both the heating capacity of a heat pump and the work input required to operate at capacity depend on the heat source (evaporator) temperature. In stand-alone space heating applications and in systems where a heat pump is used in parallel with a solar heating system, the heat source is ambient air. Since the space heating demand is a function of ambient temperature, heat pump capacity and heating requirements are closely coupled. In a series heat pump system, the heat pump heat source is the solar system storage tank. In this case, the distributions of heating load and heating capacity over the month are not strongly related. The method used in FCHART for ambient source heat pumps evaluates heat pump performance and space heating load over a range of ambient temperatures (Anderson [2]), while the series heat pump method centers on storage tank temperature (Svard [3]).

As shown in Fig. 3, the capacity of an ambient source heat pump increases with increasing ambient temperature, while the heating load decreases. The curves cross, i.e., the capacity for energy supply meets the energy demand, at a temperature called the balance point. When the ambient temperature is above the balance point, the heat pump meets the heating load and the work input is the work required to operate at capacity times the ratio of load to capacity. During the times when ambient temperature is below the balance point, the heat pump operates at capacity and thus requires the full work input. Since the energy supplied by the heat pump and the corresponding work requirement are functions of ambient temperature, FCHART integrates both quantities over an ambient temperature distribution to determine stand-alone heat pump system performance. Anderson [2] has found straightforward relationships between stand-alone heat pumps and heat pumps which operate in parallel with a solar heating system: the fractions of the heating load met by energy absorbed from the atmosphere and by heat pump work in a parallel system are equal to those for the corresponding stand-alone system, each multiplied by the fraction of the heating load not met by the solar system. Comparisons between simulations and the above methods for ambient source heat pumps show excellent agreement.

The design method used in FCHART for series heat pump systems combines the $\bar{\phi}$-method (which gives system performance as a function of tank temperature) with $\bar{\phi}$,f-charts. The solar system load is defined as the total energy which must be supplied to the heat pump evaporator in order for the heat

pump to fully meet the space heating demand. Since the heat pump operating characteristics depend on tank temperature, this load is a function of tank temperature. An initial approximation of the solar system load is made and the $\bar{\phi}$,f-chart correlation is used to find the fraction of this load met by collected solar energy. Then, the ϕ-method is used to determine the implied average monthly tank temperature, allowing a more accurate estimate of the solar system load to be made. This process is repeated until convergence is reached. Svard [13] has shown good agreement between this method and detailed simulations.

Using FCHART

The interactive FCHART program provides convenient access to the design methods described here. The program asks questions in order to determine which type of system is being considered, and allows the user to set or vary performance parameters easily. Instructions and assistance are given whenever the user types in HELP. Some sample questions and user responses are given in Fig. 4.

In addition to the LIST command which appears near the bottom of Fig. 4, FCHART features many other commands which control analysis and input/output options. The more important commands and their uses are summarized in Table 1. Among the analysis options, FCHART includes algorithms to optimize system parameters and perform life-cycle cost analyses. For example, the optimum series heat pump and direct solar heating for any locations may be determined and the life-cycle costs of the two alternatives compared. Combining efficient methods of performance evaluation with system optimization and economic analysis routines, FCHART 4.0 is a convenient and powerful tool for engineers in the solar energy field.

Table 1
FCHART Program Commands

RUN	- perform analysis of system
HELP	- provide information on program
FORGET	- forget system description and begin asking questions
OPT	- optimize system with respect to specified parameters
LOOP	- perform several analyses, varying specified parameter
TITLE	- print following title at top of output tables
SAVE	- write concise system description and parameter values into storage file
READ	- read system description and parameter values from storage file
LIST	- list system description, parameters, or weather data, e.g., LIST SYSTEM, LIST COLLECTOR, LIST DATA

ACKNOWLEDGEMENT

This paper summarizes work done by many members of the University of Wisconsin Solar Energy Laboratory. S.A. Klein and W.A. Beckman were particularly important in the development of the design methods, the program, and this paper.

REFERENCES

[1] B.Y.H. Liu and R.C. Jordan, "The Long-Term Average Performance of Flat-Plate Solar Energy Collectors," Solar Energy, 7, 53 (1963).

[2] J.V. Anderson, "Procedures for Predicting the Performance of Air-to-Air Heat Pumps in Stand-Alone and Parallel Solar-Heat Pump Systems," M.S. Thesis, University of Wisconsin, Madison (1979).

[3] H.C. Hottel and B.B. Woertz, "Performance of Flat Plate Solar Heat Collectors," Trans. ASME 64, 91 (1942).

[4] H.C. Hottel and A. Whillier, Trans. of the Conference on the Use of Solar Energy, 2, "Evaluation of Flat-Plate Collector Performance," Part I, 74, University of Arizona Press (1955).

[5] R.W. Bliss, "The Derivations of Several Plate Efficiency Factors Useful in the Design of Flat-Plate Solar Heat Collectors," Solar Energy, 3, 55 (1979).

[6] S.A. Klein, "Calculation of Flat-Plate Collector Utilizability," Solar Energy, 21, 393 (1978).

[7] A. Whillier, "Solar Energy Collection and Its Utilization for House Heating," Ph. D. Thesis, Mechanical Engineering, M.I.T. (1953).

[8] B.Y.H. Liu and R.C. Jordan, "Availability of Solar Energy for Flat-Plate Solar Heat Collectors," Chapt. V, Applications of Solar Energy for Heating and Cooling of Buildings, ASHRAE GRP 170, New York (1977).

[9] M. Collares-Pereira and A. Rabl, "Simple Procedure for Predicting Long Term Average Performance of Nonconcentrating and of Concentrating Solar Collectors," Solar Energy, 23, 235 (1979).

[10] J.E. Braun, "Seasonal Storage of Energy in Solar Heating," M.S. Thesis, University of Wisconsin (1979).

[11] W.A. Beckman, S.A. Klein and J.A. Duffie, Solar Heating Design by the f-Chart Method, Wiley, New York (1977).

[12] S.A. Klein and W.A. Beckman, "A General Design Method for Closed-Loop Solar Energy Systems," Solar Energy, 22, 269 (1979).

[13] C. Svard, M.S. Thesis, University of Wisconsin (1980).

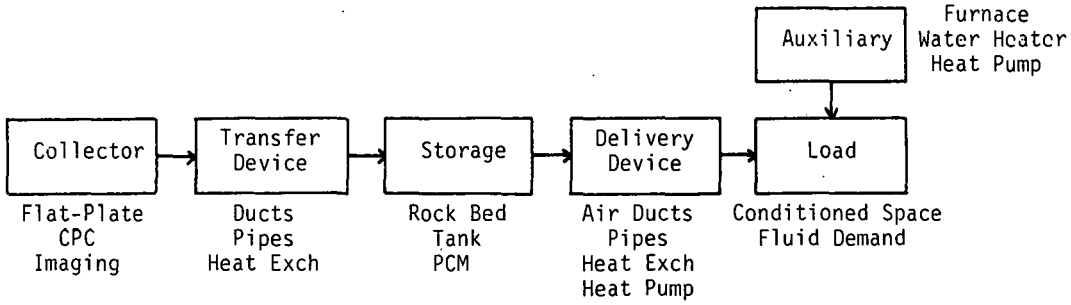

Figure 1. Components in Solar Energy Systems

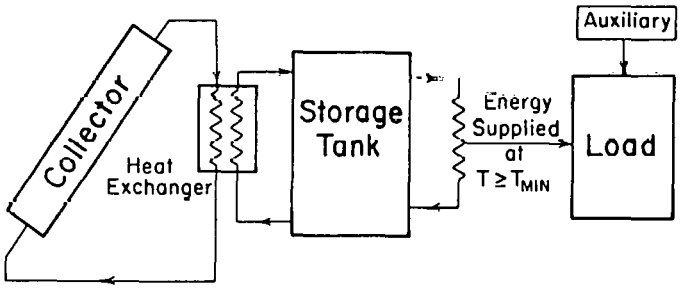

Figure 2. A Solar Heating System

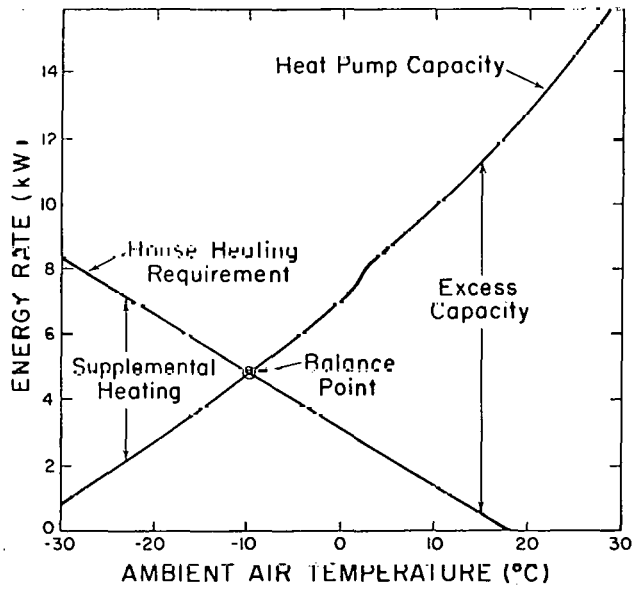

Figure 3. Heat Pump Capacity and Heating Requirement

```
    Do you have a process heating (PROC), space heating (SPACE), combined space
    and water heating (SDHW), water heating only (DHW), or passive solar only
    system (PASSIVE)?
>HELP
    The options are:
        PROC    -  process heating or air conditioning
        SPACE   -  space heating (only) system
        SDHW    -  combined space and domestic water heating
        DHW     -  domestic hot water (only) system
        PASSIVE -  passive solar or heat pump only
>SPACE
    Do you have a flat-plate, CPC, or imaging collector (FPLATE, CPC, IMAGE)?
>FPLATE
    Is there a heat exchanger between the collector and storage (HX, NHX)?
>HX
    Do you want to consider pipe losses (LOSS, NLOSS)?
>NLOSS
    Is your system air-based (AIR) or liquid-based (LIQ)?
>AIR
    Do you have a rock bed (ROCK) or phase change energy storage (PCES)?
>ROCK, LIST
    ROCK BED STORAGE PARAMETERS
    S1.  Storage capacity/collector area.......
    S2.  Storage unit height/diameter..........
    S3.  Heat loss coefficient.................
     :
     :
```

Fig. 4 Sample FCHART Questions and Answers

NOTES

A SIMPLIFIED THERMAL PERFORMANCE SIMULATION AND ECONOMIC ANALYSIS METHODOLOGY FOR DESIGN OF PASSIVE SOLAR HOMES

L. Icerman
K. Myers
Dept. of Technology and Human Affairs
Washington University
St. Louis, Missouri 63130

A. Swift
Dept. of Mechanical Engineering
Washington University
St. Louis, Missouri 63130

ABSTRACT

A simplified methodology is developed which consists of a computer simulation of the heat flow characteristics of a passive solar home for a variety of design parameters (e.g., window area, insulation levels, thermal mass) and site-specific factors (e.g., weather conditions, building orientation). Performance data from the thermal response simulation and unit cost estimates of passive design elements are incorporated into a linear programming optimization model to determine least-cost designs and to predict the corresponding heat flow characteristics. Preliminary results indicate that the linear programming model can predict heat flow characteristics of the optimal home designs to within a few percent of those obtainable from more expensive hourly simulation techniques. Application of this design methodology to a moderate-sized home in the Columbia, Missouri, area shows that many passive design elements and systems are highly cost effective in new home construction at current electric utility rates.

1. INTRODUCTION

Numerous computer models have been developed to predict the heat transmission characteristics and resulting heating and cooling loads of passive solar buildings given specific environmental inputs [1, 2]. Thermal performance simulation models have also been developed to enable the evaluation of alternative passive and active home designs [2-4]. The difficulty with using detailed performance simulations to evaluate alternative designs is that the programs are complex, require large computing capability, and each design configuration must be simulated independently in order to determine the overall impact of the passive components on the thermal performance of the building. Even when these difficulties do not represent a barrier to design evaluation, hourly thermal performance simulation methods typically do not include design cost as a parameter to facilitate the comparison of alternative passive home designs.

In order to alleviate these problems that are characteristic of standard programs, we have developed a linear programming optimization model which combines performance data from numerous hourly thermal performance simulations with cost estimates of passive design elements to predict heat flow characteristics and to determine least-cost designs. This procedure offers considerable potential cost savings for design evaluations because following the generation of a number of basic component simulations, all subsequent technical and economic design evaluations may be performed using only the linear programming model.

2. THERMAL PERFORMANCE SIMULATION MODEL DEVELOPMENT AND VALIDATION

The hourly thermal performance simulation model calculates heat transmission for residential and small commercial buildings by analyzing heat flows through the building envelope and then calculates heating and cooling requirements based on the hourly heat transmission and the preset room temperatures. In this model, the building is assumed to be one zone of equal temperature distribution, with a heated basement (no room divisions or attached garage). The major inputs to the program are hourly weather data and the building description. The weather data used are Typical Meteorological Year data for Columbia, Missouri, obtained directly from the U.S. Weather Bureau [5].

The thermal performance simulation model (see Figure 1) performs a heat flow analysis for a building based primarily on standard ASHRAE methods [6]. The model deviates from the ASHRAE methods when calculating transient heat flow through the building walls, in which case it uses the Crank-Nicolson method of numerical solution to the transient heat flow equation [7]. In addition, a Trombe wall model is included which uses a thermal net analysis [4] to calculate glass and air space temperatures for a double-glazed Trombe wall without vents. The Crank-Nicolson method [7] is then used to calculate the Trombe wall temperature profile.

Three separate validations of the thermal performance model were performed. Validation of the Crank-Nicolson method was accomplished by comparing the results of the hourly simulations with analytical results obtained using Heisler

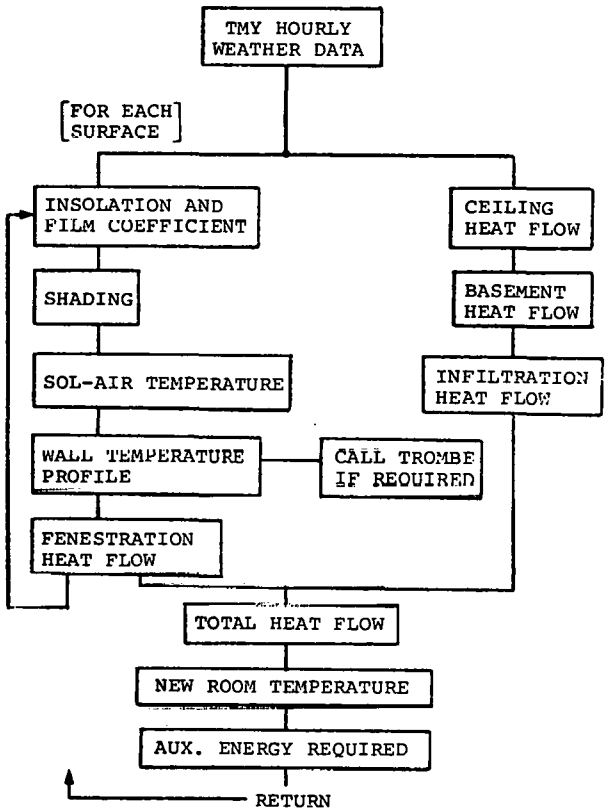

Fig. 1. Hourly Thermal Performance Simulation Model

Charts [8]. The simulation results agreed with the Heisler charts with an average error of approximately 0.7% and a maximum error of 1.3%.

The Trombe wall model was validated by comparison with results obtained by experiments with Trombe wall test rooms [4]. The simulation calculated temperatures with an average error of less than 5% and a maximum error of less than 10% for each hour.

The entire hourly simulation program was validated by comparing monthly thermal performance values from the simulation with values for an actual residence in the St. Louis area. Monthly utility bills for the winter period of January 5, 1979, to February 4, 1979, and the summer period of July 11, 1978, to August 9, 1978, were used to determine gas and electric energy consumption. In addition to using hourly ambient temperature and wind velocity data compiled by the St. Louis Weather Bureau, hourly insolation values were calculated using cloud cover and precipitation data for St. Louis as inputs to a correlation model based on Columbia, Missouri, SOLMET data [9]. The resulting heating and cooling loads were calculated to within 3% and 4% of the monthly values, respectively.

3. HOURLY SIMULATIONS

The hourly thermal performance simulation model was used to evaluate several retrofit and redesign alternatives that may be applied to typical midwestern residences. As part of these evaluations, the thermal performance and cost effectiveness of retrofit and redesign options were determined. These results were then used to demonstrate the potential for cost reductions in optimal designs produced by the linear programming model compared to the reference home described in Section 3.1.

In order to standardize the simulations and to determine average thermal response in a given location, Typical Meteorological Year data [5] were used for all simulations. A four-month heating season, November 15 to March 15, and a four-month cooling season, May 15 to September 15, were simulated using weather data for Columbia, Missouri.

3.1 Retrofit options

The reference home has approximately an 80-m^2 (850-ft^2) floor area, a heated basement, a brick-faced east wall, and asbestos siding on the other three walls. The home has 8.5 m^2 (91 ft^2) of window area (4.4 m^2 (47 ft^2) on the east and 4.1 m^2 (44 ft^2) on the west) and 0.9-m (3-ft) overhangs. One air exchange/hour and temperature swings of 21.1 to 26.7°C (70 to 80°F) and 18.9 to 24.4°C (66 to 76°F) in the winter and summer, respectively, are assumed.

Several retrofit options for the reference home were considered, with each new configuration retaining all of the properties of the previous ones. Configuration A-1 changed the winter and summer temperature swings to new values of 18.9 to 21.1°C (66 to 70°F) and 24.4 to 26.7°C (76 to 80°F), respectively. Configuration A-2 increased the ceiling insulation from R-15 to R-40. (All insulation values are expressed as thermal resistance (R) values for convenience: 1.0 R = 0.18°C-m^2/watt (1.0°F-hr-ft^2/Btu).) Configuration A-3 increased wall insulation from R-12 to R-20. Configuration A-4 replaced existing draperies with R-2 insulating shutters, which were closed on winter nights and used as sun shades in the summer. In order to determine the cost effectiveness of these options, a simple payback criterion was used to compare retrofit costs with the value of the energy saved. Retrofit option costs were estimated using Means' cost data [10]. The home was assumed to be all electric with a seasonal coefficient of performance (COP) of 1.0 for both heating and cooling. The cost of electricity was chosen to be 4¢/kwh. The results of these simulations are shown in Table 1.

TABLE 1. RESULTS OF RETROFITTING REFERENCE HOME

Configuration	A-1	A-2	A-3	A-4
Heating load reduction (%)	22	34	44	49
Cooling load reduction (%)	26	34	37	53
Total load reduction (%)	23	34	41	50
Investment required ($)	0	212	274	379
Years to payback @ 4¢/kwh	0	1.5	1.6	1.8

3.2 Redesign options

A number of redesign configurations were simulated in order to determine the performance and cost of each alternative configuration compared to the reference home design. The economic criteria selected for redesign were based on incremental, annualized costs of each option above and beyond the base cost of the reference home. The investment cost was amortized over 30 years at an effective annual mortgage rate of 10% to simulate the effect such costs would have on the mortgage payments of a homeowner. Energy tax credits, interest deductions from income taxes, and back-up heating system size reductions, all of which improve the economic attractiveness of design changes, were not considered in this analysis. The minimum annual cost, including operating and annualized capital costs, is taken to be the decision criterion to indicate the best economic choice. However, the corresponding design does not necessarily correspond to the design with the smallest energy consumption. As in the retrofit case, cost data were taken from Means [10] (see Table 2), and the home was assumed to be all electric with a seasonal COP of 1.0 for both heating and cooling.

Several redesign configurations were analyzed, with each new configuration retaining all of the properties of the previous ones. Configuration B-1 reoriented the home so that the longer brick-faced wall faced south and had the temperature swing of retrofit option A-1. Configuration B-2 increased wall insulation from R-12 to R-20 and ceiling insulation from R-15 to R-40. Configuration B-3 increased the glass area to 6.5 m^2 (70 ft^2) on the south side and reduced the glass area on the north side to 1.9 m^2 (20 ft^2). Configuration B-4 added insulating shutters (R-2) which were to be kept closed at night in the winter and to be used as sun shades in the summer. Configuration T-1 replaced the brick-faced south wall with a double-glazed, 0.305-meter (1-ft) thick, R-1.2 Trombe wall. One-third of the Trombe wall was window area for direct gain with no shutters. The Trombe wall was unvented to the structure, had a 0.9-meter (3-ft) overhang in the summer only, and was vented to the atmosphere in summer to prevent overheating. The thermal performance of these redesigns and the corresponding annual costs are presented in Table 3.

TABLE 2. PASSIVE ELEMENT COSTS

Passive element	Cost	
Insulation	$\$0.11/m^2$	($\$0.01/R\text{-}ft^2$)
Wall sections (excluding windows)	$\$21.30/m^2$	($\$1.98/ft^2$)*
Windows (double-glazed)	$\$43.04/m^2$	($\$4.00/ft^2$)
Shutters (R-2)	$\$10.76/m^2$	($\$1.00/ft^2$)
Trombe wall (double-glazed)	$\$114.39/m^2$	($\$10.63/ft^2$)**

*For wall insulation values above R-20, a double-studded wall section is assumed to cost an additional $\$1.94/m^2$ ($\$0.18/ft^2$).

**This value is based on data from Ref. [11] for a 0.305-meter (1-ft) thick Trombe wall.

The results presented in Table 3 are useful to energy conscious designers or homeowners interested in reducing home construction and operation costs. Table 3 also illustrates a basic limitation of using hourly simulations for design, because selection of an optimal design, a logical next step, would require simulations of all possible configurations for each different design option and location.

A better approach, and one used in other design methods based on hourly simulations (e.g., F-Chart design method), is to determine the relationships among significant parameters in the simulations by making numerous simulation runs and then to use these relationships to develop a short-cut method to choose the optimal design and to predict thermal performance.

4. LINEAR PROGRAMMING CONCEPTS AND OPTIMAL DESIGN

4.1 Linear programming model development

The linear programming model (see Figure 2) is based on a standard linear programming software package. The methodology is as follows:

Step 1. Determine significant parameters in the design. For passive solar residential design, typical parameters are wall and ceiling insulation R-values, window areas on each wall, and Trombe wall area.

Step 2. Choose basic dimensions and construction materials of the home.

Step 3. Specify very low wall and ceiling insulation values to represent low heat transmission conditions and reduce window area to zero.

Step 4. Perform parametric hourly thermal performance simulations by changing only one parameter at a time to determine the effect on the thermal response.

Step 5. Develop functional relationships, based on the simulation results, between beneficial net heat flow values and parameter choices. Beneficial heat flow is defined as heat gain in the winter or heat loss in the summer, since these flows displace the use of auxiliary energy.

Step 6. Determine the thermal performance effects of non-parametric variables, such as internal gains, basement losses, and infiltration rates, from the hourly simulation results.

Step 7. Assign annualized unit costs for each passive design element based on mortgage interest rates and other appropriate criteria. The value of auxiliary heating and cooling loads is determined according to fuel source, equipment efficiency, and the cost of delivered energy.

Step 8. Generate a coefficient matrix in which each column represents a parameter variable and each row corresponds to a functional relationship or design constraint.

Step 9. Apply a linear programming algorithm to solve the coefficient matrix by varying the values of all passive design parameters until a least-cost design is obtained.

Step 10. Calculate the thermal performance of the least-cost passive design from the matrix coefficients.

4.2 Advantages and limitations

This methodology, which should be useful to both analysts and designers, has several distinct advantages compared to standard thermal performance simulation codes: (i) least-cost designs may be determined and the thermal performance calculated without the use of complex hourly simulations; (ii) design constraints and economic considerations are integral parts of the design methodology; (iii) a catalog of coefficient

TABLE 3. THERMAL PERFORMANCE AND ECONOMIC ANALYSIS OF REFERENCE, REDESIGNED, AND OPTIMIZED HOMES

Configuration	Reference[a]	Redesign options					Optimized design options		
		B-1	B-2	B-3	B-4	T-1	@ 4¢/kwh	@ 8¢/kwh[b]	@ 16¢/kwh
Heating load reduction (%)	-	29	50	52	57	72	54	66	86
Cooling load reduction (%)	-	40	51	51	52	51	59	61	64
Total load reduction (%)	-	32	50	51	55	65	56	65	79
Initial design cost ($)	423	423	697	710	781	2,374	547	1,093	3,249
Annualized design cost ($/y)	45	45	74	75	83	252	58	116	345
Total annual cost[c] ($)									
@ 4¢/kwh	468	331	286	281	273	400	245	266	434
@ 8¢/kwh	890	616	497	486	462	548	432	416	523
@ 12¢/kwh	1,313	902	709	691	652	696	619	566	613
@ 16¢/kwh	1,736	1,187	921	896	842	844	806	716	687

[a]The reference home has a heating load of 6,962 kwh (23.76 million Btu), a cooling load of 3,601 kwh (12.29 million Btu), and a total load of 10,563 kwh (36.05 million Btu).

[b]The optimized design for 12¢/kwh is identical with the optimized design for 8¢/kwh.

[c]The total annual cost is the sum of the annualized design cost and annual cost of the back-up energy requirements.

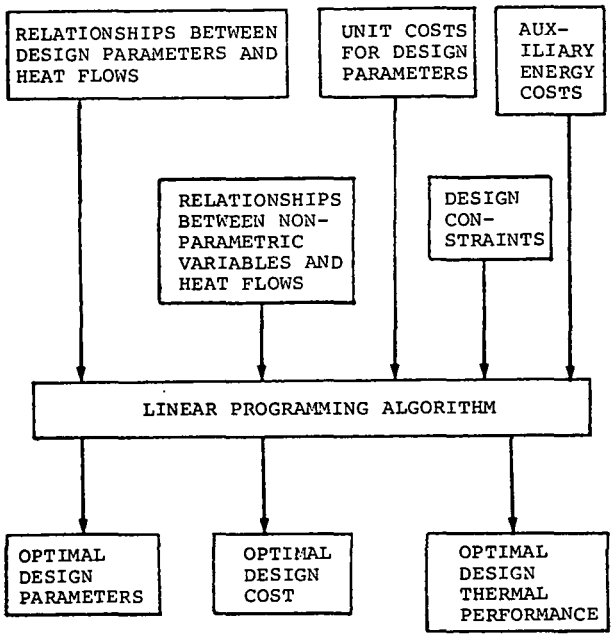

Fig. 2. Linear Programming Model

matrices may be developed for selected passive design elements and then rearranged to characterize a variety of passive designs; and (iv) since the model is really a design methodology, the results should be able to contribute to the formulation of building codes.

A current limitation of this methodology is that the matrix coefficients are specific and depend on: (i) predetermined room temperatures; (ii) fixed climatic regions; (iii) approximately constant wall area to home volume ratios; and (iv) specific residence types (e.g., one vs. two story). This limitation can be reduced in more advanced models.

4.3 An example of optimal residential design

The linear programming methodology was applied to a south facing reference home having 0.9-meter (3-ft) overhangs and insulating (R-2) window shutters. The cost data are from Means [10] given in Table 2. Four optimal designs were derived based on energy costs of 4, 8, 12, and 16 ¢/kwh. The design optimized for 4¢/kwh consists of a south wall insulated to R-20 with 1.86 m^2 (20 ft^2) of window area. The remaining walls are insulated to R-20 and the ceiling was insulated to R-35. The designs optimized for 8 and 12¢/kwh have R-40 insulation in all the walls, 3.72 m^2 (40 ft^2) of window area in the south wall, and R-50 insulation in the ceiling. The optimal design based on 16¢/kwh has a south facing 21.6-m^2 (232-ft^2) Trombe wall with 3.7 m^2 (40 ft^2) of window area. The remaining walls have R-40 insulation and the ceiling is insulated to R-50.

A number of optimized home designs have been simulated using the hourly thermal performance model to validate the thermal performance predicted by the linear programming model. The linear programming model predicted total energy needs to within a few percent of the results from the thermal performance model [12].

The thermal and economic performance of the optimized designs are presented in Table 3 so that direct comparison may be made with the redesign options. In all cases, the optimized designs have lower total annual costs than the redesigned homes. The results indicate that strategic expenditures for passive solar design elements are necessary to reach optimal thermal and economic performance goals that correspond to significantly higher energy savings and larger reductions in annual energy costs than those typically associated with modern passive solar home configurations.

5. ACKNOWLEDGMENTS

We would like to thank Warren Cargal of Solar Building Corporation of St. Louis, Missouri, for his assistance in passive design concepts and Stephen Andes of Londe, Parker, Michels of Clayton, Missouri, for his assistance in the modelling of Trombe walls. In addition, some of the early work for this paper was performed under the classroom guidance of Professor Francis Vithayathil, Washington University.

6. REFERENCES

1. Passive Solar, State of the Art, Vol. 2, Components, Simulation, and Testing, 2nd National Passive Solar Conference, pp. 349-473, Philadelphia, PA (1978).

2. Proceedings of the 4th National Passive Solar Conference, pp. 115-297, Kansas City, MO (1979).

3. S. A. Klein, et al., TRNSYS, A Transient Simulation Program, Solar Energy Laboratory, University of Wisconsin, Madison, WI (1976).

4. J. Perry, Mathematical Modelling of the Performance of Passive Solar Heating Systems, LA-UR-77-2345, Los Alamos Scientific Laboratory, Los Alamos, NM (1977).

5. I. Hall, et al., Generation of a Typical Meteorological Year, Proceedings American Section International Solar Energy Society, Vol. 2, pp. 669-675, Denver, CO (1978).

6. American Society of Heating, Refrigerating, and Air Conditioning Engineers, Handbook of Fundamentals, New York, NY (1972).

7. M. Ozisik, Boundary Value Problems of Heat Conduction, p. 402, International Textbook Company, Scranton, PA (1968).

8. F. Kreith, Principles of Heat Transfer, p. 149, International Textbook Company, Scranton, PA (1965).

9. National Oceanic and Atmospheric Administration, Regression Equations and Coefficients of the ARL Models of Global Solar Radiation, Asheville, NC.

10. Building Construction Cost Data, R. S. Means Company, Duxbury, MA (1979).

11. J. D. Balcomb, et al., Handout from the Advanced Passive Design Workshop, Omaha, Nebraska, sponsored by DOE and MASEC, July 1979.

12. K. Myers, L. Icerman, and A. Swift, Simulation and Optimization Techniques for Determining Energy Efficient and Cost Effective Passive Home Design, pp. 207-211, Proceedings of the 4th National Passive Solar Conference, Kansas City, MO (1979).

LONG-TERM SOLAR COOLING SYSTEMS PERFORMANCE PREDICTIONS VIA A SIMPLIFIED DESIGN METHOD

D.K. Anand, Professor
R.B. Abarcar, Research Associate
R.W. Allen, Professor

Solar Energy Projects
Department of Mechanical Engineering
University of Maryland
College Park, Maryland

ABSTRACT

A viable alternative to detailed computer simulation as a means of obtaining long-term solar cooling system performance is the correlation of numerous simulation results that cover a wide range of system parameters and weather conditions. The design method presented in this paper uses a solar cooling fraction, f_c-chart which was derived from detailed SHASP (Solar Heating and Air Conditioning Simulation Programs) runs of a solar cooling system operating under varying real weather conditins obtaining in various cities selected for their reasonably good values of available insolation and expected cooling loads. The combinations of diverse climatic conditions and cooling demands insure the region independency of the resulting correlation.

INTRODUCTION

The f-chart [1] is a solar heating design chart which was developed from TRNSYS [2] and is widely accepted. A similar simplified design method for cooling called the f-$\bar{\emptyset}$ charts uses the utilizability curves of Liu and Jordan [3] is proposed but is limited to constant COP cooling operation or constant thermal efficiency operation of high temperature thermal systems.

The computer simulation program called SHASP [4] has been successfully used in solar cooling systems performance predictions. The program uses a generalized chiller model where cooling capacity is dependent on the hot water supply temperature. There is a dynamic interaction between the chiller and the building cooling load which is dependent on ambient air temperature, insolation and heat generation. A wide range of system parameters and weather data are used in the detailed simulation runs and the results are correlated to develop the simplified cooling design charts.

SYSTEM DESCRIPTION

The basic solar cooling system is shown in Fig. 1. The cooling machine used is a hot water fired absorption chiller where cooling capacity is dependent on the hot water supply temperature. The cooling load is dependent on the ambient air temperature, insolation and heat generation. The control strategy used to simulate the system operation is based on a previous study of solr cooling systems [5]. Basically, all of the useful energy collected by the solar collector is sent to a liquid storage tank and stored as sensible heat. Whenever there is a cooling demand, the absorption chiller draws off hot water from storage and delivers enough cooling to satisfy the demand. If the temperature of the hot water in storage is such that the chiller cannot satisfy the load, then auxiliary is used to fully supply the generator requirements.

ANALYSIS

An energy balance of the solar cooling system yields

$$Q_u - \frac{Q_L}{COP_{av}} + Q_{aux} = \Delta E \qquad (1)$$

Eq. (1) applies to any system whose load, Q_L, can be met 100% of the time. For an undersized system, the cooling load cannot be met at all times and Q_L should be replaced by the total cooling supplied. Also, for the system considered using an absorption chiller, the auxiliary energy, Q_{aux}, is directly supplied to the generator of the chiller. Eq. (1) also applies to a system using a Rankine chiller where the auxiliary energy is supplied to the boiler of the Rankine Cycle.

On a long term basis, the change in storage tank capacity, ΔE will be negligible compared to the other energy quantities and Eq. (1) reduces to

$$Q_u - \frac{Q_L}{COP_{av}} + Q_{aux} = 0 \qquad (2)$$

The average cooling supplied when the system operates only on auxiliary, is given by:

$$Q_{C_{aux}} = COP_{av}(Q_{aux}) \qquad (3)$$

The portion of the load accountable to solar is then:

$$Q_{C_{sol}} = Q_L - Q_{C_{aux}} \quad (4)$$

$$Q_{C_{sol}} = Q_L - COP_{av}(Q_{aux}) \quad (5)$$

The solar cooling fraction can be defined as

$$f_c = \frac{Q_{C_{sol}}}{Q_L} = \frac{Q_L - COP_{av}(Q_{aux})}{Q_L} \quad (6)$$

$$f_c = 1 - \frac{Q_{aux}}{(Q_L/COP_{av})} \quad (7)$$

Using Eq. (2), the solar cooling fraction can be expressed in terms of the useful collected heat, Q_u, as:

$$f_c = \frac{Q_u}{(Q_L/COP_{av})} \quad (8)$$

The instantaneous useful heat collected by a collector array of area A_c is given by:

$$q_u = \left[F'_R\overline{\tau\alpha} - \frac{F'_R U_L (T - T_d)}{I_c}\right] I_c A_c \quad (9)$$

The total energy collected over the entire period of operation of the system is obtained by integrating Eq. (9).

$$Q_u = \int F'_R \tau\alpha I_c A_c dt - \int F'_R U_L (T - T_d) A_c dt \quad (10)$$

The long term solar cooling fraction can then be expressed as

$$f_c = \int \frac{F'_R \tau\alpha I_c A_c}{(Q_L/COP_{av})} dt - \int \frac{F'_R U_L (T - T_d) A_c}{(Q_L/COP_{av})} dt \quad (11)$$

The integrals in Eq. (11) cannot be evaluated easily since the insolation and the dry-bulb temperature are not continuous mathematical functions. Moreover, the relationship between the solar thermal system, the chiller and the load is both complex and dynamic. As an alternative to evaluating Eq. (11), detailed simulation runs are made using SHASP with real weather inputs and an average daily solar cooling fraction, f_c, for any cooling month can be calculated.

The grouping of terms in Eq. (11) suggests a correlation between the solar cooling fraction and two dimensionless parameters

$$X = F'_R U_L A_c (T_{ref} - \overline{T}_d)\Delta T/(Q_L/COP_{av}) \quad (12)$$

$$Y = F'_R \tau\alpha I_{ct} A_c/(Q_L/COP_{av}) \quad (13)$$

A reference temperature, T_{ref} = 96.1C (205F) is used since there is a limit to the maximum generator temperature of an absorption chiller due to recrystallization. Using the least squares method of curve fitting, the detailed simulation results are correlated into a single function of the dimensionless parameters of the form

$$f_c = a + bY + cX + dY^2 + eX^2 \quad (14)$$

RESULTS

The solar cooling fraction, f_c chart shown in Fig. 2 results from the correlation of detailed solar cooling simulation runs made using SHASP and real weather data for the cities of Phoenix, AZ, Ft. Worth, TX, Miami, FL, Charleston, SC, Madison, WI and Washington, D. C. These cities were selected for their diverse climatic conditions which present a wide range of combination of available insolation and expected cooling load.

The system parameters were varied over a range of values that represent what actual systems might possibly have. The ranges over which various parameters were varied are:

Collector:

$$0.53 \leq F'_R\tau\alpha \leq 0.76$$

$$3.123 \leq F'_R U_L \leq 5.452 \text{ W/m}^2 - {}^\circ\text{C}$$

$$51.1 \leq A_c \leq 92.9 \text{ m}^2$$

$$-10^\circ \leq (\emptyset - S) \leq +10^\circ$$

$$\frac{m}{A_c} = 48.8 \frac{\text{Kg}}{\text{m}^2 - \text{hr}}$$

Hot Storage:

$$48.8 \leq (M/A_c) \leq 97.9 \text{ Kg/m}^2$$

$$96.1 \leq T_{Dump} \leq 100^\circ \text{ C}$$

Absorption Chiller:

$$76.7 \leq T_{G\ min} \leq 85^\circ \text{ C}$$

The generator of the absorption chiller is fired by hot water from storage at temperatures

$$T_{G\ min} \leq T_G \leq 96.1^\circ \text{ C}$$

The polynomical regression correlation of the detailed SHASP runs give the cooling fraction as

$$f_c = 0.19207 - 0.079798X + .00201243X^2 + 0.45434Y - .0036096Y^2 \quad (15)$$

Equation (15) is used to determine the constant solar cooling fraction curves shown in Fig. 2. Outside the range of values of X and Y covered by Fig. 2, the following procedure should be used to obtain the cooling fraction:

X = 15 whenever calculated X > 15

and Y = 6 whenever calculated Y > 6

otherwise: use calculated values of X and Y

SAMPLE EXAMPLE

The following example illustrates the ease with which the solar cooling fraction can be predicted using the method discussed in this paper together with information available from other sources [6,7]. This example considers the performance of a residential solar cooling system in Ft. Worth, TX for the month of July. The system parameters are:

$A_c = 51.1\ m^2\ (550\ ft^2)$

$F_R'\tau\alpha = 0.68$

$F_R'U_L = 3.123\ \frac{W}{m^2 - {}^oC}\ (.55\ \frac{Btu}{hr - ft^2 - {}^oF})$

$M = 4377\ Kg\ (9650\ lb.)$

For a residence whose average daily July load is 366.217 MJ (347,105 Btu) the solar cooling fraction is computed as follows:

From Ref. 6, for Ft. Worth (32.5° N lat.)

$\bar{H} = 25.59\ Mj/m^2$

$\bar{K}_T = .64$

$\bar{T}_d = 29.0^o\ C$

For $\bar{K}_T = 0.64$ and $(\emptyset - S) = 0.$

$\bar{R} = .864$

The total incident radiation is

$$\bar{I}_{C_T} = (.864)(25.59) = 22.11\ \frac{MJ}{m^2 - day}$$

From Ref. 7, there are 21 hours for which the ambient air is above 23.9° C (75° F), the room set temperature. For this 21 hour period, the chiller must provide an average cooling of

$$q_E = \frac{366.217}{21} = 17.44\ \frac{MJ}{hr}\ (16{,}529\ \frac{Btu}{hr})$$

The manufacturer's catalog for an available 3 - Ton chiller shows that at the chiller generator operating at an average hot water inlet temperature of 83.49° C (182.28 F) will provide 17.44 MJ/hr of cooling with a generator input of $28.36\ \frac{MJ}{hr}$ The average chiller COP is then

$$COP_{av} = \frac{17.44}{28.36} = 0.61$$

The dimensionless parameters are calculated thus:

$$X = \frac{(F_R'U_L)\ A_c(T_{ref} - \bar{T}_d)\ \Delta t}{(Q_L/COP_{av})}$$

$$= \frac{(3.123)(51.1)(96.1 - 29)(24)}{\frac{(366.22)(277.8)}{.61}}$$

$$= 1.541$$

$$Y = \frac{(F_R'\tau\alpha)\ A_c I_{c_T}}{(Q_L/COP_{av})} = \frac{(.68)(51.1)(22.11)}{(\frac{366.22}{.61})}$$

$$= 1.280$$

Equation (15) gives a solar cooling fraction of .5964. The detailed simulation (SHASP) gives a value of 0.5897. The predicted value using the simplified method is 1% higher than the detailed simulation value.

CONCLUSION

Future work on the simplified solar cooling design method would include expanding the simulation runs to cover all the fourteen (14) representative cities for which TRW [7] has collected data. Although the differences between the predicted cooling fraction and the cooling fraction obtained via detailed simulation are all within the allowable engineering errors, there are indications that better correlations would result by grouping cities into at least two types of cooling regions. Better agreement can be expected, for example, if cities like Miami, Charleston and Washington, D. C. are grouped into one regional design chart and cities like Pheonix and Ft. Worth into another design chart. On going research is presently geared towards this goal.

ACKNOWLEDGEMENT

This work is supported by the U. S. Department of Energy, Systems Development Division under Contract No. DE AC03-79C S 30202.

NOMENCLATURE

A_c	collector area, m^2
COP_{av}	average chiller COP
ΔE	change in storage capacity
f_c	solar cooling fraction
$F'_R\tau\alpha$, F'_RU_L	collector parameters
$\overline{I}_{c_T}$	average hourly insolation on the plane of the collector $\frac{MJ}{m^2 - day}$ ($\frac{Btu}{ft^2 - day}$)
Q_{aux}	average daily auxiliary energy $\frac{MJ}{day}$ ($\frac{Btu}{day}$)
Q_L	average space cooling load
Q_u	average useful collected energy
q_E	evaporator capacity $\frac{MJ}{hr}$ ($\frac{Btu}{hr}$)
q_G	generator input $\frac{MJ}{hr}$ ($\frac{Btu}{hr}$)
$\overline{T}_d$	average daily ambient (dry-bulb temperature, ^oC (^oF)
T_C	generator hot water inlet temperature, ^oC (^oF)
X, Y	dimensionless parameters

REFERENCES

1. "FCHART, An Interactive Program for Designing Solar Heating Systems", University of Wisconsin, June 1978.

2. "TRNSYS, A Transient Simulation Program", Solar Energy Laboratory, University of Wisconsin, Madison, February 1978.

3. Klein, S.A., and W.A. Beckman, "A General Design Method for Closed-Loop Solar Energy Systems", Solar Energy, Vol. 22, pp. 269-282, 1979.

4. "SHASP, Solar Heating and Air-Conditioning Simulation Programs", Solar Energy Projects, Mechanical Engineering Department, University of Maryland, College Park, Maryland, December 1978.

5. "Control Strategy Studies of Solar Heating and Cooling Systems", Solar Energy Projects, Mechanical Engineering Department, University of Maryland, College Park, Maryland, November 1978.

6. Beckman, W.A., S.A. Klein, and J.A. Duffie, Solar Heating Design by the f-Chart Method, John Wiley and Sons, 1977.

7. "Solar Heating and Cooling of Buildings", (Phase 0), Vol. I to III, TRW Report prepared for NSF/RANN, May 31, 1974.

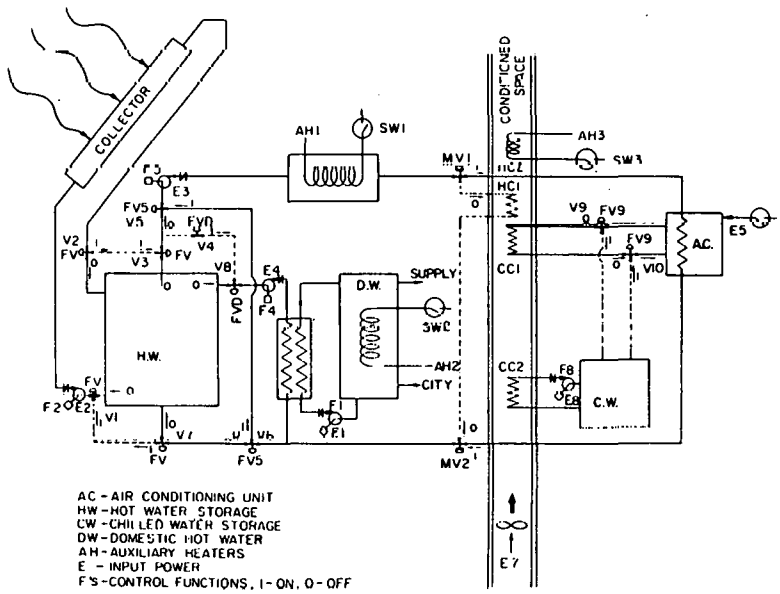

Fig. 1 Schematic Diagram of the Solar Cooling System

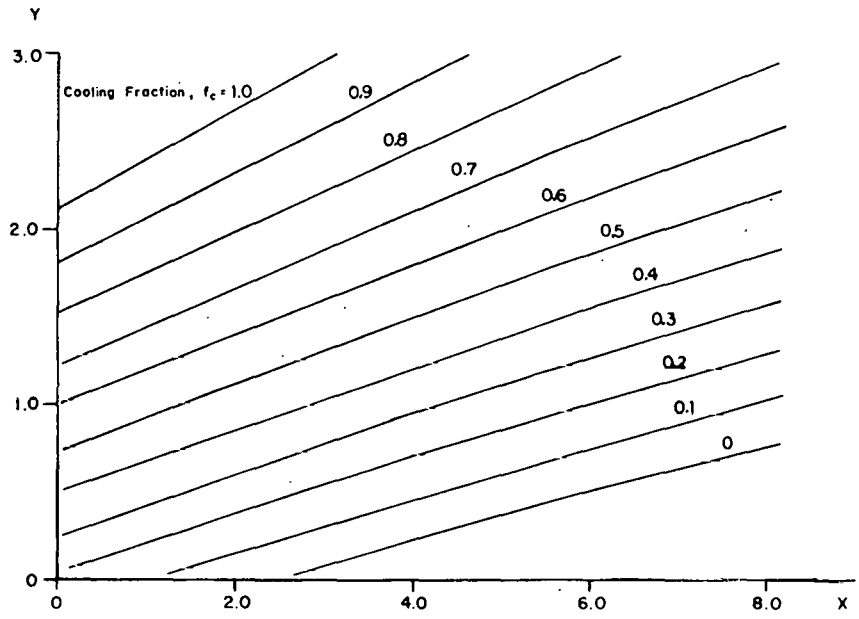

FIG. 2 SIMPLIFIED SOLAR COOLING DESIGN CHART

NOTES

PACE—PASSIVE ACTIVE CONSERVATION EVALUATOR—A NEW COMPUTER PROGRAM FOR BUILDING ENERGY ANALYSIS

John Kurtz
Booz, Allen & Hamilton Inc.

and

Lyle Groome
Solar Energy Research Institute

ABSTRACT

PACE is a computer program with wide analytical versatility currently being developed for the Solar Energy Research Institute (SERI). The version of the program currently being developed will provide comprehensive performance, economic, and financial analysis capability for active and passive residential solar energy applications. Ultimately, the program will include capability for analysis of conservation measures, thus allowing tradeoff analysis among conservation and solar options.

The PACE program combines key elements of several popular existing calculation methods and programs in forming a composite "umbrella" program. These include the F-chart method for active system performance estimation [1], the Solar Load Ratio (SLR) method for passive performance estimation [2], and the RSVP/2 solar economic analysis program [3].

PACE is a tool designed to serve a broad range of users and uses, both in the research/analysis field and in the residential building marketplace. It is a conversational interface program allowing it to be used easily by those unfamiliar with computer use. In addition, the structure of the program allows it to be used effectively by persons with greatly differing levels of solar knowledge.

The balance of this paper will cover the following aspects of the PACE program:

- The range of conditions to which the program is applicable
- An overview of the basic structure of the program
- A summary of the output reports available
- A brief look at several special features of the program
- A discussion of several key issues concerning current and future development
- Anticipated availability of the program.

PROGRAM SCOPE

The PACE program is intended to serve a wide range of users and applications. This resulted in the formulation of ambitious program development criteria.

Intended Users

The primary users envisioned for the PACE program fall into two general categories—research analysts and marketplace participants. Research users anticipated include analysts in industry, government and academic sectors for purposes of analyzing policy, economic, financial, marketing and other questions concerning residential energy use. Intended marketplace users include builders, developers, designers, mortgage lenders, home buyers, realtors, utility companies, and existing homeowners. It is expected that many of the marketplace users would use the program through a servicing organization. Possible examples of such organizations include trade associations, state energy offices, regional solar energy centers, Energy Extension Service offices, computer timesharing services, and many other possible public and privately sponsored service points. A number of these types of organizations are already using various versions of the component programs from which PACE is being constructed.

Program Applications

The ultimate objective in the development of PACE is that it be the first comprehensive energy analysis program to include active and passive solar, and conservation measures. Currently, active and passive analysis capabilities are operational. Conservation capability will be added at a later date, contingent on funding availability.

The program can be used to analyze both new and retrofit applications in both single family and multi-family residential structures. Weather data (monthly averages) for 266 cities is available in the program data base.

Active solar systems analysis capability includes domestic hot water, space heating, and combined systems. The program can accommodate air or liquid medium, low or medium temperature flat plate type collectors.

Passive solar applications capability currently includes direct gain, mass (Trombe) wall, and water wall systems. The program can be used for analysis of combinations of these passive systems and also for combinations of active hot water and passive heating systems.

Program Output

PACE provides both energy performance and economic output information. Performance information currently includes energy savings from solar applications. Economic information includes monthly cash payments, utility cost savings, economic merit indicators (e.g. payback, net present value, internal rate of return) for solar systems studied, and economic optimum solar system sizing. Because various users have different interests with respect to output information, a variety of different output reports are available providing both different aspects of the output information and different levels of detail.

Development Criteria

To address the scope of users and applications discussed above, the PACE program has been developed to fit certain criteria for flexibility and ease of use. These include:

No prior computer knowledge - The program is written in a straightforward question and answer format so that it can be used by persons with no computer knowledge.

No significant technical knowledge - PACE is written with a default structure such that it will provide reasonable value estimates for most variables if the user cannot. On the other hand, a knowledgeable user can input detailed, specific solar or other technical, economic, and financial data.

Quick and inexpensive to use - To maximize applicability and usefulness of the range of possible users, the program is designed so that it can be run quickly and at very low cost.

Comprehensive - Also to enable widespread use, PACE is designed to be applicable to any specific residential building, location (U.S.), and solar system situation—with all important solar performance and economic variables accounted for.

Flexibility - The program is designed in a modular fashion so that it can be easily updated and expanded to accommodate changes for: improved calculation techniques, additional solar or conservation applications, and new uses (such as energy auditing or building energy performance evaluation in conjunction with the DOE BEPS program).

PROGRAM STRUCTURE

In operation, the program has three basic modes—input, computation, and output. These are illustrated diagrammatically in Fig. 1 below.

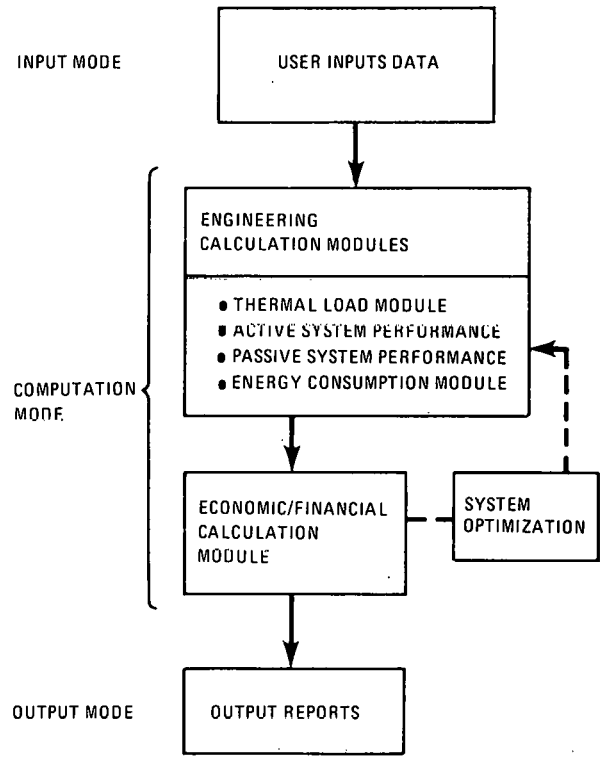

Fig. 1 PACE Program Structure

The various program sequence modes, and the modules within them, are controlled by an executive interface not shown in Fig. 1.

Input Mode

During the input mode, the user selects the type of analysis desired and provides values for variables relevant to that analysis. Data input is accomplished through a series of question/answer type input "prompts." The program asks the user questions expressed in conversational English and, for most questions, provides an average value or default response. The user then has the option of selecting the default value or choosing a preferred value. If the user does not clearly understand the question, inputting a "?" will prompt a more detailed explanation of the question, or a reference to the relevant section of the User's Manual.

During the input sequence the user provides data concerning the following areas:

Building characteristics—including building location, type, size, occupancy, and thermal characteristics.

Type of solar application—covering choices of new or retrofit, active or passive, domestic hot water and/or space heating.

Solar system specifics—including dimensions, orientation and physical properties of solar components in as much detail as is known.

Back-up system(s)—covers the type and characteristics of the back-up heating system(s).

Economic data—includes building, solar and back-up system cost data (if known) and a number of relevant economic variables such as fuel price and escalation rates, tax rates and incentives, maintenance and other expenses, discount rate and appraisal data.

Financial data—includes mortgage or other financing terms and related financing expenses.

To facilitate use by the wide range of anticipated PACE users, there are three levels of input detail available to the user. Level I is the simplest and involves the user selecting values for only the most critical variables—about 15. All other variable values are defaulted. Level II allows the user the provide input information in detail in some (user-selected) areas of particular interest, while only Level I variable questions are asked in other areas. Level III is the most detailed, in which the user is questioned about every relevant variable—typically around 50 or 60. At each level the user can easily change values of any variable, whether or not prompted to do so.

Computation Mode

In the computation mode the program performs all calculations required by the analysis inputs selected. A series of computation mode modules are involved sequentially. The computation modules include engineering modules for computing thermal load, active system performance, passive system(s) performance and energy consumption, and an economic computations module.

The thermal load module provides the user with three optional methods for determination of thermal loads.

(1) The user may compute the building thermal load off-line and input it directly to the program, in which case no further computation is required.

(2) For an existing building, the user may choose to input monthly fuel consumption data from utility bills, from which the program will provide an estimate of the thermal load.

(3) The user may have the program provide an estimate of the thermal load from the building characteristics provided. Currently this estimate will be based on the assumption that the building is constructed in accordance with 1979 HUD-MPS standards for energy conservation. To provide a more building-specific load estimate would involve many more building characteristics input variables than are presently used. This subject is discussed later in the issues section of this paper.

The active system performance module provides estimated energy supplied by active solar energy systems, if any are being considered in an analysis. Performance estimates are developed using the F-chart method [1]. The current version of the PACE program uses F-chart version 3.0, however, it is intended that this be supplanted with version 4.0 as soon as that version is available.

The passive solar performance module provides estimated energy supplied by any passive systems considered in an analysis. Passive performance estimates are developed using the Solar Load Ratio (SLR) method curves developed at the Los Alamos Scientific Laboratory [2]. SLR curves are currently available (and included in PACE) for direct gain, mass (Trombe) wall and water wall systems—each with or without night insulation.

For the analysis of passive systems, the PACE program requires additional input information concerning the dimensions and physical properties of passive components.

The energy consumption module provides an estimate of the building's actual energy consumption. This estimate is a function of the thermal load, the thermal contributions from solar sources, and the type and operational efficiency of back-up heating systems.

The economic computations module - Once engineering estimates are completed, the program proceeds to economic and financial analysis computations. First, detailed monthly cash flows are calculated, based on the engineering results, for both the building and solar systems being studied and for a similar building without the solar application. By comparing the two cash flow streams comparisons can be made with respect to:

- Financing payments (principle and interest)
- Tax payments and tax savings
- Utility costs and savings
- Insurance, maintenance, and other costs.

Using the differentials between the two cash flow streams, various economic merit indicators can be calculated. Merit indicators presently incorporated in the PACE program include:

- Net present value of (solar) investment
- Internal rate of return

- Financial management rate of return
- Number of years to payback (solar) investment
- Number of years to recover down payment on (solar) investment
- Number of years until positive cash flow is achieved (i.e. annual savings from solar investment exceeds annual costs attributable).

Output Mode

Once all engineering and economic computations called for in a selected analysis have been completed, the program provides the results to the user in the form of one or more preformatted output reports. The output reports available are summarized in the next section.

OUTPUT REPORTS

To address the needs of the wide range of users for whom the PACE program has been developed, a number of different output reports are available including:

- Engineering Summary Report—provides estimated monthly thermal loads and solar energy contributions and annual energy contribution (with and without solar) from each applicable energy source.
- Homebuyers Summary Report—presents comparative monthly costs for solar and nonsolar new single family home cases, broken down into mortgage payments, energy costs, and tax savings.
- Retrofit Summary Report—also for a single family home, presents monthly financing and energy costs for a solar application to an existing home. The information is presented in a comparative format, with and without solar.
- Lenders Summary Report—provides information very similar to that of the homebuyers report, but adds computation of certain expense to income ratios used by lenders in evaluating qualifications for granting loans. Tax savings are not shown in the lenders report, however, the amount of any Federal tax credit is indicated.
- Multifamily (Investors) Report—is geared strictly to income property applications. It is a comprehensive financial pro forma evaluation of the merit of the solar system(s) as an investment in conjunction with income producing real property. All cash flows, depreciation options, and tax considerations are included. The report allows the user the see the cumulative cash flow and annual return on investment effect if the project were sold, at any selected point in the future.
- Design Report—provides a summary of cost, energy savings, and economic merit indicator values for a specified range of different possible solar energy system sizes. The report also indicates the economic optimum size on a life cycle cost basis.
- Detailed Cash Flow Report—provides annual cash flow amounts, for as many years as desired, broken down into individual items (e.g. energy costs) and subtotals of interest (e.g. net expense after taxes). For comparison, these cash flows are provided separately for both the house with solar features and the reference house (without solar).
- Differential Cash Flow Report—shows annual additional costs and savings, broken down into major components, and net and cumulative totals attributed to the solar features—for as many years as desired.
- Graph of Cumulative Savings—illustrates graphically the pattern of cumulative total savings (or losses) attributable to the use of solar energy (shown in annual increments).
- Iteration Report—shows the change in solar performance, cost, and economic indicator values that result from changes in the value of any selected input variable (e.g. system size, system cost, fuel price, interest rate, loan term, etc.) This report is particularly useful in performing parametric analysis studies.

In addition to showing calculation results, each of the output reports also provides a summary of the main input assumptions incorporated in the computations.

SPECIAL PROGRAM FEATURES

In addition to its basic computational capabilities, the PACE program has a number of noteworthy user-oriented features including:

- An iteration routine
- Optimization of system size
- Data-checks to reduce input errors
- Adaptability to different levels of input detail.

Iteration Routine

The iteration routine is a particularly powerful analytic tool. It allows the user to quickly perform parametric (or sensitivity) studies of the effect of changes in the value of any input variable such as solar system size, system cost, conventional fuel price, future fuel escalation rate, etc. Once the user has determined a variable to be iterated (e.g. system size), a selection is made of the range of the variable to be considered (e.g. 40 sq. ft. to 160 sq. ft.), and the iteration increment to be used (e.g. 20 sq. ft. increments) in the analysis. The PACE program then computes output information such as solar energy system performance, system cost, and economic merit indicator values corresponding to each variable increment (e.g. 40 sq. ft, 60, 80, etc. to 160 sq. ft.). The results are shown on an iteration report discussed above.

The iteration report has several particularly useful applications. It can be used to determine which input variables have a significant effect on solar system performance and economics. These studies have been used in establishing the default structure of the PACE program.

The iteration routine is also useful in determining the values of certain input variables that will cause solar applications to be economically competitive with conventional energy systems. This information in turn is useful for such purposes as setting R&D goals for performance improvement and determining appropriate levels for effective economic incentives such as tax credits, low interest loans, grants, etc.

As a further aid in performing parametric analysis studies, the iteration routine can be used in conjunction with the sizing optimization routine discussed below.

Sizing Optimization Routine

For cases in which there is not a preset size for a solar energy system, the optimization routine will provide an estimate of the most economical system size on a life cycle value basis. This optimization is based on the user's selection of analysis period, discount rate, and system performance characteristics, unless the user chooses to use program-supplied default values.

Data-Check Features

Because the program has been designed to be used by marketplace participants with limited technical knowledge of solar energy systems, a system of data-checks has been included to reduce input errors. The data-check feature checks values input, as they are input by the user, against a predetermined reasonable range for the variable. If the input value is outside the reasonable range, a message is given to the user indicating that fact. The user may then choose to either change the value or proceed with the analysis despite the value being outside the range. For input values within the reasonable range, no message interrupts the flow of the program.

Knowledgeable users may wish to use the program for analysis of variables in areas well outside the current reasonable ranges used for the data-check feature. If so, the data-check can be switched off to avoid the inconvenience of interruptions from the data-check reminder messages.

Adaptability to Different Input Detail Levels

As noted above (in the section on Input Mode), there are three different basic levels of input detail that can be selected by the user, depending on knowledge and interest. Even within each of the lower two levels, the user has access to any of the well over 100 variables in the program. This allows the program to be adapted to any specific or unique information already known or of interest. Examples of such specific detail might include: the performance characteristics of a particular brand of solar collector, the inclusion of exact orientation and dimensional characteristics of a passive system, the use of unusual financing techniques such as variable payment mortgages, or the study of irregular scenarios of future energy price escalation.

CURRENT AND FUTURE DEVELOPMENT ISSUES

The PACE program is being developed in a technical and policy environment that is rapidly evolving and changing. Consequently, there is a continuous series of interesting research issues to be addressed. Several of the current issues of interest include:

- Expansion of the PACE building thermal load module is necessary to provide an evaluation tool for conservation measures and for use in conjunction with the national Building Energy Performance Standards (BEPS) being developed and promulgated by the Department of Energy.
- Passive performance estimating algorithms, such as the SLR methods, are still rudimentary in their development and limited in application breadth. For example, validated SLR routines are not yet available for sun space applications, and in the applications for which SLR curves are available the user cannot adjust the amount of thermal mass included.
- Optimization of passive system sizes is complex when (as is often the case) more than one type of passive system is included in a building. This issue is strongly interrelated with the issue of establishing reliable passive cost estimating default data.

The size of the PACE program has become an issue as the program has become more comprehensive and correspondingly larger computer core requirements (currently 60K decimal). At the same time, the marketplace is moving rapidly toward very affordable mini and micro computers. To enable use of PACE in small computers, examination is being made of ways to restructure the program in a sequence of overlays. Alternatively, study is needed to determine whether specific portions of the program could or should be broken out and packaged as smaller programs for specific market segments.

Use of PACE to develop simplified manual estimating techniques has great potential for expanding the benefits of the program more widely in the marketplace. A simplified manual estimator has already been developed for active hot water systems (and should be available shortly from the National Solar Heating and Cooling Information Center). This estimation consists of a straightforward series of look-up tables developed by computer program runs.

A complete discussion of the above issues is beyond the scope of this paper. However, work is underway in each area and will be the subject of future papers.

PACE PROGRAM AVAILABILITY

The initial version of PACE to include both active and passive analysis capability is expected to be publicly available from SERI in the summer or fall of 1980.

The immediate predecessor to PACE—RSVP/2—which provides analysis of active systems, is available from the National Technical Information Center in the form of a User's Manual, Programmer's Manual and program tape. Information for ordering can be obtained from the National Solar Heating and Cooling Information Center. RSVP is also accessible via the Cybernet computer time-sharing system operated by Control Data Corporation.

The development and availability of the complete PACE program including conservation measures, as well as active and passive solar, is presently contingent upon funding availability.

ACKNOWLEDGEMENTS

The authors acknowledge the support and funding of the Systems Development Division, Office of Solar Applications, of the U.S. Department of Energy, and in particular Mr.Michael Maybaum.for the initiation of this project. Also acknowledged is the contribution of Dr. Arthur Reiger of the U. S. Department of Housing and Urban Development, who was responsible for the development of the RSVP program at HUD, upon which the PACE program is substantially based.

REFERENCES

[1] Beckman, W.A., Klein, S.A., and Duffie, J.A., Solar Heating Design by the F-Chart Method, John Wiley & Sons, 1977.

[2] Balcomb, J.D. and Anderson, B., Passive Solar Design Handbook prepared for the U.S. Department of Energy, scheduled to be published January or February, 1980.

[3] Booz, Allen & Hamilton Inc., HUD Residential Solar Viability Program RSVP/2 USERS MANUAL prepared for the U.S. Department of Housing and Urban Development, September, 1979.

SOLCOST: A SOLAR ENERGY DESIGN PROGRAM

Dr. Dwight E. Hull
Roger T. Giellis
Thermophysics Section
Martin Marietta Aerospace
Denver, Colorado 80201

ABSTRACT

The SOLCOST solar energy design program [1] was developed in 1976 under the auspices of the U.S. Department of Energy. The program predicts the annual solar system performance for a range of collector areas and then determines the optimum collector area based on a life-cycle cost analysis. SOLCOST is based on a detailed simulation for an average day for each month. The original methodology required a reasonable estimate of the dawn collector inlet temperature to perform the average-day analysis. This approach was improved in Version 2.0 with an algorithm that automatically computed the dawn inlet temperature. This version was released in January 1979.

This paper describes in detail the SOLCOST radiation model and the thermal analysis methodology of Version 2.0. Key validation results are presented for hot water systems showing excellent agreement between SOLCOST predictions and measured system performance. Also covered is an overview of some recent modifications of the SOLCOST software that will be available in Version 3.0 (to be released in early 1980).

INTRODUCTION

The solar energy design program, SOLCOST, is a public domain computerized design tool intended for use by nonthermal specialists to size solar systems. The program predicts the annual solar fraction for a range of collector areas and then determines the optimum collector area based on a life-cycle cost analysis. The SOLCOST inputs are versatile and powerful, allowing less sophisticated users to access reasonable default values for most of the parameters.

An iterative procedure was developed for Version 2.0 to assist SOLCOST users in estimating the starting collector inlet temperature, which is the key to the SOLCOST average-day methodology. The procedure consists of an iterative process that checks the storage temperature at dawn against the previous dawn value. If the difference is outside a reasonable limit, the average-day analysis is repeated using a refined estimate of the dawn storage temperature. The important element of this one-day simulation is the energy balance on the storage tank. All energy delivered to storage either satisfies the load or is lost through the tank insulation. The methodology of this procedure is presented in detail.

The SOLCOST radiation data bank has been updated in Version 3.0 to include default clearness factors that align the SOLCOST clear-day irradiances with the SOLMET data base. The radiation algorithm is discussed in detail to document the clearness factor concept and also to describe the coupling between the radiation model and the SOLCOST average-day simulation.

SOLCOST SOLAR RADIATION MODEL

The SOLCOST methodology is based on a one-day simulation performed on the 15th day of each month. Since hourly steps are taken during the daylight hours of the simulation, radiation must be incident on the collector on an hourly basis. The simulation also requires that the collector be driven with two radiation profiles, one for a clear day and one for a totally cloudy day.

Clear-Day Methodology - The starting point for clear days was the ASHRAE model [2] in which the direct normal irradiation is estimated by

$$(1) \qquad I_{DN} = \frac{A}{\exp\ (B \sin \beta)}$$

where A is the apparent extraterrestrial irradiation at air mass = 0 and B, the atmospheric extinction coefficient, are functions of the month that take into account the earth-sun distance and the air's water vapor content. The angle β is the solar altitude angle above the horizon. The values of A and B given in Reference [2] were selected so I_{DN} would be in agreement with the Threlkeld and Jordan measured radiation values on average cloudless days [3].

To account for local values of atmospheric water content and variable aerosols, the ASHRAE model uses a parameter called clearness number to modify the direct normal solar component. Unfortunately very little direct normal radiation data are available to allow direct calculation of clearness numbers. The recent work by Randall and Whitson [4] has resulted in improved direct normal insolation estimates that are now available for 26 SOLMET sites [5].

The Department of Energy has recently recommended that the SOLMET data base be used in all solar simulation and design work. This insolation data

base has been available in SOLCOST since Version 2.0 (i.e., monthly average total insolation values). However, in Version 3.0, an additional step has been taken to further align the SOLCOST radiation model with the SOLMET data set. Specifically, monthly clearness numbers have been derived from 26 cities from the clear sky, solar noon total irradiance values used by the SOLMET developers to generate their data base (see Appendix A in [5]). Based on these clearness numbers, the set of default monthly clearness numbers given in Table 1 were calculated. Since obviously this default set does not apply to all the cities in the data bank, a parameter called the clearness factor has been estimated for each city in the data bank. This factor is a multiplier on the default monthly clearness numbers to account for location. The User's Guide for SOLCOST Version 3.0 [6] contains a map of the clearness factors that have been assigned to cities in the SOLCOST data bank.

TABLE 1 CLEARNESS NUMBERS IN SOLCOST RADIATION MODEL

January	0.98	July	0.88
February	1.01	August	0.89
March	0.98	September	0.92
April	0.95	October	0.97
May	0.92	November	0.99
June	0.90	December	0.98

The diffuse component for clear-day radiation is based on the work of Threlkeld [3,7] in which a dimensionless parameter C is defined as

$$(2) \qquad C = I_{dH}/I_{DN}$$

where I_{dH} is the diffuse radiation on a horizontal surface for a clear day. Values for C are given in [2].

In SOLCOST, Threlkeld's diffuse term is divided by the clearness number squared to account for varying atmospheric clarity

$$(3) \qquad I_{dH} = C\ CN\ I_{DN}/CN^2 = C\ I_{DN}/CN.$$

This modification of the ASHRAE model was based on the work of Kusada [8] and was experimentally checked by Hulstrum [9] for Boulder, Colorado conditions.

For tilted collectors, the incident solar energy is given by

$$(4) \qquad I_{t\theta} = CN\ I_{DN}\cos\theta + I_{d\theta} + I_r$$

where $I_{d\theta}$ = diffuse sky radiation and I_r = diffuse ground-reflected radiation.

The diffuse sky radiation is computed directly from the product of the clear-day diffuse radiation incident on a horizontal surface I_{dH} and the angle factor between the collector and the sky F_{ss}

$$(5) \qquad I_{d\theta} = I_{dH}\ F_{ss}.$$

The diffuse ground-reflected radiation I_r is computed from the product of the total horizontal radiation I_{tH} with the ground reflectance GR and the angle factor between the collector and the ground F_{sg}

$$(6) \qquad I_r = I_{tH}\ GR\ F_{sg}.$$

The default value for ground reflectance in SOLCOST is 0.2, although the user can input an array of monthly values for the ground reflectance, depending on the location and ground cover.

Cloudy-Day Methodology - For cloudy conditions, SOLCOST assumes a totally cloudy day, i.e., no direct normal radiation is incident on the collector. The diffuse radiation on a horizontal surface is calculated from the following relation taken from the work of Kimura and Stephenson [10]

$$(7) \qquad I_{dH,cl} = I_{dH}\ [CCF - K(1-CC/10)]$$

where

$I_{dH,cl}$ = cloudy-day horizontal diffuse radiation,
I_{dH} = clear-day horizontal diffuse radiation from Eq (3),
CCF = cloud cover factor,
CC = cloud cover amount,
K = variable, depending on solar altitude angle and C (ASHRAE diffuse sky factor).

For totally cloudy conditions, CC is equal to 10, and Eq (7) reduces to

$$(8) \qquad I_{dH,cl} = I_{dH}\ CCF.$$

Kimura and Stephenson determined that the cloud cover factor CCF depended on the season and the amount of cloud cover CC. They correlated their data with the expression

$$(9) \qquad CCF = P + Q(CC) + R(CC^2)$$

where the values of P, Q, and R are given in [10]. Since CC is assumed to be equal to 10, the values of CCF can be computed directly; in fact, the values of P, Q, and R have been interpolated monthly and input to the CCF array in SOLCOST.

Once the value of $I_{dH,cl}$ is determined from Eq (8), angle factors to the sky and ground are applied to compute the diffuse energy incident on the tilted collector

$$(10) \qquad I_{t\theta,cl} = I_{dH,cl} \cdot (F_{ss} + F_{sg}).$$

THERMAL ANALYSIS METHODOLOGY

The SOLCOST solar system evaluation method is based on an hour-by-hour simulation performed one day per month. Key assumptions made in the analysis include:

1) Collector efficiency is characterized by a straight line with intercept $F_r'\tau\alpha$ and slope $F_r'U_L$;

2) Unstratified liquid storage;

3) Collector inlet temperature is equal to storage tank temperature (if a heat exchanger is present, the collector parameters must be derated with the technique described by F. de Winter [11]).

The essence of the average-day approach consists of performing an hourly energy balance on the solar system with the collected solar energy term weighted with a simple factor that accounts for the long-term variability in the incident solar radiation. This weighting factor PP is a direct function of the long-term daily average horizontal insolation available at the site. It is computed from the relation

$$(11) \quad PP_i = \frac{H_h - H_{hd,cloudy}}{H_{h,clear} - H_{hd,cloudy}}$$

where

PP_i = weighting factor for month i,
H_h = daily average total horizontal insolation for month i (from SOLMET data in SOLCOST weather data bank),
$H_{h,clear}$ = SOLCOST model-generated clear-day total horizontal insolation for month i,
$H_{hd,cloudy}$ = SOLCOST model-generated cloudy-day total horizontal insolation for month i.

The terms $H_{h,clear}$ and $H_{hd,cloudy}$ are computed from integration of the clear-day and cloudy-day terms I_{clear} and I_{cloudy} generated by the SOLCOST radiation model discussed above.

Iterative Procedure for Starting Inlet Temperature - An iterative process is used to determine the long-term average dawn storage temperature for each month of the year. Four steps are performed each hour in the one-day simulation, including:

1) Step 1 - Collector efficiency given by

$$(12) \quad \eta_c = F_r'\tau\alpha - F_r'U_L\,(T_{in} - T_{amb})/I$$

where

η_c - collector efficiency,
T_{in} - collector inlet temperature,
T_{amb} - ambient temperature constructed with a cosine function of T_{min} and T_{max},
I - solar irradiance (I_{clear} or I_{cloudy}),
F_r' - intercept of collector efficiency curve (input),
$F_r'U_L$ - slope of collector efficiency curve (input).

Collector efficiencies η_{clear} and η_{cloudy} are computed for clear-day and cloudy-day values of the solar irradiance I_{clear} and I_{cloudy} using the same ambient temperature and inlet temperature for each calculation;

2) Step 2 - Useful collected solar energy

$$(13) \quad QU = [PP\,\eta_{clear}\,I_{clear} + (1-PP)\eta_{cloudy}\,I_{cloudy}]\eta_t\,CA$$

where

QU = useful solar energy from the collector,
PP = weighting factor (defined above),
η = collector efficiency,
I = solar irradiance,
CA = collector aperture area,
η_t = transport efficiency (i.e., for piping losses from collector to storage);

3) Step 3 - Load determination, a user input (on a daily basis) that is then removed from the thermal system on an hourly basis as a function of ambient temperature or by a user-specified load distribution profile;

4) Step 4 - Storage tank temperature that is assumed to be the same as the collector inlet temperature in SOLCOST. The new storage tank temperature is calculated by summing the energy added to storage (Step 2) and the energy removed from storage (Step 3) and dividing by the storage capacity and adding this to the old storage tank temperature as

$$(14) \quad TS_{new} = TS_{old} + (QU - QLOSS - LOAD)/(GF*CA*8.337)$$

where

TS_{new} = new storage tank temperature,
TS_{old} = old storage tank temperature,
QU = useful energy collected,
QLOSS = storage losses,
LOAD = system load,
GF = gallons of storage per square foot of collector,
CA = collector area.

The storage tank temperature has user-imposed upper and lower limits. This means that the storage temperature cannot rise above a specified value (default is 200°F) and cannot drop below another specified value (default is 100°F).

These four steps are repeated every hour from sunrise until sunset. At sunset the remainder of the load is removed and the final storage temperature is computed (subject to the minimum storage temperature constraint). At this point a final storage tank temperature that is the storage tank temperature after the load was removed is available. This final storage tank temperature is then compared with the storage tank temperature used to start the hour-by-hour calculation. If they differ by more than some tolerance (default is 1°F), a new starting storage tank temperature is calculated and the hour-by-hour simulation is repeated. The new starting storage tank temperature is based on the calculated final storage tank temperature, the old starting storage tank temperature, the useful energy collected, and the load. When the temperature convergence criteria are satisfied, monthly values for the energy terms are computed by simply multiplying the daily terms by the number of days in the month. This process is repeated for each month of the year.

Tables 2 and 3 show the resulting energy balance summary and the storage temperatures that are output from the SOLCOST thermal analysis for a given collector area. The number of iterations required to reach convergence is shown in the last column in Table 3. Typically only three to five iterations are necessary, resulting in a negligible impact on total run time.

TABLE 2 SOLCOST ENERGY BALANCE SUMMARY

Energy Balance by Month for 300.0-ft^2 Collector

Month	Fraction by Solar	Average Useful Solar per Day, Btu/Day-ft^2	Total Useful Solar Energy, MBtu/mo	Auxiliary Energy, MBtu/mo	Conventional System Energy, MBtu/mo
1	0.464	717.2	6.67	7.71	14.38
2	0.542	783.1	6.58	5.55	12.13
3	0.608	786.7	7.32	4.72	12.03
4	0.800	736.7	6.63	1.66	8.29
5	1.000	595.7	5.48	0.00	5.48
6	1.000	405.2	3.55	0.00	3.55
7	0.995	298.5	2.78	0.01	2.79
8	1.000	343.1	2.79	0.00	2.79
9	1.000	475.7	3.98	0.00	3.98
10	1.000	428.8	7.14	0.00	7.14
11	0.600	725.8	6.53	4.35	10.88
12	0.465	674.4	6.27	7.21	13.48
Annual	0.678		65.71	31.21	96.92

NOTE: Conversion energy and solar auxiliary energy are gross values (i.e., they include tank insulation and/or combustion loss).

TABLE 3 SOLCOST STORAGE TEMPERATURE SUMMARY

Temperature and Energy Information for 300-ft^2 Collector Area

Month	Storage Temperature			Storage Losses, Btu/day	Number of Iterations
	Dawn, °F	Maximum, °F	Average, °F		
1	100.0	129.0	114.0	7639.0	2
2	100.0	135.0	116.0	8090.0	2
3	100.0	136.0	117.0	8202.0	2
4	100.0	141.0	120.0	8789.0	2
5	125.0	155.0	138.0	12502.0	3
6	166.0	188.0	175.0	20148.0	4
7	185.0	200.0	191.0	23541.0	3
8	185.0	200.0	191.0	23669.0	6
9	176.0	200.0	186.0	22540.0	3
10	127.0	171.0	147.0	14296.0	4
11	100.0	137.0	117.0	8340.0	2
12	100.0	128.0	113.0	7595.0	2

VALIDATION RESULTS

Methodology and Data Sources - The validation results presented are based on direct comparisons of SOLCOST predictions with measured thermal performance data. Inputs to the program included measured ambient temperatures, insolation, collector $F_r'\tau\alpha$ and $F_r'U_L$ values, auxiliary water temperature, mixing valve set temperature, and the gallons of hot water delivered per day. Three test sites provided data for these validation comparisons, including:

1) NBS Solar Domestic Hot Water Test Facility in Gaithersburg, MD. Six domestic hot water systems are being tested [12] under well-instrumented operating conditions;

2) Hogate's Restuarant in Washington, DC. This is a national solar data program site that employs a 6200-square-foot collector to provide hot water to a restuarant [13];

3) Aratex Industrial Laundry in Fresno, California. This national solar data program site employs a 6500-square-foot collector to preheat hot water for a large industrial laundry.

Results - Liu and Fanney of the National Bureau of Standards have reported their comparisons between SOLCOST and the NBS experiments in [14] for the months of July 1978 through June 1979. The systems reported were (1) a double-tank direct (i.e., no heat exchanger between storage and the collectors) and a double-tank indirect system that used a wraparound external heat exchanger. Comparisons of SOLCOST annual performance predictions with the measured NBS data are tabulated.

	SOLCOST Solar Fraction	Measured Solar Fraction
Two-Tank Direct	0.47	0.51
Two-Tank Indirect	0.47	0.47

Figure 1 shows the monthly comparison of predicted versus measured solar fractions for the NBS data sets. The agreement between the two is excellent.

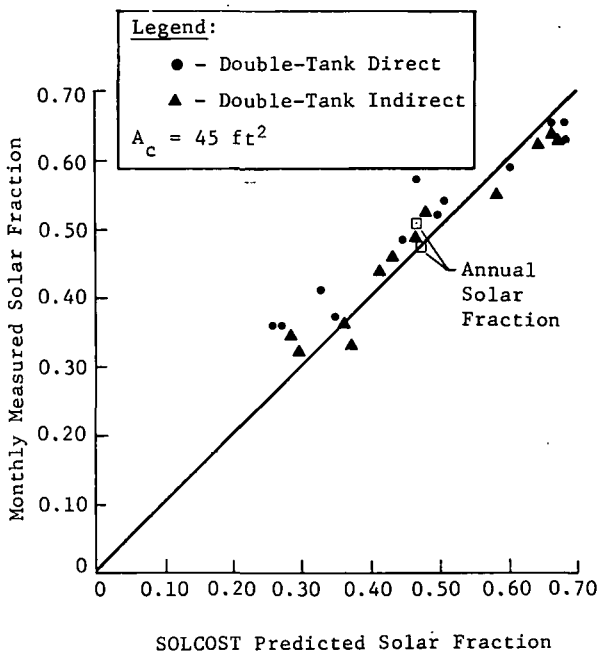

Figure 1
SOLCOST Predictions Compared with Measured Data, NBS Hot Water Systems

Figure 2 shows the monthly comparisons for the Hogate and Aratex systems. The annual measured solar fraction for Aratex was 0.16 and the SOLCOST prediction was 0.18. Data for the Hogate system were insufficient to compute the annual fraction.

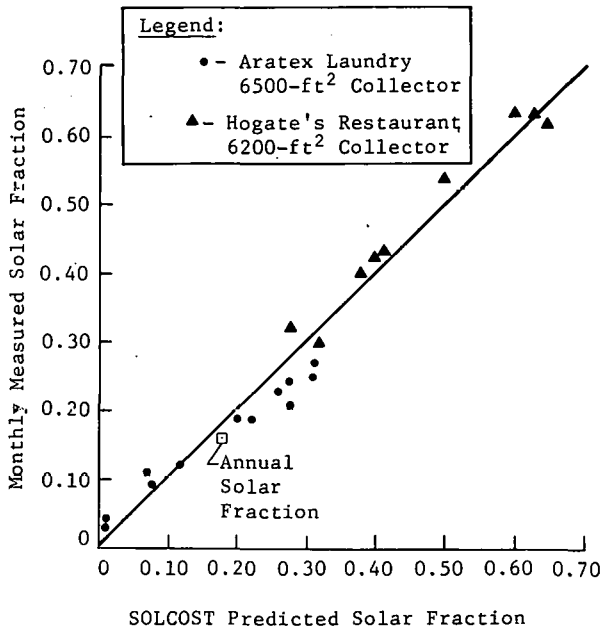

Figure 2
SOLCOST Predictions Compared with Measured Data, Large Hot Water Systems

Again the agreement between measured and predicted values is very good. Considering the fact that SOLCOST is a design tool, the accuracy of its predictions are more than adequate for its intended purpose.

SOLCOST VERSION 3.0 FEATURES

Version 3.0 of SOLCOST will be available in February 1980 with the following improvements:

1) New software for total optimization of building thermal systems, including windows, insulation, doors, and the active solar system (the optimization is based on the minimization of discounted costs over the life of the building system);

2) Automatic adjustment of the collector parameters for inclusion of heat exchangers, varying flow rates, different collectors in series or parallel, etc;

3) Revised clearness numbers in the solar radiation model that align SOLCOST clear-day hourly predictions with the SOLMET clear-day values.

Version 3.0 also contains sizing algorithms for typical components in a solar system, including pipes, ducts, manifolds, pumps, fans, and heat exchangers. If the user chooses, the cost of these components can be automatically accounted for in the SOLCOST economic analysis as a function of collector area. This improves the accuracy of the preliminary design analysis because the costs for these components vary as a function of system size. For small collector areas this can be a significant consideration.

SOLCOST can also determine the proper size for three types of heat exchangers, including (1) liquid-to-liquid counterflow, (2) air-to-liquid crossflow, and (3) liquid-to-air crossflow. These heat exchangers may be located in either the collector loop or the load distribution loop. After determining the heat exchanger rating, SOLCOST can automatically derate the collector intercept and slope parameters to account for the heat exchanger effect.

ACKNOWLEDGEMENT

This work was sponsored by the Department of Energy, Office of Conservation and Solar Applications, Education and Communications Branch under Contract EY-76-C-2876.

REFERENCES

1. M. Connolly et al.: "Solar Heating and Cooling Computer Analysis - A Simplified Design Method for Nonthermal Specialists," Proceedings of Joint Conference of the American Section of the International Solar Energy Society and the Solar Energy Society of Canada, Winnepeg Canada, August 1976.

2. ASHRAE Applications Handbook, Chapter 58, 1978 Edition.

3. J. Threlkeld and R. Jordan: "Direct Radiation Available on Clear Days," ASHRAE Transactions, Vol 64, 1958, p. 45.

4. C. Randall and M. Whitson, Jr.: Hourly Insolation and Meteorological Data Bases Including Improved Direct Normal Insolation Estimates, Aerospace Corporation, Report No. ATR-78 (7592)-1 (Sandia Document SAND78-7047), December 1977.

5. SOLMET Manual, Vol 2, TD-9724, prepared by National Climatic Center for DOE, February 1979.

6. User's Guide for SOLCOST, Version 3.0, available from SOLCOST Service Center, 2524 E. Vine Drive, Ft. Collins, CO 80204, 1980.

7. J. Threlkeld: "Solar Irradiation on Surfaces on Clear Days," ASHRAE Transactions, Vol 69, 1963, p. 24.

8. T. Kusada: "NBSLD, the Computer Program for Heating and Cooling Loads in Buildings," NBS BUILDING SCIENCE SERIES NO. 69, July 1976.

9. R. Hulstrom: Definition Study for Photovoltaic Residential Prototype System, NASA Contract No. NAS3-19768, NASA Report No. NASCR-135056, Martin Marietta Report No. MCR76-394, September 1976.

10. K. Kumura and D. Stephenson: Solar Radiation on Cloudy Days, ASHRAE Transactions, Vol 75, Part 1, 1969.

11. F. de Winter: "Heat Exchanger Penalties in Double-Loop Solar Water Heating Systems," Solar Energy, 17, p. 335, 1976.

12. V. S. Aquila: Thermal Performance Evaluation of the Hogate's Restaurant Solar Hot Water System, U.S. Department of Energy, SOLAR/2028-78/35, November 1978.

13. H. L. Armstrong, et al.: Aratex Services, Inc Industrial Laundry Solar Energy System Performance Evaluation, U.S. Department of Energy, SOLAR/2008-78/24, June-September, 1978.

14. A. Hunter and S. Liu: Comparison of Experimental and Computer-Predicted Performance for Six Solar Domestic Hot Water Systems, National Bureau of Standards, July 1979. Also to be presented at ASHRAE Semiannual meeting, Los Angeles, California, February 1980.

Session VIB

Jane Pejsa
Honeywell Corporation
Chairperson

BUILDING LOAD MODELS

A SIMPLIFIED SOLAR HEATING SYSTEM PERFORMANCE ESTIMATOR FOR RESIDENTIAL APPLICATIONS

Jane H. Pejsa
Technology Strategy Center
Honeywell Inc.
2600 Ridgway Parkway
Minneapolis, Minnesota 55413

ABSTRACT

A Simplified Solar Heating System Estimator based on specific collector characteristics and system design can be derived for residential space heating applications. Within the lower 48 United States six "solar regions" are defined. Within each region, the solar energy available over the heating season is relatively consistent. Furthermore, regionally, there is a correlation between latitude and design load of a building and the expected annual space heating load. Described herein is the technique to derive regional algorithms for the space heating load and to generate annual collector performance curves. The assumptions and limitations inherent in this simplified approach are also set forth.

INTRODUCTION

The marketing of solar space heating systems for residential applications continues to lag, in spite of the bleak future of fossil fuels. The practicability of solar heating systems has been amply demonstrated at many levels. Yet there appears to be a gap in the communication of system performance to the individual homeowner who, in the end, must make the decision to purchase or not to purchase solar hardware.

Herein is described a technique that can lead to a valuable design and marketing tool for solar collector distributors, HVAC design engineers, architects and building contractors, and indeed for the homeowner himself.

The tool itself consists of seven figures--a map delineating six solar regions of the continental United States and six regional performance graphs--from which performance of a given system design can be estimated for any residential application in the United States. Once the tool has been created for a particular system, any user can estimate the performance of a solar heating system knowing just three parameters:

- The geographic location of the system.
- The design load of the space heating system.
- The number of collectors in the system.

The technique for deriving the regional performance curves has been demonstrated successfully with an analysis of performance for one system design. The derivation is described in the following sections, with attention also given to the limitations inherent in this technique.

THE SOLAR REGION CONCEPT

During the heating season there are wide variations in the level of solar radiation across the United States. North-south variations are, of course, inherent in the earth's tilt relative to the sun and they can be minimized by tilting the flat plate collector at the appropriate angle. East-west variations, however, are climate-related and suggest at least four solar regions in the northern latitudes. In the southern latitudes these east-west variations also exist, but they are not so pronounced. Therefore, six solar regions are defined, within which there is good consistency as to seasonal radiation levels. These are shown in Figure 1.

ESTIMATION OF ANNUAL SPACE HEATING LOADS

The derivation of the regional performance charts continues with an analysis of annual space heating loads relative to design heating loads at 25 locations throughout the United States. This analysis reveals that within each of the solar regions the number of annual degree-days for a specific location can be estimated directly from the heating design day temperature. In Regions 1, 3, and 5 across the northern tier of the United States, the relationship can be approximated by a linear equation in which the design day indoor-outdoor temperature difference, ΔT, is the independent variable:

$$\text{Annual Degree Days} = K \cdot \Delta T \qquad (1)$$

The value of K varies from region to region, of course.

In Regions 2, 4, and 6 the algorithm includes latitude, ϕ, as the second independent variable. Within each of the three regions the following relationship is defined:

$$\text{Annual Degree Days} = (K_1 \cdot \phi + K_2)\Delta T \quad (2)$$

The values of K_1 and K_2 are derived from a regression analysis of a number of cities for each region. The heart of this performance estimating tool is the pair of equations (1) and (2). With the appropriate K values for each region it is possible to estimate the annual space heating load of a residential building directly from its design heating load. Note that the values of K are independent of the temperature scale, Celsius or Fahrenheit.

ESTIMATION OF SOLAR SYSTEM PERFORMANCE

In recent years the University of Wisconsin has developed the f-Chart method for computing solar system performance. It is well known and widely accepted in the solar energy field. Furthermore, there is ample documentation available as to its derivation and dependability in the design of solar heating systems [1,2]. Using this method, an analysis of system performance has been completed for a typical hydronic solar collector heating system in each of the six solar regions. The cities for which performance was estimated--New York, Atlanta, Omaha, Phoenix, Seattle, and Denver--were selected as representative of their regions in an earlier study [3].

For the f-Chart evaluations, the effective heat transmission coefficients, UA, are calculated from the design loads and design temperatures in the six locations:

$$UA = \frac{\text{Design Load}}{\text{Design } \Delta T} \quad (3)$$

The solar collector modeled is a standard 1.67 square meter (18 square foot) high-performance single-glazed collector; the system is the hydronic liquid-based space and water heating system modeled in f-Chart. Design heating loads and number of collectors in the system are varied in the analyses to derive a solar system performance table for the representative city in each region. Figures 2 through 7 present graphically the results of these analyses. Each figure includes the regional algorithm for estimating annual space heating load as a function of design space heating load. The domestic hot water load of all analyses remains at 227 liters (60 gallons) per day at 60°C (140°F).

RELIABILITY AND LIMITATIONS

Cited previously are the levels of approximation that are involved in generating the regional performance estimation curves. Inasmuch as all regions include a diversity of weather profiles, the presence of error margins is not unexpected. To quantify these margins, three f-Chart analyses of system performance have been completed for each of 36 locations: a mean error relative to the f-Chart estimates has been computed for each location. In most cases the curves generate performance estimates about as accurate as the f-Chart method itself. In 28 locations, the mean error is less than 10 percent. In seven locations the mean error is between 10 percent and 20 percent. In just one of the 36 locations analyzed does the mean error between the f-Chart analyses and the performance curve estimates exceed 20 percent--namely, in Duluth, Minnesota.

CONCLUSIONS

This technique of deriving regional performance curves for a specific residential solar heating system design can best be applied by collector manufacturers since the collector parameters are a key input to the analyses from which the curves are generated. Once the regional performance curves have been derived, they become a simple, yet dependable, marketing and design tool to size a system and to evaluate its feasibility. When initial costs and fuel prices are factored in, the set of curves can also be used to evaluate cost-effectiveness of the system. The simplicity of the inputs--building location and design heating load--assures the participation of all interested parties: the HVAC salesman, the building contractor, and the homeowner himself.

REFERENCES

[1] P. J. Hughes, W. E. Buckles and S. A. Klein, "EES Report 49-3 F-Chart User's Manual, an Interactive Program for Designing Solar Heating Systems," University of Wisconsin under SERI, June 1978.

[2] W. A. Beckman, S. A. Klein and J. A. Duffie, Solar Heating Design, John Wiley & Sons, New York, 1977.

[3] "Mixed Strategies for Energy Conservation and Alternative Energy Utilization in Buildings," Honeywell Inc., Contract for ERDA No. E(04-3)-1234.

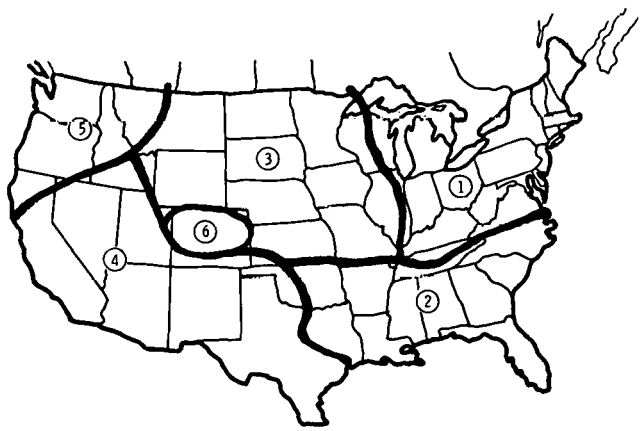

Figure 1. Six Solar Regions

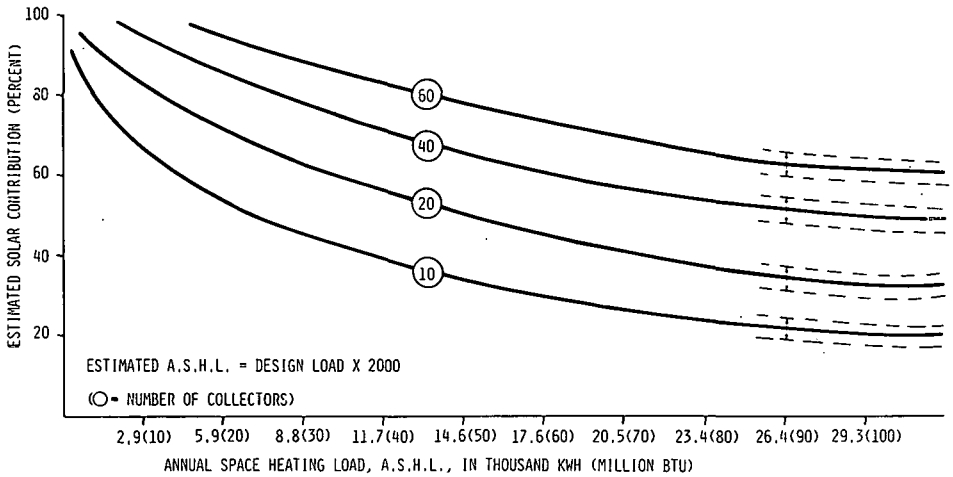

Figure 2. Solar Performance Curves for a Residential Domestic Hot Water and Space Heating System, Region 1

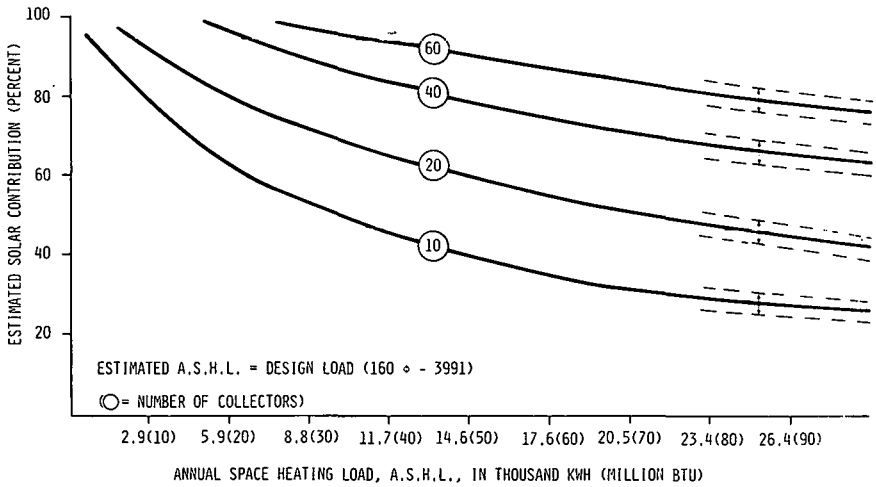

Figure 3. Solar Performance Curves for a Residential Domestic Hot Water and Space Heating System, Region 2

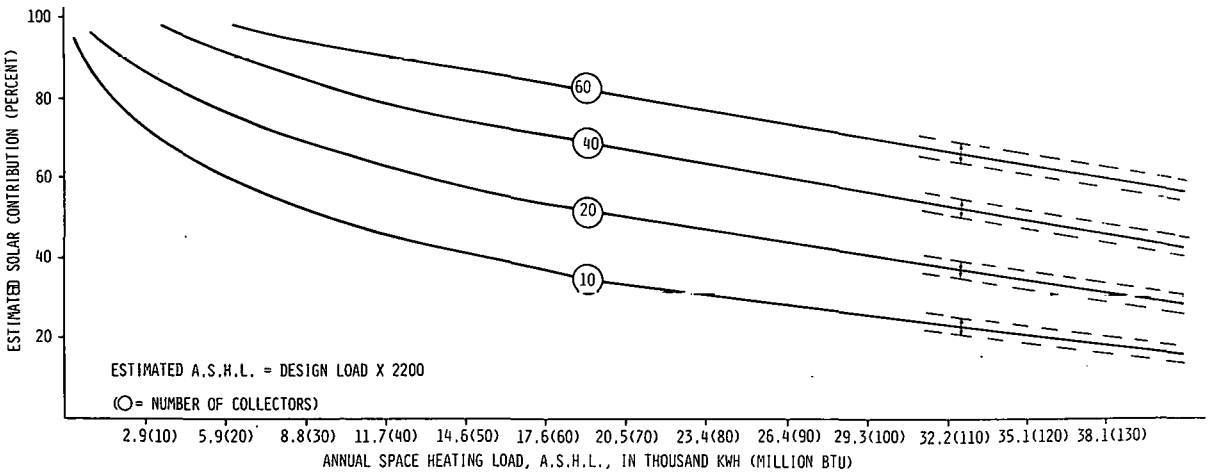

Figure 4. Solar Performance Curves for a Residential Domestic Hot Water and Space Heating System, Region 3

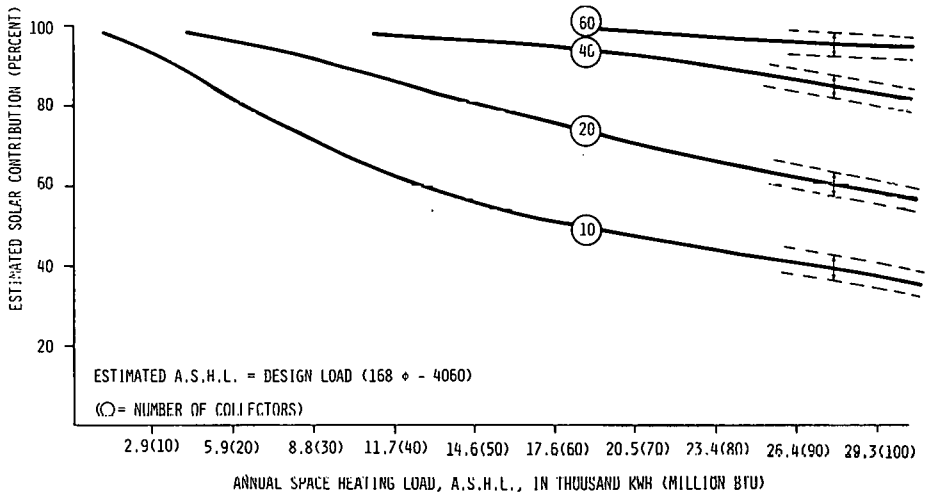

Figure 5. Solar Performance Curves for a Residential Domestic Hot Water and Space Heating System, Region 4

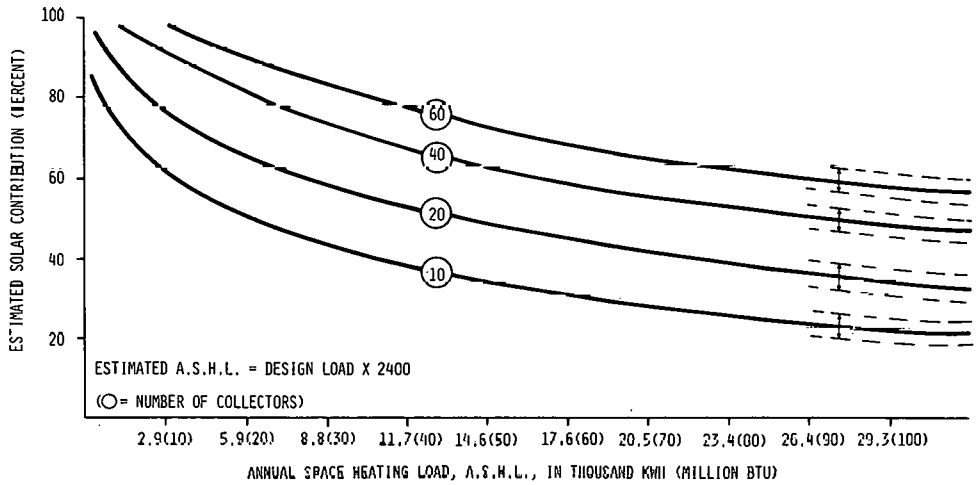

Figure 6. Solar Performance Curves for a Residential Domestic Hot Water and Space Heating System, Region 5

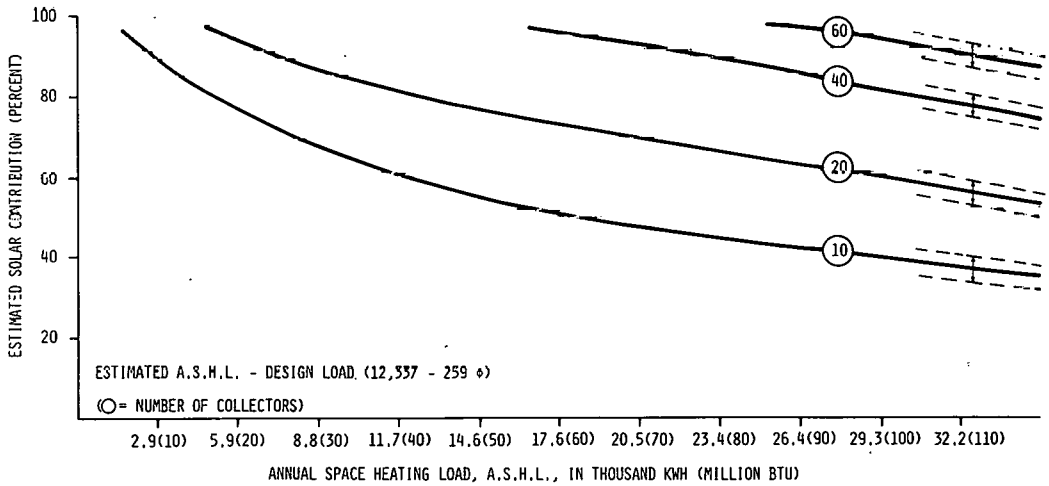

Figure 7. Solar Performance Curves for a Residential Domestic Hot Water and Space Heating System, Region 6

On Extracting Useful Building Performance Characteristics without Simulation*

A. V. Sebald
Department of Applied Mechanics and Engineering Sciences
and
Energy Center
University of California, San Diego
La Jolla, California 92093

ABSTRACT

Although simulation is a useful tool, it does not permit extraction of all the information embodied in a thermodynamic model. This paper discusses an alternative but complementary approach in which the model normally created for simulation is processed using Fourier Transforms to extract structural information which can be obtained without simulation. More importantly, such information is not produced by simulations. Simple existing computer algorithms can be used to accomplish the necessary processing even for large models (>40 nodes). The resulting structural information is useful both to determine whether building performance is satisfactory and to indicate solution paths when it is not.

INTRODUCTION

Simulation has proved to be a valuable tool in the analysis of building thermodynamics in general and passive solar energy systems in particular.[1-5] A variety of different schemes have been used to determine periodic (usually hourly) building responses to internal and external driving functions. In all cases, however, simulation amounts to an hourly solution of a series of equations representing a model of the thermal system. The trajectories of temperatures derived from this series of solutions provides much useful information. However, all information about building response is contained in the model and simulation is only one way to extract such information. Indeed, much information contained in the model is not extracted at all when simulation is used exclusively. It is the purpose of this paper to discuss a different approach meant to complement existing techniques in that respect. The principle idea is that the model contains all available, relevant knowledge about the building and the analyst's task is to extract as much insight from that model as possible. Since thermal network (TN) models provide the most exact[6] one dimensional dynamic heat transfer description in common use, it is appropriate to use them as a paradigm for discussion. All thermodynamic computer models known to the author are ultimately based on that description.

*This work was supported in part by the Solar Heating and Cooling R&D Branch of the Office of Conservation and Solar Applications of the U.S. Dept. of Energy under contract DE-AC04-79AL 10891.

The frequency domain has been used for analyzing simple passive solar buildings [10]. This paper discusses a much more comprehensive approach.

THERMAL NETWORK MODELS

Thermal Network (TN) models are analyzed in detail in Ref. [7]. A summary of those results provide a good starting point for the current discussion. In particular, the one dimensional heat transfer through any useable building medium can be modeled by a series of contiguous slabs each of which is mathematically represented by a thermal capacitance and a thermal conductance to each of its two boundaries.* As such, the differential equation governing heat transfer is given by

$$C\dot{x} = \sum_{i=1}^{2} \left[(x - T_i)\, u_i + a_i S_i \right] \qquad (1)$$

where

x = temperature at the center of the slab

C = thermal capacitance of the slab

T_i = temperature of the i^{th} boundary

u_i = thermal conductance from the i^{th} boundary to the center of the slab

S_i = heat flux incident on the i^{th} boundary

a_i = a suitable coefficient

x and T_i are temperatures at their respective locations called NODES.

Some materials (e.g. air spaces) are appropriately modeled without capacitance. An entire building can therefore be modelled by a combination of individual models of the form (1). This representation is very general in that it includes non-linear, time varying conductances. Complex models of this nature are most appropriately expressed using matrices in which two kinds of equations are of

*This approximation is valid provided the slab is thin enough. See Ref. [6].

interest. First, knowledge of the current temperature of all massive nodes (i.e. those with capacitance) is crucial since future values of all temperatures in the building depend only on current massive node temperatures and future driving functions. Second, sometimes massless node temperatures are of interest for control computations or displaying simulation results. Using a procedure detailed in Ref. [7], one writes an equation like (1) for each node in the model. Proper use of matrix algebra will eliminate uninteresting massless nodes and yield the set of matrix equations:

$$\dot{X} = Ax + Be \qquad (2a)$$

(2)

$$Y = Cx + De \qquad (2b)$$

where

X is the vector of massive node temperatures

Y is the vector of interesting massless node temperatures

e is the vector of exogenous variables (Sun, outside temperature, furnace, internal gains, etc.)

A, B, C, D are potentially time varying matrices determined by the building configuration using the simple algorithm of Ref.[7].

Equations (2) can then be used in simulations (See [7]). Indeed, they are crucial to any general simulation algorithm for systems with a large number of nodes. Some additional straightforward manipulation of the matrices A, B, C, D of (2) yields the system time constants relating any element of the input vector e to any element of the temperature vector X or Y. These time constants accurately determine simulation stability limits (see Ref. [7]). When coupled with a frequency description of the inputs, e, the time constants give information on amplitude, phase and frequency composition of important building variables X and Y (e.g. room air temperature). In fact, it may be possible to use such information either in lieu of simulation or to properly reduce the size or duration of a simulation.

In order to elucidate the method, the case of constant A, B, C, D will be considered exclusively in the sequel. Variations on these techniques also provide a great deal of information even in the time varying case. The above facts are most easily understood by analyzing a generic system like (2):

$$\text{Let } \dot{X} = AX + Be \; ; \; X(0) = X_0 \; . \qquad (3)$$

Hence (Eq. (14) of [7]):

$$X(t) = \epsilon^{At} X_0 + \int_0^t \epsilon^{A(t-\tau)} Be(\tau)\, d\tau \; . \qquad (4)$$

Rule 1: The eigenvalues λ_i of A define the system response to both initial conditions and inputs. For simplicity, the response of X in (2) is analyzed. The same techniques permit analysis of Y in (2).

Initial Conditions: ($e = 0$)

When $e = 0$, the j^{th} element of $X(t)$ can be expressed as

$$X_j(t) = \sum_{i=1}^{n} f_i(t)\, \epsilon^{\lambda_i t} \qquad (5)$$

where n is the number of elements of X and f_i are weighting (possibly time varying) coefficients dependent on both A and its eigenvalues (See [8]). There are three cases:

(i) real λ_i are the reciprocals of time constants defining rates of exponential decay.

(ii) imaginary λ_i are natural frequencies of sinusoidal oscillations.

(iii) complex λ_i describe the decay time constant and frequency of an exponentially damped sinusoid ($\epsilon^{\alpha t} \sin \omega t$).

Therefore, λ_i and f_i totally describe the speed and form of the system's response to an initial condition (e.g. some parts of the building are colder than others at the initial time).

Inputs: ($X_0 = 0$)

Taking the Fourier transforms of both sides of (3), one obtains

$$j\omega X(j\omega) = A X(j\omega) + Be(j\omega) \qquad (6)$$

or

$$X(j\omega) = (j\omega I - A)^{-1} Be(j\omega) \qquad (7)$$

The matrix $(j\omega I - A)^{-1}$ is therefore a complex coefficient determining the effect in the frequency domain of e on X. Since $(j\omega I - A)^{-1}$ is complex, each element has a magnitude and a phase. This provides a technique for estimating building response to weather and control variables of various frequency compositions. In fact, for a single X_i and a single e_k

$$C_k(j\omega) \triangleq X_i(j\omega)/e_k(j\omega) = \left|(j\omega I - A)^{-1} B\right|_{ij} \; ,$$

which is a complex number whose magnitude describes the magnitude of $X_i(j\omega)/e_k(j\omega)$ at frequency ω. In general, $G_{ik}(j\omega)$ can be expressed as a ratio of polynomials:

$$G_{ik}(j\omega) = \frac{\sum_{m=0}^{n-1} \beta_m (j\omega)^m}{\sum_{m=0}^{n} \alpha_m (j\omega)^m} \tag{8}$$

The roots of the denominator are the system eigenvalues. These are constant over all i and k. The roots of the numerator combined with the eigenvalues provide a great deal of structural information about the system. First, one factors the numerator and denominator,

$$G_{ik}(j\omega) = \frac{\prod_{m=0}^{n-1} (j\omega + z_m)}{\prod_{m=0}^{n} (j\omega + \lambda_m)} \tag{9}$$

where Π denotes the product over the specified limits. The magnitude* of $G_{ik}(j\omega)$ can then be expressed as the sum of the effects of each z_m and λ_m as follows.[7] There are three cases:

Real λ_m and z_m:

λ_m:

$$\left|\frac{1}{j\omega+\lambda_m}\right|_{db} = \left|\lambda_m\right|_{db}^{-1} + \left|\frac{1}{1+(j\omega)/\lambda_m}\right|_{db} \approx \begin{cases} \left|\lambda_m\right|_{db}^{-1} & \text{for } \omega \leq \lambda_m \\ \text{decays at 20 db per decade change in } \omega \text{ for } \omega > \lambda_m \end{cases} \tag{10a}$$

z_m:

$$\left|j\omega+z_m\right|_{db} = \left|z_m\right|_{db} + \left|1+(j\omega)/z_m\right|_{db} \approx \begin{cases} \left|z_m\right|_{db} & \text{for } \omega \leq \lambda_m \\ \text{decays at 20 db per decade change in } \omega \text{ for } \omega > z_m \end{cases} \tag{10b}$$

*$G_{ik}(j\omega)$ expressed in decibels (db) = $20 \log_{10}\left|X_i(j\omega)/e_k(j\omega)\right|$.

The error due to the above approximations is maximum at $\omega = \lambda_m$ or $\omega = z_m$ with magnitude equal to 3db (ie. .707). See [8].

Imaginary λ_m and z_m:

$$\left|\frac{1}{j\omega\ \lambda_m}\right|_{db} = \begin{cases} \left|\lambda_m\right|_{db}^{-1} \text{ at } \omega = 1 \\ \text{decays at 20db per decade change in } \omega \text{ for } \omega \neq 1 \end{cases} \tag{10c}$$

$$\left|j\omega\ z_m\right|_{db} = \begin{cases} \left|z_m\right|_{db} \text{ at } \omega = 1 \\ \text{grows at 20db per decade change in } \omega \text{ for } \omega \neq 1 \end{cases} \tag{10d}$$

Complex λ_m and z_m

These correspond to damped resonances (See discussion following (5)) and result in quadratic factors in either the numerator or the denominator of the form

$$(j\omega)^2 + 2\delta\,\omega_m(j\omega) + \omega_m^2 \triangleq Q(j\omega)$$

where ω_n is the resulting undamped resonant frequency and δ is a damping term.

λ_m:

$$\left|\frac{1}{Q(j\omega)}\right|_{db} \approx \begin{cases} \left|\omega_m^2\right|_{db}^{-1} \text{ for } \omega \leq \omega_m \\ \text{decays at 40db per decade change in } \omega \text{ for } \omega > \omega_m \end{cases} \tag{10e}$$

z_m:

$$\left|Q(j\omega)\right|_{db} \approx \begin{cases} \left|\omega_m^2\right|_{db} \text{ for } \omega \leq \omega_m \\ \text{grows at 40db per decade change in } \omega \text{ for } \omega > \omega_n \end{cases} \tag{10f}$$

The error in the last approximations depends on δ and tables are easily used [8, pg. 187]. Most buildings should have $\delta \approx 1$ for which the maximum error is about 6db.

USE OF THE ABOVE RELATIONS

Suppose that $e_k(j\omega)$ is viewed as

$$u_k(j\omega) = \sum_{s=0}^{n} \sigma_s \cos(\omega_s t + \phi_0) \quad (11)$$

This expression can be obtained by a Fourier transform or a regression in which σ_m, w_m and ϕ_m are determined. All time functions $u_k(t)$ which are physically realizable in buildings can be expressed as a sum of sinusoids. Our ultimate goal is determination of the effects of these sinusoids on the outputs $X_i(j\omega)$ and $Y_i(j\omega)$. $G_{ik}(j\omega)$ contains that information. If (8)-(10) are used to approximate the magnitude of $G_{ik}(j\omega)$, the entire goal is easy to achieve knowing only z_m, λ_m and ω_s for all m and s.

From (9), the attenuation at a given ω_s is equal to the sum of the attenuations of each λ_m and z_m at ω_s as given by (10). Similar results are available for the phase change induced by the system. In particular, since $G_{ik}(j\omega)$ is a complex number, it has a magnitude as described above and a phase. Each sinusoid as it passes through the system, (3) will have its phase ϕ_s changed by the phase of $G_{ij}(j\omega)$ at $\omega = \omega_s$. Simple rules analogous to (10) apply. More importantly, these rules require only knowledge of z_m and λ_m of (9).

Finally, if one is interested in a massless node as output (e.g. room air temperature) the linear representation of (2b) guarantees that the logic of Eqns. (3)-(11) carries through and such cases can be easily handled.

COMPUTATIONAL CONSIDERATIONS

The variables z_m and λ_m of (9) are economically obtained directly from the matrices A, B and C by use of existing computer algorithms. Simple regression routines generate least squares estimates of σ_s, ω_s and ϕ_s in (11). These routines assume that a given sequence of hourly values for an input variable e_k can be expressed as

$$e_k(t) = \sum_{s=0}^{n^*} \phi_s \cos \omega_s(t + \phi_s) + r(t) \quad (12)$$

where $r(t)$ is a noise (random) term denoting the unaccounted error in the approximation. Real data is inserted for $e_k(t)$ and the best values of σ_s, ω_s and ϕ_s are chosen to minimize the variance of $r(t)$. See Ref. [9] for details.

CONCLUSIONS

1. Thermal network (TN) models contain more information than can be extracted by simulations alone.

2. Straightforward processing of TN models using Fourier transforms permits extraction of system time constants and response to exogenous variables in order to both determine whether a building is performing satisfactorily and indicate solution paths if it is not.

3. Useful information can be obtained even if the TN model changes with time.

4. The structural information discussed in this paper is obtained directly from the same model which would be used for simulation. Once he has constructed a TN model, the analyst is therefore free to pursue either simulation or structural analysis or both - without starting over. The same model is used by both methods.

REFERENCES

[1] J. D. Balcomb and B. Anderson, Passive Solar Design Handbook, U.S. Department of Energy, Solar Heating and Cooling R&D Branch, Office of the Assistant Secretary for Conservation and Solar Energy (1979).

[2] A. V. Sebald, J. R. Clinton and F. Langenbacher, "Performance Effects of Trombe Wall Control Strategies," Solar Energy (in press).

[3] Building Loads Analysis and System Thermodynamics (BLAST) Program User's Manual, U.S. Army Construction Engineering Research Laboratory Technical Report CERL-TR-E-153 (June 1979).

[4] DOE1 User's Guide, Energy and Environment Division, Lawrence Berkeley Laboratory, Report LBL-8569, Berkeley, CA.

[5] A. V. Sebald, Ed., "Special Issue on Simulation in Solar Energy Systems," Energy: The International Journal, Vol. 4, No. 4 (August 1979).

[6] J. P. Holman, Heat Transfer, McGraw-Hill, New York (1976).

[7] A. V. Sebald, "Efficient Simulation of Large, Controlled Passive Solar Energy Systems: Forward Differencing in Thermal Networks," UCSD Energy Center Report, University of California, San Diego, La Jolla, CA 92093 (November 1979).

[8] R. C. Dorf, Modern Control Systems, Addison Wesley, Reading, Mass. (1967).

[9] T. Takenawa, "Studies in System Identification, Estimation and Forecasting," Ph.D. Thesis, Department of Applied Mechanics and Engineering Sciences, University of California, San Diego, La Jolla, CA 92093 (1979).

[10] J. M. Alcone and W. J. Kennish, "Regionalized Design Guidelines for SHAC Systems," Proceedings of 3rd National Passive Solar Conference, pp. 302-308 (1978).

COMPARISON OF BUILDING THERMAL ANALYSIS METHODS

Keith Harrington
Arga Associates
1056 Chapel St.
New Haven, Conn 06510

R. T. Lydon
Arga Associates
1056 Chapel St.
New Haven, Conn. 06510

ABSTRACT

A guide to passive solar load models is developed based on the literature. Eight basic algorithms are identified. Each is charactorized by four criteria with the user of the algorithm in mind. The criteria consist of the models base assumptions, computational costs, types of input and relevance of output to the stages of architectural design. Some concluding notes are made on the nature of test cells.

The models include Bi-Nodal R-C, Eight Nodal R-C, Mini-Nodal R-C, Full-Nodal R-C, Heat Balance - Dynamic Matrix, Heat Balance - Hybrid, Heat Balance - Fixed Matrix, and Weighting Factors. At least one example of each is given in the concluding table.

INTRODUCTION

The basic requirement of a good simulat is the delivery of the most utilizable information at the least cost. This paper will look at some of the passive solar algorithms in use, to identify both their appropriateness to various stages of the design process and their inherent costs to the user in time and computer resources. The models will be considered in light of the following criteria:

1) completeness or potential for completeness of model

2) magnitude of calculations and their rate of growth

3) clarity and volume of the input requirements

4) relation of invested time to usable output

Eight examples were chosen because they either represent a basic computational approach or they are a significant step in the scale of that approach to the problem. In all cases, what are being explored are the algorithms and their potentials and not a given program. The names are listed only as an example of a generic type.

The last page is a reference table listing each model and its comparitive attributes in a graphic form. It is hoped that this will give an overview of the discussions of these approaches.

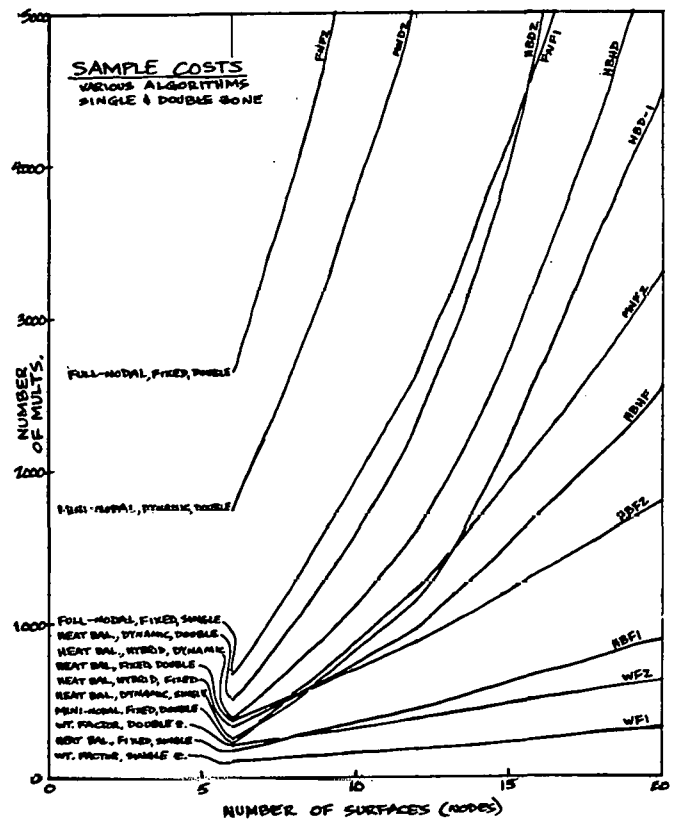

BI-NODAL R-C NETWORK

This is a solution implemented on a calculator, thus having severe size and time limitations, but it is indeed a simulation and could be of use to the designer in the early stages of concept formation to check feasiblity of some of the more direct solar approaches. It does illustrate the tendency of these smaller programs to view the passive system as a special case component to be used to adjust envelope heatloss calculations. These calculations need to be done by hand before running the program, or a rule-of-thumb figure must be used in order to arrive at an envelope heatloss coefficient. All heat transfers are reduced to one coefficient that links storage to room air.

EIGHT-NODAL R-C NETWORK

This is another calculator solution which like the model above steps through one day at a time in one hour increments, but this one pushes the limits as far as time and space on these machines. Again it is not meant to give a yearly energy budget, but rather explore the heat dynamics of a space on a user chosen design day. The assignment of its available nodes is fairly open ended but they could be used to explore a primary and secondary conductive path as well as a glazing path. The method entails a matrix inversion technique which allows for a simultaneous determination of all the nodal states. Here also the user must arrive at an overall skin U*A figure and such things as east and west solar heating of the skin would be difficult to model without allocating precious nodes to each side. Thus a great deal of the burden of appropriateness of the model falls on the user and his ability to pre-understand the dynamics of his problem. If it is straight forward then this could be a handy sizing tool. When the designer wants to know how how much mass will be needed, and is not yet concerned with it's relationship to the rest of the building's systems, this would be of considerable help.

MINI-NODAL R-C NETWORK

This is the beginning of the year-long simulation programs and is implemented on a full sized mini-computer. One advantage of the year-long run is that the design day conditions are found, these being the result of a sequence of days rather than an extreme of any one condition. The mini-computer does imply a loss of hardware accessiblity, but if used through a service improves the consistancy of the assumptions and results.

This level of the R-C network model still requires the user's identification of the major heat pathways as well as the proper selection of resistances. With the larger number of nodes available one is assured of picking up the major dynamics. Also, many of the previously lumped resistances can be broken out into values with direct physical values. Typically, though, the shell will be treated as a single load resistance. The reason for this is that with these finite difference models all nodes are included in one matrix. For example a Trombe wall which only includes three conduction paths has a total of 13 nodes. Assuming a straight simultaneous solution of the matrix each step would incur ((nodes)**3)/2 multiplications. If we adjust this to a standard problem format, that of a simple six surface room, and assume 2 iterations per hour, we arrive at a computational cost of 5N+(2N)**3, where N is the number of surfaces, in this case "6", or 1758 multiplications per hour. It can be seen that this is a two-zone model. It will be noted that it is still a multiple of five larger than the two zoned heat balance methods. One way to reduce computation is to hold the heat transfer coefficients constant and then invert the matrix. For the above example this yields 5N+2*(2N)**2 or 318 multiplications per hour, a considerable savings.

From the designer's point of view this technique is able to explore any of the processes in the building, but there is an obvious cost incentive to break the total system into specific sub-components. Also, once again the model structure itself does not enforce a level of completeness. This is left to the user familiar with electric networks and their sensitivities, thus, the recommendation of its value as a service on a consultation basis. This can also foster an educational process through discussion of choices and results with a client.

FULL-NODAL R-C NETWORK

This is the largest and most complete system model of the R-C networks and in principle would have many informational advantages. Such things as radiational exchange, convective transfers, as well as the conductive properties of all the major surfaces in a multi-zonal system could be explored. This would mean all surface temperatures and geometry based heat exchanges could be found. Thus a space could be dimensioned and real information gained about the layout and deployment of mass and collectors in the system.

To a designer with for example a space with a south solar aperture, an east-west facing mass storage partition wall and with partial earth-sheltering of the north wall, this level of detail may be needed simply to generate meaningful feedback about such a system.

With this level of specificity about the system one can input resistance values that are physical measures and completely describe the network. This provides a level of protection against improper assumptions in the input sessions. It also entails a higher cost in input preparation and problem definition. It is a tool for refining, definitely not gross designing decisions.

This is the outward bound of explicit definition of the problem, and as with the previous finite difference solutions, suffers from computational growth. With the matrix inversion multiply solution mentioned above, looking at six surfaces in each of two zones with one massive surface in each, all other pathways having two nodes each, we have 10N+2*(6N)**2 where N=6, giving 2,652 multiplications per simulated hour. If the coefficients were recalculated each step the formula would be 10N+(6N)**3 or for the standard problem 46,716 multiplications per hour! This assumes a node on each surface of each of 12 walls and two massive walls.

HEAT BALANCE - DYNAMIC MATRIX

We find a fundamentally different approach being taken here to accomplish the same degree of completeness as in the previous model. In this case a system of heat balance equations are created for the interior surfaces of each of the zones. Conduction transfer functions are set up using a response factor analysis method to model conductive heat transfer. These have the ability to model time-dependent heat transfers in both directions separately, based on a surface temperature time series. The outside heat flux is arrived at using the history up to the last hour (charge state) and then the updated outside history is used for the solution of the inside heat flux (discharge state). This has two advantages. First, heat capacitance and conduction in a massive wall can be accounted for with a single entry in the system matrix. Secondly, the splitting of directions and the updating of a wall's outside temperature using the last hour's value allows one to use a pseudo-outside temperature for interzonal conduction to the interior zone. This means that each zone can be treated as a separate matrix which helps to "charge" its neighbors. A cost figure including the time series then would be 5N+20N+(N**3)/2 , additional zones being linear multiples. This means our standard problem of two zones of six walls each would take 516 multiplications per with a one hour time step. It should be simulated hour. It should be noted that these transfer functions also allow a more reasonable modeling of a multi-layered wall.

As seen by the user, this model, as with the previous one, gives fairly detailed information about the workings of the relationships in the system. The key here is geometry, for if the design is not yet to that level, costs are incurred for feed-back on a set of specifics not yet indicated. The input, because the system is not a metaphor in a language foreign to the designer, is a set of familiar architectural definitions. All heat transfer coefficients can be dynamically recalculated each hour internally, saving the designer the chore of finding a set of fixed coefficients.

HEAT BALANCE - HYBRID

In principle this solution would consist of a combination of an abbreviated R-C network and the heat balance models. The the R-C network could model a certain class of passive elements which then could be treated as wall sections and system air inputs in the overall heat balance model. A catalog of R-C models could include such diverse elements as hydronic heating systems,radiant floor and ceiling slabs, attics, basements, vented walls, Trombe walls, water walls, roof ponds, rock storage and active solar systems. The use of these modular passive elements would eliminate the need for the heat balance model to treat them as additional zones and thereby reduce computing costs where the full geometric model is not needed. A reasonable projection of a space's loads can be averaged with the last hour's load to drive these models. The heat balance solution insures proper modeling of the geometrics and integration of the passive elements into the living zones, while also circumventing the need for one overall matrix for the whole building.

Looking at the computational costs, given two zones, one a passive element, the size is 10N+(2N)**2+20N+((N-1)**3)/2 . For the above cited problem of two zones, one a Trombe wall and one a six sided room, each hour would take 386 multiplications. This shows that if one zone is a passive element, significant savings can be gained by using an R-C network for it.

The input requirements would be about the same for this solution as the preceding one. This should be qualified, by saying that the passive elements would have to be stock networks that the user would simply dimension at run time. If the user did not have this insulation from the R-C model the input would be considerably complicated. The ability to replace the elements with alternates would be of help to a designer at the stage of making system and form decisions.

HEAT BALANCE - FIXED MATRIX

If one takes a look at the make up of the heat balance matrix, several simplifying assumptions can be made. Making these simplifications allows one to fix the properties of this matrix into a set of constant state matrices. If inverted this reduces the solution step from (N**3)/2 to N**2 . This means that the size of the computations is 5N+20N+N**2 for each zone. For the example of two six sided zones the computation would consist of 377 multiplications per hour time step. If this model were used as the heat balance side of the preceding model the size would be 10N+(2N**2)+20N+(N-1)**2 , or 349 multiplications per hour.

One of the assumptions that is needed is that the inside convective film coefficient is constant. One way to deal with this is to define two states, one where the floor is cooler than the ceiling (stable) and the other the reverse (unstable). Then an inverted matrix is kept for each condition and used as needed. The other limit is that the pure conduction U value is a constant. The only place this is a problem is in the case of insulating shades. Here again, two state matrices are kept. Thus, for each zone there are eight state matrices kept, including the two used for either floating temperature or load calculation modes.

Essentially, this model requires the same inputs as the 'dynamic matrix' model. In practice that model, which is slower, but has less limiting assumptions, probably is better for looking closely at system dynamics over 'design week' periods, whereas this model is more suited to heat budgeting a building over a year's time, given its greater algorithmic efficiency.

WEIGHTING FACTOR METHOD

This model goes one step further toward simplifying the computations and thereby gaining greater efficiency. It considers only one state for the interior space. It then builds a model like the fixed matrix' example. It then applies unit inputs in each of the possible input routes and observes the systems behavior, developing a time series to describe it. The principle of superposition allows the resulting series to be additive in their modeling of the system. As long as the original matrix is not diagonalized by lumping geometric effects this may also be used to model such elements as unvented Trombe walls. In practice, input through conduction paths are lumped and as a result inside wall surface temperatures are not available. Accepting these limitations, the algorithm is very fast, and grows only linearly as the number of surfaces grows. It's size formulation at present is 5N+10N+12 per zone. Multi-zone calculations are based on the assumption of steady state neighbors in this model. Th.s given the standard two six sided z.nes each hourly iteration requires only :04 multiplications.

This algorithm requires the same sort of building description as the heat balance type, and it then does an internal reduction of it for the simulation. The output is meant for insights into the building's year-long energy budget. In a sense this model is meant more for analysis than design, although the two do serve each other.

CLOSING NOTES

One should be reminded that this paper has surveyed only the set of load generating models. There are many other components of a good model not considered. These are independent of the models that are described above. They include such thermal inputs as infiltration, solar gain through glazing and inputs due to people, equipment and lights.

A second observation is that at least one version of each of the above models is able to track some of the LASL test cells closely. Given the fact that the major differences in model assumptions lies in the area of internal radiation exchange and convective heat transfers perhaps validation should be based on systems that can distinguish between these effects and conduction in a more definitive way. This could be done with measured 'test cells' that had a more realistic internal air volume and less regular shape. This may mean two cells for each system, one flat space and one with a deep space. This would seem particularly important in the case of the direct gain cell.

CONCLUSIONS

This paper has endeavored to explore the published state-of-the-art of passive solar load models. To that end it has discerned eight basic algorithmic types. Two of these are meant for calculators. The other six are implemented on large computers. All were considered in light of their completeness, efficiency, inputs and appropriateness of output to the various stages of building design. It has been found that all considered models make a trade-off between cost and model completeness, each to serve different ends.

ACKNOWLEDGEMENTS

The authors would like to thank Robert Frew, Donald Watson, Everett Barber and Carl Williams, all of Yale University, for their insights into the combinatorial possiblities of the subjects of Solar Energy, Architecture, and Computation.

BIBLIOGRAPHY

G.P.Mitalas, "An Assessment of Common Assumptions in Estimating Cooling Loads and Space Temperatures", ASHRAE Transactions, Pt.II,1965,P#1949

P.L.Versteegen, "Survey of Currently Used Simula tion Methods", SAI, Inc., Nov.,1978,(DOE ME-78-04-4261)

R.L.Merriam, "Building Energy Analysis Computer Programs with Solar Heating and Cooling System Capabilities", A.D.Little, Inc.,EPRI RP1269

W.L.Glennie, "Hand-Held Calculator Aids for Passive Design", SERI Reprint

J.T.Kohler and P.W.Sullivan, "TEANET: Users Manual", TEA, Inc., July 1978

R.D.McFarland, "PASOLE: A General Simulation Program for Passive Solar Energy",LASL Report (LA-7433-MS), Oct. 1978

J.D.Balcomb,R.D.Mcfarland, and S.W.Moore, "Simul ation Analysis of Passive Solar Heated Buildings --Comparison with Test Room Results",ISES June 1977, (LA-UR-77-939)

W.O.Wray and J.D.Balcomb, "Sensitivity of Direct Gain Space Heating Performance to Fundamental Parameter Variations", Solar Energy Vol.23, pp.421-425,Pergamon Press Ltd.,1979

T.Kusuda, "NBSLD, the Computer Program for Heating and Cooling Loads in Buildings", NBS Building Scicnce Series 69R, May 1978

F.Arumi-Noe, "Multi Space Thermal Coupling Algorithm of the DEROB System",Conference on Heat Transfer in Energy Conservation, Dec 1977, ASME

F.Arumi-Noe, "A Model for the DEROB/PASOLE System",2nd Nat. Passive Solar Conf.,Vol II, March 1978

K.Harrington, R.S.Frew, and C.Williams, "SOLSTICE and EQUINOX: Program Descriptions", Arga Associates, June, 1979.

E.M.Sparrow and R.D.Cess, "Radiation Heat Transfer", pp.56-63,Brooks/Cole Publishing Company, Belmont,Calif., 1966

J.E.Fromm, "A Numerical Method for Computing the Non-Linear, Time Dependent, Buoyant Circulation of Air in Rooms", Proceedings: Use of Computers for Environmental Engineering Related to Buildings, NBS Building Science Service 39, 1971

G.S.Campbell, "An Introduction to Environmental Biophysics", Springer-Verlag, New York, 1977

D.G.Stephenson and G.P.Mitalas, "Cooling Load Calculations by Thermal Response Factor Method", ASHRAE Transactions, Part I, 1967

S.C.Diamond, et al, "DOE2 Program Manual", LASL (LA-7688-M), LBL (LBL-8705), Feb 1979

Z.O.Cumali, et al., "Extension of Methods Used for Analyzing Passive Solar Systems",4th Nat. Passive Solar Conference Proceedings, Oct 1979

T.Kusuda,"Review of Current Energy Analysis Calculation Procedures",A Letter Report, Center for Building Technology, NBS, July 1971

D.Watson and K.Harrington, "Research on Climate Design for Home Builders: Breif Summary of Quant ification Results",4th Nat. Passive Solar Conference Proceedings, Oct 1979

R.T.Lydon,E.M.Barber, and R.Loope, "SUNSYM - Solar Thermal Systems Design Programs", Systems Simulation and Economic Analysis for Solar Heating and Cooling, Conference Proceedings, June 1978

D.Watson, "Solar Design",Progressive Architecture, PP.102-107, Nov 1979

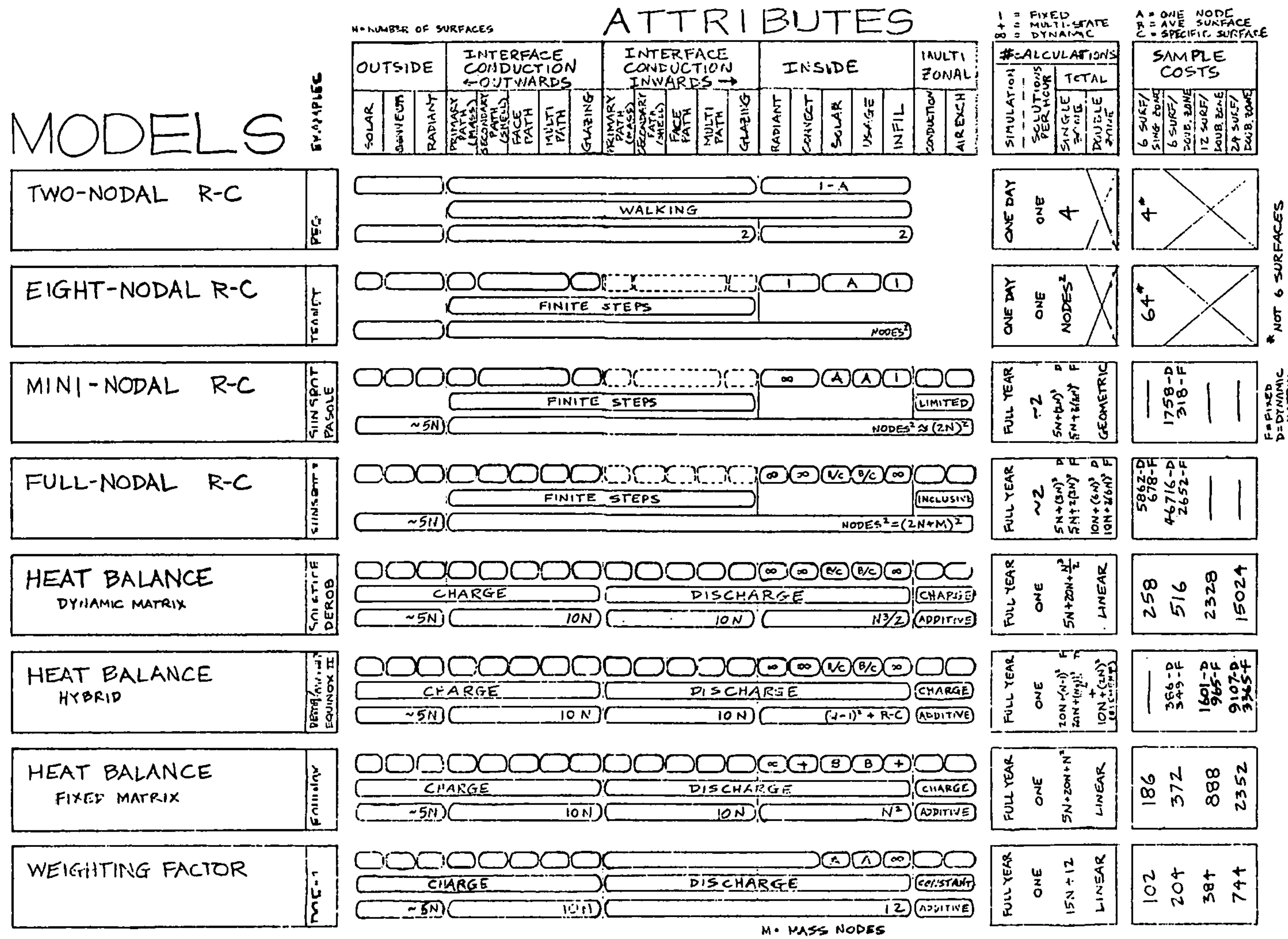

ATTRIBUTES
N = NUMBER OF SURFACES
MODELS
EXAMPLES
OUTSIDE
SOLAR
SKYVIEW
RADIANT
INTERFACE CONDUCTION ←OUTWARDS
PRIMARY PATH (MASS)
SECONDARY PATH (SHELL)
FACE PATH
MULTI PATH
GLAZING
INTERFACE CONDUCTION INWARDS →
INSIDE
RADIANT
CONVECT
SOLAR
USAGE
INFIL
MULTI ZONAL
CONDUCTION
AIR EXCH
1 = FIXED
+ = MULTI-STATE
∞ = DYNAMIC
#CALCULATIONS
SIMULATION
SOLUTIONS PER HOUR
TOTAL
SINGLE ZONE
DOUBLE ZONE
A = ONE NODE
B = AVE SURFACE
C = SPECIFIC SURFACE
SAMPLE COSTS
6 SURF/SING ZONE
6 SURF/DOUB ZONE
12 SURF/DOUB ZONE
24 SURF/DOUB ZONE
TWO-NODAL R-C
WALKING
1-A
ONE DAY
ONE
4
4*
EIGHT-NODAL R-C
FINITE STEPS
NODES²
ONE DAY
ONE
NODES²
64*
* NOT 6 SURFACES
MINI-NODAL R-C
SUNSPOT
PASOLE
~5N
LIMITED
NODES² ≈ (2N)²
FULL YEAR
~2
5N+(2N)² D
5N+2(N)² F
GEOMETRIC
1758-D
318-F
F = FIXED
D = DYNAMIC MATRIX
FULL-NODAL R-C
SUNSPOT
~5N
INCLUSIVE
NODES² = (2N+M)²
FULL YEAR
~2
5N+(3N)² D
5N+2(3N)² F
10N+(6N)² D
10N+2(6N)² F
5862-D
678-F
46716-D
2652-F
HEAT BALANCE
DYNAMIC MATRIX
SOLAR
DEROB
CHARGE
DISCHARGE
~5N
10N
10N
N³/2
CHARGE
ADDITIVE
FULL YEAR
ONE
5N+20N+N³/2
LINEAR
258
516
2328
15024
HEAT BALANCE
HYBRID
EQUINOX II
CHARGE
DISCHARGE
~5N
10 N
10 N
(J-1)² + R-C
CHARGE
ADDITIVE
FULL YEAR
ONE
366-D
349-F
1601-D
965-F
9107-D
3365-F
HEAT BALANCE
FIXED MATRIX
CHARGE
DISCHARGE
~5N
10N
10N
N²
CHARGE
ADDITIVE
FULL YEAR
ONE
5N+20N+N²
LINEAR
186
372
888
2352
WEIGHTING FACTOR
CHARGE
DISCHARGE
~5N
10N
12
CONSTANT
ADDITIVE
FULL YEAR
ONE
15N+12
LINEAR
102
204
384
744
M = MASS NODES

Dup

PREDICTING THE TIME RESPONSE OF A BUILDING UNDER HEAT INPUT CONDITIONS FOR ACTIVE SOLAR HEATING SYSTEMS*.

Mashuri L. Warren, Ammar F. Sakkal‡, and Steven R. Schiller

Solar Energy Group
Energy and Environment Division
Lawrence Berkeley Laboratory
University of California, Berkeley

ABSTRACT

A dynamic model has been developed to determine the response of a residential building to changes in heat input, and to predict room and air temperature changes. The model has been developed to simulate the response of a typical building for possible use with the LBL test facility that evaluates control strategies for active solar systems. The model must properly predict the rapid rise in room temperature resulting from addition of heat with a fan coil, must give the correct average building load, and must require only limited computational capabilities.

The building is modeled as a three node capacitance-resistance network which can be solved to determine the room air temperature, interior wall temperature, and building-shell wall temperature as a function of time in response to heat input. Capacitance terms represent the thermal masses of the air within the structure, the interior walls, and the interior surface of the outer building shell. Resistance terms represent the resistance to the heat transfer from the interior and exterior walls to the room air, from the exterior wall to the outside, and from the room air to the outside by transmittance through windows and by infiltration. The heat input is provided directly to the air (as, for example, when a heating fan coil is turned on).

The time dependent equations are solved using Laplace transforms to determine the building response to a step increase in heat input power. The dynamic response of the building's temperatures can be characterized in terms of the building heat loss coefficient, UA, and three exponential decay terms with appropriate time constants and weights. A time constant of the order of a few minutes describes the air temperature rise due to heat input balanced against losses to the building and to the outside. A time constant of the order of several hours describes the relaxation of the temperature of the building thermal mass to the outside ambient temperature. A third time constant describes the rearrangement of energy between the air and the structure.

The magnitudes of different capacitances and resistances are estimated for a typical residential structure. The time constants and the building heat loss coefficient are then determined from the model. The results are compared with an experimental measurement[1] in which the three time constants have been experimentally determined.

For predicting building temperature response and evaluating control strategies the three node resistance model offers a simple method which can be applied on a small computer and in real time. It is anticipated that this model will provide the thermal accuracy and computational speed suitably matched to the requirements of the LBL test facility for control strategies.

INTRODUCTION

The LBL solar control test facility[2,3] consists of a hydronic solar space heating system with heat input and building load simulator. The load simulator consists of an airflow channel with a heating coil similar to that in the furnace ductwork of a residential heating system.

To make meaningful comparisons between alternate control strategies using identical simulated load conditions, it is necessary to determine the building heating demand and the condition of the building thermostat based on building parameters and

* This work has been supported by the Systems Analysis and Design Branch, Systems Development Division, Office of Solar Applications, U. S. Department of Energy under Contract No. W-7405-ENG-48.

‡ presently at University of Minnesota.

weather conditions. Thus an investigation was begun to choose a model to predict average heating requirements and to describe how the room air, wall, and thermostat temperatures respond to sudden changes in heat input when the heating fan turns on or off, and to changing weather conditions. Such modeling becomes of crucial importance if one attempts to simulate the recovery from night thermostat setbacks.

While standard load calculations neglect thermal capacitance effects, some authors[4,5,6] do consider the response of room temperature to sudden heat inputs using a resistance-capacitance thermal network model with a single thermal capacitance term, characteristic of the lumped thermal mass of the building structure. This model gives the temperature response over several hours, which, for instance, can determine the temperature swing and mean temperature of a passively heated structure. Other researchers [7,8,9,10] have considered thermal network models with several nodes.

In our analysis we are constrained to models that can be implemented on our HP 9825A microcomputer which is performing many tasks. We have applied a three node model based on a physical modeling of a building. The exponential response times, and with some modest effort the appropriate weighting factors for the different exponentials are determined. By Laplace transform solution of the resulting equations, with careful attention to initial conditions, analytic expressions for the interior of the building shell, T_1, the temperatures of the room air, T_2, and the interior walls, T_3, are can be obtained, in response to a step heating input. The results of the analysis are applied to a specific building, and compared to limited data available from the literature.

THE THREE NODE MODEL

The three node capacitance-resistance network, shown in Figure 1, is used to study the dynamic response of a building to the input of heat. The thermal mass within the insulating envelope is divided into three portions: C_1, C_2, and C_3.

C_1 represents the thermal mass of the interior surface of the exterior wall at a temperature T_1. For a reasonably well insulated structure, most of the temperature drop to the outside is across the insulating layer. For short time periods the temperature dependence of the interior surface is dominated by the thermal conductance to the interior air, and not by conductance through the wall to the outside.

C_2 represents the thermal mass of the air enclosed within the volume of the residence at a temperature T_2. It is assumed in this analysis that air within the space is well mixed and is at a uniform temperature.

C_3 represents the thermal mass of the interior, walls at a temperature, T_3. For a passive solar structure this would also include the indirectly heated thermal mass.

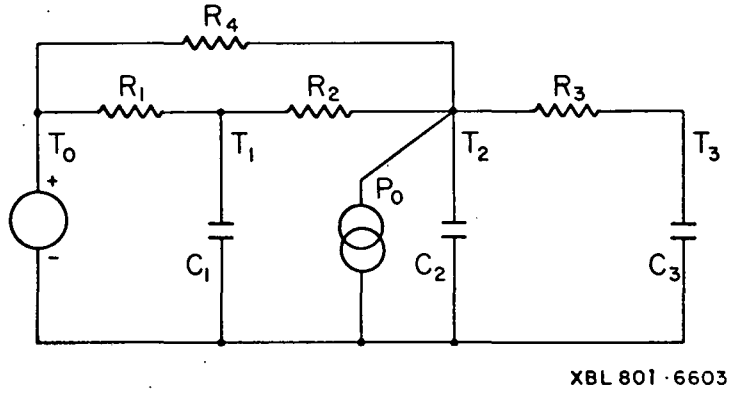

Figure 1. The thermal network used to predict temperature changes in response to heat input.

There are four heat transfer paths represented as resistances: R_1 R_2, R_3, and R_4. Each thermal resistance is the reciprocal of the effective UA calculated for each path.

R_1 represents the resistance to heat loss from the interior surface of the external building shell at temperature T_1 to the outside temperature T_o.

R_2 represents the resistance to heat transfer from the air in the space at temperature T_2 to the interior surface at temperature T_1. This is approximately equivalent to the air film resistance of the inner surface of the building shell not counting windows.

Similarly R_3 represents the resistance to heat transfer from the air at temperature T_2 to the interior structure at temperature T_3.

Finally, R_4 represents the resistance to heat loss through the windows and by infiltration.

The forcing functions driving the system are the outdoor temperature, T_o and the heat input power $P(t) = P_o$, from the fan coil or furnace ductwork which transfers energy directly to the air within the space. Direct solar gain is not included in the analysis. Both the outdoor temperature T_o and the power delivered to the load are assumed to be constant over the period of the analysis corresponding to one thermostat on period or off period. By careful treatment of initial condition the analysis is reinitialized when the thermostat control states change.

THE EQUATIONS

The equations for the temperatures, T_1, T_2, and T_3, determined from the resistance capacitance network can be solved using the Kirchhoff analysis, where the currents represent heat flows and the voltages represent temperature. Laplace transform of these equations are then performed with careful consideration of the initial conditions at time t = 0; $T_1(0)$, $T_2(0)$, and $T_3(0)$.
Assuming that the heat input, P_o, and outdoor temperature, T_o, are constant:

$$P(s) = \frac{P_o}{s} \quad ; \quad T_o(s) = \frac{T_o}{s} \quad .$$

The Laplace transform equations are:

$$\frac{T_1(s)-T_o/s}{R_1} + \frac{T_1(s)-T_2(s)}{R_2} + C_1[sT_1(s)-T_1(0)] = 0$$

$$\frac{P_o}{s} = \frac{T_2(s)-T_1(s)}{R_2} + \frac{T_2(s)-T_o/s}{R_4} + \frac{T_2(s)-T_3(s)}{R_3} + C_2[s\,T_2(s)-T_2(0)]$$

$$\frac{T_3(s) - T_2(s)}{R_3} + C_3\,[s\,T_3(s) - T_3(0)] = 0$$

These equations can be put in matrix representation.

$$\begin{vmatrix} C_1(s+1/t_1) & -1/R_2 & 0 \\ -1/R_2 & C_2(s+1/t_2) & -1/R_3 \\ 0 & -1/R_3 & C_3(s+1/t_3) \end{vmatrix} \begin{pmatrix} T_1(s) \\ T_2(s) \\ T_3(s) \end{pmatrix}$$

$$= \begin{pmatrix} C_1\,T_1(0) + \dfrac{T_o}{s\,R_1} \\ C_2\,T_2(0) + \dfrac{P_o}{s} + \dfrac{T_o}{s\,R_4} \\ C_3\,T_3(0) \end{pmatrix}$$

where t_1, t_2, and t_3 are constants:

$$t_1 = \frac{C_1}{1/R_1 + 1/R_2}$$

$$t_2 = \frac{C_2}{1/R_2 + 1/R_3 + 1/R_4}$$

$$t_3 = R_3C_3$$

ROOTS OF THE EQUATIONS

The characteristic time constants, τ_1, τ_2, and τ_3, that describe the dynamic response of the building temperatures are obtained from the roots of the determinant by solving the cubic equation:

$$\frac{t_2\,(1 + st_1)}{R_3\,C_2} + \frac{t_1t_2\,(1 + st_3)}{R_2\,C_2\,R_2\,C_1} - (1+st_1)(1+st_2)(1+st_3) = 0$$

Building Parameters.

The characteristic time constants have been determined for two specific examples; a well insulated and an uninsulated residential structure. The building parameters for these two cases are shown in Table 1.

	BTU/hr-°F				
	$1/R_1$	$1/R_2$	$1/R_3$	$1/R_4$	$1/R_{eff}$
well insulated	243	3111	653	279	504
uninsulated	1317	3111	653	629	1554

	BTU/°F		
	C_1	C_2	C_3
well insulated	2470	245	1036
uninsulated	2470	245	1036

Table 1. Building Parameters

The building modeled is a 1700 ft^2 (158 m^2) residence treated as a single zone. The well insulated structure has R-values (in ft^2-hr-°F/BTU) of 17 (floor), 32 (ceiling), and 21 (walls) with 200 ft^2 (12 % of floor area) (19 m^2) double glazed windows and an infiltration rate of 2/3 air change per hour. The uninsulated structure has R-values of 5.4(floor), 5.2 (ceiling), and 4.4 (wall) typical of frame construction with 340 ft^2 windows (20 % of floor area) and an infiltration rate of one air change per hour. From these values the thermal resistance terms are calculated.

The effective steady state heat loss rate from the air in the space to the outside is given by the series resistances R_1 and R_2 in parallel with R_4.

$$1/R_{eff} = 1/R_4 + 1/(R_1 + R_2)$$

The thermal masses in the space are estimated:

1) C_1, the thermal equivalent of 1/2 inch of sheet rock on the inner surface of the exterior walls, ceiling, and floor; 2) C_2, the thermal mass of the building air volume; and 3) C_3, the estimated thermal mass of 960 ft^2 of interior partition walls.

Time Constants.

The exact time constants predicted by the model for the building require the solution for the roots of the cubic equation and are shown in Table 2.

Typical	τ_1	τ_2	τ_3
well insulated	0.057	1.29	7.72
uninsulated	0.053	0.97	2.73
Experimental*			
minimum	0.098	0.50	10.3
maximum	0.066	0.43	6.6

Table 2. Time constants in hours. *Observed data is from Socolow and Sonderegger[1] for a Twin Rivers townhouse.

The longest time constant, τ_3, which describes the relaxation of the total building thermal mass at the effective heat loss rate, $1/R_{eff}$, is approximately given by

$$\tau_3 \cong [C_1 + C_2 + C_3] R_{eff}$$

The approximate value of τ_3 is 7.44 hrs (exact root 7.72 hrs) for the insulated case and 2.41 hrs (exact root 2.73 hrs) for the uninsulated case. The longest time constant depends both on the thermal mass in the space and the effective heat loss rate.

The shortest time constant τ_1 is related to the relaxation of the space air temperature by heat loss to the walls and to the outside through the windows and by infiltration. τ_1 is given approximately by;

$$\tau_1 \cong C_2 \, [1/R_2 + 1/R_3 + 1/R_4 \,]^{-1}$$

The approximate value for t_1 is 0.061 hrs (exact root 0.057) for the insulated case and 0.056 hrs (exact root 0.053) for the uninsulated case. The shortest time constant is sensitive to the thermal capacitance of the air and the coupling to the thermal mass in the space and does not change significantly with degree of insulation of the space.

The intermediate time constant τ_2 is related to the redistribution of energy within the space and is not readily identified.

Experimental Observation.

Socolow and Sonderegger[1] have analysed a single experiment in which a building, different from the one modeled, was "toasted" with the furnace on for 4 hours and then allowed to cool for 3.5 hours while the temperature in a hallway is observed. The hallway temperature rose from from 68 °F (20 °C) to 97 °F (36 °C) and then cooled. Their observations of the hall temperature are shown in Figure 2.

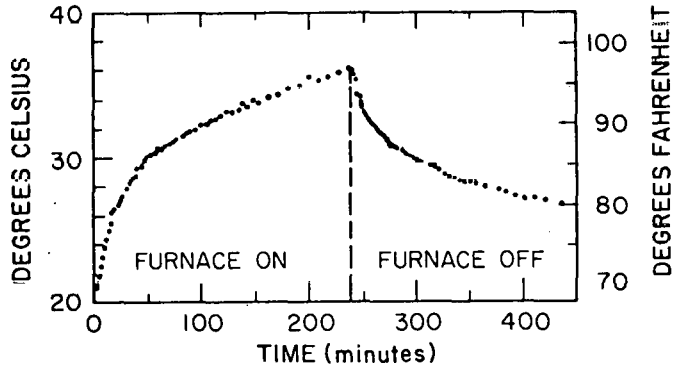

Figure 2. Hallway temperature as a function of time. Adapted from Socolow and Sonderegger[1].

Subsequent analysis of this experiment revealed three distinct time constants for the heating and cooling process. Because of limited data, their time constants depend somewhat on assumptions made as to the final temperature reached, so that they were able to give only the range of values that are shown in Table 2. As we have little information about the conditions of the experiment not too much can be made from their results. However, their measured short and long time constants are certainly close to the values obtained for the well insulated structure, and the intermediate time constant is the correct order of magnitude.

TIME RESPONSE.

The matrix equations are solved using Cramer's rule to determine the time response of the room air, $T_2(s)$, and wall temperatures, $T_1(s)$ and $T_3(s)$. Here only the solution for the room air temperature, T_2, will be presented, but the others are similar. The Laplace transform for the room air temperature is given by

$$T_2(s) = \frac{1}{|det|}\begin{vmatrix} (1/t_1 + s)C_1 & C_1 T_1(0) + T_o/sR_1 & 0 \\ -1/R_2 & C_2 T_2(0) + \frac{P_o}{s} + \frac{T_o}{s R_4} & -1 \\ 0 & C_3 T_3(0) & (1/t_3 + s)C_3 \end{vmatrix}$$

where $T_1(0)$, $T_2(0)$, and $T_3(0)$ represent the initial temperatures at time t=0. The value of the determinant is given by

$$|det| = \frac{C_1 C_2 C_3}{t_1 t_2 t_3} F'(1 + s\tau_1)(1 + s\tau_2)(1 + s\tau_3)$$

where the constant F' is given by

$$F' = 1 - \frac{t_1 t_2}{R_2^2 C_1 C_2} - \frac{t_2}{R_3 C_2} = \frac{t_2(R_1 + R_2 + R_4)}{C_2 R_4 (R_1 + R_2)}$$

The solution for the Laplace transform of the room air temperature is given by:

$$T_2(s) = \left\{ \frac{t_2(1 + st_1)(1 + st_3)}{F' C_2} \left(\frac{P_o}{s} + \frac{T_o}{s R_4} \right) + \frac{t_1 t_2 (1 + st_3)}{F' C_1 C_2 R_1 R_2} \frac{T_o}{s} + \frac{t_1 t_2 (1 + st_3)}{F' C_2 R_2} T_1(0) + \frac{t_2(1 + st_1)(1 + st_3)}{F'} T_2(0) + \frac{t_2 t_3 (1 + st_1)}{F' C_2 R_3} T_3(0) \right\} \times \frac{1}{(1 + s\tau_1)(1 + s\tau_2)(1 + s\tau_3)}$$

Transforming into the time domain under the assumption that the initial temperatures are equal $T_1(0) = T_2(0) = T_3(0) = T_{in}(0)$, the solution takes on a (relatively) simple form. For the well insulated case;

$$T_2(t) = P_o R_{eff} + T_o + \{ -0.11 P_o R_{eff} - 0.06 [T_o - T_{in}(0)] \} e^{-t/\tau_1} + \{ -0.02 P_o R_{eff} - 0.03 [T_o - T_{in}(0)] \} e^{-t/\tau_2} + \{ -0.86 P_o R_{eff} - 0.91 [T_o - T_{in}(0)] \} e^{-t/\tau_3}$$

After a long time, $t >> \tau_3$, the solution reduces to the steady state temperature.

The time dependent temperature equation can be put in a general form:

$$T_2(t) = P_o R_{eff} + T_o - \sum_j \{ w_{hj} P_o R_{eff} + w_{cj} [T_o - T_{in}(0)] \} e^{-t/\tau_j}$$

where w_{hj} and w_{cj} are the heating and cooling weighting factors for each time constant τ_j.

The calculated weighting factors for the well insulated and uninsulated cases, as well as for the observed values by Socolow and Sonderegger[1] are shown in Table 3. Without specific knowledge of the experimental measurements, comparison is difficult. However, the weighting factors calculated by our simple model for both the heating and cooling cases, bracket the values given by the experiment.

	Heating			Cooling		
	w_{h1}	w_{h2}	w_{h3}	w_{c1}	w_{c2}	w_{c3}
well insulated	0.10	0.02	0.86	0.06	0.03	0.91
uninsulated	0.32	0.16	0.53	0.11	0.28	0.61
observed	0.09	0.14	0.76	0.10	0.20	0.70

Table 3. Heating and cooling weighting factors.

SENSITIVITY ANALYSIS

Sensitivity studies were run to observe the dependence of the time constants and the weighting factors on different parameters. Comparison of different cases where the infiltration and glazing loss rates, degree of insulation, and distribution of thermal mass are varied are shown in Table 4.

	BTU/hr-°F			hours		
	$1/R_1$	$1/R_4$	$1/R_{eff}$	τ_1	τ_2	τ_3
Infiltration	243	279	504	0.057	1.29	7.72
	243	450	675	0.055	1.28	6.03
	243	629	860	0.053	1.27	4.94
Insulation	243	376	601	0.056	1.29	7.41
	750	376	980	0.056	1.15	3.96
	1317	376	1301	0.056	0.99	3.02
	BTU/°F			hours		
	C_1	C_3		τ_1	τ_2	τ_3
Capacitance	3000	500		0.057	0.79	7.41
	2000	1500		0.056	1.43	8.28
	1000	2500		0.052	1.04	10.2

Table 4. Sensitivity studies. Results for several different cases. In all studies the thermal mass of the air, C_2, and the transfer from air to wall, $1/R_2$ and $1/R_3$, were held constant.

Infiltration.

If the value of the infiltration and glazing loss parameter, $1/R_4$, is increased from 279 BTU/hr-^oF for 200 ft^2 of double glazing with 2/3 air change per hour, to 629 for 340 ft^2 of single glazing with one air change per hour, the short time constants, τ_1 and τ_2, change only by a few percent indicating that the internal rearrangement of heat is unaffected. However, the long time constant, τ_3, decreases from 7.72 hrs to 4.9 hrs as expected because of the increased loss from the thermal mass.

Insulation.

As the insulation value of the wall is decreased from heavy to minimal insulation, the short time constant is unchanged. The intermediate time constant decreases by 30 % and the long time constant falls by a factor of two. The weighting factors, shown in Table 3, also indicate that the importance of the intermediate time constant increases with decreasing insulation.

Capacitance.

If the thermal mass within the structure, $C_1 + C_2 + C_3$, is kept constant, but is shifted from the exterior wall to the interior of the space, the short time constant is almost unchanged, the intermediate time constant becomes somewhat larger, and the long time constant goes from 7.4 hrs to 10.18 hours as the thermal mass is moved further from the exterior walls.

CONCLUSIONS

This simplified building load model predicts thermal behavior of typical buildings based on physically definable building parameters. The temperature response of a building to a change in heat input, can be characterized in terms of an effective energy loss term, R_{eff}, three heating weighting factors w_{hj}, and three cooling weighting factors, w_{cj}, and three time constants, τ_j, which are straightforward to evaluate from building parameters and which are experimentally observable. The model gives predictions which agree in general with those observed in an experiment with a real building.

It is hoped that this paper will prompt interest in careful observation and evaluation of short time constants of buildings. These short time dynamics are important in implementing building temperature control strategies.

The wall and air temperatures predicted by this model can serve as forcing functions for a thermostat response model to determine when heating is required. In our analysis we have not included transit delays and heating delivery time constants, although extension of the analysis to include them is straightforward. With a active solar heating system, the rate of heat delivery depends on the storage tank temperature, so that the thermostat cycling time is not a simple function of the indoor-outdoor temperature difference. This three time constant model may also serve to model the control response of passive structures to back-up heating systems.

REFERENCES AND FOOTNOTES

[1] Robert H. Socolow and Robert C. Sonderegger, "The Twin Rivers Program on Energy Conservation in Housing: Four Year Summary Report," Center for Environmental Studies, Report No.32, August 1976, Princeton University. Excerpts in ASHRAE Trans., 83(1), (1977).

[2] Mashuri L. Warren, Steven R. Schiller, and Michael Wahlig, "Experimental test facility for evaluation of controls and control strategies," Second Annual Systems Simulation and Economic Analysis Conference, 23-25 January, 1980, San Diego, CA

[3] M. Majteles, H. Lee, M. Wahlig and M. Warren, "Experimental Test Facility for Evaluation of Solar Control Strategies," Proc. Workshop on Control of Solar Energy Systems for Heating and Cooling. Hyannis, Mass. 23-25 May, 1978. (LBL-8308) Aug. 78.

[4] W. K. Roots, M. Shridhar, R. H. Tull, and J. R. Pfafflin, "Mode-Dependent Time Constants in Three Forms of Space Heating," IEEE Transactions on Industry Applications, Vol. IA-10, No. 6 (Nov/Dec 1974), pp. 699-702

[5] R. C. Sonderegger, "Dynamic Models of House Heating Based on Equivalent Thermal Parameters," Princeton University, Center for Environmental Studies, Report PU/CES 57 (September 1977).

[6] R. O. Zermuehln, H. L. Harrison, "Room Temperature Response to a Sudden Heat Disturbance Input," ASHRAE Transactions, 71, (1965), pp. 206-210.

[7] H. L. Harrison, W. S. Hansen, and R. E. Zelenski, "Development of a Room Transfer Function Model for Use in the Study of Short-term Transient Response," ASHRAE Transactions, 74, (1968), pp.198 206.

[8] K. M. Letherman, "Functional Modeling of Room Temperature Response and Effects of Thermostat Characteristics on Room Temperature Control," in C. J. Hoogendoorn and N.H. Afgan, Energy Conservation in heating, cooling, and ventilating buildings (Washington:Hemisphere Publishing Corp., 1978), pp.393-404

[9] A. V. Sebald, F. Langenbacher, and J. R. Clinton, "On Proper Control of Direct Gain Solar Houses," Proc. 4th National Passive Conference, AS/ISES, 3-5 October 1979,

[10] A. Kaya, "Analytic Techniques for Controller Design," ASHRAE Journal, April 1976, pp. 35-39.

COMPARISON OF SIMULATION AND MEASURED PERFORMANCE OF THE SUNCATCHER HOUSE DESIGN USING SOLSIM AND SOLEST

Bruce T. Maeda Paul W. Grant

Davis Alternative Technology Associates
(D.A.T.A.)
P.O. Box 470
Davis, CA 95616

ABSTRACT

D.A.T.A.'s thermal analysis simulation program has been used to simulate the performance of the Suncatcher® passive solar home design by Living Systems. The simulations of days in December, 1978, and November, 1979, are compared to actual monitored data of the Nittler/Maeda Suncatcher. In addition, long term data for 1978 is compared to a computerized simplified performance estimation procedure more appropriate for design evaluation of passive solar and energy conserving design. This estimation procedure evaluates passive solar heating, natural cooling, and domestic hot water performance. Simulation results appear to be in good general agreement with 2°C(4°F) differences in maximum temperatures.

INTRODUCTION

The purpose of this paper is to compare the monitored performance of the passive solar Nittler/Maeda Suncatcher® House in Davis, California, to computer simulations and performance estimations. D.A.T.A.'s SOLSIM code was used to perform the simulations of the Suncatcher House. A program description is given in another paper being presented at this conference III. During the design process a passive solar performance estimation computer code, SOLEST, was used to predict the natural heating and cooling performance of the design. Using appropriate monthly and annual data the average monthly performance and auxiliary loads of the Suncatcher house were compared to the computer estimates. In addition, the actual performance was compared to Doug Balcomb's solar load ratio estimation procedures using D.A.T.A.'s LASL6 version of this method. These comparisons have been used to validate and update the computer codes.

Solar and Energy Conserving Design of the House

The Suncatcher System. The Nittler/Maeda Suncatcher was designed by Jim Plumb of Living Systems and is located in Davis' Village Homes, a subdivision featuring a variety of active and passive solar home designs. The Suncatcher design is characterized by a reflective overhang and north sloping roof surface. This configuration provides enhanced collector area for reflective solar heat gain through 8.9m^2(96ft^2) of clerestory windows. The roof and overhang surfaces form a cavity that increases winter solar gain, while preventing overheating in the summer (see Figs.1 and 2). Manually operated insulated shutters (R value of 6) inside the house reduce winter heat losses, and also decrease cooling loads by reflecting diffuse solar gain away from their exterior-facing reflective surfaces.
The water Trombe' collector consists of seven galvanized steel culverts 0.6m(2ft) in diameter and 3.0m(10ft) high, located 2.4m(8ft) behind the clerestory windows.

The water-filled tubes, centrally located within the living space, remain at temperatures within the comfort range of 18-26°C (65-78°F)and help moderate temperature in the living, dining, and hallway portions of the residence.

Direct Gain Components. Three south facing bedrooms are heated by direct solar gain through the windows, completely shaded in summer by a grape arbor. Heat storage in the bedrooms is provided by thermal mass in 208l(55gal) water filled drums and the parquet covered slab floor. The locations of these drums is indicated in Fig.3.

Natural Cooling System. To reduce Davis climate severe cooling requirement (over 800 hours annually above 27°C(80°F)] the house uses heavy wall insulation, double glazing and well-shaded, draped windows. Additional cooling needs are met with daytime heat storage in water mass and later heat rejection by cross ventilation through the south windows above the collector/storage tubes and the north side windows. Relatively consistent, cool evening and night breezes from the Carquinez Straits provide the driving force for nighttime ventilation.

Other Energy Efficient Features. Other energy efficient features include natural lighting with a light shelf above a south bedroom closet, an interior clerestory window providing additional light into the living room (on the north side of the house), a ceiling to north wall hot air circulation duct and fan, and a solar "breadbox" hot water heater. The house has fewer than normal appliances, the residents using only a stove, washer, refrigerator, and several small electric appliances. There is no dishwasher,

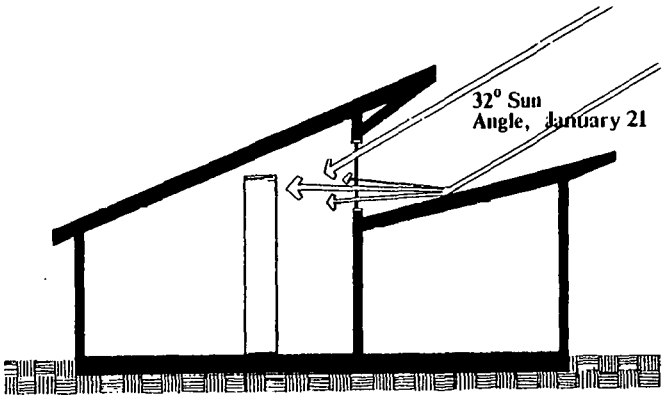

Suncatcher Ray Tracing

Fig.1

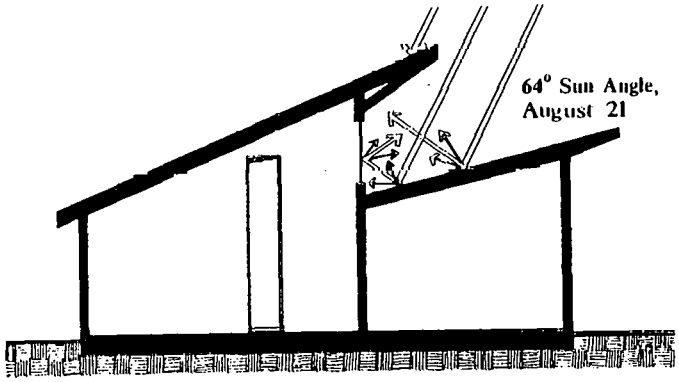

Suncatcher Ray Tracing

Fig.2

clothes dryer (other than solar), garbage disposal or trash compactor. The residents' demand for hot water and electricity is modest.

DATA ACQUISITION SYSTEM AND PROCEDURES

Sensors and Equipment

The Nittler/Maeda Suncatcher has over 130 temperature sensors located throughout the house as shown in Fig.3. Non-shielded type T iron-constantan thermocouples were used because they were installed before the grant award and were available at no cost. Although these thermocouples are not as accurate as we would like, they are adequate for measuring air temperatures. The mass temperatures, especially for the water tubes, are more crucial and may require thermistor installation for monitoring during the grant extension period. The installed sensors terminate at a reference junction with a precision thermistor monitoring the reference temperature. Additional equipment includes maximum/minimum thermometers made by Taylor Instruments and purchased from Weathertronics of West Sacramento, California. These instruments are reset by a simple push button device rather than a magnet.

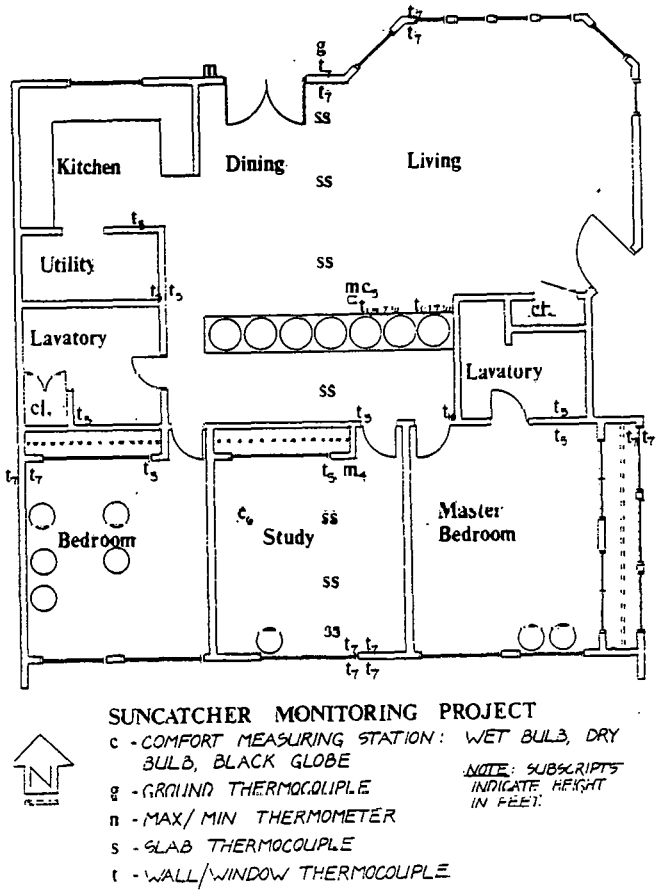

Fig.3

There are two comfort measuring stations also shown in Fig.3, both located near the interior maximum/minimum thermometer in the study and in the living room. These stations monitor wet bulb, dry bulb, and black globe temperatures (the equilibrium temperature within a black enclosure used as an indication of the average temperature at which the walls and roof are radiating). These temperatures will be combined in the final reduced data to standard comfort indices. Wind speed is taken by a Weathermeasure model W121 recording system. Data is taken manually once a day and combined with Davis daily data. A Hersey BTU flow meter is installed in the output taken manually once a week. Solar radiation is measured on a vertical plane directly behind the clerestory windows. The thermopile-type pyranometer is double-dome, Eppley model PSP. Its output is recorded hourly by the data acquisition system. Two additional gas and watt hour meters were provided by Pacific Gas and Electric, the local utility. The gas meters separately monitor the space heater and hot water heater, leaving the stove as residual value. The two additional watt hour meters measure the lighting circuits and the refrigerator energy use.

Hourly Data Acquisition and Data Acquisition System

After a variety of complications, the data acquisition system started gathering data in August, 1978, but despite several debuggings, system problems continued through May 1979; hourly data was gathered only sporatically, but with increasing reliability during this period. The data acquisition system now functions well with only sporadic, routine problems.

Data Acquisition Equipment. A single board microcomputer does all the necessary collecting, storing, and initial processing of the data gathered from temperature sensors within the house. The central processing unit is an IMSAI 8048 computer controller interfaced to multiplexing, analog to digital conversion and amplification circuits for the respective sensor input signals. The 75 channels are first selected by a CMOS analog multiplexer, then amplified with a high performance modular CMOS chopper, and finally converted from analog to digital form using a monolithic successive approximation A/D converter with 8-bit resolution. The computer controls the multiplexing, amplification and conversion, and recieves the 8-bit data words through its I/O PORT. Data is temporarily stored in random access memory (RAM) and later transferred to a paper tape punch. This microcomputer system is well suited to the relatively simple tasks required of it. Pre-processing of data is kept to a minimum since all programming is in maching language. Since interrupt capabilities of the 8048 have been pre-empted by a PROM monitor, the on-board timer is not available for providing the time during the data logging. Real time is provided by an external crystal controlled clock that is interrogated by the computer.

SOLSIM

D.A.T.A. uses the computer program SOLSIM to do hour by hour simulation of nonsolar and passive solar structures. The program can be used to simulate a wide range of structural sizes, from small models to multi-floored buildings of 10,000m^2 or more. However, it was originally designed to evaluate natural heating and cooling performance of solar homes. This program was developed by Bruce T. Maeda. The program uses many algorithms from the National Bureau of Standards Load Program, NBSLD, but has been developed along additional lines to accomodate heat storage effects of mass and radiative and cooperative cooling of mass elements. A more complete program description is given in another paper presented at this conference entitled "Solar 'Breadbox' Simulation using D.A.T.A.'s TBBX Code" [1].

Results

December 7, 1978. Calculated temperatures were compared to results for two separate days, the first comparisons being done for December 7, 1978. Some of the results of this comparison are graphically illustrated in Fig.4. The actual air temperatures fluctuate less than the calculated ones. This indicates that the mass was more effective than assumed in the input file. However, the difference in the time of peak in the air temperature indicates the opposite effect, with calculated air temperatures peaking later than measured temperatures. The measured temperatures of the mass indicate less effective storage than the calculated temperatures. The difference in temperature maximum is about 2.2°C (4°F), but generally the calculated and measured temperatures are within 1°C(2°F) of each other. The calculated and measured water mass storage temperatures differ by 2°C(3.6°F) on the average. Although the temperature error is small, the heat represented by this temperature difference is large. It appears as though infiltration and heat loss increase more than predicted during the day. This could be due to several effects that were not modeled. The most likely candidates to explain the differences include increased daytime heat loss through the high clerestory glazing due to temperature stratification. Increased infiltration in the daytime due to the stack effect also was not modeled by the program. In addition, the solar gain used was not measured, but calculated, by the program, and the actual radiant gain may have been less than that used in the calculations. These results are graphically displayed in Fig.4. This last point is instructive because closer agreement between calculated and measured temperatures is found for November 10, 1979, where measured radiation was available and adjusted accordingly, as shown in Fig.5.

November 10, 1979. In spite of a greater difference in maximum temperatures--2.8°C(5°F), the general agreement of measured and calculated temperatures for November 10, 1979 is much better than for December 7, 1978. The differences in the temperature curves are probably explained by the causes noted above. The mass temperature curves are in much better agreement due to solar radiation input closer to actual values, as indicated by data from the Davis Weather Station and clear sky radiation tables from the ASHRAE Handbook of Fundamentals. Slight adjustments in the input parameters could bring almost exact agreement with the displayed temperatures and several other calculated and measured temperatures. These adjustments could readily be made within the bounds of error of realistic physical characteristics of the weather, structure, and the storage mass elements.

SOLEST

This computer program uses a degree day method to estimate monthly and annual energy use for space heating and cooling. Degree day data is readily available for many localities. Degree-days to base 65°F are well correlated with the amount of natural gas used for space heating.

The algorithm used in the computer program for estimating energy consumption multiplies the monthly normal degree days times the "thermal area" of the residence times twenty-four to yield the monthly heat loss. However, this calculation does not account for the useful heat gain due to solar energy.

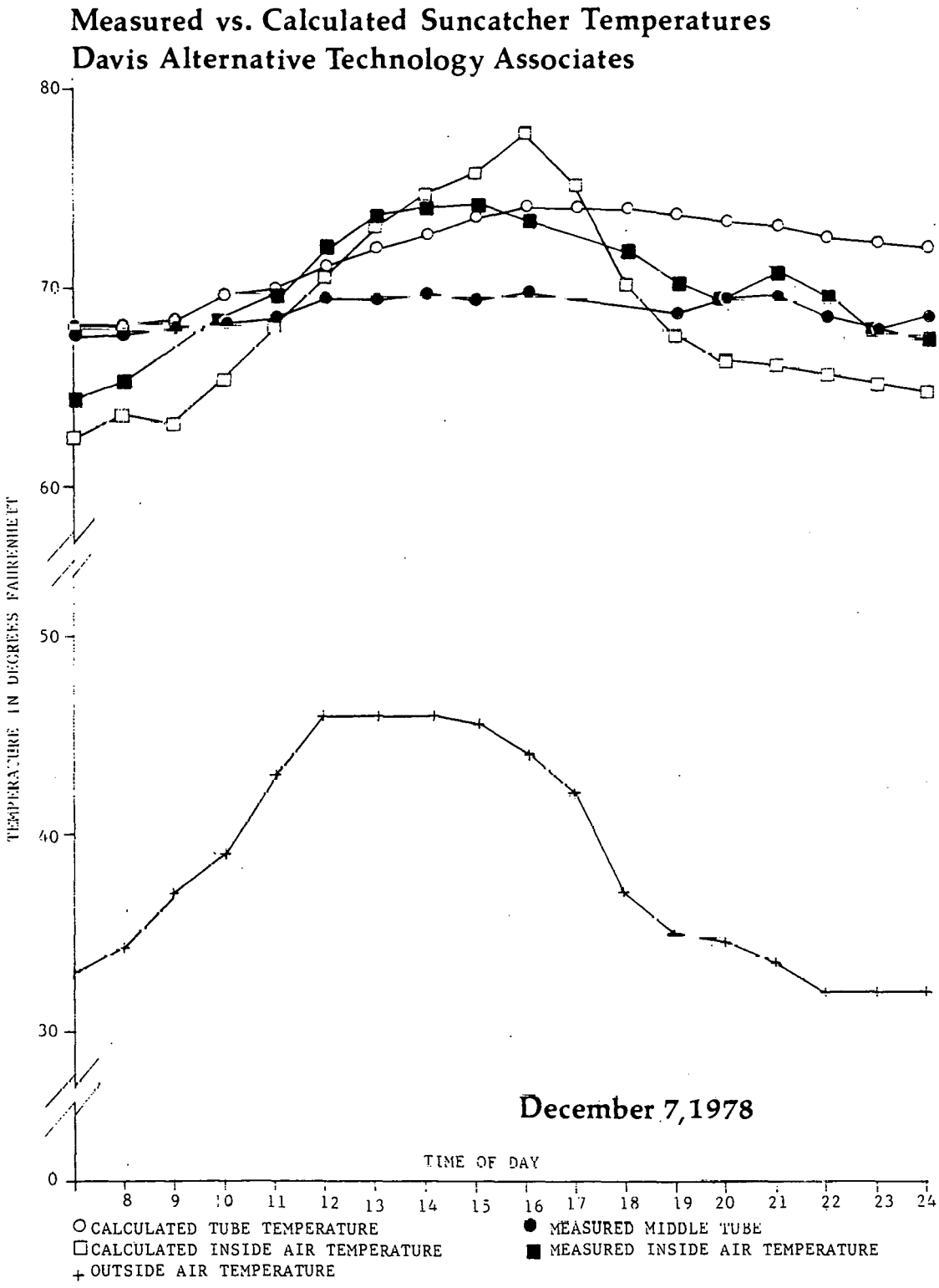
Measured vs. Calculated Suncatcher Temperatures
Davis Alternative Technology Associates
TEMPERATURE IN DEGREES FAHRENHEIT
80
70
60
50
40
30
0
December 7, 1978
TIME OF DAY
8 9 10 11 12 13 14 15 16 17 18 19 20 21 22 23 24
○ CALCULATED TUBE TEMPERATURE
● MEASURED MIDDLE TUBE
□ CALCULATED INSIDE AIR TEMPERATURE
■ MEASURED INSIDE AIR TEMPERATURE
+ OUTSIDE AIR TEMPERATURE

Fig.4

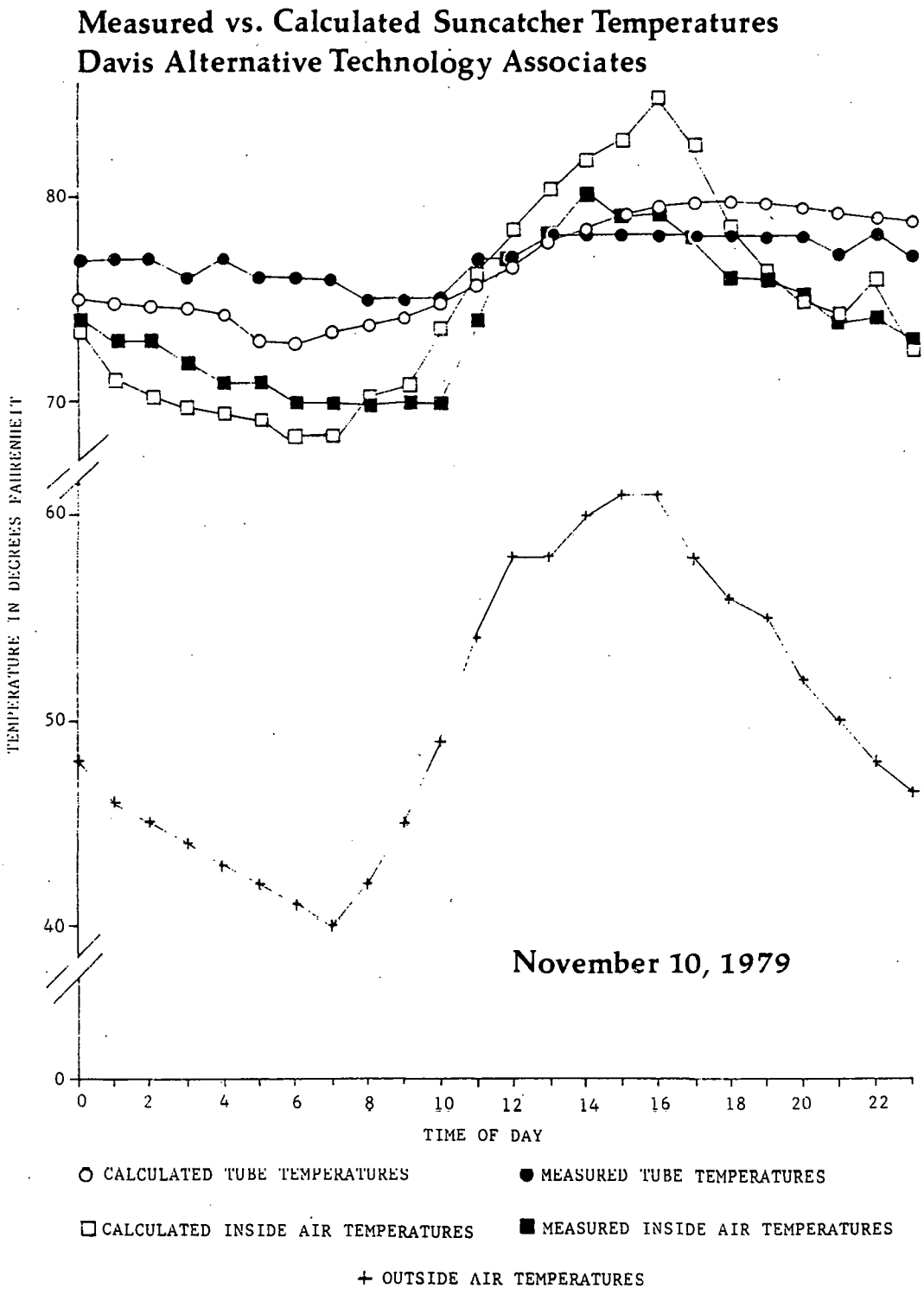
Measured vs. Calculated Suncatcher Temperatures
Davis Alternative Technology Associates
TEMPERATURE IN DEGREES FAHRENHEIT
80
70
60
50
40
0
0
2
4
6
8
10
12
14
16
18
20
22
TIME OF DAY
November 10, 1979
O CALCULATED TUBE TEMPERATURES
● MEASURED TUBE TEMPERATURES
□ CALCULATED INSIDE AIR TEMPERATURES
■ MEASURED INSIDE AIR TEMPERATURES
+ OUTSIDE AIR TEMPERATURES

Fig.5

Since all solar energy incident on glass is not usable for heating, the program calculates only the appropriate portion of average solar gain transmitted through south or nearly south glazing by first determining the "justified solar glass". Solar glass is vertical glass that faces within 90 degrees of south, or tilted glass within 50 degrees of south. Solar glass may be considered "justified solar glass" under two conditions.

1. Some of the heat from solar glass is needed to balance heat loss even on sunny days in the winter (usually cold and clear). This solar glass may be "justified" by the daytime heat loss of the structure.
2. Any additional heat from solar glass to be useful must be stored for later use in "thermal mass" in order to be "justified".

Thus solar glass may be "heat loss justified" or "thermal mass justified".

Some types of thermal mass may "justify" more glass than others. The program distinguished the following general thermal mass types:

1. Sunlit water mass in containers
2. Shaded water mass in containers
3. Trombe walls (sunlit concrete walls 30cm(12") thick with sunlit side dark colored)
4. Shaded concrete wall
5. Sunlit concrete slab, covered by hard-surfaced floor
6. Shaded concrete slab, covered by hard-surfaced floor
7. Concrete slab, rug-covered or insulatively covered

Slab thickness is assumed to be at least 10cm(4"). Greater thicknesses are assumed to be beneficial in the short run (daily) only if both sides of the slab are available for heat exchange.

After the total amount of justifiable solar glass is determined, the minimum of the justifiable solar glass and actual solar glass is taken to be the "justified solar glass". The average insolation of vertical south glazing is used to determine the heat gain through the justified solar glass.

Other glazing orientations are weighted differently in calculating solar glass. The winter heat gain due to non-solar glass is ignored to allow a margin for error on the conservative side. The winter heat gain through the justifiable solar glass is deducted from the heat loss of the structure.

The method for estimating space cooling load is somewhat different. The heat gain calculation assumes a 90 degree outside temperature. It includes heat gain from "unshaded afternoon glass", which is west-facing glazing, skylights, a portion of the unshaded south glass and, "equivalent unshaded glass". which is the sum of all glazing areas times their respective mean daily summer shading coefficients, element by element.

This gain is reduced by the "peak cooling potential" of the thermal mass heat storage of the structure. The "peak cooling potential" is based on assumed temperature differentials between the various storage types and the design temperature of the air inside the house, usually 26°C(78°F). The surface area of the exposed thermal mass is used to calculate the "peak cooling potential". The assumed temperature differentials are based on empirical data derived primarily from the climate of California's Central Valley. The cooling credit is modified by other factors as well. One factor accounts for the estimated minimum temperature on a summer's day whose peak temperature reaches the summer design hour peak. Another is the ratio of heating degree to cooling degree days in the month under consideration. The exact weight of these factors is not known, but in practice the general trend and order of magnitude is realistic and probably within the limits of error of the other calculations. These formulations are used:

$PKCR_o$ = peak cooling credit due to cooled mass

$$PKCR_1 = PKCR_o * \left[\frac{\text{80 F-expected summer min. daily temp.}}{\text{20 F}}\right]$$

$$PKCR_2 = PKCR_1 * \left[1 + \frac{\text{monthly heating degree days}}{\text{monthly cooling degree days}}\right]$$

These factors are rationally based, but not experimentally demonstrated. To ignore them because they are not experimentally demonstrated would be to assume their effect to be zero, an assumption which would certainly result in a greater error than the one induced by the errors present in our assumptions.

The heating load annualization methodology resembles short calculation annualization used by public utilities and by solar researchers, and is based on degree days and "thermal areas". The solar contribution aspect of this calculation methodology has been ignored in traditional usage. Our methodology uses average monthly radiation incident on south-facing glazing to determine the solar contributions to heating. It would be better to use solar radiation deviation measures rather than averages, but this data is either unavailable or at least very difficult and expensive to obtain. To allow for the error introduced by the use of averages, the program reduces the collected solar energy by 10%. The cooling annualization is based on the number of annual dry bulb hours greater than 27°C(80°F) or the number of annual wet bulb hours greater than 23°C(73°F). This measure has proven to be a reliable estimate of the relative cooling needs based on climate [2]. Residential structure solar radiation loads will, however, vary the energy budget more than the climatic factor. Thus, the program calculates a "full load" cooling hour using both outside temperature and radiation factors, then annualizes this "full load" hour by using dry bulb hours over 27°C(80°F) or wet bulb hours over 23°C (73°F).

LASL6

The Suncatcher house performance was also compared to another estimation procedure using the computer program LASL6. LASL6 is D.A.T.A.'s interactive microcomputer based version of Balcomb's and McFarland's Solar Load Ratio method for estimating the performance of passive solar houses. The details of this method were presented at the 2nd National Passive Solar Conference[3].

Results

Predicted Vs. Actual Auxiliary Energy Usage
(in Therms)

	Predicted (70% furnace efficiency)		Actual
	SOLEST	LASL6	
JAN	33.9	35.1	46
FEB	50.4	37.5	33
MAR	6.1	8.7	7
APR	14.1	14.3	0.8
Subtotal	105.3	95.6	86.8
NOV	4.0	16.8	11.7
DEC	38.1	50.7	30.5
Subtotal	44.1	67.5	42.2
TOTAL	147.4	163.1	137.6

Conclusions

SOLSIM can be used to effectively model the Nittler/Maeda Suncatcher house and probably other nonsolar and water or masonary Trombe wall houses in non-humid climates; however, the large number of input parameters characteristic of this and other larger simulation programs can probably be used to mock up performance without true simulations of the actual heat transfers occuring. This can be done while maintaining the physical characteristics of the structure and mass within realistic bounds. Validations must measure more parameters than the input parameters of the program, or at least have strict constraints on the magnitude of physical characteristics that are, or relate to, the program inputs. Without these constraints and measurements, it would be much more appropriate to use simpler models that approximate the complexity of the measured validation data. Indeed, simpler models may be quite adequate to provide insights into the behavior of passive systems. Complex programs are probably most useful to extend the state of the art of passive solar design by modeling untried or unproven systems, because to do this they must be able to model difficult and complex structures whose heat transfer mechanisms must be adequately represented and could defy many simplifying assumptions.

Both SOLEST and LASL6 underestimate actual performance; however, in both cases night setback of temperatures are not accounted for by the programs. It is difficult to assess the effect of this on either program. SOLEST overestimates auxiliary energy use by 7.1%; LASL6 by 18.5%. It would appear that SOLEST is more accurate, but because of effects that cannot be readily evaluated, no firm conclusions can be made. In either case both are reasonably close to the inherent error in such calculations due to the problems with estimating the infiltration load (±15-20%). Also in both cases, it appears that the programs can readily evaluate passive designs without the complexity of full year simulation.

ACKNOWLEDGEMENTS

The authors wish to express their thanks to the people who helped in making this publication possible. The basic research, monitoring of the Nittler/Maeda Suncatcher house, and some of the computer program was supported by the United States Department of Energy, Solar Heating and Cooling Branch of the Office of Conservation and Solar Application under grant #EG-77-G-04-4154 and its extension grant# DE-FG04-79CS30169. Bruce Melzer helped to edit the drafts. Martha Townsend was invaluable in typing and layout. Libby Hueter also helped to layout and prepare the final draft for publication. Marcia Cary and Patricia Karapinar rapidly and efficiently produced the graphics. The authors assume full responsibility for any errors, including incomprehensible writing.

REFERENCES

1. B.Maeda and B.Melzer,"Solar 'Breadbox' Simuations Using D.A.T.A.'s TBBX Code"; presented at the Second Annual Systems Simulation and Economics Conference, San Diego, CA Jan 23-25 1980

2. NAHB and NAHB Research Foundation, Designing, Building and Selling Energy Conserving Houses; National Association of Home Builders, Washington, DC 1977

3. J.D.Balcomb and R.D.McFarland,"A Simple Empirical Method for Estimating the Performance of A Passive Solar Heated Building of the Storage Wall Type", Proceedings of the Second National Passive Solar Conference, Vol.2; Mid-Atlantic Solar Energy Association, Philadelphia, PA 1978

NOTES

SIMULATION OF PASSIVE/HYBRID SOLAR HOMES WITH A USER-ACCESSIBLE COMPUTER-BASED DESIGN TOOL

Davis Straub
Ecotope Group
2332 E. Madison
Seattle, WA 98112
(206) 322-3753

Morry Browne
Otto Smith
System Development Group
PO Box 337
Northgate Station
Seattle, WA 98125
(206) 932-5786

ABSTRACT:

Theoretical work regarding heat transfer processes in rockbin heat storage systems has progressed in the last few years. Computer algorithms have been developed which efficiently solve the rockbin energy balance equations. Two of the most efficient and flexible theoretical formulations, one from the TRNSYS model and one designed for DOE by the Boeing Computer Services Company to be used as a component in an active systems model, have been incorporated into a designer-oriented computer model developed to simulate passive solar houses (SUNCAT). Appropriate controller logic and space conditioning algorithms have been added to SUNCAT (now Ecotope Passive/Hybrid Solar Model) to allow it to model numerous types of passive/hybrid house combinations.

The incorporation of these rockbin models into SUNCAT allows the designer to specify and size rockbins, determine the effect of different thermal connections between the rockbin and other spaces, and to see the effect of design changes on hybrid house performance over any selected time period. As an example, the yearly performance of a hybrid house is determined for three climates, Seattle, WA, Madison, WI, and Albuquerque, NM.

INTRODUCTION:

Little analytical work has been done on hybrid houses, such as houses with attached greenhouses and active rockbins (1,2), although some authors have estimated their performance (3,4). Studies of active solar hot air systems have occasioned the theoretical work on rockbin storage (5-8). While the general formulation of the theoretical problem of heat transfer within rockbins has been understood since the thirties (9), numerical techniques have only recently been applied that efficiently utilize computer resources.

ROCKBIN MODELS:

The general formulation of the rockbin model consists of two energy balance equations , one for the air and one for the rocks. (These equations arise from the assumption that energy is conserved.) They are coupled by a shared term for heat transfer between the rocks and air. These two equations when combined with some restrictive boundary conditions constitute the Schumann model (9) for which an analytical solution exists that is used to test numerical solutions.

The two energy balance equations are as follows: (See Glossary)

$$Pa*Ca*dTa/dt + (\dot{m}*Ca/A)*dTa/dx = hv*(Tr-Ta) \quad (1)$$

$$Pr*Cr*(1-e)*dTr/dt = hv*(Ta-Tr) \quad (2)$$

These equations are based on the following assumptions:

1. The principal resistance to heat flow into any one rock is from the air to the rock surface, thus the interior temperature of each rock is essentially the same as its surface temperature.

2. The air is in plug flow, thus there is no variation in air temperature or flow rates in the radial direction. This also implies uniform rock temperatures in the radial direction. Therefore a one-dimensional model suffices.

3. The conductivity between rock particles is negigible, especially in the axial direction.

4. Axial conduction or dispersion (i.e. eddy diffusion and convection) does not occur in the air phase.

5. The physical properties of the .rockbin and air are constant.

6. No mass transfer occurs.

7. No heat losses to the environment occur (4).

The solutions that we present to Equations 1 and 2 will allow for relaxation of four of these assumptions.

Two major practical problems exist in solving these equations. The first is that the air and the rocks have very different thermal capacities and therefore different time constants. A straight-forward finite difference solution of this set of equations would require many small time steps and consequently high computation costs, for numerical stabilty and convergence.The second problem is the determination of the heat transfer rate between rocks and air. It is dependent on the speed of the air around the rocks. This air speed can be related through the use of physical and empirical constants to the nominal air speed and particle shape, size and spacing (5). There is no general agreement on the determination of this heat transfer rate, hv.

Our goal is to determine the performance of a hybrid house over periods from a day to a year. We will not be interested in modeling phenomena within the rockbin that will not appreciably effect the accuracy of our solutions over those time periods. The heat capacity of air is much smaller than the heat capacity of rocks, and the first term of equation 1 may be discarded with small effect on our solution.

SOLUTIONS:

Rocks:

The first general formulation of the solution to these two equations assumes that the ratio of the heat transfer rate (between the rocks and the air) to thermal mass flow rate (net heat transfer units or NTU) is infinite. Equatuons 1 and 2 are combined and la=1r. With one stroke. the two major problems faced by a solution of the equation are accomodated, although at a cost in accuracy and ability to specify the rockbin parameters.

This formulation is presented in Hughes, et. al. (5) and forms the basis for the rockbin module in the TRNSYS model. The major justification for this approach is that for most practical rockbins under most practical air velocities experienced in solar hot air systems, NTU is large and as NTU increases the modeled performance of solar hot air systems approaches quite quickly that modeled assuming an infinite NTU (5). As the determination of NTU is itself somewhat problematic and as in some of the cases that we have investigated NTU is not large, i.e. less then 10, the assumption that NTU is large for most practical systems may not not always be justifiable. (See Figure 2, NTU's are somewhat greater then NTUC's)

With NTU infinite our two energy balance equations become:

$$dTr/dt = [-\dot{m}*Ca/(A*Pr*Cr*(1-e))]*dTr/dx \quad (3)$$

We have incorporated the TRNSYS module in our ROCKS subroutine and solved it with the forward finite difference technique.(10) The stability criteria for the rockbin does not require as small a time increment as is necessary for the explicit solution of the heat transfer equations for the house walls in SUNCAT (10).

Bcsrocks:

The second solution incorporated into our subroutine BCSROCKS is a generalization and expansion of that found in Hughes (10) and Marvin and Numma (6) from the work by a team at the Boeing Computer Services Company (7,8). Assumptions one, three, four, and seven are relaxed (seven is also relaxed in ROCKS and four could be). A pseudo-axial conduction that approximates the gradual loss of temperature stratification during periods of no air flow and a pseudo-heat transfer parameter (NTUC) to approximate axial dispersion in the air and conduction between rocks are developed. While these considerations can produce a more realistic model, NTUC must be determined and the solution is still limited in is accuracy by the determination of the heat transfer between rocks and air, hv. The Boeing team chooses Jury, et.al.'s (12) formulation of hv as the most convincing.

We have written a hand calculator program that can be used to determine NTUC from the correlation used in the BCS study. Figure 1 gives NTUC for a range of values of the ratio of air flow rate (cu.ft./min) to cross-sectional area of rockbin (sq.ft.) compared to length of rockbin (ft.) for 2" round rocks, at 80 degrees F air temperature, and a void fraction of .3.

The problem of convergence and stability are dealt with by first assuming that the rock temperature is fixed over a chosen time increment as a linear function of distance over each rock nodal point within the rockbin. The air temperatures are then determined analytically. A corrector-predictor routine (modified Euler's) is used in the time variable to determine rock temperatures for the next period. The stability criteria for BCSROCKS are more restrictive than those of our ROCKS

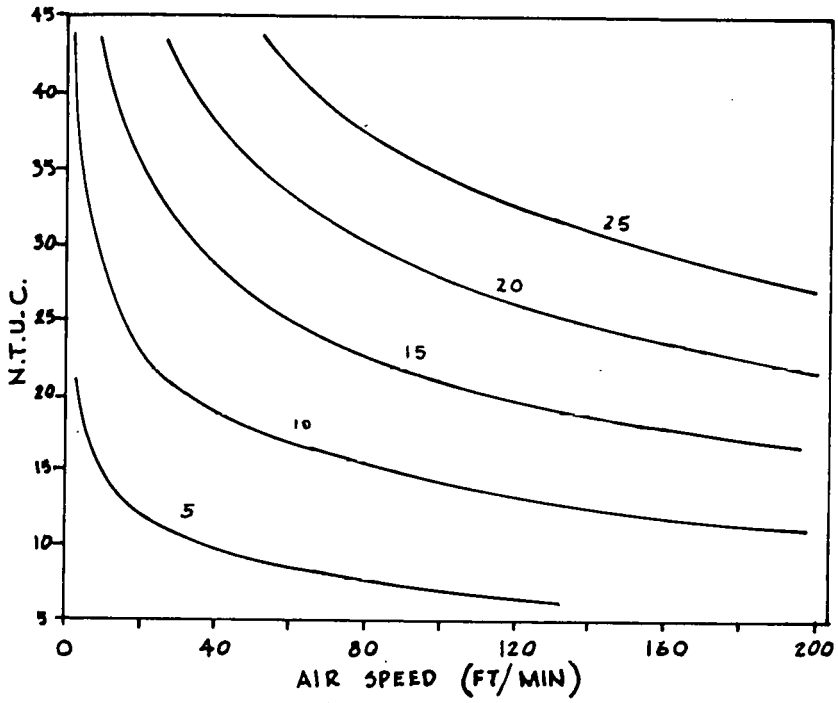

FIGURE 1

formulation, but still less restrictive than those required by the walls modelled in SUNCAT.

In Figure 2, these two models as incorporated in SUNCAT are tested for convergence to the analytical solution of the Schumann model. The boundary and initial conditions are the same as presented in Marvin and Mumma, except that fifteen nodes are used for BCSROCKS as per von Fuchs (13), five nodes are used for ROCKS as per Hughes (5). These choices are presently a matter of judgement, with the number of nodes required decreasing as NTUC decreases.

THE ECOTOPE PASSIVE/HYBRID SOLAR MODEL:

With BCSROCKS and ROCKS now incorporated into our model we are able to simulate hybrid houses. System control logic for determining and changing the state of the system has been added to SUNCAT. This allows the rockbin to heat and cool two different zones for any set temperature range, to interact with a furnace or cooler of fixed heat delivery rate and hysteresis, to interact with a convective or forced flow between the two zones, to be turned off when a lower set point is reached in the rockbin and, finally, to be bi-directional heating or cooling.

The important feature of BCSROCKS is that it unlike ROCKS allows a closer look at the effect on hybrid house performance of changes in the rockbin length, cross-sectional area, rock size, and rock shape, but requires a determination of NTUC and some added judgement on the choice of the number of nodes.

BCSROCKS predicts auxiliary heating energy use at 35.6 mBTU's/year, for the Seattle case as in Table 1. This represents a cost in prediction accuracy compared to ROCKS of $75/yearly heating bill at $10/mBTU. The additional nodes in BCSROCKS (total of ten in this case) require additional computing effort, i.e. reduced efficiency, but because the time increment need not be decreased beyond that necessary for the walls this increase is from 53.36 CPU seconds to 74.54 CPU seconds raising the price of a year run for the Seattle case in Table 1 from $6.04 to $8.48.

In Table 1, three houses are compared on the basis of their yearly heating energy use in millions of BTU's per year and their respective solar fractions. (See Appendix B for a definition of the two solar fractions used.) The first two houses have attached south-facing greenhouses, the first house utilizes a rockbin (ROCKS) for heat storage and the second uses a massive wall on the north side of the greenhouse directly in contact with the living area. Both houses show considerable energy savings over the reference house in all

climates.

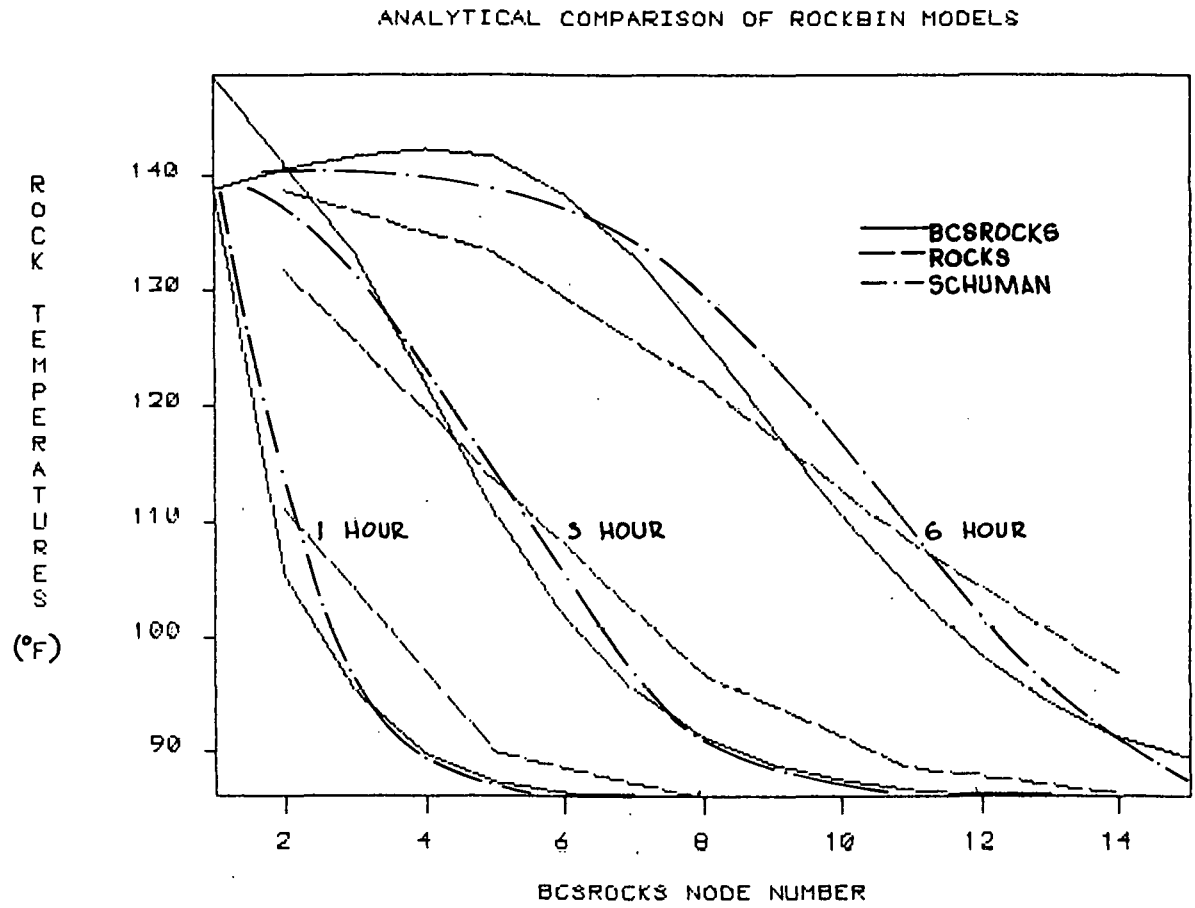

FIGURE 2

	SEATTLE		MADISON		ALBUQUERQUE	
	mBTU	sf	mBTU	sf	mBTU	sf
LWAGH	33	.32/.07	49	.28/.19	11	.67/.66
TWAGH	38	.21/-.08	56	.18/.07	14	.60/.58
REF	48	-.27	68	-.06	34	.04

LWAGH = Lightweight attached greenhouse with rockbin
TWAGH = Attached greenhouse with Trombe wall
REF = Reference non solar house (See Appendix A)
mBTU = yearly heating energy use
sf = solar fraction with respect to reference house and to no loss wall in place of solar greenhouse (14)

TABLE 1

HORIZONTAL ROCKBINS:

The major assumption that was not relaxed was that of plug flow. In addition, the equations assume that the hot air enters the rockbin from the top. This assumption allows us to forget the effects of convective flow along the axis because the hotter rocks are assumed to be at the top and convective flow is therefore minimal.

In a horizontal rockbin that is fed from the side, two effects may occur that will lessen the validity of our assumption of plug flow. The rocks may settle and provide less resistance to air flow at the top and the rocks may stratify in the plane perpendicular to the flow, especially if they are beneath a floor that is conducting heat into an adjoining space. Convective flow can follow from this stratification. Nonetheless, these situations may be adequately modeled by a one-dimensional model if the inaccuracy is of an acceptable magnitude, as in the case of the thermal capacity of the air.

Plug flow has been difficult to achieve in practice, and many rockbins used in experimental work have had severe air leaks (7,8,10). The experimental work carried on by the University of Wisconsin for BCS showed large variations in temperature across the planes within the rockbin. Channeling was apparently occuring and measures were taken to increase uniformity of flow (8). A pressure drop of 40 to 60 pascals appears to be necessary to limit channeling (8,13,15).

FURTHER WORK:

Further experimental and modeling work needs to take place to determine if the plug flow assumption is accurate enough for horizontal rockbins. Although the passive loads portion of the model has been validated against test cell data at the National Center for Appropriate Technology and the rockbin model has been validated at the University of Wisconsin, the two models together with their accompanying systems and contoller logic have not been validated and the system as a whole would benefit from a test cell type validation. In addition, a model such as we have developed here should be used to determine the performance of various types of hybrid houses with different rockbin configurations under different climate conditions, so that current design rules of thumb can be verified or updated.

CONCLUSION:

The Ecotope Passive/Hybrid Solar Model has been developed as a tool for designers to access hybrid houses. We have found that both rockbin modules can be used effectively in our model. The ROCKS module is useful when the details of rockbin design are not paramount and BCSROCKS allows greater flexibility in determining rockbin parameters with increased accuracy and reasonable costs.

ACKNOWLEDGMENTS:

George von Fuchs at Boeing Computer Services, Buck Rogers, Scott Morris, Dr. S.A. Mumma,Dr. Peterson at LASL, James Hill at NBS and Dale Lewis of Ecotope Group have all been instrumental in providing assistance to the authors.

GLOSSARY:

A	= cross sectional area of the rockbin
Ca	= heat capacity of the air
Cr	= heat capacity of rocks
e	= void fraction or space between rocks
hv	= volumetric heat transfer coefficient between rocks and air
L	= length of the rockbin
$\dot{m}$	= mass flow rate of air through rockbin
NTU	= hv*A*L/m*Ca
NTUC	= 1/[(Dp/L)*Pe + (1+Bi/5)/NTU] (variables given in 8)
Pa	= density of air
Pr	= density of rocks
Ta	= temperature of air in the rockbin
Tr	= temperature of the rocks
t	= time
x	= distance in the rockbin

REFERENCES:

1. Kohler, J.T., Sullivan, P.W., Michal, Charles J., "Simulation of Direct Gain Buildings with Active Rockbeds on a TI-59 Programmable Calculator Using TEANET," Proceedings of the 3rd National Passive Solar Conference, Volume 3,p. 424, (1979).

2. Balcomb, J.D., "Designing Fan-Forced Rock Beds," Solar Age, p. 44, (1979).

3. Niles, P.W.P. and Haggard, K.L., Passive Solar Handbook of California, Final Review Draft, (1979).

4. Mazria, E., The Passive Solar Energy Book, Rodale Press, Emmaus, Pa., (1979).

5. Hughes, P.J., Klein, S.A., Close, D.J., "Packed Bed Thermal Storage Models for Solar Air Heating and Cooling Systems," Transactions of the ASME, Journal of Heat Transfer, (1976).

6. Mumma, S.A., Marvin, W.C., "A Method of Simulating the Performance of a Pebble Bed Thermal Energy Storage and Recovery System," ASME-76-HT-73, (1976).

7. Kuhn, J.K., et.al., "Developing and Upgrading of Solar System Thermal Energy Storage Simulation Models," Technical Progress Report, For Period March 1, 1978 - August 31, 1978, Boeing Computer Services Company, (1979).

8. Kuhn, J.K., von Fuchs, G.F., and Zob, A.P., "Developing and Upgrading of Solar System Thermal Energy Storage Simulation Models," Technical Progress Report, For Period September 1, 1978 - February 28, 1979, Boeing Computer Services Company, (1979).

9. Schumann, T.E.W., "Heat Transfer: A Liquid Flowing Through a Porous Prism", Journal of the Franklin Institute, Volume 208, p. 405, (1929)

10. Chapman, A.J., Heat Transfer, The Macmillan Company, New York, (1967).

11. Hughes, P.J., The Design and Predicted Performance of the Arlington House, M.S. Thesis, Mech. Engr. Dept., University of Wisconsin, (1975).

12. Jury, S.H., and Berbano, M.C., "Heat Transfer in Packed Bed Heat Recuperators - II. The film coefficients for dry sorbent solids." Journal of the Franklin Institute, Volume 303, No. 4, pp. 329-343, (1977).

13. personal communication, George von Fuchs

14. Palmiter, L., and Hamilton, B., "A Comparison of Performance Factors for Passive Solar Heating," Proceedings of the 3rd National Passive Solar Conference, Volume 3, (1979).

13. Electrohome Ltd., Giffels Associates Ltd., Waterloo Research Institute, Solar Energy Program, A Heat Storage Subsystem for Solar Energy: Final Report - Phase 2, SolaSTOR - 6, (1979)

APPENDIX A:

The prototype houses are as follows:

living area = 2000 sq.ft.
length to width ratio = .75
1 storey
attic = R/38
walls = R/19
floor = R/19
infiltration = 1/2 air change/ hr.
windows = 150 sq.ft. non south
double glazed
set points = 67F, 80F
set back = 12F, on at 10PM off at 6PM
furnace rate = 25,000 BTU/hour

The reference house has:

R/19 south wall with 50 sq.ft. double glazed window

The two solar houses have attached greenhouses with 400 sq.ft. of south-facing vertical single glazing. South glass to load ratio of .83 sq.ft./BTU/DD.

The house with the Trombe wall has a 400 sq.ft., eight inches thick concrete wall with sixteen sq.ft. of vents, and a wall heat capacity to south glass ratio of 16 BTU/F/sq.ft.

The house with the rockbin has a 400 cu.ft. rockbin (cross-sectional area = 40 sq.ft. and length 10 ft. and a NTUC = 23.4) for a rockbin heat capacity to south glass ratio of 21 BTU/F/sq.ft., a lightweight north wall with sixteen square feet of vents and a fan rate of 800 cu.ft./min. Losses from the rockbin to the living space are assumed to be zero.

APPENDIX B:

The solar fractions as given in Table 1 are based on two different reference houses. The first solar fraction is based on the reference house described in Appendix A and assumes that a wall insulated to the standards of the rest of the house with a window area equal to the average of the other walls replaces the solar greenhouse. The second solar fraction assumes that the solar greenhouse is replaced with a wall that has no heat loss, i.e. perfectly insulated. The SUNCAT model does not take into account the effects of solar radiation striking the outside of opaque walls. It is interesting to note that in Albuquerque these solar fractions are very similar, while in other locations they are not. More discussion of the question of solar fraction is available in reference 14.

Session VIIA

Dr. Robert Busch
Bickle/CM Corporation
Chairperson

CLIMATE ANALYSIS

A COMPARATIVE STUDY OF THE TRY AND TMY METEOROLOGICAL DATA

John Anderson and Doug Madison
Solar Energy Research Institute
Golden, Colorado

ABSTRACT

This study compares the data for 20 sites common to the Test Reference Year (TRY) and Typical Meteorological Year (TMY) data sets. The TRY and TMY data was compared in terms of eight statistics that are important in determining heating and cooling loads in buildings and solar systems performance. The eight statistics include average dry-bulb and dew-point temperatures, heating and cooling degree-days, humidity ratio, and average insolation values. For most locations the average dry-bulb temperatures agreed fairly well. The heating and cooling degree-day values also were close, with standard deviations less than 10% of typical values. However, the statistics relating to ambient humidity did not agree, and the insolation values generated from the TRY data (with the ASHRAE/DOE-2 algorithm) were quite different from the TMY values. Overall, the TRY and TMY data sets are not interchangeable over a wide range of simulation problems.

INTRODUCTION

An initial stumbling block in solar system and building performance design has been the lack of widely accepted "representative" weather data. At present, two major sets of typical data dominate: the TRY, established by a technical committee of the American Society of Heating, Refrigerating, and Air-Conditioning Engineers (ASHRAE); and the TMY, which was chosen by Sandia Laboratories under contract to the Department of Energy (DOE).

To understand the differences between the TRY and TMY data sets, one must understand how each of the data sets was chosen. The TRYs were chosen on the basis of dry-bulb temperature alone [1]. Years that contained temperature extremes were eliminated from the collection of years for which data were available. Thus, the first year eliminated was that which contained the hottest July; the second year eliminated was that containing the coldest January, etc. After all but one of the available years of data had been eliminated, the remaining year was designated the Test Reference Year.

By contrast, the data for TMYs were chosen on a monthly basis [2]. Thus, a TMY is normally composed of one month from each of 12 different years. The pool of available data was narrowed to five candidate months based on a statistic that included the weighted effects of dry-bulb temperature, dew-point temperature, wind velocity, and insolation. Table 1 shows the weighting factors used. The single most typical month was chosen from among the five candidate months on the basis of the day-to-day "persistence" of the dry-bulb temperature and global radiation. The procedure that was used to select the TMY data thus gives primary consideration to insolation values and much less consideration to other factors such as dry-bulb temperature.

Table 1. Weighting Factors Used in Selecting Candidate Months for TMYs[a]

Dry Bulb			Dew Point		
Min	Mean	Max	Min	Mean	Max
1/24	2/24	1/24	1/24	2/24	1/24
Wind Velocity			Solar Radiation		
Max	Mean				
2/24	2/24			12/24	

[a]From Ref. [2].

Of course, the user's main concern with these procedures is whether they produce a data set that is representative of the long-term data for a given location. This issue has been addressed by studying each of these data sets individually. Arens et al. [5] compared the number of heating and cooling degree-days calculated from the TRY data to those calculated from the long-term data. His results showed that although the TRY data contained slightly cooler temperatures than the long-term data, the agreement was good. Freeman [6] made an exhaustive examination of the representativeness of the TMY data in terms of both the building loads and predicted solar system performance. He discovered some discrepancies in the solar system performance predicted for months with low loads, and he doubted the typicality of the diffuse radiation. However, he concluded that the agreement between the TMY and the long-term data was adequate for most simulation work, especially when the desired results were seasonal or annual values.

In this study, the TMY and the TRY data are compared for agreement in terms of eight meteorological statistics chosen on the basis of their importance in determining both building loads and active and passive solar system performance. The statistics used are:

1. Average dry-bulb temperature
2. Heating degree-days, base temp. = 65° F (18.3° C)

3. Cooling degree-days, base temp. = 65° F (18.3° C)
4. Average dew-point temperature
5. Total hourly differences between the ambient humidity ratio and the humidity ratio at 77° F and 50% relative humidity (Δw)
6. Average daily direct radiation on a horizontal surface
7. Average daily diffuse radiation on a horizontal surface
8. Average daily global radiation on a horizontal surface

These statistics were compared on both a monthly and an annual basis for 20 sites common to TRY and TMY data. These sites are shown in Fig. 1. Since both of these data sets claim to reflect the long-term meteorological trends in at least some respects, this study examines how well they agree with each other. That is, to what degree are they interchangeable?

Fig. 1. Locations of the 20 sites Common to the TRY and TMY Data Sets.

RESULTS

Dry-Bulb Temperature

Although the TMY selection procedure weighted dry-bulb temperature rather weakly, the agreement between the two data sets in this area was reasonable. The standard deviation of the differences in the monthly averages was 1.3° C, while the standard deviation of the differences between the annual values was only 0.6° C. Figure 2 shows a scatter plot of annual averages from the TRY plotted against those from the TMY. Each point on the plot represents one of the 20 locations shown in Fig. 1. The worst agreement was found for Washington, D.C., which had a monthly standard deviation of 2.09° C.

Heating and Cooling Degree-Days

The number of heating or cooling degree-days for a given period is a function of both the average dry-bulb temperature for that period and the spread of the hourly temperatures around that average. The number of degree-days provides a single measure of the overall congruence of the

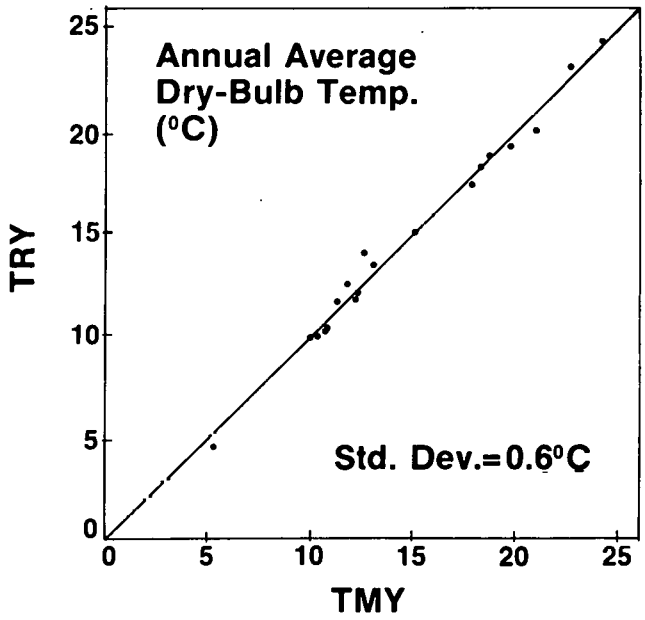

Fig. 2. TRY vs. TMY: Annual Average Dry-Bulb Temperatures (° C).

two sets of temperature data. In this study, both heating and cooling degree-days were based on a temperature of 65° F (18.3° C).

Figure 3 shows the annual heating degree-day values from the TRY data plotted against those from the TMY data. The standard deviation of the differences between the annual values was 142 degree-days, while the standard deviation for the monthly values was 40 degree-days. For a location with about 3000 heating degree-days annually or

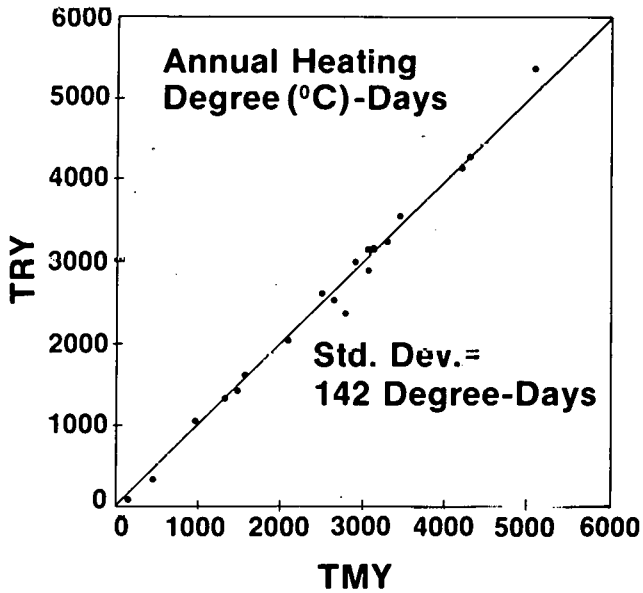

Fig. 3. TRY vs. TMY: Annual Total Heating Degree(C)-Days.

500 degree-days monthly (such as Columbia, Mo.), these values represent about 5% and 8% of the totals, respectively. TMY and TRY data agreed the least for Washington, D.C., where the TMY data predicted 16% more annual heating degree-days than the TRY data. Overall, the cooling degree-day data did not agree quite as well as the heating degree-day data. Figure 4 shows a scatter plot of annual cooling degree-days from the TRY data versus those from the TMY data. The standard deviation of the differences in the annual cooling degree-days was 80 degree-days, and the monthly standard deviation was 23 degree-days. For a location such as Nashville, Tenn., with ~1000 cooling degree-days annually and ~250 cooling degree-days monthly, these standard deviations represent about 8% and 10%,respectively, of these totals.

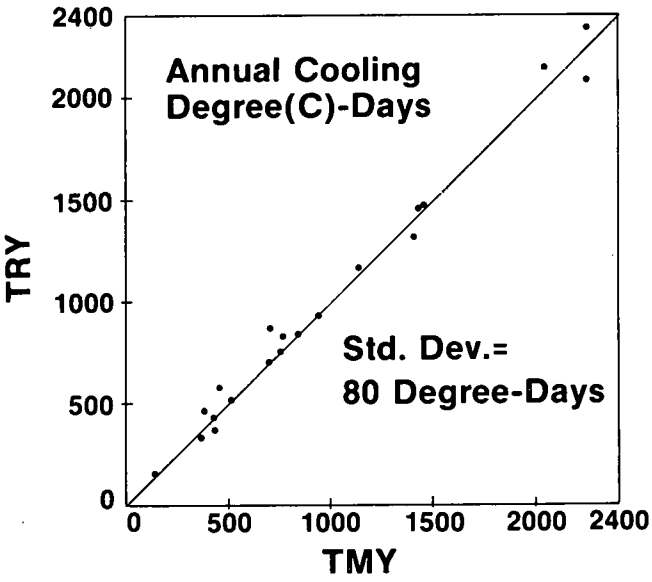

Fig. 4. TRY vs. TMY: Annual Total Cooling Degree(C)-Days.

Overall, these figures demonstrate reasonable agreement between TRY and TMY data sets for most locations. Because the method used to find the TMY offered much more month-to-month flexibility, this agreement is remarkable.

Dew-Point Temperature

Because the TRY selection process chose only on the basis of "nonextreme" dry-bulb temperatures, the typicality of meteorological factors indicative of latent cooling loads was ignored. On the other hand, the TMY selection process weighted typicality of the dew-point temperature equally with that of the dry-bulb temperature. Thus, any degree of agreement between TRY and TMY data sets in this area is fortuitous. Figure 5 shows a scatter plot of annual average dew-point temperatures. The standard deviation of the differences between the annual averages was 0.9° C, while the standard deviation of the monthly averages was 1.9° C. These values are about 50% larger than those for the dry-bulb temperature, indicating significantly worse agreement.

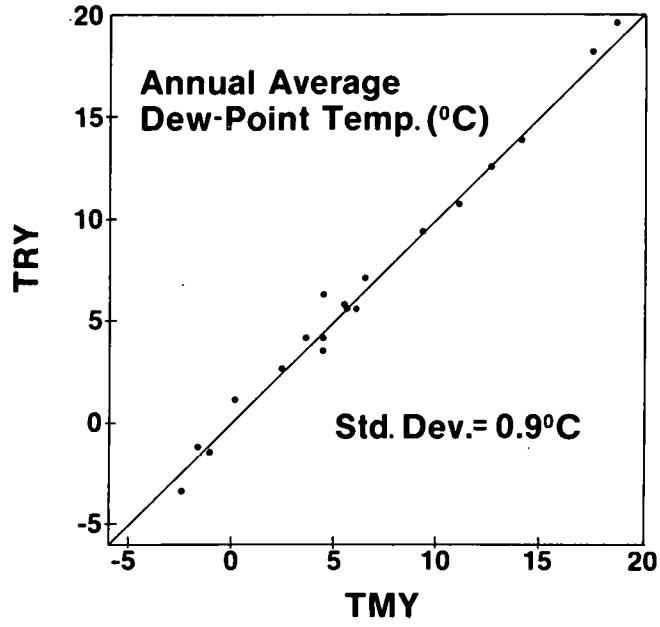

Fig. 5. TRY vs. TMY: Annual Average Dew-Point Temperature(C).

Humidity Ratio

Although the average dew-point temperature indicates the average humidity, there is no universally accepted figure that describes the spread of the individual humidity values about the average value in the way that degree-days do. To get some feeling for this spread, a quantity that represented the difference between the ambient humidity ratio (calculated from the dew-point temperature) and the humidity ratio at 77° F and 50% relative humidity (w = 0.01) was used. This humidity difference (Δw) thus represents the lb_m of water (per month or year) that would have to be removed from the air if the infiltration or ventilation rate were 1 lb_m of air per hour.

The annual totals for TRY data are plotted against those for TMY data in Fig. 6. The agreement between the data sets is poor for either large or small values, i.e., for either very humid or dry climates, and the TRY values tend to be higher than the TMY values. The annual and monthly standard deviations are 1.72 and 0.44 lb_m $H_2O/(lb_m$ air/hr), respectively. Although the annual totals reasonably agree, the monthly values do not agree well. Therefore, the two data sets will not predict the same latent cooling loads on a monthly basis, and on an annual basis, the TRY data tend to predict higher latent loads than TMY data. Since the TRY data was chosen without regard for typicality of dew-point temperatures, it seems reasonable to assume that the latent cooling loads predicted by the TMY data will be more representative of the long-term data.

Insolation

The TRY data do not contain solar insolation data. However, programs such as DOE-2 contain an ASHRAE algo-

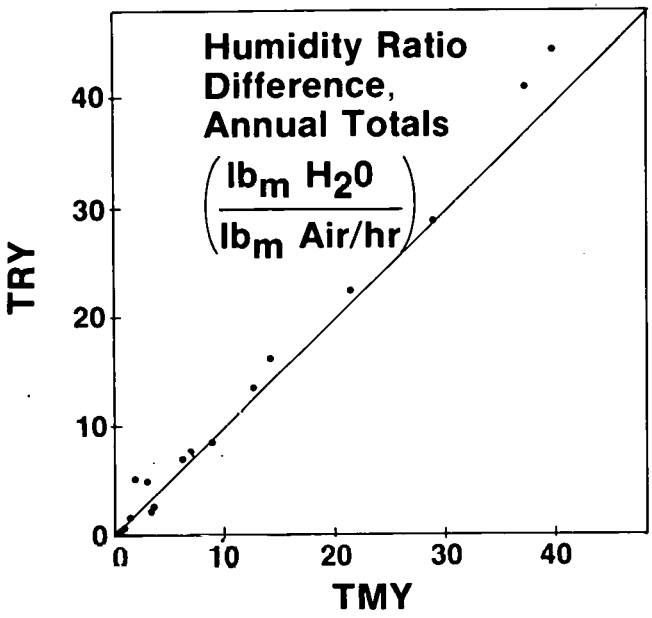

Fig. 6. TRY vs. TMY: Annual Total Hourly Difference Between the Ambient Humidity Ratio and the Humidity Ratio at 77°F and 50% Relative Humidity.

rithm [3,4] that generates direct and diffuse insolation values from the cloud cover data available in the TRY data. The values of direct and diffuse horizontal radiation generated by this algorithm were used for this comparison.

The TMY data contain values for both global horizontal (standard year corrected) and direct normal radiation. To make direct comparisons between the TMY values and the values generated from the TRY data, several calculations had to be performed. First, the direct normal radiation had to be corrected to direct horizontal radiation. Then the diffuse horizontal could be obtained by subtracting the direct horizontal from the global horizontal. In this way, three monthly average daily radiation numbers were calculated for comparison: direct horizontal, diffuse horizontal, and global horizontal.

The results of this comparison showed major discrepancies between the insolation values calculated by DOE-2 from the TRY data and the values from the TMY data. Figures 7, 8, and 9 present the annual average daily direct, diffuse, and global radiation, respectively. The direct radiation values generated from the TRY data are consistently 1.5 to 2 times higher than the TMY values for all 20 locations. On the other hand, the diffuse radiation values generated from the TRY data are consistently only 1/3 to 1/2 as large as the TMY values. Since the global radiation is the sum of the direct and diffuse, any differences in these two values are reflected in the global radiation. However, since the direct radiation values are so much larger than the diffuse values, the differences in direct radiation dominate, and the TRY-generated global radiation values are much larger than the TMY values.

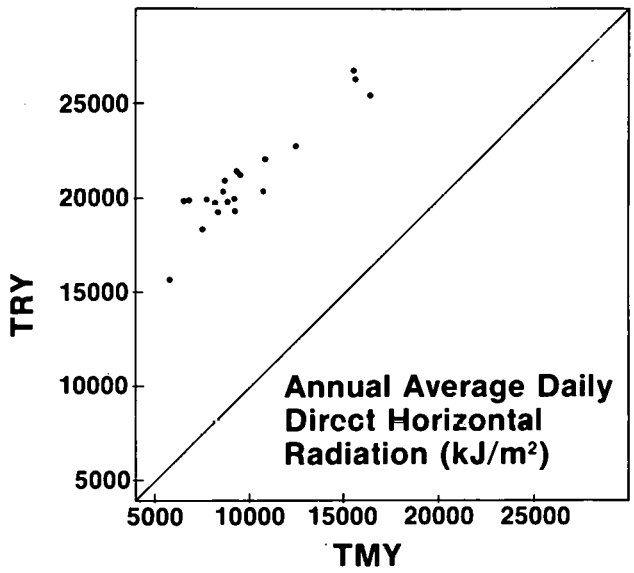

Fig. 7. ASHRAE Algorithm Using TRY Data vs. TMY: Annual Average Daily Direct Radiation on a Horizontal Surface.

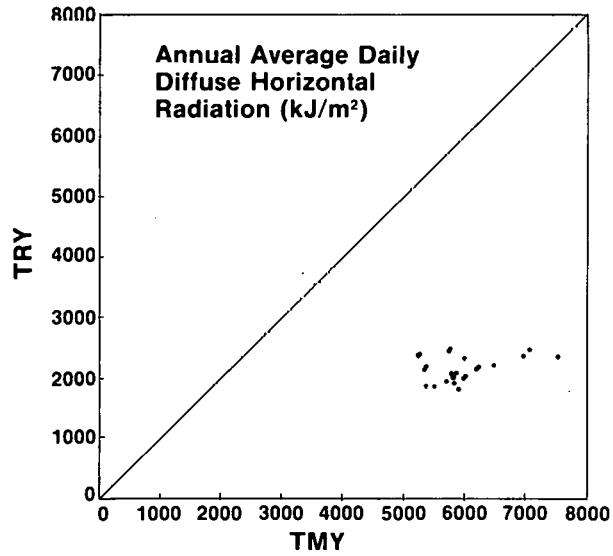

Fig. 8. ASHRAE Algorithm Using TRY Data vs. TMY: Annual Average Daily Diffuse Radiation.

This comparison of TMY insolation data with an ASHRAE/DOE-2 algorithm is not a true comparison between TMY and TRY data. Unless the TMY data are grossly unrepresentative, the algorithm is deficient in generating reasonable values.

CONCLUSIONS

The TRY and TMY data sets agree marginally well on statistics related to dry-bulb temperature, giving standard deviations within 10% of typical values for both the

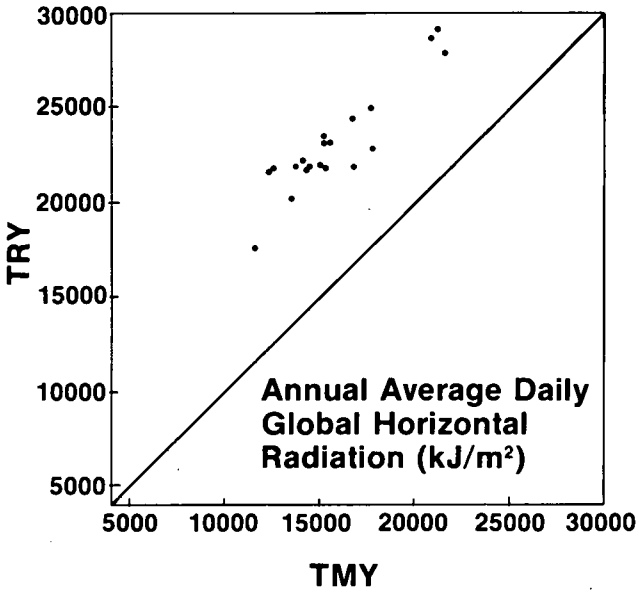

Fig. 9. ASHRAE Algorithm Using TRY Data vs. TMY: Annual Average Daily Global Radiation on a Horizontal Surface.

annual and monthly degree-day figures. However, the agreement of the statistics for humidity is not as good, and the insolation values do not agree.

To a user, the importance of these discrepancies depends upon the type of building or system that is to be simulated. For example, the heating loads predicted by the two data sets for a large commercial building whose load is dominated by internal generation and ventilation requirements should agree fairly well. The sensible cooling loads for such a building should be very similar. However, the two data sets will predict substantially different results if they are used to predict latent cooling loads, loads on skin-dominated buildings where solar gain is important, or other types of solar installations.

Of course, improvement of the ASHRAE/DOE-2 insolation generating algorithm would probably alleviate some of these problems, and if TRY data is to be used, this algorithm must be improved. However, it seems that one certainly cannot use TRY and TMY data interchangeably over a broad range of problems.

ACKNOWLEDGMENT

This work was supported by the Systems Development Division, Office of Solar Applications, DOE.

REFERENCES

1. E. Stamper. "Weather Data." ASHRAE Journal, 19(2): p. 47; February 1977 .

2. I. J. Hall et al. "Generation of a Typical Meteorological Year." Proceedings of the 1978 Annual Meeting of AS of ISES; Denver, CO; Vol. 22. 1978.

3. ASHRAE Task Group on Energy Requirements for Heating and Cooling of Buildings. Energy Calculations 1: Procedure for Determining Heating and Cooling Loads for Computerizing Energy Calculations. Algorithms for Building Heat Transfer Subroutines. New York, NY: ASHRAE; 1975.

4. Lawrence Berkeley Laboratories; DOE-2 Program Manual. Berkeley, CA: LBL; February 15, 1979.

5. E. A. Arens, D. H. Nall, and W. L. Carroll. "The Representativeness of TRY Data in Predicting Heating and Cooling Requirements." ASHRAE Journal. 20 (No. 12): p. 58 1978 .

6. T. L. Freeman. Investigation of the SOLMET Typical Meteorological Year. Proceedings of the 1979 International Congress of ISES, Atlanta, GA; May 1979.

NOTES

AN "MRT METHOD" OF COMPUTING RADIANT ENERGY EXCHANGE IN ROOMS

Joseph A. Carroll
UCSD Energy Center
La Jolla, CA 92093

ABSTRACT

The "MRT View Factor" method presented in this paper couples each surface in a room to an MRT node, which acts as a clearinghouse for all radiative exchanges. An upward adjustment in the coupling between each surface and the MRT exactly cancels that surface's self-weight in the MRT. The adjustments also happen to improve the accuracy of the conventional view factors implicitly assigned by MRT methods. The effects of surface emittance and air emittance (typically .05-.15 in residences) are modelled without difficulty. For greatest accuracy, radiation coefficients can be varied with temperature.

This method is inherently free from heat balance errors and errors in the overall radiative coupling of each surface to its environment. Errors do occur in the "implicit view factors", but errors such as this are inherent in any method which overlooks the gory details of the enclosure geometry. Coplanar surfaces cause the largest errors, and these errors can be compensated for if necessary.

1. INTRODUCTION

In simulating the thermal performance of buildings, one must predict not only T_{air} but also the Mean Radiant Temperature, for the MRT is typically nearly as important as T_{air} in determining the overall sensation of warmth experienced by occupants (1). Most simulation programs calculate radiant energy exchange using view factor techniques, which explicitly couple each pair of surfaces. The programs then separately calculate the MRT from the surface temperatures and radiant energy sources such as sunlight.

The possibility of using the MRT not only in comfort estimates but also in room heat transfer calculations led to the current analysis. The advantage of using the MRT can be considerable: coupling each of N surfaces to the MRT (which must be calculated anyway) need involve only N heat transfer calculations, while linking each surface to all other surfaces plus a radiant source of energy involves N^2 calculations.

The basic problem with applying the MRT to heat transfer is that coupling a surface to the MRT implicitly couples it to each surface which is represented in the MRT--including itself. This "self-weighting" of surface i in the MRT means that $(MRT-T_i)$ will be less than the true driving force for heat transfer, the difference $(T_{o,i}-T_i)$, where the $T_{o,i}$ is the properly weighted average of all surface temperatures other than i. As a result, radiant energy transfer will be consistently underestimated by an amount proportional to the self-weight of surface i in the MRT.

There are two ways to compensate for this error: adjust the MRT, or adjust the connections to the MRT. A recent version of BLAST does the former. At each timestep, BLAST calculates the sum of the emittance-area products and the sum of the emittance-area-temperature products. Then at each surface i, the program subtracts i's contributions to the two sums and divides the remainders to get an estimate of $T_{o,i}$.

The MRT Method proposed here uses the other strategy. The total radiative conductance U_i from each surface to the MRT includes a factor F_i which exactly compensates for its self-weight in the MRT. This strategy is faster than that used by BLAST, and turns out to be more accurate as well.

The F_i factors are analogous to view factors and thus will be called "MRT view factors". The procedure for calculating them will be shown for a cube and then generalized to deal with arbitrary polyhedra. Then the method will be applied to real (i.e., messy) enclosures. Subsequent sections will further generalize the MRT view factor method to deal with air emittance, gray surfaces, radiant sources, and large variations in temperature. The final section will show how the method can be used to greatest advantage in a forward difference algorithm.

The appendix provides a geometrical image of the MRT view factor method as a mapping of polyhedra onto a sphere. This analogy provides a guide for applying the method to the problem situations discussed in section 3.

2. MRT VIEW FACTORS

Consider a hollow cube. Each facet is an isothermal blackbody emitter, and the gas in the cube has zero emittance. If the temperature differences are small, we may estimate the MRT within the cube as the area-weighted average surface temperature.

If we want to use that MRT in calculating the radiant energy transfer within the cube, we must assign a conductance U from each surface to the MRT. We start by differentiating the radiation equation to find h_b, the blackbody radiation coefficient:

$$h_b = 4\sigma T^3 \qquad (1)$$

Since each surface i has a weight of 1/6 in the MRT, $(MRT-T_i)$ is 1/6 less than $(T_{o,i}-T_i)$. To compensate for this reduction in the apparent driving force for

heat transfer, the h_b must be scaled up by a factor of F to get an effective radiation conductance U between i and the MRT:

$$F = 1/(1-1/6) \quad (2)$$

$$U = h_b F_i \quad (3)$$

The factor F can best be described as an overall view factor from each surface to all the surfaces represented in the MRT, including the surface itself. The effective portion of F is exactly 1; the remainder of F is a futile self-coupling, an artifact which creates no errors.

This "MRT view factor" concept can be generalized to irregular enclosures as follows: the self-weight each facet i in the enclosure varies directly not with area A_i but rather with the "UA", which changes with F_i as well as with A_i. Thus the "1/6" term above must be replaced by $A_iF_i/(\text{Sum of all } A_iF_i)$, giving the following matrix equation:

$$F_i = 1/(1-A_iF_i/\text{Sum}A_iF_i), \quad (4)$$

to be solved once, at the beginning of a simulation. A simple iterative algorithm is adequate, using initial values of $F_i=1$ for the F_i terms on the right side of equation 4. The iterations converge quickly unless one facet is much larger than any of the others, and seem to converge enventually for all physically possible polyhedra.

One can easily perform a Y-Δ transformation on the resulting MRT network to compare it to a conventional view factor network. The direct coupling A_iF_{ij} from each surface i to each surface j will be:

$$A_iF_{ij} = A_jF_{ji} = A_iF_iA_jF_j/(\text{Sum}A_iF_i) \quad (5)$$

This and other MRT methods implicitly assign conventional view factors F_{ij} independently of relative position in an enclosure. Since true view factors do generally vary with relative position, this means that MRT methods introduce some view factor errors. This insensitivity to position is an unavoidable consequence of the reduction in the number of explicitly assignable conductances in an MRT network.

The individualized values of F_i for irregular polyhedra generally result in implicit view factors more accurate than those directly determined by area. The appendix shows why this is so, and also shows how one can intuitively assess how well a given geometry can be handled.

It should be noted that although there may be view factor errors in this method, the set of $(UA)_i$ to the MRT form a consistent thermal network, which allows heat transfer calculations that are inherently free from heat balance errors.

3. APPLICATION TO REAL ENCLOSURES

The above discussion has dealt with "facets" of an enclosure. Application to real rooms is simpler if one deals with "components", which may extend over several facets which view each other, or which may share a facet with another component. Procedures for those cases are described below. Then problem cases are discussed, including the case of "one-zone" models of multi-room buildings.

If different facets of a component do not see each other, they are best considered as one larger facet in the F_i calculations. In cases where mutually viewing facets of component i are comparable in area, one can simply use the total number of facets N_i of that component, and their total area A_i, in a new form of the MRT view factor matrix equation:

$$F_i = 1/(1-(A_i/N_i)F_i/(\text{Sum}A_iF_i) \quad (6)$$

The number of facets N_i need not be an integer and need not be estimated too accurately, because it is only used in the above equation and usually has only a fairly weak effect on F_i. (For components in typical rooms, F_i is usually between 1.0 and 1.3.)

Separate components which are coplanar or otherwise shielded from each other present more of a problem. The erroneous implicit view factor between them can be reassigned to other surfaces by the following strategy: the two components are treated as the fractions N_i of a larger facet. After the F_i values are calculated, then the erroneous coupling A_iF_{ij} between the pair of non-viewing components is evaluated using equation 5. Then a "negative coupling" of equal magnitude is assigned directly between that pair of components, to explicitly cancel the implicit coupling through the MRT node. This adjustment adds to the complexity of the network, and should only be used where simpler alternatives are inappropriate. The simpler alternatives and their applications are discussed below.

If both components are small in area, then the erroneous coupling will be very small. Thus one can ignore the fact that they are coplanar and simply treat them as separate facets having $N_i=1$. This is also adequate in cases where components coplanar to i have an average temperature similar to that for the surfaces actually viewed by i. Thus letting a window "see" a well insulated frame wall coplanar with it will not create large errors.

If the components are large but have similar temperatures, or similar thermal properties, then they can be considered fractional parts of one facet, but the "negative coupling" can be skipped. This might apply to the case of a shallow rockbin under part of a slab floor. (In fact, the erroneous radiative coupling may be smaller than the actual transverse conductive coupling between the floor sections.)

The only condition where the decoupling scheme seems really necessary is where coplanar components have substantial area and significantly different temperatures and thermal properties. For example, modelling a large Trombe wall as "seeing" a large window on the same building face would clearly overestimate heat losses from the wall.

Enclosures with high aspect ratio and significant temperature gradients and differences in component properties in the long direction present problems, because axial heat transfer in long enclosures is a diffusion-like process involving significant gradients along the long surfaces, and most heat transfer models are based on an assumption of isothermal surfaces. One can divide an enclosure into several distinct regions having coupled MRTs, and such a treatment should be more accurate than view factor methods unless they also partition the enclosure. The aspect ratio of each element will affect the results, and the best ratio to use has not been determined yet.

he final problem case is the most practical one: a one-zone model of a multi-room building. The following procedure should give the most representative results. Start with a list of the total areas of each type of component. Construct a single room using all of them, dividing any components which normally have some view of themselves into facets in accordance with the following two rules:

1. The sum of the N_i for large-area components should be similar to the number of major planes in a typical room in the building (usually about 6). Components may be divided into non-integer numbers of facets. Components with small areas such as windows and doors should not be included in this sum.

2. The relative size of the facets of different components should be representative of their relative size in a room. Thus the wall and window components should typically be divided into facets which each have smaller areas than the floor.

The choice of N_i values is not critical, since it has effect only on F_i, and generally only a weak effect at that. However, components with a large total area (such as interior partitions) must be divided into a reasonable number of parts, so that they are partly coupled to each other. Otherwise, their effect on other components will be exaggerated.

4. MODELLING THE EMITTANCE OF ROOM AIR

Accurate modelling of the effects of room air emittance is not necessary in most room-size enclosures. This is fortunate because of all the non-linearities. The simple formula below was developed to fit the data of Hottel (2), and estimates the average air emittance $\bar{\varepsilon}_a$ over a range of path lengths in residential enclosures as a function of room size and water vapor content, with a minor adjustment for average room surface emittance $\bar{\varepsilon}_s$. (This is included because total emittance rises slower with non-gray gases than with gray gases when the effective path length is raised by surface reflections.) The contribution of CO2 has been neglected, but Hottel's data shows it is minor. The formula is:

$$\bar{\varepsilon}_a = .08\ \bar{\varepsilon}_s\ \ln(1 + 4\ V/(A\bar{\varepsilon}_s)\ RH\ \exp(T_a/17) \qquad (7)$$

where V/A is the ratio of room volume to room surface area (in meters), RH is the relative humidity (/100%), and the exponential term represents the variation of saturation water vapor density with air temperature T_a (°C). For $\bar{\varepsilon}_a < .2$ or so, the errors in the above are usually under .02.

To show how air emittance is modelled in an MRT network, it is helpful to use the term "view factor" unconventionally. If $\bar{\varepsilon}_a = .1$, each face of a cube will be coupled radiatively to the air as if it were a cloud of particles having a viewfactor = .1 from each surface. Since the air thus reduces each of the other view factors by .1, it should do that for the implicitly determined view factors in the MRT network. The best fit will be obtained by simply assigning an area A_a to the air and treating it as another i:

$$A_a = \bar{\varepsilon}_a\ (\text{Sum of all } A_i \text{ except } A_a) \qquad (8)$$

$$(UA)_a = h_b\ A_a\ F_a \qquad (9)$$

Variations in $\bar{\varepsilon}_a$ usually have only a slight effect on the other F_i. To reduce run time in simulations which permit air emittance to vary over time, one can calculated fixed F_i values at the beginning, for a case with average absolute humidity, and then at each timestep scale the A_a with $\bar{\varepsilon}_a$.

5. GRAY SURFACES

If one assumes evenly irradiated isothermal diffuse gray surfaces, then there is no need to keep special track of reflected rays in an enclosure: they will be distributed just the same as emitted rays. For such a case, A.K. Oppenheim (3) has shown that one can properly model the effects of surface emittance merely by inserting a "surface resistance" at each surface having less than emittance surface. The proper resistance can be directly inserted into any MRT network, and the resulting U_i is:

$$U_i = h_b/(1/F_i + (1-\varepsilon_i)/\varepsilon_i) \qquad (10)$$

The limitations in the previous paragraph may seem rather severe. The same limitations apply to most view factor methods. Deviations from those conditions will result in equal errors in the MRT method and the conventional methods. Given the high emittances of most building materials, the errors are likely to be negligible, with the possible exception of errors due to large gradients in irradiation and temperature. Errors in those cases can be minimized by partitioning the enclosure, as discussed in section 3.

6. SOURCES OF RADIANT ENERGY

The term "Mean Radiant Temperature" is usually defined as the temperature of a uniform black enclosure in which an occupant or object would have the same net radiative energy transfer as occurs in an arbitrary environment. Since direct gains onto people and surfaces change the radiative balance, the true MRT will be higher (by a somewhat variable amount, depending on the surface), than the "longwave MRT", MRTL. One can model this increase for the average room surface, and also distribute the direct gain to the various surfaces in this MRT method using the following equations:

$$MRTL = \text{Sum}(T\ UA)_i\ /\ \text{Sum}(UA)_i \qquad (11)$$

$$MRT = MRTL + \dot{Q}_r/\text{Sum}(UA)_i \qquad (12)$$

$$\dot{Q}_i = (UA)_i\ (MRT - T_i) \qquad (13)$$

This distributes direct gain (and other radiant gains) based on longwave properties, and has several effects. First, one cannot directly assign the gains arbitrarily to each room surface. For ordinary high-emittance building surfaces, the gains will be automatically delivered to surfaces based on their area, with a slight bias towards larger surfaces because of their higher F_i. To sort the gain differently, one can first do the equations above, and then explicitly transfer directly from one surface to another whatever fraction of the gain one wishes to redirect. One can also use the same procedure to eliminate the two artifacts of the MRT method discussed below.

A portion of the gain will be assigned to window surfaces, based on their weight in the MRT. Since the inner surface of a window is farily well coupled to the outside environment, about 40-80% of that portion of the gain will be effectively lost to ambient.

This effect can be regarded as modelling the optical inefficiency of building enclosures as cavity absorbers: it scales properly with window area and has approximately the right magnitude (a few % in most cases). However, the model is affected by overall window conductance to ambient, while real behavior depends rather on the insolation angle, the room geometry and surface absorptances, and the "inside-out" shading coefficient of window assemblies. Thus the results of parametric studies of window U-values will be slightly less accurate than those of window area.

Another effect of sorting the gain based on longwave properties is that approximately $\bar{\epsilon}_a$ of the total gain will be delivered to the air. This effect also happens to correspond to something real: the increase in convection coefficients on strongly heated surfaces. When window coverings (drapes, shades, blinds) and other surfaces such as patches of rug are in bright sun and strongly heated, they will be coupled much better than usual to the room air. The simplest way of modelling this is to assign some small amount of the solar gain to the air node. The MRT network happens to do this automatically, if $\bar{\epsilon}_a > 0$.

A final subtlety regarding direct gain is that the MRT network calculates the impact of the gain for an average surface in a given room. As a result, the direct gain effect on people will be estimated most accurately if people share the sun with room surfaces roughly on an area-weighted basis. If the average effect is known to be different for the two, this difference can be compensated for in the comfort calculations, after the heat transfer calculations are done.

7. LARGE VARIATIONS IN TEMPERATURE

Near room temperature, radiative couplings between surfaces vary 1%/°C with variations in mean temperature. Many other properties such as capacitance, conductivity, convection coefficients, and air emittance also vary with conditions, and it is not unusual for their variations to counteract each other somewhat. For example, a passive house will tend to have higher direct gain, lower temperature, and lower absolute humidity in cold weather than in warm weather. The resulting variations in h_c, h_r, and $\bar{\epsilon}_a$ will tend to cancel each other out, so that a model which varies only the h_r may be less accurate than a simple linear model which uses the right average properties.

Even in cases where the variations do not cancel, the net error may be less than expected. An example is a linear model which always underestimates the couplings from heated surfaces. Their temperatures will then be overestimated, which reduces the error in the estimate of their effect on the MRT and their heat exchange with other surfaces.

Nonetheless, it is useful to have procedures to vary radiative couplings with temperature. Many enclosures are subject to larger variations over time than over space. In such cases, all couplings may be adjusted together at each timestep, by a factor proportional to $MRTL^3$ (degrees K): first calculate the MRTL using baseline $(UA)_i$, then adjust the UAs, then add the gain, then calculate the heat transfer at each surface. This procedure (and the next one) cause no heat balance error, because scaling the UAs does not change the MRTL if all conductances change together.

A more complicated procedure can deal accurately with cases involving significant temperature variations in space as well as over time. It scales each $(UA)_i$ by two factors nearly proportional to $T^{1\frac{1}{2}}$, and estimates the fluxes at each surface within about 1% for surfaces between 0C and 50C. It also correctly biases the MRT towards the warmer surfaces.

To vary the conductances individually, one calculates base values $(U_bA)_i$ for each conductance, for a temperature of 27C (81F). Then at each timestep, each conductance is first adjusted individually:

$$(U'A)_i = (.865 + T_i/200)(U_bA)_i \qquad (14)$$

Then the MRTL is calculated from all the T_i and $(U'A)_i$, and all conductances are adjusted again (together):

$$(UA)_i = (.865 + MRTL/200)(U'A)_i \qquad (15)$$

(In English units, the numbers in both equations above should be .775 and 360.) Then solar and other radiant gains are included and the heat transfer at each surface is calculated.

One can use the above procedure on a one-shot basis to find the best-fitting U_i for each component. The estimates of average temperature for each component should be biased towards conditions involving large temperature differences, because that is when U_i errors have the greatest effects. Using the procedure in this way would be most useful for components such as Trombe walls and windows, which are consistently warmer or cooler than the room.

8. USING MRT NETWORKS TO GREATEST ADVANTAGE

The potential advantages of the MRT view factor method in reducing computation time were mentioned in the introduction. In some applications, few of these advantages will be realized. For example central and backward difference equations must include terms for all nodes directly or indirectly tied to each other, and reducing the number of explicit connections may not speed computation very much.

Even some forward difference techniques will not take maximum advantage of this method. For example, some programs reduce the size of a network by "dissolving" all massless nodes before the simulation begins. This process should not be applied to the MRT and air nodes, because that will increase the number of conductances in a network.

An efficient algorithm for linear networks containing controls is shown below. It assumes that after the radiative and convective $(UA)_i$ have been found, a Y-Δ transformation has eliminated each massless surface node. Since dissolving a surface node couples the MRT and air nodes not only to mass i but also to each other anyway, one can include air emittance in the model without increasing run time. X is the total cross-coupling between the MRT and air nodes, and R_i and C_i are the radiative and convective couplings to mass i. Infiltration is represented as a C_i to ambient. $SumC_i$ and $SumR_i$, the sum of all the couplings from the masses to the air and MRT nodes respectively, (excluding conductance X), are also precalculated.

If the simulation permits night insulation or shading which alters the conductance of windows, the proper set of precalculated terms is chosen at the beginning of each timestep.

A "bootstrap" procedure is used to deal with the two coupled massless nodes. It looks inefficient because it works in several steps. However, if any changes in control state are required after the MRT and T_{air} are found for one control state, the intermediate steps quickly pay for themselves. The procedure will be described very briefly.

First, for both the MRT and air nodes, calculate the sums of the C_iT_i products and the R_iT_i products, $SumC_iT_i$ and $SumR_iT_i$. (This excludes the cross-connection X.) Then add all fixed heat sources into $SumC_iT_i$ and $SumR_iT_i$.

Next, include the effects of the coupling X in the air temperature by multiplying $SumR_i$ and $SumR_iT_i$ by a factor of $X/(SumR_i+X)$, and add the results to the $SumC_i$ and $SumC_iT_i$. (This has the effect of a Y-Δ transformation, temporarily eliminating the MRT.) Then one can calculate the T_{air} and MRT:

$$T_{air} = SumC_iT_i/SumC_i \qquad (16)$$

$$MRT = (SumR_iT_i + X\ T_{air})/(SumR_i+X) \qquad (17)$$

Then any necessary control decisions can be made. To include the effects of adding venting and rockbed or other fans, or backup heat, one simply adds their contribution to the sums on the right side of the two equations above and updates the T_{air} and MRT to represent the new control state.

Finally, the T_{air} and MRT are used in the finite difference equations which predict the future temperatures at each mass based on their current temperatures and rates of change.

The algorithm described above has been used in simulations of a 7-component, 20-mass system with all the control features listed above. These simulations have been done on a microcomputer, and it would not have been nearly as feasible to do such work without an MRT network such as is provided by the MRT view factor method. The advantages of this method also extend to main-frame computers, where parametric studies and multi-zone simulations become more affordable when an efficient "room" algorithm is used.

Besides direct use in simulations, the MRT view factor method may also be useful in improving the accuracy of even simpler models of room heat transfer. Models involving a "room" or "globe temperature" node differ from MRT-air models only in that they have effectively added an infinite conductance between the MRT and air nodes. A careful analysis of those methods in this light may show ways to minimize their errors.

ACKNOWLEDGEMENT

This work was supported in part by the Solar Heating and Cooling R & D Branch, Office of Conservation and Solar Applications, U.S. Department of Energy, under contract DE-AC04-79AL10891.

REFERENCES

1. P.O. Fanger, Thermal Comfort, pp. 58-67, Danish Technical Press, Copenhagen, 1970.

2. H.C. Hottel, Radiant Heat Transmission, in W.H. McAdams, "Heat Transmission," McGraw-Hill Book Company, New York, 1954. (Note: the data is from this source, but equation #7 is an empirical fit by this author, and not from Hottel.)

3. A.K. Oppenheim, "Radiation Analysis by the Network Method," pp. 725-735 in Transactions of the ASME, May, 1956.

(APPENDIX IS ON FOLLOWING PAGE)

APPENDIX. MAPPING ENCLOSURES ONTO A SPHERE

To shed light on the MRT view factor method, it is useful to introduce a geometrical interpretation. Consider a spherical enclosure. The length of a chord between any two points on the sphere is proportional to the cosine of the angle of incidence at each end of the chord. Thus the second-power distance effects exactly cancel out the cosine effects which occur at each end of the chord. Since each region on a sphere sees itself and others on a strict area-weighted basis, a simple MRT scheme will provide exact results for diffuse gray surfaces; relative position is entirely irrelevant.

Next inscribe a polyhedron such as a geodesic dome within a sphere. By using a somewhat smaller sphere, we can obtain the best fit between the sphere and the edges (rather than the corners, or the faces) of the polyhedron. We can then map the dome onto the sphere by projecting each facet i of the polyhedron onto the area S_i on the sphere, where S_i is the region shaded by facet i from radiation inside the dome. Since area S_i is a concave surface having facet i as an aperture, they have the same effective views of other surfaces. Since the sphere can be modelled without error by an MRT method, the only geometrical errors in the MRT method result from the mapping operation.

The MRT view factors F_i can now be explained as representing the ratio of area S_i (on the sphere) to A_i (on the polyhedron). The matrix equations in the paper (4 or 6) thus map an arbitrary polyhedron onto a sphere by associating each facet area A_i with an area S_i, whose effective aperture is exactly A_i. If the polyhedron may be "inflated" into the edge-fitting sphere without significantly changing the distances or orientations between the apertures, then the mapping will not introduce significant view factor errors. Thus "boxy" enclosures will be handled quite accurately. Comparing the view factors implicitly fixed by the MRT view factor method with the true view factors for simple rectangular enclosures, it was found that the errors are negligible at low aspect ratios, and increase smoothly with the aspect ratio of the enclosure. (Maximum error at ratios of 4:4:1 and 4:1:1 is about .06). It was also found that the variations in F_i always serve to reduce the errors below what they would be if the implicit view factors were directly proportional to area.

The MRT view factors also do justice to some rather unusual enclosure geometries. For a hemispherical geodesic dome having unit floor area, the small facets of the dome "shade" an area little larger than themselves, while the floor shades the entire bottom hemisphere. The MRT view factor method gives F_i values which implicitly fix view factors from any facet of .5 to the dome and .5 to the floor, despite the 2:1 area ratio; these values are the correct ones.

Consider now a shallow tent-shaped attic under a low-pitch gable roof. The MRT view factors will bias the MRT heavily towards the ceiling, so that the roof and endwall facets are coupled almost entirely to the ceiling rather than each other. For the roof facets this is accurate, due to the cosine effects involved, but the view factor from the ends to the ceiling and roof should not be biased.

The error in the shallow-attic case can easily be predicted by mapping the attic onto the best edge-fitting sphere: the mapping tilts the endwalls inwards. In this case, view factors proportional to area (such as calculated by BLAST) are more accurate for the small endwalls. The larger roof sections will be handled better by the MRT view factors, however.

The procedure which de-couples coplanar surfaces can be visualized as follows. The surfaces are considered one facet for the mapping operation. This results in more "ballooning" outwards of the facet, and more of an increase in relative area, than if the surfaces were considered as separate facets. The two regions on the sphere will be properly coupled to the rest of the sphere (since they have the right aperture area), but they will also be erroneously coupled to each other behind the aperture. This erroneous coupling is then assessed and cancelled.

The "local MRT" scheme can be compared to linear or planar arrays of soap bubbles. The common walls transmit energy perfectly but diffusely as it travels from one sphere to the next. Since the energy is diffused at each common wall, the macroscopic properties of the model (i.e., the long-range diffusivity) may not be easy to match to those of a real enclosure.

Air emittance can be visualized as a cloud of particles within the sphere, whose combined effect can be modelled by enlarging the sphere and depositing the particles on the newly-created area.

Surface emittance effects can be visualized by dividing each facet on the sphere into two portions, one having unit diffuse reflectance and the other unit emittance. The reflecting portions have no direct or indirect effect on view factors or overall heat transfer, and so can be discarded, leaving a smaller sphere.

One can also use the sphere model to see how the method implicitly fixes view factors from occupants to the enclosure. These view factors are simply proportional to the areas S_i associated with each facet i, after the various emittance adjustments have been made. The view factors from occupants to each facet will be slightly less than those from a facet to other facets, because occupants see all facets, rather than all but one.

For the geodesic dome mentioned above, the occupant view factors will be .5 each to the dome and the floor, if $\varepsilon_a = 0$ and $\varepsilon_s = 1$. If $\varepsilon_a = .1$ and $\varepsilon_s = .9$, then the floor view factor is reduced to about .41, and the "air" view factor is .09 (slightly less than ε_a). The bias towards the floor (which has only 1/3 the total area) happens to be reasonable, since that is where people usually are. However, the relative weight of dome and floor does shift in the wrong direction as air emittance is varied.

In the case of a shallow attic, the MRT view factors grossly bias the MRT toward the ceiling temperature in getting the best overall fit for view factors between surfaces. The unrepresentative MRT is a problem only if one wants to estimate thermal comfort in attics under low-pitch roofs.

THE NEW SERI DATA BASE FOR VALIDATING PASSIVE SYSTEM COMPUTER MODELS

Robert D. Busch, Ph.D.
Bickle/CM, Inc.
2403 San Mateo NE, S-8
Albuquerque, New Mexico 87110

ABSTRACT

A standardized reporting format for passive solar experimental data has been developed for SERI. Utilizing this format, data from 8 test cells and passive houses, located in 4 different climate regions, has been published and entered into the SERI data base. This information represents consistent and coherent data which can be used to validate computer models of passive solar systems and components.

The format consists of two sections:

1) A complete description of the building or structure including dimensions and material properties; and
2) Two-weeks of measurements covering clear and cloudy days.

Measured data includes: insolation, ambient outdoor temperature, indoor air temperature, and temperatures of passive components.

For the first time, developers of simulation programs have a consistent set of data available to test and fine tune their programs. Thus, the new SERI data base represents a useful source of information for the validation of computer models.

INTRODUCTION

Passive solar heating and cooling systems utilize materials, components, and assemblies that are commonly used in the construction industry. It is the creative design and application of these conventional items that creates energy savings through passive solar utilization. However, the major barrier to widespread application of passive solar concepts is a lack of coherent and consistent experimental data upon which performance analyses can be based. Without scientifically defensible experimental data, predictive tools cannot be adequately validated, and projected savings cannot be accurately calculated. Thus, the acquisition of reasonable experimental data and its presentation in a standard format are the first critical steps towards the widespread utilization of passive solar techniques.

The basic problem is the lack of scientific data in a useful form on the experimental performance of passive solar systems. Although there have been many passive solar structures built, very few of these have adequate instrumentation to provide the necessary data for assessing thermal performance. For those structures which are monitored (approximately 70 buildings [1] and 50 test cells [2], the data was not reported in a standard format and thus may not be useful to either of the target audiences.

That data from the monitored structures which has been reduced and analyzed usually results in the publication of a few parameters which "characterize" the system (e.g. solar fraction, diurnal temperature swing) but do not always adequately describe it to others interested in assessing performance. In fact, some of these performance factors have multiple definitions which are not compatible in a final comparison [3]. This creates problems for the code validator who may not have sufficient data, for the experimentalist who does not know which definition to use, and for the general public who cannot obtain consistent information on the performance of passive solar systems.

To resolve these problems requires:

a) The identification of those variables which are significant in the needs of both target audiences;

b) The creation of a standard format which assures adequate information transfer among those involved in the passive solar field; and

c) The publication of selected experimental data in the standard format.

SET OF SIGNIFICANT VARIABLES

Discussions with various code developers and an extensive literature review have identified the set of significant variables given in Table I. These variables are of primary interest in evaluation of passive solar heating. Additional parameters such as relative humidity, ground temperatures should be included for passive cooling analyses. It is important to note that this set of parameters represents those variables which are necessary to

verify a simulation model through correlation with monthly performance information. A more detailed set of data would be required for the validation of simulation algorithms. Thus, Table I lists those parameters which are significant in a "basic" level evaluation [4] for models of overall building performance, but is not necessarily sufficient for validating those models which simulate passive systems.

SIGNIFICANT VARIABLES
FOR
PASSIVE SOLAR HEATING ANALYSES

Weather Variables

- Drybulb Temperature [°C] or [°F]
- Solar Radiation, preferably incident on collector plane, also horizontal, if possible [w/m^2] or [Btu/hr-ft^2]

Building Variables

- Dimensions [m] or [ft]
- Aperture Glazing Area [m^2] or [ft^2]
- Glazing Thickness [m^2] or [ft^2]
- Glazing U-value [w/m^2-°C] or [Btu/hr-ft^2-°F]
- Glazing index of refraction and extinction coefficient
- Total Effective Mass-by material [Kg] or [Lb]
- Mass Heat Capacity [watt-hours/°C] or [Btu/°F]
- Mass Surface Area [m^2] or [ft^2]
- Solar Absorptance of Mass
- Building Heat Load Factor [w/°C] or [Btu/hr-°F]
- Infiltration [m^3/hr] or [ft^3/hr]
- Ventilation [m^3/hr] or [ft^3/hr]
- System Operating Energy [w-hr] or [Btu]
- Internal Heat Sources, occupants, appliances, etc. [w-hr] or [Btu]
- Thermostat Setpoint [°C] or [°F]

Validation Variables

- Indoor Air Temperature (Globe, Mean Radiant, Shaded, Etc.) [°C] or [°F]
- Average Storage Temperature [°C] or [°F]
- Auxiliary Energy Requirements [w-hr] or [Btu]

Table I gives those variables which are of direct importance to the modeling audience. The variables are divided into three categories:

a) Weather variables - The driving functions for the model;
b) Building variables - The input variables which describe standard conditions of the model. Normally, they represent one-time measurements, but they could also be the median of a set of values; and
c) Validation variables - The model outputs to be compared with actual performance parameters to check model validity.

Since this is a general listing of important variables, no attempt is made to prescribe a level of detail for any of the parameters. Utilizing the standard format discussed later, the experimentalist should report these variables at a level of detail suggested by the measurement procedures. Model verification can then be done at that level of detail or at a lower level by weight averaging the data. For model validation, a mix of cloudy and clear weather for approximately 7 days is preferable. Initialization usually involves simulation over 3 days, continuing with the mix of clear and cloudy days. If 3 consistent days are not available for initialization, then most models utilize the first day and exercise the model until it reaches steady conditions. Thus, if possible, it seems best to choose a 10-day period starting with three days of steady weather. However, a 7-day period with a good mix of clear and cloudy days represents another viable alternative.

Since the current project is directed at two target audiences, it is important that the data and requirements specified by the code developers be compatible with the needs of the experimentors and those assessing system thermal performance. From a review of papers on performance, the set of significant variables seems to also be adequate for assessing performance on the levels defined by the National Bureau of Standards (NBS). [5,6]

STANDARD DATA FORMAT

Many meetings, papers, etc., have discussed methods of assessing thermal performance with various levels of detail. Very few, however, have directly addressed the question of format for the data required in these calculations. Due to the lack of a standard performance evaluation methodology and the considerable amount of data which presently exists, it was necessary to develop a preliminary standard reporting format to provide a common basis for presenting the large amounts of data being generated. When a standard performance evaluation methodology is implemented, then data will be available in a consistent format for performance analyses. Modifications can be made to the format if required by utilization of the standard methodology; however, it is important that present data be put in a common format as soon as possible to provide for easy utilization. This will allow for model verification with standard data sets and also provide

consistent information for public dissemination.

Based on information from NBS and a Swedish paper, [7], a standard reporting format has been developed and is given in Table II. This is slightly different from that proposed by NBS since NBS is primarily concerned with defining the instrumentation requirements for passive solar experiments. However, once the test equipment is set up and data is acquired, then the information should be reported in the standard format of Table II to ameliorate its use by both target audiences. Because this format has been derived from documents utilized by the International Energy Agency and the National Bureau of Standards, it is expected that all the reporting formats should be relatively consistent and compatible. (To be compatible, all data should be reported in both SI and English units).

TABLE II
DESCRIPTION OF STANDARD FORMAT

Section I - General Description of System, Project, and Environment

A. Brief summary of project and objective, including location of original data and contact for the project.

B. Description of environment

1. Location of structure, ground reflections, external shading objects, etc. Site plan and photographs if available.
2. Climate including description of typical sky conditions; tabulation of degree day, design temperatures, percent possible sunshine, station altitude, average station pressure, and days of snow cover, (for cooling systems, also include ground temperatures and average annual hours with drybulb greater than 80°F); and graphs of ambient drybulb temperature, solar radiation, etc. Classify climate according to guidolines developed by AIA/RC. [8]

C. Description of building (photographs preferable)

1. Plans, elevations, etc. for structure as-built.
2. Materials and material properties - it is especially important to identify those properties which are field values and those which are derived from the literature.
3. Description of building construction and use.

D. Description of passive solar system

1. Heat and ventilation flow diagrams
2. Storage location and type
3. Normal operating modes
4. Shading diagrams and description of internal and external shading devices. Include dimensions and operating mode descriptions for shades, fins, louvers, blinds, beadwall, etc.

E. Description of data acquisition system

1. Types and locations of sensors including accuracy of measurements.
2. Data recording device with specifications
3. Frequency of measurement for each parameter

Section II - System Thermal Performance

A. Listing of Building Variables (as defined in Table I)

B. Description of Weather Variables for Selected Test Period (Tables and Graphs)

C. Graphs and Tables of the Validation Variables for the Selected Period

D. Graphs and Tables of the Thermal Performance Parameters including:

1. Solar energy collected
2. Energy balance for the test period
3. Space heating load

Since the data presented in this manner will be utilized in many ways, it is important that it be reasonably comprehensive and that a description of instrumentation and data methods be included. Many of the building variables, such as building heat load and glazing conductivity, are used in the performance calculations and may have a large effect on an overall performance factor such as solar fraction; a five percent uncertainty in the building heat load can result in a fifteen percent change in the solar fraction. Thus, it is very important that all variables which were measured in the field be distinguished from those which were estimated or derived from the literature. This allows others to define parameter sensitivities and identify possible sources of error. A complete description of the experimental methodology will provide sufficient information to assess the applicability of the data to other structures and other environments.

DATA BASE DESCRIPTION

Presently, the data base, utilizing the standard format, consists of three test cells and five residences. A brief description of each of these facilities with comments on the scope of the measurements follows.

LASL Test Cells: Data is presented from the Direct Gain and the Trombe Wall Test Cells. Measurements cover a twelve day period in January. Recorded data includes vertical solar insolation, ambient temperature, inside air temperature, and

mass temperatures. This is a good set of data to do initial code validation with.

NCAT Test Cells: Data is presented from the Direct Gain and the Trombe Wall Test Cells in Butte, Montana. Measurements cover a fourteen day period in November and include: solar radiation on a vertical surface, ambient air temperature, indoor air temperature and front and back mass surface temperatures. As presently stored in the data base, the data covers seven days with the cells vented and seven days without. This makes it difficult to use for validation, so the data will be changed in the near future to alleviate the problem.

University of Nebraska Test Cells: Data is available from the Direct Gain and Trombe Wall Test Cells in Lincoln, Nebraska. Measurements cover eight days in March and include: solar radiation, ambient air temperature, and inside cell temperatures. Inside surface temperatures will be added to the data base soon. This data is useful for validating cell performance in a different climatic region.

Doug Balcomb House: This house has a sunspace with mass wall at the back. It is located in Santa Fe, New Mexico. Data covers a fourteen day period in December and January with fourteen hours of data missing. There is almost eight days of continuous data available. Measurements include: solar insolation, ambient temperature, sunspace and house auxiliary energy usage. This is a good set of data for validating the extrapolation of code results from a direct gain cell to a sunspace house.

Bruce Hunn House: The Hunn house is located in White Rock, New Mexico near Los Alamos. It is a two story structure with a Trombe wall. Data covers a fourteen day period during late December and early January. Measured variables include: horizontal solar radiation, outdoor air temperature, indoor air temperature, and storage wall temperatures at two different heights. The data set covers an occupied and unoccupied period so the thermostat set point changes during the sixth day. Auxiliary energy information was not available, so it must be estimated on a daily basis.

Bruce Maeda House: Bruce Maeda's house is a Suncatcher design with direct gain and a waterwall. This is located in Davis, California. Measurements cover twelve days in November and December. Variables included in the data base are: vertical solar insolation, ambient air temperature, indoor air temperature for different parts of the house, wall temperatures, and watertube temperatures. This is a good set of data for testing codes which can simulate a mixture of direct gain and water storage.

Charless Fowlkes House: The Fowlkes House, utilizes a watertube storage wall, and is located in Bozeman, Montana. Data is available for a thirteen day period in January. Measured variables include: vertical solar radiation, ambient air temperature, inside air temperature, and watertube temperatures. During the period of record, the house used no auxiliary heat as it has no thermostat, only wood backup. This is an excellent set of data for validating waterwall storage models.

Williamson House: This is a direct gain clerestory house located just outside of Santa Fe, New Mexico. Measurements are available for a fourteen day period in late December and early January. The data base variables include: horizontal and vertical solar radiation, ambient air temperature, indoor direct gain wall surface temperatures, and indoor mean radiant temperature. This is a useful data set for validating simulation models of direct gain structures.

Data from these data sets have been used to validate Bickle/CM's Trombe Wall code. Results indicate that the code is reasonably accurate in predicting the overall performance of a structure. However, the validation process indicated some problems with the relative magnitudes of different heat transfer mechanisms. Because the data set is meant for basic evaluation, this validation process was not able to identify the causes for the problems; only that the problems do exist.

SUMMARY

A standardized reporting format for passive solar experimental data has been developed for SERI. Utilizing this format, data from 8 test cells and passive houses located in 4 different climate regions, has been published and entered into the SERI data base. This information represents consistent and coherent data which can be used to validate computer models of passive solar systems. Now design performance estimates can be given to the manufacturers and public with a better degree of confidence than was available in the past.

ACKNOWLEDGEMENTS

This paper is the result of comments, critiques, and support from Ron Kammerud of Lawrence Berkeley Laboratories, Bruce Hunn of Los Alamos Scientific Laboratory, Robert McFarland of Los Alamos Scientific Laboratory, Francisco Arumi of The University of Texas at Austin, Mike Weston of IBM, and Bruce Maeda of Davis Alternative Technology Associates. Their review of the interim report provided many helpful comments and clarifications for which we are grateful.

I am deeply indebted to Bill Ducas of the National Bureau of Standards for his cooperation and discussion of the standard performance variables and standard reporting formats from NBS and the International Energy Agency. He was also very helpful in identifying areas of confusion from the viewpoint of a performance evaluator.

Data in the companion volumes was provided by Larry Palmiter of the National Center for Appropriate Technology and Stan Moore of Los Alamos Scientific Laboratory. Without extensive discussions with these

two, this report could not have been compiled. I especially want to thank Larry Palmiter for providing assistance on code validation requirements and techniques. I also gratefully acknowledge the support which Doug Balcomb of Los Alamos Scientific Laboratory has provided on this project.

This work was performed under a contract from the Solar Energy Research Institute, Golden, Colorado.

REFERENCES

1. AIA Research Corporation, Passive Solar Design: A Survey of Monitored Buildings, Report #HC/CS-4113-2, Washington, D.C., October 1978.

2. Notes from Performance Data Acquisition Meeting, Los Alamos, NM, February 12-13, 1979.

3. Palmiter, L. and Hamilton, B., "A Comparison of Performance Factors for Passive Solar Heating," prepared for Third Annual Passive Solar Conference, San Jose, California, January 12-15, 1979.

4. Ducas, W. and Hill, James, "Proposed Procedure for the Data Gathering, Analysis, and Performance Reporting of Passive Solar Heated Buildings," NBS Draft, October 1, 1979.

5. Holton, J.K., "Critical Performance Standards for Passive Solar Buildings," Passive Solar: State of the Art, Vol. II, pp. 294-297, March 1978.

6. Ducas, W., et al., "Thermal Data Requirements and Performance Evaluation Procedures for Passive Buildings," Passive Solar: State of the Art, Vol. II, pp. 411-430, March 1978.

7. Isakson, P. and E. Ofverholm, "Outline: Reporting Format for Solar Heated Buildings with Comments," IEA Solar Energy Experts Meeting on sub-project 1, October 1976.

8. AIA Research Corporation, Regional Guidelines for Building Passive Energy Conserving Homes, Report #HUD-PDR-355, Washington, D.C., November 1978.

NOTES

STANDARD ASSUMPTIONS AND METHODS FOR SOLAR HEATING AND COOLING SYSTEMS ANALYSES

Cecile M. Leboeuf
Solar Energy Research Institute
Golden, Colorado

ABSTRACT

This paper presents a set of inputs, assumptions, analytical methods, and a reporting format to help compare the results of residential and commercial solar system analyses being performed by different investigators. By the common use of load data, meteorological data, economic parameters, and reporting format, researchers examining, for example, two types of collectors may more easily compare their results.

For residential heating and cooling systems, three locations were selected. The weather data chosen to characterize these cities are the Typical Meteorological Year (TMY). A house for each location was defined that is typical of new construction in that locale. Hourly loads for each location were calculated using a computerized load model that interacts with the system and specified inputs characterizing each house.

Four locations for commercial cooling analyses were selected from among the existing sites for which TMYs were available. A light commercial (nominal 25—ton cooling load) office building was defined and is used in all four locations. Hourly cooling and heating loads were computed for each city and are available on magnetic tape from the Solar Energy Research Institute (SERI).

INTRODUCTION

An analysis of a solar heating or cooling system requires as inputs meteorological data (temperatures, dew point, insolation, and wind speed) and a well-defined structure to determine the load characteristics. In the past, researchers analyzing systems have generally not modeled identical buildings in identical locations using the same weather data. Since these parameters greatly influence the performance of the system, it is difficult for researchers to draw meaningful correlations when comparing systems or analysis methods. Also, because format and content of reported information often differs among investigators, a common format would be very useful.

This paper recommends a set of locations, meteorological data, building descriptions, and load calculation methods for use in analysis of both solar and conventional energy systems. Conditions are not meant to be ideal or typical in every sense, nor do they cover all climates or structures in the United States. Parameters and algorithms specified here are system independent (except for passive systems, which employ the building as part of the heating/cooling system) and should standardize the comparison of the results of analyses of solar and conventional energy systems and of analysis procedures. Methods outlined in this paper may be used by component designers, system designers, university researchers, and private consultants. Detailed illustrations of the applicability of this information and a more comprehensive treatment of the standard assumptions may be found in Ref. 1. Copies of this preliminary report are available from SERI. Because revisions and modifications will be necessary, comments from the user community are strongly urged. Every attempt will be made to incorporate these inputs into future revisions.

Much of the information contained in this paper was excerpted from two studies performed by Science Applications, Inc. (SAI) [2,3] and required common inputs for the simulation of systems in several locations. Through the development of standard inputs and analysis methods, the systems analyzed could be compared and significant conclusions drawn.

METEOROLOGICAL INPUTS

One obstacle to solar heating and cooling studies has been the lack of an accepted year of hourly meteorological data for computer simulations. Also, there are several methods that compute beam radiation from total horizontal radiation and a few algorithms that compute radiation on a tilted surface. Because these methods usually generate different results, they hinder the comparison of the simulation results of various systems. This section recommends one set of meteorological data (called TMY) and one algorithm for computation of beam radiation and radiation on a tilted surface.

The Typical Meteorological Year

Because the simulations of solar systems usually cover a year or less, it was desirable to develop a data base with shorter-term information than the SOLMET [4] data. The Department of Energy (DOE) contracted Sandia Laboratories to develop a typical

meteorological year (TMY) for each station (except Stephenville, Tex.) using statistical selection techniques [5]. The 26 TMY tapes generated by Sandia Laboratories are available through the National Climatic Center in Asheville, N. C. By choosing a series of months that emphasize the typicality of global radiation, one can construct a year that is representative of long-term weather patterns at each of the 26 locations. Therefore, long-term average system performance can be predicted with a one-year simulation.

The American Society of Heating, Refrigeration and Air-Conditioning Engineers (ASHRAE) developed a Test Reference Year (TRY) [6] weather tape for 60 cities, in which the primary criterion for selection was ambient temperature. Although they do not include values for solar radiation, TRY tapes do indicate sky cover and cloud type. Hence, incident radiation can only be roughly estimated when one uses TRY data. Radiation is an important parameter in all solar systems analyses, as well as in conventional energy system evaluations.

Because it is a potential standard meteorological data base and contains information paramount to solar energy systems, the TMY was selected for analyses of all solar systems and performance comparisons between conventional and solar systems.

Radiation Components

The values for direct radiation that appear on the TMY tapes were computed according to the Randall algorithm, a technique developed at the Aerospace Corporation [7] and recommended by SERI.

The radiation received on an arbitrarily oriented surface, such as that of a flat-plate solar collector, is a combination of direct-beam, sky-diffuse, and ground-reflected radiation. Calculation of the direct component of the insolation for a tilted surface is a straightforward geometric transformation applied to the horizontal values that appear on the TMY tapes. However, the calculation of the ground-reflected and sky-diffuse components requires the introduction of assumptions about the nature and distribution of the sky-diffuse and reflected radiation. Many algorithms correlate global radiation with radiation on a titled surface. Tom Stoffel of SERI informed the author that an algorithm developed by Hay [8] of Canada has proved to be most accurate when compared with actual measured data on surfaces of varying tilt. This algorithm is recommended for use in computing radiation on tilted surfaces for solar systems analyses [1].

RESIDENTIAL SOLAR HEATING AND COOLING SYSTEMS

Standardized methods for modeling of residential solar heating and cooling systems are presented in this section. As described in the introduction, the purpose of these inputs is to provide a basis for comparison of systems and simulation codes under development. They are not intended for use in designing or sizing a solar system in a location other than those modeled. Although the chosen locations represent a broad spectrum of climates and weather patterns found throughout the United States, it was impossible to cover every climate. Specifications for the actual homes are based on those typical of new construction in each location. Heating and cooling loads are computed using ASHRAE transfer function techniques [9] in an interactive TRNSYS-compatible load model package [2,10]. Location-dependent and building-specific inputs may be found in Ref. 1.

Selection of Residential Locations

Candidate cities for solar heating and cooling study locations included the 26 SOLMET (TMY) cities. In an attempt to choose from these sites a variety of load profiles and climates for both heating and cooling seasons, an analysis of the distribution of loads across the United States was performed by SAI [2]. From this analysis, it appeared that three cities could reasonably characterize the types of climates found throughout the country. Next, each TMY site was examined for its existing and potential market for solar systems. A large regional population and many building starts were assumed to represent the market. The final choices for residential analyses were Fort Worth, Tex; Washington, D.C.; and Madison, Wis.

Building Descriptions

A typical single-family residence for each of the three locations was selected for analysis. In each location, the chosen house is defined by a set of building characteristics that dominate for that locale. Building characteristics are described briefly for each representative house.

Thermal insulation characteristics were obtained by using ASHRAE 90-75 [11] and Ref. 12. The values developed are based on an economic analysis recommended by the National Association of Home Builders that states a payback period of seven years will result if these insulation guidelines are followed. This procedure specifies houses that are well designed and exceed the minimum guidelines of ASHRAE 90-75. It is assumed that the major axis of the house lies east-west; thus, the structure lends itself to active solar systems. No assumptions are made as to whether the front or rear of the house has the desired southern exposure.

Following is a brief description of the characteristics of each house. More detailed descriptions may be found in Ref. 1.

The Madison house is a 158 m^2 (1700 ft^2), one-story, wood frame Rambler. It has a basement, three bedrooms, and a two-car garage. Walls have 3.35 m^2-°C/W (R-19) insulation, the roof has 5.28 m^2-°C/W (R-30), and all windows are triple glazed.

A one-story, 167 m^2 (1800 ft^2), wood frame, brick-veneered Ranch house typifies Fort Worth. Built on a slab foundation, it has three bedrooms and a two-car garage. The roof has 3.35 m^2-°C/W (R-19) insu-

lation while the walls have 1.94 m^2-°C/W (R-11); windows are double glazed.

The typical house for Washington, D.C., is a 161 m^2 (1735 ft^2) two-story wood frame Colonial with three bedrooms, a two-car garage, and a basement. All windows are double glazed; the walls and roof are insulated with 3.35 m^2-°C/W (R-19) and 5.28 m^2-°C/W (R-30), respectively.

Load Calculation

Maximum accuracy is obtained when building load calculations and Heating, Ventilating, and Air-Conditioning (HVAC) system performance calculations proceed simultaneously in an hourly system simulation, since the effect of the varying interior and environmental conditions on the conditioned space can be accounted for. However, hourly HVAC system and load simulations are prohibitively expensive for system studies in which many sensitivities are of interest unless a simplified load model is available. The ASHRAE transfer function technique [9] is a compromise between very detailed and very simple load calculations; the method approximates load time-lags due to building capacitance.

The ASHRAE transfer function technique has been employed in Version 9.2 of TRNSYS [10], which provides separate roof, wall, and room modules. These three modules were combined into one TRNSYS component module for easier application and for a reduction in computer time over the TRNSYS load package. A listing of the load module, the necessary standard inputs for each location, and a more comprehensive description of the load model theory may be found in Ref. 1.

LIGHT COMMERCIAL SOLAR COOLING

Current federal emphasis on and support of the 25-ton cooling system development prompted the definition of a light commercial application for analysis of solar cooling systems [13].

A small office building (nominal 25-ton cooling load), similar to those found in many office parks across the United States was chosen to represent the standard, bench-mark light commercial building. Locations potentially appropriate for solar cooling of commercial buildings were also selected. Finally, loads for each location were computed and stored on magnetic tape.

This section details the location selection, the building specifications, and the method of load calculation for light commercial applications.

Locations for Light Commercial Solar Cooling Analyses

It was assumed that potential markets for light commercial cooling systems could be characterized by a large number of commercial construction starts and by a fairly warm climate.

An evaluation of the SOLMET sites with respect to the climate and new construction activity constraints performed by SAI [2] resulted in the selection of four locations for light commercial cooling studies. They are: Phoenix, Ariz.; Washington, D.C.; Miami, Fla.; and Fort Worth, Tex.

Building Description

The commercial building described here, a small office building, represents what might be typical for commercial solar energy system applications in the future. A well-constructed building that has a nominal design cooling load of 25 tons, the small office building meets or exceeds ASHRAE 90-75 standards. Additional energy conservation features such as low total lighting levels and a minimum ventilation rate are incorporated.

The following specifications were developed for a building in the Washington, D.C., area. However, they are adequate to describe a typical small office building in any other geographical location. Only the gross air circulation requires a different value for each location. More details may be found in Ref. 1.

Building Type:	A typical, small, one-story office building with brick veneer and a flat roof; no overhangs or protuberances for shading.
Dimension:	A rectangle 43.9 m (144 ft) long, 21.3 m (70 ft) wide, and 3.7 m (12 ft) high; gross area, 936.5 m^2 (10,080 ft^2); the net conditioned area, 874.5 m^2 (9,413 ft^2).
Orientation:	The long axis of the building lies east-west; a single entry door is located on the north wall.
HVAC System:	A variable air volume system supplies each zone with the conditioned air necessary to meet the load; a general return plenum is above the ceiling tile; one central plant serves all zones; enthalpy control is used [14].
Climate Control:	For the cooling season, each zone thermostat is set at 26.1°C (79°F) on and 25°C (77°F) off; system is turned off rather than set back when unoccupied.
Opaque Envelope:	Walls have a 0.1 m (4 in) brick facing over 0.15 m (6 in) concrete block. A 0.01 m (0.5 in) space and 0.04 m (1.5 in) of rigid insulation are sandwiched in between. The gross U value is 545 W/m^2-°C (0.096 Btu/ft^2-°F-hr).

The roof is a metal deck covered by 0.05 m (2 in.) of rigid insulation underneath standard built-up roofing and gravel; gross U value is 488 W/m^2-°C (0.086 Btu/ft^2-°F-hr).

The floor consists of carpeting over a concrete slab on grade; a 0.05 m (2 in.) layer of polyurethane insulation surrounds the perimeter.

Windows: All windows are double glazed, solar bronze, with a U value of 3.55 W/m^2-°C (0.625 Btu/ft^2-°F-hr) and an effective solar transmissivity of 0.25. The north wall has a window area of 29.3 m^2 (315 ft^2), the south wall has a window area of 25.8 m^2 (278 ft^2), and the east and west walls each have a window area of 3.0 m^2 (32 ft^2).

Commercial Load Calculation

Calculating the hourly load for a commercial building is complicated. For residential buildings and buildings with only a few zones, loads may be calculated so that an interaction with the system is possible. Calculating such interactions for a commercial building would require a very complex computer model and a prohibitively large amount of computer resources. A complex model is required because the building is subdivided into many zones. Each zone has its own space conditioning requirements that are met by an appropriate air handling system. These systems merge at a plant that provides the necessary energy for the building. This section describes a method for analyzing solar and conventional energy systems by which commercial loads may be approximated, stored on a tape, and input hourly to an executive computer model.

Recommended for use in commercial building analyses, load tapes for the light commercial building examined here were developed with the aid of a comprehensive computer code developed by the Army call BLAST [15]. BLAST estimates hourly space heating and cooling requirements, hourly performance of fan systems, conventional heating and cooling plants, total plant energy, and solar energy system performance. The loads as seen by the central plant for the light commercial building were computed by BLAST, using the TMY data, building parameters, and the air handling system specifications. Load data thus processed for each city are available on magnetic tape from SERI. Heating as well as cooling loads are included on the tape so that year-long energy system simulations may be performed. Employment of commercial load data is more fully illustrated in Ref. 1.

ECONOMIC ANALYSIS

Life-cycle costing has been demonstrated to be a suitable method of analyzing the economic feasibility of solar energy systems [16,17]. Tax laws are different for residential and commercial systems; therefore, the systems must be analyzed dissimilarly with respect to property taxes, depreciation, and other economic parameters. However, both may be studied using life-cycle costing techniques, and the results may be contrasted with those of similar analyses for conventional systems to determine economic feasibility. Additionally, if several investigators are studying, for example, residential space heating systems using the inputs and methods suggested in this paper, then the results of their economic predictions may be compared to examine the relative economic feasibility of each system.

An excellent application of life-cycle costing to solar energy systems may be found in a paper by Audrey Perino of Sandia Laboratories [16].

Many parameters required as inputs in an economic analysis are difficult to predict precisely. Often, costs are dependent on location or are rapidly changing, which makes it difficult to specify a value. Table 1 contains a list of some parameters needed for an economic analysis of a solar energy system and includes suggested values for each. These values are the recommended standard assumptions and were suggested by Roger Bezdek in Ref. 17.

Table 1. SUGGESTED ECONOMIC INPUTS

	Residential	Commercial
Down payment, % of investment	20	30
Loan interest rate (%)	8.5	8.0
Discount rate (%)	10	10
Inflation rate (%)	5.0	5.0
Income tax rate (%)	30	50[a]
Borrowing period (yr)	30	25
Period of an analysis (yr)	20	20
Accounting lifetime (yr)	30	20

[a]Total, state, and federal.

As the economic picture becomes clearer, more accurate assumptions may be made when predicting the life-cycle cost of an alternative. In the interim, readers are encouraged to consider possible applications of life cycle cost to their problems.

REPORTING FORMAT

The International Energy Agency (IEA), a group established in 1974 to help resolve energy problems, has recently adopted a reporting format [18]. This

format for reporting on thermal performance of solar energy systems was prepared by U.S. and Swedish researchers as a part of an IEA task titled "Investigations of the Performance of Solar Heating and Cooling Systems." It is advantageous to adhere to the format in reporting solar system study results for two reasons. First, a common format will facilitate the comparison of systems by use of similar tables, units, and performance parameters. Second, fidelity to this format by U.S. investigators will demonstrate a willingness to cooperate internationally. This format should therefore be adhered to as strictly as possible.

CONCLUSIONS

Standardized inputs and methods for analyzing residential and commercial energy systems were presented. These recommendations help to provide continuity and comparability among solar research endeavors.

For residential systems, three locations (Fort Worth, Madison, and Washington, D.C.) were selected, based on demonstrated and potential markets for solar systems and on the need to characterize a variety of climates. TMY data should be used for these cities. It is recommended that analysts model their systems in each of these locations so that performance may be linked to regional variations in climate. Homes typical of new construction in each city were defined and descriptive parameters provided. An interactive load model developed from ASHRAE [9] algorithms and based on existing TRNSYS [10] modules was recommended.

Four commercial analysis locations were selected: Fort Worth, Washington, D.C., Miami, and Phoenix. One light office building (nominal 25-ton load) to be used in all locations was defined. Heating and cooling loads for each site were computed and stored on magnetic tape for use in system simulations. Again, analysts are encouraged to model their systems in all of the commercial locations to facilitate study comparisons.

TMY data for all three residential and four commercial locations (5 cities total; 2 cities are common to both), as well as loads for commercial analyses, are available from SERI on 9-track magnetic tape.

Users should address their requests to:

Design Tool Manager
Market Development Branch
Solar Energy Research Institute
1617 Cole Blvd.
Golden, CO 80401

ACKNOWLEDGMENTS

This paper was prepared under the Systems Analysis and Testing (SAT) Task, No. 3525.10 in the Analysis Division of the Solar Energy Research Institute (SERI) and was supported by Systems Development Division, Office of Solar Applications, DOE. Much of the groundwork for this document was performed by Science Applications, Inc. and their subcontractors. The author would like to acknowledge Chuck Bishop and L. Marty Murphy of SERI for their help and guidance.

REFERENCES

1. C. M. Leboeuf. Standard Assumptions and Methods for Solar Heating and Cooling Systems Analysis. Preliminary Report, SERI/TR-31-402. Golden, CO: Solar Eneregy Research Institute; January 1980.

2. P. J. Hughes and J. H. Morehouse. Comparison of Solar Heat Pump Systems to Conventional Methods for Residential Heating, Cooling, and Water Heating. McLean, VA: Science Applications, Inc., for DOE; April 1979.

3. P. L. Versteegen and J. H. Morehouse. A Thermal and Economic Comparative Analysis of Absorption and Rankine Solar Cooling Systems for Commercial Buildings. McLean, VA: Science Applications, Inc.; May 1979.

4. National Climatic Center. SOLMET User's Manual. Vol. I. Asheville, NC: 1977.

5. I. J. Hall et al. "Generation of Typical Meteorological Years for 26 SOLMET Stations." Proceedings of the 1978 Annual Meeting of AS/ISES; Denver, CO. Albuquerque, N.M.: Sandia Lab.; 1978.

6. E. Stamper. "Weather Data." ASHRAE Journal, p. 47 (February 1977).

7. Aerospace Corporation for DOE. Performance, Value and Cost of Solar Thermal Electric Receiver Plants Outside of the Southwest. Los Angeles, CA: Aerospace Corp.; May 1978.

8. J. E. Hay. "Measurement and Modeling of Shortwave Radiation on Inclined Surfaces." 3rd Conference on Atmospheric Radiation; Boston, MA: American Meteorological Society; 1978.

9. American Society of Heating, Refrigerating, and Air Conditioning Engineers. ASHRAE Handbook of Fundamentals. New York: ASHRAE;

10. "TRNSYS--A Transient Simulation Program." TRNSYS User's Manual. Report No. 38 (Version 9.2). Madison, WI: University of Wisconsin Engineering Experiment Station; October 1977.

11. Energy Conservation in New Building Design. ASHRAE Standard 90-75. New York: ASHRAE; 1975.

12. U.S. Department of Commerce, Bureau of the Census. Characteristics of New Housing. C-25-77-13. 1979.

13. U. S. Department of Energy. National Program Plan for the Solar Cooling of Buildings. Draft Report. February 1979.

14. American Society of Heating, Refrigerating and Air Conditioning Engineers. ASHRAE Systems Handbook. New York: ASHRAE; 1973.

15. BLAST--The Building Loads Analysis and System Thermodynamics Program Users Manual. CERL Technical Report. Vol I. E153. Washington, DC; June 1979.

16. A. M. Perino. A Methodology for Determining the Economic Feasibility of Residential or Commercial Solar Energy Systems. SAND 78-0931. Albuquerque, NM: Sandia Labs.; 1979.

17. R. H. Bezdek. An Analysis of the Current Economic Feasibility of Solar Water and Space Heating. Washington, DC: U. S. Department of Energy; January 1978.

18. International Energy Agency. Reporting Format for Thermal Performance of Solar Heating and Cooling Systems in Buildings. Draft. IEA; May 1979.

Session VIIB

Anthony Eden
Solar Energy Research Institute
Chairperson

SYSTEMS SIMULATION IV

Dup

OPTIMIZATION OF SOLAR ASSISTED HEAT PUMP SYSTEMS VIA A SIMPLE ANALYTIC APPROACH

John W. Andrews
Brookhaven National Laboratory
Building 701
Upton, New York
11973 USA

ABSTRACT

An analytic method for calculating the optimum operating temperature of the collector/storage subsystem in a solar assisted heat pump system is presented. A tradeoff exists between rising heat pump coefficient of performance and falling collector efficiency as this temperature is increased, resulting in an optimum temperature whose value increases with increasing efficiency of the auxiliary energy source. Electric resistance is shown to be a poor backup to such systems. A number of options for thermally coupling the system to the ground are analyzed and compared.

INTRODUCTION

Solar assisted heat pump (SAHP) systems have been studied extensively. Most of these studies [1-4] have simulated, on an hour-by-hour basis, several plausible system configurations involving solar collectors and heat pumps. All of the referenced studies assumed that electric resistance was the auxiliary heat source. Although much has been learned from these studies, it has been difficult to evaluate the sensitivity of their results to all of the assumptions that went into them. The need was seen for an approach which would be simple enough so that all of the assumptions could be stated concisely. Also, the question has been asked [5,6]: What is the optimum temperature at which solar energy should be collected and stored in SAHP systems? Such an optimum may be produced by the tradeoff between increasing heat pump coefficient of performance (COP) and decreasing collector efficiency with increasing temperature. This paper describes a method for answering the above question by means of closed-form algebraic solutions. Fundamental to the present approach is the assumption that, within acceptable limits of accuracy, the storage temperature of the solar system is a constant throughout each of the time periods (months in this paper) into which the simulation is divided. Of course, this will never be strictly true; however, in computer simulations of SAHP systems, the storage temperature during the period December through February, when most of the heating load occurs, remained most of the time within 10°C of the set minimum value. In any event, the outcome of the analysis will be an optimum storage temperature for each month; any excursions from this value will represent suboptimal operation.

COMPONENT MODELING

Collector performance is modeled via the usual Hottel-Whillier straight-line graph of efficiency vs. $(T-T_a)/I$. The collector inlet temperature is here assumed to equal the storage temperature T. Collector efficiency is given by

$$\eta = \eta_o \left(1 - \frac{1}{\chi_o} \cdot \frac{T-T_a}{I}\right) \qquad (1)$$

where T_a is the ambient temperature, I the insolation rate, and η_o and χ_o the vertical and horizontal intercepts of the efficiency curve.

The intensity of the insolation striking the collector during daylight hours is taken to be a random variable with a constant probability density for insolation values between 0 and I_{max}. That portion of received insolation falling with intensity greater than $(T-T_a)/\chi_o$ can be partially collected with efficiency increasing with increasing I. The lower-intensity insolation is lost completely. It can be shown that under these assumptions the total energy that can be collected at temperature T is given by

$$E_c = SA\eta_o \left(\frac{T_m-T}{T_m-T_a}\right)^2 \qquad (2)$$

where S is the received insolation on a unit area of collector, A is the collector area, and T_m is the maximum stagnation temperature $T_a + I_{max}\chi_o$.

The simple formula given in Eq. 2 is not intended to be exact, but in order for it to be useful it should provide results which are reasonably close to those given by more precise methods. I have therefore used Eq. 2 to calculate the solar fractions for the case given in the original f-Chart paper [7], assuming a collector operating temperature of 40°C, and I_{max} = 3410 kJ/m^2-hr. This comparison is shown in columns 1-3 and 5-12 of Table 1. On a monthly basis Eq. 2 tends to give lower solar fractions than f-Chart at low collector areas and higher estimates at high collector areas. This trend is also seen in the yearly totals, with

*Work performed under the auspices of the U.S. Department of Energy, Systems Development Division, Office of Solar Applications.

Table 1.

COMPARISON OF SOLAR FRACTIONS (f) OBTAINED USING EQ. 2 WITH THOSE OF f-CHART (f*). LOCATION: MADISON, WISCONSIN

Month	Heating & Hot Water Load (GJ)	Insolation on Tilted Collector (GJ/m^2)	Average Ambient Temperature (°C)	Far-Field Temperature (Ground Coupling) (°C)	A = 20m^2		A = 40m^2		A = 80m^2		A = 120m^2	
					f	f*	f	f*	f	f*	f	f*
Jan.	28.62	0.382	-8.1	3.3	0.08	0.11	0.16	0.23	0.32	0.42	0.48	0.56
Feb.	24.83	0.405	-6.0	0.8	0.13	0.15	0.26	0.30	0.51	0.53	0.77	0.69
Mar.	22.09	0.557	-0.2	0.1	0.18	0.25	0.36	0.47	0.72	0.76	1.00	0.91
Apr.	13.06	0.512	7.9	1.6	0.33	0.39	0.66	0.67	1.00	0.94	1.00	1.00
May	7.53	0.555	13.8	4.9	0.68	0.67	1.00	0.96	1.00	1.00	1.00	1.00
June	3.70	0.588	19.4	9.2	1.00	0.95	1.00	1.00	1.00	1.00	1.00	1.00
July	2.36	0.620	21.8	13.2	1.00	1.00	1.00	1.00	1.00	1.00	1.00	1.00
Aug.	2.63	0.600	20.9	15.9	1.00	1.00	1.00	1.00	1.00	1.00	1.00	1.00
Sept.	5.01	0.584	16.0	16.6	1.00	0.88	1.00	1.00	1.00	1.00	1.00	1.00
Oct.	10.51	0.522	10.3	15.0	0.47	0.47	0.86	0.77	1.00	1.00	1.00	1.00
Nov.	18.71	0.330	1.9	11.6	0.13	0.15	0.26	0.29	0.53	0.51	0.79	0.66
Dec.	26.02	0.357	-5.2	7.4	0.09	0.11	0.18	0.23	0.35	0.42	0.53	0.57
Year	165.07				0.25	0.28	0.41	0.44	0.62	0.65	0.78	0.76

Weather and load data (Columns 1-3 and f-Chart solar fractions)were taken from Ref. 7. Typical far-field temperatures (Column 4) were calculated for Madison using Ref. 12.

however closer agreement between the two at all collector areas. Because of its simplicity, Eq. 2 lends itself well to use in an analytical model of a more complicated system.

The coefficient of performance COP_h of the solar source heat pump is modeled as a constant fraction γ of Carnot [4]:

$$COP_h = \frac{\gamma T_c}{T_c - T} \quad . \tag{3}$$

The heat pump source temperature is assumed equal to the storage temperature T. In practice, a known curve of heat pump COP vs. source temperature can be fitted to this equation, with γ and T_c serving as parameters for the fit. This approach is taken here, with $\gamma = 0.596$ and $T_c = 345$ °K (based on data from Ref. 5). Because of the form of this equation, all temperatures must be expressed in absolute units in the work that follows.

In contrast to most computer simulations of SAHP systems to date, the auxiliary or backup energy source is not assumed at the outset to be electric resistance, with a COP of 1. Instead, the COP of the auxiliary (COP_x) is left as a parameter. We assume for now that the auxiliary COP is a constant independent of the extent to which it is used. Later, when ground coupling is considered, this assumption will have to be modified.

OPTIMUM OPERATING TEMPERATURE

It is now possible to consider the flows of energy through the system. The energy E_s delivered to the load by the solar source heat pump is equal to the sum of the collected solar energy plus the purchased energy needed to operate the heat pump, which is added to the heat delivered to the load:

$$E_s = \frac{COP_h}{COP_h - 1} E_c$$

$$= \frac{\gamma E_o (T_m - T)^2}{T_c (T - T_d)} \tag{4}$$

where $E_o = SA\eta_o T_c^2/(T_m - T_a)^2$, and $T_d = (1-\gamma) T_c$.

The purchased energy required is given by

$$E_{ps} = \frac{E_s}{COP_h}$$

$$= \frac{E_o (T_c - T)(T_m - T)^2}{T_c^2 (T - T_d)} \quad . \tag{5}$$

It is assumed here that the energy E_s delivered by the solar source heat pump does not exceed the load E_ℓ . In this case the auxiliary energy requirement is given by

$$E_x = E_\ell - E_s \quad . \tag{6}$$

The purchased energy required to operate the auxiliary is given by

$$E_{px} = \frac{E_x}{COP_x}$$

$$= \frac{E_\ell}{COP_x} - \frac{\gamma E_o (T_m - T)^2}{COP_x T_c (T - T_d)} \quad . \tag{7}$$

The total purchased energy $E_p = E_{ps} + E_{px}$ is to be minimized as a function of the solar system operating temperature by setting dE_p/dT equal to zero and solving for T. When this is done, the optimum operating temperature T_{op} is obtained:

$$T_{op} = \frac{T_r + 3T_d + \sqrt{(T_r - T_d)(T_r + 8T_m - 9T_d)}}{4} \quad (8)$$

where $T_r = (1-\gamma/COP_x)T_c$.

One should remember that this result depends upon the assumption that the energy E_s delivered by the solar source heat pump does not exceed the load E_ℓ . This requirement defines a domain of reasonable storage temperatures, the lower limit of which is the temperature T_{ox} for which enough solar energy is collected that no auxiliary is needed. Below this temperature, the theory presented above no longer corresponds to reality, since it would require a negative contribution from the auxiliary. But there can be no point in going below this temperature in practice, since heat pump performance becomes poorer and there is no compensating reduction in auxiliary usage. By setting E_s equal to E_ℓ and solving for T, the no-auxiliary storage temperature T_{ox} is obtained:

$$T_{ox} = T_m + \frac{E_\ell T_c - \sqrt{4\gamma E_o E_\ell T_c (T_m - T_d) + E_\ell^2 T_c^2}}{2\gamma E_o} \quad (9)$$

If $T_{op} > T_{ox}$, then the assumptions used in deriving T_{op} are valid and T_{op} is the optimum storage temperature. If $T_{op} < T_{ox}$, then T_{op} is unphysical and T_{ox} is the optimum. In any case, then, the optimum storage temperature T_o is given by

$$T_o = \max\left\{T_{op}, T_{ox}\right\} \quad (10)$$

A number of conclusions can be drawn from this analysis. First, if electric resistance auxiliary is used ($COP_x = 1$), then $T_r = T_d$ and

$$\frac{dEp}{dT} = \frac{2E_o(T_m - T)}{T_c^2} \quad . \quad (11)$$

The right side of Eq. 11 is positive for all $T < T_m$; therefore the purchased energy required decreases monotonically with decreasing T and there can be no optimum $T_{op} > T_{ox}$. In this case T_{ox} is always the optimum temperature, which means that the system should be operated at a temperature low enough to make resistance backup unnecessary. For low collector areas T_{ox} can be well below ambient, possibly resulting in system performance poorer than that of an air-to-air heat pump. But it does lead to the conclusion that resistance heat is a poor backup to such a system, since if it needs to be used it implies suboptimal system operation.

If a backup with a COP greater than one is used, then optimum operating temperatures can be obtained which require the use of some backup. Such an auxiliary could be provided, for example, by a separate, freezable tank of water or other phase-change material (a mini-ACES system), or, on a primary energy basis, by a fossil-fueled burner. If such an auxiliary is used, one can obtain the optimum storage temperature for the SAHP system for each month, and the amount of purchased energy required to operate the system. One can also calculate the energy required to meet the entire load with the auxiliary only, without the SAHP. For some types of auxiliary (e.g. the ice-maker) this latter strategy would involve added capital and operating costs, whereas for others (e.g. the fuel-fired burner) there would be no additional capital costs. The difference between these two numbers is the energy saved by the SAHP system. These energy savings are presented in Fig. 1, for the weather and load data of Table 1, as functions of collector area, for systems having auxiliaries with COP's of 2, 2.4, and 3. Collectors having vertical intercepts of 0.7 and horizontal intercepts of 0.02, 0.03, and 0.04 °C-m^2-hr/kJ are used. As the efficiency of the auxiliary increases, the energy which can be saved by the SAHP system decreases relative to use of the auxiliary only. There are two reasons for this. First, with a more efficient auxiliary there is simply less room for conservation since the auxiliary is now by itself relatively energy efficient. Second, the SAHP, in order to compete with the auxiliary, must operate at higher source temperatures in order to provide COP's that are attractive relative to the auxiliary. This can be seen by examining in Fig. 1 the January (lowest) optimum storage temperatures for each case. Operating at higher source and collection temperatures, the SAHP system will now collect and use less solar energy than before. In evaluating these results, it is necessary to keep in mind the assumption that was made, that the auxiliary COP was independent of the extent to which it is used. A more efficient auxiliary which uses electricity as the source of purchased energy must use a heat pump in connection with an alternate source of low-grade heat, as from

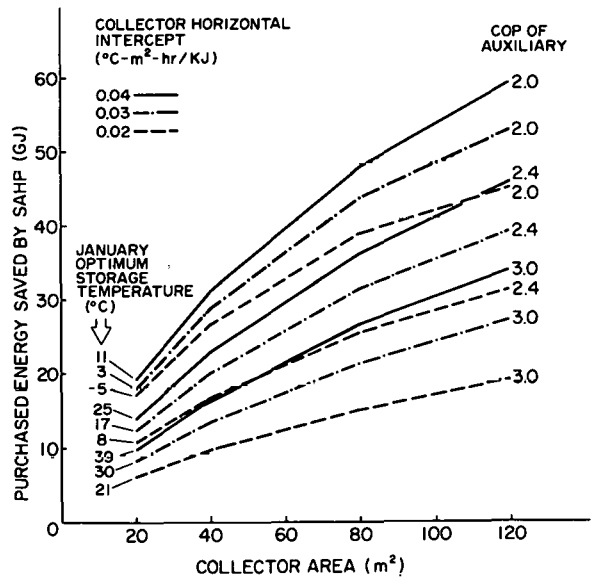

Fig. 1. Purchased Energy Saved by SAHP Relative to Use of Auxiliary Only, without SAHP

the latent heat of fusion of ice or from the ground. Such auxiliaries will in general not satisfy the above assumption of constant COP as a function of utilization, but will perform better when used less or, alternatively, will require greater initial capital cost to provide the same performance at higher levels of utilization. One possible alternate heat source, the ground, is now examined in greater detail.

GROUND COUPLING

The use of the ground as a source of low-grade heat as input to a heat pump for space and water heating is under intensive investigation in a number of countries [8-10]. A number of options for combining the use of ground-source and solar-source energy have been identified. These are:

1. Use of the ground as a long-term solar storage medium, to allow excess solar heat collected in the summer and fall to be partially recovered in the winter months.

2-4. Storage of solar heat in a separate tank, with ground heat processed to the load via the heat pump when solar heat is unavilable. At least three substrategies exist:

2. Solar heat delivered to the load directly when the tank temperature is above a set minimum (here taken to be 40°C), and processed through the heat pump when the tank temperature is less than this.

3. Solar heat delivered to the load directly only. Ground-coupled auxiliary is used when the tank temperature drops to 40°C.

4. Solar heat used to preheat the return air from the load, with use of the ground-source heat pump to raise the air temperature to the value required for comfort [3]. In this strategy the tank temperature can drop below 40°C, but must remain above that of the heated space (20°C).

5. Use of passive solar design concepts, with the ground-coupled heat pump providing hot water and auxiliary space heating.

Although the present study concentrates on heating, it should be remembered that in each of these concepts the heat pump can also provide sensible cooling and/or dehumidification, where required. The following analysis begins with option 2, and is extended to options 3 and 4. Treatment of options 1 and 5 remains for future work. Other means of combining solar with ground energy are possible, such as the burning of wood backed up by the ground-source heat pump or the use of photovoltaics to drive the ground-source heat pump. These are not considered here.

System Optimization for Option 2

In order to treat the case where ground-source heat is used as a backup to a solar-source heat pump, it is assumed that the ability of the ground to deliver heat is proportional to the difference between the temperature T_x at which heat is extracted and the temperature T_f of undisturbed ground at the same depth at the same time of the year, or far-field temperature:

$$E_g = (T_f - T_x)\, b \tag{12}$$

The constant b is a product of the inherent heat transfer capability of the ground coupling device, in kJ/hr-°C-m for linear pipes or kJ/hr-°C-m^2 for tanks or planar devices; the size of the device in linear or square meters; and the number of hours in the time period, e.g. 720 hr/month. The COP of the heat pump using ground-source energy is assumed to follow the same function of source temperature as when using solar-source energy:

$$COP_x = \frac{E_x}{E_{px}} = \frac{\gamma \bar{T}_c}{\bar{T}_c - T_x} \tag{13}$$

Two energy balance equations can be written, the one on the ground-source heat pump given by

$$E_x = E_g + E_{px} \tag{14}$$

and the one on the load given by Eq. 6 as before.

Solving these equations for E_{px} (eliminating E_x, E_g, and T_x) one obtains

$$E_{px} = \frac{(E_\ell - E_s)\,(E_\ell - E_s + bT_c - bT_f)}{b\gamma T_c + E_\ell - E_s} \tag{15}$$

where E_s is given as a function of T by Eq. 4. E_{px} is then added to E_{ps} to obtain E_p, the function to be minimized. The functional relationship between E_p and T is now complicated enough that attempting to find the minimum in the usual way results in an intractable fourth-degree equation. Instead, the minimum was found for each case by means of a computer. The COP vs. T relationship used (including parasitic power requirements) is shown in Fig. 2, which assumes processing of solar heat through the heat pump below 40°C [5] and direct heating above [11]. For the latter region of temperature, the above equations were modified to take into account the linear relationship of direct-heating COP to temperature T.

The relationship of solar collector area to ground-coupled field heat-transfer capacity, for systems optimized as to storage temperature on a monthly basis, is shown by the solid curves in Figs. 3-5 for collectors having horizontal intercepts χ_o equal to 0.02, 0.03, and 0.04 °C-m^2-hr/kJ, respectively. The weather and load data of Table 1 were used. Representative far-field temperatures were calculated at 1.5m depth at the Madison location [12]. Each curve is plotted for a constant fraction F of nonpurchased (solar and/or ground) energy. The numbers along the curve are the optimum operating temperatures for solar storage, in January, at that point on the curve.

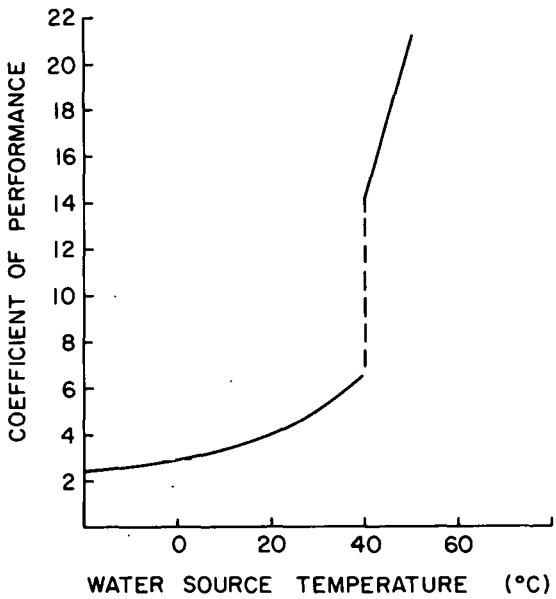

Fig. 2. System COP vs. Water Source Temperature: T<40°C, Heat Pump; T>40°C, Direct Heating.

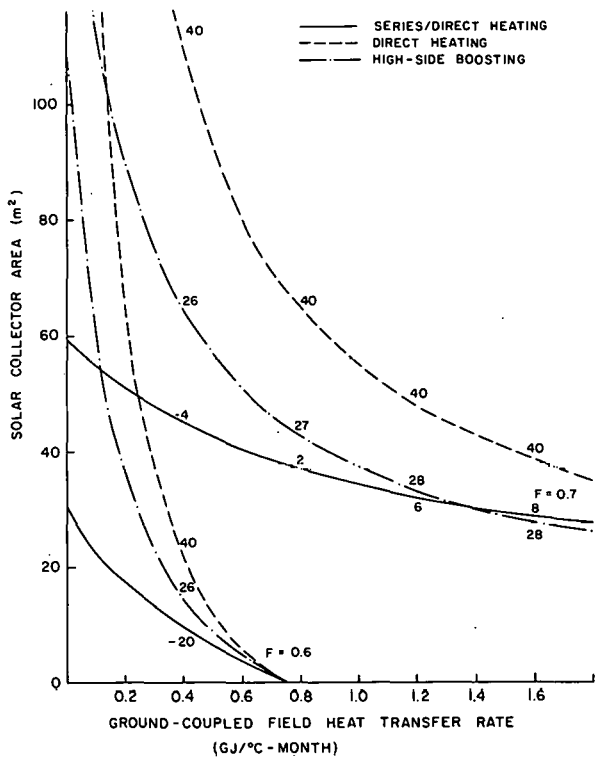

Fig. 3. Solar Collector Areas and Ground-Coupled Field Sizes Needed to Provide a Fraction F of Non-Purchased Energy. Horizontal Intercept X_o of Collector Efficiency Curve = 0.02°C-m^2-hr/kJ. Numbers on Lines Are Optimum Source Temperatures in January.

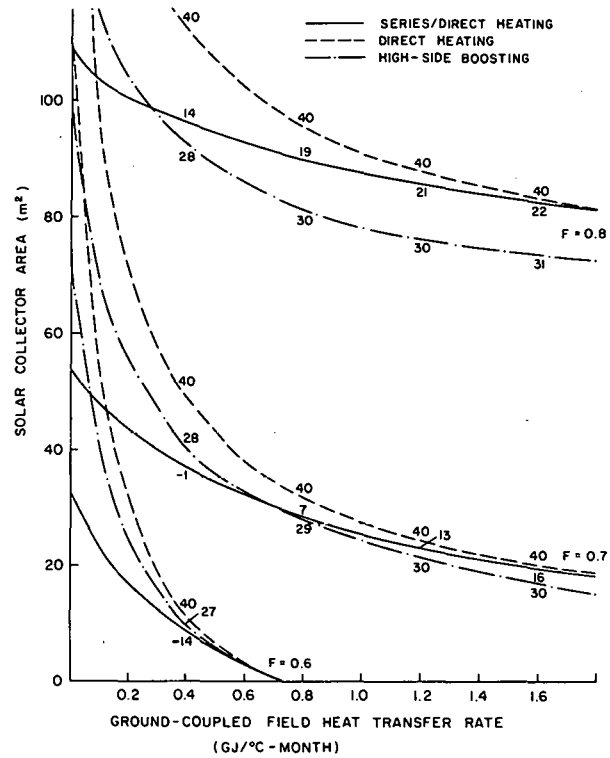

Fig. 4. Solar Collector Areas and Ground-Coupled Field Sizes Needed to Provide a Fraction F of Non-purchased Energy, X_o = 0.03°C-m^2-hr/kJ.

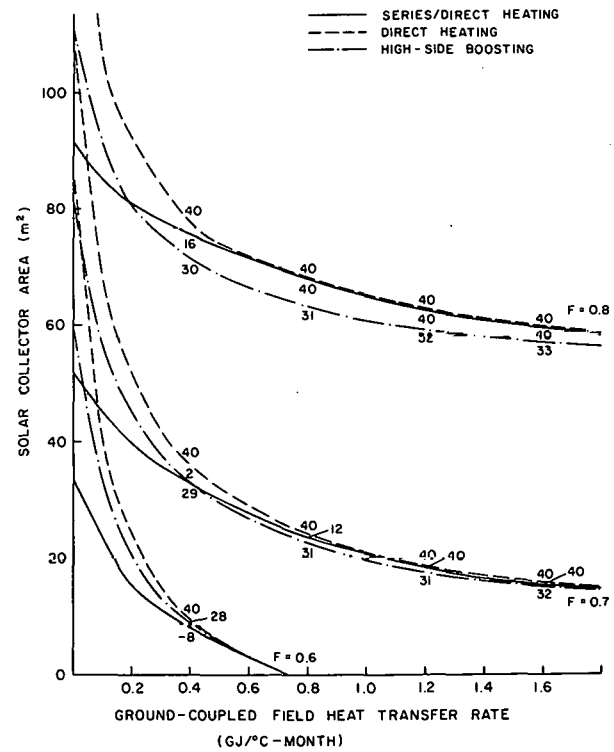

Fig. 5. Solar Collector Areas and Ground-Coupled Field Sizes Needed to Provide a Fraction F of Non-Purchased Energy, X_o = 0.04°C-m^2-hr/kJ.

Economic Optimum

The tradeoff between solar collector area and ground coupling can be represented by curves of constant cost, which are straight lines whose negative slope is equal to the ratio of unit cost of ground coupling to that of collector area. From a family of such lines of equal slope, select the one which is tangent to the curve of constant system performance. The economic optimum, for a preselected fraction of nonpurchased energy, for systems having both solar collectors and ground coupling, is the point of tangency. Bose [9a] has quoted an installed cost of $2 to $3/ft ($6.50 to $10/m) for a buried-pipe system which provides sustainable heat rates in excess of 2 Btu/hr-°F-ft pipe (12.5 kJ/hr-°C-m pipe). If collectors are assumed to cost $100/m^2 or more installed, optimum ground-coupled field capacities of approximately 1.0 GJ/°C-month or more are obtained. This is important to the discussion which follows.

Options 3 and 4

The analysis was extended to include option 3 by restricting the computer search of solar source temperatures to a domain above 40°C. Curves of constant system performance for systems optimized under these conditions are shown by the dashed lines in Figs. 3-5. Since the set of possible operating conditions under option 3 is a proper subset of those available to option 2, the option 3 curves will always lie at or above those of option 2. For option 3 the January optimum operating temperature was always 40°C, the minimum available.

An approximate treatment of option 4 was made by allowing the search for the optimum temperature under the direct heating mode to extend below 40°C, with a COP as a function of temperature which follows the same straight line as above 40°C, intercepting the horizontal axis at 20°C (slope 0.7/°C). The results of this optimization procedure are shown by the dash-dot lines of Figs. 3-5.

Results for Ground Coupling

If we focus our attention towards the right sides of Figs. 3-5, where in each case the economic optimum probably lies, the following results can be noted. For the two better collectors (Figs. 4 and 5), options 2 and 3 gave results which were not very different. Since option 3 is operationally simpler than option 2, it is to be preferred in these cases. Option 4 gives somewhat better results than the others, but the difference is not great except for F=0.08, χ_o = 0.03 (Fig. 4). For the collector having the lowest horizontal intercept (Fig. 3), option 2 requires significantly less collector area than option 3. In this case, option 4 is about equivalent in performance to option 2. Option 4, while more complex from a controls standpoint than option 3, is about as simple as option 3 as far as hardware is concerned, and is therefore probably to be preferred over option 2 in this case.

CONCLUSIONS

The following conclusions are drawn: 1) Electric resistance is a poor backup to a SAHP system. 2) As the COP of the auxiliary increases, the optimum storage temperature of the SAHP system increases, assuming that the auxiliary COP is independent of the extent to which it is used. 3) When ground coupling is used as a backup to a SAHP system, and solar energy is collected in a separate tank, it does not appear advantageous to process solar-derived heat through the heat pump. This conclusion does not apply to the case where solar energy is stored in the ground.

REFERENCES

1. T.L. Freeman, J.W. Mitchell, and T.E. Audit, Performance of combined solar heat pump systems, Solar Energy 22, 125-135 (1979).
2. P.J. Hughes and J.H. Morehouse, Comparison of solar heat pump systems to conventional methods for residential heating, cooling, and water heating, Science Applications Inc., McLean Virginia, Report 80-906-WA (1979).
3. B.C. Hwang and W.F. Bessler, Economics of solar assisted heat pump systems for residential use, International Solar Energy Society International Congress, Atlanta (1979).
4. W. Kahan and R.C. Estes, Optimization and comparison strategies for solar energy systems, Am. Soc. Mech. Eng. Pub. 79-WA/SOL-26 (1979).
5. E.A. Kush, Performance of heat pumps at elevated evaporating temperatures - with application to solar input, ASME Pub. 79-WA/SOL-19 (1979).
6. P. Vercaemert et al., A simplified procedure for performance of solar systems with heat pumps, ASME Pub. 79-WA/SOL-23 (1979).
7. S.A. Klein, W.A. Beckman, and J.A. Duffie, A design procedure for solar heating systems, Solar Energy 18, 123-4 (1975).
8. P. Metz, Experimental results from the solar ground coupling research facility at Brookhaven National Laboratory, International Solar Energy Society International Congress, Atlanta (1979).
9. J.E. Bose, Design and field testing of solar assisted earth coils, Annual Report, U.S. Dept. of Energy Contract EM-78-S-01-4257, Oklahoma State University (1979); a, p. 18.
10. Many papers on ground coupling are collected in the Proceedings of the Nordic Symposium on Earth Heat Pump Systems, Chalmers University of Technology, Göteborg, Sweden, October 1979.
11. W. Dollars et al., Development of marketable solar assisted heat pumps - residential design review, Lennox Industries Inc., Carrolton Texas, p. 1-3 (1978). Report prepared under U.S. Dept. of Energy contract EG-78-C-03-1720.
12. K. Labs, Underground building climate, Solar Age 4, No. 10, pp. 44-50 (October 1979).

SENSITIVITY ANALYSIS OF SOLAR ASSISTED HEAT PUMP SYSTEMS

Nadine M. White
Jeffrey H. Morehouse
Patrick J. Hughes
Science Applications, Inc.
8400 Westpark Drive
McLean, Virginia 22102

Theodore D. Swanson
Mueller Associates, Inc.
1900 Sulphur Spring Road
Baltimore, Maryland 21227

ABSTRACT

Space heating systems which combine the use of solar energy with an electric heat pump have been proposed as a practical approach to the cost effective utilization of solar energy. Numerous studies have been made comparing the performance of series type solar assisted heat pump (SAHP) systems, parallel type SAHP systems, stand-alone heat pumps and conventional fossil fired alternatives. Through utilization of previously developed thermal and economic models, areas for possible cost reduction and/or performance improvement in SAHP systems are identified. Major system components evaluated include collectors, heat pump, storage, heat exchangers, and controls. Variations in many of the parametric values of each of these components are evaluated.

This study identifies the heat pump and solar collectors as the components with the greatest potential for technical improvement. For the heat pump, its capacity at design point, rate of change in capacity with increasing evaporator temperature, and minimum utilizable evaporator temperature are the principal parameters. For the collectors, their $\tau\alpha$ and U_L are the principal parameters. The change in system performance due to specific parametric variations is quantified. The results of variations with only one parameter are used as a basis for studies involving multiple parametric variations. Costs associated with each change are also estimated. This permits computation of life-cycle costs for each alternative system design. The result of this work will be the identification of the most optimistic, but realistic, future SAHP designs.

1.0 INTRODUCTION

There have been many simulation studies comparing solar heat pump systems with each other, with stand-alone heat pumps and with conventional systems. This analysis differs from other studies in that it is a systematic variation of major parameters for both series and parallel solar heat pump systems and stand-alone heat pumps. In addition, these variations are compared in several different geographic locations which allow estimates of climatic effects to be included.

1.1 Objectives and Scope

The purpose of this study is to provide thermal and economic information concerning the major parameters affecting solar assisted heat pump systems. This study concentrates on the two systems shown in Figure 1, a liquid-based series and a liquid-based parallel system.

The series system includes a liquid collector, a series connected solar heat pump system for heating and cooling, electric resistance backup heating and a separate solar domestic hot water heating system with electric backup (Figure 1-a). The (parallel) system has a liquid-based solar space and water heating system in parallel with a heat pump for backup space heating and for cooling. In addition, there is electric resistance backup space and water heating (Figure 1-b). Water heating was included in these systems since it is the most competitive of residential solar applications; thus, a solar space heating and cooling system would be expected to provide water heating as well.

1.2 Approach, Modeling and Sizing Considerations

System comparisons were made for three locations: Washington, D.C.; Fort Worth, Texas; and Madison, Wisconsin. In each location, a residence typical of single family construction in the near future was defined. Typical meteorological year (TMY) hourly data were used to characterize the weather forcing function for load and system simulation.

Before comparisons could be made, both the series and parallel systems components had to be sized in a manner appropriate for the particular system and climate. Nine base cases were defined (three for each location) based on the optimally sized configurations developed in Reference (1).

For the engineering modeling study, TRNSYS with suitably reformulated heat pump and load modules was used. This program was chosen not only for its ability to impose thermal comfort standards on the systems modeled, its thorough documentation, its flexibility and varied data output, but also to provide continuity with the other heat pump system studies which provided base case data for this particular survey. Loads were calculated simultaneously with the system simulation to allow dynamic

interaction and maximum accuracy. Parasitic energy consumptions of blowers and pumps were also included in the analysis. Details of TRNSYS and the load and heat pump modules can be found in Reference 1.

2.0 EQUIPMENT HOUSES AND LOADS

A "typical" single-family residence for each of the three locations was selected for analysis in this study. The "typical" house in each location was defined by a set of building characteristics wherein each characteristic is the dominant one of that locale. The building characteristics are generally described in Table 2-1 for the type of house chosen to represent each location.

Thermal insulation characteristics were obtained by utilizing ASHRAE 90-75. The values developed were based on an economic analysis which states that a payback period of seven years will result if these insulating guidelines are followed. This procedure specifies houses that are well designed and exceed the minimum guidelines of ASHRAE 90-75. For the purposes of this study, it was assumed that the major axis of the house is on an east-west orientation. The structure is thus assured to lend itself to active solar systems. No assumptions were made as to wheter the front or rear of the house has the desired southern exposure. Sizing of the conventional equipment for these three residences was done using standard ASHRAE procedures. Details of the resulting equipment sizes can be found in Reference (1).

The domestic hot water daily use profile was based on a four-person consumption of 300 liters (80 gallons) per day. The hourly consumption utilized is shown in Table 2-2. It should also be noted that since the hot water load is directly dependent on the temperature rise of the water from inlet to delivery, monthly average water supply temperatures were used in each location. Performance data for the heat pumps is shown in Tables 2-3 and 2-4.

3.0 THERMAL ANALYSIS

While many performance measures and energy quantities important to the overall systems used were tracked during the TRNSYS simulation, this study's focus is primarily the annual energy outputs and load quantities:

1) WHPH - work input to the heat pump in the heating mode

2) WHPC - work input to the heat pump in the cooling mode

3) QA-L - the auxiliary energy transferred to the space heating load

4) DELEP - the delta change in energy purchased (either + or -) defined by the equation:

$$\Delta E_p = (WHPH + WHPC + (QA\text{-}L))\text{Parameter Variation} - (WHPH + WHPC + (QA\text{-}L))\text{ Base Case}$$

where the base used were the collector-area-optimized systems in Reference (1).

A preliminary survey of parameters important individually to the systems considered produced the listing in Table 3-1. The range of the parameters was devised so as to use the previously simulated parameter results of Reference (1) as a starting point.

The changes involved for the heat pumps involved variations in the performance data decks but not in the TRNSYS decks. For the capacity increase, the new compressor work required was calculated by keeping the COP at each temperature level the same for both new and old capacities.

4.0 PRESENTATION AND DISCUSSION OF RESULTS

The results of the thermal and economic investigations of the various parameters are presented graphically in Figures 4-1 and 4-13.

4.1 Thermal Results

Increasing the heat pump capacity over the base case did not significantly affect the annual purchased energy for the stand-alone and parallel systems. The series system indicated a slight reduction in energy usage as seen in Figure 4-1.

The delivered air temperature parameter changes indicated greatest possibilities for energy savings in the stand-alone heat pump ($\approx 4.25 \times 10^6$ KJ/year), while the parallel system showed smaller savings (2.5×10^6 KJ/year) and the liquid series systems changes were so small as to be within the noise range of the simulation's capabilities. Results are given here only for the stand-alone heat pump and the parallel system (Figures 4.2 and 4.3).

Any change in the TAU-ALPHA product of the collector resulted in an increase of energy purchased over the base case. All results were fairly substantial, from 3-10.5 x 10^6 KJ/year. In order to get significant dollar savings at the base case U_L, TAU-ALPHA would need to drop to .6. Results are shown in Figures 4.4 and 4.5.

For changes in the collector loss coefficient U_L, results were also pretty much as expected. Decreasing the loss coefficient decreased the energy purchased in both series and parallel systems. The parallel system was particularly sensitive to this type of variation with a ΔE savings of almost 7.5 x 10^6 KJ/year for a U_L of 15 in Fort Worth. Madison data illustrated the effect of increasing the U_L, with a gain in ΔE purchased of 9.8 x 10^6 KJ/year for the parallel system. The series system was less sensitive but indicated the same trend. Results for the U_L variations are shown in Figures 4.6 and 4.7.

For the collector-to-load heat exchanger variations which increased the effectiveness, only moderate energy savings (2 to 4 x 10^5 KJ/year) for either solar assisted system was noted. Decreasing the effectiveness, however, brought a quick increase in energy usage (particularly for Madison). The most dramatic increases were for the liquid series system. This is shown in Figure 4.8; the overall quantities of energy involved, however, are small.

The "rotated" heat pump performance curve results were very interesting (see Figures 4-9 to 4-11). Both the stand-alone heat pump and parallel systems showed an increase in energy used when the performance curve was "rotated" to provide better low end performance. The series system, however, indicated an improvement in energy purchased (as much as 10.5 x 10^5 KJ/year).

The storage volume changes studies indicate an advantage for the series configuration, but not for the parallel. The energy purchased increased for the parallel system, no matter whether a smaller or larger storage ratio over the base case was employed. However, the results were generally small changes ($\lesssim 10^6$ KJ/year) and not judged significant for cost purposes. The series system provides a savings in energy when a larger storage capacity is used. The savings are moderate but combined with other possible suggested changes, could aid in generally improving series efficiency. Results for the storage volume are shown in Figures 4.12 and 4.13.

4.2 Economic Results

The cost estimate associated with the specific SAHP parametric variations identified in Table 3.1 are presented in Tables 4.1 to 4.5. These tables show the change in cost per m^2 of collector area. Table 4.6 shows the capital acquisition costs (including overhead and profit) for the optimized base system collector areas. This information is presented in two forms: total cost and cost per m^2 with fixed costs. Using data given in Table 4.6, simple addition or subtraction will give new $/$m^2$ costs for the parameter variations.

It is felt that while these cost estimates are realistic, they are somewhat optimistic in that they assume existence of a mature solar industry. All costs are in 1979 dollars and include a 25 percent overhead and profit allowance for the mechanical/electrical contractor. Were a general contractor to be involved, an additional 10 percent overhead and profit should be included. These cost estimates are based on References 2 through 6 as well as field experience of the authors.

Cost estimates are not presented for several of the possible parametric variations. There are two reasons for this. For it is felt that the (equipment) cost impact is negligible. Although there will be a cost increase for changing the heat pump capacity slope, it is felt that an accurate estimate of such costs is presently impossible. As a rough guideline, a net 10 percent cost increase for each such change would be reasonable. Accordingly, instead of attempting to predetermine the cost effectiveness of such improvements, it is hoped that this study will provide a guideline as to the justifiable cost increase associated with a given improvement. For example, were the identified change in heat pump capacity slope to result in a net system life-cycle cost reduction of $500, then the upper limit for allowable equipment cost increases could be set.

5.0 SUMMARY

The thermal and economic results of single parameter variations have been presented for stand-alone heat pumps and series and parallel heat pump systems in three geographic locations. The results were presented in the form of annual purchased energy changes and initial dollar costs associated with given parameter values.

These thermal and economic parametric results are to be combined to produce system life-cycle costs which will indicate potentially beneficial parametric areas of investigation. Additionally, the optimum "mix" of parameters will identify the "optimum" system for design purposes. Further parametric investigations underway include dual-parameter (instead of single) variations; the results of these simulations will be included in the final report submitted to SERI (BOA contract # BP-9-8150-1).

REFERENCES

1. Morehouse, J. H., and Hughes, P. J., "Comparison of Solar Heat Pump Systems to Conventional Methods for Residential Heating, Cooling, and Water Heating," Final Report, Science Applications, Inc., McLean, Va., Report # 80-906-WA, April 1979.

2. T. A. King, et al, "Cost Effectiveness and Assessment Based on Commercial Demonstration Projects," 1979 DOE Operational Results Conference.

3. T. A. King and J. B. Carlock, "Construction Cost Factors Identified in Commercial Solar Energy Systems"; 1979 DOE Regional Solar Energy Updates.

4. Means Mechanical and Electrical Cost Data.

5. Dubin-Bloom Associates, "Cost Optimization and Estimating for Four Solar Collector Designs," for BNL, March 1978.

6. J. W. Andrews and A. S. Lewandowski, "Survey of Low-Cost Solar Energy Collectors for Use in Solar Assisted Heat Pump Systems," BNL report, May 1978.

Table 2-1

General Description of Housing Types Chosen for Each Location

Characteristics	Washington, D.C./ N.Y. City Corridor	Madison, Wisconsin Area	Fort Worth, Texas Area
House Type:			
House style	Colonial	Rambler	Rancher
Type of construction	Wood frame	Wood frame	Frame, brick veneer
Foundation	Basement	Basement	Slab
Number of stories	Two	One	One
Heating system	Warm air-oil	Warm air-Gas	Warm air-electric
Cooling system	Central A/C	Central A/C	Central A/C
House Size:			
Living area	161 m^2	158 m^2	167 m^2
Outside wall area	162 m^2	109 m^2	112 m^2
Window area	28 m^2	19 m^2	20 m^2
Thermal Characteristics:			
Roof insulation	Batt, 9 in.	Batt, 9 in.	Batt, 6 in.
Wall insulation	Batt, 6 in.	Batt, 6 in.	Batt, 3 1/2 in.
Floor insulation	Batt, 3 1/2 in.	Batt, 3 1/2 in.	N/A
Window type	Double pane	Triple pane	Double pane

Table 2-2

Hourly Profile of Domestic Hot Water Consumption

Time	Consumption (Liters)	Time	Consumption (Liters)
12-1 a.m.	6.4	12-1 p.m.	10.8
1-2 a.m.	0	1-2 p.m.	15.2
2-3 a.m.	0	2-3 p.m.	8.0
3-4 a.m.	0	3-4 p.m.	7.2
4-5 a.m.	0	4-5 p.m.	6.4
5-6 a.m.	0	5-6 p.m.	11.2
6-7 a.m.	4.4	6-7 p.m.	20.4
7-8 a.m.	14.0	7-8 p.m.	34.8
8-9 a.m.	21.6	8-9 p.m.	28.8
9-10 a.m.	25.6	9-10 p.m.	20.8
10-11 a.m.	20.8	10-11 p.m.	16.4
11-12 a.m.	13.6	11-12 p.m.	13.6

Table 2-3

Heat Pump Performance Data

Liquid to Air - Liquid Series System

HEATING MODE (2-SPEED COMPRESSOR)		
Source Temperature (°F)	Dry Coil Capacity, (Btu/hr)	Watt (KW)
35	39500	3.82
45	49374	4.10
55	60347	4.32
65	71319	4.55
75	82290	4.78
85	49374	2.96
95	60347	3.02
105	71319	3.08

COOLING MODE			
Sink Temperature (°F)	Dry Coil Cooling Capacity (Btu/hr)	Break Point Temperature (°F)	Watt (KW)
72	39752	58.5	3.11
77	38642	58.5	3.18
82	37278	58.5	3.27
87	35966	58.5	3.38
92	35560	58.5	3.49
97	33064	58.5	3.58

Table 2-4

Heat Pump Performance Data

Air-to-Air - Liquid Parallel System

HEATING MODE (2-SPEED COMPRESSOR)		
Source Temperature (°F)	Dry Coil Capacity (Btu/hr)	Watt (KW)
-3	23000	4.93
7	27750	5.14
17	32900	5.35
27	37200	5.56
37	25500	2.17
47	30200	2.33
57	35000	2.50
67	39600	2.56

COOLING MODE			
Sink Temperature (°F)	Dry Coil Cooling Capacity (Btu/hr)	Break Point Temperature (°F)	Watt (KW)
85	28800	61.0	2.72
95	27300	61.5	2.89
105	25900	61.8	3.03
115	24300	61.8	3.16

Table 3-1

Single Parameter Variations and Ranges

Parameter	Stand Alone Heat Pump	Liquid Series	Liquid Parallel
Storage Volume (M^3/M^2_c)	-	.6,.4,.2,.1,.075,.05	.6,.4,.2,.1,.075,.05
Heat Exchanger Effectiveness			
1) Collector to Tank	-	.8,.7,.55	.8,.7,.55
2) Tank to Load	-	.85,.77,.65	.85,.77,.65
Control Temperature (°C) (Delivered air)	32,35,38	32,35,38	32,35,38
Collector			
$\tau\alpha$	-	.88,.8,.7,.6	.83,.7,.6
U_L (KJ/HR-°C-M^2)	-	50,40,30,20	40,30,20,15
Heat Pump			
1) Capacity Increase (BTU/HR)	0,7500,15000	0,6500,15000	0,7500,15000
2) Capacity Slope Change (one case only)	$+10^3$ Btu @ 0°F with -10^3 Btu @ 66°F	$+10^3$ Btu @ 40°F with -10^3 Btu @110°F	$+10^3$ Btu @ 0°F with -10^3 Btu @66°F

Table 4-1

Storage Tank Material and Installation Costs

Storage Volume (M^3) to Collector Area (M^2) Ratio	Liquid Series SAHP $/$M^2$ of Collector	Liquid Parallel SAHP $/$M^2$ of Collector
.05	-26.00	-31.30
.075	-21.70	-26.0
.10	-17.30	-20.90
(Base) .20	0.0	0.0
.40	+34.70	+41.70
.60	+69.40	+83.40

Table 4-2

Heat Exchanger Material Costs

(Collector to Storage Heat Exchanger Only)

Effectiveness	$/$M^2$ of Collector
.55	-12.88
.70 (BASE)	0.0
.80	+14.43

Notes 1. These material costs are for both types of SAHP systems.

2. Installation costs are $85 per unit - regardless of effectiveness.

Table 4-3

Factory Built Solar Collector Material Costs

($/$M^2$ of Collector Area)

Collector Parameter $\tau\alpha$

Collector Parameter U_L (KJ/HR-M^2-°C) \ $\tau\alpha$	.88	.83	.8	.7	.6
50	-32	-54	-54	-64	-64
40	-21	-32	-32	-54	.64
30	0	-11	-21	-43	-64
20	+11	0	-11	-32	-54
15	+33	-22	0	-21	-32

Notes: 1. The above cost estimates assume that the collectors are mounted flat against a tilted roof. A factor for mounting material is included.

2. Installation costs for all collectors are $16/$m^2$ of collector area (OH&P included).

3. Base Cases: LS: $\tau\alpha$ = .88 U_L = 30, LP: $\tau\alpha$ = .83 U_L = 20

Table 4-4

Site Built Solar Collector Material Costs

($/M^2 of Collector Area)

Collector Parameter U_L (KJ/HR-m^2-°C) \ Collector Parameter τα	.88	.83	.8	.7	.6
50	-11	-11	-11	-22	-33
40	0	0	-11	-22	-22
30	0	0	0	-11	-11
20	-	-	-	-11	-11

Notes: 1. The above cost estimates assume that the collectors are mounted flat against a tilted roof. A factor for mounting materials is included.

2. Installation cost for all collectors is $22/M^2 of collector area (OHP included).

3. Bases Cases: LS: τα = .88 U_L = 30, LP: τα = .83 U_L = 20

Table 4.5

Heat Pump Equipment Costs

($/unit)

Rated Heating Capacity Increase Btu/hr	Stand Alone Heat Pump and Liquid Parallel SAHP	Liquid Series SAHP
None	0	0
7,500	+310.00	+320.00
15,000	+610.00	+630.00

Notes: 1. Installation costs are $375 for the stand-alone/parallel SAHP system, and $350 for the liquid series system (OH+P included).

Table 4.6

Capital Acquisition Costs

(1979 $)

System / Location	Stand Alone Heat Pump	Liquid Series Total Cost	Liquid Parallel Total Costs	Liquid Series Cost Breakdown	Liquid Parallel Cost Breakdown
Washington	2,913	18,618 (Collector area 60 m^2)	18,188 (Collector area 43 m^2)	$142.00/m^2 + 10,098	$222/m^2 + 8,642
Madison	2,876	19,551 (Collector area 69 m^2)	20,286 (Collector area 53 m^2)	$138.00/m^2 + 10,029	$220.00/m^2 + 8,626
Fort Worth	2,829	16,400 (Collector area 50 m^2)	14,875 (Collector area 30 m^2)	$134.00/m^2 + 9,700	$217.00/m^2 + 8,365

Notes: 1. The numbers are based on reference 1 information (from its Table 4.3).

	TOTAL ENERGY USED (KJ/YR	
	Liquid Series	Liquid Parallel
Wash	15.43 x 10^6	22.56 x 10^6
Mad.	20.19 x 10^6	32.63 x 10^6
Ft.W.	12.90 x 10^6	18.43 x 10^6

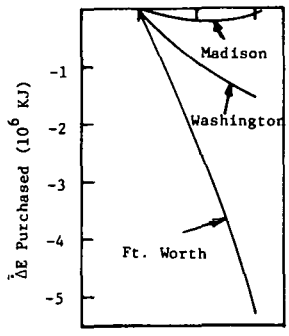

Figure 4-1. HP Capacity Increase (BTU/Hr) Liquid Series Systems All Cities

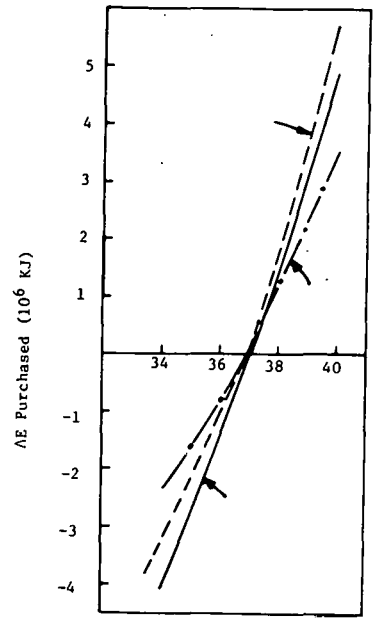

Figure 4-2. Delivered Air Temperature (°C) Stand-Alone Heat Pump All Cities

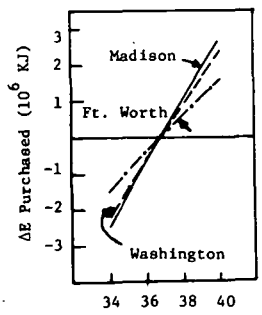

Figure 4-3. Delivered Air Temperature (°C) Liquid Parallel All Cities

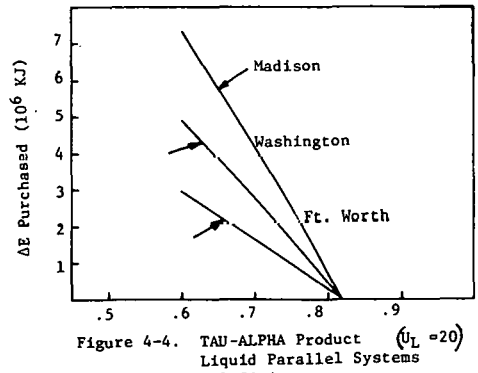

Figure 4-4. TAU-ALPHA Product (U_L =20) Liquid Parallel Systems All Cities

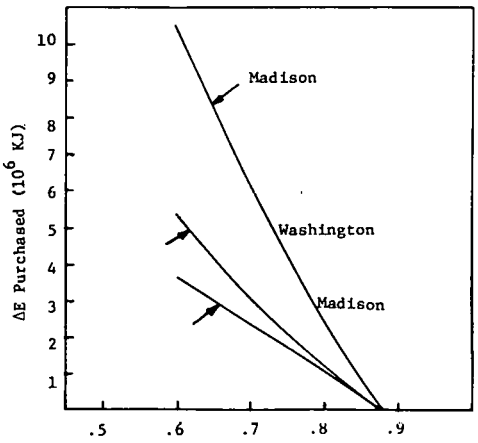

Figure 4-5. TAU-ALPHA Product (U_L = 30)
Liquid Series Systems
All Cities

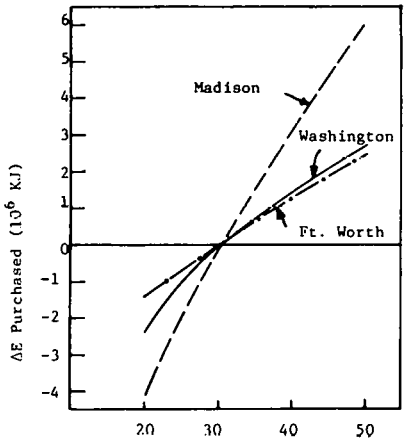

Figure 4-6. U_L of Collector at
$\tau\alpha$ = .88
Liquid Series Systems
All Cities

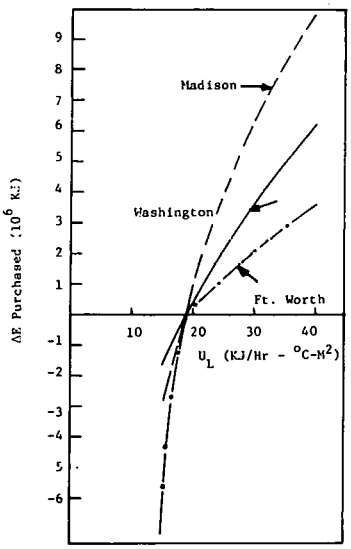

Figure 4-7. U_L of Collector at
$\tau\alpha$ = .83
Liquid Parallel Systems
All Cities

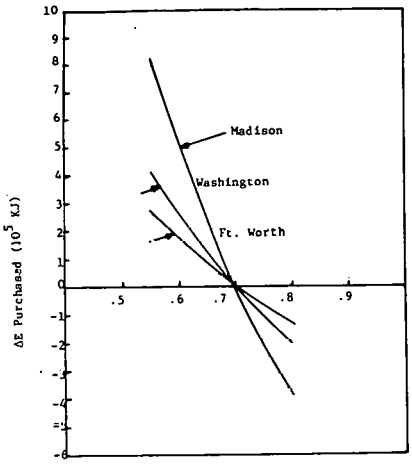

Figure 4-8. Collector to Tank Heat Exchanger Effectiveness
Liquid Series Systems - All Cities

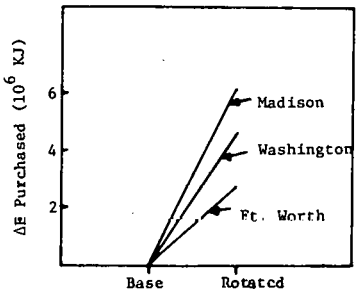

Figure 4-9. Rotated Performance Curves
Liquid Parallel-All Cities

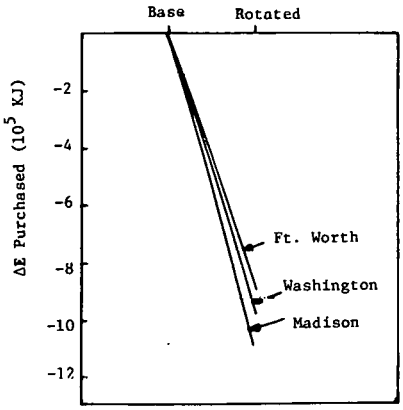

Figure 4-10. Rotated Performance Curve
Liquid Series - All Cities

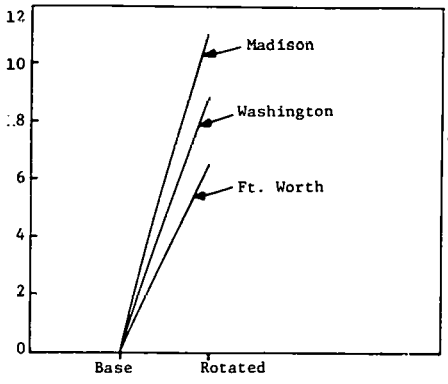

Figure 4-11. Rotated Performance Curve
Stand-Alone Heat Pump
All Cities

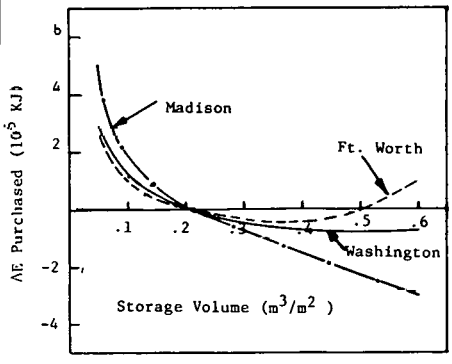

Figure 4-12. Storage Volume m^3/m^2
Liquid Series Systems
All Cities

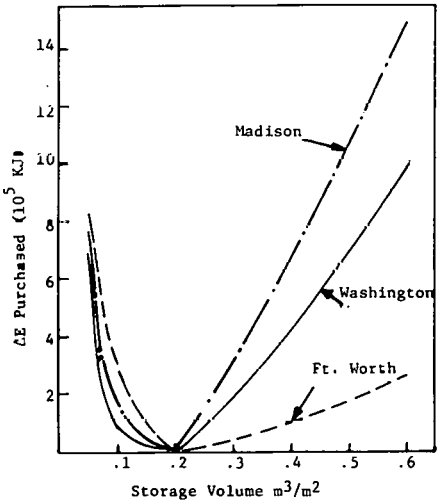

Figure 4-13. Storage Volume m^3/m^2
Liquid Parallel Systems
All Cities

Dup

SOLAR-ASSISTED HEAT PUMP - SWIMMING POOL SYNERGISTICS FOR DOMESTIC HEATING*

Terry R. Galloway
Chemical Engineering Division
Lawrence Livermore Laboratory
Livermore, California 94550

ABSTRACT

In this study for a 150m^2 home clear performance and economic advantages are shown for a solar-assisted heat pump, providing domestic hot water and space heating and cooling, when the pump uses a year-round solar-heated swimming pool as a large thermal energy reservoir. The pool can cycle seasonably between 18 and 31°C (64 and 88°F), allowing year round swimming, and provide an excellent water source for the heat pump and low cost, low temperature plastic solar panels operating at their near-optimum efficiency.

The system has been optimized by examining the performance and cost characteristics of different glazed and unglazed solar panel collector (areas from 28 to 150m^2 and orientation from horizontal to 60° tilt) for sites in San Francisco Bay Area and in San Joaquin Valley. Actual experimental data has been used whenever possible, together with numerical simulations for performance. The optimum system was found to use 75m^2 of \$44/m^2 unglazed collector at 48° tilt, a 300 GJ/year (30,000 BTU/hr) capacity heat pump, and a standard size swimming pool with a solar blanket cover. Solar energy supplied about 85% of the energy requirements at \$6.62/GJ (\$6.62/10^6BTU) in July 1979 dollars. With 20 year financing (10% interest), the payout period (re-breakeven) was projected at 7 years and net savings in year 2000 at \$42,701 (using the California State Tax Credit) compared against a conventional all-natural gas system. Discounting these savings back to July 1979, the present value of \$6,350 would be equivalent to a 9.5% return on investment.

This swimming pool - integrated solar system compares favorably against an equivalent system supplying 90% of the domestic energy needs, optimized without a pool, but with a 7600Kg (2,000 Gal) buried, uninsulated concrete tank. This system uses 18m^2 of glazed collector at \$90/m^2 and with \$11.06/GJ, pays out in 14 years, nets by year 2000 a savings of \$13,161 for a 3.6% return on investment compared to natural gas. Comparing sites in San Francisco Bay Area with little or no cooling with sites like Fresno, in the San Joaquin Valley, shows that a 75m^2 bare panel system can provide heating and cooling at comparable loads with only a slight loss in performance. For example, the 75m^2 Fresno system optimized at \$8.79/GJ with a 9.2% ROI compared against a conventional natural gas heated, electric air conditioner cooled home.

Background and Need

Large scale development of solar energy in the U.S. to serve a portion of the energy needs of single family residences, condominium, or energy-integrated communities awaits clearly advantageous economics. Before investment, the public is looking for a reasonable initial capital investment and a clear payout or breakeven in under ten years. It is the responsibility of solar energy conversion engineering community to continue to examine new solar energy system configuration ideas that make use of new or developing technology and make their findings known to the American consumers.

In this paper, we examine the synergistics of integrating swimming pools with solar-assisted heat pumps to provide solar energy at a low enough cost to serve 90% of a building's heating needs. The key here is to take advantage of the lower cost, plastic, solar collectors available on the market for swimming pool heating.

The notion of using ground-coupled swimming pools for heat storage reservoirs with and without heat pumps has been examined before (1-4). It has generally been recognized that the high cost of the pool makes including the pool as part of the solar system unattractive economically (i.e., payout periods exceeding 15 years). But when the swimming pool is justified and capitalized as a luxury, the economics improve considerably. The author has previously (5,6) examined residential space heating systems using a swimming pool coupled to a heat storage reservoir containing phase change materials, with and without heat pumps. The systems proved marginally economic. However, as presented in this paper, a swimming pool can serve as an excellent heat storage reservoir and the system optimized to provide very attractive economics, compared even to natural gas heating.

In this paper we will first describe the heat pump characteristics that are most desirable for solar-assisted operation, then the properties of low

*This work was performed under the auspices of the U.S. Department of Energy by Lawrence Livermore Laboratory under contract No. W-7405-Eng-48.

cost, low temperature solar collector panels operating with and without glazing, swimming pool heat balances and thermal dynamics. Then we put these components together into a solar-assisted heat pump-swimming pool integrated system, model its performance for the San Francisco Bay Area and San Joaquin Valley and then optimize the hardware to minimize cost. We then compare performance and cost with optimized solar-assisted heat pump-operated residential systems without using a swimming pool. Finally we identify the key areas where further developmental work would result in more cost-effective systems.

Heat Pump Characteristics:

The solar energy group at the Brookhaven National Laboratory (BNL) for the past several years has been involved in a program to develop the optimum heat pump characteristics for solar-assisted heat pump space heating applications (2,7). Three subcontracts were let to General Electric* (EG-78-C-03-1719, Heinz Joster), Lennox (EG-78-C-03-1720 Wm. Dollars) and Northrup (EG-78-C-03-1718, Amir Ecker) as an incentive for commercial development. The BNL heat pump performance curves for the "ideal" heat pump have served as the goal challenge for the commercial development. An excellent review of different heat pump configurations has been recently done at G.E. (8).

Heat pumps appear most attractive for solar-assisted applications when their coefficient of performance (COP) increases continually as the output (condenser) temperature increases in the range 35 to 80°C (90 to 180°F) and operate at water source temperatures 15 to 40°C (55 to 104°F). Large commercial-scale (10 to 1,000 times larger than for single family residences) solar-assisted heat pumps are available that do very well in this temperature range (9). As shown in Fig. 1, however, smaller units with evaporator temperatures above 50°C (125°F) and COP's above 3.8 are not presently on the market, but will be soon. For the purposes of this study, we have taken a constant COP of 3.6 as typical of present day smaller units.

The low temperature (15 to 40°C) of the water source fed to heat pumps is the key to the special compatibility of heat pumps to solar energy. At these temperatures near ambient, low cost, unglazed solar panels can be used at higher efficiencies than panels that must deliver their heat at a higher temperature (i.e., above 50°C).

Low Cost Solar Collectors:

The author has previously (5) measured the efficiency - fluid factor performance curve for low cost, low temperature plastic solar collectors with and without glazing. The results are shown in

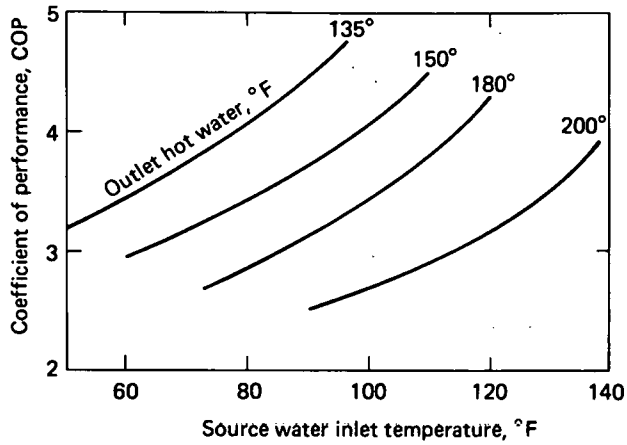

Fig. 1 Templifier heat pump performance.

Fig. 2A for a FAFCO-II plastic collector (10) that is inexpensive (i.e., $\$44/m^2$) and widely used today for swimming pool solar heating systems. This panel was then covered with a thin (1mm), inexpensive, greenhouse plastic panel (i.e., Tedlar^{R*} coated Filon panel) (11). This glazing sheet was separated 4 mm from the surface and sealed at the edges. In both cases, the back of the panel was insulated with 5 cm of glass wool. The tests were done with the panels oriented normal to the sun and with wind velocity around 2.2 m/s (5 mph). Tests showed that without flow no damage to panel resulted. The performance equations describing these tests are as follows:

$$\text{Unglazed} \quad \varepsilon = 0.81 - 25.2 \frac{\bar{T}_f - T_{air}}{S} \qquad (1)$$

$$\text{Glazed} \quad \varepsilon = 0.77 - 11.8 \frac{\bar{T}_f - T_{air}}{S} \qquad (2)$$

Where $\bar{T}_f$ is the arithmetic average between the water inlet and outlet temperature (°C); T_{air}, the ambient air temperature (°C); S, the solar insolation flux (W/m^2), and ε, the efficiency expressed as the heat flux captured divided by the solar insolation flux.

Since these tests were made, FAFCO (10) has developed and begun marketing a glazed panel, FAFCO - IV, at about $\$90/m^2$, that consists of a corrugated Tedlar coated glazing mounted over the basic FAFCO-II swimming pool collector. The reported performance (10) is nearly identical with that reported earlier (5).

In examining Fig. 2A we note that with temperature differences, $\bar{T}_f - T_{air}$, around 5°C the efficiencies are around 70% for both panels. And when temperature differences exceed 10°C, the glazed panel has clear advantages, in spite of the double per square meter costs (i.e., $\$44/m^2$ and $90/m^2$). Consequently,

*Reference to a company or product name does not imply approval or recommendation of the product by the University of California or the U. S. Department of Energy to the exclusion of others that may be suitable.

*Tedlar^R is a trademark of EI duPont de Nemours and Co.

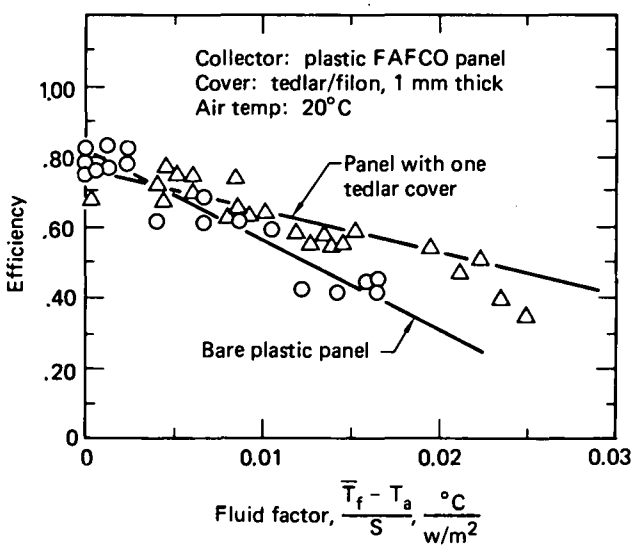

Fig. 2a Solar panel performance curves: installed tests.

we have desired to keep $\bar{T}_f - T_{air}$ below 10°C when the solar collector is limiting the energy gain of the system. Other more advanced collectors, such as double-glazed selective surface panels and evacuated tubular collectors, have efficiencies below the unglazed FAFCO-II collector in this low temperature range, as shown in Fig. 2B. Also shown is the latest substantial effect of wind velocity on the unglazed collector as predicted by FAFCO (10). For the evaluations given in this paper, we have used the data in Fig. 2A, which compares nearly exactly with the curve for 2.2m/s (5 mph) winds. In later discussions, it is important to note here that this was done to be completely conservative as our analyses.

Swimming Pool Dynamics:

Previously, the author (5) made heat balance studies using separately metered electric heat on a 68,700Kg (18,000 Gal) swimming pool with solar blanket cover (12) spanning a wide range of $\bar{T}_f - T_{air}$, temperature differences between pool surface water and ambient air, under varying solar insolation fluxes and seasonal conditions. The results including more recent data, are shown in Fig. 3, depicting energy flows necessary to maintain $\bar{T}_f$ = 21.3°C (72°F) for different $\bar{T}_f - T_{air}$ values under different solar insolation fluxes onto the surface of the pool cover.

For example, under low wind conditions and a daily average solar insolation flux of 16 MJ/m^2-d (75 BTU/hr-ft^2) or 200 w/m^2 on the horizontal surface, a $\bar{T}_f - T_{air}$ = 5°C temperature difference can be maintained with no heat input to the pool. With 10 GJ/mo (14,000 BTU/hr) input added from solar panels, the pool can be maintained 13°C above ambient. This, then, is the kind of swimming pool heat balance data we need to start system design studies.

The author also previously (5) conducted rate of heat up studies to get some estimates of the

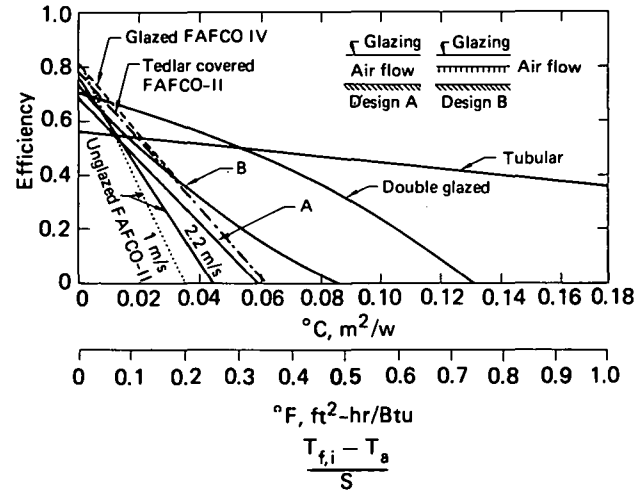

Fig. 2b Comparison with typical collectors.

importance of pool cover heat loss and ground coupling. An evaluation for the performance of the pool cover as a horizontal solar collector was determined as:

$$\varepsilon = 0.23 - 2.27 \frac{\bar{T}_f - T_{air}}{S} \qquad (3)$$

however, at these temperatures of the study, no accurate expression for ground coupling could be obtained. We were only able to note experimentally that as the unheated pool water temperature fell to low values in the winter, it never fell below 8°C (46°F) when the air temperature remained at -5°C for over 1 week. Since the ground temperature is

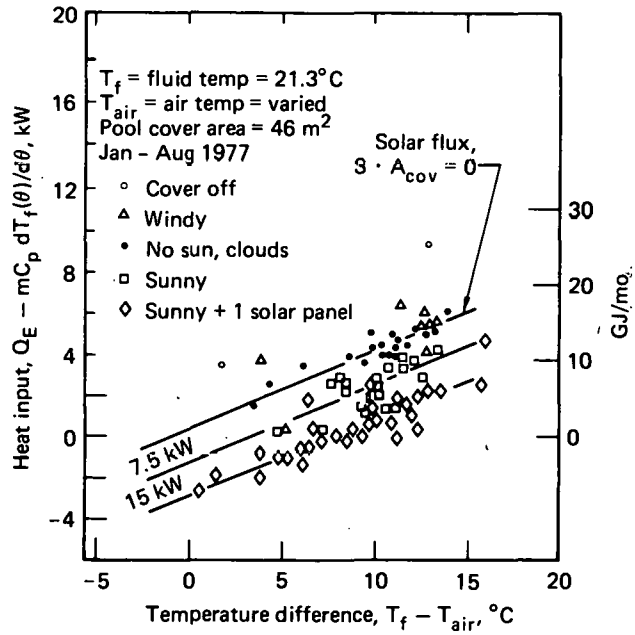

Fig. 3 Pool heat balance reveals pool cover performance.

around 13°C (55°F), this observation must be explained by ground coupling transferring ground heat into the pool. Thus, 8°C (46°F) may be taken as a useful lower limit when extracting heat from the pool for space heating. At pool temperatures around 20°C (68°F) the effective heat capacity can be taken as 0.288GJ/°C (1.5×10^5BTU/°F).

Solar-Assisted Heat Pump - Swimming Pool Integrated System:

The proposed system is shown in Fig. 4. It consists of a swimming pool with a conventional pump, filter, heater loop with a solar collector in a bypass loop, controlled by a pinch valve activated by a solar flux sensor (SFS). Cut into this loop, is a heat pump operated in series. The heat pump can be water to air, as indicated by the forced air loop for heating or cooling, or it can be a higher efficiency, water to water heat pump applying hot water to a base-board heating system. Domestic hot water can be supplied by preheating tap water via a "recovery coil" placed on the compressor output line.

The feasibility was examined of a direct heating mode where hot water from the pool is fed directly to the house space heating system. When the pool temperature is constrained between 18 and 31°C (64 and 88°F), however, it is not hot enough to efficiently heat exchange with forced air and is completely impractical for hydronic systems.* Thus, a series heat pump was used for the entire simulation.

Numerical Simulation:

Conventional monthly average simulation modeling (13) was done on this system shown in Fig. 4, including solar input and heat loss and transient heating and cooling of the pool, and the decline in solar collector efficiency with increasing fluid factor. The bases for design are shown in Table 1. The first validation task was to check out the model on the swimming pool - solar collector loop. These results are shown in Fig. 5, where the seasonal variation in pool temperature is compared with three years of experimental data. For the simulation monthly average solar flux and temperature data from the Oakland Airport (14) were used. The agreement between experimental data and prediction appears satisfactory for the monthly average methods. Significant improvements would require the treatment of daily fluctuation, which should be undertaken in the future.

*This application appears to be marginally achievable with the smaller heat pumps on the market now, because most units can not exceed output temperatures of about 40°C (104°F).

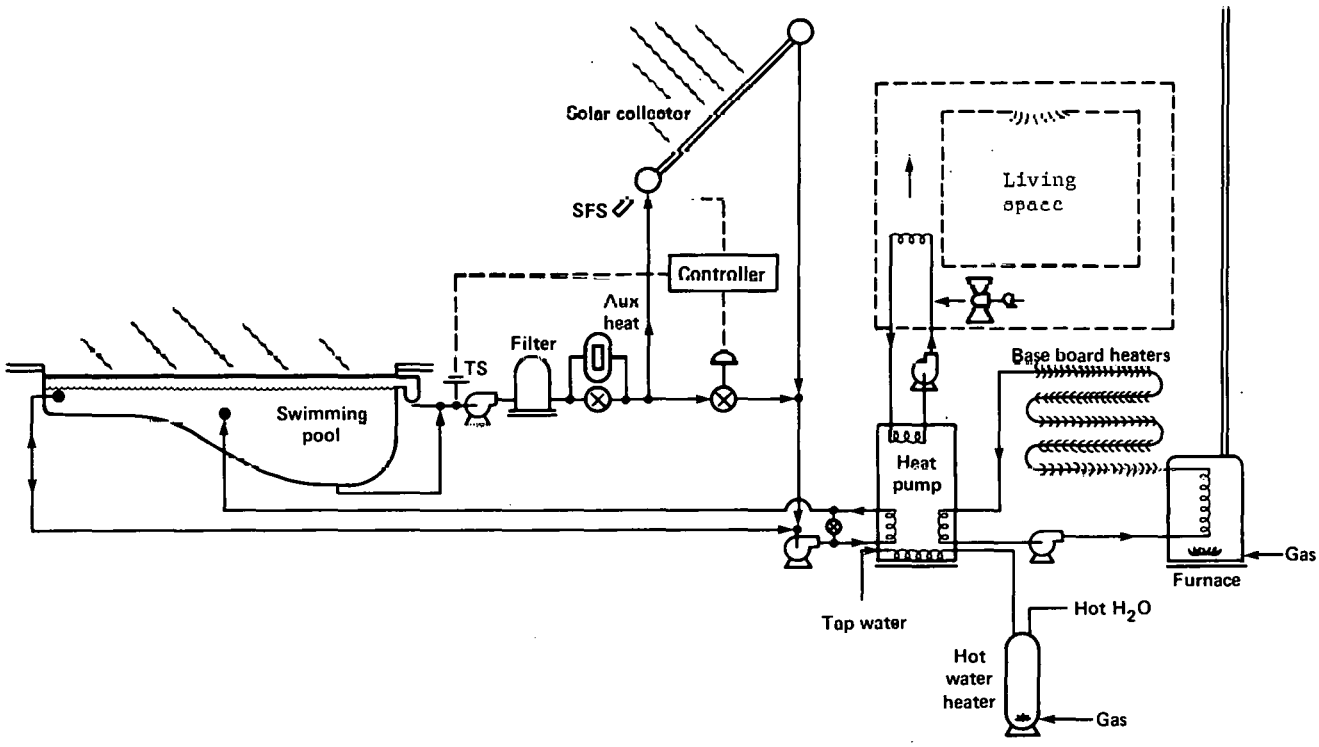

Fig. 4 Solar-assisted heat pump swimming pool integrated system.

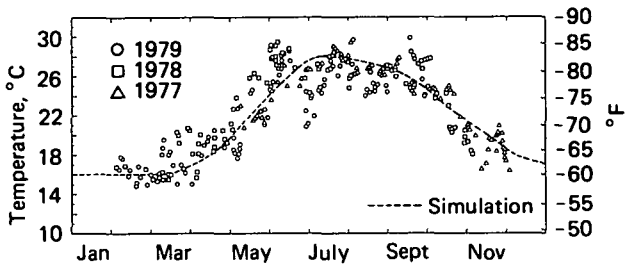

Fig. 5 Three year average pool temperature history.

The next simulation was done to illustrate the performance differences between 19m^2 of unglazed and glazed collectors, as shown in Fig. 6. As expected, the glazed panel delivers more heat and the pool heats up faster and stays warm longer than with the unglazed panel. More auxiliary heat is required for the unglazed panel in the middle of winter than for the glazed panel. Also, the unglazed panel is much more sensitive to wind on the panel surface--degrading the efficiency as shown in Fig. 2. Using the economic factors and energy costs in Table 1, solar pool heating using glazed or unglazed collector, both reached breakeven in 5½ years with a discounted cash flow return on investment (ROI) of

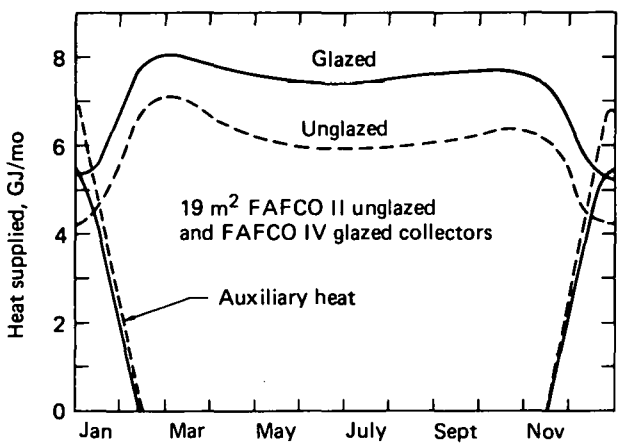

Fig. 6a Comparison of bare and glazed panels on swimming pool only.

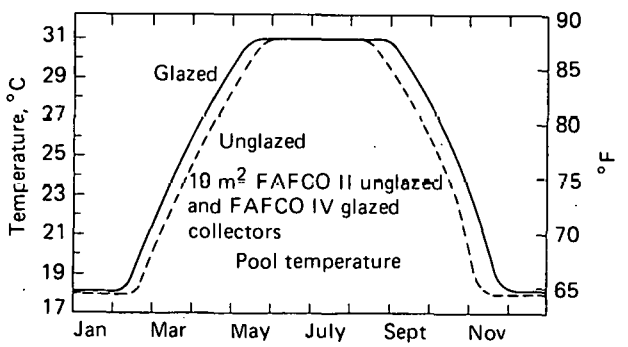

Fig. 6b Comparison of bare and glazed panels on swimming pool only.

13%, in comparison to an all gas heated system. We found that the increased costs of the glazed panels was almost exactly matched by the decrease in auxiliary gas heat required in the middle of winter, as shown in Fig. 6. These economic results are indeed attractive and are generally experienced by solar pool heating customers in this area. With this validation of this part of the model, we now move on to the challenge of space heating.

First, we shall examine the use of unglazed collectors and a series heat pump operating off a 2,000 gallon buried concrete tank. The tank is covered with insulation on the top, but the sides lose and gain heat to and from the ground as discussed earlier for swimming pools. As shown in Fig. 7, we have modeled the variation in solar heat supplied by the collector as their efficiency varies with solar flux and the difference in ambient and storage tank temperatures. These estimates are believed to be accurate to 10% since approximations for the collector fluid T_f were taken as the storage tank $\overline{T}_f$ at the inlet to the collector. And this is believed to be adequate since the ΔT was typically 10°C and collector water

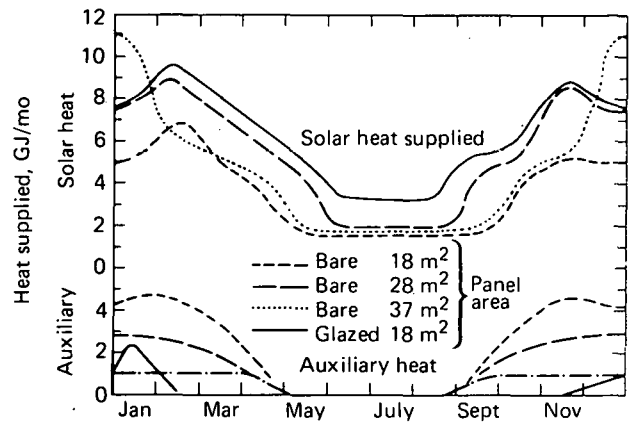

Fig. 7a Performance with bare panels, heat pump, 2,000 gallon tank.

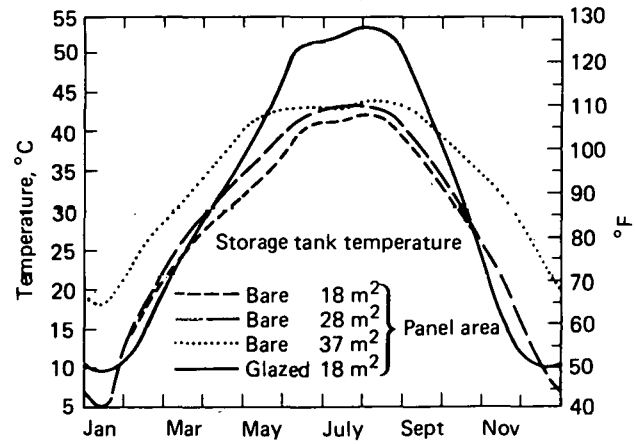

Fig. 7b Performance with bare panels, heat pump, 2,000 gallon tank.

TABLE 1. DESIGN BASES

	Symbol
Mass of water in storage = 68,700 Kg (18,000 gal) 0.288 GJ/^oC	
Unglazed FAFCO-II at \$44./m^2 and glazed \$90/m^2	
Area of collector = 18, 28, 37, 57, 62, 75, 112m^2	
Floor area of house = 150m^2	
House heat loss = 30,000 KJ/^oC - day	
Cooling load balance is heating load	
Panel 30^o tilt south and 48^o tilt south	
Heat pump Commandaire SWPH100 at \$740	C_E
Interest = 10% 0.125/yr 20 year	I
Elect power \$14/GJ 8% incr/yr \$25/GJ	C_P
Maintenance materials } 1% of capital 5% incr/yr	C_{MM}
Maintenance labor }	C_{ML}
Natural gas (California average) \$3/GJ 14% incr/yr	C_F

Oakland

H.W. Load	= 24 GJ/yr
House heat load	= 57 GJ/yr
Pool heat load	= 69 GJ/yr
	150

Fresno

Cooling load (Fresno)	= 28 GJ/yr
House heat load	= 44
H.W. Load	= 24
Pool heat load	= 60
	156

flows were high at 100kg/h-m^2. Auxiliary heat is required in the winter in order to supply domestic hot water and space heating requirement for the 150m^2 house, as shown in the center panel of Fig. 7. The corresponding variation in storage tank temperature is shown in the bottom panel of Fig. 7. Note the increased period of warmth in storage tank temperature as the panel area is increased from 18 to 37m^2. A comparison has also been made (solid curve) showing 18m^2 of glazed panel. Here the solar collection efficiency is consistently better and the swing in storage tank temperature greater, with corresponding reductions as auxiliary heat required.

The component costs for the glazed and unglazed collectors, series heat pump and 7600Kg (2,000 gal) storage tank are summarized in Tables 2A, 2B, and 3. Table 2A shows the individual costs for equipment, C_E, pumping costs, P_{CP}, collector with C_CA_C, maintenance, Cmml, the annualized solar costs $C_{s,a}$, without and with California tax credit, the financing cost, C_BI, the auxiliary natural gas cost, Q_AC_F, electric heat, EC_E, annualized auxiliary cost, $C_{A,a}$, and the total annualized costs, $C_{T,a}$. For this system, the total energy supplied for domestic hot water and space heating was 81 GJ/year and thus the cost per GJ delivered is shown as around 12/GJ. Also shown in the last column is the

TABLE 2A. COMPONENT COSTS PANEL, HEAT PUMP, 2,000 GAL TANK

Area	Glazing	C_E	P_{cp}	C_CA_C	C_{mml}	W/O Tax Credit C_{sa}	W/Tax Credit C_{sa}	C_{BI}	Q_AC_F	E_{CE}	$C_{A,9}$	C_{Ta}	Total Energy Suppl.	\$/GJ	%Solar
18m^2	Bare	\$1860	500	840	16	843	686	140	193	0	333	1019	81	\$12.60	59
28m^2	Bare	1880	500	1260	18	911	718	140	64	0	204	922	81	11.40	80
37m^2	Bare	1900	500	1680	20	968	750	140	89	0	229	979	81	12.00	66
18m^2	Glazed	1860	500	1680	16	957	737	140	29	0	169	906	81	11.00	91

TABLE 2B. COMPONENT COSTS PANEL, HEAT PUMP, POOL SYSTEM (SAN FRANCISCO BAY AREA)

System	Glazing	Equip. C_E $	P GJ/yr	C_p $	$C_c A_c$ $	$C_{mm,ml}$ $	No Tax Incent $C_{s,a}$ $	With Tax Incent $C_{s,a}$ $	$_BC_I$ $	$_AQ_PC$ $	PC_p $	$C_{A,a}$ $	$C_{T,a}$ $	Total Energy Supplied GJ/yr	$/GJ	%Solar
Fire & Pool	Bare	250	7.8	190	1260	12	392	287	30	200	483	542	$844	150	8	0
	Glazed	250	7.8	190	1680	12		310							5.63	40
28m^2	Bare	1880	20	500	1260	18	788	698	140	1360	0	1500	2158	150	14.39	57
37m^2	Bare	1900	20	500	1680	20.5	842	690	140	939	0	1079	1769	150	11.79	56
57m^2	Bare	1920	21	520	2520	27.00	977	767	140	324	0	464	1231	150	8.21	77
75m^2	Bare	1940	22	540	3360	33.00	1113	853	140	0	0	140	993	150	6.62	85
112m^2	Bare	1960	23	570	5040	45.50	1365	971	140	0	0	140	1124	150	7.49	92
150m^2	Bare	1980	24	590	6720	67.28	1613	1157	140	0	0	140	1297	150	8.65	99
62m^2	Glazed	940	22	540	6375	73	1527	1073	140	268	0	408	1481	150	9.87	85
94m^2	Glazed	960	23	570	8500	95	1847	1265	140	78	0	218	1483	150	9.89	92
							San Joaquin Valley Panel, Heat Pump, Pool System									
28m^2	Bare	1880	900	1260	18	1310	1094	140	1360	0	0	1500	2594	180	14.41	57
37	Bare	1900	900	1680	20.50	1368	1122	140	939	0	0	1079	2201	180	12.23	69
57	Bare	1920	900	2320	27.00	1482	1177	140	324	0	0	464	1641	180	9.12	76
75	Bare	1940	900	3360	33.00	1595	1731	140	0	0	0	140	1371	180	7.62	82
112	Bare	1960	900	5040	50.40	1825	1344	140	0	0	0	140	1484	180	8.24	82

TABLE 3. LIFE CYCLE ECONOMICS
(ALL SAN FRANCISCO AREA UNLESS NOTED)

System	Annual Cost	Breakeven Year	Discounted ROI	Year 2000 Savings	California Tax Credit
With 2000 gal tank					
28m^2 bare	922	14	3.5%	$12,851	Yes
18m^2 glazed	906	14	3.6	13,161	Yes
With swimming pool					
75m^2 bare	993	7	9.5	42,701	Yes
112m^2 bare	1124	8	8.9	40,073	Yes
112m^2 bare	1494	13	5.5	32,681	No
112m^2 bare$_1$	1174	8	8.5	39,081	Yes
62m^2 glazed	1481	12	5.6	32,941	Yes
62m^2 glazed	1935	15	3.1	23,861	No
75m^2 bare$_2$	1371	8	9.2	41,150	Yes

[1]With 50% increase in heat pump cost.
[2]Located in Fresno, San Joaquin Valley with 28GJ/yr cooling load.

fraction of this energy delivered that was supplied by the solar panels. Note that the unglazed panels optimize at around 28m^2 and this compares closely with the glazed panel optimum around 19m^2, both with around $11/GJ, even though the fraction solar delivered for the glazed system is up to 91%. This illustrates well the trade-off between glazed and unglazed systems. From Table 3, it can be seen that both have a discounted cash flow return on investment, ROI of 3.5%.

Now we shall examine the improved economics that are possible by using the swimming pool in place of the storage tank. Figure 8 shows the various seasonal heating loads and the simulated performance of such a system when the pool temperatures are constrained between 18 and 31°C for year-round swimming. The component costs are shown in Table 2 and the lifecycle costs in Table 3. The optimum panel area was 75m^2 and Fig. 9 shows the cash flow for such a system with breakeven in the 7th year. It realizes a discounted ROI of 9.5%, which is even more spectacular when one recognizes that these earnings are tax-free. We have also

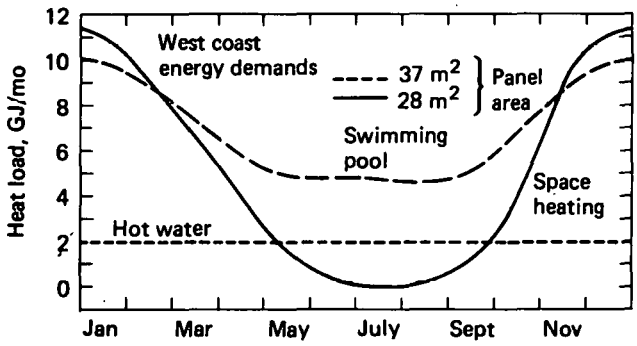

Fig. 8a Performance with bare panels, heat pump and swimming pool.

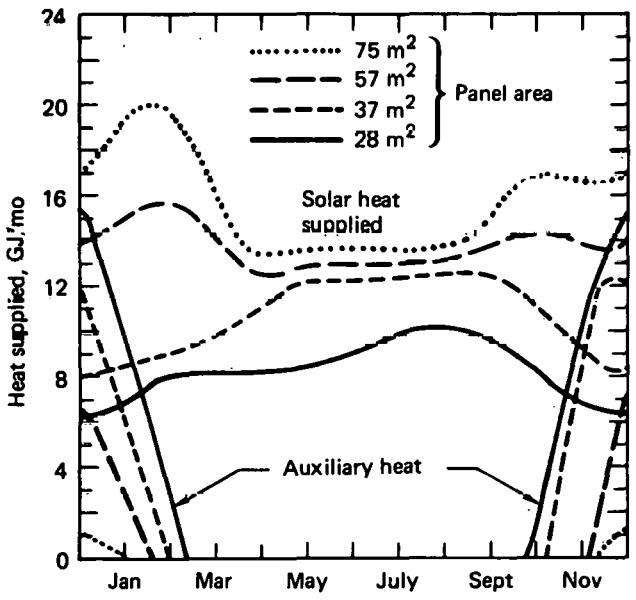

Fig. 8b Performance with bare panels, heat pump and swimming pool.

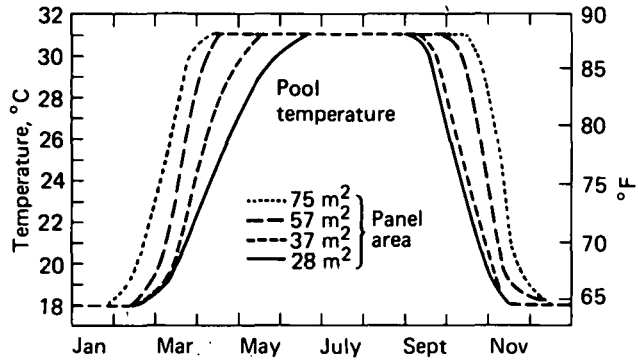

Fig. 8c Performance with bare panels, heat pump and swimming pool.

compared the sensitivity of the lifecycle costs in Table 3 to a 50% increase in heat pump cost from $1,000 to $1,500, which would be expected for a near doubling of the 1 Mg (1 ton) capacity to 2 Mg (2 ton). This increase only drops the discounted ROI from 8.9 to 8.5% for the 112m^2 collector system.

The sensitivity to the California 55% tax credit, also shown in Table 3, is found to be substantial. Without the tax credit for the 112m^2 system, the discounted ROI of 8.9% falls to 5.5% and the payment is extended to 13 years. This would be barely acceptable economics. A similar result is found for glazed panels where the discounted ROI drops from 5.6 to 3.1%, increasing the payment time from 12 to 15 years.

Finally, we examine in Table 3 and Fig. 10 the sensitivity to adding a subtantial air conditioning load as we change sites and climatology from the San Francisco Bay Area to Fresno, typifying the San Joaquin Valley. The component costs as shown on Table 2, with the optimum system again 75m^2. However, the added running time of the heat pump as an air conditioner adds substantially to the electric power consumption (from $500 to 900 per year). However, these increased operating costs for the heat pump are offset by the conventional air conditioner operating costs for the non-solar Fresno house. As a result, the discounted ROI is

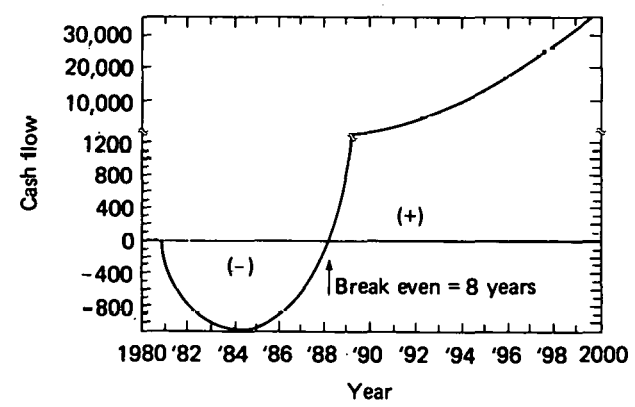

Fig. 9 Life cycle costs 75 m^2 bare panel, heat pump, pool.

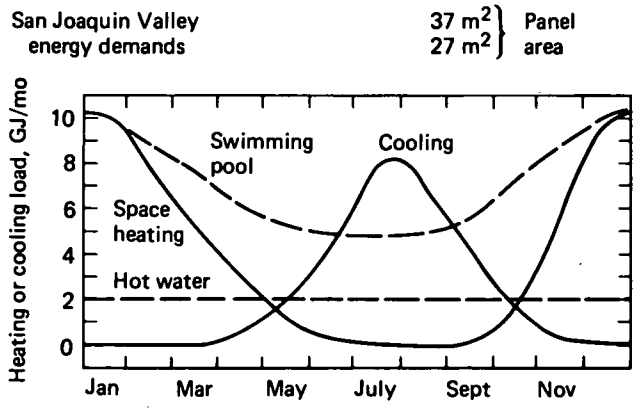

Fig. 10a Performance with bare panels, heat pump and swimming pool.

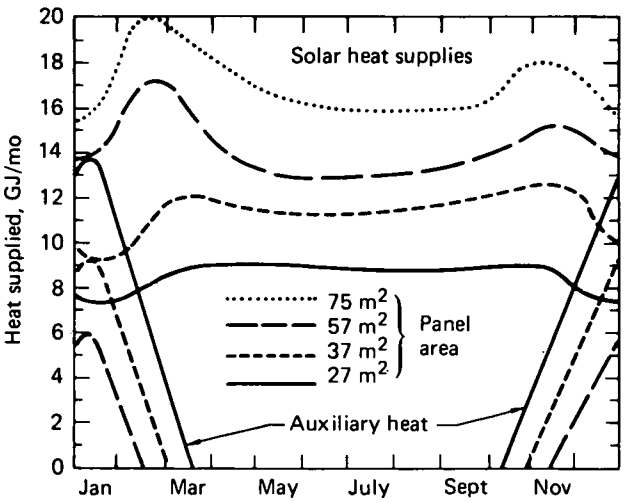

Fig. 10b Performance with bare panels, heat pump and swimming pool.

a high 9.2% with an 8 year payment. It is not as high as the similar application in the San Francisco Bay Area (i.e., 9.5%) since heat pumps in a cooling mode are not as efficient (i.e., COP) as when they are in a heating mode. But, these economics are indeed attractive anyway.

Acknowledgment

This work is in part the result of an agreement between the Oakland Public Schools and LLL where LLL provides professional resource persons on a volunteer basis in trade for the use of the school facilities. Appreciation is expressed to the LLL Solar Energy Group and Geophysics Division for valuable discussions and to the Oakland Public School system and especially the staff of Chabot Observatory for the opportunity of working at the facility. Gratefully acknowledged is the help of many students -- high school and college -- who assisted in the design and construction of computer hardware and software, photographic photometry and tedious data reduction of some 4,000 measurements, especially Tom Green, Paul Futscher, Joseph Waidl, Steve Massie, Bill Colias, David Rogers, and Fred Schumacher.

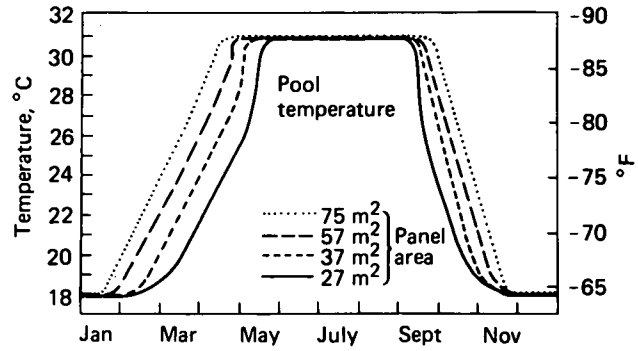

Fig. 10c Performance with bare panels, heat pump and swimming pool.

Conclusion and Future:

We have seen that when a swimming pool is already capitalized for pleasure and not charged against a solar energy system, a design can be developed for providing 90% of the domestic hot water, space heating and swimming pool year-round heating needs at very attractive economics (i.e., discounted ROI of 9.5% and 7 year payout). The design can be unglazed, inexpensive ($44/m^2) plastic solar collector that can be tilted for maximum winter heating and operate above 50% efficiency in the winter. Glazing the collectors dropped the collector area requirements and sensitivity to wind and provided good (5.6% ROI) economics for the 760 kg (2,000 gal) tank system but did not match the 9.5% ROI economics using the swimming pool system, owing to the pool constrained temperature limitation (18 to 31°C) for swimming year.

Sensitivity studies showed the 55% tax credit critical to the outstanding economics, and the next sensitivity was to local wind and temperature variations. The economics were not strongly sensitive to heat pump unit cost. The payment period is sensitive to the base case energy supply picture, for example, the price increase curve for natural gas.

Future studies should handle in more detail (i.e., hourly weather simulations), the local wind and temperature variations.

References

1. G.W. Rhodes, "Evaluation of Economic Benefit of Swimming Pools in Residential Solar Systems - National Swimming Pool Institute Summary Report," October 17, 1977. Rhodes Associates, 1032 Elwell Court, Suite 126, Palo Alto, California 94303.
2. J. G. Cottingham, "The Cost-Effective Potential of Optimumly Designed Heat Pumps for the Collection, Storage and Distribution of Solar Energy," Brookhaven National Laboratory Report, BNL-25195, November 1978.
3. D. A. Olsen, "Pool Becomes Heat Sink with Heat Pump System", Solar Engineering, p. 27-28, March 1979.
4. P. D. Metz, "The State of the Art of Sensible Heat Storage for Solar Source Heat Pump Systems," Brookhaven National Laboratory report BNL-35909, March 1979.
5. T. R. Galloway, "A Plastic Solar Panel, Heat Storage, Baseboard Heating, System for Both Swimming Pool and Home," 12th Intersociety Energy Conversion Engineering Conference Proceedings, pp. 1263-1270, August 28 to September 2, 1977, Washington, D.C.
6. T. R. Galloway, "Paraffin Wax Heat-Storage for Solar Heated Homes," 13th Intersociety Energy Conversion Engineering Conference Proceedings, pp. 963-969, August 20, 1978, San Diego, California.
7. E. A. Kush, "Experimental Performance Study of a Series Solar Heat Pump." Brookhaven National Laboratory, report BNL 26220, May 1979.
8. W. F. Bessler, and B. C. Hwang, "Performance of Solar Assisted Heat Pump Heating Systems for Residential Use," ASME experiment 79-HT-2, resented at Joint ASME/AICHE 18th National Heat Transfer Conference, San Diego, California, August 6-8, 1979.
9. A. Weinstein, R. Duncan, G. Van Zuiden, and R. Niess," Applying Heat Pump Engineering to Industrial Heat Water Needs," Solar Engineering, pp. 24-26, March 1979.
10. Available literature and private communication: FAFCO Incorporated, 235 Constitution Drive, Menlo Park, California 94025.
11. Available literature, Solar Energy Bulletin, No. SE1-76, and private communications: Filon Greenhouse Panels, Division of Vistron Corp., 12333 S. Van Ness Ave., Hawthorne, California.
12. Mac Ball Industries, 3040 Market Street, Oakland, California 94608. Hypalon Heat Saver Insulated Pool Blanket.
13. J. A. Duffie and N. A. Beckman, "Solar Energy Thermal Processes," Wiley, N.Y. 1974.
14. P. Berdahl, et al., "California Solar Data Manual," Lawrence Berkeley Laboratory, report LBL-5971, January 1978.

RESULTS OF SYSTEMS SIMULATION AND ECONOMIC ANALYSIS OF A SOLAR-POWERED TURBOCOMPRESSOR HEAT PUMP

G. Melikian, B. W. Rhodes and T. N. Obee
United Technologies Research Center
East Hartford, Connecticut U.S.A.

ABSTRACT

Since 1974, United Technologies has been actively engaged in the design, development and demonstration of solar-powered Rankine cycle heating and cooling systems for building applications. Under a recent DOE contract, UTC has built and tested an 18-ton cooling capacity, 500,000 Btu/hr heat pump over a wide range of operating conditions simulating an actual building installation. To assist in the heat pump design and analysis, UTRC has developed and used several comprehensive systems simulation and economic analysis programs. Collector array size, storage tank volume and control strategies were evaluated with these procedures. Typical results of the system simulations for buildings in six selected geographical regions are described and the economic potential for such a system is illustrated. The impact of variations in projected fuel price and component cost level on the UTC system economic potential (i.e., return-on-investment, payback period, etc.) is shown in detail.

United Technologies has designed, built and tested (Refs. 1 and 2) a unique thermally-driven heat pump, sized for multi-family residential applications. This prototype unit was specifically designed to operate at peak temperatures typical of medium-concentration collectors and to permit efficient air cooling. The basic heat pump design data was developed under prior ERDA- and DOE-sponsored programs in which the operational feasibility and performance characteristics of a laboratory Rankine-cycle turbocompressor heat pump and air conditioning system were demonstrated (Refs. 3 and 4).

Seasonal performance estimates and economic analyses of the UTC heat pump were conducted for widely differing climatic conditions and energy costs. The impact of various collector types, collector array sizes, storage tank capacities, control strategies, component cost levels, overall system configurations, energy prices and escalation rates plus tax credits and incentives were evaluated in the Ref. 2 contract. A selected summary of the Ref. 2 results are presented herein.

SYSTEM DESCRIPTION

The UTC heat pump (HP) system, shown in Fig. 1 incorporates a Rankine-cycle power loop in which a centrifugal turbine is used to drive a centrifugal compressor in a vapor compression refrigeration loop. The thermal energy to the power loop is provided at temperatures up to approximately 300 F (149 C) by a medium-concentration solar collector array. Auxiliary energy for cooling is provided by a fossil-fuel-fired furnace. Heating can be provided by direct solar, direct furnace, or furnace-driven heat pumping of low-temperature solar energy in combination with power loop heat recovery. The HP is rated at 18 tons for cooling at standard ASHRAE operation conditions of 95 F db/75 F wb and approximately 500,000 Btu/hr for heating. It utilizes low-maintenance air-cooled condensers for heat rejection and conventional HVAC design heat exchangers and controls.

PERFORMANCE SIMULATION PROCEDURES

The overall performance of the UTC heat pump system installation has been estimated by means of an analytical simulation procedure which includes performance models for each of the major components and subsystems, the thermal load characteristics of a typical multi-family residence and meteorological data for specific U.S. locations.

These models were incorporated into the basic Univ. of Wisconsin TRNSYS building heating/cooling simulation computer program (see Ref. 2). This program was extensively modified by UTRC (with UTC sponsorship) to allow simulation of new collector types and special components in the heat pump module, such as, the Rankine-cycle turbocompressor system and fan-coils operating with off-design sensible and latent loads. The performance (output and Coefficient of Performance) of the basic UTC heat pump module (Fig. 1) was calculated as a function of the module interface air or water flow conditions by means of a detailed performance prediction program developed by UTRC (previously described in Ref. 4). The results of such calculations for the prototype UTC solar-powered heat

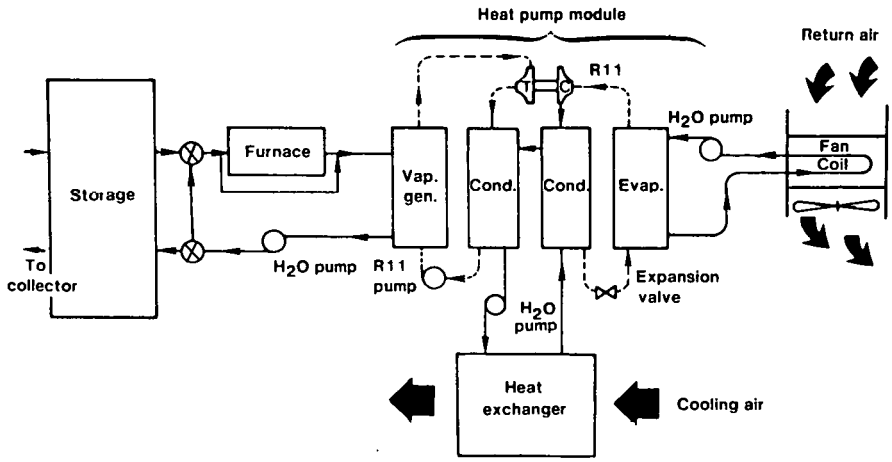

Fig. 1 Heat Pump System in Cooling Mode

pump were incorporated into the TRNSYS program for both cooling (Fig. 2) and heating (Ref. 1) mode operation. Performance models were also incorporated for the collectors, storage tank, fan-coil and auxiliaries. In addition, new computer codes were developed to; (1) model advanced east-west tracking concentrating collectors and nontracking CPC-type collectors in any orientation, (2) utilize collector instantaneous performance data correlations, (3) model a master control routine which selects the system operating mode, and (4) read special SOLMET type weather tapes.

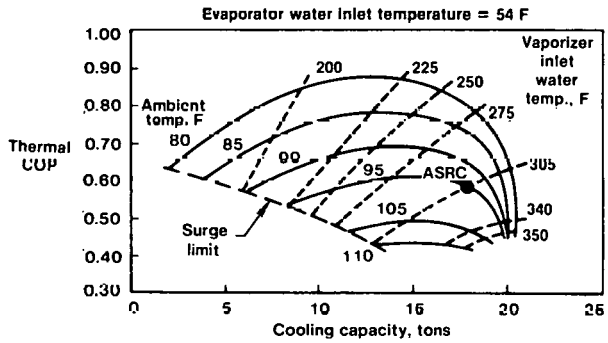

Fig. 2 Heat Pump Performance in Cooling Mode

Meteorological Data

The UTC heat pump installation performance analyses were conducted with hourly weather data. The National Bureau of Standards, under DOE sponsorship, has generated consistent weather and insolation data (SOLMET) for numerous U.S. locations for use in evaluating solar heating and cooling systems. SOLMET data tapes have been selected for typical years at six locations: New York, NY (1958); Madison, WI (1961); Fort Worth, TX (1960); Apalachicola, FL (1957); Phoenix, AZ (1962); and Santa Maria, CA (1956); which represent a wide variety of heating/cooling loads, geographic areas and solar insolation levels.

Building Thermal Model

Building heat loss/gain factors depend on the size, construction, and use of the building, as well as, on its geographical location and orientation. For this study, a building model was established to simulate the heating and cooling loads of an energy efficient (as per ASHRAE Standard 90-75) three-story multi-family residence with six (6) apartments on each floor. Each apartment comprised 800 sq ft of living space, with 5400 sq ft on each floor; a total floor area of 16,200 sq ft; a total exterior wall area of 10,000 sq ft; and a total building volume of 145,800 cu ft.

Building design point loads were based on weather data provided in the 1972 edition of ASHRAE Handbook of Fundamentals and ASHRAE Standard 90-75. The design point heating load was designed on the basis of coincident wind velocity and the 97.5 percent dry bulb temperature for a heating season. The design point cooling load was designed on the basis of the 2.5 percent temperature levels for a cooling season. Based on these design point procedures, the modeled building would require a nominal 15 to 20 ton capacity cooling system if located in a region with a climate typical of northeastern U.S. When the system installation was evaluated in other climatic areas, the size of the modeled building was modified to accommodate the 18-ton UTC cooling system.

PERFORMANCE ESTIMATES

The UTC-modified TRNSYS simulation computer program was used to determine the effects of collector characteristics (type, configuration, surface area, tilt angle, etc.), storage tank characteristics (capacity, segments, etc.) and

system operating strategies on seasonal performance of the UTC solar-powered heat pump installations in various geographical locations. These results included solar contribution (energy supplied by solar collector/total thermal energy supplied to HP system), parasitic power consumption and time in each operating mode; as well as, time profiles of all system and building conditions (temperatures, heating/cooling rates, humidity, etc.). A sampling of these results are presented herein. A typical annual energy distribution profile for a New York location is shown in Fig. 3. These results show a substantial portion of the winter heating load is delivered by solar-assisted heating pumping and essentially all of the summer cooling load is delivered by the HP in the solar-powered cooling mode. The combined impact of the building loads, solar insolation availability, and HP performance on storage tank temperature is shown in Fig. 4. These computer generated plots are for building simulation calculations made every 15 min. for an entire year; however, such detailed results are usually unnecessary for most performance and economic evaluation studies.

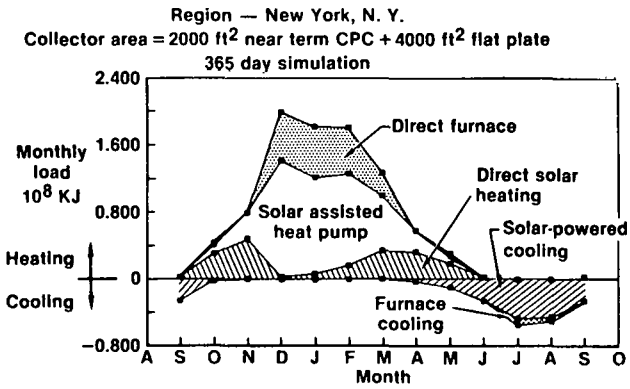

Fig. 3 Heat Pump Installation Distribution of Energy Delivered

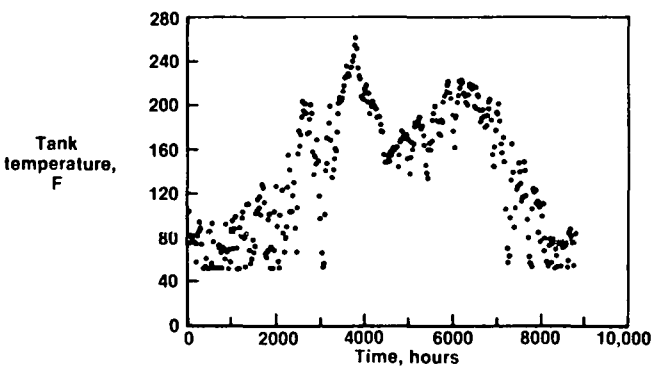

Fig. 4 Heat Pump Installation Storage Tank Temperature

System performance simulations were made in 15 minute increments for one-day/month, three-day/month, and every day for a typical year of operation. Based on these calculations, an average three-day/month simulation was developed, permitting rapid determination of annualized performance. This three-day/month simulation procedure proved to be satisfactory for performance comparisons of similar systems and identifying general trends in major parameter sensitivity analyses (such as comparisons of different types of collectors and collector size variations).

Several representative moderate temperature solar collectors were evaluated in earlier UTC studies (Ref. 1). A comparison of the annual solar contribution performance of these collectors indicated a significant advantage for advanced compound parabolic collector (ACPC) (peak efficiency of 72%) in moderate temperature (200-300 F) heat pump applications. Heating only or cooling only applications can be efficiently met with the flat plate or parabolic trough collectors. Since the ACPC collectors are still in the R&D stage and not expected to become commercially available in the near future, the UTC heat pump system was evaluated in detail with present state-of-the-art "near term" CPC collectors (peak efficiency of 64%). Although current CPC collectors are relatively expensive, they are only required for cooling mode operation of the UTC heat pump. During heating operation, (either direct solar heating or heat pump heating) a solar collector output temperature of 160 F down to 55 F is adequate. Such temperatures can be achieved with low-cost flat plate collectors. Since a majority of U.S. locataions have a short cooling season, the suitability of utilizing hybrid solar collector systems employing relatively low-cost, low-temperature flat plate collectors coupled in series with moderate temperature CPC collectors was investigated. The annual solar contribution of the UTC heat pump system utilizing the hybrid collectors is presented for the New York region in Fig. 5 and compared with advanced and near term CPC collectors. These data are presented for an optimum collector tilt angle and storage tank size ($\sim$ 1.5 gal/ft^2 of collector) as determined in performance sensitivity analysis described in Ref. 2. The flat plate collectors are tilted 60° from the horizontal providing the optimum angle during the heating season, and the CPC collectors are tilted 25° (rather than 40° when used alone) to provide the optimum angle for the cooling season. The data in Fig. 5 indicates that replacing 2000 sq ft of CPC area with an equivalent area of flat plate collector (total area equal 4000 sq ft) results in about a 10 percent degradation in annual solar contribution; however, as will be discussed later, the hybrid collector installation is typically more cost effective.

A comparison of the annual solar contribution performance obtained with the three-day per month and 365-day per year simulations is also presented in Fig. 5 for advanced CPC solar collectors. The more reliable 365-day calculation results give solar contribution values which are approximately 83 percent of the values obtained with the three-day simulation (for 4000 sq ft of total collector area). Consequently, where an accurate absolute level of performance is desired, annual performance calculations should be conducted with a 365-day simulation procedure.

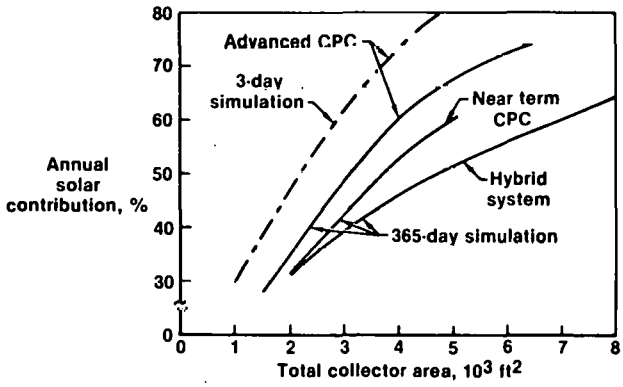

Fig. 5 Heat Pump Installation Annual Solar Contribution

Detailed annualized performance characteristics were calculated for alternative UTC heat pump installation configurations covering a range of collector and storage tank types and size. Although their average thermal COP's were similar, the optimum installations had significantly higher solar contributions and lower parasitic power consumption and operating time. A summary of the performance characteristics for an optimum installation in New York with 2000 ft^2 of near term CPC (NTCPC) and 4000 ft^2 of low-cost flat plate (FP) collector is presented in Table I. In addition, representative NTCPC collector installation characteristics are presented for New York and five (5) other locations. These performance simulations indicate a significant portion of the selected buildings heating and cooling energy needs can be supplied by solar energy, thereby reducing its annual fuel and electricity requirements. For example, the UTC solar-powered HP installation can provide a solar contribution of 50 to 60 percent with 4-6000 ft^2 of collector (Table 1).

When used in cooling dominated areas such as Phoenix and Apalachicola, the UTC system can provide a substantial fraction of the building cooling energy needs with a minimum amount of collector. For example, in Phoenix, a system utilizing 1000 sq ft of advanced CPC collector (ACPC) would result in a 45.9 percent seasonal solar contribution (SSC), while 2000 sq ft of the same collector would increase the solar contribution to 81 percent. In Apalachicola, 2000 sq ft of near term CPC collector would provide 57 percent of the building needs from solar. The lower performance of near term CPC's, the lower insolation values for Apalchicola, and a larger building contributed to the different results for Phoenix relative to Apalachicola.

In heating dominated areas such as Madison, WI, 4000 sq ft of NTCPC can provide a SSC of about 41 percent. However, in the Ft. Worth area where building heating/cooling ratios are closer to unity, 2000 sq ft of NTCPC collector can provide a SSC of about 53 percent. Detailed building indoor conditions for all six (6) regions evaluated, indicate that standard comfort conditions can be met with the UTC solar installation in addition to providing significant energy savings. A detailed evaluation of the economic potential of the UTC system has been conducted for a UTC solar HP installation in New York.

ECONOMIC ANALYSIS

Life-cycle costing was used to evaluate the economic performance of the UTC solar-powered heat pump system relative to a conventional HVAC system. The selected HVAC system includes an electric air conditioner with an overall seasonal COP of 2.3 and a fossil-fueled furnace with a seasonal efficiency of 80 percent. The baseline general economic assumptions used in these economic evaluations are presented in Table 2. Solar systems have a 20 percent investment tax credit and a conventional HVAC 10 percent. Both systems were assumed to have a 20 yr. life and 10 yr. depreciation period.

Life-cycle costing is a method of expenditure evaluation which considers the sum total of all relevant quantifiable costs (acquisition cost and running cost) associated with the expenditure during the time the purchased asset is in use. Acquisition costs (or initial capital costs) must be estimated; however, only acquisition costs of subsystem components not common to the two investments being evaluated are required by the life-cycle cost approach. The subsystem components for which acquisition costs were established are for the UTC solar HP - the solar collector, storage tank and heat pump module (includes all other components except the auxiliary furnace), and for the conventional HVAC - a unitary chiller. The furnace and indoor fan-coils are common to both systems. Installed costs for solar collectors and the heat pump module have yet to be accurately defined; therefore, these costs were varied over a range of values to display their impact on system life-cycle cost.

Location	Collector Type	Collector Area	Solar Energy Collected 10^6 Btu/yr	Average Thermal COP HP Heating	Solar Cooling	Furnace Cooling	Solar Contribution, % Heating	Cooling	Total
New York, NY	NTCPC/FP	2000/4000	610	1.94	0.85	0.66	48.6	92.4	56.3
New York, NY	NTCPC	4000	594	1.92	0.76	0.65	40.1	97.1	52.1
Phoenix, AZ	ACPC	2000	729	-	0.82	0.62	100	76.7	81.0
Fort Worth, TX	NTCPC	2000	471	2.02	0.77	0.61	49.1	56.3	53.3
Santa Maria, CA	NTCPC	2000	626	2.15	0.71	0.62	70.2	73.2	70.6
Madison, WI	NTCPC	4000	719	1.93	0.82	-	30.5	100.0	39.7
Apalachicola, FL	NTCPC	2000	420	2.10	0.79	0.62	76.9	50.5	57.2

Table 1. Alternative UTC Heat Pump Installation Performance

	Cost Model[3] Low/Moderate/High
CPC Collector Cost Range, $/ft^2	10/20/30
Flat Plate Collector Cost Range, $/ft^2	5/10/15
Cost of Electricity, ¢/kW-hr	5
Fuel Cost Range, $/$10^6$ Btu	NA/7.00/10.50
Misc. Annual Charges, % of Capital Costs	2.25
Operation and Maintenance, % of Capital Cost	2
Cost Base Year	1980
Installation Year	1985
General Inflation Rate, %	6
Escalation Rate of Fuel[1], %	6
Escalation Rate of Electricity[1], %	4
Discount Rate[2], %	10
Tax Rate, %	48
Depreciation Method	Straight Line
Ownership	Commercial

(1) These rates are above the general inflation rate

(2) Based on .53 fraction of equity in capital structure, 14% average return on equity, 48% tax rate, 10% average interest rate on debt.

(3) All costs expressed in 1980 dollars.

Table 2. Assumptions Used in Economic Analysis

Various economic indicators were used to assess the financial merit of alternative investments. These include: net present value benefit, net present value benefit ratio, cost of energy delivered, after-tax discounted rate-of-return, and payback period. The latter two indicators were selected for inclusion herein. After-tax discounted rate-of-return values greater than 10 percent are necessary for cost effective building HVAC investments. Payback period, which represents the years required to pay back an initial investment difference with future cost-saving differences (not discounted) between two alternative investments, should be less than about 10 years for a cost effective investment. These economic indicators (all after-tax values) were evaluated with respect to changes in the cost of fuel, collector cost and area, and heat pump module cost. The results of these evaluations identified the hybrid collector configuration with a total of 6000 ft^2 as the most cost effective installation.

Selective results for this configuration are shown in Figs. 6 and 7. Rate-of-return and payback period are shown as a function of the heat pump module cost for low and high collector cost values (defined in Table II) and two fuel cost levels ($7 and 10.50/$10^6$ Btu) which are approximately equivalent to $1.00 and $1.50/gal of oil. The Fig. 6 and 7 results indicate that the UTC system is cost effective at HP module costs of up to $60-$75,000 when fossil-fuel costs are $7 per 10^6 Btu and CPC installed costs approach $10.00 per sq. ft. (the low cost assumption). This collector cost is less than one-half of the current installed CPC costs. If fuel costs reach about $10 per 10^6 Btu, the allowable collector costs can increase to $20 per sq. ft. or the allowable heat pump module costs can increase to above sixty thousand dollars and still remain competitive with a conventional heating and cooling system. The heat pump module cost at which the UTC system becomes cost effective is approximately the same when evaluated by any of the economic indicators discussed earlier (see Ref. 2). This consistency suggests that the economic indicators are of equal value when used to determine cost effectiveness.

The results presented in Figs. 6 and 7 are based on the current 20 percent solar investment tax credit. The purpose of an investment tax

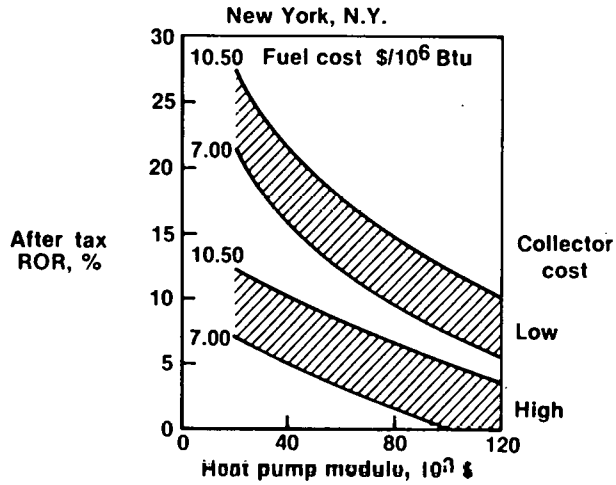

Fig. 6 UTC Heat Pump Rate-of-Return

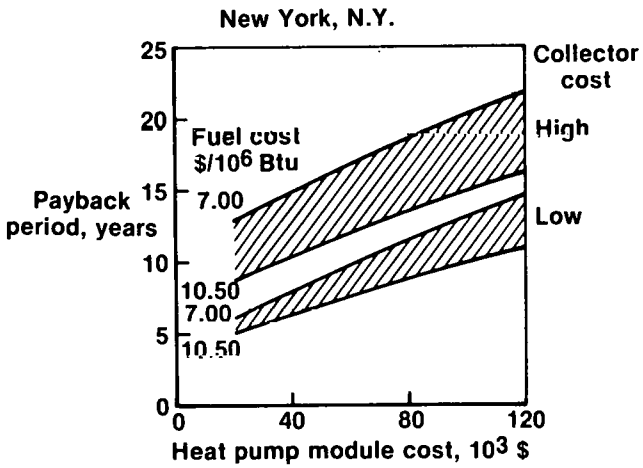

Fig. 7 UTC Heat Pump Payback Period

credit for solar heating and cooling systems is to decrease the burden of high initial capital costs. The effect of several values of the investment tax credit on rate-of-return are shown in Fig. 8 assuming moderate values of collector and fuel costs. These results indicate that an increase in tax credit (above the current regulation value) would make a significant impact on the solar HP economic attractiveness. For example, an increase in investment tax credit from 20 percent to 50 percent (as advocated by various government and industry solar experts) increases the heat pump module allowable cost by $55,000 to $90,000 (Fig. 8) at moderate values of collector and fuel cost and to over $150,000 at high fuel cost and low collector costs.

CONCLUSIONS

Detailed systems simulation and economic analysis have been developed and used by UTC to assist in the design and identify the potential of the UTC heat pump. The results indicate a significant solar contribution of 50 to 90 percent can be achieved in diverse climatic loca-

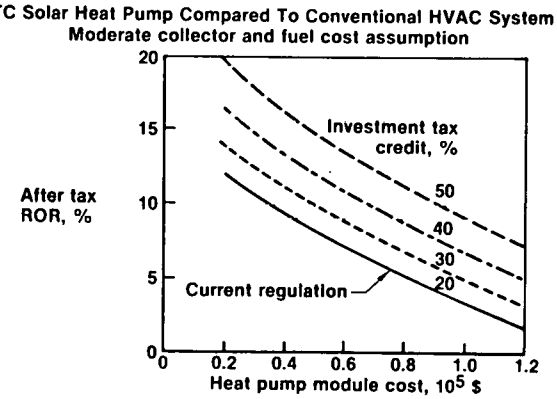

Fig. 8 Effect of Investment Tax Credit on Rate-of-Return

tions. The HP system would be cost competitive if either fuel costs increased to $10/10^6 Btu or collector installed costs decreased to $10/sq. ft. An increased investment tax credit would substantially improve the cost effectiveness and become a powerful stimulus for future installations.

ACKNOWLEDGMENTS

This program was conducted jointly by the Research Center and Hamilton Standard Division of United Technologies Corporation for DOE Office of Conservation and Solar Applications.

The authors wish to Thank Messrs. F. R. Biancardi, M. D. Meader, A. M. Landorman, C. E. Kepler of UTRC and Messrs. P. Young and J. Sitler of HSD for their assistance.

REFERENCES

1. Biancardi, F. R. and G. Melikian: "Analysis and Design of an 18-ton Solar-Powered Heating and Cooling System," Paper 789524 presented at 13th IECEC, San Diego, CA, August 1978.

2. Biancardi, F. R., et al: "Design, Development and Testing of a Solar Powered Multi-Family Residential Prototype Turbocompressor Heat Pump Final Report": Draft Report R79-953050-1, prepared under DOE Contract AC03-777-CS34510, September 1979.

3. Biancardi, F. R., et al: "Design and Operation of a Solar-Powered Turbocompressor Air Conditioning and Heating System," Paper 759031 presented at IECEC, 1975.

4. Biancardi, F. R., M. D. Meader, G. Melikian and A. M. Landerman: "Test and Evaluation of a Solar-Powered Laboratory Turbocompressor System for Building Heating and Cooling Final Report." Report R7-952529-1. Prepared under ERDA Contract EY-76-C-02-2824000, March 1977.

APPLICABILITY OF DATA FROM THE NATIONAL SOLAR DATA NETWORK FOR SIMULATION STUDIES

Leonard G. Doak, P.E. and Robert E. Waterman, PhD.
Energy Systems Department
Automation Industries, Inc.
Vitro Laboratories Division
14000 Georgia Avenue
Silver Spring, Maryland 20910

INTRODUCTION

The National Solar Data Network (NSDN) (1) is a rich source of solar system performance data for the validation of computer simulation models. Since 1977 over 900 million measurements of sensor data from NSDN sites have been collected and stored, and the quantity of this data is rapidly increasing. The number of instrumented sites is also expected to increase from the current authorized level of approximately 150 to a total of 250 by the end of 1982. This paper presents a summary of the types and quantities of data currently stored in the NSDN, projected improvements in the collection of data for the future, and suggested uses of the data for validation of solar simulation models.

THE NSDN PROGRAM

The purpose of the National Solar Heating and Cooling Demonstration Program, which includes the NSDN program, is to promote early commercialization of solar systems. The NSDN sites selected by DOE include a broad range of solar system types and geographical locations within the United States. Sensors are sampled automatically, and the data are stored at each site for one or more days. Since December 1979, the data have been transmitted over telephone lines to a central computer at Vitro Laboratories in Silver Spring, Maryland, where data reduction and analysis take place. Thermal performance of each site is analyzed and the results are reported in site specific Monthly Performance Reports. Performance over longer time periods is presented in Seasonal Reports.

Performance of the solar systems is evaluated using the energy balance concept (2). The monthly performance factors include:

- System level performance:
  - Thermal performance of the system
  - Solar fraction
  - Total energy consumed
  - Total energy saved
  - Comparison savings (passive systems only)
- Subsystem level performance:
  - Thermal performance of each subsystem
  - ECSS solar conversion efficiency
  - Solar fractions
  - Energy consumed, energy saved

Performance calculations based on the site data collected during the month is compared with predicted performance for the site using the F-Chart simulation method (3).

TYPES OF DATA COLLECTED

Three types of data are collected: 1) data from solar system sensors for thermal performance assessments, 2) weather data, and 3) data for special analyses from a few sites. Data collection emphasizes measurements that are intended to lead to performance assessments at the system level rather than at the subsystem or component levels.

Solar system sensor data consists of:

- Temperature sensors in each subsystem
- Flowmeters in each subsystem
- Auxiliary power used via wattmeters, flowmeters
- State sensors (i.e., on-off, etc.)

Weather data consists of:

- Insolation, in the plane of collector (all sites)
- Ambient temperature (outdoor, all sites)
- Wind speed and direction (some sites)
- Relative humidity (some sites)

Special sensors consist of:

- Corrosion sensors (resistance values across samples of materials in solar systems)
- Reliability data for data acquisition equipment

TYPICAL DATA STREAMS

Of the 148 sites currently authorized in the NSDN, 92 are now operating and reporting data; the remainder are under construction or otherwise incomplete. A total of 84 sites are active solar systems; 8 are passive systems. Data from NSDN sites is sampled at five minute intervals and stored on site. Parity checks are made during daily transmission of these data to the central computer, and the 5 minute data are printed out on tabulation sheets daily. These data are aggregated to form monthly tabulations that present averages or sums of the data for each day and for the entire month.

Figures 1 and 2 are truncated samples of typical printouts of data for an active solar site. The figures show daily and monthly outputs, respectively. The site in this example, Cathedral Square, is an apartment complex in Burlington, Vermont, which uses solar energy for domestic hot water heating (4).

Data from each of the 8 passive solar systems is obtained from a number of temperature sensors in rooms and in mass storage areas, as well as from extensive environmental sensors. Figures 3 and 4 are daily and monthly data printouts for a typical passive site, Hullco Construction, a residence in Prescott, Arizona (5). The daily printouts present a series of computer generated curves of the data that are sampled at 5 minute intervals. Usually a curve is generated for each sensor output. Temperature curves for a Trombe wall and related temperatures over a 24 hour period are shown on Figure 3.

ADDITIONAL DATA AND IMPROVEMENTS

The NSDN sites can serve as a source of additional performance data beyond that envisioned when the program was established. Consideration is being given to include, at some new sites, additional sensors for special measurement purposes. For active systems, sensors may be added or improved to record additional data for air flow measurements, for air infiltration, and for storage. For passive systems, sensors may be added to measure air stratification, infiltration quantities, and energy gains from wood stoves and fireplaces.

Quality of current NSDN data is sufficiently high so that energy balance equations can generally be solved for each system. During site start-up and for a few months thereafter, there may be variability in the consistency of the data from some sites. After the start-up period, site performance and data quality are consistently good. Accuracy of instrumentation meets good commercial standards. For example, temperature sensor accuracy is typically $\pm$ 0.5°F. (Users of NSDN data are reminded not to attribute precise laboratory standards to the accuracy of the data.) Improvements in NSDN data quality are being pursued via better installation procedures, and the check-out and calibration of the instrumentation. A continuing error analysis program is being conducted to analyze error sources and make improvements.

LONGEVITY OF DATA COLLECTION

Data collection began during 1977, and for over 30 sites is now in its third year. As the number of sites increases, the size of the NSDN data bank is increasing exponentially. A cumulative plot of site months of operation is shown on Figure 5. For a typical site, over 300,000 sensor measurements are made during each month. For some sites, the data collection will soon begin its fourth year. Thus, the NSDN data bank includes both quantity and longitudinal distribution of solar data.

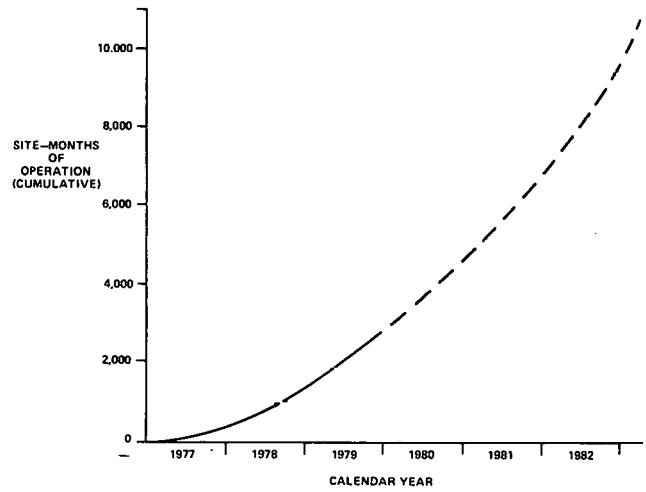

Figure 5. Cumulative site-months of operation for NSDN sites.

SIMULATION

Computer simulation of solar energy systems is an indispensable tool for research, development and evaluation of systems. For existing solar energy systems, simulation provides a method for comparing actual performance with that predicted by a mathematical model. In the design of new systems, simulation allows one to comprehensively test a large number of competing designs quickly and relatively inexpensively. The same testing, based on fabrication of a prototype system, would be time consuming and costly. Reference (12) contains concise descriptions, and cost and availability information for several widely used solar simulation programs.

Data from the National Solar Data Network can be used for simulation over a wide range of solar designs. The NSDN data includes active system

DATE 79/11/01 SITE = 168 SOAS = 151 CATHEDRAL SQ,BURLINGTON PRINT TIME 79/11/ 3 16:58:57

TAB 1 COLLECTOR LOOP PAGE 7

HR.MN.SC	T001	T001	EP100	W100	T100	T150	T150 -T100	T151	T101	T151 -T101	EP101	W101	T152	T102	T152 -T102
13.31.49	215.8	54.4	0.759	27.67	129.9	133.0	3.1	138.6	129.6	9.0	0.371	48.424	129.9	126.8	3.9
13.37.09	178.4	54.9	0.760	27.67	130.5	138.8	8.3	139.2	130.4	8.8	0.373	47.927	130.4	126.8	3.9
13.42.29	121.7	54.4	0.760	27.67	129.7	134.9	5.2	135.4	129.4	6.0	0.369	48.915	129.5	126.4	3.1
13.47.49	79.3	54.5	0.759	27.39	128.5	131.2	2.6	131.3	128.2	3.1	0.371	48.915	128.1	126.6	1.5
13.53.09	87.8	54.7	0.760	27.11	128.3	129.4	1.1	129.9	127.8	2.1	0.371	47.927	128.1	127.0	1.1
13.58.29	101.9	54.9	0.764	27.11	127.9	129.4	1.5	129.5	127.8	1.7	0.373	47.425	127.3	126.8	0.5
14.03.49	96.3	55.1	0.762	27.67	128.1	129.2	1.1	129.5	127.8	1.7	0.373	47.927	127.9	127.0	0.9
14.09.09	104.8	54.9	0.766	27.67	128.3	128.4	1.1	129.9	127.6	2.3	0.375	48.424	127.7	127.2	0.5
14.14.29	161.4	55.1	0.770	27.11	128.9	132.9	4.0	133.2	128.6	4.6	0.369	47.425	128.9	127.0	1.9

TAB 2 SOLAR STORAGE

HR.MN.SC	EP101	W101	T200	T201	T202	T203	EP300	W300	T350	T300	T350 -T300	W301	T308	T301	T351
13.31.49	0.371	48.424	129.9	127.0	123.8	124.5	0.286	19.759	125.8	125.8	0.0	868.22	54.2	56.8	119.0
13.37.09	0.373	47.927	128.5	127.4	124.2	124.7	0.287	19.911	126.2	126.4	-0.2	868.22	55.0	58.5	118.4
13.42.29	0.369	48.915	128.5	127.4	124.2	125.1	0.285	19.607	126.4	124.6	1.8	877.46	54.5	56.7	106.7
13.47.49	0.371	48.915	128.7	127.6	123.0	125.4	0.288	20.061	126.6	126.8	-0.2	878.38	54.5	57.6	105.7
13.53.09	0.371	47.927	128.7	128.2	124.8	125.2	0.286	19.759	126.6	127.0	-0.4	878.38	54.6	57.9	105.3
13.58.29	0.373	47.425	128.7	128.2	125.0	125.5	0.287	20.061	126.8	126.8	0.0	878.38	54.6	59.7	104.7
14.03.49	0.373	47.927	128.9	128.3	124.6	125.6	0.288	19.453	126.9	127.0	-0.2	878.38	54.7	61.2	104.3
14.09.09	0.375	48.424	128.9	128.2	123.6	125.5	0.291	19.208	126.6	127.0	-0.4	878.38	55.0	63.1	104.1
14.14.29	0.369	47.425	127.3	128.0	125.4	125.7	0.290	19.759	126.8	127.3	-0.6	878.38	55.2	64.0	103.8

TAB 3 DHW TANK

HR.MN.SC	EP303	W303	T307	T357	T307 -T357	EP301	EP302	W302	T202	T352	T352 -T302	T303	T304	T305	T306
13.31.49	1.245	74.569	182.5	180.8	1.6	0.178	0.313	14.138	117.6	127.7	10.1	128.5	126.3	119.5	233.5
13.37.09	1.245	74.978	179.3	176.3	2.0	0.183	0.318	13.480	118.0	127.7	9.7	128.3	126.9	119.5	233.5
13.42.29	1.238	75.912	186.4	183.6	2.8	0.176	0.315	14.138	118.8	127.7	8.9	128.3	126.7	120.6	233.5
13.47.49	1.241	75.384	181.5	179.0	1.3	0.177	0.316	13.480	116.0	128.5	12.4	128.9	126.9	120.2	233.5
13.53.09	1.245	74.978	178.5	177.1	1.5	0.186	0.318	13.812	120.3	127.7	7.3	128.5	126.7	120.0	233.5
13.58.29	1.249	74.978	185.2	182.2	3.0	0.190	0.316	14.766	119.4	128.8	9.5	128.5	126.9	121.0	233.5
14.03.49	1.247	74.158	185.6	183.6	2.0	0.190	0.321	14.455	120.1	129.2	9.1	129.5	127.3	121.6	233.5
14.09.09	1.251	74.978	178.5	177.1	1.5	0.196	0.326	13.138	119.4	129.4	10.1	129.9	127.3	121.4	233.5
14.14.29	1.249	73.745	179.3	176.7	1.6	0.196	0.322	12.788	122.3	129.6	7.3	130.1	127.7	122.0	233.5

Figure 1. Daily printout (5 minute intervals) for an active solar site. (NSDN site: Cathedral Square, Burlington, Vermont)

MONTHLY REPORT
ENERGY COLLECTION AND STORAGE SUBSYSTEM (ECSS)

SITE: CATHEDRAL SQUARE , BURLINGTON, VERMONT SOLAR/1024-79/11
REPORT PERIOD: NOVEMBER,1979

DAY OF MONTH	INCIDENT SOLAR ENERGY MILLION BTU	AMBIENT TEMP DEG-F	ENERGY TO LOADS MILLION BTU	AUX THERMAL TO ECSS MILLION BTU	ECSS OPERATING ENERGY MILLION BTU	ECSS ENERGY REJECTED MILLION BTU	ECSS SOLAR CONVERSION EFFICIENCY
1	2.658	51	0.194	N	0.024	N	0.064
2	0.049	49	0.232	C	C.CCC	C	4.411
3	0.515	42	0.188	T	0.002	T	0.411

STORAGE PERFORMANCE

SITE: CATHEDRAL SQUARE , BURLINGTON, VERMONT SOLAR/1024-79/11
REPORT PERIOD: NOVEMBER,1979

DAY OF MONTH	ENERGY TO STORAGE MILLION BTU	ENERGY FROM STORAGE MILLION BTU	CHANGE IN STORED ENERGY MILLION BTU	STORAGE AVERAGE TEMP DEG F	STORAGE EFFICIENCY
1	0.448	0.194	0.121	123	0.703
2	0.000	0.232	-0.336	118	1.000
3	0.010	0.188	-0.307	105	-12.456

HOT WATER SUBSYSTEM

SITE: CATHEDRAL SQUARE , BURLINGTON, VERMONT SOLAR/1024-79/11
REPORT PERIOD: NOVEMBER,1979

DAY OF MON.	HOT WATER LOAD MILLION BTU	SOLAR FR.OF LOAD PER CENT	SOLAR ENERGY USED MILLION BTU	OPER ENERGY MILLION BTU	AUX THERMAL USED MILLION BTU	AUX ELECT FUEL MILLION BTU	AUX FOSSIL FUEL MILLION BTU	ELECT ENERGY SAVINGS MILLION BTU	FOSSIL ENERGY SAVINGS MILLION BTU	SUP. WAT. TEMP DEG F	HOT. WAT. TEMP DEG F	HOT WATER USED GAL
1	0.358	16	0.224	0.189	1.489	N	2.482	-0.024	0.274	53	132	566
2	0.347	17	0.212	0.190	1.556	0	2.554	-0.024	0.253	54	125	568
3	0.422	12	0.212	0.190	1.697	T	2.829	-0.024	0.282	54	125	667

ENVIRONMENTAL SUMMARY

SITE: CATHEDRAL SQUARE , BURLINGTON, VERMONT SOLAR/1024-79/11
REPORT PERIOD: NOVEMBER,1979

DAY OF MONTH	TOTAL INSOLATION BTU/SQ.FT	DIFFUSE INSOLATION BTU/SQ.FT	AMBIENT TEMPERATURE DEG F	DAYTIME AMBIENT TEMP DEG F	RELATIVE HUMIDITY PERCENT	WIND DIRECTION DEGREES	WIND SPEED M.P.H.
1	1135	N	51	52	N	N	N
2	21	0	49	51	C	C	C
3	220	T	42	41	T	T	T

Figure 2. Monthly printouts of daily averages or sums for an active solar site. (NSDN site: Cathedral Square, Burlington, Vermont)

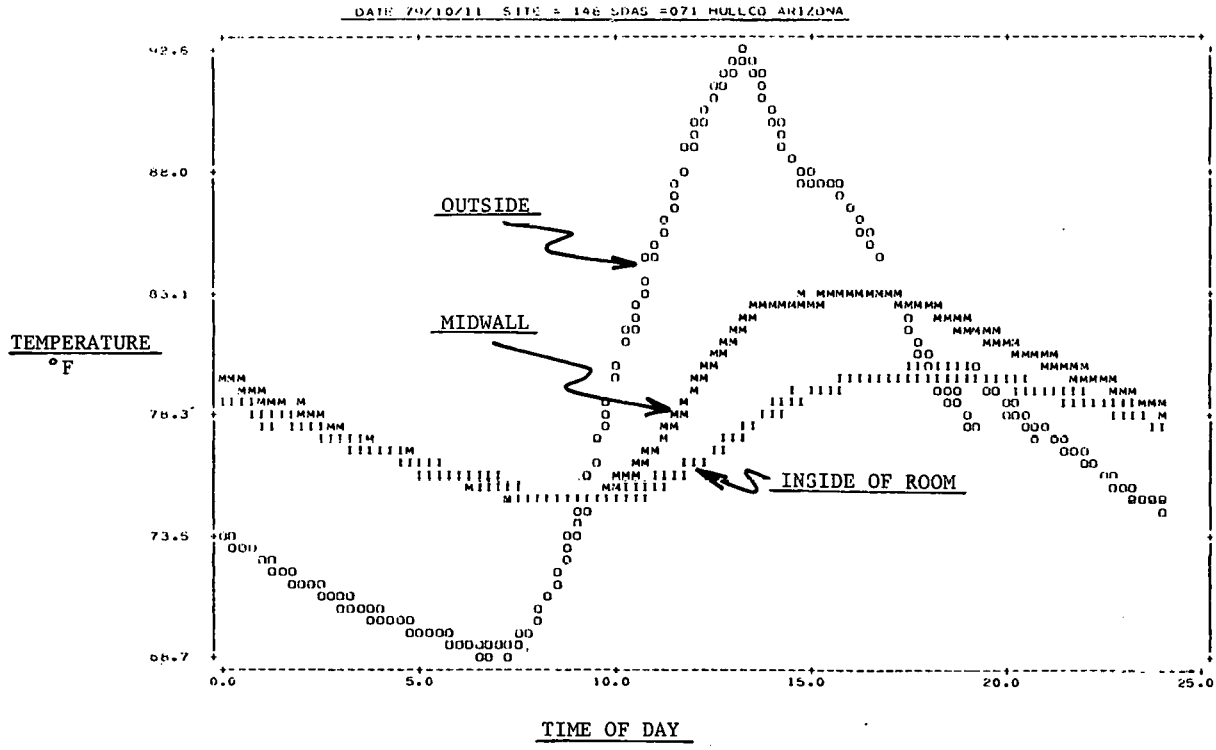

Figure 3. Daily printout (5 minute intervals) from passive solar system. (NSDN site: Hullco Construction Co., Prescott, Arizona)

MONTHLY REPORT: HULLCO CONSTRUCTION, OCTOBER 1979

PASSIVE SYSTEM ENVIRONMENT

DAY OF MON. (NBS)	BUILDING COMFORT ZONE 1	BLDG COMF ZONE 2	BUILDING TEMP MIDNIGHT DEG F	BUILDING TEMP 6 AM DEG F	BUILDING TEMP NOON DEG F	BUILDING TEMP 6 PM DEG F	INTERIOR RELATIVE HUMIDITY PERCENT	AMB TEMP DEG F (N113)	DAYTIME AMB TEMP DEG F	INCIDENT SOLAR ENERGY MILLION BTU	AVG STOR TEMP DEG F
1	77	77	77	76	78	80	24	66	84	0.688	76
2	78	77	78	76	78	80	22	66	82	0.781	76

PASSIVE SPACE HEATING

DAY OF MON. (NBS)	SPACE HEATING LOAD MILLION BTU (Q402)	SOLAR ENERGY USED MILLION BTU (Q400)	CHANGE IN STORE ENERGY MILLION BTU (Q207)	AVERAGE STORAGE TEMP DEG F	DIRECT SOLAR UTIL EFFIC	AUX THERMAL USED MILLION BTU (Q401)	BLDG TEMP DEG F (N405)	AMB TEMP DEG F (N113)	WIND AVG SPEED MPH (N114)	WIND AVG DIR DEG (N115)	SOLAR FR LOAD PCT. (N600)
1	0.101	0.101	0.013	75.5	0.148	0.000	78	66	2.0	209	100
2	0.109	0.109	0.021	75.9	0.140	0.000	78	66	1.5	0	100

SPACE HEATING SUBSYSTEM

DAY OF MON. (NBS)	SPACE HEATING LOAD MILLION BTU (Q402)	SOLAR FR. OF LOAD PCT. (N600)	SOLAR ENERGY USED MILLION BTU (Q400)	OPER ENERGY MILLION BTU (Q403)	AUX THERMAL USED MILLION BTU (Q401)	AUX ELECT FUEL MILLION BTU	ELECT ENERGY SAVINGS MILLION BTU (Q415)	BLDG TEMP DEG F (N406)	AMB TEMP DEG F (N113)
1	0.102	100	0.102	0.000	0.000	0.000	0.102	78	66
2	0.109	100	0.109	0.000	0.000	0.000	0.109	78	66

ENVIRONMENTAL SUMMARY

DAY OF MONTH (NBS ID)	TOTAL INSOLATION BTU/SQ. FT (Q001)	AMBIENT TEMPERATURE DEG F (N113)	DAYTIME AMBIENT TEMP DEG F	RELATIVE HUMIDITY PERCENT	WIND DIRECTION DEGREES (N115)	WIND SPEED M.P.H. (N114)
1	1719	66	84	35	209	2
2	1954	66	82	31	0	1

Figure 4. Monthly printout of passive performance data. (NSDN site: Hullco Construction, Prescott, Arizona)

…easurement - with air or liquid transport - for heating, cooling and domestic hot water. Collector performance models can be simulated using this data for flat-plate, concentrating and tracking collectors. Passive system measurements - as many as 45 sensors per system - can be used for simulation of many passive system designs. For example, the NSDN data bank of sensor measurements can be used in the simulation of any combination of these solar subsystems, active and passive, over a wide range of geographic and environmental conditions.

Simulation, using F-Chart (3), is one method currently being used to evaluate the performance of the NSDN demonstration sites. Typical input data to F-Chart simulation from each NSDN site includes:

- o Space heating load
- o Space cooling load
- o Hot water usage
- o Incident solar energy
- o Average ambient temperature

The output from F-Chart includes:

- o Expected solar fraction
- o Expected insolation
- o Long term climatic factors

The F-Chart output is compared with measured data to evaluate the performance of each site.

The simulation program F-Chart can also be used in conjunction with NSDN climatic data to evaluate the performance of a potential solar energy system. The applicable NSDN climatic data includes monthly average ambient temperature, available insolation and heating and cooling degree days. These data are tabulated for each site reporting in the NSDN and are included in monthly and seasonal performance reports. A list of currently available reports is included in reference (11). Examples and discussion of the use of F-Chart in connection with particular NSDN demonstration sites appear in references (7, 9, 17, 18, 19).

VALIDATION

Validation of a simulation model is usually performed to ensure some measure of agreement between the model and the actual systems represented by the model. Various approaches to the overall validation process are described in references (10, 21). A standard part of the validation procedure consists of comparing results generated by the simulation program with measured performance data from representative systems. The comparison can be carried out by a variety of methods, two of which, the open loop and closed loop model, are suggested schematically in Figures 6 and 7.

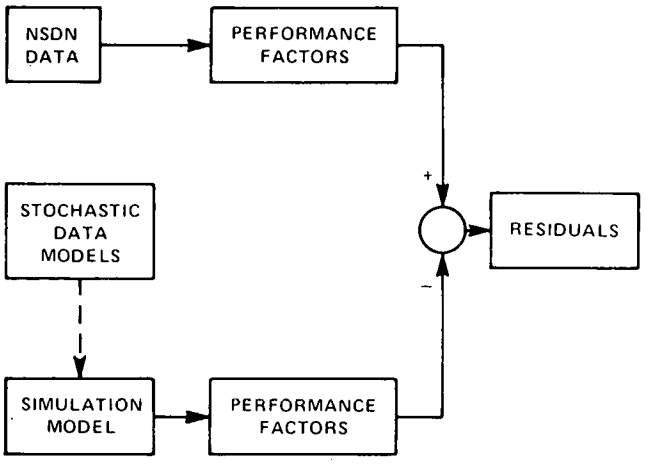

Figure 6. Open Loop Model Validation

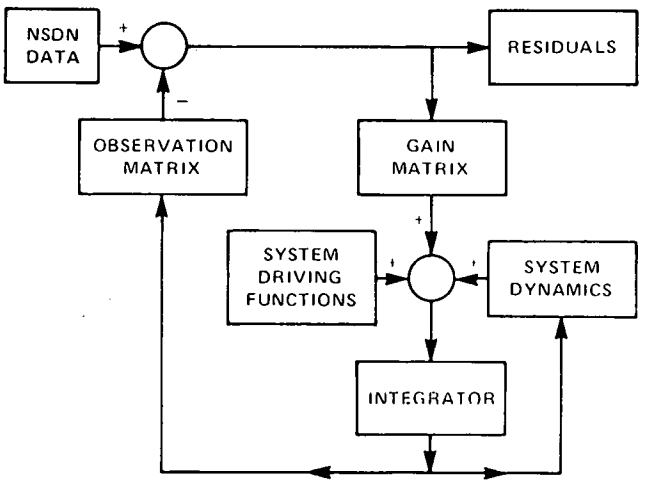

Figure 7. Closed Loop Model Validation (Kalman Filter).

The open loop method is easily implemented, but has the disadvantage that the residuals must then be subjected to further study. The closed loop simulation shown in Figure 7 is typical of a Kalman filter formulation, a method that has been used extensively by the aerospace industry. In the Kalman filter algorithm, the residuals are used at each time step to compute a statistical

weighting term that is in turn used to obtain an optimal estimate of the state of the system. A related quantity, the covariance matrix, provides a useful measure of the uncertainty in the estimated state. The manner in which particular NSDN data can be used in the Kalman filter depends to a large degree upon the application. As an example, consider the NSDN insolation data. If one is validating a model of a solar energy system then the NSDN insolation data will probably be used as part of the system driving function. On the other hand, if the application is the validation of a stochastic insolation model, then the NSDN insolation data would be used as data input to the Kalman filter.

A number of papers deal with models of solar systems and subsystems. They contain mathematical models that were developed with the aid of simulated data. NSDN data could be substituted for the simulated data in most of these instances to validate the model. For example, references (6, 14, 15, 16) deal with stochastic models of solar radiation. NSDN insolation data is available at five minute intervals and is, therefore, well suited to the task of verifying these models. NSDN data on solar energy system collector and storage loops would be useful in corroborating the results on control systems presented in (8). The heat pump simulation results presented in (13) can be checked with the aid of NSDN data on ambient temperature, system loads, and system losses.

When real data is used to validate a model, one should have a measure of the accuracy of the data being used. Towards this end, a number of sensor accuracy studies have been conducted in the NSDN Program. Continued accuracy of the data is further ensured by the NSDN instrumentation calibration procedures. Accuracy of the transmitted data is verified by a parity check, and site analysts study the scan level data for reasonableness. To date, system accuracy has received less attention than sensor accuracy. A new study has begun to assess the accuracy of NSDN data and the sensitivity of performance accuracy to data errors. The study will also be considering methods for filtering and preprocessing of the data. Reference (20) illustrates the recent use of data filters in connection with NSDN data. Additional preprocessing approaches that can be used to screen or smooth data are mentioned in (21).

SUMMARY

The NSDN data is an invaluable asset for both simulation and model validation. The data covers a wide range of system configurations and operating conditions. Data has been collected continuously for almost three years and it is being collected in a real (non-laboratory) environment. The use of this vast and increasing data base for simulation can further the goal of accelerating the widespread commercialization of solar energy.

ACKNOWLEDGEMENT

This work was sponsored by the Department of Energy, Office of Conservation and Solar Applications under Contract DE - AC01 - 79CS30027.

REFERENCES

(1) "National Solar Data Network", SOLAR/0003-77/17, December 1977.

(2) "Thermal Data Requirements and Performance Evaluation Procedures for the National Solar Heating and Cooling Demonstration Program", National Bureau of Standards, NBSIR 76-1137, August 1976.

(3) W. A. Beckman, S. A. Klein, J. A. Duffie, "Solar Heating Design by the F-Chart Method", John Wiley and Sons, New York, 1977.

(4) "Monthly Performance Report", Cathedral Square, November 1979, SOLAR/1024-79/11.

(5) "Monthly Performance Report", Hullco Construction, October, 1979, SOLAR/1043-79/10.

(6) Loren J. Lantz, C. Byron Winn, "Validation of Computer Models Used for Predicting Radiation Levels", Proc. of Annual Meeting of ISES, Denver, Co., Vol. 2.2, pp. 693-697, August 1978.

(7) J. C. Mears, Jr., J. M. Nash, J. T. Smok, "Comparison of Predicted and Measured Solar Energy System Performance", contributed to the Winter Annual Meeting of the American Society of Mechanical Engineers, New York, 1979.

(8) C. Byron Winn, Dwight Ellsworth Hull, III, "Optimal Controllers of the Second Kind", Proc. of Annual Meeting of ISES, Denver, Co., Vol. 2.1, pp. 493-498, August 1978.

(9) T. Collins, "Solar Energy: Four Sites Demonstrate Potential", IEEE Spectrum, pp. 60-65, April 1979.

(10) T. M. Knasel, W. Kennish, D. Cassel, "Status and Methodology for Validating Solar Heating and Cooling System Models, "Presented at 1979 Silver Jubilee International Congress of ISES, Atlanta, Ga., June 1979.

(11) Availability of Solar Energy Reports from NSDN, SOLAR/0020-79/37, U.S. Department of Energy, May 1979.

(12) Analysis Methods for Solar Heating and Cooling Applications, SERI/SP-35-232, 1978.

(13) Eddie R. Hoover, C. Byron Winn, "Design and Computer Simulation of Solar-Heat Pump Systems", Proc. of Annual Meeting of ISES, Denver, Co., Vol. 2.1, pp. 313-318, August 1978.

(14) Carlo Mustacchi, Vincenzo Cena, Massimo Rocchi, "Stochastic Simulation of Hourly Global Radiation Sequences", Solar Energy, Vol. 23, pp. 47-51, 1979.

(15) Gerard F. Lameiro, William S. Duff, "A Markov Model of Solar Energy Space and Hot Water Heating Systems", Solar Energy, Vol. 23, pp. 211-219, 1979.

(16) D. K. Anand, R. B. Abarcar, S. R. Venkateswaran, R. W. Allen, "System Performance Predictions for Solar Heating and Cooling Using Stochastic Weather Models", Proc. of Annual Meeting of ISES, Denver, Co., Vol. 2.1, pp. 125-130, August 1978.

(17) Kenneth L. Shenfish, "Thermal Performance of the Scattergood School Solar Energy System", Proc. of DOE's Solar Update, CONF-780701, pp. 243-254, July 1978.

(18) Richard V. Walker, "Thermal Performance of the Perl-Mack Enterprises, Inc. Solar Energy System", Proc. of DOE's Solar Update, CONF-780701, pp. 255-265, July 1978.

(19) Henry L. Armstrong, "Thermal Performance of the ARATEX Services, Inc. Solar Energy System", Proc. of DOE's Solar Update, CONF-780701, pp. 267-274, July 1978.

(20) W. H. McCumber, Jr., M. W. Weston, "Analysis of Collector Array Performance from Field Derived Measurements", Proc. of DOE's Solar Update, CONF-780701, pp. 231-241, July 1978.

(21) C. Byron Winn, Bradford W. Parkinson, Nguyen Duong, "Validation of Solar Systems Simulation Programs", Proc. of Annual Meeting of ISES, Denver, Co., Vol. 2.1, pp. 120-124, August 1978.

NOTES

Session VIIIA

Dr. William Duff
Colorado State University
Chairperson

SYSTEMS ECONOMICS IV

ECONOMIC ANALYSIS OF CONDUCTOR-INSULATOR-SEMICONDUCTOR (CIS) SOLAR CELLS

R. Singh, W.S. Duff, J.B. DuBow, and N.L. Weaver
Solar Energy Applications Laboratory
Colorado State University
Fort Collins, Colorado 80523

and

K. Rajkanan
General Instrument Corp.
Hicksville, New York 11802

ABSTRACT

At the present time a major obstacle to terrestrial applications of photovoltaics is the high cost of solar cells. Possible cost reduction may emerge only from the technological breakthrough in the material and design aspects of solar cells. Both above options are incorporated in conductor-insulator-semiconductor (CIS) solar cells which therefore offer one of the best prospects for cheap solar photovoltaic electricity. The CIS solar cells consist of a base-semiconductor covered by a very thin insulating layer (~10-30 Å) and then a top conducting layer. Recently it has been shown that single crystal silicon CIS solar cells can be fabricated with performance equivalent to p-n junction. In the case of poly and amorphous silicon, the CIS structures have yielded the highest efficiency. Thus the stage has been set for the prototype production of CIS solar cells. We have performed the feasibility study based upon the SAMICS methodology developed at the Jet Propulsion Laboratory (JPL). The economic analysis of CIS solar cells is reported based on solar grade silicon at $10/kg and amorphous silicon as alternative base-semiconductors.

INTRODUCTION

Photovoltaics, the direct conversion of solar energy to electricity, will have a significant impact on world electrical energy requirements provided the cost of the conversion system is about 10¢ to 30¢ per peak watt. Such large scale photovoltaic conversion systems will consist of many components other than the solar cell itself. The balance of the system (BOS) (e.g., energy storage, power conditioning, etc.) also needs further cost reductions. However, at the present time a major obstacle to terrestrial applications of photovoltaics is the high cost of solar cells. In the direction of cost reduction, various approaches are being considered. One such approach is the use of a new class of solar cells, namely the conductor-insulator-semiconductor (CIS) solar cell [1]. Recent experimental work has shown that single crystal silicon based CIS solar cells can be fabricated with performance equivalent to p-n junction solar cells [2]. With grating type MIS solar cells, Godfrey and Green have obtained an efficiency of 13.3% (AM1) on Wacker-Chemitronic SILSO polysilicon, which equals the best efficiency achieved in the lab for this material [3]. In the case of amorphous silicon, to date devices with the highest efficiency have been obtained using MIS structures [4]. Thus, in the case of thin film polycrystalline or amorphous thin film materials, the advantages of the CIS structures become obvious. Therefore the stage has been set for the mass production of such solar cells. Before the establishment of such a production facility, the economic analysis of CIS solar cells is desirable. It is the purpose of this paper to present the economic analysis of CIS solar cells both for polycrystalline and for amorphous silicon as the base-semiconductor. We have used the SAMICS IPEG costing procedure developed at the Jet Propulsion Laboratory in Pasadena, California.

BACKGROUND MATERIAL

The term CIS stands for conductor-insulator-semiconductor and refers to a solar cell structure consisting of a base-semiconductor covered by a very thin insulating layer (~10-30Å) and then a top conducting layer. Figure 1 is the schematic drawing of the CIS solar cell. The top layer must be transparent to let light through to the semiconductor underneath and should have low electrical re-

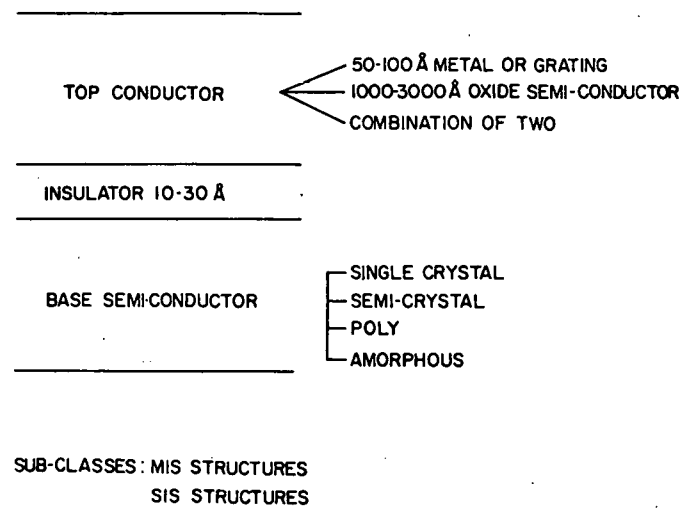

Fig. 1. CIS Solar Cell - General Structure

sistivity, since it is an electrode. This top layer can be a metal film (Al, Cr, Ti, etc.), an oxide semiconductor (ZnO, SnO_2, ITO, etc.) or a combination of these, leading to a wide variety of metal-insulator-semiconductor (MIS) [5] or semiconductor-insulator-semiconductor (SIS) [6] solar cells. The MIS solar cells can be fabricated either by transparent metal approach or by grating type approach.

To date in the case of single crystal and polycilicon, the highest efficiencies have been obtained by using grating type solar cells [2,3]. We have therefore chosen grating type silicon MIS solar cells as a representative member of the CIS family for economic analysis. A schematic diagram of the grating type MIS (or p-n) cell is shown in Fig. 2.

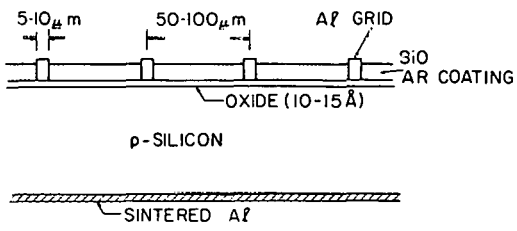

Fig. 2 Cross Section of Grating Type Structure

The analysis is equally valid for other types of MIS and SIS solar cells with slight variation in the cost component.

DESCRIPTION OF METHODOLOGY

The JPL SAMICS IPEG (Interim Price Estimation Guideline) costing formula (revised Dec. 1979 [13]) was chosen to evaluate the cell fabrication economics of CIS photovoltaic cells. The IPEG formula condenses the SAMICS methodology into a single cost equation. (The framework of assumptions upon which the equation is formulated is documented in references 7 and 8). Based on a required price approach the IPEG equation is of the following form:

$$PRICE = [0.57 * EQMT + 78 * SQFT + 2.1 * DLAB + 1.2 * (MATS + UTIL)]/Q$$

where

PRICE = Required price in dollars (1975) per cell
EQMT = Total direct capital equipment cost
SQFT = Total direct facilities floorspace needed
MATS = Total direct materials expense
UTIL = Total direct utilities expense
Q = Number of cells produced annually

(Costs expressed in 1980 dollars and 1986 dollars are deflated to 1975 dollars by a factor of 1.4 and 2.1, respectively. The cost coefficient for floorspace implies 1975 dollars [13]). The IPEG formula translates direct cost items into annualized costs per cell including implied indirect costs.

SAMICS has been validated by JPL against conventional industrial costing practices for solar cell factories varying in scale from 0.5 MW to 500 MW [11]. Estimated prices compared within 8%. As part of this analysis, a comparison was made between the results of the SAMIS III computer program (a JPL program which implements the SAMICS methodology), and the revised IPEG procedure for a test case ion implant junction fabrication sequence. The SAMIS results are reported in ref. [12]. IPEG produced results which were 16% lower than SAMIS, however in absolute terms the difference is small. Test case ion implant junction fabrication costs are .119 $(1975)/peak watt and .103 $(1975)/peak watt for SAMIS III and IPEG, respectively.

The JPL "Test Case" fabrication sequence for a 250 MW 1986 factory will be used as a cost reference for p-n junction solar cells [12]. The JPL "Test Case" is based on the growth of thin ribbon polysilicon cut into wafers 75 mm by 100 mm. The feedstock for this sheet growth is assumed to be 10 $/kg "solar grade" silicon. For comparison with CIS device fabrication, the JPL test case cell fabrication consists of the following sequence of process steps: (1) Spray deposition of aluminum back metallization and firing; (2) Plasma etch; (3) Ion implant doping and pulse annealing; (4) Silver ink printing of front and back grid pattern and firing; (5) Spray deposition of TiO_2 AR coating; and (6) Electrical test. Interconnection, encapsulation and module fabrication and packaging complete the manufacturing process.

The CIS devices are fabricated from the same wafers as in the JPL test case. For purposes of comparison the CIS cells are assumed to have a conversion efficiency of 12.9% equal to assumed for ion implant technology. Encapsulation and module fabrication costs are also assumed to be identical for both ion implant cells and CIS cells. Cost estimates for both cases reflect highly automated factories with operations optimized in the sense that overhead costs for R & D and prototype production activities typical of today's industry are eliminated.

The IPEG formula can be applied at several levels of process aggregation. In the analysis of this paper, the formula has been applied to cell fabrication as a single manufacturing step. Equipment cost, materials cost and other cost items were totaled for all cell fabrication process steps. A cell fabrication value added price was then generated via the IPEG equation.

Cost Analysis of Polycrystalline CIS Devices

The cell fabrication process sequence for a candidate CIS factory is shown in Fig. 3. In the CIS sequence doping steps have been replaced by thin film deposition and photolithography processes. The corresponding direct equipment and materials costs are indicated in Table 1. For the 250 MW factory, direct floor space requirements for equipment in the cell fabrication section is estimated to be 500 m^2. Direct assembly line labor and utilities requirements were assumed to be comparable to those implied by the JPL Test Case. Value added costs generated by the IPEG formula are tabulated in Table 2.

Comparison of the 1 MW and 250 MW CIS value added costs indicate the substantial economies of scale

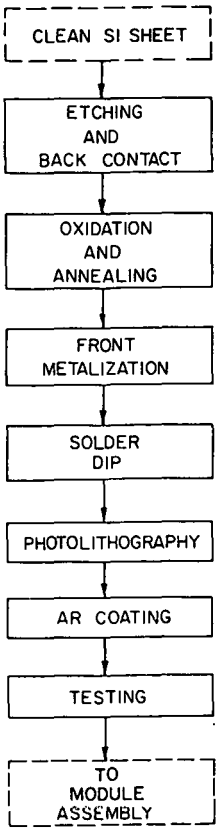

← Fig. 3. Fabrication Flow Chart for Grating Type Al-Si-SiO_x-(p-Si) Solar Cell

TABLE 1. CAPITAL COSTS AND MATERIALS/SUPPLIES COSTS BREAKDOWN FOR THE FABRICATION OF Al-SiO_x-(p-Si) SOLAR CELLS (FACTORY OUTPUT - 250 MW PER YEAR)

Process	Capital Costs (millions)	Materials/ Supplies Costs (millions)
Etching and back contact	1.0	1.65
Oxidation and alloying	0.1	0.1
Front metallization	5.5	2.0
Solder dip	0.05	1.0
Photolithography	2.15	2.0
AR coating	1.0	1.0
Testing	0.02	0.05
Total	9.82	7.8

TABLE 2. COMPARISON OF VALUE ADDED CELL FABRICATION COSTS EXPRESSED IN 1975 DOLLARS/PEAK WATT

Cost Component	1 MW CIS	250 MW CIS	250 MW (a) JPL Test Case
Equipment	0.409	0.022	0.020
Facilities	0.337	0.002	0.006
Labor	0.332	0.018	0.018
Materials	0.026	0.026	0.054
Utilities	0.020	0.004	0.004
Total	1.124	0.072	0.102

(a) JPL cost estimates stated in ref. [12] reaggregated to match IPEG cost categories

anticipated in scaling up the manufacturing sequence. Studies by JPL and RCA indicate the significant cost reductions can be achieved in scaling production from the 1 MW level to 30-50 MW. At this level substantial automation must necessarily have been achieved and cost reductions in increasing scale beyond 50 MW are less pronounced [10,11].

Figure 4 shows the breakdown of costs on a percentage basis for the 1 MW and 250 MW CIS factory. The clear difference in the two breakdowns is the reduction of facilities related cost in the 250 MW case. Capital equipment and labor also take a smaller fraction of costs with materials costs filling in the difference. The dominant reason for the "per watt" costs reductions in increasing plant size is the increase in thruput afforded by a high degree of automation. This is true for both the JPL test case and the candidate CIS factory. Once a certain level of automation is achieved, materials related costs become more dominant and it is in this regard that the CIS structure offers some advantage. As Table 2 indicates, materials costs are estimated to be 50% lower for the CIS factory versus the JPL test case.

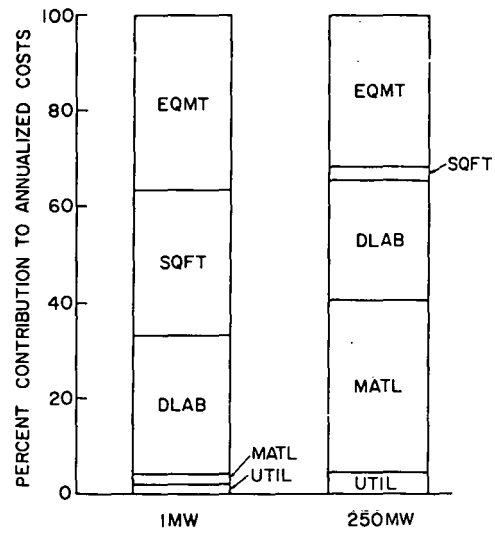

Fig. 4. Percentage Distribution of Annualized Costs for 1 MW and 250 MW CIS Factory

Based on the IPEG cost formula, the variation of cell fabrication costs with variation in each of various cost components can be estimated. The cost sensitivity diagram for the 250 MW CIS factory is shown in Fig. 5. (These results are qualitatively similar in the JPL Test Case also.) In the diagram, "inverse efficiency" means that variations with respect to the reciprocal of device efficiency have been plotted. Device efficiency has the most significant effect on "per peak watt" costs. Materials costs are the next most significant cost component. Variation in facilities and utilities related costs have the least effect on cell fabrication cost. These sensitivity results indicate most importantly that achieving high conversion efficiencies (10 to 15%) is crucial in terms of producing solar cells which can be economically competitive with other energy sources.

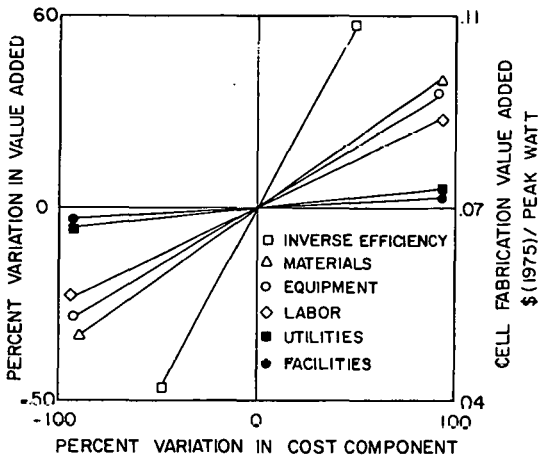

Fig. 5. Cost Sensitivity Diagram for 250 MW CIS Solar Cell Factory

With respect to the project cost of complete photovoltaic modules, the CIS modules are competitive but only slightly lower in cost than the JPL test case modules. Although CIS cell fabrication costs are 30% lower than in the test case, substrate and module fabrication costs are dominant items in total panel costs and these are assumed equal in both cases (see Table 3). Where CIS structure may offer a considerable cost advantage is with amorphous structures where substrate costs can be significantly reduced as discussed below.

Cost Analysis of Amorphous Silicon CIS Devices

A schematic diagram of the amorphous CIS solar cell appears in Fig. 6. The fabrication sequence is similar to that for the polysilicon CIS device with the addition of an amorphous silicon deposition step. The cost of amorphous silicon was taken to

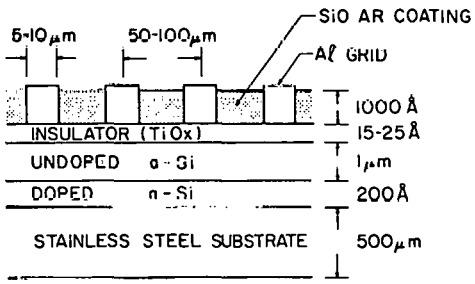

Fig. 6. Amorphous Silicon CIS Solar Cell Structure

be $2/kg. To date, amorphous devices have achieved conversion efficiencies in the range of 5 to 6% for small active area devices. In this analysis, a conversion efficiency of 10% was assumed to evaluate the economic feasibility of these devices. Devices with conversion efficiencies below 10% are severely penalized by area related costs both directly and in terms of installation cost.

Table 4 indicates the breakdown of annualized costs for amorphous CIS solar cells. Cell fabrication value added costs are estimated at 0.09 $(1975) per peak watt versus 0.07 $(1975) per peak watt for the polysilicon CIS device. The higher cost for the amorphous cell is due principally to the lower assumed amorphous device efficiency. The promise for amorphous devices lies in the elimination of the silicon wafer substrate being replaced by a stable metal substrate - typically stainless steel.

TABLE 3. COMPARISON OF SOLAR CELL MODULE COST EXPRESSED IN 1975 DOLLARS/PEAK WATT

	250 MW CIS Factory	250 MW JPL Test Case
Wafer/substrate	.18	.18
Cell fabrication	.07	.10
Module fabrication	.16	.16
Total	.41	.44

Referring to Tables 3 and 4, although reduced conversion efficiency increases cell and module fabrication costs, for the amorphous device a 20% reduction over the JPL test case is projected for total panel cost. Although contingent on producing cells of sufficiently high efficiency, amorphous CIS solar cells may ultimately prove an important option in the photovoltaics market.

TABLE 4. IPEG COST ESTIMATE FOR a-Si CIS SOLAR CELL MODULE

Cost Category	Value Added Cost $(1975)/$W_{pk}$
Substrate	0.02
Cell fabrication	
Equipment	0.033
Facilities	0.002
Labor	0.022
Materials	0.025
Utilities	0.006
Subtotal	0.09
Module fabrication	0.19
Total	0.30

CONCLUSION

In this paper we have presented the economic analysis of CIS solar cells. The 1986 DOE cost goal can be very easily met provided the polysilicon is available at $10/kg and the production of sufficiently large scale to support a high degree of automation. With 10% efficient amorphous silicon CIS solar cells, the cost is roughly 30¢, which makes photovoltaics competitive with other energy sources even at today's prices. It is worth mentioning here that in the case of polysilicon CIS solar cells, the low cost device technology is

available today and without much research and development work, a prototype production facility can be established. The devices fabricated from such a production facility can be rigorously tested for reliability and stability. Ultimately, materials cost related savings afforded by the CIS structure may favor commercialization of CIS photovoltaic cells.

ACKNOWLEDGEMENTS

The authors gratefully acknowledge Drs. R.W. Aster and D.B. Bickler of JPL in providing information helpful in the preparation of this paper.

REFERENCES

[1] R. Singh, K. Rajkanan and J.B. DuBow, "Development Trends for the Mass Production of Low Cost Conductor-Insulator-Semiconductor (CIS) Solar Cells". Proc. 2nd Miami Internatl Conf. on Alternative Energy Sources, December 1979 (in press)
[2] R.B. Bodfrey and M.A. Green. Appl. Phys. Lett., 34, 790, 1979
[3] R.B. Godfrey and M.A. Green. Japan J. Appl. Phys, April 1980 (in press)
[4] C.R. Wronski. Proc. 13th IEEE Photovoltaics Spec. Conf., Washington, D.C., p. 744, June 1978
[5] R. Singh and J. Shewchun. J. Vac. Sci and Tech., 14, 89, 1977
[6] R. Singh and J. Shewchun. J. Appl. Phys., 49, 4588, 1978
[7] R.G. Chamberlain, "A Normative Price for a Manufactured Product: The SAMICS Methodology", Vols. 1 and 2. JPL 5101-93 (JPL; Pasadena, CA), January 1979
[8] R.W. Aster and R.G. Chamberlain. "Interim Price Estimation Guidelines: A Precursor and an Adjunct to SAMIS III". JPL document 5101-33 (JPL; Pasadena, CA), September 1977
[9] R.W. Aster, "Economic Analysis of a Candidate 50¢/Wpk Flat-Plate Photovoltaic Manufacturing Technolgoy". (JPL; Pasadena, CA), December 1978
[10] RCA Laboratories, "Automated Array Assembly - Final Report". (RCA; Princeton, NJ), December 1977
[11] R.G. Chamberlain, "Recent Development in the Economic Modeling of Photovoltaic Module Manufacturing". 2nd European Communities Photovoltaic Solar Energy Conf., W. Berlin (D. Reidel; Boston) April 1979, p. 851
[12] D.B. Bickler, "A Preliminary 'Test Case' Manufacturing Sequence for 50¢/Watt Solar Photovoltaic Modules in 1986". 2nd European Community Photovoltaic Solar Energy Conf., W. Berlin (D. Reidel; Boston), April 1979, p. 835
[13] Personal communication with Robert Aster of Jet Propulsion Laboratory, December 1979
[14] Personal communication with Don Bickler of Jet Propulsion Laboratory, January 1980

NOTES

FEASIBILITY STUDY FOR ANAEROBIC DIGESTION OF AGRICULTURAL CROP RESIDUES

by

E. Ashare, M.G. Buivid, and E.H. Wilson

Dynatech R/D Company
Cambridge, Massachusetts 02139

ABSTRACT

The objective of this study was to provide cost estimates for the pretreatment/digestion of crop residues to fuel gas. A review of agricultural statistics indicated that the crop residues wheat straw, corn stover, and rice straw are available in sufficient quantity to provide meaningful supplies of gas. Engineering economic analyses were performed for digestion of wheat straw, corn stover, and rice straw for small farm-, cooperative-, and industrial scales. The small farm scale processed the residue from an average size U.S. farm (400 acres), and the other sizes were two and three orders of magnitude greater, respectively. The results of the analyses indicate that the production of fuel gas from these residues is, at best, marginally economical unless a credit can be obtained for digester effluent. The use of pretreatment can double the fuel gas output but will not be justifiable economically unless low chemical requirements or low cost chemicals can be utilized. Additional development is necessary in this area. Use of low cost "hole-in-the-ground" batch digestion results in improved economics for the small farm size digestion system, but not for the larger systems size.

INTRODUCTION

As a result of the energy crisis, a considerable effort has been expended over the last few years to develop alternate renewable sources of energy. One such source is biomass, which can be grown specifically for use as an energy crop, or which can be obtained as residues from both crops and animals. The biomass must then be converted to an easily utilized form of energy. Both thermochemical and biological processes are being considered as conversion processes for the production of liquid and/or gaseous fuels. One such process is the biological anaerobic digestion of biomass for the production of methane gas.

This study was undertaken for the Solar Energy Research Institute (SERI) to determine the economic feasibility of fuel gas production by the pretreatment/ digestion processing route for three distinct scales of operation -a small farm system, a farm cooperative scale system, and a larger scale utility/industrial system. The system of residue cost, pretreatment, digestion, and effluent processing and/or disposal is presented on an economic basis, and the cost of fuel gas is computed. An economic feasibility study and sensitivity analysis were performed by including such factors as facility size, pretreatment chemical requirements, heating requirements, energy and material balances, capital and operating costs, feedstock costs, potential for and value of recovered byproducts, and disposal of effluent stream. (A detailed description of this analysis is presented in the final report for this project, "Feasibility Study for Anaerobic Digestion of Agricultural Crop Residues", which is available through NTIS, Report No. SERI/TR-8157-1).

Anaerobic Digestion

An extensive discussion of anaerobic digestion concepts was presented by Ashare and Wilson [1]. The choice of process to be employed with crop residues - either a continuous or batch process - depends upon the composition of the residue and scale of the system.

Continuous digestion can be carried out in either a plug flow or continuous stirred tank reactor (CSTR). The major difference between these is that in the plug flow system each particle has the same residence time in the reactor, whereas in the CSTR there is a broad distribution of residence times. Experience with continuous anaerobic digestion systems has been primarily with the CSTR. The plug flow concept is still under development. Jewell et al. [2] currently are investigating the plug flow anaerobic digestion of dairy cow manure. However, these concepts have not been applied to large scale digestion of agricultural crop residues.

Pfeffer and Quindry [3] have investigated digestion of corn stover in 750 liter stirred tank reactors, and have noted difficulty in handling greater than 8% solids in the digester. Jewell et al. [2] have observed, on a pilot plant scale, that plug flow digestion of manure with wheat straw resulted in operating problems due to

straw flotation. More development work is necessary to determine both optimum digestion conditions and materials handling properties.

The use of low capital cost "hole-in-the-ground" batch digestion systems has been proposed for use with crop residues. This approach is similar to municipal solid refuse disposal, which has traditionally been accomplished in sanitary landfills. Recently, interest in this process has extended to the production of methane from biomass with a high solids content, such as agricultural crop residues. The economic success of gas extraction from existing landfills has led to an interest in increasing landfill gas yields from municipal solids wastes and other sources of biomass. Attempts are being made to accelerate gas production rates by pretreating the biomass before it is deposited into the batch digester, thereby enhancing microbial metabolism during decomposition. This technique, referred to as "controlled landfilling," incorporates an admixture of nutrients, buffer, and inoculum with the biomass source [4]. Recent laboratory scale experiments using municipal solid waste mixed with digested sewage sludge (inoculum and nutrient supply) and buffer have resulted in approximately 60% biomass conversion after 6 months at mesophilic conditions [5]. Jewell et al. [2] have shown similar results with wheat straw mixed with digested dairy manure effluent and utilizing leachate recycle. These results were obtained at mesophilic conditions, with 20% solids and approximately 0.24 gm/cm^3 (15 lb/ft^3) density of solids in the reactor. The results with the "controlled landfill" concept with both municipal solid waste and wheat straw indicate the potential of the process. Additional experimentation is necessary to determine the kinetics and gas yield for high solids batch digestion of crop residues.

Pretreatment

Fuel gas production from crop residues can be enhanced by use of a pretreatment process to produce water soluble molecular fragments. The cellulosic fraction of the residue is broken down into simple wood sugars. The complex benzene ring structure of the lignaceous fraction of the residue is broken down into low molecular weight aromatic acids and other organic fragments. Pfeffer and Quindry [3] have shown that the biodegradability of corn stover can be increased from about 35% to 70% with a NaOH pretreatment at 110°C for 4 hours. Olalade et al. [6] have shown increased biodegradability of barley straw after NaOH pretreatment. McCarty et al. [7] have also shown improved biodegradability of biomass following alkali pretreatment.

BASE LINE SYSTEMS DESIGN

One approach to systems analysis of engineering processes is to establish a base case for which the economic analysis is performed. The procedure used in this study is the selection and analysis of nine base line systems, which includes the different types of residues considered and three significantly different scales of operation, namely, small farm, cooperative, and utility/ industrial sizes. A sensitivity analysis is performed to determine the effects of changes in the various base-line systems parameters.

A summary of agricultural data [8] indicates that there are three major crop residues which should be considered: small grain straws (primarily wheat straw), corn stover, and large grain straws (primarily rice straw). These choices were based on the total U.S. residue available and on localized conditions of high residue concentration, e.g., rice straw in the Sacramento River Valley of California. The per acre yield for these residues is estimated from agricultural statistics to be 4.0 (1.6), 4.4 (1.75), and 5.8 (2.3) T/ha (tons/acre), respectively. The composition of the residues utilized in the analyses are presented in Table 1.

In this analysis, base line conditions were established for small, medium, and large scale processes. Small scale is defined as a process designed for use on a small farm, utilizing the residue produced on that farm. The medium scale system would be a cooperative venture, designed to utilize the residue from 100 small farms (two orders of magnitude greater than the small farm system). The large scale system is an order of magnitude greater than the medium size, utilizing residue from 1000 farms, a size sufficiently large for a utility or industrial complex. The average size of a small farm in the U.S. is approximately 162 ha (400 acres).

Various process options are utilized for each base line system. The options considered are presented in Table 2.

In all cases, it is assumed that manure is added with the crop residues (in the ratio of 1 part manure solids/10 parts feed solids) to provide nutrients and inoculum. The major difference between the small scale and the other two sizess is the digestion temperature and retention time. The medium and large scale systems operate at thermophilic conditions, 60°C, with a retention time of 10 days. The small scale system incorporates a mesophilic temperature of 35° with a 16-day retention time.

The digester feed solids concentration is assumed to be 10% for all cases. High solids concentration is preferred since it results in smaller reactor volume and lower effluent stream heat losses, both factors contributing to lower costs. Continuous digestion with high solids concnetration (up to 17%) in the feed has been obtained with other substrates, such as dairy cow manure [9]. However, Pfeffer and Quindry [2] have indicated some difficulty in mixing corn stover with digester solids content above 8%. A value of 10% solids is utilized for feed concentration to ensure that the digester solids concentration will be less than 8%. Note that

with effective pretreatment, a 10% feed concentration would result in significantly less than 8% digester solids and could justify the use of higher feed solids with an associated reduction in digester size and costs.

The labor requirements and costs for the base line designs will affect the annual operating costs significantly. The values used are 4 operators per shift, 3 shifts per day for the medium scale system, and 8 operators per shift, 3 shifts per day for the large system. The cost for operators was taken to be $6.00/hr. For the small scale system, it is assumed that the process will require 2 hours per day of the farmer's time, but the value of this time is taken to be $0/hr. There were also no supervision, overhead, or administration costs attributed to the small scale base line design.

The cost of crop residue will affect the economics of the conversion process significantly. For all base line cases, the value of this crop residue was taken to be $0/T. A detailed discussion of the effect of residue cost is presented in the sensitivity analysis. Significant credits or penalties can be attributed to the digester effluent stream, e.g., credit for fertilizer or refeed value. However, for the base line system, the credits and penalties are disregarded. A detailed discussion of these factors is included in the sensitivity analysis.

To ensure an objective and equitable economic evaluation of the various processes analyzed in this program, a consistent and uniform set of cost estimating criteria must be applied. Commonly used methods for profitability evaluation include rate of return on investment, discounted cash flow, present worth, and payout period. Another method which has been used previously by Dynatech R/D Company is the utility financing method, which is applicable to a specific set of conditions. In this study, the discounted cash flow (DCF) [10] and utility financing methods were used. In this analysis, the discounted cash flow method is utilized by assuming an expected rate of return on investment and determining the unit gas cost which gives a present value of zero for that rate of return. The procedure for calculating the unit gas cost based on the utility financing method was described in a report from Esso Research and Engineering Company to the Federal Power Commission [11].

Capital cost estimates used in this study were based on price levels at March 1979. Cost data were obtained from manufacturer's quotes, the literature, empirical cost correlations, and various other sources. If these data must be updated to present costs, this can be done by the use of a cost index. The index used in this study is the Chemical Engineering (CE) Plant Cost Index [12]. It is commonly accepted and used in the chemical industry. Based on a value of 100 for 1957-59, the composite CE plant cost index for the base time frame of March 1979 is 232.

BASE LINE SYSTEMS ANALYSIS

The results of the base line systems analyses are presented in Figure 1 for corn stover. Similar results are found for rice straw and wheat straw. The results give unit gas cost as a function of system size utilizing a discounted cash flow method for the returns on investment indicated. For the large scale system, the unit gas cost obtained using the utility financing method is also presented. It is apparent from these results that there is an economy of scale, i.e., unit gas cost is lowest for the largest scale system.

There are several significant performance differences between the different size systems. The medium and large scale base line systems incorporate a CSTR at 60°C and 10 days retention time which gives a fractional conversion of biodegradable volatile solids of 77%. The fractional conversion of volatile solids depends upon the fractional content of biodegradable solids in the feed; the conversions are 28, 38, and 32% for corn stover, rice straw, and wheat straw, respectively. The small scale system utilizes a CSTR at a lower temperature, 35°C, and longer retention time, 16 days. This leads to a lower fractional conversion of biodegradable volatile solids, 45%, and a lower conversion of volatile solids; 16, 23, and 19% for corn stover, rice straw, and wheat straw, respectively. If the small scale case were to utilize 60°C and 10 day retention time operation, the unit gas costs would be about 40% lower than those presented.

Another interesting comparison is the relative contributions due to fixed and operating costs. For the small, medium, and large scale systems, the ratios of operating to fixed costs contributions are approximately 0.5, 2.2, and 1.4, respectively. The small scale system has a low ratio since all labor associated costs were assumed to be zero. For the medium and large scale systems, labor and supplies costs acconted for approximately 60 and 35% of operating costs, respectively, which results in the high ratios of operating costs to fixed costs.

The major contribution to capital costs is due to digester cost, which accounts for approximately 70, 70, and 75% of capital costs for small, medium, and large scale systems, respectively. Approaches which lead to lower digester capital costs should result in significant reductions in unit gas costs.

The results of the base line systems analyses indicate which factors make large contributions to unit gas costs. Approaches to abate these costs by appropriately altering these factors are discussed in the sensitivity analysis.

SENSITIVITY ANALYSIS

A sensitivity analysis was performed to determine the effects of varying some of the base line parameters on system economics. One important

condition is the type of digester process employed. One significant change is to utilize a batch digestion process. A second change is variation in retention time of solids in the digester.

Batch Digestion

The batch digestion process can be incorporated by utilizing a controlled landfill concept with a low capital cost reactor (e.g., a hole-in-the-ground) as the batch digester. For the batch landfill system, the digestion temperature is assumed to be 35°C. For this temperature, the value of the reaction rate constant utilized is one which would yield 60% conversion of biodegradables in 6 months, as was obtained in the laboratory experiments [2,5]. Buffer chemical addition equal to 1% of the solids content is included for the batch process at a cost of $29.50/T ($30/ton). The results are presented in Figure 2 for batch digestion of corn stover, over a range of batch digestion retention times.

Analysis of the results indicates that for the range of batch digestion retention times of 6 months to 1 year, the gas cost is lower for the higher retention times. This is due to the large difference in conversion efficiences (e.g., 60% at 6 months and 83% for 1 year) and the corresponding difference in gas production.

A comparison of batch digestion with the base case CSTR system indicates several interesting results. For the medium and large sizes, the base case CSTR system results in a lower unit gas cost than does the batch process. For the small scale system, the batch process results in equivalent lower unit gas costs than for the CSTR. There are several reasons for this. First is the gas production. For the base line CSTR design, the medium and large scale systems utilize 60°C, whereas for the small scale system, a 35°C digestion temperature is incorporated. The conversion efficiency is much higher for the thermophilic mode than for the mesophilic, whether a batch or CSTR digester is employed. Thus, the gas production for the medium and large scale systems is about 15% greater than for the batch process (at 180 days retention time). For the small scale sytem, the gas production is 50% greater for the batch system (at 180 days retention time). These differences in gas production are partial contributors to the variations in unit gas costs.

A second reason for the differences in unit gas costs is the differences in capital costs of the digesters. The batch system utilizes a low cost per unit volume reactor, but because all the solids must be loaded in the reactor initially, the volume of the reactor for batch operation is significantly greater than for the CSTR mode, 20 and 35 times greater for the small and large scales, respectively. Typically, a density of 0.64 gm/cm^3 (40 lb/ft^3) is maximum for a landfill, compared to about 1 gm/cm^3 (64 lb/ft^3) for a continuous flow system. The digester cost for the large scale batch system (for corn stover) is $44 million, which is 4.5 times the $9.8 million for the base line CSTR design for corresponding conditions. This ratio is much lower than the ratio of digester volumes, due to the lower per volume digester cost for the batch system, $6.15/m^3 ($4.70/yd^3) compared to $52/m^3 ($40/yd^3) for the CSTR digester. For the small scale system, the batch digester cost is $100,000, which is 2.3 times the CSTR digester cost of $43,000.

It should be noted that the major cost item for the small scale batch system is the digester. Because this is a hole-in-the-ground digester, it is possible to reduce this cost significantly by having the farmer construct the digester. If the digester cost were reduced by 50%, the unit gas cost would also decrease by about 50%, since the digester cost contributes about 90% to the gas cost.

Since small scale batch digestion has a potential economic advantage over a continuous process, it is important to describe the scenario for this process. The crop residue is added to the digester with the appropriate addition of manure (inoculum and nutrient), buffer, and water to provide a mixture which will result in a high rate of gas production. This loading and admixing step should occur over a one month period. The digestion process will be designed to result in 60% conversion of biodegradable matter in six months. However, the digestion process could continue up to ten months, which would yield about 78% conversion, after which time the digester is unloaded and prepared for the residue obtained from the next season's crop. This unloading step should proceed over a one month period. The total cycle will be 12 months, with one month each for loading and unloading, and up to 10 months for digestion.

It should be noted that several critical factors could influence this scenario. First, it is necessary to start the batch digester at the appropraite time to ensure maximum gas production at the time of maximum need, i.e., the winter months. Also, it is essential that the periods of intensive labor (loading and unloading) for this process do not coincide with other high labor farm operations (such as crop harvesting). Meeting such conditions will probably require use of a residue storage system. The actual timing of this process will depend upon location and crop residue utilized.

The results, which indicate the relative economic advantage of the small scale batch system over the conventional CSTR, indicate that development for small farm digestion of crop residues should continue on the controlled landfill concept. This system probably has the advantage of requiring less labor once the system is initiated, a desirable characteristic for small farm operation, i.e., there is no need for daily (or less frequent but regular) loading of residue as is the case for continuous digestion.

Retention Time

The effect of varying CSTR digester retention time results in lower unit gas cost. The effect of decreasing retention time is to decrease the digester volume, and therefore the capital cost is decreased. However, lowering retention time decreases the fractional conversion and hence the gas production. The effects of these opposing factors result in decreasing gas cost with lowering of the retention time in the range of 4 to 16 days for the digestion conditions and feedstocks incorporated in this analysis. The decrease in unit gas cost is about 20% for the large scale system when going from 10 days to 6 days retention time. Pfeffer has found stable thermophilic digestion for retention times as low as 4 days for digestion of corn stover.

Pretreatment

The results for the base line systems designs show that the fractional conversion of volatile solids is extremely low, less than 40% of the heating value of biomass is obtained in the form of methane. One approach to improve the yield is to use a pretreatment step to solubilize the originally non-biodegradable volatile solids. Chemical and/or thermal processing can be used to improve the yield [3,7].

The effect of adding pretreatment to all the base line cases was analyzed, and the results are presented in Table 3 for corn stover, rice straw, and wheat straw. The conditions of pretreatment used in these analyses were 115°C temperature, 4 hours retention time, 50% conversion of non-biodegradable volatile solids to biodegradable volatile solids, and 5% loss of input biodegradable solids. The chemical pretreatment conversion of 50% was with addition of sodium hydroxide which costs about $295/T ($300/ton).

Pfeffer and Quindry [3] presented economics for pretreatment and digestion of corn stover and obtained a unit gas cost of about $9.50/GJ ($10/MM Btu), compared to about $4.10/GJ ($4.30/MM Btu) for the analysis presented in this study. However, Pfeffer's economic analysis uses net energy production, whereas in this study the gross energy output is used. The net gas output used by Pfeffer of 143 GJ/hr (135 MM Btu/hr) is about half of the gross value calculated using the composition and conversion parameters in this report. This gros value would yield a gas cost of about $4.75/GJ ($5/MM Btu), which is comparable to the results presented for this study.

The results of the analysis of pretreatment indicate that the cost of chemical significantly affects the unit gas cost. For a 5% chemical requirement the chemical cost is about 50% of operating cost for medium and large scale systems. This chemical cost is a critical factor in the unit gas cost resulting from pretreatment and digestion of crop residue and suggests approaches in pretreatment anddigestion of crop residue and suggests approaches in pretreatment processing to reduce unit gas cost. These alternative methods include use of lower cost chemicals or less chemical. However, experimental evidence indicates that use of less chemical results in lower conversion to biodegradables [7] so that the gas production is less and unit gas cost is higher. For example, if use of 2.5% NaOH were to result in only 25% conversion of non-biodegradables, the unit gas cost for pretreatment digestion of corn stover (for the intermediate size) will be approximately $5.07/GJ ($5.29/MM Btu) for the 5% NaOH pretreatment case, i.e., essentially no difference in unit gas cost.

The effect of varying pretreatment conditions was also analyzed. Other pretreatment conditions used are 150°C and 1 hour retention time, with 5% chemical added and 50% conversion. The effects of these changes are to lower the capital cost and increase the heat requirement, with the net result of approximately no change in unit gas cost, assuming a 50% conversion.

Labor Requirement

Operating labor costs contribute about 25 and 10% to the operating costs for the medium and large scale systems. In addition, other factors such as supervision, overhead, and supplies are directly related to operating labor costs. For the small farm system, these labor and associated costs were assumed to be zero. Since labor costs are such a significant factor, it is essential to determine the effects of varying the labor requirements and associated costs.

For the small scale system, the base line case utilized $0/hr for the farmer's labor cost. However, this labor should be assigned a value since it could be utilized for another profitable farm operation. The value of a farmer's labor is extremely difficult to assess, since it is very seasonal. Obviously, during harvesting the labor value is high, and in mid-winter it would be low. The effect of labor cost is shown in Figure 3, assuming $6/hr average cost, and varying the labor requirement for the digestion process. (The results in this figure can also be used to determine the effect of different hourly labor rates, e.g., 2 hrs/day at $6/hr would give the same cost as 1 hr/day at $12/hr.) For 1 hr/day labor requirements at $6/hr the gas cost will increase by about $1.40/GJ ($1.50/MM Btu).

The results for the medium size system are presented in Figure 4. A variation in operating labor requirement from the base line case of 4 men/shift to 1 man/shift is shown. The unit gas cost is reduced by about $0.38/GJ ($0.40/MM Btu) for each man/shift reduction in labor requirements. For the large scale system, the base line case utilized 8 men/shift. The results of varying the labor requirement, presented in Figure 5, are that a reduction of 1 man/shift reduces the unit gas cost by about only $0.05/GJ ($0.05/MM Btu).

It is concluded from these results that for the small and medium scale systems simple digestion

processes which require minimal operating labor are essential for economical feeasibility. The manpower required for loading feedstock for a continuous digestion process would make any reduction in labor requirement very difficult to justify.

Residue Cost

The base line systems analyses utilized a $0/T residue cost. For some biomass sources (e.g., municipal solid waste) drop charges, or negative feedstock costs, are the case, but for agricultural crop residues, it is likely that a positive cost will be attributed to the feedstock. This cost will be due to removal or harvesting the crop residues from the field and its delivery to the processing facility.

The effects of feedstock cost on unit gas cost are presented in Figure 6 for corn stover. For the medium and large scale systems, unit gas cost will increase by $2.40/GJ ($2.50/MM Btu) for every $10/T($10.16/ton) increaes in feedstock cost. For the small scale system, the increase is about $3.85/GJ ($4.06/MM Btu) per $10/T ($10.16/ton) increase in feedstock cost. It should be noted, however, that if pretreatment were used, the gas production would be about doubled, resulting in a sensitivity to feedstock cost of about half of the no-pretreatment case.

These results must be compared with estimated costs for agricultural crop residue collection and delivery. Approximate costs for crop residues have been developed by SRI Inter-national [8]: $9.85/dry metric ton ($10/dry ton) for high moisture crop residues (such as corn stover) and $5.90/dry metric ton ($6/dry ton) for low moisture residues (such as rice and wheat straws). Vetter [13] estimated the cost of harvesting and transporting corn stover to range from $15-20/dry metric ton for a range of 175-1000 metric tons per years. The output from a small farm, 160 ha (400 acres), is approximately 711 T/yr (700 tons/year). These costs include amortized costs for farm machinery required for the harvesting procedure. Horsfield and Williams [14] estimate the cost of about $5.90/T ($6/ton) to transport the straw 16 km (10 miles).

The average distance for transportation can be estimated by considering the processing facility as centrally located within the area from which the residue is collected. For the 160 ha (400 acre) small size system, the average distance to transport residue is less than 0.8 km (0.5 miles). For the cooperative size system, collecting residue from the 100 small farms, or 16,000 ha, the average distance is about 16 km (20 miles), assuming crop residue is obtained from only 10% of the area around the processing facility. For the large scale facility, the average distance is 48 km (30 miles), also assuming collection from 10% of the area. If 25% of the area were harvested, the average distances would be about 9.7 and 32 km (6 and 20 miles) for the medium and large scale systems, respectively. Thus, for the medium size system, $6/T for transportation is reasonable. For the large scale system, the transportation cost would be about $12/T, assuming a cost of about 19¢/km (30¢/mi) for the additional distance [15].

It is obvious from the range of values presented that the residue cost can range from $5-20/T. The corresponding increase in unit gas cost would range from about $1-5/GJ for the medium and large scale systems without pretreatment and about $0.50-2.50/GJ when pretreatment is utilized. For the small scale system, the collection cost would be low (no harvesting cost, only no transportation cost), contributing about $3/GJ to the gas cost.

Digester Effluent

The base line designs incorporated the assumption that there would be no credit or penalty associated with the digester effluent. Potential uses of the effluent solids include fertilizer and animal feed. The value for such uses could be significant. On the other hand, a penalty could be associated with disposal of digester effluent, particularly the waste water stream after dewatering the digester effluent to recover the solids.

The effect of credits and penalties for the effluent stream was investigated. The conditions used in the analysis were a dewatering processing step in which 95% of the solids were recovered at a concentration of 25% solids; the low solids waste stream was disposed of at a cost of $0.50/$m^3$ ($2/1000 gal), and the credit for the solids ranged from $0 to $75/T.

The results of the analysis for effects of credits and penalties are presented in Table 4 for corn stover, rice straw, and wheat straw for the medium and large size systems. The results in this table give the ROI required for zero present worth using the DCF method, assuming a gas value of $1.90/GJ ($2/MM Btu). The returns on investment obtained by this procedure are presented in Figure 7 for corn stover. From this figure it is noted that every $10/T increase in by-product value increases the return on investment by about 4%. These results indicate that for a high by-product credit value, the digester effluent will have a greater value than the value of gas. Under those conditions, it might be better to consider the gas as the by-product stream.

A comparison should be made between expected by-product credit values and the range of values used for hte sensitivity analysis. Vetter [13] indicates that corn stover would have a fertilizer value of about $4.90/dry T ($5.00/dry ton). This value is due primarily to the nitrogen, phosphorus, and potassium content, which would not change significantly during digestion. However, since some biodegradable solids are removed during digestion, the value of the effluent solids would be greater than $5/T. Digestion without pretreatment removes about 25% of the total solids, giving an effluent value of about $6.60/T ($6.70/ton). Pretreatment results in about 50% total solids reduction, giving an effluent value of about $9.85/T ($10/ton).

Pretreatment results in about 50% total solids reduction, giving an effluent value of about $9.85 /T ($10/ton). SRI [16] has indicated that a $25/T value for digested animal manure effluent would be optimistic. The range used in this sensitivity analysis appears to extend to highly optimistic values. The range more probably encountered would be $5-25/T, which would give a ROI (assuming $1.90/GJ gas value) of up to about 10% for the large scale system

ENERGY BALANCE

One of the most critical factors in any alternate energy or energy conversion process is the energy balance, i.e., some indication of the difference between energy in and energy out. There are several ways to define the energy balance. One is the ratio of process energy requirement to gross energy output (the energy content of the digester gas). If this ratio were greater than 1, the process would use more energy than it delivers and hence would be uneconomical in an energy accounting. It should be noted that this definition does not incorporate the energy content of the residue feedstock (the higher heating value of the residue). If incorporating this energy content into the energy balance is desired the ratio should be the difference between energy output and process energy requirement to energy input.

Values of the ratios (η_1) and (η_2) for the various systems and options are presented in Table 5 for corn stover, rice straw, and wheat straw and the small, intermediate, and large scale systems. The energy efficiencies presented in this table indicate that the highest energy efficiency (η_2) occurs for pretreatment followed by continuous thermophilic digestion, i.e., the conditions for the intermediate and large scale systems. These systems also have low values for η_1, the ratio ot process energy use to energy output. The lowest value of η_1 arise for the batch digestion process, since this design utilizes the heat of reaction to provide process heat, and there is no heat loss attributed to the digester effluent stream. Also, the batch systems does not require any energy for digester mixing.

For the base line small scale system with corn stover feedstock, the system utilizes about 50% of the energy it produces. The energy balance is slightly better for rice straw and wheat straw. For the base line medium and large scale systems with corn stover, the process utilizes about 20% of the energy it produces, which is better than for the small scale system. Since the medium and large scale systems operate at thermophilic conditions, the conversion and gas production are greater than for the small scale system, thus giving a more favorable energy balance.

ACKNOWLEDGEMENTS

This work was performed for the Solar Energy Research Institute, Bio/Chemical Conversion Branch, under subcontract XR-9-8157-1. The authors wish to thank Dan Jantzen of SERI for his support as technical monitor for this program. The support of R.L. Wentworth and D.L. Wise of Dynatech R/D Company is also acknowledged.

REFERENCES

1 Ashare, E.,and E.H. Wilson. 1979. Analysis of Digester Design Concepts. Dynatech R/D Company Engineering Report on DOE Contract No. EY-76-C-02-2991.*000, Report No. COO-2991-42.

2 Jewell, W.J., H.R. Capener, S. Dell'orto, K.J. Fanfoni, T.D. Hayes, A.P Leuschner, T.L. Miller, D.F. Sherman, P.J. van Svest, M.J. Wolin, W.J. Wujcik, 1978. Anaerobic Fermentation of Agricultural Residue: Potential for Improvement and Implementation. Preliminary Draft of Final Report prepared for U.S. Department of Energy - Fuels from Biomass Report EY-76-S-02-2981-7.

3 Pffeffer, J.T., and G.E. Quindry. 1979. Biological Conversion to Methane, Corn Stover Studies. Project Report, December, 1, 1977 - August 1, 1978. Submitted June 1979 to U.S. Department of Energy, Contract No. EY-76-S-02-2197.

4 Augenstein, D.C., D.L. Wise, R.L. Wentworth, and C.L. Cooney. 1976. Fuel Gas Recovery from Controlled Landfilling of Municipal Wastes. Resource Recovery and Conservation, 2: 103-117.

5 Buivid, M.G. 1979. Dynatech R/D Company, private communication, July, 1979.

6 J. Healy, W. Owen, D. Stuckey, P.J. Colberg, L.Y. Young, and P.L. McCarty. 1978. Heat Treatment of Organics for Increasing Anaerobic Biodegradability. Quarterly Progress Report for the period June 1, 1978 to August 31, 1978. Submitted to the U.S. Department of Energy, under Contract No. EY-76-S-03-PA-44.

7 Ololade, B.G., et al. 1970. Canadian J. Animal Sci., 50: 657.

8 Ernest, R.K., R.H. Hamilton, N.S. Borgeson, F.A. Schooley, and R.L. Dickenson. 1979. Mission Analysis for the Federal Fuels from Biomass Program, Volume III. Feedstock Availability. Final Report prepared for U.S. Department of Energy, Contract No. EY-76-C-03-0015 PA-131.

9 Marchaim, U. 1979. Kibbutz Industries Association, private communication, May 1979.

10 Peters, M.S., and R.D. Timmerhaus. 1968. Plant Design and Economics for Chemical Engineers. McGraw-Hill, New York.

11 Siegel, H.J., T. Kalina, and H.A. Marshall. 1972. Description of Gas Cost Calculation Methods being Used by the Synthetic Gas-Coal Task Force of the FPC National Gas Survey. Esso Research and Engineering Company, report to the Federal Power Commission.

12 Economic Indicators, Chem. Eng., 86 (28):7, December 31, 1979.

13 Vetter, R.L. 1976. Agricultural Residues as Feed Resources in Energy Relationships for a 320-Acre Iowa Farm: An Attempt to Increase Production of Grain and Meat while Rendering the Farm Energy Self-Sufficient by Generating Methane through Anaerobic Fermentation of Residues. Report No. ERDA/USDA-1946/76/FR-3.

14 Horsfield, B. and R.O. Williams, 1976. Technical and Economic Assessment of the Utilization of Rice Straw Residue from the California Sacramento Valley for On-Power Generation. Report to U.S. Department of Energy, TID-28551.

15 Koelsch, R.K., et al. 1977. Use of Crop Residues to Support a Municipal Electrical Utility in Food, Fertilizer, and Agricultural Residues. ed. R.C. Loehr. Ann Arbor Science Publishers, Inc., Ann Arbor, MI.

16 Jones, J.L., W.S. Fong, F.A. Schooley, and R.L. Dickenson. 1978. Mission Analysis for the Federal Fuels from Biomass Program. Volume V. Biochemical Conversion of Biomass to Fuels and Chemicals. Final report prepared for U.S. Department of Energy, Contract No. EY-76-C-03-0015 PA-131.

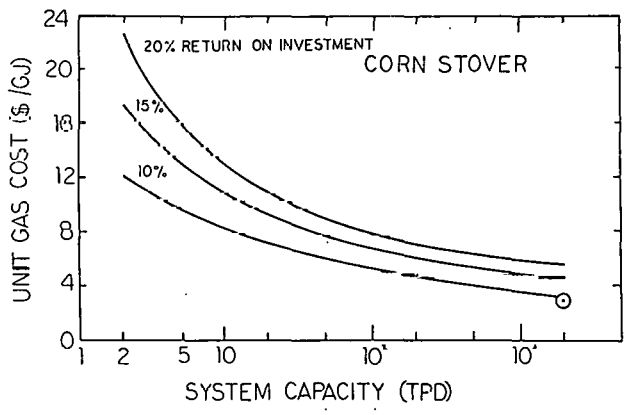

Fig. 1 Unit Gas Cost as a Function of System Capacity

Base Line Systems Analyses for Corn Stover (—— DCF Method; O Utility Financing Method

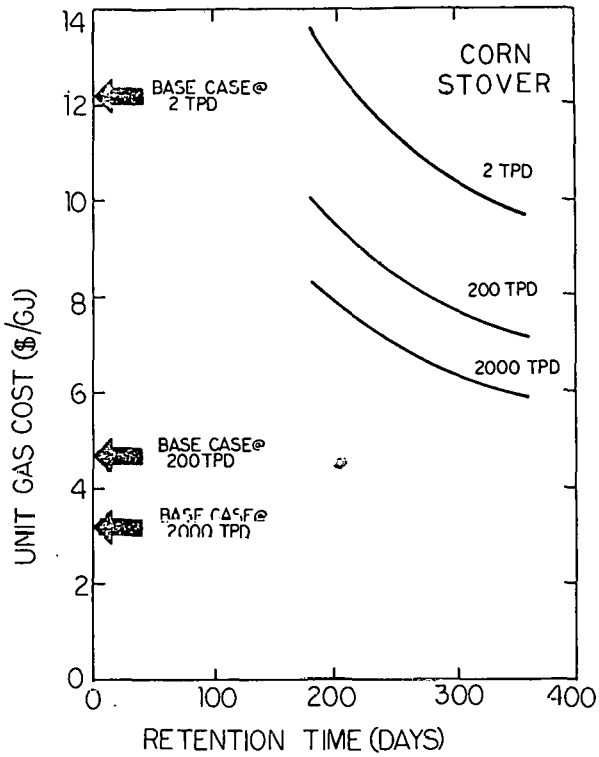

Fig.2 Unit Gas Cost for Batch Digestion of Corn Stover

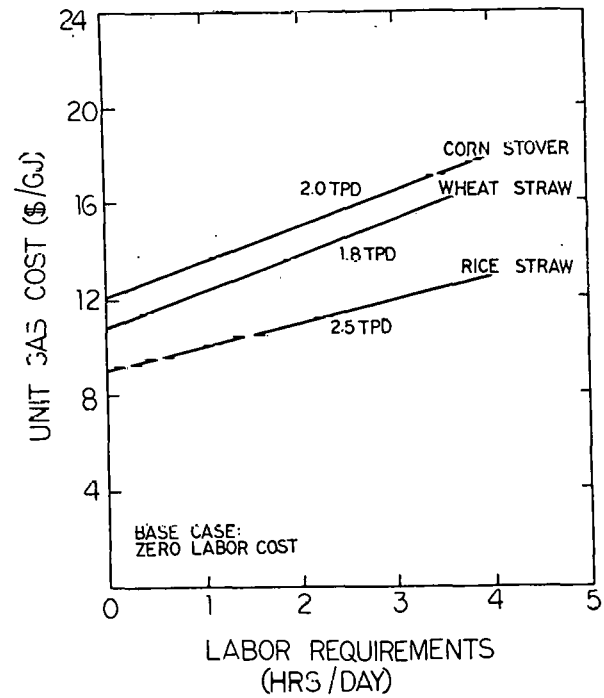

Fig.3 Effect of Labor Requirement on Unit Gas Cost for Small Scale System

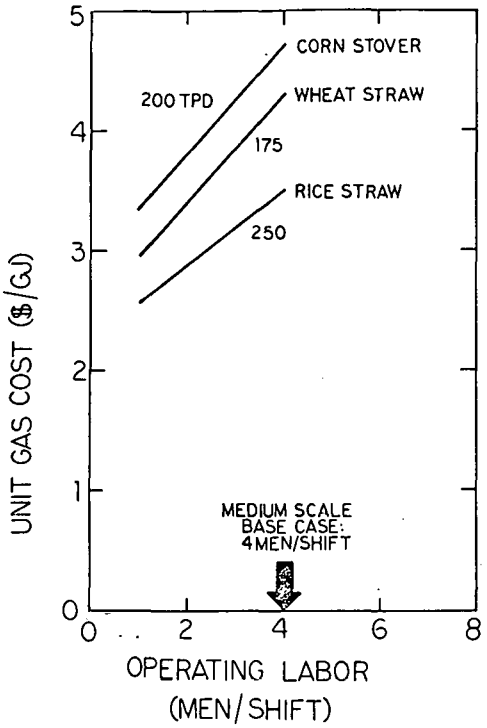

Fig. 4 Effects of Labor Requirement on Unit Gas Cost for Intermediate Scale System

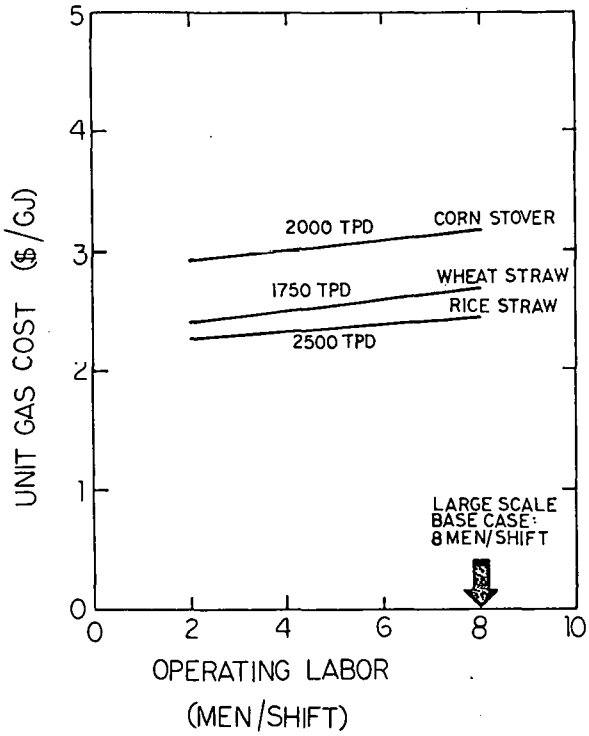

Fig. 5 Effect of Labor Requirement on Unit Gas Cost for Large Scale System

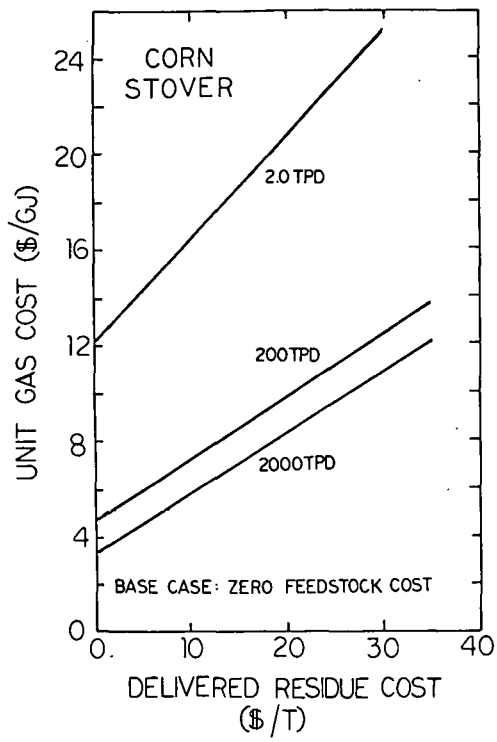

Fig. 6 Effect of Residue Cost on Unit Gas Cost for Corn Stover

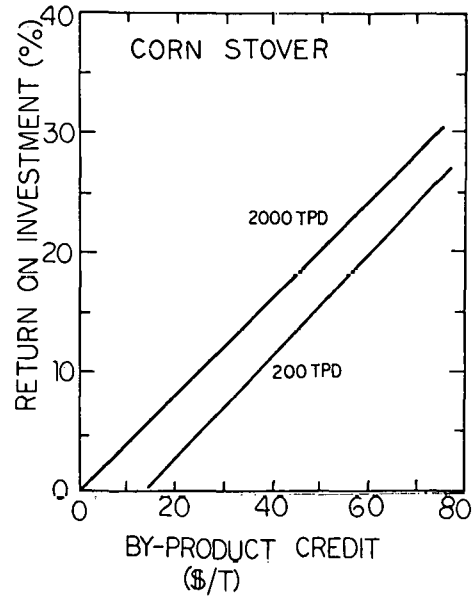

Fig. 7 Effect of By-Product Value on DCF Return on Investment (Gas Value of $2/GJ)

Table 1
Residue Composition

	Wheat Straw	Corn Stover	Rice Straw
% Solids Content	90	50	92.5
% Volatile Solids (of Total Solids)	94	95	83
% Biodegradability (of Volatile Solids	42	36	50

Table 2
Base Line Process Options

	Small Scale	Medium Scale	Large Scale
Storage	Y	Y	Y
Shredder	Y	Y	Y
Holding/Mixing	Y	Y	Y
Pretreatment	N	N	N
Digestion	C	C	C
Heat Exchange	Y	Y	Y
Dewatering	N	N	N
Gas Purification	N	N	N

Y = Option Used
N = Option Not Used
C = CSTR Digester

Table 3
Effect of Pretreatment* on Residue Digestion

	Corn Stover	Rice Straw	Wheat Straw
Small Scale			
Annual Gas Production (MM Btu)	2.68 x 10	3.2 x 10	2.4 x 10
Unit Gas Cost ($/MM Btu)	12.81	12.36	12.76
Intermediate Scale			
Annual Gas Production (MM Btu)	4.56 x 10	5.47 x 10	4.10 x 10
Unit Gas Cost ($/MM Btu)	5.29	5.10	5.15
Large Scale			
Annual Gas Production (MM Btu)	4.56 x 10	5.47 x 10	4.10 x 10
Unit Gas Cost ($/MM Btu)	4.33	4.38	4.15

* Pretreatment Conditions
NaOH Requirements = 3% of feed solids
Conversion = 50% of non-biodegradable solids
Temperature = 115°C
Retention Time = 4 hours

Table 4
Effect of By-Product Credit Value on Rate of Return on Investment

$/TON BY-PRODUCT CREDIT	% RETURN ON INVESTMENT FOR UNIT GAS COST OF $2/MM BTU					
	CORN STOVER		RICE STRAW		WHEAT STRAW	
	200 TPD	2000 TPD	250 TPD	2500 TPD	175 TPD	1750 TPD
0	-	-	-	-	-	-
25	5	10	8	12	4	12
50	16	21	18	22	16	21
75	26	30	26	30	24	30

Table 5
Energy Efficiency of Crop Residue Digestion Processes

		CORN STOVER			RICE STRAW			WHEAT STRAW		
		small	intermediate	large	small	intermediate	large	small	intermediate	large
Base Line	η_1	0.49	0.21	0.21	0.35	0.15	0.14	0.40	0.16	0.16
	η_2	0.08	0.21	0.21	0.14	0.30	0.30	0.10	0.24	
Batch Digestion (180 d retention time)	η_1	0.08	0.08	0.08	0.03	0.03	0.03	0.04	0.04	0.04
	η_2	0.71	0.71	0.21	0.29	0.29	0.24	0.24	0.24	0.24
CSTR with Pretreatment	η_1	0.35	0.14	0.14	0.33	0.13	0.13	0.33	0.13	0.13
(57 VSDB 50% conversion)	η_2	0.11	0.33	0.09	0.10	0.66	0.66	0.18	0.40	0.40
CSTR with Gas Purification	η_1			0.30			0.24			0.25
	η_2			0.18			0.27			0.22

η_1 = (process energy requirement)/(digester gas energy content)

η_2 = $\frac{\text{(digester gas energy content) - (process energy requirement)}}{\text{(feedstock energy content)}}$

Dup

THERMAL AND COST GOAL ANALYSIS FOR PASSIVE SOLAR HEATING DESIGNS*

Scott Noll and Christina Kirschner
Los Alamos Scientific Laboratory

ABSTRACT

Economic methodologies developed over the past several years for the design of residential solar systems have been based on life cycle cost (LCC) minimization. Because of uncertainties involving future economic conditions and the varied decision making processes of home designers, builders, and owners, LCC design approaches are not always appropriate. To deal with some of the constraints that enter the design process, and to narrow the number of variables to those that don't depend on future economic conditions, a simplified thermal and cost goal approach for passive designs is presented. Arithmetic and graphical approaches are presented with examples given for each. Goals discussed include simple payback, solar savings fraction, collection area, maximum allowable construction budget, variable cost goals, and Btu savings.

INTRODUCTION

Over the past several years, standardized methodologies have evolved for the analysis and economic optimization of solar hot water and residential space heating designs [1]. In most instances, the optimizing criteria has been the minimization of life cycle costs (LCC): that is, determine the particular system configuration that results in the lowest delivered cost of heat to the home (solar and backup) over the expected system lifetime. Although it is widely held that life cycle cost minimization results in the specification of an economically efficient solar design [2], there are a variety of considerations that make the results of such optimization techniques untenable and/or unuseable.

- The results of economic design optimization are generally driven by expectations concerning unknown or uncertain future conditions; these expectations take the forms of specified values for parameters such as inflation rates, fuel and tax escalation rates, discount rates, and operation and maintenance costs over time. The uncertainty of parameter values increases as the life cycle analysis period increases.

- LCC analysis usually considers the stream of costs and benefits over the expected system lifetime. Where the building ownership period is equal to or greater than the expected system lifetime, as in government owned and operated buildings, this presents no problem. Where ownership periods are shorter, as with residential property, the solar system may change hands many times. This complicates life cycle analysis because of such questions as transaction costs, uncertain resale valuation, and changing owner/system interactions. An alternative approach is ownership cycle costing, OCC, which considers costs only throughout one ownership.

- LCC analysis embodies the cycle-implicit assumption that longer term benefits of LCC minimizing designs will be realized by the party making the analysis. Where the client/owner may also be the owner/operator, (i.e. commercial buildings) the longer term benefits of design optimization will be realized by the requesting client. At the other end of the spectrum is the speculative tract-home builder of residential construction. These builders are not responsible for the ultimate operating costs of the homes they construct and therefore have no incentive to increase first costs with solar designs when a lower LCC for heating would result. Building codes and local ordinances mandating prescriptive construction standards and use of solar have been used to help circumvent these problems. On the other hand, when energy conservation and solar features are recognized as effective home marketing devices, the builders will respond to this demand with construction techniques that more closely represent optimized economic designs.

- Finally, an optimized LCC design may imply physical attributes that violate existing design, site, or budget constraints. Examples would be maximum lot frontage dimensions with sideyard set back conditions that limit the south-facing linear exposure and hence collection area; partial shading due to permanent or temporary obstructions; architectural styling considerations and restrictive covenants; maximum permissible housing costs in an area due to the predominance of non-solar market comparables, etc.

In response to these considerations, we have formulated a simplified approach that allows one to either graphically or arthimetically evaluate thermal and cost goals for residential passive solar heating designs with or without regard to LCC. In this particular consideration, economic optimization per se is not considered; rather we have presented an approach that allows for separation of current versus future parameters in order to identify specific thermal and cost conditions that are required to achieve a variety of specified conditions.

*This work was performed at LASL under the auspicies of the Department of Energy, Office of Solar Applications, Systems Development Branch.

ARTHMETIC APPROACH

The arithmetic approach to thermal and cost goals analysis is merely the algebraic equivalent of what will be shown graphically. Although accuracy is improved, the arithmetic approach is not as fast in application but is quite easily understood.

We begin with an equation that is equivalent to saying that the life cycle savings of a passive solar addition are exactly equal to zero, that is:

$$[SSF \cdot P_o \cdot PWF_f \cdot CRF \cdot LOAD \cdot DD \div 10^6] - [VC \cdot A \cdot PWF_s \cdot CRF] = 0 \quad (1)$$

The units of the two terms in brackets are in equivalent annual $/yr. The first term represents annualized savings, the second term annualized costs. Definitions of terms is provided below:

- SSF Solar Savings Fraction which bears a direct relationship to the Load Collector Ratio (LCR) as set forth by LASL's Solar Group [3].
- P_o Initial cost of fuel in $/mmBtu corrected for conversion efficiency.
- DD Average annual heating degree days (65°F Base)
- LOAD Heat loss factor of the residence for all surfaces other than the south facing passive solar collector area. (Btu/DD)
- VC $/ft^2 variable cost of passive solar construction—fixed costs are seldom a significant factor in passive solar designs--all costs are expressed in the VC term.
- A Passive solar collection area (ft^2)
- LCR Building load collector area ratio (LOAD÷A) (Btu/DD-ft^2)
- PWF_f Present worth factor for auxiliary heat fuel costs which accounts for the future fuel escalation rate, discount rate, and period of analysis.
- CRF Capital recovery factor used to convert an initial dollar amount (present value dollar amount in our example) into a stream of equal annual payments such that the discounted sum of these payments is equal to the initial dollar amount.
- PWF_s Present worth factor for solar costs used to convert the initial passive solar construction cost into the sum of discounted annual cash flows associated with passive solar system ownership. PWF_s accounts for the down payment, principal plus interest payments, mortgage interest tax deductions, property taxes and deductions, insurance, operation and maintenance expenses and resale value net of the remaining loan balance.
- SPBK Simple payback equal to add-on cost divided by first year dollar savings.

$$SPBK = \frac{VC \cdot A \cdot 10^6}{P_o \cdot SSF \cdot LOAD \cdot DD}$$

Separating equation (1) into current and future factors:

$$\frac{VC \cdot A \cdot 10^6}{P_o \cdot SSF \cdot LOAD \cdot DD} = \frac{PWF_f \cdot CRF}{PWF_s \cdot CRF} = \frac{PWF_f}{PWF_s} . \quad (2)$$

Equation (2) still represents the breakeven LCC condition. The form of equation (2) has the advantage that the left side term deals with current factors (variable construction costs, initial fuel cost, degree days, and the three components of passive solar thermal performance represented by the LASL LCR tables; SSF, A, and LOAD). The right hand side deals with the future factors. In addition, the left side term is equivalent to the most basic definition of simple payback SPBK—first cost divided by the first year dollar savings.

DEFINING THE GOALS

In the context of equation (2), a variety of criteria may be used to determine system specifications or cost and thermal goals. Some of the criteria might include:

- simple payback
- solar savings fraction
- maximum add-on budget for passive solar construction
- passive collection area
- maximum energy budgets (e.g., Building Energy Performance Standards)

Other economic criteria have been used [4] to represent conditions necessary for consumer acceptance and relate to cash flow performance. These include years of negative annual cash flow and number of years required for cumulative savings to recover the initial downpayment expense. Since year by year cash flow analysis of any particular design is required to arrive at these numbers, they are not easily calculated using the approach set forth in this paper.

Equation (2) can be used in the following way:

a) Given values for DD and SSF(LCR); calculate SPBK or VC or P_o given values for two of the three.

b) Given values for SPBK, VC, P_o and DD, calculate SSF · LCR. Since SSF and LCR are mutually dependent, one must use the LCR tables to find the combination that yields a product close to the above value.

c) Given SPBK, SSF, and DD; A or LOAD can be determined given a value for the other; then P_o or VC can be determined given a value for the other; note SPBK, P_o, and VC may be interchanged in this process.

EXAMPLES

To exemplify (a), (b), and (c) above, assume we are looking at a double-glazed direct gain passive solar design in Dodge City, Kansas, with R-9 night insulation and mass surface/glazing area ratio of

3:1. From the LCR tables [3] we have the following performance relationship between SSF and LCR.

SSF	.1	.2	.3	.4	.5	.6	.7	.8	.9
LCR	236	109	68	47	35	26	20	14	8

From local data we know:

DD = 5046

P_o = \$.05/kwh = \$14.65/mmBtu (electric resistance)

a) Find the maximum variable cost one can pay for passive solar to achieve a six year payback for a .60 solar savings fraction against an electric resistance heating fuel alternative. From equation (2):

$$\frac{VC \cdot 10^6}{P_o \cdot SSF \cdot LCR \cdot DD} = SPBK \quad \text{or}$$

$$VC = \frac{SPBK \cdot P_o \cdot SSF \cdot LCR \cdot DD}{10^6}$$

Therefore,

$$VC = \frac{6 \cdot 14.65 \cdot .60 \cdot 26 \cdot 5046}{10^6} = \$6.92/ft^2$$

b) Find the thermal performance required to achieve an eight year payback for a direct gain design costing \$16/ft^2 against the electric resistance fuel alternative.

From equation (2):

$$SSF \cdot LCR = \frac{VC \cdot 10^6}{P_o \cdot DD \cdot SPBK}$$

$$= \frac{16 \cdot 10^6}{14.64 \cdot 5046 \cdot 8} = 27$$

The LCR table indicates that at SSF = .10, LCR = 236, and SSF · LCR = 23.6. Larger SSF values imply smaller product values, so the goal can only be met by a low-level passive design where the first square feet of collection area are the most efficient on a per square foot savings basis (i.e., the LCR value is over 236 Btu/DD-ft^2).

c) Find the collector area necessary to provide a solar savings fraction of .30, with a building load of 10,000 Btu/DD. With a VC = \$15/ft^2 find the simple payback of such a design against the electric resistance heating alternative. For SSF = .30, LCR = 68, and

$$A = \frac{LOAD}{LCR} = \frac{10,000}{68} = 147 \text{ ft}^2.$$

$$SPBK = \frac{15 \cdot 10^6}{14.65 \cdot .30 \cdot 68 \cdot 5046} = 9.9 \text{ years}$$

GRAPHICAL APPROACH

Figure 1 illustrates the reference graphs for thermal and cost goal analysis. The figure is divided into five contiguous quadrants numbered I thru V. The lower left hand corner shows the units for each of the variables.

Quadrant I shows the relationship between average cost (AC), initial fuel price (P_o), and simple payback (SPBK). By defining two of these variables, the third is uniquely determined. Quadrant II shows combinations of average cost (AC) and annual heating season Btu savings per square foot of passive collection area (SSF · LCR · DD ÷ 10^3) that imply equivalent passive solar variable construction costs (VC). Again, if two of these three variables are known, the third is uniquely determined. Quadrant III accounts for heating degree days. Once degree days are specified a transformation can be made between seasonal square foot energy savings and energy savings per square foot per degree day (SSF · LCR). Although there are many algebraic comginations of LCR and SSF that would produce a given value of their product, only unique combinations of SSF and LCR are feasible for a passive design in a particular climate. This can be seen by examining the LASL LCR performance tables. In quadrant IV, the SSF-LCR performance combinations can be plotted for a particular design or designs. This is done by choosing a solar savings, fraction value, say SSF = .30, and finding the intersection of the corresponding LCR value (LCR = 68 for our direct gain example) and the SSF = .30 ray emanating from the origin. If this is done for all values of SSF from .1 to .9, and the points are connected, a feasible combination curve between SSF · LCR and LCR will be traced. This is shown in Quadrant IV. Finally, Quadrant V allows one to separate LCR into the LOAD and A components. This is useful for determining the impacts of various collector area - building load combinations or for working backwards to find collector area or building heat loss requirements.

For illustration, the counterpart of example (c) in the arthmetic section is shown in Figure 1. The numbers in parentheses, (1) thru (7), correspond to the sequence in steps when using the graphical approach. These are described in order below.

(1) As described above, plot the performance combinations for the double glazed direct gain design under consideration. Trace the resultant curve.

(2) Find the collector area necessary to provide SSF = .30 with LOAD = 10,000 Btu/DD by drawing a line from the feasible curve intersection point in QIV straight down to the LOAD = 10,000 curve in QV.

(3) Now draw a horizontal line to the left and read the intersection point off of the A axis. A = 147 ft^2 is the result.

(4) Now go back to QIV and draw a horizontal line from the SSF = .30 intersection point to the left into QIII. Continue the line until it intersects the proper DD value. If the DD

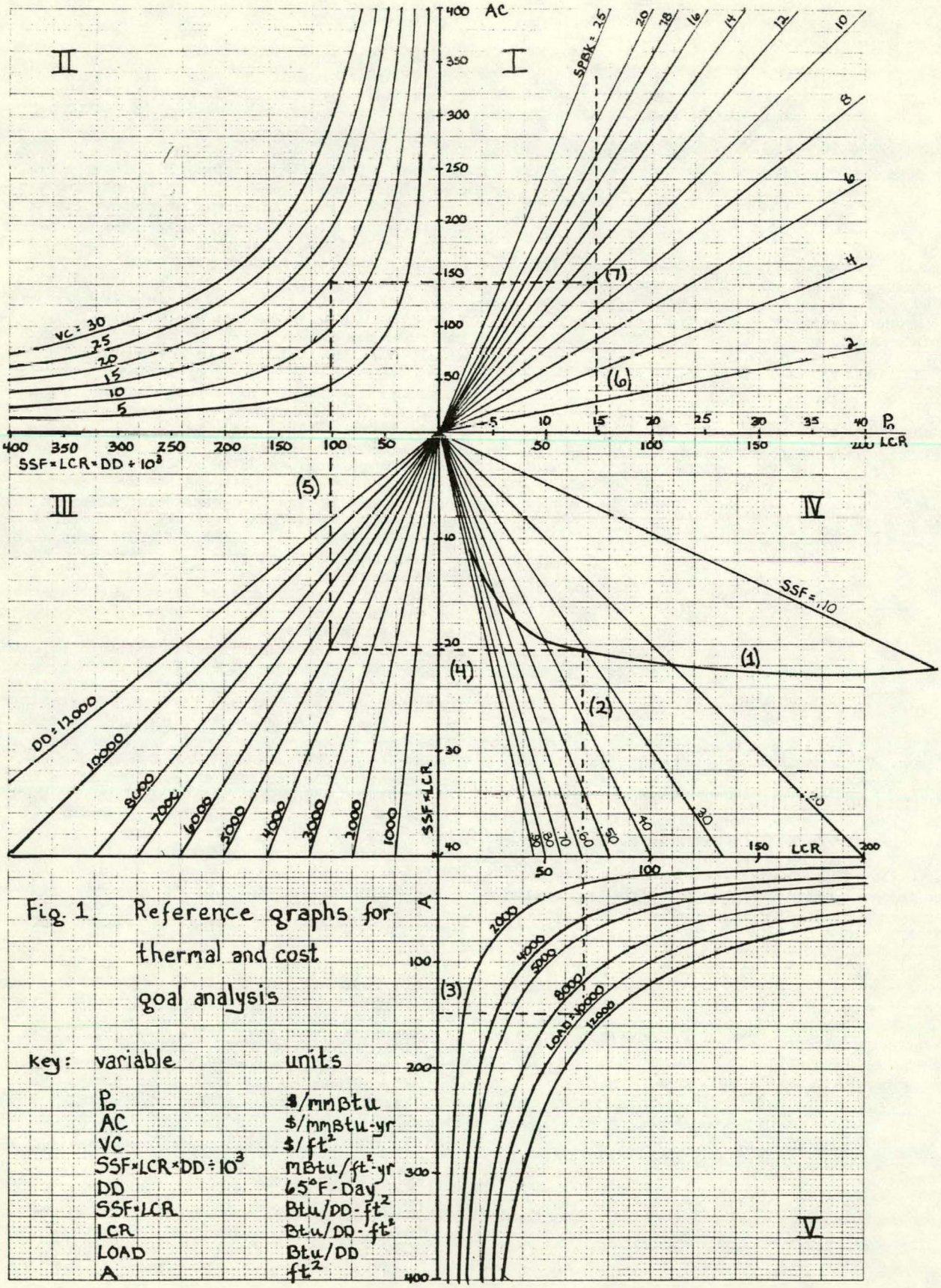

Fig. 1. Reference graphs for thermal and cost goal analysis

key:

variable	units
P_o	\$/mmBtu
AC	\$/mmBtu-yr
VC	\$/ft²
SSF×LCR×DD÷10³	MBtu/ft²-yr
DD	65°F-Day
SSF×LCR	Btu/DD-ft²
LCR	Btu/DD-ft²
LOAD	Btu/DD
A	ft²

condition falls between the given lines interpolation is necessary.

(5) Next, draw a vertical line from the intersection in QIII into QII until it intersects the correct VC value. In this example go to the curve VC = $\$15/ft^2$.

(6) Find the initial auxiliary fuel cost on the P axis in QI. Draw a vertical line straight up from that point. Electric resistance in Dodge City is $14.65/mmBtu is shown in QI.

(7) Draw a horizontal line from the correct VC point in QII (determined in (5)) into QI and find where the two lines intersect. This final intersection point determines the simple payback condition for the direct gain design under consideration. SPBK is shown to be a little bit less than 10 years which corresponds to the arithmetic results of 9.9 years.

The remaining (a) and (b) examples can be tested graphically by the reader. The accuracy of the graphical approach is not extreme, however it can be used with a minimum of effort and does not require arithmetic manipulation.

EXTENSIONS

Several extensions of the graphical approach can be made which might increase the usefulness and versatility of the method. First, the right side of equation (2) shows the ratios between the present worth factors for solar and auxiliary fuel. Another graph can be added that shows combinations of key financial parameter values that would yield particular PWF ratios. For example, two important parameters that can be analyzed are the ownership period and a resale profit factor that takes into account the relative appreciation rate of passive solar homes as compared to conventional market comparables. The limitation of this approach is that all other parameters entering the PWF formulas must be held constant to limit the problem to two dimensions. If the PWF ratio is divided by the SPBK of a particular design, the result will be a life cycle (or ownership cycle) benefit/cost ratio. Values greater than 1 indicate positive savings while values less than 1 indicate negative savings.

It also might be possible to integrate Balcomb's methodology [5] of optimal budget allocation between passive and conservation under various budget constraints. Derivative values of the LCR performance moves are available [3] to pursue this approach.

In conclusion, this paper has presented a simplified arithmetic and graphical approach for the analysis of passive solar heating design thermal and cost goals. The approaches have been shown to be consistent in application and offer the designer a means for quickly evaluating the implications of various design, performance, and economic criteria that may arise as constraints or goals to be met.

ACKNOWLEDGEMENTS

I wish to thank Dean Brunton of the University of New Mexico for his help in developing the graphical approach and Bill Robson for reviewing the paper and discovering several mistakes on the first go-around. Also, my gratitude to Marcella Dekker for her typing assistance.

REFERENCES

[1] Audrey M. Perino, "A Methodology for Determining the Economic Feasibility of Residential or Commercial Solar Energy Systems," Sandia Laboratory Report No. SAND78-0931, January, 1979.

[2] Rosalie Ruegg, "Calculating the Solar Dollar Gains: Ins and Outs of Life Cycle Costing," Solar Engineering Magazine, July, 1979, p. 11.

[3] J. D. Balcomb, et al. The Passive Solar Design Handbook, Department of Energy Draft Report No. DOE/CS-0090-D. April, 1979.

[4] R. H. Bezdek, A. S. Hirshberg, W. H. Babcock, "Economic Feasibility of Solar Water and Space Heating," Science, March 23, 1979, p. 1215.

[5] J. D. Balcomb, "Passive Solar and Energy Conservation: Working Together," presented at the Second Annual Systems Simulation and Economic Analysis Conference, San Diego, California. January 23-25, 1980.

NOTES

SOLAR TECHNOLOGY FOR CENTRAL STATION APPLICATIONS:

A REGIONAL MARKET ANALYSIS APPROACH

Barry G. Silverman*

Peter Fontaine**

Paul L. Hietanen**

Abstract. An approach to market penetration analysis is described using solar thermal, photovoltaics, ocean thermal energy conversion, hydrothermal and several more traditional electricity generation concepts in four NERC regions as an example. The technologies are characterized and the steps in the market penetration approach are described. Gas-fired, hydrothermal, synthetic fuel and coal-fired power plants exhibit the greatest market capture by 2010. Solar thermal also performs well.

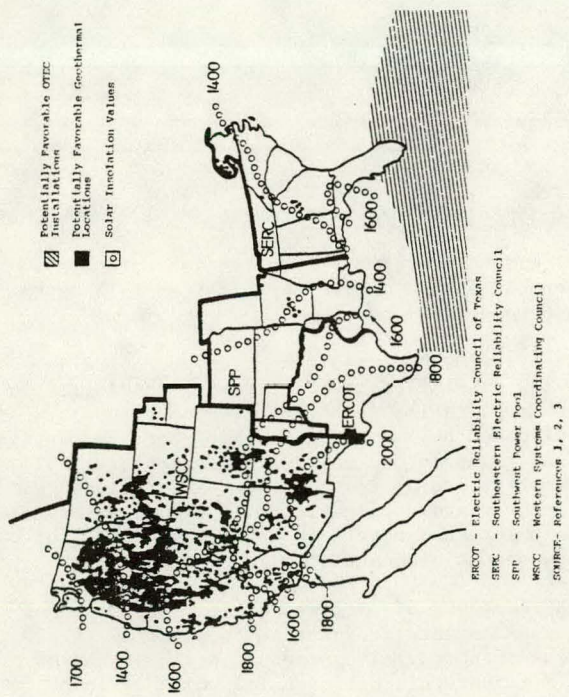

FIGURE 1. SOLAR CHARACTERISTICS OF SELECTED NERC REGIONS

*As Assistant Professor, George Washington University Dr. Silverman directs several efforts for the Santa Fe Corporation

** Analyst, Santa Fe Corporation

1.0 INTRODUCTION

The purpose of this article is to demonstrate the use of a market penetration tool that provides a systematic, credible framework for analysis and fully reproducible results. This tool is not a "black box" procedure that performs technology forecasts through "sleight of computer". Rather it is a simplified, straightforward technique that the non-model builder can readily understand and feel comfortable with.

In the present application of this tool a market penetration analysis over the period 1981 to 2010 of selected solar electric technologies -- ocean thermal energy conversion (OTEC), solar photovoltaic, solar thermal, and hydrothermal -- in central station applications is described. Advanced and conventional fossil fuel-fired, nuclear, and hydro-electric power plants are also considered.

Figure 2. APPLICABILITY MATRIX

Region	ERCOT		SERC		SPP		WSCC	
Market / Technology	Baseload	Non-Baseload	Baseload	Non-Baseload	Baseload	Non-Baseload	Baseload	Non-Baseload
OTEC	*		*		*			
Solar Photovoltaic		●		●		●		●
Solar Thermal	●	●	●	●	●	●	●	●
Hydrothermal (Liquid)							●	●
Advanced Fossil Fuels	●	●	●	●	●	●	●	●
Conventional Fossil Fuels	■	■	■	■	■	■	■	■
Nuclear LWR	■		■		■		■	
Hydroelectric			■				■	

■ Presently available technology

● Denotes near- and mid-term initial application (1981-1995)

* Denotes initial application in the long-term (1996-2010)

SOURCE: References 3, 4, 5, 6

The technology forecast is performed for four National Electric Reliability Council areas -- ERCOT, SERC, SPP and WSCC -- as indicated in Figure 1. The distribution of (a) average daily insolation, (b) feasible OTEC sites, and (c) identified hydrothermal reseviors is also portrayed in Figure 1. The applicability of the technologies considered to electric utility markets in each of the four regions is portrayed in Figure 2.

2.0 MARKET PENETRATION METHODOLOGY

The methodology for estimation of technology market penetration consists of two tasks: (1) estimate market potential for each application and (2) estimate market penetration for each technology in each application over time.

2.1 Estimate Market Potential

The market potential is the total number of new units that will need to be installed over the planning horizon. This constitutes the market place in which the candidate technologies will compete. While any level of disaggregation is possible, in the current study, market potential (and penetration) is computed for baseload and non-baseload applications on a region by region basis as follows:

$$MP_{ij}(t) = e_{ik}\, C_{ij}(t-1) + r_{ij} C_{ij}(t-1) + CO_{ij}(t) \quad (1)$$

where

$MP_{ij}(t)$ = market potential for region i and application j in year t

$C_{ij}(t-1)$ = capacity for region i and application j in year t-1

e_{ik} = rate of capacity expansion for region i and time frame k

r_{ij} = rate of scheduled replacements for region i and application j (= 3.0 percent/year)

$CO_{ij}(t)$ = conversions of existing capacity in region i and application j to alternative system in year t

$C_{ij}(t-1)$ estimates were obtained for 1978 from Ref 7. $CO_{ij}(t)$ estimates correspond to the 1978 Fuel Use Act requirements for utility conversions as computed by Trexler (ref 8). Values of e_{ik} were derived from Ref 7, 9, as follows:

	ERCOT (i=1)	SERC (i=2)	SPP (i=3)	WSCC (i=4)
Near/Mid Term (k=1)	3.2	4.2	5.1	3.9
Long Term (k=2)	2.8	3.6	4.5	3.4

FIGURE 3. CAPACITY EXPANSION, REPLACEMENT AND CONVERSION FOR BASELOAD AND NON-BASELOAD BY REGION

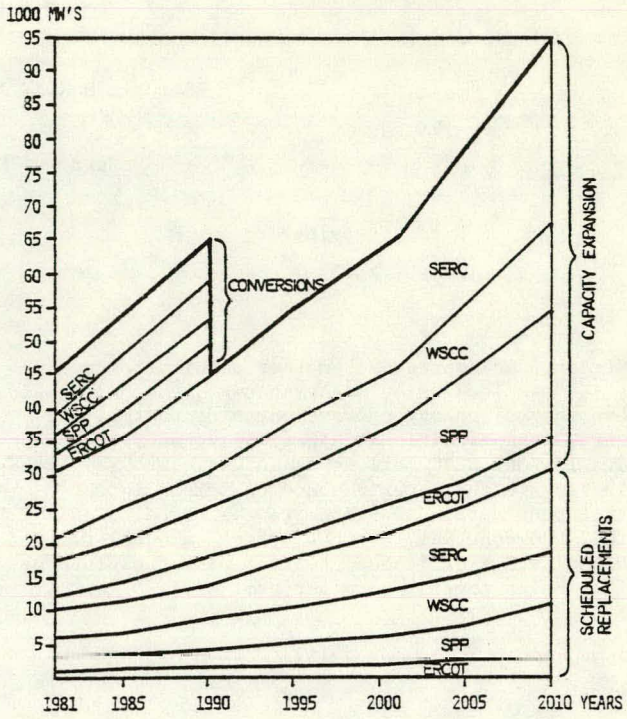

SOURCE: DERIVED FROM REFERENCES 7, 8, 9

Using these values in equation 1, the market potential estimates were computed as shown in Figure 3.

2.2 Estimate Market Penetration

The allocation of market potential to competing technologies in a given application follows the procedure outlined below.

Step 1: Characterize Competing Technologies -- Having identified the competing technologies in each application in Figure 2 the particular designs considered here are now further described in Tables 1 and 2 and in the following paragraphs. All system costs are up to the busbar and include land and storage where applicable, main and auxiliary station equipment, and materials, parts, and labor for operation and maintenance (O&M).

OTEC consists of a closed cycle with shell and tube heat exchangers designed to be sited 20 to 200 miles offshore. The proposed design requires a 38°F temperature differential which is found in southeast U.S. waters (see Figure 1). OTEC will be linked directly to the land based power grid (no storage considered) via a submarine transmission cable and will have a net power output of 400 MWe.

The solar photovoltaic system includes an array of solar cells rated at 100 MW capacity.

TABLE 1. ELECTRIC UTILITY TECHNOLOGIES - BASELOAD MARKET

Criteria / Technologies	Commercialization Date (Year)	Lead Time (Years)	Plant Life (Years)	Conversion Efficiency (%)	Capital Costs ($1978/KW)	Operation & Maintenance ($1978/KW/yr.)	Capacity Facotor (%)	Reliability (%)
OTEC	1997	6	40	5	1474	37.75	70	90
Solar Thermal	1992	4	30	39	2000	24.00	70	90-94[1]
Hydrothermal Liquid	1987	5	20	7	500	24.53	70	90
Advanced Coal	1982	5	30	34	631	21.30	70	90
Advanced Gas/Liquids	1990	3	30	50	545	27.90	70	90
Conventional Coal	P.A.*	6	30	34	661	61.70	70	80
Nuclear LWR	P.A.*	12	30	33	857	9.81	70	90
Hydro-Electric	P.A.*	4	40	80	550	5.20	60	95

*P.A. = Presently Available

[1]Range represents the differences in reliability for solar thermal in each of the regions considered.

SOURCE: References 3, 4, 6, 10-14

TABLE 2. ELECTRIC UTILITY TECHNOLOGIES - NON-BASELOAD MARKET

Criteria / Technologies	Commercialization Date (Year)	Lead Time (Years)	Plant Life (Years)	Conversion Efficiency (%)	Capital Costs ($1978/KW)	Operation & Maintenance ($1978/KW/Yr.)	Capacity Factor (%)	Reliability (%)
Solar Thermal	1992	4	30	39	1000	10.00	30	90-94[1]
Solar Photovoltaic	1986	6	20	15	1884	17.88	30	95
Advanced Coal	1982	5	30	34	631	21.30	50	90
Advanced Gas/Liquids	1985	1	30	38	300	6.13	50	90
Conventional Coal	P.A.*	6	30	34	661	35.00	50	80
Conventional Gas	P.A.*	6	20	32	435	17.96	50	90

*P.A. = Presently Available

[1]Range represents the differences in reliability for solar thermal in each of the regions considered.

SOURCE: References 3, 4, 6, 12-15

The solar thermal power station includes a tower receiver, variable focus array, heat transfer fluids, fluid transmission elements, a heat engine, and electric generating equipment. The baseload system includes up to 7 hours storage and has a capacity rating of 500 MWe.

The hydrothermal system is liquid dominated and includes heat exchanger, heat transfer fluids, fluid transmission elements, a heat engine and electric generating equipment.

Advanced coal technology includes direct combustion of crushed coal with reliable lime/limestone scrubbers. Advanced gas/liquid technologies represent a generic system using synthetic fuels.

Step 2: Estimate Maximum Market Fractions -- The maximum market fraction (MMF) is that share of the market which will be captured by a given technology in the absence of competition. That is, due to commercialization barriers (e.g., limited manufacting capacity, plant siting restrictions and restrictive building codes) most new (and existing) technologies can only capture a portion of the total market. The MMF estimates for the technologies studied here are described below.

OTEC is assigned an MMF equal to 100 percent of SERC and 50 percent of the ERCOT and SPP baseload market potential. It is assumed that in the long term (post 1995), OTEC market penetration will not be unduely constrained by efforts to resolve (a) low utility interest to date, (b) jurisdictional issues, (c) liability and accountability issues, (d) marine safety hazard issues, and (e) conflicts of ocean use.

Photovoltaics receive an MMF equal to the non-baseload market potential in all regions. Due to its inability to utilize diffuse light (i.e., light through cloud cover), solar thermal on the other hand, is assigned an MMF equal to the baseload and non-baseload market potential in ERCOT, SERC, SPP, and the southern half of WSCC.

The MMF for hydrothermal (liquid) is one-third of baseload and non-baseload in the WSCC region.

For fossil-fired power plants several MMF's exist: (a) mandatory conversion of oil-fired plants by 1990 is required by the National Energy Act: conversions in each NERC region were plotted on Figure 1. (b) conventional gas-fired power plants are assigned an MMF equal to 15 percent of the non-baseload market in each region, while advanced gas/liquids is assigned an MMF of 20 percent of both baseload and non-baseload and (c) coal-fired power plants are assigned an MMF equal to the entire baseload market and 60 percent of the non-baseload market in each region.

For a variety of reasons (e.g., lack of acceptable sites, community reaction, etc.) nuclear and hydroelectric are assigned MMF's equal to 10 percent of the baseload market except in SERC where the hydroelectric MMF is only 5 percent.

Step 3: Compute Market Scores -- A multi-attribute weighting procedure was developed as shown in the example in Figure 4 on the basis of surveys (see Ref 4 and 16) of utility decision makers regarding the critical cost/performance criteria that are evaluated in purchasing decisions. Using the data in Tables 1 and 2 and a levelized life-cycle revenue requirements algorithm the market score for each

technology in each application and region was computed. Factors used in the required revenue algorithm include: (a) a fixed charge rate of 12 percent, (b) regional fuel prices as reported by utilities to the U.S. Department of Energy (Ref 17), (c) fuel price deregulation schedules from the National Energy Act, (Ref 18), and (d) fuel specific escalation and inflation rates in each region (derived from Ref 17). Typical environmental scores, market scores and maximum market fractions for the technologies competing in the non-baseload application in the WSCC region are shown in Table 3.

Figure 4. MARKET SCORE WORKSHEET

Region/Market: ERCOT/Non-Baseload Tech: Solar Thermal

Criteria	Conventional Tech. (A)	Tech Goal (B)	Percentage Improvement $\frac{(A-B)}{A} = (C)$*	Weight (D)	Penetration Merit (C x D) = (E)
Required Revenue Cost (1978$/KW)	317.22	224.99	1.291	0.25	0.323
Procurement Cost (1978$/KW)	661	1400	0.487	0.20	0.097
Reliability* (% Available)	80	94	1.175	0.20	0.0235
Environmental Impact (Score: 0-15)	12	4	1.667	0.20	0.333
Development Lead Time (Years)	5	4	1.333	0.10	0.133
Useful Plant Life* (Years)	30	30	1.000	0.05	0.050
Total Market Score (Sum of Column E)					1.172

*For Reliability and Plant Life: (c) = 1 - $\frac{(A-B)}{A}$

TABLE 3. SLECTED MARKET INFORMATION
REGION: WSCC
MARKET: NON-BASELOAD

Technologies \ Criteria	Environmental Impact Score	Market Score	Maximum Market Fraction (%)
Conventional Coal	12	1.00	85
Solar Thermal	4	1.17	60
Solar Photovoltaic	1	0.65	100
Advanced Coal	9	1.14	60
Advanced Gas/Liq.	2	1.35	20
Conventional Gas	2	1.18	15
Hydrothermal Liquid	3	1.34	33

Step 4: Estimate Nominal Market Shares -- The purpose of this step is to apportion the markets for each region and application to the competing technologies on the basis of the market scores. The "nominal" market shares are allocated according to the algorithm depicted in Figure 5 and up to the limits imposed by the maximum market fraction. The output of this step is a fraction that represents the share of the market likely to be captured by each technology in each application and region over time.

Figure 5. MARKET ALLOCATION ALGORITHM (for Pairwise Comparisons)

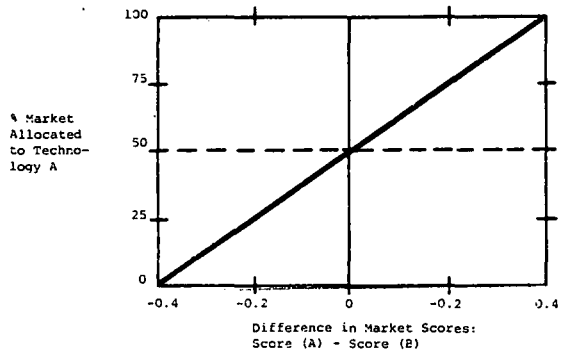

Step 5: Determine Effective Market Penetration -- When a new technology is introduced into a market, most potential buyers will fail to purchase it initially due to risk aversion tendencies. Said another way, the venturesomeness of potential buyers is initially low, and increases to 100 percent of the potential only gradually over a period of several years. This lack of venturesomeness causes a delay in the penetration as shown in Figure 6.

Figure 6. PENETRATION DELAY CURVE

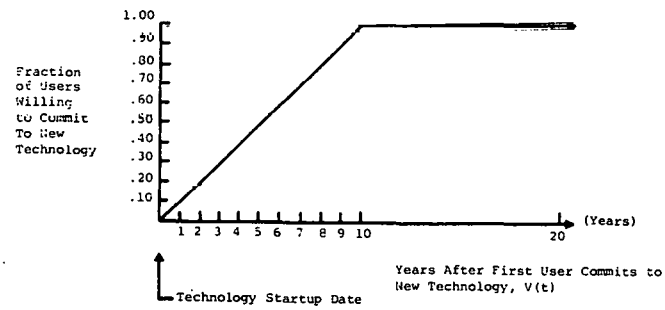

By combining penetration delay with nominal market shares and market potential, effective market penetration is estimated as:

$$PE_{ij}(t) = PD(t) \times N_{ij}(t) \times MP_{ij}(t)$$

where:

$PE_{ij}(t)$ = effective penetration in region i and application j for year t

$PD(t)$ = penetration delay (from Figure 6)

$N_{ij}(t)$ = nominal market share in region i and application j for year t

$MP_{ij}(t)$ = market potential in region i and application j for year t

The results of this study as shown in terms of a specific regional example in Figure 7 and summarized for all regions in Table 4.

Figure 7. WSCC - NON-BASELOAD MARKET PENETRATION

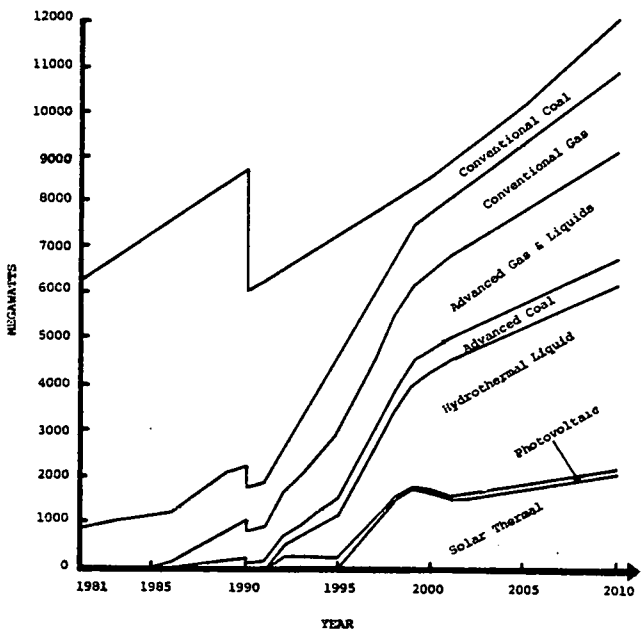

3.0 DISCUSSION OF RESULTS

The results of this market penetration exercise indicate that no one (or two) technologies should dominate the electric utility sector in the next 30 years. Instead, each market in each region should be composed of a combination of solar, advanced fossil, and conventional technologies. Specific results of the analysis are several:

- Many of the technologies analyzed have significant life-cycle cost advantage over the conventional coal system. As a result, the deployment of these technologies is constrained only by site and resource availability, manufacturing capacity, and other such factors which are incorporated into the

TABLE 4. SUMMARY OF MARKET PENETRATION ANALYSIS

		BASELOAD		NON-BASELOAD	
	TECHNOLOGY	MARKET CAPTURED (%)	INSTALLED CAPACITY (1000 MWs)	MARKET CAPTURED (%)	INSTALLED CAPACITY (1000 MWs)
ERCOT	ADVANCED COAL	44.2	39.56	18.4	20.61
	ADVANCED GAS/LIQUIDS	9.4	8.43	13.5	14.98
	CONVENTIONAL COAL	36.2	32.43	35.7	39.77
	CONVENTIONAL GAS	----	-----	14.9	16.75
	NUCLEAR LWR	8.4	7.48	----	-----
	OTEC	0.9	0.84	----	-----
	SOLAR PHOTOVOLTAIC	----	-----	0.9	0.98
	SOLAR THERMAL	0.9	0.82	16.6	18.57
SERC	ADVANCED COAL	42.2	153.67	18.3	83.79
	ADVANCED GAS/LIQUIDS	10.8	39.08	15.7	71.77
	CONVENTIONAL COAL	28.8	105.02	29.5	134.46
	CONVENTIONAL GAS	----	-----	14.8	67.54
	HYDROELECTRIC	4.9	18.23	----	-----
	NUCLEAR LWR	9.9	36.46	----	-----
	OTEC	1.6	6.02	----	-----
	SOLAR PHOTOVOLTAIC	-----	-----	1.5	6:21
	SOLAR THERMAL	1.8	6.18	20.2	92.08
SPP	ADVANCED COAL	49.1	102.86	19.9	51.47
	ADVANCED GAS/LIQUIDS	11.2	23.55	15.1	39.16
	CONVENTIONAL COAL	27.2	56.96	29.4	76.19
	CONVENTIONAL GAS	----	-----	15.0	38.86
	OTEC	1.3	2.64	----	-----
	NUCLEAR LWR	10.0	20.94	----	-----
	SOLAR PHOTOVOLTAIC	----	-----	0	0
	SOLAR THERMAL	1.2	2.49	20.5	53.09
WSCC	ADVANCED COAL	26.9	54.98	3.7	10.57
	ADVANCED GAS/LIQUIDS	10.5	21.51	12.8	36.73
	CONVENTIONAL COAL	26.6	54.34	33.2	95.14
	CONVENTIONAL GAS	----	-----	13.2	37.91
	HYDROELECTRIC	10.0	20.45	----	-----
	HYDROTHERMAL	18.5	37.88	14.8	42.29
	NUCLEAR LWR	6.7	13.78	----	-----
	SOLAR PHOTOVOLTAIC	----	-----	0.7	2.12
	SOLAR THERMAL	0.7	1.46	21.6	61.83

the maximum market fraction. For example, hydrothermal, advanced gas/liquids, conventional gas, and hydroelectric technologies all achieve a market share equal to their maximum market fractions (MMF). The analysis uses a constant set of MMFs but it should be noted that these values can change over time. For example, the advanced gas/liquids MMF should rise as synthetic fuels become increasingly available at competitive costs. On the other hand, the decline in conventional gas supplies could result in a decreasing MMF for use of conventional gas technology. This is a possible refinement for future analysis.

- As a group, the solar technologies capture small-to-moderate shares of the 8 market applications studied. In both the baseload and non-baseload WSCC markets, hydrothermal captures as much as a third of the market potential (after the year 2000). Solar thermal has strong penetration in all non-baseload applications (capturing as much as 38 percent of the potential in some years), but limited penetration (3 to 5 percent in most years) in the baseload market where storage capability is required. The high costs of OTEC and Photovoltaics permit only very small penetration of these two advanced solar technologies (0 to 4 percent of the market in the long-term).

- The analysis indicated that results are quite sensitive to inputs such as cost data and maximum market fractions. Because of the inherent uncertainty in these inputs, the results can only be viewed as one of many possible scenarios for future utility market composition. For example, estimates of Photovoltaic capital costs range from one to five thousand dollars per KW capacity. Such a dispersion of estimates translates into a significant range of possible results. Other data uncertainties exist, requiring repeated use of the market penetration analysis for several scenarios to insure adequate representation of each technology,

- Although wind and biomass technologies were not considered in this paper, they represent additional solar options which in all probability will act as fossil fuel savers in both baseload and non-baseload applications.

- The purpose of this article was not to predict the market penetration of solar technology; that is the task of solar industry experts. The purpose was to describe a tool which will help the solar expert assess market penetration in a systematic, well-organized fashion.

- The steps described in this article provide a plausible and straightforward approach that assures structural validity and fairly robust results (i.e., small changes in input assumptions will not lead to large changes in results). However, there is no cheap and quick way of producing believable market penetration assessments. If the time spent completing a procedure such as that described here is to be justified, careful monitoring and verification of the validity of the input data and assumptions is required. Delphi and other group decision techniques must be employed with the relevant parties to reach consensus on input assumptions. In the absence of a high degree of consensus, it is recommended that alternative futures be examined via scenario construction.

- Finally, the preparation of market penetration assessments is not a one time affair. Each forecase should be reviewed periodically and updated as required.

REFERENCES

1. Energy Alternatives, A Comparative Analysis, Science and Public Policy Program, University of Oklahoma, Norman, 1975.

2. Ocean Systems Multiyear Program Plan, Executive Abstract, U.S. DOE, Div. of Central Solar Technology, Washington, D.C., 1979.

3. A Comparative Evaluation of Solar Alternatives: Implications for Federal RD&D, v. I-III, SRI International, Menlo Park, 1978.

4. Analysis of Benefits Associated with the Introduction of Advanced Generating Technologies, Description of Methodologies and Summary of Results, Final Report: Electric Utility Study, Mitre Corp./Metrek Div., McLean, 1978.

5. Cost and Market Penetration Analysis of Selected Fossil Fueled Electric Power Generating Systems, v. I, Mitre Corp./Metrek Div., McLean, 1978.

6. Data provided by the U.S. DOE, Office of Coal Utilization, Washington, D.C., 1979.

7. Electric Power Supply and Demand 1978-1987 for the Contiguous United States, U.S. DOE/ERA - 0018, Washington, D.C., July 1978.

8. "The Department of Energy Atmospheric Fluidized Bed Combustion Utility Demonstration Program", E.C. Trexler, 5th International Conference on Fluidized Bed Combustion, ERDA, Washington, D.C., 1977.

9. National Energy Plan II, Executive Office of the President, Washington, D.C., 1979.

10. "Comparative Composite Cost Data on OTEC", W.G. Sherwood, F.S. Dunning, Jr., in Solar Energy and Conservation Symposuim - Workshop, _____, Miami, 1978.

11. OTEC Platform Configuration and Integration, v. I-III, Gibbs & Cox Inc., New York, 1978.

12. Energy, Non-Nuclear Energy Technologies, v. II, S. S. Penner, L. Icerman, Addison - Wesley, Reading, 1975.

13. Energy Conversion Alternatives Study, Summary Report, NASA TM-73871, prepared by NASA for ERDA and NSF, Cleveland, 1977.

14. Oral Communications with George Kaplan, U.S. DOE, Div. of Central Solar Technology, Washington, D.C. and Pat Eicher, Sandia National Laboratory, Albuquerque, 1979.

15. Evaluation of Technological Data in the DFI and PIES Models, U.S. DOE/EIA/0016-2, Washington, D.C., April 1979.

16. Electric Utilities and Equipment Manufacturers, Factors in Acceptance of Advanced Energy Conversion Technologies, A.D. Little Inc., prepared for NSF, Acorn Park, 1975.

17. Cost and Quality of Fuels for Electric Utility Plants, Energy Data Monthly Report, U.S. DOE/EIA-0075, Washington, D.C., August 1979.

18. National Energy Act, U.S. HOR, 95-2, Washington, D.C., October 1978.

19. 1978 Year-End Summary of the Electric Power Situation in the United States, Edison Electric Institute, New York, 1978.

TECHNICAL AND ECONOMIC FEASIBILITY OF SOLAR PONDS IN LARGE-SCALE AGRICULTURAL APPLICATIONS

E. I. H. Lin, W. T. Sha
Components Technology Division
Argonne National Laboratory

S. L. Soo
University of Illinois
Urbana, Illinois

ABSTRACT

Analyses are presented to show that a 1-acre salt-gradient solar pond can supply adequate heat to meet the grain drying and space heating requirements of a typical 2.02 x 10^6 m^2 (500-acre) Illinois farm. The specific corn-drying and hog-house heating needs of the 3.64 x 10^6 m^2 (900-acre) Fillman farm, Mazon, Illinois, are also shown to be amply sustainable by such a pond. Calculations are made to demonstrate that solar ponds are becoming economically competitive with fossil fuels. Their additional advantages, potential future uses and possible socio-economic impact are also discussed. Large-scale demonstration of solar ponds in agricultural applications is recommeneded.

INTRODUCTION

Salt-gradient solar ponds collect and store solar thermal energy, which can be extracted as needed for various uses throughout the year, not necessarily during sunny hours. While several engineering questions remain to be answered, the technological feasibility of solar ponds has been well established by numerous experimental studies with field ponds and laboratory models during the last two decades in many countries around the world. Economically, the cost of heat provided by solar ponds ranges from one-fourth to as low as one-fortieth of that provided by conventional solar collection and storage systems[1]. Compared with fuel oil and propane gas currently used in grain drying, a solar pond at its present level of operational efficiency is almost as competitive. With the price of fuel oil and propane gas continuously rising, and with pond efficiency further improved as a result of continuing research and development work, it seems certain that solar ponds will become even more economical and widely used, not only in additional applications related to farming, but also in low-temperature industrial processes and heating and cooling of groups of single family homes and large building complexes.

This paper presents an analysis of the technical and economic feasibility of using a large-scale solar pond to meet the heat requirements of Illinois farms. The feasibility analysis is particularly meaningful as Illinois is a major agricultural state and has severe winter climates. For example, the 1979 harvest of Illinois has been estimated at 5.36 x 10^7 m^3 (1.52 billion bushels) of corn and soybeans. Based on an average 8.5 percentage point of moisture removal, grain drying for this level of production is estimated to require 3.57 x 10^5 m^3 (81 million gallons) of LP gas, 1.28 x 10^5 m^3 (4 million ft^3 of natural gas), and 7.58 x 10^3 m^3 (2 million gallons) of fuel oil[2]. The analysis presented shows that solar ponds can be used to replace most of the fossil fuels currently used in grain drying and house/barn heating, on favorable economic terms. The heat requirement vs. availability comparison shows that a 4047 m^2 (1-acre) pond can supply adequate heat to meet the grain drying and house/barn heating needs of a 2.02 x 10^6 m^2 (500-acre) farm in Illinois. Furthermore, the added advantages of solar ponds in environmental and farming aspects are discussed. The analysis concludes with a positive recommendation of stepping up large-scale demonstration effort for solar ponds in agricultural applications.

PREVIOUS WORK AND TECHNICAL FEASIBILITY

The concept of collecting and storing solar energy by means of salinity-gradient solar ponds was first derived from observations of natural lakes with salt concentration gradients[3]. Incident solar radiation is absorbed by the lakes at various depths, and the salt concentration gradients aid in preventing global convection, thereby retaining heat in the lower regions of the lakes. Lake temperatures greater than 70°C (158°F) have been observed.

Man-made salt-gradient solar ponds (abbreviated hereinafter as solar ponds) utilize this concept and have proved to be workable, through small-scale demonstration projects, for heating buildings, swimming pools and greenhouses, for drying grains, and for electric power generation [1,3]. In a sense, the technical feasibility of solar ponds has been generally established by studies conducted over the last two decades in Israel, USSR, Chile, India, the United States, etc. To cite some examples, there are the ponds at Ohio State University[1] and the University of New Mexico[3], both of which are approximately of area 200 m^2 (0.05 acres) and depth 2.5 m (8.2 ft), were constructed in 1975, and have

since been in operation; valuable experience has been accumulated at these two experimental ponds. Among the ponds recently completed or presently under construction are[3,12]: the 10,000 m^2 (2.5-acre) pond in Israel near the Dead Sea, built in 1978 to provide winter heating and summer cooling for a resort hotel; the experimental pond in Israel near Yavne, built in 1977 and used to operate a turbine to generate 6 kW of electricity; the 400 m^2 (0.1-acre) pond with 4.5 m (15 ft) depth at Ohio State University, being constructed to provide information on heat loss and overall efficiency and to supply heat for dairy operations; and the Miamisburg, Ohio, pond, of area 2090 m^2 (0.5 acres), depth 3.5 m (12 ft), built in 1978 to heat an outdoor municipal swimming pool in the summer and a recreational building in the winter. These examples not only point out the renewed interest in a long-existing workable concept, but also the current trend in putting solar ponds to wider use.

However, before solar ponds can be commercialized, large-scale demonstrations of actual applications must be conducted. Since farming is one of the areas where solar ponds can be advantageously utilized, we shall examine heat requirements for two Illinois farms versus heat availability from a 4047 m^2 (1-acre) solar pond in what follows.

Heat Requirements

Case I. A typical 2.02 x 10^6 m^2 (500-acre) farm: Consider that corn is the major product of the farm, and that average-size houses and barns exist on the farm. The energy requirements are:

(i) Corn drying: Assuming an annual yield of 1.31 x 10^{-3} m^3/m^2 (150 bushels/acre), the total annual production of corn is 2643 m^3 (75,000 bu). Further assume that the whole crop is to be dried from an average initial moisture content of 25% to an average final moisture content of 15%. Using a grain bin dryer operated at 54°C (130°F) with an air flow of 0.02 cms/m^3 (1.5 cfm/bu) and with stirring, the heat required is 3.9 x 10^8 J/m^3 (13,000 Btu/bu), and the electricity required for the fan is 3.41 kWh/m^3 (0.12 kWh/bu)[4]. Thus, a total of 1.04 x 10^{12} J/yr (0.98 x 10^9 Btu/yr) will be required to dry corn produced on the 2.02 x 10^6 m^2 (500-acre) farm, in addition to a relatively small amount of electricity needed to drive the fan.

(ii) House Heating: Assuming the farm house has a 186 m^2 (2000 ft^2) living area, the heating requirement is about 25,000 Btu/deg F-day[5]. The heating deg F-days in Chicago from September 1 to May 31 being 6310[6], the total house heat needed is 0.17 x 10^{12} J/yr (0.16 x 10^9 Btu/yr).

(iii) Barn Heating: The heating demand of livestock buildings depends on species, ages of animals, and type of shelter[7]. In the absence of precise data, we assume conservatively that 0.32 x 10^{12} J/yr (0.3 x 10^9 Btu/yr) is needed for barn heating.

Thus, the total heat requirement for the 500-acre farm is estimated to be the sum of the above three items; i.e., 1.53 x 10^{12} J/yr (1.44 x 10^9 Btu/yr).

Case II. The 3.64 x 10^6 m^2 (900-acre) Fillman farm[8]: Located in Mazon, Illinois, the Fillman Farm grows corn and raises over 1000 hogs year round. For years, part of the corn crop has been dried on the farm using a high-temperature dryer which burns LP gas. One of the two hog houses on the farm, i.e., the 8 m x 20 m farrowing house is currently heated in winter by an array of air solar collectors. The other hog house, i.e., the 6 m x 49 m finishing house, relies on hot water heating (using fuel oil) to maintain a 21°C (70°F) temperature in winter. Rising fuel cost is making the solar pond option more and more attractive. The energy requirements by this 3.64 x 10^6 m^2 (900-acre) farm are:

(i) Corn Drying: The average annual yield for the Fillman farm is 3524 m^3 (10^5 bu) of corn, out of which 1057 m^3 (30,000 bu) are to be dried from an average initial moisture content of 25% to an average final moisture content of 15%. Again as before, each bushel requires 13,000 Btu of heat and 0.12 kWh of electricity (for the fan). This means a total of 0.41 x 10^{12} J/yr (0.39 x 10^9 Btu/yr) is required to dry corn produced on this farm, in addition to the electric power required to drive the fan.

(ii) Hog-House Heating: According to 1978-1979 record, heating of both hog houses uses 1.7 x 10^{12} J/yr (1.61 x 10^9 Btu/yr).

Summing (i) and (ii) above, the estimated total heat requirement for the 900-acre Fillman farm is 2.11 x 10^{12} J/yr (2.0 x 10^9 Btu/yr).

Heat Availability

Based on meteorological data for Lemont, Illinois[9], the total integrated annual solar radiation on the surface of a 4047 m^2 (1-acre) solar pond is 2.08 x 10^{13} J (1.97 x 10^{10} Btu). If the pond collection-storage efficiency is assumed to be 19% (some Israeli ponds show 20% - 25% efficiency[10]), then the annual heat gain will be 3.95 x 10^{12} J/yr (3.74 x 10^9 Btu/yr). Figure 1 shows solar radiation on the pond surface based on data given in [9], estimated monthly heat gain in the storage zone of the pond based on a 19% average pond efficiency, and estimated heat accumulation in the pond, as well as heat requirements for grain drying and house/barn heating on a typical 2.02 x 10^6 m^2 (500-acre) Illinois farm (Case I). Heat requirements shown in the figure are based on the conservative assumption that the heat-exchange effectiveness during heat extraction is roughly 50%. It is noteworthy that the above calculation of available heat is consistent with the two calculations presented in [11] based on different data sources.

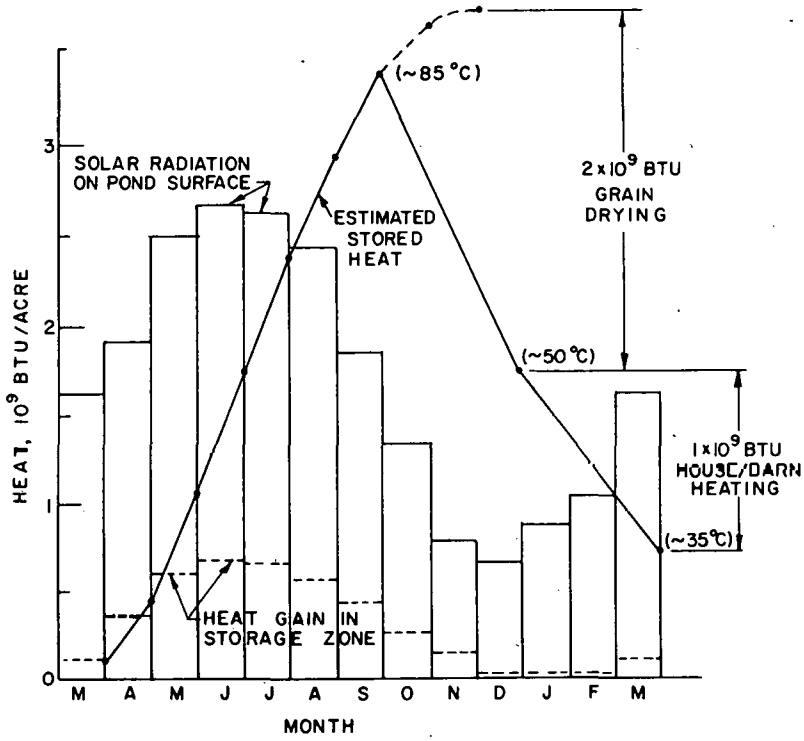

Figure 1. Solar Radiation on, and Estimated Stored Heat in a 1-acre Solar Pond in Lemont, Illinois. Heat Requirement vs. Availability for Grain Drying and House/Barn Heating.

It is thus seen that the available heat of 3.95 x 10^{12} J/yr (3.74 x 10^9 Btu/yr) from a 4047 m^2 (1-acre) solar pond is more than adequate to satisfy the heat requirements of the two farms as presented in Cases I and II.

ECONOMIC FEASIBILITY

The construction cost for a 4047 m^2 (1-acre) solar pond is estimated as follows, based on information available in [1] and [12], as well as current local labor and material costs in Illinois.

Item	Cost	Percent Construction
Land	$ 4,000	2
Liner & Installation	45,000	23
Excavation plus Labor	25,000	12
Instrumentation and Miscellaneous Items	24,000	12
Salt, 3400 tons @ $30/ton	102,000	51
Total Construction	$200,000	100

If this construction cost is amortized at an annual interest rate of 10% over a period of 20 years, the annual payment (principal plus interest) will be approximately $25,000. This is the cost of heat gain in the amount of 3.95 x 10^{12} J/yr (3.74 x 10^9 Btu/yr) as calculated above.

It thus follows that the cost of available heat from the 4047 m^2 (1-acre) solar pond is

$$\frac{\$25,000}{3.95 \times 10^{12}\ J} = \$6.33/10^9\ J\ (\$6.68/\text{million Btu})$$

On the other hand, the most favorable current market price of LP gas is $118/$m^3$ ($0.52/gal). The heat content of LP gas being 2.2 x 10^{10} J/m^3 (92,000 Btu/gal), it follows that the cost of heat from LP gas is

$$\frac{\$118/m^3}{2.2 \times 10^{10}\ J/m^3} = \$5.36/10^9\ J\ (\$5.65/\text{million Btu})$$

It must be noted that in order to make an equitable comparison between unit heat costs from solar ponds and LP gas, other factors such as the costs of solar-pond heat exchangers and LP gas dryers must also be considered. However, it is clear from the above calculations that it takes only a 19% increase in the LP gas price or an improvement from 19% to 22.5% of solar-pond efficiency to make the solar pond more economical than LP gas. Both these conditions are, of course, realizable; the former in the near future, and the latter after we gain more understanding about solar ponds from the R&D work in progress. We can thus conclude that solar ponds are becoming economically competitive with LP gas and fuel oil, and will soon surpass them.

Note that although factors such as tax advantages are not considered in the above

comparison of unit heat costs, it is felt that the simple comparison is convincing enough in pointing out the economic potential of solar ponds. A life cycle cost analysis, which is not included here, also showed that solar ponds are life-cycle cost effective. Additional advantages afforded by solar ponds built on individual farms are listed below:

(i) Long wait at local elevators for crop drying can be avoided; a long wait at harvest time causes grain spoilage, reduces farmers' profit, and prevents orderly marketing.

(ii) With ready on-site drying day or night, early harvest of high moisture wheat (moisture content up to 24-25%) is possible, which means higher wheat yields (due to reduced shattering loss at the combine header) and improved grain quality. It also facilitates raising double-crop soybean following wheat, since harvesting high-moisture wheat can move the harvest date ahead 5-7 days or more, which is important as each day of earlier soybean planting can mean 1/2 to 1 bu/acre more yield [13,14].

(iii) Solar cooling, refrigeration, and irrigation [15] using a solar pond as a heat source may not be economically feasible at the present time, but with the improvement of solar pond technology, these appear to be strong possibilities for the future.

(iv) Solar ponds reduce air pollution from burning fossil fuels. They also provide for beneficial use of farm land that is set aside to prevent overproduction.

CONCLUSION

Analyses have been presented to show that solar ponds are technically feasible for grain drying and house-barn heating on large-scale farms, and that they are becoming economically competitive with LP gas and fuel oil that are currently used in farming. Application of solar ponds to grain drying is particularly attractive, since load demand occurs at the peak of heat reserve, and heat extraction at such time alleviates heat losses which would otherwise be severe during the winter months. The replacement of fossil fuels by solar ponds will modify the fuel demand characteristics considerably, if the latter are widely adopted in farm use. It is estimated that solar ponds can replace $50 million to $90 million worth of oil and gas used on farms annually in Illinois, and over $1 billion worth nationally. It is therefore recommended that large-scale demonstration effort for agricultural applications of solar ponds be stepped up. The benefit of the recommended demonstration work is expected to extend beyond farming, as solar ponds can potentially also be applied to low-temperature industrial processes, and heating of greenhouses, school buildings, groups of single-family homes, and large residential and commercial complexes.

ACKNOWLEDGMENTS

The authors gratefully acknowledge the support given by Mr. J. M. Davis of U. S. Department of Energy, and Drs. W. W. Schertz, A. I. Michaels, and Mr. G. S. Rosenberg of Argonne National Laboratory. The manuscript was typed by Mrs. Sally Moll, and the work was performed under sponsorship of the Systems Development Division, Office of Solar Applications, U. S. Department of Energy.

REFERENCES

1. C. E. Nielsen, "Nonconvective Salt-Gradient Solar Ponds," Solar Energy Handbook (W. C. Dickinson, P. N. Cheremisnoff, Ed.) Marcel Decker (1979).

2. L. Hill et al., "Drying and Storage Requirements for Illinois Grain during 1979 Harvest," University of Illinois at Urbana-Champaign (1979).

3. F. Zangrando and H. C. Bryant, "A Salt Gradient Solar Pond," Solar Age, 21 (1978).

4. D. W. Morrison, "Energy Use in Grain Drying," Proc. Grain Conditioning Conf., University of Illinois-Urbana, pp. 2-5 (Jan 1978).

5. A. Rabl and C. E. Nielsen, "Solar Ponds for Space Heating," Solar Energy, 17 (1975).

6. F. Kreith and J. F. Kreider, Principles of Solar Engineering, McGraw-Hill (1978).

7. M. Hall, "Temperature Modifications in Livestock Buildings," Proc. Grain Conditioning Conf., pp. 40-42 (1976).

8. J. Fillman, Flying F Farms, Inc., private communication.

9. W. A. Beckman, S. A. Klein, and J. A. Duffee, Solar Heating Design, p. 150, John Wiley (1977).

10. G. Assaf et al., "Large Size Solar Ponds for Electricity Production," Proc. Int. Congress ISES (1979).

11. E. I. H. Lin, W. T. Sha and S. L. Soo, "Stability Considerations and a Double-Diffusive Convection Model for Solar Ponds," ANL-CT-79-34 (1979).

12. R. S. Bryant, R. P. Bowser and L. J. Wittenberg, "Construction and Initial Operation of the Miamisburg Salt-Gradient

Solar Pond," Proc. Int. Congress ISES (1979).

13. J. R. Barrett, S. D. Parsons, and B. A. McKenzie, "Harvesting and Drying Wheat for Profit and Quality," Conf. Proc. Alternatives for Grain Conditioning and Storage (1978).

14. E. D. Rodda, "Drying Soybeans for Profit and Quality," Conf. Proc. Alternatives for Grain Conditioning and Storage (1978).

15. Alternative Sources of Energy, May/June, p. 19 (1979).

NOTES

Dup

SOLPOND - A SIMULATION PROGRAM FOR SALINITY GRADIENT SOLAR PONDS

By
Jon Henderson
Cécile M. Leboeuf

Solar Energy Research Institute
Golden, Colorado

ABSTRACT

A computer simulation design tool was developed to simulate dynamic thermal performance for salinity gradient solar ponds. Dynamic programming techniques allow the user significant flexibility in analyzing pond performance under realistic load and weather conditions. Finite element techniques describe conduction heat transfer through the pond, earth, and edges. Results illustrate typical thermal performance of salinity gradient ponds. Sensitivity studies of salty pond thermal performance with respect to geometry, load, and optical transmission are included. Experimental validation of the program with an operating pond is also presented.

INTRODUCTION

Salinity gradient solar ponds offer the advantages of relatively high operating temperatures and long-term storage for costs significantly below those of conventional active solar systems. The outlook for greatly increased interest in solar ponds appears favorable, and commercialization may be close at hand. Because development of solar pond engineering is necessary for commercialization, work at the Solar Energy Research Institute (SERI) has addressed many of the engineering problems. This paper discusses a computer simulation program, SOLPOND, for predicting thermal performance of salty ponds. Previous analyses of salty solar ponds have discussed their optical, thermal, and hydrodynamic behavior and developed simplified, closed-form solutions of pond thermal performance [1,2]. SOLPOND offers much greater versatility. Finite element techniques model pond thermal performance, and the program performs discrete time solutions. SOLPOND allows the user considerable flexibility because weather and load profiles are handled as discrete data and optical transmission characteristics of the pond solution are considered as input data.

PROGRAM STRUCTURE

Within SOLPOND the transient thermal performance of a salinity gradient pond is modeled from a lumped-parameter thermal network. For large ponds, edge losses are small in comparison to total energy collection; such ponds are modeled with a one-dimensional finite element geometry (see Fig. 1). Each node of the corresponding thermal network describes the temperature at the related position within the pond. The upper and lower convecting layers are represented by individual finite elements because they are approximately isothermal. Several elements are used to model the thermal profiles within the nonconvecting salinity gradient or the earth below the pond. In the thermal network, the current inputs account for absorption of solar radiation within each finite element. The storage layer current source also accounts for the thermal load delivered by the pond.

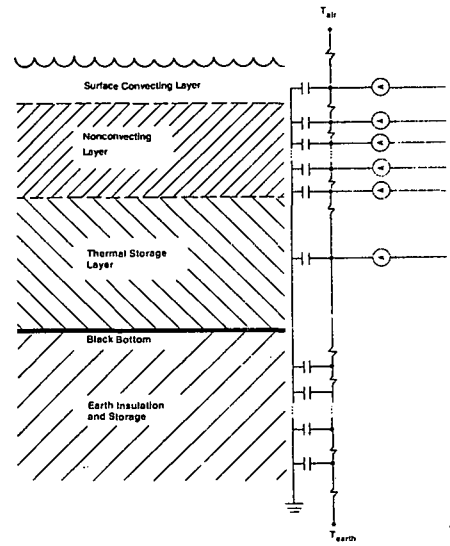

Fig. 1. One-dimensional solar pond thermal network.

The one-dimensional finite element model does not account for heat flow through the pond edges. This assumption is reasonable only for large ponds. The detrimental effects of edge losses become important when the pond perimeter-to-surface-area ratio becomes large (i.e., in a small pond). To account for edge losses, a three-dimensional anaylsis is necessary. For simplicity, SOLPOND models a circular pond. Axial symmetry of temperatures and incident solar radiation are assumed. Thus, the three-dimensional analysis is described by a two-dimensional finite element model revolved around the axis of symmetry. The element geometry is illustrated in Fig. 2.

The computation sequence in SOLPOND first calculates a time invarient discrete state transition matrix from the thermal network and then performs a time solution of the finite element temperatures. Since the discrete state

transition matrix is computed only once, time-varying factors that may exist in the thermal model are not considered. The major time-varying components that affect thermal performance are the dynamics of the salinity gradient. Because the growth and erosion of the gradient are determined by natural and maintenance effects and are not well understood, modeling of this effect is not practical.

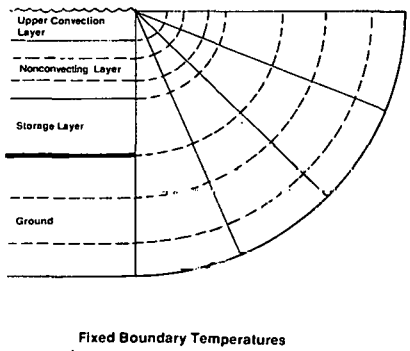

Fig. 2. Three-dimensional finite element geometry.

Additional aspects of the simulation program are as follows:

- Depths for the upper convection layer, nonconvecting layer, storage layer, load data, optical transmission, simulation time step, thermal conductivities, and heat capacities are user-selected inputs.
- Weather data that include daily averages for dry bulb temperature and modified solar radiation that accounts for reflected losses from the pond surface are available for Typical Meteorological Year (TMY) sites.
- The number of finite elements used to model the gradient layer and ground are user selected.
- To avoid numerical overstability, implicit finite difference equations compute the time solution.
- The pond storage temperature never exceeds 100°C. It is assumed that excess energy is extracted when necessary to avoid overheating.

SIMULATION RESULTS

Knowledge of the thermal performance of salty solar ponds is of fundamental importance in assessing their market potential. For any salty pond, local weather, predicted load, geometry, and optical properties will greatly affect thermal performance. The potential combinations of these properties are limitless, but a general understanding of salty solar pond thermal performance is possible by examining several simulation results. The presented results focus on aspects of pond thermal performance that would be difficult to investigate with previous simpler solar pond thermal models. From these simulations, several significant design factors affecting thermal performance are investigated. The stationary parameters used for these simulations are listed in Table 1.

Table 1. ASSUMED PARAMETER VALUES

Thermal conductivity of salt solution	0.65 (W/m°C)
Thermal conductivity of ground	1.0 (W/m°C)
Heat capacity of salt solution	3.98×10^6 (J/m^3°C)
Heat capacity of ground	2.0×10^6 (J/m^3°C)
Ground temperature 10 m below pond bottom	10 (°C)
Depth of upper convection layer	0.1 (m)
Simulation time step	14 (days)

For all the following simulations (except where noted), optimistic optical transmission properties for the pond saline solution are assumed. Transmission is computed from Nielsen's lumped representation of the solar spectrum and the associated exponential decay terms [2].

All simulation results are based on pond thermal performance after initial heating is completed. Thus, the pond thermal response results are steady-state, periodic solutions. This approach is convenient and appropriate for initial study because the pond warm-up transient is usually short-lived and of minor importance after the first summer of operation.

Effect of Load Profile

Temperature and load matching between a particular application and solar pond thermal performance is of obvious design importance. The seasonal thermal performance of the pond is sensitive to total energy extraction and the time that this extraction occurs. To illustrate this effect, three simulation results are drawn in Fig. 3. For these runs, total annual energy extraction, pond geometry, and weather data were identical. The time of year when the load was applied to the pond was the only variable in these simulations.

The summer-peaking and winter-peaking loads continuously extracted 70 W/m^2 for 22 weeks beginning in May and November, respectively. The continuous load extracted 29.6 W/m^2 throughout the entire year.

As can be seen in Fig. 3, this pond could provide the summer-peaking load at temperatures above 65°C. The same pond would have a minimum storage temperature below 25°C if it were used for the winter-peaking load.

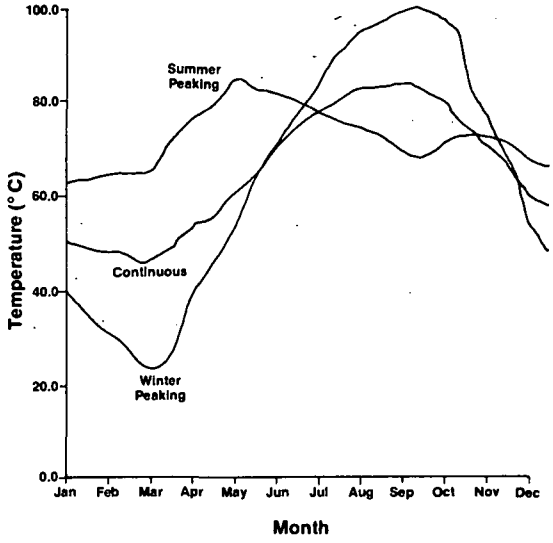

Fig. 3. Effect of seasonal load profile.

Effect of Storage Layer Depth for Winter Peaking Loads

The pond in Fig. 3 is poorly designed for a winter-peaking heating load requiring thermal energy above 35° C because the delivered energy temperature is too low during part of the operating season. One approach toward raising the minimum delivered energy temperature is to increase the thickness of the storage layer.

Figure 4 illustrates this effect for a pond used for continuously supplying a 55 W/m^2 heating load from November through March in Madison, Wis. A 5-m storage depth would be required to maintain the storage temperature above 40° C. A 3.0-m storage layer would have a minimum storage temperature near 30° C, and a pond with a 1.5-m storage layer would drop to about 15° C by the end of the heating season. If salty ponds are to be used for winter heating applications, they will have to be deeper than ponds yet constructed.

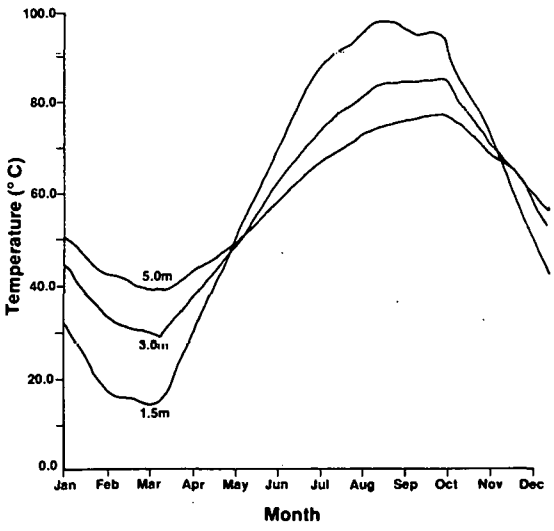

Fig. 4. Effect of storage depth.

Effect of Optical Transmission

The variation in pond thermal performance because of variation in optical transmission of the salt solution is great. Pond thermal performance is sensitive to the amount of solar radiation absorbed in the nonconvecting layer and the amount that penetrates into the storage layer. Also, the solution optical transmission can vary greatly because of salt impurities that inexpensive salts contain.

The optical transmission characteristics of the pond saline solution vary with the salt purity. Pure water characteristics establish an upper bound on optical transmission, with the dissolved salt and impurities further degrading transmission. The thermal performance of a pond using transmission properties of distilled water and Nielsen's data of a clear solution has been simulated with SOLPOND. The resulting seasonal temperature profiles are drawn in Fig. 5.

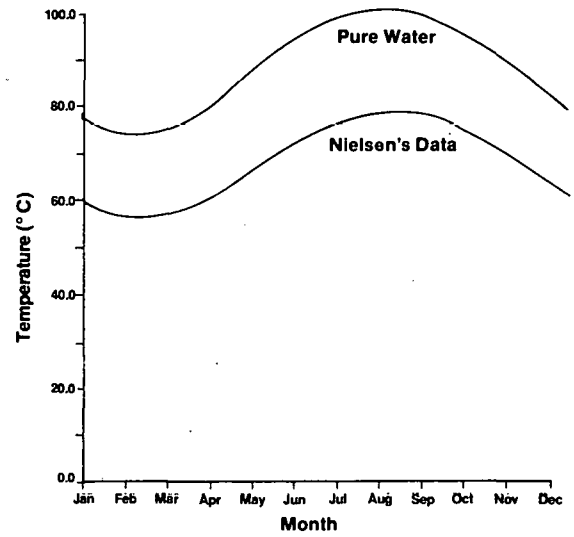

Fig. 5. Effect of optical transmission.

Nielsen's transmission data is for a highly clear salt solution. For applications using less pure salt, such as industrial byproducts, the transmission may be further degraded with a corresponding drop in pond performance. The need for high optical transmission is a major consideration in salt selection and pond maintenance.

Edge Loss Analysis

A convenient parameter for approximating average annual thermal losses through the pond edges is a perimeter heat-loss coefficient. This parameter relates the edge loss per length of perimeter to the temperature difference between the pond storage layer and the ambient air.

Using the material properties and ground temperature listed in Table 1 and a 0.3-m upper convection layer, several perimeter heat-loss coefficients have been calculated. These are presented in the graph in Fig. 6, which illustrates the dependence between pond depth profile and the perimeter heat-loss coefficient. Significant variation in the perimeter heat-loss coefficient will result if the ground conductivity differs from the 1.0 W/m°C value typical of dry ground used in the simulations; wet ground can have a thermal conductivity more than five times greater than dry ground. Other factors, such as operating temperature and load profile, affect the value of the perimeter edge loss coefficient but to a much lesser degree.

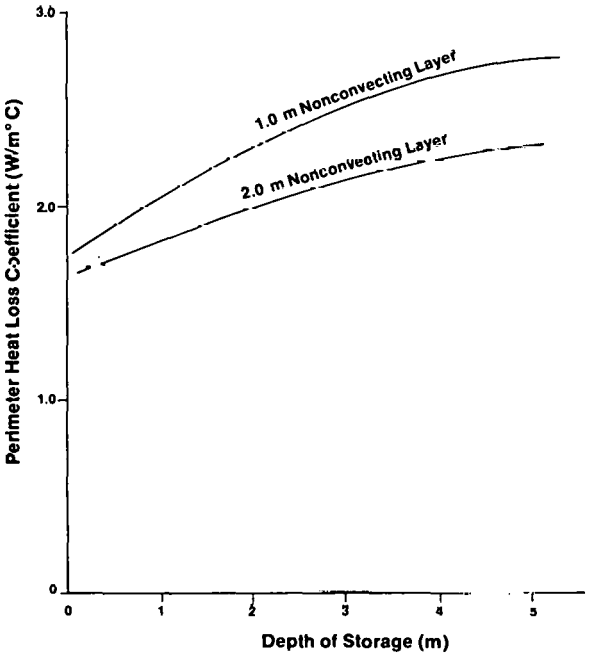

Fig. 6. Typical perimeter heat-loss coefficients for dry ground.

The importance of accounting for thermal losses through the pond edges can be highlighted by considering the degradation in delivered energy for several pond sizes. Table 2 lists the approximate load per unit surface area lost through the pond edges for three ponds having a 2.0 W/m°C perimeter heat-loss coefficient and operating 50°C above ambient. The small pond, typical in size of research ponds in the United States, loses over 3 kW through the edges, which is equivalent to a 40 W/m^2 load on a pond with negligible edge losses. This is most of the potential load. The second pond has the same surface area-to-perimeter ratio as the Miamisburg pond* and, consequently, suffers similar thermal degradation that is more than $10/Wm^2$ of pond surface for these operating assumptions. The 100-m diameter pond is large in comparison with ponds constructed in the United States and loses 4 W/m^2, which is about 10% of the delivered energy. The performance degradation from edge losses is significant for small ponds, and insulation may be desirable. SOLPOND may be used to simulate small ponds with insulation along the perimeter.

*An existing salinity gradient pond, 55 m by 37 m in size.

SOLPOND COMPARISON TO ACTUAL POND PERFORMANCE

It is desirable to test the validity of a computer modeling code by comparing simulation predictions with measured performance of a full-scale system. Only a handful of solar ponds are located within the United States, and all except the Miamisburg, Ohio pond are used for experimental purposes. About 1/2 acre in surface area, the pond in Miamisburg is significantly larger and of a more practical size than the experimental ponds. Additionally, thermal performance data have been collected for over a year. Based on data availability, size, and the ready cooperation of the associated personnel, the Miamisburg Pond was selected for this evaluation of the accuracy of SOLPOND predictions.

Thermal performance and weather data taken at the Miamisburg Pond during the period from 23 July through 5 November 1979 were used for this validation exercise. Temperature values from July 23 established the necessary initial conditions for SOLPOND. Because SOLPOND models circular ponds and the Miamisburg pond is rectangular, a circular pond with a surface-area-to-perimeter ratio equivalent to that of the Miamisburg pond was simulated.

Figure 7 shows SOLPOND predictions and measured values for storage temperatures. The lower curve was developed using a ground thermal conductivity of 5.0 W/m-°C (wet ground). SOLPOND default values were used for the remainder of the material properties. Close agreement between measured and predicted values is apparent. In the upper simulation , all of the SOLPOND default values, including ground thermal conductivity of 1.0 W/m-°C (dry ground), were used. This illustrates the degradation in performance of the Miamisburg pond caused by the greater thermal conductivity of wet earth.

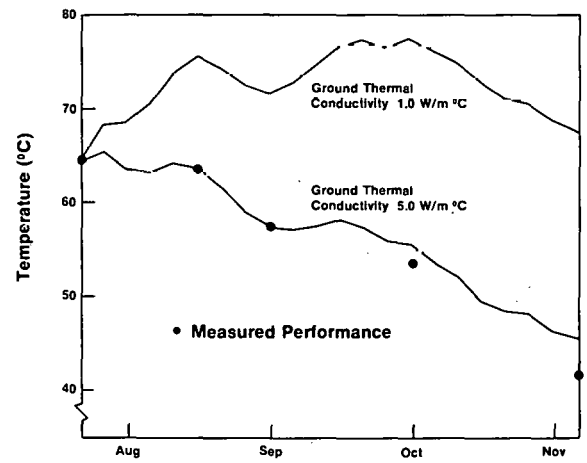

Fig. 7. Comparison of SOLPOND simulations to measured performance for the Miamisburg Pond.

Software/hardware validations are inherently limited in their accuracy for several reasons. Material anisotropies, data collection limitations, and model approximations contribute to prediction error. These general problems as they relate to this simulation are detailed next.

A precise knowledge of material properties is important for an accurate solar pond simulation. Ground properties such as thermal conductivity and specific heat vary according to the type of soil and the moisture content. Because variations may be found both regionally and locally, if one assumes constant properties throughout, the pond may introduce errors. Currently, however, ground property measurements do not exist, and values are estimates.

The optical transmission of the pond solution is another unknown. For the SOLPOND simulations, Nielsen [2] coefficients for clear water were used. A study of the optical properties of the Miamisburg solution currently underway at SERI indicates little deviation from Nielsen's data.

A third unmeasured characteristic of the pond is the surface heat-loss coefficient. However, as long as evaporation is not suppressed (by means of a cover or other device) performance is fairly insensitive to this parameter. A large value is used to provide close tracking of the pond surface temperature to the ambient temperature.

Data collection at an experimental facility is determined by a balance among hardware, design, and data reduction costs. The Miamisburg pond is well instrumented with thermocouples in the salt solution and in the ground to 1.5 m below the pond bottom. SOLPOND required initial temperatures for the salt solution and the ground around and below the pond. Many of these beginning conditions were necessarily estimated.

Also, during early 1979, a leak developed in the pond liner, causing significant losses of solution from the storage layer. Three hundred tons of salt and the associated water were lost from May to mid-October, when the leak was repaired. This fluid loss translates into a unmeasured heat loss from storage, but the loss also caused shifting in the depths of all three layers. For example, the depth of the upper convecting layer went from 0.5 m in July to 1.3 m in November. Also, the ground beneath the pond became wet, thereby raising the ground thermal conductivity.

SOLPOND was developed as a design tool to help the modeler examine the sensitivity of a variety of external parameters on solar pond behavior. SOLPOND was also designed to give maximum system information with minimum computer time, thus allowing multiple runs for a parametric study. To keep computational time small, several simplifying assumptions were used in the model.

For example, SOLPOND does not allow for changes in layer depths during a run; thus, it was necessary to interrupt the Miamisburg simulation to update the layer depth values. Material properties are also assumed to be constant, thereby discounting variation in optical transmission or ground thermal properties with time or location. However, the close agreement shown in this exercise demonstrates the viability of SOLPOND for future use.

CONCLUSIONS

A simulation program, SOLPOND, has been developed to analyze solar pond thermal performance under realistic weather and energy extraction conditions. This program was used for several illustrative examples. Simulation results highlight a pond sensitivity to seasonal load profile, storage layer depth, and optical transmission through the salt solution. Thermal losses through the pond edges were evaluated for several pond sizes and were shown to be significant for ponds as large as 100 m. A validation exercise showed close agreement between predicted thermal performance and measured data for an operating pond.

ACKNOWLEDGMENTS

This paper describes work supported by the Systems Development Division, Office of Solar Applications, Department of Energy. The authors thank Layton Wittenburg and Marc Harris of the Monsanto Company for providing data on the Miamisburg, Ohio salinity gradient pond.

REFERENCES

1. Weinberger, H. "The Physics of the Solar Pond." Solar Energy. Vol. 8. (no. 2) 45-56 (1964).

2. Rabl, A. and Nielsen, C. "Solar Ponds for Space Heating." Solar Energy. Vol 17, 1-12, (1975).

Session VIIIB

Louise Morrison
Solar Energy Research Institute
Chairperson

VALIDATION II

VALIDATION AND THE BUILDING ENERGY PERFORMANCE STANDARDS (BEPS) PROGRAM

William J. Kennish
TPI, Inc.
5010 Sunnyside Avenue
Beltsville, Maryland
20705 USA

T. M. Knasel
Patrick Hughes
Science Applications, Inc.
8400 Westpark Drive
McLean, Virginia 22102 USA

ABSTRACT

The Building Energy Performance Standards (BEPS) Program has been formulated to reduce energy consumption in buildings. However, the approach of the BEPS Program places a tremendous burden on validation and monitoring of three key phases: systems analysis, building construction, and building operation. If any confidence is to be developed in the projected results of the BEPS Program, an aggressive validation/monitoring program must be undertaken. However, this validation effort will only identify uncertainties, not remove them. The expense of such a program can be quite high and does not necessarily guarantee a successful program. (Reduction in actual energy consumption)

In the event that the current approach to implementing the BEPS Program is maintained, specific recommendations can be made in regard to the role of validation. These are discussed in the paper. An alternative approach to the current implementation plan is briefly mentioned and the impact on validation needs described.

INTRODUCTION

The Building Energy Performance Standards (BEPS) Program, now in the final stages of public review, is an attempt to curb the growing demand for energy in the operation of buildings. The proposed regulation's major distinction is that it stipulates energy usage per square foot of the building as the regulatory criteria in contrast to past building codes which focused on component selection or building design (such as specifying UA values, double pane windows, etc.). In theory, the energy usage per square foot criteria should ensure the reduction of building energy consumption to the levels prescribed in the BEPS Program. However, in practice there is a process which takes place in the design and construction of a building which may lessen the likelihood of attaining the proposed levels of energy consumption.

Figure 1 illustrates a series of events that take place from the time of conceptual design to the time of energy consumption. Once a conceptual design is proposed, the A/E firm formulates a detailed design, applying whatever analysis is available and taking other building codes into consideration. The detailed design is required to show that this building meets the BEPS requirements which call for the use of specified computer programs (initially acceptable programs plus programs which are "qualified" at a later date). If this compliance is shown, and other codes are satisfactorily met, permission is given to construct the building. The responsibility of the BEPS Program essentially terminates at this point. However, note that the goal of the program--reduced energy consumption--is still two steps away in our simplified schematic.

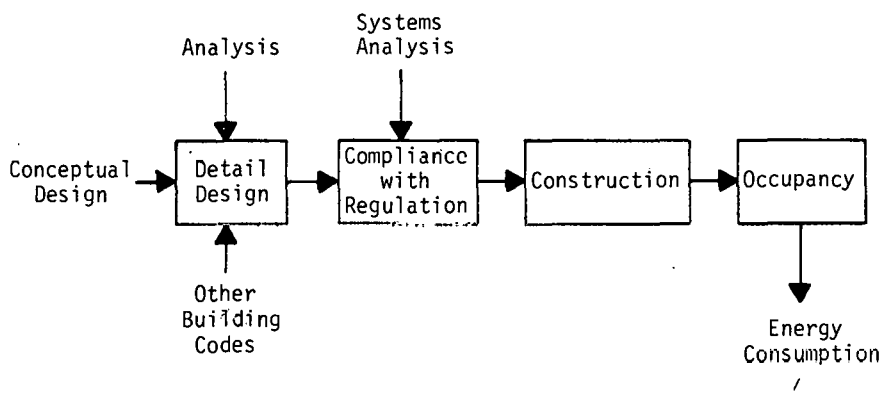

Figure 1. Sequence of Events Leading to Energy Consumption

The first of these steps is construction. When dealing with low energy buildings, the quality of construction and the use of proper materials becomes of paramount importance. The second step is occupant behavior, which affects the calculation of energy consumption. For example, in a cooling dominated commercial building the solar heat gain and occupancy levels can play important roles in establishing the cooling requirements of the building. Venetian blinds may have been installed with the expectation of providing a very small shading coefficient during cooling hours and a larger shading coefficient during sunny heating hours. But the actual use of the blinds may be quite independent of such considerations. It may also be that the tenants occupy the building with considerably more equipment and/or biological energy inputs than assumed in the compliance analysis.

Therefore it is clear that the objectives of the BEPS Program with respect to energy consumption at the design stage have significant obstacles to overcome before reaching their intended goals. The actual consumption may bear little resemblance to the original projections.

The role of validation in the process described above is vital. Although the issue of validation is far too complex and expansive to discuss in great detail here, we will attempt to discuss it at the programmatic level to indicate required research areas and potential problem areas. It should be noted that there is currently no provision for validation in the BEPS Program Plan.

THE NEED FOR VALIDATION

The heavy emphasis on the design stage in the proposed BEPS Program places a tremendous strain on the validation of all phases of the process described above. An analogous situation can be found in industrial controls. The BEPS methodology is analogous to an open loop control scheme where controls (decisions) are made and implemented with no feedback from the final result. This method works well for systems which are understood in detail and have little variation in performance. However, if the process is not well understood the results from control actions may vary significantly from the desired results. When this is the case it is necessary to incorporate feedback into the control loop to minimize the effects of uncertainties and insure the attainment of the desired results. This, of course, is typically more expensive than open loop control but often imperative.

Here is where the role of validation enters the picture. If there is to be any confidence in the projected energy savings of the BEPS Program without formulating new regulations which rely more heavily on the measured performance output of the process, then aggressive validation projects must be pursued in the following areas:

1. Systems analysis for compliance (Including qualification of alternative methods)
2. Construction effects on thermal performance
3. Occupancy effects on thermal performance

SYSTEMS ANALYSIS

The ability to accurately predict the thermal performance of a building is critical. The BEPS Program requires that the design of buildings meet certain energy/square foot objectives. But for this approach to have any credibility, the government must have a high level of confidence in the energy consumption predictions which are made to qualify a building design. Development of this high level of confidence is no easy task for several reasons:

1. Because the programs are complex and often modular, they allow many building design analyses from the same computer program. This makes a validation of the computer program at the system level an overwhelming task.
2. There may be a large degree of uncertainty associated with the inputs to the program, such as weather, thermal properties of materials, heat transfer coefficients, user errors, engineering assumptions, etc.
3. Available subsystem models do not always match with the design thereby requiring additional approximations.
4. Detailed and reliable data is not available for many buildings.
5. Construction and occupancy (to be discussed separately) can significantly affect building thermal performance.
6. Many computer programs will probably be "qualified" as allowable analysis tools thus making a comprehensive validation study for each prohibitively expensive. Qualification will be discussed in a later section.

It is easy to conclude that the validation of the systems analysis tools to be used in the BEPS Program is not only an important task but also an involved process. Furthermore, the validation of the analytical tools can only raise the level of confidence to a certain level because of inherent uncertainties associated with the proper use of the tools. A validation study cannot remove uncertainties which are a result of stochastic weather inputs, assumptions made for ease of analysis or material parameter variations. Even more important is that validation of the tools does not deal with the problem of program manipulation to obtain desired results. Indeed, due to the complexity of the analysis there are usually a sufficient number of uncertain parameters which can be selected so as to produce a wide range of predicted energy consumption. It would certainly serve no meaningful purpose if the primary result of the BEPS Program becomes the birth of "creative" energy systems analysis.

If validation of the analysis methods is to take place, several suggestions can be made:

1. Emphasize subsystem and component validation rather than total system validation. The results from subsystem studies can be applied to many different sytems whereas the results from a system study may only be applicable to that particular system.

2. The emphasis in any validation study should be on identification of which systems the computer program can be used to simulate rather than a statement of the program's "accuracy" or "validity."

3. In the process of qualifying alternative analysis methods, the emphasis should again be placed on determining which systems the methods can be used to analyze. This may include parameter ranges as well as generic system types.

4. Whenever possible standardized algorithms should be required to reduce the amount of validation necessary and to avoid unnecessary variations in predictions.

It should be noted that a verification project for DOE2 is currently underway at Los Alamos Scientific Laboratory (LASL) and represents a very important step toward any BEPS validation program. Results from the LASL work should be incorporated into the BEPS Validation Program Plan.

CONSTRUCTION EFFECTS

Many of the uncertainties discussed above are caused by uncontrolled input variations and necessary engineering approximations in the analysis phase of building design. However, as pointed out earlier, the analysis and qualification phase at present is the end of the BEPS concern even though it may not be synonymous with building energy consumption. When buildings employ conservation measures or passive and active solar systems, the construction phase plays an important role in determining the actual energy consumption. Also, if material quality, installation procedures or finishing steps do not correspond to the expectations included in the building analysis, the building's energy consumption may be substantially greater than the level used for qualification of the design. Little is gained by such a situation both from a national energy standpoint and from the standpoint of a building owner who probably paid a premium price for the building without receiving the expected operational benefit.

A validation study to document the effects of construction quality on building thermal performance would help alleviate the potential problem of quality assurance. Monitoring of the construction phase (at least on a spot check basis) may be deemed necessary to insure quality control. This type of monitoring program can be extremely expensive but the need may be sufficient to justify it.

OCCUPANCY EFFECTS

If we were to assume that the engineering assumptions made in the analysis phase had negligible effect on the accuracy of the predictions and that the building was constructed exactly as designed, there would still be a significant hurdle to overcome before attaining the energy goals. This final hurdle is the operation or occupancy effect on the thermal performance. When the building is designed, analyzed and qualified by BEPS there are many assumptions made concerning the occupancy of the building. Some of these areas are shown below:

1. Occupancy level (people/ft^2)

2. Equipment use (BTU/hr/ft^2)

3. Use of voluntary shading devices

4. Use of voluntary ventilation systems

5. Indoor set temperatures if occupant controlled

6. Hours of operation

This partial list indicates that the occupant can have a significant effect on the demands from the HVAC system. However, the selection of values for many of these input parameters is rather arbitrary and can be adjusted at the design stage to yield a wide range of energy loads.

Again, keeping in mind that the goal of the BEPS Program is to reduce energy consumption, it is obvious that an extensive validation/monitoring program should be initiated to study and hopefully control the effects of occupancy on building performance. If this is not done, then the designer is free to eliminate or reduce conservation measures by being extremely optimistic about occupant effects. Though this does not serve the objectives of the BEPS Program, it would be considered legitimate under the current proposed legislation.

Standard assumptions could be called for in the BEPS Program if more were known about occupancy effects and if less variability existed. However, this does not appear to be a feasible approach at this time. If monitoring were attempted it might prove extremely expensive and minimally productive.

CONCLUSIONS

The BEPS Program represents an attempt to reduce energy consumption in buildings. Without question, this is a necessary goal for the U.S. Government to pursue. It is not sufficient to allow only the cost of fuel to encourage the use of energy efficient designs since buildings built today affect the national energy situation for decades to come. It also seems appropriate to use energy per square foot as goals for enforcing new regulations. The format of the regulations, however, puts a tremendous burden on the

validation and monitoring of three key areas: systems analysis, construction effects and occupancy effects. If the current approach to the BEPS Program is to be maintained, then the following should be initiated as soon as possible.

1. All qualified analysis programs should be subjected to detailed validation studies to better understand the limits of use for each program. Note that this will identify the uncertainties, not remove them.

2. The effects of construction practices on building performance should be studied. This would be followed by a monitoring program of construction sites (at least on a spot check basis).

3. A further study should be undertaken to understand the effects of occupancy practices on building performance. This should also be followed by a monitoring program.

Hopefully, these efforts would assist in the attainment of the BEPS goals. However, due to the emphasis the program places on analysis, its primary accomplishment may be the creation of extremely imaginative system analysts rather than significantly affecting energy consumption.

There does exist another option for the BEPS Program which will be mentioned here due to its effect on the need for validation. If the BEPS Program focused on the end objective (actual energy consumption) the uncertainties of the earlier stages could be left to industry to deal with. For example, if the standards proposed were compared to utility bills (actual energy consumed) and fines levied if the standards were not met, then it would become the responsibility of the designer, builder, and building manager to ensure compliance with the regulation. The fines could be graduated, but stiff enough to encourage retrofits for poorly performing buildings. There are many pros and cons associated with such an approach but the beneficial effect of lessening validation requirements are obvious and should not be underestimated when considering costs of implementation.

Dup

THE DOE-2 VERIFICATION PROJECT: PHASE I RESULTS

Stephen C. Diamond and Bruce D. Hunn
Los Alamos Scientific Laboratory
Los Alamos, NM 87545

ABSTRACT

A computer program, designated DOE-2 (formerly DOE-1), has been developed to provide architect/engineers with a public domain tool for fast and economic energy analysis of buildings.

With funding from the US Department of Energy, the Los Alamos Scientific Laboratory (LASL) has developed and implemented a program plan to verify DOE-2. Phase I of this plan is an analytical verification of the DOE-2 program as a computational unit rather than as separate algorithms.

Work on Phase I of the DOE-2 Verification Project is nearly complete. Results of the crosscheck with the American Society of Heating, Refrigerating, and Air-Conditioning Engineers (ASHRAE) loads calculative procedures, as well as the results of a line-by-line check of program constants and flag-setting algorithms, are reported. Also presented are results of empirical tests of the full DOE-2 program, including comparisons with measured energy consumption, and preliminary results of a study of the user interpretation of input data on predicted results.

INTRODUCTION

The DOE-2 Verification Project began in 1978 with the preparation of a verification program plan [1] by LASL. This plan outlined the tasks to be completed and identified relevant work being conducted outside the LASL project. The methodology adopted for implementing this project was then presented [2].

Most of the DOE-2 Verification Project Phase I tasks are complete and are being evaluated. This paper summarizes the results of the more important of these tasks. A comprehensive and detailed status report is being prepared.

SUMMARY OF PHASE I RESULTS

ASHRAE/DOE-2 LOADS Crosscheck

This task, conducted by a consultant to LASL, involved the comparison of the DOE-2 LOADS program predictions with results of commonly used loads calculative methods that are described in the 1972 and 1977 ASHRAE Handbooks of Fundamentals [3,4]. The 1972 ASHRAE method uses weighting factors that are specified in the 1972 ASHRAE handbook. On the other hand, the 1977 ASHRAE method uses Cooling Load Factors that are derived from the same weighting factors as are specified in the 1972 handbook except that 1977 handbook weighting factors are used for lights. The purpose of the task was to provide DOE-2 users with a reference point for building loads calculations and not to determine the accuracy of any of the methods.

Comparisons of the predictions of DOE-2 with those of the 1972 and 1977 ASHRAE methods were made for peak and daily total cooling loads for a summer design day and for design lighting and occupancy schedules [5]. Four cooling load components were considered separately: cooling loads resulting from (1) heat gain through an opaque south-facing wall, (2) solar gain through a south-facing window, (3) lights, and (4) occupants. Results of these comparisons are presented in Figs. 1 and 2 and in Table 1.

Figure 1 shows a comparison of DOE-2 predictions and those of the two ASHRAE methods for cooling loads resulting from heat gain through a 20-cm (8-in.) brick, south-facing wall. Although this figure shows that DOE-2 predicts a peak only about 4% lower than the 1972 ASHRAE method, the loads are not in phase. Agreement is better between the DOE-2 predictions and those of the 1977 method. However, this agreement is coincidental because both the 1972 and 1977 ASHRAE methods are based on the weighting factors presented in the 1972 handbook, whereas DOE-2 uses weighting factors specified in the 1977 handbook.

Figure 2 presents a similar comparison of predicted cooling loads resulting from heat gain from lights. The significant differences shown illustrate that in this lighting case the 1972 ASHRAE method uses 1972 handbook weighting factors; the 1977 ASHRAE method uses 1977 handbook weighting factors; and DOE-2 uses weighting factors from Ref. 6.

Table 1 is a summary of results for the four load component comparisons. Although the daily sums for each method are nearly the same, there are

TABLE 1

DOE-2 LOADS/ASHRAE COMPARISON

Cooling Load Component	Relative Variation (%) DOE-2/ASHRAE 1972 Peak	DOE-2/ASHRAE 1972 Daily Sum	DOE-2/ASHRAE 1977 Peak	DOE-2/ASHRAE 1977 Daily Sum
South-facing wall (conduction)	-3.8	+0.2	-2.0	-0.1
South-facing window (solar)	-14.9	-0.2	-15.0	+2.0
Lights	+29.0	-0.01	+20.0	+0.02
Occupants	+4.5	+0.2	-0.1	-0.4

considerable differences in the predicted peak loads. DOE-2 predicts peak cooling loads that differ by as much as 29% from those predicted by the 1972 and 1977 ASHRAE methods. However, this does not mean that DOE-2 is wrong; it means that DOE-2 uses more recent sets of weighting factors than do the ASHRAE methods.

Constants and Flag-Setting Checks

An earlier version (DOE-1.4) of the DOE-2 computer program was checked on a line-by-line basis for two types of errors: those in assigned values of constants and those in flag-setting algorithms. The work was conducted by McDonnell Douglas Automation Company (MCAUTO) under contract to LASL.

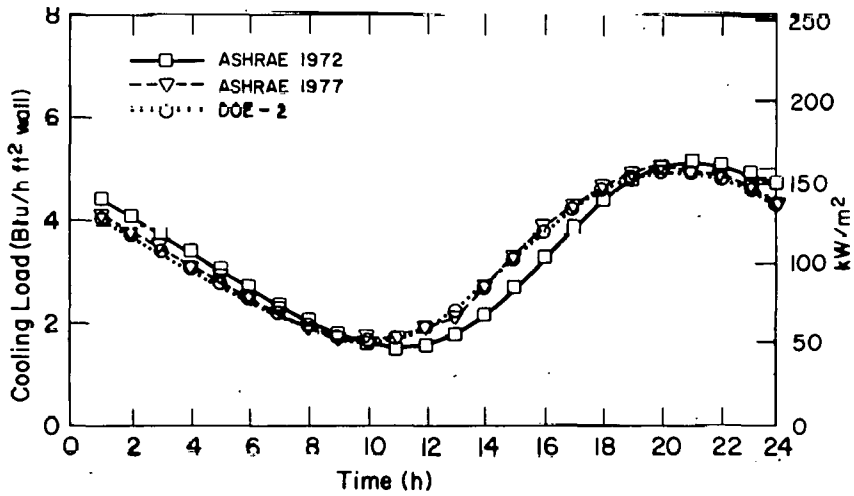

Fig. 1. Comparison of Cooling Loads for Heat Gain through South-Facing Wall--DOE 2 Versus ASHRAE Methods.

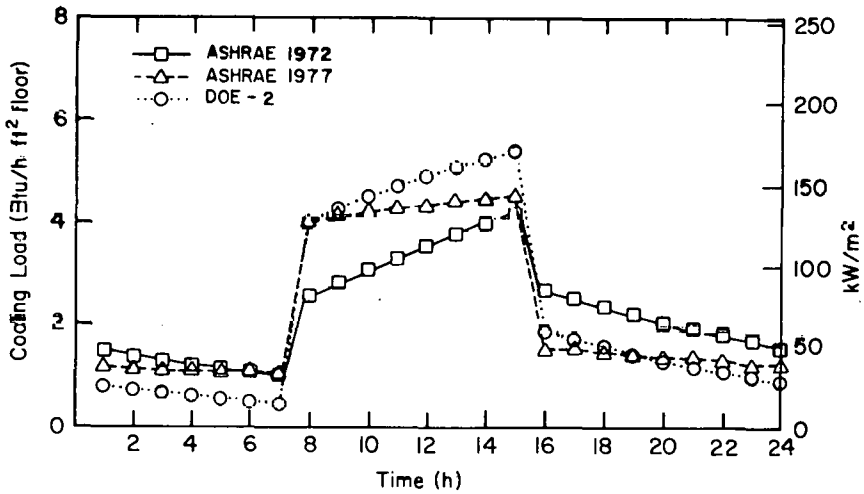

Fig. 2. Comparison of Cooling Loads for Heat Gain from Lights--DOE-2 Versus ASHRAE Methods.

The check of all program constants revealed a total of 19 errors, of which only 6 were significant. All of these errors have been corrected.

A majority of the 13 discrepancies found in the flag-setting algorithms were extraneous items inserted by the programmers for future use that did not affect the computations. These discrepancies have all been eliminated in the current (DOE-2.0A) version of the program.

PLANT Program Equipment Subroutine Check

This work was also conducted by MCAUTO, who compared PLANT program equipment performance default values to manufacturers' performance data. Commonly available published data, such as that contained in equipment brochures for system sizing, were used. Data from three different manufacturers were used, when available, to compare with each component model.

Figure 3 shows a comparison for the input versus output curve for a small boiler. Excellent agreement is shown between manufacturers' data and the DOE-1.4 simulation. Figure 4 shows the relationship between coefficient of performance (COP) and part-load ratio (PLR) for a reciprocating chiller. Note that significant differences are evident between both manufacturers' data and the program. This illustrates a point that is emphasized in the verification program plan; namely, that to determine the required component model accuracy, it is necessary to obtain the actual performance variance within a generic class of components. In this particular case, the COP varies from one manufacturer to another by as much as 17% for the same PLR. Therefore, the model cannot be expected to predict the COP to within 10% for this component.

The majority of comparisons made indicated good agreement between manufacturers' data and the equipment model subroutines. The only models with poor agreement were for waste heat from diesel-engine and gas-turbine generators. Lawrence Berkeley Laboratory (LBL) has corrected these inconsistencies in the current program version (DOE-2.0A).

Monthly-Energy-Use Field Tests

The purpose of this task is threefold: (1) to test the DOE-2 program in an overall manner, (2) to compare DOE-2 monthly and annual energy consumption with measured utility data for existing buildings in an uncontrolled environment, and (3) to introduce the human factor into the testing of the DOE-2 program.

A set of five contractor/test building pairs was selected by competitive bid to perform this task. In addition, two national laboratory/building pairs were involved. These seven pairs are

- Single-floor office building/Control Data Corporation;
- Multifloor office building/Galehouse and Associates;
- Retail store/New Mexico Energy Institute;
- Restaurant/Gamze, Korobkin, and Caloger;
- Hospital/Bickle Division of CM, Incorporated;
- School/LBL; and
- National Security and Resources Study Center (NSRSC)/LASL.

Reference simulations. The seven participants simulated their respective buildings using the DOE-2.0A program. These simulations were conducted using historical knowledge of the buildings

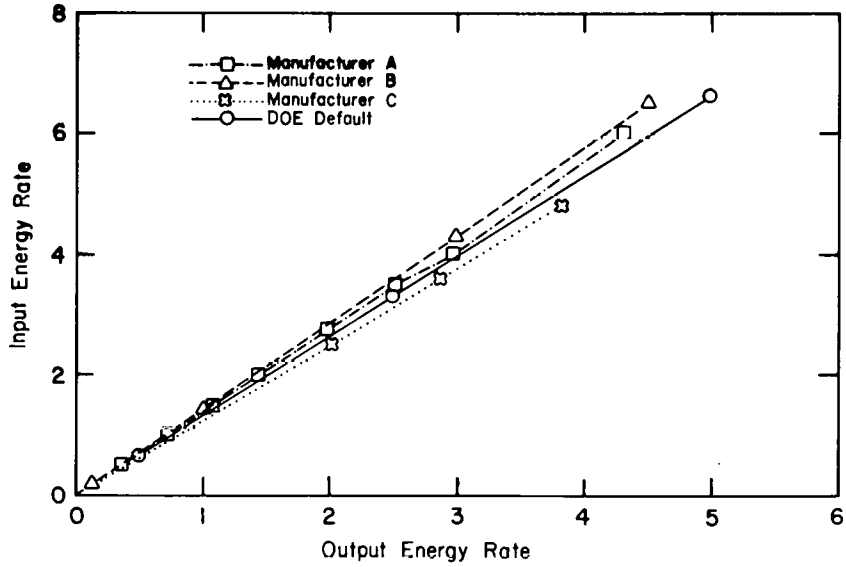

Fig. 3. DOE-2 PLANT Equipment Performance Default Curves Versus Manufacturers' Data--Small Boiler.

and their operation during the one-year test period. The period of simulation, metered data, and weather data used were all for the same calendar period. DOE-2 energy consumption predictions were compared to metered data (monthly utility bills).

A summary of reference-run results is shown in Table 2. Variation between predicted and measured values for gas or fuel-oil energy, electricity, total energy, and energy budgets is shown on an annual basis. The minimum deviation for gas/fuel-oil consumption was 1% for the restaurant, and the maximum was 19% for the retail store. The variation in prediction discrepancies for electricity consumption was less, with minimums of <1% for the multifloor office building and the school, and a maximum of 15% for the solar building (NSRSC). The prediction of annual total energy consumption (energy budget) varied the least, with a minimum of less than 1% for the restaurant and a maximum of 12% for the retail store and the solar building.

Differences in computed-versus-measured energy use were significantly higher on a monthly basis, ranging up to 45%, than on an annual basis.

User-effect simulations. Each of the buildings simulated in the reference runs, with the exception of the school building, was simulated by each of the other private contractors (round robin) that did not do the reference run on that building. Each reference-run contractor prepared a data package for his reference-run building for use in the user-effect test. This data package contained as-built engineering drawings, equipment specifications, operating schedules (for the year of simulation), and information regarding changes in the structure or schedules that have occurred since construction. It did not contain historical operating information.

The user-effect simulations have only recently been completed and have not been fully evaluated. However, Figs. 5-7 represent preliminary results for gas consumption, electricity consumption, and total energy consumption, respectively, for the restaurant (located in Chicago, Illinois). Each figure contains plots of the monthly measured data, the DOE-2 reference run, and the four user-effect DOE-2 runs. Three of the four user-effect runs for gas consumption (Fig. 5) compare well with the reference run (within ±10%) for monthly values. The outlying set of values appears to be

TABLE 2

SUMMARY OF REFERENCE RUNS RESULTS (ANNUAL)
DOE-2 PREDICTIONS VERSUS MEASURED DATA

	Gas/Fuel Oil (%)	Electricity (%)	Total Energy (%)	Predicted Energy Budget $MJ/m^2 \cdot yr$	(Btu/$ft^2 \cdot yr$)	Measured Energy Budget $MJ/m^2 \cdot yr$	(Btu/$ft^2 \cdot yr$)
Single-floor office	-15	+6	-6	1551.3	(136,695)	1659.4	(146,214)
Multifloor office	-14	<-1	-4	1327.8	(117,000)	1376.1	(121,258)
Retail store	-19	-4	-12	1709.6	(150,642)	1949.1	(171,739)
Restaurant	-1	-2	<-1	7959.2	(701,313)	8037.3	(708,203)
Hospital	-4	-14	-7	4812.5	(424,051)	5171.2	(455,657)
School	+5	<-1	+4	1075.1	(94,731)	1032.5	(90,980)
NSRSC (solar)	+15	-15	-12	492.3	(43,380)	562.1	(49,528)

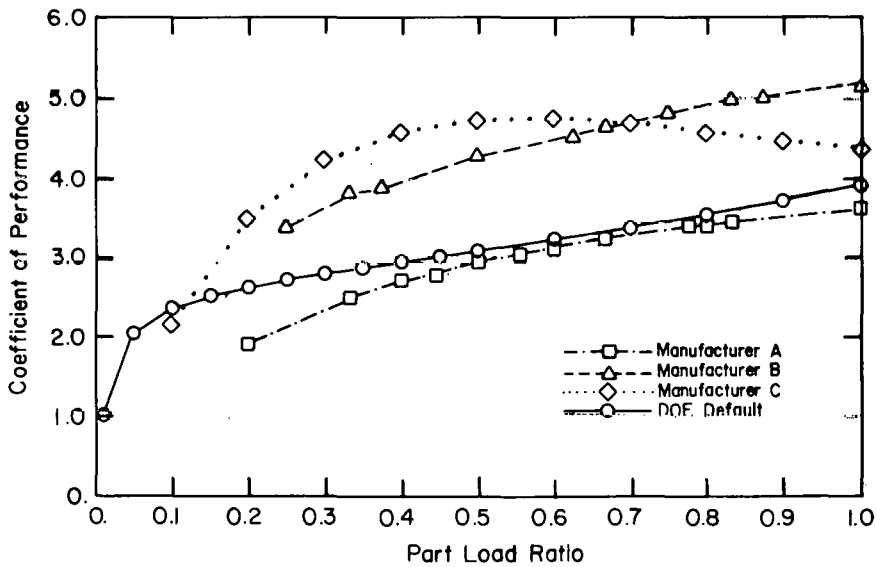

Fig. 4. DOE-2 PLANT Equipment Performance Default Curves Versus Manufacturers' Data --Reciprocating Chiller.

a result of a disagreement in the interpretation of base loads. The scatter in the user effect for monthly electricity consumption, approximately ±25% (Fig. 6), is greater than that for gas consumption.

CONCLUSIONS

Comparisons of DOE-2.0A with 1972 and 1977 ASHRAE loads-calculative methods have shown the following:

- Differences among the daily total loads predicted by the methods are small (<1%).
- Differences of up to nearly 30% occur among the peak loads predicted by the methods.

These differences result from the use of different sets of weighting factors in the three methods compared. Because predicted peak loads are widely used for equipment sizing, these differences should be quickly resolved.

DOE-2.0 is free of errors in constants and flag-setting algorithms.

Comparisons of DOE-2 PLANT equipment performance default values and manufacturers' data have

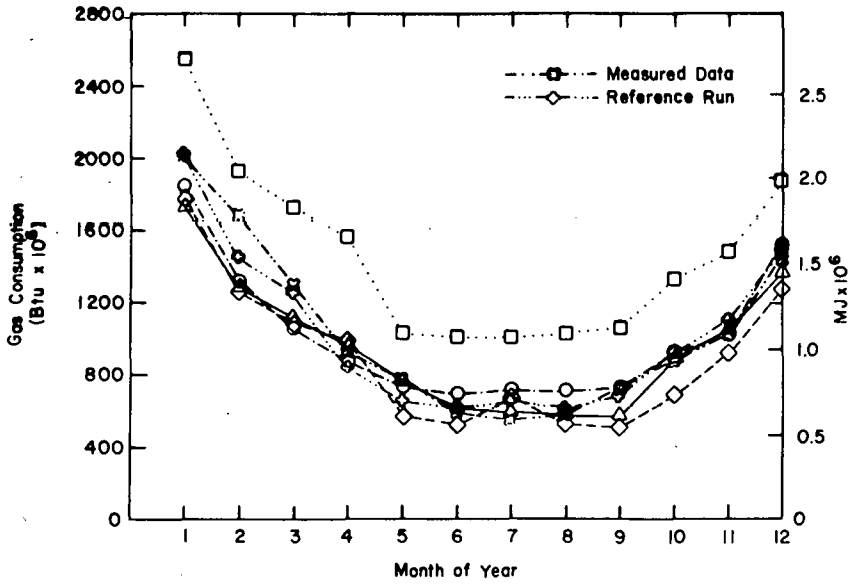

Fig. 5. DOE-2 Verification Project User-Effect Runs--Restaurant.

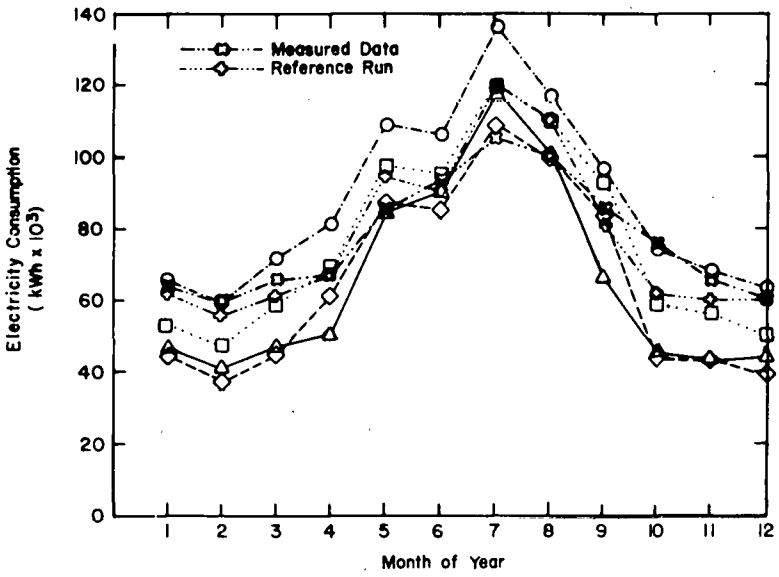

Fig. 6. DOE-2 Verification Project User-Effect Runs--Restaurant.

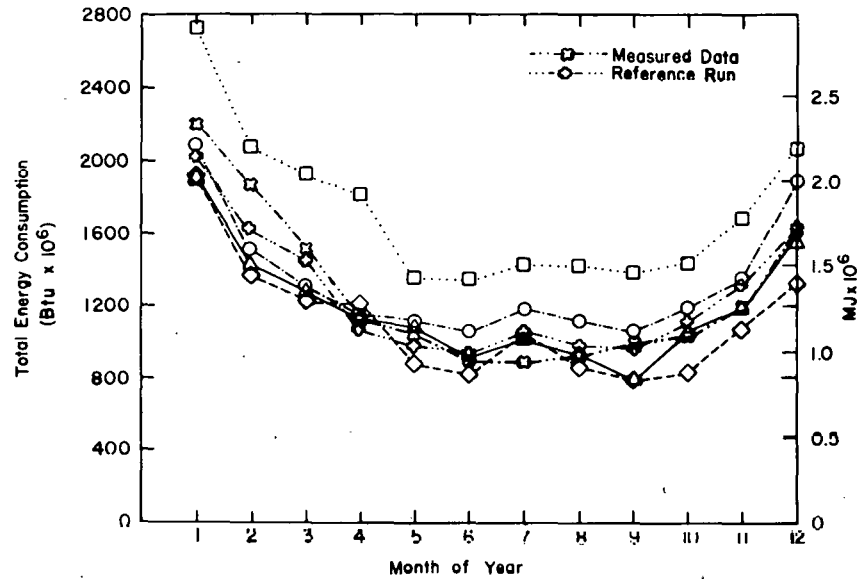

Fig. 7. DOE-2 Verification Project User-Effect Runs--Restaurant.

identified a few questionable default curves. These have been reviewed and corrected where appropriate in the DOE-2.0A program.

The reference runs made on six commercial buildings of different types indicate good agreement with measured monthly and annual energy consumption data. Predictions for the six buildings differed from measured annual data by 1-19% for gas/fuel-oil consumption, by 1-15% for electricity consumption, and by 1-12% for total energy consumption.

Preliminary data reported for one building (restaurant) indicate a user-effect difference of approximately ±10% for gas consumption and approximately ±25% for electricity consumption, both on a monthly basis.

REFERENCES

[1] Stephen C. Diamond, Bruce D. Hunn, and Thomas E. McDonald, "DOE-1 Verification Program Plan," Los Alamos Scientific Laboratory report LA-7552-MS (November 1978).

[2] Stephen C. Diamond, Bruce D. Hunn and Thomas E. McDonald, "Verification Methodology for the DOE-1 Building Energy Analysis Computer Program," Proceedings of the Systems Simulation and Economic Analysis Conference, San Diego, California (June 27-29, 1978).

[3] 1972 ASHRAE Handbook of Fundamentals, American Society of Heating, Refrigerating, and Air-Conditioning Engineers, Inc., 345 East 47th Street, New York, NY 10017.

[4] 1977 ASHRAE Handbook of Fundamentals, American Society of Heating, Refrigerating, and Air-Conditioning Engineers, Inc., 345 East 47th Street, New York, NY 10017.

[5] David W. Galehouse, "Crosscheck of DOE-2.0A LOADS Program: DOE-2 Verification Project," final report to Los Alamos Scientific Laboratory, Galehouse and Associates, Dayton, Ohio (December 10, 1979).

[6] "Procedure for Determining Heating and Cooling Loads for Computerizing Energy Calculations. Algorithms for Building Heat Transfer Subroutines," Energy Calculations 1, 1975, ASHRAE Task Group on Energy Requirements for Heating and Cooling of Buildings, American Society of Heating, Refrigerating, and Air-Conditioning Engineers, Inc., 345 East 47th Street, New York, NY 10017.

COMMIX-SA: VALIDATION, APPLICATION AND EXTENSION OF A SOLAR DESIGN TOOL

E. I. H. Lin, K. V. Liu, and W. T. Sha
Components Technology Division
Argonne National Laboratory

ABSTRACT

Two validation cases, one concerning laminar pipe flow, and the other heat discharge from a stratified water tank, are presented to show the validity of calculations by the three-dimensional thermohydrodynamic computer code COMMIX-SA. The wide range of applicability of the code and its extensions in progress to model rock beds and salt-gradient solar ponds are also briefly discussed.

INTRODUCTION

COMMIX-SA[1] is a three-dimensional thermohydrodynamic computer code developed for solar applications in general, and for analysis of thermocline storage tanks in particular. The code solves the cylindrical-coordinate conservation equations of mass, momentum and energy as an initial-boundary-value problem, using a modified ICE finite-difference technique[1]. As the usefulness of any computer code rests on the validity of its calculations, it is important that studies be made to verify the stability and accuracy of the code. Presented herein are two validation cases which serve to show that COMMIX-SA is indeed capable of producing results which are in good accord with known analytical and experimental work. Also discussed are the code's range of applicability and current work in extending it to model rock beds and salt-gradient solar ponds, which is expected to significantly add to the versatility of the solar design tool.

VALIDATION

Case 1. Laminar Pipe Flow

Steady-state laminar flow in the entrance and developed regions of a pipe is an extensively studied subject in fluid mechanics. In the developed region, the axial velocity assumes the well-known Poiseuille profile

$$w = 2\, w_{ave} \left[1 - \left(\frac{r}{R}\right)^2\right] ,$$

where w = local axial velocity; w_{ave} = average axial velocity = $Q/(\pi R^2)$; Q = volume rate of flow through pipe; R = radius of pipe; and, r = radial coordinate.

For the entrance region, numerous theoretical calculations and experimental data exist in the literature[2]. Although no perfect agreement exists between any two sets of calculations (or experimental data), the correct trend appears to have been well established. This makes the laminar pipe flow problem a suitable test case for validating COMMIX-SA.

Although the problem is axisymmetric and hence in principle a two-dimensional analysis should suffice, three-dimensional analysis was performed in order to validate the 3-D capability and, in particular, to demonstrate the workability of the singularity treatment as implemented in COMMIX-SA[1]. The simulation concerned a vertical pipe of radius R = 0.05 m, with gravity acting in the -z (i.e., downward) direction. The mesh set-up was: Δr = 0.003, 0.004, 0.005, 0.008, 3 * 0.01 (m); $\Delta\theta$ = 12 * 30°; and Δz = 0.3, 0.4, 0.5, 0.6, 0.8, 1.0, 7 * 1.2 (m).

At the pipe inlet, the velocity (w) was taken to be uniform and equal to 0.004 m/s. Isothermal analysis was performed, and the reference temperature was arbitrarily taken to be 57.2°C. The kinematic viscosity (ν) of water at this temperature is 0.503×10^{-6} m²/s. The Reynolds number (Re) is approximately equal to 795. No-slip boundary condition was employed at the pipe wall, and $\partial w/\partial z = 0$ was imposed at the pipe outlet.

Steady-state solution was obtained by going through a sequence of transient calculation using a uniform time step Δt = 0.5 sec. The initial conditions for the velocity components were: u = 0; v = 0; w = 0.004 m/s uniformly; and the initial pressure distribution accounted for the static head.

A dimensionless axial distance

$$z^* = \frac{z}{4R^2\, w_{ave}/\nu} = \frac{z}{DRe}$$

was used in presenting the results to facilitate

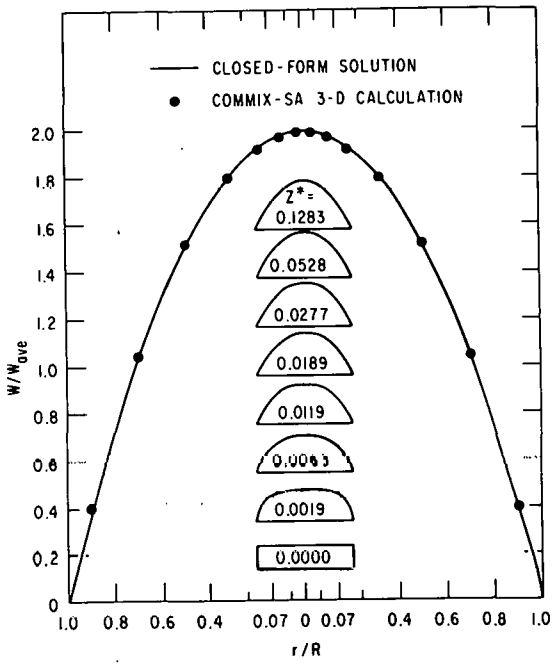

Fig. 1 Velocity Profiles in the Entrance and Fully Developed Regions of a Pipe.

comparison with previous calculations and experimental data by other investigators[2]. In the above expression, z = axial coordinate; D = diameter of pipe; ν = kinematic viscosity; and $Re \equiv w_{ave} D/\nu$ is the Reynolds number.

The calculated velocity profile in the developed region is shown in Fig. 1. Its agreement with the closed-form solution (i.e., the Poiseuille profile) is seen to be excellent. The development of the velocity profile within the entrance region as calculated by COMMIX-SA is also presented in Fig. 1. The gradual thickening of the viscous boundary layer within this region as the flow proceeds up the pipe is well illustrated.

Figure 2 shows the center-line (r/R = 0) velocity as a function of axial position. Figure 3 shows the velocity at r/R = 0.9 (near the pipe wall) again as a function of axial position. The COMMIX-SA calculations are clearly in very good agreement with the majority of previous theoretical and experimental investigations. The deviation of some previous results from the correct trend has to do either with the particular assumptions used in the analyses or with uncertain conditions involved in the experiments. They have been discussed by Campbell and Slattery[2].

The Campbell-Slattery analysis[2] is believed to be one of the best available. The COMMIX-SA results are hence compared in Fig. 4 with the Campbell-Slattery results for a number of r/R values; satisfactory agreement was achieved. It must be noted that the Campbell-Slattery analysis was based on a macroscopic momentum balance with viscous dissipation accounted for within the boundary layer; the essentially one-dimensional analysis still involved certain approximations. The entrance length calculated by COMMIX-SA is seen to be somewhat larger than that by Campbell and Slattery, due to the relatively coarse Δz mesh used in the simulation. In fact, the coarse Δz mesh also caused the fine details near the inlet to be smeared out. This explanation by coarse Δz mesh is justified because in an earlier COMMIX-SA calculation, even coarser Δz mesh was used, and there much more smearing was observed. However, since these results are adequate for the purpose of validation, it is felt that further calculation with finer resolution is unnecessary.

Case 2. Heat Discharge from a Stratified Water Tank

Few sets of wall-controlled stratification experiments in thermal energy storage tanks have been performed and documented to date. One such set which is suitable for validation of COMMIX-SA was performed at the U. S. Army Construction Engineering Research Laboratory (CERL), Champaign, Illinois[3,4]. These experiments involved heat charging or discharging from insulated cylindrical tanks at uniform initial temperatures, constant flow rates, constant inlet temperatures, and various inlet and outlet port sizes. Vertical temperature profiles were determined in these experiments from temperatures measured along the centerlines of the tanks. A heat discharge case, with its measured temperature profiles at different discharge times[4], was chosen as a basis for comparison with the corresponding COMMIX-SA simulations. The particular insulated cylindrical tank was of diameter 0.6 m and height 1.22 m. The tank was initially filled with water at a uniform temperature of 49.7°C. With quiescent initial flow conditions, discharge began when cold water at a temperature of 19.1°C was pumped into the tank from a single inlet (of diameter 0.019 m) located at 0.17 m above the bottom of the tank, while the tank water was drawn out via a single outlet (also of diameter 0.019 m) located at 0.17 m below the top of the tank. Throughout the heat discharge event, the inlet flow rate was maintained at a constant 4.92×10^{-5} m³/s (0.78 gpm), and the inlet water temperature stayed at 19.1°C.

In the COMMIX-SA simulation, the finite-difference grid set-up was: Δr = 6 * 0.06 (m); $\Delta\theta$ = 2 * 15°, 5 * 30°, 2 * 15° (half cylinder was analyzed to take advantage of existing symmetry); Δz = 2 * 0.044, 2 * 0.038, 0.029, 3 * 0.191, 0.029, 12 * 0.038, 0.057, 7 * 0.076 (m). The inlet and outlet velocities, assumed equal, were determined from the constant flow rate 4.92×10^{-5} m³/s (0.78 gpm). No-slip and adiabatic boundary conditions were employed at the tank walls. It must be noted that, as in any computer simulation, these specifications represent only a close approximation, and not an exact duplication, of the real situation.

The predictions by COMMIX-SA for the tank temperature profiles, with different Δz's, are pre-

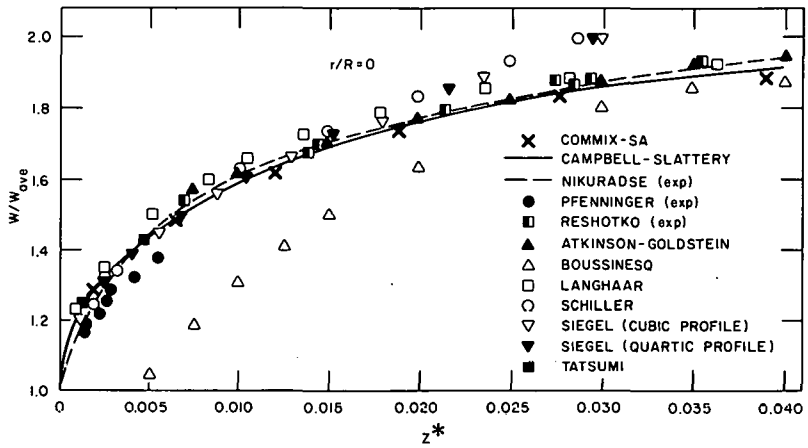

Fig. 2 Velocity as a Function of Axial Position at r/R = 0

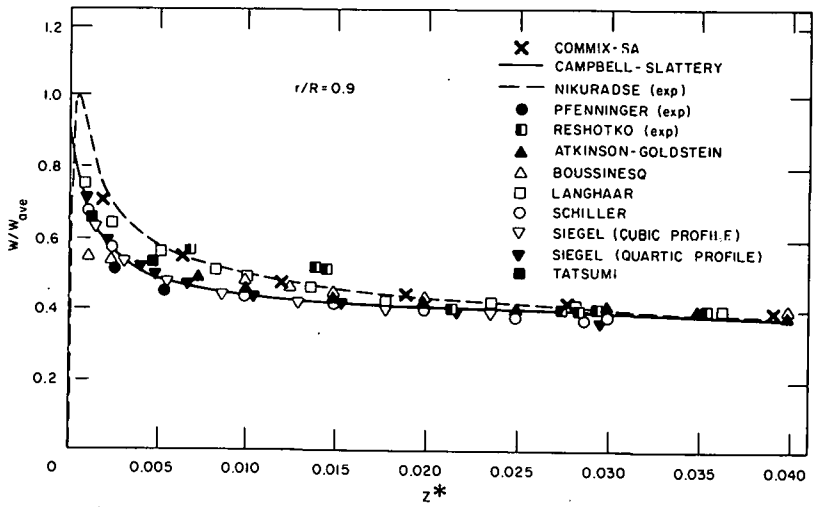

Fig. 3. Velocity as a Function of Axial Position at r/R = 0.9

sented in Figs. 5, 6, and 7, for times 10, 20, and 30 min. from start of heat discharge, respectively. Also presented simultaneously in these figures are the U. S. Army CERL data for direct comparison. From these figures, it is clear that mesh sizes, particularly Δz, have an important influence on the accuracy of the predictions. This is because discontinuities represented by the thermoclines are present in the tank temperature field. Although the discontinuities are rather mild, reasonably fine meshes are required to obtain a decent description of them. The thermoclines in this particular case have thicknesses typically in the 0.1 m - 0.15 m range, and it was found necessary to have $\Delta z \leq 1/3$ of the thermocline thickness to attain a reasonable prediction.

Refining Δz, however, increases the number of computational cells and necessitates a corresponding reduction in the time steps (to maintain numerical stability), and hence increases computation time. Moreover, there appears to be a limit to what one can gain in terms of accuracy by ever decreasing Δz, as is evidenced by the small differences between the results for Δz = 3.81 cm and Δz = 1.91 cm in Figs. 5 and 6. This latter observation is not totally unexpected, however, if one recalls that COMMIX-SA employs an upwind differencing scheme in treating the convective terms in the governing equations[1], and if one also notes that upwind differencing, while remarkably stable, is only of first order accuracy and engenders the so-called false diffusion effect. This artificial diffusion effect has been discussed in the literature [e.g., 5, 6, 7], and although several methods have been proposed to resolve the problem, none appears to have been totally satisfactory.

In spite of the minor deficiencies, reasonable agreement appears to exist between the COMMIX-SA predictions and the U. S. Army CERL data. The discrepancies between the two are attributed chiefly to the upwind-related inaccuracy, as well as experimental uncertainties, which are:

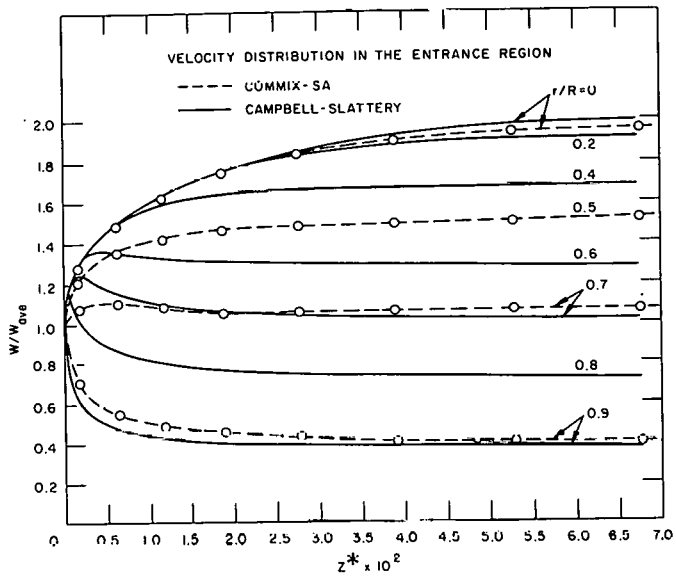

Fig. 4 Comparison of COMMIX-SA and Campbell-Slattery Calculations for Laminar Pipe Flow

(i) temperature measurement was accurate to +1.5°C; and, (ii) the temperature-inversion bulges below the thermoclines as shown in Figs. 5, 6, and 7 can not yet be validly explained[4]. While improvements regarding COMMIX-SA comutational accuracy may be expected in the future, confidence is established with respect to the validity of COMMIX-SA calculations, from results presented above for the two validation cases. It is of interest to note that with false diffusion effect in mind, one can infer, for example, that the heat-discharge response calculations by COMMIX-SA as presented in Ref. [8] were probably conservative; in other words, the actual performance of the storage tanks discussed in Ref. [8] may very well be better than predicted.

APPLICATION AND EXTENSION

COMMIX-SA was originally developed to investigate three-dimensional fluid flow and heat transfer phenomena in thermocline storage tanks. However, because of the rigor and generality of the mathematical formulation, and of the flexibility of the code structure[1], the computer program can actually be used as an analytical and design tool for a wider class of problems that initially intended. The domain of its applicability in fact extends beyond solar applications to other technological fields where detailed information about the three-dimensional thermohydrodynamic behavior of fluid systems is required. Within the area of solar applications, the utility of COMMIX-SA in analyzing behavior of liquid sensible-heat storage components, in identifying and evaluating improved storage designs, and in ranking the performance of various such devices, has been well demonstrated[8,9]. Useful extensions of COMMIX-SA to model rock beds and salt-gradient solar ponds have been under way at Argonne National Laboratory. A porous-media model is currently being developed within the COMMIX-SA framework to address the flow-channeling, plenum-design, and internal-partitioning questions associated with both vertical and horizontal rock beds. As to salt ponds modeling, COMMIX-SA is being extended to include a double-diffusive convection model which is expected to facilitate investigation of pond behavior and stability characteristics. The objective of the former task is, of course, to better understand behavior of rock beds and to improve their designs and performances; whereas for the latter, the ultimate goal is to determine practical methods which will ensure stability and increase efficiency of salt-gradient solar ponds.

CONCLUSION

Two validation cases have been presented to show the validity of COMMIX-SA calculations. In the laminar pipe flow case, excellent agreement was obtained between the calculations and the closed-form solution as well as various experimental data available for the fully-developed and entrance regions. In the stratified-tank heat discharge case, reasonable agreement was also achieved between predictions of tank temperature profiles and the corresponding experimental results. Although the false diffusion effect associated with upwind differencing caused some smearing of thermoclines, the general validity of the calculations was not adversely affected. The wide applicability of COMMIX-SA and its current extensions to model rock beds and salt-gradient solar ponds have also been briefly discussed.

ACKNOWLEDGMENTS

The authors gratefully acknowledge the support provided by Mr. J. M. Davis of the U. S. Department of Energy, and Drs. A. I. Michaels, W. W. Schertz and Mr. G. S. Rosenberg of Argonne

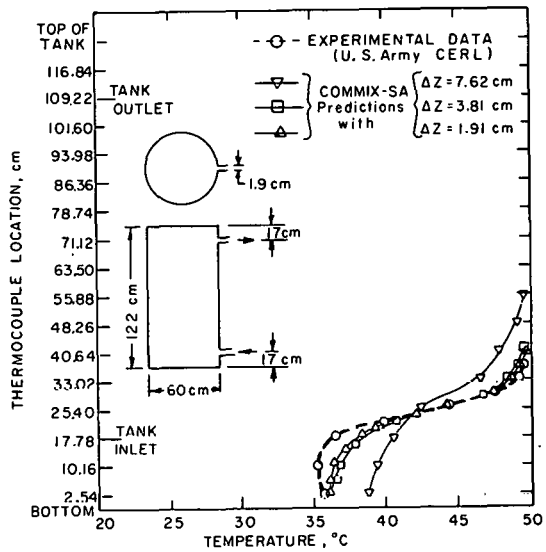

Fig. 5 Tank Temperature Profiles at t = 10 min.

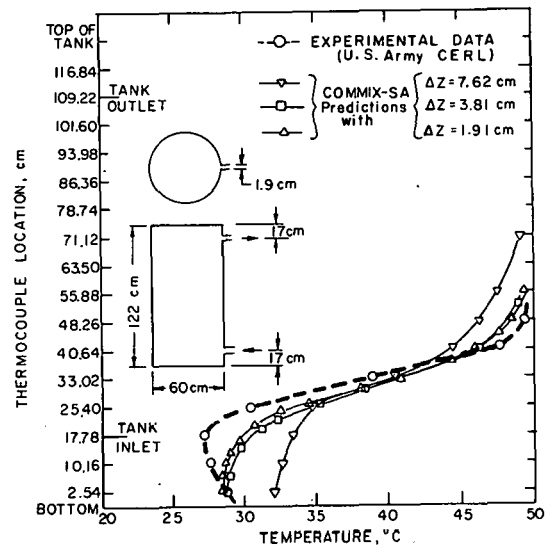

Fig. 6 Tank Temperature Profiles at t = 20 min.

National Laboratory. The manuscript was typed by Mrs. Sally Moll, and the work was sponsored by the Systems Development Division, Office of Solar Applications, U. S. Department of Energy.

REFERENCES

1. W. T. Sha, E. I. H. Lin, R. C. Schmitt, and K. V. Liu, "COMMIX-SA-1: A Three-Dimensional Thermodydrodynamic Computer Program for Solar Applications," ANL-80-8, DRAFT (Dec 1979).

2. W. D. Campbell and J. C. Slattery, "Flow in the Entrance of a Tube," J. Basic Engineering, Trans. ASME, pp. 41-46 (1963).

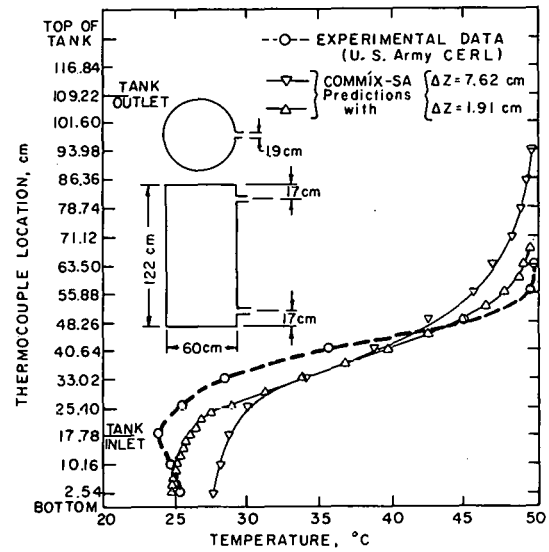

Fig. 7 Tank Temperature Profiles at t = 30 min.

3. B. J. Sliwinski, A. R. Mech and T. S. Shih, "Stratification in Thermal Storage during Charging," Proc. 6th International Heat Transfer Conference, Vol. 4, pp. 149-154 (1978).

4. B. J. Sliwinski, U. S. Army CERL, Champaign, Illinois, private communication.

5. D. B. Blackburn and J. N. Lillington, "False Diffusion Effects in the SABRE Upwind Difference Scheme and Comparisons with Central Differences in a Simple Vortex Heat Transfer Problem," AEEW-R-1072, UKAEA, England (1976).

6. L. C. Chow and C. L. Tien, "An Examination of Four Differencing Schemes for Some Elliptic-Type Convection Equations," Numerical Heat Transfer, Vol. 1, pp. 87-100 (1978).

7. B. P. Leonard, "A Stable and Accurate Convective Modelling Procedure Based on Quadratic Upstream Interpolation," Computer Methods in Applied Mechanics and Engineering 19, pp. 59-98 (1979).

8. E. I. H. Lin and W. T. Sha, "Effects of Baffles on Thermal Stratification in Thermocline Storage Tanks," Proc. Int. Solar Energy Soc. Cong., Vol. 1, pp. 586-590 (1979).

9. E. I. H. Lin, W.T. Sha and A. I. Michaels, "On Thermal Energy Storage Efficiency and the Use of COMMIX-SA for Its Evaluation and Enhancement," Proc. Solar Energy Storage Options Workshop, San Antonio, Texas, pp. 501-513 (1979).

NOTES

A COMPARATIVE ANALYSIS AND EVALUATION BY TEST OF SOLAR HEATING AND COOLING SYSTEM COMPUTER PROGRAMS

Richard L. Merriam
Arthur D. Little, Inc.
Acorn Park
Cambridge, Massachusetts 02140

Gary G. Purcell
Electric Power Research Institute
3412 Hillview Avenue
Palo Alto, California 94303

ABSTRACT

An analysis, test and comparative evaluation of solar heating and cooling programs has been undertaken to establish their usefulness to problems of interest to electric utilities. From over 31 identified available programs, eleven were selected for detailed analysis to establish their range of applications and intended capabilities. Based on program ratings relative to specific categories of applications, four programs were selected for testing. Test cases were defined for three building types: single family dwelling, light commercial building and a heavy commercial structure. Performance predictions were carried out for conventional HVAC systems, passive solar design options, active solar options and variations of these to examine the sensitivity in predictions to various design assumptions. The sensitivity analysis provided a means for assessing the probable accuracy of the programs relative to the applications explored.

All programs were tested by a single individual to minimize user-related differences in the results. However, inherent differences in the programs' intended capabilities (features considered, etc.) precluded exact comparisons since differing compromises specific to the individual programs were required to apply the programs to the defined test problems. Although good agreement was obtained between the predicted weekly or monthly loads, the hourly loads and demands were found to be significantly different. The programs were also found to differ substantially in the requirements imposed on the user and in the processing times.

INTRODUCTION

A large number of solar heating and cooling system simulation programs have become available in the past few years as a theoretical framework for the developing solar heating and cooling industry. These programs often differ significantly in terms of their capabilities and intended applications. A study has been carried out for the Electric Power Research Institute to evaluate a few of the more promising programs to establish their usefulness to the various problems of utility interest (e.g., building energy analysis, system design, demand pattern and load forecasting, and rate design).

The specific objectives of the work included: 1) identification and characterization of the major building energy analysis programs with solar capabilities; 2) in-depth analysis and rating of selected programs relative to categories of application; 3) testing of selected programs to uncover their strengths and weaknesses; and 4) evaluation of these programs from the electric utility perspective. Over thirty available programs with solar system capabilities were identified and described in detail in a separate document [1]. Eleven programs were selected for analysis, carried out on the basis of the program documentation (AXCESS, BLAST, DEROB, EMPSS, EP, F-CHART, HISPER, SOLCOST, TRACE, TRNSYS, and WATSUN). The documentations were reviewed for the presence or absence of program features in fifty-one general categories and were rated in four user-related areas. Weighting factors for the individual ratings (204 in all per program) were developed for twelve combinations of building type (residential, light commercial, heavy commercial) and generic systems (conventional, active solar, passive solar, load managed). From the overall ratings four programs were selected for detailed testing: AXCESS, DEROB, EMPSS, and TRNSYS. These programs can simulate the performance of a broad range of solar systems and building types (Fig. 1). Two of these programs were developed specifically for use by electric utilities (AXCESS and EMPSS).

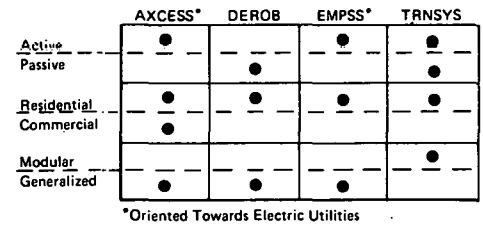

Fig. 1. Characteristics of Simulation Models Tested and Evaluated

TESTING METHODOLOGY

Benchmark test cases were developed for a single family residence, a light commercial building, and a heavy commercial building (Fig 2). The residential building description was based on an actual test house located in Columbus, Ohio; the light commercial building was adapted from the California Certification Program, while the heavy commerical

building test problem was patterned after a test case used in a recent ASHRAE test of manual methods of energy analysis. Attempts were made to describe realistic occupancy related factors and HVAC system designs without prior reference to the capabilities of the models being tested.

	Residential	Light Commercial	Heavy Commercial
BUILDING	OSU/EPRI Test House	ASHRAE Fundamental Office Building	20 Story Office Building (KASUDA)
CONVENTIONAL HVAC	Electric Furnace Central A/C Electric Hot Water	Single Duct Electric Coil Air Cooled Compressor Electric Hot Water	Terminal Re-heat Electric Coils Centrifugal Chiller Gas Hot Water
PASSIVE DESIGN		Modify Conventional	

Fig. 2 Benchmark Test Cases

All tests were performed by a single individual to minimize user related inconsistencies in the comparisons. Initial tests were carried out for the single family residence with a conventional heating and cooling system. Parametric analyses of the influence of building elements and control options were done to provide sensitivity analyses of the programs capabilities and to uncover reasons for differences in the programs predictions. Subsequent studies on the light commercial building focussed on the relative predictions of the models concerning the effects on overall energy use by incorporation of passive and active solar options. All tests were run using measured weather data for Columbus, Ohio. The approach to testing and results have been reviewed with the program authors.

RESULTS

Calculated January heating loads are shown for three of the programs in Table 1 for various parametric studies for the conventional single family residence. Both TRNSYS and EMPSS yield similar predictions over the range of conditions studied; the AXCESS model was developed specifically for commercial building applications and contains important restrictions limiting its applications to residential buildings (only one exposure per zone, fixed internal temperature). The effect of a night set back (2.2°C) is to reduce the heating load by about 4%. Table 2 summarizes comparisons between DEROB and TRNSYS predicted loads for one week in the heating season and one week in the cooling season. The predictions are in reasonable agreement when heat exchange between the basement and the conditioned space is neglected.

Table 1. Single-Family (Columbus) January Heating Loads

Factors Modeled					Calculated Loads (kWh)		
Attic	Basement	Solar Loads	Internal Loads	Setback	AXCESS	EMPSS	TRNSYS
X	X	X	X	X	3085	3236	2922
X		X	X	X	—	2555	2426
		X	X	X	2229	2114	1967
		X	X		2294	2190	2058
		X			2994	3038	3044
				X	—	3182	3205
					2996	3275	3306

Table 2. Single-Family Loads: DEROB-TRNSYS Comparison

Dates	Factors Modeled			Calculated Sensible Loads (kWh)	
	Attic	Basement	Windows	DEROB*	TRNSYS
January 1-January 7	X	X	X	466	649
	X		X	490	538
			X	428	435
				311	319
July 1-July 7	X	X	X	270	283
			X	270	337
				217	287

Monthly HVAC system energy expenditures for the conventional single family residence show good agreement in the heating season with large differences obtained in the cooling season (Fig. 3) The major difference between the EMPSS and TRNSYS predictions is related to the latent heat removel, which is underpredicted by the EMPSS model. Although close agreement between the monthly heating loads has been obtained, the predicted hourly demand patterns can be substantially different (Fig 4). Both the TRNSYS and EMPSS runs were made assuming about 366 kg/m^2 floor area of internal thermal mass; however, the methods employed by the programs for treating the thermal mass are different (TRNSYS assumes the mass is in intimate contact with the conidtioned air whereas EMPSS assumes it is a separate node with a finite thermal coupling to the air). The DEROB run was made by representing the interior partitions and the ceiling between the first and second floors of the residence. Because of the finite rates of heat exchange between the air and the interior partitions and

ceiling, the apparent thermal mass was lower, leading to a spreading of the net heating requirement over the day.

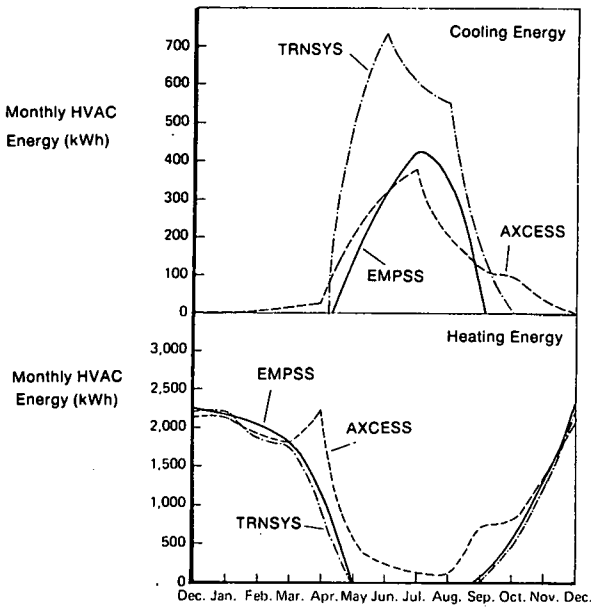

Fig. 3. Annual HVAC Energy Expenditures: Single Family (No Attic or Basement)

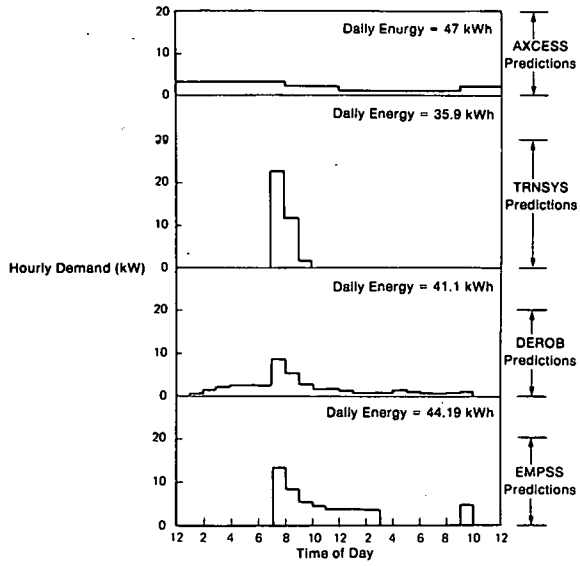

Fig. 4. Single Family (No Attic or Basement) January 7 Space Heating Energy

A number of design trade-offs for the light commercial building were investigated including direct gain and trombe wall passive options (Table 3) and active solar options (Table 4). It was assumed that the building was occupied five days a week from 7 a.m. to 5 p.m. and that the heating thermostat was set down to 12.8°C (55°F) during the unoccupied hours. Since the current version of DEROB cannot accommodate an internal heat schedule that differs by day, an average day internal heat profile was used to preserve the monthly total heat input.

Table 3. Light Commercial Building: Passive Options

	Predicted Heating Loads (kWh)	
Option	**DEROB**	**TRNSYS**
Conventional	10,653	12,483
Direct Gain	11,336	14,253
Direct Gain/Insulation	9,970	11,342
Trombe Wall	10,070	11,042
Trombe Wall/Insulation	9,897	10,683

Table 4. Light Commercial Building: Active Solar Options

	Load (10^3kWh)		Collection Efficiency		Percent Solar (%)	
	EMPSS	TRNSYS	EMPSS	TRNSYS	EMPSS	TRNSYS
Solar Heating (January)	12.9	13.1	39	38	29	28
Solar Cooling (July)	4.8	6.5	22	18	61	31

Stationary Collector With Selective Absorber

The relative performance predictions by the two passive solar programs (DEROB and TRNSYS) for the effects of incorporating passive design features in the building are in general agreement. The direct gain options consisted of a double pane south facing window occupying roughly 50% of the south wall area and a double pane skylight occupying 25% of the roof area. The trombe wall occupied 64% of the south wall (the direct gain option was not included) with an insulation covering assumed present whenever the building was unoccupied (this latter assumption was easily modeled with TRNSYS but only roughly approximated by DEROB). The two active solar systems simulated comprised a 18.6 m^2

(2,000 ft^2) stationary selective surface absorber flat plate collector with 11,360 liters (3,000 gal.) storage. Very close agreement between the predictions of the active solar system was achieved for the heating season. Predicted collection efficiencies in the cooling season differed somewhat; the percent solar figures for the cooling season are substantially different, largely due to the differing total cooling loads predicted.

Table 5 summarizes a comparison of the user related factors in terms of the total data inputs (reflective of the level of effort to use the programs) and the relative computing costs.

Table 5. User-Related Program Comparisons

	Total Data Inputs			
Building	AXCESS	DEROB	EMPSS	TRNSYS
Single Family	955	737*	334	906
Light Commercial	810	211	299	1,007

	Relative Computer Costs			
Building	AXCESS	DEROB	EMPSS	TRNSYS
Single Family	.88	11.0*	.20	1
Light Commercial	.82	2.1	.26	1

*5 volumes used to represent the single family residence.

CONCLUSIONS

The study was undertaken to investigate the applicability of the more promising computer models to a variety of buildings and generic systems. A number of general findings have emerged from the work: 1) programs are best viewed as a means for establishing the relative performance of system alternatives rather than as predictive tools; 2) in most situations use of a program involves judgements and compromises resulting in predictions that are highly user dependent; 3) proper documentation and attention to user related factors (such as complexity in input data preparation, level of choices offered to the user, input-output formats, error checking, etc.) are as important as the technical capabilities of the program; 4) the most widely accepted programs are those that are offered by organizations that provide active support in program use (through training and availability to respond to user questions); and 5) program "validation" is largely achieved through wide-spread use of a program and through the responsiveness of the program authors to problems uncovered.

REFERENCES

1. S.J. Feldman and R.L. Merriam, "Building Energy Analysis Computer Programs with Solar Heating and Cooling Systems Capabilities", EPRI report ER-1146, August 1978.

SOLCOST PROGRAM SENSITIVITY TO INPUT MODEL PARAMETERS

Loren J. Lantz
Solar Environmental Engineering Co., Inc.
2524 East Vine Drive
Fort Collins, Colorado 80524

C. Edward Hancock
Solar Environmental Engineering Co., Inc.
2524 East Vine Drive
Fort Collins, Colorado 80524

ABSTRACT

The SOLCOST Program has been used for a great deal of design and analysis work for state of the art solar systems including service hot water and space heating systems. The program predicts the thermal performance of the proposed solar system and then prepares an economic analysis for the system from the thermal results and various economic input parameters. The National Bureau of Standards (NBS) has recently collected data for several representative solar service hot water heating systems for comparing model predictions. The data sets have been some of the best collected and prepared data taken to date. As part of an ongoing validation effort for the SOLCOST Program, this data was compared with its thermal analysis predictions. However, before the SOLCOST thermal output and the reduced data from the NBS could be compared, a sensitivity analysis was accomplished to determine what the program's uncertainty to various input parameters could be. This analysis produced the distribution of the output load fraction which could be compared statistically to the recorded data. The authors were not primarily concerned with comparing two numbers but were more interested in the resulting distribution of the difference of the predicted and observed load fractions.

Assumptions were made as to the distribution of the more sensitive input parameters such as the collector efficiencies, load and the weather. Then several analyses were performed and the final distributions were calculated. For one system the expected (SOLCOST predicted) load fraction was about 62 percent on a yearly basis but the sensitivity analysis indicated that a one standard deviation about the number would be about 5 to 6 percent of the expected prediction.

The paper presents a short description of the SOLCOST Program and the NBS system which was used as a basis for comparison. The methodology including output distribution assumptions is presented along with results.

INTRODUCTION AND DISCUSSION

The SOLCOST Program [1] was developed by the Martin Marietta Corporation for the purpose of evaluating proposed solar thermal systems, including service hot water, space heating, space cooling and heat pump systems on an economic basis. The program consists of thermal and economic analysis packages. The thermal analysis portion is based on daily simulations using real observed weather data averages for a month, including average minimum, average maximum temperatures and the percent of sunshine or total horizontal radiation if available. A simulation is done for a representative cloudy day and sunny day and then a weighted average of the two results are taken producing the average expected load fraction and contributed solar energy for the month. The monthly values are tabulated and fuel rates are used to calculate expected energy costs for the solar system including auxiliary fuel. The economic analysis portion takes these energy costs for the solar system and its auxiliary source and compares them to a reference system which need not use the same fuel. The system costs, mortgage information, escalation rates and individual's economic financial picture are all considered in calculating lifetime savings. The SOLCOST Program can optimize the solar system size or calculate values for user's specified collector area. There are companion papers at this committee meeting which further describe the capabilities of the SOLCOST Program.

In 1978, the NBS configured six service hot water systems [2] with the primary purpose of collecting quality data for the purpose of comparing computer codes' thermal predictions against actual measured results. These six experimental test systems produced a great deal of high quality data making it possible to compare solar thermal predictions to real reduced data. One system was of primary interest (Fig. 1) because it was directly applicable to the SOLCOST performance model for a service hot water system. In cooperation with the NBS, Martin Marietta performed data comparisons for several months against the NBS' data with fairly good results. (See Table 1 [3]). This particular experiment gave a great deal of confidence in the SOLCOST Program's capabilities to adequately predict thermal performance and to esimtate the load fraction. However, it was desirable to proceed one step further and calculate the uncertainty inherent in the SOLCOST Program's predictions due to uncertainty in estimating system parameter inputs. The classic approach to determining the confidence interval about the expected load fraction is to perform a sensitivity analysis.

Analysis and Results

In an effort to estimate a confidence interval within which the SOLCOST predicted load fraction lie, a sensitivity analysis was conducted where various input parameters were varied randomly and

Fig. 1. NBS Double Tank Direct System

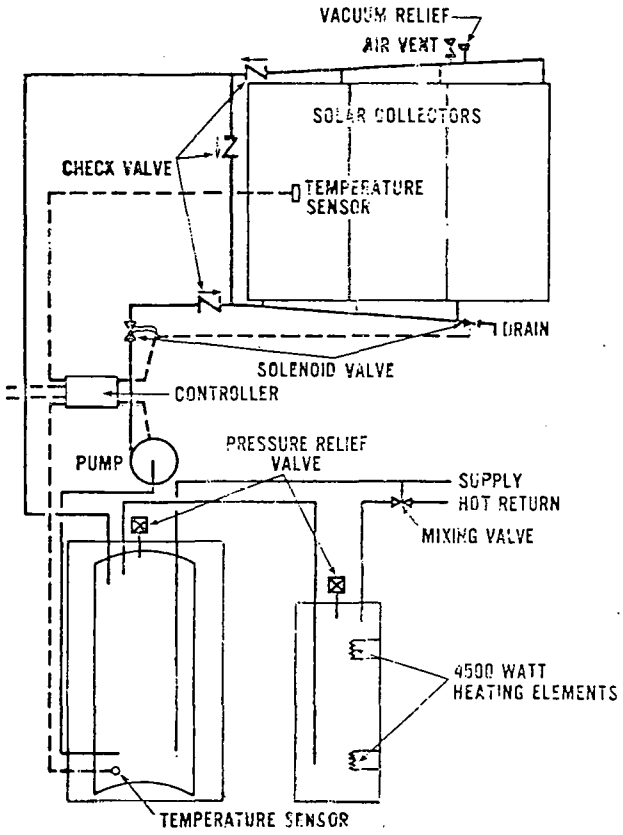

TABLE 1. SOLCOST COMPARISONS WITH NBS TEST RESULTS

	Two Tank Direct	
Month	NBS Results	SOLCOST
7	.53	.54
8	.48	.52
9	.49	.54
10	.46	.43

the final standard deviation values of the resulting distributions were calculated.* The input parameter variations are given in Table 2. The standard deviation divided by the mean values were determined purely by judgement and experience in the installation and analysis of services hot water solar systems. Later on in the paper, resulting deviation estimates will be presented as well as estimates where all of the σ/μ values were input and set equal to 10%.

The sensitivity analysis was conducted in two phases. In the first phase, each parameter listed in Table 2 was varied individually with all of the other parameters being left at their nominal values, and in the second phase all of the parameters were varied simultaneously and randomly. All distributions were assumed to be normal with the exception of the collector parameters which were sampled from the beta distribution. However, a normal distribution was used as an alternative for the beta distribution and little difference was seen.

Results of the basic sensitivity analysis are presented in Table 3. This table lists the ratio $\hat{\sigma}/\hat{\mu}$ (estimated standard deviation/estimated mean) for the predicted monthly and annual load fractions as input parameters are varied individually and all together. As an example of interpreting these results, if the expected July load fraction as predicted by SOLCOST is .54 (Table 1) and $\hat{\sigma}/\hat{\mu}$ is .09 for simultaneous variation of all inputs (Table 3), then according to the assumptions stated above, 68 percent of all July load fractions for this system will fall in the range .49 to .59. That is, the standard deviation ($\hat{\sigma}$) of the predicted load fraction is estimated as (.09)(.54) = .049 and, assuming normal distributions (there is no reason to believe a normal distribution should not be used) 68 percent of all observations lie within ± .05 of the estimated expected load fraction. Figure 2 displays a cumulative chart of occurrence for the annual solar fraction with given input variations.

TABLE 2. INPUT PARAMETERS WHICH WERE RANDOMLY VARIED

Parameter	Input Variation
Radiation	σ/μ = .07
Maximum ambient temperature	σ = 3°F
Minimum ambient temperature	σ = 3°F
Tank insulation	σ/μ = .10
Transport efficiency	σ/μ = .04
Collector efficiency at 0	σ/μ = .04
Collector efficiency at 0.5	σ/μ = .10
Load	σ/μ = .10

Many individuals use the resulting predictions from thermal analysis programs such as SOLCOST, FCHART and RSVP as if they were inbedded in cement and were accurate to four or more decimal places. Considering the predictions of SOLCOST or any other program to such degrees of accuracy is possibly providing a disservice to the analyst and the expected owner of the solar system. Variation in input parameters can be caused both by the way the equipment is manufactured and installed. It is unrealistic to expect the input parameters to the SOLCOST Program to be accurate to a very high degree. Computer modeling errors also exist. Consequently, it is important to understand and to estimate what the uncertainty is. The uncertainty caused by the weather is also displayed in this table and the resulting variation could be interpreted as microclimate variations, for example:

*Normal probability distributions were assumed.

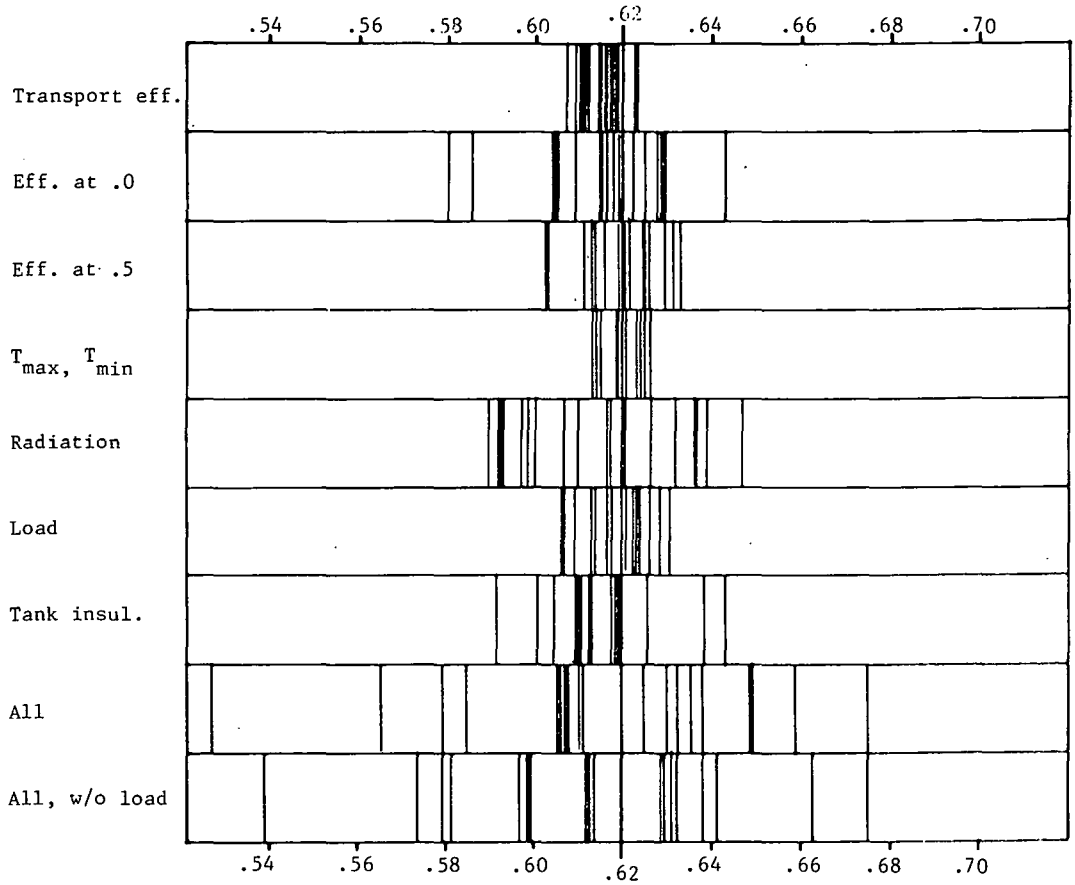

Fig. 2. Annual Solar Fraction, Sensitivity

between suburbs, rural area and downtown areas of a metropolitan center.

In an effort to determine which input parameters were more sensitive, the results were normalized in the sense that all of the standard deviations are equal to 10 percent of the desired input parameter value for input to the program. The resulting occurrence frequently was calculated and the efficiency at 0 or commonly referred to as the $F_R\tau\alpha$ product appeared to be the most sensitive parameter. These results are shown graphically in Fig. 3.

It was desirable to determine what, if any, relationship existed between the resulting standard deviation estimates when input parameters were varied singularly and the resultant standard deviation esimtates and the load fractions when all inputs were varied simultaneously. It was hoped that a resultant relationship would be visible for it would make estimation of net sensitivity calculatable without performing the entire experiment again. Table 4 depicts the resultant sensitivity as calculated in two different ways. The first column reproduces the results shown in Table 3 when all input parameters were varied simultaneously. The second column is the sensitivity as calculated by taking the sum of the squares of the individuals standard deviation estimates for the individual input parameter variations. The square root of that sum was taken and finally divided by the nominal expected load fraction. This second methodology would produce similar results if everything were normally distributed and the transformations linear in nature. There is no concrete evidence to indicate that there is any significant difference between the sensitivity calculated in the two different ways. This reduces to a great simplification, because, to analyze sensitivity, it does not become necessary to calculate the net sensitivity by simultaneously varying all of the input parameters and then by taking the sum of the square root as previously described, the new input sensitivity can be discerned quickly. This simplification also leads to an easy way to display sensitivity to input parameters on normal program output. This particular methodology has not been included in the SOLCOST Program, but is under consideration.

Conclusions and Summary

The sensitivity to many input parameters has been determined for one particular system as analyzed by the SOLCOST Program. Output variations and load fractions were determined for each month of the year and on an annual basis as could be possibly caused by uncertainty in input parameters. The output annual load fraction on a nominal basis was 62 percent. The sensitivity or the variation about this output value as caused by uncertainty in input parameters has a standard deviation of approximately 9 percent of the estimated mean value. In other words, there is a 95 percent probability that the real annual load fraction

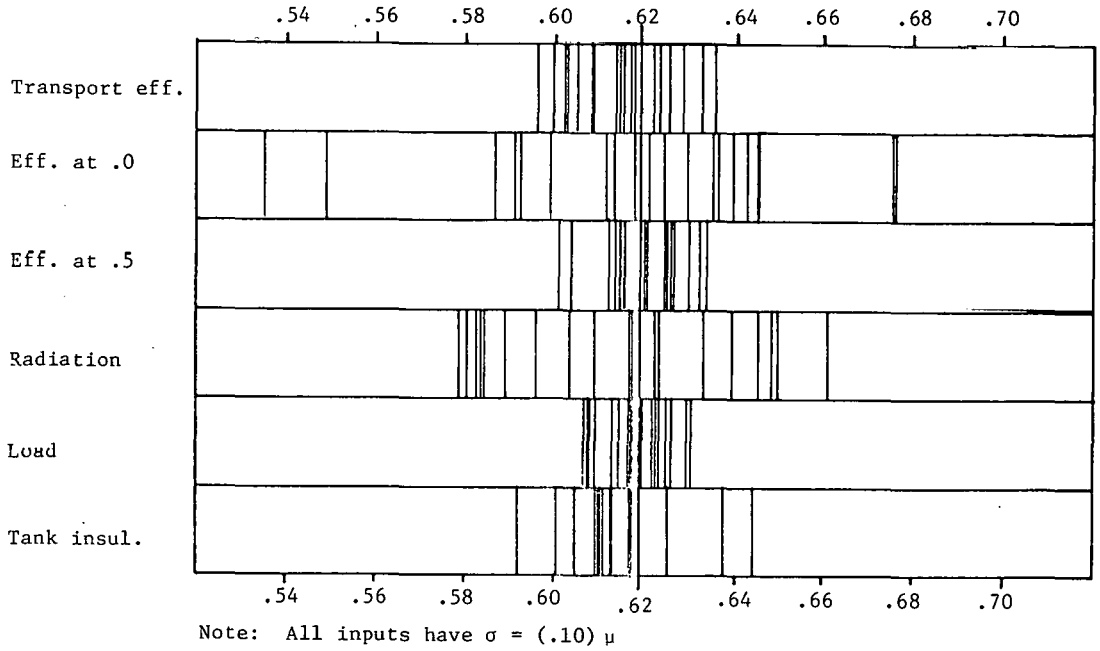

Fig. 3. Normalized Annual Solar Fraction Sensitivity

TABLE 3. RESULTING SENSITIVITY

	JAN	FEB	MAR	APR	MAY	JUN	JUL	AUG	SEP	OCT	NOV	DEC	ANNUAL
Trans. eff.	.02	.04	.02	.03	.03	.03	.03	.02	.03	.01	.04	.03	.01
Eff. .0	.01	.02	.02	.02	.04	.02	.03	.02	.04	.03	.04	.03	.03
Eff. .5	.02	.01	.02	.02	.01	.01	.01	.01	.03	.01	.03	.01	.01
$T_{max,min}$	.01	.01	.02	.02	.02	.01	.01	.02	.03	.01	.03	.01	.01
Radiation	.13	.13	.10	.11	.10	.06	.06	.09	.10	.08	.15	.13	.03
Load	.04	.05	.04	.04	.04	.04	.05	.04	.05	.04	.03	.06	.01
Tank insul.	.02	.01	.02	.02	.01	.02	.02	.03	.02	.02	.02	.01	.02
All varied simultaneously	.14	.17	.10	.12	.11	.10	.09	.08	.11	.12	.16	.17	.06

TABLE 4.† RESULTANT SENSITIVITY TO LOAD FRACTION CALCULATED TWO WAYS

Month	$\hat{\sigma}/\hat{\mu}$ (Inputs varied simultaneously)	$\hat{\sigma}/\hat{\mu}$ (Calculated by sum of squares)*
Jan	.14	.14
Feb	.17	.15
Mar	.10	.12
Apr	.12	.13
May	.11	.12
Jun	.10	.09
Jul	.09	.10
Aug	.08	.11
Sep	.11	.14
Oct	.12	.11
Nov	.16	.16
Dec	.17	.16
Annual	.06	.05

lies between .56 and .68. Also, a test was conducted to see if the net sensitivity and the annual and monthly load fractions could be calculated by adding the sum of the individual variances and then taking the square root of this sum and dividing by the nominal load fraction to see if this is by chance equal to the result obtained when simultaneously varying all input parameters. The results were quite encouraging and there is no reason to indicate that the resulting sensitivity is different as calculated by the two different methods. This is what would be expected if all input parameters were normally distributed and the transformation between input parameters and final load fraction were a linear process. It should be remembered, however, that this particular load fraction of 62 percent is not on either end of the scale, (near 0 percent or 100 percent). This particular observation may not be true if the load fraction falls within the neighborhood of these boundary points.

References

1. SOLCOST, Solar Energy Design Program for Non-Thermal Specialists, User's Guide, Version 3.0, January 1980, The SOLCOST Service Center, 2524 E. Vine Drive, Fort Collins, CO 80524

2. Fanney, A. H., "Experimental Validation of Computer Programs for Solar Domestic Hot Water Heating Systems," July 1978, NBS, Washington, D.C. 20234.

3. SOLCOST/NBS Comparisons, Interoffice memorandum from R. Giellis to the NBS, April 16, 1979.

4. Anand, D.K., et. al., "Validation Methodology for Solar Heating and Cooling Systems," Energy, The International Journal, Vol. 4, No. 4, August 1979.

* σ (resultant) = $\sqrt{\sigma_1^2 + \sigma_2^2 + \sigma_2^2 \ldots}$

where σ_i are individual standard deviations due to input parameter variations

† See also Table 3.

NOTES

A COMPARISON OF THE PREDICTED PERFORMANCE OF SEVERAL SOLAR SYSTEM SIMULATION CODES FOR AN INDUSTRIAL PROCESS HEATING SYSTEM

Thomas L. Freeman
Altas Corporation
Santa Cruz, CA 95060

ABSTRACT

Comparisons of several active solar energy system simulation codes in the solution of a series of solar industrial process heat (IPH) problems are described. A typical solar IPH system was defined in sufficient detail to allow the particpants to provide input to their codes. Several collector types and two different load temperature requirements were investigated. A variety of modeling problems and differences were found and are discussed. A sensitivity study was performed on stratified tank modeling assumptions.

After a series of iterative problem redefinitions and recomparisons of results, excellent overall agreement of both long and short term results was achieved. In the process, errors and shortcomings were identified in each of the codes and confidence in their accuracy was improved. The critical importance of user error was noted.

INTRODUCTION

The DOE System Simulation and Economic Analysis (SSEA) working group has conducted a series of simulation comparison exercises involving DOE funded solar energy system simulation computer programs in several important solar applications. This paper reports on a recently concluded set of comparisons of the predicted performance of solar industrial process heating (IPH) systems. The simulation programs involved in the IPH comparison exercise included DOE-2 (from Lawrence Berkeley Laboratory and Los Alamos Scientific Laboratory), TRNSYS (from the University of Wisconsin), and LASL (an internal Los Alamos program). All codes were run by personnel from the respective authoring laboratory. In addition, TRNSYS was independently run by Altas Corporation. The SOLTES program recently developed by Sandia Laboratory specifically for simulation of IPH systems was involved midway through the exercise, but results were not obtained in time for inclusion in this paper.

The purpose of this and the other SSEA simulation comparisons is to increase the utility of the codes by identifying and correcting errors, inconsistencies, and important holes in the capabilities. The "user effects", caused by differing interpretations of system description data and program input data requirements, and mistakes in input preparation, have been essentially eliminated during this exercise. The input to the programs and the codes themselves were changed in a number of ways as results were obtained and compared for each revision of the problem statement. For this reason the final results reported here are not indicative of the agreement or accuracy likely from a user having no independent method of verifying results.

PROBLEM STATEMENT

Although there are many similarities in the modeling of IPH systems to previous SSEA residential space and DHW systems, there are a number of important differences. The fact that IPH systems are generally much larger does not in itself require different models or modeling techniques. However, since higher temperatures are involved, models of high performance tracking and or concentrating collectors are required, storage stratification is potentially more important, and heat losses from pipes and storage are more critical (particularly since they are often located outdoors). IPH load profiles, unlike space heating profiles, are generally independent of the weather and are very repetitive on a daily basis (though frequently zero on weekends). The problem statement was therefore designed to challenge the capabilities of the codes in these areas.

The IPH system chosen for the exercise was similar in design and application to one installed by Acurex Corporation on a Campbell's Soup plant in Sacramento. A schematic of the system is shown in Figure 1. It used approximately 700 m^2 of high performance collectors, a 75 m^3 vertical cylindrical storage tank, and a hot water load profile typical of a two-shift, five-day work week in a canning factory.

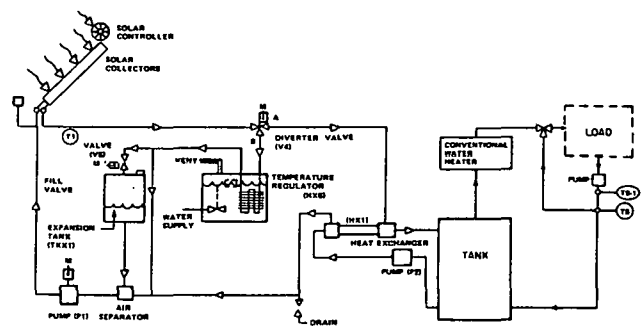

Figure 1 IPH System Schematic

Table 1 Selected Long Term Results

		OPEN LOOP, LOW TEMPERATURE LOAD								CLOSED LOOP, HIGH TEMPERATURE LOAD			
		I_{HOR} (MJ/m^2)	I_{CIN} (GJ)	I_{ACPT} (GJ)	Q_{COUT} (GJ)	Q_{SIN} (GJ)	Q_{SOUT} (GJ)	Q_{LOAD} (GJ)	SOLAR FRACT.	Q_{COUT} (GJ)	Q_{SIN} (GJ)	Q_{SOUT} (GJ)	SOLAR FRACT.
JANUARY	DOE-2	345	441	419	171	164	164	280	.58	96	86	73	.25
	TRNSYS (UW)	345	444	421	172	167	167	281	.58	98	87	74	.24
	TRNSYS (ALTAS)	345	444	423	173	166	166	281	.58	100	90	76	.25
	LASL	345	444	425	172	169	170	281	.60	90	84	72	.23
JULY	DOE-2	876	652	590	241	234	235	268	.86	183	171	166	.60
	TRNSYS (UW)	875	645	584	241	234	235	269	.86	179	168	163	.59
	TRNSYS (ALTAS)	875	645	588	242	234	234	269	.86	184	172	167	.60
	LASL	875	647	593	243	239	239	269	.88	174	167	163	.59
YEARLY TOTAL	DOE-2	7625	6980	6408	2622	2535	2472	3183	.764	1838	1700	1559	.472
	TRNSYS (UW)	7625	6987	6396	2626	2549	2485	3186	.768	1828	1693	1552	.465
	TRNSYS (ALTAS)	7625	6987	6421	2644	2565	2497	3186	.777	1880	1715	1590	.474
	LASL	7628	6980	6468	2639	2591	2531	3186	.784	1762	1685	1545	.466

The final problem statement specified General Electric evacuated tubular collectors with CPC reflectors and the associated collection subsystem, heat exchanger, plumbing, and control strategy recommended in the General Electric applications manuals. On the load side of the stratified storage tank, hot water was drawn from the tank through a heater that boosted the load delivery temperature, if required, to maintain a minimum temperature required by the process. A mixing valve downstream of the heater diluted the load delivery water, if required, to maintain this temperature.

The problem was run twice (with two different load temperature requirements). The first requirement was for the open loop, 80°C hot water delivery system actually used in the Campbell's plant shown schematically in Figure 2A. The second requirement was for a hypothetical closed loop process requiring 120°C water shown in Figure 2B. In both cases, the total energy requirements and energy demand profiles were identical. The daily load consisted of a constant flow for the first 45 minutes of each hour from 0800 hours to 2400 hours. This load was drawn every weekday of the year.

SIMULATION RESULTS

The participants furnished both "long term" and "short term" simulation results. The long term results consisted of monthly and annual integrated totals of selected performance measures for both the low temperature and high temperature versions of the problem. The short term results consisted of hourly integrated values of selected performance measures for the low temperature system only. Only the results for the final problem statement are presented here.

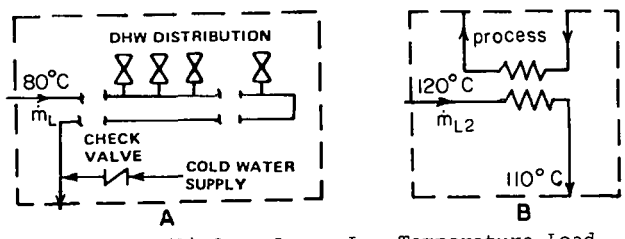

Figure 2 (A) Open Loop, Low Temperature Load
(B) Closed Loop, High Temperature Load

Long Term Results

Shown in Table 1 is a comparison of the long term results for both the low temperature and the high temperature load systems for two months of the year and for the entire year. The performance factors are defined as follows:

I_{HOR}	Global horizontal insolation
I_{CIN}	Insolation on collector surface
I_{ACPT}	Amount of I_{CIN} accepted by CPC
Q_{COUT}	Net energy gain of collectors
Q_{SIN}	Amount of Q_{COUT} input to storage
Q_{SOUT}	Useful Energy output from storage
Q_{LOAD}	Total load energy requirement
Solar Fract.	Fraction of Q_{LOAD} met by solar energy

Agreement in the long term results is generally excellent. Rarely do differences in any of the performance measures exceed 2 or 3 percent. All solar fraction predictions are within .02 in every month for both the high temperature and low temperature systems.

There are only a few noteworthy differences evident in these results. One is the slight, seasonally dependent difference in tilted radiation (I_{CIN}) between DOE-2 and the other codes, which suggests a small systematic error in the insolation tilting algorithm in DOE-2. LASL shows consistently smaller pipe losses as evident in the differences between collector output (Q_{COUT}) and storage input (Q_{SIN}). The largest disagreement is in the collector output (Q_{COUT}) for the high temperature load. The inclusion of collector capacitance effects in the LASL model probably accounts for its lower performance prediction. The TRNSYS (Altas) results seem to be consistently higher than the others. Small

differences in control system, heat exchanger, and piping loss modeling could be responsible. The effects of these differences are accentuated in situations when the radiation intensity is low and the load temperature requirement is high (as in January for the high temperature load). In such situations, the "critical" insolation level needed to provide useful energy gain is often very near the radiation available and net gain is highy sensitive to system parameters that define the "critical" insolation level.

Short Term Results

The short term results for the low temperature load system are shown in the plots of Figures 3, 4 and 5. These are hourly plots of the collector output energy and the tank top and bottom node temperatures for the first three days of January.

The collector output comparisons show near perfect agreement. The timing problems seen in previous exercises are not evident here. Small phase shifts in hourly results had been caused by small differences in the way the codes computed solar time from local standard time and the way in which time was aligned with hourly insolation data. These problems have finally been resolved in the current exercise because of two factors: 1) TMY data is already in solar time, so no transformation of time is required (provided solar time is used as the simulation time base), and 2) all participants have correctly treated the radiation data as an integrated total over the hour and have hence aligned the data with the hour angle from the preceding half timestep.

The excellent agreement in collected energy indicates that the CPC optics have been modeled in an equivalent manner and that no major differences exist anywhere else in the system, particularly on the collector side of the storage tank.

The plots of the top and bottom nodes of the two-node tank models reveal some minor differences in the codes. On the whole, LASL predicts a slightly higher degree of stratification than the other codes. TRNSYS (Altas) and DOE-2 show nearly perfect agreement throughout, while TRNSYS (UW) and LASL agree well during certain discharging periods (as in hour 30 and 55 in Figure 4). These differences are presumably due to small differences in the way the mixing assumptions have been implemented in the code, as discussed below.

DISCUSSION

The final results do not reveal significant sources of difference since most of them were finally resolved. The following discussion therefore highlights some of the modeling problems and approaches encountered in the exercise.

Insolation Data

All previous SSEA comparison exercises used an hourly weather data base assembled several years ago for

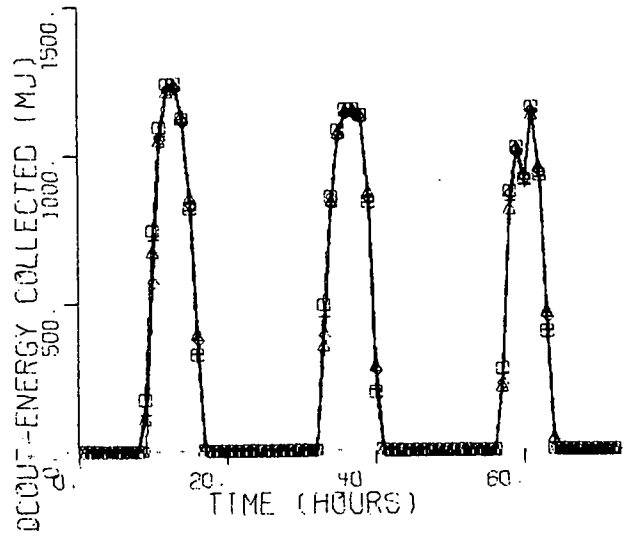

Figure 3 Hourly Plot of Collected Energy

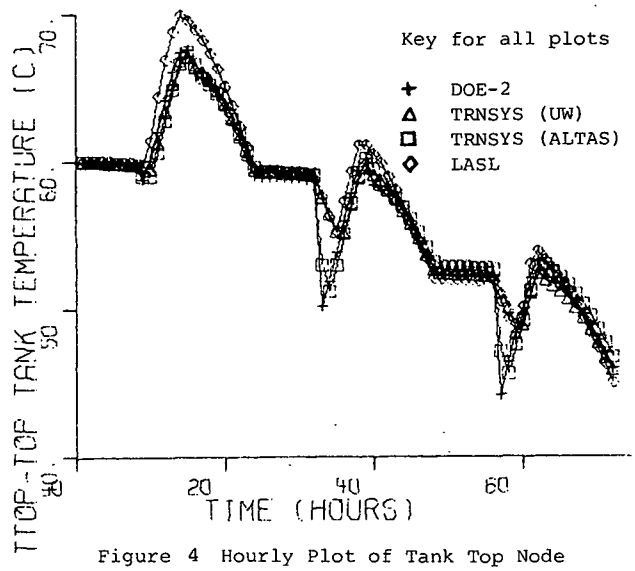

Figure 4 Hourly Plot of Tank Top Node Temperature

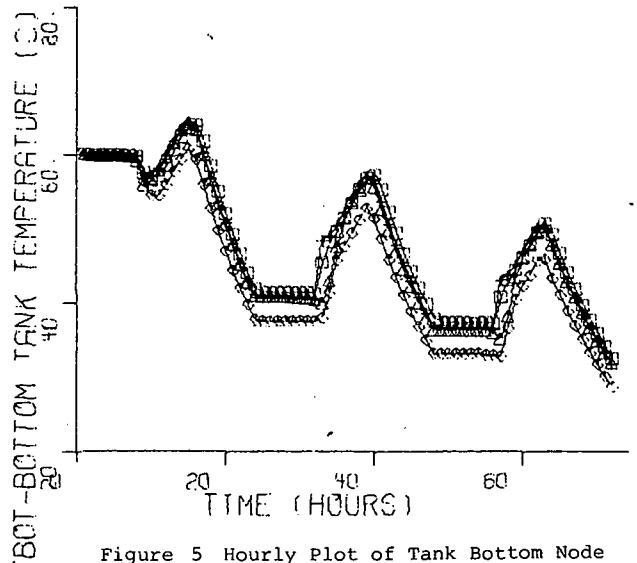

Figure 5 Hourly Plot of Tank Bottom Node Temperature

comparisons within the International Energy Agency (IEA). This data contained no beam or diffuse breakdown of the hourly total global horizontal insolation, necessitating that each code estimate it. Even though a common algorithm was specified for splitting total radiation into beam and diffuse components and for translating these components to tilted surfaces, the codes predicted somewhat different splits and hence different tilted surface insolation. This was due to several small differences in the calculation of solar time, in aligning the insolation data with solar time, in the treatment of beam radiation near sunrise and sunset, etc. Many of these problems were eliminated when the use of the Typical Meteorological Year (TMY) for Albuquerque was specified for the problem. The TMY data includes both measured total global radiation and direct normal radiation as predicted by the "Aerospace Corporation" model.

As evident from Table 1, the insolation calculated on the plane of the collectors (Q_{CIN}) was nearly identical for each code when using the TMY data. It was observed, however, that when the TMY direct radiation was compared to that predicted by three other beam-diffuse models available in TRNSYS (the Liu-Jordan, the old Boes method, and the Hottel-Bugler method) the TMY value was not generally in agreement. Because of the highly random nature of the Aerospace direct normal radiation model, hour by hour correlation with other non-random methods cannot be expected. This is apparent from Figure 6, which shows the scatter of hourly insolation data from the Albuquerque TMY tape superimposed on the "Boes" correlation used in previous SSEA exercises. Although the splits of the monthly totals come out about the same for all models, any skew in beam-diffuse breakdown for a particular month or season can have a significant impact on the predicted performance of collectors which utilize predominantly beam radiation.

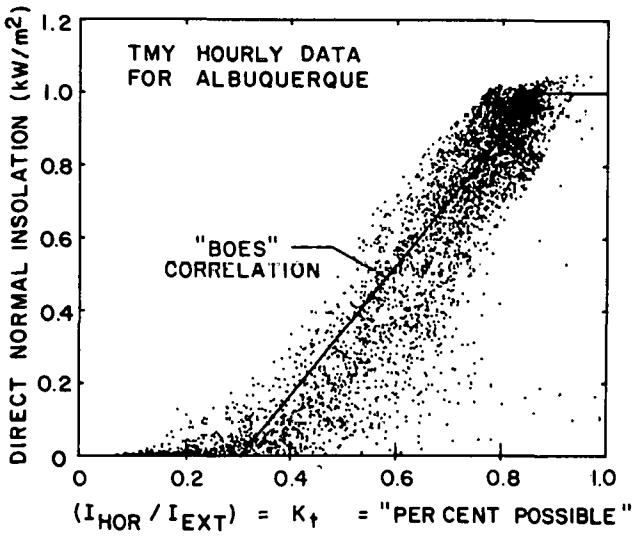

Figure 6 Albuquerque Hourly TMY Insolation Data Superimposed on the "Boes" Correlation

Working Fluid

The codes involved in this exercise share the basic assumption of constant working fluid properties. The effect is not believed to be large for the system investigated but this has not been verified since all codes made the same assumption.

Collectors

Stationary and seasonally adjusted flat plate collectors, optimally tracking CPCs with flat plate receivers, and stationary CPCs with evacuated tubular receivers were investigated at various times in the comparison. Several collector modeling approaches ranging from detailed modeling of fundamental mechanisms to various adaptations of the Hottel-Whillier-Bliss model, to purely empirical representations, were considered and tested. Each approach can be implemented in virtually any of the codes and should be selected after consideration of the purpose of the simulation and the amount of effort the user is willing to invest.

In this, as in previous SSEA comparisons, excellent agreement was found between the flat plate collector models using different modeling approaches. This should be expected because of the widely known and accepted flat plate steady-state performance theory. The only factor that causes systematic differences in the results is the treatment of collector heat capacitance. For typical flat plate collectors, consideration of collector thermal capacitance has been found to reduce the long term solar contribution in this exercise from about 1 to 3 "percent solar".

An optimally tracking flat plate collector enhanced with moderately concentrating East-West oriented CPC reflectors was investigated. Most participants developed models by extending the flat plate collector theory to include the CPC optical analysis of Rabl and Winston. A steady state collector simulation comparison test was conducted to identify sources of difference in the models. Errors were resolved and agreement in long term system performance was eventually achieved.

Since this collector model did not represent any existing practical collectors, the final problem statement specified a commmercially available CPC collector, the General Electric TC-100 evacuated tubular collectors in low concentration CPCs oriented North-South on a stationary South-facing bed. Since the detailed modeling of this array was deemed beyond the scope of this "system performance" comparison, it was agreed to use a quadratic fit of thermal performance test data taken in accordance with ASHRAE 93-77. The use of two empirically derived incidence angle modifiers was considered for the components of insolation in the vertical plane of, and in the plane perpendicular to, the CPC axis. It was decided, however, to model the beam and diffuse components of radiation accepted by the CPC as functions of solar position and then to apply the empirical efficiency equation to the radiation

List of Participants

accepted. This properly accounts for the angular acceptance of the CPC but ignores the angular dependency of the $\tau\alpha$ of the receiver.

The insolation angular acceptance model independently developed by several participants expresses the total radiation incident on a CPC receiver (I_{ACPT}) as a function of the tilted surface beam (I_B), sky diffuse (I_D), and ground reflected (ρI_{TOT}) components, and corresponding "view factors" F_B, F_D, and F_G.

$$I_{ACPT} = F_B I_B + F_D I_D + F_G \rho I_{TOT}$$

For a CPC, radiation is accepted if the component of the angle of incidence measured in the plane of the perpendicular to the CPC axis (Ω) is less than the acceptance half angle (θ). This is relatively straightforward for beam radiation since it is either all accepted or all rejected.

$F_B = 1$ if $\Omega \leq \theta$

$F_B = 0$ if $\Omega > \theta$

$$\text{where } \Omega = \tan^{-1}\left[\frac{\sin(\gamma_s - \gamma_c)\sin\theta_z}{\cos\beta\cos\theta_z + \sin\beta\sin\theta_z\cos(\gamma_s - \gamma_c)}\right]$$

for N-S axis CPCs

and γ_s = azimuth of sun

γ_c = azimuth of collector surface

θ_z = zenith angle

β = collector slope

For sky and ground radiation, however, the exact expressions are rather complex. The approximations used by most participants for F_D and F_G were:

$$F_D = (1 + \cos\beta)/2C$$
$$F_G = (1 - \cos\beta)/2C$$

These are simply the view factors of a flat plate to the sky and the ground respectively, divided by the CPC concentration ratio, C. A forthcoming paper by J.C. Mitchell of the University of Wisconsin will present exact expressions for all of these view factors for the general case of arbitrary CPC orientation.

Tank

Thermal stratification in liquid solar energy storage tanks is a physically complicated mechanism but results suggest that the relatively simple nodal models employed by each of the codes are probably adequate. The tank models employed by the various codes differ significantly only in two ways: the mixing assumptions (essentially "no mix" or "complete mix") and the number of isothermal layers modeled (from 2 to 5).

The "no mix" assumption is that liquid entering the tank finds the tank node that it is closest to in temperature (and hence density) without mixing with any intermediate nodes. The entering liquid mixes with this node and displaces liquid toward the exit node, modifying the temperatures of all "downstream" nodes. The "complete mix" assumption is that liquid entering the tank mixes completely with the node at which it enters, again displacing liquid into all nodes in the direction of the exit node. These two assumptions represent limiting cases for a given number of nodes in stratified tanks. The "no mix" assumption overpredicts stratification and system performance, while the "complete mix" assumption underpredicts stratification and performance.

A sensitivity study was performed on the mixing assumptions and number of tank nodes using the LASL code and an earlier statement of the IPH problem with the open loop, low temperature load. In the low temperature load simulations, mains supply water at 10°C entered the bottom of the tank while high temperature collectors delivered very hot water to the top. The tank had a height-to-diameter ratio of 1.75. These factors were thought to contribute to very significant stratification and to accentuate differences in stratified tank models. The results, shown in Figure 7, reveal surprisingly little difference in annual system performance, however. Modeling two nodes instead of one accounts for most of the maximum effect attributable to stratification. The "no mix" assumption and the use of more nodes always result in better performance but little improvement is seen for more than three nodes, especially in the "complete mix" case. This data does not prove which model best represents reality; that depends on the kinetic energy and geometry of the entering and exiting flowstreams. It seems likely, however, that the two-node "no mix" or the three-node "complete mix" models are the most accurate for most solar storage tanks. For IPH systems employing faster tank cycling rates or lower supply and return temperature differences, the effects of these assumptions will be even less significant than shown in Figure 7. For the final results of Table 1, the participants agreed to use two-node tank models.

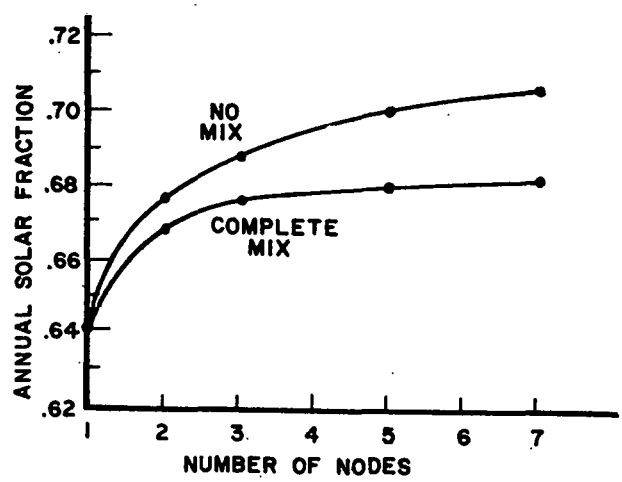

Figure 7 Effect of Tank Modeling Assumptions on Annual System Performance

Industrial Process Load

Modeling industrial process loads requires a means of specifying hourly profiles of energy or flowrate requirements for an entire year. Most industrial process loads are cyclical on a daily, weekly and seasonal basis. As a result, a general means of specifying different schedules for weekdays, weekends and holidays, for different times of the year is convenient. DOE-2 has the most flexible and user-oriented capability in this regard. TRNSYS can handle "scheduling" fairly conveniently, by multiplying the outputs of several "cyclical forcing functions".

The load profile specified in the problem statement was "on" for the first 45 minutes of each hour and "off" for the last 15 minutes. Since TRNSYS can take 15-minute timesteps, the load was modeled just as described. The other codes rely on hourly timesteps and therefore represented the load as a series of average hourly loads. For the systems investigated here, the approximation seemed to cause no significant bias in the predicted results.

Pipes

The thermal loss coefficient and heat capacitance of intercomponent piping was specified. Because the pipes were bigger and longer and because they were located out of doors, they were more significant in this problem than in previous SSEA comparison exercises. A programming error was identified in the TRNSYS model as a result. In addition, some doubt was cast on the utility of the simple "lumped" or one-node pipe model employed in TRNSYS. Several of these could be used "in series" to model a long pipe but this is a trick that a typical user would not employ. The "long term" effect of pipe capacitance and heat loss can be seen by comparing the differences between collector output (Q_{COUT}) and storage input (Q_{SIN}) in Table 1. LASL predicts significantly less loss than the other codes but the overall effect on the system performance is still minimal.

CONCLUSIONS

The predicted results of three solar system simulation codes have been successfully compared for a series of systems involving typical industrial heat applications of solar energy. After an iterative series of problem redefinitions and recomparisons of results, agreement has progressed from the order of ± 10 percent to ± 1 percent. In the process, at least one outright error was found, CPC and tracking collector modeling capability was added to the codes, and different user approaches to solving the problem were identified.

The effects of thermal storage stratification modeling assumptions have been examined. Two mixing assumptions commonly used in simulation models effectively bracket the range of stratification achieved in real storage tanks and this range is less critical to long term performance than is often believed.

Work on comparisons of these codes in the future should probably concentrate on comparing new and more sophisticated component models, since it has been shown that the mechanics of performing the system simulation are performed nearly the same by all codes. Significant differences caused by faulty modeling assumptions or coding errors are likely to exist in any new, non-trivial model. Software-software tests, particularly at the component level, are the most efficient and cost effective way of locating and correcting them.

Tracking, evacuated tube, and other high performance collector models should be systematically compared. The effects of capacitance in collectors, and plumbing could be more accurately modeled and compared. The importance of variable fluid properties should be ascertained and models for two-phase flow in high temperature systems could be developed and compared in future exercises.

The critical importance of user error has been noted. The agreement between the final results is near the limit of convergence of the numerical algorithms employed by the codes in most cases and hence is as good as can ever be expected from simulations. However, even though very experienced users were involved in this exercise, each made at least one serious input error that would have gone unnoticed without the opportunity for comparison to the results of the other participants.

Future development work in public domain codes should recognize that, in practice, user error overwhelms the differences caused by modeling assumptions and solution algorithms. There are countless ways to make errors in the preparation of input for even relatively simple systems in both TRNSYS and DOE-2. The DOE-2 user interface has been designed especially to minimize the opportunity for error and is certainly better than TRNSYS in that respect.

Acknowledgements

The author is thankful for the efforts of Jim Hedstrom, Mark Roschke, and Dave Odegard in performing the simulations and helping with the analysis. The financial support of SERI through Subcontract No. XH-9-8183-2, is gratefully acknowledged.

References

1. Freeman, T.L., "Solar Industrial Process Heat Test Problem," (November 1979 Revision), distributed to SSEA participants.

SYSTEMS SIMULATION AND ECONOMIC ANALYSIS

SECOND ANNUAL CONFERENCE

January 23-25, 1980
Bahia Hotel
San Diego, California

List of Attendees

A.

Redfield W. Allen
Mechanical Engineering Dept.
University of Maryland
College Park, MD 20742
(301) 454-4994

Dave K. Anand
Mechanical Engineering Dept.
University of Maryland
College Park, MD 20740
(301) 454-4994

John Anderson
Solar Energy Research Institute
1617 Cole Blvd. Bldg. 9/3
Golden, CO 80401
(303) 231-1015

John W. Andrews
Brookhaven National Laboratory
Building 701
Upton, NY 11973
(516) 345-7726

E. A. Aronson
Sandia Laboratories
Division 2623 Applied Math
Albuquerque, NM 87185
(505) 264- 4348

Francisco Arumí-Noé
Numerical Simulation Lab
School of Architecture
University of Texas
Austin, TX 78712
(512) 471-4911

B.

J. Douglas Balcomb
Los Alamos Scientific Laboratory
P.O. Box 1663 MS 571
Los Alamos, NM 87545
(505) 667-5061

David E. Ball
Southern Solar Energy Center
61 Perimeter Park
Atlanta, GA 30342
(404) 458-8765

Sherif A. Barakat
National Research Council of Canada
Division of Building Research
Ottawa, Ont. Canada KIAOR6
(613) 993-1421

W. A. Beckman
University of Wisconsin
Energy Laboratory
1500 Johnson Drive
Madison, WI 53706
(608) 263-1586

Ron Biggs
Public Works Canada/ Solar Programs Office
Sir Charles Bldg.
17 Riverside Drive
Ottawa, Canada 2180M2
(613) 998-9817

Nancy Birkenheuer
Solar Energy Research Institute
1617 Cole Blvd.
Golden, CO 80401
(303) 231-1256

Charles J. Bishop
Solar Energy Research Institute
1617 Cole Blvd., Building 9/3
Golden, CO 80401
(303) 231-1015

Rebecca C. Bjustrom
The MITRE Corporation
1820 Dolley Madison Blvd.
McLean, VA 22102
(703) 827-6630

John H. Blake
Olin Solar TM - Olin Brass
4745 Terrace Drive
San Diego, CA 92116
(714) 280-9774

Mike Brambley
Dept. of Applied Mechanics/Engr. Science
University of California, San Diego
La Jolla, CA 92093
(714) 452-2045

Louis L. Bucciarelli
Massachussetts Institute of Technology
Lincoln Lab, D-334, Box 73
Lexington, MA 02173
(617) 862-5500 ext. 213

A. Russ Burke
Department of Energy (OSA)
1000 Independence Avenue
Washington D. C.
(202) 252-8061

Robert D. Busch
Bickle/CM Inc.
2403 San Mateo NE Suite S-8
Albuquerque, NM 87110
(505) 884-5838

C.

Cecilia D. Cameron
Dept. of Mechanical Engineering
University of British Columbia
Vancouver, British Columbia, Canada
(604) 228-2781

Joseph Carroll
Energy Center, B-010, Urey Hall
University of California, San Diego
La Jolla, CA 92093
(714) 452-4804

Paul R. Casperson
Northeast Solar Energy Center
70 Memorial Drive
Cambridge, MA 02142
(617) 661-3500

David Chan
Northeast Solar Energy Center
70 Memorial Drive
Cambridge, MA 02142
(617) 661-3500, ext. 234

Tak S. Chan
General Electric Company
P.O. Box 8661
Philadelphia, PA 19101
(215) 962-5857

Craig B. Christensen
Solar Energy Research Institute
1617 Cole Blvd.
Golden, CO 80401
(303) 231-1455

Terry Clark
Shelteck Canada Ltd.
400-4th Street SW
Calgary, Alberta, Canada T2POJ4
(403) 232-3981

C. Brent Cluff
Water Resources Res. Ctr.
University of Arizona
Old Psychology Bldg. #28
Tucson, AZ 85721
(602) 626-1808

David S. Cowen
Institute of Gas Technology
3424 S. State Street
Chicago, IL 60616
(312) 567-5725

Marvin Crouthamel
RCA
Bldg 10-8
Camden, NJ 08102
(609) 338-3360

Henry M. Curran
Hittman Associates, Inc.
9190 Red Branch Road
Columbia, MD 21045
(301) 730-7800

D.

Roger L. Davenport
Solar Energy Research Institute
1617 Cole Blvd.
Golden CO 80401
(303) 231-1750

Mike Davis
DOE-Conservation & Solar Energy Division
1000 Independence Avenue, NW
Forrestal Bldg. Rm. 5G088
Washington D.C. 20585
(202) 252-8150

Richard B. Davis
Jet Propulsion Lab
4800 Oak Grove Drive
Pasadena, CA 91103
(213) 577-9286

John De Vries
Hittman Associates, Inc.
9190 Red Branch Road
Columbia, MD 21045
(301) 730-7800

Stephen C. Diamond
Los Alamos Scientific Laboratory
P.O. Box 1663
Los Alamos, NM 87545
(505) 667-5061

Mikos Doka-Suna
157 Louise Lane
Davis, CA 95616
(916) 758-7456

William T. Downey
Arthur D. Little, Inc.
20/509 Acorn Park
Boston, MA 02215
(617) 864-5770 ext. 2987

William S. Duff
Solar Energy Applications Lab
Solar House II, Colorado State Univ.
Fort Collins, CO 80523
(303) 491-5859/(303) 491-8618

Edward R. Durlak
Civil Engineering Lab
Code L-63
Port Hueneme, CA 91360
(805) 982-4207

E.

Anthony Eden
Solar Energy Research Institute
1617 Cole Blvd.
Golden, CO 80401
(303) 231-1990

F.

Robert B. Farrington
Solar Energy Research Institute
1617 Cole Blvd. 9/3
Golden, CO 80401
(303) 231-1938 FTS 327-1938

Donald R. Farris
Los Alamos Scientific Laboratory (LASL)
E-4, MS 429 P.O. Box 1663
Los Alamos, NM 87545
(505) 667-4967

R. Fischl
Drexel University
Department of Electrical Engineering
Philadelphia, PA 19104
(215) 895-2241

Greg E. Franta
Solar Energy Research Institute
1617 Cole Blvd.
Golden, CO 80401
(303) 231-1263

Thomas L. Freeman
Altas Corporation
500 Chestnut Street
Santa Cruz, CA
(408) 425-1211

G.

Roger T. Giellis
Martin Marietta Corporation
P.O. Box 179 MS S-0484
Denver, CO 80201
(303) 973-3853

Charles R. Grebenstein
Exxon Enterprises
P.O. Box 592
Florham Park, NJ 07046
(201) 765-4281

Lyle Groome
Solar Energy Research Institute
1617 Cole Blvd, Bldg. 9/3
Golden, CO 80401
(303) 231-1015

Barbara L. Grossman
Massachussetts Institute of Technology
Lincoln Lab, P.O. Box 73
Lexington, MA 02173
(617) 862-5500 ext. 112

H.

Robert H. Hamilton
Department of L.A.W.R.
University of California, Davis
Davis, CA 95616
(916) 752-1929

James R. Harper
Solar Energy Research Institute
1617 Cole Blvd.
Golden Co 80401
(303) 231-1009

K. Harrington
ARGA Associates
1056 Chapel Street
New Haven, CT 06510
(203) 789-0555

Thomas Hartman
Southern Solar Energy Center
61 Perimeter Park
Atlanta, GA 30341
(404) 458-8765

Robert J. Hassett
Department of Energy
1000 Independence Avenue
Washington, D.C. 22009
(202) 252-8160

James C. Hedstrom
Los Alamos Scientific Laboratory
P.O. Box 1663
Los Alamos, NM 87545
(505) 667-2621

Groipon Heffner
J.B.F. Scientific
1925 N. Lynn Street, Suite 308
Washington D.C. 22009
(703) 524-4232

Albert Heitz
Lawrence Berkeley Lab
University of California
Berkeley, CA 94720
(415) 486-4239

Dr. Tomas Held, President
Columbian Solar Energy Society
Apartado Aereo 5516
Bogota 2, Columbia
c/o Dr. Raiford (919) 855-8303

Jon Henderson
Solar Energy Research Institute
1617 Cole Blvd. Bldg. 9/3
Golden, CO 80401
(303) 231-1015

Roger Henry
Public Works Canada
Solar Programs Office
Sir Charles Bldg., 17 Riverside Drive
Ottawa, Canada 2180M2
(613) 998-9817

P. Herczfeld
Drexel University
Department of Electrical Engineering
Philadelphia, PA 19104
(215) 895-2243

George Hinman
Washington State University
Environmental Research Center
Pullman, WA 99164
(509) 335-1546 FTS 445-1546

Doug Hooker
Solar Energy Research Institute
1617 Cole Blvd.
Golden CO 80401
(303) 231-1122

Frank C. Hooper
Mechanical Engineering
University of Toronto
Toronto, Canada M5S 1A4
(416) 978-2903

Dale E. Horton
201½ S. Asbury
Moscow, ID 83843
(208) 882-6047

Dwight E. Hull
Martin Marietta Corporation
P.O. Box 179 M.S. S0484
Denver, CO 80201
(303) 973-3853

I.

Joseph J. Iannucci
Sandia Laboratories
Division 8326
Livermore, CA 94550
(415) 422-2140

ohammed Iqbal
Mechanical Engineering Dept.
University of British Columbia
Vancouver, British Columbia, Canada
(604) 228-3398

J.

Robert W. Jones
University of South Dakota
Earth Science/Physics Dept.
Vermillion, SD 57069
(605) 677-5649

Ronald D. Judkoff
Solar Energy Research Institute
1617 Cole Blvd.
Golden, CO 80401
(303) 231-1462

K.

Clayton Kemp
Flack & Kurtz, Consultant Engineers
1665 Grant
Denver, CO 80203
(303) 832-6000

William J. Kennish
TPI, Inc.
5010 Sunnyside Avenue, Suite 301
Beltsville, MD 20705
(301) 345-5200

Frank L. Kester
I.G.T.
3424 S. State Street
Chicago, IL 60525
(312) 562-3860

Kate Kramer
Solar Energy Research Institute
1617 Cole Blvd.
Denver, CO 80401
(303) 231-1009 ext. 1227

Dr. Edward A. Kush
Brookhaven National Laboratory
Bldg. 701 - Solar Technology
Upton, NY 11973
(516) 345-3567 FTS 666-3567

L.

Loren J. Lantz
Solar Environmental Engineering Co., Inc.
2524 E. Vine Drive
Fort Collins, CO 80524
(303) 221-5166

Stanley R. Leacock
Lockheed Research Lab
0/52-32 B/205
3251 Hanover Street
Palo Alto, CA 94304
(415) 493-4411

Cecile Leboeuf
Solar Energy Research Institute
1617 Cole Blvd. Bldg. 9/3
Golden, CO 80401
(303) 231-1015

Robert R. Le Chevalier
Science Applications
1546 Cole Blvd.
Golden, CO 80401
(303) 232-7900

Kwang Y. Lee
University of Houston
Electrical Engineering Dept.
Houston, TX 77004
(713) 749-1197

Craig M. Lemrow
Corning Glass Works
Houghton Park C-7
Corning, NY 14830
(607) 974-8073

Lance L. Leonaitis
Southern Solar Energy Center
61 Perimeter Park
Atlanta, GA 30341
(404) 458-8765

K. Vincent Liu
Argonne National Laboratory
9700 S. Cass Avenue
Argonne,ID 60439
(312) 972-8580

Gerald W. Lowery
Science Applications, Inc.
8400 Westpark Drive
McLean, VA 22102
(703) 827-4787

M.

J. Ward MacArthur
Honeywell, Inc. - Energy Resources Center
2600 Ridgway Parkway
Minneapolis, MN 55413
(612) 378-5416

Doug Madison
Solar Energy Research Institute
1617 Cole Blvd.
Golden, CO 80401
(303) 231-1256

John W. Massey
NASA Marshall Space Flight FA32
Huntsville, AL 35812
FTS 872-1673

Richard Paul Mazzucchi
Battelle Northwest Laboratories
P.O. Box 999
Richland, WA 99352
(509) 942-0854, FTS 444-0854

J. W. Mitchell
Solar Energy Laboratory
University of Wisconsin
1500 Johnson Drive
Madison, WI 53706
(608) 263-1586

John E. Montague
Martin Marietta Corp.
P.O. Box 179 MS S-0403
Denver, CO 80201
(303) 973-4052

John E. Moore
LASL M.S. 985
Los Alamos, MN 87544
(505) 667-6118

Jeffrey H. Morehouse
Science Applications, Inc.
1764 Old Meadow Lane
McLean, VA 22102
(703) 827-4915

Robert Morette
New York State Energy Research &
Development Authority
Rockefeller Plaza
Albany, NY 12223
(518) 465-6251

Louise Morrison
Solar Energy Research Institute
1617 Cole Blvd. Bldg. 9/3
Golden, CO 80401
(303) 231-1015

L. Marty Murphy
Solar Energy Research Institute
1617 Cole Blvd. Bldg. 9/3
Golden, CO 80401
(303) 231-1015

N.

Douglas J. Nelson
Solar Thermal Systems
Divison of Exxon Enterprises, Inc.
P.O. Box 592
Florham Park, NJ 07932
(609) 765-4271

Scott A. Noll
Modeling & Economic Analysis
Los Alamos Scientific Laboratory
S-2/MS 605 LASL
Los Alamos, NM 87545
(505) 667-2871

Douglas B. Nordham
Solar Energy Research Institute
1617 Cole Blvd.
Golden, CO 80401
(303) 231-1275

O.

Timothy N. Obee
United Technologies Research Center
Silver Lane
East Harford, CT 06118 (203) 727-7161

Colin O'Brien
Shelteck Canada Ltd.
400-4th Street SW
Calgary, Alberta Canada T2P 0J4
(403) 232-3981

P.

Larry S. Palmiter
National Center for Appropriate Technology
Box 3838
Butte, MT 59701
(406) 494-4572

Joseph Peerson
Argonne National Laboratory D-362
Argonne, IL 60439
(312) 972-6233 (FTS)

Jane H. Pejsa
Honeywell Control Systems
1700 West Highway 36
St. Paul, MN 55113
(612) 378-4313

Joseph C. Perkowski
Oxford Development Group Ltd.
Royal Trust Tower
Edmonton, Alberta, T5J 3A4
(403) 426-6340

Joseph E. Perry
Los Alamos Scientific Laboratory
Box 1663 MS 571
Los Alamos, NM 87545
(505) 667-6441

William R. Powell
JHV/APL
Johns Hopkins Road (APL)
Laurel, MD 20810
(301) 953-7100 ext. 2046

R.

Joseph E. Rasson
LBL 90-202Y P
LBL Cyclotron Road, Bldg. 90
Berkeley, CA 94720
(415) 486-5738

Boyd W. Rhodes
United Technologies Research Center
Silver Lane
East Hartford, CT 06108
(203) 727-7367

C. H. Richards
P.O. Box 1551
Cupertino, CA 95015

David J. Richards
486 Vaughn Avenue
San Jose, CA 95128
(408) 288-5626

Richard C. Rodgers, Jr.
P.O. Box 1365
Palo Alto, CA 94302
(415) 321-4768

Corbyn Rooks
U.S. Department of Energy
2607 Cass Street
La Crosse, WI 54601
(608) 782-0646

Mark A. Roschke
L.A.S.L.
Los Alamos SCI Laboratory M.S. 985
Los Alamos, NM 87544
FTS 843-3348

S.

Barry A. Saitman
Solar Office, California Energy Commission
1111 Howe Avenue
Sacramento, CA 95825
(916) 920-7393

Steven R. Schiller
Lawrence Berkeley Lab
90-2024, Lawrence Berkeley Laboratory
Berkeley, CA 94720
(415) 486-4290

S. Schweitzer
University of Maryland
Mechanical Engineering Dept.
College Park, MD 20742
(301) 454-2411

Anthony V. Sebald
University of California, San Diego
B-010
La Jolla, CA 92037
(714) 452-4706

Michael Sedmak
Booz Allen Hamilton
311-1st Street NW
Washington D.C. 20001
(202) 624-0610

Jefferson G. Shingleton
Mueller Associates, Inc.
1900 Sulphur Spring Rd.
Baltimore, MD 21227
(301) 247-5666

J. D. Stack
Sacramento Municipal Utility District
6201 S. Street
Sacramento, CA 95819
(916) 452-3211

Shirley A. Stadjuhar
Solar Energy Research Institute
1617 Cole Blvd.
Golden, CO 80401
(303) 231-1110

Davis Straub
Ecotope Group
2332 E. Madison
Seattle, WA 98112
(206) 322-3753

Norman E. Suhs
Tennessee Valley Authority
240 Chestnut Street Tower 2
Chattanooga, TN 37401
(615) 755-6506

Santhanam Sundaram
Jacobs-Del Solar Systems, Inc.
251 South Lake Avenue
Pasadena, CA 91101
(213) 449-2171

Ted D. Swanson
Mueller Associates, Inc.
1900 Sulphur Spring Road
Baltimore, MD 21227
(301) 247-5666

T.

Edgar C. Tacker
University of Houston
Electrical Engineering Department
Houston, TX 77004
(713) 749-4416

Rob W. Taylor
San Diego Gas & Electric
101 Ash Street
San Diego, CA 92101
(714) 232-4252

Peter B. Thomas
Gould Inc., Energy Research Laboratory
40 Gould Center
Rolling Meadows, IL 60008
(312) 640-4465

Ronald G. Toelle
U.S. Government
NASA/George C. Marshall Space Flight Center
ATTN: FA33/Solar Energy
Marshall Space Flight Center
Huntsville, AL 35812
(205) 453-2054

Terrance N. Troy
National Bureau of Standards
Room A-166, Technology Building
Washington, D.C. 20234
(301) 291-3179

W.

Dan S. Ward
Solar House I
Colorado State University
Fort Collins, CO 80523
(303) 493-1563

Anthony W. Warren
Boeing Computer Services Company
Mail Stop 9C-01
Seattle, WA 98124
(206) 575-5095

Mashuri L. Warren
Lawrence Berkeley Lab
90-2024
Berkeley, CA 94720
(415) 486-6364

Robert E. Waterman
Vitro Labs
14000 Georgia Avenue
Silver Springs, MD 20910
(301) 871-3269

R. W. Weaver
Jet Propulsion Laboratory
4800 Oak Grove Drive
Pasadena, CA 91103
(213) 792-9117

Frank C. Weinstein
Franklin Research Center
1030-15th Street NW
Washington, D.C. 20005
(202) 223-8105

Lee S. Windheim
Leo A. Daly Company
45 Maiden Lane
San Francisco, CA 94108
(415) 421-8657

Michael D. Wysocki
University of Texas
Department of Architecture
Austin, TX 78743
(512) 471-4911

Richard L.T.Wolfson
Middlebury College
Physics Department
Middlebury, VT 05753
(802) 388-7956

William O. Wray
Los Alamos Scientific Laboratory
Mail Stop 571
Los Alamos, NM 87545
(505) 667-2625

Stephen K. Young
Science Applications, Inc.
8400 Westpark Drive
McLean, VA 22102
(703) 821-8133

Edward Ashare
Dynatech R/D Company
99 Erie St.
Cambridge, MA 02139
617/868-8050

J. W. Baughn
University of California/Davis
Department of Mechanical Engineering
Davis, CA 95616
916/752-0580

Natalia A. Blackburn
McCaughey & Smith
130 Centennial Way Ste.C
Tustin CA 92680
714/ 838-1980

Roger Bezdek
DOE - MS CS60 - Room 5G044
1000 Independence Avenue
Washington, DC 20585
FTS 8-252-8098

J. R. Clinton
Solar Energy Analysis Laboratory
4325 Donald Avenue
San Diego, CA 92117
714/270-3781

Bernard A. Coyle
City College
50 Phelan Ave.
San Francisco, CA 94112
415/591-3335

J. Clair Ellis
The Aerospace Corporation
P.O. Box 92957
Los Angeles, CA 90009
213/648-5494

Waqidi Falicoff
Southwest Solar Corporation
441 North Oak St.
Inglewood, CA 90301
213/673-8140

Terry R. Galloway
Lawrence Livermore Laboratory
P.O. Box 808
Livermore, CA 94550
415/422-6456

Roger B. Harwell
TEAM, Inc.
120 West Broadway #41
Tucson, AZ 85701
602/622-7408

F. Ann Herlevich
SERI
1617 Cole Blvd.
Golden, CO 80401
303/231-1810

Dave Kearney
SERI
1617 Cole Blvd.
Golden, CO 80401
303/231-1114

Patrick J. Keegan
Rho Sigma, Inc.
11922 Valerio St.
North Hollywood, CA 91605
213/982-6800

Frank Kreith
SERI
1617 Cole Blvd.
Golden, CO 80401
303/231-1109

John Kurtz
Booz Allen & Hamilton, Inc.
4330 East West Highway
Bethesda, MD 20014
301/951-2227

E.I.H. Lin
Argonne National Laboratory
9700 South Cass Ave.
Argonne, IL 60439
312/972-6032

Bruce T. Maeda
Davis Alternative Technology Assoc.
P.O. Box 503
Davis, CA 95616
916/756-9300

Joseph C. McMurrin
Jet Propulsion Laboratory
M/S 507-228
4800 Oak Grove Drive
Pasadena, CA

Richard L. Merriam
A.D. Little Inc.
Acorn Park
Cambridge, MA 02140
617/862-5770 x 887

Fred Morse
U.S. DOE
1000 Independence Ave. N.W.
Washington, DC 20585
202/252-8084

Peter Offenhartz
EIC Corporation
55 Chapel S. E.
Newton, MA 02158
617/965-2710

Wayne Place
Lawrence Berkeley Lab
Room 90-2024
Berkeley, CA 94720
FTS 451-6620

Gary G. Purcell
Electric Power Research Institute
3412 Hillview Ave.
Palo Alto, CA 94303
415/855-2168

Maurice Raiford
Dept. of Mechanical Engineering
North Carolina Agr. and Tech.
Greensboro, NC 27411
919/855-8303

Harry W. Sigworth Jr.
Pacific Gas & Electric Co.
245 Market St. Room 1700
San Francisco, CA 94106
415/781-4211 x4945

Barry G. Silverman
Santa Fe Corporation
4660 Kenmore Ave.
Alexandria, VI 22304
703/823-2233

Patricia Smith
Sedway-Cooke
325 Pacific Ave.
San Francisco, CA 94111
415/433-0966

Thomas J. Tatum
JAYCOR/Energy Division
1401 Camino Del Mar
DelMar, CA 92111
453/6580 x263

Michael A. Wahlig
Lawrence Berkeley Lab
90-2024 1 Cyclotron Road
Berkeley, CA 94720
415/486-5787

Michael D. Walzel
University of Houston
SPA Room 113
Houston, TX 77004
713/749-1154

Ronald D. White
U.S. DOE
1000 Independance Ave. N.W.
Washington, DC 20585
202/252-6433

Bruce A. Wilcox
Berkeley Solar Group
3026 Shattuck Avemue
Berkeley, CA 94705
415/843-7600

C. Byron Winn
CSU
Dept. of Mechanical Engineering
Fort Collins, CO 80523
303/491-6783

Jay J. Yoon
Systems Control, Inc.
1801 Page Mill Road
Palo Alto, CA 94304
415/494-1165 x 252

Agenda

Second Annual Systems Simulation and Economic Analysis Conference

January 23-25, 1980
Bahia Hotel
San Diego, California

Agenda

January 22

7:00 - 9:00 p.m.	Registration	Mezzanine

January 23

7:00 - 8:00 a.m.	Registration	Mezzanine
8:30 a.m.	Registration moves to Mission Bay Lounge	
8:00 a.m.	Opening Remarks - Dr. Fred Morse - Department of Energy	Mission Bay Ballroom

Concurrent Sessions:

	a	b
	Session Ia - Systems Simulation I Mission Room Dr. William Beckman, Chairperson — University of Wisconsin	**Session Ib - Systems Economics I** Bay Room Mr. Clair Ellis, Chairperson - Aerospace Corporation
8:40 a.m.	System Analysis for Multizone Buildings J. Ottenstein, J.W. Mitchell and W.A. Beckman—University of Wisconsin	Energy Conservation and Passive Solar: Working Together J.D. Balcomb—Los Alamos Scientific Laboratory
9:00 a.m.	SERI DOE-2 Solar Simulator Study A. Eden—Solar Energy Research Institute	Selection of Economically Optimum Solar Energy Heating Systems by Analysis and Simulation R.C. Estes and W. Kahan—The Singer Company
9:20 a.m.	Systems Analysis of the Thermal Performance of Operating Systems D. S. Ward—Colorado State University	Simulation and Cost Optimization of the Solar Assisted Annual Cycle Energy System (ACES) J.W. MacArthur and K. Nguyen—Energy Resources Center -Honeywell
9:40 a.m.	Analysis of Community Solar Systems for Combined Space Heating and Domestic Hot Water Using Annual Cycle Thermal Energy Storage F.C. Hooper, J.D. McClenahan, R.J.D. Cook—University of Toronto, F. Baylin and R. Monte—Solar Energy Research Institute	An Optimization Technique for Minimizing the Cost of Self-Powering Industrial HVAC Systems D. S. Cowen—Institute of Gas Technology
10:00 a.m.	Simulations and Experiments on the Arlington House System M.A. Daugherty and J.W. Mitchell—University of Wisconsin	The Application of Simulation Modeling to the Cost and Performance Ranking of Solar Thermal Power Plants L. Rosenberg—Jet Propulsion Laboratory
10:20-10:40 a.m.	Break	
	Session IIa - Controls I Mission Room Dr. Mashuri L. Warren, Chairperson — Lawrence Berkeley Laboratory	**Session IIb - Validation I** Bay Room Dr. William Kennish, Chairperson—TPI Inc.
10:40 a.m.	Control Strategies for Dual Tank Storage Systems: an Experimental Comparison R. Wolfson and H. Harvey—Middlebury College	Real-World Validation of SHAC Models L.S. Morrison—Solar Energy Research Institute
11:00 a.m.	Enhancement of Performance of Active Solar Systems by Optimal Control and System Identification Techniques C. Baer, D. Pryor, C.B. Winn—Colorado State University	Field Validation of the Derob System: The Bruce Hunn Residence F. Arumi' -Noe', D.O Northrup—University of Texas
11:20 a.m.	Analytic Techniques for Development of Control Strategies for Passive Solar Building M. Fichor, P. Horozfold, R. Fischl - Drexel University	Validation of Solar System Simulation codes by the International Energy Agency T.L. Freeman—Atlas Corporation J.C. Hedstrom—Los Alamos Scientific Laboratory
11:40 a.m.	Optimal Control of Combined Photovoltaic/Thermal Solar Heating and Cooling Systems E.O. Bazques, D.K. Anand, R.W. Allen—University of Maryland	Analysis of User Effects on the DOE-2 Solar Simulator J.L. Peterson, S.C. Diamond—Los Alamos Scientific Laboratory
12:00 Noon	Solar Flat Plate Collector Control System Sensitivity Analysis P.R. Herczfeld, R. Fischl, S. Konyk—Drexel University	The Sea-Lab Passive Test Building Project J.R. Clinton—Solar Energy Analysis Laboratory
12:20 - 1:40 p.m.	Conference Luncheon	Mercedes Room and Del Mar Room

	Session IIIa - Systems Simulation II Mission Room Dr. Dan S. Ward, Chairperson—Colorado State University	**Session IIIb - Systems Economics II** Bay Room Dr. J. Douglas Balcomb, Chairperson—Los Alamos Scientific Laboratory
1:40 p.m.	Feasibility Evaluation for Solar Industrial Process Heat Applications S.A. Stadjuhar—Solar Energy Research Institute	Economics of Solar Domestic Hot Water Heaters in California M.F. Young, J.W. Baughn—University of California, Davis
2:00 p.m.	Computer-Aided Solar Thermal Systems Analyses for Industrial Process Heat (IPH) Applicationss S. Sundaram, C.F. Roos, B.G. Eldridge—Jacobs-Del Solar Systems, Inc.	A comparative Analysis of Six Generic Solar Domestic Hot Water Systems R.B. Farrington—Solar Energy Research Institute
2:20 p.m.	A Micro-Computer Code for Direct-Coupled Photovoltaic Pumping System Simulation B.A. Blevins, R.B. Rogers—New Mexico Solar Energy Institute	Comparison of Solar Power Systems: Thermal and Electric J.J. Iannucci—Sandia Laboratories, Livermore CA.
2:40 p.m.	Flat-Plate Photovoltaic Array Simulation and Design Analysis R.W. Weaver—Jet Propulsion Laboratory	Inflation and Taxes in Benefit-Cost Analysis. J.C. Ellis—The Aerospace Corporation
3:00 p.m.	Method for Predicting Long-Term Average Performance of Photovoltaic Systems Y. Gupta, S. Young—Science Applications, Inc.	Solar Assisted Heat Pump Swimming Pool Synergistics for Domestic Heating T.R. Galloway—Lawrence Livermore Laboratories
3:20 p.m.	Performance Studies of Combined Photovoltaic/Thermal Solar Heating and Cooling Systems S.R. Venkateswaran, D.K. Anand—University of Maryland	SERI: On-Line Models Library and Solar Models Data Base N. BirkenHeuer, K. Kramer—Solar Energy Research Institute
4:00 - 4:45 p.m.	Informal Discussions	
6:00 - 7:00 p.m.	Cocktail Party - Cash Bar	Bay Room
January 24		
8:00 a.m.	Opening Remarks - Dr. Roger Bezdek - Department of Energy	Mission Bay Ballroom
Concurrent Sessions:	**a**	**b**
	Session IVa - Controls II Mission Room Dr. Byron Winn, Chairperson—Solar Environmental Engineering Corp.	**Session IVb - Systems Economics III** Bay Room Dr. Ashley Emery, Chairperson—University of Washington
8:30 a.m.	Implementation of an Optimal Controller of the Second Kind B. Winn, C.B. Winn—Colorado State University	The Effects of Ownership Options, Government Policies, and Operational Alternatives on the Economic Viability to Specific Investors of Investment in Small Power Systems J.V.V. Kasper—University of California, L.A. R.B. Davis—Jet Propulsion Laboratory
8:50 a.m.	The Comparison of Proportional and On/Off Collector Loop Control Strategies Using a Dynamic Collector Model S.R. Schiller, M.L. Warren—Lawrence Berkeley Laboratory, D.M. Auslander—University of California/Berkeley	SOLSTOR Results for a Photovoltaic/Battery System with Time-of-Day Pricing and Setback B.C. Caskey, D.L. Caskey—Sandia Laboratories
9:10 a.m.	Optimal Identification of Parameters in Passive Solar Buildings D. Pryor, C. Beer, C.B. Winn—Colorado State University	Economic Worth of On-Site Solar Electric Generation to Central Utility Stations Y. Gupta, R. Knowles, O. Merrill, S. Young—Science Applications, Inc.
9:30 a.m.	Control System Analysis for Off-Peak Auxiliary Heating of Passive Solar Systems H.S. Murray, J.D. Balcomb—Los Alamos Scientific Laboratory J.L. Melsa—Notre Dame University	Economies of Scale in the Acquisition of Solar Energy C.Dick, C. Grobonstein—Exxon Enterprises, Inc.
9:50 a.m.	Experimental Test Facility for Evaluation of Controls and Control Strategies M.L. Warren, S.R. Schiller, M. Wahlig—Lawrence Berkeley Laboratory	The Thermal and Economic Implications of the City of Seattle Energy Code A.F. Emery, D.R. Heerwagen, C.J. Kippenhan—University of Washington
10:10 - 10:40 a.m.	Break	
	Session Va - Systems Simulation III Mission Room Dr. James Baughn, Chairperson—University of California - Davis	**Session VB - Component Simulation Models** Bay Room Dr. John Andrews, Chairperson—Brookhaven National Laboratory
10:40 a.m.	Simulation and Design Methods for a Solar Central Receiver Hybrid Power System M.D. Walzel—University of Houston	Transient Modeling of Lithium Bromide Water Absorption Machines and Their Validation R.B. Abarcar, D.K. Anand, R.W. Allen—University of Maryland
11:00 a.m.	BALDR-1, A Solar Thermal System Simulation J.G. Finegold, F.A. Herlevich—Solar Energy Research Institute	Solar "Breadbox" Simulation Using D.A.T.A.'s TRNX Code B. Maeda—Davis Alternative Technology Associates
11:20 a.m.	Performance of Distributed Active Solar Power Systems P.A. Curto, W.E. Jacobsen, A.S. Cherdak—MITRE	TRNSYS Simulation of Chemical Heat Pumps for Solar Heating, Cooling and Storage P. O'D. Offenhartz—EIC Corporation
11:40 a.m.	Output Power of Wind Machines W.R. Powell—Applied Physics Laboratory, Johns Hopkins University	A Comparison of Two Techniques for the Simulation of PV Systems L.L. Bucciarelli, B.L. Grossman—MIT Lincoln Laboratory
12:00 Noon	Solar District Heating Model for an Azimuth-Tracking Floating Concentrator on a Seasonal-Heat-Storage Reservoir C.B. Cluff, R.B. Kinney—University of Arizona, Water Resources Research Center	Modeling and Economic Analysis of Air Leaks in a Solar Air Heating System J.G. Shingleton, D.E. Cassel,—Mueller Associates, Inc., M.E. McCabe—National Bureau of Standards
12:20 - 1:40 p.m.	Lunch Break	

	Session VIa - Simplified Analyses Mission Room Mr. Thomas Freeman, Chairperson — Altas Corporation	**Session VIb - Building Load Models** Bay Room Dr. Jane Pejsa, Chairperson — Honeywell Corporation
1:40 p.m.	Calculation and Optimization of Solar Energy Collectors for Process Heat P. Bendt, A. Rabl—Solar Energy Research Institute	A Simplified Solar Heating System Performance Estimator for Residential Applications J.H. Pejsa—Honeywell, Inc.
2:00 p.m.	FChart Version 4.0: The University of Wisconsin Solar Energy Design Program J.C. Mitchell—University of Wisconsin	On Extracting Useful Building Performance Characteristics Without Simulation A.V. Sebald—University of California, San Diego
2:20 p.m.	A Simplified Thermal Performance Simulation and Economic Analysis Methodology for Design of Passive Solar Homes L. Icerman, K. Myers, A. Swift—Washington University	Comparison of Building Thermal Analysis Methods K. Harrington, R.T. Lydon—ARGA Associates
2:40 p.m.	Long Term Solar Cooling Systems Performance Predictions Via a Simplified Design Method D.K. Anand, R.B. Abarcar, R.W. Allen—University of Maryland	Predicting the Time Response of a Building Under Heat Input Conditions for Active Solar Heating Systems M.L. Warren, A.F. Sakkal, S.R. Schiller—Lawrence Berkeley Laboratory
3:00 p.m.	A Model for Performance and Economic Analysis of Active and Passive Solar Energy Systems B. Karpay, J. Kurtz—Booz-Allen & Hamilton Inc.	Simulation and Performance of Double Envelope Houses in Cold Climates B. Maeda—Davis Alternative Technology Associates
3:20 p.m.	Solcost: A Solar Energy Design Program D.E. Hull, R.T. Giellis—Martin Marietta Aerospace	Simulation of Passive/Hybrid Solar Homes with a User-Accessible Computer-Based Design Tool D. Straub, O. Smith, M. Browne—Ecotope Group
4:00 - 5:30 p.m.	Informal Discussion	

January 25

8:00 a.m.	Opening Remarks — Department of Energy	Mission Bay Ballroom
Concurrent Sessions	**a**	**b**
	Session VIIa - Climate Analysis Mission Room Dr. Robert Busch, Chairperson — Bickle/CM Corporation	**Session VIIb - Systems Simulation IV** Bay Room Mr. Anthony Eden, Chairperson — Solar Energy Research Institute
8:30 a.m.	Regional Differences in Solar Radiation Availability R.J. Bahm—University of New Mexico	Optimization of Solar Assisted Heat Pump Systems Via a Simple Analytic Approach J.W. Andrews—Brookhaven National Laboratory
8:50 a.m.	A Comparative Study of the TRY and TMY Meteorological Data J.V. Anderson, D. Madison—Solar Energy Research Institute	Sensitivity Analysis of Solar Assisted Heat Pump Systems P.J. Hughes, J.H. Morehouse—Science Applications, Inc., T.D. Swanson—Mueller Associates, Inc., W.J. Kennish—TPI, Inc.
9:10 a.m.	An "MRT Method" of Calculating Radiant Heat Transfer J. Carroll—UCSD Energy Center	Performance Design Correlation Study of Solar Assisted Heat Pump System Installed in Maryland R.E. Dame—Mega Engineering
9:30 a.m.	The New SERI Data Base for Validating Passive System Computer Models R.D. Busch—Bickle/CM Corporation	Results of Systems Simulation and Economic Analysis of Solar-Powered Turbocompressor Heat Pump G. Melikian, B.W. Rhodes, T.N. Obee—United Technologies
9:50 a.m.	Standard Assumptions and Methods for Solar Heating and Cooling Systems Analysis C. Leboeuf—Solar Energy Research Institute	Application of Data from the National Solar Data Network (NSDN) to Simulation Studies L. Doak, R. Waterman—Automation Industries, Inc., Vitro Laboratories
10:10 - 10:40 a.m.	Break	
	Session VIIIa - Systems Economics IV Mission Room Dr. William Duff, Chairperson — Colorado State University	**Session VIIIb - Validation II** Bay Room Ms. Louise Morrison, Chairperson — Solar Energy Research Institute
10:40 a.m.	Economic Analysis of Conductor-Insulator-Semiconductor (CIS) Solar Cells R. Singh, W.S. Duff, J.B. DuBow, N.L. Weaver—Colorado State University	Validation and the Building Energy Performance Standards (BEPS) Program W. Kennish—TPI, Inc, T.M. Knasel—Science Applications, Inc.
11:00 a.m.	Feasibility Study for Anaerobic Digestion of Agricultural Crop Residues E. Ashare, M.G. Buivid, E.H. Wilson Dynatech R/D Company	The DOE-2 Verification Project: Phase I Results S.C. Diamond, B.D. Hunn— Los Alamos Scientific Laboratory
11:20 a.m.	Thermal and Cost Goals for Passive Solar Designs F. Roach, S. Noll—Los Alamos Scientific Labs S. Ben-David, C. Kirschner—University of New Mexico	COMMIX-SA: Validation, Application and Extension of a Solar Design Tool E.I.H. Lin, K.V. Liu, W. T. Sha—Argonne National Laboratory
11:40 a.m.	Solar Technology Market Penetration Analysis: An Approach B.G. Silverman, P. Fontaine—Santa Fe Corporation	A Comparative Analysis and Evaluation by Test of Solar Heating and Cooling Computer Models R.L. Morriam Arthur D. Little, Inc.
12:00 Noon	Technical and Economic Feasibility of Solar Ponds in Large-Scale Agricultural Applications E.I.H. Lin, W.T. Sha,—Argonne National Laboratory. S.L. Soo—University of Illinois, Urbana	Solcost Program Sensitivity to Input Model Parameters L.J. Lantz, E. Hancock—Solar Environmental Engineering Co.
12:20 p.m.	Solpond - A Simulation Program for Salinity Gradient Solar Ponds J. Henderson, C. Leboeuf—Solar Energy Research Institute	A Comparison of the Predicted Performance of Several Solar System Simulation Codes for an Industrial Process Heating System T.L. Freeman—Altas Corporation
12:40 p.m.	Closing Remarks	Mission Bay Ballroom
1:00 p.m.	Adjournment	

CANCELED PRESENTATIONS

January 23, 1980

9:00 a.m. Selection of Economically Optimum Solar Energy Heating Systems by Analysis and Simulation
R. C. Estes and W. Kahan
The Singer Company

10:00 a.m. The Application of Simulation Modeling to the Cost and Performance Ranking of Solar Thermal Power Plants
L. Rosenberg
Jet Propulsion Laboratory

11:40 a.m. Optimal Control of Combined Photovoltaic/Thermal Solar Heating and Cooling Systems
E. O. Bazques, D. K. Anand, R. W. Allen
University of Maryland

11:40 a.m. Analysis of User Effects on the DOE-2 Solar Simulator
J. L. Peterson, S. C. Diamond
Los Alamos Scientific Laboratory

2:20 p.m. A Micro-Computer Code for Direct-Coupled Photovoltaic Pumping System Simulation
B. A. Blevins, R. B. Rogers
New Mexico Solar Energy Institute

January 24, 1980

1:40 p.m. Calculation and Optimization of Solar Energy Collectors for Process Heat
P. Bendt, A. Rabl
Solar Energy Research Institute

January 25, 1980

9:10 a.m. Performance Design Correlation Study of Solar Assisted Heat Pump System Installed in Maryland
R. E. Dame
Mega Engineering

CHANGES IN PRESENTATIONS

January 23, 1980 Session IIIb - Systems Economics II Bay Room

3:00 p.m. Solar Assisted Heat Pump Swimming Pool Synergistics for Domestic Heating
T. R. Galloway
Lawrence Livermore Laboratories
WILL BE PRESENTING IN SESSION VIIb - 9:10 a.m. - January 25, 1980.

3:20 p.m. Solar Models Data Base
Kate Kramer
Solar Energy Research Institute
WILL BE PRESENTING AT Session IIIb - Systems Economics II at 3:00 p.m.

GRAPHICAL CLIMATE DISPLAYS

by

Raymond J. Bahm
Bickle/CM
2403 San Mateo NE
Suite S-8
Albuquerque, New Mexico 87110
(505) 884-5838

INTRODUCTION

The 3-dimensional displays in this report provide a simple, rapid method of characterizing the climate at a location. These displays provide qualitative information on the performance which might be expected from particular types of solar space heating systems and can be used to aid in preliminary decisions of solar space heating systems and other mechanical and architectural designs.

SOLTEMP DISPLAYS

The solar and temperature climate at a particular location can be characterized by mapping the combination of solar radiation availability and mean daily temperatures onto a single three-dimensional graph. The lower axis is mean daily temperature, degrees F. The axis on the left in the figure represents the daily total solar radiation availability as a percent of extraterrestrial (ETR) solar radiation. The vertical axis shows the relative frequency of occurrence of the combined solar availability and mean daily temperature. This is called the Sol-Temp Data Space.

Warm days are represented to the left of the graphs, and cold days to the right. Sunny days are at the upper portion of the graphs and cloudy days on the lower portion.

OPERATION OF SOLAR SPACE HEATING SYSTEMS

The operation of a typical active solar heating system can be characterized on the Sol-Temp Space by referring to the figure below. The area to the left of the heavier line represents days when the solar system is not used (average daily temperature is above 65°F; no heating is required). The area to the upper right of the space, above line A, represents days when the solar system has full output capabilities because there is plenty of available solar radiation. Days when the solar system doesn't collect any energy, because there is not sufficient available energy to overcome collector and other system losses, are represented to the lower right of the space, below line B. Thus, B represents a lower threshold for active system operation. The area between lines A and B represents days when the system performance is a strong function of the various system design parameters--storage size, collector area, outdoor temperature, etc. In this region the system performance should be very sensitive to the availability of solar radiation. The actual positions of lines A and B will be a function of the system parameters. For typical active systems, A is at about 60 percent ETR and B at about 25 percent ETR.

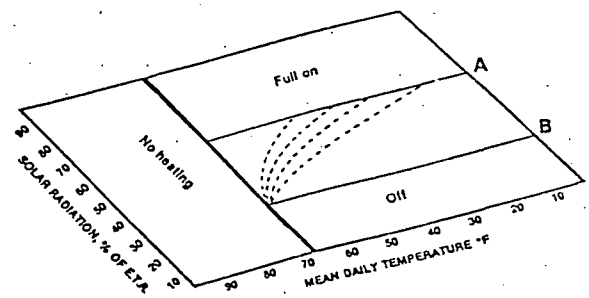

Passive solar space heating systems can have a variety of characteristics, and cannot be characterized as easily as active systems. Passive systems are often described as collecting energy even at very low levels of radiation--about 5% of ETR. It may, therefore, be worth considering passive designs in climates like those of the Northeastern U.S.

A COMPARISON OF FOUR CITIES

Specific climatic characteristics of four cities are compared in the following displays. In addition to the Sol-Temp displays three other examples of displays are shown.

Each display type was prepared to answer specific questions. A large variety of display types are possible. At this point only a few of these

possible displays have been prepared.

This set of displays is part of a program to develop graphical tools which can aid the architect, engineer and other designers in making preliminary design decisions.

The first step in our program is to formulate those questions about climate which require answers early in the design process. We invite you to help with this step by identifying typical designer's needs. The next step is to prepare displays which attempt to provide answers to these questions. The third step is to actually use the displays generated during the design process, thereby evaluating their effectiveness. We believe this is the most important step in developing useful design tools. The last step is to prepare and effectively disseminate these displays for use by the design community.

DATA SOURCES

The data for these displays were taken from the SOLMET data tapes available from the U.S. Department of Commerce, National Oceanic and Atmospheric Administration, Environmental Data and Information Service, National Climatic Center, Asheville, NC.

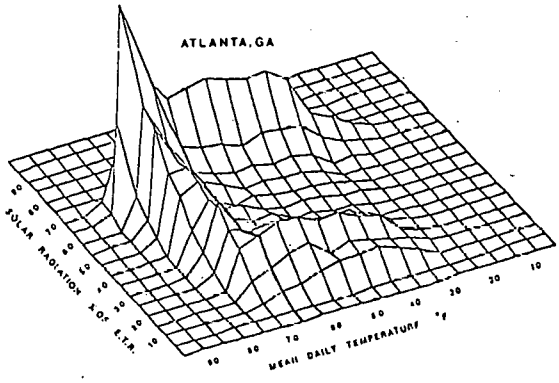

ATLANTA

RADIATION VS TEMPERATURE ANALYSIS

- Cool - Clear Conditions 60% of Heating Season
- Active Solar System Not Useful for 30% of Heating Season
- Coldest Weather Occurs with Clearest Conditions
- Passive System Designed to Capture Maximum Diffuse Radiation May be Useful When Active Systems Are Not.
- "Valley" in Center of Plot Implies Active Systems Either "On" or "Off"
- Passive Systems Designed to Capture Maximum Diffuse Radiation Prone to Overheating if Vents Not Provided.
- Climate Seems to Have Two Winter States, Very Sunny or Overcast.

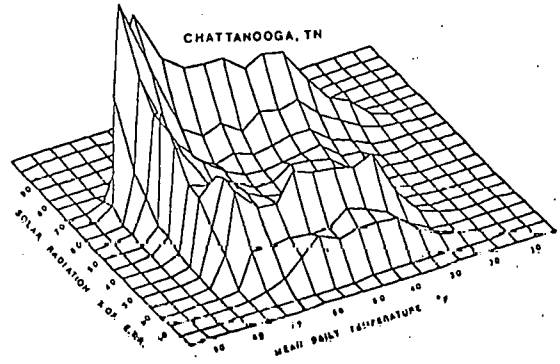

CHATTANOOGA

RADIATION VS TEMPERATURE ANALYSIS

- Cold - Clear Conditions 50% of Heating Season
- Active Solar Systems Not Useful 30% of Heating Season
- Passive Greenhouse Systems May be Useful when Active Systems are not if the Passive Systems are Designed to Capture Maximum Diffuse Radiation.
- "Valley" in Center of Plot Implies Active Systems Either "On" or "Off".
- Passive Systems Without "Venting" Capabilities Prone to Overheating If Designed to Capture Maximum Diffuse Radiation.
- Diversity of Peaks Indicates a Moderately Diverse Climate.

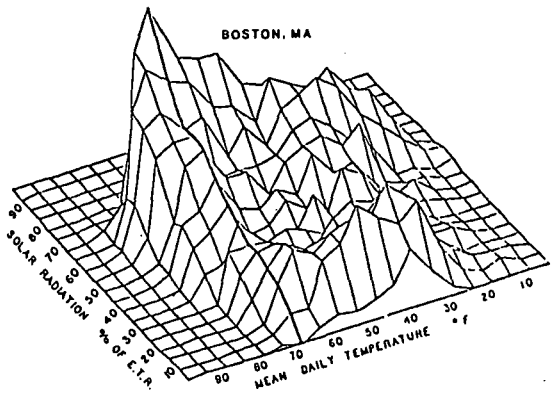

BOSTON

RADIATION VS TEMPERATURE ANALYSIS

- Large Percentage of Heating Season Occurs Below 20% ETR. Thus Active Systems Not Useable During These Periods.
- Center of Plot Quite "Hilly" Indicating System Performance Very Sensitive to Design Parameters - Storage Size, Collector Area, Controls, etc.
- Coldest Days, i.e., Below 20°F Mean Daily Temperature, Occur When Sunniest i.e., 60% ETR or Greater
- Large Amounts of Diffuse Radiation During Colder Periods Favor Passive Systems Designed to Maximize Collection of Diffuse Radiation.
- Vents Should be Provided for Passive Systems which Maximize Collection of Diffuse Radiation to Prevent Overheating During Sunny Days.
- Large Diversity of Peaks Indicates Very Diverse Climate.
- Large Portion of Winter Has Heavy Overcast.

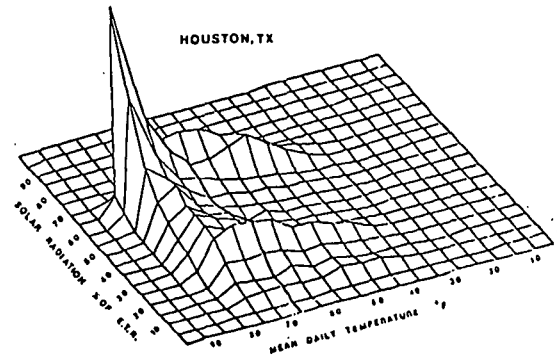

HOUSTON

RADIATION VS TEMPERATURE ANALYSIS

- Cool - Clear Conditions 50% of Heating Season
- Active Solar Systems Not Useful 15% of Heating Season
- "Valley" in Center of Plot Implies Active Systems Either "On" or "Off"
- Climate Seems to Have Two Winter States, Sunny or Moderately Overcast, but Rarely Heavy Overcast.
- Climate is Not Very Diverse With Much of Time Requiring Cooling
- Passive Systems Which Capture Maximum Diffuse Radiation Require Venting to Prevent Overheating.

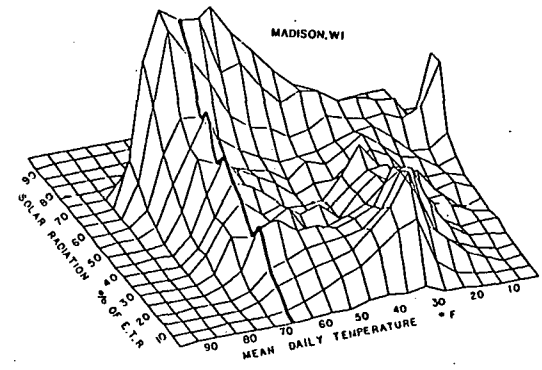

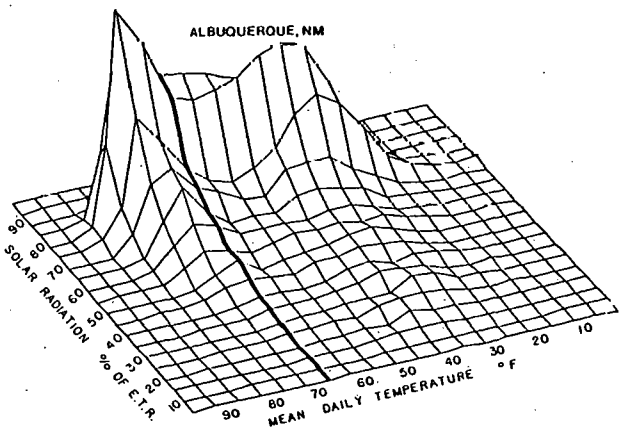

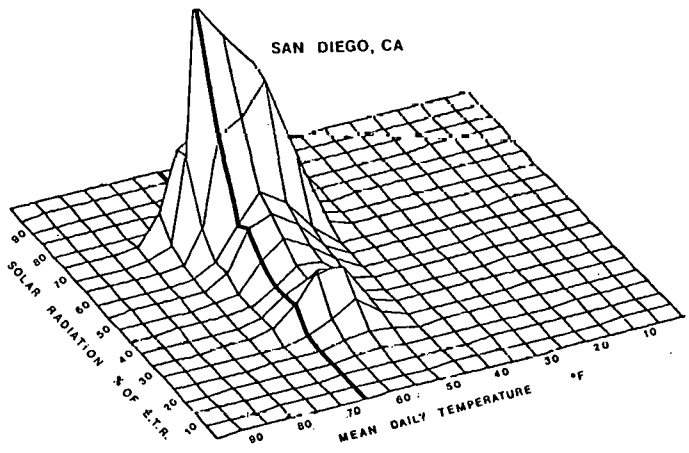

*U. S. GOVERNMENT PRINTING OFFICE: 1980-0-677-175/135